PHYSICAL REVIEW

VOLUME 5 NUMBER 2

1915

THE
PHYSICAL REVIEW

A journal of experimental and theoretical physics established by E. L. Nichols in 1893

SECOND SERIES, VOL. 95, NO. 2 JULY 15, 1954

Absolute Temperature Scale between 4.2° and 5.2°K†

R. BERMAN* AND C. A. SWENSON
Cryogenic Engineering Laboratory, Massachusetts Institute of Technology, Cambridge, Massachusetts
(Received March 29, 1954)

The vapor pressure of helium has been determined between 4.25° and 5.1°K, using a constant volume gas thermometer. An equation is proposed which fits the experimental data closely, and gives temperatures which differ by a maximum of 0.02° from the currently accepted values. The reliability of the value of the boiling point of helium and the thermodynamic consistency of the properties of liquid helium near the boiling point are discussed.

INTRODUCTION

THE currently accepted temperature scale[1] between 4.2° and 5.2°K is largely based on five vapor pressure measurements by Kamerlingh-Onnes and Weber,[2] all above 4.9°. The assumed shape of the vapor pressure curve is not determined solely by these points, but also by the fact that it must join smoothly onto the more accurately known portion of the curve below 4.2°.

It has recently been suggested by Worley, Zemansky, and Boorse[3] that this accepted curve could be in error by as much as 0.06° at 4.8°. They found that an interpolation formula for the resistance of carbon resistors, which fitted vapor pressure data between 1.8° and 4.2° and at the hydrogen triple point, gave temperatures which were lower than the accepted values for helium vapor pressures above one atmosphere, and were in close agreement with values given by an extrapolation of the equation of Keesom and Lignac[4] (which fits the vapor pressure data closely between 2.2° and 4.2°).

We had need for accurate values of dP/dT in this region in order to calculate values of the vapor density from previous experiments.[5] It was noticed that values of dP/dT at 4.3° as calculated from the accurately known portion of the accepted scale and from the formula valid above 4.2° were in disagreement. This suggested that the two curves did not join sufficiently smoothly near the boiling point, where both should apply. Thus doubts were cast on the equation which had been used to fit the data of Kamerlingh-Onnes and Weber.

We have successfully used carbon resistance thermometers for thermal conductivity work between 4° and 80°K, but the discrepancies noticed by Worley *et al.* were not evident since the resistance thermometers were calibrated directly against a gas thermometer over the whole range during the course of each experiment, and an interpolation formula was not required. As our apparatus contained a vapor pressure bulb for calibrating the gas thermometer, it was possible to adapt it for an accurate determination of the helium vapor pressure between 4.2° and 5.2°K.

APPARATUS

Figure 1 is a schematic drawing of the apparatus. The copper gas thermometer (volume roughly 100 cc) is supported on the liquid helium vessel by a length of thin-walled copper-nickel tubing. The heat conduction along this tube is quite small, and the actual cooling of the gas thermometer is achieved by a method similar to that described by Swenson and Stahl.[6] The liquid helium is kept under a slight overpressure by means of

† This work was supported in part by the U. S. Army Air Force, Wright Air Development Center, and in part by the U. S. Army, Office of Ordnance Research.
* On leave from the Clarendon Laboratory, University of Oxford, Oxford, England.
[1] H. van Dijk and D. Schoenberg, Nature **164**, 151 (1949).
[2] H. Kamerlingh-Onnes and Sophus Weber, Leiden Comm. **147b** (1915).
[3] Worley, Zemansky, and Boorse, Phys. Rev. **93**, 45 (1954).
[4] W. H. Keesom, *Helium* (Elsevier Publishing Company, Amsterdam, 1942), p. 196.
[5] R. Berman and J. Poulter, Phil. Mag. **43**, 1047 (1952).
[6] C. A. Swenson and R. H. Stahl, Rev. Sci. Instr. (to be published).

an external bubbler, and by opening the needle valve the gas thermometer can be cooled by liquid helium forced through the copper coil which is silver-soldered to its base. The rate of cooling can be easily controlled by the needle valve, and once a desired temperature is reached, it can be maintained constant through the use of a heater which is attached to the inlet of the copper coil. Changes in temperature are detected rapidly by a carbon resistance thermometer used in conjunction with a Leeds-Northrup Type K potentiometer. The resulting temperature control was such that during the course of a gas thermometer reading (about 20 min), the drift in the vapor pressure of the helium corresponded to less than 0.001°.

The gas thermometer is connected to a 15-mm bore mercury manometer by stainless steel tubing, 0.5-mm inside diameter. The mercury level in the right-hand limb of the manometer is kept constant by adjusting the pressure in the mercury reservoir. The levels are read using a Société Genevoise cathetometer and a 110-cm calibrated Invar scale. The micrometer head of the cathetometer telescope was marked in 0.01-mm intervals, and readings of a mark on the invar scale could be reproduced to a few tenths of a division. However, owing to the greater difficulty of setting on the mercury meniscus, the reproducibility was seldom better than 1 division, or 0.01 mm. This was, for our smallest gas pressure, equivalent to about 0.002°.

The copper vapor pressure bulb (1.5 cc) soldered to the top of the gas thermometer was used initially with nitrogen and hydrogen to calibrate the gas thermometer, and finally to obtain the vapor pressure of liquid helium. It is not necessary to measure the vapor pressures to great accuracy, since in the range with which we were concerned, the vapor pressure changes were about a thousand times greater than the changes in the gas thermometer pressure.

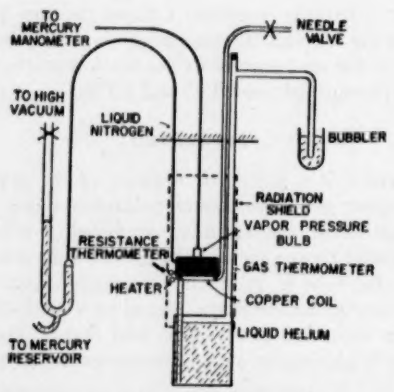

FIG. 1. A schematic drawing of the apparatus. The vacuum jacket and surrounding liquid nitrogen bath are not shown.

REDUCTION OF THE READINGS TO ABSOLUTE TEMPERATURE[7]

An idealized constant volume gas thermometer would consist only of a volume at the temperature to be measured, and of a dead volume in the manometer at room temperature. The ratio of volumes should be as large as possible, and in our case was about 33:1. The pressure-temperature relationship for a gas thermometer is given mainly by two factors, the quantity of gas in the system, and the dead volume ratio. These can be determined by measuring the pressure in the system at two known thermometer temperatures. We chose temperatures near the boiling points of nitrogen and hydrogen, since the vapor pressure-temperature relationships for these substances have been measured accurately by other workers.[8,9]

The system cannot in practice be divided into two such discrete volumes and one must take into account temperature variations of the capillary which connects the two volumes. In our apparatus the major contribution to this effect is due to the gas in the capillary between the liquid nitrogen bath and the gas thermometer. The result is a temperature-dependent addition to the dead volume, which varies from 8 percent when the thermometer is near 80°, to 12 percent at 20°, and 14 percent at 4°K. These figures were calculated, assuming a linear variation with temperature of the thermal conductivity of the stainless steel in the range from 4° to 80°K.[10] The effects of these corrections are quite small, and represent less than 0.001° near 4°.

The system is not truly of constant volume because of the thermal expansion of the copper thermometer. This effect is again small (0.001° near 4°K), and the volume change between 80° and 20°K was taken to be 0.075 percent.[11,12] The deformation of the thermometer due to pressure changes was also checked and found to be less than one or two parts in 10^5, so that it could be neglected.

No corrections were necessary for the changes in the amount of helium adsorbed on the copper surface, since an estimate showed that they were very small.[13] In any event, since data were taken for pressures differing by a factor of four, such effects, if appreciable, would have become evident.

The major reason for taking data at three different filling pressures (giving sensitivities of 0.5, 1, and 2 cm

[7] For further details see, for example, H. J. Hoge and F. G. Brickwedde, J. Research Natl. Bur. Standards **22**, 351 (1939).
[8] W. H. Keesom and A. Bijl, Physica **4**, 305 (1937).
[9] Keesom, Bijl, and van der Horst, Proc. Koninkl. Akad. Wetenschap. Amsterdam **34**, 1223 (1931).
[10] R. Berman, Phil. Mag. **42**, 642 (1951).
[11] Calculated from Grüneisen's law, assuming cubic expansion of 48×10^{-6} at room temperature and a Debye Θ of 330° for copper. For our purposes the deviation from this law for copper at low temperatures, discussed by Bijl and Pullan (see reference 12), is sufficiently small to be neglected.
[12] D. Bijl and H. Pullan, Phil. Mag. **45**, 290 (1954).
[13] For steel, see H. P. R. Frederikse and C. J. Gorter, Physica **16**, 402 (1950).

Hg/degree) was to test the validity of two rather significant corrections which had to be applied. These were for the nonideality of the helium gas and the thermomolecular effect in the capillary leading from the thermometer. The thermomolecular effect was negligible for the calibration data, but the nonideality was still appreciable even at 80°K.

Typical values for the corrections near 4° were as follows: For the smallest filling of the thermometer, neglecting the nonideality would produce an error of 0.023°, and neglecting thermomolecular effects would produce an error of 0.007° in the opposite direction. For the largest filling, the corresponding figures are 0.104° and 0.0005°. These corrections were calculated from the virial coefficient[14] and thermomolecular data[15] given in Keesom's book.

The hydrostatic head correction for both the height of the liquid and height of the vapor above the liquid in the vapor pressure thermometer was small enough to be neglected.

In two of the cases (fillings of 2 and 4 cm Hg pressure) the quantity of gas in the system was determined by measurements close to the hydrogen boiling point, using the vapor pressure data of Keesom, Bijl, and van der Horst.[9] In the third case no hydrogen point data were taken, and the thermometer filling was determined using the accepted (1948 Cambridge) vapor pressure tables for a point at 4.245°K.

RESULTS

The data from all three runs could be represented by the following equation with a mean deviation of 0.002° and a maximum error of 0.007°:

$$\log_{10}p_{\rm cm}=0.97864-(2.77708/T)+2.5\log_{10}T \quad (1)$$

(where p is measured in cm Hg at 20°C). The constants of this equation were determined by passing a least-squares straight line through a plot of $(\log_{10}p_{\rm cm}-2.5\log_{10}T)$ *vs* $1/T$.

Figure 2 gives the deviation of our individual experimental points from the above equation. As can be seen, the scatter is independent of thermometer pressure and, hence, confirms the accuracy of our corrections.

The deviations from our equation of the original experimental points and proposed curve of Kamerlingh-Onnes and Weber[2] are also shown. This curve is of importance, since it is used exclusively by Keesom in his book to describe measurements between 4.2° and 5.2°K. The third curve gives the deviations of the accepted scale from our equation. Considering the experimental data on which this curve is based, the agreement is indeed satisfactory. Equation (1) fits smoothly onto the accepted scale at 4.25° and reproduces it fairly well at lower temperatures, with a deviation of 0.01° at 3.5°K. It actually reproduces the accepted scale more faithfully between 4.0° and 4.3° than does the formula of Keesom and Lignac.[4] This latter equation, when extrapolated to temperatures above 4.3°, gives temperatures that are increasingly low, with an error of 0.05° at 4.8°K.

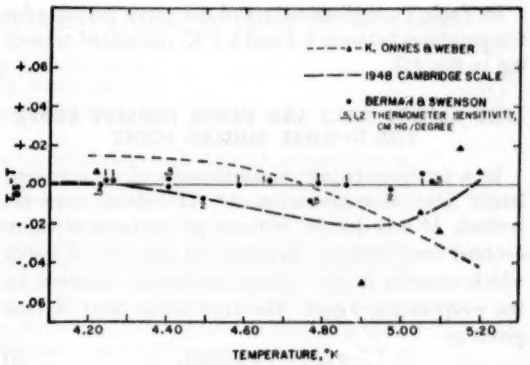

FIG. 2. The deviations of various experimental data and vapor pressure formulas from our proposed scale. T_{BS} is the temperature as given by Eq. (1).

Recent investigations of the absolute temperature scale below 4.2°[16] have assumed the value of the boiling point of helium to be 4.216°. This temperature is the result of three measurements by Keesom and Schmidt[17] based on the boiling point of normal hydrogen (20.381°). When we use the same vapor pressure data for hydrogen,[18] we confirm their helium boiling point to 0.002°. This is true for each of the two runs in which we calibrated the gas thermometer near 20°K. Woolley, Scott, and Brickwedde,[19] however, give a boiling point of hydrogen which is roughly 0.01° higher, and this, if correct, would increase the helium boiling point by 0.002°. The liquid helium temperature scale near 4°K, based on liquid hydrogen data, is therefore subject to this basic uncertainty, which is of the same order as the experimental accuracy of Keesom and Schmidt[17] and of ourselves.

The critical temperature as given by Kamerlingh-Onnes and Weber is roughly in agreement with our data. We did not make a separate determination of the critical point, but have assumed the critical pressure of 171.8 cm Hg (at 0°C) reported by them, and find a temperature of 5.206(±0.003)°K corresponding to this pressure. The critical pressure apparently has not been checked since these original determinations in 1911.[20]

[14] W. H. Keesom, *Helium* (Elsevier Publishing Company, Amsterdam, 1942), p. 49.
[15] See reference 14, p. 122.
[16] R. A. Erickson and L. D. Roberts, Phys. Rev. **93**, 957 (1954). We are grateful to Dr. Roberts for a preprint of their paper.
[17] W. H. Keesom and G. Schmidt, Physica **4**, 828 (1937).
[18] Since our vapor pressure measurements were taken within an hour after condensing the hydrogen from a cylinder, we have assumed that our hydrogen consisted of the normal mixture.
[19] Woolley, Scott, and Brickwedde, J. Research Natl. Bur. Standards **41**, 379 (1948).
[20] H. Kamerlingh-Onnes, Leiden Comm. **124b** (1911).

In Table I are given values of the vapor pressure for temperatures between 4.2 and 5.2°K, calculated according to Eq. (1).

THE LATENT HEAT AND VAPOR DENSITY ABOVE THE NORMAL BOILING POINT

In a previous paper[5] measurements of an apparent latent heat of evaporation, L^*, of helium were described. L^* was defined in terms of the mass of vapor evolved upon heating, ignoring the quantity of vapor which remains in the volume previously occupied by the evaporating liquid. The true latent heat is then given by

$$L = L^*(1-\rho_V/\rho_L), \tag{2}$$

where ρ_V and ρ_L are the vapor and liquid densities, respectively. It was shown that the only directly determined value of this vapor density in the neighborhood of the normal boiling point was not compatible with values derived from the virial coefficients or by the extrapolation of isotherms. It is, however, possible to calculate the vapor density directly from the values of L^* if reliable values of dP/dT are known, since by combining the Clausius-Clapeyron equation

$$\frac{dP}{dT} = \frac{L}{T(\rho_V^{-1}-\rho_L^{-1})} \tag{3}$$

TABLE I. The vapor pressure, vapor and liquid densities, and latent heat of evaporation for saturated helium above 4.2°K.

1 T °K	2 P cm Hg at 20°C	3 ρ_V 10^{-3} g/cc	4 ρ_L g/cc	5 L cal/mole
4.2	75.09	1.69_5	0.1263	19.7_6
4.25	78.74	1.77_5	0.1251	19.4_8
4.3	82.50_5	1.86	0.1238	19.1_8
4.35	86.39	1.95	0.1226	18.8_5
4.4	90.39	2.05	0.1214	18.5
4.45	94.51	2.15	0.1202	18.1
4.5	98.75	2.27	0.1189	17.6
4.55	103.1		0.1177	
4.6	107.6		0.1165	
4.65	112.2		0.1153	
4.7	117.0		0.1142	
4.75	121.8			
4.8	126.8			
4.85	131.9			
4.9	137.2			
4.95	142.6			
5.0	148.1			
5.05	153.8			
5.1	159.6			
5.15	165.6			
5.2	171.6			
5.206	172.5 (Critical pressure for Hg at 20°C)			

with Eq. (2), we obtain

$$\rho_V = (TdP/dT)/L^*. \tag{4}$$

We have calculated values of ρ_V from the values of L^*, and the values of dP/dT derived from Eq. (1), and give these in column 3 of Table I. The discrepancy noted previously[6] between calculated vapor densities and the direct measurements of Mathias *et al.*[21] is actually increased by the change in temperature scale. Below 4.2° values calculated in this way are in excellent agreement with values derived from the virial coefficients, as given, for example, by Erickson and Roberts.[16]

In column 4 of Table I are given values of ρ_L found by Kamerlingh-Onnes and Boks,[22] corrected to our proposed temperature scale. Using our values of ρ_V and these values of ρ_L, we have calculated the true latent heat above the normal boiling point. The agreement with the smoothed values given by Keesom[23] is good, although above 4.2°K this is somewhat fortuitous, since the values of both ρ_V and dP/dT used by Keesom differ by several percent, but in opposite directions, from the values we have derived. At 4.0° and 4.2°K our values of latent heat also agree to within 0.5 percent with values calculated from the free energies by Erickson and Roberts.[16]

SUMMARY

These experiments have shown that the currently accepted values of the boiling point and critical point of helium are quite accurate. The deviations from the accepted scale above 4.3°K which were suggested by Worley, Zemansky, and Boorse[3] (0.06°) were confirmed as to sign, but were actually only one-third as great. This would seem to cast doubt on the validity of using an interpolation formula for carbon resistors between 4.2° and the triple point of hydrogen, unless the behavior of the specific resistor has been checked previously against a gas thermometer.

We have also shown that at the boiling point of helium the vapor density, virial coefficients, and vapor pressure curve are in thermodynamic agreement. A further check on the second virial coefficient is given by the fact that our boiling point, obtained with pressures of several centimeters of mercury in the gas thermometer, agrees so precisely with that obtained by Keesom and Schmidt,[17] who used pressures several hundred times less.

[21] Mathias, Crommelin, Kamerlingh-Onnes, and Swallow, Leiden Comm. **172b** (1925).

[22] H. Kamerlingh-Onnes and J. D. A. Boks, Leiden Comm. **170b** (1924).

[23] See reference 14, p. 231.

Theory of the Aurora Based on Magnetic Self-Focusing of Solar Ion Streams

W. H. Bennett and E. O. Hulburt
Naval Research Laboratory, Washington, D. C.

(Received December 3, 1953)

It is assumed that the sun emits a jet of an electrically neutral mixture of fast electrons and positive ions, and that the space between the sun and earth is filled with an ionized, electrically neutral gas. As the jet proceeds the fast electrons are slowed down and scattered by encounters with the space ionization, being continually replaced by slow electrons from space. The stream of positive ions continues as an electric current, but at all times the stream and surrounding gas are closely electrically neutral. Due to the magnetic field of the electric current, the fast moving positive ions are continually compressed into the stream and the fast electrons and slower ions are ejected from the stream. This is "magnetic self-focusing." The stream develops into a narrow core which if correctly aimed enters the earth's magnetic field and is diverted to auroral zones according to the calculations of Störmer. Meinel's observations indicate that the primary solar particles in the stream are mainly protons of speed greater than 3×10^8 cm sec^{-1}. A speed of order of 10^{10} cm sec^{-1} of the protons is required for correct Störmer orbits into auroral latitudes and penetration to 60- to 80-km levels in the upper atmosphere. For a stream which carries sufficient energy for an aurora, the density of space ionization between the sun and earth is calculated to be at least 10^{-5} electron ion pairs cm^{-3} to support magnetic self-focusing and not more than 10^9 pairs cm^{-3} for the fast protons to be able to reach the earth. It is suggested that the auroral rays are not the solar proton stream but are formed when the protons are stopped in the upper atmosphere. Due to the charges and absorbed energy of the protons, oxygen and nitrogen particles of the atmosphere are ejected outward to great heights along the lines of magnetic force and form the auroral rays and streamers.

INTRODUCTION

THE identity of the primary particles incident upon the earth's upper atmosphere and responsible for the aurorae has remained in question[1] until recently when Meinel reported his measurements[2] of the H_α line in the quiet arc which occurs at the beginning of an auroral display. Meinel observed a broadening but no Doppler shift in the H_α line when observing towards the magnetic horizon, but found and measured a Doppler shift when observing towards the magnetic zenith. He was able to show that protons reach the earth's atmosphere with velocities of at least 3.3×10^8 cm/sec corresponding to more than 50 000 electron volts of proton energy.

The hydrogen which is responsible for the H_α line having the observed Doppler shift would have to approach the earth as ions in order for the earth's magnetic field to be able to restrict such particles to the auroral zone of about 23° of latitude around the magnetic poles of the earth. Calculations of the kind first published by Störmer[3] show that such ions would have to have velocities of at least 10^{10} cm sec^{-1} corresponding to energies of the hydrogen ions of 65 Mev. Meinel pointed out that these much larger velocities are not precluded by his observations because an incoming hydrogen ion would first have to be slowed down by collisions in the earth's atmosphere to the order of 10^8 cm sec^{-1} before it could attach a slow atmospheric electron into the excited atomic state from which H_α could be radiated. The maximum intensity in Meinel's Doppler-shifted H_α line occurs at a velocity of 4×10^7 cm/sec and the intensity falls steadily to approximately zero at a velocity of 3.3×10^8 cm/sec. The likelihood of electron attachment is negligible until the relative velocity of ion and electron has decreased to the order of magnitude of the Bohr-orbital velocity of the electron in the atom to be formed[4] which for the excited state necessary for the H_α radiation is about 7×10^7 cm/sec. That high-velocity ions were present in the upper atmosphere in auroral latitudes was discovered by Meredith, Van Allen, and Gottlieb[5] by means of cosmic-ray equipment on high-altitude rockets. They observed ionic particles having a penetrating power greater than that of 18-Mev protons at north magnetic latitudes 64° and 74°, which are near the region of maximum auroral frequency, and did not observe such ionic particles at north magnetic latitudes 89° and 56°, which are remote from the auroral zone.

A 65-Mev proton has a penetrating power of approximately 26 meters of air at normal pressure and temperature. If these protons were to enter the earth's atmosphere vertically they would penetrate to an altitude of 40 kilometers whereas auroral arcs are usually seen at higher altitudes than this. Störmer calculations of the paths of such protons in the earth's magnetic field show that the paths are turned away from the vertical and that the protons spiral or curve around the magnetic lines of force while approaching the earth, reaching the end of their allotted 26 meters

[1] A recent review, "The Aurorae," V. C. A. Ferraro in Advances in Physics, a supplement of the Phil. Mag. **2**, (7), 265–320 (1953).
[2] A. B. Meinel, Astrophys. J. **113**, 50 (1951), and Mém. soc. roy. sci. Liège **12**, 203 (1952).
[3] C. Störmer, Kristiania Ske. Vid. Selsk **1**, 3 (1904) and Arch. sci. phys. et nat. **32**, (1911–12). See also Thomas H. Johnson, Revs. Modern Phys. **10**, 193 (1938) and R. A. Alpher, J. Geophys. Research **55**, 437 (1950).
[4] See N. F. Mott and H. S. W. Massey, *The Theory of Atomic Collisions* (Clarendon Press, Oxford, 1949), second edition, Chap. XII, Sec. 2.
[5] Meredith, Van Allen, and Gottlieb kindly gave us advance information of their results.

of air (at N.T.P.) at altitudes above 40 kilometers. Meinel found that H_α comes from lower altitudes than the oxygen and nitrogen auroral emissions.

Although the 10^{10} cm sec^{-1} protons must be slowed down to the order of 10^8 cm sec^{-1} before attachment of electrons to radiate H_α is likely, protons moving at an intermediate velocity of say 10^9 cm sec^{-1} are moving at the same velocity as 250-ev electrons, and this is the right order of magnitude of velocity for the ionizing particles to excite optically the atmospheric molecules and produce the main auroral displays.

Many of the features of auroral phenomena were explained in the early work of Birkeland[6] and Störmer[3] on the supposition that streams of particles of one polarity of charge moved from the sun to the earth. The theory was developed to explain the restriction of the incoming ions to auroral zones around the magnetic poles by the earth's magnetic field, the delay between the passage of a sun spot past the line of centers between the sun and earth and the incidence of the auroral disturbance at the earth, the correlation between auroras and magnetic storms, and the location of auroras at 80 to 140 kilometers in altitude.

Explanations of the auroras involving streams of charged particles were rejected by Schuster[7] and Lindemann[8] (now Lord Cherwell) and later by Chapman and Ferraro[9] for the reason that such streams would disperse due to mutual electrostatic repulsion of the particles in the stream. To overcome this objection, various theories[9–11] have been advanced based on electrically neutral streams of particles of both signs of charge, but the theories have not been carried completely or satisfactorily to the point of explaining how the particles are diverted to auroral latitudes. In this paper a theory is presented which is based on an effect not heretofore considered in auroral stream theories, namely the magnetic self-focusing action of ionized streams first presented in 1934 and developed in a more general form recently.[12]

SELF-FOCUSING STREAM THEORY

It is generally supposed that interplanetary space is filled with an electrically neutral mixture of positive ions and electrons but the various estimates of the density of this matter differ by several orders of magnitude. In the theory of magnetically self-focusing streams it is shown[12] that a stream of charged particles of only one sign entering a region containing an electrically neutral mixture of charges of both signs with random velocities small compared with the velocity of the particles in the entering stream can form a magnetically self-focusing stream. The condition that must be met in order for the stream to be self-focusing is that the total electric current i in the stream of fast particles must be greater than

$$i \geqq 2c^2(\theta_1+\theta_2)/eu, \tag{1}$$

where θ_1 is the average kinetic energy of the particles in the entering stream due to components of velocity transverse to the axis of the stream, θ_2 is the average transverse energy of the residual slow particles of opposite sign, u is the average velocity in the direction of the stream of the particles in the entering stream, e is the charge of each such particle, and c is the velocity of light.

When a current of high-speed protons, large enough to be magnetically self-focusing, emerges from the sun and proceeds into the electrically neutral mixture in interplanetary space, the protons introduce an excess positive charge which repels the residual slow positive ions from the stream. The residual slow ions have negligibly small magnetic forces acting on them because their velocities are small, while the high-speed ions are attracted towards each other magnetically. The residual slow ions ejected from the stream produce electric fields in the electrically conducting medium permeating the interplanetary space and the charges in that medium shift under the influence of those electric fields to relieve those electric fields. The residual slow electrons are held in the stream by the excess positive charge in the stream. Any of these electrons with which high-speed protons collide and which recoil in the direction of motion of the protons will be magnetically repelled by the preponderant magnetic field of the high-speed protons, and so the stream continues to repel slow ions and fast electrons keeping only the fast protons and slow electrons. Streams which are established in a gas at low pressure are essentially stable as discussed in reference 12.

In order to estimate the magnitude of the minimum electric current which a stream of 10^{10} cm sec^{-1} protons must have in order to be self-focusing, it is necessary to know the value of the average kinetic energy of the protons due to components of velocity transverse to the axis of the stream. These transverse components arise both by virtue of the thermal spread in velocity of the protons around the mean velocity of the protons in the stream and also because of the divergence of the stream away from the axis of the stream as the stream starts away from the sun. Table I gives some representative values of minimum currents in amperes of 10^{10} cm sec^{-1} protons required for self-focusing, for various temperatures of the protons and various maximum slopes of the direction of motion of protons from the axis in a diverging cone of protons. From Table I it is seen that the divergence of the stream of protons as it emerges from the sun is probably the principal

[6] K. Birkeland, Arch. sci. phys. et nat. **4**, 497 (1896).
[7] A. Schuster, Proc. Roy. Soc. (London) **85**, 44–50 (1911).
[8] F. A. Lindemann, Phil. Mag. **38**, 669–684 (1919).
[9] S. Chapman and V. C. A. Ferraro, Terrestial Magnetism and Atm. Elec. **36**, 77–97; **46**, 1–6 (1941) and S. Chapman, Ann. geophys. **6**, 205–224 (1952).
[10] D. F. Martyn, Nature **167**, 92 (1951).
[11] H. Alfvén, Kgl. Svenska Vetenskapsakad. Handl., 3rd Ser. **18**, No. 3, 1–39 (1939) and No. 9, 1–39 (1940).
[12] W. H. Bennett, Phys. Rev. **45**, 890–897 (1934); Phys. Rev. (to be published).

factor determining the minimum current of protons which the stream must contain in order to become self-focusing and so to reach the earth in an intense enough bundle to produce an aurora.

ORIGIN OF A STREAM

It is assumed that the jet of material which first emerges from the sun consists of an electrically almost neutral mixture of fast protons and fast electrons moving along together at about the same velocity, so that the electric current in the jet is zero; such a jet would not be magnetically self-focusing. The jet would diverge increasingly with increasing altitude above the sun's surface both because of the random thermal velocities of the particles and also under the effects of the gradients of radiation density—the same kind of effect which caused the material in the jet to rise out of the sun and attain such a high velocity in the first place. The jet moves out through the sun's atmosphere which may be supposed to consist mostly of an electrically neutral mixture of slow electrons and slow protons which decreases in density with altitude.

The effects of collisions of the rapidly moving electrons and protons in the outermost parts of the jet with the slow electrons and protons in the sun's atmosphere are calculated using the methods published by Thomas.[13] By using Thomas' equation (4.31) for the time rate at which a charged particle of mass m_1 and large velocity v_1 loses momentum when moving through an atmosphere of slow charged particles of mass m_2 and particle density N_2 per unit volume, the mean rate of deceleration of the particle of kind 1 may be written

$$dv_1/dt = 4\pi e^4 A\{\log(2B/\log B) - \gamma - 1\}N_2/v_1^2 m_1, \quad (2)$$

where $A=(m_1+m_2)/m_1m_2$, $B=3v_1^6/4\pi A^3e^6N_2$, and $\gamma=0.5772$ is Euler's constant.

In Table II are given some values, calculated from (2), of the deceleration of 10^{10} cm sec^{-1} electrons and of 10^{10} cm sec^{-1} protons in densities N of slow electrons and N of slow protons. Given also are the total deceleration of the electrons and protons in mixtures of the two polarities of slow particles and the ratios of the decelerations in various densities of slow particles. It is seen that the electrons are slowed down at more than 5000 times the rate at which the protons are slowed down at all densities of the atmosphere. As the jet of material rises out of the sun, the electrons in the jet are retarded and scattered out of the jet more than 5000 times as rapidly as the protons are, whenever the jet of material has decreased in density enough to permit the atmosphere to penetrate into the jet. In such outermost parts of the jet, the excess of fast protons over fast electrons which accompanies such selective scattering and slowing of electrons, produces a positive electric current outward from the sun. This selective scattering and slowing of the electrons continues with a continuing increase in positive electric current outward from the sun in the jet until the current has risen to exceed the critical current for magnetic self-focusing given by Eq. (1). At this point, the magnetic field of the magnetically self-focusing stream exerts a repellent force on the remaining fast electrons in the jet strong enough to repel them all from the stream, keeping only the slow electrons which were already there before the stream arrived or which drift into the stream from the outside of the stream assisted by the electric attraction of the excess positive charge in the magnetically self-focusing stream. From this point on, the stream is self-focusing and does not spread out to a greater mean square radial distribution than the stream had where self-focusing first set in. Once self-focusing has set in, the magnetic field produced from there on also reacts backward along the on-coming material to eject the fast electrons and assists to some extent in propagating the self-focusing conditions backwards towards the sun. As the self-focusing conditions propagate backwards towards the sun, the divergence of the material in the jet is decreased, and the current which must be exceeded in order to attain self-focusing conditions is correspondingly reduced, as illustrated in Table I.

In addition to the effect of the sun's atmosphere in

TABLE I. Minimum current of 10^{10} cm sec^{-1} protons for magnetic self-focusing for various proton temperatures and various cone angles. (ξ = half-angle of the cone.)

Proton temperature	tan ξ 0.001	0.01	0.1
10 000°K	5.9 amp	570 amp	57 000 amp
100 000	7.3	570	57 000
1 000 000	21	590	57 000

TABLE II. Deceleration in cm sec^{-2} of 10^{10} cm/sec electrons and protons in electrically neutral mixtures of slow electrons and protons of density N.

N	1 cm^{-3}	10^6 cm^{-3}	10^{12} cm^{-3}	10^{18} cm^{-3}
Fast electrons due to slow electrons	1.2	9.6×10^{5}	7.3×10^{11}	5.1×10^{17}
Fast electrons due to slow protons	0.6	4.9×10^{5}	3.8×10^{11}	2.8×10^{17}
Fast protons due to slow electrons	3.3×10^{-4}	2.7×10^{2}	2.1×10^{8}	1.5×10^{14}
Fast protons due to slow protons	4.5×10^{-7}	0.4	3.2×10^{5}	2.6×10^{11}
Total deceleration of electrons	1.8	1.5×10^{6}	11.1×10^{11}	7.9×10^{17}
Total deceleration of protons	3.3×10^{-4}	2.7×10^{2}	2.1×10^{8}	1.5×10^{14}
Decel. of electrons / Decel. of protons	5400	5400	5400	5300

[13] L. H. Thomas, Proc. Roy. Soc. (London) **121**, 464 (1928).

scattering electrons out of the mixed jet rising out of the sun, the atmosphere also exercises another selective effect which can be deduced from Eq. (2). If there are some ions of other elements than hydrogen in the jet of material, these will not be slowed down and scattered out as much as the protons and so the stream of positive ions which eventually emerges from the sun's atmosphere will be richer in ions of the heavier elements than is the matter in the sun. Such heavier ions are held in the magnetically self-focusing stream at least as strongly as the protons, and if they are multiply charged, as they will doubtless be, they will be held in magnetically even more strongly. Such heavy ions would probably be separated from the proton stream when the stream enters the magnetic field of the earth, but whether they actually exist or where they would go is speculative.

INTERPLANETARY MATTER

Intense auroral displays produce an intensity of visible light at the ground of the order of magnitude of moonlight which is approximately 1 erg cm^{-2} sec^{-1}. If one supposes that an average display reaches one percent of this intensity at its maximum, and that the order of one percent of the energy of the incoming protons produces visible light, a stream of 10^{10} cm sec^{-1} protons spread over an area 1000 km in diameter would contain a current of about 15 amperes. This is probably less than the actual auroral currents.

In order for a stream to form, it must be able to acquire slow electrons from the interplanetary matter in approximately the same density as the density of the fast protons in the stream. In Table III are given values of this density for streams of 10^{10} cm sec^{-1} protons for various currents and various equivalent stream radii, that is the radius which the stream would have if the stream were to be redistributed into a cylinder of uniform density equal to the density at its most dense part. The density of interplanetary matter does not necessarily have to be as large as the values given in Table III, because the stream of fast protons can attract slow electrons to some extent from the surrounding space.

It might be supposed that the rapidly moving protons will collide with the slow electrons in the stream, giving them increasing velocities in the direction of the stream so that the magnetic field of the stream would magnetically repel these speeded up electrons and throw them out, or that the collisions would increase the kinetic energy of the electrons due to transverse components of velocity and so increase the value of θ_2 in Eq. (1) that the current in the stream would become less than the critical current causing the stream to disperse. The following calculations indicate that neither of these possibilities is important. Consider a stream of fast protons of uniform density out to a radius r and zero beyond travelling through interplanetary matter consisting of a density n slow electrons cm^{-3} originally mixed with an equal density of slow ions. The slow electrons may be supposed to have reached thermal equilibrium characterized by a temperature T which is probably between 200°K and 10 000°K. The gas kinetic rate at which slow electrons will enter unit length of the stream is $n(kT/2\pi m)^{\frac{1}{2}}2\pi r$. The number of slow electrons in unit length of the stream is approximately $n\pi r^2$. The average time τ spent by a slow electron in the stream is the quotient of these two expressions, or $\tau=(\pi m/2kT)^{\frac{1}{2}}r$. For $r=1000$ km, τ is 23 and 3.2 sec for $T=200°$ and 10 000°K, respectively. Assume an exaggeratedly large density, 0.2 fast proton cm^{-3}, in the stream. Then from Eq. (2) the average rate at which a slow electron acquires a velocity in the direction of the stream is 0.12 cm sec^{-2}, and the average changes in velocity are 2.8 and 0.4 cm sec^{-1}, respectively, which are negligibly small compared to the velocity 10^{10} cm sec^{-1}.

From Thomas' Eq. (4.33), can be calculated the average rate at which a slow electron can acquire an increase in kinetic energy due to transverse components of velocity, θ_2 in Eq. (1). The average gain in θ_2 while an electron is in the stream is of the order of 0.003 ev which is negligible compared with the values of θ_1 to be expected from the divergence of the stream while forming.

From Eq. (2) one may estimate the density of interplanetary ionization which would slow down 10^{10} cm sec^{-1} protons by 10 percent and 100 percent in travelling from the sun to the earth, a distance of 1.5×10^{13} cm. It is found that the densities are of order 10^9 and 10^{10} slow electrons cm^{-3}, respectively, which are improbably large values. It is concluded that the present theory of self-focused streams requires a density of interplanetary matter between the rather wide limits of 10^{-5} and 10^9 ion electron pairs cm^{-3}.

TABLE III. Minimum density of ions and electrons per cm^3 in interplanetary space necessary to support a self-focused stream.

Current amperes	Equivalent stream radius 10 km	100 km	1000 km
10	0.0018	0.000018	0.00000018
100	0.018	0.00018	0.0000018
1000	0.18	0.0018	0.000018

DISCUSSION

Although many of the foregoing calculations are based on protons of speed 10^{10} cm sec^{-1}, it is hardly necessary to remark that the present theory is not limited to protons. As far as the theory is concerned the incoming ions could be of other kinds than protons and of other speeds than 10^{10} cm sec^{-1} within limits. Protons of speeds 10^{10} cm sec^{-1} spiral to the earth along the lines of magnetic force, the radii of the spiral being about 20 and 30 km at altitudes 100 and 1000

km, respectively. But the auroral rays, which lie approximately along the magnetic lines, emit mainly the radiations of oxygen and nitrogen and do not emit the hydrogen spectrum with observable intensity. The rays are observed up to 800 km, and it is not believed that the upper atmosphere normally extends to such a high altitude. It is suggested that the auroral rays arise from a secondary action. The charge carried by the ionizing stream of protons which are stopped in the earth's atmosphere at about 70-km altitude must be neutralized by motion of charges in the earth's ionized upper atmosphere—else impossibly large electrical fields would rapidly be produced around the place where fast protons are being stopped. At altitudes below about 90 km, the charge motion in the earth's atmosphere will consist mostly of positive ions moving upwards and negative ions moving downwards. There will be few free electrons here because the atmospheric oxygen is mostly molecular and dissociative attachment with free electrons to form negative atomic oxygen ions rapidly removes free electrons from the air in such conditions as these, as has recently been shown by Loeb.[14] The mobilities of negative ions and positive ions are approximately equal, and so the negative ion current downwards is about equal to the positive ion current upwards. The positive ions moving upwards continue to move upwards carrying material in the form of ions to as high altitudes as the electron field will sustain them and this field could well reach to 800-km altitude. The downward current of negative ions below altitudes of 90 km must be sustained by an equal downwards current of negative charges from higher altitudes, although above about 120 km most of the atmospheric oxygen is atomic instead of molecular and negative ion formation is unlikely. The much greater mobility of free electrons at these higher altitudes enables the electrons to move more easily and to neutralize the electric field more nearly completely at these higher altitudes, but the downward current of these free electrons cannot exceed the downward current of negative ions at the lower altitudes unless there is recombination of electrons with positive ions at the intermediate altitudes and such recombination is negligible at these low densities. Both the incoming electrons and the outgoing positive ions must spiral around the earth's magnetic lines of force. These streams are the auroral rays. This view appears to offer a reasonable explanation of the appearance of the lines of ionized nitrogen and oxygen observed in the spectrum of auroral rays up to 800 km. It further follows that groups of auroral rays, such as those which often develop out of a quiet auroral arc above 80 km are not filamented structures caused by irregularities of the solar emission but rather by irregularities of the terrestrial atmosphere.

A solar proton speed of 10^{10} cm sec^{-1} is greater than the value 10^{8} cm sec^{-1} of certain older estimates,[15] which were based on the statistical observation that 15 to 30 hours, or of order 10^{5} sec, elasped between the time that a sun spot passed the meridian and the onset of an associated auroral display or magnetic storm. Dividing 1.5×10^{13} cm by 10^{5} sec gives a particle speed of order 10^{8} cm sec^{-1}. Such a calculation assumes that the particles travel in straight lines from the sun to the earth and is incorrect if they do not do so. Paths of protons near the earth are not straight but are bent by the terrestrial magnetic field in a direction contrary to the motion of solar rotation (an oversimplified statement, the exact path is very complicated); hence the long delay of the protons in reaching the earth is only apparent. However, to calculate the delay quantitatively requires knowledge of the geometrical shape of proton orbits in the earth's magnetic field which is not as yet available.

The present view throws doubt on the particle theory of magnetic storms of Chapman and Ferarro[9] which assumed an ionized, electrically neutral stream of particles which spread out from the sun uniformly in a vast cone and envelop the earth. Unless the particle density of interplanetary space is very low, less than about 10^{-5} cm^{-3}, such a stream would become self-focusing, and would not progress as a vast cone and would not produce the magnetic effects which they have calculated.

[14] See L. B. Loeb, Phys. Rev. **86**, 256 (1952).

[15] See L. Harang, *The Aurorae* (Chapman and Hall, Ltd., London, 1951), p. 143.

Origin of Nitrous Oxide in the Atmosphere

P. HARTECK AND S. DONDES
Department of Chemistry, Rensselear Polytechnic Institute, Troy, New York
(Received March 23, 1954)

The origin of nitrous oxide in the atmosphere is due to the reaction between nitrogen molecules and oxygen atoms formed by the photochemical dissociation of ozone in the atmosphere. The steady state of 5×10^{-7} nitrous oxide in the atmosphere is due to the photochemical equilibrium between nitrous oxide formation and nitrous oxide decomposition, the latter in the upper atmosphere.

NITROUS oxide is present in the atmosphere in a concentration of 5×10^{-7}, similar to the amount of hydrogen present but greater than the ozone content.[1] In a letter to the *Journal of Chemical Physics* we have indicated that experimentally, the following reaction (I) has been accomplished and has a heat of activation of only about 12 kcal.[2]

$$N_2+O+M=N_2O+M. \quad (I)$$

The reason for the presence of nitrous oxide in the atmosphere, has, to date, not been explained. We believe the presence of nitrous oxide in the atmosphere to be due to a photochemical equilibrium between nitrous oxide formation and nitrous oxide decomposition, as follows:

$$O_3+h\nu_{(II)}=O_2+O, \quad (II)$$

$$O_2+O+M=O_3+M, \quad (III)$$

$$O_2+O+M=O_3^*+M, \quad (IIIa)$$

$$N_2+O_3^*=N_2O+O_2, \quad (Ia)$$

$$N_2O+h\nu_{(IV)}=N_2+O \text{ or } NO+N.^3 \quad (IV)$$

If the sum of the light quanta absorbed by ozone is known[4,5] ($h\nu_{II}=5\times10^{15}$/cm² sec), the nitrous oxide production can be readily calculated, which will be, in turn, equivalent to the photochemical decomposition of nitrous oxide in the stationary state.

$$\frac{+d(N_2O)}{dt}\text{ produced}=\frac{h\nu_{II}\times k_I\times(N_2)}{k_{III}\times(O_2)}$$

$$=\frac{-d(N_2O)}{dt}\text{ decomposed}=h\nu_{IV}, \quad (V)$$

with

$$k_I/k_{III}=(f)e^{-12\,000/RT};\ (N_2)/(O_2)=4;$$

$$h\nu_{II}=5\times10^{15};\ (f)=10;$$

$$\frac{+d(N_2O)}{dt}\text{ produced}=5\times10^{15}\times4\times(f)$$

$$\times\exp\left(\frac{-12\,000}{1.985\times300}\right)=3.5\times10^8.$$

k_{III} and k_I, are the reaction velocity constants for reactions (III) and (I), respectively. $h\nu_{II}$ and $h\nu_{IV}$, are the absorbed light quanta per cm²/per sec, in the daytime, for ozone and nitrous oxide, respectively. The temperature of the atmosphere ranges from 220° to 320°K, but since the higher temperatures are more effective, we have used a temperature of 300°K in these calculations.[6] The (f) factor is used to include some degrees of freedom which may be effective in reaction (V).

An evaluation of the absorption coefficients of nitrous oxide, oxygen, and ozone, shows, that only in the wavelength region of 1900A to 2050A, the nitrous oxide absorbs reasonably and is photochemically dissociated, and indicates that of the 10^{13} light quanta per cm² per sec, available from the sun's irradiation, only 10^8 to 10^9 per cm² per sec are absorbed. This result compares very favorably with that calculated in Eq. (1).

With about 10^{19} nitrous oxide molecules per cm² present in the atmosphere, the time of relaxation can be calculated as

$$10^{19}/(1.5\times10^7\times3\times10^8)=2\times10^3 \text{ years},$$

where 1.5×10^7 is one-half the number of seconds in one year, and 3×10^8 is the number of light quanta absorbed by nitrous oxide per cm² per second. Since the concentration of nitrous oxide in water at 10°C is almost the same as in the gas phase, the nitrous oxide in the atmosphere would be washed out once in about 10^4 years.

The explanation presented above presumes that the nitrous oxide would not be attacked or be produced biologically. This question could readily be answered by an analysis of waters of different origins. We are presently investigating other possible reactions of nitrous oxide in the atmosphere, which may play a minor role, as

$$NO_2+N=N_2O+O.^7 \quad (VI)$$

It seems that the exact knowledge of the nitrous oxide behavior [i.e., heat of activation, diffusion, separation, and (f) factor] in nature, as with carbon-14 and tritium, would enhance the finer details of the behavior of the atmosphere.

Acknowledgment is made to the U. S. Atomic Energy Commission for its kind assistance and support of this project.

[1] L. E. Miller, J. Chem. Educ. **31**, 112 (1954); G. P. Kuiper, *The Atmospheres of the Earth and Planets* (University of Chicago Press, Chicago, 1949).
[2] P. Harteck and S. Dondes, J. Chem. Phys. **22**, 758 (1954).
[3] Henriques, Duncan, and Noyes, J. Chem. Phys. **6**, 518 (1938).
[4] Watanabe, Inn, and Zelikoff, J. Chem. Phys. **21**, 1026 (1953); Johnson, Purcell, Tousey, and Watanabe, J. Geophys. Research **57**, 157 (1952).
[5] Zelikoff, Watanabe, and Inn, J. Chem. Phys. **21**, 1643 (1953).
[6] Reaction (IIa) considers that the formation of ozone in a three-body collision first forms an activated ozone molecule (the heat of formation being 23 kcal). Therefore, reaction (Ia) may not be neglected in comparing it with reaction (I), especially not at the lower temperatures.
[7] P. Harteck and S. Dondes, J. Chem. Phys. **22**, 953 (1954).

Second Sound Attenuation in Liquid Helium II

W. B. HANSON*† AND J. R. PELLAM‡
National Bureau of Standards, Washington, D. C.
(Received April 1, 1954)

Second sound attenuation was measured in the hundred kilocycle per second frequency range with a continuous wave method. Measurements were carried out over the temperature interval from 1.25°K to 2.17°K. The short wavelengths employed and the absence of walls near the second sound beam caused geometrical attenuation and wall losses to be negligible compared to the actual liquid attenuation.

The attenuation was found to be amplitude independent for the small amplitudes employed. The expected increase of attenuation with the square of the frequency was experimentally verified up to 0.27 Mc/sec. Excellent agreement with Khalatnikov's latest theory was obtained for both the magnitude and temperature dependence of the attenuation. The attenuation was found to increase rapidly as the λ point was approached and apparently becomes infinite there.

I. INTRODUCTION

THE phenomenon of second sound propagation in liquid helium II is well known. Early theoretical[1,2] and experimental[3,4] investigations demonstrated the anomalous heat flow characteristics of helium II and showed that the ordinary heat conduction equation does not apply. Instead a true reversible wave equation is involved, and the resulting thermal propagation displays the usual characteristics of true wave behavior.

The first-order properties of these thermal waves, called second sound, have been studied intensively since their discovery by Peshkov in 1946. Thus the velocity behavior has been determined reliably from the λ point (2.19°K) down to about 0.5°K and has been observed down to temperatures of the order of 0.01°K. Although until recently no serious attempts have been made to measure such second-order properties of these waves as attenuation, this quantity has been under consideration from the theoretical standpoint for some time. Experimental developments have now progressed to the point where reliable attenuation measurements can be achieved, and the purpose of the present investigation was to measure this absorption as a function of frequency and temperature.

The subject of second sound attenuation has been examined by several authors. The *temperature amplitude attenuation coefficient* α under consideration is defined by the relationship

$$\tau(x)=\tau(0)e^{-\alpha x} \tag{1}$$

for plane wave propagation, where $\tau(x)$ is the temperature deviation from the ambient as a function of distance x. The contribution to attenuation attributable to the ordinary viscosity of the normal fluid component was given in 1948 by Pellam[5] as

$$\alpha_{\text{vis}(1)}=\frac{2}{3}\frac{\omega^2}{\rho v_2^3}\frac{\rho_s}{\rho_n}\eta, \tag{2}$$

in terms of the angular frequency ω ($\omega=2\pi\nu$), the wave velocity of second sound v_2, and the component densities ρ_n and ρ_s of normal fluid and superfluid. Since the coefficient of ordinary viscosity η of normal fluid has since been termed "first viscosity" by Khalatnikov,[6] the above contribution to the attenuation coefficient is indicated by the subscript vis(1).

As has been recently shown by Khalatnikov, two additional processes contribute to the attenuation of second sound in liquid helium II. The presence of these additional mechanisms became apparent to Khalatnikov in connection with his analysis of earlier observations of *first sound* attenuation in liquid helium II. In 1947 Pellam and Squire[7] had measured the absorption of ordinary (first) sound in liquid helium II and found not only an anomalously high value of attenuation, but also an *increase* with decreasing temperature. Although Andronikashvilli's 1948 viscosity measurements could explain the above-mentioned temperature dependence of the first sound absorption, the complete disagreement in actual order of magnitude was interpreted by Khalatnikov as evidence of complicated dynamic interactions not involved in the ordinary viscosity.

Khalatnikov was able to explain this excessive first sound absorption in terms of a new viscous process associated with both normal fluid and superfluid which he called "second viscosity." He showed that this second viscosity should be the predominant factor in first sound absorption below 2.0°K and that the absorption should continue to increase as the temperature was lowered. This was later verified by Atkins and

* Submitted in partial fulfillment of the requirements for the degree of Doctor of Philosophy at the George Washington University.

† Now at the N.B.S. Cryogenic Engineering Laboratory, Boulder, Colorado.

‡ Now at California Institute of Technology, Pasadena, California.

[1] L. Tisza, Compt. rend. **207**, 1035, 1186 (1938).

[2] E. M. Lifshitz, J. Phys. (U.S.S.R.) **8**, 110 (1944).

[3] V. P. Peshkov, J. Exptl. Theoret. Phys. (U.S.S.R.) **10**, 389 (1946).

[4] Keesom, Saris, and Meyer, Physica **7**, 817 (1940).

[5] J. R. Pellam, Phys. Rev. **75**, 1183 (1949).

[6] I. M. Khalatnikov, J. Exptl. Theoret. Phys. (U.S.S.R.) **20**, 243 (1950).

[7] J. R. Pellam and C. F. Squire, Phys. Rev. **72**, 1245 (1947).

Chase.[8] In the case of second sound the absorption due to second viscosity should be only of the same order of magnitude as that resulting from the normal fluid viscosity. Thus the total second sound absorption due to viscosity was given by Khalatnikov[6] in 1950 as

$$\alpha_{\text{vis}}=\left(\frac{\omega^2}{2\rho v_2^3}\right)\left(\frac{4}{3}\eta+\zeta_{II}\right)\frac{\rho_s}{\rho_n}, \tag{3}$$

where ζ_{II} is a second viscosity coefficient.

A more complete analysis of second sound attenuation should include still a third mechanism, namely the loss resulting from diffusive thermal flow within the normal component. Recently (1952) Khalatnikov[9] has extended his theory to include this process, so that finally

$$\alpha=\frac{\omega^2}{2\rho v_2^3}\left[\left(\frac{4}{3}\eta+\zeta_{II}\right)\frac{\rho_s}{\rho_n}+\frac{K}{C}\right], \tag{4}$$

where the additional term represents this second-order thermal process.[10] Here C is the ordinary specific heat capacity of liquid helium II and K, which is analogous to the ordinary thermal conductivity coefficient, is a parameter deduced from the theory on the basis of the same arbitrary constants employed for computing the viscosity coefficients. Although this second-order thermal flow has no appreciable effect on first sound absorption it provides the major contribution to second sound absorption and outweighs the combined effect of first and second viscosity by a factor of roughly two and one-half.

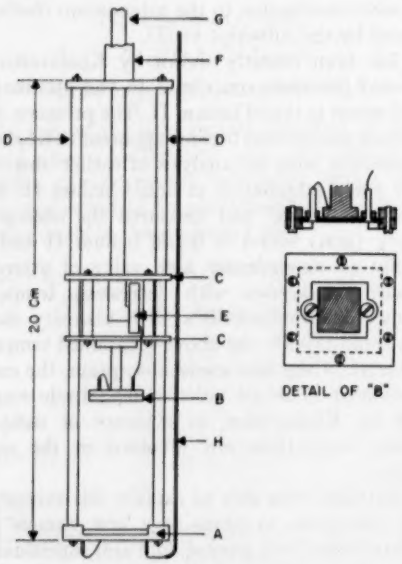

FIG. 1. Second sound cell.

II. EXPERIMENTAL

The frequency range of second sound generation and detection was extended into the submegacycle region during these investigations for two reasons. First, a very high frequency was necessary in order to affect the high wave-preservation properties of these waves sufficiently to produce a measurable attenuation (assuming a frequency squared dependence). Second, in order to preclude possible extraneous losses resulting from interactions between the waves and any containing walls, it was necessary to employ waves of sufficient "directionality" to constitute one-dimensional propagation in the extended medium. Evidently, unless a high order of directionality is attained, the *geometrical attenuation* resulting from beam spreading could actually result in greater pseudoattenuation than that avoided by eliminating constraining walls. It was only necessary, however, to extend the frequencies to sufficiently high values to reduce such geometrical attenuation to an appropriate negligible value. Observations made under such conditions, where geometrical attenuation was effectively outweighed by true attenuation within the second sound wave, presumably gave results associated solely with the properties of the liquid helium II.

a. Second Sound Cell

The geometrical requirements of such a system were satisfied by the configuration represented in Fig. 1. Here the second sound cell is shown consisting of a fixed transmitter A and a movable receiver B. The transmitter A consisted of a thin (0.0005-in.) layer of carbon on a Bakelite backing, to which electrical contact was established in the usual manner with silver paste strip electrodes along two opposite ends of a one-inch square. A square section was used to provide uniform heat flow density throughout the whole wave front. Since the dimensions of this transmitter were always greater than 100 wavelengths of the second sound, an effectively true plane wave of uniform intensity was generated. A cover flange was used to secure the transmitter (and receiver as well) to the flat brass backing plate.

The same type of arrangement was used for the receiver B except that the thickness of the carbon layer was reduced with fine emery paper to increase its thermal response. This receiver, about 1.2 cm on a side, was parallel to the transmitter to within about one thousandth of an inch and maintained its alignment to far greater precision. (This was necessary as the wavelengths were sometimes of the order of only two thousandths of an inch.) Using a receiver of smaller dimensions than the transmitter not only reduced the

[8] K. R. Atkins and C. E. Chase, Proc. Phys. Soc. (London) **A64**, 826 (1951).

[9] I. M. Khalatnikov, J. Exptl. Theoret. Phys. (U.S.S.R.) **23**, 34 (1952).

[10] In 1949 Dingle derived an identical expression for losses due to thermal conduction. By using the value of the heat conductivity coefficient measured for liquid helium I, where the diffusive heat flow is not masked by the internal mass flow, he obtained numerical values of the correct order of magnitude.

alignment problem but also restricted the examination of the second sound beam to the central portions where any fringing or slight beam-spreading tendencies would be least effective. The receiver element was mounted on the frame C which made sliding contact with the four stainless steel alignment rods D. Also mounted on this frame was a small brass compartment E, containing the resistor in series with the receiver and the input circuit to the preamplifier.

The outer Monel tube F provided the mechanical support for the second sound cell and was soldered to the Dewar cap. The inner Monel tube G extended through a packing gland at the top of the Dewar. It provided the means for changing the receiver distance, which could be varied between limits of one-half centimeter and about fifteen centimeters from the transmitter, and also contained the leads to the receiver. The small Monel capillary tube H provided an electrical shield for the input lead to the transmitter.

b. Electronic Equipment

The main experimental problem encountered in the measurements was that of generating and receiving second sound at sufficiently high frequency to provide an observable attenuation. Following this the problem was primarily one of reducing the electrical "cross talk" inherent in such a continuous-wave method to a magnitude that would not obscure the received second sound signals.

The system is represented in the block diagram of Fig. 2. The input frequency $\nu/2$ leading to the transmitter A originated in a crystal oscillator because the frequency ν of the second sound (the input frequency is doubled since heating occurs during *both* halves of the electrical cycle) had to be sufficiently stable to remain in the approximately four cycle per second pass band of the wave analyzer. Although there could be no electrical shielding between the transmitter and receiver, the problem of cross talk was largely self-eliminated by the inherent filter properties of the second sound system. That is, the receiver system was tuned to detect signals at twice the driving voltage frequencies, so that direct electrical pickup of the original frequency did not occur. Electrical cross talk could occur only as the result of anharmonicity in the driving voltage, since the receiver circuit was necessarily tuned to this second harmonic.

In order to prevent this component in the driving voltage from reaching the transmitter, two tuned high-Q filter circuits were inserted directly following the amplifier. These filters discriminated against the second harmonic before the voltage was impressed across the resistance R of the transmitter. In spite of these precautions, enough cross talk occurred at second sound frequencies to complicate the measurement procedure.

The temperature-sensitive resistor R_2 comprising the receiver formed part of a bolometer circuit in which the

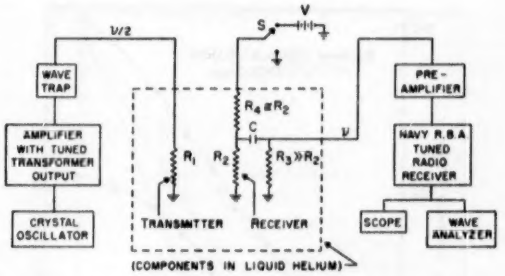

FIG. 2. Block diagram.

bias voltage could be switched off in order to observe the cross talk. In order to improve the signal-to-noise ratio the input circuit to the first stage of amplification was placed in the liquid helium. The received signal at frequency ν was then further amplified and detected by means of a radio receiver delivering an output signal at one kilocycle per second to the wave analyzer. This receiving unit was capable of measuring electrical signals of the order of a few millimicrovolts.

c. Measuring Technique

The technique employed for these measurements involved essentially a free travelling-wave system. This was achieved in practice by operating at sufficiently high second-sound frequencies, and with sufficient transmitter-receiver separation, that the wave attenuation effectively precluded multiple reflections. In this manner certain of the desirable features of both the continuous-wave and the pulse methods were realized. That is, the narrow-band characteristics of this continuous-wave technique provided high receiver sensitivity, while the self-annihilation of the waves provided as effective a distinction between direct and multiply reflected waves as is customarily accomplished with pulses by "separation in time." The method required only that measurements be carried out within the narrow operating range within which direct signals were observable, but multiple reflections eliminated.

This requirement could be met most satisfactorily by recording data at a series of fixed receiver positions, making use of the dependence of second-sound velocity on temperature for controlling the phase relationship between the true second-sound signal and the cross talk. For any particular receiver location, the input power was adjusted to a suitable level to provide observable signals at that position. The receiver sensitivity being maintained constant throughout for a given frequency, the observed signals of the entire series were then reducible to "constant-input data" and plotted on an arbitrary scale. The steps in this process are illustrated in Figs. 3, 4, and 5.

At a given receiver position the continuous wave was turned on and the temperature of the liquid helium II was allowed to increase slowly, while the signal dis-

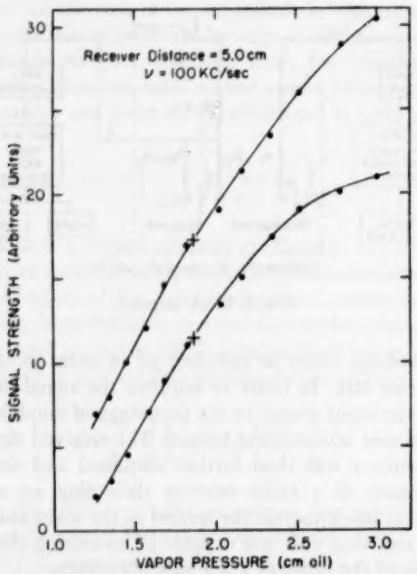

FIG. 3. Received signal plotted *versus* helium vapor pressure at a fixed receiver distance of 5.0 cm, showing maximum and minimum curves which occur as a result of the presence of cross talk. The increase in the curve separation at higher temperature shows the effect also of multiple reflections as the attenuation becomes less.

played on the wave analyzer was recorded as a function of the helium vapor pressure (temperature). These readings consisted of a series of maxima and minima as shown in Fig. 3, depending upon whether the phase of the second sound upon arrival at the receiver coincided with (or opposed) that of the cross talk. For any given receiver position the signal produced by cross talk was independent of temperature and could be read directly by bypassing the bolometer dc voltage source. Accordingly any spreading in the separation between the maxima and minima was evidence of multiple reflections between the transmitter and receiver. This is illustrated in Fig. 3, where the excess separation between maxima and minima at the higher temperatures, for which the attenuation is less, indicates the arrival of "second-trip waves" at the receiver. The effects of such "second-trip waves" may be recognized in this manner and were usually eliminated by suitable frequency-distance combinations. In any case, their presence in small proportion to the primary wave served only to increase the fluctuations without affecting the mean value.

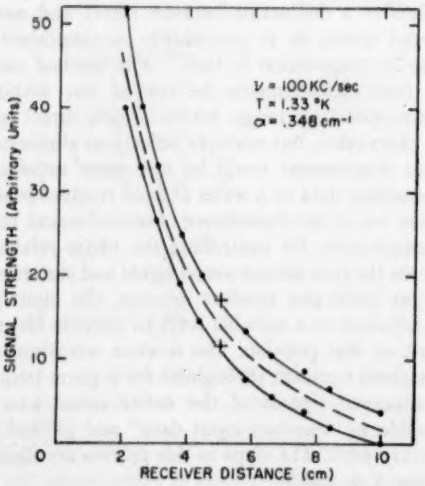

FIG. 4. Received signal strength plotted *versus* transmitter-receiver separation. The dashed curve is taken to represent the true second sound amplitude with cross talk and weakly reflected signals averaged out.

During a run a set of such curves (as in Fig. 3) were taken at different receiver distances but with constant receiver sensitivity. The attenuation was then evaluated by replotting maxima and minima, as a function of the distances employed, for each of several chosen temperatures. An example is shown in Fig. 4, where the data are plotted for a temperature of 1.33°K, the points being taken from the smooth curves represented by Fig. 3. Finally the dashed curve in Fig. 4 is taken to represent the actual second sound amplitude as a function of distance with the cross talk averaged out.

Replotted on a semilog basis, a straight-line dependence is obtained (the central curve corresponds to the dashed curve of Fig. 4). This behavior of the final data appears to substantiate the reliability of the general method, including the procedure for nullifying the effects of multiple reflections. The consistency of the data in this connection is illustrated by the results given in Fig. 5. For example, the signal strengths plotted at value 10 on the arbitrary scale used here have been sufficiently attenuated beneath the value at the transmitter (zero distance) that the first echo, after two additional transits, would arrive at the receiver attenuated to one or two percent of the primary signal. Consistency of the observed slopes, however, for points both above and below such a value show the negligible effects due to reflections.

d. Extraneous Attenuation

Various precautions were taken to insure that all the observed signal diminution with distance was attributable to true liquid attenuation rather than to any effects associated with the equipment or the geometry.[11] For example, it has been mentioned earlier that the second sound waves were "beamed" in order to avoid the effects of any constraining tube walls. The transmitter, which was one inch square, was centered within a dewar of about $2\frac{3}{4}$ inches inside diameter, thus allowing nearly one inch of liquid between the second

[11] Geometrical and other effects can easily overshadow the true liquid attenuation of second sound. This was evidently the case in an early investigation near the λ point by one of the authors (see reference 5) in which values exceeding the present ones were observed. A realization of the need for measurements free of such possible effects instigated the present research.

sound beam and the nearest wall (except for the guide rods). Attenuation effects due to wall losses were thus eliminated for all practical purposes.

Under these conditions losses resulting from beam spreading were undoubtedly the most serious factor encountered. For order of magnitude, one can consider the angle of spreading to equal the ratio of wavelength to transmitter dimension, so that this effect would be most important at the lower frequencies and in the region where the velocity is highest. For example, at a frequency of 100 kc/sec, and for the maximum wave velocity (about 20 meters/sec), the wavelength λ becomes about $\frac{1}{5}$ millimeter. For the transmitter width (a) of 25 mm, a spreading angle $\theta=\lambda/a$ of 0.008 radian represented the upper limit. Simple geometrical considerations lead to the coefficient of attenuation due to geometry,

$$\alpha_{\text{geom}}=2\theta/a=2\lambda/a^2, \tag{5}$$

for small-angle spreading (where one remembers that the coefficient of power attenuation is twice the coefficient of amplitude attenuation). We thus obtain for the maximum geometrical attenuation $\alpha_{\text{geom}}=0.006$ for the case of worst spreading (or $\log_{10}\alpha_{\text{geom}}/\omega^2=-13.8$).

By comparison, the minimum value of α measured in this region was about 0.11 cm^{-1}, or about twenty times the amount of the attenuation due to spreading. Usually this geometrical attenuation amounted to less than one or two percent of the true liquid attenuation, which was somewhat less than the experimental scatter. Actually the presence of this extraneous attenuation would tend always to increase the measured value but by an amount insufficient to warrant corrections.

III. RESULTS

a. Amplitude Dependence

In Fig. 6 the attenuation is plotted *versus* amplitude for a temperature of 1.38°K and for a frequency of 100 kc/sec. Within the range shown, which includes all amplitudes employed for these experiments, the attenuation is *evidently completely independent of amplitude.* Actually the magnitudes of heat current density (and associated temperature amplitude) which are given represent upper limits to the true values. That is, at the high frequencies employed it is likely that a considerable fraction of the rf heat component was dissipated in the carbon layer and did not contribute to the second sound amplitude; i.e., the bulk carbon could not follow the rapid temperature fluctuations but only a thin layer at the surface. This situation was considered primarily responsible for the rapid decrease in signal strength as frequency was increased; although signals were observed at frequencies as high as 350 kc/sec, the signal strength was not large enough to permit meaningful measurements. Accordingly, the values along the abscissa of Fig. 6 exceed the true magnitudes by the amount of such generator losses at 100 kc/sec.

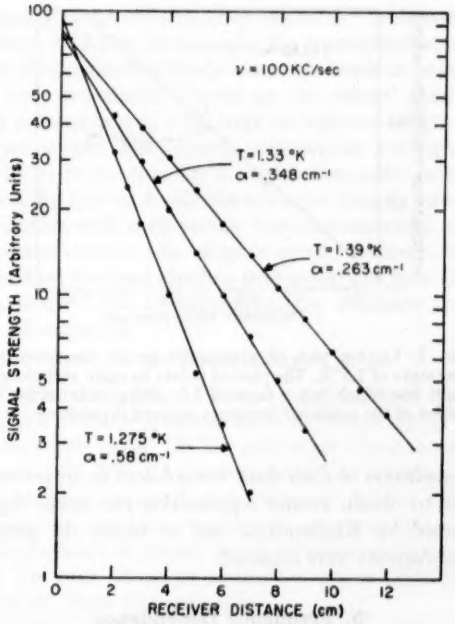

FIG. 5. Semilog plot of second sound amplitude *versus* receiver distance. The attenuation coefficient is equal to the negative of the slope of the straight lines. The rapid variation of attenuation with temperature in this region is evident.

Some recent work by Atkins and Hart[12] (employing the pulse method at a carrier frequency of the order of 20 kc/sec) has been published while this paper was being written, and they report that attenuation does increase with amplitude. This observation was very likely the result of working at sufficiently high heat-current levels that nonlinear effects were important (their amplitudes were much greater[13] than those used in the present work). Such nonlinear effects required an

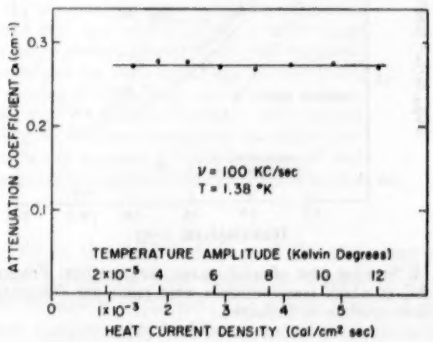
ATTENUATION COEFFICIENT α (cm⁻¹)
ν = 100 KC/sec
T = 1.38 °K
TEMPERATURE AMPLITUDE (Kelvin Degrees)
HEAT CURRENT DENSITY (Cal/cm² sec)

FIG. 6. Plot demonstrates independence of second sound attenuation on temperature amplitude for the amplitude range used in these experiments. Abscissa values represent upper limits to the actual temperature amplitudes.

[12] K. R. Atkins and K. H. Hart, Phys. Rev. **92**, 204 (1953).
[13] K. R. Atkins (private communication).

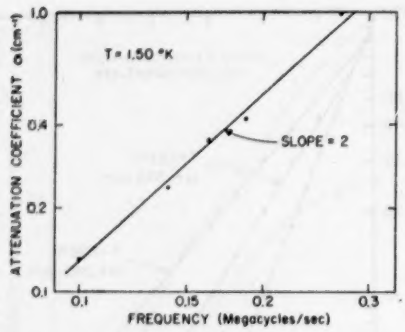

FIG. 7. Log-log plot of attenuation *versus* frequency at a temperature of 1.5°K. The plotted points lie quite well along the straight line which has a slope of 2.0, giving quantitative confirmation of the predicted frequency-squared dependence.

extrapolation of their data toward zero input power in order to obtain results representing the linear region assumed by Khalatnikov and to which the present measurements were confined.

b. Frequency Dependence

As may be seen from the theory, the attenuation of second sound should vary as the square of the frequency; according to Khalatnikov this dependence should obtain, in the temperature interval covered, up to a frequency of about 100 Mc/sec. The measured values of attenuation reported here give quantitative confirmation of this frequency squared behavior.[14] This is illustrated for a temperature of 1.5°K in Fig. 7, where α is plotted *versus* frequency on a log-log scale and the straight line has been drawn in with a slope of two. Although data are given here for but a single temperature, the general validity of the relationship is demonstrated in Fig. 8, where α/ω^2 is plotted as a function of temperature for a composite set of frequencies. The internal consistency shown by these data could logically exist, within the range of frequencies employed, only by strict conformity to the frequency-squared law.

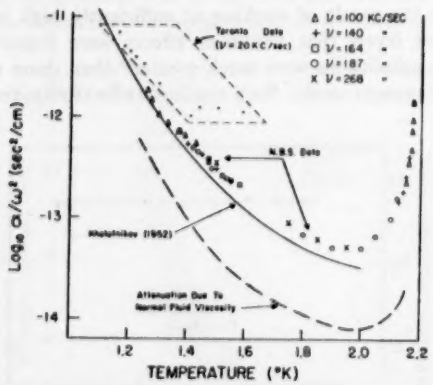

FIG. 8. Semilog plot of α/ω^2 *versus* temperature. Frequencies ($\nu=\omega/2\pi$) at which measurements were made are designated by the various symbols as indicated.

[14] The low-frequency measurements of Atkins and Hart suggest a similar behavior. Their published data were given only at 20 kc/sec, but they remark "at 10 kc/sec and 30 kc/sec it was more difficult to evaluate the beam spreading correction, but the results indicate the small attenuation varies approximately as the square of the frequency." It is not clear, in view of the difficult beam-spreading corrections, to what extent these small attenuations verify the law.

c. Temperature Dependence

In Fig. 8 the quantity α/ω^2 is plotted *versus* temperature. Data taken at the various frequencies employed are indicated by different symbols, and the composite curve formed by these points represents a unique, frequency-independent relationship. It will be observed that no data occur within roughly one-tenth of a degree on either side of 1.65°K. As explained earlier, the measurement technique utilized the variation of second sound velocity with temperature, and this gap occurs in the region where second sound velocity is a maximum. The trend of the results is quite clear, however, throughout the entire temperature range from 1.25°K to 2.17°K. The coherence of the data obviated the need for a connecting smooth curve drawn through the points, but values taken from such a curve are presented for reference in Table I.

TABLE I. Attenuation values taken from smooth curve drawn through the experimental points (curve not shown on Fig. 8).

Temperature (°K)	$\alpha/\omega^2\times10^{13}$ (sec²/cm)	Temperature (°K)	$\alpha/\omega^2\times10^{13}$ (sec²/cm)
1.275	14.1	1.80	0.72
1.30	11.2	1.85	0.59
1.35	7.9	1.90	0.51
1.40	5.6	1.95	0.49
1.45	4.25	2.00	0.51
1.50	3.10	2.05	0.66
1.55	2.35	2.10	1.00
1.60	1.82	2.125	1.45
1.65	1.41	2.15	2.51
1.70	1.10	2.16	4.0
1.75	0.89	2.17	8.9

The dashed curve of Fig. 8 represents the attenuation to be expected from the normal fluid viscosity as given[5] by expression (2), and employing the values of viscosity coefficient η measured by Hollis-Hallett.[15] This curve follows the trend of the data at all temperatures, but in magnitude actually represents only about one sixth of the total attenuation present.

[15] A. C. Hollis-Hallett, Proc. Roy. Soc. (London) **A210**, 404 (1952).

The solid curve represents Khalatnikov's final (1952) prediction as given by expression (4), adding to expression (2) the dynamic terms both in viscosity ("second viscosity") and thermal conductivity. Actually this latest work of Khalatnikov's was unknown to the authors until after the experiments had been completed. *The agreement with the experimental results is remarkably good both in magnitude and in temperature dependence.* Khalatnikov did not extend the curve above 2.0°K because above this temperature the density of excitations is so high that the ideal gas approximations for the phonons and rotons can no longer be considered valid. The increase predicted[5] on the basis of the decrease in wave velocity (α proportional to $\rho_s/\rho_n v_2^3 \sim 1/v_2$) is apparent, however, in the 2.0°K λ-point range.

The data shown within the parallelogram in the upper left-hand portion of Fig. 8 were reported recently by Atkins and Hart[13] for a frequency of 20 kc/sec. Though they plotted values of α for this frequency on a linear scale, we have for comparative purposes replotted this data on the same $\log_{10}(\alpha/\omega^2)$ basis originally employed by Khalatnikov. At their lowest temperatures the data clearly indicate the rapid rise in attenuation with decreasing temperature predicted by Khalatnikov. Above 1.4°K, however, the effects of the large beam spreading at the low frequency employed[16] become more evident. At 1.6°K for example, the geometrical attenuation is apparently already about six times as large as the true attenuation (based on the present results). As a consequence of these large background effects the scatter of their data becomes comparable (see log plot of Fig. 8) to the true liquid attenuation under investigation. By moving Khalatnikov's curve linearly upward to coincide with their points, they demonstrated good agreement within the range covered. Actually they could have obtained absolute determinations from their data below 1.3°K by subtracting the necessary background correction.

d. Conclusions

(1) The attenuation of second sound has been measured as a function of temperature and frequency in the submegacycle range. (2) The results are found to agree substantially with the predictions of Khalatnikov. (3) The frequency-squared dependence of second sound attenuation has been established quantitatively. (4) No dependence of second sound attenuation on amplitude has been observed at the low-power levels employed for these measurements.

[16] The geometrical spreading increases as $1/\nu$ and the second sound attenuation increases as ν^2; thus the ratio of the magnitudes of the two effects ($\alpha_{true}/\alpha_{geom}$) varies as ν^3. At 100 kc/sec, as opposed to 20 kc/sec, the relative importance of the beam spreading is down by a factor of $(5)^3=125$.

PHYSICAL REVIEW VOLUME 95, NUMBER 2 JULY 15, 1954

Temperature-and-Field Emission of Electrons from Metals*

W. W. Dolan and W. P. Dyke
Physics Department, Linfield College, McMinnville, Oregon
(Received April 9, 1954)

Both the current density and the distribution in energy of electrons emitted from metals are calculated for various combinations of temperature, applied surface electric field, and work function. A wider range of those variables than previously achieved is made possible by use of numerical integration. The integrand is the usual function based on the free-electron theory of metals and the wave-mechanical barrier transmission coefficient of Sommerfeld and Bethe which assumes a classical image force and a plane surface. Results, which are presented in graphical form, are consistent with the Fowler-Nordheim field emission equation for low temperatures, and with the Richardson thermionic emission formula at low fields. Predicted emission at temperatures up to 3000°K is compared with cold emission at fields between 10^7 and 10^8 v/cm. A qualitative comparison is made between the present results and previous experiments on the transition between field emission and the vacuum arc.

INTRODUCTION

ELECTRONS are emitted from metals under the action of both temperature and electric field. When the temperature is high and the field is low, the process is thermal emission, which is described by the familiar Richardson equation; the effects of intermediate fields on thermal emission are well known as the Schottky effect. When the field is high and the temperature is low, the process is field emission, described by the Fowler-Nordheim equation; the added effect of intermediate temperature has been considered by several authors, as indicated below.

When both temperature and field are high, the emission process is strongly dependent on both variables and is properly described as neither thermal nor field emission; therefore the descriptive term "temperature-and-field emission," or, in abbreviated form, "*T-F*

* This work was supported by the U. S. Office of Naval Research.

emission," is used herein. No previous work readily applicable to the general ranges of both variables has been found.

Effects attributed to *T-F* emission were seen during the transition from field emission to vacuum arc[1,2] when the electric field was 7×10^7 v/cm and the temperature apparently exceeded 3000°K, which are higher values of the combined variables than those found in earlier works. The experimental methods of reference 2 can be extended to a quantitative study of both *T-F* emission and vacuum arc mechanisms, and such study is desirable for several reasons. The properties of *T-F* emission are unique, and new or improved electron sources have frequently contributed to advances in both basic science and electronics, the industry in which free electrons are employed. The vacuum arc phenomena have basic importance though they have not been well understood. Furthermore, the arc has important contact with practice; first, it provides a useful means for altering the shape and purity of the microscopic tips of field emitters; second, it sets an upper limit to the field emission current density which can be supplied without damage to the emitter; and third, it is an undesirable form of electrical breakdown in cases where insulation is required.

The present paper concerns a numerical evaluation of the usual integral describing the temperature-and-field dependent emission of electrons from metals. Earlier evaluations of the integral, while in desirable analytical form, suffered from approximations necessary to that type of solution and from the restriction of the validity of the solution to limited ranges of one or more of the variables. In the present work both the current density and the distribution in energy among the emitted electrons are calculated for electric fields F encountered in usual field emission experiments, i.e., $2\times10^7<F<7\times10^7$ v/cm, and for several temperatures in the range $0°<T<3000°$K. The effect of several values of work function on current density is considered.

Qualitative comparisons are made between the present calculations and earlier experimental data concerning the transition from field emission to the vacuum arc. The comparison indicates that prior to arc the emitter temperature was at least 3000°K, a conclusion which strengthens the previously proposed mechanism for arc initiation; measurement of the emitter temperature during intermittent operation has not been otherwise possible because of the microscopic emitter size[3] and transient nature of the heating problem.[4] A more quantitative experimental test of the present calculations will be presented in a forthcoming paper.

From the calculated distribution in energy among emitted electrons, certain conclusions are drawn regarding mechanisms,[5] other than resistive heating,[4] by which the emission process can add energy to, or subtract it from, the metal.

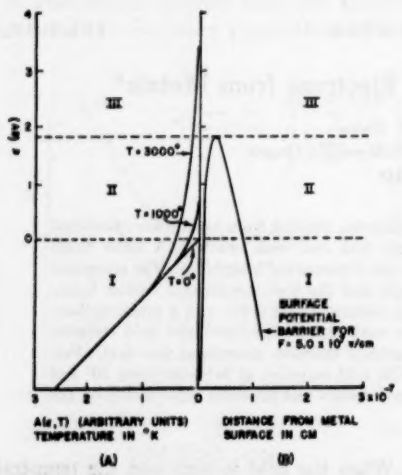

FIG. 1. Schematic drawing showing, on the left, the electron supply function $A(\epsilon,T)$ for several values of the temperature T and, on the right, the potential barrier for a typical value of the electric field, the vertical line at 0 representing the metal surface: Region I, below the Fermi level $\epsilon=0$ (field emission); Region II, between the Fermi level and top of barrier; Region III, above barrier (thermal emission); if emission from Region II is appreciable, the total emission is called $T-F$ emission.

THEORETICAL METHOD

The present problem requires knowledge of the values of electron current density and the distribution in energy of electrons emitted from metals at fields up to about 10^8 v/cm and temperatures up to and exceeding 3000°K. Although several early investigators gave attention to this question,[6-8] and the qualitative description of the solution was correctly predicted by Houston,[8] the only careful prior treatment of the general problem was that of Guth and Mullin,[9] which, however, was applicable at the fields in question only for restricted ranges of temperature. A recent contribution by Nakai[10] using numerical methods was of limited usefulness because of its neglect of the image force in defining the surface potential barrier.

Assumptions of the present work include: (1) a simple one-band electron model expressed by the Fermi-Dirac statistics; (2) a smooth metal surface, neglecting effects of atomic scale; (3) a classical image force; (4) the coefficient for transmission of electrons through the

[1] W. P. Dyke and J. K. Trolan, Phys. Rev. **89**, 799 (1953).
[2] Dyke, Trolan, Martin, and Barbour, Phys. Rev. **91**, 1043 (1953).
[3] Dyke, Trolan, Dolan, and Barnes, J. Appl. Phys. **24**, 570 (1953).
[4] Dolan, Dyke, and Trolan, Phys. Rev. **91**, 1054 (1953).
[5] W. B. Nottingham, Phys. Rev. **59**, 906 (1941).
[6] R. H. Fowler and L. W. Nordheim, Proc. Roy. Soc. (London) **A119**, 173 (1928).
[7] R. A. Millikan and C. C. Lauritsen, Proc. Natl. Acad. Sci. U. S. **14**, 1 (1928).
[8] W. V. Houston, Phys. Rev. **33**, 361 (1929).
[9] E. Guth and C. J. Mullin, Phys. Rev. **61**, 339 (1942).
[10] J. Nakai, Technol. Repts. Osaka Univ. **1**, 213 (1951).

surface potential barrier in the form used by Sommerfeld and Bethe.[11] The latter assumption permits comparison of present results with the generally accepted Fowler-Nordheim equation[12] for cold field emission. Furthermore, as compared with transmission coefficients proposed by other authors,[9,12,13] the coefficient used by Sommerfeld and Bethe has a great advantage in simplicity, while none of the alternate forms found in the literature differed from it by more than a factor of 2 at pertinent energy levels.

Under these assumptions, the current density J for all fields F and temperatures T can be expressed by the single integral

$$J=\int_{-\infty}^{\infty} cA(T,\epsilon)D(F,\epsilon)d\epsilon, \qquad (1)$$

where the variable ϵ is the difference between the electron energy and the reference energy at the conduction (Fermi) level, and the energies are those associated with the component of velocity normal to the metal surface. The function $A(T,\epsilon)$ describes the supply of electrons to the surface from the Fermi sea, and $D(F,\epsilon)$ is the transmission coefficient discussed above. Both are used here in the forms presented in reference 11, namely,

$$A(T,\epsilon)=\ln[1+\exp(-\epsilon/kT)],$$
$$D(F,\epsilon)=\exp[-6.85\times10^{7}(\phi-\epsilon)^{\frac{3}{2}}f(y)/F]. \qquad (2)$$

Other symbols in Eq. (2) include Boltzmann's constant k, the work function ϕ, and Nordheim's elliptic function $f(y)$[12,14] depending on ϕ, ϵ, and F. The constant c in Eq. (1) has the form $4\pi mkT/h^3$, where h is Planck's constant and m is the mass of the electron.

The function A is represented graphically in Fig. 1. The vertical line at the center of the figure indicates the metal surface; on the left is the supply function A for three values of T, and on the right is the surface potential barrier for a typical field.

Field currents originate from Region I, i.e., $\epsilon<0$, where the electron supply is large but the barrier transmission coefficient is small, and integration of Eq. (1) over this region (for $T=0$) yields the Fowler-Nordheim equation. Thermionic currents originate from electrons escaping over the barrier (Region III) where the supply is small but the transmission coefficient is large. Integration of Eq. (1) over Region III, for F small, yields the Richardson equation. For many combinations of T and F an appreciable part of the emission originates from energy levels in Region II, i.e., between the Fermi level and the top of the barrier, and is properly neither thermal emission nor field emission. This distinction was pointed out earlier by LePage and DuBridge.[15] In the latter case, the total emission is designated herein "temperature-and-field emission," which for convenience is abbreviated T-F emission.

Analytic evaluation of the integral of Eq. (1) over the general range is difficult. In the work of Guth and Mullin[9] it led to the use of certain approximations which limited the range of fields over which the solution was valid at high temperatures. The present work makes use of a simple numerical integration using Simpson's parabolic rule. While this method lacks mathematical elegance as compared with analytic procedures, it is believed that the errors involved are less than those imposed by the approximations of any known analytic method; at the same time the present method offers the advantage of simplicity both in performance and in understanding.

Values of A and D were computed for given combinations of ϕ, T, and F. The product AD was tabulated, and graphed as a function of ϵ as exemplified in Fig. 2, which is discussed below. The integration, equivalent to finding the area under such a curve, was extended to a range such that the extreme ordinates of each curve were one percent of the maximum ordinate; thus the contribution from the omitted portion of the curve was negligible. The intervals $\Delta\epsilon$ used in the process varied, for different temperatures, from 0.1 to 0.3 ev.

DISCUSSION OF RESULTS

1. Energy Distribution of the Emitted Electrons

A few examples of calculated energy distributions for emitted electrons, such as the curves of Fig. 2, have been published by Henderson and Dahlstrom,[16] Mueller,[17] Gomer,[18] and (for the triangular barrier neglecting image force) by Nakai.[10] The first and second of these references were in connection with experimental investigations of the distribution at room temperature; no treatment of the general case was found.

Examination of Fig. 2 reveals the following properties of the distributions: (1) For field emission with $2\times10^{7}<F<7\times10^{7}$ v/cm and low temperature, the maximum of the distribution curve is found near the top Fermi level $\epsilon=0$. (2) For T-F emission at intermediate temperatures beginning near 1000°K, the abscissa of the maximum moves toward higher energies, and the base of the distribution grows broader. The ordinate of the maximum also increases greatly, though this fact is concealed by Fig. 2, in which the amplitudes of all curves are arbitrarily normalized. (3) For T-F emission at high temperatures, for example 3000°K, the maximum is near the top of the potential barrier.

Another point of view for the interpretation of the combined effect of T and F on the energy distribution curves for emitted electrons is offered by Fig. 3. The solid curves show distributions for various fields at a

[11] A. Sommerfeld and H. Bethe, *Handbuch der Physik* (Verlag Julius Springer, Berlin, 1933), Vol. 24, No. 2, p. 441.
[12] L. W. Nordheim, Proc. Roy. Soc. (London) **A121**, 626 (1928).
[13] N. H. Frank and L. A. Young, Phys. Rev. **38**, 80 (1941).
[14] Burgess, Kroemer, and Houston, Phys. Rev. **90**, 515 (1953).
[15] W. R. LePage and L. A. DuBridge, Phys. Rev. **58**, 61 (1940).
[16] J. E. Henderson and R. K. Dahlstrom, Phys. Rev. **55**, 473 (1939).
[17] E. W. Mueller, Z. Physik **120**, 270 (1943).
[18] R. Gomer, J. Chem. Phys. **20**, 1772 (1952).

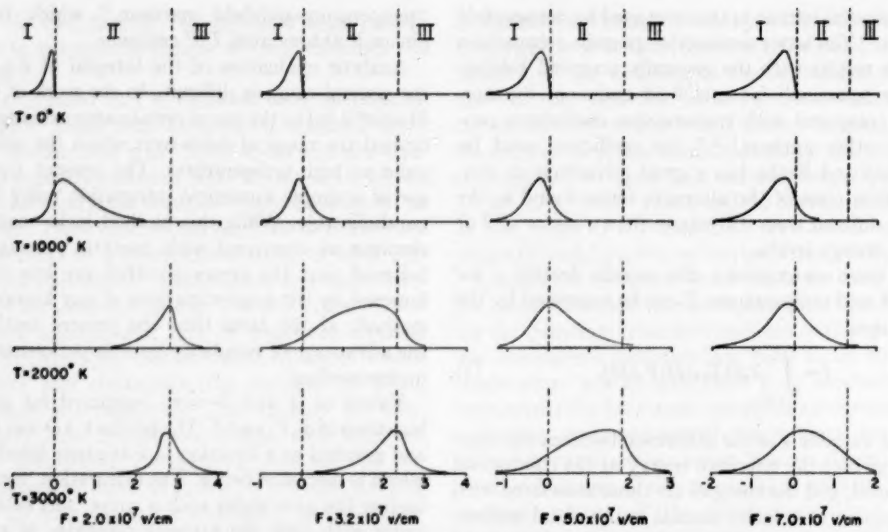

FIG. 2. Theoretical energy distributions for emitted electrons at indicated fields and temperatures, for $\phi = 4.5$ ev, with amplitudes arbitrarily normalized to a common maximum; abscissas ϵ in ev relative to the top Fermi level at 0. Regions I, II, and III correspond to those in Fig. 1.

constant temperature of 3000°K; these coincide at energy levels above the potential barrier for each field as expected. The dotted curves, on the other hand, indicate distributions for various temperatures at the constant field 5.0×10^7 v/cm. In each case, the curves build up to the curve of largest amplitude shown in the figure, that for $F = 5.0\times10^7$ v/cm and $T = 3000$°K. The corresponding curve for $F = 10^8$ v/cm and $T = 3000$°K, if drawn to the same scale, would have an amplitude more than a hundred times greater than the largest shown in the figure.

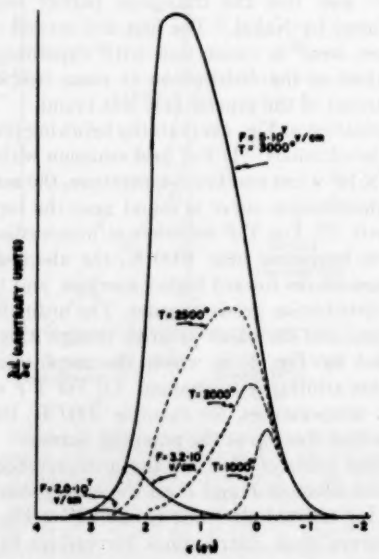

FIG. 3. Energy distributions for emitted electrons with $\phi = 4.5$ ev and at various fields for a constant temperature $T = 3000$°K (solid curves); a constant field of 5×10^7 v/cm at various temperatures (dashed curves).

2. Current Density as a Function of Field and Temperature

Current densities predicted by Eq. (1) for various values of F and T at a work function of 4.5 ev (the average value for clean tungsten) are exhibited graphically in Fig. 4. Current density was calculated at five values of F from 2×10^7 to 10^8 v/cm for each of the temperatures indicated. It is evident that the enhancement of electron emission due to added thermal energy is much larger at low than at high fields, as was recognized in principle by earlier authors.

It is also clear from Fig. 4 that the temperature effect is slight at values of T less than 1000°K for the range of fields shown, but increases rapidly for higher T. This is of interest in connection with the early experimental attempts to establish such a temperature effect. Millikan and Eyring[19] detected at 1100°K a slight effect whose magnitude was consistent with the present results; however, de Bruyne[20] failed to observe any effect up to 1944°K. Earlier work did not benefit from recent techniques which insure clean electrode surfaces and may, therefore, be in doubt in some cases.

The results embodied in Fig. 4 were compared with those computed by the present authors from the formula of Guth and Mullin[9] for the ranges of T and F in which the latter is valid. The correspondence between the two

[19] R. A. Millikan and C. F. Eyring, Phys. Rev. **27**, 51 (1926).
[20] N. A. de Bruyne, Phil. Mag. **5**, 574 (1928a).

was found to be within the difference introduced by the choices of the coefficient D in the two cases. Comparison with Nakai's result[10] is not sufficiently informative to merit inclusion here because of the neglect of the image force in his work, and the small number of computations reported. It is worth note that the trend of Nakai's few tabulated values is similar to that given here.

3. Dependence of Temperature Effect on Work Function

Calculations heretofore presented assumed a work function $\phi=4.5$ ev, the accepted average value for clean tungsten. In order to compare the effect of temperature on current density for several values of ϕ and F, a limited number of tabulations of J were made for $\phi=6.3$ ev, one of the highest values reported[21] and assigned to the average value for platinum, and $\phi=3.0$ ev, a value found experimentally for tungsten partially coated with barium.[22] The trend of these results is exhibited in Fig. 5 in which $\log_{10}(J/J_0)$ is plotted against T for the three values of ϕ. The comparison is made at constant field (Fig. 5a) and at constant J_0, the value when $T=0$ (Fig. 5b). In the case of a constant field the effect of high temperature can be interpreted as reducing the disparity between current densities emitted from materials of different work functions; for example, at $T=0°$K and $F=2\times10^7$ v/cm, the ratio of current densities for work functions of 3.00 and 6.30 ev is approximately 10^{16}, whereas at 2000°K it is about 10^8 and at 3000°K less than 10^6.

CONCLUSIONS

Several conclusions of a qualitative nature may be drawn from a comparison between the foregoing data and earlier experiments relating to the transition between field emission and the vacuum arc.[1,2] Just prior to arc initiation, an increase in current density over that expected from field emission was observed and attributed to T-F emission. Comparison of the observed increase with that predicted herein, using the known value of electric field, provides further evidence that the emitter temperature was high just prior to arc. High temperature is thought to be an arc-initiating factor; however, direct measurement of the temperature has not been possible in view of the transient nature of temperature[4] and microscopic size of the heated portion of the cathode tip.[3,4] Quoting from reference 2, "the expected change in [cold cathode] current density was a factor of 1.6 while the observed change in intensity in the [emission pattern] ring was in excess of an order of magnitude based on an estimate aided by a densitometric analysis of the photographic negatives of the emission patterns." An equivalent statement is that

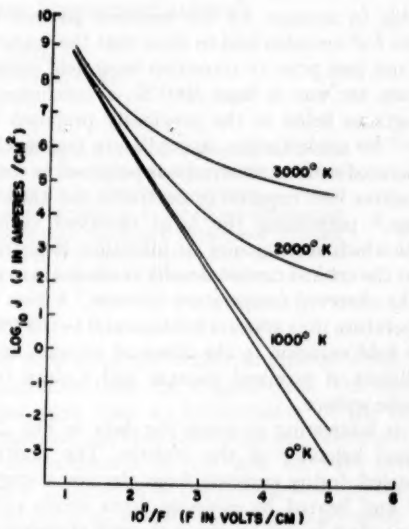

FIG. 4. Graph relating calculated current density J to electric field F at various temperatures T, for $\phi=4.5$ ev.

the observed current density was at least a factor of 6 larger than that expected from the cold cathode, the increase being attributed to temperature, which from various data was estimated to exceed 3000°K. The electric field was known to be 6.3×10^7 v/cm at the emitter surface from which the emission pattern ring originated. For these values of T and F, Fig. 4 predicts an increase of current density by a factor of 5.0 over the value expected for the cold tungsten cathode, which is in agreement with that observed in the foregoing experiment, within the experimental error. Thus it is

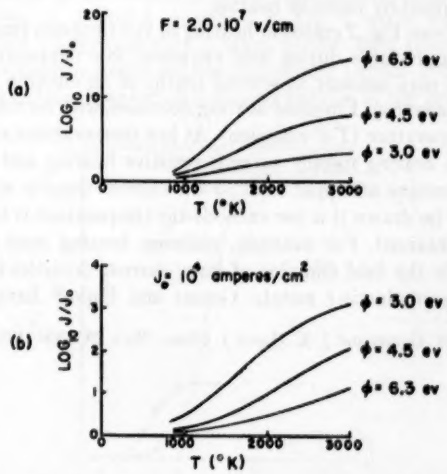

FIG. 5. Graphs showing the dependence of the ratio J/J_0 on temperature T and work function ϕ at (a) a constant electric field $F=2.0\times10^7$ v/cm and (b) a constant value for $J_0=10^6$ amp/cm^2; J is calculated electron emission current density and J_0 is field current density for $T=0°$K.

[21] L. A. DuBridge, Phys. Rev. **31**, 236 (1928).
[22] Barbour, Martin, Dolan, Trolan, and Dyke, Phys. Rev. **92**, 45 (1953).

possible to account for the emission pattern ring as due to T-F emission and to show that the emitter temperature just prior to transition from field emission to vacuum arc was at least 3000°K, a conclusion which strengthens belief in the previously proposed mechanism[1,2] for arc initiation. According to that mechanism evaporated emitter material was proposed as the source of positive ions required to neutralize the known space charge,[22] permitting the large observed current increase which accompanies arc initiation. Resistive heating at the critical current density is adequate to account for the observed temperature increase.[4] A high emitter temperature thus appears fundamental to the transition from field emission to the observed vacuum arc under conditions of excellent vacuum and a clean tungsten cathode surface.

It is interesting to relate the data in Fig. 2 to the thermal behavior of the emitter. The emitter will be cooled during emission from electron energy levels $\epsilon>0$ and heated by emission from levels $\epsilon<0$. The former effect is well known in thermal emission and the latter mechanism was proposed by Nottingham[5] for the case of field emission. It is apparent from Fig. 2 that combinations of T and F exist such that either process can occur during electron emission from the tungsten cathode. For example, cooling occurs when the mean of the energy distribution curve lies at $\bar{\epsilon}>0$; in this case, electron vacancies at the mean level $\bar{\epsilon}$ are replaced by lower energy electrons from the conduction level $\epsilon=0$ at the expense of the thermal energy of the emitter. Conversely, as Nottingham has suggested, the metal will be heated when the mean of the energy distribution curve has a value $\bar{\epsilon}<0$. Such energy transfer to or from the cathode, called "emission heating" or "emission cooling" hereinafter, must be added to that supplied by resistive heating.

From Fig. 2 emission heating of the tungsten emitter is appreciable during field emission (low temperature) and may amount to several tenths of an electron volt per electron. Emission heating decreases with increasing temperature (T-F emission). At low temperatures emission heating usually exceeds resistive heating and will determine an upper limit to the current density which can be drawn if a low cathode-tip temperature is to be maintained. For example, emission heating may preclude the field emission of large current densities from superconducting metals. Gomer and Hulm[23] have reported preliminary studies from superconducting tantalum at low current densities.

For intermediate current densities, for example those obtained with $F=5\times10^7$ v/cm, emission cooling exceeds resistive heating for all T above a certain value, thus placing a limit on the value of T expected from resistive heating for a given current density. This limit can be calculated by the methods of reference 4 when emission cooling is considered along with resistive heating and thermal conduction.

It is interesting to note that emission cooling is small compared with resistive heating during the final stages of the transition between field emission and the vacuum arc, for a typical emitter. Therefore emission cooling appears inadequate to prevent the large emitter temperature increase believed to have initiated the arc for such emitters. Consider, for example, the data from emitter 0–38, reference 2, for which the transition occurred for $F=7.4\times10^7$ v/cm and $T=3000$°K, approximately. From Fig. 2, $\bar{\epsilon}$ may be estimated to have the value 0.2 ev for this case, which represents the energy per electron subtracted from the emitter by emission cooling. On the other hand, resistive heating is about 5 times larger than emission cooling under the same conditions, as may be shown by the methods of reference 4.

A worthy project would be the solution of the transient temperature rise at the field-emitter tip, using the methods of reference 4 with two refinements requiring consideration of (1) resistivity as a function of temperature, (2) emission heating, which is large at low T, and emission cooling, which is significant under some conditions at high T. Proper evaluation of the effects of emission heating requires knowledge of its distribution throughout the emitter volume, about which there has been some question.[24]

The data in Fig. 4 can be tested by the experimental techniques used in reference 2 when in addition the emitter is heated from a supply in its support filament. Results of such tests will be reported in a future paper.

The data of Fig. 2 can be tested by the method of Henderson and Dahlstrom[16] together with modifications of their method suggested by Mueller[17] and techniques suggested in the preceding paragraph. Measurement of the distribution in energy among the emitted electrons would provide another method for measuring cathode temperature.

[23] R. Gomer and J. K. Hulm, J. Chem. Phys. **20**, 1500 (1952).

[24] G. M. Fleming and J. E. Henderson, Phys. Rev. **59**, 907 (1941).

Threshold Field Properties of Some Superconductors*

E. MAXWELL† AND O. S. LUTES
National Bureau of Standards, Washington, D. C.

(Received January 26, 1954)

Some refined measurements of the critical field curves for tin, thallium, indium, and mercury have been completed and the results compared with the specific predictions of the Gorter-Casimir and the Koppe versions of the two-fluid model of superconductivity. Neither version is completely adequate, although each has points in its favor. The Koppe prediction of a universal critical field curve for all superconductors is not verified. The Gorter-Casimir α model has greater flexibility than the Koppe model, and although it is capable of giving a fair description of the critical field data, it is in some respects also inconsistent with the data. The isotope effect in thallium has been observed and is consistent with the half-power law.

INTRODUCTION

THE threshold field curve, which defines the phase boundary between the normal and superconducting states, is a fundamental characteristic of superconductors. From the thermodynamics of the superconducting phase transition it follows that the difference in free energies of the normal and superconducting states is proportional to the square of the critical field. Consequently one can check the applicability of thermodynamic reasoning to the problem by quantitatively comparing threshold field data with calorimetric data for mutual consistency. Such comparisons have been made in the past by other observers, and the correctness of the thermodynamic treatment has been adequately confirmed.

This paper is primarily concerned with another aspect of the threshold field curve. Since the threshold field is determined once the free energies of the normal and superconducting states are given it provides a means of testing theoretical models of superconductivity in which the free energy is explicitly given as a function of temperature. The two-fluid model of superconductivity is such a model, and in the present paper we shall use some recently obtained precise critical field measurements on tin, mercury, indium, and thallium to compare with some specific forms of the two-fluid model.

Because of the relatively high precision of the present data it becomes practicable to try to interpret some of the finer details of the critical field curve. In a recent paper[1] a very general form of the two-fluid model was described and some of the present experimental data were briefly presented in a preliminary form. In this paper we shall be more directly concerned with describing the experimental aspects of the investigation and giving a more detailed analysis of the data.

The data for tin were given in an earlier paper[2] in connection with an investigation of the isotope effect. We give here some additional parameters which have been calculated from the original data. The thallium data also stem from an investigation of the isotope effect and have not been previously published in detail. These measurements on tin and thallium revealed systematic departures of the critical field curves from parabolic form of a kind which were generally consistent with some forms of the two-fluid model. It was therefore also thought advisable to investigate the behavior of indium and mercury with high precision techniques. A limited comparison of this sort using the tin data has been given by Bender and Gorter.[3]

EXPERIMENTAL METHOD

The method of measurement was the null magnetic method described in an earlier paper.[2] The identical apparatus was used for the thallium measurements. For mercury and indium an apparatus with another pickup coil system was used which differed from the one described chiefly with respect to number of turns and coil resistance. Some typical transition curves observed in the course of these experiments are given in Figs. 1, 2, and 3 as well as in Fig. 4 of the earlier paper.[2] The critical field is taken as that field at which the specimen would become completely normal if there were no rounding-off of the upper portion of the transi-

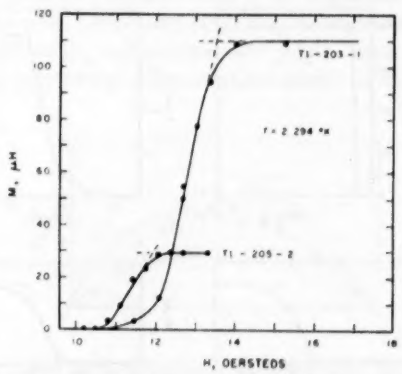

FIG. 1. Transition curves for thallium.

* Supported by the Office of Scientific Research, Air Research and Development Command under contract with National Bureau of Standards.

† Now at Lincoln Laboratory, Massachusetts Institute of Technology, Cambridge 39, Massachusetts.

[1] P. M. Marcus and E. Maxwell, Phys. Rev. **91**, 1035 (1953).

[2] E. Maxwell, Phys. Rev. **86**, 235 (1952).

[3] P. L. Bender and C. J. Gorter, Physica **18**, 597 (1952).

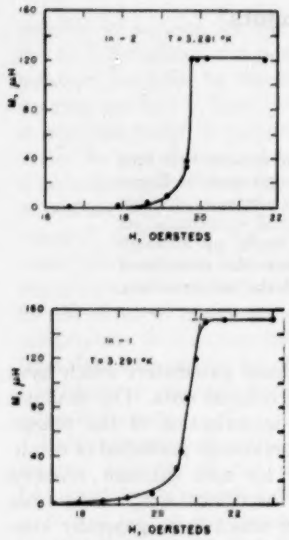

FIG. 2. Transition curves for indium. In-1 cast in Pyrex capillary; In-2 single-crystal free rod of indium.

tion curve. The steep slope of the transition curve is extrapolated to the level of M (the mutual inductance setting for balance) in the normal state, and the corresponding value of the field is taken as the critical field.

In some cases where the transitions were sharp, as for the mercury and indium single crystals, it was possible to fix the critical field to within about one tenth of an oersted. In the case of thallium, however, some of the transitions were less sharp and have a probable uncertainty of three or four tenths of an oersted. The errors due to nonuniformity of the field and to uncertainty in the calibration constant of the magnet are each less than $\frac{1}{4}$ percent.

THE SPECIMENS

Some of the physical properties of the specimens are given in Table II. The isotopic tin and thallium samples were reduced from the oxide form and the chemical purity figures refer to the original oxides. The samples were melted *in vacuo* after reduction and subsequently recrystallized in the course of which process the purity was probably somewhat enhanced. The natural metal samples were in all cases Johnson-Matthey Specpure materials.

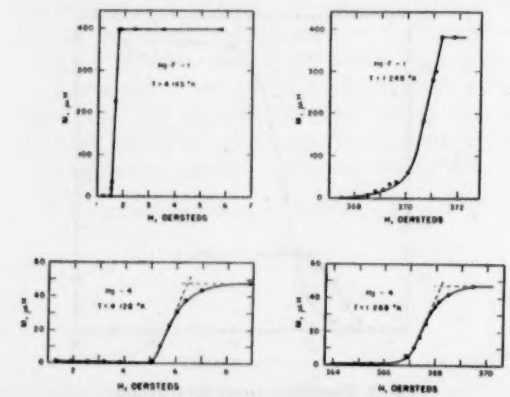

FIG. 3. Transition curves for mercury. Hg-4 sample in Pyrex tube; Hg-*F*-1 free rod of mercury.

The tin and thallium samples were kept in the Pyrex glass capillaries in which they were crystallized. Since tin does not stick to clean Pyrex this probably resulted in no appreciable strain when the specimens were cooled down. Thallium, however, does stick somewhat to glass so there is a possibility that strain may have been present. One of the indium samples In-1 was crystallized in a Pyrex capillary in which it was sealed off and used. Since indium also tends to stick to glass a second sample In-2 was cast and crystallized, and then the glass was etched off in HF. The crystal was kept and used in a loosely fitting glass tube.

Mercury sample Hg-4 was enclosed in Pyrex and frozen just prior to using. The second sample, Hg-*F*-1, was a free rod and was made by slowly freezing mercury in a glass tube lines with thin paper. The freezing mixture was a mixture of dry ice in alcohol, and the tube was slowly lowered into the bath so as to promote slow crystal growth. After freezing, the rod was slipped out of the enclosing tube, the paper lining removed and the frozen rod reinserted so that it was free of the walls. The rod was kept cold until used.

RESULTS

The collected results of the critical field measurements are given in Tables I, II, and III. The original tin data were tabulated in the earlier paper.[2] Some minor changes have been made in the values of some of the tin constants. In the earlier analysis where relative changes were more important, the computations were based heavily on difference measurements whereas in the present paper each of the isotope curves has been considered by itself.

The transitions were for the most part reasonably sharp and the frozen-in moments were no more than a few percent. The thallium data are probably the poorest, as shown both by the scatter of the points in Fig. 5 and by the breadth of the transitions in Fig. 1. This may be, in part, due to strain resulting from adhesion to the glass walls of the capillary and in part to chemical impurity.

The effect of strain may be gauged from the comparative data of the two indium specimens and the mercury specimens. In-1 was used in the original glass capillary in which it had been cast whereas the glass was removed from In-2 by etching in hydrofluoric acid. The transitions are slightly sharper for In-2, and there is a small but observable change in the critical field curve, including a small reduction in the initial slope and a lowering of the transition temperature.

TABLE I. Threshold field data for the specimens.

Tl-5		Tl-205-2		Tl-203-1		In-2		In-1	
T°K	H oersteds	T°K	H oersteds	T°K	H oersteds	T°K	H oersteds	T°K	H oersteds
2.370	2.95	2.358	3.70	2.384	1.35	1.219	238.5	1.287	237.7
2.350	4.87	2.351	4.40	2.381	2.08	1.230	237.7	1.698	205.8
2.330	7.86	2.344	5.32	2.375	2.73	1.648	207.7	1.967	181.8
2.294	12.33	2.334	6.76	2.374	2.74	1.862	188.5	2.295	146.7
2.171	28.2	2.330	7.46	2.372	2.92	2.023	173.7	2.353	141.3
2.001	47.9	2.310	9.80	2.370	3.45	2.300	144.4	2.900	74.0
1.805	69.8	2.297	11.42	2.358	4.98	2.624	107.3	3.136	42.5
1.598	91.2	2.294	11.93	2.351	5.96	2.875	75.0	3.291	21.1
1.524	99.2	2.170	27.8	2.344	6.44	3.110	43.7	3.364	9.90
1.257	122.4	2.001	47.3	2.334	7.95	3.237	26.1	3.392	5.87
		1.994	47.7	2.330	8.67	3.281	19.80	3.411	3.17
		1.805	69.0	2.310	10.92	3.321	13.70		
		1.745	75.6	2.297	12.76	3.379	5.30		
		1.598	90.2	2.294	13.52				
		1.464	103.2	2.170	29.0				
		1.257	122.3	2.001	48.9				
				1.994	49.4				
				1.745	77.1				
				1.464	104.4				
				1.237	123.9				

Hg-4		Hg-F-1	
T°K	H oersteds	T°K	H oersteds
1.268	368.2	1.249	371.3
1.913	323.3	1.935	326.8
2.456	267.8	2.512	260.6
2.888	212.8	2.924	208.8
3.292	154.5	3.385	137.8
3.580	107.5	3.750	78.0
3.862	57.7	3.992	31.9
3.986	34.1	4.098	10.85
4.014	28.6	4.145	1.84
4.064	19.1		
4.067	18.0		
4.098	11.6		
4.128	6.46		
4.148	2.32		

Both of these effects are usually associated with strain, i.e., the less the strain the lower are both T_c and $(dH/dT)_{T_c}$. The same is true for Hg-4 and Hg-F-1, the former of which was enclosed in a glass capillary while the latter was a free rod and possibly also a single crystal. The transitions were appreciably sharper for Hg-F-1 and the transition temperature slightly lower. There was little difference in the initial slope.

It is quite possible that the thallium data may have been influenced somewhat by strain. The tin was probably strain free because of the fact that tin does not usually adhere to clean glass.

The critical field curves are closely parabolic in the lower range of temperatures, but all except those for mercury clearly deviate from the simple parabolic form at higher temperatures. The mercury curve is however closely parabolic over the entire range. The over-all departures from the parabola, $h=1-t^2$, are exhibited in Figs. 4 to 7 where the differences between a parabola drawn through H_0 and T_c, and the observed data, are plotted in normalized form. H_0 is the critical field at absolute zero, T_c is the zero-field transition temperature, and h and t are the reduced field and temperature H/H_0 and T/T_c, respectively. The differences, although small, are quite observable. The significance of the solid and dashed curves will be explained later.

The critical field curves all have this feature in common. At low temperatures they are parabolic and at temperatures near $T=T_c$ they are all linear. We can therefore specify four observable parameters for each curve, H_0, T_c, $[dH/d(T^2)]_{T=0}$ and $(dH/dT)_{T_c}$, without reference to the detailed intermediate form of the curve. These quantities are tabulated in Table II, and were obtained by least squares adjustment of straight lines to selected portions of the data, namely $H_c(T^2)$ near $T=0$ and $H_c(T)$ near $T=T_c$. It turns out that both slopes are related to interesting physical quantities in the two-fluid description of a superconductor. If $H_c(T)$ is expressed as a polynomial in T, then the slope $[dH/d(T^2)]_{T=0}$ is the coefficient of the leading term. Other coefficients may be evaluated from T_c, $(dH/dT)_{T_c}$ and intermediate points. Some fourth degree polynomial representations found in this way

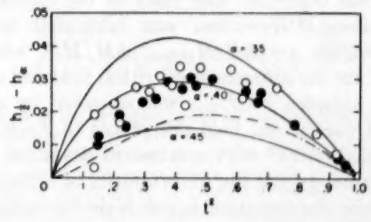

FIG. 4. Plot of the deviation of the critical field data for tin from the parabola $1-t^2$. The solid curves are the deviations calculated for the α model. The broken curve is the deviation calculated from Koppe's model. ○ Sn-112-1; ● Sn-124-1.

TABLE II. Observed threshold field curve parameters.

Sample	T_c °K	H_0 oersteds	$-\left(\frac{dH}{dT}\right)_{T_c}$ oersteds/°K	$-\left[\frac{dH}{d(T^2)}\right]_{T=0}$ oersteds/°K²	Remarks
Sn 112-1	3.8090	312.3	144.3	23.42	42 mm×0.33 mm
	(0.0089)	(0.63)	(1.3)	(0.66)	99.58% pure
Sn 118-1	3.7452	303.3	139.8	22.92	57 mm×0.39 mm; Cast and used in Pyrex capillaries;
	(0.0010)	(1.52)	(0.49)	(0.13)	99.19% pure probably single crystals
Sn 124-1	3.6657	298.4	141.0	23.98	23 mm×0.31 mm
	(0.0027)	(0.54)	(1.54)	(0.18)	99.91% pure
Tl-5	2.3917	172.8	125.8	31.85	64 mm×0.5 mm
(nat. Tl)	(0.0025)	(1.4)	(5.6)	(0.71)	specpure thallium
Tl-205-2	2.3861	171.4	129.2	31.62	37 mm×0.35 mm; Cast and used in Pyrex capillaries;
($M=205.02$)	(0.0010)	(1.1)	(2.0)	(0.50)	99.73% pure presumably single crystals
Tl-203-1	2.3956	170.0	130.5	30.40	52 mm×0.51 mm
($M=203.33$)	(0.0007)	(1.1)	(1.7)	(0.33)	99.74% pure
In-1	3.4314	278.9	149.6	25.16	52 mm×1 mm; single crystal cast in Pyrex capillary and kept
(nat. In)	(0.0010)	(0.78)	(1.8)	(0.21)	in glass envelope; specpure indium.
In-2	3.4178	275.0	142.2	24.68	45 mm×1 mm; single crystal cast in Pyrex capillary and glass
(nat. In)	(0.0019)	(0.46)	(1.5)	(0.14)	etched off in HF; specpure indium.
Hg-4	4.1596	404.5	196.2	22.81	62 mm×1 mm; 99.999 Hg in Pyrex capillary.
	(0.0011)	(2.7)	(2.1)	(0.49)	
Hg-F-1	4.1538	410.7	196.9	23.56	50 mm×2.5 mm; 99.999 Hg free rod (presumably single
	(0.0008)	(4.0)	(1.6)	(0.70)	crystal).

(Figures in parentheses are the standard deviations of the numbers above them.)

are as follows:

$$\text{Sn} \quad h=1-1.078t^2-0.103t^3+0.181t^4,$$
$$\text{In} \quad h=1-1.051t^2-0.123t^3+0.1745t^4,$$
$$\text{Tl} \quad h=1-1.053t^2-0.152t^3+0.206t^4,$$
$$\text{Hg} \quad h=1-t^2.$$

From the observable parameters we can also calculate values for γ, the molar specific heat coefficient associated with the electrons in the normal state. These values, calculated from Eq. (3) below, are as follows:

$$\text{Sn} \quad \gamma=4.45\times10^{-4} \text{ cal/deg}^2 \text{ mole},$$
$$\text{Hg} \quad \gamma=5.3\times10^{-4} \text{ cal/deg}^2 \text{ mole},$$
$$\text{In} \quad \gamma=4.0\times10^{-4} \text{ cal/deg}^2 \text{ mole},$$
$$\text{Tl} \quad \gamma=3.65\times10^{-4} \text{ cal/deg}^2 \text{ mole}.$$

ISOTOPE SHIFT IN THALLIUM

In the course of these experiments the isotope shift between the two thallium samples, of mass 205.01 and 203.33, was observed. The value of the exponent ϵ in the relation $M^{\epsilon}H_0=\text{const}$ was calculated using the approximation $\epsilon=(\Delta H/H_1)_{T=0}/(\Delta M/M_2)$, where ΔH and ΔM are the differences in critical field and mass for the two samples. $(\Delta H)_{T=0}$ was obtained by extrapolation of the critical field differences to $T=0$. It was found that $\epsilon=0.49$ with a standard deviation of ±10 percent arising from the uncertainties of extrapolation. Thus while the precision is not high the value of the exponent is consistent with the half-power relation previously observed in tin[3] and mercury.[4]

[4] Reynolds, Serin, and Nesbitt, Phys. Rev. 84, 691 (1951).

DISCUSSION

Before discussing the relation of these results to the two-fluid model we shall briefly summarize some of the features of this model from the standpoint of the treatment referred to earlier.[1] From this point of view superconductivity is associated with changes in the energies of the electrons near the surface of Fermi distribution, which may be described by saying that a fraction of the electrons enter a condensed state, losing their thermal excitation and entropy. The degree of condensation is described by a parameter ω which by definition takes on values between 0 and 1 as the transition temperature goes from T_c to 0. The excited and condensed fractions are treated like two phases in thermal equilibrium. The distribution between the two phases varies so that first, at $T=T_c$, all electrons are in the excited phase and then gradually condense as the temperature is lowered, until at $T=0$ all are in the condensed state. Excluding lattice terms the free energy of the superconducting state is

$$F_s=-\beta\omega-\tfrac{1}{2}\gamma T^2K(\omega), \tag{1}$$

where the first term is the condensation energy and the second is the thermal excitation term. β is given by $H_0^2V_m/8\pi$, in which V_m is the molar volume. $K(\omega)$, a function of ω, is the effective normal fraction, and takes on values from 1 to 0 as T goes from T_c to 0. Minimizing F_s with respect to ω yields the equilibrium condition

$$K'(\omega_e)=K'(0)(T_e/T)^2, \tag{2}$$

in which ω_e is the equilibrium value of ω and also a

generalized form of the Kok relation

$$K'(\omega_e)=-\frac{H_0^2V_m}{T_c^2 4\pi K'(0)}. \tag{3}$$

Some explicit forms for the critical field curve and some related derivatives may be readily obtained. These are

$$h^2=\omega_e+t^2[1-K(\omega_e)]/K'(0), \tag{4}$$

$$dh/dt=h/t-\omega_e/ht, \tag{5}$$

$$K(\omega_e)=1-K'(0)\left[\frac{d(h^2)}{d(t^2)}\right]=1-K'(0)\left[2h\frac{dh}{d(t^2)}\right], \tag{6}$$

in which h and t are the normalized critical field and transition temperature, H/H_0 and T/T_c. It follows from these that

$$K'(0)=\left[\left(\frac{d(h^2)}{d(t^2)}\right)^{-1}\right]_{t=0}=\left[\left(2h\frac{dh}{d(t^2)}\right)^{-1}\right]_{t=0}, \tag{7}$$

$$\left(\frac{dh}{dt}\right)_{t=1}=-\left[-\left(\frac{d\omega_e}{dt}\right)_{t=1}\right]^{\frac{1}{2}}. \tag{8}$$

It will be apparent that $h(t)$ is determined once $\omega_e(t)$ and $K(\omega_e)$ are known. Conversely if the detailed form of $h(t)$ is known, both $\omega_e(t)$ and $K(\omega_e)$ may be determined. Moreover the quantities $K'(0)$ and $(d\omega_e/dt)_{t=1}$ may be evaluated if H_0, T_c, and the slopes $[dH/d(T^2)]_{T=0}$ and $(dH/dT)_{T_c}$ are known.

We shall compare the observed form of $h(t)$ and the quantities $K'(0)$ and $(d\omega_e/dt)_{t=1}$ with those calculated on the basis of two special forms of the two-fluid model, the α model of Gorter and Casimir,[5] and the Koppe[6] model.

The α model is a purely *ad hoc* description, and while the Koppe model is based on ideas proceeding from Heisenberg's theory of superconductivity, it too may be considered on an *ad hoc* basis. However it makes a definite assumption about the statistics of the electron distribution and consequently goes back a little further than the α model.

In the α model $K(\omega)$ is given by

$$K(\omega)=(1-\omega)^\alpha, \tag{9}$$

where α is a parameter of the superconductor. When $\alpha=\frac{1}{2}$ the critical field curve reduces to the well-known parabolic case, and both the electronic entropy and specific heat follow a T^3 law. Most previous treatments and applications of the α model have assumed that $\alpha=\frac{1}{2}$. However by taking α as a general parameter we get an extra degree of freedom which is useful in describing the departures from parabolic form which are actually observed. A more detailed discussion of the α model has been given in the paper referred to earlier.[1] We need only remark here that for the α model Eqs. (4), (7), and (8) become

$$h^2=1-\frac{t^2}{\alpha}+\left(\frac{t}{\alpha}-1\right)t^{2/(1-\alpha)}, \tag{10}$$

$$K'(0)=-\alpha, \tag{11}$$

$$(d\omega_e/dt)_{t=1}=-2(1-\alpha). \tag{12}$$

Koppe's model postulates a definite form for $K(\omega)$ based on the assumption that the density of electron states has a discontinuity at the Fermi level. Koppe's expression for $K(\omega)$ cannot be given in closed form but has been evaluated numerically[7] and is a function of only reduced variables. Consequently the same $K(\omega_e)$ and $h(t)$ apply to all superconductors according to Koppe. This model gives a critical field curve which is not quite parabolic but which has the same curvature as the parabola at $t=0$, namely $[dh/d(t^2)]_{t=0}=-1$.

Both the α model and the Koppe model are compared with the data in the difference plots Figs. 4 to 7. The solid curves are the difference between a parabola passing through H_0 and T_c and the α-model curves for various values of α. The broken-line curve is that predicted by the Koppe model.

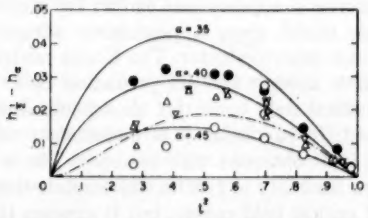

FIG. 5. Plot of the deviation of the critical field data for thallium from the parabola $1-t^2$. The solid curves are the deviations according to the α model and the broken line that according to the Koppe model. The open points represent data normalized with a value of H_0 obtained by passing a parabola through the points near $t=0$. The solid points represent data normalized with a value of H_0 found by passing a cubic through all the points. ○, ● Tl-203-1; ▽, Tl-5; △, Tl-205-2.

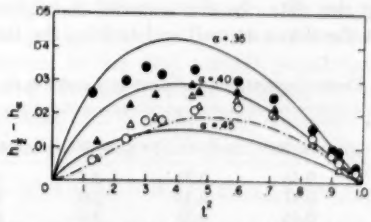

FIG. 6. Plot of the deviation of the critical field data for indium from the parabola $1-t^2$. The solid curves are the deviations according to the α model and the broken line that according to the Koppe model. The open points represent data normalized with a value of H_0 obtained by passing a parabola through the points near $t=0$. The solid points represent data normalized with a value of H_0 found by passing a cubic through all the points. △, ▲ In-1; ○, ● In-2.

[5] C. T. Gorter and H. B. G. Casimir, Physik. Z. **35**, 963 (1934).
[6] H. Koppe, Ann. Physik **1**, 405 (1947).
[7] See references 1 and 5, also B. B. Goodman, Cambridge thesis (unpublished).

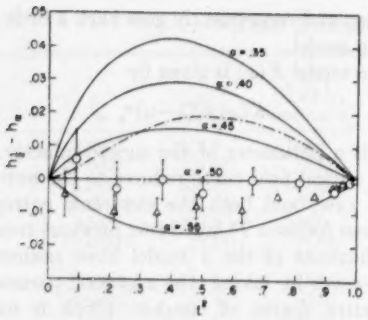

FIG. 7. Plot of the deviation of the critical field data for mercury from the parabola $1-t^2$. △ Hg-4, ○ Hg-*F*-1.

The Koppe model appears to be a satisfactory representation for the indium data and a fair representation for the thallium, for which the precision is somewhat poorer. However it is not consistent with the mercury data, which is closely parabolic, or with the tin data which has somewhat greater curvature.

The α model, with its extra parameter, is somewhat more flexible than the Koppe model, but it too is inconsistent with some features of the data. It should be noted that the experimental data in the plots of Figs. 4–7 define curves whose curvature is sensitive to small changes in the value of H_0 used for normalization. The data represented by the open points were normalized using a value of H_0 found by passing a parabola through the data in the region of $T=0$. The solid points were obtained using a value of H_0 found by passing a cubic through all of the points. The first technique is probably better and the parameters of Tables II and III were determined by this method. The tin plots of Fig. 4 were also normalized in this way. The mercury data were normalized by passing a parabola through all the points. There was no significant difference between this parabola and that fitted locally to the points near $T=0$.

We can apply some internal consistency checks to see how well the α and Koppe models succeed in describing the data. In the α-model description α is related to the slopes at $t=0$ and $t=1$ by the following relations:

$$K'(0)=\{2[dh/d(t^2)]_{t=0}\}^{-1}=-\alpha, \tag{13}$$

$$(dh/dt)_{t=1}=-(2/1-\alpha)^{\frac{1}{2}}. \tag{14}$$

If the α model is a good representation the α determined by (13) and (14) should be the same as that giving the best fit in Figs. 4–7. In Table III we have tabulated the quantities $-K'(0)$ and $1-2[(dh/dt)_{t=1}]^{-2}$ for each of the specimens. For the mercury data, which is parabolic and which would check in any case, there is of course agreement. For the other three metals however $-K'(0)$ runs from 0.46 to 0.49 whereas the α computed from $(dh/dt)_{t=1}$ is considerably lower, of the order of 0.3–0.4. In fact if one now examines the deviation plots of Fig. 4 there is a trend in the data in the direction of increasing α, as t^2 goes from 1 to 0. Stated in another way, for $t^2<0.4$ the data is closely linear in t^2 whereas the α-model curves exhibit greater curvature. It appears therefore that the α model, with constant α, represents the data in an approximate fashion but is not an accurate description.

TABLE III. Derived quantities pertinent to α and Koppe models.

Sample	$-K'(0)$	$1-2\times[(dh/dt)_{t=1}]^{-2}$	$[(dh/dt)_{t=1}]^2$	$\frac{-K'(0)}{[(dh/dt)_{t=1}]^2}\times$
Sn-112-1	0.46	0.35	3.1	1.42
Sn-118-1	0.47	0.33	3.0	1.41
Sn-124-1	0.46	0.33	3.0	1.39
Tl-5	0.47	0.34	3.0	1.44
Tl-205-2	0.48	0.38	3.2	1.54
Tl-203-1	0.49	0.41	3.4	1.65
In-1	0.47	0.41	3.4	1.60
In-2	0.48	0.36	3.1	1.49
Hg-4	0.50	0.50	4.0	2.0
Hg-*F*-1	0.50	0.50	4.0	2.0

It is noteworthy that Koppe's model predicts a critical field curve which has the same curvature as the simple parabola at $t=0$. In Koppe's model $K(\omega_e)$ decreases exponentially as $t\to 0$. In this region the critical field curve is an insensitive tool with which to explore $K(\omega_e)$. Measurements of specific heat and thermal conductivity below 1°K would be revealing and some recent determinations[8] of the latter have indeed indicated exponential behavior. Goodman[8] has suggested that this behavior is essentially a characteristic of a system with a finite gap between the ground state and the lowest excited state.

In the treatment of the general two-fluid model[1] the specific heat discontinuity is given by

$$(C_s-C_n)/\gamma T_c=-K'(0)[(dh/dt)_{t=1}]^2. \tag{15}$$

This quantity is tabulated for all of the specimens in Table III. Koppe has predicted that this quantity is numerically equal to $\pi^2/(12\ln^2 2)=1.7118$ for all superconductors, which is apparently not borne out.

In conclusion it appears that neither the α model nor the Koppe model gives a completely adequate description of a superconductor. The Koppe model is not quite flexible enough and its prediction of a unique reduced critical field curve for all superconductors is not verified. In particular it is inconsistent with the parabolic form observed with mercury. The α model has enough flexibility to give an approximate characterization of critical field curves, but it appears that the model with constant α is an oversimplified description.

The authors are indebted to Dr. H. P. R. Frederikse for valuable comment and discussion.

[8] B. B. Goodman, Proc. Phys. Soc. (London) **A66**, 217 (1953); J. G. Daunt, Proc. Schenectady Cryogenics Conference, 1952 (unpublished).

Susceptibility Tensor and the Faraday Effect in Ferrimagnetics

ROALD K. WANGSNESS
United States Naval Ordnance Laboratory, White Oak, Maryland
(Received April 14, 1954)

The components of the susceptibility tensor have been calculated for the two-sublattice model of a ferrimagnetic in which damping is neglected, and the results related to the theory of the Faraday effect in these materials. It is shown that in most cases the only change necessary is the replacement of the electron gyromagnetic ratio by the effective gyromagnetic ratio of the material. The effect of the sublattice structure is more apparent when the material has a compensation point, for then the rotation can change sign two or more times as a function of temperature or composition. The rotation to be expected for an unmagnetized antiferromagnetic is also determined, and some of the simpler results are generalized to the case in which there are an arbitrary number of sublattices. Other possible sublattice effects are also briefly considered.

INTRODUCTION

IF the electronic magnetic moments in a ferromagnetic material are subjected to a magnetic field having a constant component in the z direction and a small oscillating component in the xy plane, then it has been shown[1-4] that the gyroscopic behavior of the spins leads to expressions for the transverse components of the magnetization of the form

$$\left.\begin{aligned} M_x &= \xi_x H_x - i(\zeta/\omega)H_y, \\ M_y &= +i(\zeta/\omega)H_x + \xi_y H_y, \end{aligned}\right\} \tag{1}$$

where ω is the circular frequency of the oscillating field.

A consequence of this tensor character of the susceptibility is that the index of refraction for a circularly polarized plane wave propagated in the z direction depends upon the sense of rotation of the field vectors. If a linearly polarized wave is incident upon the material, its two components of opposite circular polarization will travel through the material with different phase velocities. Their resultant at any point is still a linearly polarized wave, but one whose plane of polarization has been rotated through an angle proportional to the distance traversed in the medium, a result which is familiar from the usual description of the Faraday effect. One finds the angle of rotation after a distance l to be given by

$$\theta = (2\pi\epsilon_{eff}^{\frac{1}{2}}/c)l\zeta,$$

provided that ξ_x, ξ_y, and (ζ/ω) are all small compared to unity, and where $\epsilon_{eff}=\frac{1}{2}(|\epsilon|+\epsilon_1)$ if one assumes the dielectric constant to be a complex scalar. In an appropriate set of units, therefore, the rotation per unit length of path is simply given by

$$\theta = \zeta. \tag{2}$$

In the common case in which the applied frequency ω is sufficiently large compared to the ferromagnetic resonance frequency, it is easily shown[4] that

$$\zeta = -\gamma M, \tag{3}$$

where γ is the gyromagnetic ratio of the ferromagnetic electrons and M is the equilibrium component of the magnetization in the direction of the constant field. A principal reason for the simplicity of the results given by (2) and (3) is that damping terms which affect the response of the magnetization to the oscillating field have been neglected; in general, if damping is included, then ζ, ξ_x, and ξ_y all become complex, as has been shown by Hogan,[3] with a resulting complication in the expression for the rotation. For our purposes, the explicit inclusion of damping terms in the equations of motion is not necessary, and for simplicity will be neglected, although it will occasionally become convenient to include damping in an implicit manner as is often done in the elementary theories of optical dispersion.

Experimental results[3] obtained by using various ferrites are in good agreement with the predictions given by (3). This can be the more readily understood since it has been shown[5] that the resonance frequency of ferrimagnetics can, in most cases, be quite accurately taken to be of the same form as that given by the standard theory of ferromagnetic resonance. It is necessary, however, that the gyromagnetic ratio of a single electron, γ, be replaced by the effective gyromagnetic ratio, γ_{eff}, defined as the ratio of the total magnetic moment to the total angular momentum of the specimen. In the simplest case in which the ferrimagnetic material can be adequately described as being comprised of two magnetic sublattices, we have

$$\gamma_{eff} = M/S = (M_1+M_2)/[(M_1/\gamma_1)+(M_2/\gamma_2)]. \tag{4}$$

As a result, it is reasonable to expect that the expression (3) for the Faraday rotation should actually be written for ferrimagnetics as

$$\zeta = -\gamma_{eff}M, \tag{5}$$

[1] D. Polder, Phil. Mag. **40**, 99 (1949).
[2] F. F. Roberts, J. phys. et radium **12**, 305 (1951).
[3] C. L. Hogan, Bell System Tech. J. **31**, 1 (1952); Revs. Modern Phys. **25**, 253 (1953).
[4] G. T. Rado, Phys. Rev. **89**, 529 (1953).
[5] R. K. Wangsness, Phys. Rev. **91**, 1085 (1953); **93**, 68 (1954). Hereinafter, these papers will be denoted by I and II, respectively, and numbers in following parentheses will refer to the corresponding equation of the paper.

which reduces to (3) in the ferromagnetic case in which one assumes the sublattice gyromagnetic ratios to be equal.

Ordinarily, this change can be expected to have no great effect upon the observed rotation since the γ_i of the sublattices are of the same magnitude, and also the magnetization of one sublattice is dominant over the complete range of temperature or composition considered. An interesting situation arises, however, when the ferrimagnetic in question possesses a compensation point for magnetization, that is, a temperature or composition at which the magnetizations of the two sublattices are equal and oppositely directed. This means that the dominant magnetization changes from one sublattice to the other as the compensation point is passed through and the net magnetization will change sign provided that any constant external magnetic field is sufficiently small. Both of these possibilities have been realized experimentally.[6,7] Further, one can expect the γ_i to be different so that there will also exist a compensation point for angular momentum which, in general, will not coincide with that for magnetization. Thus, in the range between these two points, M and S will be parallel rather than antiparallel as normally occurs, and we see from (4) that the effective gyromagnetic ratio of the material will have a sign opposite to that of the magnetic electrons themselves. Such an effect would not be observed by the usual absorption type resonance experiments, but (5) indicates that it should be detectable by a change in sign of the Faraday rotation.

We shall now illustrate the effect of these qualitative considerations by considering a definite example. In Fig. 1 are shown values of magnetization and γ_{eff} which

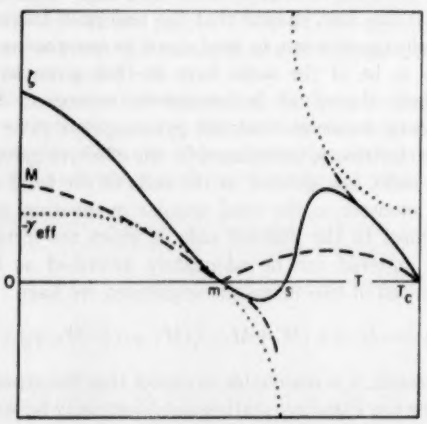

FIG. 1. Qualitative dependence of the magnetization, effective gyromagnetic ratio, and Faraday rotation upon temperature. m and s are compensation points for magnetization and angular momentum, respectively.

[6] E. W. Gorter and J. A. Schulkes, Phys. Rev. **90**, 487 (1953).
[7] L. R. Maxwell and S. J. Pickart, Phys. Rev. **92**, 1120 (1953).

are similar to those which have been observed as a function of temperature for $Li_{0.5}Fe_{1.25}Cr_{1.25}O_4$.[6,8] The temperatures m and s are the compensation temperatures for magnetization and angular momentum, respectively; the magnetization is taken to be positive for all temperatures since the constant field which is used in the Faraday effect is assumed to be large enough to ensure that the net magnetization will always be aligned parallel to this field. The negative sign of γ_{eff} makes ζ positive in the normal regions and a reversal in sign is then inferred from (4) for the temperature range between m and s although it is known[5] that such a definition of γ_{eff} in this range is not exact. Then, according to (5), the rotation can be obtained by a simple multiplication of the curves; the resulting curve is also shown in the figure. We note that (4) and (5) together would make the rotation infinite and discontinuous at s; actually, of course, this cannot be the case, and we should expect that the qualitative effect of any real damping would be to join these branches in a smooth manner (as in the case of optical dispersion) with the result that the actual rotation at s would be zero as shown. The general trend is clear, however, and we see that a consequence of the concept of effective gyromagnetic ratios is that as the temperature is varied the observed rotation should change sign near m and again near s.

In the following sections, we shall justify these simple considerations by a more rigorous discussion. First, we shall calculate the exact expressions for the components of the susceptibility tensor for a two-sublattice system, and then consider the expressions obtained for the rotation in the special case in which the material apparently behaves in resonance experiments as a true ferromagnetic. After this we shall consider in some detail the effects that the existence of compensation points would have on the curve shown in Fig. 1. The rotation to be expected for an antiferromagnet will also be obtained from the results for the general two-sublattice case. Finally, we shall generalize our results as far as possible for the case in which we are dealing with an arbitrary number of sublattices.

When it is necessary to discuss a specific example, we shall restrict ourselves to a material exemplified by the temperature dependence shown in Fig. 1, although the discussion can be easily adapted to other cases, such as may occur as a function of composition.

THE SUSCEPTIBILITY TENSOR

We shall use the notation of I and II, except that the resonance frequencies discussed there will now be denoted by ω_0, so that ω represents the frequency of the external field.

If H_x and H_y are assumed to be proportional to $e^{i\omega t}$, then we assume that M_x and M_y also vary as $e^{i\omega t}$, so

[8] J. S. van Wieringen, Phys. Rev. **90**, 488 (1953).

that the equations of motion become

$$\begin{aligned}
&i\omega M_{1x}-\tfrac{1}{2}(A_y+B_y+C_y+D_y)M_{1y}\\
&\qquad+\tfrac{1}{2}(A_y-B_y+C_y-D_y)M_{2y}=-\gamma_1 M_1 H_y,\\
&i\omega M_{2x}+\tfrac{1}{2}(A_y-B_y-C_y+D_y)M_{1y}\\
&\qquad-\tfrac{1}{2}(A_y+B_y-C_y-D_y)M_{2y}=-\gamma_2 M_2 H_y,\\
&i\omega M_{1y}+\tfrac{1}{2}(A_x+B_x+C_x+D_x)M_{1x}\\
&\qquad-\tfrac{1}{2}(A_x-B_x+C_x-D_x)M_{2x}=\gamma_1 M_1 H_x,\\
&i\omega M_{2y}-\tfrac{1}{2}(A_x-B_x-C_x+D_x)M_{1x}\\
&\qquad+\tfrac{1}{2}(A_x+B_x-C_x-D_x)M_{2x}=\gamma_2 M_2 H_x.
\end{aligned}$$

If we introduce the new variables

$$M_j=M_{1j}+M_{2j},\quad \Delta_j=M_{1j}-M_{2j}, \tag{6}$$

where $j=x,y$ and the notation

$$\gamma_\pm=\gamma_1 M_1\pm\gamma_2 M_2, \tag{7}$$

the equations become

$$\left.\begin{aligned}
&i\omega M_x-B_y M_y-C_y\Delta_y=-\gamma_+ H_y,\\
&i\omega\Delta_x-D_y M_y-A_y\Delta_y=-\gamma_- H_y,\\
&B_x M_x+C_x\Delta_x+i\omega M_y=\gamma_+ H_x,\\
&D_x M_x+A_x\Delta_x+i\omega\Delta_y=\gamma_- H_x.
\end{aligned}\right\} \tag{8}$$

When we solve Eqs. (8) for M_x and M_y, we find them to be of the form given in (1), where

$$\left.\begin{aligned}
\xi_x&=\mathfrak{D}^{-1}(\mathfrak{L}_x\mathfrak{R}_y-\mathfrak{K}_y\omega^2),\\
\xi_y&=\mathfrak{D}^{-1}(\mathfrak{L}_y\mathfrak{R}_x-\mathfrak{K}_x\omega^2),
\end{aligned}\right\} \tag{9}$$

$$\zeta=-(\omega^2/\mathfrak{D})(\gamma_+\omega^2-\mathcal{P}), \tag{10}$$

and where

$$\begin{aligned}
\mathcal{P}&=A_x(\gamma_+A_y-\gamma_-C_y)+C_x(\gamma_+D_y-\gamma_-B_y)\\
&=A_y(\gamma_+A_x-\gamma_-C_x)+C_y(\gamma_+D_x-\gamma_-B_x)\\
&=S(\gamma_1\gamma_2 P)^2+\gamma_1\gamma_2 M_1M_2\{P[\gamma_1(n_{1x}+n_{1y})\\
&\quad+\gamma_2(n_{2x}+n_{2y})]+\gamma_1M_1n_{1x}n_{1y}+\gamma_2M_2n_{2x}n_{2y}\},
\end{aligned} \tag{11}$$

$$\begin{aligned}
\mathcal{K}_j&=\gamma_+B_j+\gamma_-C_j=(\lambda-N_j)(\gamma_1-\gamma_2)^2M_1M_2\\
&\quad+(\gamma_1^2M_1+\gamma_2^2M_2)Q_j+\gamma_1^2M_1^2n_{1j}+\gamma_2^2M_2^2n_{2j},
\end{aligned} \tag{12}$$

$$\mathfrak{L}_j=\gamma_+A_j-\gamma_-C_j=\gamma_1\gamma_2[PM+M_1M_2(n_{1j}+n_{2j})], \tag{13}$$

$$\begin{aligned}
\mathfrak{R}_j&=A_jB_j-C_jD_j=\gamma_1\gamma_2\{(\lambda-N_j)(M_1^2n_{1j}+M_2^2n_{2j})\\
&\quad+Q_j(P+M_1n_{1j}+M_2n_{2j})+M_1M_2n_{1j}n_{2j}\},
\end{aligned} \tag{14}$$

and $\mathfrak{D}$, the determinant of the coefficients of the homogeneous equations corresponding to (8), is given by

$$\mathfrak{D}=(\omega^2-\omega_0^2)(\omega^2+\omega_0^2-2F). \tag{15}$$

If desired, Eqs. (11)–(14) can be written in terms of the macroscopic effective demagnetizing factors due to anisotropy by using II(9), but for many of our purposes it will be sufficient simply to know the components of the susceptibility tensor when anisotropy is neglected. Thus, if we set $n_{ij}=0$, we find from (9) and (10) that

$$\zeta=-(\omega^2/\mathfrak{D})[(\gamma_1M_1+\gamma_2M_2)\omega^2-S(\gamma_1\gamma_2P)^2], \tag{16}$$

and

$$\begin{aligned}
\xi_j=\mathfrak{D}^{-1}\{&(\gamma_1\gamma_2)^2P^2MQ_j-\omega^2[(\lambda-N_j)(\gamma_1-\gamma_2)^2M_1M_2\\
&+Q_j(\gamma_1^2M_1+\gamma_2^2M_2)]\}.
\end{aligned} \tag{17}$$

THE APPARENT FERROMAGNETIC CASE

It was shown in II that when the product of the molecular field coefficient and the net magnetization is large compared to the components of the applied and anisotropy fields the resonance frequency has essentially the same form as that given by the theory of ferromagnetic resonance; namely, $\omega_0^2=\gamma_{eff}^2Q_xQ_y$. In this approximation, $P=\lambda M$ and $2F=(\lambda\gamma_1\gamma_2S)^2$ according to II(2). Generally we will also have $|2F|\gg\omega^2,\omega_0^2$ so that

$$\mathfrak{D}\simeq(\omega^2-\omega_0^2)(-2F),$$

and then we find that (16) and (17) become

$$\zeta_f=-\omega^2\gamma_{eff}M/(\omega^2-\gamma_{eff}^2Q_xQ_y), \tag{18}$$

$$\xi_{jf}=-\gamma_{eff}^2MQ_j/(\omega^2-\gamma_{eff}^2Q_xQ_y). \tag{19}$$

In most of the experiments which have been performed on the Faraday effect in ferrites, the external field has been kept small enough so that ω is large compared to the ferromagnetic resonance frequency. In addition, it is usually a good approximation to assume that $|\gamma_{eff}M|\ll\omega$.[3,4] Under these conditions, Eq. (18) is seen to reduce to the usual expression given in (5) and that $|\xi_{jf}|\ll1$ as expected. Thus, the results of this section verify our previous qualitative derivation of the formula (5) which has been amply tested by experiment. Equation (5) does differ from the usual formula in that it involves γ_{eff} which, however, under these conditions cannot be expected to differ much from the gyromagnetic ratio of the sublattice constituents and hence will be close to that of a free electron. Equation (18) also predicts the change in sign to be expected of the rotation as the field is increased to make the resonant frequency finally larger than ω; this effect is familiar from the study of the paramagnetic Faraday effect and has been experimentally observed in ferrites.[9]

EFFECT OF A COMPENSATION POINT

It is quite difficult to discuss the dependence of (16) upon temperature both exactly and in very general terms because no quantitative description of the temperature variation of the individual sublattice magnetizations seems to exist. What we shall do instead is to extrapolate our previous results as well as possible through the region of the compensation points and augment this by more precise discussions at the compensation points where exact calculations are more easily done.

I. Qualitative Discussion

The usual experimental procedure is to represent ω_0 as the product of the appropriate function of the ob-

[9] Second article in reference 3.

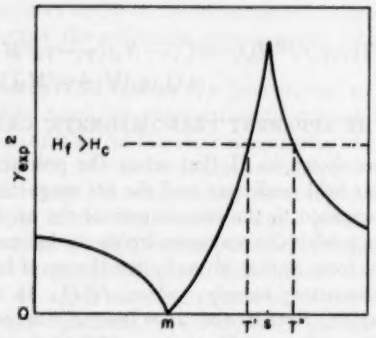

FIG. 2. Dependence of squared experimental gyromagnetic ratio upon temperature. Dashed lines locate two additional temperatures at which rotation will vanish for large enough external field.

served field needed for resonance and an experimental gyromagnetic ratio which we shall write as γ_{exp}; thus, $\omega_0^2=\gamma_{exp}^2Q_xQ_y$. In contrast to the prediction of infinity given by (4) at the point where $S=0$, the limited experimental data and the theoretical results given by I(22) and II(18–19) indicate that γ_{exp}^2 is large but finite at the compensation point for angular momentum. The general behavior to be expected of γ_{exp}^2 is shown in Fig. 2.

It is, therefore, probably not too unreasonable to expect that a fairly accurate representation of the rotation as a function of temperature can be given by the following generalization of (18),

$$\zeta_q=-\omega^2\gamma_{exp}M/(\omega^2-\gamma_{exp}^2H_f^2), \tag{20}$$

where we have put $H_f^2=Q_xQ_y$.

There are now essentially two cases to be considered corresponding to whether or not the constant field is large enough to make H_f greater than a critical field H_c which is determined by the maximum value of γ_{exp} and is defined by the equation

$$H_c^2=\omega^2/\gamma_{exp\ max}^2. \tag{21}$$

Using (21), we can then write (20) as

$$\zeta_q=-\gamma_{exp}M/[1-(H_f\gamma_{exp}/H_c\gamma_{exp\ max})^2]. \tag{22}$$

Equation (22) indicates in general that there will be an infinite discontinuity in ζ_q when $\gamma_{exp}^2=(H_c/H_f)^2\gamma_{exp\ max}^2$. Accordingly, when damping is taken into account, we would actually expect the rotation to pass through zero at this point.

Now when $H_f<H_c$, the denominator in (22) will never vanish, and if we assume that the sign of γ_{exp} has the same temperature dependence as shown in Fig. 1 for γ_{eff}, then the rotation predicted by (22) is as shown by the solid curve in Fig. 3. This, of course, is similar to that found in Fig. 1.

On the other hand, when $H_f>H_c$, there are two temperatures T' and T'' at which we can expect the denominator of (22) to vanish. The method of finding T' and T'' is illustrated in Fig. 2. This result means that ζ_q will change sign a total of four times: at m, T', s, and T''. This leads to a temperature dependence of ζ_q similar to that shown by the solid curve in Fig. 4. As H_f decreases to H_c, the points T' and T'' approach each other and eventually coincide so that there will be a smooth transition from the curve of Fig. 4 to that of Fig. 3.

II. $M=0$

With $M_2=-M_1$, we know that, with the neglect of anisotropy, $\omega_0^2=0$, and $-2F\simeq-[(\gamma_1-\gamma_2)\lambda M_1]^2\gg\omega^2$ from II(14) and II(12), so that (16) becomes

$$\zeta_m=\frac{-(\gamma_1-\gamma_2)M_1(\omega^2+\gamma_1\gamma_2H^2)}{\{\omega^2-[(\gamma_1-\gamma_2)\lambda M_1]^2\}}. \tag{23}$$

Since in most cases the applied field is small and the molecular field ($|\lambda M_1|$) large compared to the field needed for resonance at the applied frequency, Eq. (23) can generally be approximated further as

$$\zeta_m=-\omega^2/[\lambda^2(\gamma_2-\gamma_1)M_1]. \tag{24}$$

III. $S=0$

For this case, it simplifies matters to assume that we are dealing with the usual experimental case in which the sample has axial symmetry about the direction of the constant field so that $Q_x=Q_y=Q$. Then we find from II(16, 18, 19) that

$$\omega_0^2=-\lambda\gamma_2(\gamma_1-\gamma_2)M_1Q=F$$

and therefore $\mathfrak{D}=(\omega^2-F)^2$. Equation (16) is then found to reduce to

$$\zeta_s=\frac{-(\gamma_1^2-\gamma_2^2)\omega^4M_1}{\gamma_1[\omega^2+\lambda\gamma_2(\gamma_1-\gamma_2)M_1Q]^2}. \tag{25}$$

The approximate form of (25) corresponding to (24) is

$$\zeta_s=\frac{-(\gamma_1+\gamma_2)\omega^4}{\lambda^2\gamma_1\gamma_2^2(\gamma_1-\gamma_2)M_1Q^2}. \tag{26}$$

IV. The General Aspect of the Rotation

Using the results of the last two sections, we can now get an estimate of the relative signs and magnitudes

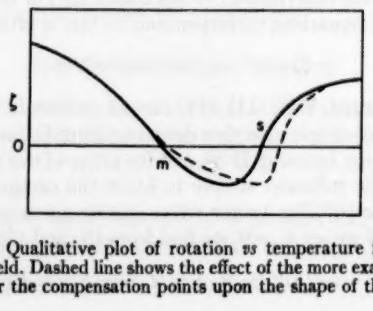

FIG. 3. Qualitative plot of rotation *vs* temperature for small applied field. Dashed line shows the effect of the more exact calculations for the compensation points upon the shape of the curve.

of ζ at the two compensation points. It will be sufficient for our purposes to use (24) and (26). We find that

$$\zeta_s/\zeta_m = -(\gamma_1+\gamma_2)\omega^2/(\gamma_1\gamma_2 Q^2). \tag{27}$$

It is immediately evident from (27) that ζ has opposite signs at these two points so that the rotation has changed sign at least once between m and s. A satisfactory estimate of the relative magnitudes is obtained by taking $\gamma_1 \simeq \gamma_2 \simeq \gamma$, so that

$$|\zeta_s/\zeta_m| = (\omega/\gamma Q)^2;$$

however, we shall continue to write

$$Q = H + (N-N_s)M = H + (N-N_s)(\gamma_1-\gamma_2)(M_1/\gamma_1).$$

If we substitute as fairly representative the values $H=500$, $N-N_s=5$, $(\gamma_1-\gamma_2)/\gamma_1=0.1$, $M_1=600$, and $\omega/\gamma=3000$, we find a value for the ratio of about 14.

We have yet to determine the magnitude and sign of, say, ζ_m, relative to the normal value ζ_f given in (18). If we assume that the applied frequency is large compared to the ferromagnetic resonance frequency we find from (18) and (24) that

$$\zeta_m/\zeta_f = \omega^2/[(\gamma_2-\gamma_1)\gamma_{eff}\lambda^2 M_1 M]. \tag{28}$$

In order to make further use of (28), we must choose which of the sublattice magnetizations is to be regarded as being dominant at a given temperature, although it is easily seen that our final results are independent of our particular choice. We shall assume that M_1 is the dominant magnetization from $T=0$ to the compensation point for magnetization. In other words, for $T<m$, we assume that $|M_1|>|M_2|$, and for $T>m$, that $|M_1|<|M_2|$. Now the condition for $S=0$ is that $|M_2/M_1| = |\gamma_2/\gamma_1|$. If $S=0$ is to occur at a temperature below that for which $M=0$, then we see that $|\gamma_2|<|\gamma_1|$. On the other hand, if $S=0$ is to occur at a temperature above that for which $M=0$, then we must have $|\gamma_2| > |\gamma_1|$. Since it is this latter case which corresponds to the situation pictured in Fig. 1, we see that we have $(\gamma_2-\gamma_1)\gamma_{eff}>0$, so that ζ_m and ζ_f always have the same sign according to (28).

In order to estimate the relative magnitudes of ζ_m and ζ_f, we shall assume that $\gamma_{eff}\simeq\gamma$ and $M\simeq\frac{1}{2}M_1$ in addition to the numerical estimates used in the last paragraphs. Then we find that

$$\zeta_m/\zeta_f \simeq 20(\omega/\gamma H_E)^2 \simeq 0.02,$$

where we have put $-\lambda M_1 = H_E \simeq 10^4$ oersted.

In summary, we have found that ζ_m is very small although not yet zero and shows no sign change, while ζ_s is of the same order of magnitude as the usual rotation but is always of the opposite sign. We are now able to redraw Figs. 3 and 4 somewhat more accurately. The first crossover near m will occur at a slightly higher temperature while the crossovers shown at s in Figs. 3 and 4 should occur at somewhat higher and lower temperatures, respectively. Hence, the general aspect of the rotation for the two cases should be more like that shown by the dashed lines in Figs. 3 and 4. The curves are meant to be purely qualitative and there is no necessary quantitative significance in the values of the relative maxima and minima.

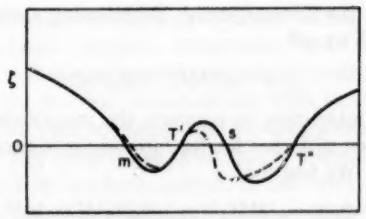

FIG. 4. Qualitative plot of rotation *vs* temperature for large applied field. Dashed lines shows the effect of the more exact calculations for the compensation points upon the shape of the curve.

As yet, there are no substantial experimental data which can be compared with these predictions, although preliminary results obtained on a sample of $Li_{0.5}Fe_{1.25}Cr_{1.25}O_4$ by Brown and Hebbert of this Laboratory[10] apparently show a behavior similar to that of Fig. 3. Some of the difficulties encountered in measuring the rotation of waves propagated in a wave guide rather than as plane waves and which complicate the interpretation of the results have been discussed by Hogan.[9]

THE ANTIFERROMAGNETIC CASE

It is easy to adapt our general results to the case in which the material is antiferromagnetic; however, if we were simply to take $\gamma_1=\gamma_2$ and $M=0$, the rotation would be zero by (23). Actually, we must now take anisotropy into account since it is known to have so important a role in antiferromagnetic resonance. We shall assume, as in II, that $\gamma_i=\gamma$ and $n_{ij}=n_j$. According to II(9), this last assumption not only implies equal anisotropy constants but equal values of M_i^2, i.e., $M=0$. As a result, we are omitting corrections of higher order in H since M is not exactly zero when $H=0$; this will be seen from our results below which will still give a value of ζ proportional to H in spite of our assumption that $M=0$.

With these assumptions, we easily find from (10) that

$$\zeta_a = -2\omega^2\gamma^3 M_1^2(n_x+n_y)H/\mathfrak{D}, \tag{29}$$

where $\mathfrak{D}$ can be evaluated by the use of II(20) and the preceding equation for F.

For convenience, we shall simplify this equation somewhat by introducing the anisotropy and exchange fields in the usual way by setting $n_j=H_a/M_1$, and $-\lambda M_1 = H_E$; we shall also assume that $H_E \gg H$.

If we now keep only the largest terms in II(20) and preceding equations, we find as usual that

$$\omega_0^2 = 2\gamma^2 H_E H_a = F,$$

[10] R. W. Brown and R. S. Hebbert (private communication).

so that $\mathfrak{D}=(\omega^2-\omega_0^2)^2\simeq\omega_0^4$. Substituting these results into (29) we get

$$\zeta_a=-\omega^2HM_1/(\gamma H_aH_E^2). \tag{30}$$

It is interesting to compare the magnitude of this expression with that for the ferromagnetic region given by (18). We find that

$$\zeta_a/\zeta_f=\omega^2HM_1/(\gamma\gamma_{eff}H_aH_E^2M)\approx 10^{-3}$$

if we continue to use the same numerical approximations as before, and, in addition, take $H_a\approx 10^3$. The expected value for the rotation in the antiferromagnetic case is thus much smaller than that for the ferromagnetic case. On the other hand, if we compare (30) with the value to be expected in the paramagnetic region above the Curie temperature where we can write $\zeta_p=-\gamma M=-\gamma\chi H$, we find that

$$\zeta_a/\zeta_p=\omega^2M_1/(\gamma^2\chi H_aH_E^2)\approx 1$$

if we assume the value of the susceptibility to be about 6×10^{-4}. Since these last two quantities are of the same order of magnitude, one would not expect to observe an abrupt change in the rotation as the material is cooled below the Curie temperature in contrast to what is observed for the absorption.[11]

This interesting result that one could expect to find a Faraday rotation for an antiferromagnet even if $M=0$ is another case which illustrates how important is the anisotropy for the determination of the electrodynamic properties of the antiferromagnetic case. This is most easily illustrated by considering the explicit form taken by the general Eqs. (8) in this case. They are easily found to be

$$\begin{aligned}
&i\tilde{\omega}M_x-HM_y-H_a\Delta_y=0,\\
&i\tilde{\omega}\Delta_x-2H_EM_y-H\Delta_y=-2M_1H_y,\\
&HM_x+H_a\Delta_x+i\tilde{\omega}M_y=0,\\
&2H_EM_x+H\Delta_x+i\tilde{\omega}\Delta_y=2M_1H_x,
\end{aligned}$$

where $\tilde{\omega}=\omega/\gamma$ and where we have written $H_a+2H_E\simeq 2H_E$. Upon inspection of these equations, we see that the existence of a nonzero H_a is the only thing that keeps us from treating M_x and M_y independently from Δ_x and Δ_y, and thus serves as the necessary coupling which brings the exchange field into the resonance frequency and also makes the transverse components of the magnetization depend on the oscillating components of the applied field. This is vividly illustrated when one calculates ξ and ζ and finds them both proportional to H_a, while the exchange field enters in only through the determinant of the coefficients.

AN ARBITRARY NUMBER OF SUBLATTICES

The calculation of detailed results equivalent to those of the last sections for the case in which we are dealing with an arbitrary number of sublattices would seem to be too complex to be possible. Instead, we shall show only that the simplest results as given in (18) and (19) are probably very accurately also true in this case.

For simplicity, we shall not include demagnetizing and anisotropy fields so that the equation of motion for the ith sublattice becomes

$$d\mathbf{M}_i/dt=\gamma_i\mathbf{M}_i\times(\mathbf{H}+\textstyle\sum_k\lambda_{ik}\mathbf{M}_k),$$

where the λ_{ik} are molecular field coefficients satisfying the relation $\lambda_{ik}=\lambda_{ki}$. Summing this equation over all sublattices, we find that

$$d[\textstyle\sum_i(\mathbf{M}_i/\gamma_i)]/dt=(\sum_i\mathbf{M}_i)\times\mathbf{H}, \tag{31}$$

since $\sum_{ik}\lambda_{ik}\mathbf{M}_i\times\mathbf{M}_k=0$. If we let $M=\sum_i M_{ix}=\sum_i M_{iy}$, $M_j=\sum_i M_{ij}$, and assume as usual that M_j and H_j are small and proportional to $e^{i\omega t}$, we find from (31) that

$$\left.\begin{aligned}
i\omega\textstyle\sum_i(M_{ix}/\gamma_i)&=-MH_y+HM_y,\\
i\omega\textstyle\sum_i(M_{iy}/\gamma_i)&=MH_x-HM_x.
\end{aligned}\right\} \tag{32}$$

For small deviations from the z direction we can expect M_{ij} to be proportional to M_i, and, in the limit of strong molecular fields, the constants of proportionally ϑ_i will be the same for all sublattices.[12] Then we can write

$$\textstyle\sum_i(M_{ij}/\gamma_i)=\vartheta\sum_i(M_i/\gamma_i)=(\sum_i M_{ij})/\gamma_{eff},$$

so that Eqs. (32) become

$$\begin{aligned}
i\omega M_x&=-\gamma_{eff}MH_y+\omega_0M_y,\\
i\omega M_y&=\gamma_{eff}MH_x-\omega_0M_x,
\end{aligned}$$

where $\omega_0=\gamma_{eff}H$.

When these last equations are solved for M_x and M_y, we find the results to have the form (1) where

$$\zeta=-\omega^2\gamma_{eff}M/(\omega^2-\gamma_{eff}{}^2H^2),$$

and

$$\xi=-\omega_0\gamma_{eff}M/(\omega^2-\omega_0^2),$$

which essentially agree with (18) and (19).

DISCUSSION

The results of our calculations in the previous sections have been seen to support in general the qualitative discussion given in the introduction. It would be possible, of course, to obtain better approximations to our very general results, but since most of the effects which have been predicted have not yet been observed experimentally, this is not really necessary at present.

On the other hand, a thorough discussion of ferrimagnetic resonance and allied effects requires for completeness that damping be included in as simple and accurate a manner as possible. When this is done, a possible sublattice effect to be considered is that the relaxation times for the various sublattices are very likely unequal because of the different nature of their

[11] Trounson, Bleil, Wangsness, and Maxwell, Phys. Rev. **79**, 542 (1950); L. R. Maxwell and T. R. McGuire, Revs. Modern Phys. **25**, 279 (1953).

[12] J. Smit and H. P. J. Wijn, *Advances in Electronics* **VI** (to be published).

surroundings. These probably unlike quantitative interactions between the ions and the crystalline lattice as well as among the magnetic ions themselves may then result in different approaches to thermal equilibrium. In this connection one may be able to devise a method of measuring the relaxation times of the individual sublattices; a possible approach may consist of a careful study of line widths and saturation properties of a series of compounds of varying composition in which one alters the constituents of the sublattices in a known and regular manner.

The apparent inertial mass of a moving ferromagnetic domain wall, which was first discussed by Döring,[13] is known to be a consequence of the connection between the electronic angular momentum and magnetic moment and arises from the precessional motion of the spins in the internal demagnetizing fields of a moving wall. In fact, the apparent mass per unit area depends on γ and it is tempting to think that in a ferrimagnetic γ_{eff} should be involved instead. If this were actually the case, then it may be observable as a dependence of the natural resonance frequency due to wall motion upon the temperature or composition.

I wish to thank Dr. T. R. McGuire and Dr. G. T. Rado for some helpful discussions, and Mr. R. W. Brown and Mr. R. S. Hebbert for permission to mention their preliminary experimental work.

[13] W. Döring, Z. Naturforsch. **3a**, 374 (1948); G. T. Rado, Phys. Rev. **83**, 821 (1951).

PHYSICAL REVIEW VOLUME 95, NUMBER 2 JULY 15, 1954

Backscattering of Kilovolt Electrons from Solids*

ERNEST J. STERNGLASS†
Cornell University, Ithaca, New York
(Received November 13, 1953)

The total number and energy distribution of backscattered electrons at 0.2–4 kev incident energy (V) have been measured for six elements using electrostatic retarding potential techniques. For atomic number $Z \lesssim 30$, backscattering was found to be essentially independent of V and almost linearly dependent on Z. For $Z \gtrsim 30$, backscattering decreases with decreasing V below 2–3 kev to values less than those for elements of $Z \simeq 30$, and it no longer is a simple function of Z. The ratio of the mean energy of the backscattered electrons to that of the primaries is found to be close to one-half for $Z=6$ and to increase only slightly for the heavier elements. These results are shown to indicate a dominant role of inelastic processes in the scattering of intermediate energy electrons, in contrast to scattering at very high energies, where elastic interactions control the phenomenon.

I. INTRODUCTION

PRESENT experimental and theoretical knowledge of the interaction of intermediate energy electrons with complex atoms is still very limited, in contrast to the situation at energies very large or very small relative to atomic binding energies. Measurements of the total number and energy distribution of electrons backscattered from solids such as reported on below offer a means of shedding new light on the relative importance of elastic and inelastic processes in the intermediate energy region. Such information is of importance in the formulation of a theory of backscattering more complete than existing theoretical treatments.[1] Aside from its practical interest, data on the backscattering process is also of value in the development of theories of bremsstrahlung production, cathode-luminescence, secondary emission, and bombardment-induced conductivity, where information on the primary beam spreading and total energy loss in the material is required. In particular, knowledge of the number of backscattered electrons at low energies would for the first time allow a separation of the true, low-energy secondary electrons from the total yield of emitted electrons for comparison with theory.[2]

At present, reliable data on the number of backscattered electrons[3] exist only for a few elements below

* This paper constitutes part of a thesis submitted in partial fulfillment of the requirements for the Ph.D. degree at Cornell University. Portions of the work were carried out at the U. S. Naval Ordnance Laboratory, White Oak, Maryland, and at the Westinghouse Research Laboratories, East Pittsburgh, Pennsylvania. A report on preliminary work was presented at the November, 1950, meeting of the Electron Physics Division of the American Physical Society, by Sternglass, Frey, and Grannis [Phys. Rev. **85**, 391 (1952)].

† Now at the Westinghouse Research Laboratories, East Pittsburgh, Pennsylvania.

[1] W. Bothe, Ann. Physik **6**, 44 (1949); see also article in *Handbuch der Physik* (Springer, Berlin, 1933), Vol. 24, part 2, p.1 for summary of earlier work.

[2] See the review article on Secondary Emission by K. G. McKay, *Advances in Electronics* (Academic Press, New York, 1948), Vol. 1.

[3] The term "backscattered electrons" as used here refers to all electrons emitted from a bombarded target whose energy is greater than 50 ev in accordance with the usual convention. This definition is designed principally to eliminate the true, low-energy secondary electrons, more than 95 percent of which have energies less than 30 ev for all solids and which will be referred to simply as "secondary electrons." It must be remembered that, because of the indistinguishability of electrons, the so-called "backscattered electrons" defined in this manner include some high-energy secondaries formed in close electron-electron collisions.

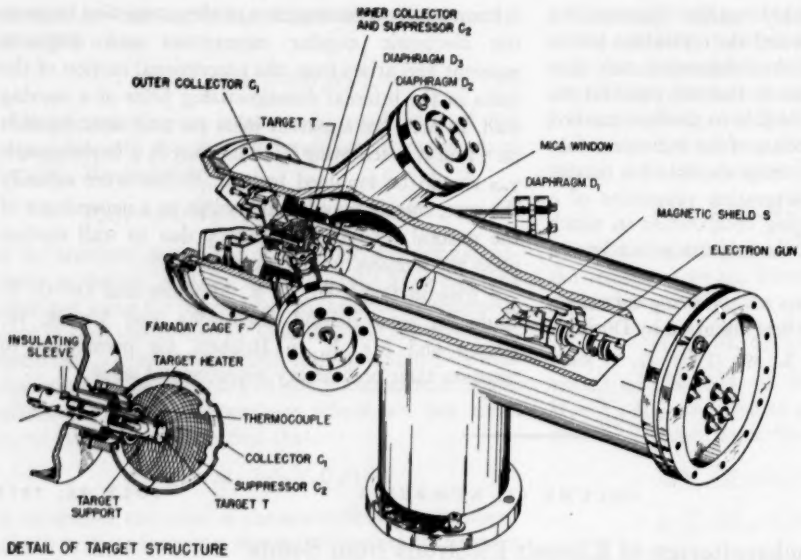

FIG. 1. Cut-away drawing of experimental tube and electrode arrangement.

200 ev[4–7] and above 2000 ev,[8–10] whereas accurate information on the energy distribution is available only below 200 ev[11,12] and above 370 kev,[13] except for some isolated measurements between 16 and 32 kev.[14] The investigation reported below was undertaken to fill the gap in the range from 200 ev to 2000 ev, where the effects of atomic binding energies on the scattering process can be expected to be most pronounced.

II. CHOICE OF EXPERIMENTAL TECHNIQUES

Since one of the chief purposes of the present investigation was to obtain a measure of the total number of backscattered electrons per primary particle, a spherical target-collector geometry was decided upon. In such an arrangement, the total current to the collector for an opposing potential of 50 volts gives a direct measure of the number of backscattered electrons. When this is subtracted from the total collector current measured with an aiding field, the true low-energy secondary yield, which serves as a convenient check on the target condition, is also obtained.

The spherical collector arrangement is not suitable for measuring the energy distribution of the backscattered electrons because of the defocusing action of the large retarding fields required. For this reason, it was decided to leave the region in front of the target field-free and to use a separate Faraday cage maintained at a variable opposing potential to determine the energy spectrum of a sample scattered into a fixed direction. Although the spectrum of the backscattered electrons is known to depend to some extent on the angle of observation,[14] the additional information to be obtained by varying this angle did not justify the increased complexity required in the present study. Possible diffraction effects, taking place only for the small number of perfectly elastically reflected electrons, will not be important and can in any case be easily detected by varying the primary energy.

A retarding method of measuring the electron energies was chosen in preference to a deflection one principally because of its simplicity and greater current intensity.

III. DESCRIPTION OF EXPERIMENTAL APPARATUS

A. Demountable Tube and Vacuum System

Inasmuch as the backscattering phenomenon is fundamentally a volume property, it is not very sensitive to small amounts of surface adsorbed gases. Since only chemically inactive metals were to be measured, a demountable vacuum tube could therefore be employed.

A cut-away drawing of the experimental tube is shown in Fig. 1. Three side arms with interchangeable windows are provided for observation and the mounting of auxiliary electrodes in addition to the openings at both ends on which the target and associated electrodes are mounted. The tube was designed so that no waxes, greases or rubber gaskets were required in its construction. A special type of re-usable packing gland seal employing a wire tin gasket was adapted for

[4] H. Bruining, Physica **5**, 913 (1938).
[5] I. Gimpel and O. Richardson, Proc. Roy. Soc. (London) **A182**, 17 (1943).
[6] O. Krenzien, Z. Physik **126**, 365 (1949).
[7] H. P. Myers, Proc. Roy. Soc. (London) **A215**, 329 (1952).
[8] P. Palluel, Compt. rend. **224**, 1492 (1947).
[9] B. F. J. Schonland, Proc. Roy. Soc. (London) **A104**, 235 (1923); **108**, 187 (1925).
[10] K. H. Stehberger, Ann. Physik **86**, 825 (1928).
[11] H. W. Farnsworth, Phys. Rev. **31**, 405 (1928).
[12] E. Rudberg, Phys. Rev. **50**, 138 (1936).
[13] W. Bothe, Z. Naturforsch. **4a**, 542 (1949).
[14] J. O. Brand, Ann. Physik **26**, 609 (1936).

all the openings in the tube as shown in Fig. 1. A mercury pump (D.P.I. MHG-50) with liquid-air trap was used in preference to an oil diffusion pump, because earlier experiments had demonstrated that a film of amorphous carbon builds up on the target under electron bombardment when oil is employed. The system was capable of reaching ultimate pressures as low as 2×10^{-7} mm of Hg.

B. Electrode Structure

The basic features of the electrode structure are shown in the drawing of Fig. 2. The arrangement consists of an electron gun (G), which produces a beam of electrons that passes through a magnetic shield (S), and a series of apertures (D_2 and D_3) sufficiently large so as not to limit the beam. The electrons emitted from the target (T) are collected by a set of concentric spherical electrodes composed of an outer collector (C_1) and a wire mesh electrode (C_2), which acts as a suppressor screen. A small portion of the backscattered electrons pass to the Faraday cage (F), through an opening in the collector located at an angle of 45° relative to the direction of incidence.

The electron gun is a standard cathode-ray type using electrostatic focusing and deflection (DuMont 5B) with the ordinary oxide cathode replaced by a special sintered molybdenum cathode kindly supplied by the RCA Laboratories. To forestall any possible deposition of cathode material on the target, the gun is tilted at an angle of approximately 3° so that the target cannot "see" the cathode.

The beam deflection plates in conjunction with the system of apertures D_1, D_2, and D_3 serve also as a velocity selector to remove any slow electrons from the primary beam. The shield S serves not only to eliminate disturbing magnetic fields but also to prevent stray electrons from reaching the target and collector structure. A mica-covered window permits observation of the target and visual focusing of the beam by means of a phosphor screen deposited on diaphragm D_2. D_3 is held at a negative potential of 22.5 volts with respect to D_2, so as to stop any secondaries that may have been formed at the edge of D_2 by stray primaries.

The target structure proper is shown in the detail drawing of Fig. 1. The upper portion of the target support is hollow so as to accommodate a small, noninductively wound tungsten wire heater. Heat conduction is reduced by means of a ribbed construction as well as by the use of poorly conducting mild steel which has the additional advantage of reducing any possible stray magnetic fields from the heater winding.

The inside of the collector C_1 and the wires of C_2 are covered with a baked-on coating of colloidal graphite to reduce secondary emission and backscattering from the collector at high primary energies.

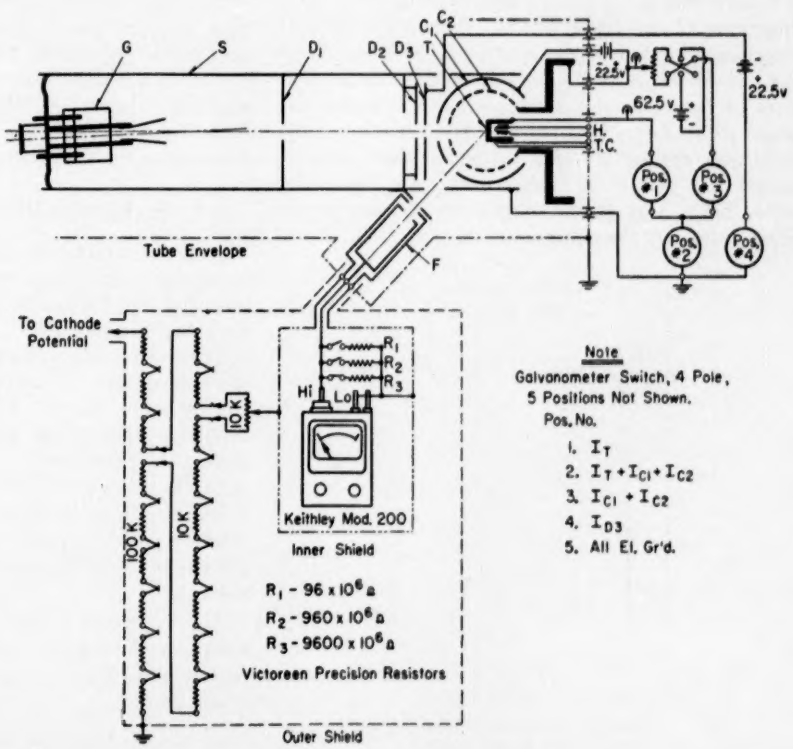

FIG. 2. Schematic diagram of measuring circuits for secondary emission and backscattering measurements.

The suppressor screen is made from 16 mesh copper screen with 68 percent open area.

The Faraday cage F consists of two concentric insulated aluminum cylinders with caps that carry the defining apertures. The inner cylinder is coated with colloidal graphite so as to reduce the number of electrons lost through the opening to a minimum. The outer cylinder serves as an electrostatic shield for the collecting cylinder.

C. Measuring Circuits for Secondary Electron Yields and Energy Spectra

The circuit arrangement for measuring the total backscattered fraction η and the true secondary yield Δ is shown in the upper right-hand portion of Fig. 2. It is based on the fact that the total yield of all electrons, $\delta=\eta+\Delta$ is equal to the ratio of the total emitted current I_e collected with an aiding potential to the beam current I_0 striking the target. η is given directly by the ratio of I_e to I_0 when an opposing potential $E_{C_2-T}=50$ volts is applied, except for certain corrections to be discussed below. In addition to these quantities, the ratios of I_e to I_0 as the opposing potential is varied from 0 to 50 volts give the integrated energy distribution curve for the true secondaries, subject to certain corrections to be outlined later.

Inasmuch as the ratios rather than the absolute values of the currents to the electrodes are important, it was decided to use a single galvanometer (2.5×10^{-10} amp/mm, 12 sec period) and switch it to the different positions indicated in the diagram. The precision of the measurements as obtained by repeated determinations of the yield on a given portion of a target was found to be about ±0.5 percent. The variation of the yield over the surface of a particular target did not exceed ±1 percent at primary energies above 500 volts. Below this energy, difficulties of focusing the beam increased the uncertainty in the value of the yield somewhat, so that no reliable measurements could be made at energies below 200 volts.

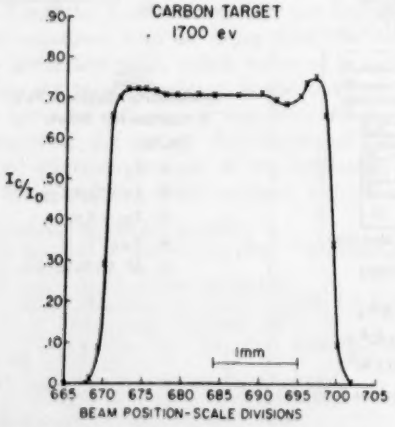

FIG. 3. Variation of collector to beam current ratio across a typical target.

The target-collector potential E_{C_2-T} was varied over a range from 0 to 60 volts. The potential was measured by means of a Simpson Multi-Range voltmeter calibrated against a Weston precision standard voltmeter to an accuracy of ±2 percent on the 50, 10, and 2.5 v scales.

Measurements of the yield with the target-heater current switched rapidly on and off showed that there was no detectable effect of any uncompensated stray magnetic field on the yield measurements. The target temperature was measured by means of a Leeds and Northrup potentiometer connected to an iron-constantan thermocouple below the target disk.

D. Measuring Circuit for Backscattered Electron Spectra

The circuit for determining the spectrum of the backscattered electrons is shown in the lower left-hand side of Fig. 2. An electrometer (Keithley Model 200) is used to measure the current collected by the Faraday cage at any given potential of the cage relative to the target. The potential is accurately selected in fixed fractions of the incident primary voltage by a cascaded divider, the high end of which is connected directly to the electron gun cathode.

In order to avoid leakage currents and prevent electrostatic disturbances on the electrometer at the high voltages used (up to 2000 volts), the whole electrometer is enclosed in a metal box (inner shield of Fig. 2) maintained at the potential of the Faraday cage and guard-ring. Relative electrometer readings could be duplicated to a precision of approximately 5 percent of full scale-value.

E. Electron Beam Control Circuits

Since the target, associated electrode structure, and measuring circuits were required to operate at ground potential, the electron gun cathode had to be held at high negative potentials.

The accelerating potentials were measured by means of a special type of high-voltage vacuum-tube voltmeter employing a circuit described by Schneeberger,[15] calibrated against the high-voltage standards of the Bureau of Standards' x-ray laboratory. Below 2000 volts, the voltages were read by a standardized Simpson voltmeter. It is estimated that the primary voltage readings could be relied upon to an accuracy of ±2 percent below 2000 v, and to ±4 percent above 2000 volts.

The deflection voltage supply is of conventional design, employing full-wave rectification and a balanced output using ganged helipots for precision positioning of the beam.

[15] R. J. Schneeberger, Rev. Sci. Instr. **19**, 40 (1948).

IV. ANALYSIS OF ELECTRODE STRUCTURE CORRECTIONS

In order to obtain meaningful values of the backscattering coefficient η and accurate energy distribution curves for the secondaries, two types of effects must be considered and corrected for if necessary. The first type is related to the emission of electrons from the collecting electrodes and influences primarily the value of η. The second type is connected with field-configuration effects due to departure from ideal spherical symmetry, space-charge, and contact potential, which influence only the form of the energy distribution of the low energy electrons emitted by the target. Since this quantity is not of primary concern in the present paper, these latter effects will not be discussed further.

The disturbing effects of electrons ejected from the collector structure by backscattered electrons from the target can be divided into those due to high-energy and low-energy electrons emitted from the spherical collector. The importance of high-energy electrons leaving the collector is determined both by the number of such electrons, i.e., the value of η for the collector material, and by the geometry of the target-collector arrangement. In the present case, η for the collector structure was made as small as possible by coating it with colloidal graphite for which $\eta=0.07$. Even at high opposing potentials, when all of the electrons arriving at the collector are high-energy electrons, the loss in the collected current cannot exceed about 7 percent. By arranging the collector to have the form of a nearly complete sphere surrounding a small target, all except the small fraction of the ejected high-energy electrons which are intercepted by the target assembly are collected by another portion of the collector, and therefore, do not subtract from the collector current. The geometry of the structure is such that only about 3 percent of the re-emitted electrons would be expected to strike the target, resulting in a net loss of only 0.2 percent.

It is important to observe in this connection that when the collector material is a metal of high η such as nickel or molybdenum, and if the geometry is of the plane-parallel form, where the target subtends nearly the whole solid angle seen by an electron emitted from the collector, the correction may be as large as 20 percent because of this factor alone.[16]

The error due to the emission of secondaries from the collector is somewhat more difficult to eliminate or correct for. Since it is desirable to have a collector surface that has a low yield at all energies, a baked-on coating of colloidal graphite was used in the present experiments. The yield of low-energy secondaries from this coating is, however, still so large that other means are required to reduce the emission. A spherical suppressor screen, analogous to the one used in a pentode, was constructed for this purpose. By applying a sufficiently large opposing potential between the outer collector sphere and the suppressor screen, it is possible to prevent nearly all secondaries formed at the outer collector from returning to the target. The small number of secondaries formed on the suppressor screen itself cannot in general be prevented from reaching the target, and it is therefore necessary to correct for this effect (see Appendix).

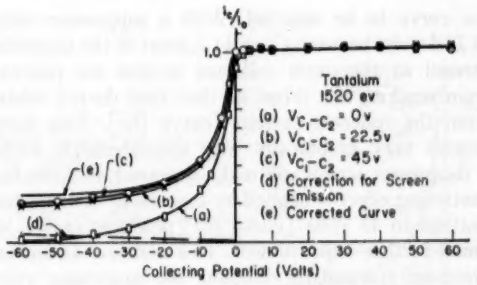

FIG. 4. Plot of measured collector current *vs* collector voltage to test performance of suppressor grid.

V. ADJUSTMENT AND TEST OF EQUIPMENT

A. Primary Beam

Beam collimation and absence of all stray current effects was tested by measuring the current to the collector structure, I_c, as a function of beam position. A typical "cross section" curve of this type is shown in Fig. 3 for the case of an amorphous carbon deposit. It is seen that the collector current cuts off sharply at the edges, indicating absence of stray currents to the collector and providing a measure of the effective beam diameter ($\sim$0.2 mm in this case). The constancy of the yield from point to point across the center of the target is noteworthy, indicating a high degree of precision in independent yield determinations.

A particular point on the target could be selected and observed without drift of the beam over a period of approximately two hours to an accuracy of $\pm$0.1 mm.

B. Spherical Collector Structure

The performance of the target-collector arrangement is most directly tested by plotting the collector current *vs* collector potential curve. By varying the suppressor voltage, the effectiveness of the suppressor screen and the penetration of the field through the suppressor can be judged, as shown in Fig. 4. Without any suppressor voltage, the emission from the collector is so strong that it masks the presence of backscattered electrons almost completely, since I_c/I_0 approaches zero for large negative voltages [curve (a)]. Even when the applied potential between target and inner collector is reduced to zero, some electrons from the collector can still reach the target, causing the knee of

[16] A situation of the type described exists in the arrangement used by Trump and Van de Graaff, J. Appl. Phys. 18, 327 (1947), so that the values of η measured cannot be considered as completely reliable.

the curve to be rounded. With a suppressor voltage of 22.5 volts between C_1 and C_2, most of the secondaries formed at the outer collector surface are prevented from reaching the target so that they do not subtract from the collector current [curve (b)]. This demonstrates very graphically why measurements without a suppressor screen will make it appear as if the backscattering effect is negligible. Increasing the suppressor voltage to 45 volts [curve (c)] produces only a very small further improvement. This additional number of electrons stopped by doubling the suppressor voltage can be entirely accounted for by the small number of secondary electrons from the collector that possess energies in excess of 22 volts. This fact, together with the observation that the additional increase in collector current is of constant value independent of target to collector potential, shows that the penetration of the suppressor field into the measuring region is negligibly small.

The sharpness of the knee of curve (c) and its location at zero collecting potential to within approximately one-half volt, confirms the expected absence of significant contact potential and space charge effects. The correction due to electrons emitted from the suppressor screen wires is indicated by curve (d), which, when added to curve (c), results in the final plot, curve (e). Inspection of curve (e) shows an almost complete leveling off of the current to the collector with increasing opposing potential. This indicates the presence of an appreciable number of high energy electrons that cannot be stopped by an opposing potential of 50 volts. It is apparent that although the correction due to emission of secondaries from the suppressor screen is of crucial importance for the absolute value of the backscattering coefficient, η, it is only a minor effect as far as the shape of the energy distribution curve for the true secondaries is concerned.

C. Target Condition

The plot of collector current against collecting potential serves as a valuable check on the condition of the target surface. Contamination by the presence of excessive amounts of adsorbed gases results in an increasing collector current with aiding collecting potential, presumably due to field effects. This lack of saturation of collector current has been repeatedly observed before outgassing of the surface in the course of the present experimental work.

In a study such as the present one, where a demountable vacuum system is employed, still another type of contamination must be guarded against. This is the formation of an amorphous carbon deposit due to the cracking of organic molecules on the surface by the incoming electron beam, as referred to above. Such deposits have been widely observed by electron microscopists and identified as composed essentially of pure carbon that shows no detectable crystal structure.[17] Early experiments carried out by the author, in which an oil diffusion pump was used in place of the mercury diffusion pump, indicated that in the course of only a few minutes of bombardment the secondary emission yield as well as the backscattered fraction from a nickel target decreased to that of pure carbon. The effect was found to be essentially proportional to the beam current and the contamination was found to be confined exactly to the position of the beam. Efforts to eliminate this effect by means of charcoal and liquid air traps succeeded only in reducing the rate of formation by a small factor, so that it was finally decided to go over to a mercury pumping system. With mercury as a pumping fluid, bombardment of the target over a period of many hours showed no noticeable change in the yield, i.e., less than $\frac{1}{2}$ percent. This would appear to indicate that certainly the major contribution to the organic deposit formation comes from the pumping oil and not from small amounts of organic contamination on the metal parts of the demountable system. For each target used in the present study, measurements of the yield of secondary and backscattered electrons were made at a series of points across the target face at the beginning and end of the run. The secondary yield values were compared with the best values given in the literature in order to insure that no carbon deposits had been formed. In addition, measurements of the backscattered fraction were made with the target maintained at 200° to 400°C so as to reduce the adsorption of organic molecules to a minimum.

VI. EXPERIMENTAL PROCEDURE

The targets of molybdenum, tantalum, and platinum studied in the present investigation were prepared from 10-mil sheet stock which was carefully cleaned in acetone after being polished with fine rouge. Another target was made out of soft steel electrolytically polished and cleaned. A coating of zinc was plated onto this target and evaporated from the surface in the vacuum system before measurement.[18] The copper target was prepared from electrolytic copper sheet stock, polished and cleaned a few minutes before insertion into the tube. The graphite target was prepared from an aqueous solution of colloidal graphite deposited on a 30-mil nickel disk baked out for 6 hours at 100°C before insertion in the vacuum system. In each case, after pumping down to approximately 10^{-6} mm pressure, the targets were heated to about 500°C for a period of one to two hours and then maintained at a temperature of approximately 400°C for a period of about 12 hours.

[17] J. Hillier, J. Appl. Phys. **19**, 226 (1948).

[18] Because of the rapid rate of evaporation relative to that of diffusion, it is believed that the amount of Zn in the Fe is sufficiently small to be negligible as far as any effects on the high-energy electron scattering is concerned, particularly since the atomic number of Zn is not very different from that of Fe.

The yield of secondary electrons and backscattered electrons for a series of points across each target was obtained after cooling to room temperature in order to check the uniformity of the surface. An energy distribution curve was then obtained for points in the center of the target, to check for the presence of adsorbed gases or of an oxide layer, as described above. If the surface was found to be in satisfactory condition according to these criteria, yield curves for both δ and η as a function of primary energy were taken simultaneously by alternatively applying 50 volts negative and positive collecting potentials at a given primary energy. At each primary energy the beam was focused and centered visually and electrically. By deflecting the beam out of the collector apertures, the residual current to collector and target, due to stray currents and leakage, was noted.

The energy distribution of the backscattered electrons was measured in the following manner. The primary beam was centered on the target until the electrometer connected to the Faraday cage indicated a maximum collected current with the potential of the Faraday cage at target potential and with 50 volts opposing potential applied between target and the spherical collector screens. The proportionality between beam current and electrometer deflection was checked so that measurements of the beam current could serve to correct for possible fluctuations in the primary current reaching the target in the course of a run. The Faraday cage potential was then adjusted in fixed steps by means of the voltage divider and the electrometer deflection observed. A final check was provided by the indication of zero current to the Faraday cage with full negative accelerating potential applied to it.

VII. TYPICAL RESULTS—PLATINUM

Figure 5 shows typical results for the total yield δ and the backscattered fraction η as functions of the primary energy in the case of a Pt target. Also shown is a curve for δ representing an average value of the two most reliable sets of data available in the literature.[19,20] It is seen that the low-temperature curve for δ agrees closely with earlier results at room temperature, so that an additional check on the condition of the target is obtained. The values of δ decrease with increasing temperature, whereas those of η are independent of target temperature. A similar behavior was found for tantalum and carbon. In each case, the total yield δ changed in a reproducible manner with temperature while the high-energy component η remained unchanged. The temperature effect on the yield will form the subject of a separate communication.[21] It will therefore be merely stated here that it is satisfactorily explained in terms of an increase in low-energy secondary absorption proportional to the absolute temperature, in accordance with the author's theory of secondary emission.[22]

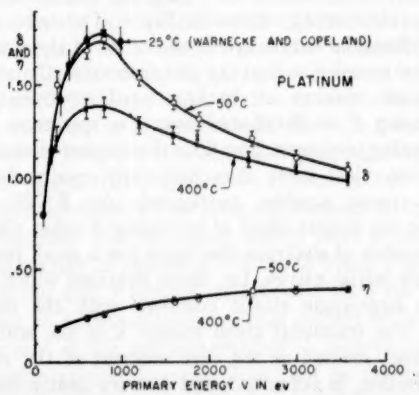

FIG. 5. Total yield δ and backscattered fraction η as function of primary energy and temperature for platinum. Present data compared with average of curves obtained by R. Warnecke, reference 20, and P. L. Copeland, reference 19.

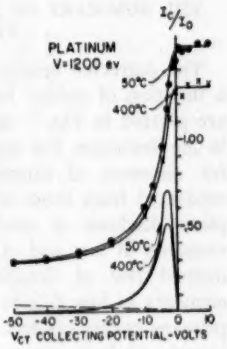

FIG. 6. Integral and differential energy distribution curves for secondary electrons from platinum as function of temperature. Integral curves corrected for emission from collector by amount indicated by dashed line.

Typical secondary electron energy distribution curves, on which the separation of the backscattered fraction is based, are shown in Fig. 6. From these curves it is apparent that the temperature influences only the low-energy secondaries to any appreciable extent. Examination of these curves brings out the importance of backscattering in the total yield. It is seen that in the case of a heavy element such as platinum, η amounts to as much as $\frac{1}{3}$ of the total yield at 3.6 kev, or an appreciable fraction of the quantity usually referred to as total secondary electron emission.

The results of the measurements on the energy distribution of the backscattered electrons for the platinum target at four different primary energies are shown in Fig. 8D and will be discussed below.

---

[19] P. L. Copeland, Phys. Rev. **40**, 122 (1932).

[20] R. Warnecke, J. phys. et radium **7**, 270 (1936).

[21] A summary of the temperature effect in metals was presented by the author at the January meeting of the American Physical Society [Phys. Rev. **90**, 380 (1953)]. Note that in the abstract the percent changes in Δ should read 0.07, 0.06 and 0.05 percent per °K, instead of 0.7, 0.6, and 0.5.

[22] E. J. Sternglass, thesis, Cornell University, February 1951 (to be published). See also the summary in the report of the 13th Annual Electronics Conference, Massachusetts Institute of Technology, 1953 (unpublished).

VIII. SUMMARY OF DATA ON BACKSCATTERED FRACTION

The corrected results of the measurements on η as a function of energy for C, Fe, Cu, Mo, Ta, and Pt are plotted in Fig. 7 together with the available data in the literature. For the sake of greater clarity, curves for elements of atomic number $Z>30$ have been separated from those of $Z<30$. Inspection of the two plots discloses a markedly different behavior for elements of low and of high Z, with a fairly sharply defined line of demarcation near $Z\simeq 30$. For the elements of low Z, η is essentially independent of the primary energy, as has been observed for all Z at high energies.[5,9] In contrast to this, for elements of $Z>30$, η decreases strongly with decreasing energy beginning at 2–3 kev, so much so in fact that η for an element of $Z=73$ (Ta) becomes less than half of the value for an element of $Z=29$ (Cu).

The present data appear to fit rather well to those of Palluel, which extend from 2–16 kev,[8] except that Palluel's values are uniformly between 5 and 10 percent higher. This disagreement is partly explained by the fact that Palluel counted all emitted electrons in excess of 40 ev as backscattered electrons. The more usual convention followed here draws the line between secondaries and scattered electrons at 50 ev, thereby including fewer high energy secondary electrons in the quantity η. The earlier results of Bruining,[4] Gimpel and Richardson,[5] and Myers,[7] at very low energies, which did not seem to follow any definite pattern, now fit in well with data at higher energies. It is noteworthy that appreciable backscattering exists down to the very lowest energies, in disagreement with the behavior expected by some authors.[23]

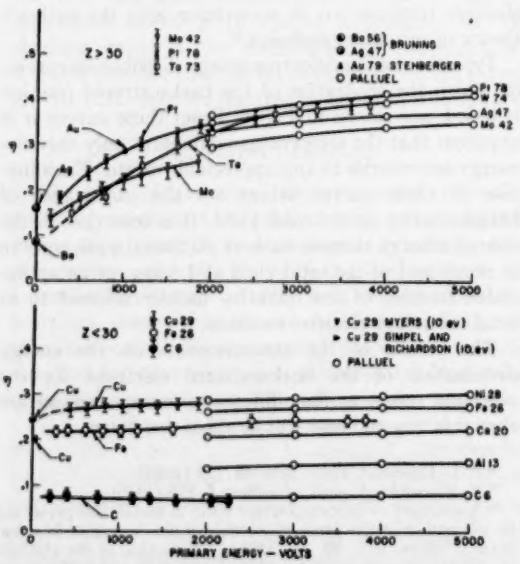

FIG. 7. Variation of backscattered fraction η with incident energy. Upper diagram—elements of $Z>30$. Lower diagram—elements of $Z<30$. Bruining, reference 4; Gimple and Richardson, reference 5; Myers, reference 7; Palluel, reference 8; Stehberger, reference 10; barred symbols, present work.

IX. SUMMARY OF DATA ON ENERGY DISTRIBUTION

The energy spectra of the backscattered electrons for carbon, iron, tantalum, and platinum targets at different incident energies are shown in Fig. 8. The experimental points have been plotted on a relative energy scale, and they have been normalized to refer to equal numbers of scattered electrons. Inspection of these plots show that there does not exist any significant dependence on primary energy. The small spread of the experimental points at different energies can be attributed to experimental errors and to the fact that the reduction to a relative scale affects the data at different primary energies to different degrees as long as these energies are not very much larger than 50 ev. The differential distribution curves were in each case derived from the data at the three highest energies, which must be considered the most reliable because of beam focusing considerations.

X. DISCUSSION OF RESULTS

The evidence obtained on the backscattering process as contained in the spectrum of the high energy electrons and their total number makes it possible to obtain greater insight into the physical process involved in this phenomenon.

As far as the energy distribution is concerned, the principal features are the relative constancy of its shape with energy between 500 and 2000 ev, the predominance of electrons that have experienced appreciable energy losses, the absence of a large group of elastically scattered electrons, and the slow increase of the mean energy with increasing atomic number.

The last three points are illustrated by the plots of the distribution curves for C, Fe, Ta, and Pt at 0.5–2 kev incident energy shown in Fig. 9. The areas under the differential curves are in the ratios of the η values at these energies, so that the plot shows directly how the increased number of backscattered electrons, with increasing Z is distributed over the spectrum. It is interesting to observe how little the number of electrons that have lost more than half their energy changes with atomic number, particularly for $Z\lesssim 26$ (Fe). By far the largest effect of increasing Z takes place in the number of electrons that have lost a small fraction of their initial energy, i.e., those electrons which have made large-angle elastic collisions with the nuclear field. The fractional mean energy $\bar{k}$ of the scattered electrons, defined as the first moment of the energy distribution, is actually found to vary nearly linearly with atomic number Z. A useful empirical relation for $\bar{k}$ based on the present data and accurate to ± 5 percent

[23] P. Palluel, Compt. rend. 224, 1551 (1947).

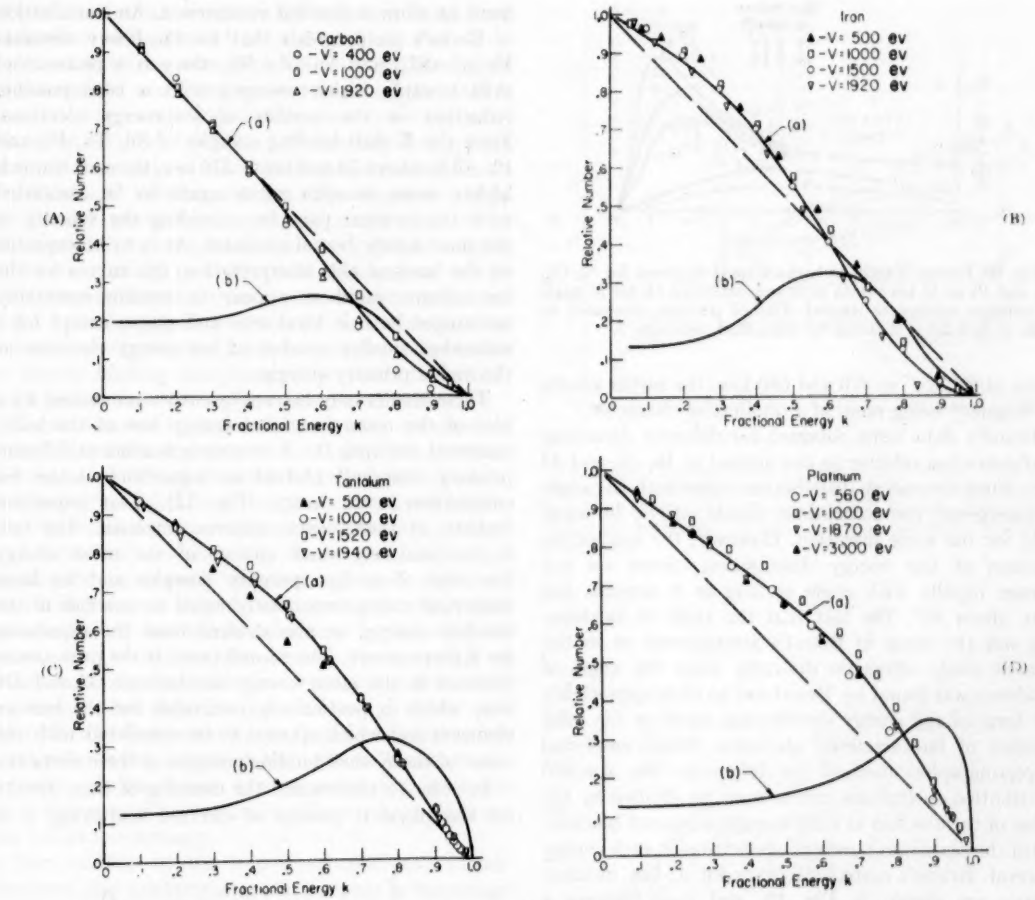

FIG. 8. Energy distribution curves for backscattered electrons from carbon (A), iron (B), tantalum (C), and platinum (D). Curves (a)—Integral curves averaged for all except lowest energies; Curves (b)—Differential curves obtained from (a).

for the primary energies V between 0.2 and 32 kev, is given by the expression $\bar{k}=0.45+2\times10^{-3}Z$.

The absence of a distinct group of perfectly elastically reflected electrons generally observed at low energies ($V\lesssim300$ ev) is at first somewhat surprising. It is, however, in agreement with Becker's results for the case of 70 to 800 ev electrons impinging upon Pt.[24] Becker found that the relative number of all backscattered electrons which have experienced no energy loss decreases with increasing energy from a value of approximately 23 percent at 70, ev, to about 8 percent at 200 ev, and 3 percent at 500 ev. Since the total number of backscattered electrons at 500 ev is only 22 percent of the incident number, it is evident that elastically reflected electrons could not be expected to show up in measurements of the present type at the high energies involved.

[24] A. Becker, Ann. Physik **78**, 253 (1925).

It is of interest to compare the energy distribution curves obtained with those measured at higher energies by other investigators. The only available data of this nature which lend themselves to direct comparison are those of Brand[14] in the 16–32 kev energy region, and

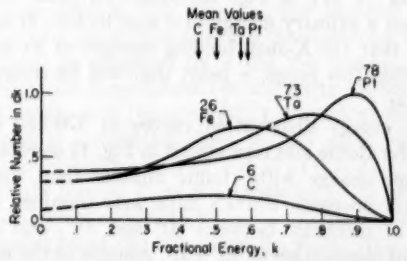

FIG. 9. Energy spectra of backscattered electrons for C, Fe, Ta, and Pt in energy range from 0.5–2 kev. Areas in ratio of total backscattered fraction η.

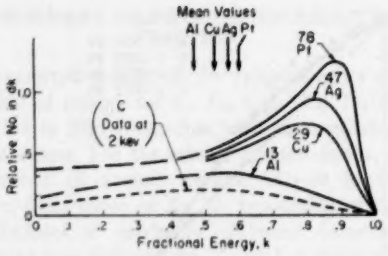

FIG. 10. Energy spectra of backscattered electrons for Al, Cu, Ag, and Pt at 32 kev. Data of Brand, reference 14, for 8° angle of emission relative to normal. Dashed portions estimated on basis of data for η obtained by Schonland, reference 9.

those of Bothe,[13] at 370 and 680 kev, the earlier results of Wagner[25] being more of a qualitative character.

Brand's data were obtained for different directions of observation relative to the normal at 16, 24, and 32 kev. Since the energy distribution varies with the angle of emergence, the comparison should strictly be made only for the same direction. However, the qualitative features of the energy distribution curves do not change rapidly with angle as long as it remains less than about 45°. The fact that the angle of incidence was not the same in Brand's arrangement as in the present study offers no difficulty since the angle of incidence was found by Brand not to alter appreciably the form of the energy distribution curve or the total number of backscattered electrons. Brand employed a photographic method to determine the spectral distribution so that his curves must be divided by the value of the abscissa at each energy to convert blackening of the plate into numbers of electrons in each energy interval. Brand's corrected curves for 32-kev incident energy are shown in Fig. 10, and they indicate a surprising similarity to the present data taken at much lower energies plotted in Fig. 9. The change in shape with increasing atomic number is of the same character and the areas under the curves of elements of the same or similar Z are approximately equal. The greatest difference in shape between Brand's and the present data is found for the elements of $Z \sim 30$ (Fe and Cu). A distinct shift of the most probable energy towards higher values, which can be seen in the plot for 32 kev of Fig. 10, occurs for these elements between a primary energy of 2 and 16 kev. It is to be noted that the K-shell binding energies of Fe and Cu lie within this range, a point that will be returned to later on.

The energy distribution curves at 370-kev energy given by Bothe and reproduced in Fig. 11 show a much stronger change with atomic number than the data at lower energies. Bothe's data were obtained for an angle of incidence between 20° and 35°, and for an angle of observation of 50°±15° relative to the normal, sufficiently close to the present experimental arrangement to allow a detailed comparison. An examination of Bothe's plots reveals that for the heavy elements Pb ($Z=82$), and Sn ($Z=50$), there is a pronounced shift towards higher energies with a corresponding reduction in the number of low-energy electrons. Since the K-shell binding energies of Sn, Ta, Pt, and Pb, all lie above 29 and below 370 kev, the shift towards higher mean energies seems again to be associated with the incident particles exceeding the velocity of the most firmly bound electrons. As is to be expected on the basis of this interpretation, the curves for the low atomic numbers appear to remain essentially unchanged both in total area and shape, except for a somewhat smaller number of low-energy electrons at the higher primary energies.

These results may be conveniently summarized by a plot of the mean fractional energy loss of the backscattered electrons $(1-\bar{k})$ *vs* atomic number at different primary energies[26] plotted on logarithmic scales for comparison with theory (Fig. 12). Two important features of these curves deserve emphasis. The first is the relatively small change of the mean energy loss with Z at low primary energies and its large numerical value, very nearly equal to one-half of the incident energy, as also evident from the expression for $\bar{k}$ given above. The second point is the pronounced decrease in the mean energy loss between 32 and 370 kev, which is particularly noticeable for the heavier elements and which appears to be correlated with the value of the K-shell binding energies of these elements.

In order to understand the meaning of these results for the physical process of electron scattering, it is

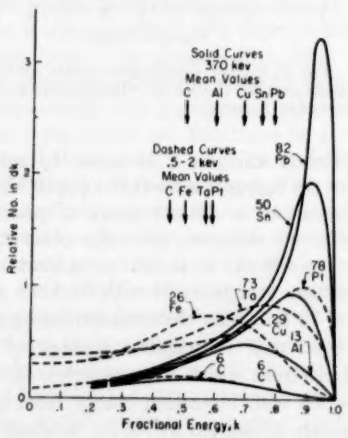

FIG. 11. Energy spectra of backscattered electrons for C, Al, Cu, Sn, and Pt at 370 kev. After Bothe, reference 13, parallel-beam incidence at 20–35°, angle of observation 50°. Present data at 0.5–2 kev shown dashed for comparison.

[25] P. B. Wagner, Phys. Rev. **35**, 98 (1930).

[26] Mean energies at 32 kv were estimated from Brand's data on the basis of his curves as completed from a knowledge of the total backscattered fraction measured by Schonland (see reference 9). The mean value plotted in each case is the center of gravity of the distribution function determined graphically.

helpful to refer to the data on the variation of the total backscattered fraction η with V, Fig. 7.

If backscattering were predominantly due to nuclear Coulomb field scattering even at low energies, then η should in every case be greater for elements of higher Z. However, as Fig. 7 shows, for elements of $Z \gtrsim 30$, η may drop to values less than those for elements of $Z \lesssim 30$ at low incident energies. The simplest way in which such an apparent anomaly would seem to be explainable is to consider the scattering at low energies to be due mainly to the atomic electrons, or to the scattering accompanying energetic inelastic collisions. This is to be expected since the cross sections for inelastic scattering at incident energies comparable to atomic binding energies greatly exceed the elastic cross section for a strongly screened nuclear field.

If one assumes that the electrons play a dominant role in the scattering process at least at low energies, the fact that heavy elements scatter relatively little in this energy region becomes at once understandable. The theory of inelastic collisions worked out by Bohr[27] and Bethe[28] shows that only those atomic electrons participate significantly in inelastic processes that have velocities less than that of the incoming particle. More specifically, in the case of electrons incident on the atom, the maximum effectiveness in scattering is reached only for those atomic electrons that have binding energies less than $1/e$ times the energy of the incident particle. As a result, it is to be expected that at low incident energies, atoms of high atomic number may actually contain fewer *effective* scattering electrons than elements of low atomic numbers whose electrons are bound less strongly.

The validity of the hypothesis that the atomic electrons play a determining role not only in the energy loss but also in the scattering process of an incident electron beam may be tested in a number of different ways. According to this view, at low energies there should exist a correlation between the scattering power of an atom as measured by η and the number Z_0 of electrons in the atom whose binding energy is less than approximately $\frac{1}{3}$ of the energy of the incident particle. That such a correlation does in fact exist may be seen by comparing a plot of η *vs* Z at 0.3, 1, 2, and 5 kev, with a plot of Z_0 *vs* Z at energies 1/2.7 of these values as shown in Fig. 13.[29]

Examination of the two diagrams shows that below a value of $Z \simeq 25$ the number of effective electrons

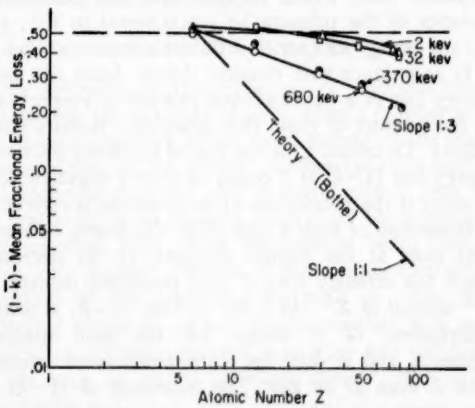

FIG. 12. Dependence of the mean energy loss of electrons backscattered from solids on the atomic number. Points at 32 kev estimated from measurements by Brand, reference 14. Values for 370 and 680 kev determined from measurements by Bothe, reference 13.

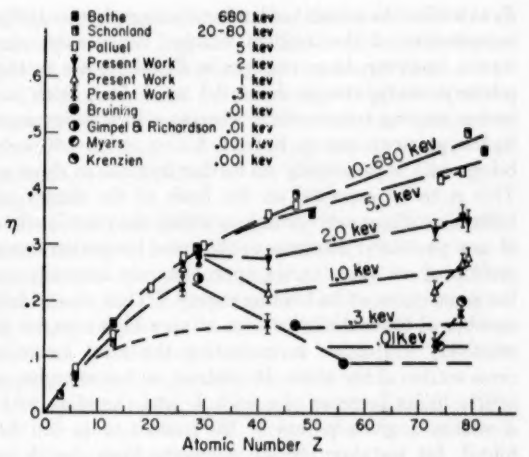

FIG. 13(a). Backscattered fraction η as function of atomic number Z at different primary energies. Bothe, reference 13; Schonland, reference 9; Palluel, reference 8; Bruining, reference 4; Gimpel and Richardson, reference 5; Myers, reference 7; Krenzien, reference 6.

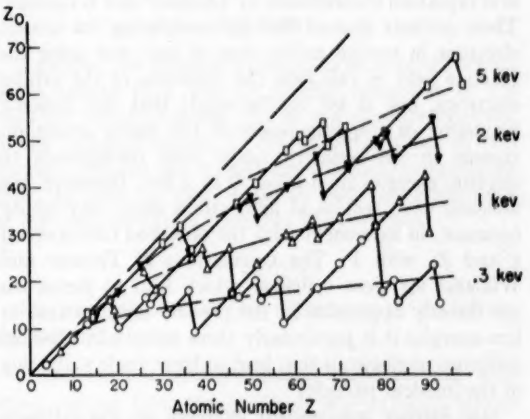

FIG. 13(b). Number of outer shell electrons Z_0 of binding energy less than a given value as function of atomic number Z. Limiting binding energies for each curve taken as 1/2.7 of indicated incident electron energy.

[27] N. Bohr, Phil. Mag. **25**, 10 (1913); Kgl. Danske Videnskab. Selskab, Mat.-fys. Medd. **18**, No. 8 (1948).
[28] H. A. Bethe, Ann. Physik **5**, 325 (1930).

[29] Data on the binding energies were taken from the tables of Hill, Church, and Mihelich, Rev. Sci. Instr. **23**, 523 (1952).

Z_0 as well as the amount of backscattering η is essentially independent of the incident energy. For heavier elements, however, large changes in Z_0 take place in the primary energy range from 0.3 to 2 kev, with an accompanying increase in η, whereas a further increase in the primary energy beyond 5 kev up to 680 kev brings with it practically no further increase in Z_0 or η. This is to be expected on the basis of the theory of inelastic collisions, according to which the contribution of any particular electron to the total ionization cross section of an atom varies approximately inversely as the square-root of its binding energy.[27] Thus, the added number of inner shell electrons at very high energies is relatively ineffective in increasing the total inelastic cross section of the atom. In contrast, at low energies, a nearly linear increase of η with Z_0 and therefore with Z within a given period of the atomic table can be found, for instance for the elements from $Z=73$ to $Z=79$, so that the important role of the atomic shell electrons is clearly brought out.

The increase of the inelastic cross section of heavy atoms with increasing primary particle velocity was first explained theoretically by Thomas[30] and Williams.[31] These authors showed that by considering the atomic electrons in motion rather than at rest, and using the Hartree field to calculate the velocities of the orbital electrons, one is led to the result that the inelastic scattering or stopping power of the heavy atoms increases in the velocity range that corresponds to electron energies from about 0 to 2 kev. However, the inelastic cross section of light atoms stays very nearly constant, in agreement with the observed constancy of η and Z_0 with V. The calculations of Thomas and Williams for close collisions which lead to ionization are directly applicable in the present case, because at low energies it is particularly these essentially classical collisions of electrons that lead to large angle scattering of the incident particle.[32]

Still further independent evidence on the intimate connection between inelastic scattering and back-diffusion comes from data on the variation of the stopping power of atoms for α particles with increasing particle velocity, since stopping of α particles is almost entirely due to inelastic collisions. Experimental values of the stopping power of particles obtained by Gurney[33] show that for heavy elements (Au and Ag) the stopping power increases up to an equivalent electron energy of about 1200 volts. In contrast, the stopping power is constant or even decreases slightly with increasing velocity for elements of low Z, again in agreement with the observed variation of η with V.

The dominant role of inelastic atomic collisions also explains the experimental evidence on the shape of the energy distribution curves and its dependence on atomic number discussed above. In the case of those "inelastic" collisions that make the greatest contribution to the total value of η, the mean fractional energy loss of the electrons emerging from the entrance surface will be close to one-half. The qualitative reason for this is that for every primary that loses more than one-half of its energy in a single collision there will be a fast secondary of more than one-half the initial energy, which is counted as a backscattered primary particle. Since for an energy loss of one-half in a collision with an essentially free atomic electron both particles make an angle of 45° to the direction of incidence and both are counted as backscattered electrons, the energy distribution curve will tend to show a maximum near its center.

In contrast to this, a purely elastic collision with the nuclear field leads to backscattered electrons of energy equal to that of the incident particle and produces no energetic "knocked-on" electrons. Therefore, the actual shape of the spectrum and its mean energy are a measure of the relative importance of inelastic and elastic scattering processes, and of the total number of "knocked-on" atomic electrons emerging with large kinetic energies. An examination of the energy spectra reveals that inelastic scattering processes must outweigh the elastic processes by a large factor, since even at the highest energies used in the present experiments the mean fractional energy loss is much larger than required by Bothe's theory based on elastic scattering alone, even for the heaviest elements. This can be seen as follows. Bothe has shown[13] that the mean fractional energy loss of the backscattered electrons should depend approximately inversely upon Z on the basis of the following two assumptions: (1) The deviations are due only to elastic scattering by an unscreened nuclear Coulomb field, which requires that the penetration distance of the primary be proportional to Z^{-2}; and (2) the energy loss per unit distance is proportional to Z in accordance with classical theory. Since the mean energy loss of a backscattered primary is proportional to the product of these two quantities, Bothe's result follows. Therefore, a log-log plot of the mean fractional energy loss $(1-\bar{k})$ *vs* Z ought to show a negative slope of unity if the assumption of no screening is correct.

Inspection of such a plot (Fig. 12) shows, however, that even at the highest energies, $(1-\bar{k})$ decreases much less strongly with Z than predicted, namely, as $Z^{-\frac{1}{4}}$ instead of Z^{-1}. At 2 kev or less, $(1-\bar{k})$ is nearly independent of Z except for the very heaviest elements, and it does not vary much more strongly with Z even at 32 kev. The constancy of $(1-\bar{k})$ at low energies is, however, to be expected if inelastic collisions dominate. For these collisions, the penetration distance of the primary electron is proportional to $1/Z_0$ and the mean energy loss in this distance is proportional to Z_0, so that the product is independent of Z_0 and Z.

The fact that $(1-\bar{k})$ varies only slowly with Z even

[30] L. H. Thomas, Proc. Cambridge Phil. Soc. **23**, 713 (1926).
[31] E. J. Williams, Nature **119**, 489 (1927).
[32] C. B. O. Mohr and F. H. Nicol, Proc. Roy. Soc. (London) **A142**, 320 (1933).
[33] R. W. Gurney, Proc. Roy. Soc. (London) **A107**, 340 (1925).

at energies as high as 680 kev means that screening is strong and cannot be neglected. If one uses the expression for elastic scattering by a screened Coulomb field according to the Thomas-Fermi model in the limit of high energies,[34] one finds that the scattering mean free path varies only as $Z^{-\frac{1}{3}}$, thereby bringing the theory into agreement with experiment. Noteworthy is the fact that at energies below those of the K-shell electrons, the actual screening of the nuclear field appears to be stronger than predicted by the Thomas-Fermi model. This is indicated by the fact that the mean energy of the backscattered electrons obeys the $Z^{-\frac{1}{3}}$ dependence required by the Thomas-Fermi model only *after* the K-shell energy is exceeded.

These considerations point towards a theory of backscattering at energies comparable to those encountered in atomic binding, where the scattering and slowing down of a particle beam is calculated primarily in terms of inelastic collisions. Elastic collisions by the screened nuclear field result in a correction significant only for the heavier elements.

The importance of inelastic collisions brought out above would also appear to indicate why the existing descriptions of backscattering of electrons from metal surfaces at very low energies[35] have failed to describe the observed effects correctly. The theory of MacColl is based on a highly idealized model of a metal surface in which there is no provision for interaction with atomic electrons. Only coherent or elastic scattering at a uniform potential step, determined by the work-function plus Fermi energy, is considered. This model leads to very small percentages of backscattering (<2 percent at 10 ev), to a rapid drop of η with increasing energy, and to a dependence upon work function and Fermi energy, none of which are in agreement with the data summarized in Fig. 7.

CONCLUDING REMARKS

The evidence on the variation of backscattering with energy for elements of large atomic number and the small dependence of the mean energy of the scattered electrons on the atomic number indicate clearly that inelastic processes play a much greater part in the scattering of an electron beam than has generally been assumed. Thus, when the incident beam energy is not very greatly in excess of the K-shell excitation potentials of the scattering material, or when the scattering atoms are of low atomic number, it is not possible to calculate electron scattering and diffusion on the basis of elastic collisions alone.[36] This is in sharp contrast to the situation that exists for heavy particles, where inelastic collisions can safely be regarded as contributing only to the energy loss.

The data obtained on the energy distribution of the backscattered electrons further indicate that when elastic scattering does become important at high energies, the screening of the nuclear field cannot be neglected.

From a practical standpoint, the present results demonstrate that the backscattering phenomenon is appreciable not only at high primary energies but also down to the very lowest bombarding energies. It must, therefore, be taken into account whenever accurate calculations of electron beam penetration or energy dissipation in solids are to be made.

The author wishes to express his appreciation to Mr. S. C. Frey and Mr. F. H. Grannis for their assistance in the preliminary experimental work, to Dr. L. R. Maxwell, Dr. D. Bleil, and Dr. R. L. Longini for helpful advice and encouragement, and to Dr. L. P. Smith for guidance and support throughout the course of the present work.

APPENDIX

Basically, the emission of secondaries from the screen wires results in a loss of current measured in the collector circuit. Letting I_{CM} be the measured current in the collector circuit, I_C the corrected value of this current, and I_{CS} the current due to emitted secondaries from the collector mesh wires, all these being functions of the collector-target potential V_{CT}, one has

$$I_C = I_{CM} + I_{CS}. \tag{1}$$

The value of I_{CS} is in turn determined by the following factors:

1. the current of high-energy backscattered electrons coming from the target at any primary energy V, $I_0 \cdot \eta(V)$, where I_0 is the primary current;
2. the fraction of all these electrons which strike the screen wires. This is equal to the fraction of the area covered, p_C;
3. the true secondary emission coefficient of the screen material, Δ_{CS}, measured at the mean energy of the backscattered electrons, $V\bar{k}$, where $\bar{k}$ is the mean fractional energy of the backscattered electrons leaving the target;
4. the fraction of the emitted secondaries from the collector wires that actually get to the target at a given value of V_{CT}, $K(V_{CT})$.

Thus, I_{CS} is given by the expression

$$I_{CS} = I_0 \cdot \eta(V) \cdot p_C \cdot \Delta_{CS}(V\bar{k}) \cdot K(V_{CT}). \tag{2}$$

Because of the fact that there are essentially no secondaries of energy $\gtrsim 50$ ev, η is given by the expression

$$\eta = I_C(-50 \text{ ev})/I_0, \tag{3}$$

[34] L. I. Schiff, *Quantum Mechanics* (McGraw-Hill Book Company, Inc., New York, 1949), p. 169.

[35] L. A. MacColl, Bell System Tech. J. **30**, 888 (1951).

[36] Because neither screening nor inelastic scattering is taken account of in present theories of backscattering, it is, for instance, impossible to draw definite conclusions on the interaction of positrons with matter from measurements on the total backscattering relative to that for electrons [See H. H. Seliger, Phys. Rev. **78**, 491 (1950) and W. Miller, Phys. Rev. **82**, 452 (1951)].

which, by virtue of Eqs. (1) and (2), becomes

$$\eta=\frac{I_{CM}(-50\text{ ev})}{I_0}\frac{1}{1-p_C\cdot\Delta_{CS}\cdot(V\dot{k})\cdot K(-50\text{ ev})}. \quad (4)$$

In this expression, Δ_{CS} may be found by a measurement of the yield from a target of colloidal graphite prepared in the same manner as the material covering the screen wires. Only the determination of the quantity $K(V_{CT})$ offers any problem; all the other quantities are known directly.

Fortunately, because p_C and Δ_{CS} are generally small quantities, a small error in the calculated value of K will enter only as a second-order correction to the magnitude of η. This allows certain simplifying approximations to be made that permit an analytic treatment of this correction.

Briefly, the fraction of the electrons from the collector screen that reach the target is not unity, because, although there exists an attractive field directed toward the target for such electrons when η is being measured, some of the secondaries miss the target and return to the collector. The reason many of these electrons miss the target is that they possess appreciable initial velocities, the directions of which do not in general lie within the solid angle subtended by the target at the collector surface. Since the force-field between target and collector is, to a first approximation, of the inverse square law type, one is dealing essentially with the familiar problem of planetary orbits in a gravitational field, and one may use simple considerations of conservation of angular momentum and energy to arrive at an estimate of K, as shown below. Letting r_T be the radius of the target, assumed to be of spherical form, r_C the radius of the inner collector C_2, V_0 the initial energy with which the secondary leaves C_2, and φ the angle of emergence of the secondary electrons relative to the normal, there will evidently be a minimum angle $\varphi_{\min}$ at which the orbit will just touch the target. All electrons emitted into a cone with half-angle $\varphi_{\min}$ will therefore be captured, so that the fraction of all electrons with $\varphi<\varphi_m$ is just equal to $K(V_{CT})$. Using conservation of angular momentum and energy for the condition of grazing incidence leads to the relation

$$\sin\varphi_m=\frac{r_T}{r_C}\left[\frac{V_0+V_{CT}}{V_0}\right]^{\frac{1}{2}}. \quad (5)$$

In the present case the secondaries are emitted from circular wires so that the emission is isotropic. This means that the fraction of electrons emitted into a cone of half-angle $\varphi_{\min}$, K, is equal to $(1-\cos\varphi_m)$, by simple geometrical considerations. Combining this with Eq. (5), one arrives at a simple expression for the fraction reaching the target, K, in terms of V_0, V_{CT}, and the radii of target and collector:

$$K=1-\left[1-\left(\frac{r_T}{r_C}\right)^2\frac{V_{CT}+V_0}{V_0}\right]^{\frac{1}{2}}. \quad (6)$$

Since the average energy of secondary electrons from metals is known to be approximately 4–5 volts, whereas $(r_T/r_C)^2=\frac{1}{16}$, this expression may be simplified for small V_{CT} to

$$K=\tfrac{1}{2}\left(\frac{r_T}{r_C}\right)^2\left(1+\frac{V_{CT}}{V_0}\right). \quad (7)$$

This shows that the correction I_{CS} which must be added to the measured collector current I_{CM} increases approximately linearly with V_{CT}. The complete expression for I_C/I_0 at any voltage V_{CT} is

$$\frac{I_C}{I_0}=\frac{I_{CM}}{I_0}+\eta(V)\cdot p_C\cdot\Delta_{CS}(V\dot{k})\cdot\tfrac{1}{2}\left(\frac{r_T}{r_C}\right)^2\left(1+\frac{V_{CT}}{V_0}\right). \quad (8)$$

For $V_0=4.5$ ev, roughly equal to the average energy of secondaries from carbon, the present arrangement leads to a value $K=0.5\pm10$ percent at $V_{CT}=-50$ ev. A simple calculation shows that an error of as much as 20 percent in K results in an error of only 1–2 percent in the value of η for typical values of Δ_{CS}, thereby justifying the approximations made in the above calculation.

Surface Studies of Solids by Total Reflection of X-Rays*

L. G. PARRATT
Cornell University, Ithaca, New York
(Received March 22, 1954)

Analysis of the shape of the curve of reflected x-ray intensity *vs* glancing angle in the region of total reflection provides a new method of studying certain structural properties of the mirror surface about 10 to several hundred angstroms deep. Dispersion theory, extended to treat any (small) number of stratified homogeneous media, is used as a basis of interpretation.

Curves for evaporated copper on glass at room temperature are studied as an example. These curves may be explained by assuming that the copper (exposed to atmospheric air at room temperature) has completely oxidized about 150A deep. If oxidation is less deep, there probably exists some general reduction of density (e.g., porosity) and an electron density minimum just below an internal oxide seal. This seal, about 25A below the nominal surface plane, arrests further oxidation of more deeply-lying loose-packed copper crystallites.

All measurements to date have been carried out under laboratory atmospheric conditions which do not allow satisfactory separation or control of the physical and chemical variables involved in the surface peculiarities. The method, under more controlled conditions of preparation and treatment of the surface, promises to be useful.

I. INTRODUCTION

SINCE x-rays in total reflection from a mirror surface penetrate very little into the mirror medium, peculiarities in the reflected intensity reveal structural peculiarities of the surface itself. Analysis of the reflected intensity may provide a new and fruitful method for studying surface properties that involve variations of electron density with depth, e.g., corrosion, porosity, aging, or annealing, and perhaps for studying smoothness on a scale between that of the optical microscope and the electron microscope.

A typical experimental arrangement for this method is sketched in Fig. 1. The intensity reflected from a smooth surface of a thick mirror of glass, for example, varies with the incident glancing angle ϕ as shown in Fig. 2 for an x-ray wavelength 1.39A (the Cu $K\beta_1$ line). For this curve, the observed cut-off or critical angle ϕ_c is 12.3 minutes of arc or 3.58×10^{-3} radian.

The critical angle and the shape of the observed curve are determined essentially by the electron density and are otherwise independent of the amorphous or crystalline structure, or of the orientation of crystallites on (or in) the surface. If the mirror interface is a sharply defined boundary between two uniform homogeneous media, the dispersion theory predicts the reflection curve. The predicted curve for air and glass is shown in Fig. 2. In general, the experimental and theoretical curves are in qualitative but not detailed agreement.

The proposed method consists of (1) a comparison of an observed curve with a theoretical curve, and/or (2) a comparison of the observed curves for differently produced surfaces, or for a given surface before and after some specific treatment. The shape of the theoretical curve depends sensitively upon the particular model one chooses for the surface; by adjusting the model to give a theoretical curve in closer agreement with experiment, one learns which properties of the surface are responsible for the various peculiarities of the observed curve.

In the present paper, the theory is outlined and a few exemplary experimental curves are discussed, in particular a curve for evaporated copper on a glass substrate. Some quantitative results and conclusions are possible but satisfactory utilization of this method must await (as must most other methods for the study of surfaces) improved experimental techniques in the production and control of the surfaces.

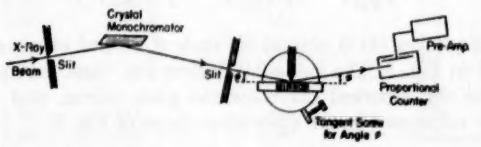

FIG. 1. Experimental arrangement for the x-ray total reflection method of studying smooth solid surfaces.

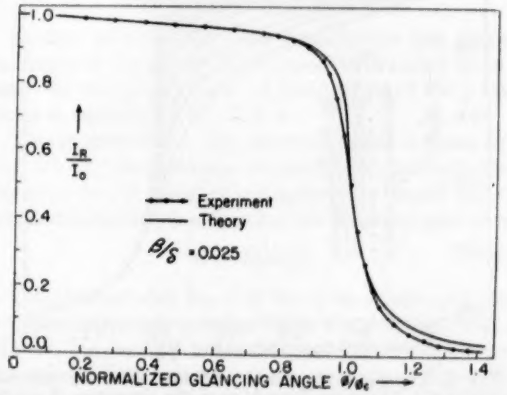

FIG. 2. Intensity reflected from polished glass at small angles of incidence. The angle ϕ_c is the critical angle for total reflection.

* This research was supported by the United States Air Force through the Office of Scientific Research of the Air Research and Development Command.

II. DISPERSION THEORY

Two Homogeneous Media

For any glancing angle, the expressions for the electric vector of the incident beam $E_1(z_1)$, of the reflected beam $E_1^R(z_1)$, and of the refracted beam $E_2(z_2)$ at a perpendicular distance z from the surface, are

$$\left.\begin{aligned} E_1(z_1)&=E_1(0)\exp\{i[\omega t-(k_{1,x}x_1+k_{1,z}z_1)]\}\\ E_1^R(z_1)&=E_1^R(0)\exp\{i[\omega t-(k_{1,x}x_1-k_{1,z}z_1)]\}\\ E_2(z_2)&=E_2(0)\exp\{i[\omega t-(k_{2,x}x_2+k_{2,z}z_2)]\}\end{aligned}\right\}, \quad (1)$$

where k_1 and k_2 are the propagation vectors (of magnitudes $2\pi/\lambda_1$ and $2\pi/\lambda_2$) outside and inside the mirror, respectively, z is taken as positive into the mirror, x, z is the plane of incidence, refraction, and reflection of the beam, and the athwart direction y is parallel to the mirror surface. For x-rays, the glancing angle ϕ_1 (written hereafter without the subscript) is always very small, and we write

$$k_{2,x}^2+k_{2,z}^2=k_2^2=r_2^2k_1^2=r_2^2(k_{1,x}^2/\cos^2\phi)\doteq k_{1,x}^2(1-2\delta_2-2i\beta_2+\phi^2),$$

where $r_2=1-\delta_2-i\beta_2$ is the refractive index of the mirror, $r_1=1$ for air or vacuum, and where we neglect second and higher powers of δ_2 and β_2 since they are each of the order of 10^{-5} or less. $\beta_2=\lambda\mu_2/4\pi$ where μ_2 is the linear (incoherent) absorption coefficient of the mirror.

From the boundary condition for the tangential components of the electric vectors, $k_{2,x}=k_1$, and with the approximation $k_{1,x}\doteq k_1$ for small ϕ, it follows that

$$k_{2,z}\doteq k_1(\phi^2-2\delta_2-2i\beta_2)^{\frac{1}{2}}.$$

For convenience, we write

$$f_2=(\phi^2-2\delta_2-2i\beta_2)^{\frac{1}{2}}.$$

The expression for the refracted beam becomes

$$E_2(z_2)=E_2(0)\exp[i(\omega t-k_{2,x}x_2)]\exp[-ik_1f_2z_2]. \quad (2)$$

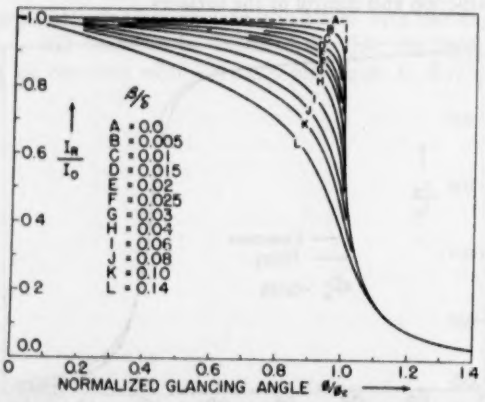

FIG. 3. Two-media theoretical reflection curves for selected values of β/δ. The shape depends upon the absorption of x-rays in the mirror. For no absorption, the reflection coefficient is unity for $0<\phi/\phi_c<1$, then drops abruptly.

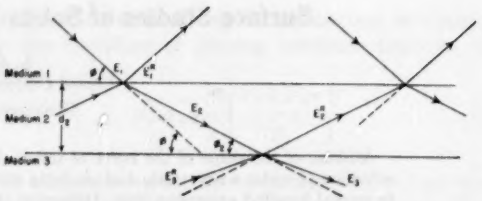

FIG. 4. Sketch of reflection and refraction for stratified homogeneous media.

Shape of the Reflection Curve: Two Media

The Fresnel[1] coefficient for reflection, $F_{1,2}$, can be written

$$F_{1,2}=\frac{E_1^R}{E_1}=\frac{\sin\phi-r_2\sin\phi_2}{\sin\phi+r_2\sin\phi_2}\doteq\frac{\phi-f_2}{\phi+f_2}=\frac{f_1-f_2}{f_1+f_2}, \quad (3)$$

where

$$f_1=(\phi^2-2\delta_1-2i\beta_1)^{\frac{1}{2}}=\phi.$$

The first part of Eq. (3) is written for the σ component of polarization, but, within the approximations made in the second part, no distinction need be made between the σ and π components.

To obtain the expression for the intensity ratio, we write

$$f_2=A-iB,$$

where

$$A=\frac{1}{\sqrt{2}}\{[(\phi^2-\phi_{c2}^2)^2+4\beta_2^2]^{\frac{1}{2}}+(\phi^2-\phi_{c2}^2)]^{\frac{1}{2}}\},$$

$$B=\frac{1}{\sqrt{2}}\{[(\phi^2-\phi_{c2}^2)^2+4\beta_2^2]^{\frac{1}{2}}-(\phi^2-\phi_{c2}^2)]^{\frac{1}{2}}\},$$

and from Snell's law, *viz.*, $r_2=\cos\phi/\cos\phi_2$, we write $\delta_2=\frac{1}{2}\phi_{c2}^2$ where ϕ_{c2} is the critical angle of incidence for which the angle inside the mirror is just zero. Inserting these relations in Eq. (3) and multiplying the numerator and denominator by the complex conjugate, we get the ratio of reflected to incident intensity,

$$\frac{I_R}{I_0}=\left|\frac{E_1^R}{E_1}\right|^2=\frac{(\phi-A)^2+B^2}{(\phi+A)^2+B^2}=\frac{h-(\phi/\phi_{c2})\sqrt{2}(h-1)^{\frac{1}{2}}}{h+(\phi/\phi_{c2})\sqrt{2}(h-1)^{\frac{1}{2}}}, \quad (4)$$

where

$$h=\left(\frac{\phi}{\phi_{c2}}\right)^2+\left\{\left[\left(\frac{\phi}{\phi_{c2}}\right)^2-1\right]^2+\left(\frac{\beta}{\delta}\right)^2\right\}^{\frac{1}{2}}.$$

Equation (4) is plotted for each of several values of β/δ in Fig. 3. The value 0.025 gives the "best match" with the observed curve for the glass mirror, and is the value used in the theoretical curve of Fig. 2.

[1] E.g., A. H. Compton and S. K. Allison, *X-Rays in Theory and Experiment* (D. Van Nostrand Company, Inc., New York, 1935), p. 307. Fresnel theory for homogeneous media is presumed to hold for "granular" matter even though the x-ray wavelengths are of the order of magnitude of the atomic "grain" size: The penetration of the x-rays (discussed later) is large compared with this "grain" size.

N Stratified Homogeneous Media

One conjecture as to the difference between the experimental and the two-media theoretical curves for a metal surface involves the role of a possible oxide surface layer. Another conjecture, in case the surface material is deposited as a thin film on a substrate of different material, involves the effect of the substrate. Other conjectures may involve a complicated model of the surface structure that requires more than two laminal media for representation. So, we next derive the theoretical expression for the shape of the reflection curve for N ($N \geqslant 2$) stratified homogeneous media having smooth boundary interfaces.

We denote the thickness of each lamina n ($n \leqslant N$) by d_n. The thickness of medium 1 (air or vacuum) is of no concern.

The continuity of the tangential components of the electric vectors (see Fig. 4) for the $n-1$, n boundary may be expressed as

$$a_{n-1}E_{n-1}+a_{n-1}^{-1}E_{n-1}{}^{R}=a_n^{-1}E_n+a_nE_n{}^{R}, \quad (5)$$

$$(a_{n-1}E_{n-1}-a_{n-1}^{-1}E_{n-1}{}^{R})f_{n-1}k_1 = (a_n^{-1}E_n-a_nE_n{}^{R})f_nk_1, \quad (6)$$

where the amplitude factor a_n for *half* the perpendicular depth d_n is, from Eq. (2),

$$a_n=\exp\left(-ik_1f_n\frac{d_n}{2}\right)=\exp\left(-\frac{\pi}{\lambda}f_nd_n\right). \quad (7)$$

In Eqs. (5) and (6), the vector amplitudes E_{n-1}, $E_{n-1}{}^{R}$ and E_n, $E_n{}^{R}$ refer to the values midway through medium $n-1$ and n, respectively.

The solution of the simultaneous Eqs. (5) and (6) is obtained by dividing their difference by their sum and writing the result as a recursion formula

$$R_{n-1,\,n}=a_{n-1}{}^{4}\left[\frac{R_{n,\,n+1}+F_{n-1,\,n}}{R_{n,\,n+1}F_{n-1,\,n}+1}\right], \quad (8)$$

where

$$R_{n,\,n+1}=a_n{}^{2}(E_n{}^{R}/E_n)$$

and

$$F_{n-1,\,n}=\frac{f_{n-1}-f_n}{f_{n-1}+f_n}.$$

One solves Eq. (8) for $E_1{}^{R}/E_1$ by starting at the bottom medium, medium N, and noting that $R_{n,\,n+1}=0$ since the thickness of this medium is infinite. One also notes that a_1 is unity, and therefore $R_{1,2}=E_1{}^{R}/E_1$.

The ratio of reflected to incident intensity, I_R/I_0, is obtained by separating Eq. (8) for $R_{1,2}$ into its real and imaginary terms and multiplying by the complex conjugate. This step is symbolized by

$$I_R/I_0=|E_1{}^{R}/E_1|^{2}. \quad (9)$$

The algebra is straightforward but very tedious for $N>3$. Evaluations of Eq. (9) for N up to 6 have been carried out and are discussed later.

TABLE I. Penetration $z_{1/e}$ in copper, in A. $[I_z(z_{1/e})/I_z(0)=1/e]$

ϕ/ϕ_c	1.281A	1.392A	1.540A
0.10	17.7	18.6	17.8
0.25	18.2	19.1	18.3
0.50	20.3	21.4	20.4
0.75	26.3	28.0	26.7
0.90	38.2	42.4	40.5
0.95	48.1	59.0	56.2
0.99	62.0	118	111
1.00	66.5	181	164
1.01	71.4	276	243
1.05	93.3	567	490
1.10	121	808	699
1.20	168	1170	1008
1.30	209	1464	1263
1.40	246	1724	1489
$\delta=$	16.72×10^{-6}	17.85×10^{-6}	24.05×10^{-6}
$\beta=$	23.5×10^{-7}	3.76×10^{-7}	5.58×10^{-7}

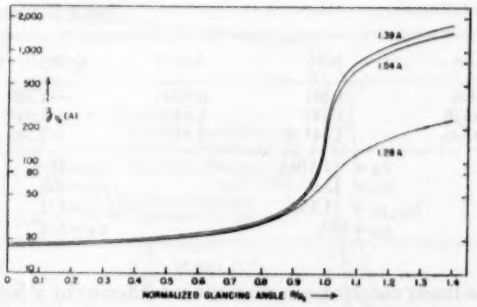

FIG. 5. Calculated $1/e$ penetration depths in copper. Penetration is very small for $\phi/\phi_c \lesssim 0.9$ and here is not sensitive to the photoelectric absorption coefficient. For $\phi/\phi_c > 1$ the penetration is given essentially by the usual absorption relation.

Penetration: Two Media

So that we may have some quantitative idea of the thickness of the surface layer involved, we shall determine the theoretical depth of penetration of the x-ray beam in medium 2 when $d_2=\infty$.

The expression for the refracted beam is given by Eq. (2). For the intensity at depth z, we multiply the exponent by its complex conjugate. The depth $z_{1/e}$ at which the intensity is reduced to $1/e$ is readily seen to be

$$z_{1/e}=\lambda/4\pi B. \quad (10)$$

Calculations with Eq. (10) for three wavelengths for a copper mirror are listed in Table I and are plotted in Fig. 5. The δ and β values indicated in the table are the normal bulk copper values, taken from Table II. Note that wavelengths are selected on either side of the K-absorption discontinuity $\lambda_K=1.379$A, so that

TABLE II. Calculations for δ for copper.

Line	λ(A)	λ/λ_K	$g_K \operatorname{Re}(J_K-1)$	$g_{L_I} \operatorname{Re}(J_{L_I}-1)$	$g_{L_{II,III}} \operatorname{Re}(J_{L_{II,III}}-1)$	$g_M \operatorname{Re}(J_M-1)$	$\delta(\times 10^6)$
$WL\beta_1$	1.281	0.930	−2.340	−0.017	0.170	0.030	16.72
$CuK\beta_1$	1.392	1.010	−4.949	−0.020	0.190	0.034	17.85
$CuK\alpha_1$	1.541	1.117	−2.565	−0.025	0.213	0.039	24.05

$\lambda_K = 1.379$A, $p_K = 11/4$, $g_K = 1.33$, $\rho = 8.936$ g/cm³,
$\lambda_{L_I} = 12.0$, $p_{L_I} = 2.0$, $g_{L_I} = 1.5$, $M = 63.57$ g/mole,
$\lambda_{L_{II,III}} = 13.15$, $p_{L_{II,III}} = 5/2$, $g_{L_{II,III}} = 4.0$,
$\lambda_M = 160$, $p_M = 5/2$, $g_M = 20$.

the linear absorption coefficients are different by a factor of more than 6. Until ϕ/ϕ_c becomes very close to unity, the thickness of the layer involved in the reflection process is small, of the order of 20 to 50A. After the critical angle is reached, the penetration depth becomes rapidly large and is soon the value calculated from the familiar absorption relation,

$$\frac{I_2(z_{1/e})}{I_2(0)} \doteq \exp(-\mu_2 x_{1/e}) \doteq \exp\left[-\frac{\mu_2}{\phi_2} z_{1/e}\right] = \exp\left[-\frac{\mu_2}{(\phi^2-2\delta_2)^{\frac{1}{2}}} z_{1/e}\right].$$

Actually, the *effective* thickness for our interest in reflected intensity is even less than $z_{1/e}$ (especially since the involvement is weighted exponentially with depth), the top surface layer being much more important than successively deeper layers.

However, as discussed later, the mirror is probably not homogeneous. For example, porosity, or an oxide layer on copper, would cause the penetration [for $I_2/I_2(0) = 1/e$] to be somewhat greater than the calculated value.

Theoretical Values of δ

The quantum-mechanical theory for the complex refractive index, in terms of the various q shells of electrons, gives

$$r = 1-\delta-i\beta = 1-A'\lambda^2\frac{\rho}{M}\sum_q \int_{\omega_q}^{\infty} \frac{\omega^2 (dg/d\omega_v)_q}{\omega^2-\omega_v^2-i\eta_q\omega} d\omega_v, \quad (11)$$

where

$$A' = Ne^2/2\pi m_e c^2 \doteq 2.7019\times 10^{10},$$

N = Avogadro's number; e = electronic charge; m_e = electronic mass; c = velocity of light; ρ = density; M = molecular weight; $\omega = 2\pi\nu$, ν = incident x-ray frequency; $\omega_v = 2\pi\nu_v$, ν_v = frequency of dispersion oscillators; $\omega_q = 2\pi\nu_q$, ν_q = frequency of the q-absorption discontinuity; $(dg/d\omega_v)_q$ = density of dispersion oscillators, q-type electrons, near ω_v; and η_q = damping factor. The density of the dispersion oscillators follows the absorption relation λ^{p_q} for q-type electrons, and the area under the curve of the absorption spectrum gives the oscillator strength g_q. The damping factor η_q is given by a combination of the classical radiation damping and the width of the q state: For copper and the wavelengths of the present work, the damping factor is safely neglected.[2]

The real part of the integral term of Eq. (11) gives

$$\delta = A'\lambda^2\frac{\rho}{M}[Z+g_K \operatorname{Re}(J_K-1)+g_{LI} \operatorname{Re}(J_{LI}-1) + g_{LII,III} \operatorname{Re}(J_{LII,III}-1)+g_M \operatorname{Re}(J_M-1)], \quad (12)$$

where $A'\lambda^2(\rho Z/M)$ is the normal dispersion term (Z is the atomic number), and the others are the significant anomalous dispersion terms for copper at $\lambda = 1.39$A. The real part of (J_q-1) is shown integrated in reference 2.

Calculations for δ are listed in Table II. The various constants used in these calculations are given under the table and are discussed in reference 2.

III. EXPERIMENTAL CURVES

A moderately thick (about 2000A) copper film was deposited by evaporation[3] on the glass surface studied in Fig. 2. OFHC copper (pieces of 25-mil wire) was evaporated during a time of about 20 minutes from an array of four 15-mil tantalum helical filaments 20 cm from the substrate and spaced linearly to give a film of very nearly uniform thickness along the 14-cm surface. The curve recorded for this film with the Cu $K\beta_1$ line, $\lambda = 1.39$A, is shown in Fig. 6.

The experimental curve of Fig. 6 is typical of about 30 copper curves, with many different moderately thick films and different glass substrates, that have been

[2] L. G. Parratt and C. F. Hempstead, Phys. Rev. **94**, 1593 (1954).

[3] The optically polished glass surface was cleaned as follows: Washed thoroughly with Lakeseal laboratory soap, rinsed with tap water, swabbed with 30 percent hydrogen peroxide (CP), stroked lightly with a cheesecloth swab soaked with acetone (CP) several times until no "breath figure" could be seen, then, finally, subjected in the vacuum to a glow discharge for several minutes.

No special effort was made in the present work to control the rate of evaporation or condensation, temperature of the substrate during or after the condensation, traces of gases and of unidentified material on the substrate or in the evaporation chamber, nor subsequent adsorption or chemisorption on the surface.

Backstreaming of the pumping fluid, Octoil S, was reduced by two water-cooled baffles in series in the pumping line. A liquid N_2 trap was supported inside the evacuation chamber.

The pressure during evaporation was always less than 10^{-6} mm Hg, and about 3×10^{-7} before and after evaporation, as measured with a Bayard-Alpert type ionization gauge.

recorded with $\lambda = 1.39$A, and of about 20 curves with $\lambda = 1.54$A. (Films of mean thickness less than about 200A show special features which will be discussed in a later paper.) The Fig. 6 curve is also more or less typical of many gold, silver, and aluminum mirrors.

In this Section we consider four general problems in the interpretation of an experimental curve: (1) instrumental effects, (2) smoothness of the mirror, (3) matching the two-media theoretical curve to the experimental curve, and (4) the experimental value of δ.

Instrumental Effects

The observed curve, especially in the region of maximum slope, is of course perturbed to some extent by such instrumental effects as imperfect collimation and heterochromaticity of the incident x-ray beam, and any inaccuracy in either coordinate scale. These effects are believed to be negligibly small in the present work.

The beam was collimated and monochromatized by (1) a slit 0.01 cm wide placed near the x-ray tube and 37 cm from the calcite monochromator crystal, see Fig. 1, (2) the diffraction pattern of the calcite crystal (about 11 seconds full width at half-maximum), and (3) a second slit 0.003 cm wide placed between the crystal and the mirror at a position 23 cm from the axis of the crystal. The second slit, about 1 cm from the near end of the mirror, served to cut off the angular and spectroscopic "tails" of the beam and also to reduce the linear width of the beam incident on the mirror. The mirror subtended the entire beam at $\phi \geqslant 1 \times 10^{-3}$ radian.

Although the x-ray tube was operated at 35 kv, the spectral pass band, less than one x.u. wide at half-maximum, was so narrow that we can safely ignore the continuous radiation in higher orders of Bragg reflection from the calcite crystal.

The incident angle ϕ was measured on the drum of a tangent micrometer screw. Increments in ϕ were accurate to better than 2 seconds of arc. The zero of the angle scale was determined from photographs of the direct beam and of the reflected beam with each of several values of ϕ as follows: Measurements of the distances between the photographic images were made with a comparator and the zero angle obtained by extrapolation. The zero angle accuracy was about ± 4 seconds of arc.

The intensity scale (response of the proportional counter system[4]) was found to be linear within 0.5 percent if the counting rate did not exceed 1000 counts per second (5-microsecond resolving time).

[4] We have also used Geiger counter and ionization chamber systems. A proportional counter system with a resolving time less than 5 microseconds is recommended. Geiger counter systems were found unsatisfactory [Parratt, Hempstead, and Jossem, Rev. Sci. Instr. **23**, 1 (1952)], and the ionization chamber method has an unfavorable combination of sensitivity, stability and response time. The proportional system, with a channel discriminator as we use it, provides a very effective method for reducing the magnitude of the background intensity.

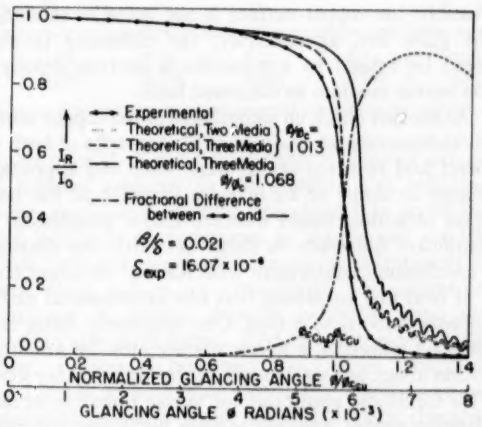

FIG. 6. Comparison of experimental and theoretical reflection curves for copper (2000A thick) on glass for $\lambda = 1.39$A. The experimental surface is evaporated copper on polished glass. In the normalized abscissas scale, ϕ_c is the experimental value. Explanation of the difference between the curves involves conjectures as to peculiarities of the experimental surface.
(The maxima and minima for $\phi/\phi_c > 1$, three media curve, comprise an interference pattern between beams reflected from the copper and from the glass substrate.)

The incident intensity was measured by recording the direct beam with the mirror temporarily slid out of position.

Mirror Smoothness

Lack of smoothness of the mirror is probably most sensitively detected in the region of maximum slope of the curve. The theoretical curves are based on a surface model of perfect smoothness, so a comparison of the experimental and theoretical curves, properly matched for β/δ, should provide a first test for smoothness.

Since the curves of Fig. 2 show very satisfactory agreement at the inflection point, the glass substrate appears to be smooth.[5,6] The maximum slopes of the experimental and theoretical curves for copper, Fig. 6, are also in rather satisfactory agreement but the experimental slope is slightly smaller than the theoretical.

[5] The curve of Fig. 2 was taken with a glass mirror optically flat to about a tenth of a wavelength of green light over the critical central few centimeters, and to one wavelength over the full length, 14 cm, of the mirror. Flatness to about 500A is necessary to avoid reflection distortion [see C. M. Lucht and D. Harker, Rev. Sci. Instr. **22**, 392 (1951)].

[6] Electron microscope studies show freshly polished glass surfaces with a smoothness of about 10A over very short distances, and infrequent scratch grooves as deep as 500A [R. C. Williams and R. C. Backus, J. Appl. Phys. **20**, 98 (1949)]. Multiple-beam interferometry shows surface planeness to within 1/150 of a wavelength (of visible radiation) over a test area of about 4-mm diameter [O. S. Heavens, Proc. Phys. Soc. (London) **B64**, 419 (1951)].
However, over a few thousand angstroms extent along at least some optically polished glass mirrors, x-ray reflection work by W. Ehrenberg, J. Opt. Soc. Am. **39**, 746 (1949), has indicated a ripple-type of surface with peak to trough depth about 10A and a ripple length of about 2 mm. Such ripple structure, if present, would give some broadening of the inflection part of the observed curve.

Possibly the copper surface is not quite as smooth as the glass but, alternatively, the difference in slope could be caused by a nonuniform electron density of the mirror medium as discussed later.

As another check on smoothness of the copper mirror, microdensitometer analyses of photographs of both the direct and reflected beams were made. An appreciable change in shape or an increase in width of the beam upon reflection would indicate mirror roughness. No significant difference in shape or width was detected, a conclusion in agreement with Kiessig[7] on nickel films.

It is at first surprising that any experimental surface appears smooth to x-rays. One frequently hears that, for good reflection, a mirror surface must be smooth to within about one wavelength of the radiation involved.[8] This condition, applicable for visible radiation at large glancing angles, apparently does not apply for x-rays at very small glancing angles.

Best Match of Curves

With spurious instrumental factors and mirror roughness discounted, the shape of the observed curve must be explained in terms of some model of the mirror structure. Without prior knowledge of the actual structure, we shall assume the simplest model, *viz.*, two homogeneous media with a sharp plane interface. The difference between the experimental curve and a *matched* two-media curve, with conjectures as to a better model, is discussed later. First, we must effect the two-media match, i.e., for a homogeneous copper lamina on a glass substrate.

In the region $\phi/\phi_c \lesssim 0.6$, the experimental and theoretical curves, Fig. 6, are both rather flat. In this region, we have essentially total reflection from any electron density greater than about 40 percent of the normal bulk copper value. This is a reasonable density limit with any surface model later considered, so we expect that here the curves should match. We match also at one point[9] in the inflection region, at, say, $I_R/I_0=\frac{1}{2}$ (which point we shall call $\phi_{\frac{1}{2}}$), but we do not try to match the maximum slope. With these match criteria, we find that the ratio β/δ is rather rigidly fixed.

If the actual electron density in the mirror is not constant with depth, the intensity match at $\phi_{\frac{1}{2}}$ (i.e., at $\phi/\phi_c=1.013$ as shown later) is not quite consistent with the $\phi/\phi_c \lesssim 0.6$ match. For example, if the density increases with depth, the effective penetration of the x-ray beam would cause the curve in the region $\phi/\phi_c \lesssim 1$ to be somewhat lower than the theoretical two-media curve matched at $\phi/\phi_c=1.013$. (Of course, in the match, ϕ_c is the experimental value; if the value for the normal bulk copper were used, the theoretical curve would pass through $\phi_{\frac{1}{2}}/\phi_c=1.068$; this curve for three media is also shown in Fig. 6.) However, a few percent uncertainty as to the proper ϕ/ϕ_c value at which to make the match in the inflection region is of little moment so far as the β/δ value is concerned.

It is interesting to check the matching value of β/δ with the ratio obtained from the normal bulk values.[10] These values, from Table I, give $\beta/\delta=0.021$, in perfect agreement with the matching value.

A three-media curve, Eq. (8), for 2000A normal bulk copper on glass differs from the two-media curve by including the effect of penetration to, and reflection from, the glass. The three-media curve does not differ significantly from the two-media curve in the match regions, but in the region $\phi/\phi_c>1$ the curve oscillates in an interference pattern.[11] In Fig. 6, both the matched two- and three-media curves are shown.

Experimental δ

Use of the normalized abscissa scale ϕ/ϕ_c in Figs. 2 and 6 implies prior knowledge of the value of ϕ_c (or of δ). With the value of β/δ from the "best match" just discussed, a rather precise value of ϕ_c may be read from the ϕ curve by the following method. With the experimental point $\phi_{\frac{1}{2}}$, easily and unambiguously determined, and with the value of β/δ, we obtain ϕ_c from Eq. (13) which is a version of Eq. (4).

$$\frac{\phi_{\frac{1}{2}}}{\phi_c}=\left\{\frac{1+(\beta/\delta)^2}{1+9(\beta/\delta)^2}\left[\frac{1}{2}+\frac{3\sqrt{2}}{8}(1+(\beta/\delta)^2)^{\frac{1}{2}}\right]\right\}^{\frac{1}{2}}. \quad (13)$$

The ratio $\phi_{\frac{1}{2}}/\phi_c$ is not a sensitive function of β/δ, as can be seen from Table III, and the uncertainty in the "best match" estimate of β/δ is usually not serious. In case this uncertainty is significant, we may make a new plot with ϕ/ϕ_c as abscissas, using the tentative value of ϕ_c, and effect a better "best match," i.e., a more accurate value of β/δ and, from Eq. (13), a final value of ϕ_c.

An experimental precision better than 1 percent is practical in the determination of δ $(=\frac{1}{2}\phi_c^2)$.

From the experimental curve of Fig. 6, $\beta/\delta=0.021$ and $\phi_{\frac{1}{2}}=(19.78\pm0.1)$ minutes of arc; we calculate from Eq. (13) that $\phi_{\frac{1}{2}}/\phi_c=1.013$ and deduce $\phi_c=19.5$ minutes or 5.67×10^{-3} radian. From this ϕ_c, $\delta=(16.07\pm0.2)\times10^{-6}$ for copper for $\lambda=1.39$A.

Of course, if the electron density in the mirror is not

[7] H. Kiessig, Ann. Physik **10**, 715 (1931).

[8] Electron diffraction studies of evaporated copper surfaces show randomly oriented single crystallites of about 70A or more on an edge [e.g., see H. Levinstein, J. Appl. Phys. **20**, 306 (1949), and references].

[9] It is common practice to assume this match point in determining δ. E.g., see reference 7; A. J. Lameris and J. A. Prins, Physica **1**, 881 (1934), and references.

[10] Normal bulk values may be used in this check since (a) both β and δ vary linearly with density, and (b) the shape of the theoretical curve depends only upon the ratio β/δ [see Eq. (4)].

[11] No significant oscillations were observed in the experimental curve of Fig. 6, although, when recorded with more closely-spaced points, some curves do show faint oscillations.

The oscillating interference pattern is more pronounced with films somewhat thinner than 2000A. See also H. Kiessig, Ann. Physik **10**, 769 (1931); F. Odenbach, Ann. Physik **38**, 469 (1940); and R. Riedmiller, Ann. Physik **20**, 377 (1934).

TABLE III. Calculations from Eq. (13).

β/δ	0	0.02	0.03	0.04	0.06	0.08	0.10	0.12	0.14	0.18
ϕ_i/ϕ_e	1.015	1.013	1.011	1.009	1.007	0.991	0.976	0.961	0.947	0.911

constant with depth, the experimental δ corresponds to some sort of average density over the depth penetrated by the x-ray beam.

IV. CONJECTURES ABOUT SURFACE PROPERTIES

The experimental value of δ for the copper surface is 10 percent less than the normal bulk copper value. Therefore, with no intent now to match the experimental curve in the inflection region, we should draw the three-media curve for 2000A copper on glass through the point $\phi/\phi_e=1.068$ where ϕ_e is the experimental value. This is the solid curve in Fig. 6. The discrepancy between the experimental curve and this solid curve is shown as the fractional difference, the short-long dash curve. In this section we shall conjecture as to the properties of the surface responsible for this difference.

Before proceeding to specific structural models of the surface, let us inquire as to a likely *a priori* general nature of the surface.

Spongy Surface Structure

During the production of a copper mirror by evaporation and condensation onto a polished glass substrate, we suppose that little crystals build up at numerous places and with perhaps various crystallographic orientations. As the mean film thickness increases, neighboring crystallites touch each other and presumably form a somewhat loosely packed spongy structure.[8] As the mean thickness continues to increase, the deeper-lying atoms or crystallites are subjected to stronger forces to rearrange into larger crystals and into shapes and orientations leaving a smaller net volme of intercrystalline space.[12] In general, the rate and extent of such an annealing or rearranging process are functions of time, of temperature (during and after production), of substrate structure, and of various conditions of the evaporation, e.g., sanitation of the substrate, rate of condensation, pressure, and type of residual gas present.[13] Because of the intercrystalline space, the average density near the surface is less than the normal bulk value and presumably increases with depth (excepting the uncertain region at the substrate interface). The phrase "loose packing" shall be used to refer to this type of attenuated average density.

Loose packing is also a characteristic of many ground and polished surfaces. In the grinding and polishing process, mechanical rupture and distortion occur for many hundreds of angstroms in depth, and on the surface there may be short-range physical transport of atoms, atom groups, or crystallites. The degree of attenuation of density depends generally upon the crystallite size (and shape). Perhaps very close to the surface, a layer of extremely small atom groups or crystallites is present in an essentially liquid or amorphous state having a higher average density (because of close packing) than obtains for the region of loose-packed larger crystallites immediately beneath.

Oxidation

Oxidation of a copper mirror also results in an attenuated density if the oxide forms a skin-layer on the general surface plane. A 70A copper single crystal on a Formvar substrate has been observed[14] to oxidize (Cu_2O) to a depth xA in t minutes in oxygen at 20 mm Hg pressure at room temperature according to the relation

$$x=4+6.5\log_{10}t, \quad t>2 \text{ minutes}, \tag{14}$$

which, after 4 hours, gives $x=20$A, and a limiting growth thickness of about 50A after many years.[15] A thick abraded copper specimen oxidized to a maximum depth of only 90A below the general plane of the surface after 21 months exposure to pure dry oxygen at room temperature.[16]

Interior oxidation may also occur: Oxygen may penetrate through the intercrystalline space in the spongy aggregate structure and corrode the surfaces of the deeper-lying crystallites. Interior oxidation is no doubt largely responsible for the fact that the specific area[17] is appreciably greater than unity.[18] Such oxidation, if the oxide does not fluff (break loose), results in an increase in electron density but not as high density as the normal bulk value for pure copper.

The copper mirrors of the present study were removed from the evaporation chamber, taken to another room

[12] We assume that the x-ray scattering from the aggregate of loosely packed (and/or partially oxidized) crystallites is essentially coherent as for a medium of gradually changing density but that is otherwise homogeneous.

[13] Perhaps some of the rearrangement results from the escape or ejection of gas or other impurity atoms that were entrained during the condensation.

That greater porosity exists for thin than for thick films is shown by M. S. Blois, Jr., and L. M. Rieser, Jr., J. Appl. Phys. **25**, 338 (1954).

[14] A. H. White and L. H. Germer, Trans. Electrochem. Soc. **81**, 305 (1942). See also W. E. Campbell and U. B. Thomas, Trans. Electrochem. Soc. **91**, 623 (1947).

[15] It is unlikely that any other type of corrosion is important. An extremely thin layer of CuO may form on the surface of Cu_2O without much consequence; some Cu_2S is probably also present but with a presumed small effect.

[16] W. E. Campbell and U. B. Thomas, Trans. Electrochem. Soc. **76**, 303 (1939).

[17] The specific area, studied in catalysis, is the ratio of the free surface to the area of the general plane.

[18] O. Beeck, Revs. Modern Phys. **17**, 61 (1945), and others, also suggest that the oxygen is adsorbed in the interior surface of evaporated metal films.

and mounted on the x-ray spectrometer. A minimum of about 15 minutes exposure to laboratory air was unavoidable before the curve was recorded. Some rearranging of atoms or crystallites in the surface and some oxidation, both during and after preparation, were inevitable.

Specific Conjectures

With the above general conjectures as to the nature of our surfaces, we turn to specific models in an attempt to understand the difference between the experimental and three-media curves of Fig. 6.

First, we note that in the region $\phi/\phi_c > 1$, the experimental curve falls below the theoretical curve. (This discrepancy is also a characteristic of each of several moderately thick gold, silver and aluminum mirrors with glass substrates. Our studies with these surfaces are not yet complete.) One is first tempted to say that an appreciable part of the x-ray beam penetrates through the metal film to the metal-glass interface where the beam is refracted into the glass and is lost. Indeed, the ratio of refractive indices of copper and glass precludes total reflection from the copper-glass interface for $\phi > \phi_{c_{glass}}$. However, appreciable intensity is theoretically reflected from the glass, as is evidenced by the interference pattern of the three-media curve of Fig. 6. The theoretical curve includes, of course, both refraction into and partial reflection from the glass but the net average effect yields a curve which is about the same as for pure infinitely thick copper.[19]

We note also a similar but smaller discrepancy with the glass mirror, Fig. 2, for which there is no substrate.

We conclude that the substrate is not responsible for the discrepancy (except the oscillations) between the experimental and theoretical curves of Fig. 6.

(A) *General Reduction of Density*

A general reduction of (electron) density throughout the entire copper, such as by uniform porosity or by uniform partial oxidation during the evaporation process, would result in a reduction of δ.

If the 2000A film were pure copper with a uniform porosity such that the average density were about 8 instead of 8.936 g/cm^3, this model would give the observed value of δ. If instead, the entire 2000A film were completely oxidized and not loose packed, the expected δ (for Cu_2O) would be 14.16×10^{-6}, i.e., 20.6 percent less than for normal bulk copper. But if the oxidation of individual crystallites were not complete, so that the average electron density were about midway between the values for Cu_2O and Cu, this partial-oxide model would account for the observed value of δ.

But neither of these models, uniform porosity or uniform partial oxidation, would account for the discrepancies in the two regions $0.6 \lesssim \phi/\phi_c < 1$ and $\phi/\phi_c > 1$. In fact, these regions would be emphasized as *separate* regions if the theoretical curve (Fig. 6) were drawn for ϕ_1/ϕ_c at a value a little less than 1.068—the new fractional difference curve would have a pronounced minimum in it near $\phi/\phi_c = 1$ indicating the likelihood of *two* different types of surface peculiarities in addition to the uniform reduction of density.

It seems likely that uniform general reduction of density, while perhaps present to a certain degree, is not the dominating feature of the mirror surface.[20]

(B) *Oxide Layer of Limited Depth and of Varying Density*

A more promising model is the following. Assume, first, that oxidation is complete and uniform to a certain depth, with no loose packing in the oxide or in the underlying pure copper. Three-media theoretical curves for this model are shown in Fig. 7 for each of several oxide thicknesses.[21] The constants used in the calculations for these curves are listed in Table IV. The curve for 150A thickness gives δ in good agreement with experiment, and also exhibits a reduced intensity, but not the right curve shape, in the $\phi/\phi_c > 1$ region. The discrepancy in the $\phi/\phi_c < 1$ region is reasonably well accounted for.

Examination of the curves of Fig. 7, keeping in mind the penetration of the x-ray beam as the angle of incidence increases, indicates that, if a very small amount of loose packing or fluffing of the oxide were allowed at the surface and if the sharp Cu_2O-Cu interface were relaxed into a gradual transition region, a model could probably be found which would give good agreement with experiment. The theoretical curve for one trial six-media model is compared with the experimental curve in Fig. 7; the details of the model are indicated in the figure. Additional laminae are evidently needed to approximate the transition from Cu_2O to Cu. Note that inclusion of the glass substrate introduces the oscillations, fainter now than in Fig. 6.

This model, with additional laminal media to approximate gradual changes in density, would be satisfactory if oxidation does, in fact, agree with this pattern. Let us review our *a priori* expectations: (1) the oxide on the surface of a single copper crystal is not expected to penetrate more than about 20A [from Eq. (14)] at room temperature; (2) an evaporated copper surface

[19] It is interesting to note that an incorrect three-media theoretical curve which takes into account only the real part of the amplitude factor a_m, Eq. (7), shows no oscillations and lies below the two-media curve in the range $\phi > \phi_c$ by a few percent. The imaginary or phase factor raises the curve, and indeed, raises it a greater amount for thinner films in the range just beyond ϕ_c.

[20] More or less uniform reduction of density was concluded by H. Kiessig, reference 7. See also references 11 and 13, and R. W. James, *The Optical Principles of the Diffraction of X-Rays* (G. Bell and Sons, Ltd., London, 1950), pp. 171–177.

[21] Each of the three-media curves of Fig. 7 contains interference maxima and minima in the region $\phi/\phi_c > 1$ not included in the figure; e.g., the second maximum in the 150A curve appears just beyond $\phi = 10^{-2}$ radian.

[If the imaginary (or phase) factor of Eq. (7) is deleted, the curves corresponding to those of Fig. 7 for 5 to 150A show a sharp minimum near $\phi_c(Cu_2O) = 5.32\times10^{-3}$ radian, and show very close agreement with the pure copper curve for $\phi/\phi_c > 1.02$.]

consists of single crystals perhaps 70A or more in size; (3) the evaporated copper surface is probably somewhat spongy; and (4) interior oxidation is probably present. Although at somewhat elevated temperatures complete oxidation of evaporated copper takes place a hundred or so angstroms in depth,[22] there is some question whether *complete* oxidation takes place in many or any of the 70A (or larger) single crystals at room temperature.

Experimental curves with fresh 2000A copper mirrors usually have essentially the same shape as curves recorded after several months exposure to atmospheric air at room temperature. Occasionally, however, after ageing a mirror, the curve shows some slight decrease in reflected intensity in the region $0.3 \lesssim \phi/\phi_c \lesssim 0.95$, but not in the region $\phi/\phi_c \gtrsim 1$. (This intensity decrease with age, or with temporarily elevated temperature, is much more pronounced with thinner films.) The change in the curve may indicate that further oxidation (or some fluffing) of the partially oxidized smaller crystallites near the extreme surface occurs, but, in terms of this model, oxidation does not appear to progress more deeply into the mirror surface after the first few minutes of exposure to atmospheric air.

With the depth and completeness of oxidation in some doubt, we proceed to an alternative model.

(C) *Reflection Trap*

In the proposed spongy aggregate of copper crystallites, the average crystallite size increases, and the intercrystalline space decreases, with depth into the surface. The lattice constant of Cu_2O (4.26A) is larger than that of copper (3.61A), and the copper crystallite in the surface swells greatly as it changes to Cu_2O. This is responsible for the possible fluffing of the oxide.[23] At some critical depth, the intercrystalline space first fills up with oxide. The mechanical forces involved in fluffing may at this depth effect a seal rather than continue fluffing which would now require a rather violent eruption of the large mass of material above the seal. If such a seal is formed, further free admittance of oxygen below the seal is stopped and oxidation here practically ceases.[24] The copper crystallites below the seal remain loose packed with a thin covering of oxide. With continued exposure to oxygen, the seal extends upward toward the surface, becoming thicker. Whether the seal reaches the surface before general fluffing above the seal occurs is not now important.

Formation of such a seal may be at least partially responsible for the rather sudden decrease after a minute or so in the observed rate of oxidation,[14] of oxygen take-up,[25] and/or of the heat of adsorption.[26] This subject is too complex for adequate treatment now.[27]

In terms of this model, the electron density may vary with depth somewhat as roughly sketched in Fig. 8 for pure but loose-packed copper and for partially oxidized copper. (In the figure, the heart of every partially oxidized crystallite is shown as remaining pure copper —this and other details of the figure are not to be taken too literally.) Although the term "seal" has been used and is indicated in Fig. 8, our interest is limited now

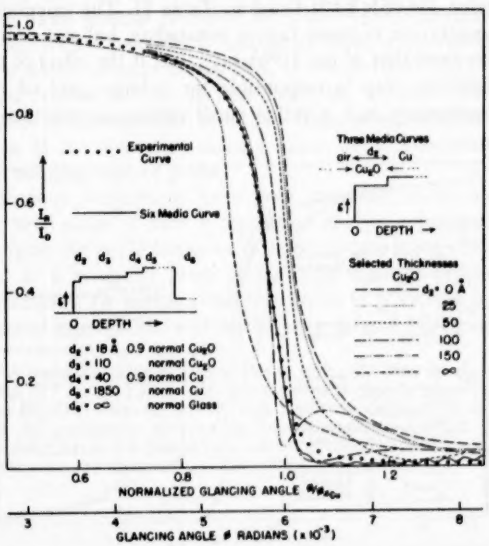

FIG. 7. Three-media reflection curves for homogeneous cuprous oxide on homogeneous copper, and one six-media curve for $\lambda = 1.39$A. The experimental curve is included for comparison.

TABLE IV. Dispersion constants for $\lambda = 1.39$A.

Normal copper	Cu_2O	Glass
$\rho = 8.936$ g/cm³	6.0 g/cm³	...
$\delta = 17.85\times10^{-6}$	14.16×10^{-6}	6.40×10^{-6}
$\phi_c = 20.54$ min	18.29 min	12.3 min
5.98×10^{-3} rad	5.32×10^{-3} rad	3.58×10^{-3} rad
$\beta = 3.76\times10^{-7}$	3.43×10^{-7}	1.60×10^{-7}

[22] Garner, Gray, and Stone, Proc. Roy. Soc. (London) **A197**, 294 (1949), Disc. Faraday Soc. No. 8, 246 (1950); and M. Bound and D. A. Richards, Proc. Phys. Soc. (London) **51**, 256 (1939).

[23] F. C. Frank and J. H. van der Merwe, Proc. Roy. Soc. (London) **A200**, 125 (1950), suggest that, in general, if the molar volume of the oxide exceeds 115 percent of the molar volume of the metal, the oxide nucleates at several centers and may break away. K. Leu, Ph.D. thesis, University of London, 1951 (unpublished), reports that when exposed to laboratory air up to temperatures of 135°C, the cuprous oxide on single copper crystals grows as an amorphous layer. H. Frisby, Compt. rend. **226**, 572 (1948) and **228**, 1291 (1949), and others, find Cu_2O on the (110) plane of a single copper crystal grows with orientation perfectly parallel to that of copper. It is yet difficult to know what happens.

[24] Oxidation below the seal continues but much more slowly, at a rate determined, perhaps, by the mobility of the cation (Cu^+) through thick oxide. [See K. Hauffe, Prog. Metal Phys. **4**, 71 (1953).]

[25] J. A. Allen and J. W. Mitchell, Disc. Faraday Soc. No. 8, 309 (1950), and references.

[26] Beeck, Cole, and Wheeler, Disc. Faraday Soc. No. 8, 314 (1950), and references.

[27] See R. Gomer and C. S. Smith, *Structure and Properties of Solid Surfaces* (The University of Chicago Press, Chicago, 1953), for review of current status of this and related subjects.

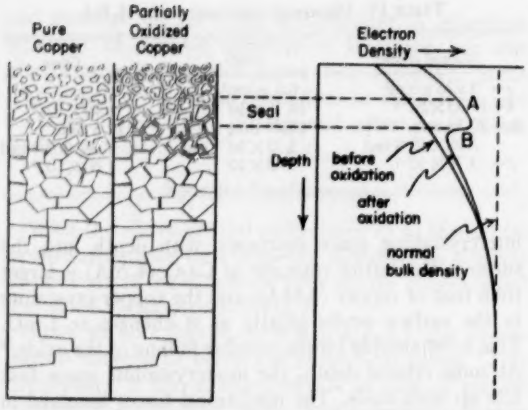

FIG. 8. Rough sketch of loose-packed surface structure of evaporated copper before and after partial oxidation. A seal of oxide is presumed to form; just below the seal the electron density is a minimum. The indicated loose packing and specific area are without doubt exaggerated for an evaporated copper surface produced and kept at room temperature.

to an electron density maximum and minimum whether or not an oxygen-impervious seal is present.[28]

The significant feature of this model is that part of the x-ray beam travelling upward in the mirror medium, suffers partial reflection at the underside of the density maximum (seal). For a certain range of angle, this beam, trying to break through the seal from underneath, is totally reflected back into the mirror where it is again reflected. The beam is thus partially caught in a "reflection trap."

The effect of such a reflection trap depends upon the details of the configuration of electron density in the surface. For five arbitrary configurations, each containing a density maximum and minimum, we have evaluated Eq. (8); the resulting theoretical reflection curves are shown in Fig. 9. The constants used are listed in Table V; since δ and β each varies linearly with electron density, they are listed together. The first configuration of Fig. 9 or Table V contains an exaggerated trap—an excessive reduction of effective electron density. The second, compared with the first, shows that the effect of the trap is sensitive to thickness d_2. The third and fourth configurations have shapes more like the experimental curve, with the minimum intensity in each case, however, too low and too narrow. The addition of two more laminae, the fifth configuration, helps in these regards. The ϕ_c for the fifth configuration, is about 5.83×10^{-3} radian and the experimental value is 5.67×10^{-3}, a discrepancy in δ of about 5 percent.

No doubt, with additional trial configurations, with generally smaller densities, and with perhaps more laminae to approximate gradually changing density, we could find a reflection trap configuration that would give excellent agreement with experiment in δ and in curve shape. The significant conclusion now is that the agreeing configuration would probably be like the one we would guess for the proposed phenomenon—thus the reflection trap model is believed to be reasonable.

(Inclusion of the glass substrate as a seventh medium would introduce the interference oscillations but otherwise probably not seriously alter the curve shapes.)

The discussion has so far dealt with wavelength 1.39A. Curves recorded with $\lambda=1.54$A yield a δ value (22×10^{-6}) which is 8.3 percent less than the theoretical value (24.05×10^{-6}) listed in Table II. The calculated penetration of these rays is somewhat, but not much, less than that of the 1.39A rays; but if the effect of the reflection trap is responsible for a large part of the discrepancy in δ, a rather small change in penetration

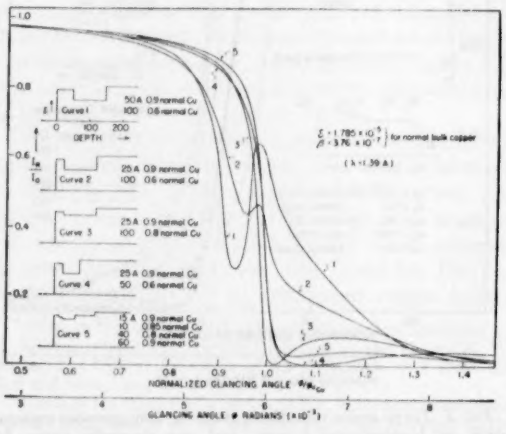

FIG. 9. The effect of a reflection trap in the surface. Curves for five different configurations of electron density are shown. The seal in the evaporated copper surface may be about 20A below the nominal surface plane to yield a curve in agreement with experiment.

[28] An electron density minimum may also be produced by the degree of close-packing of crystallites of gradually increasing size with depth. For example, on the extreme surface of optically polished glass, the "crystallite" size may be almost as small as individual molecules—a liquid-like surface with essentially no intercrystalline space. Also, in competition with oxidation or the liquid-like surface to effect the density maximum, we may have limited-depth intercrystalline adsorption of oils or other unidentified materials from the laboratory air. For copper, oxidation is possibly the principal effect; for glass, we cannot distinguish without better controlled conditions between the other two effects.

Professor T. J. Gray of Alfred University recently pointed out in a private conversation that the electrons which move from inside the copper (or oxide) surface to attach to the oxygen in chemisorption result in an excess of electrons at the surface (n-type material) and of holes inside the surface (p-type material). This contributes to the electron density maximum and minimum configuration but the relative magnitude of this contribution is probably small.

Another interesting possibility is the following. In the early stages of film deposition the copper crystallites may grow vertically and then "bridge over" enclosing holes at the substrate. If, as the film thickness increases, such vertical aggregation with subsequent latteral "bridging over" continues to occur, enclosing holes that are much smaller than those adjacent to the substrate, and if the more deeply embedded holes tend to collapse (except probably at the substrate), we may always have a reflection trap very close to the surface. This conjecture may be more reasonable than an interior oxide seal for evaporated metal surfaces.

may result in a rather large shift in the experimental δ.[29] The observed shift is in the right direction to support the hypothesis of the reflection trap and its large influence in the percentage discrepancy in δ.

V. SUMMARY

The method of x-ray total reflection has been discussed for the study of certain surface properties of solids. Dispersion theory has been extended to treat any (small) number of stratified homogeneous media, and has been applied in an interpretation of experimental curves.

The measured refractive index term δ is significantly less than the theoretical value (on the model of a single homogeneous mirror medium), and the experimental and theoretical curves are appreciably different in other regards. Three structural models of the surface have been discussed in an effort to account for the difference in the curves.

The discussion has been made in detail for a 2000A thick evaporated copper film on a polished glass substrate. For this surface it is not reasonable that the copper film has only a general, uniform reduction of density; such a model accounts for only one discrepancy between the theoretical and experimental curves. A consistent accounting can be made, however, if the copper surface has oxidized completely to a depth of about 150A with a small amount of loose packing or porosity on the surface and with a gradual transition region Cu_2O to Cu. The requisite complete-oxidation depth may be reduced somewhat if oxide is combined with some general porosity. But, since single crystals of copper are believed to oxidize at room temperature to a depth of only about 20A, it seems likely that a third feature of the surface must be invoked. This feature is the so-called reflection trap, an actual minimum in the dispersion density about 20 to 50A below the nominal surface plane.

Various conjectures have been proposed as to the physical cause of such a dispersion density minimum. Perhaps the oxide forms an interior oxygen-impervious seal in a generally loose packed aggregate of copper crystallites. Or perhaps the film grows in thickness by vertical aggregation with subsequent lateral "bridging over" enclosing holes which tend to collapse as they become more deeply embedded in the surface. The holes may be rather large only at a depth 15 to 50A beneath the nominal surface plane (and perhaps at the copper-glass interface).

Curves for evaporated gold, silver, aluminum, and for optically polished glass were also mentioned with similar general conclusions. For the glass mirror (and perhaps to a certain extent for the metal mirrors) the maximum dispersion density in a loose packed surface may be caused by a dense amorphous surface layer or by a limited-depth adsorption of unidentified materials resulting from exposure to laboratory air.

The measurements to date have all been carried out under laboratory atmospheric conditions. These conditions do not allow satisfactory separation and control of the physical (and chemical) variables believed to be involved in the surface. For this reason, the method has been explored only qualitatively to date: We cannot yet choose a realistic combination of the three surface features for copper (a) uniform porosity, (b) an oxide layer of limited depth and of varying density, and (c) a reflection trap. However, under more controlled conditions of preparation and treatment of the surface, we can restrict the number and/or range of the variables at our disposal in selecting a surface model to be used in theoretical calculations. Then the method promises to be useful in surface studies of solids.

TABLE V. Arbitrary electron density configurations: homogeneous laminae: reflection trap. δ, β = fraction of the values for normal bulk copper, Table I.

	First configuration		Second configuration		Third configuration		Fourth configuration		Fifth configuration	
Medium	d(A)	δ, β	d(A)	δ, β	d(A)	δ, β	d(A)	δ, β	d(A)	δ, β
1 (air)	...	0	...	0	...	0	...	0	...	0
2 (Cu)	50	0.9	25	0.9	25	0.9	25	0.9	15	0.9
3 (Cu)	0	...	0	...	0	...	0	...	10	0.85
4 (Cu)	100	0.6	100	0.6	100	0.8	50	0.6	40	0.8
5 (Cu)	0	...	0	...	0	...	0	...	60	0.9
6 (Cu)	∞	1.0	∞	1.0	∞	1.0	∞	1.0	∞	1.0

VI. ACKNOWLEDGMENTS

The author is pleased to acknowledge his indebtedness to Mr. C. F. Dam, Mr. J. O. Porteus, and Mr. C. F. Hempstead for recording many of the curves, to Mr. Gerry Neugebauer, Mr. Robert Braden and the Cornell Computing Center for computations, and to Mr. Edmond Brown and Dr. E. L. Jossem for many pleasant and stimulating discussions.

[29] A tentative value of δ from curves with gold films on glass, 28.6×10^{-6} for $\lambda=1.39$A, is 30 percent smaller than is predicted from Eq. (11) when the normal bulk density is assumed. In this case the penetration at $\phi=\phi_c$ is, from Eq. (10), $z_{1/e}=60$A. If this reduction in δ is caused by a reflection trap, the "seal" must be very close to the general surface plane.

Possible Macroscopic Effects of Single Lattice Defects

JEROME ROTHSTEIN
Columbia University, New York, New York
(Received February 15, 1954)

A spiral dislocation with axis perpendicular to the lattice planes of a layer lattice converts the disconnected sheets to a connected helicoid. Crystal properties dependent on propagation effects and so strongly anisotropic in the layered crystal may approach isotropicity as intra-plane parameters can now dominate inter-plane propagation. A single defect may thereby have a macroscopic effect on semiconduction and photoduction, magnetic susceptibility, specific heat, and other properties. Substances in which such effects may exist are listed.

MOST effects of lattice defects are proportional to defect density, at least for small ratios of number of defects to number of lattice points. Color centers in alkali halides, structure-sensitive photoconductivity, and semiconductivity, provide such examples for vacancies, interstitials, and impurities, while work-hardening depends similarly on dislocation density. The screw or spiral dislocation, however, seems to be qualitatively different from these in that a single one might engender macroscopic change in a number of observable properties.

The role of dislocations in crystal growth has been discussed by Frank,[1] and supporting evidence for the theory put forth by Griffin,[2] Verma and Amelinckx,[3] Forty,[4] and Dawson and Vand.[5] The dislocations increase the rate of growth and produce growth contours visible in a microscope. The purpose of the present note is to call attention to the possibility of large effects on electric, magnetic, and other properties of fully grown layered crystals due to a single spiral dislocation. It seems probable that these dislocations are unique in this respect.

Consider, for purposes of illustration, a single crystal of graphite. Its pronounced anisotropicity is related to the large c/a ratio. The planar system of conjugated single and double bonds in lattice planes perpendicular to the c axis produces large electronic conductivity and diamagnetic susceptibility for electron flow parallel to these planes. Electron flow parallel to the c axis has a high activation energy and gives small susceptibility values. A screw dislocation whose axis lies parallel to the c axis converts the disconnected parallel sheets into a connected helicoid. A circuit about the dislocation, remaining on a sheet, then yields a translation parallel to the c axis from an initial to an adjacent lattice plane. Electron flow is then possible, within the system of conjugated bonds, without the necessity of surmounting the high interplanar activation energy.

TABLE I. Some layer lattices.

Type	Formula
CdI_2	Ag_2F, dibromides of Co, Fe, Mg, Mn, V, di-iodides of Ca, Cd, Co, Fe, Ge, Mg, Mn, Pb, Ti, V, Yb, dihydroxides of Ca, Cd, Co, Fe, Mg, Mn, Ni, disulfides of Pt, Sn, Ti, Zr, diselenides of Pt, Ti, Zr, ditellurides of Co, Ni, Pd, Pt, Ti, AlB_2, and Tl_2S (distorted CdI_2), $Co(OH)_{1.8}Br_{0.5}$, $Co(OH)_{1.8}Cl_{0.5}$, $Ni(OH)_{1.8}Cl_{0.4}$
$CdCl_2$	dibromides of Cd, Ni, dichlorides of Cd, Co, Fe, Mg, Mn, Ni, Zn, NiI_2, $Cd(OH)_{1.25}Cl_{0.75}$
BiI_3	$FeCl_3$, $CrBr_3$, AsI_3, SbI_3, BiI_3
MoS_2	MoS_2, WS_2
Other	$CrCl_3$, LiOH, $Al(OH)_3$, H_3BO_3, BN, graphitic compounds, $HgCl_2$, $HgBr_2$, yellow HgI_2, mica, and other minerals

The dc conductivity and static magnetic susceptibility are thus expected to lose their anisotropicity to a considerable extent, with parameters in the base plane being now approximately applicable in directions perpendicular thereto. At optical frequencies or higher, one would, of course, expect the effect of a single dislocation to be small again. At intermediate frequencies, the transition between the approximately isotropic dc regime and the anisotropic optical regime could well be accompanied by dispersion effects. A classical treatment of the electromagnetic properties of a conducting helicoid might be of value in indicating the kind of cutoffs, stop and pass bands, etc., to be expected.

The specific heat at low temperatures might also be affected by a spiral dislocation. The crystal is "clamped" in the neighborhood of the dislocation axis, but vibrations perpendicular to the lattice planes formerly constituting running waves confined to a plane now can spiral through the crystal. This might be expected to shift the vibration spectrum toward lower frequencies (as well as changing its shape), and thus to modify the reststrahlen also. Particle size effects on specific heat and elastic constants should be larger for crystals with a spiral dislocation.

It may be difficult to realize a spiral dislocation in graphite,[6] but there are many other layered crystals which occur naturally or which can be grown, for which

[1] F. C. Frank, Discussions Faraday Soc. **5**, 48 (1949).
[2] L. J. Griffin, Phil. Mag. **41**, 196 (1951).
[3] A. R. Verma and S. Amelinckx, Nature **167**, 939 (1951).
[4] A. J. Forty, Phil. Mag. **42**, 670 (1951), **43**, 481 (1952).
[5] I. M. Dawson and V. Vand, Nature **167**, 476 (1951).

[6] Spiral dislocations of the type contemplated have been observed in some graphite crystals by F. H. Horn, Nature **170**, 581 (1952).

such effects could be sought.[7] Some of these are listed in Table I. For those which are semiconductors, one arrives at conclusions similar to the conclusions of the previous discussion. With others, one would expect an anisotropic photoconductivity or extrinsic semiconductivity to tend toward isotropicity in the presence of a spiral dislocation. This "short-circuiting" of the anisotropicity might also be observed for diffusion, ionic conduction, and the like.

Note added in proof.—Many spiral dislocations have large Burgers' vectors, corresponding to axial displacement of many lattice distances. For such dislocations one has a set of interleaved helicoids rather than a single one (like a screw with a multiple thread) and similar considerations apply.

[7] CdI_2 seems like a particularly favorable case to investigate, as dislocations of the type contemplated have been much studied, e.g., A. J. Forty, reference 4, and Phil. Mag. 43, 72 and 377 (1952). Spiral dislocations in beryl and CdI_2 are reported by B. J. Applebe and H. F. Kay, Phil. Mag. 44, 105 (1953). For a general survey (with much information on SiC) and many references see A. R. Verma, *Crystal Growth and Dislocations* (Academic Press, Inc., New York, 1953).

PHYSICAL REVIEW VOLUME 95, NUMBER 2 JULY 15, 1954

Comparison of Various Approximate Exchange Potentials

FRANK HERMAN AND JOSEPH CALLAWAY,* *David Sarnoff Research Center, RCA Laboratories Division, Princeton, New Jersey*

AND

FORMAN S. ACTON, *Department of Mathematics, Princeton University, Princeton, New Jersey*

(Received April 9, 1954)

A modification of Slater's simplification of the Hartree-Fock equations is proposed, in which an averaged exchange potential is defined for each set of states having a common angular momentum. For a germanium atom we have calculated the approximate exchange potentials according to Slater's averaging procedures and according to our own, and have compared these with the usual Hartree-Fock exchange potentials.

SLATER[1] has recently shown how the Hartree-Fock equations can be approximated by a set of Schrödinger-type equations each containing the same "averaged" exchange potential. The Hartree-Fock equations as modified by Slater are more easily solved than are the original Hartree-Fock equations. It is natural to ask: is it possible to obtain approximate exchange potentials for the individual states better than the one represented by Slater's single averaged exchange potential and at the same time retain most of the simplicity and convenience of Slater's formulation?

That the exchange potentials of the states having a common angular momentum should bear a greater resemblance to each other than to the exchange potentials corresponding to states having other l was suggested to the authors by Herring.[2] Accordingly, we have defined an averaged exchange potential for each set of electronic states having a common l. Each of these averaged exchange potentials is formed from the Hartree-Fock exchange potentials belonging to the occupied states having a particular value of l.

With a view to comparing the various approximate exchange potentials, we calculated the Hartree-Fock, the Slater averaged, the s, p, and d averaged, and the free-electron exchange potentials for a germanium atom. Each of these potentials was computed from an orthonormalized set of radial wave functions $Q_{nl}(r)$ derived from the self-consistent wave functions $P_{nl}(r)$ obtained by Hartree and Hartree for the $(4s)^2(4p)^2$ state of the germanium atom.[3]

We made no attempt to determine self-consistent eigensolutions or potentials using any of the various exchange potential approximations.[4] Each of the potentials we did evaluate may be regarded as the starting potential in the first cycle of a self-consistent iteration procedure. Although a comparison of the potentials corresponding to self-consistent solutions would be more significant, we feel that some insight on the relative merits and special features of the various approximate exchange potentials may be gained by placing our potentials side by side.

The exact Hartree-Fock and the Slater averaged exchange potentials appearing in the wave equation for

* Present address: Palmer Physical Laboratory, Princeton University, Princeton, New Jersey.

[1] J. C. Slater, Phys. Rev. 81, 385 (1951).

[2] C. Herring (private communication); see also H. B. Huntington, Phys. Rev. 61, 325 (1942).

[3] W. Hartree and D. R. Hartree, Phys. Rev. 59, 306 (1941). We will express the orthonormalized wave function corresponding to state nlm in the form $\psi_{nlm}(\mathbf{r})=r^{-1}Q_{nl}(r)Y_l^m(\theta,\phi)$, where $\mathbf{r}=r,\theta,\phi$, and the $Y_l^m(\theta,\phi)$ are normalized spherical harmonics.

[4] A self-consistent solution for the Cu^+ ion has been obtained by Pratt using the free-electron approximation for the exchange potential; see G. W. Pratt, Jr., Phys. Rev. 88, 1217 (1952).

$\psi_{nlm}(\mathbf{r}_1)$ may be written as

$$V_{HF;nlm}^{\text{exch}}(\mathbf{r}_1)=\frac{\sum_{n'l'm'}\int\psi_{nlm}^*(\mathbf{r}_1)\psi_{n'l'm'}^*(\mathbf{r}_2)(2/r_{12})\psi_{n'l'm'}(\mathbf{r}_1)\psi_{nlm}(\mathbf{r}_2)d\mathbf{r}_2}{\psi_{nlm}^*(\mathbf{r}_1)\psi_{nlm}(\mathbf{r}_1)}, \quad (1)$$

and

$$V_{\text{Slater}}^{\text{exch}}(\mathbf{r}_1)=\frac{\sum_{n'l'm'}\sum_{n''l''m''}\int\psi_{n'l'm'}^*(\mathbf{r}_1)\psi_{n''l''m''}^*(\mathbf{r}_2)(2/r_{12})\psi_{n''l''m''}(\mathbf{r}_1)\psi_{n'l'm'}(\mathbf{r}_2)d\mathbf{r}_2}{\sum_{n'l'm'}\psi_{n'l'm'}^*(\mathbf{r}_1)\psi_{n'l'm'}(\mathbf{r}_1)}, \quad (2)$$

for all *nlm* [see reference 1, Eqs. (4) and (7), respectively].[5] In (1), the summation is restricted to all occupied states $n'l'm'$ having the same spin as the state *nlm*. In (2), the summations in both numerator and denominator are carried over all occupied states having the same spin as the state under consideration.

The averaged exchange potential constructed by us for the states having angular momentum l may be derived from (2) by requiring that $l'=l$ in both numerator and denominator.

The free-electron exchange potential [see reference 1, Eq. (10)] is given by

$$V_{f.e.}^{\text{exch}}(\mathbf{r}_1)=6\left[\frac{3}{4\pi}\sum_{n'l'm'}\psi_{n'l'm'}^*(\mathbf{r}_1)\psi_{n'l'm'}(\mathbf{r}_1)\right]^{\frac{1}{3}}, \quad (3)$$

for all *nlm*. The summation is confined to states having the same spin as the state being considered. Throughout this paper, distances will be measured in Bohr units, potentials, in rydbergs.

In our study of the germanium atom, we chose to deal with the ${}^4S\,(4s)^1(4p)^3$ (valence) state. The spin of each of the four valence electrons is "up." We evaluated the exchange potentials for electrons having both upward and downward spin. In Table I we list selected values of the electronic Coulomb potential $V_{\text{elec}}^{\text{coul}}(r)$, the net Coulomb potential [defined as $64/r-V_{\text{elec}}^{\text{coul}}(r)$], the free electron exchange potential $V_{f.e.}^{\text{exch}}(r)$, and the various averaged exchange potentials.

The following features of Table I should be noted: (a) The $V_l^{\text{exch}}(r)$, $l=0, 1, 2$, differ from each other at all values of r. The different behavior is significant only at moderately large values of r, where the exchange potentials have magnitudes comparable with the

TABLE I. Coulomb and approximate exchange potentials for germanium atom in ${}^4S\,(4s)^1(4p)^3$ state. The exchange potentials for electrons of spin up and down are shown at the left and right, respectively, of the appropriate columns. (The four valence electrons are all assigned upward spin.) The entries directly below the exchange potential column headings are the arithmetic means. The radial distance r is measured in Bohr units, the various potentials, in rydbergs.

r	$V_{f.e.}^{\text{exch}}(r)$	$V_{\text{Slater}}^{\text{exch}}(r)$	$V_{l=0}^{\text{exch}}(r)$	$V_{l=1}^{\text{exch}}(r)$	$V_{l=2}^{\text{exch}}(r)$	$V_{\text{net}}^{\text{Coul}}(r)$	$V_{\text{elec}}^{\text{Coul}}(r)$
0.01	67.30	62.61	62.66	45.38	36.40	6099.64	300.36
0.02	54.52	55.85	56.13	37.48	29.64	2913.52	286.48
0.05	30.67	35.21	38.52	23.19	17.65	1034.58	245.42
0.10	19.54	19.36	24.26	17.97	12.10	435.35	204.65
0.20	12.59	13.79	14.89	14.02	7.584	161.73	158.27
0.40	6.852	6.126	7.076	7.100	5.070	49.24	110.76
	7.015 6.689						
0.60	5.417	5.420	6.263	5.903	4.733	20.29	86.38
	5.527 5.307						
0.80	3.861	4.303	5.140	4.768	3.753	10.17	69.83
	3.867 3.855						
1.00	2.831	3.273	4.006	3.780	2.881	5.96	58.04
	2.921 2.741	3.257 3.290	3.822 4.190	3.754 3.806	2.888 2.874		
1.20	2.340	2.495	2.950	2.976	2.268	3.86	49.47
	2.716 1.963	2.454 2.535	2.397 3.503	2.843 3.108	2.295 2.241		
1.40	2.091	1.862	2.336	2.292	1.855	2.65	43.06
	2.746 1.436	1.724 1.999	1.643 3.029	1.944 2.639	1.907 1.803		
1.60	1.905	1.560	2.050	1.866	1.574	1.89	38.11
	2.743 1.066	1.497 1.622	1.400 2.700	1.406 2.325	1.653 1.495		
2.00	1.593	1.175	1.786	1.535	1.242	1.01	30.99
	2.575 0.612	1.188 1.163	1.258 2.313	1.092 1.978	1.371 1.113		
2.40	1.330	0.976	1.631	1.449	1.065	0.57	26.10
	2.297 0.363	1.045 0.908	1.180 2.082	0.966 1.932	1.241 0.889		

[5] The Hartree-Fock radial wave equations may be readily constructed with the aid of the information contained in D. R. Hartree and W. Hartree, Proc. Roy. Soc. (London) A156, 45 (1936). The Hartree-Fock and the Slater averaged exchange potentials appropriate to the radial wave equations for the $Q_{nl}(r)$ may be determined by writing the forms analogous to Eqs. (1) and (2), respectively.

TABLE II. Comparison of Hartree-Fock and various averaged exchange potentials. $U_{nl}^{HF}(r)$ is defined as $[Q_{nl}(r)]^2$ multiplied by the Hartree-Fock exchange potential appropriate to state nl [see Eq. (1)]. Similarly, $U_{nl}^{\text{Slater}}(r)$ is defined as $[Q_{nl}(r)]^2 V_{\text{Slater}}^{\text{exch}}(r)$, and $U_{nl}^{(l)}(r)$ as $[Q_{nl}(r)]^2 V_l^{\text{exch}}(r)$. In all cases, we have listed the exchange potentials appropriate to electron states with upward spin, i.e., with the same spin as the four valence electrons. In the case of germanium, $U_{3d}^{HF}(r)$ is identical to $U_{3d}^{(l=2)}(r)$.

r	U_{1s}^{HF}	U_{1s}^{Slater}	$U_{1s}^{(0)}$	U_{2s}^{HF}	U_{2s}^{Slater}	$U_{2s}^{(0)}$	U_{3s}^{HF}	U_{3s}^{Slater}	$U_{3s}^{(0)}$
0.01	428.7	419.3	419.6	29.71	37.28	37.31	3.863	5.237	5.241
0.02	812.1	791.9	796.0	50.93	64.01	64.34	6.507	8.935	8.981
0.05	518.2	471.3	515.7	9.580	10.69	11.70	0.9712	1.207	1.321
0.10	62.67	44.56	55.81	32.12	29.36	36.78	3.853	4.709	5.898
0.20	0.7535	0.2812	0.3035	75.55	69.61	75.15	3.597	4.045	4.367
0.40				5.162	3.507	4.039	6.488	6.476	7.458
0.60				0.2259	0.1101	0.1270	11.86	10.26	11.83
0.80				0.0109	0.0021	0.0025	5.773	4.838	5.783
1.00							1.945	1.521	1.785
1.20							0.5684	0.4007	0.3915
1.40							0.1584	0.0900	0.0496
1.60							0.0431	0.0233	0.0218
2.00							0.0034	0.0015	0.0016

r	U_{2p}^{HF}	U_{2p}^{Slater}	$U_{2p}^{(1)}$	U_{3p}^{HF}	U_{3p}^{Slater}	$U_{3p}^{(1)}$	$U_{3d}^{HF} = U_{3d}^{(2)}$	U_{3d}^{Slater}
0.01	0.2727	0.3773	0.2734	0.0379	0.0511	0.0370		
0.02	2.665	3.972	2.666	0.3604	0.5341	0.3585		
0.05	26.24	39.18	25.80	2.916	5.071	3.340	0.0314	0.0157
0.10	75.84	79.96	74.23	6.463	8.636	8.017	0.4442	0.2774
0.20	57.79	56.70	57.66	0.9620	1.067	1.085	3.931	2.161
0.40	3.172	2.264	2.622	7.373	6.792	7.865	6.895	5.707
0.60	0.1478	0.0765	0.0833	10.07	9.266	10.09	6.561	5.728
0.80	0.0094	0.0022	0.0025	5.246	4.740	5.252	3.877	3.379
1.00				1.994	1.715	1.976	1.936	1.718
1.20				0.6936	0.5415	0.6273	0.8982	0.8403
1.40				0.2337	0.1473	0.1662	0.3818	0.4222
1.60				0.0775	0.0462	0.0434	0.1939	0.2140
2.00				0.0091	0.0044	0.0040	0.0502	0.0580

net Coulomb potential. (b) $V_{\text{Slater}}^{\text{exch}}(r)$ resembles $V_{l=0}^{\text{exch}}(r)$ at small r, as expected. (c) $V_{\text{f.e.}}^{\text{exch}}(r)$ approximates $V_{\text{Slater}}^{\text{exch}}(r)$ remarkably well at small and intermediate values of r.

In Table II we have listed selected values of the various exchange potentials (for states having spin up) multiplied by $[Q_{nl}(r)]^2$, $nl = 1s \cdots 3d$.

An inspection of Table II reveals that the Hartree-Fock exchange potentials are approximated more closely by the $V_l^{\text{exch}}(r)$ than by $V_{\text{Slater}}^{\text{exch}}(r)$ for most of the core states over most of the range of r.

As expected, the results indicate that our modification of Slater's treatment of the Hartree-Fock equations yields better approximate exchange potentials for the core states than Slater's single averaged exchange potential. The fact that the free electron exchange potential resembles $V_{\text{Slater}}^{\text{exch}}(r)$ so well (see Table I) bears out Slater's view[1] that the exchange potential depends more upon the local charge density than upon the detailed nature of the wave functions of the occupied states.[6]

The authors wish to express their appreciation to Dr. D. O. North of the RCA Laboratories for his interest, encouragement, and counsel during the course of this work. The authors are grateful to Dr. L. P. Smith and Mr. R. Serrell of the RCA Laboratories and to Dr. C. Herring of the Bell Telephone Laboratories for valuable criticism.

The numerical computations were performed on an IBM Card-Programmed Calculator at the Computation Laboratory of the James Forrestal Research Center, Princeton University, as part of an investigation of the energy band structure of the germanium crystal being conducted by one of us (F.H.). The authors wish to thank Mr. R. H. Goerss and Mr. J. G. C. Templeton of Forrestal for carrying out the machine computations.

[6] A comparison of Slater's averaged exchange potential and the free-electron exchange potential has recently been made by H. J. Juretschke, Phys. Rev. 92, 1140 (1953) for the case of the surface region of a free-electron metal.

Centrifugal Distortion in Asymmetric Top Molecules. III. H_2O, D_2O, and HDO†

D. W. POSENER* AND M. W. P. STRANDBERG
Department of Physics and Research Laboratory of Electronics, Massachusetts Institute of Technology, Cambridge, Massachusetts

(Received March 1, 1954)

Structural and potential constants obtained from infrared data are used with the theory of vibration-rotation interaction to obtain rotational and distortion parameters for the molecules H_2O, D_2O, and HDO; transition frequencies calculated using these parameters are compared with those observed in the microwave region, and, in the case of HDO Q-branch lines, a simple relation between the two sets is obtained. The validity of approximation theories as applied to HDO Q-branch transitions is discussed. Methods of analyzing the observed spectrum of HDO are described, and so-called "observed" parameters for this molecule are obtained; the rotational constants are found to be $a=7.0396\pm0.0005\times10^5$ Mc/sec, $b=2.7360\pm0.0005\times10^5$ Mc/sec, $c=1.9186\pm0.0005\times10^5$ Mc/sec, $\kappa=-0.6841\pm0.0002$.

1. INTRODUCTION

THE careful investigation of the infrared spectrum of water by a number of workers[3–7] has led to its rotational spectrum becoming probably the most thoroughly studied of any asymmetric top molecule. Moreover, its equilibrium structure and force constants, through quartic terms, are also known to various degrees of accuracy, from analysis of the vibrational spectrum.

This molecule, familiar to all, and simple enough at first sight, shows many interesting and complicated effects in its spectrum. Not the least of these arises from the fact that the molecule is so light that vibration and rotation cause comparatively large distortion of the equilibrium structure, and this has to be taken into account in any detailed description of the spectrum.

Contributions to the theory of centrifugal distortion in polyatomic molecules have been made by a number of authors,[8–16] but only a very little comparison with experiment has been carried out because most molecules are so heavy that the effects of centrifugal distortion in their spectra are almost negligible. The distortion effects observable in the water spectrum are so large, however, that a detailed check of the theory is possible in this case; the microwave method is particularly suited to such a study because its accurate frequency measurements immediately show up small perturbations (centrifugal distortion is, after all, a high-order effect). The present work is a contribution to such an investigation.

A number of microwave absorption lines due to some isotopic modifications of water have been reported by various workers.[17–24] Many of these transitions were found either by chance or as the result of searching in the general region of the positions predicted from infrared data. Tables[25] of such predictions are particularly useful in the case of HDO, although based on rigid rotor calculations, because distortion effects in adjacent energy levels partially cancel and thus observed a-type Q-branch transitions are found fairly close to the predicted rigid values. Moreover the relative abundance of HDO Q-branch lines in the microwave region makes this isotopic variety a much more useful subject for study than H_2O or D_2O, since more information can be extracted from it. Accordingly,

† Supported in part by the Signal Corps, the Air Materiel Command, and the U. S. Office of Naval Research, and in part by a grant from the Commonwealth Scientific and Industrial Research Organization, Australia. A detailed account is given in reference 1; a preliminary report appeared as reference 2.

* Present address: Division of Electrotechnology, Commonwealth Scientific and Industrial Research Organization, Sydney, Australia.

[1] D. W. Posener, Massachusetts Institute of Technology Research Laboratory of Electronics Technical Report No. 255, May 14, 1953 (unpublished).
[2] D. W. Posener and M. W. P. Strandberg, J. Chem. Phys. **21**, 1401 (1953).
[3] Randall, Dennison, Ginsburg, and Weber, Phys. Rev. **52**, 160 (1937).
[4] Fuson, Randall, and Dennison, Phys. Rev. **56**, 982 (1939).
[5] B. T. Darling and D. M. Dennison, Phys. Rev. **57**, 128 (1940).
[6] H. H. Nielsen, Phys. Rev. **59**, 565 (1941).
[7] G. W. King, J. Chem. Phys. **15**, 85 (1947).
[8] E. B. Wilson, Jr., and J. B. Howard, J. Chem. Phys. **4**, 260 (1936); E. B. Wilson, Jr., J. Chem. Phys. **4**, 313 (1936); E. B. Wilson, Jr., J. Chem. Phys. **4**, 526 (1936); E. B. Wilson, Jr., J. Chem. Phys. **5**, 617 (1937).
[9] W. H. Shaffer and H. H. Nielsen, Phys. Rev. **56**, 188 (1939).
[10] H. H. Nielsen, Phys. Rev. **60**, 794 (1941); H. H. Nielsen, Phys. Rev. **61**, 540 (1942).
[11] W. H. Shaffer and R. P. Schuman, J. Chem. Phys. **12**, 504 (1944).
[12] R. B. Lawrance and M. W. P. Strandberg, Phys. Rev. **83**, 363 (1951).
[13] R. E. Hillger and M. W. P. Strandberg, Phys. Rev. **83**, 575 (1951).
[14] H. H. Nielsen, Revs. Modern Phys. **23**, 90 (1951).
[15] D. Kivelson and E. B. Wilson, Jr., J. Chem. Phys. **20**, 1575 (1952).
[16] D. Kivelson and E. B. Wilson, Jr., J. Chem. Phys. **21**, 1229 (1953).
[17] C. H. Townes and F. R. Merritt, Phys. Rev. **70**, 558 (1946).
[18] Golden, Wentink, Hillger, and Strandberg, Phys. Rev. **73**, 92 (1948).
[19] Strandberg, Wentink, Hillger, Wannier, and Deutsch, Phys. Rev. **73**, 188 (1948).
[20] M. W. P. Strandberg, J. Chem. Phys. **17**, 901 (1949).
[21] D. W. Posener, Massachusetts Institute of Technology Research Laboratory of Electronics Quarterly Progress Reports: July 15, 1952, p. 28; October 15, 1952, p. 20; January 15, 1953 (unpublished), p. 14.
[22] C. I. Beard and D. R. Bianco, J. Chem. Phys. **20**, 1488 (1952).
[23] Jen, Bianco, and Massey, J. Chem. Phys. **21**, 520 (1953).
[24] Weisbaum, Beers, and Herrmann, Phys. Rev. **90**, 338 (1953); Y. Beers and S. Weisbaum, Phys. Rev. **91**, 1014 (1953); S. Weisbaum and Y. Beers (private communication).
[25] King, Hainer, and Cross, Phys. Rev. **71**, 433 (1947); hereafter referred to as KHC II.

the present work is concerned primarily with the HDO microwave spectrum and its analysis.

An attempt at such an analysis has previously been made,[26] but inadequacy of the then known data prevented it from being very successful. Concurrently with the present work, Weisbaum and Beers have investigated this problem and published a preliminary report;[24] their results will be discussed below.

2. ROTATIONAL ENERGIES OF MOLECULES

Nielsen[10,14] has derived expressions for the energies of the general vibrating-rotating molecule. We wish to express some of his results in terms of the phase choice of KHC I;[27] our notation is similar to that of reference 14, though we have made minor alterations; the details of some of our equations do, however, differ somewhat from those given in the works cited.

We use a central-force coordinate system in which to express the potential energy. Let s_{ij} and s_{ij}^e be the distance and equilibrium distance, respectively, between the i-th and j-th nuclei in the molecule, and let $r_{ij}=s_{ij}-s_{ij}^e$ be the "relative displacement" from equilibrium. The potential energy, through cubic terms, may be written $V=V_0+V_1$, where V_0 is the quadratic term and V_1 the cubic term. For the water-type molecule, numbering the central (oxygen) nucleus "1," and writing $r_1, r_2, r_3 \equiv r_{12}, r_{13}, r_{23}$, respectively, we have:

$$V_0=K_{11}(r_1^2+r_2^2)+K_{33}r_3^2+2K_{12}r_1r_2+2K_{13}(r_1+r_2)r_3$$
$$=\tfrac{1}{2}\textstyle\sum_s \omega_s^2Q_s^2=\tfrac{1}{2}\hbar\sum_s \omega_s q_s^2, \tag{1}$$

where Q_s is the s-th normal coordinate, $\omega_s=2\pi\nu_s=2\pi c\tilde{\nu}_s$ is the sth normal angular frequency, and $q_s=(\omega_s/\hbar)^{\frac{1}{2}}Q_s$. The cubic term is

$$V_1=K_{111}(r_1^3+r_2^3)+K_{112}r_1r_2(r_1+r_2)+K_{113}r_3(r_1^2+r_2^2)$$
$$+K_{133}r_3^2(r_1+r_2)+K_{333}r_3^3+K_{123}r_1r_2r_3$$
$$=\sum_{s\le s'\le s''} k_{ss's''}Q_sQ_{s'}Q_{s''}=\sum_{ss's''} k_{ss's''}q_sq_{s'}q_{s''}. \tag{2}$$

By neglecting effects due to the electronic contribution to the rotational energy,[28] and omitting discussion of degeneracies, Coriolis, and other vibrational effects (which do not interfere with the ground states of the molecules under discussion), the rotational energies, to the second order of perturbation theory, may be obtained as follows.

The Hamiltonian is

$$H_R=\tfrac{1}{2}\textstyle\sum_{gg'}\sigma_{gg'}{}^vP_gP_{g'}$$
$$+\tfrac{1}{4}\textstyle\sum_{gg'g''g'''}\tau_{gg'g''g'''}P_gP_{g'}P_{g''}P_{g'''}, \tag{3}$$

where

$$\sigma_{gg'}{}^v=(\delta_{gg'}/I_{gg'}{}^e)-\textstyle\sum_s(v_s+\tfrac{1}{2})b_s^{(gg')},$$
$$\tau_{gg'g''g'''}=-\tfrac{1}{2}(1/I_{gg}{}^eI_{g'g'}{}^eI_{g''g''}{}^eI_{g'''g'''}{}^e)$$
$$\times\textstyle\sum_s(a_s^{(gg')}a_s^{(g''g''')})/\omega_s^2,$$
$$b_s^{(gg')}=(1/I_{gg}{}^eI_{g'g'}{}^e)(\hbar/\omega_s) \tag{4}$$
$$\times[A_{ss}^{(gg')}-\textstyle\sum_{g''}(a_s^{(gg'')}a_s^{(g'g'')})/I_{g''g''}{}^e$$
$$-4\textstyle\sum_{s'}\zeta_{ss'}^{(g)}\zeta_{ss'}^{(g')}\omega_s^2/(\omega_s^2-\omega_{s'}^2)$$
$$-3\omega_s\textstyle\sum_{s'}k_{sss'}a_{s'}^{(gg')}/(\hbar\omega_{s'})^{\frac{1}{2}}].$$

Here g, g', etc., stand for x, y, z in the equilibrium principal axis system, $I_{gg'}{}^e$ is an equilibrium moment or product of inertia, P_g is the component of total angular momentum along the g-th axis, the v_s are vibrational quantum numbers defining the vth vibrational state, $\delta_{gg'}$ is the Kronecker delta, and $a_s^{(gg')}$, $A_{ss}^{(gg')}$, and $\zeta_{ss'}^{(g)}$ have been defined elsewhere.[1,14]

Since the $b_s^{(gg')}$ are small, we may write

$$I_{gg'}{}^v=1/\sigma_{gg'}{}^v\approx I_{gg}{}^e[\delta_{gg'}+I_{gg}{}^e\textstyle\sum_s(v_s+\tfrac{1}{2})b_s^{(gg')}],$$

from which a useful expression for the inertia defect[5] of a planar molecule can be obtained. With the usual convention $I_{aa}\leqslant I_{bb}\leqslant I_{cc}$, and with

$$\Delta_v=I_{cc}{}^v-I_{aa}{}^v-I_{bb}{}^v, \tag{5}$$

it is easily shown that

$$\Delta_v\approx-\textstyle\sum_s(v_s+\tfrac{1}{2})(\hbar/\omega_s)\{(a_s^{(cc)})^2/I_{cc}{}^e$$
$$-[(a_s^{(aa)})^2+(a_s^{(ab)})^2]/I_{aa}{}^e$$
$$-[(a_s^{(bb)})^2+(a_s^{(ab)})^2]/I_{bb}{}^e$$
$$+4\textstyle\sum_{s'}(\zeta_{ss'}^{(c)})^2\omega_s^2/(\omega_s^2-\omega_{s'}^2)\}. \tag{6}$$

For the water molecule this approximation is good to a few percent.[1]

In a symmetric top representation, with the phase choice of KHC I, the matrix elements of the Hamiltonian (3) become:

$$(K|H_R|K)=R_0+R_2K^2-D_KK^4,$$
$$(K|H_R|K\pm1)=[g(J,K\pm1)]^{\frac{1}{2}}(2K\pm1)\{\tfrac{1}{2}(B_{yz}{}^v\pm iB_{zx}{}^v)$$
$$+(R_8^{(x)}\pm iR_8^{(y)})J(J+1)$$
$$+(R_9^{(x)}\pm iR_9^{(y)})[K^2+(K\pm1)^2]\},$$
$$(K|H_R|K\pm2)=[g(J,K\pm1)g(J,K\pm2)]^{\frac{1}{2}}\{(R_4\pm iR_4')$$
$$-(R_5\pm iR_5')[K^2+(K\pm2)^2]\}, \tag{7}$$
$$(K|H_R|K\pm3)=[g(J,K\pm1)g(J,K\pm2)g(J,K\pm3)]^{\frac{1}{2}}$$
$$\times(2K\pm3)(R_7^{(y)}\pm iR_7^{(x)}),$$
$$(K|H_R|K\pm4)=[g(J,K\pm1)g(J,K\pm2)g(J,K\pm3)$$
$$\times g(J,K\pm4)]^{\frac{1}{2}}(R_6\pm iR_6'),$$

[26] W. H. Lewis, thesis, Massachusetts Institute of Technology, 1951 (unpublished).

[27] King, Hainer, and Cross, J. Chem. Phys. **11**, 27 (1943); hereafter referred to as KHC I.

[28] B. F. Burke and M. W. P. Strandberg, Phys. Rev. **90**, 303 (1953).

where

$$\begin{aligned} R_0&=\tfrac{1}{2}(B_{xx}^{v}+B_{yy}^{v})J(J+1)-D_J J^2(J+1)^2,\\ R_2&=B_{zz}^{v}-\tfrac{1}{2}(B_{xx}^{v}+B_{yy}^{v})-D_{JK}J(J+1),\\ R_4&=\tfrac{1}{4}(B_{yy}^{v}-B_{xx}^{v})+\delta_J J(J+1),\\ R_4'&=\tfrac{1}{2}B_{xy}^{v}+\delta_J' J(J+1), \end{aligned} \tag{8}$$

$$B_{gg'}^{v}=\tfrac{1}{2}\hbar^2\sigma_{gg'}^{v(\mathrm{eff})}=\hbar^2/2I_{gg'}^{v(\mathrm{eff})}, \tag{9}$$

$$\sigma_{gg'}^{v(\mathrm{eff})}=\sigma_{gg'}^{v}-D_{gg'},$$

$$g(J,K\pm1)=J(J+1)-K(K\pm1), \tag{10}$$

and

$$\begin{aligned} D_{xx}&=\beta(\tau_{zzzz}+\tau_{yyyy}-2\tau_{zzyy}+4\tau_{xyxy}\\ &\qquad -12\tau_{yzyz}+8\tau_{xzxz}),\\ D_{yy}&=\beta(\tau_{zzzz}+\tau_{yyyy}-2\tau_{zzyy}+4\tau_{xyxy}\\ &\qquad +8\tau_{yzyz}-12\tau_{xzxz}),\\ D_{zz}&=-\tfrac{3}{4}(D_{xx}+D_{yy})+5\beta(\tau_{yzyz}+\tau_{xzxz}),\\ D_{xy}&=20\beta\tau_{yzxz},\\ D_{yz}&=-5\beta(\tau_{yzzz}-\tau_{yzyy}-2\tau_{xyxz}),\\ D_{xz}&=5\beta(\tau_{xzzz}-\tau_{xzyy}+2\tau_{xyyz}),\\ D_J&=-2\beta^2(3\tau_{zzzz}+3\tau_{yyyy}+2\tau_{zzyy}+4\tau_{zyzy}),\\ D_K&=D_J-16\beta^2(\tau_{zzzz}-\tau_{xxzz}-\tau_{yyzz}-2\tau_{yzyz}-2\tau_{xzxz}),\\ D_{JK}&=-D_J-D_K-16\beta^2\tau_{xzzz},\\ \delta_J&=-4\beta^2(\tau_{xzzz}-\tau_{yyyy}),\\ \delta_J'&=8\beta^2(\tau_{xzzy}+\tau_{yyxy}),\\ R_5&=-2\beta^2(\tau_{xzzz}-\tau_{yyyy}+2\tau_{yyzz}-2\tau_{zzzz}\\ &\qquad +4\tau_{yzyz}-4\tau_{xzxz}),\\ R_5'&=4\beta^2(\tau_{zzzy}+\tau_{yyzy}-2\tau_{xxzy}-4\tau_{yzxz}),\\ R_6&=\beta^2(\tau_{zzzz}+\tau_{yyyy}-2\tau_{zzyy}-4\tau_{zyzy}),\\ R_6'&=-4\beta^2(\tau_{zzzy}-\tau_{yyzy}),\\ R_7^{(x)}&=-4\beta^2(\tau_{zzzx}-\tau_{xzyy}-2\tau_{zyyz}),\\ R_7^{(y)}&=-4\beta^2(\tau_{zyzz}-\tau_{zyyy}+2\tau_{zyxz}),\\ R_8^{(x)}&=4\beta^2(\tau_{yzzz}+3\tau_{yzyy}+2\tau_{zyxz}),\\ R_8^{(y)}&=4\beta^2(3\tau_{xzzz}+\tau_{xzyy}+2\tau_{xyyz}),\\ R_9^{(x)}&=-R_8^{(x)}+8\beta^2\tau_{yzzz},\\ R_9^{(y)}&=-R_8^{(y)}+8\beta^2\tau_{xzzz}, \end{aligned} \tag{11}$$

$$\tag{12}$$

in which $\beta=\hbar^2/8$.

The effective reciprocal moments B_{gg}^{v} are usually denoted by a, b, and c, and ordered so that $a\leqslant b\leqslant c$. "Off-diagonal" terms may appear in molecules of low symmetry, e.g., HDO. For the latter molecule, in a I^r representation, the $b_s^{(xz)}$ are nonvanishing, and a B_{xz}^{v} exists; then the first term of the Hamiltonian is not a sum of squares, but can be made so by a simple rotation of axes (which also mixes up the τ's of the second term).[1,8]

Following the notation of KHC I, we can rewrite certain terms in the rotational matrix (7) thus:

$$\begin{aligned} R_0&=\tfrac{1}{2}(a+c)J(J+1)+\tfrac{1}{2}(a-c)FJ(J+1)\\ &\qquad -D_J^2(J+1)^2,\\ R_2&=\tfrac{1}{2}(a-c)(G-F)-D_{JK}J(J+1),\\ R_4&=\tfrac{1}{4}(a-c)H+\delta_J J(J+1), \end{aligned} \tag{13}$$

where, for a I^r representation, $F=\frac{1}{2}(\kappa-1)$, $G-F=-\frac{1}{2}(\kappa-3)$, $H=-\frac{1}{2}(\kappa+1)$, and $\kappa=(2b-a-c)/(a-c)$.

For the particular case of HDO in a I^r representation, after transforming the $B_{gg'}^{v}$ to principal axes, it is convenient to write

$$H_R=\tfrac{1}{2}(a+c)J(J+1)-D_J J^2(J+1)^2+\tfrac{1}{2}(a-c)E, \tag{14}$$

where E is the *reduced energy matrix* with elements

$$\begin{aligned} E_{K\,K}&=FJ(J+1)\\ &\quad+[(G-F)-D_{JK}J(J+1)]K^2-D_K K^4,\\ E_{K\,K\pm1}&=\pm i[g(J,K\pm1)]^{\frac{1}{2}}(2K\pm1)\{\tfrac{1}{2}R_7^{(x)}\\ &\quad+R_8^{(y)}J(J+1)+R_9^{(y)}[K^2+(K\pm1)^2]\},\\ E_{K\,K\pm2}&=[g(J,K\pm1)g(J,K\pm2)]^{\frac{1}{2}}\{\tfrac{1}{2}H+\delta_J J(J+1)\\ &\quad-R_5[K^2+(K\pm2)^2]\},\\ E_{K\,K\pm3}&=\pm i[g(J,K\pm1)g(J,K\pm2)\\ &\quad\times g(J,K\pm3)]^{\frac{1}{2}}(2K\pm3)R_7^{(x)},\\ E_{K\,K\pm4}&=[g(J,K\pm1)g(J,K\pm2)\\ &\quad\times g(J,K\pm3)g(J,K\pm4)]^{\frac{1}{2}}R_6, \end{aligned} \tag{15}$$

in which D_{JK}, D_K, δ_J, R_5, R_6, $R_7^{(x)}$, $R_8^{(y)}$, and $R_9^{(y)}$ now stand for the original distortion constants divided by $\frac{1}{2}(a-c)$; they are the *reduced distortion constants*. The above result is equally applicable to H_2O and D_2O, but the vanishing of $R_7^{(x)}$, $R_8^{(y)}$, and $R_9^{(y)}$ for these molecules very considerably simplifies computational problems.

It is apparent that the major complexity of the problem lies in the reduced energy matrix. This can be transformed to a basis of Wang functions, using the transformation X of KHC I in the usual manner. In the presence of $(K|K\pm1)$ and $(K|K\pm3)$ elements, the resulting matrix can now be factored into two submatrices only, corresponding to symmetric (+) and antisymmetric (−) Wang functions, and these submatrices are of order $J+1$ and J, respectively; they

take the forms

$$(+)=\begin{pmatrix} H_{00} & H_{01} & H_{02} & H_{03} & H_{04} & 0 & 0 & \cdots & \cdots \\ H_{10} & H_{11}^{+} & H_{12}^{+} & H_{13}^{+} & H_{14} & H_{15} & 0 & \cdots & \cdots \\ H_{20} & H_{21}^{+} & H_{22}^{+} & H_{23} & H_{24} & H_{25} & H_{26} & \cdots & \cdots \\ H_{30} & H_{31}^{+} & H_{32} & H_{33} & H_{34} & H_{35} & H_{36} & \cdots & \cdots \\ H_{40} & H_{41} & H_{42} & H_{43} & H_{44} & H_{45} & H_{46} & \cdots & \cdots \\ 0 & H_{51} & H_{52} & H_{53} & H_{54} & H_{55} & H_{56} & \cdots & \cdots \\ 0 & 0 & H_{62} & H_{63} & H_{64} & H_{65} & H_{66} & \cdots & \cdots \\ \cdots & \cdots & \cdots & \cdots & \cdots & \cdots & \cdots & \cdots & \cdots \\ \cdots & \cdots & \cdots & \cdots & \cdots & \cdots & \cdots & \cdots & \cdots \end{pmatrix},$$

$$(-)=\begin{pmatrix} H_{11}^{-} & H_{12}^{-} & H_{13}^{-} & H_{14} & H_{15} & 0 & \cdots & \cdots \\ H_{21}^{-} & H_{22}^{-} & H_{23} & H_{24} & H_{25} & H_{26} & \cdots & \cdots \\ H_{31}^{-} & H_{32} & H_{33} & H_{34} & H_{35} & H_{36} & \cdots & \cdots \\ H_{41} & H_{42} & H_{43} & H_{44} & H_{45} & H_{46} & \cdots & \cdots \\ H_{51} & H_{52} & H_{53} & H_{54} & H_{55} & H_{56} & \cdots & \cdots \\ 0 & H_{62} & H_{63} & H_{64} & H_{65} & H_{66} & \cdots & \cdots \\ \cdots & \cdots & \cdots & \cdots & \cdots & \cdots & \cdots & \cdots \\ \cdots & \cdots & \cdots & \cdots & \cdots & \cdots & \cdots & \cdots \end{pmatrix}, \quad (16)$$

where

$$H_{0\,K}=2^{\frac{1}{2}}E_{0\,K}, \quad (K=1,2,3,4)$$
$$H_{K\,K'}{}^{\pm}=E_{K\,K'}\pm E_{-K\,K'}, \quad (17)$$

and otherwise

$$H_{K\,K'}=E_{K\,K'}.$$

Here

$$E_{-K\,-K-1}=E_{K\,K+1}, \qquad E_{-K\,-K+1}=E_{K\,K-1},$$
$$E_{K+1\,K}=-E_{K\,K+1}, \qquad E_{K+3\,K}=-E_{K\,K+3}, \quad (18)$$

etc.

Although these matrices may present a formidable appearance for large J values, they can be handled, for computation purposes, by an extension of the continued-fraction method described by KHC I for the rigid rotor case; a detailed account of the procedure is given in Appendix D of reference 1.[29]

3. THEORETICAL PARAMETERS

Our "theoretical" computations are based on the following geometrical model of the water molecule:[30] $r_{OH}=0.9584\times10^{-8}$ cm, $\angle HOH=104°27'$. For atomic masses we take $m(H)=1.67341233\times10^{-24}$ g, $m(D)=3.34428232\times10^{-24}$ g, $m(O^{16})=26.55872000\times10^{-24}$ g. As fundamental constants we use[31] $c=2.9979\times10^{10}$ cm/sec, $h=6.62363\times10^{-27}$ erg sec. On the assumption that the equilibrium geometry and the potential constants are invariant to isotopic substitution, the latter constants may be obtained from infrared data;[5,32] using the normal "frequencies" (in cm^{-1}): H_2O, $\bar{\nu}_1=3825.32$, $\bar{\nu}_2=1653.91$, $\bar{\nu}_3=3935.59$; D_2O, $\bar{\nu}_1=2758.06$, $\bar{\nu}_2=1210.25$, $\bar{\nu}_3=2883.79$, we obtain (in dyne/cm$\times10^5$) $K_{11}=9.04949641$, $K_{12}=0.52397791$, $K_{13}=-1.20497839$, $K_{33}=2.04835571$. Reference 5 also gives the cubic constants for H_2O (in cm^{-1}), $\alpha_1=-322$, $\alpha_2=-47$, $\alpha_3=1$, $\alpha_4=216$, $\alpha_5=-909$, $\alpha_6=160$; these are related to our $k_{ss'a''}$ according to $k_{111}=hc\alpha_1$, $k_{112}=k_{121}=k_{211}=-hc\alpha_3/3$, $k_{122}=k_{212}=k_{221}=hc\alpha_4/3$, $k_{133}=k_{313}=k_{331}=hc\alpha_5/3$, $k_{233}=k_{323}=k_{332}=-hc\alpha_6/3$, $k_{222}=-hc\alpha_2$; from them we get (in dyne/cm$^2\times10^{12}$) $K_{111}=-84.56753212$, $K_{112}=57.47345798$, $K_{113}=-35.92925361$, $K_{133}=24.61366648$, $K_{333}=-2.51799700$, $K_{123}=-96.56701865$.

Here, as in the sequel, parameters are frequently quoted to significant figures far in excess of the accuracy warranted by the data (for example, the cubic potential constants are known to perhaps one significant figure only). However, it appears to be undesirable to attempt to work only to estimated accuracies since this may easily lead to a rounding-off errors. Accordingly, we quote here the actual numbers used in our computations.

A detailed listing of intermediate quantities is given in reference 1. Here we record only those parameters which enter directly into the rotational matrix; Table I shows these (in a I^r representation).

TABLE I. "Theoretical" parameters. (a) Before principal axis transformation. (b) After principal axis transformation.

	H_2O	D_2O	HDO (a)	HDO (b)
	Effective rotation constants (Mc/sec $\times10^5$)			
a	8.3172247	4.6128487	6.97845341	6.97876766
b	4.3413336	2.1741669	2.72550273	2.72522145
c	2.7779216	1.4504848	1.91859173	1.91863695
$d=B_{zz}{}^{\rho}$	0	0	−0.03262965	0
	Inertia defect (g cm$^2\times10^{-40}$)			
Δ_0	0.07609087	0.10381619	0.08676075	0.08676075
	Asymmetry parameter			
κ	−0.43552032	−0.54231577	−0.68105413	−0.68120013
	Distortion constants (Mc/sec)			
D_J	28.92348858	7.45681896	9.01676826	9.14172899
D_K	729.36580935	225.00743493	279.94933771	287.08933921
D_{JK}	−112.71978845	−32.66381366	41.47209724	36.81321390
δ_J	14.00262952	3.46850038	3.24683339	3.33311881
R_3	31.16163450	8.12053047	9.03150455	−7.87718656
R_4	−3.05588799	−0.69525362	−0.54839883	−0.57220390
$R_7{}^{(x)}$	0	0	3.05952301	3.11603472
$R_8{}^{(y)}$	0	0	−8.00882857	−9.19943988
$R_9{}^{(y)}$	0	0	50.81694501	49.91730954

[29] For an effectively similar treatment in the case of vanishing $(K|K\pm1)$ and $(K|K\pm3)$ matrix elements, see also B. L. Crawford, Jr., and P. C. Cross, J. Chem. Phys. **5**, 621 (1937).

[30] G. Herzberg, *Infrared and Raman Spectra of Polyatomic Molecules* (D. Van Nostrand Company, Inc., New York, 1945), p. 489.

[31] J. A. Bearden and H. M. Watts, Phys. Rev. **81**, 73 (1951).

[32] W. H. Shaffer and R. R. Newton, J. Chem. Phys. **10**, 405 (1942).

TABLE II. H_2O microwave absorption lines.

Transition	Observed	Frequency (Mc/sec) KHC II	RDGW[a]	"Theoretical" (this work)
$2_{20}\rightarrow3_{13}$	...	184 000	182 000	187 471
$5_{23}\rightarrow6_{16}$	22 235.22±0.05	23 380	20 400	24 588

[a] See reference 3.

4. MICROWAVE SPECTRUM OF H_2O

The K-band "radar water line" at 22 235 Mc/sec,[17,18] because of the $5_{23}\rightarrow6_{16}$ transition of H_2O, has been observed by a number of workers, and is the only microwave line known to belong to this molecule.

Examination of the KHC II tables shows that no other H_2O lines are likely to be found below about 180 000 Mc/sec ($2_{20}\rightarrow3_{13}$ transition); the difficulties of working in this region, however, make it desirable that a better prediction be available before searching is carried out. The one known H_2O line does not give us enough information to improve our knowledge—the KHC II tables, based on $\kappa=-0.436426$, predict it at the rigid rotor frequency of 23 400 Mc/sec, some 1000 Mc/sec too high, and the term values of reference 3 show it at 20 400 Mc/sec, so it is apparent that better parameters are needed. The present work shows no better agreement with experiment; with the parameters of Table I our calculations give the results shown in Table II.

We will show in Sec. 6 that we can expect the "theoretical" parameters to give a good estimate of the distortion, so it is interesting to compare our calculated energy levels with those of RDGW,[3] as in Table III; here the "distortion correction" is the total energy (as shown) minus the calculated rigid rotor energy.

There is little else we can say about H_2O at present, but it is hoped that eventually better values of the parameters will be deducible from the results of investigations of other isotopic modifications.

5. MICROWAVE SPECTRUM OF D_2O

The $2_{20}\rightarrow3_{13}$ and $5_{32}\rightarrow4_{41}$ transitions of D_2O were found in the course of a general search,[21] though only the first of these was identified; both lines were subsequently reported independently.[22] Their frequencies, together with those calculated from the parameters of Table I, are shown in Table IV.

TABLE III. H_2O energy levels.

Level	RDGW[a] Energy (Mc/sec ×10⁶)	RDGW[a] Distortion correction (Mc/sec ×10⁶)	This work Energy (Mc/sec ×10⁶)	This work Distortion correction (Mc/sec ×10⁶)
2_{20}	4.080100	−0.004800	4.066769	−0.008787
3_{13}	4.262100	−0.001500	4.254240	0.001449
5_{23}	13.386000	−0.026382	13.352540	−0.040304
6_{16}	13.407000	−0.015000	13.377127	0.025789

[a] See reference 3.

In the FRD work, distortion corrections were obtained semiclassically; in Table V we compare the distortion corrections calculated here with those given by FRD.

It is expected that additional useful work can be done on D_2O. Two weak lines in the water spectrum have been observed[23] at 30 182.57±0.1 and 30 778.62 ±0.1 Mc/sec, and these are as yet unidentified. In the next section we investigate probable HDO transitions, and find none in this region, though these calculations are not conclusive. Thus there is a good chance that these two lines may be due to D_2O.

6. MICROWAVE SPECTRUM OF HDO

A. Introduction

Until recently there has been little infrared work carried out on HDO because of the difficulty of untangling its lines from those of H_2O and D_2O. From one such infrared analysis, however, KHC II deduced $\kappa=-0.685$, from which they constructed their rigid rotor tables of expected HDO microwave transitions.

TABLE IV. D_2O microwave absorption lines.

Transition	Observed	Frequency (Mc/sec) FRD[a]	"Theoretical"[b]
$2_{20}\rightarrow3_{13}$	10 919.39±0.05[b] 10 919.8 ±0.1[c]	7500	10 670
$5_{32}\rightarrow4_{41}$	10 947.13±0.05[b] 10 947.4 ±0.1[c]	16 000	17 472

[a] The KHC II tables give rigid rotor term values taken from FRD (reference 4); in Tables IV and V we quote the FRD "corrected" levels.
[b] This work.
[c] Reference 22.

Previous to this publication, the only microwave line of HDO known was the $5_{33}\rightarrow5_{32}$ transition.[17,19] On the basis of these tables, however, Strandberg[20] located the $2_{21}\rightarrow2_{20}$, $3_{22}\rightarrow3_{21}$, and $4_{14}\rightarrow3_{21}$ lines, and estimated $\kappa=-0.696$.

Three other lines were then found by workers in this Laboratory[33]; the $4_{32}\rightarrow4_{31}$ line, the $7_{44}\rightarrow7_{43}$ line, and an unidentified line at 26 880 Mc/sec. During the present investigations the latter was found to have been originally discovered by McAfee[34] who assigned it to a D_2O transition; it is the conclusion of this work that it is the $6_{24}\rightarrow7_{17}$ transition of HDO.

Concurrently with the present work, Weisbaum and Beers[24] discovered a number of lines in the S-band region, and identified the transitions $6_{43}\rightarrow6_{42}$, $9_{55}\rightarrow9_{54}$, $12_{67}\rightarrow12_{66}$, and $4_{22}\rightarrow5_{05}$; we were advised of these investigations privately, though the final identity of

[33] Microwave Spectroscopy Laboratory, Research Laboratory of Electronics, Massachusetts Institute of Technology (unpublished work).
[34] K. B. McAfee, Jr., Doctoral thesis, Harvard, 1949 (unpublished).

the lines was not reasonably certain until a late stage in the present work.

We have now observed the $8_{45}\rightarrow 8_{44}$, $10_{56}\rightarrow 10_{55}$, and $11_{57}\rightarrow 11_{56}$ transitions.

The $8_{45}\rightarrow 8_{44}$ line has been independently reported,[23] and these workers also conclude from the Stark effect that the 26 880-Mc/sec line is to be assigned to the HDO $6_{24}\rightarrow 7_{17}$ transition.

The present state of experimental knowledge of the HDO microwave spectrum is summarized in Table VI.

B. "Theoretical" Frequencies

In principal, transition frequencies may be calculated by diagonalization of the rotational matrix to find the appropriate energy levels, then taking differences. We call this "exact" calculation, though in practice it may involve finding characteristic values by numerical approximation method; in our computations we have used sufficient significant figures to get within the experimental error.

TABLE V. D_2O energy levels.

Level	FRD Energy (Mc/sec×10⁶)	FRD Distortion correction	This work Energy (Mc/sec×10⁶)	This work Distortion correction
2_{20}	2.2193	0	2.2184	−0.003049
3_{13}	2.2268	−0.009000	2.2291	−0.000694
4_{41}	8.0641	−0.001200	8.0665	−0.049868
5_{32}	8.0481	−0.026400	8.0490	−0.016747

As indicated in Sec. 3, the main problem is the determination of the "reduced energies"; unless otherwise stated, the following discussion will be in terms of "reduced" parameters.

In the original assumption that $(K|K\pm 1)$ and $(K|K\pm 3)$ matrix elements could be safely neglected, we carried out some "exact" calculations for Q-branch transitions, using the appropriate constants of column a of Table I. With $\nu^0(J_K)$ and $\nu(J_K)$ the observed and calculated frequencies, the results are shown in Table VII.

It is noticed that the differences (last column of Table VII) increase in an apparently fairly regular manner within each K family; a significant relationship is obtained by simply taking the ratios $r(J_K)=\nu(J_K)/\nu^0(J_K)$, which are substantially constant (to about five significant figures) for a given value of K. If we use r_K to denote the average of $r(J_K)$, for different J but the same K, we find, for $r=2$, 3, 4, 5, 6, that $r_K=1.00937$, 1.02013, 1.03163, 1.04242, 1.05445, respectively, and that $r_6/r_4=1.02212$, $r_4/r_2=1.02205$, $r_5/r_3=1.02185$, or, $r_K/r_{K-2}=1.0220$, approximately. (The values of r_K/r_{K-1} are less consistent.)

At the time of these calculations, only the identities and frequencies of the lines 2_2, 3_2, 4_3, 5_3, 7_4, 8_4 had been definitely established. Assuming the ratio r_K/r_{K-2} (i.e., r_4/r_2) was significant, we predicted the 6_4, 9_5, and 12_6 lines at 2394.2, 3045.1, and 2961.2 Mc/sec, respectively. The agreement with the then tentatively reported frequencies of these lines appeared so good that we extended the predictions to the 6_3, 10_5, and 11_5 lines,

TABLE VI. HDO observed microwave absorption lines.

Transition	Frequency (Mc/sec)	Reference
	Q-branch transitions	
$2_{21}\rightarrow 2_{20}$	10 278.99	20
$3_{22}\rightarrow 3_{21}$	50 236.90	20
$3_{21}\rightarrow 3_{30}$	824.64±0.05	24[a]
$4_{23}\rightarrow 4_{31}$	5702.78	33
$5_{33}\rightarrow 5_{32}$	22 309 ±5	17
	22 307.67±0.05	19
$6_{43}\rightarrow 6_{42}$	2394.56±0.05	24[a]
$7_{44}\rightarrow 7_{43}$	8576.89	33
	8577.7 ±0.1	This work
$8_{45}\rightarrow 8_{44}$	24 884.77±0.05	This work
	24 884.85±0.1	23
$9_{55}\rightarrow 9_{54}$	3044.71±0.10	24[a]
$10_{56}\rightarrow 10_{55}$	8836.95±0.1	This work
$11_{57}\rightarrow 11_{56}$	22 581.1 ±0.2	This work
$12_{67}\rightarrow 12_{66}$	2961 ±1	24[a]
	P- and *R*-branch transitions	
$4_{14}\rightarrow 3_{21}$	20 460.40	20
$4_{23}\rightarrow 5_{05}$	2887.4 ±0.1	24[a]
$6_{24}\rightarrow 7_{17}$	26 880.44	34
	26 880.38±0.05	This work[b]
	26 880.47±0.1	23

[a] This table quotes the latest reported measured values (see reference 24), which were not available to us at the time our work was carried out. The $3_{22}\rightarrow 3_{31}$ line was discovered subsequently, and is included here for completeness.

[b] Our identification of this transition is based partly on Stark (see reference 21) and Zeeman (see reference 28) effect data, and partly on the results of analysis of the remainder of the spectrum (see below).

TABLE VII. HDO *Q*-branch "theoretical" frequencies (1).

Transition[a] J_K	Frequency (Mc/sec) Observed[b] $\nu^0(J_K)$	Calculated $\nu(J_K)$	$\nu^0(J_K)-\nu(J_K)$
2_2	10 278.99	10 375.742	−96.752
3_2	50 236.90	50 705.828	−468.928
4_3	5702.78	5817.548	−114.768
5_3	22 307.67	22 756.857	−449.187
6_3	...	65 714.268	...
6_4	2394.6	2470.073	−75.473
7_4	8577.7	8849.329	−271.629
8_4	24 884.77	25 673.369	−788.599
9_5	3044.7	3174.077	−129.377
10_5	8836.95	9211.967	−375.017
11_5	22 581.1	23 536.847	−955.747
12_6	2961	3122.212	−161.212

[a] Here and in the sequel we will usually use J_K to denote the Q-branch transition $J_{K-1}, \kappa_1\rightarrow J_{K-1}, \kappa_1{}'$, with K standing for K_{-1}, the index denoting the K value of the limiting prolate symmetric rotor.

[b] "Observed" frequencies listed here are those actually used in computations, before the later measurements of Table VI were available.

thus:

6_3,	64 417 Mc/sec;
10_5,	8836 Mc/sec;
11_5,	22 577 Mc/sec.

A search for the latter two lines subsequently showed them at 8837 and 22 581 Mc/sec, respectively.

We may also "extrapolate" similarly to predict the 1_1 line at 80 743 Mc/sec, but the prediction is probably not quite so accurate here because the dependence on the distortion constants is less complicated functionally.

This simple "extrapolation method" of predicting Q-branch frequencies of HDO therefore seems to be quite reliable. It appears to have the significance that the major contribution to $\nu^0(J_K)-\nu(J_K)$ comes from variations in $\frac{1}{2}(a-c)$ and κ. This is reasonable since the transition frequencies are most sensitive to small percentage variations in the effective moments, and these in turn depend partly on the anharmonic potential constants (which are not known accurately); moreover, the distortion constants should be fairly reliable because the harmonic portion of the potential is known accurately.

Thus we conclude tentatively that the "theoretical" distortion corrections are good approximations to the true corrections.

The foregoing calculations have neglected the effects of $(K|K\pm1)$ and $(K|K\pm3)$ matrix elements. The major contribution from these arises from the off-diagonal moment I_{zz}^0; its removal by a principal axis transformation leads to the parameters of column b, Table I, which provide the frequencies $\nu^t(J_K)$ of Table VIII. In this tabulation, $\nu(J_K)$ denotes frequencies computed on a similar basis to those of Table VII, i.e., with $R_7^{(z)}$, $R_8^{(y)}$, and $R_9^{(y)}$ set equal to zero; the last column, $\nu^e(J_K)=\nu^t(J_K)-\nu(J_K)$, lists the correction frequencies due to the 1- and 3-off matrix elements.

Relations between the r_K now no longer hold so nicely as before, either for $\nu(J_K)/\nu^0(J_K)$ or $\nu^t(J_K)/\nu^0(J_K)$; this fact seems to be due to some large error appearing in the original I_{zz}^0. However, the magnitude of the $\nu^e(J_K)$ shows that the effects of $R_7^{(z)}$, $R_8^{(y)}$, and $R_9^{(y)}$ certainly cannot be neglected. We note that the energy level contributions, due to these parameters, arise mainly from the $(K|K\pm1)$ elements [particularly the terms in $R_9^{(y)}$—as may be expected from Table I], and increase with K; for the 12_6 levels the correction is some $-15\,000$ Mc/sec—about 0.5 cm^{-1}, which is of sufficient magnitude to interest the infrared spectroscopists.

Including 1- and 3-off matrix elements, "theoretical" frequencies for the three P- and R-branch transitions of Table VI are shown in Table IX; we cannot yet draw any useful conclusions from these results.

TABLE VIII. HDO Q-branch "theoretical" frequencies (2).

Transition	Calculated frequency (Mc/sec) $\nu(J_K)$	$\nu^t(J_K)$	$\nu^e(J_K)$
2_2	10 369.484	10 369.413	−0.071
3_2	50 670.284	50 670.692	0.408
4_2	5812.013	5811.893	−0.116
5_2	22 727.785	22 729.495	1.710
6_4	2466.454	2466.551	0.097
7_4	8830.310	8835.272	4.962
8_4	25 599.113	25 611.148	12.035
9_5	3163.981	3167.166	3.185
10_5	9168.512	9182.991	14.479
11_5	23 394.123	23 426.396	32.273
12_6	3099.340	3114.354	15.014

C. Approximate Calculations

A much simpler method of calculating Q-branch transitions between K-doublet levels can be obtained by expanding the matrices to first order in the distortion parameters;[13,15] we refer to the method as the HSKW formula, for short, and use the following notation. Let

$$\begin{aligned}\Delta^{(1)}(J_K)=&2KJ(J+1)\delta_J/H\\&+(K-1)J(J+1)D_{JK}/(G-F)\\&-(4/3)K(K^2+2)R_6/H\\&+(2/3)K(K-1)(2K-1)D_K/(G-F)\\&+(8/3)K(K^2-1)(G-F)R_6/H^2\end{aligned}\quad(19)$$

be the first-order approximation to the (reduced) distortion correction. Then, to first order, the transition frequency is given by

$$\nu^{(1)}(J_K)=\nu^R(J_K)[1+\Delta^{(1)}(J_K)],\quad(20)$$

where $\nu^R(J_K)$ is the calculated rigid rotor frequency. This is, in effect, the HSKW formula in terms of reduced distortion constants.

The HSKW formula is not claimed to be anything more than a first order approximation; we will show its limitations for the case of HDO, where the distortion effects are large, and where the approximation cannot be expected to agree perfectly with the exact calculation.

Since (19) neglects 1- and 3-off matrix elements, it is fair to compare $\nu^{(1)}(J_K)$, as calculated by (20), with $\nu(J_K)$ of Table VIII. In Table X we show $\nu^{(1)}(J_K)$, together with the "exact" calculated distortion correction $\nu^d(J_K)=\nu(J_K)-\nu^R(J_K)$, the difference $\nu(J_K)-\nu^{(1)}(J_K)$, and the percentage difference $p=100\times[\nu(J_K)-\nu^{(1)}(J_K)]/\nu^d(J_K)$. It is clear that for the "theoretical" parameters, at least, the agreement be-

TABLE IX. HDO P- and R-branch "theoretical" frequencies.

Transition	Frequency (Mc/sec) Observed	Calculated
$4_{14}\rightarrow3_{21}$	20 460.40	−13 397.134
$4_{22}\rightarrow5_{05}$	2888	10 761.553
$6_{24}\rightarrow7_{17}$	26 880.38	27 811.867

tween the exact and HSKW methods is quite good for low J and K, but cannot be pushed too far.

D. Methods of Analysis of the Spectrum

It is apparent that we must first analyze the Q-branch spectrum; only two parameters $\frac{1}{2}(a+c)$ and D_J are then needed to account for other transitions.

In our attempt to analyze the microwave spectrum of HDO so as to obtain "true" molecular constants we have been guided by the behavior of the "theoretical" (infrared) parameters. For example, it is apparent from our discussion of these that the HSKW formula should agree with "exact" calculations to a few percent; *it is our experience that, in the fitting process, the "theoretical" distortion parameters cannot be varied by more than a few percent without giving rise to serious discrepancies between the HSKW approximation and "exact" calculations* (even though the distortion corrections remain substantially constant as required by the extrapolation method).

We have tried several methods of obtaining a "fit," always using the "exact" calculations to check our results. In these, we have assumed the $\nu^e(J_K)$, as given in Table VIII, to be constant, and have made allowance for them, thus attempting to fit the seven parameters $x_i=\frac{1}{2}(a-c)$, κ, D_{JK}, D_K, δ_J, R_5, and R_6.

(a) *Variation of all parameters*

Assuming a fit can be obtained by making only small changes in the parameters x_i, we may write

$$\nu^0(J_K)-\nu^e(J_K)=\nu(J_K)+\Delta\nu(J_K), \tag{21}$$

and

$$\Delta\nu(J_K)=\sum_i \frac{\partial\nu(J_K)}{\partial x_i}\Delta x_i. \tag{22}$$

The $\partial\nu/\partial x_i$ are readily calculable to sufficient accuracy. Solution of this set of simultaneous equations for the Δx_i, and iteration of the process, gives results which do not converge and which show large discrepancies between the $\nu(J_K)$ and $\nu^{(1)}(J_K)$. Similar difficulties arise when the $\nu^e(J_K)$ are neglected. It thus appears that close agreement cannot be obtained with seven parameters.

(b) *Variation of* $\frac{1}{2}(a-c)$, κ, *only*

Keeping the "theoretical" distortion parameters constant [though modifying the reduced parameters with change of $\frac{1}{2}(a-c)$], we can simplify the method (a) by varying only $\frac{1}{2}(a-c)$ and κ, using a least squares reduction of the equations. This gives frequency differences of the order of one percent of the distortion corrections, and is the method finally used.

If we were to follow the Hillger and Strandberg method,[18,26] we would now use the HSKW formula to vary the distortion parameters so as to improve the fit.

TABLE X. HDO Q-branch "theoretical" frequencies (3).

Transition J_K	Frequency (Mc/sec) $\nu^{(1)}(J_K)$	$\nu^4(J_K)$	$\nu(J_K)-\nu^{(1)}(J_K)$	p
2_2	10 369.603	−50.026	−0.119	0.24
3_2	50 671.812	−322.733	−1.529	0.47
4_3	5812.112	−79.667	−0.099	0.12
5_3	22 727.744	−390.265	0.041	−0.011
6_4	2466.391	−71.639	0.063	−0.088
7_4	8829.172	−311.383	1.138	−0.37
8_4	25 588.117	−1082.154	10.996	−1.02
9_5	3161.580	−197.722	2.401	−1.21
10_5	9158.796	−676.855	9.716	−1.44
11_5	23 345.677	−2008.58	48.446	−2.41
12_6	3091.899	−369.063	7.441	−2.02

As in method (a), however, we find that any such attempts—when checked by "exact" calculations—are doomed to failure.

The same difficulties were experienced when 1- and 3-off matrix elements were completely neglected.

(c) *Variation of* $\frac{1}{2}(a-c)$, κ, *keeping* $\Delta^{(1)}(J_K)$ *constant*

This method involves small changes in the "fundamental" distortion parameters, since $\Delta^{(1)}(J_K)$ is a function of $\frac{1}{2}(a-c)$ and κ. It does not seem to be much more satisfactory than (b), though it does give somewhat better agreement between $\nu(J_K)$ and $\nu^{(1)}(J_K)$. However, although the "theoretical" percentage differences p of Table X are small, there does not appear to be any reason why the true ones should be exactly the same magnitude—convenient though this might be.

As a result of these investigations we conclude that it is not possible to get a "perfect" fit with seven parameters. The next approximation, inclusion of $(K|K\pm1)$ and $(K|K\pm3)$ matrix elements, gives little better results; we believe this is due to considerable error in the $\nu^e(J_K)$ and/or neglect of other approximations, e.g., in the vibrational diagonalization of the energy matrix. Unfortunately, there seems to be no convenient way of varying the $\nu^e(J_K)$ so as to be able to consider them adjustable in the fitting process; in principal, this can be done by making small changes in the three additional parameters $R_7^{(s)}$, $R_8^{(y)}$, and $R_9^{(y)}$, and calculating the effect on the ν's; since we have been unable to find a simple way of doing this, it is apparent that a considerable amount of labor would be involved.

At this stage, then, we have to be satisfied with agreement to a few percent of the distortion corrections. Method (a) does not give this since the changes in the magnitude of the parameters which are required to force a fit become too large for the method to be valid. Methods (b) and (c) do give reasonable agreement, though there is little to decide between the two. We arbitrarily choose method (b), because it involves variation only of the effective moments, whose "theo-

TABLE XI. HDO Q-branch frequencies (4).

J_K	$\nu^t(J_K)$ (Mc/sec)	$\nu^e(J_K)$ $-\nu^t(J_K)$ (Mc/sec)	$\nu^d(J_K)$ (Mc/sec)	p	$\nu^D(J_K)$ (Mc/sec)	P
2_2	10 275.660	3.330	−50.099	−2.2	−50.170	−6.6
3_3	50 232.692	4.208	−322.636	−1.4	−322.228	−1.3
4_2	5701.757	1.023	−79.600	−3.3	−79.716	−1.3
5_3	22 307.350	0.320	−388.924	−2.8	−387.214	−0.083
6_4	2395.019	−0.419	−71.277	−4.2	−71.180	0.59
7_4	8582.081	−4.381	−308.872	−3.8	−303.910	1.4
8_4	24 865.250	19.520	−1096.841	−1.5	−1084.806	−1.8
9_5	3041.952	2.748	−196.823	−4.2	−193.638	−1.4
10_5	8829.125	7.825	−666.128	−4.8	−651.649	−1.2
11_5	22 538.263	42.837	−1972.977	−5.4	−1940.704	−2.2
12_6	2961.394	−0.394	−360.668	−5.9	−345.654	0.11

retical" accuracy is more liable to suspicion because of their dependence on the anharmonic potential constants.

E. Results of Analysis of the Spectrum

Starting from Table VIII, but omitting the data on the 10_5 and 11_5 lines (which were not then known), a least squares solution for $\Delta[\frac{1}{2}(a-c)]$ and $\Delta\kappa$ was obtained from the nine equations of the form of (22), leading to the following "observed" HDO parameters: $\frac{1}{2}(a-c)=2.55544755\times10^5$ Mc/sec, $\kappa=-0.68410904$, $D_{JK}=1.44057795\times10^{-4}$, $D_K=11.23440546\times10^{-4}$, $\delta_J=0.13043190\times10^{-4}$, $R_5=-0.30825076\times10^{-4}$, and $R_6=-0.02239153\times10^{-4}$. From these we get the $\nu(J_K)$ (as in Table VII), which give, with the $\nu^e(J_K)$ of Table VIII, the $\nu^t(J_K)=\nu(J_K)+\nu^e(J_K)$ of Table XI. Here also p and $\nu^d(J_K)$ have the same meaning as in Table X, while $\nu^D(J_K)=\nu^t(J_K)-\nu^R(J_K)$ is the total distortion correction, and $P=100\times[\nu^t(J_K)-\nu^t(J_K)]/\nu^D(J_K)$ is the percentage discrepancy (referred to the total distortion) between observed and calculated frequencies.

The worst (percentage) discrepancy occurs for the 2_2 line, which also has the least distortion; we believe this is a result of the least squares analysis, which weights this line the least.

Although P for the 11_5 line (which was not included in the analysis) is of the same order of magnitude as for the other lines, the actual frequency difference, 42 Mc/sec, between calculated and observed frequencies is much larger than we would expect from consideration of the extrapolation method discussed earlier; by keeping $\Delta^{(1)}(J_K)$ constant—method (b) of the preceeding sub-section—the difference is reduced to only about 3 Mc/sec, but the fit on the 8_4 line becomes worse (about 25 Mc/sec), and the over-all picture is about the same.

TABLE XII. HDO "observed" rotation-distortion constants.

$\frac{1}{2}(a+c)$	4.48416164 ×10⁵ Mc/sec	δ_J	3.33311881 Mc/sec
$\frac{1}{2}(a-c)$	2.55544755 ×10⁵ Mc/sec	R_5	−7.87718656 Mc/sec
κ	−0.68410904	R_6	−0.57220390 Mc/sec
D_J	11.56583333 Mc/sec	$R_7^{(a)}$	3.11603472 Mc/sec
D_{JK}	36.81321390 Mc/sec	$R_8^{(a)}$	−8.19943988 Mc/sec
D_K	287.08933921 Mc/sec	$R_9^{(a)}$	49.91730954 Mc/sec

It is interesting to refer to Table X and note how small changes in $\Delta^{(1)}(J_K)$, because of the variation of $\frac{1}{2}(a-c)$ and κ, markedly affect p, even though $\nu^d(J_K)$ is almost the same in the two cases.

We believe the general agreement shown in Table XI is as good as one can get using the present methods. Slight improvement might be obtained by now feeding in the 10_5 and 11_5 data, but this will not lead to any significant change in our final results.

With the Q-branch spectrum "solved," it is a simple matter to analyze the P- and R-branch lines. Since we have concluded that the "theoretical" distortion constants are good approximations to the true ones, we ought to get fairly consistent values of $\frac{1}{2}(a+c)$ from the $|\Delta J|=1$ transitions on the assumption that D_J is also good. With the value of D_J given in column b of Table I, the three lines of Table VI give an average $\frac{1}{2}(a+c)$ of $(4.4827\pm0.0020)\times10^5$ Mc/sec, which is apparently good to about four significant figures (we take this to be a measure of just how reliable our major parameters are). This average value gives the following frequencies: $4_{14}\rightarrow3_{21}$, 21 058.871 Mc/sec; $4_{22}\rightarrow5_{05}$, 2740.896 Mc/sec; $6_{24}\rightarrow7_{17}$, 28 133.594 Mc/sec. Although the agreement cannot be described as excellent, it is a great improvement on Table IX, and argues for some consistency in our work, as well as providing support for the identification of the 26 880-Mc/sec line. It shows that the distortion constants are fairly good, and that reasonable correlation with experiment can be obtained by changes in the effective moments alone.

Further improvement is obtained if we allow D_J to vary; a least squares solution for $\frac{1}{2}(a+c)$ and D_J gives 4.48416164×10^5 and 11.56583333 Mc/sec, respectively, from which the calculated frequencies now become $4_{14}\rightarrow3_{21}$, 20 515.856 Mc/sec; $4_{22}\rightarrow5_{05}$, 2983.326 Mc/sec; $6_{24}\rightarrow7_{17}$, 26 843.995 Mc/sec. The differences between observed and calculated frequencies are now −55.456 Mc/sec, −95.326 Mc/sec, and 36.385 Mc/sec, respectively.

Since these results are obtained in a very straightforward manner, the agreement must be regarded as quite good, even though we have had to change D_J by some 25 percent.

Table XII summarizes the results of the foregoing analysis of the HDO microwave spectrum, the distortion constants quoted being the "fundamental" values.

From $\frac{1}{2}(a+c)$, $\frac{1}{2}(a-c)$, and κ, the effective moments and reciprocal moments of inertia are easily obtained and are shown in Table XIII.

There is less than one percent difference between "theoretical" and "observed" values, and this change in three parameters, together with a comparatively large variation in D_J, has been all we have introduced to get a reasonably good fit to the spectrum.

Some rotational energy levels, calculated from the constants of Table XII, are shown in Table XIV. The effects of $(K|K\pm1)$ and $(K|K\pm3)$ matrix elements have not been taken into account exactly here, though

in some cases the corresponding "theoretical" energy corrections have been included.

Using Table XIV, some of the $|\Delta J|=1$ transitions expected from KHC II have been calculated, and are shown in Table XV. Attempts to observe the $7_{07}\rightarrow 6_{24}$ line, in the vicinity of 12 200 Mc/sec, have so far been unsuccessful.

F. Discussion of Results

Although the agreement between observed and finally calculated $|\Delta J|=1$ transitions is considered good, the large change we had to make in D_J is inconsistent with our assumption that the "theoretical" distortion constants are very close to the true ones. But it is apparent that the parameters entering into the Q-branch frequencies must be known more accurately before we can draw precise conclusions about $\frac{1}{2}(a+c)$ and D_J; the values we get for these two constants are therefore to be regarded as containing the lumped errors of the other parameters, and this has to be born in mind when examining the results of Table XIII.

TABLE XIII. HDO effective moments and reciprocal moments of inertia.

	Theoretical	Observed
a	6.97876766×10^{5} Mc/sec	7.03960919×10^{5} Mc/sec
b	2.72522145×10^{5} Mc/sec	2.73595687×10^{5} Mc/sec
c	1.91863695×10^{5} Mc/sec	1.92871409×10^{5} Mc/sec
I_a	1.20206397×10^{-40} g cm^2	1.19167485×10^{-40} g cm^2
I_b	3.07825449×10^{-40} g cm^2	3.06617597×10^{-40} g cm^2
I_c	4.37233588×10^{-40} g cm^2	4.34949132×10^{-40} g cm^2
Δ	0.09201742×10^{-40} g cm^2	0.09164050×10^{-40} g cm^2

We would like to have Q-branch parameters that are good enough to calculate "exactly" frequencies which will agree with observations to within something like 1 Mc/sec, if not better. Any such agreement obtained by the use of approximation methods (e.g., the HSKW method) must be checked by "exact" calculations, otherwise the constants obtained cannot be considered the true molecular parameters, but are merely constants in a semiempirical formula. We believe that the results obtained by Weisbaum *et al.*[24] should be described in the latter manner.

The present work has shown that such desirable Q-branch parameters are unachievable if only the seven quantities $\frac{1}{2}(a-c)$, κ, D_{JK}, D_K, δ_J, R_5, and R_6 are considered. Remaining discrepancies turn out to be of the order of magnitude of the corrections introduced by taking $R_7^{(z)}$, $R_8^{(y)}$, and $R_9^{(y)}$ into account, but inclusion of these corrections still leaves much to be desired. The assumption of the essential correctness of the "theoretical" distortion parameters leads one to expect that only small changes in $R_7^{(z)}$, $R_8^{(y)}$, and $R_9^{(y)}$ should be tolerated, and it is unlikely that such small changes would lead to significant differences in the corrections $\nu^e(J_K)$. Thus it is probable that either our theories and/or calculations involving $R_7^{(z)}$, $R_8^{(y)}$, and $R_9^{(y)}$ are incorrect, or that we must look elsewhere to improve our results; this means examination of higher terms in the vibration-rotation theory, e.g., terms in the Hamiltonian of the order of $\mathbf{P}^6$, where $\mathbf{P}$ is an angular mo-

TABLE XIV. HDO rotational energies.

Level	Energy (Mc/sec X10^6) Rigid W^R	Nonrigid W^N	Distortion W^N-W^R
2_{21}	3.282311	3.276432	−0.005879
2_{20}	3.292637	3.286708	−0.005929
3_{22}	4.681712	4.673735	−0.007977
3_{21}	4.732267	4.723968	−0.008299
4_{14}	4.707305	4.703452	−0.003853
4_{22}	6.684485	6.671355	−0.013130
4_{32}	8.925689	8.890918	−0.034771
4_{31}	8.931471	8.896619	−0.034852
5_{05}	6.682430	6.674338	−0.008092
5_{24}	8.848938	8.834291	−0.014648
5_{23}	9.163016	9.141062	−0.021954
5_{33}	11.285626	11.241421	−0.044205
5_{32}	11.308320	11.263728	−0.044592
6_{06}	9.225386	9.210664	−0.014722
6_{24}	12.169757	12.133066	−0.036691
6_{33}	14.186789	14.127912	−0.058877
6_{43}	17.392922	17.272528	−0.120394
6_{42}	17.395389	17.274923	−0.120466
7_{07}	12.145962	12.120853	−0.025109
7_{17}	12.184437	12.159910	−0.024527
7_{16}	14.288870	14.245622	−0.043248
7_{35}	17.429084	17.349701	−0.079383
7_{44}	20.707197	20.561306	−0.145891
7_{43}	20.716083	20.569888	−0.146195
8_{45}	24.504725	24.324235	−0.180490
8_{44}	24.530675	24.349100	−0.181575
8_{53}	28.685244	28.376901	−0.308343
9_{46}	28.786442	28.560607	−0.225835
9_{55}	32.950146	32.584549	−0.365597
9_{54}	32.953382	32.587591	−0.365791
10_{56}	37.702535	37.268638	−0.433897
10_{55}	37.712015	37.277468	−0.434547
11_{67}	42.944157	42.424541	−0.519616
11_{66}	42.968636	42.447079	−0.521557
12_{67}	53.721091	52.829222	−0.891869
12_{66}	53.724398	52.832183	−0.892215

TABLE XV. HDO predicted P- and R-branch frequencies.

Transition	Frequency (Mc/sec)
$7_{07}\rightarrow 6_{24}$	12 198
$5_{24}\rightarrow 4_{31}$	62 447
$5_{23}\rightarrow 6_{06}$	69 602
$6_{43}\rightarrow 7_{35}$	74 778
$6_{33}\rightarrow 7_{16}$	117 710
$8_{53}\rightarrow 9_{46}$	183 710

TABLE XVI. HDO parameters.

Rotation-distortion constants						
$\frac{1}{2}(a+c)$	4.484	±0.002 ×10⁵ Mc/sec	δ_J	3.333	±0.005	Mc/sec
$\frac{1}{2}(a-c)$	2.555	±0.005 ×10⁵ Mc/sec	R_4	−7.877	±0.010	Mc/sec
κ	−0.684	±0.03002	R_4	−0.572	±0.005	Mc/sec
D_J	9.1	±1.5 Mc/sec	$R_7^{(z)}$	3.12	±0.05	Mc/sec
D_{JK}	36.8	±0.5 Mc/sec	$R_8^{(y)}$	−8.20	±0.05	Mc/sec
D_K	287	±5 Mc/sec	$R_9^{(y)}$	50.0	±0.5	Mc/sec

Effective moments and reciprocal moments of inertia		
a	7.0396 ±0.0005 ×10⁵	Mc/sec
b	2.7360 ±0.0005 ×10⁵	Mc/sec
c	1.9186 ±0.0005 ×10⁵	Mc/sec
I_a	1.1917 ±0.0005 ×10⁻⁴⁰	g cm²
I_b	3.0662 ±0.0005 ×10⁻⁴⁰	g cm²
I_c	4.3495 ±0.0005 ×10⁻⁴⁰	g cm²

mentum operator. Rough calculations, based on orders of magnitude, indicate that such terms probably will be negligible for the present work, but one cannot be conclusive about this without going into considerable detail.

It is our opinion that any improvement in the present results will have to be obtained with the aid of a high-speed digital computer to set up exactly and solve equations of the type of (22). Notwithstanding the conclusions of the previous paragraph, it may still be possible to get a satisfactory solutions by including variations of $R_7^{(z)}$, $R_8^{(y)}$, and $R_9^{(y)}$, the corresponding $\partial\nu/\partial x_i$ being obtained by computer diagonalization of the complete matrices; this possibility ought to be considered early in any extension of this work, since even small changes in the $\nu^c(J_K)$ could conceivably bring about a neat fit—the transition frequencies are much more sensitive to changes in certain parameters (e.g., κ) than in others.

The good agreement we get for $|\Delta J|=1$ transitions gives some confidence in our final results. However, it must be pointed out that the consistency vanishes if the 26 880-Mc/sec line is not the $6_{24}\rightarrow 7_{17}$ transition, or if the 2888-Mc/sec line is actually the $5_{05}\rightarrow 4_{22}$ transition. Our information[34] is that the latter is the $4_{22}\rightarrow 5_{05}$ line, though we are not aware of any evidence (e.g., Stark data) to show the relative positions of the levels.

To conclude this sub-section, we give in Table XVI what we consider to be reasonable HDO parameters; these are obtained by rounding off the constants of Tables XII and XIII; the accuracies indicated have been estimated by us on the basis of our experience with the problem.

7. CONCLUSION

By analysis of the microwave rotational spectrum of HDO we have obtained approximate values of the molecular parameters which are in fairly good agreement with the theoretically calculated constants. The "theoretical" values, derived from infrared data on H_2O and D_2O, together with some observed microwave frequencies enabled us to calculate HDO Q-branch frequencies with rather unexpected accuracy; it must be considered very gratifying that we can do this in view of the rather tortuous calculations that have had to be carried out in going from one isotopic molecule to another.

Distortion effects in this type of molecule have been found to be large, so large that to get detailed agreement between theory and observation (in the microwave region) one must use higher approximations in the theory than had previously been considered necessary. Our results are by no means final, and possible methods of improving them have been indicated.

During preparation of this paper several other authors have reported infrared[35] and microwave[36] work on the water molecule, and comparison with the present account be of interest when detailed descriptions are published.

8. ACKNOWLEDGMENTS

The authors are grateful to Dr. Y. Beers and Dr. S. Weisbaum for making available to us their results prior to publication; to J. D. Kierstead who assisted with the experimental work; and to Miss H. Paul who carried out some of the computations.

One of us (D.W.P.) would like to acknowledge a grant from the Commonwealth Scientific and Industrial Research Organization, Australia.

[35] Benedict, Gailar, and Plyler, J. Chem. Phys. 21, 1301 (1953); Benedict, Gailar, and Plyler, J. Chem. Phys. 21, 1302 (1953).

[36] W. Gordy, J. Chim. Phys. 50 (9), C114 (1953); Duke University Report No. 3, Aug. 1, 1953, to Nov. 1, 1953 (unpublished)

Microwave Spectrum of TeCS and Masses of the Stable Tellurium Isotopes*

W. A. HARDY† AND G. SILVEY
Columbia University, New York, New York
(Received March 31, 1954)

The microwave spectrum of TeCS has been examined in the rotational transitions $J=6\leftarrow5$, $J=7\leftarrow6$, and $J=8\leftarrow7$. Seven isotopes were observed and from their absorption frequencies mass ratios have been calculated. The mass values are compared with mass spectrographic data and with the recent mass surfaces of Green. The odd-even mass variation is 1.5 milli-mass-units for both Te^{123} and Te^{125}. The Te−C bond distance is 1.904 A and the C−S distance 1.557 A. The molecular dipole moment was measured as 0.172 ±0.002 Debye unit.

THE microwave spectrum of the molecule thiocarbonyl telluride was provisionally analyzed in this laboratory in 1952, but with the apparatus then available the frequency measurements of the spectrum were not sufficiently accurate to allow a satisfactory determination of the tellurium mass ratios.[1] Thus, for Te^{123} the experimental error allowed for the odd-even mass variation was 1.2 milli-mass-units reflecting a 50-kilocycle uncertainty in the measurement of the weak absorption lines due to this isotope. Subsequent to the construction of a highly refined, albeit conventional type, Stark modulation spectrometer the TeCS spectrum was remeasured with increased precision and this paper reports more accurate mass ratios together with the rotational constants of the TeCS molecule. Some account is also given of the spectrometer used in this work.

a. ROTATIONAL CONSTANTS OF TeCS

Microwave rotational transitions of the linear molecule TeCS were observed corresponding to $J=6\leftarrow5$, $J=7\leftarrow6$, and $J=8\leftarrow7$, where J is the rotational quantum number. To each of these belongs an isotopic family due to tellurium nuclei with $A=122$, 123, 124, 125, 126, 128, and 130. Te^{120}, although stable, is only 0.09 percent abundant and was not observed.

The frequency f of the rotational transition of a triatomic linear molecule from the energy level specified by rotational quantum number J to $J+1$ is given by

$$f=(2B_v\pm q_l)(J+1)-D[4(J+1)^3-2(J+1)l^2],$$

$$B_v=B_e-\alpha_1(v_1+\tfrac{1}{2})-\alpha_2(v_2+1)-\alpha_3(v_3+\tfrac{1}{2}), \qquad (1)$$

$$B_v=B_{000}-\alpha_1v_1-\alpha_2v_2-\alpha_3v_3.$$

Here B is the reciprocal moment of inertia (times $h^2/2$), D is the centrifugal distortion constant, the α's are rotation-vibration parameters representing the change in the moment of inertia of the molecule in any of the vibrational states specified by the v's, and l is a quantum number refering to the component of angular momentum parallel to the symmetry axis of the molecule. It is different from zero only for the vibrational states of v_2, and $l=\pm1$ for $v_2=1$, giving the usual l-type doublets. The rotation of the molecule removes the degeneracy of the two bending modes allowed for $v_2=1$, and q_l is a splitting constant giving the separation of the doublets. It can be shown that for $v_2\geqslant2$, q_l is essentially zero.[2] B_v is the observed reciprocal moment of inertia, B_{000} that of the molecule in its ground state, and B_e is the equilibrium value neglecting zero-point vibrations.

Molecular parameters are given in Table I from which the TeCS spectrum may be calculated for any transition by the use of (1). Frequencies calculated using this table are exact to better than 40 kc/sec. (Although later measurements of the TeCS spectrum were more precise, Table I includes some earlier data that would have been inconvenient to redetermine in the later work.)

There were two difficulties attendant to the observation of this spectrum which require special mention. The first is the spontaneous decomposition of TeCS at temperatures above its melting point, −54°C. Accordingly, the measurements were made by holding the temperature of the wave-guide absorption cell in the range −55°C to −45°C by circulating chilled acetone around the cell. Under these conditions the molecule was semistable and the spectrum could be observed up to periods of several hours. Deposits of tellurium metal did, however, accumulate in the wave guide. The second and more formidable difficulty concerns the small molecular dipole moment of TeCS, 0.172 Debye unit, with the result that not only is the absorption coefficient considerably smaller than that of comparable molecules, but the Stark modulation fields available were unable to produce Stark splittings greater than a

TABLE I. Molecular parameters of TeCS to be used in Eq. (1). For all the isotopes an average centrifugal distortion constant D was taken as 95 cps. These parameters have the units of Mc/sec.

A of Te	B_{000}	α_3	q_l
130	1559.9303	3.2446	0.6599
128	1565.7022	3.2551	0.6649
126	1571.6524	3.2657	0.6706
125	1574.6925	3.2712	0.6728
124	1577.7898	3.2764	0.6752
123	1580.9261	3.2818	0.6776
122	1584.1224	3.2870	0.6786

* Work assisted by the U. S. Atomic Energy Commission.
† National Science Foundation Pre-doctoral Fellow.
[1] Silvey, Hardy, and Townes, Phys. Rev. **87**, 236 (1952).
[2] H. H. Nielsen, Phys. Rev. **75**, 1961 (1949).

fraction of a line width in the ground state of the molecule. It was necessary to make the microwave measurements on the rotational transitions of the excited vibrational states with $v_2=1$ in order to take advantage of the greater Stark effect in this state because of the near degeneracy of the l-type doublets.

The measured frequencies of the two l doublets with $v_2=1$ in the $J=8\leftarrow7$ transition are given in Table II for each of the tellurium isotopes observed. All these lines were measured with a fixed Stark modulation electric field intensity of 1610 volts/cm. The doublet separations and the change in doublet separation for a unit change in A (the tellurium mass number) are also given. Although the measurements are consistent, the actual absorption frequencies may be displaced from those measured because of Stark distortion of the line shapes. However, this shift is less than 25 kc/sec and will not affect the later determination of the mass ratios because the doublets are exactly symmetric about their average frequency and such a distortion will be cancelled. The measurements listed in Table I were taken by sweeping very slowly over the lines with a stabilized klystron and presenting both the line and frequency standard markers on a recording chart. Using this technique the error in the average of the doublet frequencies is less than 10 kilocycles.

The second-order Stark effect of the TeCS molecule in its ground state is very small both because of the necessarily high J values for microwave transitions and because of the small dipole moment. Lines corresponding to ground-state transitions were only observed after the application of a 700-volt Stark modulation square wave added to a 1200-volt dc source, representing a maximum modulation electric field intensity of 4370 volts/cm in the guide. Even so, the line was only partially separated from its Stark component and could not be used for accurate frequency measurements.

In a strong electric field a linear molecule in a bending vibrational mode behaves like a slightly asymmetric top, permitting a component of angular momentum parallel to the field and thus allowing a first-order Stark effect of considerably larger magnitude than the second-order effect discussed in the previous paragraph.

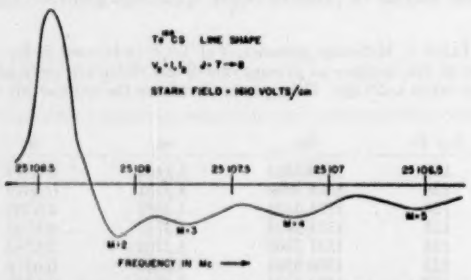

FIG. 1. The line shape of an l doublet of TeCS in a Stark field of 1610 volts/cm. In the presentation, the undisplaced line is shown as positive and the Stark components are negative. The minima are shown identified by their M component.

TABLE II. TeCS l-type doublet measured frequencies in the $J=8\leftarrow7$ rotational transition. The doublet separations and the change in the doublet separations per change in mass number are also given. All frequencies are given in Mc/sec.

A of Te	$v_2=1,1_1$	$v_2=1,1_2$	Δf	$\Delta(\Delta f)/\Delta A$
130	25 005.326	25 015.884	10.558	
				0.040
128	25 097.805	25 108.444	10.639	
				0.045
126	25 193.132	25 203.861	10.729	
				0.035
125	25 241.844	25 252.608	10.764	
				0.039
124	25 291.465	25 302.268	10.803	
				0.038
123	25 341.714	25 352.555	10.841	
				0.018
122	23 392.929	25 403.788	10.859	

The energy levels in terms of the component M of angular momentum parallel to the electric field E have been given for the bending modes as[3]

$$W=W_{e0}\pm\tfrac{1}{2}[(\Delta W)^2+4\mu^2E^2\varphi^2]^{\frac{1}{2}}. \qquad (2)$$

Here φ is a matrix element connecting the l-type doublets with $\varphi=M/[J(J+1)]$, W_{e0} is the energy in the absence of doublet splitting, and ΔW is the separation of the doublets in a given J level.

A plot, taken from an actual trace of one of the doublet components and used in the determination of the molecular dipole moment, is shown in Fig. 1. Even at the Stark modulation field strength of 1610 volts/cm used here about one-third of the line is lost due to cancellation by Stark components that are shifted by less than a line width. By measuring the frequencies of the observed minima both the electric dipole moment and the M components corresponding to the minima were determined using (2). The dipole moment was found to be

$$\mu=0.172\pm0.002 \text{ Debye unit.}$$

Calculations using the observed line widths as parameters showed that the observed minima corresponded exactly to their Stark components with negligible error due to overlap of these components and the undisplaced line. The electric field strength in the wave guide was calibrated by measurement of the Stark shift of the molecule OCS whose dipole moment was measured accurately by Shulman and Townes.[3]

The values of α_2 given in Table I and used in the determination of B_{000} are calculated using the separation between the average of the doublet frequencies for which $v_2=1$ and the unsplit line with $v_2=2$. Within the accuracy of the measurement of the ground state transitions no Fermi-type resonance effects were observed. No quardupole hyperfine structure was detected for the odd tellurium isotopes, in agreement with the

[3] R. Shulman and C. H. Townes, Phys. Rev. 77, 500 (1950).

spins of $\frac{1}{2}$ measured for these nuclei by the use of optical hyperfine structure.[4]

From the moment of inertia data the Te−C bond distance was determined as 1.904 A and the C−S bond distance as 1.557 A. These values may be interpreted in terms of the percentage contributions of the resonant structures $Te=C=S$, $Te^{+}\equiv C-S^{-}$, and $Te^{-}-C\equiv S^{+}$, together with the usual values of bonding radii of the respective atoms.[5] The small dipole moment of TeCS makes it likely that the last two structures contribute in nearly equal amounts, and the actual percentage must be about 20 percent to give the observed C−S bond distance. The Te−C bond distance then yields the value 1.23 A for the tellurium triple bond radius, which compares favorably with the value 1.20 A that would be interpolated from Pauling's values of bond radii. This indicates that Pauling's bond radii for tellurium taken from solid tellurium are fairly accurate.

b. MASS DATA

If the molecular bonds were rigid, the moment of inertia data would enable the exact determination of the isotopic tellurium masses in terms of any two masses, assumed given, from the expression

$$\frac{m^1-m}{m^2-m}=\frac{M^1}{M^2}\left(\frac{B^2}{B^1}\right)\left(\frac{B-B^1}{B-B^2}\right). \tag{3}$$

The superscripts indicate the isotopes chosen as standards and the M's refer to the total molecular mass. Geschwind has analyzed the errors in these ratios arising from the use of the effective B values (which include molecular vibrational effects) rather than the use of the equilibrium B_e's, and has shown that even in extreme cases the error would be less than a few tenths of a milli-mass-unit.[6] Accordingly, the mass ratios reported in this paper have been determined by substitution of the observed effective B values in (3); it is probable that the error introduced by this approximation is less than a tenth of a milli-mass-unit. It must be noted that all microwave mass ratio determinations using polyatomic molecules involve this assumption, and that there has been excellent agreement with mass spectroscopic and nuclear reaction data.

TABLE III. Mass defects $(M-A)$ for the stable tellurium isotopes expressed in millimass units.

A of Te	Halsted	Data of Hogg-Duckworth[a]	Green *et al.*	Microwave†
130	−51.47±0.10	−52.3±0.4	−49.44	−50.5±0.2
128	−53.51±0.13	−56.2±0.6	−52.68	−53.5
126	−55.80±0.07		−55.21	−55.6±0.2
125	−55.40±0.31		−55.35	−55.0±0.2
124	−57.22±0.11	−60.8±0.4	−57.05	−57.2
123	−56.32±0.39		−56.75	−56.1±0.2
122	−58.07±0.08	−60.1±0.6	−58.05	−57.8±0.2

[a] These results depend slightly on the mass value assumed for carbon. See reference 8.
† Using Halsted masses for Te^{128} and Te^{124}.

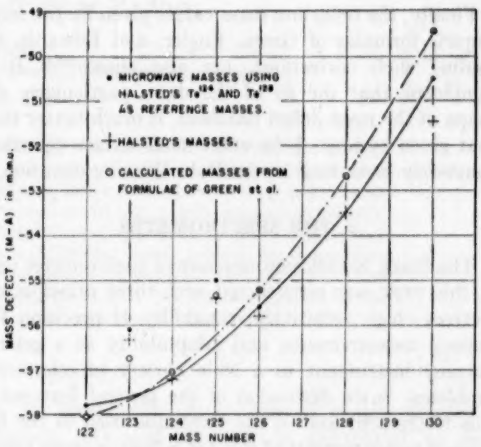

FIG. 2. The mass defects of tellurium shown as a function of tellurium mass number.

The tellurium mass data is given in Table III and the mass defect is plotted as a function of the mass number of tellurium in Fig. 2. It will be seen that the data of Halsted and that of Hogg and Duckworth do not agree within the experimental errors quoted by these authors.[7,8] Although the two reference masses used in computing the microwave mass ratios were chosen from the Halsted masses because of the smaller quoted uncertainty, comparison of these data is strongly conditioned by the specific masses chosen. For example, the choice of Te^{124} and Te^{128} used in the data indicates a disagreement with the Halsted data of 1.0 mMU for Te^{130}. Alternately, a choice of Te^{124} and Te^{130} as reference masses causes a disagreement of 0.7 mMU for Te^{128} and 0.5 mMU for Te^{122}. The above discrepancies may be seen from Table III to be considerably larger than the experimental errors quoted for the separate measurements, and accordingly no attempt has been made to combine data to achieve "adjusted" mass values.

On the other hand, the odd-even mass variations determined from the microwave data are relatively unaffected by the trend for even isotopes that is set by the choice of reference masses, and one of these may be directly compared with nuclear reaction data. Thus, the $Te^{125}(\gamma,n)$ threshold is determined by Sher, Halpern, and Mann as 6.5±0.2 Mev, comparing very favorably with the 6.4±0.2 Mev deduced from the microwave data.[9] The odd-even mass variation for Te^{125} is 1.5±0.2 mMU and for Te^{122} it is the same.

[4] Mack, Marakawa, Ross, Pick, and van den Bosch, Phys. Rev. **83**, 654 (1951).
[5] L. Pauling, *Nature of the Chemical Bond* (Cornell University Press, Ithaca, 1939).
[6] S. Geschwind, thesis, Columbia University, 1951 (unpublished).
[7] R. Halsted, Phys. Rev. **88**, 666 (1952).
[8] B. G. Hogg and H. E. Duckworth, Can. J. Phys. **30**, 628 (1952).
[9] Sher, Halpern, and Mann, Phys. Rev. **84**, 387 (1951).

Finally, the tellurium mass values given by the semi-empiric formulas of Green, Engler, and Edwards, including shell corrections, are also shown.[10,11] It is significant that the fit of the data, particularly the shape of the mass defect parabola, is much better than that given by any of the other mass-surface equations commonly used, such as the Bohr-Wheeler equation.

c. THE SPECTROMETER

The Stark modulation microwave spectrometer used in this work was constructed with three principal objectives—high sensitivity, capability of precision frequency measurements, and adaptability as a general purpose instrument to a wide variety of microwave problems. Some discussion of the general features of this instrument and of the technique used in the frequency measurements of the TeCS lines is given below. The spectrometer consists basically of a 14-foot waveguide cell with an inner septum that is Stark modulated at a frequency of 89 kc/sec. A minimum sensitivity of 3×10^{-10} cm^{-1} has been demonstrated and the line width at half-maximum intensity is 150 kc/sec.

Townes and Geschwind have derived an expression for the limiting sensitivity of a microwave spectrometer which may be written for this instrument as $\alpha_{\min}=4\times10^{-11}(N\Delta f)^{\frac{1}{2}}$.[12] Here N is a noise figure and Δf is the band width of the detecting system. It must be noted that although increased sensitivity may be achieved by the use of very small band widths, the time required for observation of an accurate line shape is at least ten times the reciprocal band width. Further, it is assumed that the microwave radiation is very nearly monochromatic and varies in a smooth and continuous manner during the tracing of the line. In practice, this requirement (particularly for the $2K33$- and QK-type klystrons used in this work) is rather formidable. For example, a 25 to 40 CFM blower directed upon the klystron in a gentle stream produces more than 300 kilocycles microphonic modulation. In the present apparatus the klystron is rigidly fixed upon a shock-mounted 250-lb concrete block and is connected to the wave guide cell by flexible wave guide. Cooling is effected by means of oil flowing at a constant rate within a jacket surrounding the shell of the klystron. Mechanical tuning of the klystron cavity is accomplished by a gear reduction, remotely activated by selsyns to avoid vibration, that provides mechanical tuning with a precision of better than 30 kc/sec and with negligible backlash. Finally, the klystron power supply is regulated to within 10 millivolts of ripple and drift. These precautions have enabled us to achieve a clean microwave signal with a frequency width of about 15 kc/sec and with very slow drift. This increased the sensitivity and also gave considerably more accurate frequency measurements. A continuous high sensitivity search over a region of more than 100 Mc/sec while mechanically tuning the klystron at a rate of 5 (Mc/sec) per minute could be automatically recorded in a very satisfactory manner.

For band widths of the order of 1 cycle/sec additional stability is obtained by stabilizing the klystron with respect to a frequency standard harmonic, using discriminator detection and dc control of the klystron repeller voltage. This technique makes the microwave signal still more nearly monochromatic and permits arbitrarily slow sweeping over the absorption line. It was used in the measurements of the l-type doublets of TeCS. Further decrease of the band width is limited in the present apparatus by saturation of the lock-in detector due to noise voltages when the receiver gain is increased to enable detection of weaker absorptions than 3×10^{-10} cm^{-1}.

Features which increase the utility of the spectrometer include a temperature control of the wave-guide cell from -70°C to 95°C and the use of a wave-guide cell constructed entirely of copper, brass, and Teflon to permit analysis of reactive molecules such as fluorides.

d. CHEMISTRY

The TeCS was prepared[13] by the action of an arc under CS_2 between a graphite anode and a tellurium-graphite cathode, the latter containing 10–15 percent graphite. The material was purified by distillation at -78°C. Considerable amounts and several varieties of unknown impurities were obtained and were only partially removed by further fractional distillation.

e. ACKNOWLEDGMENT

The authors wish to acknowledge the courtesy of Dr. A. E. S. Green and Mr. Kiuck Lee for sending us their tellurium mass values calculated from the mass-surface equations of Green *et al.*[10,11]

[10] A. E. S. Green and N. A. Engler, Phys. Rev. **91**, 40 (1953).
[11] A. E. S. Green and D. F. Edwards, Phys. Rev. **91**, 46 (1953).
[12] C. H. Townes and S. Geschwind, J. Appl. Phys. **19**, 795 (1948).
[13] A. Stock and P. Praetorius, Ber. deut. chem. Ges. **47**, 131 (1914).

Coulomb Energy and Nuclear Radius

B. G. JANCOVICI
Palmer Physical Laboratory, Princeton University, Princeton, New Jersey
(Received April 5, 1954)

The apparent discrepancy between the values ($1.45\times10^{-13}A^{\frac{1}{3}}$ cm) for the nuclear radii derived from mirror nuclei and those ($1.2\times10^{-13}A^{\frac{1}{3}}$ cm) derived from μ-mesonic atoms was investigated. The conventional calculation of the Coulomb energy difference ΔE_c between mirror nuclei is improved in two respects: the usual uniform model is replaced by the more elaborate shell model with a finite square well potential, and the exchange terms are taken into account. An equivalent Coulomb radius R_c is defined by $R_c=(6/5)(Ze^2/\Delta E_c)$; an equivalent meson radius is defined by $R_M=(5/3)^{\frac{1}{2}}\langle r^2\rangle_M^{\frac{1}{2}}$, where $\langle r^2\rangle_M^{\frac{1}{2}}$ is the mean square radius of the electrical charge distribution. The two extreme cases of the pairs (F^{17},O^{17}) and (O^{15},N^{15}) are investigated. The computation gives $R_c/R_M=1.18$ in O^{17}, $R_c/R_M=1.07$ in N^{15}. These results are smaller by about 8 percent than the experimental ratios. However, the experimental discontinuity in R_c at the closure of the p shell is reproduced.

I. INTRODUCTION

THE experiments which determine the nuclear radii may be divided into two groups: fast nucleon scattering, α-decay lifetimes, yields of charged particle initiated nuclear reactions, probe the range of nuclear forces, whereas Coulomb energy differences for mirror nuclei, electron scattering, μ-mesonic atom x-rays probe the electrical charge distribution. It is difficult to compare values for the radius of the nucleus as given by methods which belong to different groups, as these methods do not measure the same quantity. On the other side, it is desirable to get consistency inside the same group. The present paper is concerned with the determination of the electrical charge distribution.

Whereas Coulomb energy differences between mirror nuclei were usually explained in terms of a radius of the order of $1.45\times10^{-13}A^{\frac{1}{3}}$ cm, electron scattering,[1] and more recently, μ-mesonic x-rays[2] were fitted by a smaller radius of the order of only $1.2\times10^{-13}A^{\frac{1}{3}}$ cm. Actually, mirror nuclei experiments are concerned with light nuclei, while the most accurate measurements with μ-mesonic atoms are carried out with heavier nuclei. However, the results in each range of A extrapolate very well, and it seems very likely at the present time that the radius from meson experiments would be $1.2\times10^{-13}A^{\frac{1}{3}}$ cm for lighter nuclei. To explain this discrepancy, several authors pointed out that the assumed nuclear model of a uniformly charged sphere was too crude an approximation.

Actually, the electron scattering and the μ-mesonic atom x-rays measure essentially the mean quadratic radius $\langle r^2\rangle_M^{\frac{1}{2}}$ of the charge distribution,[1,3] which is related to the radius R of the uniform sphere model by

$$\langle r^2\rangle_M^{\frac{1}{2}}=(3/5)^{\frac{1}{2}}R, \tag{1}$$

whereas the Coulomb energy difference ΔE_c between mirror nuclei of charges Z and $Z+1$ is related to the same radius R by

$$\Delta E_c=(6/5)(Ze^2/R). \tag{2}$$

If the assumption of a constant charge density is dropped, (1) and (2) may be considered as mere definitions of an equivalent meson radius

$$R_M=(5/3)^{\frac{1}{2}}\langle r^2\rangle_M^{\frac{1}{2}}, \tag{3}$$

and of an equivalent Coulomb radius

$$R_c=(6/5)(Ze^2/\Delta E_c). \tag{4}$$

R_M and R_c are now just a convenient way of expressing $\langle r^2\rangle_M^{\frac{1}{2}}$ and ΔE_c; one can expect that R_M and R_c will, in general, have different values.

It has been proved[3,4] that, if the same charge distribution is assumed for every proton, any departure from the uniform model would lead to $R_c<R_M$, thus making the discrepancy between the two experiments worse. However, qualitative considerations[3] showed that there was some hope to improve things by using a shell model, in which the charge distribution is not the same for all protons, and also by taking into account the exchange terms in the calculation of ΔE_c. If, in a first approximation, the electrostatic field is considered as a perturbation, ΔE_c is the electrostatic energy of the last proton in the Coulomb field of the other protons. The last proton has a smaller binding energy and is often in a higher angular momentum state than the other ones; its wave function extends toward the periphery of the nucleus, where the electrical potential is smaller, and ΔE_c is lowered. The exchange terms also lower ΔE_c. Hence, for a given R_M, a shell model is expected to give a smaller ΔE_c and a bigger R_c than the uniform model. However, a quantitative check of this argument will prove that these effects are not large enough to remove the discrepancy.

It will be shown in the present paper that one has to expect, on the basis of the above model and an $R_M=(5\langle r^2\rangle_M/3)^{\frac{1}{2}}=1.2\times10^{-13}A^{\frac{1}{3}}$ cm, larger Coulomb energies (and hence smaller R_c) than the experimental data give.

Two extreme cases have been investigated: the pairs (F^{17},O^{17}) and (O^{15},N^{15}). In F^{17}, the last proton is in a d state outside the closed s and p shells, thus providing

[1] Lyman, Hanson, and Scott, Phys. Rev. **84**, 626 (1951).
[2] V. L. Fitch and J. Rainwater, Phys. Rev. **92**, 789 (1953).
[3] L. N. Cooper and E. M. Henley, Phys. Rev. **92**, 801 (1953).
[4] F. Bitter and H. Feshbach, Phys. Rev. **92**, 837 (1953).

a highly "favorable" case for computing a small ΔE_e and hence a large R_e. Conversely, in O^{15}, the last proton is part of a closed p shell, and provides an "unfavorable" case.

II. THE SQUARE WELL MODEL

A square well potential was assumed; its radius was arbitrarily taken as $R=1.4\times10^{-13}A^{\frac{1}{3}}$ cm. The initial choice of R is not very important, the ratios R_M/R and R_e/R are not expected to depend significantly on the absolute value of R. The same will be true then of R_M/R_e which is the quantity given by the experimental data.

Let $\psi_l(r)$ by r times the radial part of the wave function for a nucleon of orbital angular momentum l. It is normalized to unity so that

$$\int_0^\infty |\psi_l(r)|^2 dr = 1. \tag{5}$$

It is convenient to express lengths in units of the well radius R, and to set $\rho=r/R$. Inside the well, ψ_l is of the form

$$\psi_l(\rho) = A_l R\rho j_l(\xi_l\rho) \quad \text{for} \quad \rho \leqslant 1. \tag{6}$$

A_l is a normalization coefficient; ξ_l is given in terms of the reduced mass M of the nucleon, its binding energy $|E|$, and the well depth V, by

$$\xi_l = R[2M(V-|E|)/\hbar^2]^{\frac{1}{2}}; \tag{7}$$

j_l is a spherical Bessel function as defined by Schiff.[5] The functions j_l are tabulated.[6]

If the binding energy plus centrifugal barrier of a proton is large as compared to the Coulomb barrier, the deformation of the wave function by the Coulomb barrier can be neglected and the wave function outside the well is correctly represented by

$$\psi_l(\rho) = B_l R\rho h_l(i\eta_l\rho) \quad \text{for} \quad \rho \geqslant 1. \tag{8}$$

B_l is a normalization coefficient;

$$\eta_l = R[2M|E|/\hbar^2]^{\frac{1}{2}}; \tag{9}$$

h_l is a spherical Hankel function.[5] The functions h_l are not tabulated but are easily expressed in terms of rational fractions and exponential functions.

The preceding argument does not apply in the case of the last nucleon of F^{17}, the binding energy of which is very small. In this case one can argue in the following way. The only difference between the Hamiltonians of F^{17} and O^{17} is the Coulomb energy C of the last nucleon. The Hamiltonians are, respectively, $H+C$ and H; the corresponding wave functions are Ψ_F and Ψ_O, which satisfy

$$(H+C)\Psi_F = E_F\Psi_F, \tag{10a}$$

$$H\Psi_O = E_O\Psi_O, \tag{10b}$$

where $|E_F|$ and $|E_O|$ are the binding energies of F^{17} and O^{17}. As far as ground states are concerned, the wave functions minimize energies so that

$$E_O \equiv \langle\Psi_O|H|\Psi_O\rangle < \langle\Psi_F|H|\Psi_F\rangle, \tag{11a}$$

$$E_F \equiv \langle\Psi_F|H+C|\Psi_F\rangle < \langle\Psi_O|H+C|\Psi_O\rangle, \tag{11b}$$

and

$$\langle\Psi_F|C|\Psi_F\rangle < E_F - E_O < \langle\Psi_O|C|\Psi_O\rangle. \tag{12}$$

It could be shown that $\langle\Psi_O|C|\Psi_O\rangle - \langle\Psi_F|C|\Psi_F\rangle$ is much less than 2 percent of E_F-E_O. Consequently, a perturbation theory calculation gives fair results with either Ψ_F or Ψ_O. Actually, $\langle\Psi_F|C|\Psi_F\rangle$ was calculated providing thus a lower limit for E_F-E_O.

The Coulomb wave function used for Ψ_F is

$$\psi_2(\rho) = B_2\mathfrak{F}(R\rho). \tag{13}$$

The well depth is adjusted to fit the experimental binding energy of the last nucleon: this binding energy determines by (9) and (8) or by (13) the wave function outside the well, except for the normalization coefficient B_l. The continuity requirement at $\rho=1$,

$$\left[\frac{1}{\rho j_l(\xi_l\rho)}\frac{d}{d\rho}\rho j_l(\xi_l\rho)\right]_{\rho=1} = \left[\frac{1}{\rho h_l(i\eta_l\rho)}\frac{d}{d\rho}\rho h_l(i\eta_l\rho)\right]_{\rho=1}, \tag{14}$$

or, in the special case of the last proton of F^{17},

$$\left[\frac{1}{\rho j_2(\xi_2\rho)}\frac{d}{d\rho}\rho j_2(\xi_2\rho)\right]_{\rho=1} = \left[\frac{1}{\mathfrak{F}(R\rho)}\frac{d}{d\rho}\mathfrak{F}(R\rho)\right]_{\rho=1}, \tag{15}$$

determines ξ_l, and by (7), the well depth V.

The other wave functions are then determined. Their ξ_l and η_l parameters are obtained from (14) and from the relation

$$\xi_l^2 + \eta_l^2 = R^2 2MV/\hbar^2. \tag{16}$$

The normalization coefficients A_l and B_l are required to fit (5) and the requirement that ψ_l be continuous at $\rho=1$. The integrals on Bessel or Hankel functions,

TABLE I. The Coulomb function $\mathfrak{F}(r)$. $\mathfrak{F}(r)$ is r times the radial part of the wave function for a d proton of reduced mass 16/17, in the field of a central charge $Z=8$, with a binding energy 0.586 Mev.

$10^{13}r$ cm	$\mathfrak{F}$	$10^{-13}(d\mathfrak{F}/\mathfrak{F}dr_{cm})$	$10^{13}(1/\mathfrak{F}^2)\int_r^\infty \mathfrak{F}^2 dr_{cm}$
3.077	1.195	−7.638	0.7535
3.692	0.7621	−6.708	
4.308	0.5141	−5.991	0.9547
4.923	0.3612	−5.438	
5.538	0.2618	−5.004	1.124
6.154	0.1944	−4.655	
6.769	0.1473	−4.370	1.267
7.385	0.1134	−4.131	
8.000	0.08845	−3.930	1.391

[5] L. I. Schiff, *Quantum Mechanics* (McGraw-Hill Book Company, Inc., New York, 1948), p. 77.

[6] *Tables of Spherical Bessel Functions* (Columbia University Press, New York, 1947).

which are required for fitting (5) can be evaluated analytically.[5]

The mean square radius $\langle r^2\rangle_{Av}^{\frac{1}{2}}$ of the charge distribution is then computed for the residual nucleus of charge Z by

$$\langle r^2\rangle_{Av}=(1/Z)R^2\sum\int_0^\infty|\psi|^2\rho^2d\rho, \qquad (17)$$

where the summation extends over all Z protons. The integrals in (17) are easily evaluated analytically by expressing Bessel and Hankel functions in terms of trigonometrical and exponential functions.

The Coulomb energy of the last proton is also computed, exchange terms being included, by Slater's method,[7] leading through (4) to the Coulomb equivalent radius. All integrals involved in this calculation had to be carried out numerically.

III. APPLICATION TO TWO EXTREME CASES

A. $F^{17}\rightarrow O^{17}$

The last nucleon, decaying from a proton to a neutron, is in a d state, outside closed s and p shells.

Well depth

The well radius is initially chosen as $R=3.6\times10^{-13}$ cm. The binding energy of the last proton was taken as $|E|=0.586$ Mev. Outside the well the wave function will be a Coulomb function $\mathfrak{F}(r)$; inside the well, the wave function is taken as a Bessel wave function. The Coulomb wave function $\mathfrak{F}(r)$ was computed by Breit and his collaborators[8] and kindly made available to the author for the above energy, a reduced mass 16/17; an angular momentum $l=2$. $\mathfrak{F}(r)$ is tabulated in Table I, together with its logarithmic derivative and its square integral. One obtains from (15), $\xi_2=4.59$, and from (7), $V=41.2$ Mev.

Wave functions of F^{17}

The wave functions in this well are as follows:

s wave functions

$$\rho\leqslant1:\quad\psi_0=(10.29/R)^{\frac{1}{2}}\rho j_0(2.55\rho),$$
$$\rho\geqslant1:\quad\psi_0=(14200/R)^{\frac{1}{2}}\rho h_0(i3.80\rho);$$

p wave functions

$$\rho\leqslant1:\quad\psi_1=(20.50/R)^{\frac{1}{2}}\rho j_1(3.61\rho), \qquad (18)$$
$$\rho\geqslant1:\quad\psi_1=(1343/R)^{\frac{1}{2}}\rho h_1(i2.88\rho);$$

d wave function,

$$\rho\leqslant1:\quad\psi_2=(30.64/R)^{\frac{1}{2}}\rho j_2(3.61\rho),$$
$$\rho\geqslant1:\quad\psi_2=(23.89/R^3)^{\frac{1}{2}}10^{-13}\mathfrak{F}(R\rho).$$

[7] E. U. Condon and G. H. Shortley, *The Theory of Atomic Spectra* (Cambridge University Press, Cambridge, 1953), Chap. VI.

[8] Breit, Hull, Johnson, Huebner, Benedict, and Smolen (private communication).

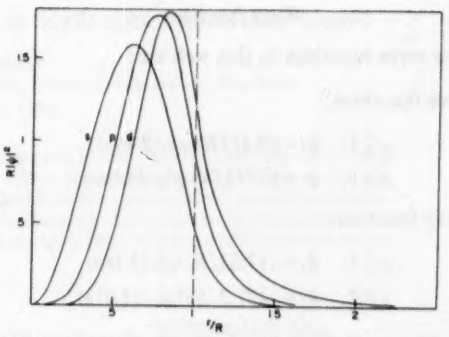

FIG. 1. The wave functions of F^{17}. ψ is r times the normalized radial wave function. The ordinate is $|\psi|^2$ in units of the reciprocal radius of the well.

The squares of these functions (probability of presence at distance r from the origin) are plotted in Fig. 1. 6.5 percent of the s charge distribution, 15 percent of the p one, and 29 percent of the d one are outside the well.

Effective meson radius of O^{17}

The mean square radius is found to be $0.6833R$ for an s wave function and $0.8090R$ for a p one. From (17) and (3) the effective meson radius is found to be $R_M=1.01R$.

Effective Coulomb radius

In Condon and Shortley's notation, the direct Coulomb energy of the d proton is

$$2F^0(d,s)+6F^0(d,p)=8.62(e^2/R). \qquad (19)$$

The exchange Coulomb energy is

$$-(1/5)G^2(d,s)-(2/5)G^1(d,p)-(9/35)G^3(d,p)$$
$$=-0.52(e^2/R); \qquad (20)$$

the total Coulomb energy is thus $\Delta E_c=8.10(e^2/R)$, and by (4), the equivalent Coulomb radius is $R_c=1.19R$.

We thus obtain $R_c/R_M=1.18$.

B. $O^{15}\rightarrow N^{15}$

The β transition is from the configuration s^2p^6; s^2p^5 to s^2p^5; s^2p^4. It is convenient to look at it as a transition of a p hole in closed s and p shells.

Well depth

The well radius is chosen as $R=3.45\times10^{-13}$ cm. The standard value $|E|=8$ Mev was taken for the binding energy of the p nucleons. Corrections of reduced mass were neglected, and also any deformation of the wave functions by the Coulomb field. From (11), one obtains $\xi_1=3.48$, and, from (7), $V=34.6$ Mev.

Wave functions

The wave functions in this well are:

s wave functions,

$$\rho \lesssim 1: \quad \psi_0 = (9.47/R)^{\frac{1}{2}} \rho j_0(2.49\rho),$$
$$\rho \gtrsim 1: \quad \psi_0 = (3373/R)^{\frac{1}{2}} \rho h_0(i3.19\rho); \tag{21}$$

p wave functions.

$$\rho \lesssim 1: \quad \psi_1 = (17.52/R)^{\frac{1}{2}} \rho j_1(3.48\rho),$$
$$\rho \gtrsim 1: \quad \psi_1 = (127.2/R)^{\frac{1}{2}} \rho h_1(i2.07\rho).$$

The squares of these functions are plotted on Fig. 2. 8.8 percent of the s charge distribution, 22 percent of the p one are outside the well.

Effective meson radius of N^{15}

The mean square radius is found to be $0.7030R$ for an s wave function and $0.8767R$ for a p one. From (17) and (3) the effective meson radius is found to be $R_M = 1.07R$.

Effective Coulomb radius

The direct Coulomb energy of a p proton is

$$2F^0(d,s) + 5F^0(p,p) = 7.78(e^2/R). \tag{22}$$

The exchange Coulomb energy is

$$-(1/3)G^1(p,s) - (2/5)G^2(p,p) = -0.48(e^2/R). \tag{23}$$

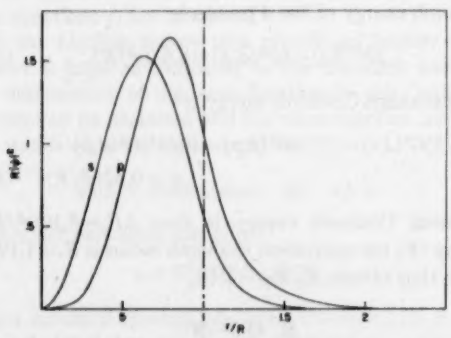

FIG. 2. The wave functions of O^{15}. ψ is r times the normalized radial wave function. The ordinate is $|\psi|^2$ in units of the reciprocal radius of the well.

TABLE II. Values of R_c/R_M.

	Square well	Oscillator well	Experimental
$F^{17} \rightarrow O^{17}$	1.18	1.20	1.27
$O^{15} \rightarrow N^{15}$	1.07	1.08	1.17

The total Coulomb energy is thus $\Delta E_c = 7.30(e^2/R)$, and by (4), the Coulomb radius is $R_c = 1.15R$. We thus get $R_c/R_M = 1.07R$.

IV. THE OSCILLATOR WELL MODEL

It is interesting to see how much the final results R_c/R_M are dependent on the special potential well which is assumed. The same calculations can be carried out, exactly and easily, using Talmi's methods,[9] for the less accurate model of an infinite oscillator well. The results are then $R_c/R_M = 1.20$ for F^{17}, and $R_c/R_M = 1.08$ for O^{15}.

V. DISCUSSION OF RESULTS AND COMPARISON WITH EXPERIMENTAL DATA

The theoretical results and the experimental values are listed in Table II. The experimental values for R_c/R_M are obtained from the experimental R_c and an assumed $R_M = 1.2A^{\frac{1}{3}} \times 10^{-13}$ cm. It is seen that the shell model reproduces the experimental discontinuity in R_c at the closure of the p shell. However, the value of R_c/R_M remains too small by 8 or 9 percent. The oscillator potential's results are very close to the square well's and show that it is not possible to suppress the discrepancy by changing the potential. The results are not very sensitive to the exact form of the potential. Thus, there is still an unexplained discrepancy between the values given for nuclear radii by mirror nuclei and by μ-mesonic atoms.

VI. ACKNOWLEDGMENTS

I am deeply indebted to Professor Wigner who suggested this problem to me and gave me constant guidance and interest during the whole work. I wish to thank Dr. Talmi for many stimulating discussions, and for communicating to me various unpublished results on oscillator well wave functions. Lastly, I am very grateful to Professor Breit and his collaborators who are entirely responsible for the Coulomb wave function material listed on Table I.

[9] I. Talmi, Helv. Phys. Acta **25**, 185 (1952).

Absorption of Tritium Beta Particles in Hydrogen and Other Gases

LEON M. DORFMAN
Knolls Atomic Power Laboratory, General Electric Company, Schenectady, New York*
(Received April 5, 1954)

The absorption curves for tritium beta particles in hydrogen and helium have been determined by using a spherical ion chamber in which the particular gas serves both as the absorber and the ionization medium. The absorption curves give half-thickness values of 0.031 mg/cm² for hydrogen and 0.061 mg/cm² for helium. From the saturation currents obtained with a given amount of tritium the relative energy requirement per ion-pair has been measured for hydrogen, helium, oxygen, and argon. These values are compared with recent values in the literature.

INTRODUCTION

THE conventional method of determining the absorption curves for nuclear beta particles and thus measuring the half-thickness or mass absorption coefficient involves the use of thin metal foils and end-window counters or ionization chambers. Because of the relatively large stopping power of even the thinnest foils the method is restricted to beta particles with energies greater than approximately 0.1 Mev. The results, moreover, are strongly dependent on the geometric arrangement of the source, absorber, and counter.

For very soft beta particles, such as the tritium betas, with end-point energy[1,2] 18 kev and average energy[3] 5.69 kev, no absorption curves or half-thicknesses have been measured. It was desirable to have such information for the interpretation of results obtained in a kinetic investigation[4] of the hydrogen-tritium exchange. At the time an estimate of the mass absorption coefficient for tritium beta particles in hydrogen was made by extrapolation of the known energy-half thickness curve[5] and correction for absorber material on the basis of proportionality to Z/A, the ratio of atomic number to mass number.

A series of experiments has since been carried out in which the absorption curves for tritium beta particles in hydrogen, helium, and oxygen have been determined. The method involves the use of a spherical ionization chamber in which the particular gas serves both as the absorber material and the medium for the ionization produced by the beta particles. In addition to the absorption measurements, comparison of the saturation currents obtained with a given pressure of tritium gives a relative measure of the energy requirement per ion-pair in these various gases.

* The Knolls Atomic Power Laboratory is operated by the General Electric Company for the U. S. Atomic Energy Commission.

[1] Curran, Angus, and Cockroft, Phil Mag. **40**, 53 (1949).
[2] G. C. Hanna and B. Pontecorvo, Phys. Rev. **75**, 983 (1949).
[3] Jenks, Ghormley, and Sweeton, Phys. Rev. **75**, 701 (1949).
[4] L. M. Dorfman and H. C. Mattraw, J. Phys. Chem. **57**, 723 (1953).
[5] C. D. Coryell and N. Sugarman, *Radiochemical Studies: The Fission Products* (McGraw-Hill Book Company, Inc., New York, 1951), Book 1, National Nuclear Energy Series Plutonium Project Record, Vol. 9, Div. IV, p. 18.

EXPERIMENTAL

The ionization chamber for the detection of current was used in conjunction with a vibrating reed electrometer, Applied Physics Corportion, Model 30-R. Currents on the order of 10^{-11} amp were measured by determining the voltage drop across a high external resistance. A vacuum-sealed Victoreen resistor having a resistance of 1.02×10^{8} ohms was used. The resistor and the connections to the electrometer head were electrically shielded. The voltage reading, which is proportional to the ionization current being measured, was taken directly from the meter on the face of the electrometer.

The spherical ion chamber, of simple design, consisted of a glass bulb, silvered on the inside to provide a conducting shell. A negative potential was applied to this silvered surface. The collecting electrode consisted of a 40-mil tungsten wire and was operated at ground potential. A silver guard ring connected to ground prevented current leak from the shell to the central wire. Most of the data were obtained with an ion chamber having an internal diameter of 57.0 mm. A single set of readings was taken with a larger ion chamber having an internal diameter of 73.0 mm.

A stable source of the voltage applied to the chamber was provided by a set of B batteries. With these the applied potential could be varied in convenient steps from 22 to 300 v.

The ionization chamber was connected through a vacuum stopcock to the vacuum system and through a sidearm to a variable level manometer. The arrangement is shown in Fig. 1. The tritium gas consisted of a hydrogen-tritium mixture containing 4.6 percent tritium as determined mass spectrometrically. This gas was introduced into the chamber to a pressure, between 7 and 80 microns, which was read on a McLeod gauge. The gas in which the absorption was to be measured was introduced through a one-way bubbler valve consisting of a pool of mercury on a sintered glass disk. In this way there could be no back diffusion of tritium from the fixed volume which was kept constant by adjustment of the manometer level. A number of readings was taken on the electrometer at each pressure.

Purified gases were obtained in the following manner. Hydrogen was purified by sorption on a uranium bed and subsequent pumping, and could be evolved as

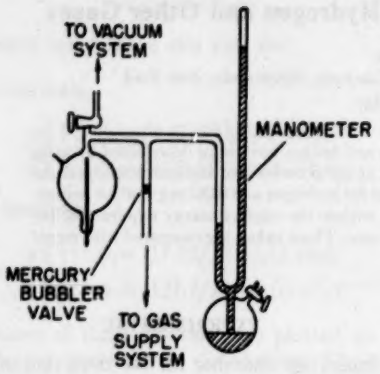

FIG. 1. Ion chamber—vacuum system arrangement.

needed. Pure, dry oxygen was obtained by thermally decomposing potassium permanganate, and passing the evolved gas through a glass coil immersed in liquid nitrogen. Tank helium was used directly. The only detectable impurity in the helium as determined mass spectrometrically was nitrogen, amounting to less than 0.02 percent. Argon was dried by passage through a trap immersed in liquid nitrogen. Mass spectrometric analysis showed the only impurity to be nitrogen, amounting to 0.13 percent.

The ion chamber could be evacuated to a pressure of less than 10^{-5} mm before each set of measurements. Background current, due to contamination of the apparatus with tritium, could easily be kept to 10^{-13} amp or less and was always negligible. It was, however, essential to keep that part of the vacuum system from which the gases were introduced absolutely free of tritium.

In determining the energy requirement per ion-pair in these various gases the same 4.6 percent tritium mixture was used with each gas. A set of readings was taken for each gas with nearly equal tritium pressures to cancel out any irregularities in the McLeod gauge.

RESULTS AND DISCUSSION

Care was taken in all measurements with the ionization chamber to avoid two specific sources of error namely, recombination, particularly in the high-pressure region, and gas multiplication in the low-pressure region. To this end the tritium pressure used was always less than 4 microns. At this pressure, with a potential of 300 v applied to the chamber, the beta-particle intensity was not high enough to give any measurable recombination even at one atmosphere pressure. This could be readily checked in that the ratio of saturation current to tritium pressure was constant for each individual gas. With hydrogen the ionization current amounted to 2.2×10^{-7} amp per mm of tritium. To avoid gas multiplication lower applied voltages were used in the low-pressure region. Indeed, the applied potential was varied for each pressure to insure that the meter reading was taken on a voltage plateau.

Data were obtained by successively increasing the pressure and determining the ionization current at each pressure by reading, on the meter, the voltage drop across the Victoreen resistor. The saturation current is reached as the absorption of beta particles in the gas phase approaches completion.

The absorption may be represented by an approximately exponential law, the result of continuous spectrum and scattering, which for the usual type of experiment may be written

$$A_d = A_0 e^{-\mu d}, \tag{1}$$

where A_0 is the activity measured without absorber, A_d the activity measured through absorber thickness d, and μ is the absorption coefficient. In the present case, where the pressure of a gaseous absorber, rather than the thickness, is increased, the data may be expressed by

$$V_P = V_S(1-e^{-\mu c P}), \tag{2}$$

where V_P, the voltage drop (or meter reading), is proportional to the ionization current at pressure P, V_S is the voltage reading at saturation current, and c is a constant which includes the cell factor and pressure-density conversion factor, or

$$\ln(1-V_P/V_S) = -\mu c P. \tag{3}$$

The absorption curves for hydrogen and helium, represented in this manner, are shown in Figs. 2 and 3

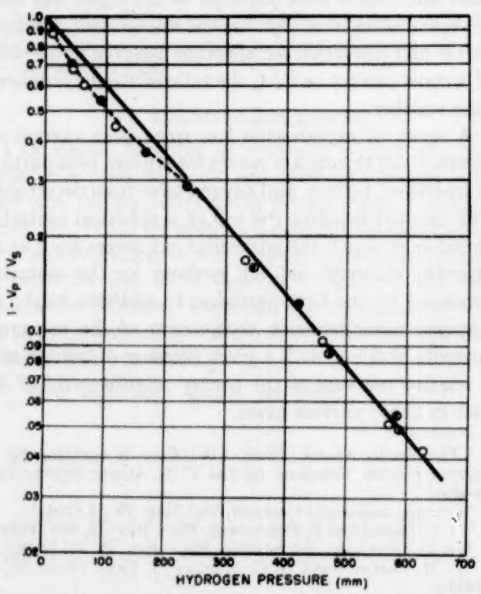

FIG. 2. The absorption curve for tritium beta particles in hydrogen. Chamber diameter 57 mm; temperature 25°C. The different points are for different tritium pressures: ○ 1.9 microns; ● 0.37 micron; ◑ 0.38 micron; ◐ 1.3 microns.

in which $1-V_P/V_S$ is plotted against pressure on a semilogarithmic scale. The different points on the hydrogen curve are for substantially different tritium pressures, ranging from 0.3 to 2 microns. These data were obtained with the small ion chamber. There is a slight deviation from linearity, which is more pronounced in the low-pressure region, where the values of V_P/V_S are somewhat higher than those fitting the linear plot. This deviation is attributable to scattering of the beta particles which strike the silvered shell and are reflected back to the gas phase, causing further ionization.

The pressures corresponding to the half-thickness have been taken from the straight line at the point where $1-V_P/V_S=0.5$. The values are:

$$P_{\frac{1}{2}}=135 \text{ mm for hydrogen,}$$

$$P_{\frac{1}{2}}=133 \text{ mm for helium.}$$

A similar curve, obtained for oxygen at substantially lower pressures, is shown in Fig. 4. The precision is not as good as for the two more transparent gases, giving

$$P_{\frac{1}{2}}=23\pm4 \text{ mm for oxygen.}$$

The half-thickness and mass absorption coefficient may be determined from these results as follows. The source of the beta radiation is uniformly distributed throughout the spherical volume. It may be shown[6] that the average distance from all points within a sphere

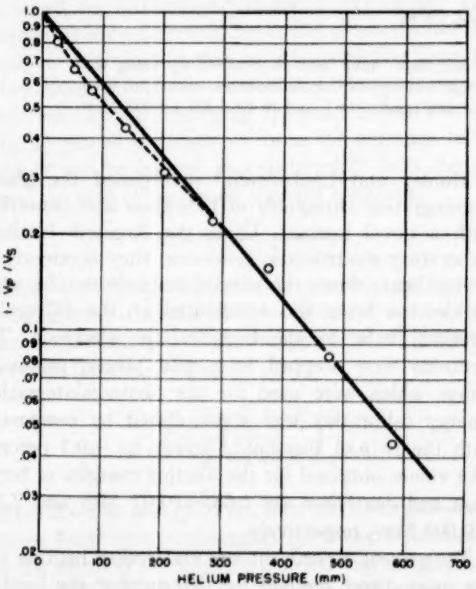

FIG. 3. The absorption curve for tritium beta particles in helium. Chamber diameter 57 mm; temperature 25°C. Tritium pressure, 2.0 microns.

[6] S. C. Lind, *The Chemical Effects of Alpha Particles and Electrons* (The Chemical Catalog Company, Inc., New York, 1928), p. 94.

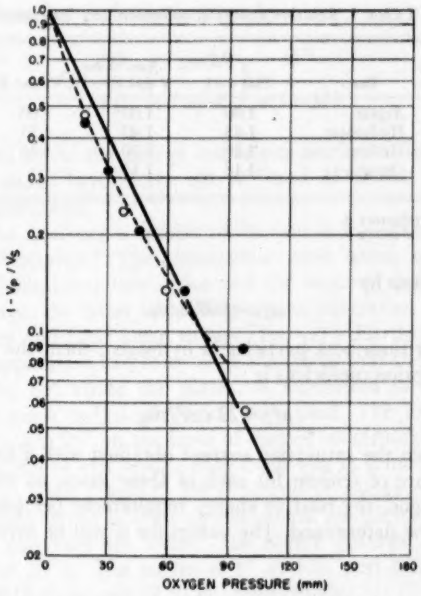

FIG. 4. The absorption curve for tritium beta particles in oxygen. Chamber diameter 57 mm; temperature 25°C. Tritium pressures: ○ 2.0 microns, ● 0.30 micron.

to the shell is 0.75 times the radius. With the small ion chamber, diameter 57 mm, this gives half-thickness values of

$$d_{\frac{1}{2}}=0.031 \text{ mg/cm}^2 \text{ for hydrogen,}$$

$$d_{\frac{1}{2}}=0.061 \text{ mg/cm}^2 \text{ for helium,}$$

$$d_{\frac{1}{2}}=0.08 \text{ mg/cm}^2 \text{ for oxygen.}$$

The measurements for hydrogen have been repeated with the larger ion chamber to check on the inverse proportionality of $P_{\frac{1}{2}}$ to radius. The data for this chamber give $P_{\frac{1}{2}}'=108$ mm. The fact that $P_{\frac{1}{2}}$ is inversely proportional to the radius, and hence $d_{\frac{1}{2}}$ independent of radius, is thus verified since $P_{\frac{1}{2}}/P_{\frac{1}{2}}'=1.25$ and $r_2/r_1=1.28$.

The half-thickness values for hydrogen and helium show very close agreement with the empirical fact that $d_{\frac{1}{2}}$ is proportional to A/Z, the ratio of mass number to atomic number. Comparison of the half-thickness for helium and oxygen with the range[7] in aluminum for 18-kev beta particles indicates these experimental values to be approximately 1/10th the range, which is 0.7 mg/cm². The half-thickness for oxygen fits a straight line through the half-thickness-energy data of Engelkemeier.[5] This last consistency may be purely fortuitous, since the geometry considerations with aluminum absorbers are quite different from those in the present experiment.

The mass absorption coefficient is related to the half-

[7] L. E. Glendenin, Nucleonics 2 (No. 1), 12 (1948).

TABLE I. Relative energy requirement per ion-pair.

Gas	This work	W_{gas}/W_{argon} V and C[a]	W, V, and K[b]
Argon	1.00	1.00	1.00
Hydrogen	1.45	1.41	1.55
Helium	1.28	1.20	1.26
Oxygen	1.18	1.19	—

[a] See reference 8.
[b] See reference 9.

thickness by

$$\mu/\rho = 0.693/d_{\frac{1}{2}}. \quad (4)$$

For tritium beta particles in hydrogen, then, the mass absorption coefficient is

$$\mu/\rho = 22 \text{ cm}^2/\text{mg}.$$

From the saturation current obtained with a known pressure of tritium for each of these gases, as well as for argon, the relative energy requirement per ion-pair may be determined. The values for w will be inversely proportional to the saturation current. These results are given in Table I which contains the numbers relative to argon. The results are compared with those of Valentine and Curran[8] for electrons and Wilzbach *et al.*[9] for tritium beta particles. There is reasonably close agreement among the values. The spread in the results for helium may be due to the trace impurity effect which has been pointed out in the recent work of Jesse and Sadauskis.[10] No attempt has been made to derive absolute values of the energy requirement from the data.

ACKNOWLEDGMENT

The author is grateful to Dr. D. L. Douglas for the advice he has given concerning the construction of the ion chamber and the operation of the electrometer.

[8] J. M. Valentine and S. C. Curran, Phil. Mag. **43**, 964 (1952).
[9] Wilzbach, Van Dyken, and Kaplan, Argonne National Laboratory Report No. 5143, October, 1953; Anal. Chem. **26** (5), 880 (1954).
[10] W. P. Jesse and J. Sadauskis, Phys. Rev. **94**, 764 (1954).

PHYSICAL REVIEW VOLUME 95, NUMBER 2 JULY 15, 1954

Photodisintegration Thresholds of Deuterium and Beryllium*†

J. C. NOYES,‡ J. E. VAN HOOMISSEN,‡ W. C. MILLER, AND B. WALDMAN
Department of Physics, University of Notre Dame, Notre Dame, Indiana

(Received March 22, 1954)

The photodisintegration thresholds of deuterium and beryllium have been determined by using the bremsstrahlung produced by monoergic electrons. The absolute energy of the electrons was measured with a cylindrical electrostatic analyzer. The binding energy of deuterium was found to be 2.227±0.003 Mev and that of beryllium was found to be 1.662±0.003 Mev.

INTRODUCTION

THE photodisintegration thresholds of deuterium and beryllium have been measured using a number of methods. Stephens,[1] in 1947, presented an exhaustive discussion of the work done on deuterium up to that time. Since 1948 two important experiments have been performed.

Bell and Elliott[2] measured the energy of the gamma ray accompanying the capture of a neutron by a proton. Their spectrometer was calibrated with the 2.615±0.001 Mev gamma ray[3] of ThC″. Their value for the binding energy of the deuteron is 2.230±0.007 Mev.

Mobley and Laubenstein[4] determined the photodisintegration thresholds of beryllium and deuterium with a novel method. Using the Argonne National Laboratory electrostatic generator, they accelerated a proton beam down the normal accelerator tube while an electron beam was accelerated up the differential pumping tube to the high voltage electrode. The electrons were stopped in a gold target, producing x-rays which were used for the photodisintegration. Energy calibration was accomplished by *comparison* with the Li(p,n) threshold,[5] known to ±0.1 percent. The values obtained for the binding energies of beryllium and deuterium are 1.666±0.002 Mev and 2.226 ±0.003 Mev, respectively.

The present experiment was undertaken because it is the most direct method for determining the binding energies. It is an absolute method requiring no nuclear reaction data for calibration.

* Supported in part by the joint program of the U. S. Office of Naval Research and the U. S. Atomic Energy Commission.
† Preliminary report: Phys. Rev. **85**, 727 (1952). A more extensive account of this work appears in a technical report.
‡ Now at Boeing Aircraft, Seattle, Washington.
[1] W. E. Stephens, Revs. Modern Phys. **19**, 19 (1947).
[2] R. E. Bell and L. C. Elliott, Phys. Rev. **79**, 282 (1950).
[3] J. L. Wolfson, Phys. Rev. **78**, 176 (1950); W. L. Brown, Phys. Rev. **83**, 271 (1951); G. Lindstrom, Phys. Rev. **87**, 678 (1952).
[4] R. C. Mobley and R. A. Laubenstein, Phys. Rev. **80**, 309 (1950).
[5] Herb, Snowden, and Sala, Phys. Rev. **75**, 246 (1949).

EXPERIMENTAL ARRANGEMENT

The photodisintegration thresholds of beryllium and deuterium were determined as follows: Electrons from the electrostatic generator entered a 90-degree cylindrical electrostatic analyzer, which served as an energy selector. The electrons which emerged from the analyzer struck a thick gold target, producing a continuous x-ray spectrum with an upper energy limit equal to the electrons' energy. The x-rays above threshold disintegrated the beryllium or deuterium, producing neutrons. The neutron yields at various electron energies up to 30 kev above threshold were extrapolated to zero yield. On converting the energy corresponding to zero yield into the center-of-mass system, the binding energies of beryllium and deuterium were obtained.

The uncertainty in threshold energy as determined by this experiment is about 0.1 percent. To realize this accuracy the uncertainties in individual measurements contributing to the threshold measurement had to be kept well below this value. The energy measurement depended only upon a knowledge of the geometry of the analyzer system, and the determination of the deflecting voltage.

A. Electrostatic Analyzer

The theory of the electrostatic analyzer has been reviewed by Bainbridge.[6] Honnold and Miller[7] have developed the relativistic ion optics of an electrostatic analyzer with application to this particular analyzer. They have shown that electrons of kinetic energy T_0 and velocity $\beta_0 c$ emerging from an object slit (see Fig. 1) placed a distance l' from the entrance to the field O' will be imaged at a distance l'' from the exit from the field O'' given by the lens equation,

$$(l'-g)(l''-g)=f^2, \tag{1}$$

where $f=a/[\kappa \sin(\kappa\Phi)]$ = focal length, $g=f\cos(\kappa\Phi)$ = coordinates of focal points, $\kappa=(2-\beta_0^2)^{\frac{1}{2}}$, and a = mean line trajectory, provided the potential difference X between the plates P_1 and P_2 is

$$X=\frac{T_0}{e}\left(\frac{T_0+2R}{T_0+R}\right)\frac{d}{a}, \tag{2}$$

where R = rest energy of electron and d = separation of plates. Furthermore, the energy resolution is determined by the width of the slits in the object and image planes, W' and W'', respectively. For the case where these widths are in the ratio of the lateral magnification of the lens the resolution is given by

$$\frac{dT}{T_0}=\left(\frac{T_0+2R}{T_0+R}\right)\frac{W''}{a(1-M)}, \tag{3}$$

where dT is the energy increment needed to displace the image beyond the slit W'' and M is the lateral magnification.

The analyzer is similar to the one at the University of Wisconsin.[8] The dimensions were based on the available laboratory space and the required deflection voltage, the latter depending on the separation of the plates and their mean radius [Eq. (2)]. Furthermore, the separation had to be large enough so that the beam would not strike the plates. A separation of $\frac{5}{16}$ in. and mean radius of 24 in. were used. The angle Φ was made 90° on the basis of ease of construction and direction of exit beam. This angle was in a horizontal plane. Since l' and l'' are functions of energy, it was decided in the interest of mechanical simplicity to fix one and vary the other. The object distance l' was set at 30 in. The values of l'' at 1.67 and 2.22 Mev were 16.65 in. and 17.54 in., respectively.

The two analyzer plates P_1 and P_2 were cut from one piece of steel. In cross section they were $1\frac{3}{16}$ in. thick and $2\frac{1}{4}$ in. wide and were supported on 6 Mykroy cylinders fastened to a 30-in. by 36-in. steel surface plate. The analyzer plates and slit systems were enclosed in a vacuum housing.

There were four pairs of beam-defining slits used with the analyzer. The object slits S_1, were in the object plane, 30-in. from the entrance end of the analyzer. Two pairs of slits, S_2 and S_3, were located at the entrance and exit ends of the analyzer, and were spaced 0.100 in. from the ends of the analyzer plates. Slits S_2 and S_3 served to define the electric field at the ends of the analyzer. The fourth pair of slits, S_4, was in the image plane. Since the image distance varied with beam

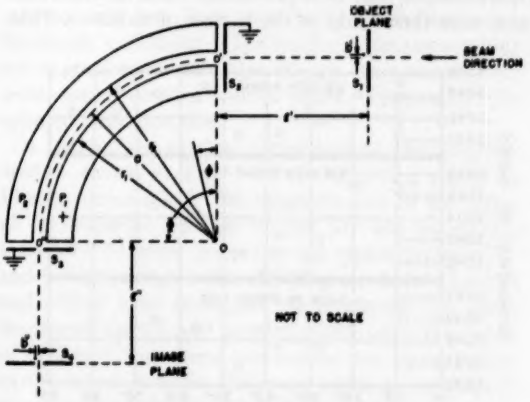

FIG. 1. Plan of electrostatic analyzer.

[6] K. T. Bainbridge in *Experimental Nuclear Physics*, edited by E. Segrè (John Wiley and Sons, Inc., New York, 1953), Vol. 1.
[7] V. R. Honnold and W. C. Miller, Nuclear Physics Technical Report No. 2, University of Notre Dame, 1953 (unpublished).
[8] Warren, Powell, and Herb, Rev. Sci. Instr. 18, 559 (1947).

energy provision was made to vary the distance of S_4 from the analyzer by means of a carriage driven by a screw.

B. Alignment

The inner analyzer plate P_1 was bolted into place on its three Mykroy insulators and two sets of measurements were made on the surface of radius r_1. First, relative variations of the radius of curvature at three different depths from the top surface of the analyzer were obtained by means of a traveling dial gauge moving perpendicularly to the surface plate. The dial gauge was zeroed at a position $\frac{1}{8}$ in. from the top of the analyzer, then readings were taken at a position $\frac{5}{8}$ in. from the top (center of analyzer) and at a position $1\frac{1}{16}$ in. from the top surface. The measuring apparatus was then moved to another angular position, the gauge re-zeroed at the $\frac{1}{8}$ in. depth, and deviations again noted at the other two depths. These sets of three relative measurements were made at a total of eleven angular positions, approximately 9° apart.

The second set of measurements on this surface was a determination of the variation of radius of curvature as a function of angular displacement from the entrance end, the variations in radius being measured relative to the entrance end. The traveling dial gauge was fastened to a radius arm pivoted at *0*, Fig. 1, and was zeroed at a point $\frac{1}{8}$ in. below the top of the analyzer plate at the entrance end (0°). Variations from zero were then observed at the ten other angular positions previously mentioned, all at the same depth of $\frac{1}{8}$ in.

From these sets of measurements one could compute the relative variations of radius from a point $\frac{1}{8}$ in. below the top of the analyzer plate at the entrance end.

The outer analyzer plate P_2 was then moved into position and separated from the inner plate by three machined steel spacers of 0.3042 in. thickness. The plate was adjusted for a snug fit of the spacers, then was bolted down and the spacers removed. The same measurements that were previously made on the inner plate were then made on the surface of radius r_2. This outer plate had been machined much more accurately than the inner plate, as no variations in radius from upper to lower position could be detected. The variations in radius as a function of angle at a depth of $\frac{1}{8}$ in. from the top surface were recorded.

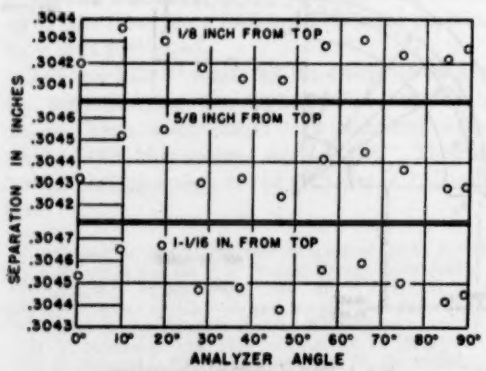

FIG. 2. Measurements of analyzer plate separation as a function of the angle from the analyzer entrance.

Assuming then that the separation of the two plates at the top at 0° was 0.3042 in., one could compute the separation between the two plates at the eleven angular positions and at three different depths from the top of the analyzer plates. These are shown in the graph of Fig. 2. From this graph the separation of the plates in the usable portion of the analyzer ($\frac{5}{8}$ in. depth) was taken as 0.3044±0.05 percent.

Absolute measurement of the radius of curvature of the inner plate was made with a cathetometer. The inner radius r_1 is 23.851 in.±0.005 percent. The outer radius r_2 is 24.155 in.±0.005 percent, and the geometric mean radius a is 24.002 in.±0.01 percent.

The next alignment step was the location of the entrance slit S_1 on a line tangent to the arc $O'O''$ and perpendicular to the line OO'. This was done by triangulation.

Herzog[9] has shown that for an analyzer spacing of 0.304 in., the fringe field at the ends of the analyzer can be considered equal to zero if the field confining slits S_2 and S_3 are opened to a separation of 0.060 in. and spaced from the analyzer ends by 0.075 in. The spacing was adjusted with feeler gauges. However, during the running of the experiment it was found necessary to increase the spacing, due to voltage breakdown from the analyzer plates, and to open slit S_2 wider to permit more beam current to enter the analyzer. The final experimental data were taken with both slits at a distance 0.100 in. from the analyzer ends, with S_2 opened to 0.075 in. and S_3 opened to 0.060 in. The effect of these changes was to increase the effective analyzer angle slightly, due to greater fringing at the ends. The change in analyzer angle causes a negligible shift in the image distance l'' and in the magnification M, and hence in the resolution.

Slit S_4 was set at the proper value of l'' and its position in the image plane (transverse to the beam) was adjusted so that the beam current passing through it was a maximum. This method of location of S_4 compensates for the increased angle of the analyzer due to the fringe fields.

It can be shown by use of Honnold and Miller's[7] Eq. (18) that for the particular conditions of this experiment slit S_3 limits the electron beam energy to about ±3 kev. More recently, further experiments to check this method of positioning S_4 were undertaken by Bhattacherjee, Waldman, and Miller.[10] Their data show that the position of slit S_4 for maximum current through it corresponds to the location of S_4 on the

[9] R. Herzog, Z. Physik **89**, 447 (1934); **97**, 596 (1935); Physik. Z. **41**, 18 (1940).

[10] Bhattacherjee, Waldman, and Miller, Phys. Rev. **95**, 404 (1954).

tangent line to the circular orbit in the analyzer drawn at the *effective* end of the electrostatic field.

C. Measurement of Voltage

A tapped resistance voltage divider was placed from each analyzer plate to ground. The potential difference between the plates was computed from the measured potential difference between the two taps.

The resistors for the voltage dividers were manufactured by the Shallcross Manufacturing Company. Each divider consisted of twenty-five one-megohm two-watt resistors and a 750-ohm tap resistor. The resistors were of 1 percent accuracy and 0.01 percent stability.

One of these one-megohm resistors was chosen as a standard and the ratio of each of the fifty resistors in the dividers to the standard was measured with a simple circuit containing a Leeds and Northrup-type K potentiometer and a Vibrating Reed Electrometer as a null detector. The two 750-ohm tap resistors were connected in series and their ratio to the standard one megohm was measured. This was done in two steps through two precision resistors (10K and 100K) in order to keep the resistance ratios to a maximum of ten. From these ratios the ratio of the fifty one megohm resistors to the two 750-ohm tap resistors was computed. The accuracy of this ratio is ± 0.02 percent. The voltage between the analyzer plates was the product of this ratio and the potentiometer voltage.

The resistor temperature coefficient was 0.002 percent per degree C. A test voltage of 1000 volts applied to one of the one-megohm resistors produced a temperature change of 20°C, or an increase of resistance of 0.04 percent. Since 700 volts was the largest voltage drop per resistor needed during the photodisintegration experiments, the maximum error in the voltage divider ratio due to resistor temperature coefficient was approximately 0.02 percent. This error would result if the tap resistance did not change value due to heating, while the one-megohm resistors heated up. An air circulating system minimized this effect.

The voltage divider resistors were mounted in groups of three between corona-free shields supported by 1-in. Lucite insulating columns. Each stack assembly was inclosed in a 7-in. diameter Lucite cylinder 24 in. high, similar to the method of Henkel and Petree.[11] The whole assembly was sealed after a desiccant had been placed inside to reduce the effect of humidity. A blower circulated air inside the stacks.

The potentiometer used to measure the voltage across the tap resistors was a Rubicon Portable Precision Potentiometer. The limit of error of the potentiometer was the voltage corresponding to one slide wire division plus 0.05 percent of the voltage reading of the dial switch. The potentiometer measured a standard cell to within 0.02 percent of its Bureau of Standards certified value.

The voltage supply for the analyzer plates was composed of two 30 kv power supplies in series, additional filters, the resistor voltage dividers, and a stabilizing network. In series with the output of the positive supply was a series regulator tube whose bias was controlled by the light from the galvanometer in the potentiometer circuit. The stabilization of the analyzer voltage effected by this feedback system and by deriving the input ac power from a Sorensen Regulator was such that, with no beam through the analyzer, the voltage varied less than 3 volts out of 30 000 volts. During operation, small breakdowns would cause the voltage to jump at times, but the average stability was of the order of 0.02 percent or 0.03 percent.

MAGNETIC FIELD

A small magnetic field in an analyzer used for electrons will affect the energy determination. The radial component of this field, directed from one plate to the other, would produce beam deflection perpendicular to the plane of the analyzer. Deflection in this direction would not affect the accuracy of the experiment, but would tend to bend the beam out of the analyzer. On the other hand, the vertical component of magnetic field would produce deflection in the plane of the analyzer.

The steel analyzer plates were degaussed until the vertical component was comparable to the earth's field. The radial component was sufficiently small so that the electron beam was not deflected out of the central portion of electric field.

The magnetic field was measured by two methods, one used before the threshold determinations, the other used afterward. In the first method, the measurement of the magnetic field in the gap, was made with a flip coil and ballistic galvanometer. In the second method the magnetic field was measured by the peaking strip method and has been described by Bhattacherjee, Waldman, and Miller.[10] The results of the two methods are in good agreement even though the measurements were spaced many months apart. Presumably the magnetic field is stable.

A plot of the vertical component of the magnetic field is shown in Fig. 1 of the following paper by Bhattacherjee *et al.*[10] The magnetic field in the region of the analyzer between 0° and 55° has an average value of 0.12 gauss up and in the region between 55° and 90° an average value of 0.20 gauss down. Honnold and Miller[7] have developed the relativistic ion optics for crossed electric and magnetic fields using the results of Millett.[12] Thus these two regions can be considered as two lenses in series. Electrons which satisfy Eq. (2) would suffer deflections in both regions. Moreover, in the region between S_1 and S_2, and again between S_3

[11] R. L. Henkel and B. Petree, Rev. Sci. Instr. **20**, 720 (1949).

[12] W. E. Millett, Phys. Rev. **74**, 1058 (1948).

and S_4 where the electric field is zero, the electrons will be deflected by mainly the earth's field. Honnold and Miller have shown that the effect of these magnetic fields is to deflect the beam passing through the analyzer toward larger radius of curvature. Thus the value of the kinetic energy computed by use of Eq. (2) must be reduced. The corrections are 3.5 kev for the deuterium threshold and 3.4 kev for the beryllium thresholds (see Table I).[13]

EXPERIMENTAL PROCEDURE

The general plan of the electrostatic generator, analyzer, and counters is shown in Fig. 3. The target was a $\frac{1}{16}$ in. thick gold disk, a "thick" target for the energies under consideration. The material to be disintegrated, beryllium or deuterium oxide, was placed in a cavity in a cylindrical lead shield, of 6 in. outer diameter and $8\frac{1}{2}$ in. length. The cavity containing the sample was $3\frac{1}{4}$ in. in diameter and 7 in. long, concentric with the cylinder. A $\frac{3}{4}$ in. hole was drilled along the cylinder axis, from the base to the cavity.

The lead shield containing the sample, was oriented with its axis horizontal, and pushed up to the gold target so that the target projected approximately $\frac{3}{8}$ in. inside the cavity. By shielding in this manner, only x-rays from the direction of the target could disintegrate the sample.

The lead shield was encased in a block of paraffin 10 in.×11 in.×15 in. A BF_3 (enriched boron 10) neutron counter was inserted in a hole in the paraffin directly above the target and sample, with its axis horizontal and perpendicular to the direction of the beam. By placing the counter above the target, the highly forward-directional x-rays from the target caused little background in the counter.

A Geiger counter was located directly behind the $\frac{3}{4}$-in. hole in the lead shield. It was well shielded by lead from all directions except on the line to the target.

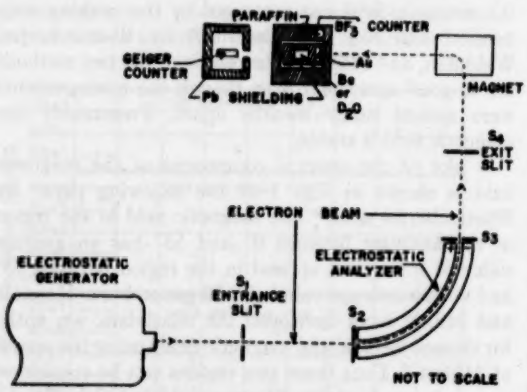

FIG. 3. Schematic layout of apparatus.

This counter was used to monitor the x-rays from the target.

For the beryllium disintegration experiment, a cylinder of Be, 2 in. in diameter and 2 in. long, weighing 192 grams, was placed in the shield next to the target. A resolution of 2 kev was used, which required slit widths of 0.041 in. and 0.031 in. for S_1 and S_4 respectively.

The beam impinging on the gold target produced bremsstrahlung. A sufficient number of monitoring x-ray counts was taken to insure good statistical accuracy. The number of neutron counts in the time required to accumulate a standard number of x-ray counts was then recorded. This number of neutron counts, less background, furnished one point on the yield curve.

To change the analyzer voltage it was sufficient merely to change the potentiometer to the new setting, the high gain of the stabilizer causing the analyzer voltage to follow. At this new voltage the neutron counts for the standard number of x-ray counts were again recorded. This process was continued to below threshold, where only background neutrons were recorded. (Background *ca* 20 counts/1000 sec.)

The target assembly was originally installed just beyond the image slit S_4. It was found that when the generator voltage was slightly high, so that the beam entered the analyzer but struck the outer half of slit S_3, a greater number of neutron counts was recorded than when the beam was directed down the middle. This was caused by x-rays from slit S_3 disintegrating the sample. To eliminate this the target was moved to the position shown in Fig. 3, adequate shielding being interposed between slits S_3 and S_4 and the sample. The necessary change in direction of the beam was effected by an electromagnet. This magnet served merely to change the beam direction by 90°, and was not used in energy determination. It was located 49 in. from S_4, a distance great enough so that its small stray field would have no effect on the beam in the analyzer. The target was 14 in. from the exit edge of the magnet.

The disintegration of deuterium was carried out in the same manner as for the beryllium. The sample was 130 grams of heavy water D_2O, 99.9 percent pure, sealed in a brass container. A resolution of 3 kev at 2.2 Mev was obtained by opening slits S_1 and S_4 to 0.063 in. and 0.048 in., respectively.

A greater slit opening was found necessary at the higher energy because of the poorer stability of the voltage of the electrostatic generator. The generator potential was stabilized by both a capacitive stabilizer[14] and a slow-acting spray voltage regulator,[15] which together maintained an average long-time generator stability of about ±0.4 percent. A poor stability

[13] The major portion of this correction is due to the deflection produced by the earth's field in the region outside the analyzer plates.

[14] Miller, Waldman, Noyes, and Van Hoomissen, Phys. Rev. 77, 758 (1949).

[15] A. O. Hanson, Rev. Sci. Instr. 15, 57 (1944).

required a longer period of time to obtain a given normalizing x-ray count, and hence meant a larger background count in the Geiger counter, with greater attendant errors.

THEORY

The deuteron problem is well known and has been solved exactly as far as the limits of error in this experiment are concerned. Bethe[16] in a summary of the work done on the problem shows that the deuteron near threshold is photomagnetically disintegrated. He gives the following expression as the photomagnetic disintegration cross section,

$$\sigma_m=\frac{2\pi}{3}\frac{e^2}{\hbar c}\frac{\hbar^2}{M}\frac{(W_1E)^{\frac{1}{2}}(W_1^{\frac{1}{2}}+W_0^{\frac{1}{2}})^2}{(E+W_1)(E+W_0)Mc^2}(\mu_P-\mu_N)^2, \quad (4)$$

where $E=h\nu-W_1$, W_1 is the deuteron binding energy, W_0 is the fictitious binding energy for the singlet state, and μ_N and μ_P are the nuclear magnetic moments of the neutron and proton respectively. This expression involves E which has a definite value for a given incident x-ray energy. We are concerned with all x-ray energies in the energy interval between threshold and the energy of the electrons. We call this interval y and integrate this cross section over y. The result is

$$\sigma_x=k'[4638.22y^{\frac{1}{2}}+(3297.78y-6500.5023)\tan^{-1}0.671156y^{\frac{1}{2}}-(1088.485y+69.66304)\tan^{-1}3.9528050y^{\frac{1}{2}}], \quad (5)$$

where σ_x is a measure of the total probability of a disintegration taking place, and k' is a slowly varying function of the incident x-ray energy and is a constant over the range of energies under consideration. It should be noted that this expression is dependent only on y. A plot of σ_x/k' against y on log-log paper results in a straight line with a slope of 2.365. Thus a linear plot of the 2.365th root of the neutron yield against the electron beam energy should result in a straight line. The extrapolation of this line to zero neutron yield determines the threshold energy.

In applying the above theoretical relations the energy must be referred to the center-of-mass system. In the case of deuterium 1.3 kev must be subtracted from the electron energy (for the 30-kev interval).

Because of the complexity of the beryllium nucleus, the situation viewed from the theoretical standpoint is not nearly so clear-cut as in the case of deuterium. Guth and Mullin[17] developed the photodisintegration cross section for Be^9. Making the proper approximations due to near-threshold energies in their expression and integrating over y gives

$$\sigma_x=Af(E_i)\int_{E_0}^{E_i}(E-E_0)^{\frac{1}{2}}(E_i-E)dE,$$
$$\sigma_x=B(E_i-E_0)^{5/2}=By^{5/2}, \quad (6)$$

where E_i is the energy of the incident electron beam, E is the x-ray energy, E_0 is the threshold energy, $f(E_i)$ is a slowly varying function of energy and is constant over y, and A and B are constants. σ_x is a measure of the total probability of a disintegration taking place and is therefore directly proportional to the neutron yield in a disintegration experiment. Thus theory predicts that the neutron yield should vary directly as the 5/2 power of y.

As mentioned above it is necessary to subtract a center-of-mass correction of 0.2 kev.

TABLE I. Summary of errors.

Ratio of separation of plates to mean radius (d/a)		
Inner radius (r_1)		0.005%
Outer radius (r_2)		0.005%
Mean radius (a)		0.01 %
Separation of plates (d)		0.05 %
	Total	0.05 %
Voltage measurement		
Voltage divider ratio		0.02 %
Potentiometer		0.05 %
Voltage stabilization		0.03 %
	Total	0.06 %
Magnetic field correction		
Correction of 3.5 kev ±10%		0.02 %
	Grand total	0.08 %
Energy resolution due to slit widths (at 2.23 Mev)		0.13 %
	(at 1.66 Mev)	0.12 %

EVALUATION OF DATA

Using the procedure described in the experimental section six runs were made to determine the binding energy of beryllium. Slit widths corresponding to 2-kev resolution of the beam energy were used. Because of this, 2-kev steps in beam energy from 20 kev above threshold down to threshold were used.

Each run was plotted individually on a log-log plot and the best straight line for the 20-kev beam variation was chosen. The average slope of these straight lines was close to 2 instead of the theoretical value of 5/2. Because of this the square root of the neutron yield was plotted against beam energy on a linear plot and these straight lines extrapolated to zero neutron yield to determine the threshold.

Figure 4 is a plot of neutron yield *vs* corrected electron energy. The correction consisted of −3.4 kev for the magnetic field effect and −0.2 kev for the motion of the center-of-mass. Figure 5 is a plot of the square root of the neutron yield *vs* corrected electron energy.

[16] H. A. Bethe, *Elementary Nuclear Theory* (John Wiley and Sons, Inc., New York, 1947).
[17] E. Guth and C. J. Mullin, Phys. Rev. **76**, 234 (1949).

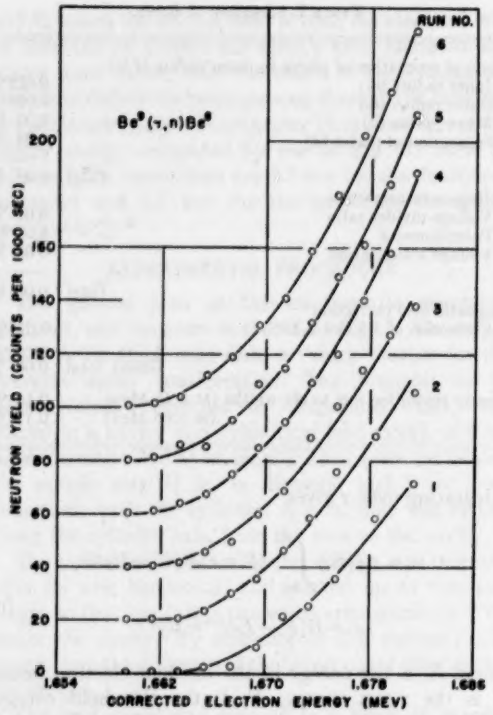

FIG. 4. Neutron yield for photodisintegration of beryllium. The ordinates for the different runs have been shifted for clarity.

Table II summarizes the determination of the binding energy from the data.

The internal consistency of these data is not as good as that for the deuterium determination nor does the yield follow the theoretical 5/2 power. In virtue of this we do not feel justified in attaching an error of less than 3 kev to the binding energy.

Four runs were made to determine the binding energy of deuterium. A run consisted of measuring the neutron yield at various beam energies from 35 kev above threshold down to threshold. Five-kev steps in beam energy in the upper energy region and three-kev steps in the lower energy region were used. Each run was analyzed individually using the method outlined above.

Figure 6 is a plot of neutron yield *vs* corrected electron energy. The correction consisted of -3.5 kev for the magnetic field effect and -1.3 kev for the motion of the center-of-mass. Figure 7 is a plot of the 2.365th root of the neutron yield *vs* corrected electron energy. In an attempt to use another method for the location of the threshold a log-log plot of neutron yield *vs* excess electron energy was made.[4] In the region of the log-log plot which distinguished between possible thresholds, the errors associated with each point were so large on the log scales as to obliterate the distinction.

TABLE II. Neutron binding energies for beryllium, in Mev.

Run number	1	2	3	4	5	6
Binding energy	1.6640	1.6624	1.6617	1.6606	1.6606	1.6598
Average	1.662±0.003 Mev					

TABLE III. Neutron binding energies for deuterium, in Mev.

Run number	1	2	3	4
Binding energy	2.2270	2.2272	2.2271	2.2270
Average	2.227±0.003 Mev			

Table III summarizes the determination of the binding energy from these figures.

The results of the four runs show a much better internal consistency than that indicated by the stated error of 3 kev. As shown in the experimental section the limiting error in this experiment was the energy resolution of the analyzer. This energy resolution was determined by the slit openings used, and was ±3 kev in this case.

DISCUSSION

Li *et al.*[18] have made a compilation of the nuclear disintegration energies of light nuclei. They considered

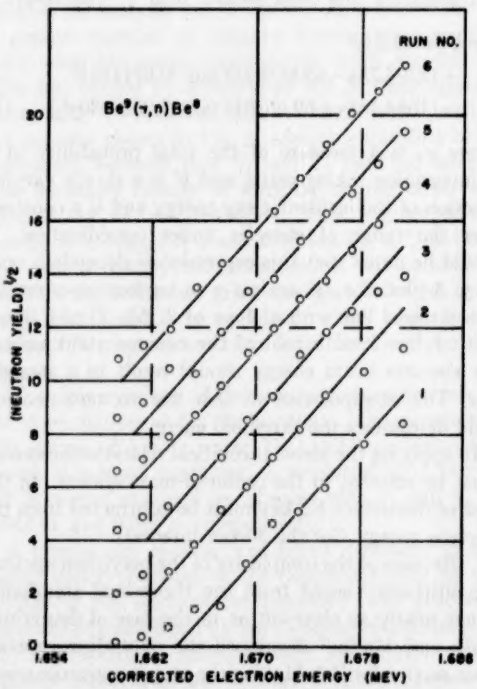

FIG. 5. (Neutron yield)$^{\frac{5}{2}}$ for photodisintegration of beryllium. The ordinates for the different runs have been shifted for clarity.

[18] Li, Whaling, Fowler, and Lauritsen, Phys. Rev. **83**, 516 (1951).

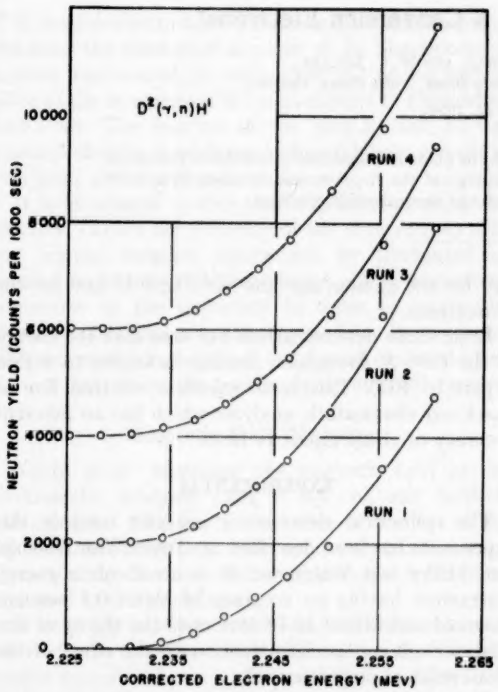

FIG. 6. Neutron yield for photodisintegration of deuterium. The ordinates for the different runs have been shifted for clarity.

only recent experiments and their value for the binding energy of deuterium is a weighted mean of all the nuclear experiments measuring that binding energy directly. Van Patter[19] has extended the work of Li *et al.* His weighted mean for the direct experimental determinations of the deuteron binding energy includes the preliminary Notre Dame value which neglected the magnetic field corrections. Both Li and Van Patter computed a binding energy determined as an internally consistent weighted mean of all the nuclear cycles involving light nuclei that could be combined to give

TABLE IV. Neutron binding energies for deuterium and beryllium, in Mev.

	B.E. of deuterium	B.E. of beryllium
Notre Dame	2.227±0.003	1.662±0.003
Bell and Elliott	2.230±0.007	
Mobley and Laubenstein	2.226±0.003	1.666±0.002
Li *et al.* (weighted exp mean)	2.227±0.002	1.666±0.002
Van Patter (weighted exp mean)[a]	2.228±0.002	1.665±0.002
Li *et al.* (internally consistent mean)	2.226±0.002	1.666±0.002
Van Patter (internally consistent mean)	2.226±0.002	1.666±0.002

[a] Includes preliminary Notre Dame values of 2.231 and 1.664 Mev.

[19] D. M. Van Patter, Massachusetts Institute of Technology Technical Report No. 57, 1952 (unpublished).

n+H−D. Their values, along with those of Bell and Elliott, and Mobley and Laubenstein are presented in Table IV.

Using the HH−D mass difference of 1.445±0.002 Mev from mass spectroscopic data,[20] and our binding energy of deuterium, the n−H difference is 782±4 kev. This, together with the atomic mass of hydrogen,[18] leads to a value of 1.008982 for the mass of the neutron.

In order to provide a check of the accuracy of our electrostatic analyzer, Bhattacherjee, Waldman, and Miller[10] measured the conversion electron energy accompanying the disintegration of Cs^{137}. Their value for the transition energy of 662.6±0.9 kev is in agreement with the 661.60±0.14 kev value of Muller, Hoyt, Klein, and Dumond,[21] and the 661.65±0.15 kev value of Lindstrom, Siegbahn, and Wapstra.[22]

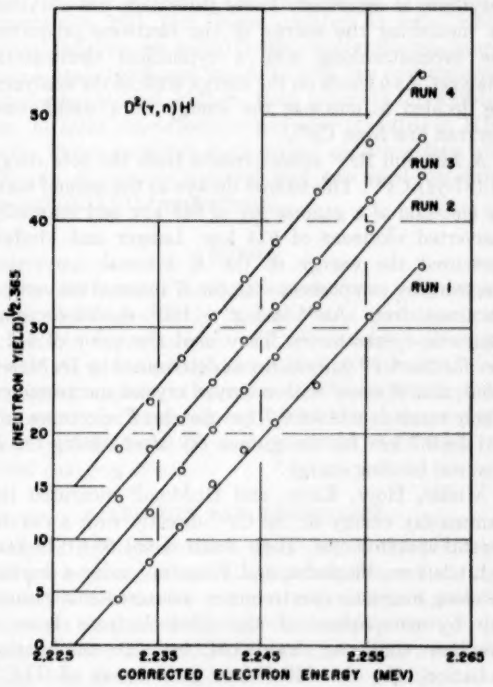

FIG. 7. (Neutron yield)$^{1/2.365}$ for photodisintegration of deuterium. The ordinates for the different runs have been shifted for clarity.

The authors wish to thank T. F. Ruane for the numerical integration of Eq. (4). One of us (J.E.V.), received support during the course of the experiment from the Research Corporation, another (J.C.N.), was a predoctoral fellow of the U. S. Atomic Energy Commission.

[20] T. R. Roberts, Phys. Rev. **81**, 624 (1951).

[21] Muller, Hoyt, Klein, and DuMond, Phys. Rev. **88**, 775 (1952).

[22] Lindstrom, Siegbahn, and Wapstra, Proc. Phys. Soc. (London) **B66**, 54 (1953).

Energy Determination of Cs^{137} K Conversion Electrons*

S. K. Bhattacherjee,† B. Waldman, and W. C. Miller
Department of Physics, University of Notre Dame, Notre Dame, Indiana
(Received March 22, 1954)

The electrostatic analyzer, previously used to determine the photodisintegration thresholds of deuterium and beryllium, has been used to measure the absolute energy of the K-conversion electrons from Cs^{137}. A value of 625.2±0.9 kev was obtained, in agreement with the measurements of others.

INTRODUCTION

In the preceding paper,[1] the determination of the photodisintegration thresholds of deuterium and beryllium is described. These thresholds are obtained by measuring the energy of the electrons producing the bremsstrahlung with a cylindrical electrostatic analyzer. As a check on the energy scale of the analyzer, we decided to measure the energy of a well-known electron line from Cs^{137}.

A 2.60-min Ba^{137} isomer results from the beta decay of (37-yr) Cs^{137}. This isomer decays to the ground state by emission of a gamma ray of 661 kev and internally converted electrons of 624 kev. Langer and Moffat[2] measured the energy of the K internal conversion electrons by comparison with the K internal conversion electrons from Au^{198} using a 180° double-focusing magnetic spectrometer. They used the value of 411.2 kev for the Au^{198} gamma ray as determined by DuMond, Lind, and Watson[3] with a curved crystal spectrometer. Their result is 623.9±0.7 kev for the K electrons and 661.4±0.7 kev for the gamma ray after adding the K electron binding energy.[4]

Muller, Hoyt, Klein, and DuMond[5] measured the gamma-ray energy of the Cs^{137} directly with a curved crystal spectrometer. Their result is 661.60±0.14 kev.

Lindstrom, Siegbahn, and Wapstra,[6] using a double-focusing magnetic spectrometer, measured this gamma ray by comparison of the photoelectrons from a uranium converter irradiated by (a) annihilation radiation, (b) the 510.85-kev gamma ray of ThC″, and (c) the Cs^{137} gamma ray. With the same instrument the energy of the Cs^{137} K conversion electrons was determined by comparison with the conversion electrons of the previously mentioned ThC″ line. The same authors measured the energy of the K conversion electrons of Cs^{137} in a small 180° magnetic spectrograph, calibrating the magnetic field with the proton magnetic resonance absorption. Their final result is 661.65±0.15 kev for the gamma ray and 624.21±0.15 kev for the K electrons.

From these determinations one sees that the energy of the Cs^{137} K conversion electron is known to within 1 part in 4000. This is an excellent electron line to check our electrostatic analyzer which has an inherent accuracy of about 1 part in 1000.

EXPERIMENTAL

The cylindrical electrostatic analyzer used in this experiment has been described by Noyes, Van Hoomissen, Miller and Waldman.[1] It is an absolute energy instrument having an accuracy of about 0.1 percent. Honnold and Miller[7] have developed the theory of this analyzer, giving special attention to the effect of the small residual magnetic field.

Since this analyzer was used originally to analyze the electron beam of our electrostatic generator, the following additional measurements and modifications had to be made for use as a spectrometer: (a) the final detection slit had to be relocated, (b) the low energy of the electrons required a more accurate mapping of the magnetic field, (c) a suitable electron detection device had to be incorporated.

Location of Detection Slit

The plan of the analyzer is shown in Fig. 1 of Noyes *et al.*[1] There are four pairs of beam and field defining slit systems. The object slit S_1 is in the object plane 30 in. from the entrance end of the analyzer. Slits S_2 and S_3, located at the entrance and exit ends of the analyzer, serve to limit the extent of the electric field. Herzog[8] has shown that for the gap width of 0.304 in., the fringe field at the ends of the analyzer can be considered zero if S_2 and S_3 have total widths of 0.150 in. and are spaced 0.060 in. from the plates P_1 and P_2. Slit S_4 is in the image plane located 11.3 in. from the exit end of the analyzer.

The process of placing slits S_1 and S_4 on the tangents to the analyzer at the entrance and exit ends respectively, is very tedious as described by Noyes *et al.* The distance l'' between S_3 and S_4 depends upon the electron energy and must be variable if one desires to use the analyzer as a beta spectrometer. After changing

* Supported in part by the joint program of the U. S. Office of Naval Research and the U. S. Atomic Energy Commission.
† Now at Tata Institute, Bombay, India.
[1] Noyes, Van Hoomissen, Miller, and Waldman, preceding paper [Phys. Rev. 95, 396 (1954)].
[2] L. M. Langer and R. D. Moffat, Phys. Rev. 78, 74 (1950).
[3] DuMond, Lind, and Watson, Phys. Rev. 73, 1392 (1948).
[4] Hill, Church, and Mihelich, Rev. Sci. Instr. 23, 523 (1952).
[5] Muller, Hoyt, Klein, and DuMond, Phys. Rev. 88, 775 (1952).
[6] Lindstrom, Siegbahn, and Wapstra, Proc. Phys. Soc. (London) B66, 54 (1953).
[7] V. R. Honnold and W. C. Miller, Nuclear Physics Technical Report No. 2, University of Notre Dame, 1953 (unpublished).
[8] R. Herzog, Z. Physik 89, 447 (1934).

l'' it is advisable to have a rapid and reliable means of checking the transverse location of S_4. Consequently, a point was located (to within 0.01 in.) on the surface plate at the intersection of both tangents to the median line orbit. The location of the slits S_1 and S_4 was accomplished by a telescope and plumb bobs erected at this point and at either S_2 or S_3.

It is of interest to note that this location of S_1 was identical (within the accuracy of our observation) with the original location determined by triangulation.[1] During the course of the experiment, slit S_4 was moved transverse to the trajectory in order to study the intensity distribution in the image plane. It was found that the maximum height of the K peak occurred when S_4 was located on the previously determined tangent line.

Magnetic Field Mapping

Noyes *et al.*[1] measured the magnetic field in the electrostatic analyzer using a flip coil and ballistic galvanometer. Due to the limitation of the size of the flip coil the deflections were only a few millimeters. Consequently, the more sensitive peaking strip[9] method was used in this experiment.

A strip ($\frac{1}{16}$ in.$\times\frac{3}{8}$ in.$\times$0.005 in.) of Delta-max was inserted into the center of a 1000 turn coil of No. 40 copper wire wound on a Lucite spool (0.40 in.$\times$0.15 in.). This probe was small enough to clear the plates of the analyzer and was mounted on the arm pivoted at O for the mapping between O' and O''.

The probe was used as one of the arms of a Maxwell bridge. The oscillator was a Hewlitt Packard 200-C and the detector was a Hewlitt Packard 300-A Wave Analyzer. It can be shown that any even order harmonic generated in such a probe is practically a linear function of the external magnetic field. Consequently, the oscillator was set at 5 kc/sec and the analyzer at 10 kc/sec. The bridge is balanced with the probe in zero field with both oscillator and detector at 10 kc/sec. The oscillator is then set at 5 kc/sec and its second harmonic remains balanced. Since the Maxwell bridge is frequency independent (for linear elements) the fundamental is almost balanced and thus does not saturate the detector.

This device was calibrated in the field of a standard solenoid for an oscillator voltage of 10 volts at 5 kc/sec. The calibration curve is linear up to 1.5 gauss (the largest field used) and has a slope of 5.6 milligauss/millivolt.

The direction of the magnetic field was determined by superposing a small field of known direction on the probe. An increase in output voltage indicates parallel fields, a decrease indicates antiparallel fields. This small field was obtained by a dc current (from a high impedance source to maintain bridge balance) through the coil of the probe.

The distribution of the magnetic field in the regions between S_1 and S_2, between S_2 and S_3 (0° to 90°), and between S_3 and S_4 is shown in Fig. 1. These measurements agree with the preliminary measurements made by Noyes *et al.* using the small flip coil and ballistic galvanometer.

Honnold and Miller[7] have used these results in their analysis of the effect of this small residual magnetic field on the energy determinations made with this electrostatic analyzer. For the case of the Cs^{137} conversion electrons the energy determined from Eq. (2) of Noyes *et al.* must be decreased by 2.9 kev.

Electron Detection

Due to the high source strength, a directional detector must be used to reduce the background. Preliminary experiments with two Geiger counters in coincidence proved satisfactory. A dual Geiger counter was machined from a brass block and was filled with the conventional argon-ethyl alcohol mixture. Both halves of the counter had the same characteristics and were operated at 1150 volts. The coincidence background counting rate was 100 per 10 minute interval and remained constant throughout all the experiments.

Source

The electrostatic analyzer subtends a very small angle and consequently necessitates a strong source. A distilled water solution of Cs^{137} chloride was evaporated on a one-mil aluminum foil, 0.04 in.$\times$0.5 in., depositing a source of approximately 2 to 3 millicuries. The source, on its aluminum foil backing, was mounted directly behind slit S_1 and grounded electrically to avoid charging effects.

RESULTS AND DISCUSSION

Figure 2 (Experiment I) is a plot of the net coincidence rate *versus* potentiometer reading of voltage across the electrostatic analyzer plates. Slits S_2 and S_3, which act as guard slits at the entrance and exit of the analyzer, were set at 0.15 in., a value which made the fringe field zero.

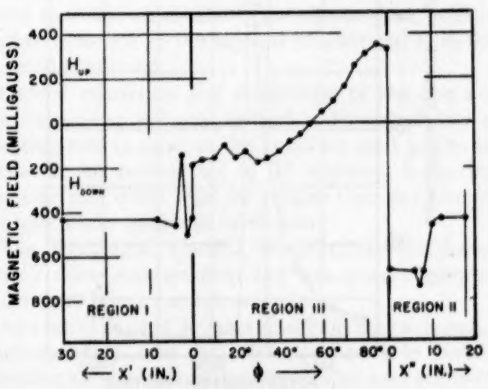

FIG. 1. Vertical component of magnetic field along the electron trajectory.

[9] Adams, Dressel, and Towsley, Rev. Sci. Instr. 21, 69 (1950).

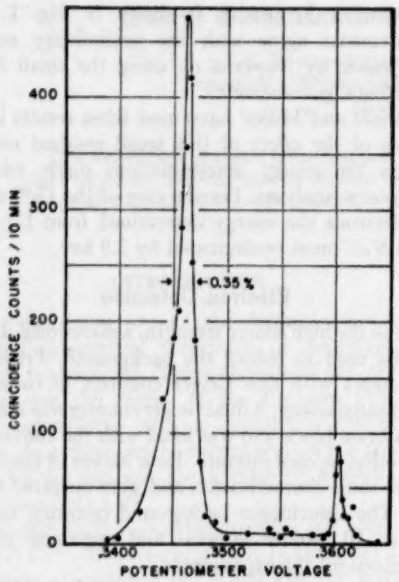

FIG. 2. Experiment I, Conversion electron spectrum. Guard slits S_2 and S_3 set at 0.15 in.

In order to obtain a greater intensity slits S_2 and S_3 were widened to 0.20 in. Figure 3 (Experiment II) is a plot of the data. The increased width of S_2 and S_3 resulted in an increased analyzer angle but this correction is too small to be considered.

Since the sources were relatively thick, the high energy edges of the lines were extrapolated to the abscissas. The potentiometer readings measure the voltage across the analyzer plates and can be converted into the energy of the electrons by Eq. (2) of Noyes *et al.* Table I gives the results of the K and L line energies as determined above.

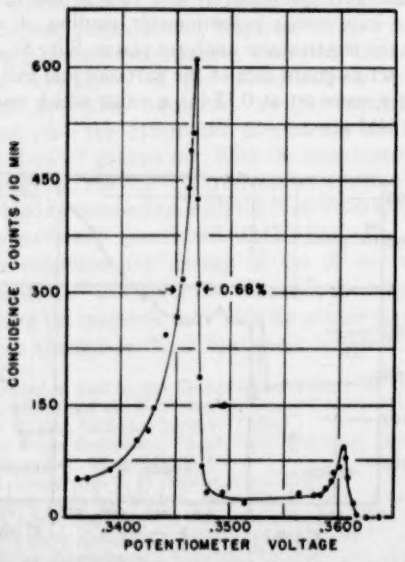

FIG. 3. Experiment II, Conversion electron spectrum. Guard slits S_2 and S_3 set at 0.20 in.

The energy resolution of the analyzer for the slit widths used can be calculated from Eq. (3) of Noyes *et al.* For the K line of Cs^{137} it is 0.9 kev. This means the energy spread admitted by the last slit (S_4) is ± 0.9 kev and is the limiting factor in determining the accuracy of this experiment.

TABLE I. Experimental energy values of K and L lines of Cs^{137}.

Exp.	Line	Potentiometer reading	Electron energy (kev)	Average electron energy (kev)	Magnetic field correction (kev)	Corrected electron energy (kev)	K and L electron binding energies (kev)	Gamma ray energy (kev)
I	K	0.3465	627.77	628.10	2.90	625.2	37.43	662.6
II	K	0.3468	628.44					
I	L	0.3606	658.72	659.06	2.80	656.3	5.99	662.3
II	L	0.3610	659.41					
						$E_L - E_K$ =31.10	$K - L_I$ =31.44	

The L lines were not resolved from the M lines in either Experiments I or II, so that the energy determinations were made by extrapolating the high energy edges of the L peaks at their half-widths. As stated above, the slit-width of S_2 and S_3 in Experiment II had an effect of increasing the fringe field and hence of effectively increasing the analyzer angle. This requires a correction of less than a tenth of a kilovolt. Therefore, arithmetic means were taken for the K-electron and L-electron energies corresponding to these two experiments. The difference between E_K and E_L is 31.10 kev and is to be compared to the binding energy difference between the K and L shells of Ba^{137}. From the data of Hill, Church, and Mihelich[4] this is 31.44 kev. Table II lists the results of this investigation along with those of other workers.

TABLE II. Cs^{137} electron and gamma ray energies.

References	K-conversion electron energy (kev)	Gamma ray energy (kev)
Langer and Moffat[a]	623.9 $\pm$0.7	661.4 $\pm$0.7
Muller, Hoyt, Klein, and DuMond		661.60$\pm$0.14
Lindstrom, Siegbahn, and Wapstra	624.21$\pm$0.15	661.65$\pm$0.15
Present investigation	625.2 $\pm$0.9	(662.6 $\pm$0.9)[b]

[a] May be adjusted for more recent Au^{198} value by adding 0.9 kev.
[b] Calculated with Ba^{137} K binding energy of 37.43 kev (see reference 4).

CONCLUSION

The agreement between the results of the present investigation and those of other investigators is satisfactory. One may now have increased confidence in the absolute energy determinations by our electrostatic analyzer.

One of us (SKB) wishes to acknowledge a Fulbright Grant from the Institute of International Education.

Gamma-Ray Absorption Coefficients for NaI, Cu, Ta, and W†

P. R. HOWLAND AND W. E. KREGER
United States Naval Radiological Defense Laboratory, San Francisco, California

(Received March 29, 1954)

Gamma-ray absorption coefficients have been measured over a range of energies from 0.279 Mev through 1.113 Mev for NaI, Cu, Ta, and W, using an energy-selective scintillation detector. Measurements were made for the absorber position which gave the maximum coefficient, and the results are in good agreement with theory.

INTRODUCTION

SEVERAL recent papers[1–5] have reported experimental gamma-ray absorption coefficients in the region of 1 Mev which are consistently several percent below theoretical values for heavy elements above tin in the periodic table. Since the Klein-Nishina cross section is highly reliable and the pair cross section is small, the theoretical photoelectric cross section would have to be reduced from 10 to 15 percent in order to agree with experiment in this region.

Rudnick,[6] in reinvestigating the absorption coefficient of tantalum for the two Co^{60} gamma rays, found a definite dependence of absorption coefficient on absorber position. Agreement was found between the experimental and theoretical values when the measurement was made at the position which gave the maximum absorption coefficient. It is Rudnick's conclusion that the position of maximum absorption coefficient gives the most reliable experimental result because this position minimizes the various scattering errors.

In the present work several absorption coefficients near 1 Mev have been investigated with an improved experimental technique in an attempt to ascertain whether there are any significant differences between experimental and theoretical values that cannot be assigned to experimental error. It was felt that an improvement in experimental technique could be obtained by employing the scintillation detector method of Colgate[4] and by making experimental measurements in the position giving maximum absorption coefficient, within the limits of the geometry concerned. It should be noted that Colgate's experimental measurements at 0.6616 Mev, made by measuring absorption coefficients as a function of position and taking the maximum value, gave good agreement with theory. However, his measurements at 1.33 Mev, using Co^{60}, were made under a fixed geometry which was apparently not the position of maximum absorption coefficient. However, even when theoretical scattering corrections were applied, the experimental values for elements above tin in the periodic table ($Z>50$) were lower than the theoretical values by amounts several time the experimental error. It is of course possible that insufficient allowance was made for the amount of 1.173-Mev gamma rays detected.[3]

EXPERIMENTAL EQUIPMENT

Detector and Collimator

Figure 1 is a schematic of the collimating apparatus. It is essentially the same as that described by Davisson and Evans[1] with the exception that the Geiger counter is replaced by a scintillation detector. A 1.5-in diameter NaI(Tl) crystal, together with a RCA 5819 photomultiplier is used as the detecting element. A resolution of 11.3 percent was obtained for the Cs^{137} gamma ray at 0.6616 Mev. The output of the photomultiplier was fed into a Radiation Instrument Corporation non-overloading amplifier and then into a Johnstone[7] single-channel differential pulse-height analyzer. The counting channel had a voltage width of ten percent of the voltage at the photopeak maximum. Initially, this channel was adjusted to have the photoelectric peak maximum at its center. The counting rate in the channel was recorded for various absorber thicknesses. An energy-selective detector of this type has a high detecting efficiency for the primary gamma-ray quanta and rejects all scattered radiation except that scattered through small angles. By setting the channel width base line on or above the photoelectric peak, a further reduction in the amount of scattered radiation detected is effected.

Careful regulation and monitoring of the line and photomultiplier voltages insured a reproducibility of counting rate as good as the statistics used in the experiment for periods up to 15 minutes. Long-time counting rate drifts were no greater than ±1 percent per hour under optimum conditions.

The equipment reached temperature equilibrium after a three-hour warmup and was always operated under equilibrium conditions.

As a result of good detector shielding, the background counting rates were less than one part in several thousand and no background corrections were required.

† Supported by Bureau of Ships, U. S. Navy.

[1] C. M. Davisson and R. D. Evans, Phys. Rev. **81**, 404 (1951).
[2] Shimizu, Hanai, and Okamoto, Phys. Rev. **85**, 290 (1952).
[3] G. R. White, Natl. Bur. Standards (U. S.) Rept. No. 1003, May 13, 1952 (unpublished).
[4] S. Colgate, Phys. Rev. **87**, 592 (1952).
[5] S. J. Wyard, Proc. Phys. Soc. (London) **66**, 382 (1953).
[6] N. Rudnick, Mass. Inst. Technol. Laboratory for Nuclear Science and Engineering, Progress Report, May 31, 1952 (unpublished), p. 180.
[7] C. W. Johnstone, Nucleonics **11**, No. 1, 36 (1953).

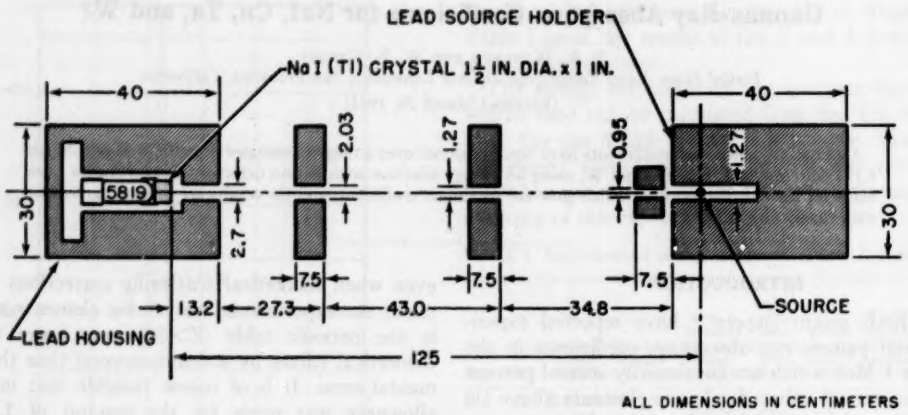

FIG. 1. Geometrical arrangement of collimators.

Counting rate linearity was checked by the method of adding sources and the maximum counting rates were kept in the linear range.

Sources

Radioactive sources obtained from Oak Ridge were placed in Pyrex glass vials of 7-mm outside diameter and 1-mm wall thickness with the exception of the Zn^{65} source whose glass vial had an outside diameter of 8 mm. The tips containing the radioactive material were rounded and of the same wall thickness as the cylindrical sides.

The Hg^{203} source was 50 mC of high specific activity mercury metal reduced from an acid solution with metallic zinc. It was approximately 1 cm in length.

The Au^{198} source was 50 mC of gold foil weighing 0.016 g. The foil was rolled and placed within the tip of its glass container.

The 50-mC source of Cs^{137} was in the form of an evaporated solid. The active portion was less than 3 mm in length.

The Zn^{65} source was 40 mC in strength and was also an evaporated solid extending to a length of about 0.7 cm in its glass vial.

Absorbers

Absorber densities were determined to an estimated accuracy of 0.04 percent. The densities were determined from the dimensions and weights of the various absorbers after machining to the desired sizes. The copper absorbers were made from electrolytic copper bar and were 1 in. in diameter. Spectrochemical analysis showed only trace impurities. The sodium iodide obtained from the Harshaw Chemical Company was in the form of small blocks 2×2×1 in. The density in this case was taken as 3.667 g/cc.[8] The blocks were sealed in light polyethylene bags during the measurements. The absorption coefficient correction due to the bags was found to be negligible. The tantalum and wolfram absorbers were obtained from the Fansteel Metallurgical Corporation and were ground to a diameter of ¾ in. They were certified pure to at least 99.9 percent.

[8] Bell, Davies, Hughes, Jordan, and Randall, Oak Ridge Laboratory Rept. No. 1415, 1953 (unpublished).

EXPERIMENTAL RESULTS

Table I compares experimental and theoretical absorption coefficients.

Since good agreement between theoretical and experimental absorption coefficients for copper has been reported,[1–5] copper absorption coefficients were measured as a check on the reliability of the present experimental equipment. No significant dependence of absorption coefficient on absorber position was noted in the case of copper. This indicated that the degradation of the primary gamma rays by the collimators was negligible since the amount of collimation between source and absorber increased as the absorber was moved nearer the detector. Similar results were presented by Rudnick.[6] There was no measurable dependence of the copper absorption coefficient on the position of the pulse-height analyzer channel with respect to the photoelectric peak. The results of the copper measurements indicated satisfactory operation of the equipment. The measurements for thallium-activated sodium iodide were included because of the widespread use of sodium iodide as a gamma-ray detector. Good agreement with theory is obtained. Bell[8] measured slightly lower values under a somewhat different geometry.

A definite dependence of absorption coefficient on absorber position was found in the case of tantalum and wolfram at both 0.6616 Mev and at 1.113 Mev. The coefficients were measured at the position giving the maximum value. Some dependence of absorption coefficient on channel position was also noted and for this reason the channel base line was set at the highest energy portion of the photoelectric peak consistent with

TABLE I. Comparison of experimental and theoretical gamma-ray absorption coefficients.

Energy Mev	Element	Position[a] cm	Experimental Meas cm²/g	Correction	Final cm²/g	Theoretical White cm²/g	Theoretical Davisson and Evans cm²/g
0.279 (Hg^{203})	NaI	83.5	0.182 ±0.001	0.0009	0.183 ±0.001	0.183	0.195
0.4118 (Au^{198})	W	58.5	0.1736±0.0005	0.0029	0.1765±0.0005	0.1768	0.1821
0.6616 (Cs^{137})	Cu	83.5	0.0724±0.0002	0.0003	0.0727±0.0002	0.0724	0.0725
	NaI(Tl)	83.5	0.0759±0.0003	0.0006	0.0765±0.0003	0.0763	0.0763
	Ta	58.5	0.0925±0.0003	0.0010	0.0935±0.0003	0.0936	0.0959
	W	62.0	0.0937±0.0002	0.0011	0.0948±0.0002	0.0955	0.0970
1.113 (Zn^{65})	Cu	83.5	0.0555±0.0003	0.0002	0.0557±0.0003	0.0554	0.0556
	NaI(Tl)	83.5	0.0541±0.0003	0.0003	0.0544±0.0003	0.0541	0.0551
	Ta	45.5	0.0598±0.0002	0.0006	0.0604±0.0002	0.0603	0.0606
	W	45.5	0.0606±0.0002	0.0007	0.0613±0.0002	0.0607	0.0611

[a] Distance from detector face to absorber face nearest detector.

good statistics. This apparently reduced the amount of scattered radiation detected and tended to give slightly higher coefficients.

THEORETICAL VALUES OF THE ABSORPTION COEFFICIENTS

Theoretical values for the absorption coefficients were obtained by interpolation, using the results of Davisson and Evans[9] and White.[10] Both these papers give calculations of absorption coefficients for gamma rays following the theoretical formulas of several authors. The absorption processes considered are photoelectric effect, Compton scattering as given by the Klein-Nishina formula, pair production in the field of the nucleus, and Rayleigh or coherent scattering. All other processes by which photons interact with matter have been neglected as being too small to effect the results. These include radiative corrections to the Klein-Nishina formula and others which have been discussed by various authors.[1–5]

Interpolations for energies and elements used in the experiment are made for the photoelectric and pair production partial absorption coefficients from accurate plots of the values quoted by Davisson and Evans.[9] The Compton scattering partial absorption coefficients were calculated using their formula 19. To these three partial absorption coefficients we have added a calculated coherent scattering coefficient[11] to give total absorption coefficients for the elements and energies used. The values for NaI(Tl) were obtained from the coefficients of Na, I, and Tl using formula 64 of reference 9 to calculate the values for the crystal. A 0.2 percent Tl content by weight was assumed.

The values according to White[10] are interpolations from plots of $(\mu/\rho)A$ *versus* Z at energies from 0.2 Mev to 1.5 Mev as taken from White's tables. From these plots the values of $(\mu/\rho)A$ are taken at the Z's of interest and plotted against energy. From these curves the values for the total absorption coefficients are obtained at the energies and for the elements used. Values for NaI are taken from a plot of White's values of μ/ρ for NaI.

CORRECTIONS

The theoretical absorption coefficients with which the experimental results are compared are calculated on the basis that any absorption or scattering process that acts on a gamma-ray photon in the absorber removes it from detection. However, the radiation detected actually includes a small amount of scattered radiation from the absorber. Although energy discrimination is used, it is possible to detect photons which have been scattered through as much as 15° under these energy discrimination conditions. Collimation reduces this scattering angle in the absorber to about 2° for scattered radiation which is detected, and it is therefore necessary to correct the intensity detected for that amount which undergoes Compton and coherent scattering in the absorber.

If I_0 is the intensity reaching the detector with no absorber present and I_1 and I_2 are the intensities reaching the detector with absorbers 1 or 2, respectively, present, then $I_1=I_0\exp(-\mu x_1)+I_{s1}$, where I_{s1}=intensity scattered into detector by Compton and Rayleigh scattering and μ=total absorption coefficient. Also

$$I_2=I_0\exp(-\mu x_2)+I_{s2},$$

so that

$$\ln(I_1/I_2)=-\mu(x_1-x_2)+\ln(1+s_1)/(1+s_2),$$

where

$$s_1=I_{s1}/I_0\exp(-\mu x_1),$$

and

$$s_2=I_{s2}/I_0\exp(-\mu x_2),$$

[9] C. M. Davisson and R. D. Evans, Revs. Modern Phys. **24**, 79 (1952).
[10] Gladys R. White, Natl. Bur. Standards Rept. No. 1003, 1952 (unpublished).
[11] W. Franz, Z. Physik **98**, 314 (1935).

with the result that

$$\mu = 1/(x_2 - x_1)\{\ln(I_1/I_2) - \ln(1+s_1)/(1+s_2)\}.$$

The values for s_1 and s_2 are calculated using the method described in reference 1 and 4. These scattered intensities include the coherent and Compton-scattered radiation and depend on the maximum angle of scatter in the absorber of a photon which can reach the detector. Values of $\ln(1+s_1)/(1+s_2)$ are given in Table I. These corrections were minimized experimentally by placing the absorber in the position which gave the largest effective absorption coefficient.

DISCUSSION

The results of this experiment using differential energy selection indicate very good agreement with theory when the absorption coefficient is maximized by appropriate positioning of the absorber.

As a result it seems likely that the present theoretical expression[12] for the photoelectric cross section is reliable near 1 Mev for heavy elements through $Z=74$ (wolfram).

The authors desire to thank Mr. R. A. Taylor for invaluable help with regard to electronic problems.

[12] Hulme, McDougall, Buckingham, and Fowler, Proc. Roy. Soc. (London) **A149**, 131 (1935).

PHYSICAL REVIEW VOLUME 95, NUMBER 2 JULY 15, 1954

New Isotopes of Niobium: Nb^{89} and Nb^{89m}†

R. M. DIAMOND
Department of Chemistry, Harvard University, Cambridge, Massachusetts

(Received April 1, 1954)

A new 1.9±0.3-hour activity was found in niobium fractions isolated from proton irradiated niobium and zirconium metal foils. By identification of the 78-hour daughter activity, the mass assignment has been made to Nb^{89}. Evidence indicates that the decay is a simple positron emission of 2.9±0.4 Mev maximum energy. Evidence was also obtained for the existence of the $\frac{1}{2}-$ isomeric state in Nb^{89} which decays with a 0.8±0.3-hour half-life by positron emission to the similar 4.4-minute state in Zr^{89}.

OBSERVATION of the niobium fraction obtained from ~60-Mev proton bombardment of niobium metal in the internal beam of the Harvard synchrocyclotron indicated the presence of a new activity of approximately two-hour half-life. In order to identify and characterize this activity, niobium metal foils were irradiated for periods of 45–60 minutes with protons of maximum energy varying from ~50 Mev (roughly the threshold for the reaction) to ~75 Mev, and zirconium metal foils were bombarded for similar periods with protons of 40–45 Mev maximum energy.

After irradiation, the niobium target foils were dissolved in a mixture of nitric and hydrofluoric acids containing molybdenum, zirconium, and yttrium carriers. Zirconium was then separated from the solution as barium fluozirconate by the addition of barium ion, and this precipitation was repeated once or twice more. Upon dilution with water, yttrium fluoride also precipitated from the supernatant. After centrifugation, the niobium was precipitated with ammonia, washed, and dissolved in concentrated hydrochloric acid. This solution was made approximately $3M$ in HCl by first saturating with HCl gas and then diluting with the appropriate amount of water. Two extractions with tributyl phosphate removed the molybdenum, and the aqueous phase was again saturated with HCl gas. Niobium was then separated from residual zirconium and yttrium by extraction from the HCl solution with diisopropyl ketone. The zirconium target foils were treated in a somewhat similar manner except that they were dissolved in hydrofluoric acid alone, the barium fluozirconate precipitation was done at least three times, and there was no necessity for the molybdenum extraction with tributyl phosphate.

Samples of the niobium fractions so obtained were followed on an end-window (3.5 mg/cm²) Geiger counter, and resolution of the decay curves indicated a two-hour activity plus the known 14.7-hour Nb^{90} and longer activities. An aluminum absorption curve taken immediately after the chemical separation showed that the major particulate radiation seemed to consist of positrons of 2.9±0.4-Mev maximum energy. Counting samples of the niobium fraction through 620 or 571 mg/cm² of aluminum cut down the fraction of interfering activities (mainly Nb^{90}) and showed that these high energy positrons had a 1.9±0.3-hour decay. There was also a suggestion of a small amount of a shorter-lived activity. The decay of samples followed with a scintillation counter employing a well-type NaI(Tl) crystal gave a similar value for the half-life and indicated more strongly the possible presence of an additional gamma activity of just under one-hour half-life. An example of the decay curves obtained is shown in Fig. 1. Crude gamma integral pulse-height curves taken with the scintillation counter indicated a greater percentage of annihilation radiation associated

† This work was supported by the U. S. Atomic Energy Commission.

with the two-hour activity than with that of Nb^{90}, in fact, annihilation radiation seems to be the principal type of gamma associated with the former activity.

To determine the mass assignment of the new niobium activity and to confirm the value of the half-life, an effort was made to separate quantitatively the daughter activity at timed intervals, and then to follow the decay for identification. The parent-daughter separation was attempted at first by either precipitation of zirconium as the barium fluozirconate or extraction of the niobium into diisopropyl ketone. Neither of these methods is very satisfactory quantitatively, but both showed that there was an ~80-hour daughter activity and that the parent had a half-life between 1½ and 3½ hours. A much better separation technique makes use of the difference in behavior of hydrochloric acid solutions of niobium and zirconium on strong base anion resins; the former ions stick much more strongly than the latter.[1] Aliquots of the chemically purified niobium fractions were placed on Dowex-2 anion exchange resin columns and washed free of their zirconium and yttrium daughters with 7*M* HCl. At periodic intervals the daughters that have grown back into the parent fraction were separated by further elutions with small amounts of 7*M* HCl. Eight such sets of five to nine separations per set were done on samples from several bombardments, the time intervals used in a set varying from 30 minutes to two hours, and the yields of the daughter activities were followed in the scintillation counter. The result of a typical set of data is shown in Fig. 2 where the activity of the daughters is plotted against time. These curves are extrapolated back to the time of the parent-daughter separation, and the slope of a straight line drawn through these extrapolated points gives in the eight sets of data values for the half-life of the parent ranging between 1.8 and 2.4 hours. This is in good agreement with the value 1.9±0.3 hours obtained from observation of the direct decay of the niobium fraction.

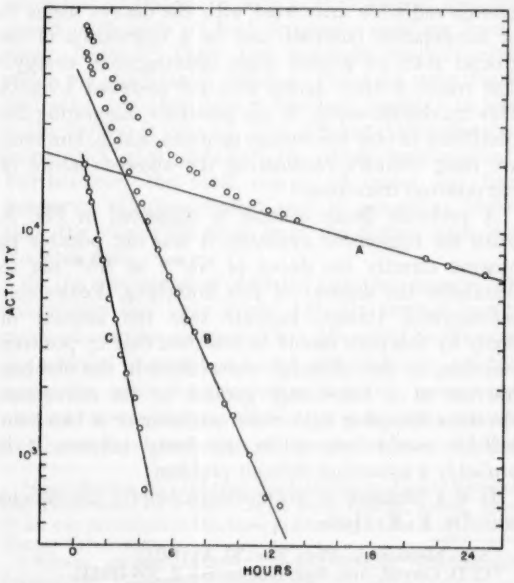

FIG. 1. Decay of niobium sample followed with a scintillation counter using a NaI(Tl) crystal. Curve *A*, resolution of 14.7-hour Nb^{90}. Curve *B*, resolution of 1.9-hour Nb^{89}. Curve *C*, resolution of 0.8-hour Nb^{89}.

[1] Huffman, Iddings, and Lilly, J. Am. Chem. Soc. **73**, 4474 (1951).

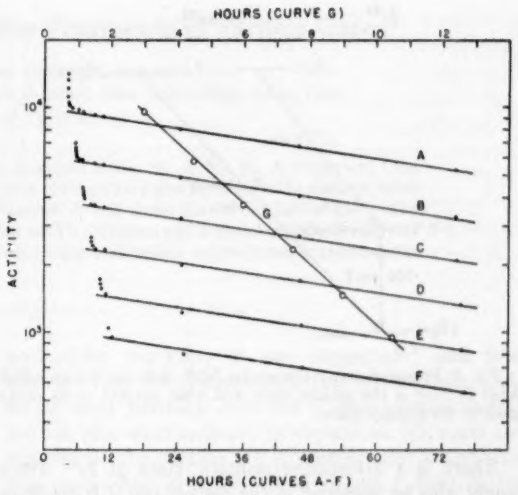

FIG. 2. Yield of Zr^{89} and Zr^{89m} daughters at successive 1½-hour separations from niobium parent, curves *A* to *F*. Curve *G* is a plot of the yields of Zr^{89} extrapolated to the times of separation, giving 2.2 hours for the half-life of Nb^{89}.

It was observed that after a small amount of short-lived activity died out, the daughter activities decayed with an ~80-hour half-life. This would have to be 78-hour Zr^{89}, or possibly 80-hour Y^{87} formed through the chain $Zr^{87} \xrightarrow{1.6\ hr} Y^{87m} \xrightarrow{14\ hr} Y^{87}$.[2] However, integral gamma pulse-height curves taken with the scintillation counter showed that the gamma radiation consisted of two groups of about one-half and somewhat less than one Mev energy which correspond to the annihilation radiation of Zr^{89} and the 913-kev gamma of the 14-second Y^{89m} in equilibrium with it and not to the 485- and 390-kev gammas of Y^{87} and Sr^{87m}.[2] This was confirmed by chemical separation of niobium, zirconium, and yttrium from samples of the daughter; the activity followed the zirconium fraction. Therefore, the parent nuclide must be Nb^{89}.[3]

[2] Hollander, Perlman, and Seaborg, Revs. Modern Phys. **25**, 469 (1953).

[3] E. K. Hyde (private communication). Kofstad, Mathur, and Hyde have identified Zr^{87} and Zr^{89} by scintillation spectrometry in the zirconium milkings of niobium fractions isolated from high energy proton and helium ion bombardments of silver, zirconium, and yttrium targets. Independently of the present investigation and, in fact, previously, Levine and Hyde have observed an ~2 hour positron emitter of 3.0–3.2 Mev maximum energy in the niobium fraction from zirconium irradiated with 40–60 Mev protons.

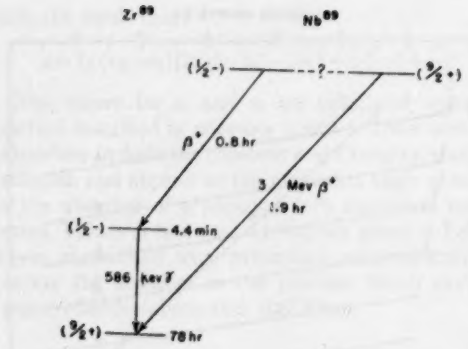

FIG. 3. Proposed decay scheme for Nb^{89}. It is not known which level in Nb^{89} is the excited state and what percent of its decay goes to the ground state.

There is a 4.4-minute isomeric state of Zr^{89} which might also be involved in the decay, and if it could be observed would certainly confirm the mass assignment to 89. As was mentioned above, a small amount of short-lived activity was indeed observed in the daughter activities, and by getting samples from the resin columns to the scintillation counter within 5–10 minutes of the start of the separation, the characteristic 4.4-minute decay of Zr^{89m} was easily resolvable from the 78-hour Zr^{89}.[4] Investigation of the quantitative relationships between these decays however showed some anomalies. Making reasonable assumptions for the relative counting efficiencies of the 586-kev gamma of Zr^{89m} and of the radiations of Zr^{89} and the Y^{89m} in equilibrium with it showed that the amount of Zr^{89m} was too small by a factor of the order of 25 to account for all of the Zr^{89}. What is of greater significance is that this factor varied with the time since bombardment, becoming larger the longer the period of time. Analyses of six sets of 5–9 milkings apiece showed that the 4.4-minute Zr^{89m} was coming from a parent decaying with a 0.8±0.3-hour half-life, and hence independently of the two-hour Nb^{89}.

From consideration of the single-particle shell model of the nucleus,[5] Nb^{89} would be expected to have either a 9/2+ or a $\frac{1}{2}-$ ground state with the other spin level as a low-lying isomeric state. As has been pointed out by Goldhaber and Hill,[6] the odd-mass niobium isotopes show a regular behavior in the pattern of these isomeric states. The spacing between the $\frac{1}{2}-$ excited state and 9/2+ ground state decreases with decreasing neutron number from 750 kev at Nb^{97} to a minimum of −105 kev (the $\frac{1}{2}-$ level actually lies the lower and is the ground state) at Nb^{91} which has a closed shell of 50 neutrons. Thereafter, the $\frac{1}{2}-$ level is expected to rise again so that at Nb^{89} the levels should be close and with either one possible as the ground state. The existence of this pair of isomeric states in Nb^{89} explains the observation of parents with differing half-lifes decaying into Zr^{89} and Zr^{89m}. Furthermore, since these last nuclides are also a 9/2+, $\frac{1}{2}-$ isomeric pair, one would not expect either of the niobium isomers to decay directly to both levels in zirconium, but only to the corresponding one, that is the 9/2+ state in niobium to the 9/2+ state in zirconium and the $\frac{1}{2}-$ state to the $\frac{1}{2}-$ state. The experimental results described above then indicate that the 9/2+ to 9/2+ transition to Zr^{89} has a 1.9-hour half-life and that the $\frac{1}{2}-$ to $\frac{1}{2}-$ decay to Zr^{89m} has a 0.8-hour period. The direct transition by positron emission from one of the isomeric states in niobium to the corresponding one in zirconium is an allowed transition with the transforming nucleon remaining in the same shell. Calculation of the log *ft* value for the 2.9-Mev positron of the predominant 1.9-hour transition gives 6.1,[7] which is at the upper limit for an allowed transition but agrees with the value 6.0 for the similar 9/2+ to 9/2+ transition of Zr^{89} to Y^{89m}. Support for the idea of such direct transitions is furnished by the observation that the major gamma radiation associated with the decays seems to be annihilation radiation and by a calculation of the ground state to ground state disintegration energy.[8] The result, 4 Mev, agrees with the observed 2.9±0.4 Mev maximum energy of the positrons, suggesting the possibility of only low-energy gammas, which, however, are most unlikely considering the allowed nature of the positron transition.

A probable decay scheme is suggested in Fig. 3. With the equipment available, it was not possible to observe directly the decay of Nb^{89m} to Nb^{89} nor to determine the amount of this branching. Reasonable assumptions, though, indicate that the amount of decay by this path should be less than that by positron emission, so that although observation in the niobium fraction of a low-energy gamma or its conversion electrons decaying with either an hour or a two-hour half-life would help settle the decay scheme, it is probably a somewhat difficult problem.

It is a pleasure to acknowledge helpful discussions with Dr. E. K. Hyde.

[4] E. K. Hyde (private communication). Mathur and Hyde have confirmed by scintillation spectrometry the presence of Zr^{89m} in the zirconium milkings of niobium fractions isolated from proton bombardment of niobium.

[5] M. G. Mayer, Phys. Rev. **78**, 16 (1950).

[6] M. Goldhaber and P. D. Hill, Revs. Modern Phys. **24**, 179 (1952).

[7] S. A. Moszkowski, Phys. Rev. **82**, 35 (1951).

[8] C. D. Coryell, Ann. Rev. Nuclear Sci. **2**, 305 (1953).

Relative Ionization Yields for Fission Fragments in Various Gases*

LLOYD O. HERWIG† AND GLENN H. MILLER
Department of Physics and Institute for Atomic Research, Iowa State College, Ames, Iowa
(Received April 15, 1954)

The ionizations resulting from U^{235} fission have been measured in He, Ne, A, Kr, N_2, A+3 percent CO_2, and A+5 percent N_2. Comparison of these values with those obtained for alpha particles in the same chamber fillings permit the calculation of ionization defect differences. It was found that about half of the 7-Mev defect previously ascribed to argon-CO_2 mixtures was due to CO_2. Nitrogen and krypton exhibited relatively large defects. No significant difference was observed between argon and helium. Several possible explanations for this are suggested and discussed.

I. INTRODUCTION

IN the experiment herein reported, the ionizations produced by U^{235} fission products in various gases and gas mixtures have been measured in a gridded ionization chamber. In each case, the ionizations from alpha particles were also measured. The data which are presented are the fission-alpha ionization ratios, which may be used as a means of comparing the fission fragment ionization efficiencies in the various gases. It might be expected that these ratios would depend on the stopping gas for reasons which follow.

It has been possible to obtain the mass distribution of fission products by several independent methods. Radiochemical analysis of these products has yielded such a distribution.[1] On the other hand, this distribution has been deduced from data taken with a double ionization chamber, in which simultaneous measurements were made on both fragments resulting from a single fission.[2,3] These two methods yielded curves which are significantly different. From the same double ionization chamber data it has been possible to infer a distribution in velocity. This is in significant disagreement with that obtained by direct measurement.[4] Furthermore, the total energy of fission has been measured calorimetrically[5] and is somewhat higher than the values obtained from the double ionization chamber data.

In the measurement of fission fragment energies the assumption had been made that the average energy required to make an ion pair in a gas would be the same for a fission fragment as for an alpha particle. On this basis, the value for the fission fragment energy was obtained by multiplying the energy of an alpha particle by the ratio of the ionizations produced by the fission and alpha particles. It was suggested[3,6] and later shown[4,7] that the discrepancies just pointed out could be at least partially removed if the average energy per ion pair were assumed to depend on the mass and velocity of the particle. In particular, the assumption was made that in argon about 6 and 7 Mev of the average light and heavy fragment energies respectively did not show up as ionization due to the changing ionization efficiency. A theoretical treatment was successful in predicting the order of magnitude of the undetected energies.[8] The basis of this prediction was the atomic collision, in which the ionizing particle interacts with the entire stopping atom, rather than with a single atomic electron. The fraction of the energy of the incident particle which can be transferred in such a collision depends on the ratio of the masses of the two particles. If the ratio is near unity, the incident particle can lose most of its energy in such a process. In the case of fission products, heavy gases such as argon and krypton are expected to be favorable for larger energy transfer, while light gases such as helium and hydrogen are not favorable. For an incident particle of high velocity in any gas, the probability of an atomic collision is small compared to that for electronic interaction, and atomic collisions are only expected to become important when the penetrating particle has a velocity of the order of v_0 or less.

$$(v_0=e^2/h\cong 2\times 10^8 \text{ cm-sec}^{-1}).$$

The recoil atoms will also have velocities of this order or less, and so are expected to have only a low ionization efficiency.

It is convenient to discuss the change in the energy per ion pair in terms of an ionization defect.[8] The ionization defect is added to the energy calculated from the ionization to give the true energy. Thus

$$E_f=w_\alpha I_f+\Delta E_f. \quad (1)$$

E_f is the initial fission fragment energy, I_f is the ionization resulting when it is stopped completely in the gas, w_α is the energy per ion pair for the alpha particles,

* Contribution No. 318 from the Institute for Atomic Research and Department of Physics, Iowa State College, Ames, Iowa. Work was performed in the Ames Laboratory of the U. S. Atomic Energy Commission.

† Present address: Atomic Power Division, Westinghouse Laboratories, Pittsburgh, Pennsylvania.

[1] Plutonium Project, Revs. Modern Phys. **18**, 513 (1946).

[2] M. Deutsch and M. Ramsey, Atomic Energy Commission Report No. MDDC-945, 1946 (unpublished).

[3] D. C. Brunton and G. C. Hanna, Can. J. Research **A28**, 190 (1950).

[4] R. B. Leachman, Phys. Rev. **87**, 444 (1952).

[5] M. C. Henderson, Phys. Rev. **58**, 774 (1940).

[6] R. B. Leachman, Phys. Rev. **79**, 197 (1950).

[7] R. B. Leachman, Phys. Rev. **83**, 17 (1951).

[8] J. K. Knipp and R. C. Ling, Phys. Rev. **82**, 30 (1951).

and ΔE_f is the ionization defect. It has already been pointed out that ionization defects of about 6 and 7 Mev were expected for the most probable light and heavy fission fragments in argon.

The differences in the ionization defects resulting from measurements using two different gases may be found even though the defect for either gas alone may not be measured readily. Initially, it was thought that the defect for helium should be negligible compared to that in argon, and so the difference for these two gases should be a good measure of the argon defect.

II. THE METHOD

It is necessary to have some measure of w_a in each gas used. Therefore, in each case the ionizations resulting from the alpha particles from natural uranium were measured. The energies of these are 4.18 and 4.76 Mev for U^{238} and U^{234}, respectively.[9] For each of two gases, 1 and 2, Eq. (1) may be written and E_f eliminated. This gives:

$$(\Delta E_f)_1-(\Delta E_f)_2=(w_aI_f)_2-(w_aI_f)_1. \qquad (2)$$

Since $w_a=E_a/I_a$, the quantities on the right are either known or can be measured. The method then consists of measuring the ratio of the most probable ionizations for fission and alpha particles in various gases. Since only the ratios are important, it is not necessary to make an absolute measurement, and the pulse heights corresponding to the maxima in the distributions may be inserted in the expression.

III. EQUIPMENT

A. The Ionization Chamber

The chamber has been described in detail elsewhere,[10] but a brief description is appropriate here. It used electron collection and employed a Frisch grid.[11] The shielding inefficiency was 6 percent and the theoretical minimum ratio of the grid-collector field to the grid-source field for complete electron collection was 1.32. The gas was purified continuously by circulation through Ca-Mg alloy chips maintained at about 470°C. This type of purifier is thought to be quite effective in the removal of molecular impurities.[12] Previous to filling, the chamber was outgassed by pumping for a period of 20 hours or more at a temperature of about 100°C, with the purifier about 40°C above its normal operating temperature. The pressure in the chamber at the end of the pumping period was always of the order of 10^{-5} mm Hg, and was limited by the vacuum attainable in the pumping system. The filling process always included the use of a cold trap.

The grid-source and grid-collector spacings were 8 and 1.25 cm, respectively. The electrode diameters were about 25 cm. The large dimensions were necessary in order to stop the alpha particles in the grid-source region for reasonable pressures in helium. The natural uranium source was in the form of UO_2, and contained about 60 μg-cm^{-2} of active material. It was prepared by a special spraying process[13] and no significant nonuniformity could be detected by either radioautograph or macroscopic alpha scanning. The source diameter was 12 cm. A collimator was placed in contact with the source which restricted the maximum angle made by an emerging particle with the normal to about 77 deg. This source has since been replaced by an uncollimated source made by the same technique and having a thickness of about 18 μg-cm^{-2}.

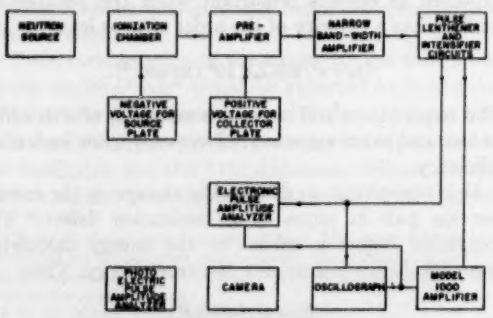

FIG. 1. Block diagram of apparatus.

B. The Electronic Equipment

The block diagram of the measuring equipment is shown in Fig. 1. The conditions of the problem placed several rather unusual restrictions on the electronic circuits. The large length of the grid wires resulted in vibrations which produced sizable microphonics signals. These had, for the most part, frequencies below 750 cps. The large electrode spacings, along with the low electron drift velocities in the purified inert gases resulted in pulse rise times as great as 15 μsec, with about 6-μsec variation due to the angular distribution of particles from the source. It was then necessary to compromise in the amplifier between the long clipping time needed to minimize rise-time effects and the short clipping time necessary to remove microphonics resulting from the grid wires. The amplifier used had equal rise and clipping times of 30 μsec, with several rejection filters tuned to frequencies below the lower half-power point. It has been shown that for such an amplifier the output pulse height has only a small

[9] British Atomic Energy Project Reports, BR-521 and BR-522, 1944 (unpublished).

[10] Herwig, Miller, and Utterback, Rev. Sci. Instr. (to be published).

[11] D. H. Wilkinson, *Ionization Chambers and Counters* (Cambridge University Press, Cambridge, 1950), first edition, pp. 74–77.

[12] L. Colli and U. Facchini, Rev. Sci. Instr. 23, 39 (1952).

[13] Herwig, Miller, and Utterback, Atomic Energy Commission Report No. ISC-472 (unpublished).

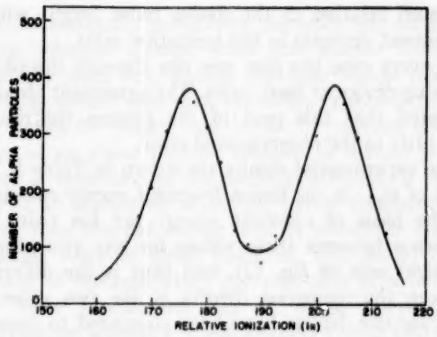

FIG. 2. Typical alpha-particle pulse-height distribution.

dependence on the pulse rise-time.[14] The pulse from this amplifier was shaped to have a flat top about 135 μsec in duration. After further amplification the signal was applied to the vertical deflection plates of a cathode ray tube. The beam in this tube was intensified for a few microseconds during the flat-topped portion, and the corresponding dot was photographed on a continuously moving film with a Dumont-Fairchild 314-A camera. The pulse-height distribution was obtained by analyzing the film in a photoscanning device.[15] In order to avoid the delay involved in this system of analysis, a 20-channel electronic analyzer was also employed.[16] This made possible the rapid examination of alpha saturation curves. The data reported in the present experiment were obtained by the photographic method.

Both alpha and fission pulse heights were obtained in terms of the pulse voltages from a standard pulse generator. These pulses were obtained by charging a condenser from an electronically regulated power supply and discharging it through a network by means of a WE 275B relay. These pulses were applied to the source electrode, and appeared on the collector due to the interelectrode capacitance. The resulting pulses were recorded on the film in the same manner as the ionization pulses.

C. The Neutron Source

The fast neutrons needed for U^{238} fission were obtained from the Ames Laboratory kevatron using the *d-d* reaction. The neutron yield was estimated to be of the order of 10^8 neutrons per second. With the chamber as close to the target as possible, a fission rate of about one per second was obtained.

IV. EXPERIMENTAL RESULTS

A typical distribution of the alpha-particle pulse heights is shown in Fig. 2. The relatively poor resolution of the peaks was due largely to the higher frequency microphonics from the grid wires in the chamber. In spite of this it was possible to locate the peaks in a systematic manner, so that the values agreed within about 0.5 percent for different runs. The selection of the peaks was accomplished using the method of diameters.[17] About 8000 events were recorded for each distribution, requiring a time of about 10 minutes.

In Fig. 3 is shown a typical fission distribution. It is believed that the relatively large width of the distribution was due to source thickness. Chamber microphonics could have no effect in this case, due to the fact that the pulses were about a factor of 20 larger than those resulting from alpha particles. The maxima of these distributions were also located by the method of diameters. In addition, a median calculation was used as a check. In this method the extrapolated value of the upper edge of the light peak was used as a reference in each case. Pulses having heights greater than 74 percent of the extrapolated pulse height were counted in the upper peak. With this quite arbitrary division, the median pulse height of each group in argon agreed with the maximum obtained by the method of diameters. It was then found, using the same criterion for the division of the pulses, that the results of the two methods were in good agreement for the other gases. For the light peak the maximum difference between values found by the two methods was about one percent, while for the heavy peak it was as high as two percent. It is to be expected that the uncertainty in locating the broader heavy peak would be greater.

Saturation curves for fission fragments in several gases are shown in Fig. 4. Alpha-particle saturation curves are not shown, but are quite similar. They are shown and discussed in an earlier reference.[10] The pressures were chosen so that the alpha-particle range was nearly the same in all of the gases. It has been pointed out[18] elsewhere that the values obtained for the

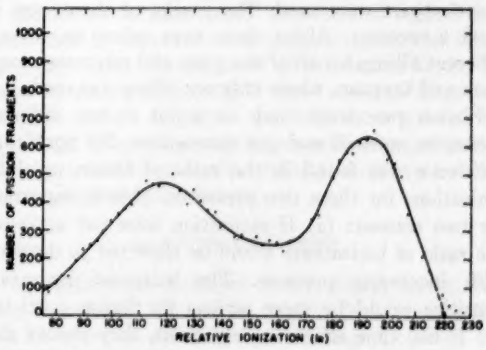

FIG. 3. Typical fission fragment pulse height distribution.

[14] Reference 11, p. 103.
[15] Hunt, Rhinehart, Weber, and Zaffarano, Rev. Sci. Instr. (to be published).
[16] W. E. Glenn, Nucleonics 9, No. 6, 24 (1951).
[17] T. E. Cranshaw and J. A. Harvey, Can. J. Research A26, 250 (1948).
[18] L. O. Herwig and G. H. Miller, Phys. Rev. 94, 1183 (1954).

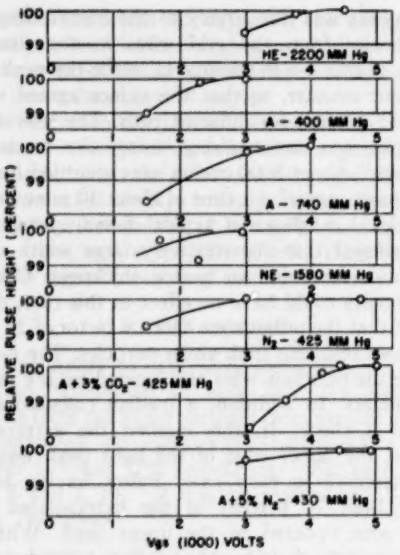
HE - 2200 MM Hg
A - 400 MM Hg
A - 740 MM Hg
NE - 1580 MM Hg
N₂ - 425 MM Hg
A + 3% CO₂ - 425 MM Hg
A + 5% N₂ - 430 MM Hg
RELATIVE PULSE HEIGHT (PERCENT)
Vgs (1000) VOLTS

FIG. 4. Saturation curves for fission fragments in various gases.

energy per ion pair for alpha particles are quite satisfactory, an indication of saturation and also of good gas purity.

For each gas filling used, at least two fission runs were made. Usually a run consisted of about 20 000 fissions and required about seven hours. The amplifier gain was checked periodically during this time. There was always a period of at least 24 hours between two fission runs using the same chamber filling. The alpha saturation curve and distribution were checked at intervals for each filling. In the case of the inert gases, the chamber filling was allowed to purify for at least 48 hours before any data were taken. In no case was any significant change in the behavior of a filling noted. For argon, several fillings spaced about a month apart were used. The results of these were in good agreement. Alpha data were taken on several different fillings for all of the gases and mixtures except neon and krypton, where only one filling was used.

Fission runs were made in argon at two different pressures, one-half and one atmosphere. No significant difference was found in the ratio of fission to alpha ionizations for these two pressures. This is important for two reasons: (a) If saturation were not attained, the ratio of ionizations would be expected to decrease with increasing pressure. The increased ionization densities would be more serious for fission particles. (b) If rise time effects were present, they should also decrease the ionization ratio at higher pressure. This would occur because the worst case would be that of an alpha particle at one-half atmosphere. At one atmosphere, the alpha-particle pulse height would be increased relative to the fission pulse height with a consequent decrease in the ionization ratio.

In every case the film was run through the photoscanning device at least twice. The agreement obtained indicated that this part of the process contributed very little to the observational error.

The experimental results are shown in Table I. The value of $w_\alpha I_f$ is the fission fragment energy calculated on the basis of constant energy per ion pair. The difference between these values for any two gases is the right side of Eq. (2), and thus is the difference between the ionization defects in the two gases. In this case the defects have been compared to those in argon+CO_2, since this mixture was used in the results previously cited.[3,4] The fission ionization energies have not been corrected for source absorption which may be as high as four Mev. Source absorption results in a systematic error which is independent of the chamber filling and does not enter into the differences of ionization defects. The main contribution to the error is the uncertainty in the location of the peaks.

V. DISCUSSION

A. Significance of the Results

It had been expected that the fission ionization defects in helium would be as much as five Mev less than those in argon. It may be seen from Table I that no such differences were observed in the present experiment. This will be discussed later.

It is interesting to note that in nitrogen rather large defects resulted. This was not anticipated but is perhaps not surprising. The molecular energy levels offer a rather good mechanism for energy loss by atomic interaction. This may be particularly important for a low velocity particle, where the ionization probability is very much reduced.

This leads to the most important point, which is the rather large difference resulting from the addition of three percent CO_2 to argon. This is particularly significant since the ion chamber measurements mentioned in the introduction, which form the basis for the ionization defect calculations, were made with argon-CO_2 mixtures. It is rather difficult to understand how a small amount of CO_2 can produce such a large effect. Other peculiar effects have been noted in argon-CO_2 mixtures and may have some bearing on this result.[10] It is interesting to note that the addition of five percent of N_2 to argon does not produce a very marked effect.

In view of the argon-CO_2 mixture behavior, the expected difference between argon and helium would be reduced to about three Mev. There seem to be several possible reasons for not observing such a large effect. 1. The effective charge of fission fragments is believed to be lower in helium than in other gases.[19,20]

[19] N. O. Lassen, Kgl. Danske Videnskab. Selskab, Mat.-fys. Medd. 26, No. 5 (1951).
[20] G. I. Bell, Phys. Rev. 90, 548 (1953).

Since the ionization probability depends very strongly on the effective charge while the atomic collision probability does not, atomic collisions would play a somewhat greater role than otherwise expected. It has been shown by Jesse[21] that about 25 percent of the energy of an alpha particle stopped in helium is expended in excitation of the metastable states. If there really is an ionization defect for fission fragments in helium, then this percentage may be somewhat higher for fission than for alpha particles. This would offer a means of demonstrating the existence of a defect, since these metastables can be made to produce ionization by adding a small amount (~0.1 percent) of an impurity, such as argon. If the above hypothesis is correct, then the addition of an impurity should result in an increase in the ratio of fission to alpha ionizations.

2. In the comparison of the results herein contained with the results which would be expected on the basis of the atomic collision mechanism, the effect of such collisions on the stopping of alpha particles has been neglected. If these collisions are important, then it is necessary to see what effect they could have. The energy of an alpha particle may be related to its ionization in the following way.

$$E_\alpha = w^e I_\alpha + \Delta' E_\alpha. \tag{3}$$

Here w^e is the high-velocity asymptotic energy per ion pair, which is believed to be independent of the charge, mass, and energy of the ionizing particle (subject only to the condition that the velocity is high; $v \gg v_0$). The quantity w^e does depend, however, on the stopping gas. It is then necessary to replace w_α in (2) by w^e, and ΔE_f by $\Delta' E_f$. The last term, $\Delta' E_f$, is the true ionization defect, since it is based on the ideal value, w^e. By the use of Eq. (3), w^e may be eliminated, and the following result is then obtained:

$$(\Delta' E_f - \frac{I_f}{I_\alpha}\Delta' E_\alpha)_1 - (\Delta' E_f - \frac{I_f}{I_\alpha}\Delta' E_\alpha)_2 = (w_\alpha I_f)_2 - (w_\alpha I_f)_1. \tag{4}$$

TABLE I. Fission ionization energies and relative ionization defects.

	$(w_\alpha I_f)_s$ Mev		$(w_\alpha I_f)_s - (w_\alpha I_f)_{A+3\%\ CO_2}$ Mev	
gas	light	heavy	light	heavy
Helium	92.9±0.5	61.8±0.7	3.4±0.7	5.4±1.0
Neon	92.0±0.5	60.0±0.7	2.5±0.7	3.6±1.0
Argon	92.5±0.5	60.9±0.7	3.0±0.7	4.5±1.0
Krypton	89.6±0.7	56.0±1.0	0.1±0.9	−0.4±1.2
N_2	88.9±0.5	58.0±0.7	−0.6±0.7	1.6±1.0
A+3% CO_2	89.5±0.5	56.4±0.7	0	0
A+5% N_2	91.5±0.5	59.9±0.7	2.0±0.7	3.5±1.0

[21] Wm. P. Jesse, Atomic Energy Commission Report No. ANL-4944, 1952 (unpublished), p. 2.

Thus, the difference in ionization defects given by Eq. (2), which comes directly from experimentally determined quantities, is in reality different from the true value by the alpha-particle defect terms.

It is possible, but improbable, that the alpha-particle terms could account for failure to find a difference between argon and helium. It would be necessary for the alpha defect in argon to be about 0.15 Mev greater than the corresponding defect in helium. In the following section, arguments are given against the existence of defects of such a magnitude.

The results for neon indicate that it is very little different from argon or helium. Since no great difference is noted for these two gases, it would be rather suprising if neon exhibited a marked defect. On the other hand, krypton showed a rather large effect. This would be expected on the basis of the atomic collision theory, since krypton is very close to the peak of the light fragment distribution.

Unfortunately, very few data are available for the energy dependence of energy per ion for alpha particles. Measurements have been made in argon by Jesse *et al.*[22] and by Cranshaw and Harvey.[17] These results are not in good agreement. In the first case heavy ion collection was used and no significant ionization defect was found. ($\Delta' E_\alpha$ probably less than 25 kev.) In the second experiment, electron collection was employed and a defect of about 85 kev was observed.

Several measurements have been made on particles coming from the $B^{10}(n,\alpha)Li^7$ reaction in argon-CO_2 mixtures.[23–25] The first two of these indicate an ionization defect for the mixture of the order of 50 kev. The result of the third experiment is in agreement with the first two. However, it was shown in addition that as the pressure was reduced, the ratio of the ionizations of the alpha particle and the lithium recoil approached the ratio of the energies of these two particles. This is an indication, but not proof, that there is negligible alpha-particle defect in argon. If there were such a defect, a relatively greater one would be expected for the slower lithium recoil. The ratio of ionizations would then be expected to be in poor agreement with the energy ratio. On the basis of the fission results it would be rather surprising if there were as large an ionization defect for alpha particles in argon as in argon-CO_2. This laboratory is presently engaged in an investigation of the ionization defects for alpha particles in various gases and mixtures.

ACKNOWLEDGMENT

The authors are indebted to Dr. Julian Knipp for many stimulating discussions, and to Mr. Nyle Utterback for technical assistance in obtaining the data.

[22] W. P. Jesse, H. Forstat, and J. Sadauskis, Phys. Rev. **77**, 782 (1950).
[23] G. C. Hanna, Phys. Rev. **80**, 530 (1950).
[24] Franzen, Rhodes, and Stephens, Phys. Rev. **87**, 141 (1952).
[25] J. DeJuren and H. Rosenwasser, Phys. Rev. **92**, 544 (1953).

Independent Particle Model and the Nuclear Photoeffect*

J. S. LEVINGER AND D. C. KENT
Louisiana State University, Baton Rouge, Louisiana
(Received April 7, 1954)

The very low value calculated by Levinger and Bethe for the harmonic mean energy for the nuclear photoeffect is increased by a factor of 3 for Cu and 4 for Ta if correlations between nucleons due to the Pauli principle are included in the calculation using an independent particle model (IPM). Our calculation removes the discrepancy between the sum-rule result and Burkhardt's calculation using the IPM for Cu. If we use a smaller nuclear radius, and include the increase of mean energy due to exchange forces, we find reasonable agreement between experimental results for Cu and Ta and the harmonic mean energies calculated for an IPM in a finite square well: i.e., 18 Mev for Cu and 12 Mev for Ta.

I. INTRODUCTION

IN a previous paper[1] (here referred to as LB) one of the present authors and H. A. Bethe calculated the effects of exchange forces on the integrated cross section and on the mean energies for electric dipole transitions in the nuclear photoeffect. LB used an approximate independent particle model (IPM) in which the nucleons were treated as a degenerate Fermi gas, with no correlations among the different nucleons. The calculated integrated cross section was in reasonable agreement with experiment.[2,3] The mean energy $\bar{W}$ was not in clear disagreement with experiment; but the calculated harmonic mean energy W_H was extremely low. LB therefore argued that there must be strong correlations among the nucleons: e.g., as in an alpha-particle model.

In the past several years the shell model, or IPM, has had striking successes in many fields of nuclear physics, including some calculations concerning the nuclear photoeffect.[4] We therefore wish to re-examine the argument against the IPM advanced by LB. A more pressing reason for this reexamination is Burkhardt's IPM calculation[5] of electric dipole transitions for the neutrons in the Cu^{63} nucleus. He finds that the cross section for photon absorption has a sharp peak at about 9 Mev. This result is in marked contrast with the LB values (for ordinary forces) of 2.9 Mev for W_H and 16 Mev for $\bar{W}$, corresponding to a very broad curve of cross section *vs* photon energy. In particular Burkhardt does not find the absorption of low-energy photons corresponding to the low value of W_H given by LB. While there is some difference between the details of IPM used by Burkhardt and LB, this difference seems much too minor to explain these major discrepancies between Burkhardt's direct calculation of the absorption cross section, and LB's sum-rule calculation of mean energies for photon absorption.

We discuss below the nucleon correlations present even in the IPM due to the Pauli principle. These correlations have a large effect on sum-rule calculations of the mean energies. Including these correlations we find good agreement between Burkhardt's results and our revised sum-rule calculation. (The two calculations must agree, provided that the same nuclear model is used.[1,4])

In the next section we set up the calculation of mean energies including nucleon correlations based on the Pauli principle. In Sec. III we find the mean energies using the LB model of a degenerate Fermi gas. In the following section we find the mean energies for an IPM in a square well for Cu and Ta and compare with Burkhardt's results, and with experiment. We also present IPM calculations of the nucleon density as a function of radius.

II. PAULI PRINCIPLE CORRELATIONS

Using the notation of LB we define two mean energies: the harmonic mean energy,

$$W_H=\sum_n f_{on}/[\sum_n f_{on}/(E_n-E_o)]$$
$$=\sigma_{\rm int}\Big/\Big[\int(\sigma/W)dW\Big], \quad (1)$$

and the mean energy,

$$\bar{W}=\sum_n f_{on}(E_n-E_o)/\sum_n f_{on}=\int\sigma W dW/\sigma_{\rm int}. \quad (2)$$

Here o refers to the ground and n to the various excited states; E_n-E_o equals the photon energy W for a transition from o to n, and $\sigma_{\rm int}=\int\sigma dW$.

The summed oscillator strength $\sum_n f_{on}$ is independent of correlation among the nucleons. It has the value NZ/A for ordinary forces, and is increased by about $0.8x$, where x is the fraction of attractive exchange (Majorana) force. For the present let us restrict the discussion to ordinary forces, as was done by Burkhardt in his calculation for Cu. The denominator in Eq. (1) and the numerator in Eq. (2) are both dependent on correlations among the nucleons.

The denominator of Eq. (1) is given in LB as

$$\sum_n f_{on}/(E_n-E_o)=(2M/\hbar^2)$$
$$\times\sum_n\{[(N/A)\sum_i\mathfrak{x}_i-(Z/A)\sum_j\mathfrak{x}_j]_{on}\}^2. \quad (3)$$

* A preliminary account is given in Phys. Rev. **93**, 932 (1954).
[1] J. S. Levinger and H. A. Bethe, Phys. Rev. **78**, 115 (1950).
[2] L. W. Jones and K. M. Terwilliger, Phys. Rev. **91**, 699 (1953).
[3] R. Nathans and J. Halpern, Phys. Rev. **93**, 437 (1954).
[4] J. S. Levinger, Ann. Rev. Nuclear Sci. (to be published).
[5] J. L. Burkhardt, Phys. Rev. **91**, 420 (1953).

Here i stands for protons and j stands for neutrons; the matrix element is calculated for the complete nuclear wave function. Consider, for example, the term for pairs of protons. Omitting the constant factors, and using closure to express the sum over n in terms of the ground-state wave function alone we have

$$\sum_n (\sum_i z_i)_{on}(\sum_i z_i)_{no} = (\sum_i z_i^2)_{oo} + (\sum_{i\neq i'}\sum z_i z_{i'})_{oo} = D + B. \quad (4)$$

In the last term on the right i is unequal to i'. If there is no correlation in the ground state between pairs of protons, these off-diagonal terms give zero. The diagonal terms were calculated by LB using the model of uniform proton density in a sphere of radius R.

$$D = (\sum_i z_i^2)_{oo} = (1/5)ZR^2. \quad (5)$$

This expression, together with a similar expression for the terms in Eq. (3) involving neutrons was used in LB to give the value for the harmonic mean energy as

$$W_H = 5\hbar^2/2MR^2 = 46A^{-\frac{1}{3}}\ \text{Mev}. \quad (6)$$

The numerical result is given for $r_o = 1.5$, and is proportional to r_o^{-2}. (The nuclear radius $R = r_o A^{\frac{1}{3}} \times 10^{-13}$ cm.) As stated above, the value of 2.9 Mev for the harmonic mean energy for photon absorption by Cu is in serious disagreement with Burkhardt's calculated value of 8.4 Mev, and in even worse agreement with experiment.

However, even in the IPM there is correlation among the nucleons, since two nucleons of the same charge must have antisymmetric total (spatial and spin) wave functions. In three-fourths of the cases the spin wave functions are symmetric, and therefore the spatial wave functions are antisymmetric. The negative contribution to the last term on the right of Eq. (4) from these triplet states is larger than the positive contribution from the singlet states. Then the denominator of Eq. (1) is decreased, and the harmonic energy is increased.

Consider a pair of protons in states k and l, respectively. If the spatial wave function normalized to 2 particles is antisymmetric, we have in Eq. (4):

$$(z_i z_{i'})_{oo} = \int [\psi_k(r_i)\psi_l(r_{i'}) - \psi_k(r_{i'})\psi_l(r_i)]^2 z_i z_{i'} d^3r_i d^3r_{i'}. \quad (7)$$

Terms such as

$$\int [\psi_k(r_i)]^2 [\psi_l(r_{i'})]^2 z_i z_{i'} d^3r_i d^3r_{i'}$$

vanish because of the definite parity of the single particle wave functions. The exchange terms do not vanish. For an antisymmetric spatial wave function, Eq. (7) gives

$$(z_i z_{i'})_{oo} = -2\int \psi_k(r_i) z_i \psi_l(r_i) d^3r_i \int \psi_l(r_{i'}) \times z_{i'} \psi_k(r_{i'}) d^3r_{i'} = -2(z_{kl})^2. \quad (8)$$

For a spatially symmetric wave function occurring in $\frac{1}{4}$ of the cases we find the same result but with the sign changed. The complete result for the off-diagonal terms is then

$$B = (\sum_i \sum_{i'} z_i z_{i'})_{oo} = -\sum_k \sum_l (z_{kl})^2. \quad (9)$$

The correction term B then involves the squared electric dipole matrix element with single particle wave functions for transitions between occupied states. [Eq. (9) could also be derived by using a product of single-particle wave functions for the ground state, and taking account of the Pauli principle by subtracting transitions from one occupied level to another, which should not be counted in the $\sum_n$ of Eq. (3).]

In the approximation that $N = Z$, used in this paper, the correction factor C to the harmonic mean energy is

$$C = (1 + B/D)^{-1}. \quad (10)$$

Here B, the negative contribution of the off-diagonal terms for pairs of protons, is given by Eq. (9), while the contribution D of the diagonal terms is given in Eq. (5).

The contribution of off-diagonal terms to the numerator of Eq. (2) for the mean energy can be calculated in an analogous manner, using matrix elements for p, the momentum component along the polarization direction of the photon. We find a correction factor C' less than unity given by

$$C' = 1 + B'/D', \quad (11)$$

$$B' = -\sum_k \sum_l (p_{kl})^2, \quad (12)$$

$$D' = (\sum_i p_i^2)_{oo}. \quad (13)$$

LB assumed no correlations, and therefore calculated just the term D', giving a mean energy for the degenerate Fermi gas model of 4/5 the Fermi energy, or 16 Mev for $r_o = 1.5$.

III. FERMI GAS MODEL

Calculations of the correction factors C and C' to the LB values for W_H and $\bar{W}$, respectively, must be based on some specific model for the nucleon wave functions. In this section we use the model of a degenerate Fermi gas of constant density in a sphere of radius R. This model is different from Burkhardt's, so our result will not be in perfect agreement with his. This model is not self-consistent, as the nucleon density cannot be constant inside the nucleus, suddenly changing to zero at the nuclear surface. It turns out that surface terms are of importance in these

TABLE I. Correction factor for harmonic mean energy, using Fermi gas model.[a]

Mass number A	Function $g(y)$	Correction factor C_F
35	0.246	1.64
69	0.295	1.88
119	0.329	2.10
174	0.356	2.30
283	0.384	2.57

[a] The function $g(y)$ and the correction factor C_F are given in Eq. (15) of the text.

calculations, particularly for the correction factor C'; so that the Fermi gas model is not reliable for quantitative results. Still, it gives semiquantitative results applicable to all nuclei.

The matrix element z_{kl} depends on q, the magnitude of the difference of the propagation vectors for nucleons in states k and l:

$$z_{kl}=(3i\cos\theta'/q)j_2(qR). \tag{14}$$

Here θ' is the angle between the vector q and the direction of polarization of the photon, while j_2 is a spherical Bessel function. We see that the matrix element has a maximum value of order of magnitude R, corresponding to pairs of states k and l where q is small, of magnitude $1/R$. This matrix element is squared, and summed over all pairs of states k and l by integrating over the distribution function[6] for q, giving

$$B=-(ZR^2/\pi)g(y),$$

$$y=(9\pi A)^{\frac{1}{3}},$$

$$g(y)=\int_0^y[j_2(x)]^2(1-x/y)^2(2+x/y)dx, \tag{15}$$

$$C_F=(1+B/D)^{-1}=[1-(5/\pi)g(y)]^{-1}.$$

In this approximate model the correction factor is independent of the parameter r_o for the nuclear radius, since both B and D are proportional to r_o^2. The correction factor C_F for the harmonic mean energy W_H is given for various values of A in Table I. We see that C_F is about two for moderate and heavy nuclei, and increases with A. Then $W_H=C_F(W_H)_{LB}$ decreases with A less rapidly than $A^{-\frac{1}{3}}$.

We have also calculated the correction factor C' for the mean energy $\bar{W}$, but this result is unreliable, since it becomes negative for large A. The surface effects, poorly treated by our Fermi gas model, are of more importance for the calculation of C' than of C, and even lead to appreciable errors in the calculation of C, as we find below by comparison with our calculation of C using a square well IPM.

TABLE II. Proton binding energies in Mev for IPM in square well.[a]

Shell	Cu($N=Z=34$)		Ta($N=Z=92$)	
	$r_o=1.5$	$r_o=1.2$	$r_o=1.5$	$r_o=1.2$
$1h^{22}$	...	...	8.0	8.0
$3s^2$	...	...	8.03	8.21
$2d^{10}$	...	...	9.29	10.06
$1g^{18}$	...	...	12.72	15.21
$2p^6$	...	...	14.48	17.97
$1f^{14}$	10.0	10.0	16.92	21.71
$2s^2$	14.15	16.35	19.13	25.08
$1d^{10}$	16.7	20.2	20.55	27.28
$1p^6$	22.4	28.9	23.61	31.99
$1s^2$	27.0	35.9	26.04	35.74
Well depth V_o	31.4	42.6	28.38	39.35

[a] The binding energy of 10 Mev for $1f$ protons in Cu, and 8 Mev for $1h$ protons in Ta is estimated from experiments. This determines the well depth V_o, and the binding energies of the other protons. The Coulomb potential is neglected. The radius parameter $r_o=RA^{-\frac{1}{3}}\times10^{13}$, where R is the radius of the square well.

[6] A. Winslow, Ph.D. thesis, Cornell University, 1952 (unpublished).

IV. IPM FOR SQUARE WELL POTENTIAL

Calculations of the corrections to the mean energies due to Pauli principle correlation have also been made using IPM wave functions in a square well potential. Calculations were made for two nuclei, called here by the approximate names of Cu($N=Z=34$) and Ta($N=Z=92$). These nuclei have closed sub-shells in the square-well IPM (no spin-orbit coupling) which simplifies the sums over k and l. We have calculated for two different values of the parameter r_o for the radius of the square well: $r_o=1.5$, and $r_o=1.2$. The former value was used by Burkhardt in calculations on Cu. The latter value of r_o is near that of recent Stanford[7] and Columbia[8] measurements. We find below that the correction factors C and C' are insensitive to the value chosen for r_o, though there is some dependence on r_o in contrast to the Fermi gas model treated above. Since the LB values for W_H and $\bar{W}$ are each proportional to r_o^{-2}, the mean energies calculated here keep a strong dependence on the value chosen for r_o. We shall find that use of the smaller value for r_o does give reasonable agreement between IPM calculations and experiment; but this agreement may well be fortuitous.

We shall first present our results on the IPM energy

TABLE III. Oscillator strengths for transitions between occupied shells for Cu.[a]

	$1s^2$	$1p^6$	$1d^{10}$	$2s^2$	$1f^{14}$
$1s$	...	−2.06	...	...	...
$1p$	2.06	...	−6.77	−1.27	...
$1d$	...	6.77	...	...	−13.67
$2s$	...	1.27	...	...	...
$1f$	...	...	13.67	...	...
Summed	2.06	5.98	6.90	−1.27	−13.67
Unused	−0.06	0.02	3.10	3.27	27.67

[a] The summed oscillator strength for a level equals the sum of oscillator strengths for transitions to occupied levels of higher energy minus the oscillator strengths to occupied levels of lower energy. The unused oscillator strength represents the strength of all transitions to unoccupied levels. (The unused oscillator strength should be non-negative; the value −0.06 for the $1s^2$ level shows lack of sufficient accuracy in the calculations.)

[7] Hofstadter, Fechter, and McIntyre, Phys. Rev. 92, 978 (1953).
[8] V. L. Fitch and J. Rainwater, Phys. Rev. 92, 789 (1953).

TABLE IV. Oscillator strengths for transitions between occupied shells for Ta.[a]

	$1s^2$	$1p^6$	$1d^{10}$	$2s^2$	$1f^{14}$	$2p^6$	$1g^{18}$	$2d^{10}$	$3s^2$	$1h^{22}$
$1s$	...	−1.95	...	...	...	−0.05	...	...	...	...
$1p$	1.95	...	−6.45	−1.20	...	...	...	−0.15	−0.06	...
$1d$	...	6.45	...	...	−14.20	−2.35	...	...	...	...
$2s$	...	1.20	...	...	...	−3.11	...	...	...	...
$1f$	...	...	14.20	...	...	...	−23.08	−3.55	...	...
$2p$	0.05	...	2.35	3.11	...	...	...	−8.78	−2.41	...
$1g$	...	...	...	...	23.08	...	...	...	...	−35.91
$2d$	...	0.15	...	...	3.55	8.78	...	...	...	...
$3s$	...	0.06	...	...	...	2.41	...	...	...	...
$1h$	...	...	...	...	...	...	35.91	...	...	...
Summed	2.00	5.91	10.10	1.91	12.43	5.68	12.83	−12.48	−2.47	−35.91
Unused	0.00	0.09	−0.10	0.09	1.57	0.32	5.17	22.48	4.47	57.91

[a] For interpretation see notes on Table III.

levels, and matrix elements z_{kl} for electric dipole transitions. We then calculate the correction factor C for the harmonic mean energy by performing the sums over k and l. We shall compare this correction factor with that found above using the Fermi gas model. We then give the correction factor C' for the mean energy, and finally compare various calculations and experimental results for Cu and Ta.

The energy levels for protons in Cu and in Ta are given in Table II for two different radii for the square well. In each case we have determined the well depth by using rough experimental values for the binding energy of the least tightly bound proton or neutron. Note that we are making the approximation $N=Z$, and neglecting both the Coulomb potential and spin-orbit coupling.

The matrix elements z_{kl} needed for the calculation of the off-diagonal terms B and B' are found using the method of Courant[9] and others. In Tables III and IV we give the oscillator strengths of each shell for electric dipole transitions of protons between the various occupied shells. (Results for $r_o=1.5$ are very close to the tabulated values for $r_o=1.2$.) We have summed over the m values for the closed shells using an equation given by Bethe[10] and have also summed over spins. The oscillator strengths are presented as a square matrix with elements above the diagonal negative since the energy difference is negative. The oscillator strength summed for each shell is found by adding each column, giving the next to the bottom row of the tables. The difference between the oscillator strength summed for the shell and the number of protons in the shell gives the "unused oscillator strength" given in the bottom row of the tables. We see that the lower levels have used almost all of their oscillator strength, transferring it to the higher levels, with the result that for Ta the 32 protons in the $2d$ and $1h$ levels have about 90 percent of the total oscillator strength of 92. (Since the oscillator strength is merely transferred from one level to another, the sum of the unused oscillator strength is the total number of protons.)

We now find the correlation correction to the harmonic mean energy by calculating B, given by Eq. (9), for the sum of the squared dipole matrix elements between occupied levels, using the oscillator strengths tabulated in Tables III and IV. While the summed oscillator strength for transitions between bound levels cancels to zero, this cancellation clearly does not occur for the sum of $(z_{kl})^2$, or $(p_{kl}{}^2)$. The numerical results for B are given in Table V for the two nuclei and two values of r_o treated in this paper. The diagonal term was found by numerical integration of the proton density distribution to find its moment of inertia. In all four cases the value found for D/R^2 is quite close to the value $Z/5$ given by a uniform charge distribution in a sphere of radius R. The correction factor C for the harmonic mean energy is then found by Eq. (10). The last column gives C_F, using the Fermi gas model of the previous section. We see that the correction factor C found for the IPM in a square well is much larger than the more approximate correction C_F. The difference in the two correction factors is due to the difference in the matrix elements z_{kl}, and remains large even for nuclei with very many nucleons. The IPM square well correction factor C is very insensitive to the value of r_o, and increases with A about as

TABLE V. Correction factor for W_H using IPM in square well.[a]

		B/R^3	D/R^3	Correction factor C	Previous section C_F
Cu	$r_o=1.5$	−4.26	6.63	2.8	1.9
	$r_o=1.2$	−4.58	7.0	2.9	
Ta	$r_o=1.5$	−13.7	18.0	4.2	2.3
	$r_o=1.2$	−13.9	18.5	4.0	

[a] The off-diagonal terms B are given by Eq. (9) using the oscillator strengths of Tables III and IV. The diagonal terms D are about equal to $Z/5$ corresponding to a sphere of radius R and uniform charge density. The correction factor $C=(1+B/D)^{-1}$ is compared with the correction factor C_F using a Fermi gas model, given in Table I.

[9] E. Courant, Phys. Rev. 82, 703 (1951).

[10] H. A. Bethe, *Handbuch der Physik* (J. Springer, Berlin, 1933), Vol. 24/1, Eq. (39.14).

TABLE VI. Mean energies for photon absorption by Cu.*

	LB $r_o=1.5$	Burkhardt $r_o=1.5$	This paper $r_o=1.5$	This paper $r_o=1.2$	Exchange $r_o=1.2$	Experiment
Harmonic mean W_H	2.9 Mev	8.4	8.1	12.7	17.8	20.
Mean $\bar{W}$	16. Mev	10.5	9.0	13.	32.	25.
$\int(\sigma/W)dW$	0.34 barns	0.11	0.12	0.08	0.08	0.08

* For LB see reference 1; for Burkhardt see reference 5. [We have included the protons in Burkhardt's value for $\int(\sigma/W)dW$.] The calculations of this paper are based on Table V for W_H, Eq. (11) for $\bar{W}$, and LB, Eq. (47) for the integrated cross section. The values for exchange forces ($x=\frac{1}{2}$) are based on LB. Experimental values are estimated from Jones and Terwilliger, reference 2.

$A^{0.4}$ thus decreasing greatly the $A^{-\frac{1}{3}}$ dependence of W_H found by LB.

The correction factor C' for the mean energy $\bar{W}$ is calculated in a similar manner. The off-diagonal terms B' [Eq. (12)] are calculated using the oscillator strengths for transitions between occupied levels given in Tables III and IV. The diagonal terms D' for the expectation value of the kinetic energy are fairly close to the value given by LB for a degenerate Fermi gas. They can be found more accurately using the kinetic energy for a nucleon of binding energy E as $b(V_o-E)-(1-b)E$, where b is the fraction of the time that the nucleon spends in the square well potential of depth V_o. The value of b is about 0.9 as calculated by numerical integrations. The correction factor $C'=1+B'/D'$ has the value of about 0.5 for Cu and 0.4 for Ta. C' is insensitive to r_o and to A.

Using the correction factors C and C' for the harmonic mean energy W_H and the mean energy $\bar{W}$, respectively, we obtain the results given in Tables VI and VII for the mean energies for photon absorption by Cu and Ta. In Table VI for Cu ($N=Z=34$) the column labelled LB is calculated neglecting the Pauli principle correlation. We observe the large discrepancy between LB's results and Burkhardt's mentioned in our first section. The results of this paper, for $r_o=1.5$, are in reasonable agreement with Burkhardt's values. (We should note that our models are quite similar, but not identical, as Burkhardt includes spin-orbit coupling, which we have neglected. Incidentally, we believe that Burkhardt treats spin-orbit coupling in an inconsistent manner. Instead of treating each level as split into two different levels for different relative orientations of L and S, Burkhardt treats each level as a single level, but fills them in the order of the Mayer-Jensen spin-orbit coupling model.) The next column gives W_H and $\bar{W}$ increased by a factor of $(1.5/1.2)^2=1.56$, using the smaller nuclear radius. Finally, the next to the last column gives still larger calculated mean energies, using the LB corrections for half exchange force. [This calculation, based on reference 1, Eqs. (43) and (46), uses $r_o=1.37$. W_H is insensitive to r_0, but $\bar{W}$ is quite sensitive to r_o. Also, we have here modified the LB equations to include the Pauli principle correlation.] The calculated mean energies are compared with experimental values, estimated from measurements of neutron yield made by Jones and Terwilliger.[2] [These mean energies are found by making an approximate correction for neutron multiplicity, and integrating to 70 Mev. See reference 4 for a discussion of the appropriate upper energy in the integrals of Eqs. (1) and (2). The value for W_H should be fairly good, but that for $\bar{W}$ is unreliable.]

We see that the three successive increases in the LB value of W_H, due to Pauli principle correlations, use of a smaller radius, and exchange forces, gives a calculated value of W_H of 17.8 Mev for Cu in reasonable agreement with the experimental value of about 20 Mev. The calculated value of $\bar{W}$ is 32 Mev if exchange effects are included, or rather higher than the experimental value of about 25 Mev. Here neither the calculated or experimental values can be considered reliable. (Our main purpose in calculation of $\bar{W}$ is to compare with Burkhardt for ordinary forces, and to show that for pure ordinary forces the photon absorption curve exhibits quite a sharp peak, since $\bar{W}$ is close to W_H.)

We also compare calculated and experimental values of the integrated cross section $\int(\sigma/W)dW$, as here the calculated value does not depend on exchange forces, but only on the nuclear wave function. Again we see the discrepancy between the LB and Burkhardt values. (We have added the proton contribution to Burkhardt's calculation of the neutron contribution to this integral.) The results of this paper for $r_o=1.5$ are in good agreement with Burkhardt. (This check is redundant, as this paper and Burkhardt agree on the value of σ_{int} and W_H, and therefore must also agree on the value of $\int(\sigma/W)dW$.) The calculated value using $r_o=1.2$ is in good agreement with the Jones and Terwilliger measurements, where we have included the effects of proton emission.

In Table VII we compare calculations and experiment for Ta($N=Z=92$). The LB value for W_H is only 1.4 Mev, but it is increased by the Pauli principle correlation, by use of a smaller nuclear radius and by half exchange forces to give 12.2 Mev, in reasonable agreement with an experimental value of about 15 Mev. The calculated mean energy $\bar{W}$ is smaller than experiment, if exchange forces are omitted, and larger than experiment if half exchange forces are included; but as discussed above, neither the calculations nor measurements of $\bar{W}$ are reliable. The integrated cross section $\int(\sigma/W)\,dW$ is in good agreement with experiment if we use the smaller radius $r_o=1.2$.

TABLE VII. Mean energies for photon absorption by Ta.*

	LB $r_o=1.5$	This paper $r_o=1.5$	This paper $r_o=1.2$	Exchange $r_o=1.2$	Experiment
Harmonic mean W_H	1.4 Mev	6.0	8.7	12.2	15.
Mean energy $\bar{W}$	16. Mev	6.5	10.4	30.	20.
$\int(\sigma/W)dW$	1.9 barns	0.45	0.31	0.31	0.32

* For interpretation see notes on Table VI.

We note in passing that for pure ordinary forces Ta, like Cu, shows a sharply peaked photon absorption curve, since $\bar{W}$ is not much larger than W_H. [For $r_0=1.5$ this corresponds to several strong transitions to bound levels: 61 percent of the total oscillator strength is used up by the $1h$–$1i$ transition (5.2 Mev), 20 percent of the oscillator strength is used in the $2d$–$2f$ transition (5.6 Mev), 17 percent by transitions to other bound levels, and only 2 per cent by transitions to the continuum.]

Thus we find in Tables VI and VII that the IPM in a square well, with $r_0=1.2$ and half exchange forces, gives reasonable agreement between calculations and experiment for the harmonic mean energy of photon absorption by Cu and Ta. Our conclusion is in disagreement with Burkhardt's, who argued that his calculations showed that the IPM was unsuccessful for calculations of the nuclear photoeffect in Cu. We have increased his mean energy by about a factor of two, by using a smaller nuclear radius and by including half exchange forces, thus removing almost all the discrepancy between his calculations and experiment.

Of course the IPM is an extreme idealization. In the high-energy photoeffect, for example, one of us[11] found good evidence for strong nucleon-nucleon correlations, as in a quasi-deuteron. We have only tried to show that the IPM might well be a reasonable starting point for less approximate calculations of the nuclear photoeffect. We should point out that since we have used sum-rules, we have only used the IPM for the nuclear ground state, and do not concern ourselves here as to whether the IPM applies to the excited states reached by photon absorption.

In Table VIII we present our calculations of the nuclear density $\rho(r)$ *vs* the radial distance in units of the radius of the square well potential (i.e., r/R). The density is normalized to $\int_0^\infty \rho(r) r^2 dr = 1$. This calculated density might be of interest for comparison with recent Stanford measurements[7] of the nuclear form factor for electron scattering. Our work is in reasonable agreement with Malenka's[12] exact calculations for an infinite square well, and approximate calculations for a potential intermediate between a square well and an oscillator potential. In Fig. 1 we plot the nuclear density for Ta with $r_0=1.2$.

Touschek[13] estimated the position of the lowest level of a nucleus that could make electric dipole transitions to the ground state. It is clear that there is at least one dipole level below the excitation energy W_H. However, W_H depends on the possible correlation of nucleus into subunits, such as alpha particles. Touschek estimates the position of lowest dipole level by summing up to an excitation energy which should include transitions for the nucleons not in alpha particles, but sufficiently low so that the alpha particles are not dissociated. He finds

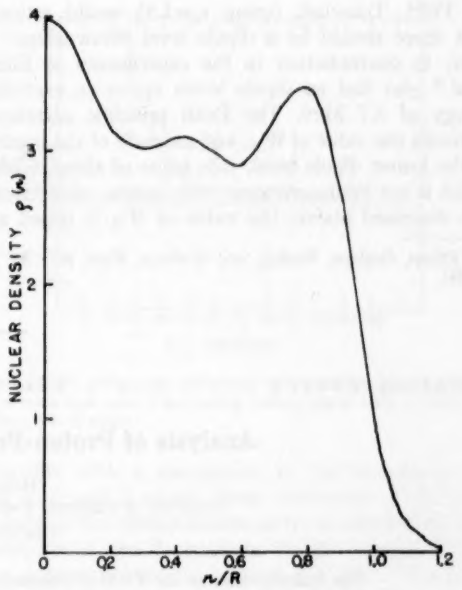

FIG. 1. Nuclear density $\rho(r)$ *vs* radial distance r/R for Ta. The nuclear density $\rho(r)$ is calculated using the IPM for Ta($N=Z=92$) for a square well potential with radius parameter $r_0=1.2$. Numerical values are given in Table VIII.

that the position of the lowest dipole level is insensitive to the correlation of nucleons in alpha particles, and has approximately the very low LB value, given by Eq. (6) of this paper. Our present work shows that one must include the Pauli principle correlations among nucleons, greatly increasing the value of W_H above that given in Eq. (6). This increase by a factor of three to four gives an estimate of the lowest dipole level which is no longer in disagreement with experiment. For example,

TABLE VIII. Nuclear density for Cu and Ta, for IPM in square well.[a]

	Nuclear density $\rho(r)$			
	Cu($N=Z=34$)		Ta($N=Z=92$)	
r/R	$r_0=1.5$	$r_0=1.2$	$r_0=1.5$	$r_0=1.2$
0	3.68	3.50	4.15	3.99
0.1	3.47	3.32	3.77	3.65
0.2	2.97	2.86	3.24	3.13
0.3	2.54	2.47	3.10	3.01
0.4	2.55	2.45	3.18	3.10
0.5	3.00	2.87	3.08	2.99
0.6	3.65	3.47	2.99	2.91
0.7	3.88	3.73	3.36	3.26
0.8	3.35	3.29	3.49	3.47
0.9	2.14	2.18	2.59	2.60
1.0	0.847	0.947	0.899	0.983
1.1	0.226	0.315	0.158	0.217
1.2	0.067	0.106	0.039	0.053

[a] The well-depths and the IPM energy levels are given in Table I. The nuclear density $\rho(r)$ is normalized for radial integration: $\int_0^\infty \rho(r) r^2 dr = 1$. With this normalization, the numerical value would be 3 for a nucleus of constant density.

[11] J. S. Levinger, Phys. Rev. **84**, 43 (1951).
[12] B. J. Malenka, Phys. Rev. **86**, 68 (1952).
[13] B. F. Touschek, Phil. Mag. **41**, 849 (1950).

for Pb^{208}, Touschek (using $r_0=1.5$) would estimate that there should be a dipole level below about 1.4 Mev, in contradiction to the experiments of Elliott *et al.*[14] who find no dipole levels up to an excitation energy of 3.7 Mev. The Pauli principle correlation increases the value of W_H, and estimate of the position of the lowest dipole level, to a value of about 6 Mev, which is not in disagreement with present experiments. (As discussed above, the value of W_H is raised still further by use of a smaller radius, and by including exchange forces.)

We believe that we have shown that the IPM is not in clear disagreement with experiments on the nuclear photoeffect. The IPM should provide a good starting point for making less approximate calculations.

[14] Elliott, Graham, Walker, and Wolfram, Phys. Rev. **93**, 356 (1954).

ACKNOWLEDGMENT

We wish to thank J. L. Burkhardt for communication of his results, and for helpful discussions on these problems.

PHYSICAL REVIEW VOLUME 95, NUMBER 2 JULY 15, 1954

Analysis of Proton-Proton Scattering at 9.7 Mev*

HAROLD H. HALL†
University of California Radiation Laboratory, Livermore, California
(Received April 6, 1954)

The Berkeley data on the 9.7-Mev differential scattering cross section have been subjected to a phase shift analysis. An S phase shift in agreement with earlier work has been found, but with somewhat better precision. This value agrees with that expected from a Yukawa potential.

This experiment shows some suggestion of a repulsive P-state interaction, while the Los Alamos data show a similar but attractive P-state interaction. It is observed that the apparent discrepancy in the small-angle differential scattering cross section is large enough to warrant further measurements in the small-angle region.

THE scattering of protons by protons near 10 Mev has been measured by several experimenters.[1–3] This report summarizes the analysis of the most recent experiment.

The differential scattering cross section obtained by Cork and Hartsough[3] has been fitted in a least-squares sense to a two-parameter phenomenological angular distribution by simultaneous adjustment of the S and P phase shifts.[4] Two systems of weighting were used, Method I weighting observations at a given angle by the reciprocal square of the fractional absolute error, and Method II using the reciprocal square of the fractional statistical error. Method I gave nearly equal weights, the ratio of maximum to minimum weight being 2.6. Method II assigned markedly unequal weights, the corresponding ratio being 31. The phase shifts resulting from the two assignments were in good agreement, as shown by Table I.

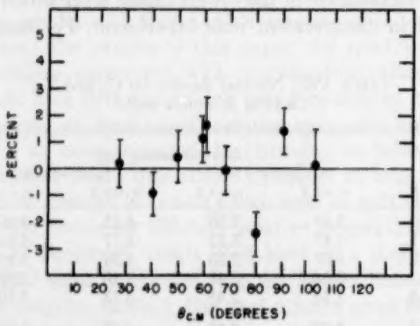

FIG. 1. The percentage difference between the experimental cross section and the least-squares fitted theoretical cross section involving only S and P scattering, as a function of angle.

Inasmuch as the differences are negligible, further comments will be restricted to the first set of phase shifts for simplicity.

The fitting of nine observations by a two-parameter function is over-determinate, so the character of the residuals, $(\sigma_{exp}-\sigma_{th})/\sigma_{th}$, is a gauge of the goodness of fit achieved. Figure 1 exhibits these residual deviations together with the absolute uncertainties, both expressed in percent.

There is no apparent suggestion that the residuals have the angular distribution characteristic of D scattering, since this would require opposite signs above and below 55° for a small D phase shift.

Figure 2 presents the matter in a somewhat more revealing light. Here the isolated points represent the

* This work was performed under the auspices of the U. S. Atomic Energy Commission.
† Now with Headquarters Strategic Air Command, Operations Analysis, Offutt Air Force Base, Omaha, Nebraska.
[1] R. R. Wilson, Phys. Rev. **71**, 384 (1947).
[2] Allred, Armstrong, Bondelid, and Rosen, Phys. Rev. **88**, 433 (1952).
[3] Bruce Cork and Walter Hartsough, University of California Radiation Laboratory Report UCRL-2373, 1953 (unpublished).
[4] H. H. Hall and J. L. Powell, Phys. Rev. **90**, 912 (1953).

percentage difference between the experimental measurements and the purely S-wave part of the phenomenological cross section. Again the vertical bars give the absolute error of each measurement. The continuous curve represents the percentage contribution to the calculated cross section by the small P phase shift, K_1.

While K_1 is small, it makes a rather large contribution, measured in probable errors, at $\theta_{c.m.}=27.53°$. It is clear that one would have difficulty in explaining the smallest-angle scattering without the help of K_1. There is, however, only one angle at which K_1 is really important in these terms, and one must recognize that at 80° one fails almost as badly in fitting the data, where K_1 is of no practical assistance.

It has been observed that the same analysis,[5] applied to the 9.73-Mev data of reference 2, requires $K_1=+0.9°$; again with the smallest-angle measurements dictating the sign and magnitude of this phase shift. It seems impossible to assess the reliability of these determinations of K_1 realistically without further measurements of the scattering cross section in the neighborhood of 20° c.m., where a P phase shift of 1.0° contributes approximately 10 percent of the differential cross section. Although most of the measurements reported in references 2 and 3 are consistent with pure S scattering, an experiment extending through the position of the maximum in the relative P-wave contribution would be particularly valuable in determining whether either of these experiments exhibits a real small-angle effect.

TABLE I. Phase shifts obtained by least-squares fitting, using two methods of weighting.

Weighting	K_0 (degrees)	K_1 (degrees)
I Absolute error	56.48	−0.55
II Statistical error	56.36	−0.53

The goodness of the over-all fit was tested by making a chi-square analysis of the residual deviations of Fig. 1. Straightforward application of the test shows that the remanent deviations are large compared to the estimated precision of measurement. Therefore it is improbable that the experimental errors are perfectly

[5] H. H. Hall, thesis, University of Wisconsin, 1952 (unpublished).

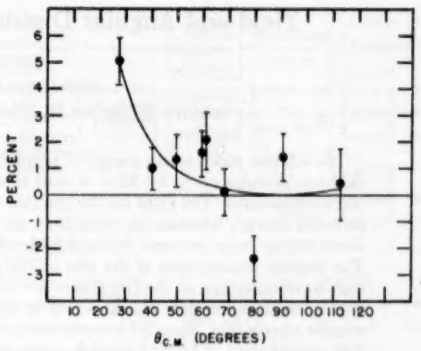

FIG. 2. The percentage difference between the experimental cross section and pure S scattering with a phase shift of 56.48°, as a function of angle.

compatible with a description of the scattering in terms of S and P waves. Some indication of the uncertainty in the determination of K_0 is afforded by an observation of the fluctuations in the "apparent" S phase shift as defined by Jackson and Blatt.[6] On this basis, one-half degree appears to be a reasonable assignment for the uncertainty in K_0. The S phase shift of $56.5\pm0.5°$ deduced from Cork's experiment is in agreement with the value $57.8\pm1.2°$ reported in reference 2, and further improvement in the large-angle measurements seems unnecessary.

By linear interpolation in Table IX of Yovits, Smith, Hull, Bengston, and Breit,[7] and use of Eq. (7.6) in Breit, Condon, and Present,[8] one finds the value of the f function associated with $K_0=56.5\pm0.5$ to be 16.17 ± 0.25. The Yukawa well, fitted to a large body of proton scattering data in reference 7, predicts a value of 16.30 for the f function at 9.73 Mev. The same calculation based on the best fit to the recent Wisconsin data[4] predicts $f=16.25$. This very good agreement supports the belief that the Yukawa well shape is the best of the commonly used shapes for describing the energy dependence of proton scattering in S states up to 10 Mev.

[6] J. D. Jackson and J. M. Blatt, Revs. Modern Phys. **22**, 77 (1950).

[7] Yovits, Smith, Hull, Bengston, and Breit, Phys. Rev. **85**, 540 (1952).

[8] Breit, Condon, and Present, Phys. Rev. **50**, 825 (1936).

Yield and Angular Distribution of Protons from $Li^6(d,p)Li^7$†

WILLIAM E. NICKELL*
State University of Iowa, Iowa City, Iowa

(Received September 21, 1953; revised manuscript received March 4, 1954)

The relative yields *versus* energy of protons from the reactions $Li^6(d,p)Li^7$, Li^{7*} have been measured for deuteron energies up to 3.0 Mev. A marked difference in the energy dependence of the yields for the two reactions is noted. The yield for the reaction $Li^6(d,p)Li^7$ shows a broad maximum centered about 1.1-Mev deuteron energy, whereas the yield from the $Li^6(d,p)Li^{7*}$ reaction shows a slow increase throughout the whole energy range covered. Above 2.5 Mev the yield from $Li^6(d,p)Li^{7*}$ exceeds the yield from $Li^6(d,p)Li^7$. The angular distributions of the two proton groups have been observed at 0.825, 2.0, and 3.0 Mev. The angular distributions of the two groups are quite similar at all energies covered. The Butler analysis of the angular distribution data indicates that in both reactions the neutron is captured with one unit of orbital angular momentum. Since Li^6 has even parity and spin 1, this gives odd parity for the ground state and the first excited state of Li^7 and possible values of $\frac{1}{2}$, $\frac{3}{2}$, and 5/2 for the spins of the ground state and the first excited state. These possible values include the known spin of $\frac{3}{2}$ for the ground state and the currently accepted spin of $\frac{1}{2}$ for the first excited state.

I. INTRODUCTION

THE bombardment of lithium six by deuterons gives rise to two reactions producing long range protons.[1–4] The reactions are

$$Li^6+H^2 \rightarrow Li^7+H^1+Q_1,$$
$$Li^6+H^2 \rightarrow Li^{7*}+H^1+Q_2,$$

where $Q_1=5.020$ Mev and $Q_2=4.542$ Mev. Deuteron bombardment of natural lithium targets as was done in the present experiment does give rise to other reactions producing protons and alpha particles but none of them are of such energy as to interfere with the measurements on the two proton groups above. The angular distribution of these two groups of protons has been studied by several investigators.[5–9] The studies have been made for deuteron energies up to 1.4 Mev. There are some minor discrepancies[10] among the data of different investigators but all data except that by Neuert[5] show fore and aft asymmetry, more protons being observed in the forward direction. Neuert's data were at the very low deuteron energy of 180 kev. His conclusion was that the distribution was spherically symmetric within his statistical error, which, however, was rather large. Yield data have been reported up to 1.8-Mev deuteron energy.[7] The previously reported data indicate a general increase of the asymmetry with increased deuteron energy; also a maximum at approximately 35° to the deuteron beam becomes more pronounced. The present investigation extends the angular distribution and yield measurements up to 3.0 Mev and interprets the results in terms of the theory by Butler.[11]

II. APPARATUS

The deuteron beam for this work was supplied from the pressurized Van de Graaff generator at the State University of Iowa. Beam intensities of several microamperes are attainable, but usually much lower intensities were used. A very intense beam may cause undesirable changes in the target or target backing due to heating.

The target chamber (see Fig. 1) is a brass cylinder approximately $3\frac{1}{4}$-in. inside diameter with $\frac{1}{8}$-in. diameter observation ports at 10° intervals from 0° to 30° and at 15° intervals thereafter to 135°. Targets were prepared by evaporation in vacuum of natural metallic lithium from an electrically heated furnace mounted in the target chamber. The thickness of lithium de-

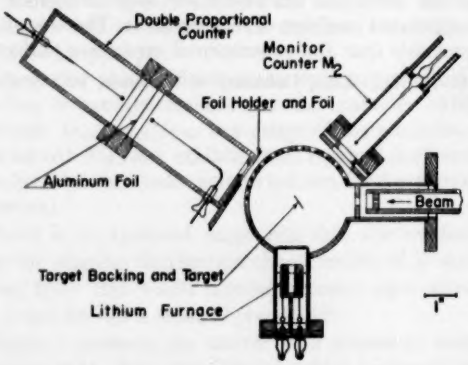

FIG. 1. Target chamber and counters.

† This work was supported in part by the U. S. Atomic Energy Commission.

* Now at South Dakota State College, College Station, South Dakota.

[1] J. D. Cockcroft and E. T. S. Walton, Proc. Roy. Soc. (London) **A144**, 704 (1934).
[2] Delsasso, Fowler, and Lauritsen, Phys. Rev. **48**, 848 (1935).
[3] Lawrence, Livingston, and Lewis, Phys. Rev. **44**, 56 (1933).
[4] Oliphant, Shire, and Crowther, Nature **133**, 377 (1934).
[5] H. Neuert, Physik. Z. **38**, 122 (1937).
[6] William E. Nickell, thesis, The State University of Iowa, 1943 (unpublished).
[7] W. Whaling and T. W. Bonner, Phys. Rev. **79**, 258 (1950).
[8] Krone, Hanna, and Inglis, Phys. Rev. **80**, 603 (1950).
[9] D. N. F. Dunbar and F. Hirst, Australian J. Sci. Research. **A4**, 268 (1951).
[10] D. N. F. Dunbar and F. Hirst, Phys. Rev. **83**, 164 (1951).
[11] S. T. Butler, Proc. Roy. Soc. (London) **A208**, 559 (1951).

posited was controlled by the furnace power and the time of exposure to the furnace. Targets of 20- to 40-kev thickness for the deuteron beam were used. Target thicknesses were estimated from counting rate *versus* integrated beam current data and known cross-section data.[7] The current integrator utilizes the standard scheme of collecting charge on a condenser and discharging the condenser when a predetermined voltage is reached. Each discharge is registered on a mechanical register. No attempt was made to determine target thicknesses with precision since the purpose was only to make targets thin enough to allow separation of the two proton groups. Considerable difficulty was encountered in making targets. In many cases there appeared to be something other than lithium present which contributed protons of range comparable to the range of the lithium protons. This contaminant is believed to have been nitrogen but this was not definitely determined. Whether a target was considered satisfactory was determined from the ratio of protons, of range greater than the shorter of the two groups under investigation, to the alpha particles from the reaction $Li^6(d,\alpha)He^4$. These alpha particles are so energetic that it is extremely unlikely any other reaction will produce alpha particles of comparable range. Consequently the proton-to-alpha ratio is a good measure of the relative abundance of contaminant. Various targets showed a wide range in the ratio of protons to alpha particles. The targets used were those which gave a ratio near the lowest of all targets made. The targets used for the 0.825-Mev data were evaporated directly onto an eight sided stainless steel block. This block was carried on the end of a shaft extending through "O" ring seals in one end of the chamber so that it could be rotated and positioned from outside. At 2.00 Mev and above, the background counting rate from the bare stainless steel block made it unsuitable and thin silver plates were attached to serve as target backing. Silver foils were used as target backing for the forward angle observations. These silver foils were held on a different block but one similar to that described above. Particles observed in the forward directions 0° to 30° passed through the thin backing.

The protons were detected in a double proportional counter (see Fig. 1) designed for this experiment and operated at 36 cm of mercury pressure. The counter gas used was a mixture of 95 percent argon and 5 percent carbon dioxide flowed continuously through the counters. Figure 2 is a block diagram of the counting apparatus. Pulse size discrimination was by the coincidence analyzer discriminators. The double proportional counter base was provided with locating pins and the counter table with locating holes to match so that the counter could be quickly and accurately located to face any desired observation port. The counter table was attached to the target chamber.

Monitoring of the deuteron beam was accomplished

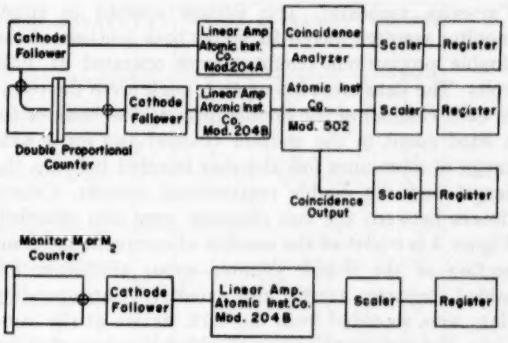

FIG. 2. Block diagram of counting apparatus.

by detection of the alpha particles from the reaction $Li^6(d,\alpha)He^4$ in another proportional counter (see Fig. 1). The monitor counter M_2 shown in Fig. 1 was used in taking the forward angle data. Another counter M_1 similar to M_2 was mounted at 90° to the deuteron beam; it was used in taking the data at 45° and larger angles. The monitor counters were calibrated against each other at each energy since they were used at different angles to the deuteron beam and the solid angles seen by the counters were different.

III. PROCEDURE IN TAKING DATA

The first step was to determine by trial the proper thickness of aluminum foil to insert between the monitor counter and the target so as to have the alpha particles detected near the end of their range. The alpha particles then make pulses near the maximum possible for given counter pressure and voltage operating conditions. Counter pressure was set to 36 cm of mercury and counter voltage and amplifier gain were adjusted to give approximately 70-volt pulses for alpha particles. A number *versus* discriminator curve was then taken to determine the best discriminator setting to use so as to count practically all alphas and exclude all of the very numerous protons which also enter the counter.

Sufficient aluminum foil was inserted between the double proportional counter and the target to exclude the aforementioned alpha particles. The counter voltages and associated amplifier gains were then adjusted to give output pulses of approximately 35 volts for protons. A number *versus* discriminator setting curve was then run for each of the two channels to determine the best discriminator setting to use. The object in this last setting is to use the highest discriminator level possible without missing any of the protons. Using a lower level would insure counting all protons but would greatly increase the background counting rate because of neutrons.

The adjustments mentioned above having once been determined were left fixed. All counters were operated at the pressure 36 cm of mercury held constant by a

Cartesian manostat. The voltage applied to either monitor counter was 1050 volts; both sections of the double proportional counter were operated at 1225 volts. The data recorded at each angle were the count in each channel of the double proportional counter for a fixed count in the monitor channel and for a wide range of aluminum foil absorber inserted between the target and the double proportional counter. Coincidences between the two channels were also recorded. Figure 3 is a plot of the number of counts in the front section of the double counter *versus* aluminum foil added between target and counter. Corresponding data were recorded from the back section at the same time. For a given thickness of added aluminum foil the two sections operate approximately 12 mg/cm² of aluminum apart on such a curve; part of this is due to 8.60 mg/cm² of aluminum between the two sections and the remainder is due to the depth of the front section. No such complete curve of counts *versus* added foil need be determined for every angle. A brief preliminary survey along such a curve allows one to determine the amount of added foil necessary to put the back section of the counter in the region enclosed in dotted lines. This portion of the curve may then be investigated very carefully and at the same time data for the portion farther back are obtained from the front section.

Inspection of Fig. 3 shows that for added foil thickness greater than 80 mg/cm² the count remains constant. This is background due to neutrons and changes very little even for as much as $\frac{1}{16}$ in. of aluminum added. As the amount of added foil is decreased the count rises rapidly for a ways and then very slowly. The count in this region of nearly constant count is background plus the long range protons under investigation. Still further decrease in the added foil brings further rise in the count until at 56 mg/cm² a steady count again obtains and further decrease causes no increase in the count. The count here is background plus both groups of protons. Of course the amount of absorber can be decreased enough to admit protons from contaminant reactions such as $C^{12}(d,p)C^{13}$ and $O^{16}(d,p)O^{17}$. A curve such as Fig. 3 for each angle serves to determine the net number of protons of each group. Actually, as mentioned above, only parts of such a curve were generally obtained.

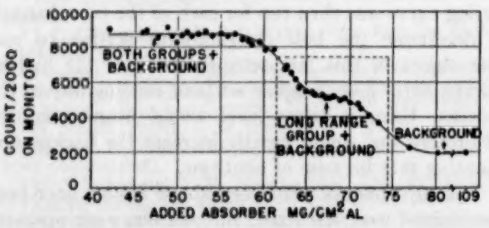

FIG. 3. Number of counts *versus* added absorber thickness.

Experimentally it is found that the net count in the back section is approximately 8 percent lower than the count in the front section at a corresponding location along the curve. This is due to multiple scattering of some particles so that they do not enter the back section, and to stopping of some particles by the wire and bead in the front section. The effect of this is that, in obtaining the number of short-range protons by subtracting the net long range group measured in the back section from the net total measured in the front section, too large a number is obtained. A correction for this effect has been made to all of the data at 0.825 Mev and at 2.00 Mev. Complete curves were determined from the front section at 3.00 Mev for 90° and smaller angles but not for larger angles. The 8 percent loss in the back section was then taken into account in determining the count to be used for the larger angles.

In addition to the angular distribution data taken as described above, data of yield *versus* integrated deuteron beam were taken at 0° and deuteron energies 1.0, 1.4, 1.8, 2.0, and at 0.1-Mev intervals to 3.0 Mev. In taking these data, the thickness of aluminum foil between the counter and target was adjusted so that the front section of the counter received both proton groups. Following each such run, a background run was taken with enough added foil to stop both groups. The ratio of each group to the total was known at 2.0 Mev and at 3.0 Mev from the angular distribution data. The ratio was also determined at 2.5 Mev and at 1.0 Mev. The ratio found at 1.0 Mev was in good agreement with that determined by Whaling and Bonner.[7] Their ratio results were used at 1.8 Mev and lower energy to divide the total count into short- and long-range groups.

The only use made of the coincidence count between the front and back sections of the double proportional counter was as a check on the efficiency of the front section when taking data with only a small amount of absorber. Under these conditions the energy of protons in the front section is relatively high and consequently the proton pulse size is reduced. Good agreement between the net count in the back section and the coincidence count was taken as evidence that the front section was counting all the protons passing through it.

IV. RESULTS AND DISCUSSION

Angular distributions of the two groups of protons separately have been determined over the range of angles 0° to 135° at 2.0 Mev and at 3.0 Mev. The distribution of each group at 0.825 Mev was determined over the range 45° to 135°. In general sufficient counts were taken at each point on the curve (see Fig. 3) used to obtain the data at each angle and bombarding energy to get statistical accuracy of better than 1½ percent. Because of straggling, the two proton groups are not completely separated and there is no level plateau

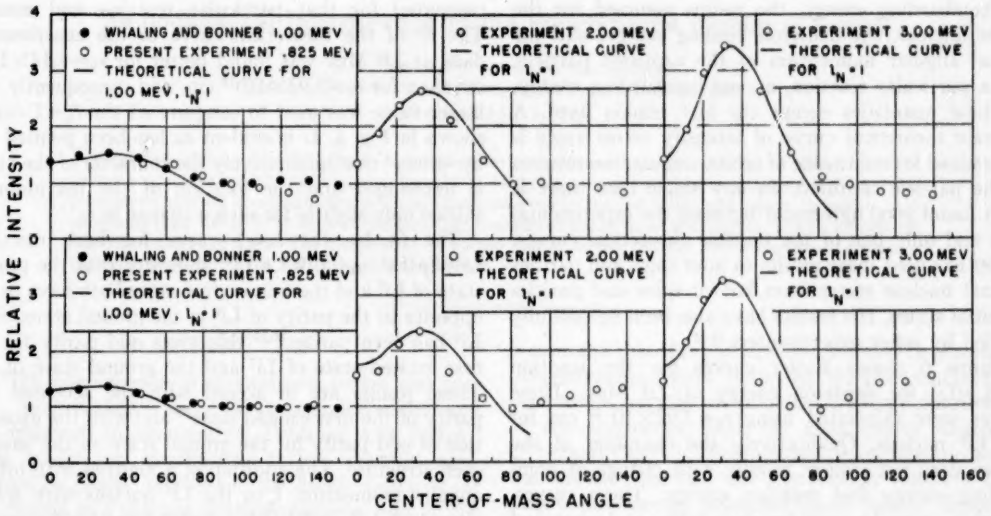

FIG. 4. Angular distribution of the two proton groups in the center-of-mass system of coordinates. The short-range group is shown in the three top curves and the long-range group in the three bottom curves. In all cases the data are normalized to unity at 90°. The theoretical curves are computed from the Butler theory using $r_0=4.14\times10^{-13}$ cm.

on the curve corresponding to the long-range group alone. There is then some error in selecting the most nearly level portion or, in most instances, in selecting the inflection point on the curve. It is estimated that the probable error in the final results is less than 4 percent.

The results of the angular distribution measurements are shown in Fig. 4. The relative intensity normalized to unity at 90° is plotted as ordinate and the center-of-mass angle as abscissa. The proper center-of-mass intensity correction factors have been applied to all data. The results of Whaling and Bonner[7] at 1.0 Mev are shown in Fig. 4 along with the results of the present experiment at 0.825 Mev. The agreement with their results for both groups is quite satisfactory except for the short-range group at backward angles. Their results for the short-range group show an increase in the backward direction reaching a maximum at approximately 130° and then a decrease, whereas for this low energy the present experiment shows no such increase for the backward angles. In their experiment, as well as in the present experiment, the short-range data are obtained as a difference between two numbers and are consequently subject to larger error than are the data for the long-range group; nevertheless the difference seems larger than can be explained by errors. The data at 2.00 Mev and at 3.00 Mev show greater fore and aft asymmetry than has been observed at lower energies, together with a more pronounced maximum at approximately 32° to the deuteron beam.

The relative yield *versus* energy data are shown in Fig. 5. The agreement with the results of Whaling and Bonner[7] over the energy range common to both experiments is quite good. Their results are also shown in Fig. 5. The relative yields of the two groups differ considerably in their dependence on the incident deuteron energy. The yield from the reaction leading to the ground state shows a broad maximum centered about 1.1 Mev. The other group shows increasing yield throughout the energy range covered. The yield of the short-range group, which at low bombarding energy is less prominent, becomes equal to the long-range group at 2.5 Mev, and above this energy exceeds the long-range yield.

Butler[11] has developed a theory and formulae from which the angular distributions to be expected from a stripping process in (d,p) and (d,n) reactions can be calculated. The theoretical expression involves the masses of the reacting particles, the reaction energy,

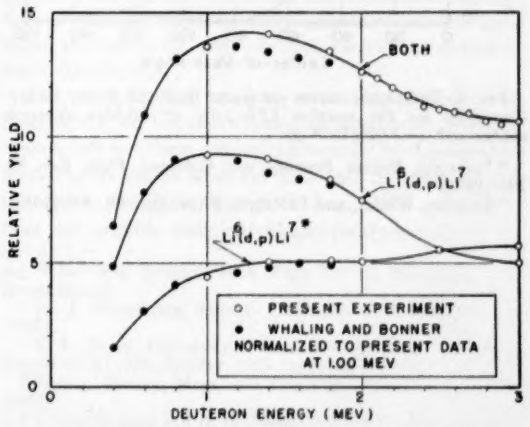

FIG. 5. Relative yield of long- and short-range protons at 0°.

the bombarding energy, the radius assumed for the target nucleus, the deuteron binding energy, and the orbital angular momentum of the captured particle. For a particular reaction, at one bombarding energy, all these quantities except the last remain fixed. A separate theoretical curve of intensity *versus* angle is determined for each value of orbital angular momentum of the particle captured. In any single case there is often found good agreement between the experimental data and only one of the possible theoretical curves. Butler has used these results to infer spins and parities of final nuclear states from known spins and parities of initial states. His results have also been successfully applied by other experimenters.[12,13]

Figure 6 shows Butler curves for the reaction $Li^6(d,p)Li^7$ for deuteron energy of 2.0 Mev. These curves were calculated using $r_0=3.92\times10^{-13}$ cm for the Li^6 nucleus. Qualitatively the character of the curves does not change rapidly with change of bombarding energy and reaction energy. These curves, therefore, may be used for data taken at higher and lower energies and even for data on the reaction $Li^6(d,p)Li^{7*}$ to the extent of determining which of the possible curves will best fit the experimental data. Examination of the experimental data shown in Fig. 4 indicates a best fit by the $l_n=1$ type curve at each energy and for each group. The solid curve shown on each plot of experimental data is the $l_n=1$ curve computed for that particular reaction and energy. The fit of the theoretical curve to the experimental data at 2.0 Mev was found better for $r_0=4.14\times10^{-13}$ cm than for $r_0=3.92\times10^{-13}$ cm, and consequently this larger value was used to compute all the $l_n=1$ curves shown in Fig. 4. It is evident as has been pointed out by others[14] that qualitatively the character of the curve is unchanged and the location of the maximum is shifted only slightly for such a change in r_0.[15]

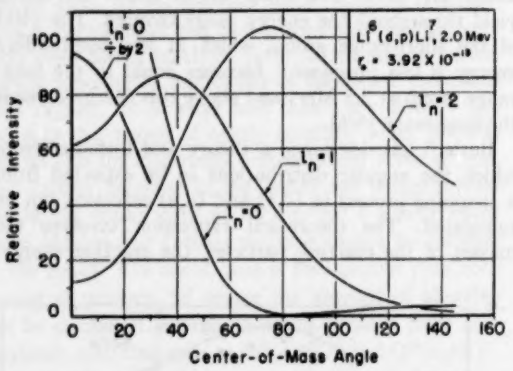

FIG. 6. Theoretical curves computed from the Butler theory. Computed for the reaction $Li^6(d,p)Li^7$ at 2.0-Mev deuteron energy and $r_0=3.92\times10^{-13}$ cm.

The fit by the $l_n=1$ curve for both reactions $Li^6(d,p)Li^7$ and $Li^6(d,p)Li^{7*}$ indicates that the ground state of Li^7 and the first excited state both have parity opposite to the parity of Li^6 in the ground state. Since Li^6 has even parity,[16,17] this gives odd parity for the first excited state of Li^7 and the ground state of Li^7. These results are in accord with the accepted odd parity of the first excited state[17] and with the expectation of odd parity for the ground state on the basis of shell structure. The addition of a neutron with orbital angular momentum 1 to the Li^6 nucleus with spin 1 gives 1/2, 3/2, and 5/2 as possible spins for the ground state and the first excited state of Li^7. The spin of Li^7 in the ground state is 3/2 and the currently accepted spin of the first excited state is 1/2.[17,18] Both of these values are included in the possible values determined by the present experiment.

The author wishes to express his sincere appreciation to Professor James A. Jacobs for his guidance and many valuable suggestions during the course of the experiment. He wishes to thank Mr. Philip R. Malmberg and Mr. George S. Carson for assistance in connection with the general maintenance of the statitron and the electronic circuits. Mr. Philip Shapiro's assistance during the long runs of data taking is sincerely appreciated. The cooperation of the personnel of the physics department instrument shop under the direction of Mr. J. G. Sentinella is gratefully acknowledged.

[12] Fulbright, Bruner, Bromley, and Goldman, Phys. Rev. **88**, 700 (1952).

[13] Bromley, Bruner, and Fulbright, Phys. Rev. **89**, 396 (1953).

[14] F. Ajzenberg, Phys. Rev. **88**, 298 (1952).

[15] The fit by the $l_n=1$ type curve for each of the two groups is in agreement with the findings of Holt and Marsham (private communication from J. R. Holt dated July 30, 1953). They used 8-Mev deuterons and find that their data for each of the two groups can be well fitted by a theoretical curve having $l_n=1$ and $r_0=5.0\times10^{-13}$ cm. Their curve reaches a maximum at approximately 25° to the deuteron beam.

[16] J. M. Blatt and V. F. Weisskopf, *Theoretical Nuclear Physics* (John Wiley and Sons, Inc., New York, 1952), p. 281.

[17] F. Ajzenberg and T. Lauritsen, Revs. Modern Phys. **24**, 321 (1952).

[18] R. G. Uebergang and N. W. Tanner, Australian J. Phys. **6**, 53 (1953).

Radiochemical Investigation of the Spontaneous Fission of Cm^{242}†

E. P. STEINBERG AND L. E. GLENDENIN
Chemistry Division, Argonne National Laboratory, Lemont, Illinois

(Received April 1, 1954)

Spontaneous fission of Cm^{242} has been investigated by radiochemical determination of the yields of 21 fission products ranging in mass number from 91 to 140. Fission is observed to be asymmetric. The yield-mass curve exhibits somewhat narrower peaks than observed in induced fission and a peak-to-trough ratio of greater than 700 to 1. Prominent fine structure is observed in the mass distribution, and an analysis of this phenomenon is made. The distribution of nuclear charge in spontaneous fission appears to be essentially the same as that in low-energy induced fission.

I. INTRODUCTION

THE phenomenon of spontaneous fission was considered theoretically by Bohr and Wheeler[1] and first observed in uranium by Petrzhak and Flerov.[2] Later studies on spontaneous fission, recently summarized by Segrè,[3] established the decay constants for this process in a number of heavy nuclides, and, in the case of U^{238}, a value for the average number of neutrons emitted per fission. It is of great interest to compare the characteristics of the mass distribution resulting from this process with that of induced fission. Extensive radiochemical investigations of the latter have shown a pronounced asymmetry in fission with the probabilities of symmetrical fission modes ("trough") and, perhaps, very asymmetric modes ("wings") increasing with excitation energy of the fissioning nucleus. It might, therefore, be expected that spontaneous fission, occurring in the ground state, would exhibit a lower trough and narrower distribution of mass than induced fission. Anomalous yields have been observed in induced fission in the mass region of the 82-neutron shell[4,5] and its complement.[6,7] This so-called "fine structure" is presumably associated with a preference for a closed-shell configuration in the fission act[5,6] and the excessive evaporation from primary fission fragments of the loosely bound neutrons just outside closed shells.[8,9] It is expected that this phenomenon will also be prominent in spontaneous fission. Ionization chamber studies have been made recently on the kinetic energy distribution of the fragments from the spontaneous fission of U^{238} [10] and Cm^{242}.[11,12] Predominantly asymmetric fission was indeed observed, not significantly different from that of low-energy neutron-induced fission. However, the rather poor resolution inherent in the ionization method precludes a significant comparison of the width of the mass distribution and frequency of symmetric fission modes in spontaneous and induced fission.

More detailed information on the mass distribution in spontaneous fission has been obtained by Thode and co-workers[13,14] and by Wetherill[15] using the highly sensitive mass spectrometric technique. These investigators examined the isotopic composition of the rare gases krypton and xenon produced in various minerals by spontaneous fission of U^{238} and Th^{232}. The observed abundances of the fission-produced isotopes of these elements indicate a narrower mass distribution with lower frequency of fission modes near symmetry as would be expected. Evidence was also presented for an abnormally high yield (fine structure) at mass 132, as might be expected from the closed-shell effects mentioned above. Although a rough yield-mass curve may be deduced from the relative isotopic abundances of the krypton and xenon alone under the reasonable assumption of identical yields at complementary masses, these mass spectrometric data do not provide a complete mass distribution.

The radiochemical method, which supplies detailed information on the distribution of mass and charge in fission, has not been applied previously to the study of spontaneous fission since the slow rate of decay by this process in available materials (e.g., U^{238} and Th^{232}) does not provide sufficient fission product activity for

† This investigation was carried out during the summer of 1952 at the Radiation Laboratory, University of California, Berkeley, California. Preliminary material for presentation at the Gordon Research Conference, New Hampton, New Hampshire (June, 1953) was issued as U. S. Atomic Energy Commission Document AECD-3520 (unpublished).

[1] N. Bohr and J. A. Wheeler, Phys. Rev. **56**, 426 (1939).

[2] K. A. Petrzhak and G. N. Flerov, Compt. rend. acad. sci. (U.S.S.R.) **28**, 500 (1940); J. Phys. (U.S.S.R.) **3**, 275 (1940).

[3] E. Segrè, Phys. Rev. **86**, 21 (1952).

[4] H. G. Thode and R. L. Graham, Can. J. Research **A25**, 1 (1947); MacNamara, Collins, and Thode, Phys. Rev. **78**, 129 (1950).

[5] D. R. Wiles, M.Sc. thesis, Dept. of Chemistry, McMaster University, Hamilton, Ontario, August, 1950 (unpublished); Wiles, Smith, Horsley, and Thode, Can. J. Phys. **31**, 419 (1953).

[6] Glendenin, Steinberg, Inghram, and Hess, Phys. Rev. **84**, 860 (1951).

[7] D. R. Wiles, Ph.D. thesis, Department of Chemistry, Mass. Inst. Technol., Cambridge, Massachusetts, November, 1953 (unpublished).

[8] L. E. Glendenin, Laboratory for Nuclear Science and Engineering, Mass. Inst. Technol. Tech. Rept. No. 35, December, 1949 (unpublished).

[9] A. C. Pappas, Laboratory for Nuclear Science and Engineering, Mass. Inst. Technol. Tech. Rept. No. 63, September, 1953 (unpublished).

[10] W. J. Whitehouse and W. Galbraith, Phil. Mag. **41**, 429 (1950).

[11] R. L. Shuey, University of California Radiation Laboratory Report UCRL-959, October, 1950 (unpublished).

[12] Hanna, Harvey, Moss, and Tunnicliffe, Phys. Rev. **81**, 466 (1951).

[13] J. MacNamara and H. G. Thode, Phys. Rev. **80**, 471 (1950).

[14] W. H. Fleming and H. G. Thode, Phys. Rev. **92**, 378 (1953).

[15] G. W. Wetherill, Phys. Rev. **92**, 907 (1953).

accurate measurements. With the recent availability of milligram quantities of Cm^{242}, which has a highly favorable spontaneous fission rate (4.66×10^5 fissions/min mg),[12] it became feasible for the first time to investigate the spontaneous fission process in detail by the radiochemical method. The great advantage of Cm^{242} is illustrated in Table I, where the spontaneous fission rates[3,12] and the activity of a typical fission product (saturation disintegration rate for a 6 percent fission yield) for Th^{232}, U^{238}, and Cm^{242} are compared. It is apparent that the determination of yields in the region of symmetric spontaneous fission, which are expected to be even lower than those in neutron-induced fission of U^{235} (about 0.01 percent), would require formidable quantities of Th^{232} or U^{238}. For example, at least a ton of U^{238} would be required to obtain a measurable activity of a fission product with a yield of 0.01 percent, whereas only one milligram of Cm^{242} would suffice.

Although the fission rate of Cm^{242} is adequate for a convenient radiochemical study of spontaneous fission, there are other factors which must be considered. Most important, of course, is the absence of appreciable fission product activity from any source other than spontaneous fission. Neutrons arising from spontaneous fission and from the (α,n) reaction, particularly in light elements, could induce fission, for example, in Am^{242} (thermal neutron fission cross section = 6000 barns[16]) which is likely to be present in the Cm^{242} source. Since induced fission may produce fission products in the region of the trough in yields perhaps as high as 0.1 percent (much higher than those expected for spontaneous fission), an induced fission rate equal to 10 percent of that of spontaneous fission would result in apparent observed spontaneous fission yields in this region of about 0.01 percent. This value is just at the limit of detection for spontaneous fission yields from a one-milligram source of Cm^{242}. It is shown by the following calculation that the contribution of neutron-induced fission is at most only 2 percent and probably much lower, and is hence a negligible source of error.

The production of 1.6 neutrons per spontaneous fission by the α, n reaction in an aqueous solution of Cm^{242} is estimated by taking a thick target yield in oxygen of one neutron per 10^7 alpha particles of about 6 Mev energy.[17] No other light elements with appreciable (α,n) yields are present in solution with the possible exception of slight boron impurities from Pyrex glass containers. As a conservative approximation, the total neutron yield from (α,n) reactions is taken as three neutrons per spontaneous fission (equivalent to allowing boron to be present in the very unlikely concentration of about 0.2 molar). In addition, the emission of three neutrons accompanies each spontaneous fission (see Sec. III), giving a total upper estimate of about six neutrons produced in the solution per spontaneous fission. An upper limit to the effect of these neutrons in inducing fission in a 10-ml aqueous solution containing about one milligram each of americium and curium (see Sec. IIA) may be estimated by assuming that all of the neutrons are thermalized and absorbed. The probability of a neutron colliding with an atom of americum or curium and inducing fission during the approximately 30 collisions required for thermalization is about 2×10^{-3}. The probability of inducing fission after thermalization is equal to the ratio of the total thermal neutron fission cross section of americium and curium to the total thermal neutron absorption cross section of the solution and is about 10^{-3}. Thus, for six neutrons per spontaneous fission, the ratio of induced to spontaneous fissions is the order of 2 percent. Since a majority of the neutrons will certainly escape the solution after a few collisions, the above result is at least an order of magnitude high.[18] Other causes of induced fission such as gamma rays, cosmic rays, etc., are much less important.

The intense alpha radioactivity of Cm^{242} (7.37×10^{12} alphas/min mg)[19] also presents some problems in radiochemical operations. Facilities and techniques for handling such sources have been developed by the Nuclear Chemistry and Health Chemistry groups at the University of California Radiation Laboratory, and these were made available for this investigation. In general, decontamination factors of the order of 10^{10} would be required to reduce the alpha activity to a reasonably low level in an isolated fission product sample. The standard radiochemical procedures for isolation of fission products[20] are easily adapted to this need. Gas evolution and the slight temperature rise in solutions of such intense alpha radioactivity are minor problems.

The foregoing considerations indicate the feasibility of a radiochemical study of the spontaneous fission process in Cm^{242} with only minor modifications from the well-established techniques employed in the studies of induced fission. The present investigation was therefore undertaken to establish, within the limitations of

TABLE I. Comparison of spontaneous fission rates.

Nuclide	Fissions/min mg	Saturation activity of Ba^{140} (dis/min)
1.4×10^{10}-yr Th^{232}	2.5×10^{-6}	1.5×10^{-7}
4.5×10^{9}-yr U^{238}	4.14×10^{-4}	2.5×10^{-5}
162.5-day Cm^{242}	4.66×10^{5}	2.8×10^{4}

[16] Street, Ghiorso, and Thompson, Phys. Rev. **85**, 135 (1952).

[17] H. L. Anderson, "Neutron from Alpha Emitters" (National Research Council Committee on Nuclear Science, December, 1948) Prelim. Rept. No. 3 of Nuclear Science Series (unpublished).

[18] We are indebted to Dr. B. I. Spinrad of the Physics Division, Argonne National Laboratory and Prof. A. Turkevich of the Inst. for Nuclear Studies, Univ. of Chicago, for helpful discussions on this subject.

[19] Hanna, Harvey, and Moss, Phys. Rev. **78**, 472 (1950).

[20] *Radiochemical Studies: The Fission Products* (McGraw-Hill Book Company, New York, 1951), National Nuclear Energy Series, Plutonium Project Record, Div. IV, Vol. 9.

time and amount of Cm^{242} available, as complete a mass distribution as possible with particular attention to the frequency of symmetrical fission modes, the presence of fine structure, and charge distribution.

II. EXPERIMENTAL

A. General Procedure

The Cm^{242} source used in this work was isolated by Dr. S. G. Thompson and Dr. G. H. Higgins and personnel of the Health Chemistry group of the University of California Radiation Laboratory from americium which had been irradiated in the Canadian pile at Chalk River. Cation and anion exchange techniques were employed for the separation of the curium (along with some of the americium) from the intense fission product rare earth activities produced mainly by fission of Am^{242}. The final sample prepared for our use consisted of approximately 1 mg each of curium (90 percent Cm^{242}, 5 percent Cm^{243}, and 5 percent Cm^{244}) and americium (75 percent Am^{241}, 2 percent Am^{242}, and 23 percent Am^{243}), with Cm^{242} accounting for more than 99 percent of the alpha activity and about 97 percent of the spontaneous fissions (3 percent being due to Cm^{244}).

All radiochemical operations were carried out in enclosed, vented glove-boxes ("Berkeley box") commonly employed for the safe handling of intense sources of alpha activity.[21] Since the curium source continuously produces spontaneous fission product activities and may contain additional fission product activities produced during the pile irradiation of the Am^{241} and incompletely removed in the purification of the curium, it was necessary to remove all activities of the element of interest before the determination of spontaneous fission yields. In general, this was accomplished by successive quantitative separations of added carrier from the curium solution, the last removal establishing the zero time for growth of activities of the element from spontaneous fission. A known weight of carrier was then added, and the fission rate of the solution was determined by alpha counting a small aliquot and applying the known alpha-to-fission ratios for Cm^{242} and Cm^{244}. Periods of growth varying from about one day to two weeks were employed to suit the half-life ranges of the nuclides under investigation. The fission rate was corrected for decay of Cm^{242} during the growth period where necessary.

The growth period was ended by separation of the carrier from the curium. After making sure that no more than 0.1 percent of the curium accompanied the carrier, the latter was transferred to a secondary Berkeley box so that final decontamination from curium and purification from other fission products was made in an environment free from the bulk of the intense alpha activity. Before removal from the secondary box for final precipitation and mounting, the fission product sample was always assayed for alpha activity to verify the adequacy of decontamination from curium. The final precipitate in each case was collected on a small circle of filter paper, weighted to determine the chemical yield, mounted at the center of a 2.5×3.25 in. cardboard support, covered with thin Cellophane, and its counting rate measured with an end-window Geiger counter. A ring of anticoincidence counters was used to reduce background. The radiochemical purity of each fission product was determined by its absorption and decay characteristics.

The observed counting rates were corrected for chemical yield, decay, fractional saturation during the growth period, and the presence of other activities due to genetically related or isotopic species. Empirical self-absorption and self-scattering factors[22] were used to correct for the effects of sample weight (usually about 20 mg), and an exponential absorption correction was made for absorption in the Cellophane covering over the sample, in the air layer between the source and the counter, and in the counter window. A geometry factor of 24.0 percent was determined by the RaDEF calibration method[23] for the source position used.

B. Individual Determinations

Strontium (9.7-hr Sr^{91} *and* 2.7-hr Sr^{92})

Precipitations of $Sr(NO_3)_2$ with fuming HNO_3 were made to remove all strontium activities from the curium solution. After a growth period of 65.6 hr, strontium was again removed as nitrate and purified[24] from contaminating fission products and curium by $Fe(OH)_3$ and $BaCrO_4$ removals, and finally precipitated as $SrCO_3$ for mounting and counting. The last $Fe(OH)_3$ precipitation was made about two hours after the end of the growth period, removing the yttrium activities (17-min Y^{91} and 11-hr Y^{91}) resulting from the complete decay of the 2-min Sr^{91} and 7-min Sr^{93} and establishing a zero time for the growth of the 51-min Y^{91m} and 3.5-hr Y^{92}.

The determination of 9.7-hr Sr^{91} and 2.7-hr Sr^{92} was made by analyses of decay and absorption curves taking into account the activities of the 51-min Y^{91m} and 3.5-hr Y^{92} daughters, and a long-lived component of low intensity probably due to 53-day Sr^{89} and 61-day Y^{91}.

Molybdenum (67-hr Mo^{99})

Precipitations of molybdenum as sulfide were employed to start growth periods of 72.0 and 89.5 hr. A modified alpha-benzoinoxime procedure[25] was then used for the isolation of molybdenum. An initial sulfide separation was followed with a specific tellurium removal by reduction to metal with SO_2. The molybdenum was then precipitated with alpha-benzoinoxime, purified

[21] See, e.g., B. B. Cunningham, Nucleonics **5**, No. 5, 83 (1949).

[22] Engelkemeir, Seiler, Steinberg, and Winsberg, reference 20, Paper 4.

[23] T. B. Novey, Rev. Sci. Instr. **21**, 280 (1950).

[24] L. E. Glendenin, reference 20, Paper 236.

[25] N. E. Ballou, reference 20, Paper 257.

by repeated precipitations of $Fe(OH)_3$, and finally isolated as $PbMoO_4$.

Since complete decay of the shorter-lived molybdenum activities occurred before final isolation and counting of the samples, only the 67-hr Mo^{99} was observed. The molybdenum samples were counted through 12.5 mg/cm² of aluminum to filter out the low-energy conversion electrons from 5.9-hr Tc^{99m}. Allowance for this additional absorber was made in the absorption correction.

Ruthenium (40-*day* Ru^{103}, 4.5-hr Ru^{105}, *and* 1.0-yr Ru^{106})

Ruthenium activities were removed from the curium solution by sulfide precipitations in preparation for growth periods of one and two days. The ruthenium was again precipitated as sulfide to end these growth periods and was purified[26] by distillation into NaOH from acidic $KMnO_4$, removal of $Fe(OH)_3$, and reduction to metal with magnesium. A longer period of 6.8 days was employed for the growth of the 40-day Ru^{103} and 1.0-yr Ru^{106} and was started and ended by distillation of ruthenium from $HClO_4$ solution.[26]

The 4.5-hr Ru^{105} was determined in the three runs by analyses of decay and absorption curves. Corrections were made for the presence of 45-sec Rh^{105m} and 36.5-hr Rh^{105} daughters. After complete decay of the 4.5-hr Ru^{105}, rhodium was removed from the ruthenium sample, the ruthenium remounted, and the relative contributions of 40-day Ru^{103} and 1.0-yr Ru^{106} (in equilibrium with 30-sec Rh^{106}) determined by analysis of an absorption curve.

Palladium (13.1-hr Pd^{109} *and* 21-hr Pd^{112})

Palladium was isolated by the dimethylglyoxime procedure[27] after initial removal from the curium by sulfide precipitation. During the first day of a 67-hr growth period it was observed that the palladium carrier was reduced to metal (presumably by decomposition products formed by the action of the intense alpha radiation on the solution). The metallic palladium was dissolved to insure exchange with fission-produced species and reprecipitated as the sulfide at the end of the growth period. After purification by dimethylglyoxime precipitations and $Fe(OH)_3$ removals, a AgCl precipitation was made to establish zero time for the growth of 3.2-hr Ag^{112}, and the palladium was finally precipitated with dimethylglyoxime.

The activities due to 13.1-hr Pd^{109} and 21-hr Pd^{112} (through its 3.2-hr Ag^{112} daughter) were determined by analyses of decay and absorption curves.

Cadmium (53-hr Cd^{115})

Cadmium was separated from the curium as the sulfide to start and end the growth period. Purification[28] was achieved by several removals of basic iron acetate from buffered solution (*p*H 5) and PdS from 6*N* HCl solution, and cadmium finally isolated as the sulfide. A final precipitation of basic iron acetate to remove indium was made near the end of the procedure to establish zero time for the growth of 4.5-hr In^{115m} and 2-hr In^{117}. Since the fission yields of cadmium isotopes were expected to be low, a relatively long growth period of 8 days was used to obtain essentially saturation activities.

The activity due to 53-hr Cd^{115} was determined from an analysis of a growth and decay curve taking into account the contributions of the 4.5-hr In^{115m} daughter and a long-lived activity, presumably 43-day Cd^{115m}, present in low intensity.

Antimony (93-hr Sb^{127} *and* 4.2-hr Sb^{129})

Antimony was oxidized with Br_2 to Sb(V) and separated from the curium by sulfide precipitation from 1*N* HCl solution to start and end a 7.1-day growth period. Purification was achieved by precipitations of molybdenum alpha-benzoinoxime, tellurium (by reduction with SO_2), and $Fe(OH)_3$. Separation from tin was made by sulfide precipitations of Sb(III) in the presence of HF. A removal of tellurium as sulfide from 6*N* HCl solution was made near the end of the procedure to establish zero time for the growth of tellurium daughter activities, and the antimony was isolated for mounting as Sb_2S_3.

Analyses of decay and absorption data were made to obtain the relative contributions of 93-hr Sb^{127} and 4.2-hr Sb^{129} to the total activity. The beta-decay scheme of Sb^{129} has not been reported. Absorption data obtained in this work indicate it to be complex with an initial half-thickness in aluminum of about 36 mg/cm², and this value was used for the absorption corrections. Branching ratios for the decay of 93-hr Sb^{127} to 9.3-hr Te^{127} and of 4.2-hr Sb^{129} to 70-min Te^{129} were taken as 84 percent and 80 percent, respectively.

Tellurium (30-hr Te^{131m} *and* 77-hr Te^{132})

Tellurium was removed from the curium solution as sulfide to start a 69-hr growth period. After ending the growth period by precipitation as sulfide, the tellurium was reprecipitated by reduction to the elementary state with SO_2 and set aside to allow the 9.3-hr Te^{127} to decay to a negligible intensity. The tellurium was then purified[29] by $Fe(OH)_3$ removals and finally precipitated by reduction with SO_2 to establish zero time for the growth of 2.4-hr I^{132}.

[26] L. E. Glendenin, reference 20, Paper 260.
[27] J. A. Seiler, reference 20, Paper 264; L. E. Glendenin, reference 20, Paper 265.
[28] R. P. Metcalf, reference 20, Paper 268; L. E. Glendenin, reference 20, Paper 265.
[29] T. B. Novey, reference 20, Paper 273; L. E. Glendenin, reference 20, Paper 274.

Analyses of decay and absorption data were made to determine the contributions of the chains, 30-hr Te^{131m}→ 25-min Te^{131}→8.0-day I^{131} and 77-hr Te^{132}→2.4-hr I^{132}. A low intensity background activity probably due to 32-day Te^{129m} was also observed.

Iodine (8.0-day I^{131}, 21-hr I^{133}, 52.5-min I^{134}, *and* 6.7-hr I^{135})

Iodine and tellurium activities were removed from the curium solution to start the growth period. The curium solution was made just basic with NaOH and a known amount of I^- carrier added. After a growth period of 20.33 hr the solution was acidified to dissolve the $Cm(OH)_3$ and any incorporated fission-produced elements, made basic, and boiled to remove H_2O_2. The basic hypochlorite procedure[30] was then employed for the isolation of radiochemically pure iodine activities.

Since the 21-hr I^{133} and 6.7-hr I^{135} decay to radioactive xenon daughters which complicate the analysis of the total iodine decay curve, it is customary to prepare an iodine stock solution from which aliquots are withdrawn periodically, the xenon activities boiled out, and the iodine activity determined. The total iodine activity available in the present investigation was insufficient for the application of this technique. Therefore, after the initial decay of the 52.5-min I^{134}, the iodine sample (as AgI) was periodically dissolved with KCN, the xenon activities boiled out, and the iodine remounted as AgI for counting. In this way it was possible to obtain from a single sample a total iodine decay curve which could be analyzed for the various iodine isotopes. The activity contributed by 2.4-hr I^{132} formed directly in fission and from 77-hr Te^{132} was taken into account. The observed 8.0-day I^{131} activity was corrected for the fraction (about 20 percent) produced from 30-hr Te^{131m} during the iodine growth period to obtain the fission yield of I^{131} formed independently of the 30-hr Te^{131m}.

Cesium (13.7-day Cs^{136})

The separation of cesium activities from the curium solution in preparation for the growth period was accomplished by $Cm(OH)_3$ precipitation from hot NaOH solution. After a period of 14 days $Cm(OH)_3$ was again precipitated to end the growth. Cesium was purified[31] by a silicotungstic acid precipitation, several perchlorate precipitations, exhaustive $Fe(OH)_3$ removals, and finally isolated as $CsClO_4$ for mounting and counting. Decay and absorption data indicated the presence of a single activity due to 13.7-day Cs^{136}. The absence of detectable 33-yr Cs^{137} activity is consistent with the growth period used.

[30] Glendenin, Metcalf, Novey, and Coryell, reference 20, Papers 278 and 279.

[31] L. E. Glendenin and C. M. Nelson, reference 20, Paper 283.

Barium (85-min Ba^{139} *and* 12.8-day Ba^{140})

Precipitations of $Ba(NO_3)_2$ with fuming HNO_3 were made to remove all barium activities from the curium solution. After growth periods of 17.5 hours and 65.5 hours, barium was again removed as nitrate and purified[32] by precipitations as $Ba(NO_3)_2$ and $BaCl_2$, removals of $Fe(OH)_3$, and isolation as $BaCO_3$ for mounting and counting. The last $Fe(OH)_3$ removal established zero time for the growth of La^{140}.

Since sufficient time was allowed for decay of the short-lived species prior to the final isolation of barium, the only significant activities observed were 85-min Ba^{139}, 12.8-day Ba^{140}, and 40-hr La^{140}. These were determined by analyses of decay curves.

Cerium

An attempt to determine the yields of cerium fission products was unsuccessful due to major contamination by 282-day Ce^{144} produced during the pile irradiation and incompletely separated from the curium. Time was not available for the necessary purification of curium from the rare earths.

III. RESULTS AND DISCUSSION

The fission yield of a nuclide may be defined as the percentage of fissions which lead to its formation. Thus,

$$Y_N = (D_N/F)100, \qquad (1)$$

where Y_N is the fission yield of nuclide N, D_N is its saturation disintegration rate (equal to the rate of formation), and F is the fission rate. In the case of induced fission, F is usually determined by fission counting during the irradiation. Alternatively, an arbitrary value may be assumed for the yield of a particular nuclide, others determined relative to it, and the sum of all fission yields then normalized to 200 percent. In the present investigation, the alpha-to-fission ratios for Cm^{242} and Cm^{244} are known[33] and F is readily obtained from an accurate alpha assay of the source. Appropriate corrections applied to the observed beta counting rates give D_N and hence, absolute fission yields.

The results of the determination of the yields of 21 nuclides produced in the spontaneous fission of Cm^{242} are presented in Table II, column 2, and plotted (circles) against mass number in Fig. 1. The estimates of reliability given in the table are based on the relative complexity of the absorption and decay data, the difficulty of calculating beta disintegration rates from observed counting rates, and the number of determinations. Since the limitations of time prevented replicate determinations in all but a few cases (Mo^{99}, Ru^{105}, Ba^{139}, and Ba^{140}), the estimated errors have been increased substantially over those normally accepted as representative of the radiochemical method. In determining

[32] L. E. Glendenin, reference 20, Papers 236 and 288.

[33] Hollander, Perlman, and Seaborg, *Table of Isotopes*, Revs. Modern Phys. **25**, 469 (1953).

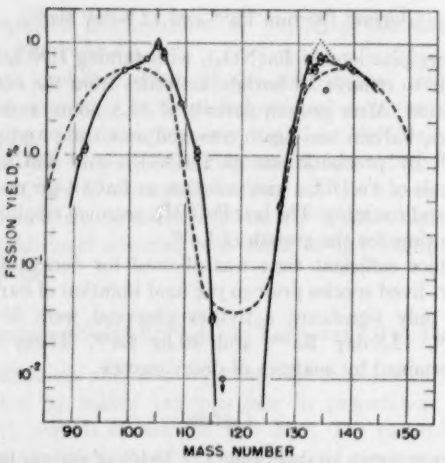

FIG. 1. Yield-mass curves for spontaneous fission of Cm^{242} (solid line) and pile-neutron induced fission of Pu^{239} (dashed line). Circles represent observed yields and triangles estimated total chain yields. The dotted line is the predicted shape of the heavy group. (See discussion of Table IV.)

the total fission yield of a chain of given mass number, an attempt is usually made to choose for analysis a member of the chain near stability where any independent formation of nuclides beyond that member would be negligible. This was not always feasible in the present investigation, and it was therefore necessary in a number of cases to calculate these expected independent yields to obtain total chain yields. The calculated independent yields are given in column 3 of Table II and are based on the charge distribution postulate of equal charge displacement from stability[8,9,34] for complementary products, and a value of 3.0 for the average number of neutrons emitted per fission (see discussion below and Table III). Total chain yields (plotted as triangles in Fig. 1) are given in column 4 with the estimated reliabilities increased somewhat from those of column 2 to reflect the uncertainty in the calculated independent yields.

A few of the values in Table II deserve special comment—namely, Cd^{115m}, Cd^{117}, Te^{131m}, I^{131}, and Cs^{136}. In the cadmium determination the sample contained about 30 counts per minute of an activity with the growth and decay characteristics of the chain 53-hr $Cd^{115}\rightarrow$4.5-hr In^{115m} and a few counts per minute of an unidentified long-lived component. Since the latter may have been due in part to contamination and was in too low an intensity to be adequately characterized, no fission yield determination for 43-day Cd^{115m} was attempted. An assumed value of 0.003 percent is listed in Table II based on a fission yield ratio of 43-day Cd^{115m} to 53-hr Cd^{115} of about 10 percent as has been observed in pile neutron fission[35,36] of U^{233}, U^{235}, and Pu^{239} as well as in 14-Mev neutron fission[36] of U^{235}. Although no activity attributable to the chain 3.0-hr $Cd^{117m}\rightarrow$50-min $Cd^{117}\rightarrow$2-hr In^{117}, was observed in the decay curve, an estimate of the maximum activity which could have escaped detection (10 counts per minute) was used to set an upper limit of 0.01 percent for the fission yield of Cd^{117m}.

The observed yield of 30-hr Te^{131m} represents about one-half of the total chain yield—the remainder presumably proceeding through the isomeric ground state (25-min Te^{131}) to 8.0-day I^{131}. It is interesting to note that an analysis of the expected yields of primary fission products in this region (Table III) predicts a value for mass 131 at tellurium (2.2 percent) close to that observed for Te^{131m} (2.3±0.5 percent). This is also true in the case of slow neutron fission of U^{235}.[9,34] These data may be interpreted as indicating a very small branch in the decay of 23-min Sb^{131} to 30-hr Te^{131m} (not inconsistent with observation[9,37]) and the apparently exclusive formation of the excited state as a primary fission product. The spins of Te^{131m} and Te^{131} are 11/2 and 3/2, respectively, and the favored formation of the higher spin state is in accord with the observations of Biller[38] on the yields of primary products of bismuth fission. It was found that the higher spin state of isomeric pairs was always formed in higher yield, often to the apparent exclusion of the lower spin state. Levy[39] studied this phenomenon further and proposed a reasonable mechanism based on the preferred formation of higher spin states at high excitation and the tendency toward only small spin changes during de-excitation.

The nuclide Cs^{136} is "shielded" by stable Xe^{136} from formation through beta decay so that the observed fission yield is only that fraction of the total chain yield formed directly in fission at Cs^{136}. Such independent yields have been utilized in developing an empirical hypothesis for the distribution of nuclear charge in fission[34] consistent with observations in slow neutron-induced fission of U^{235} and Pu^{239} and also apparently applicable[40] to 14-Mev neutron-induced fission of U^{235}. This hypothesis may be applied to the spontaneous fission of Cm^{242} to estimate the value of $\bar{\nu}$, the average number of neutrons emitted per fission, in the following manner. The observed yield for Cs^{136} (0.8±0.12 percent) represents 11±2 percent of the assumed total chain yield (7.0±1.0 percent). From the charge distribution curve[34] this value corresponds to a $Z-Z_p$ difference of 1.5, or a value of 53.5±0.1 for Z_p, the most probable charge of the primary fission product of

[34] Glendenin, Coryell, and Edwards, reference 20, Paper 52.
[35] Reference 20, Appendix *B*.
[36] A. C. Wahl and N. A. Bonner, Phys. Rev. **85**, 570 (1952).
[37] G. B. Cook, Atomic Energy Research Establishment (Harwell, England) Report AERE-C/R-729, June, 1951 (unpublished).
[38] W. F. Biller, University of California Radiation Laboratory Report UCRL-2067, January, 1953 (unpublished).
[39] H. G. Levy, University of California Radiation Laboratory Report UCRL-2305, August, 1953 (unpublished).
[40] G. P. Ford, U. S. Atomic Energy Commission Document AECD-3597, November, 1953 (unpublished).

mass 136. By definition,[34]

$$Z_P = Z_A - \tfrac{1}{2}(Z_A + Z_{A^*} - Z_F), \quad (2)$$

where Z_A is the most stable charge for mass A, Z_F is the charge of the fissioning nucleus, and Z_{A^*} is the most stable charge for the complementary mass A^*; and

$$A^* = A_F - A - \bar{\nu}, \quad (3)$$

where A_F is mass number of the fissioning nucleus. Using a value[34] of 56.2 for Z_A at mass 136, Eq. (2) gives 45.2±0.2 for Z_{A^*}, corresponding to 103.0±0.5 for A^*, and a value of 3.0±0.5 for $\bar{\nu}$ from Eq. (3). This is in good agreement with a recently reported value of 3.0±0.4 determined by direct measurement[41] and lends support to the application of the charge distribution hypothesis to spontaneous fission. A value for ν may also be obtained from the difference in mass of the fissioning nucleus and the sum of complementary masses. From Fig. 1 it may be seen that the value of ν in the mass region near symmetry is smaller than $\bar{\nu}$, as has also been observed in the case of neutron-induced fission of U^{235}.[42] The above calculations may be reversed to obtain independent yields. Such calculations were made, using $\bar{\nu}=3.0$, to estimate the independent yields of nuclides of a chain beyond the member chosen for analysis (Table II, column 3).

A comparison of the yield-mass curves for spontaneous fission of Cm^{242} and pile neutron-induced fission of Pu^{239} is presented in Fig. 1. Spontaneous fission of Cm^{242} is seen to be asymmetric, but with somewhat higher and narrower peaks. Although the amount of Cm^{242} available was not sufficient to produce a measurable activity of fission products in the region of symmetrical fission (mass numbers 116–124), the upper limit set at mass 117 indicates a peak-to-trough ratio at least as large as that observed in the thermal-neutron-induced fission of U^{235} (about 680), and perhaps considerably larger. A decrease in the peak-to-trough ratio and a broadening of the mass distribution have been observed with increasing energy of excitation in induced fission,[43] and therefore it is to be expected that spontaneous fission (no excitation) would exhibit a larger peak-to-trough ratio and a narrower mass distribution. It has also been observed that the light group distribution shifts toward higher masses with increasing mass of the fissioning nucleus while the heavy group remains relatively constant, with perhaps a slight shift in the direction of smaller masses.[44] It is seen that this trend continues with Cm^{242}, the heaviest nuclide for which fission yields have been determined.

An interesting feature of the yield-mass curve for spontaneous fission of Cm^{242} is the occurrence of pronounced fine structure as indicated by the abnormally high yields in the regions around masses 105 and 134. This phenomenon appears to be associated with a nuclear structure preference in fission for fragments containing 82 neutrons[5,6] and excessive evaporation from primary fission fragments of the neutrons with abnormally low binding energy just outside closed shells.[8,9] The effect was first observed in mass spectrometric investigations[4,6] and subsequently in radiochemical studies of U^{235} fission,[7,9,45] although it was not apparent in the earlier radiochemical studies of U^{235} or Pu^{239} fission.[46]

A comparison of the yield-mass curves for spontaneous fission of Cm^{242} and U^{238} is given in Fig. 2. The data for U^{238} are the relative yields of the stable krypton and xenon isotopes produced by spontaneous fission of U^{238} in uranium minerals.[15] A dashed curve has been drawn through the data assuming symmetrical reflection about mass 118 (i.e., two neutron emitted per fission) and normalized to 200 percent yield summation. Although the region of symmetrical fission was not investigated, the upper limit at mass 129 again indicates a large peak-to-trough ratio for spontaneous fission. The apparently high yield at mass 132 also indicates fine structure in the mass region of the 82 neutron shell.[14,15] Similar results[15] were obtained for the krypton and xenon yields from spontaneous fission of Th^{232}.

The mass distribution of the light group in the spontaneous fission of Cm^{242} is plotted in Fig. 3 with that for pile neutron-induced fission of U^{235} [6,42] shown for com-

TABLE II. Fission yields in spontaneous fission of Cm^{242}.

Nuclide	Observed fission yield (%)	Calculated independent fission yield of daughter (%)	Total fission yield of chain (%)
9.7-hr Sr^{91}	0.94 ±0.3	0.01	0.95 ±0.3
2.7-hr Sr^{92}	1.1 ±0.3	0.1	1.2 ±0.3
67 -hr Mo^{99}	5.7 ±0.7	0	5.7 ±0.7
40 -day Ru^{103}	7.2 ±1.5	0	7.2 ±1.5
4.5-hr Ru^{105}	9.5 ±0.9	0.4	9.9 ±1.0
1.0-yr Ru^{106}	7.4 ±0.8	1.0	8.4 ±1.0
13.1-hr Pd^{109}	2.9 ±0.4	0	2.9 ±0.4
21 -hr Pd^{112}	0.95 ±0.15	0.15	1.1 ±0.2
53 -hr Cd^{115}	0.033±0.01	0	
43 -day Cd^{115m}	(0.003)[a]	0	0.036±0.01
3.0-hr Cd^{117m}	<0.01	0	<0.01
93 -hr Sb^{127}	0.35 ±0.1	0.02	0.37 ±0.1
4.2-hr Sb^{129}	1.3 ±0.3	0.4	1.7 ±0.4
30 -hr Te^{131m}	2.3 ±0.5	...	
8.0-day I^{131}	2.0 ±0.4[b]	0	4.3 ±0.7
77 -hr Te^{132}	5.8 ±0.9	1.6	7.4 ±1.3
21 -hr I^{133}	5.7 ±0.8	0.3	6.0 ±0.9
52.5-min I^{134}	6.9 ±1.0	1.1	8.0 ±1.3
6.7-hr I^{135}	3.9 ±0.6	3.4	7.3 ±1.4
13.7-day Cs^{136}	0.80 ±0.12	...	...
85 -min Ba^{139}	6.6 ±0.7	0	6.6 ±0.7
12.8-day Ba^{140}	5.9 ±0.8	0	5.9 ±0.8

[a] Assumed yield from known branching ratio in induced fission.
[b] Yield independent of 30-hr Te^{131m}.

[41] F. R. Barclay and W. J. Whitehouse, Proc. Phys. Soc. (London) A41, 447 (1953).
[42] Glendenin, Steinberg, Hayden, Inghram, and Flynn (to be published).
[43] See, e.g., Turkevich, Niday, and Tompkins, Phys. Rev. 89, 552 (1953), for discussion and references.
[44] E. P. Steinberg and M. S. Freedman, reference 20, Paper 219.
[45] Yaffe, Day, and Greer, Can. J. Chem. 31, 48 (1953).
[46] Reference 20, pp. 537–542.

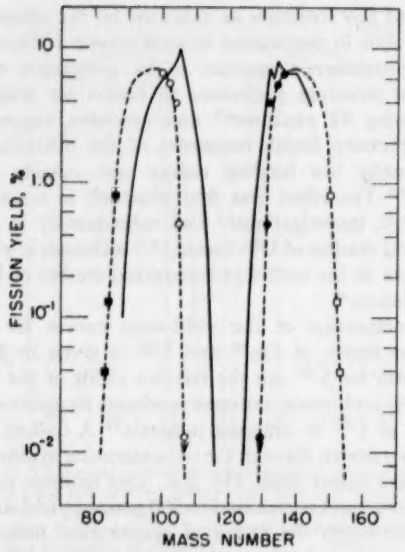

FIG. 2. Yield-mass curves for spontaneous fission of Cm^{242} (solid line) and U^{235} (dashed line). Solid squares and circles represent data for krypton and xenon isotopes, respectively; open squares and circles represent mirror points ($\nu=2$).

parison. Fine structure is seen to occur around mass 100 in the U^{235} curve and mass 105 in the case of Cm^{242}. The fact that these mass numbers are complementary in both cases to the mass region of the primary heavy fission products which contain 82 neutrons (about mass 134) and that there are no important nuclear shell closures in the mass region of the light group peaks are considered as evidence that the fine structure observed in the light group represents the effect of preference for an 82-neutron configuration in the fission act itself. The effect is seen to be more prominent in the case of Cm^{242} than in U^{235} indicating that the nuclear structure preference in fission may diminish with increasing excitation energy of the fissioning nucleus. It is reasonable that this selectivity in the fission process would diminish with increasing excitation energy as has been suggested by Wiles.[5]

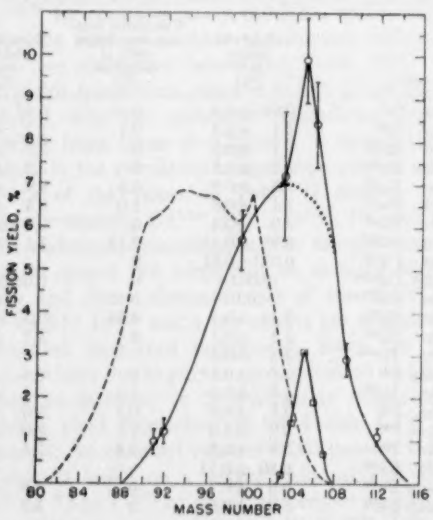

FIG. 3. Fission yields of the light groups in spontaneous fission of Cm^{242} (circles and solid line) and pile-neutron induced fission of U^{235} (dashed line). The dotted line (representing a hypothetical "smooth" yield curve) has been subtracted from the solid line to give the distribution of "excess" yields plotted as squares.

A hypothetical "smooth" curve (dotted line in Fig. 3) has been subtracted from the solid curve of Fig. 3 to give approximate "excess" yields (plotted as squares) due to the 82-neutron shell preference in the spontaneous fission of Cm^{242}. If it is assumed that for these fission modes the heavy fragment containing 82 neutrons emits one prompt neutron and its complement emits two (total $\nu=3$), it is possible to determine the identity of the primary fission products occurring in excess yield as presented in Table IV. The complementary fragments (before neutron emission) are given in columns 2 and 3, and the corresponding products (after neutron emission) in columns 1 and 4. The excess yields of these products obtained from Fig. 3 are listed in column 5. According to this analysis the excess yields due to the 82-neutron preference effect in fission amount to about 7 percent. A summation of the fission yields represented by the solid line in Fig. 3 gives 103 percent, in excellent agreement with the theoretical value of 100 percent.

A complete analysis of the distribution of fission yields in the 82-neutron shell region (mass numbers 131–141) is presented in Table III. The independent yields (by direct formation) of fission products along the chains have been calculated using assumed "smooth" chain yields complementary (with $\nu=3$) to those of the light group (dotted line of Fig. 3) and the charge distribution based on equal charge displacement. These yields represent what might be considered as the "normal" distribution in fission in the absence of perturbations due to the closed shell of 82 neutrons. The excess yields (from Table IV) are given in parentheses at their respective chain positions and may be seen to approximate closely the corresponding "normal" yields in distribution and magnitude. It seems reasonable to interpret these parallel distributions as indicative of a fundamental charge distribution in fission for all modes with a superposed selectivity for an 82-neutron configuration.[47] The arrows in Table III represent the extra evaporation from primary fission fragments of the 83rd ($S+1$), 85th ($S+3$), and 87th ($S+5$) neutrons, i.e., the odd neutrons having abnormally low binding energies[9] due to their location just outside a closed shell.

The data in Table III may be used to calculate expected cumulative yields at any chain member as well

[47] This conclusion has been used as an assumption by D. R. Wiles in an independent and somewhat similar treatment of fine structure in induced fission of U^{235} and U^{238}. (See reference 7.)

TABLE III. Analysis of fission yields in the 82-neutron shell region.[a]

Mass No.	Z_p	Independent fission yield in chain (%) $_{50}$Sn	$_{51}$Sb	$_{52}$Te	$_{53}$I	$_{54}$Xe	$_{55}$Cs	$_{56}$Ba	$_{57}$La	$_{58}$Ce	"Smooth" chain yield (%)	Nuclide determined	Calculated yield (%)	Observed yield (%)
131	51.6	0.4	2.0	2.2	0.7						5.3	Te^{131m}	2.2	2.3 ±0.5
			(0.7)									I^{131}	3.1[b]	2.0 ±0.4[b]
132	52.0	0.06	1.5	3.0	1.5	0.06					6.1	Te^{132}	5.3	5.8 ±0.9
		↑S+1		(1.9)										
133	52.3	0.01	1.1	2.9	2.2	0.3					6.5	I^{133}	8.5	5.7 ±0.8
			↑S+1		(3.1)									
134	52.7		0.4	2.2	3.0	1.1	0.01				6.7	I^{134}	9.8	6.9 ±1.0
				↑S+1		(1.4)								
135	53.1		0.05	1.5	3.3	1.9	0.1				6.9	I^{135}	6.1	3.9 ±0.6
					↑S+1		(0.2)							
136	53.5			0.7	2.8	2.8	0.7				7.0	Cs^{136}	0.9	0.80±0.12
				↑S+3		↑S+1								
137	53.9			0.1	1.9	3.3	1.5	0.05			6.9	—	6.8[c]	—
					↑S+3		↑S+1							
138	54.3			0.01	1.1	2.9	2.2	0.4			6.6	—	6.5[c]	—
						↑S+3		↑S+1						
139	54.7				0.4	2.2	2.8	1.0	0.01		6.4	Ba^{139}	6.2	6.6 ±0.7
							↑S+3		↑S+1					
140	55.2				0.02	1.2	2.8	1.8	0.2		6.0	Ba^{140}	5.7	5.9 ±0.8
						↑S+5		↑S+3		↑S+1				
141	55.6					0.4	2.1	2.3	0.7	<0.01	5.5	—	—	—

[a] Parentheses denote excess yields due to 82-neutron shell preference in fission. Vertical arrows indicate yield branching by extra neutron emission from fragments containing 83(S+1), 85(S+3), and 87(S+5) neutrons.
[b] Yield of I^{131} independent of 30-hr Te^{131m}.
[c] Total chain yield.

as total chain yields by summation of the appropriate independent yields (both "normal" and "excess"), taking into account the losses and gains in yield indicated by the arrows. Good agreement between yields calculated in this manner and those observed for the nuclides indicated is apparent in the last two columns of the table, except for the yields of the iodine isotopes. The fact that the observed yields of the latter are all about 67 percent of the calculated values may be significant. Difficulties in exchange between carrier- and fission-produced species of iodine are well known,[30] and it is possible that the presence of H_2O_2 or other decomposition products from the action of the intense alpha radioactivity in the curium solution may have interfered with the achievement of complete interchange. Until this point can be clarified by further study of the iodine chemistry in such solutions or by the determination of the cumulative yields at the xenon isotopes, the calculated total chain yields for mass numbers 133–136 have been used to predict the shape of the fine structure in the heavy group (dotted line in Fig. 1).

Further experiments on spontaneous fission are planned using larger sources of Cm^{242} and Cm^{244}. In particular, it would be desirable to extend the study of charge distribution (by determination of independent yields along chains and yields of shielded nuclides) and of mass distribution in the regions of the trough, fine structure, and the rare earth elements.

TABLE IV. Distribution of "excess" yields due to 82-neutron shell preference in fission.

Light product	Light fragment	Heavy fragment (82 neutrons)	Heavy product	Approximate "excess" yield (%)
$_{41}Nb^{103}$	$_{41}Nb^{105}$	$_{55}Cs^{137}$	$_{55}Cs^{136}$	0.2
$_{42}Mo^{104}$	$_{42}Mo^{106}$	$_{54}Xe^{136}$	$_{54}Xe^{135}$	1.4
$_{43}Tc^{105}$	$_{43}Tc^{107}$	$_{53}I^{135}$	$_{53}I^{134}$	3.1
$_{44}Ru^{106}$	$_{44}Ru^{108}$	$_{52}Te^{134}$	$_{52}Te^{133}$	1.9
$_{45}Rh^{107}$	$_{45}Rh^{109}$	$_{51}Sb^{133}$	$_{51}Sb^{132}$	0.7
$_{46}Pd^{108}$	$_{46}Pd^{110}$	$_{50}Sn^{132}$	$_{50}Sn^{131}$	...

We wish to express our appreciation to Professor G. T. Seaborg and Professor I. Perlman and the staff of the Nuclear Chemistry Group at the University of California Radiation Laboratory for their interest and hospitality during the course of this work. In particular, we wish to thank Dr. S. G. Thompson for his generous cooperation and advice and N. Garden and members of the Health Chemistry Group for their help in providing facilities for handling the intense source of alpha radiation. We are also grateful to Dr. M. Kalkstein and A. E. Larsh, Jr., for the construction and maintenance of the counting equipment and to Dr. E. K. Hulet for his kind help and cooperation.

Gamma Radiation from Reactions Induced by Polarized Particles

J. M. KENNEDY AND W. T. SHARP
Atomic Energy of Canada Limited, Chalk River, Ontario, Canada
(Received March 25, 1954)

The formulas of Simon which involve gamma radiation have been simplified by carrying out sums over parameters that do not represent observed properties of the radiation.

GENERAL expressions for the tensor moments of radiation emitted from a reaction in terms of the tensor moments of the incoming radiation have been given by Simon.[1] When one of the radiations is electromagnetic, these formulas involve explicit sums over the unobserved "orbital angular momentum" l of the γ ray. In this note it is indicated how these sums can be eliminated; the resulting formulas are more convenient for applications.

The particular sum that arises is

$$E_\kappa(L_1p_1,L_2p_2;\ Lq)=\sum_{l_1,l_2} i^{l_1-l_2}\delta(l_1p_1)\delta(l_2p_2)\times(L_11-11|l_10)(L_21-11|l_20)\times G_\kappa(L_1l_11;\ L\ \ q;\ L_2l_21).$$

Here, p_i, the "intrinsic parity" of the radiation, is 0 for magnetic radiation and 1 for electric, and $\delta(l_i,p_i)$ is 0 or 1 according as $L_i+l_i+p_i$ is odd or even. G_κ is the coefficient defined by Simon;[1] it is essentially a sum over products of an X coefficient[2] and two Clebsch-Gordan coefficients. By using the identity:

$$(L1-11|l0)\delta(l,p)=\tfrac{1}{2}[(L1-11|l0)-(-1)^p(L11-1|l0)],$$

the sum over l_1 and l_2 may be carried out by recoupling the Clebsch-Gordan coefficients and using the orthogonality of the X coefficients

$$\sum_{g,h}(2g+1)(2h+1)X\begin{pmatrix}a&b&c\\d&e&f\\g&h&i\end{pmatrix}X\begin{pmatrix}a&b&c'\\d&e&f'\\g&h&i\end{pmatrix}=\delta_{cc'}\delta_{ff'}[(2c+1)(2f+1)]^{-1}.$$

The result is

$$E_0=\tfrac{3}{4}(-1)^{L_1+1}[(2L_1+1)(2L_2+1)]^{\frac{1}{2}}(11-11|q0)\times(L_1L_21-1|L0)[1+(-1)^{L_1+L_2+p_1+p_2+q+L}],$$

$$E_{\pm1}=0,$$

$$E_2=\tfrac{3}{4}(-1)^{L_1+p_2}[(2L_1+1)(2L_2+1)]^{\frac{1}{2}}(L_1L_211|L2)\delta_{q2}=(-1)^{L_1+L_2+p_1+p_2+L}E_{-2}.$$

E_κ appears in the various formulas for reactions involving incoming or outgoing γ rays in Sec. 6 of reference 1. For example, Eq. (6.4) for the tensor moments of an outgoing γ ray from a reaction induced by a particle can be written

$$T_{\kappa'q'}\sim\sum i^{L_2'-L_1'}(-1)^{J_2+s_2+L_1'+q'-L+i-I-I'+\kappa'}\times R^*(\alpha l_1s_1,\alpha'L_1'p_1';\ J_1\pi_1)R(\alpha l_2s_2,\alpha'L_2'p_2';\ J_2\pi_2)\times W(is_1is_2;\ Iq)W(J_1L_1'J_2L_2';\ I'L)\times[(2J_1+1)(2J_2+1)]^{\frac{1}{2}}D_{\kappa\kappa'}{}^{(L)}(\phi,\theta,0)T_{\kappa q}\times G_\kappa{}^*(J_1l_1s_1;\ L\ \ q;\ J_2l_2s_2)E_{\kappa'}(L_1'p_1',L_2'p_2';\ Lq'),$$

where the normalizing factors outside the summation sign have been omitted for brevity. The special case of angular distributions from unpolarized incident beams may be obtained by setting $q=\kappa=q'=\kappa'=0$. The result for an incoming particle and outgoing γ ray is

$$T_0{}^0\sim\sum\tfrac{1}{2}\sqrt{3}(2i+1)^{-\frac{1}{2}}i^{L_2'-L_1'+L}(-1)^{s-I'+1}\times R^*(\alpha l_1s,\alpha'L_1'p_1';\ J_1\pi_1)R(\alpha l_2s,\alpha'L_2'p_2';\ J_2\pi_2)\times Z(l_1J_1l_2J_2;\ sL)P_L(\cos\theta)\{W(L_1'J_1L_2'J_2;\ I'L)\times(L_1'L_2'1-1|L0)[(2J_1+1)(2J_2+1)(2L_1'+1)\times(2L_2'+1)]^{\frac{1}{2}}\},$$

where the sum is over those L for which $L_1'+L_2'+p_1'+p_2'+L$ is even. This result is in accord with the results of other authors.[3] The quantity in braces is, apart from sign, the tabulated coefficient $Z_1(L_1'J_1L_2'J_2;\ I'L)$.[4]

[1] A. Simon, Phys. Rev. **92**, 1050 (1953).
[2] A. Simon and T. A. Welton, Phys. Rev. **90**, 1036 (1953); U. Fano, National Bureau of Standards Report 1214 (unpublished); tables of X coefficients for limited values of the parameters have been prepared by the present authors and are included in Chalk River Report AECL 97.
[3] G. Racah, Phys. Rev. **84**, 910 (1951); L. C. Biedenharn and M. E. Rose, Revs. Modern Phys. **25**, 729 (1953).
[4] Sharp, Kennedy, Sears, and Hoyle, Chalk River Report AECL 97 (unpublished).

Stopping Power of Organic Foils for 6 Mev Alphas*

JOHN PHELPS, W. F. HUEBNER, AND FRANKLIN HUTCHINSON
Sloane Physics Laboratory, Yale University, New Haven, Connecticut
(Received March 2, 1954)

The stopping power of several thin organic foils has been measured relative to air at 6 Mev. A simple cut-off method provided a direct comparison with air using natural alphas from ThC'. Mean atomic stopping powers relative to air are: polythene, 0.422; polyvinyl alcohol, 0.515; cellulose acetate, 0.617; regenerated cellulose, 0.597; Mylar, 0.627. Values are also given for the mg per cm² of each foil equivalent in stopping power to one cm of air. The experimental stopping powers are reproducible to within two percent and average about three percent below values calculated using the additive law and mean excitation potentials for H, C, N, and O taken from the literature.

INTRODUCTION

THE theory of the energy loss of heavy charged particles in matter has been developed by Bethe,[1] Bloch,[2] and others, and recently reviewed in detail.[3,4] A particle (in the energy region of a few Mev) passing through matter loses energy at a rate which is given by the familiar expression

$$-\frac{dE}{dx}=\frac{4\pi e^4 z^2}{mv^2}N\left[Z\ln\frac{2mv^2}{I}-C_K\right]. \quad (1)$$

The notation here is the usual one to be found in reference 1; I is the mean excitation potential which is characteristic of the absorber and C_K is a correction term which takes into account the decreased contribution of the K electrons in the stopping of slow particles.

It is customary to define the "stopping power" of a material as a quantity proportional to the rate at which a charged particle loses energy in traversing the material. In this experiment it has been found convenient to use a mean atomic stopping power relative to air, which is defined below. It was early determined by Bragg and others that the stopping power of a molecule was nearly equal to the sum of the stopping powers of the component atoms. This rule, known as Bragg's additive law for stopping powers, has generally been confirmed by later experiments, although the results are still somewhat conflicting in the case of some liquids, notably water.[5] It is to be expected that chemical binding effects will cause slight deviations from the strict additive rule. This has been verified experimentally at very high energies in the careful work of Thompson,[6] who found variations of about one percent.

The majority of stopping power measurements has been made on metal foils, which are easily prepared and which provide a convenient and reliable, although not especially accurate, means of measuring nuclear particle energies. In recent years, particularly since World War II, advances in applied chemistry have yielded a number of organic compounds in the form of thin foils. It seemed worth while to make a preliminary check of the additive law for several of these foils in the energy region of a few Mev, using a very simple experimental method of moderate accuracy. Two or three of these foils are now finding application in experimental nuclear physics, in some cases displacing aluminum or other metal foils. A secondary aim of the present investigation, therefore, was to obtain values of the stopping powers of the foils in a form convenient for experimentalists.

EXPERIMENTAL METHOD

The stopping power of the foils was determined by direct comparison with air, using a "cut-off" method. The essentials of the apparatus are shown in Fig. 1. The so-called thorium active deposit was collected on a small metal button to provide a convenient source of ThC' alphas of initial energy 8.78 Mev. The button was mounted at the top of the brass cylinder and directly over the window into the proportional counter below. O-ring seals allowed the air pressure inside the cylinder to be varied at will. The foils were mounted on a rotating platform suspended inside the cylinder by means of a control rod projecting through the top plate. The platform contained five identical holes so that four foils could be mounted at one time and the fifth hole left uncovered. An O-ring seal allowed the platform to be rotated, thus changing foils, and also raised and lowered without unsealing the cylinder. The distance from the source to the foils could be read directly from a scale mounted on the top plate. Alphas from the button travelled down the cylinder, through the foil if one was present, and through the window into the proportional counter. The distance from source to counter was 10 cm and the aperture into the counter was 1 cm in diameter. The thickness of the foils, in mg per cm,² was determined using a microbalance and

* Research supported in part by the U. S. Atomic Energy Commission.
[1] H. A. Bethe, Ann. Physik **5**, 325 (1930).
[2] F. Bloch, Z. Physik **81**, 363 (1933).
[3] H. Bethe and J. Ashkin, in *Experimental Nuclear Physics*, edited by E. Segrè (John Wiley and Sons, Inc., New York, 1953), Chap. 2. See this and reference 4 for earlier papers.
[4] S. K. Allison and S. D. Warshaw, Revs. Modern Phys. **25**, 779 (1953).
[5] See, for example, reference 4, p. 787.
[6] Theos Jardin Thompson, University of California Radiation Laboratory, Report UCRL-1910, 11 August 1952 (unpublished).

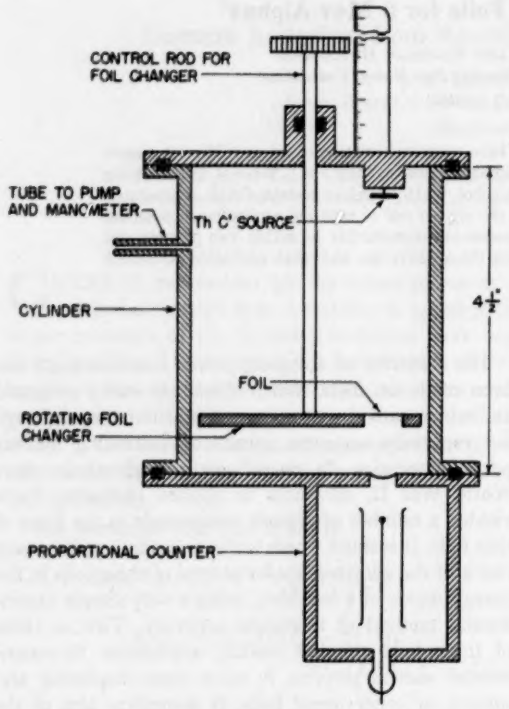

FIG. 1. Essentials of the apparatus.

samples of known area. Cut-off curves of counting rate as a function of pressure were made with and without foils in the path of the alphas, and the stopping power of the foils was computed from the displacement of the curves along the pressure axis.

A Mylar foil provided a satisfactory window for the proportional counter, which was filled with 15 cm of argon. The cylinder pressure was not allowed to drop below the counter pressure so that the window was always concave upwards. The source-foil distance was set at 8.0 cm for most of the runs, although some Mylar data were taken at 4.0 cm. An ordinary mercury manometer was used to read the cylinder pressure to within one mm. To prevent adsorption of water, the foils were kept in a vacuum desiccator when not in use. A liquid air trap was provided between the air inlet and cylinder to eliminate any effects of water vapor in the air. The temperature of the cylinder was held constant to plus or minus one degree C and was recorded separately for each run. In operation four of the five holes were usually covered with different weighed samples of the same foil.

A typical pair of cut-off curves is shown in Fig. 2. About 1000 counts were recorded for each point, and individual curves were repeated a number of times. The stopping power of a given foil was calculated from the change in the pressure needed to stop the alpha particle having the mean range. The pressure which just stopped this alpha was determined from the cut-off curves by two observers using different methods, with excellent agreement. The mean cut-off pressure was used, instead of the more common "extrapolated" pressure obtained by extrapolating the straight part of the cut-off curve to the axis, to avoid errors introduced by non-uniformities in the foils. The slopes of the cut-off curves with foils were only slightly less than the cut-off slopes without foils, showing that the foils used were quite uniform. Use of the extrapolated pressures would have decreased the measured stopping powers by less than one percent. Some data taken with polystyrene and nylon were rejected because of non-uniform foils and are not included here. The foil samples used, of polythene, polyvinyl alcohol, cellulose acetate, regenerated cellulose, and Mylar, were all approximately three cm in air equivalent. Similar samples of aluminum were used as a check on the apparatus and method.

CALCULATIONS

The mean atomic stopping power relative to air, used in this experiment, is defined by

$$s=\bar{B}/\bar{B}_{\text{air}}, \tag{2}$$

where, following the usual scheme,

$$B=Z\ln(2mv^2/I)-C_K \tag{3}$$

is the "stopping number." Values of I and C_K were taken from the literature and (3) was used to obtain B for carbon, nitrogen, oxygen, and argon. The slightly different treatment of hydrogen is discussed below. B was then averaged over all the atoms of each foil and over all the atoms of air to obtain the numerator and

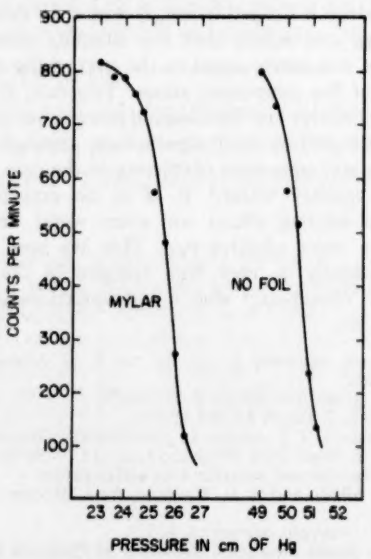

FIG. 2. Typical cut-off curves.

denominator of (2). Values of s so computed were then compared with the experimental values.

If Δp is the difference, in cm of Hg, in cut-off pressures with and without foils in the path of the particles, it is easily shown that the cm of air equivalent (for standard air at 76 cm and 15°C) of the foil is given by

$$\Delta x_0 = (288.2l\Delta p)/(76T), \tag{4}$$

where Δx_0 is the air equivalent of the foil, T the absolute temperature, and l the distance from source to counter window; l was measured to be 9.95±0.03 cm. If the values of Δx_0 obtained from (4) are divided into the thickness Δt of the foil in mg per cm², the quantity $\Delta t/\Delta x_0$ gives the mg per cm² which are equivalent in stopping power to one cm of air.

Experimentally, the mean atomic stopping power relative to air is given by

$$s = N_0\Delta x_0/N\Delta x, \tag{5}$$

where N is the number of atoms of all kinds per cm³ in the foil, N_0 the corresponding quantity for air, and Δx the linear path length in the foil which is equivalent in energy loss to Δx_0 cm of standard air. This definition of s follows from (2) and (1) if it is kept in mind that Δx and Δx_0 each correspond to the same energy decrement ΔE. Equation (5) also follows directly if s is simply interpreted as the average effectiveness of foil atoms relative to air atoms in slowing down the particle. If N' is the number of atoms of all kinds per gram in the foil and Δt the thickness of the foil in g per cm², (5) becomes

$$s = N_0\Delta x_0/N'\Delta t. \tag{6}$$

The number N' is easily computed from the known chemical composition of the foils, N_0 is known for standard air, and the measured values of $\Delta x_0/\Delta t$ are inserted in (6) to give the experimental stopping powers.

The values of I taken from Thompson's thesis[6] were adjudged to provide the most reliable calculated values of the stopping powers (see discussion below). The different types of binding were taken into account following Thompson's scheme. A question concerning the composition of the Mylar was settled by a chemical analysis. The values of $C_K(\eta,\theta)$ for carbon, nitrogen, and oxygen were taken from Walske's curves.[7] To find B for hydrogen, the expression

$$B_K = 2\ln\eta_K + 2.57861 - 2\eta_K^{-1} - (22/3)\eta_K^{-2} \tag{7}$$

TABLE I. Stopping powers of the elements.

Element	Position	$s=\bar{B}/\bar{B}_{air}$
H	saturated	0.204
H	unsaturated	0.211
C	saturated	0.857
C	unsaturated	0.864
N	molecular	0.974
O	molecular	1.075
O	−O−	1.072
O	O=	1.103

[7] M. C. Walske, Phys. Rev. **88**, 1283 (1952).

TABLE II. Stopping powers relative to air at 6 Mev.

Foil	Composition	Mg per cm² equivalent to one cm air	Experimental stopping power relative to air	Calculated stopping power relative to air	Percent deviation from calculated value
Polythene	CH_2	0.962	0.411	0.422	−2.6
Polyvinyl alcohol	C_2H_4O	1.06	0.501	0.515	−2.7
Cellulose acetate	$C_8H_{10}O_5$	1.12	0.607	0.617	−1.6
Regenerated cellulose	$C_6H_{10}O_5$	1.14	0.571	0.597	−4.4
Mylar	$C_{10}H_8O_4$	1.13	0.608	0.627	−3.0
Aluminum	Al	1.55	1.470	1.527[a]	−3.7

[a] Calculated assuming $I_{Al}=150$ ev.

given by Walske[7] for twice the stopping number of a hydrogen atom was equated (neglecting the last two terms) to twice the stopping number obtained using (3) (with $C_K=0$ for high energy) and Thompson's values. η_K is proportional to the particle energy, and this fixed the constant of proportionality. The η_K then evaluated for 5.9 Mev was inserted in the complete expression (7) to obtain B for hydrogen.

Since all of the foils used were approximately three cm in air equivalent and most of the runs were made with the foils mounted 8 cm from the source, the incident and emergent energies were nearly the same for all measurements at this distance, and the energy at the midpoint of the foils was 5.9±0.1 Mev. The stopping powers are specified for this energy. Moreover, since the mean atomic numbers of the foils do not differ greatly from that of air, the stopping power varies very slowly with energy. The results for the few runs made on Mylar at 4 cm from the source (midpoint alpha energy approximately 7 Mev) were corrected to 5.9 Mev.

RESULTS AND CONCLUSIONS

The values of s for H, C, N, and O calculated from Thompson's results are presented in Table I, which shows the influence of chemical binding according to Thompson's scheme. The experimental and calculated stopping powers of the foils are shown in Table II. The measured stopping powers are reproducible to less than two percent; this estimate of the experimental error does not take into account the possible existence of an undetected systematic error.

The uniformly low experimental results suggest the possibility of such a systematic error. Possible effects due to scattering and impurities in the air and foils were considered and rejected, as were also possible systematic errors in measurement of temperature, pressure, path length, and thickness of the foils. The disagreement among published stopping power values[8] for H, C, N, and O is somewhat greater than the disagreement between experimental and calculated results for the foils

[8] See, for example, S. Livingston and H. A. Bethe, Revs. Modern Phys. **9**, 264 (1937); L. H. Gray, Proc. Cambridge Phil. Soc. **40**, 72 (1944); J. O. Hirschfelder and J. L. Magee, Phys. Rev. **73**, 207 (1948).

in this experiment. It should be noted, however, that the earlier experiments yield, in general, still higher values for the stopping powers than are obtained from Thompson's I values and Eqs. (2) and (3). Some of these earlier results represent average values over the whole range of the particle rather than instantaneous values. The discrepancies in earlier results are the chief justification for the use of Thompson's accurate work as a standard of comparison in this experiment. It is of interest to note that if $I_{Al}=170$ ev, following the suggestion of Sachs and Richardson,[9] a calculated value of $s=1.47$ is obtained, in good agreement with the results of this experiment. The fact that we have used relative stopping powers, however, does not give any additional support to the hypothesis of an energy-dependent I.[10]

Grateful acknowledgment is made to E. I. du Pont de Nemours and Company for providing the foil samples used. The authors are indebted to Mr. Edgar Hubbard for assistance with the calculations, and to Mr. Shaler Knowles for help in construction of the apparatus.

[9] D. C. Sachs and J. R. Richardson, Phys. Rev. **89**, 1163 (1953).

[10] See reference 4, p. 816.

PHYSICAL REVIEW VOLUME 95, NUMBER 2 JULY 15, 1954

Disintegration of K^{43}†

TORSTEN LINDQVIST* AND ALLAN C. G. MITCHELL
Physics Department, Indiana University, Bloomington, Indiana

(Received March 26, 1954)

The nuclear spectrum of K^{43} (22.0 hr) has been studied with the help of a magnetic lens spectrograph. K^{43} decays to Ca^{43}, emitting gamma rays having energies 0.369, 0.627, 0.219, 0.393, and 1.00 Mev, the last three being weak. Five beta-ray groups were found, of energies 1.839, 1.218, 0.927, 0.460, and 0.243 Mev with relative abundance of 1.6, 5.4, 83.1, 5.4, and 4.5 percent, respectively. A disintegration scheme is proposed. The K^{43} was prepared by the reaction $A^{40}(\alpha,p)K^{43}$.

I. INTRODUCTION

OVERSTREET, Jacobson, and Stout[1] were the first to report on K^{43}. They bombarded argon gas with 40-Mev alpha particles. The argon was allowed to flow slowly through a 20-foot long gas chamber, connected to the cyclotron. They reported a half-life of 22.4 hr, two beta groups of energies 0.25 and 0.81 Mev measured in a magnetic spectrograph with permanent field and also by an absorption method, and a gamma ray of energy 0.4 Mev, measured by absorption in lead. Since no detailed information exists on the disintegration scheme of this isotope, it was decided to make a study of its radiations in a nuclear spectrograph.

In addition, the spin of the ground state of Ca^{43} has been measured to be 7/2, and the shell model would predict a state of $d_{3/2}$ for the ground state of K^{43}. The experiments of Overstreet, Jacobson, and Stout have been taken to imply that the transition from K^{43} to the ground state of Ca^{43} is allowed while from the shell model one would expect a transition characterized by $\Delta j=\pm 2$, yes. These considerations furnish an additional reason for making the investigation.

II. PREPARATION OF SOURCES

The isotope K^{43} was prepared by the reaction $A^{40}(\alpha,p)K^{43}$. Argon gas from a commercial tank was put into a gas chamber of size 17 in.×4 in.×1½ in. Between the cyclotron tank and the gas chamber there was, in the first experiment, a 1-mil Al foil. The gas was bombarded by 22-Mev alpha particles in the Indiana University cyclotron. The major portion of the active potassium settled out on the walls of the chamber. Following the bombardment the chamber was washed with distilled water to give a solution of the active potassium. After the first run it was found that in addition to the 22-hr K^{43} there was also a small amount of the 12.4-hr K^{42}, obtained from the reaction $A^{40}(\alpha,pn)K^{42}$. In order to suppress this reaction, the beam was passed through two 2-mil copper foils, which reduced the beam energy by 4 to 5 Mev. Since the (α,pn) reaction decreases more rapidly with alpha-particle energy than does the (α,p) reaction, it was possible to suppress the K^{42} activity entirely with the result that only the 22-hr period was observed.

The chemical separation was carried out by the ion exchange column method.

The half-life was checked each time with a separate source and was found to be 22.0 hr.

III. THE GAMMA-RAY SPECTRUM

The gamma rays were investigated by measuring the distribution of photoelectrons from lead and

† Supported by the joint program of the U. S. Office of Naval Research and the U. S. Atomic Energy Commission.

* On leave from Physics Department, University of Uppsala, Uppsala, Sweden.

[1] Overstreet, Jacobson, and Stout, Phys. Rev. **75**, 231 (1949).

uranium radiators with the help of a magnetic lens spectrometer. The surface density of the lead radiator was 8 mg/cm² and that of the uranium radiator 90 mg/cm². Figure 1 shows the distribution of the photoelectrons from the uranium radiator. Photoelectron lines corresponding to five gamma energies were found and are shown in Table I. The energies for γ_2, γ_3, and γ_4 were determined from the experiments using the lead radiator. The K and L photolines were well resolved except for the L_3 which was partly hidden under the L_2. The energies for γ_1 and γ_5 were determined using the uranium radiator (see Fig. 1), where the K and L lines for γ_1 are easily seen while only the K line for γ_5 is seen. The decay of the lines was followed and was found to be 22 hr. The 1-Mev line, too weak to furnish more than a rough estimate of the half-life in the beta spectrometer, was followed in a scintillation spectrometer and was also found to be of the same half-life. The relative intensities were determined from

TABLE I. Gamma rays from K^{43}.

Notation	Energy, Mev	Relative intensities
γ_1	0.219±0.004	1
γ_2	0.369±0.003	67
γ_3	0.393±0.004	6
γ_4	0.627±0.006	100
γ_5	1.00 ±0.02	4

TABLE II. Beta-ray groups of K^{43}.

Group	E Mev	Relative abundance %	log(ft)	Spin and parity	Transition
I	1.839±0.030	1.6	10.00[a]	$\Delta j=\pm 2$, yes	First forbidden
II	1.218±0.025	5.4	7.36	$\Delta j=\pm 1,0$ yes	First forbidden
III	0.827±0.020	83.1	5.54	$\Delta j=\pm 1,0$ no	Allowed
IV	0.460±0.020	5.4	5.87	$\Delta j=\pm 1,0$ no	Allowed
V	0.243±0.030	4.5	4.94	$\Delta j=\pm 1,0$ no	Allowed

[a] Log$[(W_0^2-1)ft]$.

a run with the lead radiator using the photoelectron cross sections obtained from Gray's formula.[2]

IV. THE BETA-RAY SPECTRUM

In order to investigate the distribution in energy of the electrons a thin source was prepared by dissolving the potassium in distilled water and allowing a drop of this solution to evaporate onto a thin Zapon foil. The GM counter used in the lens spectrometer was fitted with a thin window of stretched Teflon having a cutoff at about 10 kev.

The electron distribution was analyzed by making a Fermi plot of the data. The results are shown in Fig. 2. The spectrum can be analyzed into five groups. The results obtained are shown in Table II. The beta group of highest energy, Group I, was found to have a forbidden shape. The Fermi plot for this group was corrected by the forbidden shape factor $S_n(W)$, corresponding to a transition in which $\Delta j=\pm 2$ and there is a change of parity,

$$S_n(W)=(W^2-1)+(W_0-W)^2=C_{IT}(W),$$

where W and W_0 are the energies and end-point energies, respectively. In addition the value of $\log[(W_0^2-1)ft]$ for this group was determined to be 10.0 from these experiments, which is just the value to be expected for this type of transition.

The decay was followed over the entire spectrum and was found to be 22 hr.

Internal conversion electrons were also looked for, but only the 0.627-Mev gamma ray showed a very weak line. The internal conversion coefficient for this

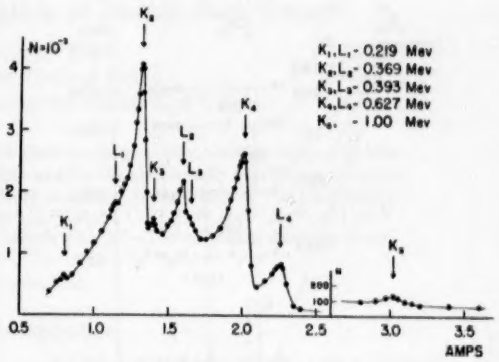

FIG. 1. Photoelectrons ejected by gamma rays of K^{43} from uranium radiator.

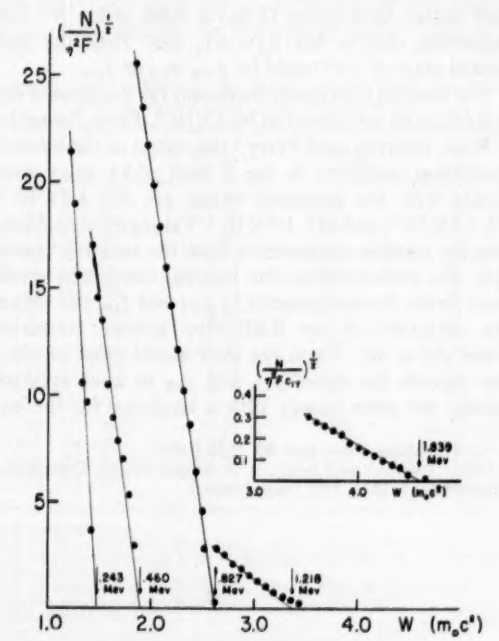

FIG. 2. Fermi plot of the beta rays of K^{43}.

[2] L. H. Gray, Proc. Cambridge Phil. Soc. **27**, 103 (1931).

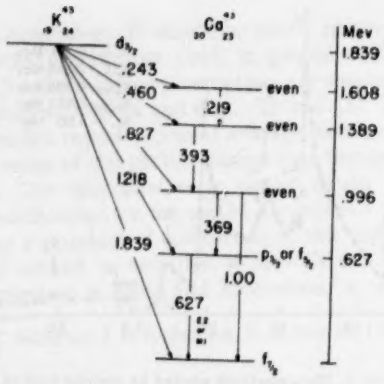

FIG. 3. Decay scheme of K^{43}.

gamma ray was estimated to be 2.10^{-4}, with a rather large error.

V. DISCUSSION

The decay scheme consists of five beta-ray groups together with five gamma rays which fit well into the scheme shown in Fig. 3. The highest energy beta-ray group shows a shape characteristic of a transition for which $\Delta j=\pm 2$, with a change of parity. Since the spin and magnetic moment of the ground state of Ca^{43} has been measured by Jeffries,[3] who gives a spin of 7/2 and a configuration $f_{7/2}$, the spin and parity of the ground state of K^{43} must be $\frac{3}{2}$ and even. Thus the experiments are in agreement with an assignment of $d_{3/2}$ to the ground state of K^{43}, as predicted by the shell model. Beta group II has a value of log $ft=7.36$ suggesting that it has $\Delta j=\pm 1$, yes. Thus the first excited state of Ca^{43} could be $p_{1/2}$, $p_{3/2}$ or $f_{5/2}$.

The internal conversion coefficient for the gamma ray at 0.627 Mev was found to be 2×10^{-4}. From the tables of Rose, Goertzel, and Perry,[4] the values of the internal conversion coefficient in the K shell which agree most closely with the measured values are $E1$, 1.0×10^{-4}; $E2$, 3.1×10^{-4}; and $M1$, 1.7×10^{-4}. Taking into consideration the possible assignments from the beta-ray transition, the evidence from the internal conversion coefficient limits the assignments to $p_{3/2}$ and $f_{5/2}$ and makes the character of the 0.627-Mev gamma transition either $E2$ or $M1$. From the shell model point of view, one expects the states $p_{3/2}$ and $f_{5/2}$ to have approximately the same energy with a tendency for the $p_{3/2}$ state to be lower. It thus seems reasonable to assign the configuration $p_{3/2}$ to the 0.627-Mev state and $E2$ to the 0.627-Mev line as a first preference.

The main beta-ray group (Group III) is allowed. From this information the only reasonable assignments to the state at 0.996 Mev are $d_{5/2}$ and $d_{3/2}$. The transitions to the higher states are also allowed so that these states should have even parity and spins of $\frac{1}{2}$, $\frac{3}{2}$, or 5/2. Since internal conversion coefficients were not measured it is impossible to assign definite configurations to these states.

The present experiments give a determination of the total disintegration energy, namely 1.839 Mev. Haxel, Jensen, and Suess[5] have given curves for the total disintegration energy of radioactive isotopes having the same isotopic number $I=N-Z$ plotted against neutron number. The disintegration energy for K^{43} determined in this experiment fits very nicely onto

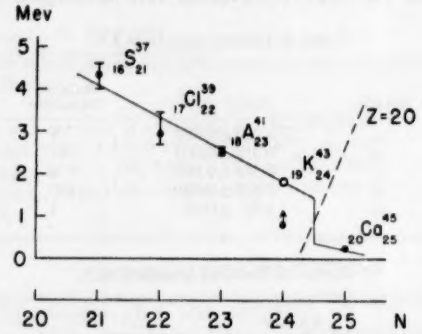

FIG. 4. Total disintegration energies in the neighborhood of $Z=20$. The solid circles and the curve are taken from Haxel, Jensen, and Suess (reference 5). The open circle is the present result for K^{43}.

the curve for S^{37}, Cl^{39}, A^{41}, K^{43}, Ca^{45}, all having $I=5$. This portion of the curve of Haxel, Jensen, and Suess is shown in Fig. 4. It will be noted that there is a sharp break in the disintegration energy curve at $Z=20$, in agreement with shell model predictions. The point for K^{43} used by Haxel, Jensen, and Suess, obtained from older data, is shown for reference.

The authors are indebted to Dr. M. B. Sampson and the cyclotron group for making the bombardments and to Mr. Arthur Lessor for making the chemical separation. One of us (T.L.) wishes to acknowledge a grant from the Swedish Atomic Committee and a fellowship from the Sweden-America Foundation.

[3] C. D. Jeffries, Phys. Rev. **90**, 1130 (1953).
[4] Rose, Goertzel, and Perry, U. S. Atomic Energy Commission Report ORNL 1023, 1951 (unpublished).
[5] Haxel, Jensen, and Suess, Ergeb. exakt. Naturwiss. **26**, 244 (1952).

Mass Differences for Isobars Capable of Double-Beta Decay*

JOHN T. MCCARTHY
Western Reserve University, Cleveland, Ohio

(Received December 2, 1953; revised manuscript received April 5, 1954)

A list has been prepared of nuclei with $A \leqslant 150$ for which there is a large energy available for double-beta decay. Mass differences were found from experimental data and by calculation with the Wigner formula. In no case is the energy for double-positron emission as large as 1 Mev. About 2 Mev or more is available for the emission of two negative electrons by Ca^{48}, Ge^{76}, Se^{82}, Zr^{96}, Mo^{100}, Cd^{116}, Sn^{124}, Te^{130}, Xe^{136}, and Nd^{150}. Calculations with the mass formula appear adequate for isobars with $\Delta Z=2$ when proper attention is paid to magic-number discontinuities.

A SYSTEMATIC search has been conducted for the nuclei of stable isobars which are most likely to exhibit the phenomenon of double-beta disintegration. One of the main factors upon which the probability of double-beta decay depends is the difference in mass between the initial and final isobaric atoms involved in the process. Therefore an attempt has been made to get an estimate of as many of these mass differences as possible from mass-spectrographic and disintegration-energy data. Also calculations have been made with the Wigner semiempirical mass formula. The results of these calculations agree rather well with the experimental data and are especially interesting and useful in the cases in which the data are conflicting or unavailable. For application to isobars this formula[1,2] contains a single parameter L whose numerical value is to be evaluated from experimental data for various regions of the periodic table.

Only seven pairs of stable isobars ($\Delta Z=2$) exist for atoms with $A \leqslant 58$. Calculations in this region were made with the numerical values of L obtained by Collins *et al.*[1] Good agreement is obtained between the calculated and experimental mass differences for the five pairs for which very good mass-spectrographic data are available. Unless the calculations for the other two pairs ($A=36$, 46) are terribly in error, it seems that in this region the double-beta process with the emission of two particles is energetically possible only for Ca^{48}.

For calculations at larger mass numbers the procedure was to select the isobaric atoms ($\Delta Z=2$) for which the mass differences can be calculated from experimental data with reasonable assurance. Both stable and unstable atoms were used. For each pair of isobars the value of L was calculated from the Wigner equation. The results are shown in Fig. 1, where the values of L are plotted against A. The large discontinuities, similar to those obtained by Collins *et al.*[1] and Halsted,[2] are associated with the "magic numbers" $N=50$ and $Z=50$ and are in agreement with other evidence for the existence of shells in the nucleus. The optimum values of L for the data represented by Fig. 1 are given by the equations

$$Z \geqslant 28 \text{ and } N \leqslant 50, \quad LA = 43.56 + 0.2194A,$$
$$Z \leqslant 50 \text{ and } N > 50, \quad LA = 61.08 + 0.2205A,$$
$$Z \geqslant 50 \text{ and } N < 82, \quad LA = 70.26.$$

The first two of these were found by applying the method of least squares and the third was found by taking a simple average of the nearly constant values of LA. Good results were obtained when mass differences for about 100 isobars ($\Delta Z=2$) were calculated by using the values of L found from these three equations. In the great majority of cases the calculated and experimental values for the mass differences agree within 0.2 or 0.3 mMU. Results are very poor only for a few pairs of unstable isobars, represented by crosses on the graph. As noted by Halsted,[2] the formula is not reliable for isobars with $\Delta Z=1$.

Experimental data are comparatively sparse and inaccurate for the isobars with $A>138$. Some calculations have been made but up to the present the results do not seem reliable. In this region Moch[3] predicted,

TABLE I. Mass differences for stable isobars which are most likely to exhibit double-beta disintegration.

A		ΔM_{calc} mMU	ΔM_{exp} mMU	Ref.
48	Ti−Ca	−4.50	−4.66	a
76	Se−Ge	−1.86	−2.5	b
78	Kr−Se	2.80	3.19	b
82	Kr−Se	−3.04	−2.7, −3.5	b, c
96	Mo−Zr	−4.12	−3.6	b
96	Ru−Mo	3.12	3.0	b
100	Ru−Mo	−2.48	...	
106	Cd−Pd	3.16	3.0	d
116	Sn−Cd	−2.96	−2.7	d
124	Te−Sn	−2.24	−2.1	d
124	Xe−Te	3.14	3.0	d
130	Xe−Te	−2.60	−3.5, −2.9	d, e
130	Ba−Xe	2.66	2.74	f
136	Ba−Xe	−2.76	...	
136	Ce−Ba	2.26	...	
150	Sm−Nd	...	−4.3	g

[a] See reference 1.
[b] B. G. Hogg and H. E. Duckworth, Can. J. Phys. **31**, 942 (1953).
[c] C. M. Huddleston and A. C. G. Mitchell, Phys. Rev. **88**, 1350 (1952).
[d] See reference 2.
[e] B. G. Hogg and H. E. Duckworth, Can. J. Phys. **30**, 628 (1952).
[f] Smith, Mitchell, and Caird, Phys. Rev. **87**, 454 (1952).
[g] See reference 4.

* Work supported by the National Science Foundation.

[1] Collins, Nier, and Johnson, Phys. Rev. **86**, 408 (1952).

[2] R. E. Halsted, Phys. Rev. **88**, 666 (1952).

[3] R. Moch, J. phys. radium **13**, 618 (1952).

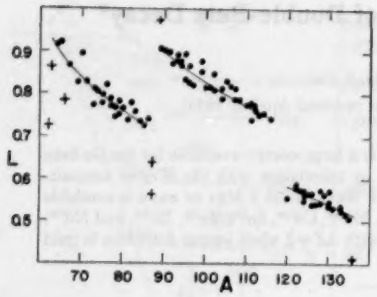

FIG. 1. Calculated values of the potential energy parameter L of the Wigner formula for isobars with $\Delta Z=2$. Crosses indicate anomalous results.

by means of semiempirical mass formulas, that the energy available for double-beta decay would be much smaller than in the lower regions. Hogg and Duckworth,[4] however, have recently found a large mass difference between Nd^{150} and Sm^{150}.

[4] B. G. Hogg and H. E. Duckworth, Can. J. Phys. **32**, 65 (1954).

Table I contains a summary of the stable isobars which have been found with mass differences greater that about 2 mMU (1.86 Mev). The agreement between calculated and experimental values is seen to be adequate for our purpose.[5] It is believed that this table is a reliable guide in the choice of elements for experimental study of possible double-beta activity. In Table I are found ten nuclei capable of emitting two negative electrons with a combined energy of about 2 Mev or more. Among the isobars for which no experimental information is available, calculations show that only Mo^{100} and Xe^{136} are good candidates for double-beta emission. Six nuclei have been found for which double-positron emission is energetically possible, as shown by the six positive values in the table. When the necessary four electron masses are subtracted from these values, it is seen that in all cases the two positrons would share an energy less than 1 Mev. This process would therefore have an extremely long half-life.

[5] *Note added in proof.*—The second, third, and fourth mass differences in the above table have been recently measured as -2.02, 2.81, and -3.18 mMU, respectively, by Collins, Johnson, and Nier in Phys. Rev. **94**, 398 (1954).

PHYSICAL REVIEW VOLUME 95, NUMBER 2 JULY 15, 1954

Interactions between Some Two-Nucleon Configurations*

MARTIN G. REDLICH†
Palmer Physical Laboratory, Princeton University, Princeton, New Jersey
(Received April 12, 1954)

The shell model wave functions may often be mixtures of those for two or more configurations. Calculations based upon a harmonic oscillator central potential with scalar Gaussian interactions between nucleons indicate that there is substantial interaction between various two-nucleon configurations of the $1d_{5/2}$, $2s_{1/2}$, $1d_{3/2}$ shell. The admixtures of the $1f_{7/2}$ subshell, which belongs to the next main level, are, however, small. A mixture of several neighboring configurations accounts for the ft value of $F^{18}(\beta^+)O^{18}$ better than any single configuration.

I. INTRODUCTION

THE j-j coupling shell model of the nucleus has had remarkable success in accounting for many qualitative regularities in nuclear structure. Moreover, it is possible to calculate quantitatively on the basis of this model numerical values of several properties of those nuclei which have both closed neutron and proton shells±one nucleon, and to do so in a rather unambiguous way. All available data except one, the magnetic moment of Bi^{209}, are in approximate agreement with such calculations.

The situation is far different for the many other nuclei. It is necessary to make additional assumptions regarding configurations, the order of filling of subshells, and many other details. It has not appeared possible to account with any set of assumptions even roughly for the quantitatively measured properties of these nuclei, which have two or more nucleons outside double closed shells. Indeed, not even the properties of nuclei within any single shell have been accounted for in a consistent way.

In view of the similarity between the atomic and nuclear shell models, it might be expected that states of many-particle nuclei are, in general, superpositions of states of two or more configurations. This effect is well known for complex atoms; for example, superpositions of states of configurations $4d^n$, $4d^{n-1}5s$, and $4d^{n-2}5s^2$ are common. Such mixing occurs when interconfiguration matrix elements of the electrostatic interelectron potential operator $\sum_{i>j}(e^2/r_{ij})$ are not zero. The mixing may therefore be said to be due to "configuration interaction."

* This work was supported in part by the U. S. Atomic Energy Commission and the Higgins Scientific Trust Fund.
† Hercules Fellow, 1952–1953. Now at the University of Wisconsin, Madison, Wisconsin.

If there are two or more electrons outside closed shells, each of them is moving in a central field determined by (1) the nucleus and closed shells, and (2) the other outer electrons. The contribution of these other electrons is in general not a central potential, and therefore the orbital angular momentum of an individual outer electron may be not even approximately a good quantum number.

Calculations of this effect for nuclei have been made on the basis of the j-j coupling shell model with a harmonic oscillator central potential and scalar Gaussian internucleon potentials. These assumptions are today often made,[1] because it seems useful to explore the consequences of any model of the nucleus which might have some validity and which is amenable to calculation.

II. FRAMEWORK OF THE CALCULATION

Calculations were made for two-particle configurations of the $1d_{5/2}$, $2s_{1/2}$, $1d_{3/2}$ shell. The potential energy of one particle with coordinates (r_1,θ_1,φ_1) is

$$V(r_1)=(\hbar\nu r_1)^2/2m, \tag{1}$$

where m = the nucleon mass, and ν was determined from

$$\langle r_1^2\rangle=\int_0^\infty r_1^2 R_{1d}^2(r_1)dr_1=\frac{7}{2\nu}=(1.43A^{\frac{1}{3}}\times10^{-13})^2; \tag{2}$$

i.e., the $1d_{5/2}$ particle is assumed to be just at the outer edge of the nucleus. Here $R_{1d}(r_1)/r_1$ is the radial part of the harmonic oscillator wave function $\psi_{1dm}(r_1)=[R_{1d}(r_1)/r_1]Y_2^m(\theta_1,\varphi_1)$. Calculations were made for $A=18$. This choice of ν leads to an energy difference between main harmonic oscillator levels of $\hbar\omega=\hbar^2\nu/m=10.3$ Mev.

The interaction between two particles a distance $r=|\mathbf{r}_1-\mathbf{r}_2|$ apart is

$$V_X(r)=V_0[\exp(-ar^2)]P_X, \tag{3}$$

where $P_W=1$, P_M = space-exchange operator, P_B = spin-exchange operator, and $P_H=P_MP_B$. The parameters V_0 and a were taken from the data for the neutron-proton system in the triplet state.[2] These lead to $V_0=-70.8$ Mev, and $a^{-1}=2.245\times10^{-26}$ cm^2. It is well known (see, e.g., reference 2) that the experimental data for low energies can equally well be accounted for by other potentials, for example, the Yukawa potential. The equivalent Yukawa potential for $V_W(r)$ with the parameters just given is

$$-\frac{98.1}{10^{13}r}\exp\left(-\frac{10^{13}r}{1.015}\right)\text{ Mev}. \tag{4}$$

This may be compared with the two-nucleon potential given in a recent book.[3] That potential has both central and tensor terms, each of the form (4). The denominator of the exponential of the central part is 1.176 instead of 1.015; i.e., the ranges are approximately equal, as would be expected. The depth of the central part, however, is 46.8 instead of 98.1. This depth would be expected to be smaller since there is a tensor force term which has about the same depth as the central term, and which contributes to the binding energy of the deuteron.

It should be noted that if there is only one outer nucleon, there is no possibility of interaction except with the core, since $V_X(r)$ is a two-particle operator. For two particles, however, there may be configuration interaction. To make calculations of this effect, it is necessary to evaluate matrix elements of the type

$$\langle j_1j_2JT|V_X(r)|j_3j_4JT\rangle. \tag{5}$$

Here j_k is the total angular momentum of a single nucleon (with orbital angular momentum l_k); J and T are total angular momentum and isotopic spin (with components J_z and T_z) of the two two-particle configurations. By means of transformation coefficients $\langle j_1j_2J|l_1l_2LS\rangle$, which were given by Racah,[4] the matrix elements (5) can be expanded in terms of similar ones for L-S coupling. These, in turn, can be expressed as series of certain radial integrals, which can readily be calculated for the present model by the methods of Talmi.[1] Details of the calculations and formulas for some radial integrals and matrix elements of type (5) may be found elsewhere.[5] The radial integrals depend upon the parameters ν and a only through $\beta=(a/\nu)+\frac{1}{2}$. $\beta=\infty$ corresponds to zero range, and $\beta=\frac{1}{2}$ to infinite range. $\beta=2.277$ for the parameters used here.

III. INTERACTIONS BETWEEN MAIN HARMONIC OSCILLATOR SHELLS

Let us examine whether there is mixing between two configurations belonging to different main harmonic oscillator levels. The third main level contains the subshells $1d_{5/2}$, $2s_{1/2}$, and $1d_{3/2}$; the fourth, $1f_{7/2}$ and others

TABLE I. Matrix elements, $\times(-1)$, in Mev, for some two-particle configurations.

		$\langle aa,JT\|V_W\|cc,JT\rangle$			$\langle aa,JT\|V_M\|cc,JT\rangle$		
				$a=1d_{5/2}$			$a=1d_{5/2}$
T	J	$a=c=1d_{5/2}$	$a=c=1f_{7/2}$	$c=1f_{7/2}$	$a=c=1d_{5/2}$	$a=c=1f_{7/2}$	$c=1f_{7/2}$
0	1	3.26	3.00	−2.72	0.94	0.43	−0.61
	3	1.77	1.49	−1.37	1.16	0.60	−0.75
	5	2.84	1.74	−1.40	2.84	1.41	−1.40
	7		2.36			2.36	
1	0	4.55	4.08	−3.78	2.90	2.08	−2.20
	2	2.08	1.98	−1.75	0.10	0.02	−0.06
	4	1.24	1.13	−0.98	−0.11	−0.10	0.08
	6		0.87			−0.19	

[1] I. Talmi, Helv. Phys. Acta **25**, 185 (1952). Earlier references are quoted there.

[2] J. M. Blatt and J. D. Jackson, Phys. Rev. **76**, 18 (1949).

[3] R. G. Sachs, *Nuclear Theory* (Addison-Wesley Press, Cambridge, 1953), p. 153.

[4] G. Racah, Physica **16**, 651 (1950).

[5] M. G. Redlich, Princeton dissertation, 1954 (unpublished).

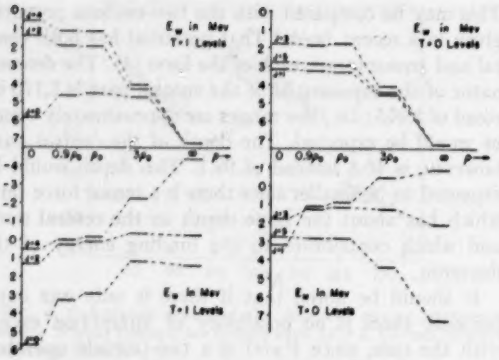

FIG. 1. The effects of changes in the range of nuclear forces on the levels of $(1d_{5/2})^3$.

which are empirically found to lie higher. Both diagonal and off-diagonal matrix elements are given for all states of $(1d_{5/2})^2$ and $(1f_{7/2})^2$ in Table I. Space-and-spin-exchange (H) and spin-exchange (B) interactions are readily obtained from this table by the formulas

$$\langle A|V_H|C\rangle=(-1)^T\langle A|V_W|C\rangle, \quad \text{and}$$
$$\langle A|V_B|C\rangle=(-1)^T\langle A|V_M|C\rangle.$$

Parity conservation prohibits configuration interaction between $(1d_{5/2})^2$ and $1d_{5/2}1f_{7/2}$. It is evident from Table I that mixing between $(1d_{5/2})^2$ and $(1f_{7/2})^2$ is largest for $T=1$, $J=0$ and ordinary (W) forces. From first-order perturbation theory, the amplitude of admixture of $(1f_{7/2})^2$ is

$$\alpha(1f_{7/2}^2)=\frac{3.78}{-2\times 10.3}=-0.183. \qquad (6)$$

This amplitude is small because the denominator, which is the difference between the energies of the main harmonic oscillator levels times the number of particles, is large. The interconfiguration matrix elements are actually about equal to the diagonal ones. Even for this state, α^2 equals 0.034, so that mixing is small.

It is easy to see that this result has qualitatively more general validity. Calculations of reference 5 indicate

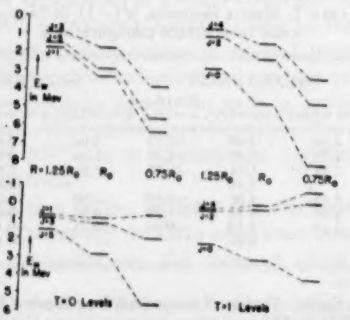

FIG. 2. The effects of changes in the nuclear radius on the levels of $(1d_{5/2})^2$.

that for short ranges the matrix elements for two-particle configurations decrease with an increasing number n of nodes, and further, that for a given set of n, l, j, they decrease with increasing atomic number A as $\beta^{-3/2}$, i.e., roughly as $\nu^{3/2}\sim A^{-1}$. It is seen from Sec. IV (Fig. 1) that the results for the range of nuclear forces chosen here do not in general differ much from those for zero range. The difference $\hbar\omega$ between main levels is proportional to $\nu\sim A^{-2/3}$. Thus α varies very roughly as $A^{-1/3}$. On the basis of the present model, admixtures of two-particle configurations from a higher main shell are therefore in general even smaller than (6) for $A>18$.

Is the actual energy difference between $1d_{5/2}$ and $1f_{7/2}$ levels about equal to the calculated 10.3 Mev? Recent experiments[6] on O^{17}, which has one neutron outside double closed shells, revealed the existence of a $7/2-$ state at 3.85 Mev. The ground state has $5/2+$, corresponding to $d_{5/2}$, and its magnetic moment is in excellent agreement with that assignment. There is, however, a $\frac{1}{2}-$ state at 3.06 Mev. It seems likely that this is due to a breakup of the closed shells; for instance, the configuration might be $(1p_{1/2})^{-1}(1d_{5/2})^2$. It is possible that the $7/2-$ state also belongs to this configuration, since $(1d_{5/2})^2$ can give states with J up to 5. Even if the $7/2-$ state in O^{17} does belong to the next main shell, the $1f_{7/2}-1d_{5/2}$ energy difference may be much larger for other nuclei in this region. The fact that the $1d_{3/2}$ shell is filled before the $1f_{7/2}$ shell for ground states would be consistent with such a change. The O^{17} data indicate a $\frac{3}{2}+$ state, presumably $1d_{3/2}$, at 5.08 Mev; i.e., above the $7/2-$ state.

IV. THE EFFECTS OF CHANGES IN THE PARAMETERS

Let us examine next whether the choice of parameters used here is critical. This question is of some importance, since the results of the present calculations have at best qualitative significance. If rather small changes in the parameters, which would still be entirely consistent with experimental results, change the matrix elements substantially, one should doubt the validity of the general results.

To change the range of nuclear forces, the potential will be taken as

$$V_X(r)=V_0(\rho)\,[\exp(-r^2/\rho^2)]P_X.$$

While ρ is varied from the value $\rho_0=1/\sqrt{a}$ used in the previous calculations, the expectation value of $V_W(r)$ for two nucleons, both in a $1s$ state, is kept constant:

$$\langle 1s^2|V_W(r)|1s^2\rangle=V_0(\rho)/\beta(\rho)^{3/2}2^{3/2}=\text{constant}.$$

The effect of variation of ρ from 0 (δ-function potential) to ∞ (forces of ∞ range) upon the levels of $(1d_{5/2})^2$ is shown for W and M forces in Fig. 1. There is only slight variation in energies and no change in order of the levels in the neighborhood of ρ_0. Similar results

[6] R. K. Adair, Phys. Rev. 92, 1491 (1953).

would hold for the integrals $\langle(1d_{5/2})^2J|V_X|(1f_{7/2})^2J\rangle$, and hence for the admixture $\alpha(1f_{7/2}^2)$ of formula (6).

Only one crossover occurs, for M forces: The state with $J=1$, $T=0$ lies lowest for $\rho=0$, but highest for $\rho=0.9\rho_0$ and all larger ranges. The explanation is readily seen. Let $\langle(1d_{5/2})^2J|V_M|(1d_{5/2})^2J\rangle^{\pi\pi}=[J]$ and, for L-S coupling, $\langle 1d^{2\,2S+1}L|V_W|1d^{2\,2S+1}L\rangle=(^{2S+1}L)$. Then

$$[1]=0.28(^3S)-0.56(^1P)+0.16(^3D);$$
$$[3]=0.62(^3D)-0.36(^1F)+0.02(^3G); \quad (7)$$
$$[5]=(^3G).$$

For a δ-function potential $(^1L)=0$ if L is an odd number. This is so because the wave function is space antisymmetric for odd L and is therefore 0 when the two particles are at coincidence. The δ-function potential is 0 except at coincidence. The matrix elements (^1L) with odd L rapidly increase with increasing ρ, until at ∞ range they equal those with even L. It is plain from formulas (7) that the effect of this increase will be largest for $[1]$, and hence the crossover between the $J=1$ level and the $J=3$ and 5 levels occurs.

For the $(1d_{5/2})^2$ configuration, the state with $J=1$ is the lowest of the $T=0$ states for W forces and all ranges $<\infty$, but only for very short range M forces. The ground state of F^{18}, which is expected to have this configuration, probably has $J=1$ and $T=0$. A state with these (T,J) may be the lowest even for $\frac{1}{2}(V_W+V_M)$ if admixtures of neighboring configurations are taken into account (see Sec. V).

The effect of a change in the nuclear radius R for constant range ρ_0 is shown in Fig. 2. The value $R=R_0$ was used in the calculations for Table I. A change of 25 percent from R_0 in either direction changes the magnitude of the energies of $(1d_{5/2})^2$ levels substantially but leaves their order and generally their relative positions about the same. For these three radii the interconfiguration integrals of V_W for $T=1$, $J=0$ and corresponding values of $\alpha(1f_{7/2}^2)$ are

R	$1.25\,R_0$	R_0	$0.75\,R_0$
$\langle(1d_{5/2})^2, J=0\|V_W\|(1f_{7/2})^2, J=0\rangle$	2.39	3.78	6.22 Mev
$\alpha(1f_{7/2}^2)$	−0.181	−0.183	−0.170.

The change in mixing is thus very small, even though the interconfiguration integral changes substantially. This is so because

$$\alpha(1f_{7/2}^2)=\langle(1d_{5/2})^2, J=0|V_W|(1f_{7/2})^2, J=0\rangle/(-2\hbar\omega),$$

and ω increases with decreasing R as R^{-2}. Similar results can be expected for other (T,J).

V. INTERACTIONS WITHIN THE 1d, 2s SHELL

There are six two-particle configurations in the $1d_{5/2}$, $2s_{1/2}$, $1d_{3/2}$ shell. They lead to the states listed in Table II. The energy differences between the single-particle levels are assumed to be due to spin-orbit splitting and to equal in magnitude the ones observed in O^{17} between $\frac{5}{2}+$ and $5/2+$ states (5.08 Mev) and $\frac{1}{2}+$ and $5/2+$ states (0.875 Mev). It is assumed, contrary to evidence from O^{17} discussed in Sec. III, that the $1f_{7/2}$ levels lie much higher. Let us define an operator $\Delta(j_1)$ as follows:

$$\langle j_1j_2JT|\Delta(j_1)|j_1'j_2'JT\rangle=a(j_1)\delta(j_1,j_1')\delta(j_2,j_2');$$
$$a(j_1)=\begin{cases}0 & \text{if } j_1=5/2\\ 0.875 \text{ Mev} & \text{if } j_1=1/2,\\ 5.08 \text{ Mev} & \text{if } j_1=3/2.\end{cases}$$

Table II. States of the two-particle configurations in the 1d, 2s shell. Expectation values of $\frac{1}{2}(V_W+V_M)+\Delta(j_1)+\Delta(j_2)$ are listed in Mev, $\times(-1)$, for all states permitted by the Pauli principle for space, spin, and isotopic spin.

Configuration	$T=\mathcal{C}$ $J=1$	0 2	0 3	0 4	0 5	1 0	1 1	1 2	1 3	1 4
$1d_{5/2}^2$	2.10		1.47		2.84	3.72		1.09		0.57
$1d_{3/2}^2$	−8.39		−7.78			−7.68		−9.32		
$2s_{1/2}^2$	1.46					1.46				
$1d_{5/2}1d_{3/2}$	−0.47	−2.81	−3.80	−2.23			−5.08	−4.53	−5.08	−2.80
$1d_{5/2}2s_{1/2}$		0.17	1.74					0.69	−0.87	
$1d_{3/2}2s_{1/2}$	−3.35	−4.39					−5.95	−4.91		

Calculations have been made for the $(T,J)=(1,0)$ and $(0,1)$ states. These are expected to be the quantum numbers of the ground states of F^{18} and O^{18}. The interaction was taken as $\frac{1}{2}(V_W+V_M)$. The matrices of $\frac{1}{2}(V_W+V_M)+\Delta(j_1)+\Delta(j_2)$ are given in Table III. The predominant configurations for $(T,J)=(0,1)$ are $1d_{5/2}^2$, $1d_{5/2}1d_{3/2}$, and $2s_{1/2}^2$. Diagonalization of the part of the submatrix for these configurations leads to the maximum eigenvalue $\lambda_{01}=4.03$ Mev. The wave function $\Psi(T,J)$ is easily calculated. Admixtures of the other two configurations are small and can be calculated by first-order perturbation theory. Then

$$\Psi(0,1)=0.732\psi(d_{5/2}^2)+0.477\psi(d_{5/2}d_{3/2})+0.464\psi(s_{1/2}^2)$$
$$-0.131\psi(d_{3/2}^2)-0.009\psi(d_{3/2}s_{1/2}). \quad (8)$$

Diagonalization of the (1,0) matrix yields $\lambda_{10}=5.05$ Mev. The wave function is

$$\Psi(1,0)=0.895\varphi(d_{5/2}^2)+0.370\varphi(s_{1/2}^2)+0.243\varphi(d_{3/2}^2). \quad (9)$$

Mixing is high for some states of larger J also. For instance, the matrix of $\frac{1}{2}(V_W+V_M)+\Delta(j_1)+\Delta(j_2)$ for (0,3) is given in Table IV. This time the predominant configuration is $d_{5/2}s_{1/2}$ with a very large admixture of $d_{5/2}^2$, and small admixtures of the other two configurations.

The expectation values in Table II for the $T=0$ states would indicate, at least for the equal mixture of

Table III. Matrices of $\frac{1}{2}(V_W+V_M)+\Delta(j_1)+\Delta(j_2)$, in Mev, $\times(-1)$.

	$T=0, J=1$						$T=1, J=0$		
	$d_{5/2}^2$	$d_{5/2}d_{3/2}$	$s_{1/2}^2$	$d_{3/2}^2$	$d_{3/2}s_{1/2}$		$d_{5/2}^2$	$d_{3/2}^2$	$s_{1/2}^2$
$d_{5/2}^2$	2.10	2.15	0.82	−1.61	−0.60	$d_{5/2}^2$	3.72	3.04	1.21
$d_{5/2}d_{3/2}$	2.15	−0.47	1.24	−0.51	0.79	$d_{3/2}^2$	3.04	−7.68	0.98
$s_{1/2}^2$	0.82	1.24	1.46	−0.44	0	$s_{1/2}^2$	1.21	0.98	1.46
$d_{3/2}^2$	−1.61	−0.51	−0.44	−8.39	1.12				
$d_{3/2}s_{1/2}$	−0.60	0.79	0	1.12	−3.35				

forces used here, that for a pure $d_{5/2}^2$ configuration a state with $J=5$ is the ground state. This is in contradiction to the allowed ft value of the $F^{18}(\beta^+)O^{18}$ transition. It is readily seen from Fig. 1 that a shorter range would, in fact, give the $J=1$ state as the lowest even for space-exchange (M) forces. However, the preceding calculation, which yielded $-\lambda_{01}=-4.03$ Mev, points the way to a more plausible explanation. The $J=5$ state belongs only to $(d_{5/2})^2$, and so its energy remains -2.84 Mev when configuration interaction is taken into account. Similarly, the (0,4) state belongs only to $d_{5/2}d_{3/2}$ and has energy 2.23 Mev. A glance at the (0,3) matrix shows that its largest eigenvalue will be less than 4.03 Mev. The same can be expected for (0,2). Thus, the present model accounts directly for the probable spin of F^{18}. It should be noted that the (0,1) state is the lowest, even though its predominant configuration is $(d_{5/2})^2$. The $(d_{5/2})^2$ probability, $|\alpha(d_{5/2}^2)|^2=54$ percent, while $s_{1/2}^2$ and $d_{5/2}d_{3/2}$ admixtures are only of the order of 20 percent.

VI. THE TRANSITION $F^{18}(\beta^+)O^{18}$

The wave functions (8) and (9) may be used to calculate the ft value for the following transition:[7]

$$F^{18} \quad \beta^+\longrightarrow \quad O^{18} \quad ft=4170\pm330 \tag{10}$$

$N, Z=9, 9$	$10, 8$	
$J_i=1$ (assumed)	$J_f=0$ (measured)	
$T_i=0$ (from experiment)	$T_f=1$	(from assumption that there are just two neutrons outside double closed shells).

The reaction $Ne^{20}(d,\alpha)F^{18}$ has been observed; therefore the ground state of F^{18} must have $T=0$. Its J could be only 0 or 1, since the ft value for the transition to O^{18}, which has $J=0$, lies in the allowed favored range. A state with $T=0$ and $J=0$ does not occur for any two-particle configuration.

The Fermi matrix element is 0 and, using constants obtained from single-particle and single-hole transitions,[8] one obtains

$$ft=\frac{5300}{\frac{1}{2J_i+1}\sum_{M_i,M_f}\sum_{q}|\langle\alpha_i J_i M_i|A_q^{(1)}|\alpha_f J_f M_f\rangle|^2}. \tag{11}$$

TABLE IV. Matrix of $\frac{1}{2}(V_W+V_M)+\Delta(j_1)+\Delta(j_2)$, in Mev, $\times(-1)$, for $T=0$, $J=3$.

	$d_{5/2}^2$	$d_{5/2}d_{3/2}$	$d_{3/2}^2$	$d_{5/2}s_{1/2}$
$d_{5/2}^2$	1.47	0.91	−0.63	1.18
$d_{5/2}d_{3/2}$	0.91	−3.80	0.84	−0.91
$d_{3/2}^2$	−0.63	0.84	−7.87	0.20
$d_{5/2}s_{1/2}$	1.18	−0.91	0.20	1.74

[7] Data are taken from F. Ajzenberg and T. Lauritsen, Revs. Modern Phys. 24, 321 (1952).

[8] G. L. Trigg, Phys. Rev. 86, 506 (1952); A. Winther and O. Kofoed-Hansen, Kgl. Danske Videnskab. Selskab, Mat.-fys. Medd. 27, No. 14 (1953).

TABLE V. The double-bar matrix element $\mathfrak{A}=(j_ij_i', J_i=1, T_i=0 \,\|\, A^{(1)} \,\|\, j_fj_f', J_f=0, T_f=1)$ for several transitions.

$j_ij_i'\rightarrow j_fj_f'$	$d_{5/2}^2\rightarrow d_{5/2}^2$	$s_{1/2}^2\rightarrow s_{1/2}^2$	$d_{3/2}^2\rightarrow d_{3/2}^2$	$d_{5/2}d_{3/2}\rightarrow d_{5/2}^2$	$d_{5/2}d_{3/2}\rightarrow d_{3/2}^2$
$\mathfrak{A}$	$-\sqrt{\frac{14}{5}}$	$-\sqrt{6}$	$\sqrt{\frac{6}{5}}$	$-\sqrt{\frac{8}{5}}$	$-\sqrt{\frac{12}{5}}$

Here α_i and α_f stand for the remaining quantum numbers (including isotopic spin) of the initial and final states. $M_i=J_{iz}$. $A_q^{(1)}$ is q component of the Gamow-Teller irreducible tensor operator. Using a well-known relation, one obtains, in the notation of Racah,[9]

$$\langle\alpha_iJ_iM_i|A_q^{(1)}|\alpha_fJ_fM_f\rangle=(-1)^{J_i+M_i}(\alpha_iJ_i\,\|\,A^{(1)}\,\|\,\alpha_fJ_f)\times V(J_iJ_f1;-M_iM_fq). \tag{12}$$

Then the denominator of (11) becomes

$$\frac{1}{2J_i+1}|(\alpha_iJ_i\,\|\,A^{(1)}\,\|\,\alpha_fJ_f)|^2. \tag{13}$$

It is evident that if the initial and final states are superpositions of states for different configurations, it is permissible in calculating the ft value to add the double-bar matrix elements (with proper phases and coefficients) instead of the $\langle\alpha_iJ_iM_i|A_q^{(1)}|\alpha_fJ_fM_f\rangle$. The double-bar matrix elements, $\mathfrak{A}$, are readily calculated by the methods of reference 9 and given in Table V for transitions between the several configurations involved in the transition (10). Since $A_q^{(1)}$ operates only on the spins and isotopic spins of single particles, $\mathfrak{A}=0$ for all transitions occurring between states of (8) and (9) except those listed in Table V.

The theoretical ft value for $d_{5/2}^2\rightarrow d_{5/2}^2$ is thus 5680; for $s_{1/2}^2\rightarrow s_{1/2}^2$ it is 2650. The observed value 4170 lies between them. For the transition (8)→(9), $ft=3190$. This is close to the $s_{1/2}^2\rightarrow s_{1/2}^2$ value, even though the $s_{1/2}^2$ admixtures are small, because the cross terms (like $d_{5/2}d_{3/2}\rightarrow d_{5/2}^2$) in the total matrix element are large and have the same sign as the direct terms. It is significant that configuration interaction does increase the matrix elements over those of $d_{5/2}^2\rightarrow d_{5/2}^2$. That the increase is too great is less important; with a change in the interaction, or in the distances between the single-particle levels, none of which is accurately known, it is surely possible to obtain just the observed ft value.

It is with pleasure that I thank Professor Eugene P. Wigner for suggesting this investigation and for his continued advice and interest. I am grateful to Dr. Igal Talmi for his advice and many valuable discussions.

[9] G. Racah, Phys. Rev. 62, 438 (1942).

Europium Activation Studies with Monochromatic Neutrons*

R. E. Wood†
Brookhaven National Laboratory, Upton, New York
(Received April 1, 1954)

Resonances in the europium slow neutron cross section at −0.011, +0.327, 0.461, 1.055, 2.74, 3.35, and 7.36 ev have been assigned to Eu^{151}. This was done by observing the intensity of the 9.3-hour activity of Eu^{152} produced as a function of neutron energy. The remainder of the europium resonances below 10 ev were assumed to be due to Eu^{153}; i.e., 1.76, 2.47, 3.84, 6.25, and 8.98 ev. The fraction of the compound nuclei decaying to the isomeric state of Eu^{152} was found to vary by a factor of four for different resonances in Eu^{151}. These fractions were obtained for six of the seven resonances in Eu^{151}.

I. INTRODUCTION

EUROPIUM activation studies with monochromatic neutrons were undertaken for two reasons; first, to obtain isotopic assignments of the many resonances found by Sailor, Landon, and Foote.[1] This was accomplished by irradiating Eu_2O_3 foils with monochromatic neutrons from the B.N.L. crystal spectrometer[2] and by observing the intensity of the 9.3-hour activity of Eu^{152} produced as a function of neutron energy. Previous measurements have shown resonances in Eu^{151} at −0.011 ev[3,4] and +3.3 ev,[5] and a resonance in Eu^{153} at 0.54 ev[4] (0.461 ev).

The second reason for studying europium activation was to observe variations from resonance to resonance in the decay of the compound nucleus if they exist. This was accomplished by measuring a relative population ratio of the isomeric state for each resonance. The population ratio of a given state is defined here as the fraction of the compound nuclei decaying to that state. Absolute population ratios of the isomeric state can be determined by measuring either the ratio of the isomeric activity to the ground state activity, or the ratio of the absorption cross section for the isomeric state to the total absorption cross section. It was considered impractical to measure absolute population ratios in this case; thus, relative population ratios were obtained by measuring a relative absorption cross section for the isomeric state. Preliminary population ratio variations have been observed in In^{116} by Sailor,[6] in Br^{80} and Rh^{104} by Capron and Verhoeve-Stokkink,[7] and more recently in Tl^{198} by Bergstrom, Hill, and dePasquali.[8]

II. EXPERIMENTAL DETAILS

Two thin Eu_2O_3 foils, whose thicknesses were approximately 0.009 and 0.016 g/cm,^{2} were used in the measurements. These foils were prepared by mixing finely powdered Eu_2O_3 with acetone and a small amount of Krylon plastic. Upon standing, the Eu_2O_3 settled out on a filter paper and the acetone evaporated. This left a reasonably uniform layer of Eu_2O_3 firmly held to the filter paper by means of the plastic binder. An average sample thickness for each filter paper was obtained by weighing. Small foils were punched from the filter papers for the activation measurements, and their thicknesses were accurately determined by transmission measurements at 0.461 ev where the cross section had been carefully measured.[1] A 12 percent variation was found in the foil thicknesses from one filter paper, but the average thicknesses obtained from the transmission measurements agreed well with those obtained by weighing. It is estimated that the error in sample thickness is less than 10 percent; however, this error would cause a negligible uncertainty in the results as the foil thickness enters only as a small correction.

The $(12\bar{3}1)$ planes of Be were used as the neutron monochromator for all irradiations excepting four points at low energy for which the (220) planes of NaCl were used. The thinner foils were irradiated at five energies in the range, 0.3 to 0.5 ev, using poor collimation. To increase intensity and to allow higher resolution by improved collimation, a single large foil was made from the thicker set of foils; this foil was used in all subsequent irradiations (0.07 to 9.0 ev). The background activity was determined in independent irradiations by rotating the crystal monochromator 1° from the Bragg angle during irradiation. To reduce the activity from environmental neutrons, the foils were shielded with 1.0 inch of B_4C at all times except while in the counter. The activity after irradiation was counted by a conventional end-window Geiger Meuller counter. A daily check of the counter sensitivity and operation was made with a cobalt source. The relative neutron flux at each energy was determined by correcting the spectrum measured with the spectrometer counter for the calculated BF_3 counter efficiency.

* Research performed under contract with the U. S. Atomic Energy Commission.
† Doctoral candidate from the University of Utah.
[1] Sailor, Landon, and Foote, Phys. Rev. **93**, 1292 (1954).
[2] L. B. Borst and V. L. Sailor, Rev. Sci. Instr. **24**, 141 (1953).
[3] William J. Sturm, Phys. Rev. **71**, 757 (1947).
[4] Borst, Ulrich, Osborne, and Hasbrouck, Phys. Rev. **70**, 557 (1946).
[5] M. Goldhaber (unpublished); see reference 20 in William J. Sturm, Phys. Rev. **71**, 757 (1947).
[6] V. L. Sailor (private communication).
[7] P. C. Capron and A. J. Verhoeve-Stokkink, Phys. Rev. **81**, 336 (1951).
[8] Bergstrom, Hill, and dePasquali, Phys. Rev. **92**, 918 (1953).

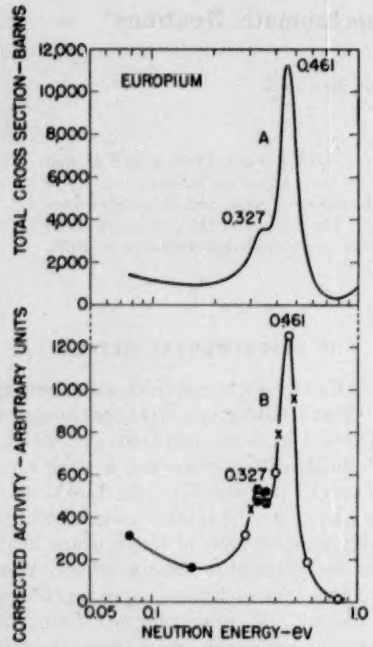

FIG. 1. Comparison of the total cross section below 1.0 ev, curve *A*, and the observed activities after all corrections have been applied, curve *B*. The crosses represent the thin-sample data and the open circles the thick-sample data using the Be crystal. The solid circles are for the thick sample using the NaCl crystal. The uncertainties due to counting statistics are smaller than the plotted points.

III. ANALYSIS

The objective of the analysis was to obtain a corrected activity which would be proportional to the absorption cross section for the isomeric state. The decay of the induced activity was followed as a function of time and the activity at the end of the irradiation was calculated on the assumption that only a 9.3-hour activity was present. The saturated activity (i.e., the activity which would be produced for an infinite irradiation time) was determined from the relation

$$A_\infty = C(A_0 - A_r)/(1-e^{-\lambda t}),$$

in which A_0 represents the activity of the foil at the end of the irradiation, t the total time of the irradiation, A_r the activity remaining in the foil from the previous irradiation, and C a normalization constant for the spectrometer beam monitor. The saturated background activity was then subtracted to give the activity produced by Bragg reflected neutrons.

Assuming that at any neutron energy the total cross section is equal to the sum of contributions from several resonances (i.e., $\sigma_t = \sigma_1 + \sigma_2 + \cdots$), the saturated 9.3-hour activity produced by Bragg reflected neutrons can be represented by the following:

$$A_\infty = K\Phi[1-\exp(-N\sigma_t)] \times [\sigma_1 R_1/\sigma_t + \sigma_2 R_2/\sigma_t + \cdots]. \quad (1)$$

The term $[1-\exp(-N\sigma_t)]$ is the fraction of the incident monochromatic neutron flux, Φ, absorbed in a foil of thickness, N, atoms/cm². The contribution to the activity from one resonance is $\sigma_1 R_1/\sigma_t$, where R_1 is the absolute population ratio of the isomeric state (9.3-hour activity) for that resonance, and so on with R_2, etc. The proportionality constant K includes the absolute value of the flux, area of foil irradiated, efficiency of the beta detector, absorption of beta particles in foil, and back scattering of beta particles from the aluminum foil mounting. It was thus possible to determine relative population ratios (KNR_1, $KNR_2 \cdots$) for closely spaced resonances by using the appropriate number of terms from the following equation:

$$KN[\sigma_1 R_1 + \sigma_2 R_2 + \cdots] = \frac{A_\infty}{\Phi} \frac{N\sigma_t}{[1-\exp(-N\sigma_t)]}. \quad (2)$$

All cross sections used in this paper were taken from the analysis of Sailor *et al.*[1] The total cross section was used as the absorption cross section since the resonance scattering was negligible for the resonances under study.

IV. RESULTS AND DISCUSSION

All of the results agreed quite well with the assumed 9.3-hour half-life. There was the possibility that the buildup of long-lived Eu activities should not be neglected in the calculations since the same foil was used repeatedly. It was found that this built-up activity was less than 1.5 counts per minute after all of the irradiations were completed. This was less than 3 percent of the total background, which confirmed the assumption that it could safely be ignored.

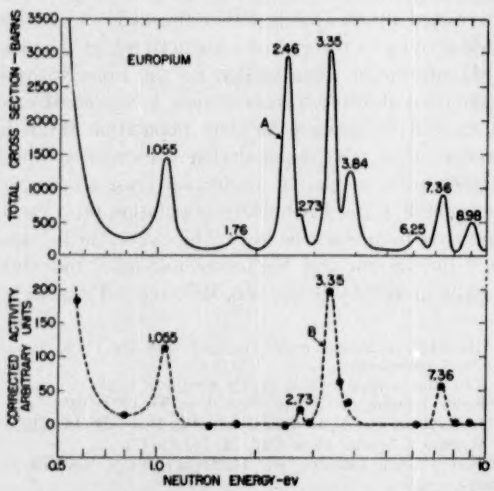

FIG. 2. Comparison of the total cross section between 1.0 and 10 ev, curve *A*, and the observed activities after all corrections have been applied, curve *B*. Activations were made at a sufficient number of points to determine the resonance structure for Eu^{151} as indicated by the dashed line. The uncertainties due to counting statistics are smaller than the plotted points.

The corrected activities, which were proportional to the absorption cross section for the isomeric state of Eu^{152}, are shown in Figs. 1 and 2; the proposed resonance structure for Eu^{151} is also indicated. The resonances at −0.011, +0.327, 0.461, 1.055, 2.73, 3.35, and 7.36 ev have been assigned to Eu^{151}; the remaining resonances below 10 ev have been assigned to Eu^{153}; i.e., 1.76, 2.47, 3.84, 6.25, and 8.98 ev. All of the assignments are statistically definite with the possible exception of the resonance at 6.25 ev. The previous assignments at −0.011 ev[3,4] and +3.3 ev[5] have been corroborated, but the assignment of the 0.54 (0.461) ev[4] resonance to Eu^{153} has been found to be in error.

It was necessary to apply an arbitrary normalization constant to two of the three sets of data shown in Fig. 1, because of differences in resolution and foil size. The thin-sample data were normalized to the point at 0.360 ev, and the data with the NaCl crystal were normalized to the average of the points at 0.327 and 0.360 ev. The average normalization of two points was used for the NaCl data because the resolution was too poor to measure the true shape of the curve as measured with the Be crystal.

The differences in the shape of the activity curve compared to the total cross section curve in Fig. 1 clearly demonstrate differences in the population ratios for the three resonances below 1.0 ev. To calculate the population ratios for the two resonances at 0.327 and 0.461 ev, it was assumed that only these two resonances contribute to the activity in the range 0.28 to 0.60 ev. Calculating the cross sections from the parameters obtained by Sailor *et al.*[1] leads to an equation in two unknowns for each of the eleven activations with the Be crystal. These eleven equations were solved by the method of least squares, giving the results shown in Table I for the 0.327- and 0.461-ev resonances. The standard deviation from the least squares solutions was less than the estimated error indicated in Table I. The activity and cross section due to the resonances at 0.327 and 0.461 ev were then subtracted from the measured activity and cross section at 0.077 and 0.155 ev using the known parameters and population ratios. Assuming the remaining activity and cross section to be due to the resonance at −0.011 ev, the population ratio given in Table I was obtained for this resonance. The estimated error on this ratio was much larger than that indicated by the average of the two points used. The remaining population ratios were obtained by using the measured total cross section directly. No attempt was made to make resolution corrections on either the total cross section or the activations. This correction becomes important at 1.0 ev and becomes increasingly more important the higher the energy.

TABLE I. Relative population ratios of the isomeric state of Eu^{152} for different resonances in Eu^{151}. The quoted errors are based upon the statistics of the points, the number of points used in the calculations, and an estimate of effects not considered in the analysis. No errors are listed for the highest energy resonances because the effects of resolution are very important, and the resolution for the activation studies was not well known.

Resonance energy[a] (ev)	Relative population ratio
−0.011	0.24±0.03
+0.327	0.19±0.02
0.461	0.11±0.01
1.055	0.08±0.03
2.73	...
3.35	~0.06
7.36	~0.06

[a] The negative energy resonance value is taken from reference 3, the other values from reference 1.

An absolute population ratio of 0.19±0.03 for the isomeric state of Eu^{152} was obtained by Hayden, Reynolds, and Inghram[9] for a Eu sample subjected to slow neutron irradiation in a graphite moderated pile. Using the results obtained in this study with their absolute population ratio, it is possible to obtain absolute population ratios for all of the resonances. These results have not been listed because of the unknown flux distribution in the irradiation of their sample.

It might be expected that the population ratios would fall into two groups depending on the spin of the compound nucleus. The results of this study are consistent with this hypothesis within the limits of error quoted, but it is interesting to note that the population ratios appear to decrease with increasing resonance energy. It would be very interesting to perform this same experiment on other elements and see if similar results were obtained.

V. ACKNOWLEDGMENTS

The author is grateful to Dr. L. B. Borst and Dr. V. L. Sailor for suggesting the experiment; also for their help and advice in the planning and execution of the experiment.

[9] Hayden, Reynolds, and Inghram, Phys. Rev. 75, 1500 (1949).

The Directional Correlation of the γ Rays of A^{38}†

J. J. KRAUSHAAR,* J. W. MIHELICH, AND A. W. SUNYAR
Brookhaven National Laboratory, Upton, New York

(Received March 11, 1954)

The angular correlation of the γ rays in A^{38} following the β-decay of Cl^{38} has been measured. The correlation function is in agreement with that expected for the spin sequence $3(D)2(Q)0$ or possibly $1(D,Q)2(Q)0$ with a 2.5 percent quadrupole intensity (out of phase). Gamma-ray lifetime arguments strongly favor the $3-2-0$ spin sequence.

THE β decay of Cl^{38} has been investigated in detail by Langer.[1] Hole and Siegbahn[2] have established the existence of two successive γ rays in A^{38} with energies of 1.60 and 2.15 Mev. Langer reported that the ground-state transition has the unique $\Delta I=2$, (yes) shape. Taking the ground-state spin of A^{38} as zero, this establishes the Cl^{38} ground state as a $2-$ level. The lowest-energy β transition to the 3.75-Mev level in A^{38} has a log $ft=4.93$,[3] which suggests it has an allowed character. Hence the 3.75-Mev level would have odd parity. Inasmuch as the intensity of the crossover transition has been shown[4] to be less than 3×10^{-4}, Langer concluded that the spin of the upper level in A^{38} is most likely $3-$.

The angular correlation of the γ rays was measured by early investigators,[5] but the accuracy of their experiments prevented any definite conclusions. Later, Steffen[6] measured the angular correlation, and he interpreted his results as indicating that the spin of the levels were 3, 2, 0 with both γ rays quadrupole. The theoretical angular correlation for this assignment is shown in Fig. 1. From general considerations of transition probabilities, Steffen concluded that all three levels were of the same parity, in disagreement with the β-decay data.

The conclusions from the β-decay and angular correlation data could be consistent if the upper γ ray were $M2$. However, an upper limit of 4×10^{-10} sec has been placed on the half-life of the second excited state of A^{38}, which is of the order of 10 times less than would be expected for such an $M2$ transition on empirical grounds.[7] Because of these inconsistencies, it was decided to remeasure the angular correlation of the γ rays in A^{38}.

The experimental apparatus and method used have been described previously.[8] The counters had 1.2 cm of Lucite and 2.5 mm of Pb in front of them. In addition, the bias on each counter was set at about 600 kev to preclude counting any coincidences arising from annihilation radiation due to internally created pairs. The sources were prepared by irradiating LiCl in the Brookhaven reactor for 20 minutes. The active powder was dissolved in a small amount of water to form sources whose volume ranged from 0.05 to 0.25 ml. In order to correct for decay, the coincidence counts were normalized to the single counts of the movable counter. No deviation from a pure exponential decay was found in 7 half-lives. The uncorrected experimental points are shown in Figs. 1 and 2. The indicated errors are standard deviations. A least-squares fit of the data to the correlation function $W(\theta)=1+a_2\cos^2(\theta)$ yields a value of $a_2=-0.105\pm0.008$ when corrected for the angular resolution of the counters. The angular resolution function of our counters was determined by using a well-collimated beam of the γ rays of A^{38}. The magnitude of the geometrical correction is given by $Q_2/Q_0=0.954$ and $Q_4/Q_0=0.859$ in the notation of Lawson and Frauenfelder.[9]

The β-decay data of Langer[1] limits the spin of the

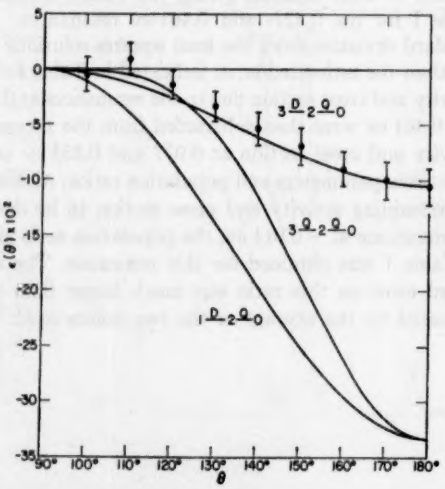

FIG. 1. Theoretical angular correlation curves for $3(D)2(Q)0$, $3(Q)2(Q)0$, and $1(D)2(Q)0$. The experimental points for A^{38} are drawn without angular resolution correction.

† Work supported by the U. S. Atomic Energy Comimssion.
* Now at Stanford University, Stanford, California.
[1] L. M. Langer, Phys. Rev. **77**, 50 (1950).
[2] N. Hole and K. Siegbahn, Arkiv. Mat. Astron. Fysik **33A**, No. 9 (1946).
[3] King, Dismuke, and Way, Oak Ridge National Laboratory Report ORNL-1450, 1952 (unpublished); A. M. Feingold, Revs. Modern Phys. **23**, 10 (1951).
[4] V. Meyers and A. Wattenberg, Phys. Rev. **75**, 992 (1949).
[5] Kikuchi, Watase, and Stoh, Z. Physik **119**, 185 (1942); R. Beringer, Phys. Rev. **63**, 23 (1943).
[6] R. M. Steffen, Phys. Rev. **80**, 115 (1950).
[7] A. W. Sunyar (unpublished).
[8] J. J. Kraushaar and M. Goldhaber, Phys. Rev. **89**, 1081 (1953).
[9] J. S. Lawson and H. Frauenfelder, Phys. Rev. **91**, 649 (1953).

second excited state of A^{38} to 3, 2, or 1. The spin of the first excited state is limited to 2 or 1 on γ-ray lifetime arguments. With these spin limitations and assuming a zero spin for the A^{38} ground state, the value we obtain for a_2 is compatible with the following cascades:

(a) 2–1–0 with either ~4 percent or ~79 percent quadrupole intensity (in phase).[10]

(b) 1–1–0 with either ~99 percent or ~1.3 percent quadrupole intensity (out of phase).

(c) 3–2–0 with <0.02 percent (in phase) or <0.01 percent (out of phase) quadrupole intensity.

In addition, a least-squares fit of the data to the correlation function $W(\theta)=1+a_2\cos^2\theta+a_4\cos^4\theta$, after the angular resolution correction described above, yields $a_2=-0.024\pm0.037$ and $a_4=-0.094\pm0.042$. These coefficients are compatible only with the 1–2–0 cascade with a 2.5 percent quadrupole intensity (out of phase). We should point out that the errors attached to the a_2 and a_4 coefficients are purely statistical. We therefore cannot definitely state whether the a_4 coefficient is zero or nonvanishing. It is worth noting that a small spurious coincidence rate ($\leq$1 percent) arising from scattering or from some other unknown cause can account completely for the possible presence of an a_4 term in the angular correlation.

The four possible cascades compatible with the experimental data can be reduced to two if the well-founded empirical rule,[11] that the first excited state of an even-even nucleus has spin 2 and even parity, is valid in this case. We may then consider only the cascades $3(D,Q)2(Q)0$ and $1(D,Q)2(Q)0$. The latter would seem unreasonable in view of the fact that the crossover transition has not been seen experimentally.[4] (Its intensity would be less than 3×10^{-4} of the cascade intensity.) It may be noted here that for the 1–2–0 levels of Nd^{144} the dipole crossover transition occurs with ~3 times the intensity of the cascade transition.[12] The degree to which the crossover transition has been excluded in A^{38} is consistent with empirical lifetime-

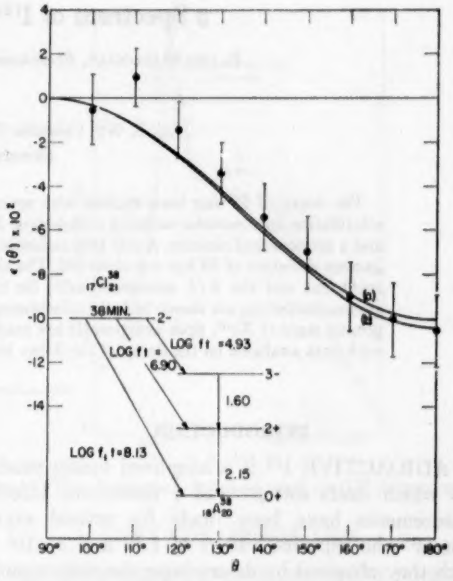

FIG. 2. Angular correlation curves for A^{38} and proposed decay scheme. Curve (*a*) is a least-squares fit of $1+a_2\cos^2\theta$ to the experimental points shown. Curve (*b*) is the theoretical correlation for a $3(D)2(Q)0$ cascade. The geometry-corrected least-squares fit is for practical purposes indistinguishable from curve (*b*).

energy relations for *E*3 transitions and the known upper limit on the lifetime of the 3.75-Mev state. We therefore feel the spin assignments 3−, 2+, and 0+ for the levels of A^{38} are most consistent with all available experimental information, although the accuracy of our angular correlation data cannot by itself exclude the $1(D,Q)2(Q)0$. If the cascade is the $3(D,Q)2(Q)0$ cascade, then within our experimental error, the first transition in the cascade is pure dipole. The decay scheme is shown in Fig. 2.

It is of interest to note that the assignment of odd parity to the level of spin 3 is in agreement with the conclusions of Glaubman[13] and Talmi[14] regarding the parity of odd spin states of even-even nuclei.

We wish to thank Mrs. P. Levy for performing nu merical integrations.

[10] D. S. Ling and D. L. Falkoff, Phys. Rev. **76**, 1639 (1949).
[11] M. Goldhaber and A. W. Sunyar, Phys. Rev. **83**, 906 (1951). Horie, Umezawa, Yamaguchi, and Yoshida, Progr. Theoret. Phys. Japan **6**, 254 (1951). Gertrude Scharff-Goldhaber, Phys. Rev. **90**, 587 (1953). P. Preiswerk and P. Stahelin, Helv. Phys. Acta **24**, 623 (1952).
[12] D. E. Alburger and J. J. Kraushaar, Phys. Rev. **87**, 448 (1952).
[13] M. Glaubman, Phys. Rev. **90**, 1000 (1953).
[14] I. Talmi, Phys. Rev. **90**, 1001 (1953).

β Spectrum of I^{129} and Its Decay Scheme*

E. DER MATEOSIAN, *Brookhaven National Laboratory, Upton, New York*

AND

C. S. WU, *Columbia University, New York, New York*

(Received April 5, 1954)

The decay of I^{129} has been studied with several instruments including a magnetic lens spectrometer, a scintillation spectrometer utilizing a technique in which the activity is introduced into a NaI(Tl) crystal, and a proportional counter. A soft beta radiation whose end-point value is measured to be 150±5 kev and a gamma radiation of 38 kev are observed. The shape of the beta spectrum is studied and the K-conversion coefficient and the K/L conversion ratio for the 38-kev gamma radiation are determined. The beta and gamma radiations are shown to be in coincidence and an upper limit is set for a possible beta branch to the ground state of Xe^{129}. Spin assignments are made which agree with shell model theories of the nucleus and with data available on the decay of the 8-day isomer of Xe^{129}.

INTRODUCTION

RADIOACTIVE I^{129} is a long-lived fission product which emits soft β^- and γ radiations. Lifetime measurements have been made by several experimenters[1] who reported values of 1.72 and 3×10^7 yr, which they obtained by determining the disintegration rates of weighed amounts of I^{129}. Absorption[1] and proportional counter[2] techniques have been used to measure the maximum energy of the β spectrum, and values close to 0.12 Mev have been given. The soft γ radiation has been reported to be 0.039 Mev.[2]

The β decay of I^{129} leads to Xe^{129}. Information about the first two excited states of this isotope has been obtained through study of the decay of the 8-day isomer of Xe^{129}. At first a 196-kev gamma radiation was observed associated with this isomer which was identified as a magnetic 4-pole transition. In order to build a decay scheme consistent with the measured ground-state spin of $\frac{1}{2}$ and shell model theories, Goldhaber and Sunyar[3] postulated a low-lying intermediate state. Following shell model theories, the second excited state was assumed to be an $h_{11/2}$ level and the first excited state a $d_{3/2}$ level. Thus, the 196-kev $M4$ transition could be the $h_{11/2}\rightarrow d_{3/2}$ transition and a $d_{3/2}\rightarrow s_{1/2}$ transition would follow to the ground state. Recently, a second transition of 40 kev in the decay of $_{54}Xe^{129m}$ was confirmed by observing its L-conversion line in a magnetic spectrometer.[4] Presumably, the 40-kev line observed in $_{54}Xe^{129m}$ and the 39-kev line in I^{129} are the same $d_{3/2}\rightarrow s_{1/2}$ transition in $_{54}Xe^{129}$.

The spin of the ground state of I^{129} has been measured and given to be 7/2 (the shell model predicts $g_{7/2}$). If the β transition observed in I^{129} leads to the first excited state in Xe^{129}, the spin and parity change involved in the β transition ($g_{7/2}\rightarrow d_{3/2}$) is $\Delta I=2$, (no), which belongs to the second forbidden parity unfavored group. A beta branch from the $g_{7/2}$ ground state of I^{129} to the $s_{1/2}$ ground state of Xe^{129} ($\Delta I=3$, no) is not completely ruled out on the basis of theoretical lifetime estimations. Considerations based upon the known ft value of Be^{10} would indicate a branching ratio of 10^{-3} for the ground-state transition. It appeared to us, therefore, that a determination of the β branching ratio in I^{129} would be of interest, and, further, that a theoretical interpretation of the forbidden shape of the beta spectrum would add to the knowledge of the second forbidden parity unfavored group, of which, to date, ony four other cases[5] (Cl^{36}, Tc^{99}, Cs^{137}, Cs^{135}) are known to exist and have been investigated. Photon studies were made to complete our knowledge concerning the decay scheme of I^{129}.

CHARACTERISTIC X-RAYS AND GAMMA RADIATION

A preliminary investigation of the soft photon radiations of I^{129} with a NaI(Tl) scintillation spectrometer revealed the presence of photons with 30-kev energy. By the use of Cd, In, Sn, and Sb critical absorbers, it was established that these photons were

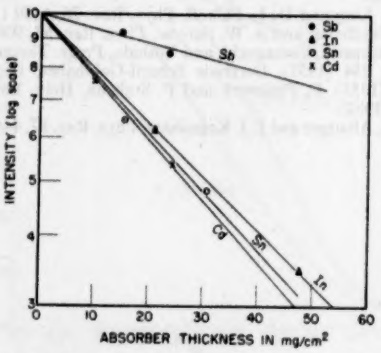

FIG. 1. Critical absorption of x-rays and γ rays of I^{129} in Sb, Sn, In, and Cd. The break between Sb and the rest indicates the presence of Xe x-rays.

* Work supported by the U. S. Atomic Energy Commission.

[1] Katcoff, Schaeffer, and Hastings, Phys. Rev. 82, 688 (1951); Parker, Creek, Herbert, Lantz, and Martin, Oak Ridge National Laboratory Report ORNL-286, September, 1949 (unpublished).

[2] C. J. Borkowski and A. R. Brosi, Oak Ridge National Laboratory Report ORNL-607, 1950 (unpublished).

[3] M. Goldhaber and A. W. Sunyar, Phys. Rev. 83, 906 (1951).

[4] S. Thulin and I. Bergstrom, Phys. Rev. 85, 1055 (1952).

[5] C. S. Wu, Physica 18, 989 (1952).

Xe K x-rays. The experimentally obtained characteristic absorption curves are shown in Fig. 1.

The soft radiations were then carefully examined with a krypton-filled proportional counter. A pronounced Xe K_α line (with a slight bump due to the K_β line) was revealed, but, in addition, the existence of a weak line at 38 kev was shown (Fig. 2). This agrees with the findings of Borkowski and Brosi.[2]

If it is assumed that the observed Xe K x-rays are due to the internal conversion of the 38-kev gamma radiation, the K-conversion coefficient for this gamma ray can be estimated by comparing the sum of the areas under the K_α, K_β and escape peaks with that of the 38-kev line after corrections for window absorption, counter efficiency, and fluorescence yield have been

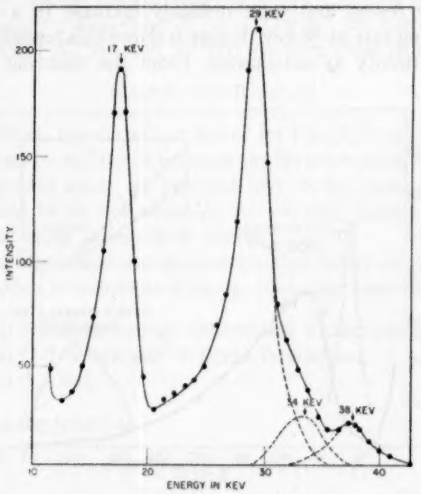

FIG. 2. Proportional counter observation of the radiations of I^{129}. The 29-kev and 17-kev peaks are due to the xenon K_α line and an escape peak, while the broadening of the 29-kev peak at 34 kev may be due to the xenon K_β line. A definite indication of a 38-kev gamma ray is shown.

applied. The K-conversion coefficient thus obtained is 22 ± 4.

Table I lists theoretical K-conversion coefficients for various multipoles, computed with the help of the calculations of Spinrad and Keller,[6] for radiations with energies approaching the K-shell binding energies. The use of these calculations in the case of I^{129} is justified by the nearness of the K-shell binding energy Xe (34.6 kev) to the energy of the 38-kev radiation.

The observed value of 22 ± 4 for α_K is in agreement with either $M1$ or $E2$ radiation. Evidence based on the K- to L-conversion ratio of the 38-kev radiation which will be presented below indicates $M1$ to be the preferred assignment. This is in agreement with a $d_{3/2}\rightarrow s_{1/2}$ transition.

[6] B. I. Spinrad and L. B. Keller, Phys. Rev. **84**, 1056 (1951).

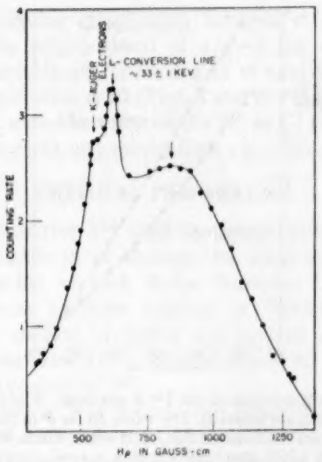

FIG. 3. The momentum distribution of the I^{129} β spectrum.

THE L-CONVERSION LINE

The β spectrum and electron conversion lines were studied with the Columbia University magnetic lens spectrometer. The investigation of a low-energy β spectrum of a highly forbidden transition is a difficult task. Because of its extremely long half-life ($t_{1/2}=3\times10^7$ yr) the specific activity of the I^{129} sample was very low. The source was prepared by depositing 200 $\mu g/cm^2$ of KI onto a Formvar film whose thickness was 10 $\mu g/cm^2$. Even though the purity of the I^{129} was 85 percent, the source was equivalent to only ~0.05 $\mu C/cm^2$, so that an extended source 1 cm in radius was necessarily used. The resolution was on this account broadened to 6–8 percent. The counter used had a Formvar window of ~25 $\mu g/cm^2$.

Figure 3 shows the momentum distribution of the spectrum. The line appearing at $H\rho=620$ is the L-conversion line of the 38-kev gamma radiation. This same L-conversion line was also observed by Thulin and Bergstrom[4] in the Xe^{129m} e^- spectrum. The energy of the gamma ray calculated from the conversion line is $E_\gamma=E_{L^-}+W_L=33+4.6=37.6\pm1$ kev. The little peak on the left side of the L-conversion line is due to K-Auger electrons.

A comparison of the area under the L-conversion line with the area under the beta spectrum enables us to determine α_L, the L-conversion coefficient. This combined with the above measured value of α_K gives us a value for the K/L conversion ratio, which is about 10:1. Whereas $\alpha_K=22\pm4$ is in agreement with either

TABLE I. Theoretical K-conversion coefficients.

Electric Multipole	α_K	Magnetic Multipole	α_K
$E1$	8	$M1$	19
$E2$	23	$M2$	300
$E3$	40		

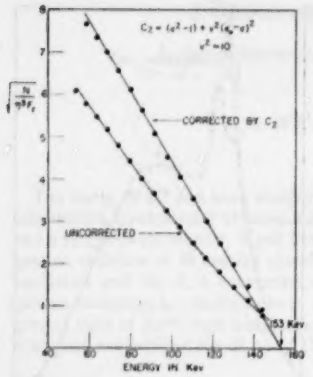

FIG. 4. The Kurie plot of the I^{129} β spectrum. N is the counting rate per momentum interval. The value 10 for v^2 in the correction factor C_2 agrees with the value of $v^2=9.5$, which fits the Cs^{135} beta spectrum which also results from a $g_{7/2}\rightarrow d_{3/2}$ transition.

$M1$ or $E2$, the K/L ratio indicates the 38-kev gamma ray to be an $M1$ transition (for $E2$ the K/L ratio is[7] around $\sim$0.2). Therefore, the preferred assignment for the 38-kev transition is $d_{3/2}-s_{1/2}$.

The Beta Spectrum

The continuous beta spectrum yields an end point higher than those previously reported. It is 150$\pm$5 kev. The Kurie plot is not linear but shows a slight curvature convex toward the energy axis (Fig. 4). The distortion due to the source thickness and broad resolution used was checked by using a S^{35} source prepared by mixing the S^{35} with KI and covering a circular area of 1-cm radius with 200 μg/cm^2 of $S^{35}-KI$ mix. It was found that distortion above 50 kev was negligible (Fig. 5).

It is important to ascertain experimentally whether a beta branch to the ground state of Xe^{129} is negligibly small. A verification of this would be to show that each beta particle emitted in the decay of I^{129} is followed by a 38-kev gamma radiation. The technique[8] developed at the Brookhaven National Laboratory of growing NaI(Tl) crystals with a trace of the radioactive substance mixed in it enables one to answer this question. Because of the nearly 100 percent efficiency in detecting the 38-kev line in the NaI(Tl) crystal, the pulse height detected should be proportional to the sum of the beta-particle energy and the gamma energy, because each beta particle emitted to the excited state of Xe^{129} is followed by a 38-kev emission. The minimum pulse height in the beta distribution, due to those β particles emitted with practically zero energy, should be equivalent to 38 kev. This implies that the pulse distribution should give practically zero intensity at the low-energy region and then suddenly increase to a high counting rate at 38 kev. Figure 6 shows this remarkable discontinuity as anticipated. From the counting rate

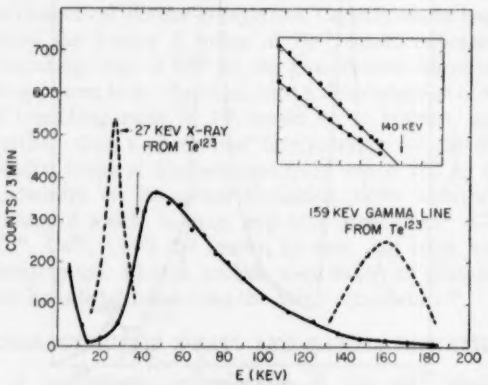

FIG. 6. Energy distribution of the I^{129} β spectrum as seen with an internal source scintillation spectrometer. The insert shows Kurie plots of the spectrum, the upper plot of the two being corrected by $C_2=(\epsilon^2-1)+v^2(\epsilon_0-\epsilon)^2$, where $v^2=10$.

below the 38-kev region, one could put an upper limit to the β branch to the ground state of Xe^{129} of less than 1 percent. This is in agreement with the theoretical estimation based on the available ft value of Be^{10} which is also a $\Delta I=3$, (no) transition. The ft value of Be^{10} after being corrected for its average value of $\bar{D}_2$ is around 10^{12} sec. Now the average value[9] of $\bar{D}_2$ for the ground-to-ground transition in I^{129} is 1.5×10^{-4}. If one assumes that the corrected ft value of all transitions with $\Delta I=3$, (no) should have about the same order of magnitude, then the uncorrected f_0t for this transition will be $\sim10^{16}$ sec. It is a factor of 10^3 larger than the observed $f_0t\sim10^{13}$ sec. This implies that the branching ratio must be of the order of $10^{-2}-10^{-3}$.

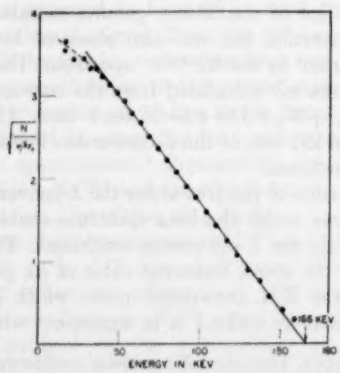

FIG. 5. The Kurie plot of the S^{35} β spectrum. This spectrum was used to check distortion due to source thickness and broad resolution. A source was prepared by mixing S^{35} with enough KI ($\sim$100 μg/cm^2) to simulate conditions existing for the I^{129} source. The spectrum shows negligible distortion above 50 kev.

[7] M. Goldhaber, Physica 18, 1091 (1952).

[8] Scharff-Goldhaber, der Mateosian, Goldhaber, Johnson, and McKeown, Phys. Rev. 83, 480 (1951); E. der Mateosian and A. Smith, Phys. Rev. 88, 1186 (1952).

[9] J. Davidson, Phys. Rev. 82, 48 (1951).

INTERPRETATION OF THE β SPECTRUM

Recent analysis of the superallowed transitions have shown that the contributions from the Gamow-Teller (G-T) and Fermi interactions in the β-decay process are comparable. This means that the beta-decay interaction is not a single interaction but rather a linear combination of approximately equal parts of G-T and Fermi interactions.

In the past, one has been able to fit the parity unfavored second forbidden β spectra by tensor or polar vector interaction alone. The reason behind this possibility is the very close energy dependences between the correction factors associated with the various matrix elements. For instance, if the transition energy$\ll$ Coulomb barrier energy, then the correction factors for the nuclear matrix elements of R_{ij}, $R_{ij}T_{ij}$ are related by $C_{Rij}\approx -2C_{Rij}{}^{*}{}_{T}{}_{ij}=4C_{Tij}$. Likewise, the correction factors of $R_{ij}{}^{*}A_{ij}$ and $T_{ij}{}^{*}A_{ij}$ are very close in shape,

$$C_{Rij}{}^{*}{}_{Aij}\approx -2C_{Tij}{}^{*}{}_{Aij}.$$

Therefore, the correction factor for the (S,T) combination can be written in terms of the tensor or polar vector interaction alone. It explains why it has been found possible to fit the observed $\Delta I=2$ (no) spectra with one of these interactions alone.

The algebraic form of the correction factor for second forbidden interactions with the following assumptions:

(i) transition energy $\ll$Coulomb barrier energy,
(ii) G-T interaction $\approx$Fermi interaction,
(iii) $S_{ijk}\equiv 0$,

can be expressed as

$$C_2=p^2+v^2q^2=(\epsilon^2-1)+v^2(\epsilon_0-\epsilon)^2,$$

where

$$v^2=\left[\frac{2(\alpha Z/2\rho)(R_{ij}+\tfrac{1}{2}iT_{ij})-A_{ij}}{(\alpha Z/2\rho)(R_{ij}+\tfrac{1}{2}iT_{ij})-A_{ij}}\right]^2=\left(\frac{2\eta-a}{\eta-a}\right)^2.$$

One outstanding relationship between v^2 and a/η is that in the neighborhood of $a/\eta=1$ the value of v^2 becomes very large. The value of v^2 used in C_2 to fit the I^{129} β spectrum is 10 (Figs. 4 and 6). This is in good agreement with the value of $v^2=9.5$ in C_2 for the Cs^{135} β spectrum which also results from a $g_{7/2}\rightarrow d_{3/2}$ transition.

CHEMICAL PREPARATION

The radioactive I^{129} used in this investigation was made available to us through the kind arrangement of Dr. Parker of Oak Ridge National Laboratory. The I^{129} was a dilute solution of $NaOH+Na_2SO_3$. The total amount of iodine was around 2 mg. The isotopic concentration is approximately 85 percent of I^{129} and 15 percent of I^{127}.

To prepare a NaI source, the iodine was first extracted with CCl_4. To the CCl_4 layer, 10 cc of distilled water containing about 5 mg Zn dust was added. The mixture was shaken and the aqueous layer was separated and filtered through a medium filter stick. The solution was passed through a cation exchange resin (Dowex-50, Na-form) to convert it to NaI. However, NaI is not suitable for use in magnetic spectroscopic investigation as the NaI source will quickly become deliquescent as soon as it is exposed to moist air. For this purpose a portion of the I^{129} was converted to KI by ion exchange and a source of approximately 200 $\mu g/cm^2$ was evaporated onto a thin Formvar film.

ACKNOWLEDGMENT

The authors wish to express their deep appreciation to Mr. E. Alperovitch of the Chemistry Department of Columbia University for his valuable assistance in the chemical preparation of the source, and also to Dr. F. Boehm, Mr. A. Schwarzschild, Mr. R. Gold, and Mr. M. McKeown for their assistance in making the measurements. Interesting discussions with Dr. M. Fuchs, Dr. M. Goldhaber, Dr. L. J. Lidofsky, and Dr. D. C. Peaslee are gratefully acknowledged.

Polarization in High-Energy *p-n-n* Double Scattering*

PETER HILLMAN,† VAUGHN CULLER, AND N. F. RAMSEY
Harvard University, Cambridge, Massachusetts

(Received April 8, 1954)

An exploratory polarization experiment on the double scattering of high-energy neutrons has been performed. A 100-Mev proton beam gives exchange neutrons in the first scattering, and these neutrons are rescattered and counted. Two high-efficiency liquid scintillation counters are used to detect the neutrons, which have an average effective counted energy of about 45 Mev. Various combinations of scatterers were used. In all cases the asymmetry 2ϵ was less than 6 percent.

I. INTRODUCTION

IN several recent experiments on the double scattering of high-energy nucleons, the second scattering cross section in certain cases showed a strong azimuthal asymmetry[1]; those experiments involving exchange scattering have, however, revealed only small effects.[2] The nonexchange experiments utilized proton beams scattered successively off various nuclei. In the exchange experiments, on the other hand, the first and second scatterings were (p,n) and (n,p) exchange reactions, respectively. In the present experiment, neutrons from (p,n) reactions in beryllium, carbon, and copper were scattered by carbon and copper nuclei and counted directly with high-efficiency liquid scintillation counters.

II. APPARATUS AND PROCEDURE

A sketch of the arrangement used is shown in Fig. 1. Normally, the first scatterer is placed in the 100-Mev internal proton beam of the Harvard synchrocyclotron. Exchange neutrons emerging at an angle of 30° to the incident proton beam are collimated to a width of about 2 in. before striking the 1½-in. diameter cylindrical second scatterers. Neutrons scattered by 30° in the plane of the incident proton beam are then counted.

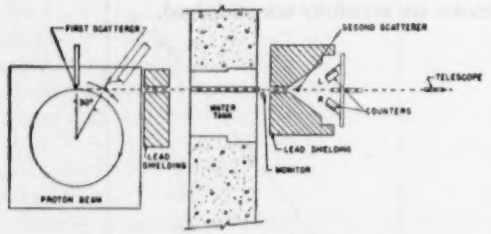

FIG. 1. Experimental arrangement.

Since it is in practice very difficult to insure the identical structure and symmetrical placement of the counters in the two directions (particularly considering the rapid change of cross section with scattering angle), the two counters are mounted on a rigid structure, sketched in Fig. 2, and frequently rotated by 180° about the beam line. Each result is then compared only with that of the *same* counter in the opposite position. A fixed cathetometer visually aimed at the first scatterer through a flat Lucite window in the cyclotron vacuum tank is used to align all collimators and, after each "flip," the counter framework. Optical distortion by the window was checked to be negligible.

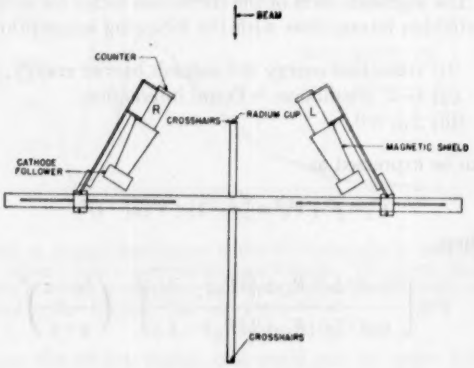

FIG. 2. Counter framework.

Each counter consists of a terphenyl-in-xylene scintillator solution[3] 8 in. long and 1½ in. in diameter held in direct contact with an RCA 5819 photomultiplier in a polished aluminum container.[4] The counters are protected from changes of gain due to the effect of earth and cyclotron magnetic fields on the photomultipliers by mu-metal shields. Gain stability is also insured directly by placing a one-millicurie radium source in a niche in the counter framework and resetting each counter to a given counting rate before each cycle. The gain was checked at the end of each cycle, and considering the much greater pulse-height slope of the radium counts, as compared with the neutron

* This work was assisted by the joint program of the U. S. Office of Naval Research and the U. S. Atomic Energy Commission.

† Now at Atomic Energy Research Establishment, Harwell, England.

[1] Oxley, Cartwright, and Rouvina, Phys. Rev. **93**, 806 (1954); Proceedings of the Fourth Annual Rochester Conference on High-Energy Nuclear Physics (preliminary version), University of Rochester, 1954 (to be published).

[2] J. M. Dickson and D. C. Salter, Proc. Phys. Soc. (London) **A66**, 721 (1953); L. F. Wouters, Phys. Rev. **84**, 1069 (1951); Rochester Conference Proceedings (see reference 1).

[3] H. Kallmann and M. Furst, Phys. Rev. **79**, 857 (1950).

[4] Hillman, Stahl, and Ramsey, Phys. Rev. (to be published).

counts, was found to remain satisfactorily steady. The pulses are fed into a cathode follower which drives some 200 feet of RG62U cable leading to the cyclotron control room. They are then fed through an Atomic Instrument Company linear amplifier (Model 204) into an Atomic Scale of 64 (Model 101-A) where they are discriminated, scaled, and fed into a register. A monitor consisting of a 3-crystal proton telescope with a polyethylene radiator is placed in front of the second scatterer to normalize counting rates to beam strength.

Lead shielding was carefully piled symmetrically to avoid spurious radium normalization or counting effects from backscattering, and care was taken to insure symmetrical alignment of all apparatus. Two direct checks on the geometry were also made. First, a run was made using a 0° (p,n) reaction (see Fig. 1), which must yield unpolarized neutrons, as a first scattering. Second, the variations in the left-right ratios with lateral motion of the second scatterers, the 0° first scatterer, and the 30° first scatterers were roughly measured and used to estimate geometrical errors.

TABLE I. Typical data sheet.

Run No.	First scatt.	Second scatt.	Length of run, min	Counts Counter 1 (right)	Counts Counter 2 (left)	Monitor
1	Radium norm.		1	3472	3545	...
2	C 30°	C	15	4003	4288	4837
3	C 30°	Empty	15	1361	1471	4654
4	C 30°	Cu	15	3793	4047	4511
5	C 30°	Cu	15	3788	4111	4676
6	C 30°	Empty	15	1291	1348	4317
7	C 30°	C	15	4227	4601	5293
8	Radium check		1	3655	3686	...
9	Noise		5	93	111	0

The detected energy and composition of the secondary beam were roughly checked by finding the effects of interposed carbon and lead attenuators. The beam was confirmed to consist largely of neutrons, with an average energy of about 60 Mev. The average effective counted energy of the tertiary beam was estimated to be about 45 Mev.

III. CALCULATIONS AND RESULTS

A typical raw data sheet for one "cycle" is shown in Table I. A complete "run" for each pair of scatterers comprises four such cycles with 180° azimuthal flips after cycles 1 and 3. Noise counts are first subtracted from all readings, which are then normalized to the monitor readings. Background is then subtracted to give the true counting rate per monitor count. Dead-time losses are negligible.

TABLE II. Values of $2e$ for various scatterer combinations. The second scattering angle was 30° in all cases.

First scatterer	First scattering angle	Second scatterer	$2e$(%)
Be	0°	C	4 ±3½
		Cu	2 ±3½
Be	30°	C	5 ±4
		Cu	0 ±3½
C	30°	C	2 ±4½
		Cu	−1½±4½
Cu	30°	C	4 ±4½
		Cu	1 ±4

The values of the quantity[5] $2e$ for each counter for each pair of scatterers are computed from the averages of cycles 1 and 4, and 2 and 3. Results obtained with the two counters and on two separate occasions agreed satisfactorily, and the final averages are given in Table II.

Errors in $2e$ arise from (1) counting statistics, including random counter drift, amounting to 1½ to 2½ percent; (2) positioning of the scatterers, estimated at about ½ percent for the first scatterer and 2 percent for the second; and (3) counter nonrigidity and misalignment, about ½ percent. The errors given in Table II are then the total estimated mean errors.

It is concluded that polarization effects, if present, are small. The significance of the fact that the values for the carbon second scatterer are in all cases slightly higher than for the copper is not known. The smallness of the effects may be ascribed to one or more of the following: (1) the choice of scattering angles; (2) the large spread of neutron energies, and hence of types of collisions involved; and (3) the possibility that n-n and/or exchange scatterings at our energies are weakly polarizing, particularly considering the probable decrease of polarization effects at lower energies and the apparent smallness of the exchange polarization even at higher energies.[1] Further experiments on polarization effects with various particle combinations are now in progress at this Laboratory.

We would like to acknowledge with thanks the aid of Mr. R. H. Stahl, whose kind assistance was greatly appreciated; of Mr. Paul F. Cooper, Jr., who did valiant night duty in running the experiment; and of the cyclotron staff and operating crew.

[5] $2e$ is defined as $(R-L)/\frac{1}{2}(R+L)$, where R and L are the true normalized right and left counting rates with right and left as indicated in the figures.

Fine Structure in the $C^{12}(\gamma,n)C^{11}$ and $O^{16}(\gamma,n)O^{15}$ Activation Curves

L. KATZ, R. N. H. HASLAM, R. J. HORSLEY, A. G. W. CAMERON, AND R. MONTALBETTI
Department of Physics, University of Saskatchewan, Saskatoon, Canada

(Received April 7, 1954)

A careful examination of the $C^{12}(\gamma,n)C^{11}$ and $O^{16}(\gamma,n)O^{15}$ reactions, resulting from irradiating samples with betatron bremsstrahlung, has revealed discontinuities in the yields as a function of peak bremsstrahlung energy. These discontinuities are interpreted to indicate the presence of strong photon absorption levels in the C^{12} and O^{16} nuclei. In C^{12} the discontinuities were found at 19.3, 19.8, 20.1, 20.5, 20.7, 21.1, 21.6, 22.4, and 22.8 Mev, and in O^{16} they were found at 15.9, 16.4, 16.7, 16.9, 17.1, 18.9, 19.3, 20.7, and 21.9 Mev. The experimental results are discussed in detail and are interpreted qualitatively.

INTRODUCTION

THE work grew out of a calibration of the energy scale of the University of Saskatchewan 25-Mev betatron, following a modification in the integrator-expander circuit of this machine[1] early in 1952. It happened that more points were taken at smaller energy intervals near the threshold of the $O^{16}(\gamma,n)O^{15}$ reaction than had been the previous practice. Several well-defined discontinuities in slope were found in a plot of the induced O^{15}, 2.0-minute positron activity against betatron operating energy.

Further work has shown that the energies at which these discontinuities ("breaks") occur are reproducible to within experimental accuracy. Early measurements showed that the first four breaks of the $O^{16}(\gamma,n)O^{15}$ activation curve were reproducible under varying experimental conditions. Five separate experiments involving such changes as reference voltage in the integrator expander and helipot potentiometer gave reproducible results.[2] Since then further breaks have been found at higher energies in the $O^{16}(\gamma,n)O^{15}$ reaction. Breaks have also been found in the $C^{12}(\gamma,n)C^{11}$ activation curve and in similar curves for other light elements in the region up to calcium. They have not been resolved in elements as heavy as copper. In the light elements they have been found in experiments in which the residual activity was measured as well as in experiments in which the neutrons resulting from the reaction were detected. It has been shown that the "break" energies are not functions of the instrumentation of the betatron. In this paper the work on the $C^{12}(\gamma,n)C^{11}$ and $O^{16}(\gamma,n)O^{15}$ reactions will be reported since these two reactions are the most extensively investigated to date. Other reactions are reported in the accompanying paper.

The breaks in our activation curves are apparently of the same nature as those found by Miller and Waldman[3] in the excitation of low-energy levels in indium by x-rays. The straight line portions observed by those workers in their activation curves were interpreted by Guth[4] in terms of thick-target spectra. The implications of similar straight line portions in our results are not yet clearly understood. We believe the breaks indicate that in the light nuclei photon absorption takes place, at least in part, into well-defined nuclear levels of the target nucleus. It is suspected that the "line" absorption indicated by the breaks is superimposed on a continuum of absorption which constitutes the experimentally well-established "giant-resonance."

EXPERIMENTAL TECHNIQUE

The basic experiment consists of the irradiation of a number of samples at various betatron energies. However, to establish the fine structure it is necessary that the activities induced in the various samples be determined very accurately relative to one another and that the energies of the irradiation be held steady to within a few kiloelectron volts.

For the oxygen activation curve cylindrical samples of boric acid ($H_2B_4O_7$) were used. These were formed by compressing the boric acid powder without binder, under a pressure of about 7 ton/in.[2] The cylinders were about 5 cm long, 2.2-cm inside and 4.0-cm outside diameter. The carbon samples were cut from polystyrene tubes 2.6-cm outside diameter and 2-mm wall thickness. They were 7.5 cm long.

The samples were counted with Victoreen IB85 cylindrical Geiger counters, over which they had been designed to fit with a slight clearance. Usually two setups were used with the oxygen samples and up to four with the carbon samples. These were intercalibrated by moving a sample among them as its activity decayed.

The samples were irradiated in the betatron beam with the cylindrical axis parallel to the beam. Each sample was given a definite irradiation dose as measured by an ionization chamber whose output was integrated. The time of irradiation for each sample was carefully measured.

The activity induced in the oxygen samples (O^{15}) has a half-life of 2.0 minutes. The counting started one minute after the end of irradiation and continued for four minutes. In the case of carbon samples the

[1] Katz, McNamara, Forsyth, Haslam, and Johns, Can. J. Research A28, 93 (1950).
[2] Haslam, Katz, Horsley, Cameron, and Montalbetti, Phys. Rev. 87, 196 (1952).
[3] W. C. Miller and B. Waldman, Phys. Rev. 75, 425 (1949).
[4] E. Guth, Phys. Rev. 59, 325 (1941).

induced activity (C^{11}) has a half-life of 20.5 minutes. The counting of these started 10 minutes after the end of irradiation and continued for 10 minutes. The total number of counts which were recorded in each of these periods (less tube background) when corrected for irradiation time was taken as representing the activity induced in the samples.

Care was taken during each irradiation to hold the dose rate from the betatron constant. However, the dose rate varies by a factor of ten as the betatron operating energy is changed by a factor of two. Thus, the irradiation time t_R required to give a definite dose of irradiation Q to the samples at different energies varied. The average photon flux incident on a sample in a given irradiation is Q/t_R. Thus, the recorded number of counts were corrected to unit dose rate (arbitrary) and to saturation by multiplying each reading by $t_R/[1-\exp(-\lambda t_R)]$.

BETATRON ENERGY STABILITY

Experience has shown that an instability in the operating energy of the betatron of 40 to 50 kev will cause the experimental points to scatter so badly that all but the strongest breaks in the activation curve will be smeared out. It has been found that under favorable operating conditions the stability of the betatron energy is better than ±5 kev. In our early work on the fine structure in activation curves, these good operating conditions were erratically obtained, and it was often necessary to check the stability by the method outlined below. Recently, however, the factors limiting the betatron stability have in the main been delineated and improved, and it is now possible to obtain satisfactory measurements at any time.

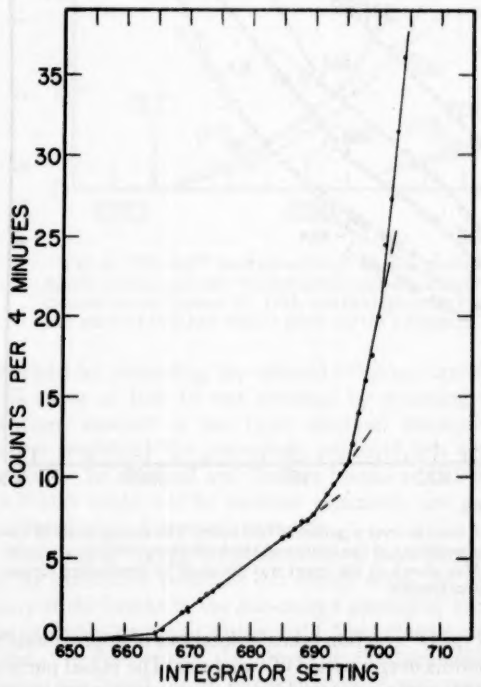

FIG. 1. $O^{16}(\gamma,n)O^{15}$. Oxygen activation curve near threshold. The fast-rising portion of this curve has a slope corresponding to an increase of 5 percent in counting rate per 10-kev change in peak bremsstrahlung energy.

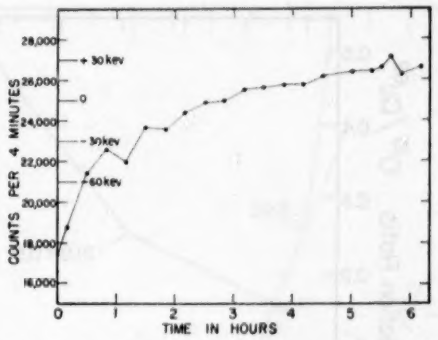

FIG. 2. Betatron energy stability. After the initial warmup period, the peak bremsstrahlung energy remained constant to ±5 kev, except for the slow drift, over a period of a few hours.

A part of the oxygen activation curve near threshold is reproduced in Fig. 1. In this region the induced activity is a strong function of the betatron operating energy. It is possible to choose a point on this curve for monitoring the betatron energy which is sufficiently far from threshold to give good counting statistics and yet show an increase of five percent in activity for a change of 10 kev in energy. The results of one of our early experiments to measure betatron stability are shown in Fig. 2. The boric acid samples were irradiated at constant energy setting and were given the same irradiation dose. The initial rising portion of the curve is interpreted as a drift in operating energy resulting from warming up of the betatron magnet or a drift of the reference voltage of the integrator-expander circuit. After this initial period the energy remained constant to within ±5 kev (2 percent change in counting rate or about 500 counts). The slow residual energy drift is easy to detect[5] and to correct for.

EXPERIMENTAL RESULTS

The earliest sets of measurements of the oxygen and carbon activities usually extend over relatively small energy intervals owing to the tendency of the betatron to lose its good energy stability after a few hours of running time. Also, on different days there was a tendency for the "zero point" of the energy scale to shift slightly with respect to the setting of the integrator helipot. For these reasons, the usual technique in a given set of measurements was to remeasure the energy position of a previously known break and then to measure as much more of the activation curve as

[5] Robinson, McPherson, Greenberg, Katz, and Haslam (to be published).

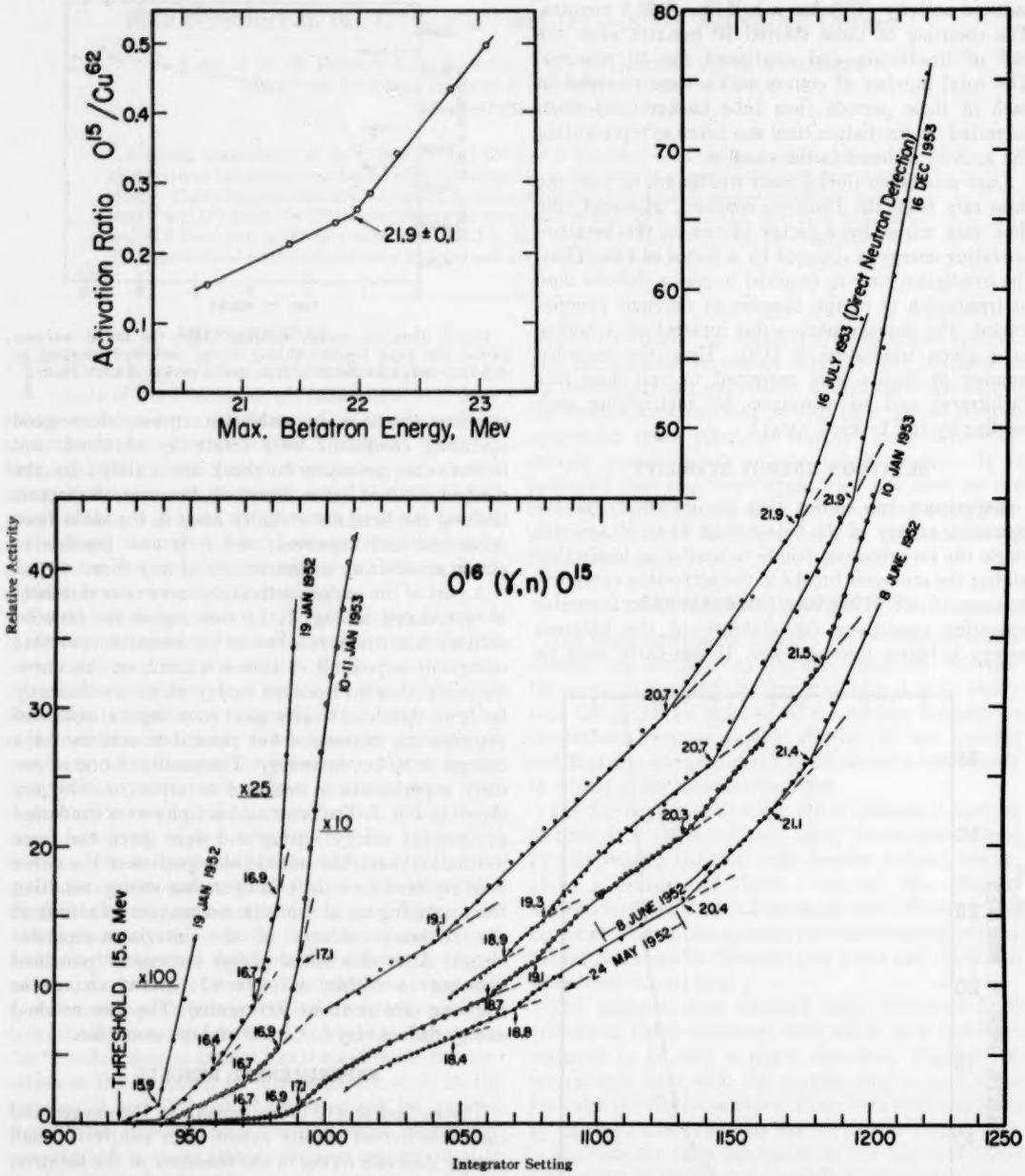

FIG. 3. Oxygen activation curves taken at intervals of approximately 6 months over a period of two years. The energy scale of the betatron was established most reliably in the latter part of 1953 and the positions of the breaks in the high-energy region are to be taken from the curves of July and December, 1953. The break at 21.9 Mev shown in the insert was obtained by irradiating copper and oxygen samples simultaneously and plotting the ratio of the induced activities.

possible before the betatron became unstable. Thus, in order to build up a composite activation curve from the early measurements, it has been necessary to normalize these separate runs both in energy and intensity.

In Fig. 3, we show representative curves of the $O^{16}(\gamma,n)O^{15}$ reaction taken at intervals of approximately 6 months over a period of two years. The initial portion of the curve was established with great care in our early measurements, and only the curves taken on January 19, 1952, and January 10, 1953, are shown. All the curves except the one of July 16, 1953, were

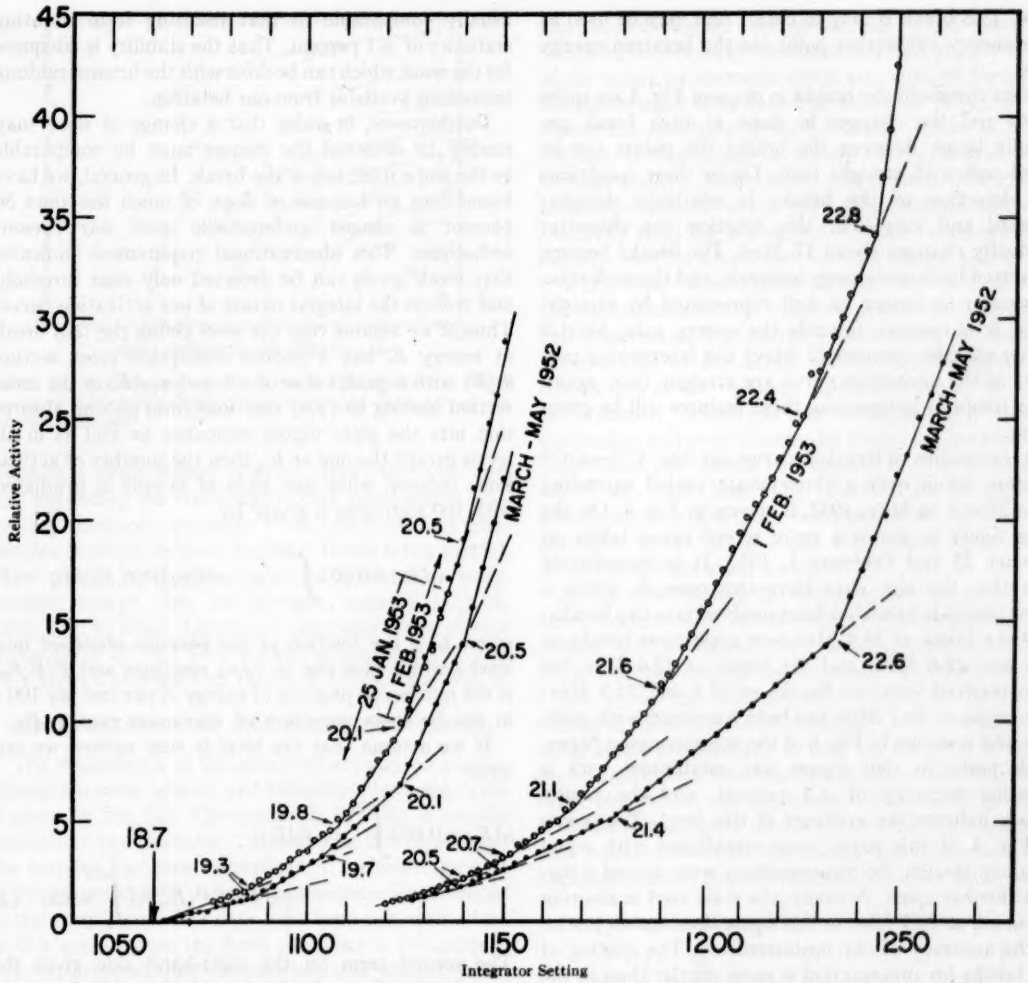

FIG. 4. $C^{12}(\gamma,n)C^{11}$ residual activity. Carbon activation curves. The early set of measurements extended over a two-month period, and only the composite curve is shown. The low-energy region of the newer curve was taken in one continuous run on January 25, 1953, and the high-energy portion on Februrary 1. In two cases a single level in the older curve was resolved into two weaker levels by the Februrary 1 measurements.

obtained by measuring the induced O^{15} β-ray activity. The curve of July 16 was obtained by detecting the neutrons emitted in the (γ,n) reaction. Because of poorer sensitivity the low-energy region of this curve could not be obtained and the two breaks at 18.9 and 19.3 Mev could not be resolved separately but gave one break at an intermediate energy.

Since the $O^{16}(\gamma,n)O^{15}$ threshold has always been one of the calibration points on our energy scale, the positions of the breaks in the low-energy portion of Fig. 3 are probably known to within ± 0.1 Mev. On the other hand, the positions of the breaks in the high-energy region are based on an extrapolation of our energy scale and are thus not known nearly as accurately —certainly not better than ± 0.2 Mev. The data of December 16, 1953, are the most reliable; the older curves are included only to emphasize the reproducibility of the general features of these curves.

The most serious discrepancy in our measurements occurred in a level which the early work placed at 21.5 Mev but which more recent curves show at 21.9 Mev. This particular level has been studied in great detail using our most recent techniques for establishing an accurate betatron energy scale.[5] In one of the experiments copper and oxygen (boric acid) samples were irradiated simultaneously, then counted alternately with the same G.M. counter. The ratio of the induced O^{15} to Cu^{62} activities resulting from the (γ,n) reactions is shown in the insert of Fig. 3. Each point on the curve represents a total of about 20 000 counts for the oxygen sample and 50 000 counts for the copper sample. The break thus established was found to be at 21.9 ± 0.1

Mev. This break is easy to detect and may be used as a secondary calibration point for the betatron energy scale.

Near threshold the breaks in slope of Fig. 3 are quite sharp and the changes in slope at each break are usually large. Between the breaks the points can be fitted well with straight lines. Under these conditions the detection of the breaks is relatively straightforward and easy. For this reaction the character gradually changes above 17 Mev. The breaks become separated by larger energy intervals, and the activation curve can no longer be well represented by straight lines: it is concave towards the energy axis. At still higher energies (around 21 Mev) the intervening portions of the activation curve are straight once again. An attempt at interpreting these features will be given below.

A composite activation curve for the $C^{12}(\gamma,n)C^{11}$ reaction taken over a three-month period extending from March to May, 1952, is shown in Fig. 4. On the same figure is shown a more recent curve taken on January 25 and February 1, 1953. It is immediately seen that the new data have two cases in which a single previous break has been resolved into two breaks; thus the break at 21.4 Mev now appears as breaks at 21.1 and 21.6 Mev, and the break at 22.6 Mev has been resolved into two breaks at 22.4 and 22.8 Mev. The break at 20.7 Mev has been examined with great care and is shown in Fig. 6 of the accompanying paper. Each point in that figure was established with a counting accuracy of ± 1 percent, and the results clearly indicate the existence of this level. The points in Fig. 4 of this paper were established with equal accuracy though the measurements were spaced somewhat further apart. Actually, the scale used in showing the break at 20.7 Mev in this figure does not do justice to the accuracy of our measurements. The spacing of the breaks for this reaction is more regular than in the case of oxygen, and there is no pronounced concavity towards the energy axis.

DISCUSSION OF RESULTS

It is difficult to estimate the resolving power of this method for detecting a true discontinuity of slope. There will be some scattering of the points on the activation curve owing to energy instability of the betatron and to the finite number of counts which are taken. We estimate that other causes of scattering, such as variations in dose delivered to the sample, differences in samples, or irradiation geometries are negligible compared to the two causes mentioned above. The effect of most of such scattering is to change the appearance of the activation curve from a series of straight segments to a continuous curve. Our experience has shown that an energy instability of ± 50 kev in the energy is sufficient to destroy the evidence for most of the breaks reported here. However, the scattering resulting from an energy instability of ± 5 kev is usually comparable to that resulting from counting statistics of ± 1 percent. Thus the stability is adequate for the work which can be done with the bremsstrahlung intensities available from our betatron.

Furthermore, in order that a change of slope may readily be detected the change must be comparable to the slope itself below the break. In general, we have found that an increase of slope of much less than 50 percent is almost undetectable with our present techniques. This observational requirement indicates that weak levels can be detected only near threshold and reflects the integral nature of our activation curve. Thus, if we assume that the level giving rise to a break at energy E_i has a photon absorption cross section $\sigma_i(E)$ with a peak value of σ_i^0, and $\sigma_{\gamma n}(E)$ is the cross section leading to (γ,n) reactions from photon absorption into the giant dipole resonance as well as in all levels except the one at E_i, then the number of activations induced when one mole of sample is irradiated with 100 roentgens is given[6] by

$$\alpha(E_0)=0.602\int_0^{E_0}[\sigma_{\gamma,n}+G\sigma_i]P(E,E_0)dE, \quad (1)$$

where G is the fraction of the photons absorbed into level i which give rise to (γ,n) reactions and $P(E,E_0)$ is the number of photons of energy E per cm^2 per 100 r in the betatron spectrum of maximum energy E_0.

If we assume that the level is very narrow we can write

$$\alpha(E_0)=0.602\int_0^{E_0}\sigma_{\gamma n}PdE + 0.602GP(E_i,E_0)\int_0^{E_0}\sigma_i dE. \quad (2)$$

The second term on the right-hand side gives the contribution from the level, and thus the change in slope at E_i is proportional to

$$GP(E_i,E_0)\int_0^{E_0}\sigma_i dE \Big/ \int_0^{E_0}\sigma_{\gamma n}PdE. \quad (3)$$

The fact that breaks are seen up to over 7 Mev above threshold shows that there are levels at these higher energies which involve an integrated cross section comparable to the total integrated cross section up to that energy.

An additional limitation on the resolving power of the method comes from the spacing of the breaks themselves. It requires at least three points to indicate the linearity of a portion of the activation curve. For a convincing demonstration there should be many more points than this on the linear portion. The natural scattering of the points about such a line makes it difficult to establish either the linearity or the

[6] L. Katz and A. G. W. Cameron, Can. J. Phys. **29**, 518 (1951).

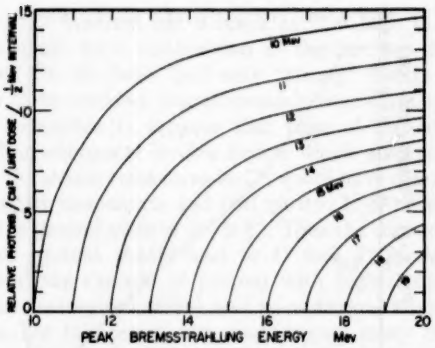

FIG. 5. Isochromats obtained from the theoretical Schiff spectrum shape normalized to unit integrated current from the ion chamber used.

slope of a small energy interval (less than ~50 kve, but depending on conditions). One particularly misleading situation can occur when two breaks of comparable strength lie close together. If one is not careful, these will be measured as a single break at an intermediate energy. See, for example, data of July 16, 1953, Fig. 3, which because of poor sensitivity gave a single break at 19.1 Mev instead of levels at 18.9 and 19.3 Mev. There are also two such examples in Fig. 4.

INTERPRETATION OF THE ACTIVATION CURVES

The dependence of the observed activity on photon absorption cross section and bremsstrahlung spectrum is given by Eq. (1). The spectrum $P(E,E_0)$ is usually normalized per "roentgen." However in this experiment the activity has been normalized to an arbitrary unit of integrated current from a transmission ion chamber in the x-ray beam. The data have been left normalized in this way because the doses delivered to the samples were very reproducible when the betatron was controlled by the integrated reading of the ion chamber.

For the purpose of analyzing the principle features of the photonuclear activation curves obtained here, it would be useful to have plots of the isochromats for the spectrum $P(E_i,E_0)$. That is $P(E_i,E_0)$ is plotted as a function of E_0 for given values of E_i, with the photon numbers properly normalized to unit integrated current of the ion chamber. Since our analysis is intended to reveal the fine structure in the photon absorption cross section, the shape of the isochromats near the upper end of the bremsstrahlung spectrum are of particular interest. This is immediately evident from Eq. (3).

To date there are no reliable data on the shape of the bremsstrahlung spectrum near its upper end for a betatron operated with the thick target as supplied by the Allis Chalmers Company and under the conditions of orbit expansion usually used. This spectrum will differ from that predicted theoretically because of energy loss within the thick target by the radiating electron, secondary bremsstrahlung from electrons which have previously radiated, and multiple traversals of the target by electrons which are captured back into the stable orbit after an initial traversal. A plot of the theoretical spectrum given by Schiff[7] shows it to be concave to the energy axis near its upper end[8] with perhaps a slight discontinuity at the peak. The above-mentioned effects would tend to straighten out this concavity resulting in a spectrum which decreases more linearly near its upper end with increasing energy.[8]

With these observations in mind we have plotted the isochromats in Fig. 5 making use of the theoretical Schiff spectrum. The curves were obtained by making a cross plot of the Schiff spectrum tables given in Appendix I of the "photon difference" paper by Katz and Cameron,[6] which has been multiplied by a varying conversion factor to change the basis of normalization from "roentgen" to the ion chamber integrated current which was used here. The effect of the changes in bremsstrahlung spectrum outlined above on the isochromats would be to make them more linear with energy near their lower ends.

Let us now consider the appearance of the activation curve which would result from a photonuclear cross section which consisted only of fairly widely spaced discrete levels. A set of such assumed levels is shown in Fig. 6(a). In Fig. 6(b) the isochromats of the bremsstrahlung spectrum corresponding to the energies of these levels are plotted, as well as the sum of these isochromats. This sum would constitute the activation curve observed in an experiment. The resulting shape of the activation curve consists of a number of segments, each concave towards the energy axis, separated by discontinuities of slope. This appearance is reminiscent

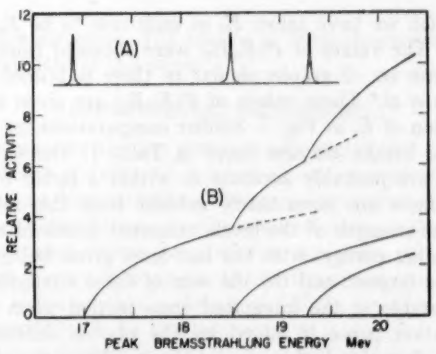

FIG. 6. Schematic representation to show how narrow levels and the isochromats can give rise to discontinuities in the activation curve.

[7] L. I. Schiff, Phys. Rev. **83**, 252 (1951).

[8] It is of interest to note that all the measurement of spectrum shape to date [H. W. Koch and R. E. Carter, Phys. Rev. **77**, 165 (1950); K. Phillips, Proc. Phys. Soc. (London) **A65**, 57 (1952); and Motz, Moller, and Wychoff, Phys. Rev. **89**, 968 (1953)] can be fitted with a straight line in the upper energy region to within experimental accuracy. This region extends over about the upper ⅓ of the curve.

of the shape of the $O^{16}(\gamma,n)O^{15}$ activation curve at intermediate energies. A straightening of the isochromats in their initial portion for reasons outlined above, followed by a curved portion, may well give rise to the observed activation curves.

Equation (2) may be used to calculate the approximate value of $\int\sigma_i dE$ at each break. The first term on the right-hand side of this equation represents the activation curve without the contribution from the level at E_i and may be expected to lie at energies $E_0>E_i$ along the extrapolation of the curve. The second term on the right-hand side thus represents the distance between the extrapolated and measured curves. Let this distance be $\Delta\alpha(E_0)$; then from (2) we find

$$G\int_0^{E_0}\sigma_i dE=\frac{\Delta\alpha(E_0)}{0.602P(E_i,E_0)}. \quad (4)$$

Values of this integral at the various breaks in the oxygen curve are given in Table I. For ease of com-

TABLE I. Integrated cross sections under the breaks.

Carbon		Oxygen	
E_i Mev	$G\int\sigma_i dE$ Mev-barn	E_i Mev	$G\int\sigma_i dE$ Mev-barn
19.3	0.23×10^{-3}	15.9	0.06×10^{-3}
19.8	0.66	16.4	0.05
20.1	1.2	16.7	0.18
20.5	1.4	16.9	0.95
20.7	2.0	17.1	0.80
21.1	5.2	18.9	0.66
21.6	5.8	19.3	1.5
22.4	5.5	20.7	2.1
22.8	33.0	21.9	7.5
	0.055 Mev-barn		0.014 Mev-barn

putation we have taken E_0 in each case to be $E_i+\frac{1}{2}$ Mev. The values of $P(E_i,E_0)$ were obtained from an accurate set of graphs similar to those published by Johns *et al.*[9] These values of $P(E_i,E_0)$ are given as a function of E_i in Fig. 7. Similar computations for the carbon breaks are also listed in Table I. The values listed are probably accurate to within a factor of 2. Two facts are immediately evident from this table: (a) the strength of the levels measured increases with increasing energy, with the last level given being by far the largest; and (b) the sum of these strengths is comparable to the integrated cross section when the activation curve is solved by the photon difference method[6] as if it had no fine structure. Thus, the most recent value of $\int_0^{24}\sigma_{\gamma n}dE$ for carbon given by Montalbetti *et al.*[10] is 0.029 Mev-barn and $\int_0^{22}\sigma_{\gamma n}dE$ for oxygen is 0.015 Mev-barn. These values are to be compared to 0.055 and 0.014 Mev-barn, respectively, from Table I. These results would imply that a substantial fraction of the $O^{16}(\gamma,n)O^{15}$ and $C^{12}(\gamma,n)C^{11}$

[9] Johns, Katz, Douglas, and Haslem, Phys. Rev. 86, 1062 (1950).
[10] Montalbetti, Katz, and Goldemberg, Phys. Rev. 91, 659 (1953).

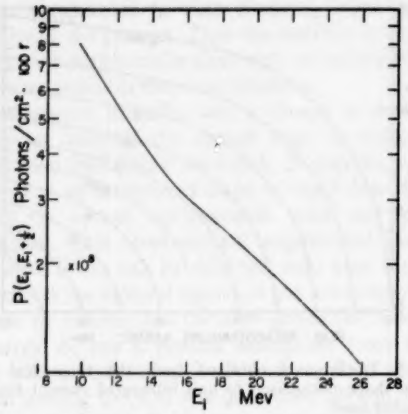

FIG. 7. Number of photons at the indicated energy per cm² per 100 r of irradiation, if the peak bremsstrahlung energy is ½ Mev higher than the indicated energy.

reaction cross section takes place by photon absorption into nuclear levels which are located at the energies of the breaks in the activation curves.

In Fig. 8 we have plotted the cross-section curve for the $O^{16}(\gamma,n)O^{15}$ reaction previously published[10] and have superposed on it our activation curve showing the positions of the levels and their relative strengths for comparison.

It would be desirable to check the existence of the resonances found here by some independent method. Unfortunately the excitation energies involved are so high that very little work has been done in this energy region with other kinds of bombarding particles. In a study of the reaction $B^{11}(p,n)C^{11}$, Blaser *et al.*[11] have found excitation energies of 19.4, 20.7, 21.4, and 21.8 Mev in the compound nucleus C^{12}. The first two of these agree well with the break positions found for

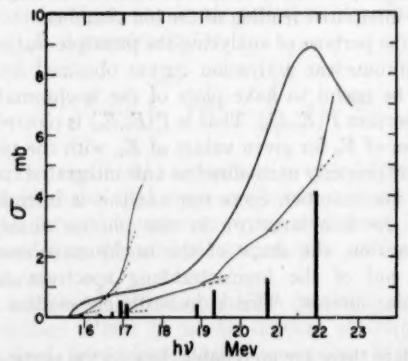

FIG. 8. $O^{16}(\gamma,n)$. Gamma-neutron cross section in O^{16} obtained from the activation curve using the photon difference method of analysis. Superposed on this cross section is the activation curve showing the positions of the breaks and a series of lines representing the relative integrated area under the corresponding breaks as listed in Table I.

[11] Blaser, Boehm, Marimier, and Scherrer, Helv. Phys. Acta 24, 30 (1951).

$C^{12}(\gamma,n)C^{11}$ reaction but a break at 21.6 Mev in our curve might be a combination of the last two resonances. On the basis that only "strong" breaks are likely to be resolved (except possibly near threshold), it is reasonable to suppose that most of the corresponding resonances involve electric dipole absorption. Thus the strong resonances in C^{12} would have one unit of angular momentum and odd parity. It is believed that the ground state of B^{11} is $\frac{3}{2}^-$. Thus the capture of *S*-wave protons should lead to 1^- and 2^- levels in C^{12}, and the capture of protons with higher orbital angular momentum would lead to additional kinds of states. For this reason one would expect many more resonances to be found in the $B^{11}(p,n)C^{11}$ reaction than in the $C^{12}(\gamma,n)C^{11}$ reaction. The fact that the opposite is true is somewhat disturbing, but Blaser *et al.* did not have high-energy resolution for their protons, and it is possible that they missed many resonances.

Goward and Wilkins[12] have examined the $C^{12}(\gamma,3\alpha)$ and $O^{16}(\gamma,4\alpha)$ reactions using nuclear plates and have found fine structure in the cross sections for these reactions. In the $C^{12}(\gamma,3\alpha)$ reaction they found cross section peaks at 19.6, 20.7, 21.9, 23.1, and 24.3 Mev [as well as some below our (γ,n) threshold]. They were not able to resolve any levels in the oxygen reaction over the energy region covered by our experiments. It is difficult to estimate the accuracy to which the positions of these C^{12} levels have been determined. The authors state that their resolution was probably of the order of 1 Mev, and possibly for this reason our results indicate about twice as many levels in the same energy range.

[12] F. K. Goward and J. J. Wilkins, Atomic Energy Research Establishment Report A.E.R.E. G/M 127 Harwell, Berks, England, March 24, 1952 (unpublished).

PHYSICAL REVIEW VOLUME 95, NUMBER 2 JULY 15, 1954

Fine Structure in the Neutron Yield Curves from (γ,n) Reactions in Li^7, C^{12}, O^{16}, and F^{19}

J. GOLDEMBERG* AND L. KATZ
Department of Physics, University of Saskatchewan, Saskatoon, Canada

(Received April 7, 1954)

Fine structure previously observed in the β^+ activation curves of C^{11} and O^{15} resulting from the betatron induced reactions $C^{12}(\gamma,n)C^{11}$ and $O^{16}(\gamma,n)O^{15}$ is shown to be present in the neutron yield curves from these reactions by detecting the emitted neutrons. The position of this fine structure as a function of betatron operating energy is the same in both cases to within experimental accuracy. The $Li^7(\gamma,n)Li^6$ and $F^{19}(\gamma,n)F^{18}$ were examined and discontinuities in the neutron yield curves were found at 9.6, 10.8, 12.4, 14.0, and 17.5 Mev for the first reaction and 11.0, 11.5, 11.9, and 15.3 for the second.

INTRODUCTION

IN the accompanying paper we report on the fine structure observed in the *activity* curves resulting from the $C^{12}(\gamma,n)C^{11}$ and $O^{16}(\gamma,n)O^{15}$ reactions induced by betatron irradiation. In those experiments the activity of the residual nuclei C^{11}(20.5 min) and O^{15}(2.0 min) are plotted as a function of maximum bremsstrahlung energy. Since the presence of fine structure in the curves was indicated by changes in slope, their real existence and precise location requires that they be reproduced under varying experimental conditions and with different measuring techniques. For this reason and because many of the light nuclei do not have convenient half-lives for measuring their residual activity an apparatus previously built for detecting neutrons emitted in (γ,n) reactions[1] was slightly modified to give a high counting rate for improved accuracy and neutron yields for a number of elements were examined for fine structure. The results of these measurements are reported in this paper.

EXPERIMENTAL TECHNIQUES

To measure the fine structure reported in this paper an energy stability of ± 5 kev in the control of the maximum bremsstrahlung energy is imperative during any one irradiation. A dispersion of over ± 30 kev, though not wiping out this fine structure, certainly makes it very difficult to detect. Recent experiments have indicated that a change of 1°C in the operating temperature of the betatron core, or a change in frequency of 0.15 cps in our 180-cps supply corresponds to an energy change of about 5 kev. All measurements reported were taken under conditions where we believe a stability of ± 5 kev was achieved.

A sketch of the experimental setup with all pertinent dimensions is shown in Fig. 1. The operation of this system has been previously described.[1] To obtain high counting rates two BF_3 counters were connected in parallel and large samples were used. Photon absorption in the samples does not alter the neutron yield curve

* Now at Departamento de Fisica, Faculdade de Filosofia, Ciencias e Letras, Universidade de Sao Paulo, Sao Paulo, Brazil, South America.

[1] Montalbetti, Katz, and Goldemberg, Phys. Rev. **91**, 659 (1953).

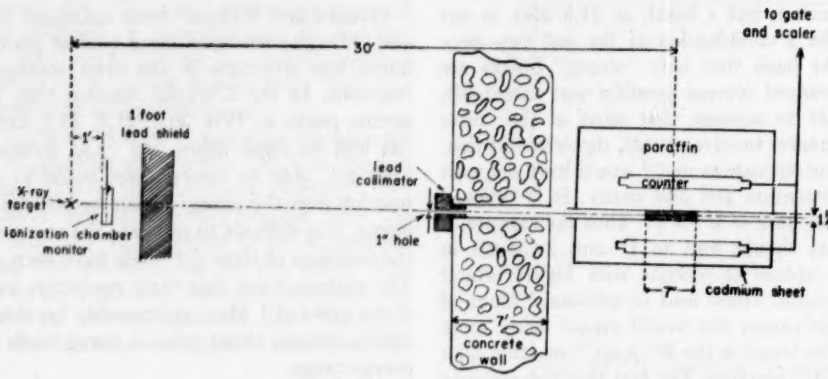

FIG. 1. Experimental arrangement.

shape, since at these energies the effective electronic absorption coefficients do not change appreciably with energy.[1] The background counting rate amounted at most to 1 percent of the number of recorded counts in an actual run.

Monitoring of the delivered dose was done with a flat chamber close to the betatron. Separate runs were also made with a monitor which subtended the same solid angle at the betatron target as the sample had under irradiation conditions. This convinced us that the presence of the observed fine structure was not the result of our monitoring procedure.[2]

RESULTS

The neutron yield curves for the reactions $Li^7(\gamma,n)Li^6$ and $F^{19}(\gamma,n)F^{18}$ are shown in Figs. 2 and 3. The discontinuities or "breaks" are clearly visible and the energies at which they occur are marked on the figures.

The results of these experiments are summarized in Table I. Taylor, Robinson, and Haslam[3] have examined the fine structure in the $F^{19}(\gamma,n)F^{18}$ activation curve by measuring the 1.87-hr F^{18} positron activity. Their results are also included in Table I. Since their method is more sensitive near threshold, they have been able to resolve two extra breaks at 10.6 and 11.2 Mev. They also found a level at 12.2 Mev which careful experiments failed to reveal in our work. This is particularly puzzling since this level is in an energy region where our neutron detection method has a sensitivity equal to the beta detection method.

In order to prove that the breaks were in no way dependent on our experimental technique or the characteristics of the betatron, measurements were repeated on the neutron yields for lithium and fluorine in the energy range from 13 to 15 Mev. These measurements were made on the same night when experimental conditions might be expected to have remained reasonably unchanged. Each curve was measured twice in two independent runs. The results are shown in Fig. 4. As expected from our previous results, it is apparent from this figure that a break occurs at 14 Mev in lithium but not in fluorine. This conclusion is substantiated in a more concise way through fitting straight lines by least squares to the points right and left of the arrow (Fig. 4).

The neutron yield curve for the $C^{12}(\gamma,n)C^{11}$ reaction is shown in Fig. 5. This reaction had been previously examined by detecting the positron activity from C^{11} and present results confirm those previously obtained, within the limitations of our method. Some of the levels were not found exactly in the same position, but this depends on the calibration of the betatron energy scale at the time of the experiment and variations of ± 0.1 Mev are certainly to be expected. A similar experiment on the neutron yield from the $O^{16}(\gamma,n)O^{15}$ reaction confirmed the breaks previously found by residual activity at 19.1, 20.7, and 21.9 Mev. The results of these measurements are shown in Fig. 3 of the preceding paper.

TABLE I. Positions of breaks in lithium and fluorine neutron yield curves and comparison with other data.

Lithium		Fluorine		
			$F^{19}(\gamma,n)F^{18}$	
$Li^7(\gamma,n)Li^6$ (Mev)	$Li^7(\gamma,\delta)He^4$ (Mev)	$O^{18}(p,n)F^{18}$ (Mev)	Present work (Mev)	Taylor *et al.*[a] (Mev)
9.6	9.6	10.59	—	10.6
10.8	—	10.84	—	—
12.4	—	10.99	11.0	10.9
14.0	~14	11.07	—	—
17.5	16.7	11.18	—	11.2
		11.27	—	—
		11.6	11.5	11.5
		12.0	11.9	11.9
		—	—	12.2
		12.8, 13.3, 13.8, 14.3	—	—
		—	15.3	15.3

[a] See reference 3.

[2] It has been found by some investigators (D. W. Kerst, private communication) that under certain conditions the γ-ray beam suffered a sudden change in its direction of emergence from the betatron. This change was related to the energy at which the betatron was operated. Such sudden displacement of the beam would result in a break in the activation curve if the monitor and sample were not in line with the betatron target even though each subtended the same angle at the target. In our case the breaks were reproducible under a variety of monitoring procedures.

[3] Taylor, Robinson, and Haslam, Can. J. Phys. **32**, 238 (1954).

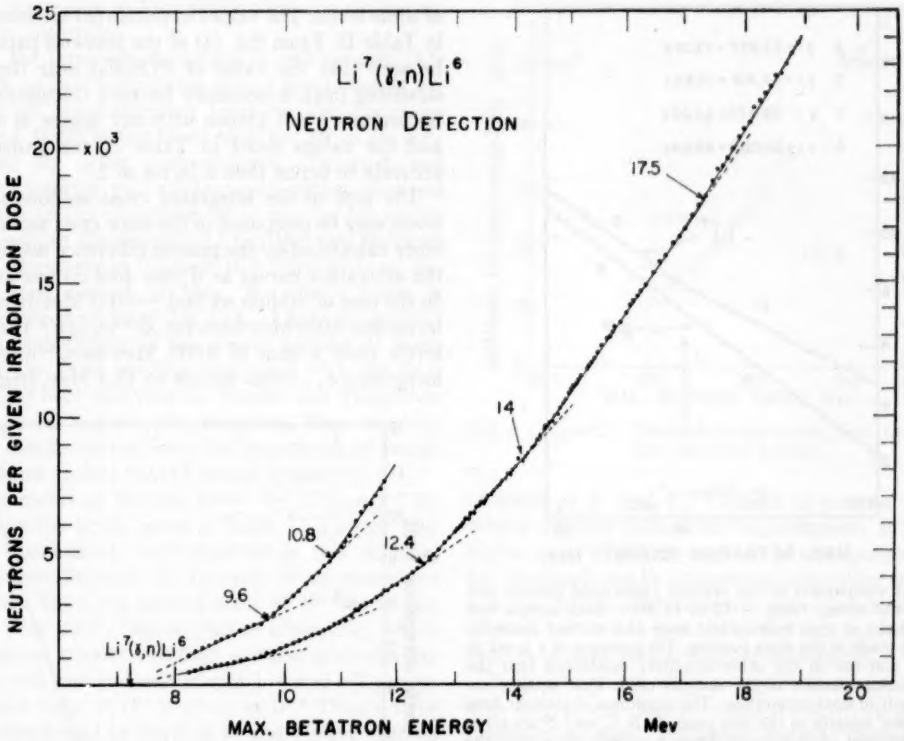

FIG. 2. Neutron yield curve of lithium showing the positions of the observed breaks. The break at 14 Mev is shown in Fig. 4 in greater detail.

A level found previously at 20.7 Mev in carbon has been carefully examined in steps of 11 kev, whereas usually steps of 44 kev are used. The results of this more detailed experiment are shown in Fig. 6 and by

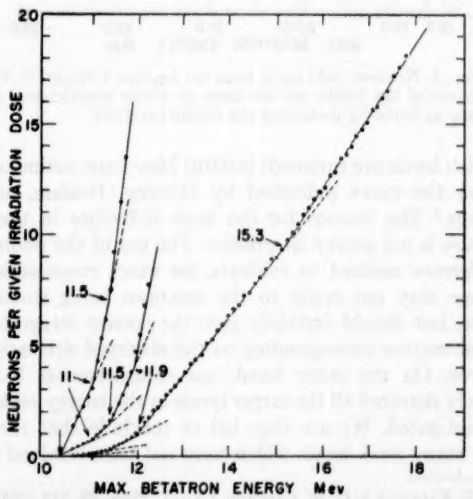

FIG. 3. Neutron yield curve of fluorine showing the positions of the observed breaks. The lower-energy region is shown on an enlarged scale.

themselves constitute strong evidence for the existence of "breaks" in neutron yield curves. The difficulty in fitting a smooth curve to the points is evident.

DISCUSSION

We interpret the breaks in these curves to indicate that nuclear photon absorption takes place, at least in part, into discrete levels in the target nuclei. The reason for this belief stems from the following considerations: the cross section for the nuclear reaction may be written as follows,

$$\sigma_{\gamma,n}=\sigma_c(\gamma)G(n),$$

where $\sigma_{\gamma,n}$ is the cross section for the (γ,n) reaction, $\sigma_c(\gamma)$ is the cross section for photon absorption, and $G(n)$ is the probability that a neutron will be emitted in preference to any other de-excitation process. The number of neutrons emitted during any betatron irradiation is given by the equation

$$\alpha(E_0)=\int_0^{E_0} P\sigma_{\gamma,n}dE=\int_0^{E_0} P\sigma_c(\gamma)G(n)dE,$$

where P is the number of photons of energy E incident on the sample per unit area when the betatron is operated at an energy E_0. The presence of fine structure

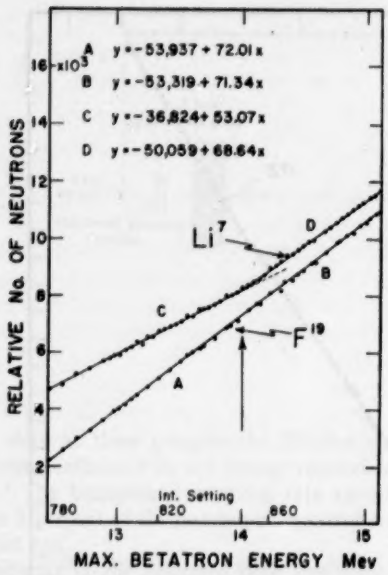

FIG. 4. A comparison of the neutron yields from fluorine and lithium in the energy range of 12 to 15 Mev. Each sample was measured twice in two independent runs and all four measurements were made in the same evening. The presence of a break in one curve and not in the other definitely establishes that the breaks are characteristic of the samples used. That is, they are not the result of instrumentation. The equations of straight lines fitted by least squares to the four parts *A*, *B*, *C*, and *D* are given in the upper part of this curve. These equations show that the slopes in *A* and *B* are the same, to within experimental accuracy, but are different in *C* and *D*.

in $\alpha(E_0)$ can thus be attributed to experimental technique or discontinuities in P, $\sigma_e(\gamma)$, or $G(n)$. The various experiments reported in this note eliminate any effect due to technique or P, and thus the observed breaks have their origin in either $\sigma_e(\gamma)$ or $G(n)$.

It is difficult to see how discontinuities in $G(n)$ can result in an increase in $\alpha(E_0)$ with energy. The usual picture is to visualize the outset of new competing processes with increasing energy, thereby causing a decrease in $\alpha(E_0)$. We are thus forced to conclude that the observed discontinuities imply fine structure in $\sigma_e(\gamma)$, that is, discrete photon absorption levels in the parent nucleus.

Applying the same type of analysis as in the case of C^{12} and O^{16}, it is possible to calculate the approximate integrated cross section $G\int\sigma_i dE$ associated with each of these levels. The values so calculated are summarized in Table II. From Eq. (4) of the previous paper it will be seen that the value of $P(E_i,E_0)$ near the bremsstrahlung peak is necessary for such calculations. This isochromat is not known with any degree of accuracy and the values listed in Table II are probably not accurate to better than a factor of 2.

TABLE II. Integrated cross section of the levels.

Lithium		Fluorine	
E_i (Mev)	$G\int\sigma_i dE$ (Mev-barn)	(Mev)	$G\int\sigma_i dE$ (Mev-barn)
9.6	0.2×10^{-3}	11.0	0.2×10^{-3}
10.8	0.3	11.5	0.3
12.4	0.7	19.5	0.9
14.0	0.6	15.3	0.5
17.5	0.8		1.9×10^{-3}
	2.6×10^{-3}		

The sum of the integrated cross sections for these levels may be compared to the same cross section previously calculated by the photon difference method[4] from the activation curves as if they had no fine structure. In the case of lithium we find ~0.003 Mev-barn for the levels and 0.020 Mev-barn for $\int_0^{17.5}\sigma_{\gamma,n}dE$.[5] The fluorine levels yield a sum of 0.002 Mev-barn,[5] whereas the integrated $\sigma_{\gamma,n}$ cross section to 15.5 Mev (region over

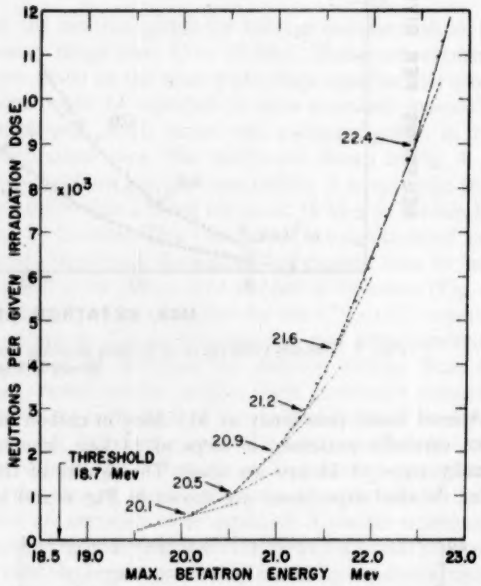

FIG. 5. Neutron yield curve from the reaction $C^{12}(\gamma,n)C^{11}$. The positions of the breaks are the same to within experimental accuracy as found by measuring the residual activity.

which levels are summed) is 0.010 Mev-barn, estimated from the curve published by Horsley, Haslam, and Johns.[6] The reasons for the large difference in these values is not known at present. The use of the photon difference method to evaluate the exact cross-section shape may not apply to the reactions being studied here, but should certainly give the correct integrated cross section corresponding to the observed activation curve. On the other hand, our measurements have surely detected all the larger levels in the energy region investigated. We are thus led to conclude that there are many weak levels which have not been resolved or

[4] L. Katz and A. G. W. Cameron, Can. J. Phys. **29**, 518 (1951).
[5] Contributions from the levels at 10.6 and 11.2 Mev found by Taylor *et al.* (see reference 3) have been included in this value.
[6] Horsley, Haslam, and Johns, Phys. Rev. **87**, 756 (1952).

that the levels observed are superposed on a continuum of photon absorption.

From the foregoing discussion, it will be seen that our work to date constitutes only a spectroscopic exploration of the absorption levels in the nuclei investigated. Some of the levels observed by us are substantiated by other measurements. Titterton and Brinkley,[7] working with photographic plates, obtained some levels in the absorption of γ rays by Li^7 nuclei. They measured the reaction $Li^7(\gamma,t)He^4$ and obtained levels at the energies 9.6 and 16.7 Mev with an unresolved level around 14 Mev. We obtain levels in lithium at the energies of 9.6, 10.8, 12.4, 14.0, and 17.5 Mev. The significance of the greater number of levels found in the (γ,n) reaction compared with the (γ,t) reaction has been analyzed by Peaslee and Telegdi[8] in the light of the isotopic spin formalism. They conclude that the measurements favor the hypothesis of charge independence against that of charge symmetry.

Measurements of fluorine using the $O^{18}(p,n)F^{18}$ reaction gave the levels listed in Table I.[9] Though considerably more levels were observed in this reaction, the agreement between the two sets of measurements is excellent. Since the ground state of F^{19} has a spin of $\frac{1}{2}$ and even parity, dipole photon absorption, which is the process usually assumed in these photonuclear reactions, will lead to levels of spin $\frac{1}{2}$, $\frac{3}{2}$ and *odd* parity. The ground state of O^{18} is given as 0^+.[9] Thus *s*-wave protons should lead to levels of $\frac{1}{2}^+$ and *p*-wave protons

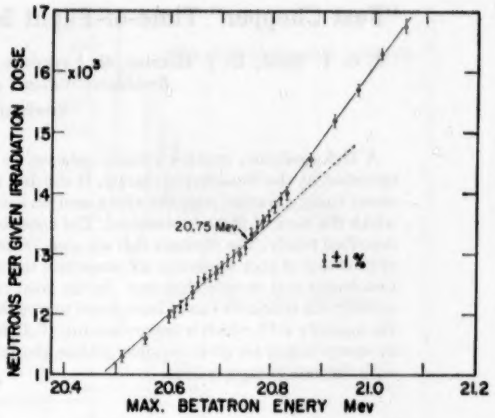

FIG. 6. $C^{12}(\gamma,n)C^{11}$. The break in the carbon yield curve at 20.75 Mev examined in detail.

to levels of $\frac{1}{2}^-$ and $\frac{3}{2}^-$. Capture of protons of higher orbital angular momentum should result in levels of higher spin. Where the two sets of measurements overlap, the levels can be assumed to have either spin $\frac{1}{2}$ or $\frac{3}{2}$ and *odd* parity. Furthermore, these levels cannot be reached by *s*-wave protons or for that matter by any protons of even orbital angular momentum.

It may be worth while to report that measurements with copper and heavier elements failed to show fine structure in their activation curves. Owing to the crudeness of our experimental method we can only conclude that the excitation levels in these elements, if present, are very close together (closer than 0.2 Mev) or represent a negligible fraction of photon absorption.

[7] E. W. T. Titterton and T. A. Brinkley, Proc. Phys. Soc. (London) **66**, 398, 194 (1953).
[8] D. C. Peaslee and V. L. Telegdi, Phys. Rev. **92**, 126 (1952).
[9] F. Ajenberg and T. Lauritsen, Revs. Modern Phys. **24**, 321 (1952).

"Fast Chopper" Time-of-Flight Measurement of Neutron Resonances*

F. G. P. SEIDL, D. J. HUGHES, H. PALEVSKY, J. S. LEVIN, W. Y. KATO,† AND N. G. SJÖSTRAND‡
Brookhaven National Laboratory, Upton, New York

(Received March 23, 1954)

A high-resolution neutron velocity selector, or "fast chopper," has been constructed and is in routine operation at the Brookhaven reactor. It consists of a high-speed rotor that produces bursts of neutrons of about 1-μsec duration, together with a neutron detector at the end of a 20-meter flight path and circuits with which the time of flight is measured. The construction and operating characteristics of the equipment are described briefly. The methods that are used for analysis of sample transmission curves in the energy regions of good and of poor resolution are presented, together with curves used to correct for the effects of Doppler broadening and sample thickness. In the good resolution region the measured total cross section in the vicinity of a resonance can be interpreted to give the total width Γ and $g\Gamma_n$. In the poor resolution region only the quantity $\sigma_0\Gamma^2$, which is proportional to $g\Gamma_n\Gamma$, is obtained. Measured parameters for levels in the 2 to 200 ev energy region are given for silver, iodine, thorium, gold, manganese, and cobalt. The results are compared with theoretical expectations.

I. INTRODUCTION

ALTHOUGH the characteristic features of low-lying levels of some heavy nuclei are reasonably well known from radioactive decay schemes, little detailed information is available on the properties of the levels at excitation energies corresponding to the binding energy of a nucleon. With the use of slow neutrons it is possible in principle to determine the properties of individual nuclear energy levels at an excitation energy just above the neutron binding energy, which is of the order of 7 Mev. For those nuclei in which the first virtual level occurs only one or two electron volts above neutron binding energy, the properties of the level have been determined reasonably well by neutron cross-section measurements. Because of the limited energy resolution available with neutrons, however, it has not been possible until recently to measure the resonance properties for individual levels higher than a few electron volts. Some information has been obtained on the *average* properties of resonances from cross sections at higher energies, which are functions of the level parameters averaged over many resonances. Such studies[1] have shown, for example, that the spacing of levels about one Mev above neutron binding energy exhibits sharp discontinuities at "magic number" nuclei, although it varies smoothly with atomic weight for other nuclei.

In order to exploit the possibility of obtaining detailed information on many levels in individual isotopes by means of neutron resonances, it was important to increase the resolving power of the measuring instruments over that available a few years ago in order to isolate the individual resonances. Study of individual isotopes has assumed greater interest with accumulating evidence that the shell structure of nuclei has a marked effect on the nuclear energy levels. According to the liquid-drop model, used almost exclusively to interpret nuclear structure some years ago, no significant differences would be expected from isotope to isotope other than the minor ones arising from differences in neutron binding energy, which depend in turn on odd-even effects and location relative to the valley of stability. From this point of view there would be no great importance in making detailed measurements on individual isotopes, for any one would be a good representative of others in the same general region of the periodic table.

At the time the present work was begun it seemed certain that, contrary to the liquid-drop model, the ground states and the first few excited states of many nuclei were determined largely by the shell structure of the nucleus. It was not known to what extent the shell structure determined the energy levels at high excitation, however. It seemed likely that at sufficiently high excitation the effect of the shells would disappear and a liquid-drop model would be more appropriate. The capture cross sections[1] at 1 Mev, which gave the average level spacings at energies 1 Mev higher than neutron binding energy, indicated that the shell structure had some effect on the level spacing even after the difference in excitation energy (caused by binding energy discontinuities) was taken into account. The possibility of shell structure extending to high excitation energy was a strong reason for efforts to improve the resolution of neutron spectrometry and for measurements with individual isotopes. During the progress of the work here reported, new developments in nuclear models[2–4] have increased the importance of resonance measurements, because they serve to test the predictions based on these models.

Many of the previous measurements of neutron resonances at low energy had been performed with cyclotron time-of-flight equipment[5,6] or neutron crystal

* Work performed under contract with the U. S. Atomic Energy Commission.

† Now at Argonne National Laboratory, Lemont, Illinois.

‡ Guest physicist from Aktiebolaget Atomenergi, Stockholm, Sweden.

[1] Hughes, Garth, and Levin, Phys. Rev. **91**, 1423 (1953).

[2] Feshbach, Porter, and Weisskopf, Phys. Rev. **90**, 166 (1953).

[3] A. Bohr and B. R. Mottelson, Kgl. Danske Videnskab. Selskab, Mat.-fys. Medd. **27**, No. 16 (1953).

[4] R. G. Thomas (private communication).

[5] Bacher, Baker, and McDaniel, Phys. Rev. **69**, 443 (1946).

[6] Melkonian, Havens, and Rainwater, Phys. Rev. **92**, 702 (1953). This paper gives complete references to earlier papers by this group.

spectrometers[7–14] used with piles. The resolutions available with these two methods were of the same order of magnitude and were sufficient to give the parameters of individual resonances below about 10-ev neutron energy. Recently other time-of-flight instruments of greatly improved resolution have been put into use, namely fast choppers,[15–22] linear electron accelerators,[23–25] and betatrons.[26] The manner in which the improved resolution of these instruments has revealed increased resonance detail is illustrated in Fig. 1, which gives the total cross section of silver as reported in the literature during the last few years.

The most convenient unit for comparing the resolving power of these instruments, whether of the time-of-flight or crystal diffraction variety, is microseconds per meter, that is, the uncertainty in neutron flight time divided by the flight path in meters. The variation of the instrumental resolution with neutron energy is the same for the time-of-flight and the crystal diffraction instruments; hence they all can be compared in units of μsec/m.[27] There is a great difference, however, in the variation of counting rate with energy for the two types of instruments: the intensity per unit time decreases rapidly with energy in the crystal diffraction method but remains almost constant with energy in the time-of-flight instruments. The energy spreads for several values of instrumental resolution are given in Table I as functions of neutron energy. The energy spread is proportional to the resolution (μsec/m) and increases rapidly with neutron energy (as $E^{\frac{1}{2}}$). Most of the cyclotron time-of-flight work was done in the 0.5–1.0 μsec/m resolution range, and the recent instruments have reached approximately 0.1 μsec/m.

In the present paper the Brookhaven chopper will be described briefly; then the methods that have been developed for analyzing resonances will be discussed in detail. Results for several isotopes, as well as the bearing of these results on current nuclear models, will be presented.

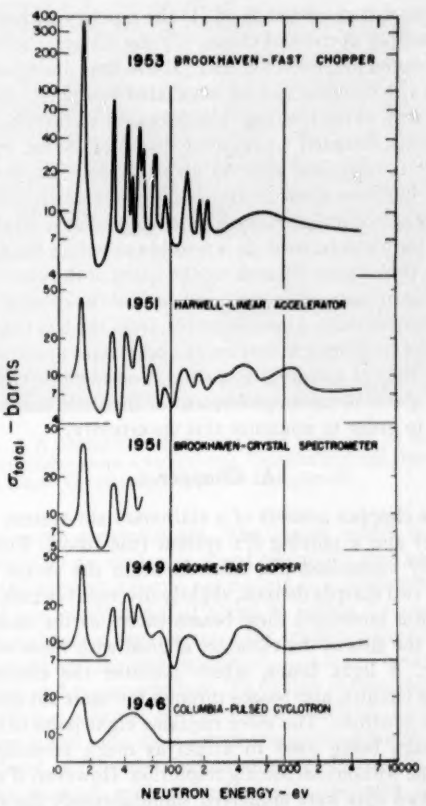
1953 BROOKHAVEN - FAST CHOPPER
1951 HARWELL - LINEAR ACCELERATOR
1951 BROOKHAVEN - CRYSTAL SPECTROMETER
1949 ARGONNE - FAST CHOPPER
1946 COLUMBIA - PULSED CYCLOTRON
σtotal - barns
NEUTRON ENERGY - ev

FIG. 1. The total cross section of silver as a function of neutron energy. This figure illustrates the manner in which the improved resolution available in recent years has revealed increased resonance detail in the energy region below 200 ev.

II. APPARATUS

The fast chopper is a mechanical shutter that produces neutron bursts of very short duration by mechanical interruption of a pile neutron beam. The pulses signalling the arrival of the neutrons at a distant detector are sorted into narrow time channels according to the time elapsed after the burst. In this way neutrons of discrete velocities are selected from a beam containing a wide velocity spread, although no true "monochromatic" beam has been produced. The resolution of such time-of-

TABLE I. The energy spreads in ev for several values of instrumental resolution.

Instrumental resolution (μsec/m)	Neutron energy (ev) 1	5	10	50	100	500	1000
0.1	0.0028	0.031	0.088	0.98	2.8	31	88
0.5	0.014	0.155	0.44	4.9	14	155	440
1.0	0.028	0.31	0.88	9.8	28	310	880

[7] W. H. Zinn, Phys. Rev. **71**, 752 (1947).
[8] W. J. Sturm, Phys. Rev. **71**, 757 (1947).
[9] Borst, Ulrich, Osborne, and Hasbrouck, Phys. Rev. **70**, 557 (1946).
[10] L. B. Borst and V. L. Sailor, Rev. Sci. Instr. **24**, 141 (1953).
[11] V. L. Sailor and L. B. Borst, Phys. Rev. **87**, 161 (1952).
[12] V. L. Sailor, Phys. Rev. **91**, 53 (1953).
[13] Foote, Landon, and Sailor, Phys. Rev. **92**, 656 (1953).
[14] R. L. Christensen, Phys. Rev. **92**, 1509 (1953).
[15] W. Selove, Phys. Rev. **84**, 869 (1951).
[16] W. Selove, Rev. Sci. Instr. **23**, 350 (1952).
[17] G. S. Pawlicki and E. C. Smith, Phys. Rev. **87**, 221 (1952).
[18] Seidl, Hughes, and Palevsky, Phys. Rev. **89**, 897 (1953).
[19] Hughes, Seidl, Palevsky, and Levin, Phys. Rev. **90**, 363 (1953).
[20] R. R. Palmer and L. M. Bollinger, Phys. Rev. **91**, 450 (1953).
[21] Bollinger, Thomas, and Palmer, Phys. Rev. **91**, 452 (1953).
[22] Bollinger, Harris, Hibdon, and Muehlhause, Phys. Rev. **92**, 1527 (1953).
[23] A. W. Merrison and E. R. Wiblin, Nature **167**, 346 (1951).
[24] A. W. Merrison and E. R. Wiblin, Proc. Roy. Soc. (London) **A215**, 278 (1952).
[25] Hodgson, Gallagher, and Bowey, Proc. Phys. Soc. (London) **A65**, 992 (1952).
[26] Yeater, Gaerttner, and Baldwin, Phys. Rev. **91**, 451 (1953).
[27] The instrumental resolution of the crystal spectrometer arises from the finite spread in diffraction angle, but this spread corresponds to a fixed uncertainty in μsec/m.

flight equipment depends on (1) the rapidity with which the chopper opens and closes, (2) the distance between the chopper and detector, and (3) the time limits within which the detector and its associated equipment define the arrival of the neutron. The Brookhaven fast chopper has been designed to improve the first factor by its ability to open and close in about 1 μsec. The second factor has been made as favorable as possible by taking advantage of an intensity high enough that a 20-meter flight path can be used. It is possible to reduce the effect of the third factor by making the speed of the electronic equipment faster than the burst time of the chopper. An inherent difficulty arises, however, from the fact that the detector itself may introduce an appreciable uncertainty in the time of arrival of a neutron. Considerable effort is being given to the improvement of the detection apparatus in order to minimize this uncertainty.

A. Chopper

The chopper consists of a stationary slit system (the stator) and a moving slit system (the rotor). From a crudely collimated pile neutron beam the stator produces two sharply defined, slightly divergent beams, and the rotor intercepts these beams except at the moment when the slits of the rotor are aligned with those of the stator. A light beam, which initiates the electronic timing circuits, also passes through the same slit system as the neutrons. The rotor contains eight pairs of slits, the pairs being used to attain as much intensity as possible without sacrificing resolution. However, if more than two slits were employed simultaneously the rotor would not be sufficiently opaque to neutrons.

The shape of the slit system, Fig. 2, is such that each pair of rotor slits opens only once per revolution. The curvature of the trailing edge of the slit is designed to allow the passage of only those neutrons above a certain velocity, the slit closing after the neutrons of minimum velocity have passed through the rotor. Were it not for this elimination of slow neutrons they would reach the detector at the same time as the fast neutrons of the next burst, and this "overlap" would necessitate removal of some of the pairs of slits or a reduction in the flight path.

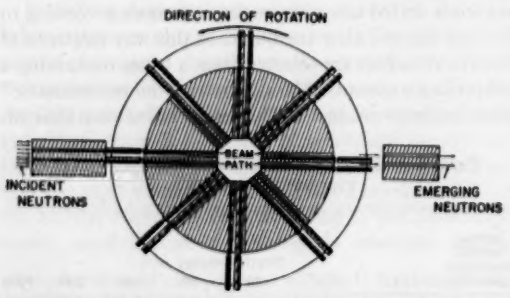

FIG. 2. A schematic plan view of the fast chopper rotor and entrance and exit stators. The shaded areas indicate plastic that is opaque to neutrons. The shape of the slit system is such that each pair of rotor slits opens only once per revolution.

Actually the intensity of even the high-energy neutrons is decreased somewhat by the movement of the rotor during the time these neutrons traverse it. As a result a decrease in intensity, which is minor at high velocities and complete at the cutoff velocity, is produced. The many factors involved in the conflicting requirements of rapidity of the burst, provision of sufficient neutron stopping material for opacity, and large solid angle for intensity, were the subject of extensive analysis of neutron passage through various shutter systems; the present design is the result of these extensive computations.[28]

Because of the many conflicting needs the rotor itself has a somewhat complicated structure, Fig. 3. The assembly containing the slits is made up of a total of 176 pieces of plastic held by two aluminum (14*S*-*T*6) alloy

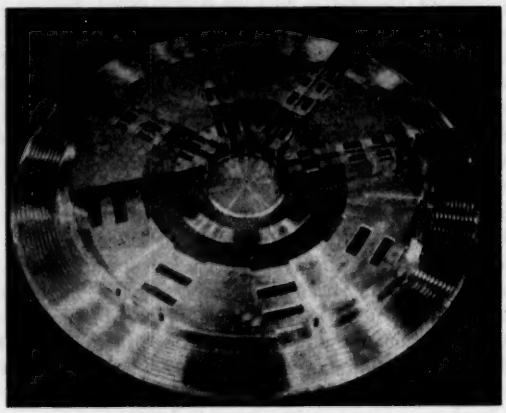

FIG. 3. A photograph of the partly assembled rotor. The 4 pairs of arms enclose the narrowest regions of 4 pairs of rotor slits. The rotor is made up of many pieces of plastic held between two aluminum forgings. It has a 30-in. diameter and weighs 250 pounds.

forgings. It has a 30-in. diameter and weighs 250 pounds. As the present chopper is intended for use in the energy region 10 ev to 10 kev, hydrogen in the form of high-strength phenolic laminate was chosen as the neutron-stopping material because of its high stopping power and low density. With the present design, actual operation showed that for about the first 2° after closing of the slits a slight leakage of high-energy (2-Mev) neutrons occurs by penetration through the phenolic material. These fast neutrons reach the detector in a short time, and at a rotor speed of 6000 rpm, cause some additional background for flight times less than about 40 μsec, corresponding to neutron energies above 1.3 kev. Another obvious difficulty in the use of phenolic laminate as neutron-stopping material is that even between neutron bursts the gamma-ray intensity in the beam is not

[28] The important design factors and the method of construction of the rotor are described in detail by F. G. P. Seidl in a forthcoming Brookhaven National Laboratory report, BNL-278 (*T*-46) (unpublished).

greatly reduced and the neutron detector must therefore have a high discrimination against gamma rays. Some reduction of gamma-ray intensity is obtained by incorporating lead or tungsten in the stator. Tungsten would be useful in stopping the 2-Mev neutrons, but is too heavy for use in the rotor.

The rotor is designed to operate steadily at a speed of 12 000 rpm, at which speed the calculated burst is approximately an isosceles triangle with full width at half-maximum equal to 0.7 μsec. Although the small size of the slit is a result of the attempt to produce a burst of short duration, the intensity being decreased thereby, an advantage results in that exceedingly small samples can be used, in actual practice as small as 20 mg. Lucite sample holders, designed for powdered samples of various thicknesses and of area slightly larger than the slit area (0.0115 in.$\times$1 in.) are used.

A photograph of the rotor and its housing is shown in Fig. 4. The vertical rotation axis represents a distinct difference between the present chopper and those of previous designs, this axis having been chosen because the mechanical problems of operating a high-speed rotor are much simpler for a vertical suspension. The rotor is operated from a dc motor by a $\frac{3}{16}$-in. drive shaft that passes through an oil vacuum seal. The rotor operates at a pressure of about 50 μ of Hg because of the prohibitive drag at atmospheric pressure. The oil vacuum seal is located at the upper part of the drive shaft, which is polished to a high finish. The fact that the present rotor has now operated at 6000 rpm for 18 months with no difficulty illustrates the mechanical simplicity of the vertical suspension. A second rotor has now been built and is being tested for higher speeds; at the present time it has been run at 11 000 rpm for 5 hr. Experimentally some resonance vibration is apparent when the rotor is turning at extremely slow speeds. Above 1000 rpm the rotor spins about its own center of mass with the drive shaft flexing if necessary in order to follow the rotor, and no observable resonance effects are encountered. None of these minor oscillations cause any difficulty in bringing the rotor up to speed, although as a precautionary measure the stator, which is located as close to the rotor as possible at full speed, is removed about $\frac{1}{4}$ in. during the period of acceleration. In case of power failure, or any unusual operation of the electronic circuits, the stator is also moved away automatically.

B. Control and Timing Circuits

Both the electronic circuits to control the chopper and those to time the arrival of neutrons at the detector use a signal from a photomultiplier at the exit collimator of the chopper. By means of mirrors and prisms, light from a tungsten-filament source mounted on the entrance stator is sent down the neutron-beam slits and is reflected onto the photomultiplier, thus ensuring that the neutron burst and light signal are coincident.

The chopper rotor is driven by a dc motor, powered

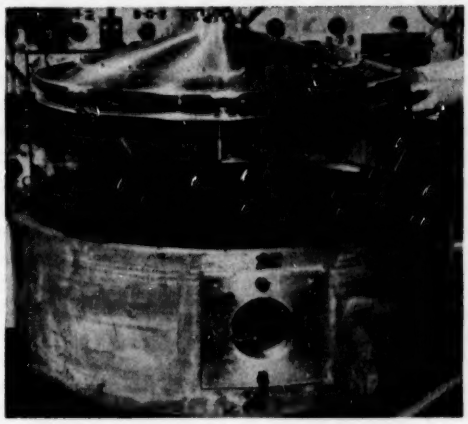

FIG. 4. A photograph of the assembled rotor and its housing. The rotor spins about a vertical axis. Entrance and exit stators are not in place. The pile shield is in the background.

by a motor-generator set. The motor speed is kept constant by an electronic speed controller that accelerates the rotor at 200 rpm per minute to a predetermined speed and maintains that speed to within 0.1 percent. To slow down or stop the rotor the armature circuit may be opened and the rotor will slowly lose speed because of friction and motor windage. To hasten the deceleration the driving motor is used as a generator and the stored energy in the rotor then drives the motor-generator set. The level of this electrical damping is adjustable.

The over-all control system also includes several standard safety features, the main overload protection being a magnetic circuit breaker. Interlocked with the breaker are circuits that open the armature circuit if the vacuum in the chopper housing falls below a predetermined level, if the voltage across the motor rises above a pre-set level, or if any of the voltage supplies for the rotor drive or control system fail. The rotor and its control circuits have now been in operation for about 8000 hr with a minimum of maintenance and repair.

The detector in use at the present time consists of a bank of 2-in. diameter BF_3 proportional counters containing enriched boron. Thirty-five of these counters, connected in parallel, are arranged to fill a volume 10 in. wide, 24 in. high, and 5 in. in the direction of the neutron travel. The efficiency of this bank of counters is extremely low at high energy, for example it is only 0.3 percent at 1-kev neutron energy. The effect of the finite flight path in the detector on the resolution will be discussed later. Although the small sample size is a distinct advantage of the fast chopper in that it allows the use of such rare materials as separated isotopes, the large size of the neutron detector is a disadvantage for it requires many BF_3 counters in the present design or extremely large scintillation counters in other possible designs.

The timing of the neutrons is performed by turning on

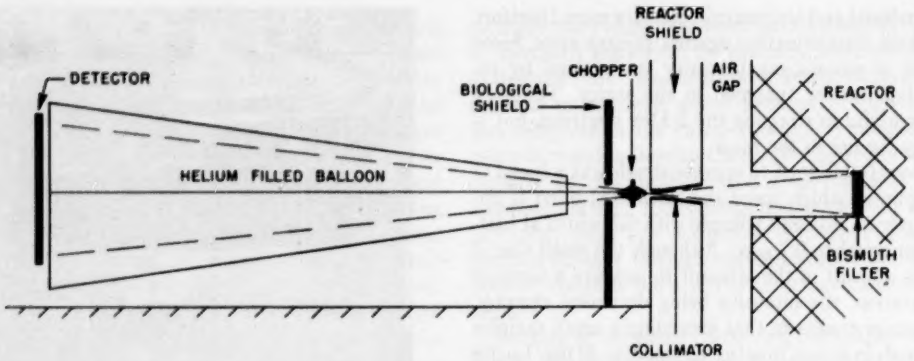

FIG. 5. A schematic elevation view of the arrangement of the chopper at the pile. All dimensions except those of the chopper are approximately to scale. The vertical scale is about 5 times the horizontal scale. The distance between the chopper and the detector is 20 meters.

an oscillator with the light pulse from the photomultiplier, then turning it off with the pulse resulting from the detection of the neutron, a method that results in unusually simple, reliable circuits.[29] The flight time is measured by counting the number of oscillations with a double-decade scaling circuit arranged in a 10×10 matrix. Some time later (but before the next light pulse) a scanning pulse transmits the position where this scaling matrix has come to rest to a bank of 100 registers, one corresponding to each matrix point. The scalers are reset and the system is then ready for another light pulse. The position of the 100 channels may be delayed with respect to the light pulse in steps of 10 channels by means of a coincidence circuit that switches off all pulses from the detector until a pre-set number of oscillations have been counted. The counting of the delay is done by the same 10×10 matrix scaler that generates the channels; in this case it is used as a predetermined count scaler.

Since the transmission and recording of the time of flight can be done in times long compared to the channel width ($\frac{1}{4}$, 1, 2, or 4 μsec channels are available) no fast coincidences are required; the only critical parts of the circuits are the fast scalers which are of standard design. The inability of this system to detect more than one neutron per burst is only a very minor drawback, for the number of detected neutrons of all velocities is very small, only 1/30 per burst at 6000 rpm. The probability of a second count occurring in a particular 100-channel region in the same burst is 1/100 or less, and the resulting loss of counts can be easily calculated.

C. Experimental Arrangement at the Pile

The arrangement at the pile of the chopper, as well as the beam collimator and the detector, is shown schematically in Fig. 5. The particular experimental hole used for the chopper is 4 in. wide by 12 in. high, and extends approximately to the center of the pile. At the far end of the hole, inside the pile lattice, a 12-in. cube of bismuth metal is placed to decrease the intensity of gamma-radiation in the beam. The thermal flux in the pile lattice at the base of the hole is 5×10^{12} neutrons/cm^2 sec. The resonance neutron flux, which is the flux of direct interest for the fast chopper, has a distribution in energy inversely proportional to the energy, i.e., the well-known dE/E spectrum that exists in a graphite moderator. The intensity of the dE/E spectrum relative to the thermal flux is typical of a graphite pile; the number of neutrons in each decade of the dE/E spectrum is given by 1/7 of the thermal flux. The effect of the bismuth block on the neutron intensity was investigated at the time of installation of the chopper and it was found that the presence of the bismuth did not reduce the thermal or resonance flux appreciably, although the gamma-ray intensity was reduced approximately twofold.

In order to lessen the number of neutrons emerging into the open room a series of collimators is located inside the beam hole. These collimators serve to reduce the size of the beam from 4 in.×12 in. high at the base of the hole to two beams, each $\frac{1}{2}$ in.×$1\frac{1}{2}$ in. high with centers separated by 1 in., at the exit end of the hole. The collimation thus forms two incident beams directed toward the slits of the chopper stator. Even with this beam collimation the neutron intensity is extremely high in the region of the incident stator, and it is necessary to surround the chopper with extensive neutron shielding to keep the neutron intensity in the immediate vicinity below physiological tolerance. The chopper is also surrounded with sandbags and steel plates that serve as an explosion shield; this shield provides additional neutron protection as well.

Samples are inserted in the chopper stator as already described at a point where the beam reaches its smallest size. After leaving the chopper the beam expands in size until it attains an area of about 1 ft×3 ft at the neutron detector 20 meters from the incident end of the rotor. In

[29] The electronic analyzer is described in detail in a forthcoming Brookhaven National Laboratory report by Graham, Higinbotham, and Rankowitz.

this 20-meter flight path the air scattering would be sufficient to reduce the neutron intensity approximately by a factor of two. Practically all this loss is prevented by means of a plastic balloon, filled with helium, extending from the chopper to the detector.

Although some neutron shielding was used around the detector when the chopper was first put in use, at the present time all shielding has been removed from the vicinity of the detector. It was found that even small amounts of shielding near the detector caused some scattering of neutrons back into the detector. These scattered neutrons would have a flight path greater than 20 meters and hence be recorded in an incorrect velocity channel. It was possible to eliminate the shielding at the counters by improving that at the chopper itself, for essentially all the background at the detector arises from neutrons emerging from the fast chopper collimator rather than from general room background.

III. PERFORMANCE CHARACTERISTICS

The equipment is very reliable and operates 24 hr a day, seven days a week, without attention except for sample changing and recording of data. Should a power failure or any change in operating conditions occur that causes the automatic circuits to stop the rotor, part of a run is lost, but as the shutdown is automatic, no attendance is necessary.

The actual counting rate obtained for the open beam is shown in Fig. 6 as a function of flight time; this rate agrees well with an actual calculation based on the resonance flux, the geometry of the chopper, and the efficiency of the detector. The peaks at 1.5 and 2.6 μsec/m are associated with the 12-in. cube of bismuth which is in the pile; the dips at 3.9 and 4.8 μsec/m are due to resonances in the various structural materials that are in the beam. For flight times greater than 3 μsec/m it is seen that the counting rate per channel is nearly constant, exhibiting only a slow decrease with increasing time of flight. This slow decrease represents the so-called chopper function, which is a result of the fact that the slits close partially during the time required by the neutrons to pass through the chopper. Disregarding the chopper function, it is easily seen that the counting rate per channel for a dE/E spectrum and a $1/v$ detector should be constant with time of flight. The flux incident on the counter is dE/E, hence the counting rate will be proportional to $dE/E^{\frac{1}{2}}$, but since the dE represented by a constant channel width dt is proportional to v^3, the counting rate per channel will be constant.

The background, which is also shown in Fig. 6, is about 4 percent of the counting rate at 5-μsec/m flight time and consists about equally of neutrons scattered from the fast chopper hole and alpha disintegrations in the walls of the counters. The background is measured by inserting a 4-in. paraffin block in the beam at the exit stator. Detailed tests, involving intensity measurements as a function of paraffin thickness with the chopper stationary as well as rotating, have shown that the 4-in. paraffin block does not affect the background itself for flight times greater than 2 μsec/m. For most of the cycle (times greater than 2 μsec/m) none of the background originates in the beam itself (such as would be true for background consisting of gamma rays in the beam penetrating the chopper). For times less than 2 μsec/m, however, the background is higher because of the presence of some fast neutrons (about 2 Mev) that penetrate the chopper while it is in a closed position but before the full thickness of plastic has moved into the beam. Background measurements have also been made with thick samples in which the transmission at a resonance was zero for several resolution widths. Although these determinations indicate a slightly higher background rate than that obtained from the paraffin measurements, the difference is not sufficient to affect the accuracy of transmission measurements.

In operation the counting rate is recorded for a given number of counts on a monitor counter rather than as a function of time; the monitor is necessary because of fluctuations in pile intensity. It consists of a single cadmium-shielded BF_3 counter located inside the shielding of the chopper, where it is sensitive primarily to resonance neutrons from the fast chopper hole that are scattered by the stator. Except in special cases where greater accuracy is required, sample runs are made sufficiently long to obtain 2 to 3 percent statistical accuracy per channel in regions between resonances. Comparable accuracy can be obtained much more quickly for the open beam run because for flight times greater than 3 μsec/m the open beam intensity is a slowly varying function, and a smooth curve can be fitted to the data. Background measurements are made periodically during both open beam and sample runs.

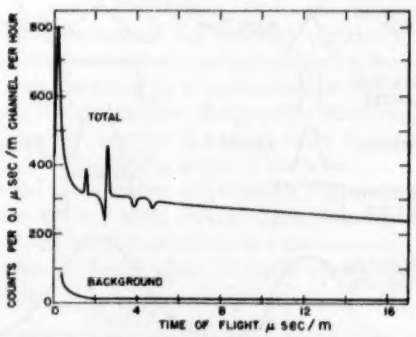

FIG. 6. The open beam and background counting rates as a function of neutron time of flight. The peaks at 1.5 and 2.6 μsec/m are associated with the bismuth filter in the reactor; the dips at 3.9 and 4.8 μsec/m are caused by resonances in structural materials in the beam. The open intensity continues to decrease slowly for flight times greater than 16 μsec/m. The background intensity, which is constant for flight times greater than 2 μsec/m, increases at small flight times because of leakage of fast neutrons.

Although a short burst of neutrons is of fundamental importance in the attainment of high resolution, there are several other points in the apparatus where uncertainties in timing may occur, and it is therefore necessary to ensure that these additional uncertainties in timing are reduced at least to values comparable with the burst time. The additional contributions to the timing uncertainty consist principally of the width of the electronic counting channel, the flight time in the detector, and the delay in the collection of the pulses in the detector. In the present equipment the counting channels are adjustable in steps and the most efficient use of the equipment is attained when the channel time is about equal to the length of the burst. Under present conditions the shortest channel time used is 1 μsec, but ½-μsec channels can be employed when the other timing uncertainties are reduced sufficiently to warrant their use. The time uncertainties involved in the operation of the neutron counters are difficult to decrease and at the present time constitute the major uncertainty in timing, being actually longer than the burst itself.

There exists a variation in collection time in the BF_3 counters which depends on the radial position of the boron disintegration in the counter; the time distribution of this variation for uniform incident flux is a rectangle about 4 μsec wide. This counter "jitter" adds a large amount to the width of the resolution function, an amount that is constant in time for all neutron velocities. The finite length of the counter in the direction of the neutron flight path (13 cm) contributes a constant *fractional* uncertainty of 0.13/20, or 0.6 percent, to the flight time. For high energies this uncertainty in time is small compared to the counter jitter but for low velocities (below 10 ev) the flight time in the counter is the major contribution to the timing uncertainty.

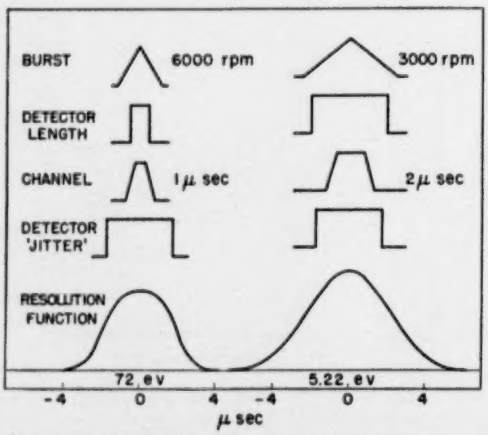

FIG. 7. The calculated resolution function for neutron energies of 72 ev and 5.2 ev. The separate timing uncertainties which contribute to the resolution function are shown. The full width at half-maximum of the resolution function is 0.18 μsec/m (3.0 ev) at 72 ev and 0.25 μsec/m (0.083 ev) at 5.2 ev.

The manner in which the various timing uncertainties combine to give the final resolution function is shown in Fig. 7 for neutron energies of 72 ev and 5.2 ev.[30] An experimental check of this calculated resolution function was made by comparison with a carefully measured transmission function of a sample of silver. The experimental transmission curve for a silver resonance at 72 ev was chosen for the comparison because it should exhibit a shape determined almost completely by the resolution function, for the actual width of the silver resonance is much less than the resolution width at 72 ev. The expected transmission curve for this silver resonance, based on its measured "strength" ($\sigma_0\Gamma^2$ value—to be described later) combined with the 72-ev resolution function of Fig. 7, is compared in Fig. 8 with the measured transmission. It is seen that good agreement exists between the measured transmission curve and that calculated from the resolution function. Thus it appears that the separate contributions to the resolution function are reasonably well known, and that the effective resolution of the instrument for actual transmission measurements is correctly given by the calculation based on these separate components.

Future improvement of the resolution of the entire apparatus obviously depends primarily on improvement in neutron detectors. At the present time development of BF_3 and scintillation detectors for use with the chopper is being actively pursued.[31] A multiple BF_3 counter is being constructed, in which a large number of small diameter proportional counters are mounted in a large container in a common BF_3 atmosphere. The small cathode diameter of these counters as well as the large diameter of the center wire should give a time jitter of 0.5 μsec, which is sufficiently small for the present operating conditions. As this bank of counters is to be 9 cm long in the direction of the neutron travel, the flight time in the counter will still add an appreciable amount to the resolution function for work below 30 ev.

Scintillation counters should be superior to BF_3 counters in both time jitter and size because the time jitter is negligible and a solid scintillator containing enriched boron can be made sufficiently thin that the flight time in the counter will also be negligible. At the present time a combination of fused B_2O_3 and small crystals of ZnS in the form of a large sheet about 1 cm thick seems to be the most promising counter material.[31] The scintillations are detected by a series of photomultipliers connected in parallel and mounted in contact with the sheet. This type of counter is capable of giving high efficiency, of the order of 10 percent for neutrons up to 1 kev, and extremely short time jitter and flight time uncertainties. Until the timing uncertainties of the detector are greatly reduced there is no advantage to be

[30] For the measurements to be described the burst width was actually about 40 percent greater than the calculated value shown in Fig. 7 because of a vertical misalignment of the slits in the stator and rotor. This misalignment has now been corrected. All calculations from Fig. 8 on are based on the wider burst width.

[31] Palevsky, Sjöstrand, and Hughes, Phys. Rev. 91, 451 (1953).

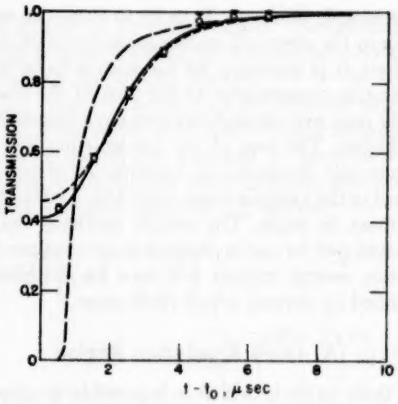

FIG. 8. An experimental check of the calculated resolution function. The — — — curve, calculated from the $\sigma_0\Gamma^2$ value of the 72-ev level in silver, is the transmission curve that would be observed with infinite resolution. The solid and - - - curves were obtained by convoluting the above curve with the resolution function calculated for counter jitters of 3.5 and 4.0 μsec, respectively. The experimental points, obtained with a 6.6 g/cm² sample of metallic silver, agree well with the transmission curve calculated for a 3.5-μsec jitter.

gained by operating the chopper above its present routine speed of 6000 rpm.

The 4-μsec jitter in the BF_3 counters causes an average delay of 2 μsec in the arrival of the detector pulse at the analyzer. In order to correct for this and other time delays that might be present in the electronics, a zero correction has been determined by making transmission measurements on the 20-kev group of resonances in titanium.[32] The zero correction is about 3 μsec in magnitude; because of aging of the light source and its associated electronics it can change by about ½ μsec over long periods of time. The correction can easily be redetermined at regular intervals by noting the position of the 2.6-μsec/m peak in the open beam intensity, the energy of this peak having been determined relative to that of the titanium resonances. The energy of this group of resonances has been determined by accelerator measurements to within at least ±2 kev, which corresponds to ±½ μsec for a 20-meter flight path. Since the position of a resonance can be determined with a precision of ±½ μsec and the uncertainties in the length of the flight path and the frequency of the analyzer oscillator are each less than 0.1 percent, it is felt that measurements of flight times can be made with an accuracy of ±1.2 μsec, or ±0.06 μsec/m.

IV. ANALYSIS OF RESONANCES

Transmission curves obtained with the fast chopper exhibit dips corresponding to resonances in the total cross section of the sample material. Although the separate cross sections, scattering and absorption, that constitute the total cross section are not obviously obtainable from a transmission measurement, we shall see that most of the information needed to determine these cross-section components can in principle be obtained from a measurement of the total cross section. As the relationship between the transmission and the total cross section is extremely complicated, the latter cannot easily be obtained and the analysis is carried out directly on the measured transmission curve. The number of dips observed in a particular energy range gives the level density directly, and further analysis enables the determination of some of the parameters of the resonances.

The cross-section resonances are described by the well-known Breit-Wigner formula, which gives the cross-section variation with energy for energies in which a single resonance level predominates. In the present work it is not necessary to take into account the more complicated formulas that relate to the effect of multiple levels. The one-level Breit-Wigner formula for the cross section as a function of energy, for absorption and for scattering, has the forms[33]

$$\sigma_a=\pi\lambda_0^2 g(E_0/E)\frac{\Gamma_n\Gamma_\gamma}{(E-E_0)^2+(\Gamma/2)^2}, \quad (1)$$

and

$$\sigma_s=4\pi\lambda_0^2 g\left|\frac{\Gamma_n/2}{E-E_0+i\Gamma/2}+\frac{R}{\lambda_0}\right|^2+4\pi(1-g)R^2, \quad (2)$$

where

$$g=\frac{1}{2}\left[1\pm\frac{1}{2I+1}\right]. \quad (3)$$

In these equations E is the energy of the neutron, $2\pi\lambda_0$ is the wavelength of a neutron with energy E_0, the energy at resonance, and Γ_n, Γ_γ, and Γ are the neutron, radiation, and total widths of the level. The g factor is a function of the spin I of the target nucleus and is double-valued, corresponding to the two possible spins of the compound nucleus, $I\pm\frac{1}{2}$. The scattering cross section is more complicated than the absorption cross section because of the coherent addition of the resonance and potential scattering amplitudes, the latter arising from scattering by a hard sphere of the nuclear radius, R. The interference effects in the scattering are useful, however, because in certain cases they aid in evaluation of the neutron width of the level.

The total cross section σ_T, which is the sum of the absorption and scattering cross sections, determines the change in transmission observed as a resonance dip, the transmission T being given at each energy by the relationship

$$T=I/I_0=\exp(-n\sigma_T), \quad (4)$$

where I and I_0 are the counting rates observed with and without the sample, containing n atoms per cm². If the transmission could be measured with infinite resolution, Eq. (4) would give the cross section as a function of

[32] Hibdon, Langsdorf, and Holland, Phys. Rev. 85, 595 (1952).

[33] J. M. Blatt and V. F. Weisskopf, *Theoretical Nuclear Physics* (John Wiley and Sons, Inc., New York, 1952), pp. 328, 391–4, and 426.

energy directly, from which the level parameters Γ and σ_0 (the peak cross section) could be obtained. Even in this ideal case, however, the separation of the total width Γ into the radiation and neutron widths would require a subsidiary measurement (of the peak scattering cross section or the ratio of scattering to total cross section, for example) because Γ and σ_0 give only $g\Gamma_n$ rather than Γ_n itself. In actual practice, the determination of level parameters is complicated greatly by the finite resolution, which broadens the observed resonance dip, and also by the Doppler effect. Because of the latter, even those neutrons of a single velocity have a velocity spread relative to the target nuclei which are in thermal motion.

The methods of analysis that are used are conveniently divided into those appropriate for two energy regions: a low-energy region of good resolution, where the individual parameters can be determined separately, and a higher-energy region where, as a result of poor resolution, only the combination of parameters $\sigma_0\Gamma^2$ can be determined. In the region of good resolution the actual width and peak height of the resonance can be measured directly from the cross-section curve, if the observed transmission can be corrected for the instrumental resolution. For an energy somewhat higher than that for which the true shape can be obtained, the area of the transmission dip for a thin sample, which gives $\sigma_0\Gamma$, can be combined with $\sigma_0\Gamma^2$ obtained from a thick sample to calculate Γ and σ_0.

In the high-energy region the resolution width is much larger than the natural width of the resonance; hence the shape of the dip in the transmission curve is determined almost completely by the resolution function and the sample thickness. In order to obtain an appreciable dip in the observed transmission curve under such conditions, it is necessary for the sample to be so thick that the true transmission at the peak of the resonance is nearly zero, even though the measured transmission is much higher. The area of the transmission dip in this case gives only the particular combination of parameters $\sigma_0\Gamma^2$, and in the analysis some correction for the Doppler effect must be made. The specific methods that have been developed for use in analysis of the chopper data in these two energy regions will now be described and exemplified by several actual resonances.

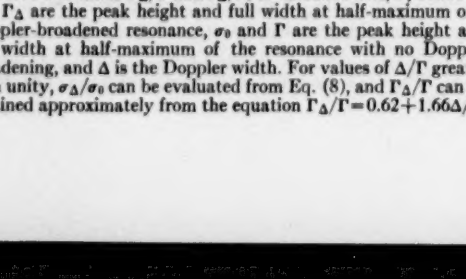

FIG. 9. The ratios Γ_Δ/Γ and σ_Δ/σ_0 as functions of Δ/Γ, where σ_Δ and Γ_Δ are the peak height and full width at half-maximum of a Doppler-broadened resonance, σ_0 and Γ are the peak height and full width at half-maximum of the resonance with no Doppler broadening, and Δ is the Doppler width. For values of Δ/Γ greater than unity, σ_Δ/σ_0 can be evaluated from Eq. (8), and Γ_Δ/Γ can be obtained approximately from the equation $\Gamma_\Delta/\Gamma=0.62+1.66\Delta/\Gamma$.

A. Good Resolution Region

For those cases in which it is possible to obtain the individual parameters of a resonance from transmission curves two general methods of analysis are employed. The first of these makes use of the details of the shape of the observed resonance; the second involves only the areas above transmission dips for several samples of varying thicknesses.

In the first method of analysis the observed transmission curve is corrected for the effects of instrumental resolution, this correction being small in instances where the instrumental resolution is less than the width of the resonance. A formula satisfactory for a small correction can be obtained easily. The true transmission T_{true} is expanded in a power series about the time of flight t for each point; this power series is convoluted with the resolution function $R(t)$ to obtain a series for the observed transmission T_{obs}, and this series is then inverted. For a resolution function that is symmetrical in time, as is the case with the Brookhaven fast chopper, the terms involving odd derivatives drop out and the resulting equation is:

$$T_{\text{true}}(t)=T_{\text{obs}}(t)-\frac{1}{2}T_{\text{obs}}''(t)\int x^2R(x)dx+T_{\text{obs}}^{iv}(t)\times\left[\frac{1}{4}\left(\int x^2R(x)dx\right)^2-\frac{1}{24}\int x^4R(x)dx\right]-\cdots, \quad (5)$$

where $\int R(x)dx=1$. The integrations are to be carried out over the complete extent of the resolution function; hence it is necessary that this function not have long "wings" if the correction is to be small. For those resonances analyzed by the present method the necessary derivatives were obtained with sufficient accuracy by numerical or graphical means, and the correction was sufficiently small that no more terms were needed than are shown in Eq. (5). The true cross section as a function of neutron energy or time of flight follows immediately from the corrected transmission curve by means of Eq. (4).

In general, the cross-section curve obtained in the manner just described will not be that predicted by the Breit-Wigner formula, but will be distorted by the

thermal motion of the target nuclei. The calculation of this Doppler broadening of neutron resonances has been performed by Bethe and Placzek.[34,35] If the $(E_0/E)^{\frac{1}{2}}$ factor (i.e., the $1/v$ factor) and interference effects are neglected in the single level Breit-Wigner formula, and if the target nuclei are assumed to have a velocity distribution characteristic of a free gas, the Doppler-broadened resonance cross section will be

$$\sigma=\frac{\sigma_0}{\Delta\sqrt{\pi}}\int_0^\infty\left[1+\left(\frac{E'-E_0}{\Gamma/2}\right)^2\right]^{-1}\times\exp\left[-\left(\frac{E'-E}{\Delta}\right)^2\right]dE', \quad (6)$$

where the Doppler width Δ is given by

$$\Delta=2(kTE_0m/M)^{\frac{1}{2}}. \quad (7)$$

Here m is the mass of the neutron, M the mass of the target nucleus, T the temperature of the target, and k the Boltzmann constant. Lamb[36] has treated the case of a Debye solid and has shown that if Γ is much greater than $k\theta$, where θ is the Debye temperature, the solid may be treated as a gas at a temperature somewhat greater than its actual temperature. This temperature difference becomes small as the sample temperature becomes much larger than the Debye temperature. Tables and curves of the Doppler-broadened cross section, σ/σ_0, are given by Born,[37] who also gives series for calculating this function and references to other mathematical treatments. In his notation σ/σ_0 is $\psi(x,\eta)$, where $x=(E-E_0)/\frac{1}{2}\Gamma$ and $\eta=\Delta/\frac{1}{2}\Gamma$.

For the method of resonance analysis under consideration, in which the shape of the transmission dip is important, two features of the Doppler-broadened cross section are considered: its peak value σ_Δ and its full width at half maximum, Γ_Δ. The first is easily evaluated analytically from Eq. (8),

$$\sigma_\Delta=\sigma_0\left(\frac{\Gamma}{\Delta}\right)\exp\left[\frac{1}{4}\left(\frac{\Gamma}{\Delta}\right)^2\right]\int_{\frac{1}{2}\Gamma/\Delta}^\infty\exp[-u^2]du. \quad (8)$$

The width is obtained from tables of the function $\psi(x,\eta)$ in the reference by Born[37] and from calculations performed by the authors to extend the range beyond that of the tables. In Fig. 9 are given curves of σ_Δ/σ_0 and Γ_Δ/Γ as functions of Δ/Γ.

In practice, values of Γ_Δ and σ_Δ are obtained from the observed transmission after correction for instrumental resolution in the manner already described. The true parameters, Γ and σ_0, can then be computed by successive approximations using the information from Fig. 9. No attempt is made to obtain σ_0 and Γ by a detailed fit of $\psi(x,\eta)$ to the experimental cross-section curve throughout the entire resonance, as it is felt that the extra labor involved in such an analysis is not warranted by the possible increase in accuracy. Before describing the application of the present "shape" method to a specific resonance, the "area" method will be considered, after which measurement of the 5.2-ev resonance in Ag^{109} by both methods will be described.

The shape method of analysis just discussed requires accurate knowledge of the instrumental resolution function and sufficiently good resolution to observe the details of the resonance shape. In contrast, the method based on the areas above transmission dips is independent of any knowledge of the resolution function and requires only good enough resolution to be able to make statistically significant measurements on a thin sample, one for which $n\sigma_\Delta\gtrsim 1$. As a result the area method can be used at somewhat higher energy than the shape method. The accuracy attainable with it, however, is reduced by the fact that only combinations of parameters are obtained.

The area method has been discussed extensively by Melkonian, Havens, and Rainwater.[6] In essence, if the incident neutron intensity changes slowly over the width of the resolution function R, the area "above" a transmission dip (between the transmission curve and unity) is given by

$$A=\int_0^\infty(1-T)dE=\int_0^\infty dE\int_0^\infty[1-e^{-n\sigma(E')}]R(E'-E)dE'. \quad (9)$$

If $\Gamma/2E_0\ll 1$, the lower limits can be replaced by $-\infty$ and the order of integration interchanged, so that

$$A=\int_{-\infty}^\infty[1-e^{-n\sigma(E')}]dE'\int_{-\infty}^\infty R(E'-E)dE, \quad (10)$$

and, since

$$\int_{-\infty}^\infty R(E'-E)dE=1,$$

$$A=\int_{-\infty}^\infty[1-e^{-n\sigma(E)}]dE, \quad (11)$$

which is independent of instrumental resolution.

If the $(E_0/E)^{\frac{1}{2}}$ factor and the Doppler broadening can be neglected in the single-level Breit-Wigner formula, then the integral for the area can be evaluated in terms of Bessel functions of imaginary argument,[38]

$$A=\tfrac{1}{2}\pi n\sigma_0\Gamma\,[\exp(-\tfrac{1}{2}n\sigma_0)][I_0(\tfrac{1}{2}n\sigma_0)+I_1(\tfrac{1}{2}n\sigma_0)]. \quad (12)$$

For a non-negligible Doppler broadening, the integral must be evaluated by series expansion or numerical

[34] H. A. Bethe and G. Placzek, Phys. Rev. **51**, 450 (1937).
[35] H. A. Bethe, Revs. Modern Phys. **9**, 69 (1937), see p. 140.
[36] W. E. Lamb, Jr., Phys. Rev. **55**, 190 (1939).
[37] M. Born, *Optik* (Julius Springer, Berlin, 1933), p. 482.
[38] R. Ladenburg and F. Reiche, Ann. Physik **42**, 181 (1913).

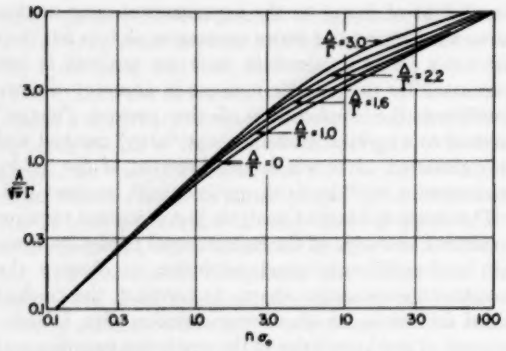

FIG. 10. The ratio $A/\pi^{\frac{1}{2}}\Gamma$ as a function of $n\sigma_0$ for various values of Δ/Γ, where A is the area "above" a transmission dip and n is the sample thickness in atoms/cm². For $n\sigma_0 \ll 1$ the slopes of these curves approach unity; for $n\sigma_0 \gg 1$ the slopes approach $\frac{1}{2}$.

integration. This calculation has been carried out for a wide range of parameters by von Dardel and Persson,[39] and by Melkonian *et al.*[6] These authors assume a single-level Breit-Wigner formula, neglecting the $(E_0/E)^{\frac{1}{2}}$ factor and the interference of resonance with potential scattering. Graphs of $A/\pi^{\frac{1}{2}}\Gamma$ as a function of $n\sigma_0$ for various values of Δ/Γ are shown in Fig. 10. The increase in the area of a transmission dip with increasing temperature (i.e., with increasing Δ) results from the decrease in the effect of "self-protection" that is associated with all but extremely thin samples. Thus the increased temperature makes a sample effectively thinner by reducing the peak height of the resonance; for an extremely thick sample, however, the reduction has little effect.

In the area method, preliminary estimates of σ_0 and Γ are obtained from values in the literature, or from a rough preliminary measurement. These values are then used to select sample thicknesses such that $n\sigma_\Delta \lesssim 1$ for one sample, and $n\sigma_\Delta \gtrsim 10$ for the other, and transmission curves are measured. The analysis to be described is then performed approximately (and none of the corrections discussed are made) in order to obtain rough values of $\sigma_0\Gamma^2$ and $g\Gamma_n/\Gamma$, which are needed in making the corrections necessary in the complete analysis.

The experimental transmission curves for the sample thicknesses described do not reach unit transmission away from the resonance. This fact arises from potential scattering, which is present away from the resonance, or at times simply from instrumental changes in the absolute magnitude of the open beam and sample counting rates. These nonresonance effects are eliminated by multiplying each transmission curve by an appropriate constant to make the transmission approach unity far from the resonance. For a thin sample this constant is easily determined by examination of the wings of the experimental transmission curve. However, for a thick sample this process may be more difficult since, owing to the presence of other resonances, it may not be possible to make measurements sufficiently far away from the resonance for the transmission to be unity.

The resonance shape may also be distorted if there is more than a few percent scattering present in the resonance because of the interference between resonance and potential scattering. In this case, the procedure adopted for normalizing the transmission is to calculate the expected shape of the wings including interference effects, far enough away from the resonance so that effects of Doppler broadening and instrumental resolution can be neglected. In this region the cross section is given by

$$\sigma_T - \sigma_{\text{pot}} = \left(\frac{E_0}{E}\right)^{\frac{1}{2}} \frac{\sigma_0\Gamma^2}{4(E-E_0)^2} + \frac{[\sigma_{\text{pot}}(\sigma_0\Gamma^2)(g\Gamma_n/\Gamma)]^{\frac{1}{2}}}{E-E_0}, \quad (13)$$

where the first term on the right-hand side arises from the resonance and the other term from the resonance-potential scattering interference. The potential cross section as it appears in the interference term is obtained with sufficient accuracy from published values;[40] the other parameters needed are just those that have already been estimated. The necessary normalizing factor is then obtained by comparing the experimental transmission curve with the calculated curve.

After the transmission curve has thus been normalized to eliminate nonresonance effects, the area above the curve between energies E_0-E_1 and E_0+E_1 is measured.

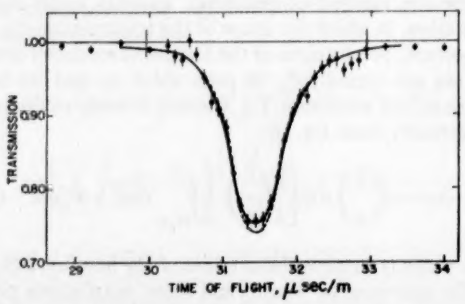

FIG. 11. The normalized transmission as a function of neutron time of flight for the 5.2-ev level in silver, obtained with a thin sample for which $1/n = 72\,200 \times 10^{-24}$ cm²/atom for Ag^{109}. The solid curve, which is used in the "area" analysis, is drawn through the experimental points; additional data outside of the region shown in the figure verify the fact that the curve approaches unit transmission far from resonance. The vertical lines at approximately 30 and 33 μsec/m indicate the points beyond which the area is calculated rather than measured. The broken curve, which is used in the "shape" analysis, is obtained by correcting the solid curve for instrumental resolution by means of Eq. (5) and the 5.2-ev resolution function of Fig. 7. All errors are given as standard deviations.

[39] G. von Dardel and R. Persson, Nature **170**, 1117 (1952).

[40] *Neutron Cross Sections*, U. S. Atomic Energy Commission Report AECU-2040 (Office of Technical Services, Department of Commerce, Washington, D. C., 1952).

The energy E_1 is selected such that it is much greater than Γ, Δ, and the instrumental resolution, but much less than E_0, and the transmission at E_0-E_1 and E_0+E_1 is greater than 0.9. The area measurement is not continued to higher transmissions because the statistical accuracy of $1-T$ becomes very poor and the effects of other nearby resonances may be important. The neglected area in the wings can be calculated far better from the preliminary $\sigma_0\Gamma^2$ value than it can be measured. Under the conditions set for E_1, the area neglected is given by:

$$\text{Area neglected}=n\sigma_0\Gamma^2/2E_1, \tag{14}$$

with half of this area lying on each side of the resonance. This calculated correction is added to the measured area to give the total area above the transmission curve. A second reason for cutting off the area measurement as discussed above is worthy of mention. The $(E_0/E)^{\frac{1}{2}}$ factor and the interference effects have been neglected in the calculation of the Doppler-corrected area curves (Fig. 10), although both these effects are present in the experimental transmission curve. However, for an area measured in an energy interval symmetrical about E_0, with E_1 small compared to E_0, the contributions to the measured area of the neglected factors cancel to a first approximation if the sample studied is not very thick.

When the area above the transmission curve has been obtained for a given sample, a curve of σ_0 as a function of Γ can then be plotted for that sample. This is done by assuming values of Δ/Γ (and therefore Γ, since Δ can be calculated) and reading $n\sigma_0$ from the appropriate curve of Fig. 10. If the points are plotted on log-log paper with σ_0 as the ordinate and Γ as the abscissa, a slope of minus one is obtained for a thin sample ($\sigma_0\Gamma=$const.), while a slope of minus two corresponds to a thick sample ($\sigma_0\Gamma^2=$const.). For curves obtained from samples of different thicknesses and plotted on the same graph, the point of intersection gives the value of σ_0 and of Γ for the particular resonance. Should these parameters indicate values of $\sigma_0\Gamma^2$ and $g\Gamma_n/\Gamma$ substantially different from those assumed in calculating the corrections to the areas, the analysis can be repeated once more with the new values of the parameters in the corrections. Because of the smallness of the corrections, a single repetition is usually sufficient.

As a test of the "shape" and "area" methods of analysis, a careful study was made of the 5.2-ev level in Ag^{109}. This resonance has been studied most recently by Selove,[15] who used methods and sample thicknesses chosen to avoid the corrections resulting from Doppler broadening. Although the resolution of the Brookhaven chopper is such that the direct shape method can be used on this level to give accurate results, the area method was also applied as a test of the accuracy of the area method.

The transmission curve shown in Fig. 11, which is used for the shape method, was obtained with a silver foil 0.0002 in. thick, for which $1/n=72\,200\times10^{-24}$ cm^2/atom for Ag^{109}. The solid curve is drawn through the experimental points, and the broken curve is obtained by correcting for instrumental resolution, by means of Eq. (5) and the 5.2-ev resolution function from Fig. 7.[30] The correction to the quantity $(1-T)$ is about 5 percent at the minimum of the dip, and is primarily due to the second derivative term; the fourth derivative term is important only in the region where the second derivative is zero. From the corrected curve the transmission at the peak of the resonance is found to be 0.739 ± 0.007. The factors that enter into this error are the statistical accuracy of the experimental curve (±0.005), the statistical accuracy of the normalization of the wings (±0.003), and an estimate of the accuracy of the correction for instrumental resolution (±0.004). (All errors are given as standard deviations.) The experimental peak cross section σ_Δ is $21\,800\pm700$ b, while the full width at half-maximum cross section is 14.4 ± 0.7 μsec, or in energy units, $\Gamma_\Delta=0.239\pm0.011$ ev. Most of the error in the width arises from the uncertainty in the location of the halfway point; the remainder arises from the uncertainty in the shape of the curve in that region.

TABLE II. The parameters of the 5.22-ev resonance in Ag^{109}.

	"Shape" analysis	"Area" analysis	"Best" values	Selove's results[a]
E_0 (ev)	5.22 ± 0.04		5.22 ± 0.04	5.17 ± 0.08
σ_0 (b)	$26\,900\pm1100$	$31\,000\pm3000$	$27\,300\pm1000$	$25\,000\pm3000$
Γ (ev)	0.177 ± 0.014	0.157 ± 0.009	0.168 ± 0.008	0.17 ± 0.02
Γ_n (mv)[b]			12.2 ± 0.5	11 ± 2
$\sigma_0\Gamma$ (ev b)	4750 ± 400	4800 ± 200	4600 ± 200	4300 ± 400
$\sigma_0\Gamma^2$ (ev^2 b)	840 ± 140	755 ± 25	775 ± 25	750 ± 60

[a] See reference 15.
[b] 1 mv $=10^{-3}$ ev.

For silver at room temperature (295°K) Lamb's calculations indicate an effective temperature only 2.6 percent higher than the actual temperature. This effective temperature gives a value of Δ of 0.071 ev at the resonance energy of 5.2 ev. Correction of the observed width for this Doppler broadening gives a true width Γ of 0.177 ± 0.014 ev. The main contribution to the uncertainty in Γ is the error in Γ_Δ; the effect of a 5 percent uncertainty in Δ would be negligible. The ratio Δ/Γ is then 0.40 ± 0.03, σ_Δ/σ_0 is 0.81 ± 0.02, and σ_0 is therefore $26\,900\pm1100$ b. These experimental results, summarized in the first column of Table II, are in good agreement with Selove's results, which are shown in the fourth column of this table.

For the analysis of this resonance by the area method, the transmission curve already given in Fig. 11 is used for the thin sample measurement. It should be noted that for $E_1\ll E_0$ the area above the transmission dip may be evaluated on a plot of transmission against time of flight, since the substitution $dE=(2E_0/t_0)dt$ is then valid. The area can be measured with sufficient accuracy by the use of a planimeter. For the curve of Fig. 11 the area is evaluated between (t_0-19) μsec and (t_0+21) μsec, which represents an energy interval $E_1=0.33$ ev. The area obtained is 0.080 ± 0.003 ev; the error results

from the statistical accuracy of the experimental curve (± 0.002 ev) and of the normalization (± 0.002 ev). The correction for the area in the wings is 0.016 ± 0.001 ev, which is based on the final value for $\sigma_0\Gamma^2$. The error in the wing correction includes an estimate of the uncertainty introduced through neglecting the effects of Doppler broadening and instrumental resolution in the calculation of this correction, as well as a 4 percent uncertainty in $\sigma_0\Gamma^2$. The total area is therefore 0.096 ± 0.003 ev, the wing correction contributing 16 percent.

In Fig. 12 is shown the transmission curve for the thick sample used in the area analysis. This sample is approximately 30 times thicker than the thin sample, having a $1/n = 2110 \times 10^{-24}$ cm^2/atom. In this case the value of E_1 chosen, 1.6 ev, is not small compared to E_0, and it is necessary to evaluate the area on a plot of transmission *vs* neutron energy. The area obtained is 0.949 ± 0.017 ev; 0.012 ev of the error is due to the statistical accuracy of the curve and 0.010 ev to a 0.3 percent uncertainty in the normalization. The correction for the area in the wings is 0.113 ± 0.007 ev, its error arising from the same uncertainties as in the thin-sample case. The total area is therefore 1.06 ± 0.02 ev, the wing correction being 11 percent.

Curves of σ_0 as a function of Γ, with a Δ of 0.071 ev, are given in Fig. 13 for the thick and thin samples just discussed. The broken lines, which represent the uncertainty caused by the errors in the areas, indicate the error in σ_0 for a given value of Γ. The intersection of the two solid lines gives the parameters of the resonance as $\sigma_0 = 30\,800$ b and $\Gamma = 0.157$ ev. Although the order of magnitude of the errors in these quantities can be estimated from the broken lines, a better estimate can be obtained by realizing that the thick and thin sample areas are really measurements of $\sigma_0\Gamma^p$, where p is nearly 2 for the thick sample, and nearly 1 for the thin sample. The values of p, obtained in Fig. 13 from the slopes of the curves at their point of intersection, are 1.91 and 1.06. The quantities which are measured in this example are therefore $\sigma_0\Gamma^{1.91} = 892 \pm 27$ and $\sigma_0\Gamma^{1.06} = 4310 \pm 170$, where σ_0 is in barns and Γ is in ev. From these numbers the uncertainties in σ_0 and Γ are found to be ± 3000 b and ± 0.009 ev, respectively.

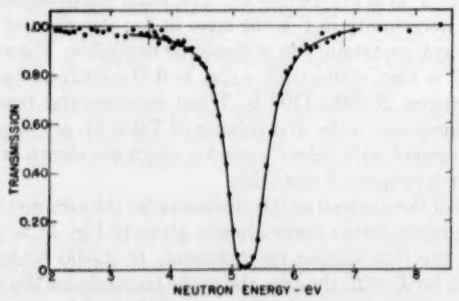

FIG. 12. The normalized transmission as a function of neutron energy for the 5.2-ev level in silver, obtained with a thick sample for which $1/n = 2110 \times 10^{-24}$ cm^3/atom for Ag^{109}. The vertical lines at approximately 3.5 and 7 ev indicate the energies beyond which the area is calculated rather than measured. The curve is normalized by means of Eq. (13) because the effects of the interference term and $(E_0/E)^{\frac{1}{2}}$ factor are appreciable in the wings. The statistical errors are smaller than the points except in the regions where they are indicated.

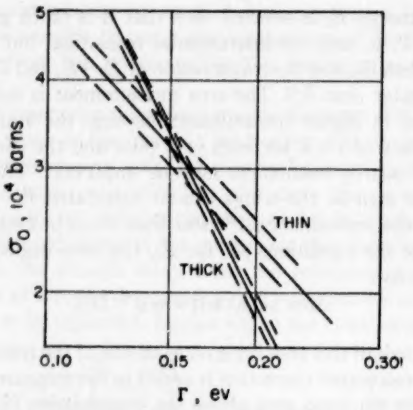

FIG. 13. A plot of σ_0 as a function of Γ for the area analysis of the 5.2-ev level in Ag^{109}. "Thin" and "thick" refer to samples for which $1/n = 72\,200 \times 10^{-24}$ and 2110×10^{-24} cm^3/atom, respectively, for Ag^{109}. The broken lines indicate the error in σ_0 for a given value of Γ. The intersection of the two solid lines gives $\sigma_0 = 30\,800$ b and $\Gamma = 0.157$ ev.

The results of the area measurements are summarized in the second column of Table II. The third column of this table gives "best" values of the parameters of the 5.2-ev level in Ag^{109} obtained by a least-squares fit to the quantities in the first and second columns which were actually measured, that is, σ_0 and Γ for the shape analysis, and $\sigma_0\Gamma^{1.06}$ and $\sigma_0\Gamma^{1.91}$ for the area analysis. From the table it can be seen that the two methods of analysis give results that agree well with each other, and with those of Selove, which are shown in the fourth column. Earlier measurements of the parameters of this resonance, quoted by Selove, agree with Table II but are less accurate. Since Ag^{109} has a spin $I = \frac{1}{2}$, the two choices for the angular momentum of the resonance are $J = 0$ or 1. The expected values of Γ_n/Γ for these possibilities, calculated from the "best" values of σ_0 and E_0, are 0.22 ± 0.01 or 0.073 ± 0.003 for $J = 0$ or 1, respectively. Experimentally, values of Γ_n/Γ are 0.04 as measured by Harris *et al.*,[41] and 0.11 as measured by Sheer *et al.*[42] The correct choice seems to be $J = 1$, which gives a value for Γ_n of 12.2 ± 0.5 mv.

In those cases where corrections for instrumental resolution are small and either the shape or area methods are applicable, the relative accuracy of the two methods is of interest. The area method requires the measurement of a thick sample in addition to the thin sample that is required in both methods, but this fact is not a great disadvantage; the additional time required is

[41] Harris, Muehlhause, and Thomas, Phys. Rev. **79**, 11 (1950).
[42] Sheer, Moore, and Heindl, Phys. Rev. **91**, 449 (1953); U. S. Atomic Energy Commission Report CU-116, 1952 (unpublished).

relatively short since it is much easier to obtain the desired percentage accuracy in area for the thick sample than for the thin sample. As far as the amount of time involved in the analysis is concerned, it is not significantly different for the two methods. With the factors just described taken into account, the following conclusions can be drawn from the analysis of the 5.2-ev Ag resonance:

1. The two methods seem to give equally good values of Γ.
2. If the corrections for instrumental resolution are relatively small, and if $\Delta/\Gamma \lesssim 1$ so that σ_Δ/σ_0 is not very sensitive to errors in Δ/Γ, then the analysis of the resonance shape gives a more accurate value of σ_0.
3. The quantities $g\Gamma_n$ and $\sigma_0\Gamma^2$, which are measures of the area above transmission dips in the limiting cases of thin and thick samples, are best measured by the area method in most cases.

For this example the choice of method of analysis therefore depends on whether the parameters desired are characteristics of the shape of the resonance (σ_0 and Γ), or of the area above the transmission dips ($\sigma_0\Gamma$ and $\sigma_0\Gamma^2$). More generally, the choice would depend upon the energy region, which determines the extent of the distortion of the resonance shape by resolution and Doppler broadening.

B. Poor Resolution Region

At energies where the resolution width is much larger than Γ, the observed transmission curve at a resonance is determined more by the shape of the resolution function and the sample thickness than by the resonance itself. The "shape" method of analysis just described for determination of the level parameters is thus not applicable because of the large corrections that would be necessary to obtain the true shape of the resonance. It also becomes difficult to make the thin-sample transmission measurement necessary for the "area" method because any sample that gives a transmission significantly less than unity (as seen with the actual resolution) is in reality a thick sample. As a result of these experimental conditions, the parameters σ_0 and Γ cannot be determined separately in practice, and only the combination $\sigma_0\Gamma^p$, where p is very nearly 2, is readily obtainable. This quantity results from a thick sample measurement because the cross section in the wings of the resonance, which is proportional to $\sigma_0\Gamma^2$, determines the measured transmission for a thick sample. The actual transmission near the center of the resonance is practically zero; hence its precise value has little effect on the measured transmission.

Corresponding to the decreased information available, there is some simplification in the method of analysis applied to the measured transmission curves, in comparison to the procedure for the good resolution region already described. For example, the wing correction to the area becomes less important, because at high energy the resolution function is much wider than the resonances, whose widths increase only slowly with energy compared to the rapid increase of the resolution width. For predominantly capture resonances the observed transmission rises rapidly to that corresponding to potential scattering, and for the resolution shown in Fig. 7 the wing correction may be neglected for resonances in heavy elements ($A \geq 100$) above about 30 ev.

It is, however, still necessary to make corrections for the effects of Doppler broadening and sample thickness in the calculation of $\sigma_0\Gamma^2$ from the area above the transmission dip for a thick sample. Figure 10, which gives these corrections, can be easily transformed to a form more useful for work with thick samples. The results of this transformation are families of curves giving a correction factor y as a function of the measured area A in ev, for various values of Γ and the Doppler broadening Δ [Eq. (7)]. The correction factor y is defined as

$$y = (\sigma_0\Gamma^2)_{\text{measured}}/\sigma_0\Gamma^2, \tag{15}$$

where

$$(\sigma_0\Gamma^2)_{\text{measured}} = A^2/n\pi. \tag{16}$$

Sets of the correction curves are shown in Figs. 14, 15, and 16 for $\Gamma = 0.05$ ev, 0.10 ev, and 0.20 ev, respectively, which cover the range usually encountered in this parameter. The correction unfortunately depends on Γ, the unknown width of the resonance, but the sample thickness can usually be chosen to make this dependence rather small.

The curves of Figs. 14–16 are convenient for use in measurement of $\sigma_0\Gamma^2$, because they give the magnitude of the Doppler and sample thickness correction much

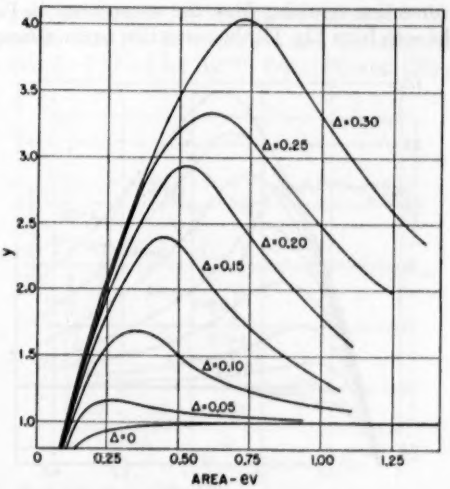

FIG. 14. The correction factor y defined by Eq. (15), as a function of the area above a transmission dip for total width $\Gamma = 0.05$ ev and various values of the Doppler width Δ.

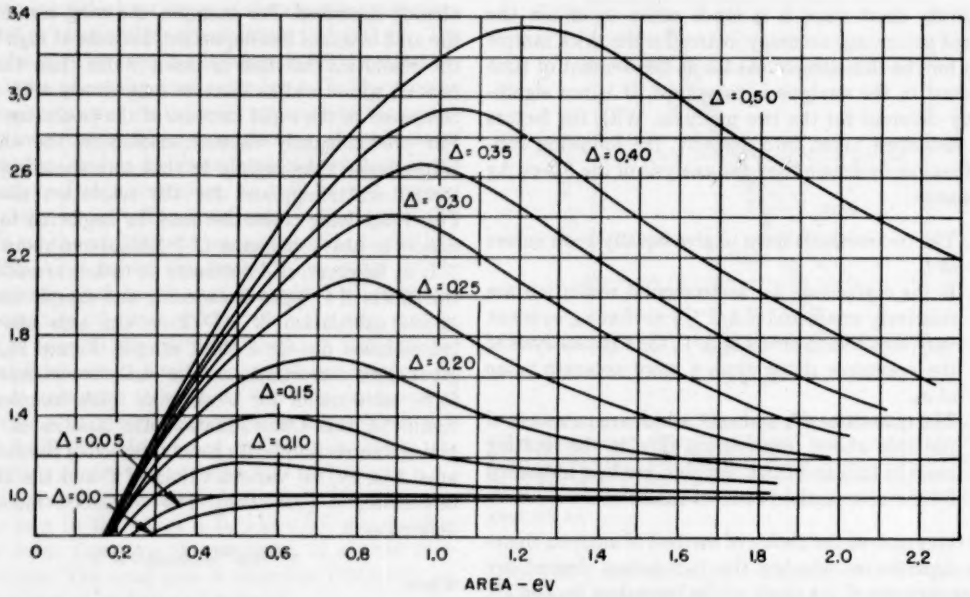

FIG. 15. The correction factor y defined by Eq. (15), as a function of the area above a transmission dip for total width $\Gamma=0.10$ ev, and various values of the Doppler width Δ. For large areas (thick samples) and $\Delta \gtrsim \Gamma$ the correction is small and relatively insensitive to Δ.

This family of curves can be used for values of Γ other than 0.10 ev. For a new set of quantities, Γ', A', and Δ', the value of y is found on the curve for $\Delta=\Delta'/10\Gamma'$ at $A=A'/10\Gamma'$. For example, if $\Gamma'=0.13$ ev, $A'=1.17$ ev, and $\Delta'=0.26$ ev, then $A=1.17/10(0.13)=0.9$, $\Delta=0.26/10(0.13)=0.2$, and from the figure, $y=1.60$.

more directly than do the curves of Fig. 10. In addition they make it possible to estimate readily the error in the correction resulting from uncertainty in the chosen Δ, and thus they aid in choice of a sample thickness to lessen the correction. Plots of y as a function of A for various values of Γ, for a given Δ (an example of which is shown in Fig. 17) can be used to estimate the error in the correction resulting from the uncertainty in Γ. As can be seen from Fig. 17, the correction to the measured $\sigma_0\Gamma^2$ can be obtained with good accuracy for samples of appropriate thicknesses, in spite of the uncertainty in Γ. Fortunately, measurements in the good resolution region indicate that values of Γ_γ do not vary greatly from resonance to resonance in a single isotope nor from isotope to isotope.[43] As a result, the correction y may be made with confidence.

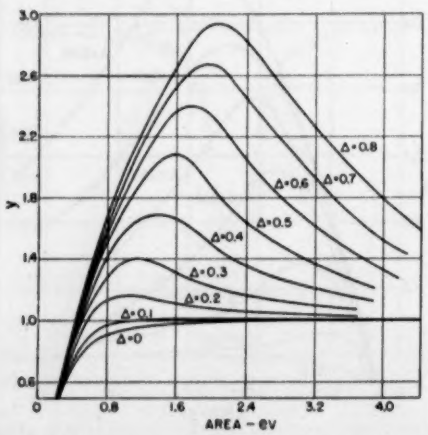

FIG. 16. The correction factor y as a function of the area above a transmission dip for total width $\Gamma=0.20$ ev and various values of the Doppler width Δ.

The procedure for determining $\sigma_0\Gamma^2$ by the area method is one that can be applied to many resonances in a routine manner. The area of a resonance dip, measured as already described, is first used to calculate $\sigma_0\Gamma^2_{\text{measured}}$ from Eq. (16). For the assumed Γ and a Δ, calculated from Eq. (7), the correction factor is obtained from Figs. 14, 15, or 16, by interpolation if necessary. The true value of $\sigma_0\Gamma^2$ is then obtained by dividing $(\sigma_0\Gamma^2)_{\text{measured}}$ by the correction factor y. Should this correction be large, the measurement is usually repeated with a thicker sample in order to make y closer to unity. Figure 17 shows that for a larger area, i.e., a thicker sample for a given resonance, there is a smaller correction, and one that is less sensitive to errors in Γ. It should be noted that with a very thick sample the wing corrections may become appreciable; thus some compromise must be made in sample thickness. The sample should be sufficiently thick for a given resonance to make the correction factor close to unity and insensitive

[43] D. J. Hughes and J. A. Harvey, Nature 173, 942 (1954).

to changes of Γ, and at the same time not so thick that the wing correction becomes large.

The quantity $\sigma_0\Gamma^2$, obtained by the procedure just described, is not of much interest as such, but it is useful to combine it with an assumed Γ_γ, and hence obtain $g\Gamma_n$. As we shall see later the fluctuations in $g\Gamma_n$ are extremely large compared to the relative constancy of measured values of Γ_γ; hence, assumption of Γ_γ does not involve a serious error. The estimate of the neutron width is made by means of the relation,

$$\sigma_0\Gamma^2=4\pi\lambda_0^2 g(\Gamma_n\Gamma_\gamma+\Gamma_n^2); \tag{17}$$

thus

$$\Gamma_n=\tfrac{1}{2}[(\Gamma_\gamma^2+\sigma_0\Gamma^2/\pi\lambda_0^2 g)^{\frac{1}{2}}-\Gamma_\gamma]. \tag{18}$$

For most of the resonances investigated scattering is much less than capture, in which case Eq. (18) reduces to

$$\Gamma_n=\frac{\sigma_0\Gamma^2}{4\pi\lambda_0^2 g\Gamma_\gamma}. \tag{19}$$

The statistical weight g of the resonance is known only in relatively few cases. As can be seen from Eq. (3), if I is zero, $g=1$, and g approaches $\frac{1}{2}$ for large I. For purposes of estimating Γ_n, g is taken to be unity for target nuclei of spin zero, and $\frac{1}{2}$ for all other cases. The maximum error introduced by this assumption is for $I=\frac{1}{2}$, for which the calculated value of Γ_n may be in error by as much as a factor of two. The Γ_n obtained from Eq. (19) seems to depend linearly on the reciprocal of the assumed Γ_γ but the dependence is actually weaker, being linear only for an infinitely thick sample. This result follows from the fact that the assumed Γ_γ is also used in the evaluation of the correction factor y to obtain $\sigma_0\Gamma^2$, and the dependence of Γ_n on Γ_γ is partially canceled. In comparing neutron widths for resonances at different energies, it is useful to eliminate the proportionality of Γ_n to $E_0^{\frac{1}{2}}$ by calculating the reduced neutron width

$$\Gamma_n^0=\Gamma_n(\epsilon/E_0)^{\frac{1}{2}}. \tag{20}$$

For convenience, ϵ is taken as 1 ev.

An example of the analysis used in the poor resolution region is furnished by the 31-ev resonance in Ag^{109}. In Fig. 18 the transmission is plotted as a function of time of flight for a 6.6 g/cm² sample of silver of normal isotopic composition. The transmission far from the resonance, which is reasonably flat at a value of 0.785 $\pm$0.005, is taken as the transmission representing the potential scattering; this transmission corresponds to a cross section of 6 barns. The area of the dip below the potential scattering is measured as 5.9$\pm$0.5 μsec, which, when normalized to unity transmission to remove the contribution of the potential scattering, becomes 7.6 $\pm$0.7 μsec, or 1.8$\pm$0.2 ev in energy units. The "measured," or uncorrected, $\sigma_0\Gamma^2$ resulting from this area, by Eq. (16), is 60$\pm$12 ev² b. The Doppler width Δ is 0.17 ev, calculated as before.

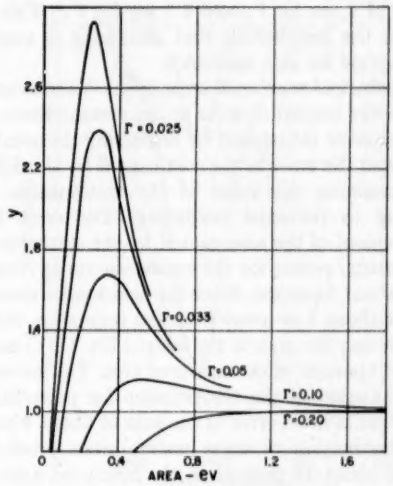

FIG. 17. The correction factor y as a function of the area above a transmission dip for $\Delta=0.10$ ev and various values of Γ. Plots of this type are useful for estimating the error in the correction fatcor that results from an uncertainty in Γ.

In order to calculate the correction factor y, it is necessary to assume a value for Γ. Fortunately the correction factor is not in general very sensitive to the assumed value of Γ if the sample is sufficiently thick. For the present example Γ is taken to be 0.13 ev, a value based on the average of directly measured Γ_γ's in the good resolution region,[43] and on the assumption that $\Gamma\approx\Gamma_\gamma$. From the curves of Figs. 14–16, y is found to be 1.09 and the true $\sigma_0\Gamma^2$ becomes 55$\pm$10 ev² b. To indicate the sensitivity of this result to the assumed Γ, calculations are also made for $\Gamma=0.05$ ev and 0.2 ev. These results, summarized in Table III, indicate that in this example y is indeed insensitive to the choice of Γ. On the assumption that $\Gamma=\Gamma_\gamma=0.13$ ev, and the approximation that $g=\frac{1}{2}$ ($I=\frac{1}{2}$ for Ag^{109}), Eqs. (19) and (20) give

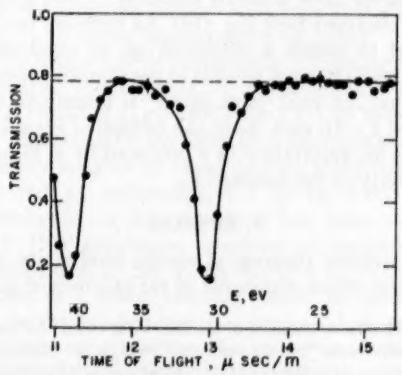

FIG. 18. A plot of transmission as a function of neutron time of flight for a 6.6 g/cm² sample of normal silver. The area obtained from this curve is used in the example of Sec. IV B to calculate $\sigma_0\Gamma^2$ for the 31-ev resonance in Ag^{109}. The data are not normalized; the broken line indicates the transmission for potential scattering.

a value of 9 mv for Γ_n and 1.7 mv for Γ_n^0. This result confirms the assumption that scattering is much less than capture for this resonance.

The principal sources of error in the determination of $\sigma_0\Gamma^2$ are the statistical error in the measurement of the area, the error introduced by neglecting the area in the wings, and the error in the area caused by the difficulty in determining the value of the transmission corresponding to potential scattering. The error in the measurement of the area caused by the statistics of the experimental points for the resonance under consideration is about 3 percent. Since the area measurement was stopped about 5 ev away from the resonance, the error in neglecting the area in the wings [Eq. (14)] amounts to about 5 percent of the measured area. The uncertainty in the location of the transmission for potential scattering results in an error in the area of about 4 percent. The combination of these uncertainties produces an error of about 10 percent in the measured area. Since $\sigma_0\Gamma^2$ is proportional to the square of the area, the error in the determination of $\sigma_0\Gamma^2$ caused by uncertainties in the area measurement is about ± 20 percent. As was shown, variation of the assumed Γ by a factor of two changes $\sigma_0\Gamma^2$ by an amount small compared to this 20 percent. Also any uncertainty in the measurement of sample thickness is usually small compared to other errors.

The 31-ev resonance in silver is sufficiently well separated from its neighbors with the present resolution that they do not give rise to any uncertainties in the analysis. At somewhat higher energies, the rapidly increasing spread of the resolution function makes it difficult to locate a transmission between resonances that corresponds to potential scattering, and at still higher energies it is difficult even to distinguish the individual resonances. This increasing difficulty in analysis will be exemplified for silver and other elements in Sec. V.

For many of the resonances analyzed in Sec. V the assumption that $\Gamma_\gamma \gg \Gamma_n$ is not valid. A value of Γ is obtained for these levels by assuming Γ_γ and adding to it a Γ_n obtained from Eq. (18). An iteration process is required to obtain a consistent set of numbers. For several levels it is not feasible to use samples sufficiently thick that the final value of $\sigma_0\Gamma^2$ is insensitive to the assumed Γ_γ. In such cases the estimated error in $\sigma_0\Gamma^2$ includes an uncertainty in y produced by a 20 percent uncertainty in the assumed Γ_γ.

V. RESULTS

An extensive program of energy level study is now under way which makes use of the methods of analysis described in the previous section. In this work the identification of energy levels with individual isotopes usually necessitates the use of separated isotopes, and in this respect the small sample size of the fast chopper is a great advantage. Total cross sections alone have been measured; the only uncertainty in the determination of parameters that results from this procedure is the uncertainty in g; and at the present stage of neutron spectroscopy this is not significant. The main advantage of additional measurements of scattering or absorption, which would give g, would be in the resulting knowledge of the level spin J.

The general program consists of measurement of individual level parameters at low energy, where good resolution makes such determinations possible, together with measurement of $\sigma_0\Gamma^2$ alone for resonances in the poor resolution region. This latter quantity is used to obtain values of Γ_n, on the assumption that the variation of Γ_γ from resonance to resonance is so much less than that of Γ_n that values of Γ_γ obtained from low energy resonances may be used in the analysis. The results of the measurements to date show that this assumption is justified and that the values of Γ_n thus obtained are reasonably accurate. When higher resolution is available with the fast chopper, individual parameters can be measured for additional resonances and the validity of the assumption concerning Γ_γ investigated in more detail. The results for several elements will be considered at present and the findings concerning level densities and widths discussed briefly. Additional measurements with the fast chopper, not included in this report, have been presented recently.[44–48]

TABLE III. The dependence of the final value of $\sigma_0\Gamma^2$ for the 31-ev resonance in Ag^{109} on the assumed Γ used in the calculation.

Γ	0.05 ev	0.13 ev	0.20 ev
y	1.13	1.09	1.05
$\sigma_0\Gamma^2$	53 ev^2 b	55 ev^2 b	57 ev^2 b

A. Manganese and Cobalt

When the fast chopper was first put into operation, some measurements were made on medium weight nuclei with well-separated resonances to test its performance. Manganese and cobalt were suitable for this purpose since their level spacings were sufficiently great that the first few resonances should not overlap and furthermore both had been investigated with other velocity selectors. The fact that the resonances in both these elements are almost completely scattering[41] also simplified the analysis greatly.

A previously unknown resonance, shown in the cross-section curve of Fig. 19, was found in Mn^{55} at 1120 ± 60 ev. This level had not been observed before because of the very poor resolution available in this energy region which lies between those that were covered by the time-of-flight[49] and Van de Graaff[32] measurements, also

[44] Hughes, Kato, and Levin, Phys. Rev. **92**, 1094 (1953).
[45] Kato, Hughes, and Levin, Phys. Rev. **93**, 931 (1954).
[46] J. S. Levin and D. J. Hughes, Bull. Am. Phys. Soc. **29**, No. 4, 57 (1954).
[47] R. S. Carter and J. A. Harvey, Bull. Am. Phys. Soc. **29**, No. 4, 57 (1954).
[48] Pilcher, Carter, and Stolovy, Bull. Am. Phys. Soc. **29**, No. 4, 57 (1954).
[49] Rainwater, Havens, Wu, and Dunning, Phys. Rev. **71**, 65 (1947).

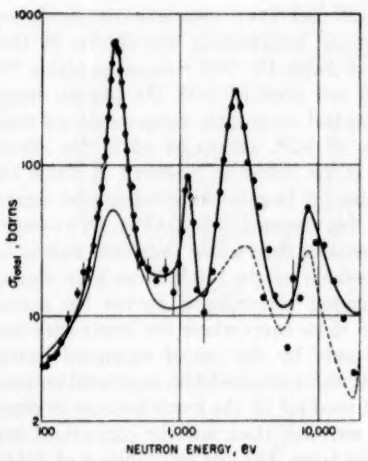

FIG. 19. The total cross section of Mn^{55} as a function of neutron energy. A 0.46 g/cm² sample of manganese was used to make the measurements above 150 ev. A previously unknown resonance was found at 1120 ev; this level lies between the energy region well covered by the earlier time-of-flight measurements (see reference 49) (light solid line) and that well covered by Van de Graaff measurements (see reference 32) (broken line). The fast chopper measurements bridge this gap, and below 4 kev provide better resolution than is available with present-day Van de Graaff measurements. The peak heights shown in this figure are not the true peak heights of the resonances, but are distorted by the instrumental resolution; higher values would be observed with a thinner sample.

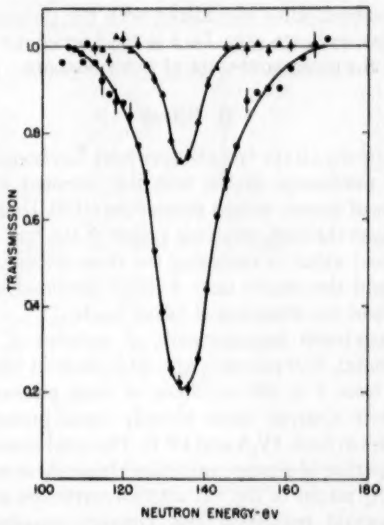

FIG. 20. The normalized transmission as a function of neutron energy for thin ($1/n = 22\,200\times10^{-24}$ cm²/atom) and thick ($1/n = 2230\times10^{-24}$ cm²/atom) samples of Co^{59}. These measurements were used in the area analysis of Sec. V A to obtain parameters of the 134-ev resonance.

shown in Fig. 19. This example illustrates the value of the fast chopper in bridging the gap that formerly existed between these two types of measurements. The presence of this resonance has since been confirmed by measurements with other time-of-flight instruments.[50,51]

Parameters were determined for the level at 346±11 ev by fitting the shape of the cross-section curve between 150 ev and 250 ev with a single-level Breit-Wigner formula that included interference between resonance and potential scattering; the thickness of the Mn metal sample was 2.4 g/cm². In this energy region the cross section is dominated by the 346-ev level and the effects of instrumental resolution are negligible. The analysis yielded $\sigma_0\Gamma^2 = (3.0\pm0.6)\times10^6$ ev² b, and since the resonance is almost completely scattering, it follows that $g^1\Gamma_n = 20\pm2$ ev. The spin of Mn^{55} is 5/2; therefore $\Gamma_n = 31\pm3$ ev or 26 ± 3 ev for $J=2$ or 3, in agreement with the work of Harris *et al.*[52] They selected $J=3$ as the correct value of the spin of the compound state. If most of the 13-barn thermal cross section is associated with the 346-ev level, then this measurement gives a value of 0.5±0.1 ev for the radiation width of the resonance.

Measurements were made on the 134±2 ev resonance in Co^{59} in order to determine σ_0 and Γ by the "area" method and to see if J could thus be determined for this level. Although Doppler broadening is negligible ($\Delta/\Gamma \approx 0.1$), a resolution of 0.18 μsec/m was not adequate for use of the "shape" method of analysis because this resolution width was almost twice the width of the resonance. Normalized transmission curves are shown in Fig. 20. The areas above the transmission dips, including a correction for the area in the wings, were 3.22±0.16 ev and 17.9±0.5 ev for samples with $1/n = 22\,200\times10^{-24}$ and 2230×10^{-24} cm²/atom, respectively. The samples used were solutions of $CoSO_4$ in heavy water. Neither sample was so thick that the interference between resonance and potential scattering would introduce any appreciable error in the analysis. Parameters for this level, obtained from these areas, are $\sigma_0 = 9700\pm1800$ b, $\Gamma = 5.2\pm0.7$ ev, $\sigma_0\Gamma = 51\,000\pm3000$ ev b, and $\sigma_0\Gamma^2 = 260\,000\pm16\,000$ ev² b. The value of $\sigma_0\Gamma^2$ agrees with previously published values.[24] Reference 24 also includes references to earlier measurements on cobalt.

As the spin of Co^{59} is known to be 7/2 and as the level is primarily scattering (Γ_n/Γ about 0.95),[41] the two possible values of σ_0 are 8200 b for $J=3$, or 10 600 b for $J=4$. Unfortunately the value of σ_0 here obtained is not sufficiently accurate to chose between these two values and permit an assignment of J for the level. Earlier measurements on this resonance had been made by Seidl.[53] This experiment consisted of measuring the transmission of a thin cobalt foil as a function of the thickness of a boron absorber placed in the neutron beam, by using a detector that was selectively sensitive to neutrons scattered by the cobalt resonance. The results of the experiment were consistent with either $\Gamma = 2.0\pm0.1$ ev and $J=4$ or $\Gamma = 5.0\pm0.5$ ev and $J=3$.

[50] L. M. Bollinger (private communication).
[51] Albert, Yeater, and Gaerttner (private communication).
[52] Harris, Hibdon, and Muehlhause, Phys. Rev. **80**, 1014 (1950).
[53] F. G. P. Seidl, Phys. Rev. **75**, 1508 (1949).

These values, when considered with the present measurements, indicate that $J=3$ is the best choice for the spin of the compound state of this resonance.

B. Silver

Practically all the fast chopper work has been devoted to the resonances in the first few hundred volts for isotopes of atomic weight greater than 100. Under these conditions the high resolving power of the fast chopper is of great value in analyzing the close resonances that occur and the results have a direct application to the theories of the structure of heavy nuclei.

Transmission measurements of samples of normal silver metal, 99.9 percent pure, were made in the energy region from 5 to 200 ev. Some of these measurements and their analysis have already been presented as examples in Secs. IV A and IV B. The total cross section as a function of energy, calculated from these measurements by means of Eq. (4) with no correction made for instrumental resolution and Doppler broadening, is shown in Fig. 21. The cross-section curve thus obtained is of course only a qualitative description of the true cross section, for as has been seen the resonances are distorted by instrumental resolution and Doppler broadening. Measurements on silver by other experimenters are given in references 15 and 24.

Transmission measurements were also made with electromagnetically enriched samples of silver isotopes, obtained from the Isotopes Division at Oak Ridge National Laboratory. Transmission curves for these separated isotopes, as well as for normal silver, are shown in Fig. 22. The high isotopic purity of these samples (>96 percent of the isotope of interest) made it a simple procedure to assign all the resonances below 100 ev. The resonance observed in normal silver at about 41.5 ev was found to be two levels, one in Ag^{109} at 40.8 ev, and the other in Ag^{107} at 42.4 ev. The two resonances between 50 and 60 ev were also completely separated. The isotopic assignments are shown in the second column of Table IV. The resonances above 100 ev are probably not resolved with the present instrumental resolution and no isotopic assignments are made.

Values of $\sigma_0\Gamma^2$, calculated as in the discussion of Sec. IV B, are shown in column 7 of Table IV. In the corrections for Doppler broadening and sample thickness, Γ_γ was assumed to be 0.13 ev, an average value of experimentally determined radiation widths in the region of atomic weight 110.[43] Areas were obtained from the measured transmission curves for normal silver except in those cases where the levels were adequately resolved only by the use of separated isotopes. The areas that were measured with separated isotope samples were not used for all the levels because in general these samples were not thick and the corrections were therefore rather large. The last two columns of Table IV give values of $2g\Gamma_n$ and $2g\Gamma_n^0$, calculated from Eqs. (19) and (20) by assuming $\Gamma_\gamma=0.13$ ev. Since g is unknown for all but the 5.2-ev level ($I=\frac{1}{2}$ for both isotopes of silver), these columns correspond to Γ_n and Γ_n^0 under the approximation that $g=\frac{1}{2}$. In the calculation of the *average* reduced neutron width, $\bar{\Gamma}_n^0$, little error is introduced by this approximation. Except for the one small resonance at 45.6 ev the values of Γ_n^0 are reasonably constant.

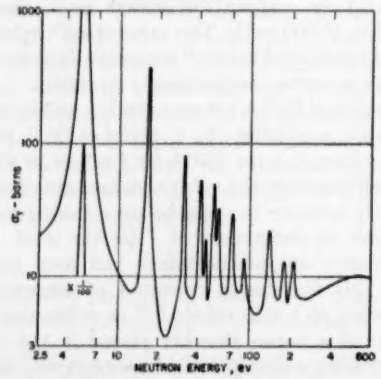

FIG. 21. The total cross section of Ag as a function of neutron energy. The 42-ev "level" is composed of two resonances, one in each isotope. Above 100 ev individual levels were not resolved. Observed cross sections near resonance are not the true values, but are lowered by the effects of instrumental resolution and Doppler broadening.

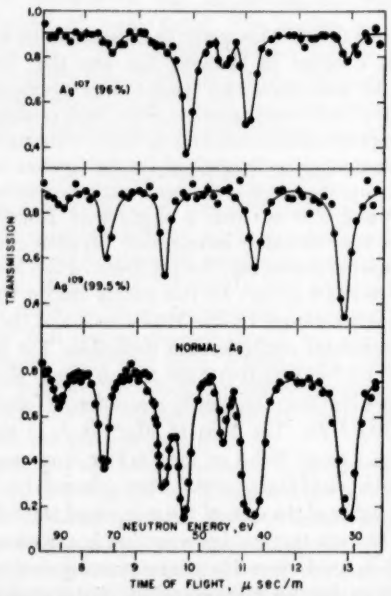

FIG. 22. The transmission as a function of neutron time of flight for samples of isotopically enriched silver and of normal silver. The Ag^{107} sample contained 1.20 g/cm² of Ag^{107}, the Ag^{109} sample 0.82 g/cm² of Ag^{109}, and the sample of normal silver 3.4 g/cm² of Ag^{107} and 3.2 g/cm² of Ag^{109}. The calculated contribution of the 4 percent Ag^{109} to the transmission of the Ag^{107} sample agreed with the dips observed at 31, 57, and 72 ev. The 42-ev "level" appeared to be too wide in the normal Ag sample, but in the enriched samples it was resolved into two levels (one in each isotope) at somewhat different energies.

TABLE IV. A summary of the parameters of the levels from 0 to 100 ev in Ag^{107} and Ag^{109}. Γ_γ is assumed to be 0.13 ev.

E_0 ev	Isotope	Area ev	$(1/n)\times10^{24}$ cm³/atom	Δ ev	y	$\sigma_0\Gamma^2$ ev² b	$2g\Gamma_n$ mv	$2g\Gamma_n^0$ mv
5.22±0.04[a]	109			0.071		775±25	12.2± 0.5	5.3 ±0.2
16.6 ±0.15	107	1.9 ±0.2	52.4	0.13	1.03	60± 7[b]	5.6± 0.8	1.4 ±0.2
31.1 ±0.4	109	1.8 ±0.2	56.3	0.17	1.09	52± 6[b]	9 ± 2	1.6 ±0.3
40.8 ±0.6	109	0.82±0.12[c]	220	0.20	1.41	34±10	8 ± 3	1.2 ±0.4
42.4 ±0.6	107	1.1 ±0.2[c]	150	0.20	1.31	45±15	10 ± 4	1.6 ±0.6
45.6 ±0.7	107	0.85±0.08	52.4	0.21	1.50	8± 2	2.1± 0.6	0.31±0.09
52.2 ±0.8	107	2.9 ±0.6	52.4	0.22	1.04	140±40		
		2.0 ±0.2[c]	150		1.13	165+40		
					Average	150±30	36 ±10	5.0 ±1.4
56.8 ±0.9	109	2.5 ±0.5	56.3	0.23	1.09	100±40		
		1.3 ±0.2[c]	220		1.31	90±30		
					Average	95±25	24 ± 6	3.2 ±0.8
72.5 ±1.3	109	3.0 ±0.3	56.3	0.27	1.10	150±30	47 ±15	5.5 ±1.8
88.5 ±2	109	1.34±0.14	56.3	0.29	1.55	21± 5	10 ± 3	1.1 ±0.3

	Ag^{107}	Ag^{109}
$\bar{\Gamma}_n^0$	2.1 mv	3.0 mv
D	50 ev	33 ev

[a] The results for this resonance are taken from the third column of Table II, with $g=\frac{1}{2}$. The numbers in the last two columns are Γ_n and Γ_n^0.
[b] Average of four measurements with samples of different thicknesses.
[c] Measured with isotopically enriched samples.

These values can be expected to vary by a factor of three just because of the fact that the J value of the levels are not known. Above 100 ev the reduced neutron widths become much larger; this fact is taken to indicate that the observed "levels" are multiple, the actual levels not being resolved.

On the assumption that all the resonances below 100 ev have been resolved, the average spacing of levels D was calculated. This spacing refers to levels of a single J that are a result of $l=0$ interactions and that lie at an excitation energy just above the neutron binding energy. The level spacing was estimated by dividing the energy interval considered by the number of levels found in that interval, and doubling this number on the assumption that half of the levels are in each spin state. The level spacing is 50 ev and 33 ev in Ag^{107} and Ag^{109}, respectively. Arithmetic averages of the reduced neutron widths $\bar{\Gamma}_n^0$, for these isotopes are 2.1 mv and 3.0 mv, respectively. It is almost certain that for the energy region below 100 ev all levels for $l=0$ interactions in these isotopes have been found. At 100 ev any resonance with a Γ_n^0 larger than 1/20 of $\bar{\Gamma}_n^0$ would have been seen; at lower energies even weaker resonances would have been detected.

C. Iodine

Transmission measurements of samples of elemental iodine, 99.9 percent pure, were made in the energy region from 15 to 200 ev; it is known from the work of other experimenters[24] that there are no neutron resonances below 15 ev. A cross-section curve is shown in Fig. 23. The resonance structure is much more clearly resolved here than in earlier measurements by others. The parameters of the resonances up to 100 ev, measured in the manner described for silver, are summarized in Table V. Above 100 ev the levels were not well resolved and therefore were not analyzed, whereas below 100 ev it seems certain that all $l=0$ resonances are represented. The calculated parameters are based on a value of Γ_γ of 0.10 ev.

On the assumption that all the resonances below 100 ev have been resolved, the average level spacing for states of a given J in iodine is 29 ev. The average value of Γ_n^0 for these levels is 2.8 mv. The observed values of $2g\Gamma_n^0$ show fluctuations of a factor of 20; as the spin of I^{127} is 5/2, lack of knowledge of J can produce variations of only a factor of 1.4. It can be concluded that the fluctuations in Γ_n^0 are much larger than those which have been observed in Γ_γ;[43] thus, any minor fluctuations in Γ_γ will not appreciably affect the calculation of Γ_n^0.

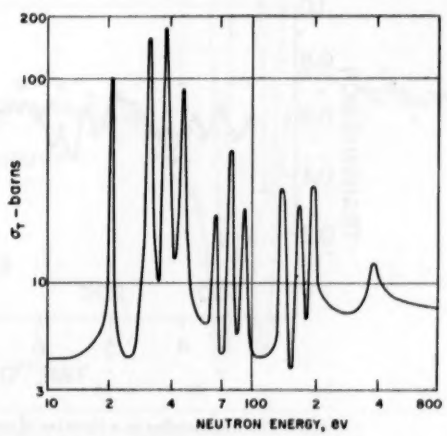

FIG. 23. The total cross section of I^{127} as a function of neutron energy. There are no resonances below 20 ev; above 100 ev individual levels were not resolved. Observed cross sections near resonance are not the true values, but are distorted by the effects of instrumental resolution and Doppler broadening.

TABLE V. A summary of the parameters of the levels from 0 to 100 ev in iodine. Γ_γ is assumed to be 0.10 ev.

E_0 ev	Area ev	$(1/n)\times10^{24}$ cm²/atom	Δ ev	y	$\sigma_0\Gamma^2$ ev² b	$2g\Gamma_n$ mv	$2g\Gamma_n^0$ mv
20.5±0.3	0.70±0.07	80.0	0.13	1.24	10± 3	1.6± 0.5	0.35±0.11
31.4±0.5	2.1 ±0.2	80.0	0.16	1.03	105±30	21 ± 7	3.8 ±1.3
37.7±0.7	2.7 ±0.3	80.0	0.17	1.04	180±50	38 ±13	6.0 ±2.0
46 ±1	1.8 ±0.3	80.0	0.19	1.13	75±30	21 ± 9	3.2 ±1.4
66 ±2	1.0 ±0.4	25.2	0.23	1.70	5^{+9}_{-3}	$2.3^{+4}_{-1.5}$	$0.3^{+0.5}_{-0.2}$
78 ±2	1.7 ±0.4	80.0	0.25	1.26	60^{+50}_{-30}	30^{+25}_{-15}	$3^{+3}_{-1.5}$
91 ±3	2.6 ±0.8	25.2	0.27	1.07	50^{+50}_{-25}	30^{+30}_{-15}	$3^{+3}_{-1.5}$
		$D=29$ ev			$\bar{\Gamma}_n^0=2.8$ mv		

D. Gold

Transmission measurements of samples of high-purity gold metal were made in the energy region from 3 to 300 ev. A transmission curve for a sample thickness of 12.3 g/cm² is shown in Fig. 24 for energies above 30 ev. Below 30 ev there is only one resonance, at 4.9 ev. The asymmetry of the 61.5-ev level and the slope of the transmission curve between 30 and 50 ev are caused by interference between resonance scattering and potential scattering. This interference term falls off slowly, only as the first power of the reciprocal of $E-E_0$. The asymmetry occurs because the interference term changes sign at resonance.

The parameters of the 4.94-ev level were obtained by analysis of the shape of the transmission dip for a 0.00465 g/cm² sample, by using the method described in Sec. IV A. The maximum observed cross section was 25 000±800 b and the observed width at half the maximum cross section was 0.23±0.01 ev. Correcting for instrumental resolution gave $\sigma_\Delta=26\,500\pm1000$ b, and $\Gamma_\Delta=0.20\pm0.01$ ev. For a Doppler width of 0.051 ev the parameters of this level are $\sigma_0=30\,600\pm1500$ b, and $\Gamma=0.163\pm0.015$ ev. These values are in good agreement with the measurements of other experimenters.[54] As the spin of Au^{197} is $\frac{3}{2}$, the choices for the angular momentum of the compound nucleus are $J=1$ or 2, which give expected values for Γ_n/Γ of 0.15±0.01 or 0.093±0.005, respectively. Experimental values obtained for Γ_n/Γ are 0.14 by Harris *et al.*,[41] and 0.12±0.01 by Tittman and Sheer.[55] It thus appears that the accuracy of the measurements is not sufficient to make a definite assignment of J.

The parameters of the resonances up to 200 ev are summarized in Table VI. The calculated parameters are based on a value of Γ_γ of 0.15 ev. On the assumption that all the resonances below 200 ev have been resolved; the average level spacing for a single J in gold is 57 ev. The average value of Γ_n^0 for all the levels measured is 5 mv, with fluctuations of about the same magnitude as observed in iodine.

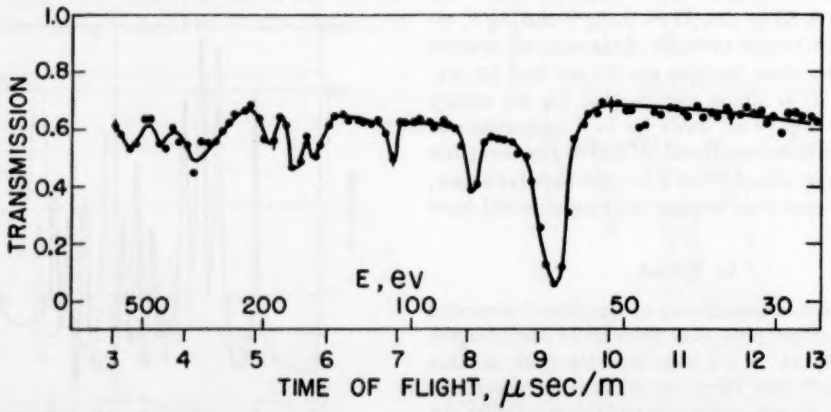

FIG. 24. The transmission as a function of neutron time of flight for a 12.3 g/cm² sample of Au^{197} metal. The only resonance below 30 ev is at 4.9 ev; above 200 ev individual levels were not resolved. The slope of the transmission curve between 30 and 50 ev and the asymmetry of the 61-ev level are caused by interference between resonance and potential scattering.

[54] H. H. Landon and V. L. Sailor, Phys. Rev. **93**, 1030 (1954).
[55] J. Tittman and C. Sheer, Phys. Rev. **83**, 746 (1951).

TABLE VI. A summary of the parameters of the levels from 0 to 200 ev in gold. Γ_γ is assumed to be 0.15 ev.

E_0 ev	Area ev	$(1/n)\times10^{24}$ cm²/atom	Δ ev	y	$g\Gamma_n^0$ ev² b	$2g\Gamma_n$ mv	$2g\Gamma_n^0$ mv
4.94±0.04[a]					800±150	19 ± 2	8.5±0.9
61.5 ±1.0	6.5±1.0	33.5	0.18	1.00	450±130	90 ±30	11 ±3
80.2 ±1.5	2.1±0.4	33.5	0.20	1.09	41± 17		
	1.9±0.3	26.7		1.10	28± 9		
				Average	32± 8	12 ± 4	1.4±0.4
110 ±3	1.4±0.3	33.5	0.24	1.27	16± 8		
	1.2±0.3	26.7		1.33	9± 5		
				Average	12± 4	6.5± 3	0.6±0.3
153 ±4	2.7±0.7	33.5	0.28	1.10	70± 40	43 ±25	3.5±2
168 ±5	4.0±0.9	33.5	0.29	1.04	170± 80	90 ±40	7 ±3
194 ±6	2.5±0.7	33.5	0.32	1.17	55± 35	43 ±30	3 ±2
		D=57 ev			$\bar{\Gamma}_n^0$=5 mv		

[a] Parameters of this resonance are obtained by the "shape" analysis discussed in Sec. V D.

E. Thorium

Thorium was investigated because it is the heaviest monoisotopic element available and it was desired to make measurements over a large range of atomic weights. Transmission measurements of thorium metal were made in the energy region from 5 to 200 ev. Representative transmission curves, shown in Fig. 25 for sample thicknesses of 3.60, 11.0, and 22.1 g/cm², revealed several interesting features. The previously reported resonance[25] at about 20 ev was clearly resolved into two levels, separated by 1.7 ev. Furthermore, these two levels and the 71-ev level showed an asymmetry characteristic of the interference between resonance and potential scattering, which indicates that Γ_n is not negligible compared to Γ_γ. Thorium is a particularly favorable case in which to observe this interference phenomenon because it is monoisotopic and has zero spin; therefore the resonance scattering interferes with the entire potential scattering.

The parameters of the levels in thorium from zero to 140 ev are summarized in Table VII; above this energy

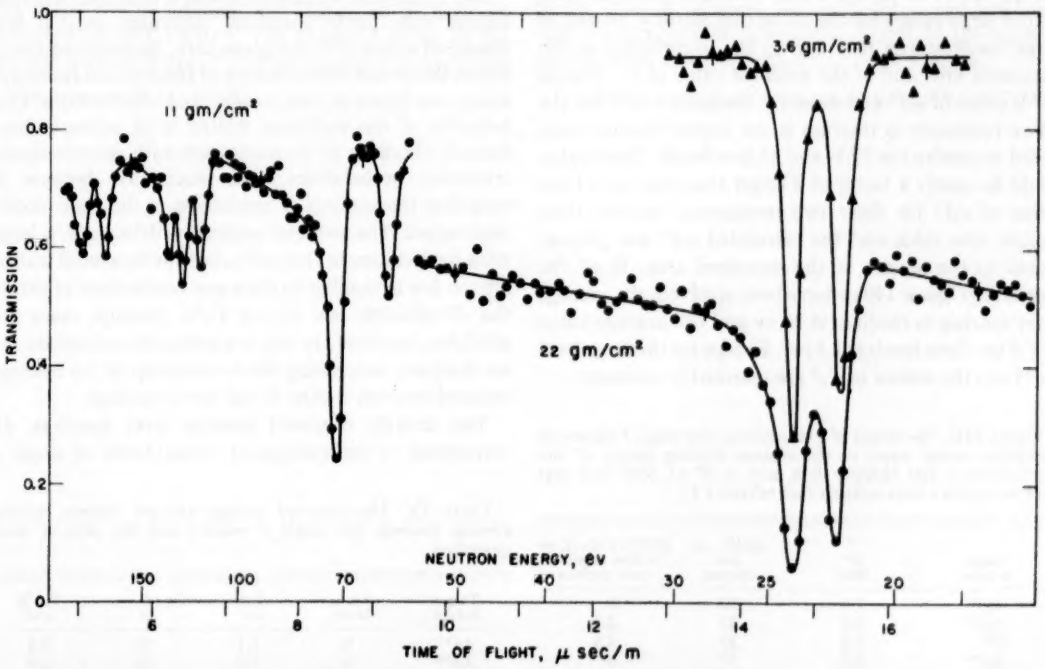

FIG. 25. The transmission as a function of neutron time of flight for samples of Th^{232} metal. There are no resonances below 20 ev; above 140 ev individual levels were not resolved. The two levels between 20 and 25 ev, which are well resolved with the thinnest sample, were not previously resolved by other experimenters. The asymmetry characteristic of interference between resonance and potential scattering is clearly seen in these two levels and the 71-ev level.

TABLE VII. A summary of the parameters of the levels from 0 to 140 ev in thorium. Γ_γ is assumed to be 30 mv.

E_0 ev	Area ev	$(1/n)\times10^{24}$ cm²/atom	Δ ev	y	$\sigma_0\Gamma^2$ ev² b	Γ_n[a] mv	Γ_n^0 [a] mv
22.1±0.2	0.55±0.05	107	0.10	1.52	7± 2	1.8± 0.5	0.4±0.1
23.8±0.3	0.70±0.06	107	0.10	1.28	13± 4	3.5± 1.1	0.7±0.2
60.5±1.0	1.6 ±0.4	17.5	0.16	1.20	12± 5		
	1.1 ±0.2	35		1.60	8± 5		
				Average	10± 4	6.4± 2.5	0.8±0.3
70.8±1.3	1.9 ±0.3	107	0.17	1.04	120±40	44 ±20	5.2±2.5
117 ±3	1.2 ±0.2	35	0.23	2.04	7± 4	8 ± 5	0.8±0.5
127 ±3	1.6 ±0.3	35	0.24	1.33	20±10	20 ±10	1.7±0.9
133 ±3	1.3 ±0.3	35	0.24	1.88	10± 5	12 ± 6	1.1±0.6
		$D=20$ ev		$\bar{\Gamma}_n^0=1.5$ mv			

[a] Since $g=1$ for thorium, the last two columns give Γ_n and Γ_n^0, rather than $2g$ times these quantities.

the levels were not well resolved. The calculated parameters are based on a value of Γ_γ of only 30 mv,[43] which is much smaller, because of the large A, than the radiation widths of the other elements investigated in this paper. It should be noted that the fractional errors in the values of $\sigma_0\Gamma^2$ are larger than those for most of the other elements studied. The reason for this is twofold: first, the prominence of the interference between resonance and potential scattering requires the use of relatively thin samples in order that the measured area be due to the resonance cross section alone; second, Δ/Γ is very large for most of these levels (greater than 3 for all except the 71-ev level). These factors combine to give rather large values for the correction factor y, as well as large uncertainties in y due to the uncertainty in the measured area and in the assumed value of Γ_γ. The 64 ev² b value of $\sigma_0\Gamma^2$ measured by Hodgson *et al.*[25] for the 23-ev resonance in thorium is not correct because they failed to resolve the 22.1- and 23.8-ev levels. Their value could be nearly a factor of 2 larger than the sum of the value of $\sigma_0\Gamma^2$ for these two resonances, because their sample was thick and the calculated $\sigma_0\Gamma^2$ was proportional to the square of the measured area. If all the resonances below 140 ev have been resolved, the average level spacing in thorium is 20 ev and the average value of Γ_n^0 for these levels is 1.5 mv. Except for the large level at 71 ev, the values of Γ_n^0 are reasonably constant.

TABLE VIII. The values of level spacings (for single J values) at excitation energy equal to the neutron binding energy E^* determined from fast chopper data, and at E^*+1 Mev from fast neutron capture cross sections (see reference 1).

Target isotope	E^* Mev	$D(E^*)$, ev fast chopper	$D(E^*+1$ Mev), ev 1-Mev capture cross sections
Ag^{107}	7.4	50	6
Ag^{109}	7.0	33	2.7
I^{127}	7.3	29	3.3
Au^{197}	6.5	57	6[a]
Th^{232}	4.9	20	

[a] This value was computed from the capture cross section given in reference 1 by assuming $\Gamma_\gamma=0.15$ ev, rather than 0.03 ev assumed in that paper.

F. Discussion

The few isotopes whose level parameters have just been described represent only a beginning in the compilation of data needed for comparison with the results of nuclear structure theory. A definite attempt has been made in this work, however, to insure that all resonances of spin $I\pm\frac{1}{2}$ have been found in given energy regions. The results would be of little use if further improvement in resolution revealed still more levels in the same energy region. A number of isotopes not reported here have also been carefully studied with the fast chopper and the results presented briefly.[44–48]

One result that was soon evident is that the radiation widths show little variation. Although only a few measured values of Γ_γ are given here, the near-constancy is best shown in a recent survey of Hughes and Harvey,[43] which was based on fast chopper and other results. This behavior of the radiation widths is of interest theoretically, because of its connection with electric dipole transition probabilities, and practically, because it simplifies the analysis of resonances in the poor resolution region. The reduced neutron widths show a large variation relative to that of Γ_γ, but the measured widths are too few in number to draw any conclusions as yet on the distribution law of the Γ_n^0's. Enough cases are available, however, to reach significant conclusions, as we shall see, concerning the relationship of the average reduced neutron widths to the level spacings.

The directly observed average level spacings, D, correspond to the spacings of virtual levels of single J

TABLE IX. The observed average reduced neutron widths, average spacings (for single J values), and the ratio of these quantities.

Target isotope	No. of levels	$\bar{\Gamma}_n^0$ mv	D ev	$\bar{\Gamma}_n^0/D$ $\times10^4$
Ag^{107}	4	2.1	50	0.4
Ag^{109}	6	3.0	33	0.9
I^{127}	7	2.8	29	1.0
Au^{197}	7	5	57	0.9
Th^{232}	7	1.5	20	0.8

values ($I+\frac{1}{2}$ or $I-\frac{1}{2}$) at an excitation energy just above neutron binding energy. The observed cases are far too few to study variation of level spacing with even-odd effects, shell structure, etc. However, a rough comparison is possible with the level spacings inferred by Hughes, Garth, and Levin[1] from the capture cross sections for 1-Mev neutrons. These cross sections give the average level spacings at an excitation 1 Mev higher than neutron binding and contain some contributions from capture of neutrons with $l>0$. The radiation widths must also be assumed in the determination of the level density but this assumption now seems well justified.

In Table VIII are listed the level spacings obtained from the fast chopper results and from the 1-Mev cross sections. Both sets of D values for the isotopes studied seem to show little variation with atomic weight. The change in measured D with 1 Mev in energy is definite, about a factor of 10 for all the isotopes. It is difficult to estimate what part of this factor can be attributed to the contribution of higher l's in the 1-Mev results, and what part represents a decrease in level spacing for $l=0$. The results on level spacing are as yet too sketchy but they will be of definite value in relation to nuclear structure theory when many more are available.

It is instructive to consider the ratio of the average Γ_n^0 to D, which according to the strong-interaction theory of nuclear cross sections, should be independent of atomic weight and of neutron energy.[56] The value of this ratio, for a potential-well depth of 20 Mev, is predicted to be 1.4×10^{-4}. The observed ratios of the average reduced widths Γ_n^0 to the average spacing D are given in Table IX, from which it can be concluded that the observed ratio is indeed of the order of magnitude predicted and is reasonably constant. The average value for the ratio is 0.8×10^{-4}, which is slightly less than the value based on a 20-Mev well depth. However, it should be noted that the predicted value of 1.4×10^{-4} is based on the assumption of equidistant levels.[57] Any departure from this assumption would decrease the predicted value of the ratio; for example, for a random distribution of levels the predicted ratio is reduced by a factor of two.

[56] See reference 33, pp. 386–90.

ACKNOWLEDGMENTS

The authors wish to express their appreciation to the following people: Richard F. Randall, for his assistance in testing and maintaining the fast chopper and its associated equipment; the Electronics Division of Brookhaven National Laboratory, for work in the design, construction, and maintenance of the time-of-flight electronic analyzer; Charles P. Baker, for the use of his analyzer while the fast chopper analyzer was being constructed; Robert C. Garth and Herbert R. Muether, for their help in the early experimental work; Jane S. Levin, June C. Morris, and Marilyn S. Smith, for their assistance with the large amount of computation and plotting required in the analysis of the data and the preparation of curves; Edward Melkonian of Columbia University, for making the results of his calculations available to us before their publication. We also wish to thank John A. Harvey for his helpful criticism and valuable suggestions during the course of the experimental work and the preparation of this paper.

[57] Feshbach, Peaslee, and Weisskopf, Phys. Rev. 71, 145 (1947).

Phase-Shift Calculation of High-Energy Electron Scattering*

D. R. YENNIE, D. G. RAVENHALL, AND R. N. WILSON
Department of Physics, Stanford University, Stanford, California

(Received March 22, 1954)

The details of a phase-shift calculation of high-energy electron scattering by nuclei are given, together with some preliminary results. A new method for summing the Legendre series for the Coulomb scattering amplitude is described. The results indicate that the first Born approximation does not give cross sections accurate enough for a reliable interpretation of the experiments. From a comparison of the few theoretical cross sections already obtained with the experiments in gold at 125 Mev, very tentative conclusions about the nuclear charge distribution are drawn. It is pointed out that an analysis of results at two or more energies will be a much more sensitive test of possible charge distributions.

I. INTRODUCTION

EXPERIMENTS on the elastic scattering of high-energy electrons by nuclei carried out by Hofstadter, Fechter, and McIntyre,[1] and by Pidd, Hammer, and Raka[2] exhibit clearly the finite extension of the nuclear charge distributions. Analyses of the results of Hofstadter's group by Hofstadter *et al.*[1] and by Schiff,[3] using the first Born approximation, led to the tentative conclusion that the charge distribution was peaked at the center of the nucleus, tapering gradually towards the edge. In view of the fact that the Born approximation is not accurate for heavy elements, we have carried out a phase-shift analysis of the process. A brief report of preliminary results has already been made.[4] We wish in this paper to give an account of our methods and of the trend of our results. Our calculations have been of an exploratory nature, with a view to fitting the experimental data at 125 Mev,[1] and we can as yet draw no definite conclusions about nuclear charge distributions. To do so will require a thorough examination of the new and more accurate results of Hofstadter's group at several energies, and we hope to report on this in the near future.

The literature on electron scattering by nuclei is very extensive, and we shall not survey all of it here. That relating to estimates of the effect of the finite nuclear size using the first Born approximation has been summarized in Schiff's paper.[3] Phase-shift analyses of this process for the energy region where only one Coulomb phase shift is modified by the finite nuclear size have been made in papers by Elton,[5] Acheson,[6] and Feshbach.[7] Bitter and Feshbach[8] showed that experiments in this region can measure only one parameter of the nuclear charge distribution, namely its root-mean-square radius. Until very recently the only calculation for an energy high enough to require the modification of several Coulomb phases, thus yielding a cross section characteristic of the particular shape of the nuclear charge distribution, has been that of Parzen,[9] but unfortunately his results are not correct.[10] Other calculations in this energy range have now been made by E. Baranger,[11] and Brenner, Brown, and Elton.[12]

The model we use is the Dirac equation for an electron in the electrostatic potential of a static, spherically symmetric charge distribution. The cross section is obtained by a numerical calculation of the phase shift of each partial wave. It is unfortunate that the complexity of the calculation tends to obscure the relationship between the details of the charge distributions and of the corresponding cross sections. A method which avoided the decomposition into partial waves might give more insight into the process. We do not take into account the interaction of the electron with nuclear magnetic or electric quadrupole moments, or the effect of nuclear excitation. Calculations by Schiff[13] using the first Born approximation suggest that the first is not important at the energies under consideration, and that the other two are small except with particular elements at large angles. We also ignore quantum electrodynamic radiative corrections. Schwinger's analysis[14] predicts a very small change in the angular dependence of the differential cross section (of the order of one or two percent), but this also is on the basis of the first Born approximation.

In Part II we give an account of scattering theory for the Dirac equation, neglecting the mass term, as is justified at high energies. As an excuse for presenting such a well-studied topic again, we claim that our version, in which the omission of the mass term is made before the reduction to partial waves, is simpler and more transparent than the usual treatment. The only

* Supported in part by the U. S. Office of Scientific Research, Air Research and Development Command.

[1] Hofstadter, Fechter, and McIntyre, Phys. Rev. **91**, 422 (1953); **92**, 978 (1953).

[2] Pidd, Hammer, and Raka, Phys. Rev. **92**, 436 (1953).

[3] L. I. Schiff, Phys. Rev. **92**, 988 (1953).

[4] Yennie, Wilson, and Ravenhall, Phys. Rev. **92**, 1325 (1953).

[5] L. R. B. Elton, Phys. Rev. **79**, 412 (1950); Proc. Phys. Soc. (London) **A63**, 1115 (1950); **A65**, 481 (1952); **A66**, 806 (1953).

[6] L. K. Acheson, Phys. Rev. **82**, 488 (1951).

[7] H. Feshbach, Phys. Rev. **84**, 1206 (1951).

[8] F. Bitter and H. Feshbach, Phys. Rev. **92**, 837 (1953).

[9] G. Parzen, Phys. Rev. **80**, 355 (1950).

[10] An error was discovered by E. Baranger (see reference 11).

[11] E. Baranger, Phys. Rev. **93**, 1127 (1954). We wish to thank Mrs. Baranger for an interesting discussion of her work and ours.

[12] Brenner, Brown, and Elton (to be published). We thank Dr. Brown for communicating these results to us prior to their publication.

[13] Reference 3, and L. I. Schiff (private communication).

[14] J. Schwinger, Phys. Rev. **75**, 898 (1949).

new feature is our summing of the series for the Coulomb scattering amplitude. It is with reluctance that we introduce a new notation for the quantum number characterizing the partial wave. We think it clearer and more consistent to use j than the k, κ, and l of previous authors, since j^2, the familiar total angular momentum operator, is actually diagonal in the representation used.

The results are presented in Part III, together with a brief comparison with the work of other authors, and the qualitative conclusions that we feel able to draw at present.

II. THEORY

1. Dirac Equation at High Energies

We shall be concerned with the scattering of electrons at very high energies ($E>50\ mc^2$). We then expect that it should be possible to neglect the rest energy of the electron in comparison with its total energy. It is physically obvious that such an approximation should not introduce any qualitative changes into the scattering properties of the electron, and in fact the only quantitative changes introduced are of relative order (m^2c^4/E^2).[6,12]

In the Dirac equation,

$$(\boldsymbol{\alpha}\cdot\mathbf{p}c+\beta mc^2+V)\psi=E\psi, \tag{1}$$

we choose a representation for the Dirac matrices which will facilitate neglecting the mass term:

$$\alpha_i=\rho_3\sigma_i, \quad \beta=\rho_1.[15] \tag{2}$$

If we write ϕ and χ for two two-component wave functions, the Dirac equation can then be written

$$\begin{aligned}(\boldsymbol{\sigma}\cdot\mathbf{p}c+V-E)\phi&=-mc^2\chi,\\ (-\boldsymbol{\sigma}\cdot\mathbf{p}c+V-E)\chi&=-mc^2\phi.\end{aligned} \tag{3}$$

Neglecting the mass, we obtain two sets of uncoupled equations:

$$(\boldsymbol{\sigma}\cdot\mathbf{p}c+V-E)\phi=0, \tag{4a}$$

$$(-\boldsymbol{\sigma}\cdot\mathbf{p}c+V-E)\chi=0. \tag{4b}$$

That such two-component equations should exist can be seen directly from the original Dirac equation (1) by noting that when the term involving β is neglected, the remaining three hypercomplex quantities α_i can be represented by two component σ matrices. Solutions of both (4a) and (4b) are needed, however, in order to have a complete set of states for Eq. (1).[16]

Consider plane wave solutions of Eqs. (4a) and (4b) in the absence of a potential:

$$\begin{aligned}\phi&=u\exp(i\mathbf{k}\cdot\mathbf{x}),\\ \chi&=v\exp(i\mathbf{k}\cdot\mathbf{x}),\end{aligned} \tag{5}$$

where

$$\begin{aligned}\boldsymbol{\sigma}\cdot(\hbar c\mathbf{k})u&=Eu,\\ \boldsymbol{\sigma}\cdot(\hbar c\mathbf{k})v&=-Ev.\end{aligned} \tag{6}$$

For a given $E(>0)$ and $\mathbf{k}$, these two solutions correspond to the two different spin states of the electron. Loosely speaking, for the first solution the spin is parallel to the momentum while for the second it is antiparallel. The normalized solutions of (6) are

$$\begin{aligned}u&=\begin{pmatrix}\cos\tfrac{1}{2}\theta\\ \sin\tfrac{1}{2}\theta\exp(i\varphi)\end{pmatrix},\\ v&=\begin{pmatrix}-\sin\tfrac{1}{2}\theta\exp(-i\varphi)\\ \cos\tfrac{1}{2}\theta\end{pmatrix},\end{aligned} \tag{7}$$

where θ and φ are the polar angles specifying the direction of $\mathbf{k}$.

If we reintroduce the potential (which for the moment we assume has a finite extent), scattering states will have the asymptotic form[17]

$$\begin{aligned}\phi&\sim\begin{pmatrix}1\\0\end{pmatrix}e^{ikz}+r^{-1}f_1(\theta,\varphi)\begin{pmatrix}1\\ \tan\tfrac{1}{2}\theta\exp(i\varphi)\end{pmatrix}e^{ikr},\\ \chi&\sim\begin{pmatrix}0\\1\end{pmatrix}e^{ikz}+r^{-1}f_2(\theta,\varphi)\begin{pmatrix}-\tan\tfrac{1}{2}\theta\exp(-i\varphi)\\ 1\end{pmatrix}e^{ikr}.\end{aligned} \tag{8}$$

It is easily seen that for a spherically symmetric potential the scattering in a given direction will be the same for both spin orientations.[18] In the following, we will therefore restrict our attention to Eq. (4a).

2. Scattering Theory of the Dirac Equation at High Energies

Any solution of Eq. (4a) can be decomposed into partial waves characterized by the total angular momentum and its z component:

$$\phi=\sum a_{jm}\phi_{jm}, \tag{9}$$

with

$$J^2\phi_{jm}=j(j+1)\hbar^2\phi_{jm}, \tag{10}$$

[15] P. A. M. Dirac, *The Principles of Quantum Mechanics* (Oxford University Press, Oxford, 1947), third edition, p. 256.

[16] A discussion of the relation between our analysis and that of previous authors is given in the Appendix.

[17] Acheson (see reference 6) has already shown that the two components of the scattered wave differ by only a factor $\tan\frac{1}{2}\theta\exp(i\varphi)$. His proof is based on relationships between spherical harmonics occurring in the expansions of the components. Our derivation gives the underlying reason for this.

[18] This may be seen as follows: If $\phi(\mathbf{x})$ is a solution of (4a), then $\chi(\mathbf{x})=\phi(-\mathbf{x})$ is a solution of (4b). If the incident wave part of $\phi(\mathbf{x})$ is traveling in the positive z direction, the incident wave part of $\chi(\mathbf{x})$ is traveling in the minus z direction. If now we rotate the second solution through 180° about the x axis, we have both incident waves traveling in the positive z direction and the intensity of the scattered waves in a given direction is the same for both solutions. Further analysis along this line shows that when we consider the scattering of electrons from randomly oriented nonsymmetric nuclei there can be no polarization of the scattered electrons; this refers only to static moments, of course. At lower energies where the mass cannot be neglected, polarization in scattering by a spherically symmetric potential is possible.

and

$$J_z\phi_{jm}=m\hbar\phi_{jm}, \tag{11}$$

where

$$\mathbf{J}=\mathbf{r}\times\mathbf{p}+\tfrac{1}{2}\boldsymbol{\sigma}\hbar.$$

For a plane-wave incident in the z direction

$$J_z\begin{pmatrix}1\\0\end{pmatrix}e^{ikz}=\tfrac{1}{2}\hbar\begin{pmatrix}1\\0\end{pmatrix}e^{ikz}, \tag{12}$$

so that we need be concerned only with the states $\phi_{j,\frac{1}{2}}$. The spin-angular parts of these states have the forms

$$\chi_j^1=\begin{pmatrix}(j+\frac{1}{2})P_{j-\frac{1}{2}}(\cos\theta)\\-P_{j-\frac{1}{2}}^1(\cos\theta)\exp(i\varphi)\end{pmatrix},$$
$$\chi_j^2=\begin{pmatrix}(j+\frac{1}{2})P_{j+\frac{1}{2}}(\cos\theta)\\P_{j+\frac{1}{2}}^1(\cos\theta)\exp(i\varphi)\end{pmatrix}. \tag{13}$$

The partial wave solutions of (4a) then take the form

$$\phi_{j,\frac{1}{2}}=r^{-1}[G_j(r)\chi_j^1+iF_j(r)\chi_j^2]. \tag{14}$$

In deriving the equations satisfied by F_j and G_j, the following identities are useful:

$$\boldsymbol{\sigma}\cdot\mathbf{L}\chi_j^1=\hbar(j-\tfrac{1}{2})\chi_j^1,$$
$$\boldsymbol{\sigma}\cdot\mathbf{L}\chi_j^2=-\hbar(j+\tfrac{3}{2})\chi_j^2, \tag{15}$$

$$\boldsymbol{\sigma}\cdot\mathbf{r}\chi_j^1=r\chi_j^2,$$
$$\boldsymbol{\sigma}\cdot\mathbf{r}\chi_j^2=r\chi_j^1, \tag{16}$$

$$\boldsymbol{\sigma}\cdot\mathbf{p}=r^{-2}(\boldsymbol{\sigma}\cdot\mathbf{r})(\mathbf{r}\cdot\mathbf{p})+ir^{-2}(\boldsymbol{\sigma}\cdot\mathbf{r})(\boldsymbol{\sigma}\cdot\mathbf{L}). \tag{17}$$

It is then easily found that[16]

$$\frac{dG_j}{dr}-\frac{(j+\frac{1}{2})}{r}G_j+\frac{(E-V)}{\hbar c}F_j=0,$$
$$\frac{dF_j}{dr}+\frac{(j+\frac{1}{2})}{r}F_j-\frac{(E-V)}{\hbar c}G_j=0. \tag{18}$$

It is convenient to handle these equations in dimensionless form. We therefore set

$$x=kr \tag{19}$$

and

$$v=V/E, \tag{20}$$

where

$$k=E/\hbar c.$$

Then

$$\frac{dG_j}{dx}-\frac{(j+\frac{1}{2})}{x}G_j+(1-v)F_j=0,$$
$$\frac{dF_j}{dx}+\frac{(j+\frac{1}{2})}{x}F_j-(1-v)G_j=0. \tag{21}$$

For use in the scattering calculation, we need those solutions of Eq. (21) which are regular at the origin.

We shall next review briefly the standard scattering theory for the non-Coulomb case, and finally modify the results thus obtained to take into account the peculiar nature of the Coulomb field. At large distances we expect to find an asymptotic solution of the form

$$\phi\sim\begin{pmatrix}1\\0\end{pmatrix}e^{ikz\cos\theta}+x^{-1}kf(\theta)\begin{pmatrix}1\\\tan\frac{1}{2}\theta\exp(i\varphi)\end{pmatrix}e^{ikz}$$
$$=\phi_{\text{inc}}+\phi_{\text{scatt}}. \tag{22}$$

The differential cross section is then given by

$$d\sigma/d\Omega=|f|^2(1+\tan^2\tfrac{1}{2}\theta)=\sec^2\tfrac{1}{2}\theta|f|^2. \tag{23}$$

Using the well-known expansion of plane waves,[19] we may express the incident wave as a sum of partial waves of the form (14):

$$\phi_{\text{inc}}=\sum_{j-\frac{1}{2}=0}^{\infty}\left(\frac{\pi}{2x}\right)^{\frac{1}{2}}i^{j-\frac{1}{2}}[J_{j}\chi_j^1+iJ_{j+1}\chi_j^2]. \tag{24}$$

The total wave, determined by the condition that its incoming wave part is the same as that of (24), is

$$\phi=\sum_{j-\frac{1}{2}=0}^{\infty}x^{-1}i^{j-\frac{1}{2}}e^{i\eta_j}[G_j\chi_j^1+iF_j\chi_j^2]. \tag{25}$$

The phase shifts η_j are determined by comparing the asymptotic radial functions in (25) with those in (24):

$$(\pi x/2)^{\frac{1}{2}}J_j(x)\sim\sin[x-\tfrac{1}{2}(j-\tfrac{1}{2})\pi],$$
$$G_j\sim\sin[x-\tfrac{1}{2}(j-\tfrac{1}{2})\pi+\eta_j]. \tag{26}$$

Combining Eqs. (25), (24), and (22) we find that the scattered wave is given by

$$f(\theta)=\frac{1}{2ik}\sum(e^{2i\eta_j}-1)(j+\tfrac{1}{2})(P_{j-\frac{1}{2}}+P_{j+\frac{1}{2}})$$
$$=\frac{1}{2ik}\sum e^{2i\eta_j}(j+\tfrac{1}{2})(P_{j-\frac{1}{2}}+P_{j+\frac{1}{2}}). \tag{27}$$

In going from the first form of Eq. (27) to the second, the terms dropped sum to zero, except in the forward direction ($\theta=0$).[20]

In the case of a Coulomb potential produced by an extended nucleus, the potential outside the nucleus takes the form

$$v=-\gamma/x,$$

where

$$\gamma=Ze^2/\hbar c. \tag{28}$$

The potential inside the charge distribution may be

[19] G. N. Watson, *Theory of Bessel Functions* (MacMillan Company, New York, 1946), revised edition, p. 128.

[20] This is best seen by putting $a_l^{(0)}=2l+1$ in Eq. (46) below. This gives $a_l^{(1)}=0$.

calculated by using the expression

$$-v(x)=4\pi\gamma x^{-1}\int_0^x \rho(x')x'^2dx'+4\pi\gamma\int_x^\infty \rho(x')x'dx', \quad (29)$$

where the dimensionless charge density ρ has the normalization

$$4\pi\int_0^\infty \rho x^2dx=1. \quad (30)$$

The results of the scattering theory must be modified slightly because of the long-range nature of the Coulomb potential. The proper asymptotic form of the scattered wave is

$$\phi_{\text{scatt}}=x^{-1}kf(\theta)\begin{pmatrix}1\\ \tan\tfrac{1}{2}\theta\exp(i\varphi)\end{pmatrix}e^{i(x+\gamma\ln 2x)}, \quad (31)$$

while the individual partial waves have the form

$$G_j(x)\sim\sin[x+\gamma\ln 2x-\tfrac{1}{2}(j-\tfrac{1}{2})\pi+\eta_j]. \quad (32)$$

The scattering amplitude $f(\theta)$ is still given by (27).

A complication of the Coulomb potential is that the phase shifts do not approach a limit as j increases. In fact, the magnitude of the phase shift increases roughly like $(\gamma\ln j)$ with increasing j. Nevertheless it is possible to sum the series (27).[21,22] An improved method for carrying out this summation is given in Sec. 4.

3. Method of Calculation

The computational problem is, of course, to integrate Eqs. (21) to determine the phase shifts, and from these to calculate the differential cross section. In this section we shall outline the method, and leave the computational details to Sec. 4 and the Appendix.

Unless we wish to use simple special expressions for the potential v, it is not easy to obtain the solutions of (21) in a closed form, or even as a power series expansion. Except for the pure Coulomb case (point charge), we therefore rely on numerical methods to integrate (21). These methods are presented in detail in the Appendix. It suffices to say here that in each step of the integration all the derivatives of F_j and G_j through the fourth are treated correctly. In future calculations we plan to include all derivatives through the sixth.

Starting with a regular solution obtained by a power series expansion about the origin, the differential equations (21) are integrated from $x=0.1$ to a point x_0 (the "fitting-on radius") which lies outside the nuclear charge distribution. At x_0 the pair of functions $G_j(x_0)$, $F_j(x_0)$ is fitted to two pairs of linearly independent Coulomb functions

$$\begin{aligned}G_j(x_0)&=C_jG_{j,R}(x_0)+D_jG_{j,I}(x_0),\\ F_j(x_0)&=C_jF_{j,R}(x_0)+D_jF_{j,I}(x_0).\end{aligned} \quad (33)$$

Here the subscript R (I) denotes a Coulomb function which is regular (irregular) at the origin. Both the regular and irregular Coulomb functions used here are given by power series expansions about the origin. The series used are given in the Appendix.

The asymptotic forms of the Coulomb functions are well known:

$$\begin{aligned}G_{j,R}&\sim\sin[x+\gamma\ln 2x-\tfrac{1}{2}(j-\tfrac{1}{2})\pi+\eta_j{}^c],\\ G_{j,I}&\sim\sin[x+\gamma\ln 2x-\tfrac{1}{2}(j-\tfrac{1}{2})\pi+\eta_j{}'^c],\end{aligned} \quad (34)$$

the Coulomb phase shifts being given by[23]

$$\exp 2i\eta_j{}^c=\frac{\rho_j-i\gamma}{j+\tfrac{1}{2}}\frac{\Gamma(\rho_j-i\gamma)}{\Gamma(\rho_j+i\gamma)}e^{\pi i(j+\frac{1}{2}-\rho_j)}, \quad (35)$$

$$\exp i(\eta_j{}'^c-\eta_j{}^c)=\frac{1-i\tan\pi(j+\tfrac{1}{2}-\rho_j)\coth\pi\gamma}{|1-i\tan\pi(j+\tfrac{1}{2}-\rho_j)\coth\pi\gamma|}e^{-\pi i(j+\frac{1}{2}-\rho_j)}, \quad (36)$$

where

$$\rho_j=[(j+\tfrac{1}{2})^2-\gamma^2]^{\frac{1}{2}}.$$

The phase shift of the function G_j is given by

$$\tan(\eta_j-\eta_j{}^c)=\frac{\sin(\eta_j{}'^c-\eta_j{}^c)}{(C_j/D_j)+\cos(\eta_j{}'^c-\eta_j{}^c)}. \quad (37)$$

Tables of Coulomb phase shifts and functions are being prepared and will be published in a separate paper. Some sample phase shifts are presented in Table I.

We now estimate the precision required in the calculation of the phase shifts. According to Eq. (27), an error of $\Delta\eta_j$ in η_j introduces the following error into the scattering amplitude:

$$\Delta_jf=k^{-1}\Delta\eta_je^{2i\eta_j}(j+\tfrac{1}{2})(P_{j-\frac{1}{2}}+P_{j+\frac{1}{2}}). \quad (38)$$

In any particular case it is possible to use this relation

TABLE I. Values of phase shifts for gold. The phase shift of the regular Coulomb functions $\eta_j{}^c$ are defined in Eq. (35), and the difference in phase between the irregular and regular Coulomb functions $\eta_j{}'^c-\eta_j{}^c$ in Eq. (36). $\delta_j{}^1$ and $\delta_j{}^2$ are the additional phase shifts caused by the finite nuclear charge distributions uniform, $kR=4.0$ and Gaussian, $b=2.12$, respectively. $\delta_j=\eta_j-\eta_j{}^c$ is defined by Eq. (37).

j	$\eta_j{}^c$	$\eta_j{}'^c-\eta_j{}^c$	$\delta_j{}^1$	$\delta_j{}^2$
1/2	0.40736	−1.17386	−0.85820	−0.71689
3/2	−0.23797	−0.54728	−0.27143	−0.18795
5/2	−0.53303	−0.36074	−0.07633	−0.04846
7/2	−0.72659	−0.26951	−0.01494	−0.01064
9/2	−0.87098	−0.21523	−0.00199	−0.00199
11/2	−0.98623	−0.17918	−0.00017	−0.00030
13/2	−1.08218	−0.15350	−0.00001	−0.00004
15/2	−1.16438	−0.13426	−0.00000	−0.00000
17/2	−1.23628	−0.11931	−0.00000	−0.00000

[21] N. F. Mott, Proc. Roy. Soc. (London) **A135**, 429 (1932).
[22] H. Feshbach, Phys. Rev. **88**, 295 (1953).
[23] N. F. Mott and H. S. W. Massey, *The Theory of Atomic Collisions* (Oxford University Press, Oxford, 1952), second edition, p. 79.

to get a fairly accurate estimate of the error in the differential cross section. For simplicity, however, we shall make some crude approximations in estimating the errors. For the charge distributions considered in the present calculations the greatest errors occur in the first few phase shifts. We therefore estimate the total error in $|f|$ to be given by a small multiple m of the error arising from $\Delta\eta_{\frac{1}{2}}$:

$$\Delta|f| = mk^{-1}|\Delta\eta_{\frac{1}{2}}|E(\theta), \tag{39}$$

where m is of the order 2 or 3, and $E(\theta)$ is a factor of order 1 which decreases to zero at $\theta=\pi$. Analysis of the quantity $(P_{j-\frac{1}{2}}+P_{j+\frac{1}{2}})$ exactly for small j and asymptotically for large j shows that a suitable form for $E(\theta)$ is $\cos\frac{1}{2}\theta$. This gives for the error in the differential cross section

$$\frac{\Delta(d\sigma/d\Omega)}{d\sigma/d\Omega} = \frac{2m|\Delta\eta_{\frac{1}{2}}|}{k(d\sigma/d\Omega)^{\frac{1}{2}}}. \tag{40}$$

It is seen that the fractional error tends to be greatest where the cross section is least.

For the purpose of comparison with the present experiments it is generally sufficient to require that the relative error in the calculated cross section be less than 10 percent at the largest angle compared. Since the differential cross section decreases rapidly with increasing angle, the relative error at smaller scattering angles will then be quite negligible. We therefore require

$$|\Delta\eta_{\frac{1}{2}}| < 0.02k(d\sigma/d\Omega)_{\min}^{\frac{1}{2}}. \tag{41}$$

Equation (41) has two interpretations: given the cross section approximately, it tells us how accurately the phase shifts must be calculated; or when (as in practice) we know $|\Delta\eta_{\frac{1}{2}}|$, it tells us roughly the limit of the reliability of our calculations. In the present calculations we have estimated $|\Delta\eta_{\frac{1}{2}}|$ to be smaller than 0.0002 radian, based on the operations involved in obtaining $\eta_{\frac{1}{2}}$; accordingly our calculations should be sufficiently accurate whenever $k(d\sigma/d\Omega)^{\frac{1}{2}}>0.01$.

There is some empirical evidence that this estimate of the error may be too pessimistic. This is provided by the calculations for exponential and Gaussian charge distributions which yield nearly straight lines for $\log(d\sigma/d\Omega)$ *vs* θ plots. These curves continue to be linear in a region where, according to Eq. (40) and the estimate $|\Delta\eta_{\frac{1}{2}}|=0.0002$ radian, the error should be comparable in magnitude to the cross section itself! If the error were actually as large as predicted by Eq. (40), the curves should have a tendency to level off at large angles.

There are two main sources of error in the present calculation. The first is the lack of accuracy of the Coulomb functions at the fitting-on radius, due to their calculation by means of a series expansion about the origin. Cancellations which occur in the summing of the series make the final sum have a greater relative error than any of the individual terms. This error can be reduced only by computing the terms more accurately; such calculations are now in progress. The second source of error is the wave function integration. This error can be reduced by using a smaller interval or by improving the accuracy of each integration step. These two sources of error contribute about equally to the phase shift errors $\Delta\eta_j$.

4. Scattering Amplitude Series

In this section we present a new method for summing the scattering amplitude series. In previous calculations, it has been the practice to calculate first the Coulomb scattering amplitude, Eq. (27) with phase shifts given by Eq. (35), and then the corrections to it due to the finite nuclear size:

$$f = f_c + (f - f_c), \tag{42}$$

where

$$f - f_c = \frac{1}{2ik}\sum(\exp 2i\eta_j - \exp 2i\eta_j^c)(j+\tfrac{1}{2})(P_{j-\frac{1}{2}}+P_{j+\frac{1}{2}}). \tag{43}$$

Since $(\eta_j-\eta_j^c)$ approaches zero with increasing j, the series (43) converges quite rapidly even though η_j and η_j^c do not individually approach zero. One sees from the Born approximation[3] that at high energies and large angles the scattering amplitude f is much smaller in magnitude than the Coulomb scattering amplitude f_c. This implies that there is almost complete cancellation between the two terms of Eq. (42), and that they must both, therefore, be known to high precision. We were unable to use the published tables of Feshbach,[22] where kf_c is given to only three decimal places and at large angular intervals.

We can discover the reason for the poor convergence of the series (27) for the case of a Coulomb potential by looking at the corresponding problem in the nonrelativistic case, where the Coulomb scattering amplitude is known analytically:

$$f_{\text{N.R.}}(\theta) = \frac{\alpha}{2k\sin^2\frac{1}{2}\theta}\exp[2i\alpha\ln\sin\tfrac{1}{2}\theta + 2i\bar{\eta}_0] \tag{44}$$

$$= \frac{1}{2ik}\sum_{l=0}^{\infty}(2l+1)[\exp(2i\bar{\eta}_l)-1]P_l(\cos\theta), \tag{45}$$

where

$$\bar{\eta}_l = \arg\Gamma(l+1-i\alpha), \tag{46}$$

and

$$\alpha = Ze^2/\hbar v.$$

The series (45) with the phase shifts (46) can be rearranged in form so that it closely resembles the series (27) with the phase shifts (35).[21] For our present purposes, however, it is not necessary to do this. From Eq. (44) we see that $f_{\text{N.R.}}(\theta)$ has a singularity in both magnitude and argument at $\theta=0$. This accounts for the poor convergence of the series (45). Since for large j values the relativistic phase shifts are nearly the same as the nonrelativistic ones for $l=j-\frac{1}{2}$, the rela-

tivistic series probably has a similar type of singularity. We accordingly transform $f(\theta)$ to make it less singular for small values of θ. This is accomplished by multiplying $f(\theta)$ by a function which vanishes at $\theta=0$ and then expanding the new function in a series of Legendre polynomials.

Let us represent $f(\theta)$ by

$$2ikf=\sum a_l P_l(\cos\theta). \tag{47}$$

Then the mth "reduced" series is defined by:

$$(1-\cos\theta)^m 2ikf=\sum a_l^{(m)} P_l(\cos\theta). \tag{48}$$

Using the recurrence relations for Legendre polynomials, we find that

$$a_l^{(i+1)}=a_l^{(i)}-\frac{l+1}{2l+3}a_{l+1}^{(i)}-\frac{l}{2l-1}a_{l-1}^{(i)}. \tag{49}$$

For large l, it turns out that

$$|a_l^{(i+1)}|=O(|a_l^{(i)}|/l^2), \tag{50}$$

so that after a few reductions the series converges quite rapidly. We have found three reductions ($m=3$) to be optimum for our present calculations. For gold, the results are illustrated in Table II, where the coefficients of the series in Eq. (47) are compared with those of the third reduction.

III. DISCUSSION OF THE RESULTS

To obtain the cross section for a given charge distribution at an energy khc we must use in Eq. (29) the corresponding dimensionless function $\rho(x)$, x being the radial coordinate measured in units of $k^{-1}=\lambda\!\!\!^{-}$. Equations (21) and (22), together with Eq. (29), then present the scattering problem in dimensionless form, with $kf(\theta)$ as a dimensionless scattering amplitude. The energy khc thus enters the calculation in two ways: first, in the determination of the radial scale of $\rho(x)$; second, in the absolute magnitude of the cross section. For another energy $k'hc$, this particular $\rho(x)$ corresponds to a physical charge distribution whose dimensions are altered by a factor k/k', and whose cross section is altered by a factor $(k/k')^2$. In the following discussion the term "shape" refers to the various analytic forms used for $\rho(x)$, and "size" refers to the value of the radial parameter involved.

We have considered the following shapes:

exponential, $\rho(x)=\rho_0 e^{-x/a}$;

Gaussian, $\rho(x)=\rho_0\exp[-(x/b)^2]$;

uniform, $\rho(x)=\rho_0$, $x<kR$, $=0$, $x>kR$;

smoothed uniform, $\rho=\rho_0[1+e^{K(x-c)}]^{-1}$;

wine-bottle, $\rho=\rho_0(1+(x/d)^4)[1+e^{K(x-c)}]^{-1}$.

Most of the calculations reported here are for gold ($Z=79$, $\gamma=Ze^2/hc=0.5765$). A few are for copper ($Z=29$, $\gamma=0.2116$) and for aluminum ($Z=13$, $\gamma=0.09486$).

TABLE II. Coefficients of the Legendre series for the Coulomb scattering amplitude. a_l are those for the original series in Eq. (47), and $a_l^{(3)}$ are the third reduced coefficients defined by Eq. (49).

l	Rea_l	Ima_l	Re$a_l^{(3)}$	Im$a_l^{(3)}$
0	0.68608	0.72753	−0.40271	0.64187
1	2.46374	−0.18893	0.46429	−0.39809
2	3.22837	−3.54238	0.28802	−0.66577
3	1.92010	−6.59828	−0.48598	0.40511
4	−0.38223	−8.89930	0.10826	0.02838
5	−3.19735	−10.44940	0.01935	−0.00448
6	−6.26093	−11.32514	0.00547	−0.00298
7	−9.41473	−11.61261	0.00194	−0.00162
8	−12.55937	−11.39191	0.00078	−0.00091
9	−15.63076	−10.73364	0.00034	−0.00053
10	−18.58706	−9.69883	0.00016	−0.00032
11	−21.40100	−8.33997	0.00007	−0.00020
12	−24.05511	−6.70216		
13	−26.53869	−4.82425		
14	−28.84572	−2.73981		

5. Comparison with the First Born Approximation

The differential cross section predicted by the first Born approximation is

$$\frac{d\sigma}{d\Omega}=\left(\frac{\gamma}{2k}\right)^2\frac{\cos^2\tfrac{1}{2}\theta}{\sin^4\tfrac{1}{2}\theta}\left|\int\rho(x)e^{i\mathbf{q}\cdot\mathbf{x}}d^3x\right|^2,$$

where $|\mathbf{q}|=2\sin\tfrac{1}{2}\theta$, and ρ, as in Eq. (30), has unit volume integral.[3] The scattering amplitude is real. For simpler shapes the "form factor" $F=\int\rho(x)\exp(i\mathbf{q}\cdot\mathbf{x})d^3x$ has the following forms:

exponential, $F=(1+q^2a^2)^{-2}$;

Gaussian, $F=\exp(-q^2b^2/4)$;

uniform, $F=3(\sin qkR-qkR\cos qkR)/(qkR)^3$.

The cross sections for the first two shapes are, on a semilog plot, smooth functions of θ; for the uniform shape, on the other hand, F has zeros (where $qkR=\tan qkR$) and the cross section is a wildly varying function of θ. In Figs. 1, 2, and 3 the dashed curves are the Born approximation cross sections for a uniform shape $kR=5.4$, exponentials $a=0.91$ and $a=1.06$, and Gaussians $b=2.12$ and $b=3.4$, respectively.

The cross sections obtained from the phase-shift analysis are, for gold, usually considerably different from the first Born approximation cross sections.[4] For the uniform shape, the first zero of the Born cross section appears only as a slight undulation, and the second zero barely as a minimum, which is shifted to a slightly smaller angle. In Fig. 1 is shown the cross section for the uniform shape $kR=5.4$, together with the cross section for the same shape in copper, suitably normalized to have the same Born cross section. For copper the agreement with the Born approximation is much better than for gold, as is to be expected.

The results of the phase-shift analysis for the ex-

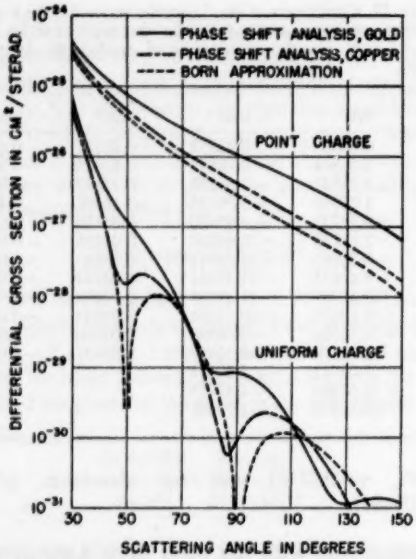

FIG. 1. Differential cross sections at 150 Mev for scattering by a point charge and by the uniform charge distribution $kR=5.4$, for gold and copper. The cross sections for copper have been multiplied by a factor that makes their first Born approximations the same as those for gold.

ponential shape are shown in Fig. 2. The cross section is a smooth function of θ, but has a considerably greater over-all slope than the Born cross section. Thus fitting experimental results with the phase-shift analysis predicts a smaller nucleus than fitting with the Born approximation.

For the Gaussian shape with $b=2.12$, the phase-shift

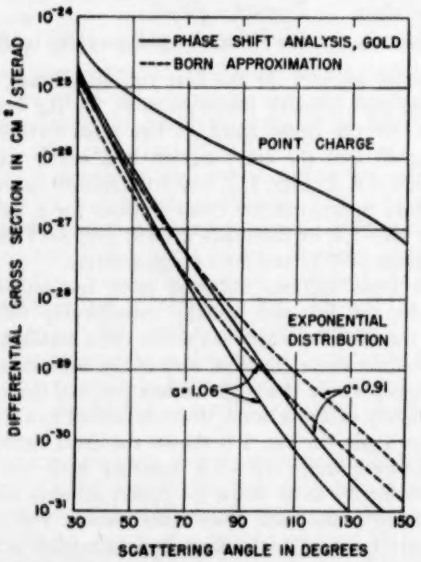

FIG. 2. Cross sections at 150 Mev for scattering by the exponential shapes $a=0.91$ and $a=1.06$, for gold.

analysis cross section, shown in Fig. 3, is almost identical with the Born cross section, whereas for $b=3.4$ it slopes less steeply. The phase-shift analysis results for the exponential and uniform shapes could be understood, as suggested previously,[4] in terms of the increase in wave number as the electron entered the attractive field of the nucleus. The results for Gaussian shapes, however, lie if anything in the opposite direction, so that such a simple interpretation is ruled out.

The difference between the phase-shift analysis and the first Born approximation is even more pronounced in the scattering amplitude, which in the phase-shift analysis is, of course, complex. In Figs. 4 and 5 we exhibit this complex behavior by making polar plots of $\log_{10}|f(\theta)|$ *versus* argument $(f(\theta))$. The values $\theta=30°$, $50°$, $70°$, $\cdots$ are indicated on each curve. In Fig. 4 are

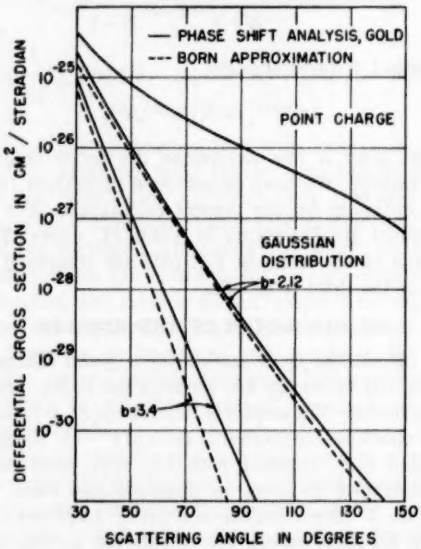

FIG. 3. Cross sections at 150 Mev for scattering by the Gaussian shapes $b=2.12$ and $b=3.4$, for gold.

the results for point scattering on Al, Cu, and Au, and for the uniform shape $kR=5.4$, in Cu and Au. In the first Born approximation the scattering amplitude lies along the horizontal axis. For a cross section with zeros it crosses the origin. The exact point-scattering amplitude is almost real for Al, and becomes more and more complex as Z increases. The scattering amplitude for the uniform shape $kR=5.4$ is for Cu a flattened spiral whose major axis is at about $30°$ to the horizontal axis and the Born approximation amplitude, while for Au it is an unflattened spiral. The filling in of the zeros in the Born approximation cross section and the fact that the exact scattering amplitude is complex are thus the same phenomenon. In Fig. 5 are scattering amplitudes for a number of charge shapes in gold. We find that for a given shape the polar plot is remarkably independent of size. For the Gaussian shape, for instance, the curves

for $b=3.4$ and $b=2.12$ are almost the same. The difference in the corresponding cross sections occurs because values of θ on the $b=3.4$ curve are shifted relative to the corresponding values of θ on the $b=2.12$ curve. Another peculiar fact is that the exponential shape $ka=0.91$ and the Gaussian shape $kb=2.12$ have very different scattering amplitudes but almost identical cross sections.

The first Born approximation cross sections are thus of little value in suggesting the correct sizes to use when fitting the data. The fact that the phase-shift analysis yields cross sections which are always smoother functions of θ means that a much wider range of shapes gives a tolerable fit with experiment than was suggested by the use of the Born approximation.

6. Interpolation

It is useful to be able to estimate the effect on the cross section of changing the size slightly, without doing a large number of trial calculations. For the smooth cross sections yielded by the Gaussian shapes, it is possible to interpolate by fitting cross sections at a particular value of θ to a polynomial in the size parameter. Since we usually need only relative cross sections, our procedure is to fit the ratio of the values of $\log_{10}[d\sigma(\theta)/d\Omega]-\log_{10}[d\sigma(\theta')/d\Omega]$ given respectively by the phase-shift analysis and the first Born approximation to a polynomial in the size parameter b. Extrapolating in this way from cross sections for $b=3.4$ and $b=2.69$ gives a cross section for $b=2.12$ which by later comparison with the phase-shift analysis we have found to be accurate to about 2 percent. The cross section for the Gaussian shape $b=3.05$ shown in Fig. 10 was obtained by this method.

Such a method is clearly unsuitable for cross sections given by uniform shapes. For these we make use of the fact that the "form factor" $\mathfrak{F}(\theta,kR)$ defined in terms of the phase-shift analysis cross sections by

$$\{\mathfrak{F}(\theta,kR)\}^2=\{d\sigma(\theta)/d\Omega\}/\{d\sigma(\theta)/d\Omega\}_{\text{point}}$$

has properties very similar to those of the form factor $F(\theta,kR)$ of the first Born approximation.[24] There, F is a function of $2kR\sin\frac{1}{2}\theta$ whose analytic form is the same for all kR (see the beginning of Sec. 5), so that $F(\theta,kR)$ and $F(\theta',kR')$ for two sizes have equal values when $kR'\sin\frac{1}{2}\theta'=kR\sin\frac{1}{2}\theta$. Hence in the first Born approximation the cross sections for all sizes can be obtained from a knowledge of the point cross section and the form factor F for one size. In the case of the phase-shift analysis we find that the two angles defined by

$$\mathfrak{F}(\theta,5.4)=\mathfrak{F}(\theta',4.0)$$

are connected by the relation $\sin\frac{1}{2}\theta/\sin\frac{1}{2}\theta'=\text{constant}\pm 4$ percent over the angular range 30° to 150°. The "constant" is roughly $(4.0/5.4)^{0.8}$. Hence to within 4 percent $\mathfrak{F}$ can be written $\mathfrak{F}(g(kR)\sin\frac{1}{2}\theta)$, and, as with the first Born approximation, is (approximately) a universal function independent of size. When obtained by the phase-shift analysis for a particular size it can be used for other slightly different sizes. Of the family of uniform shapes shown in Fig. 6, the $kR=4.0$ curve was obtained by the phase-shift analysis, and the rest by this interpolation method, as was also the uniform $kR=5.8$ curve of Fig. 10.

[24] This was suggested to us by Dr. McIntyre.

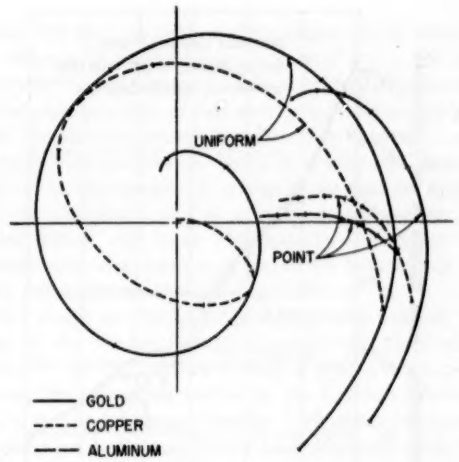

FIG. 4. Plots of $\log_{10}|f(\theta)|$ *versus* $\arg f(\theta)$, in polar coordinates, for point scattering in gold, copper, and aluminum, and for the uniform shape $kR=5.4$ in gold and copper. The values $\theta=30°$, 50°, 70°, ··· are indicated on each curve.

7. Comparison with Other Calculations

Calculations of other authors seem to confirm our results fairly well. Numerical errors have been discovered in the published work of Parzen.[9,10] In any case it seems physically rather unlikely that the phase-shift

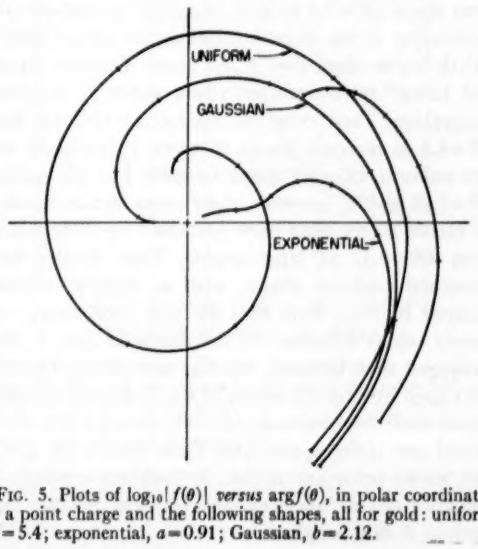

FIG. 5. Plots of $\log_{10}|f(\theta)|$ *versus* $\arg f(\theta)$, in polar coordinates, for a point charge and the following shapes, all for gold: uniform, $kR=5.4$; exponential, $a=0.91$; Gaussian, $b=2.12$.

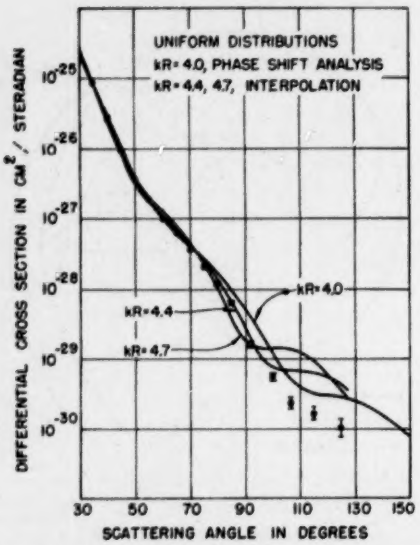

FIG. 6. Cross sections at 125 Mev for scattering by three uniform shapes, $kR=4.0$, 4.4, 4.7, for gold, together with the experimental data. All have been normalized to the same value at 35°. The ordinate scale refers to the $kR=4.0$ curve. This was obtained by the phase-shift analysis, the other two by interpolation. The nuclear radii corresponding to these shapes have r_0 values of 1.09×10^{-13} cm, 1.19×10^{-13} cm, 1.27×10^{-13} cm, where $R=r_0A^{\frac{1}{3}}$. From Eq. (40) the estimated error in the $kR=4.0$ curve is 10 percent when $d\sigma(\theta)/d\Omega\cong3\times10^{-28}$ cm² per steradian, i.e., when $\theta\cong120°$. For θ larger than 120° the error is larger.

analysis cross sections should be many times the first Born cross sections. A phase-shift analysis in which the phase shifts were obtained by the W.K.B. approximation has been made by Baranger.[11] The cross section she obtains for the uniform shape $kR=5.0$, in mercury, $Z=80$, resembles closely our cross section for the uniform shape $kR=5.4$ in gold, although its plateau (corresponding to the Born approximation second zero) is a little higher than that of our curve. Brenner, Brown, and Elton[12] have obtained phase shifts by numerical integration. Their cross section for the uniform shape $kR=4.4$ in mercury seems to agree very closely with our uniform $kR=4.4$ shape in gold. For the uniform $kR=5.28$ shape, however, their cross section tends to be rather larger than ours (obtained by interpolation from $kR=5.4$) at large angles. Their results for a smoothed uniform shape, with a slightly different analytic function from that we have used, check very closely our conclusions on this shape in Sec. 8. Both Baranger, and Brenner, Brown, and Elton, however, have used Feshbach's values of the Coulomb scattering amplitude[23] for mercury, $Z=80$. Results for $Z=80$ should not differ appreciably from results for $Z=79$, but, as we point out in Sec. 4, Feshbach's values are probably not accurate enough to yield reliable cross sections at large angles.

8. Cross Sections for Gold at 125 Mev

Experimental results for gold at 125 Mev are included in Figs. 6, 7, and 8. They are part of the new data obtained recently by Hofstadter's group.[25] They indicate a cross section which decreases steadily with θ (on this semilog plot) out to about 120°, with a slight dip at about 60°. We have found a wide variety of charge shapes all of which give cross sections having roughly this character, although these cross sections do not all fit the experimental results equally well. Since it appears that a comparison with experiment at several

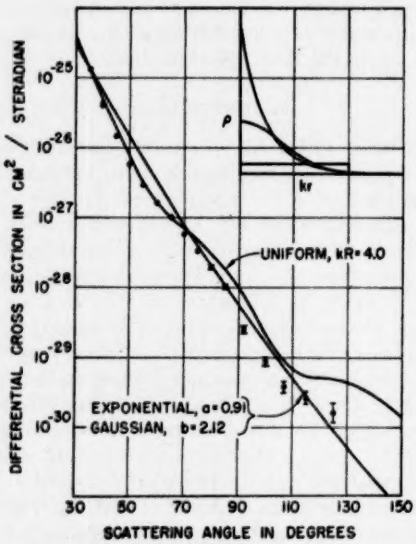

FIG. 7. Cross sections at 125 Mev for scattering by the uniform shape $kR=4.0$, the exponential $a=0.91$, and the Gaussian $b=2.12$, for gold, together with the experimental data. When all are normalized to the same value at 35° the cross sections for the Gaussian and exponential shapes coincide. The ordinate scale refers to the Gaussian shape. The rms radii of the three shapes are, respectively, 3.10λ, 3.16λ, and 2.60λ Inset are scale drawings of ρ.

energies is required to obtain the charge distribution accurately, we want in this paper only to give the trend that our present calculations suggest.

In Fig. 6 the cross sections of a family of uniform charge distributions are plotted together with the experimental results. That for $kR=4.0$ is obtained from our phase-shift analysis, the others by the interpolation method given in Sec. 6. Since the measured cross section is only relative, the scale of the interpolated curves has been altered so that they have the same value at 35° as the cross section for $kR=4.0$, and the

[25] The data with which we compared our calculations as they were made were means of the earlier published cross sections (see reference 1) and later unpublished ones, all obtained before improvements in the experimental apparatus enabled Hofstadter's group to obtain their new and more accurate data. These means of the old data agreed very well with the new data, although their probable error was of course much larger. We are grateful for Professor Hofstadter's permission to quote the new results before their publication.

experimental 35° point has been plotted here also. It seems from Fig. 6 that it will be difficult to fit both the general slope in the range 35°–80°, and the fact that there is no plateau, with a uniform charge distribution.

Figure 7 contains the cross sections for the exponential $a=0.91$, Gaussian $b=2.12$, and uniform $kR=4.0$ charge distributions, normalized at 35°, together with the experimental results. It is remarkable that over the whole range of θ used, the cross sections for the first two shapes are so closely proportional that in this figure we are unable to distinguish between them. Indeed, for angles less than 90° the cross sections of all three shapes are not very different. As regards comparison with experiment, it is seen that the cross sections of the exponential and Gaussian do decrease steadily with angle, but they have no dip at 60°. A shape having some of the features of each of those of Fig. 7 seems to be indicated. The root-mean-square radius may be taken as a measure of the relative size

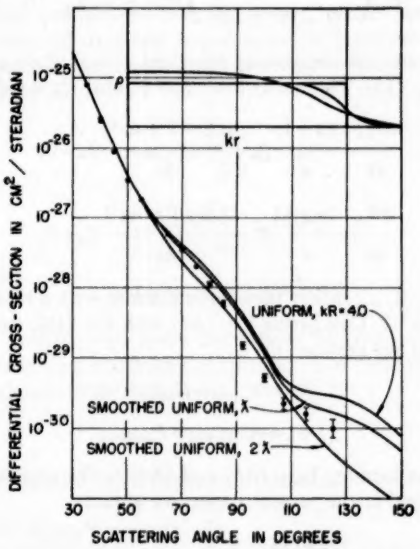

FIG. 8. Cross sections at 125 Mev for scattering by the uniform shape $kR=4.0$ and two smoothed uniform shapes: $K=4.40$, $c=3.86$; and $K=2.20$, $c=3.51$, for gold, together with the experimental data. The "smoothing distances" of the second and third shapes are λ and 2λ at this energy. The rms radii of the three shapes are all 3.10λ. Inset are scale drawings of ρ.

of these charge distributions. In units of k^{-1} it is respectively 3.16, 2.60, and 3.10 for these three shapes.

The smoothed uniform shape represents a charge distribution intermediate between uniform and exponential. The two cross sections in Fig. 8 are for smoothed uniform shapes having the same rms radius as the uniform $kR=4.0$ distribution. They have smoothing distances of 1 and 2, in units of k^{-1}. (We define smoothing distances as the distance over which ρ decreases from 0.9 $\rho(0)$ to 0.1 $\rho(0)$.) The shape with a smoothing distance of 1, that is λ, has a cross section almost the same as that of the uniform shape, whereas the shape with a smoothing distance of 2 (i.e., 2λ) has a cross section which approaches that of an exponential. It thus appears that at this energy only smoothed uniform shapes with smoothing distances between λ and 2λ have cross sections distinctly different from those of uniform or exponential. It seems likely that by appropriately choosing c and K a cross section can be obtained which will have the features shown by the experimental one. Such a shape would have about the same rms radius as those of Fig. 8.[25a]

As a shape in which charge is dispersed towards the edge of the nucleus we have considered the "wine-bottle."[26] As Fig. 9 shows, such a shape, with $d=c$, having the same rms radius as the uniform $kR=4.0$, and a maximum charge density 1.46 times its central density, has a cross section almost identical with the uniform $kR=4.0$ shape.

The experimental data at 125 Mev can probably be fitted with quite a range of charge distributions. The situation is much more definite, however, if a fit is made at two energies. For example, Fig. 10 shows the cross sections at 180 Mev given by the Gaussian and uniform nuclear charge distributions whose cross sections at 125 Mev are shown in Fig. 7. These were obtained by the interpolation methods described in Sec. 6. Experimental results at 180 Mev should be able to discriminate between them.

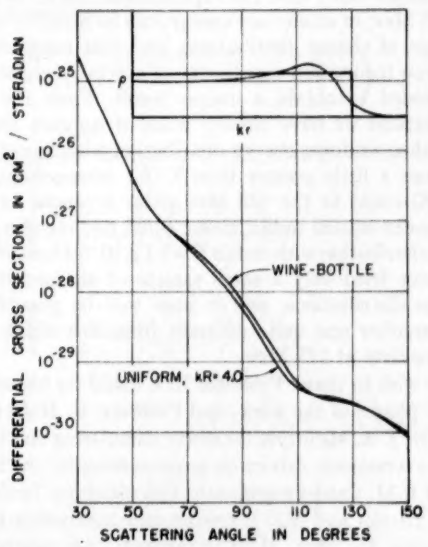

FIG. 9. Cross sections at 125 Mev for scattering by the uniform shape $kR=4.0$ and the "wine-bottle" shape with $K=5.45$ and $c=d=3.67$, for gold. These shapes have the same rms radius, and the second has a maximum charge density 1.46 times the central density. Inset are scale drawings of ρ.

[25a] *Footnote added in proof.*—Later calculations indicate that the rms radius will be a little larger (about 5 or 10 percent) than those of the charge distributions of Fig. 8.

[26] Such a charge distribution has been suggested by E. Feenberg, Phys. Rev. 59, 593 (1941).

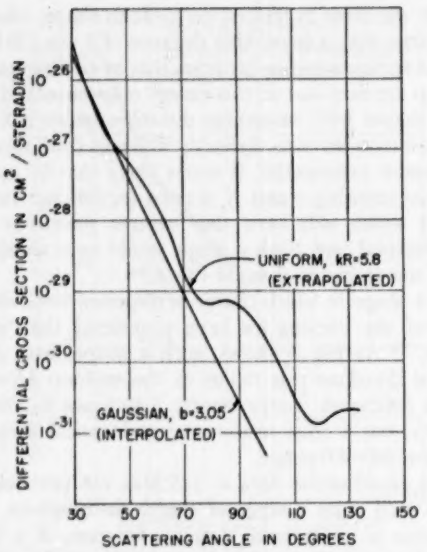

FIG. 10. Cross sections at 180 Mev for scattering by the Gaussian and uniform nuclear charge distributions whose cross sections at 125 Mev are shown in Fig. 7. At 180 Mev they correspond to the uniform $kR=5.8$ and Gaussian $b=3.05$ shapes. The cross sections were obtained by the interpolation methods of Sec. 6.

9. Conclusions

It seems likely that the experimental results in gold at 125 Mev, or at any one energy, can be fitted by quite a range of charge distributions, and that comparisons between theory and experiment at several energies will be needed to obtain a unique result. From the few calculations we have already made it appears that a smoothed uniform charge distribution with smoothing distance a little greater than λ (for terminology, see Sec. 8) could fit the 125 Mev data. It would have a root-mean-square radius about equal to that of a uniform distribution with radius $R=1.1\times10^{-13}A^{\frac{1}{3}}$ cm.[28a] But we have tried only a small sample of all conceivable charge distributions, and it may well be possible to find another one quite different from this which also fits the data at 125 Mev.

We wish to thank Professor L. I. Schiff for his advice on all phases of the work, and Professor R. Hofstadter and Dr. J. A. McIntyre for many stimulating and fruitful conversations. Advice on programming for the Stanford I.B.M. Card-Programmed Calculator by Professor J. G. Herriot and Mr. J. Carter, and instruction in its operation by Mrs. H. Van Heusen, are much appreciated.

APPENDIX

1. Comparison of the Present Treatment of the Dirac Equation with Those of Other Authors

Most previous treatments of the electron-scattering problem are based on the separation of the Dirac equation given by Darwin.[27] It seems worth while to show here the connection between Darwin's treatment and ours.

In place of (1), Darwin uses

$$(-\boldsymbol{\alpha}'\cdot\mathbf{p}c-\beta'mc^2+V)\psi'=E\psi', \tag{A1}$$

where[15]

$$\alpha'_i=\rho_1\sigma_i, \quad \beta'=\rho_3. \tag{A2}$$

The two representations are connected by

$$-\alpha_i'=U^{-1}\alpha_iU, \quad -\beta'=U^{-1}\beta U, \tag{A3}$$

where

$$U=U^{-1}=(1/\sqrt{2})(\rho_1-\rho_3). \tag{A4}$$

The partial wave solutions of (A1) take the form

$$\psi_n'=r^{-1}\begin{pmatrix}-i\mathfrak{F}_n(r)\chi_{n+\frac{1}{2}}{}^2\\ \mathfrak{G}_n(r)\chi_{n+\frac{1}{2}}{}^1\end{pmatrix}(n=0,\,1,\,2,\,\cdots), \tag{A5}$$

$$\psi_{-n-1}'=r^{-1}\begin{pmatrix}-i\mathfrak{F}_{-n-1}(r)\chi_{n-\frac{1}{2}}{}^1\\ \mathfrak{G}_{-n-1}(r)\chi_{n-\frac{1}{2}}{}^2\end{pmatrix}(n=1,\,2,\,3,\,\cdots), \tag{A6}$$

where the two-component functions χ^1 and χ^2 are given by Eq. (13). The radial functions $\mathfrak{F}_n$ and $\mathfrak{G}_n$ satisfy

$$\begin{aligned}&\frac{d\mathfrak{G}_n}{dr}-\frac{(n+1)}{r}\mathfrak{G}_n+\frac{(E-V+mc^2)}{\hbar c}\mathfrak{F}_n=0,\\ &\frac{d\mathfrak{F}_n}{dr}+\frac{(n+1)}{r}\mathfrak{F}_n-\frac{(E-V-mc^2)}{\hbar c}\mathfrak{G}_n=0.\end{aligned} \tag{A7}$$

$\mathfrak{F}_{-n-1}$, $\mathfrak{G}_{-n-1}$ satisfy the same equations with n replaced by $-n-1$. Comparing Eq. (A7) with Eq. (18), we find that in the limit $m\to0$

$$\begin{aligned}\mathfrak{G}_n&=\mathfrak{F}_{-n-2}=G_{n+\frac{1}{2}},\\ \mathfrak{F}_n&=-\mathfrak{G}_{-n-2}=F_{n+\frac{1}{2}}.\end{aligned} \tag{A8}$$

Transforming Eqs. (A5) and (A6) to the representation used in the present paper, we obtain

$$\begin{pmatrix}\phi_{j,\frac{1}{2}}\\ 0\end{pmatrix}=\frac{1}{\sqrt{2}}(\psi_n-i\psi_{-n-2}), \tag{A9}$$

$$\begin{pmatrix}0\\ \chi_{j,\frac{1}{2}}\end{pmatrix}=\frac{1}{\sqrt{2}}(\psi_n+i\psi_{-n-2}). \tag{A10}$$

The states (A5) and (A6) have definite parity while (A9) and (A10) do not.

The index n in Eqs. (A5) and (A6) seems to have been selected because it is the order of the spherical harmonics in the third and fourth components of ψ_n' and ψ_{-n-1}' and not because of its connection with any particular quantum number. An alternative is to use the quantum number $k(=\pm(j+\frac{1}{2}))$, defined by the operator

$$\hbar k=\beta'(\boldsymbol{\sigma}'\cdot\mathbf{L}+\hbar). \tag{A11}$$

[27] C. G. Darwin, Proc. Roy. Soc. (London) **A118**, 654 (1928).

This notation has been used by Acheson.[6] His radial functions $f_{\pm\kappa}$ and $g_{\pm\kappa}$ are related to those of Darwin as follows:

$$f_\kappa=\mathfrak{F}_{\kappa-1}, \quad g_\kappa=\mathfrak{G}_{\kappa-1}(\kappa=k=j+\tfrac{1}{2}), \tag{A12}$$

$$f_{-\kappa}=\mathfrak{F}_{-\kappa-1}, \quad g_{-\kappa}=\mathfrak{G}_{-\kappa-1}(\kappa=-k=j+\tfrac{1}{2}). \tag{A13}$$

With this notation the radial equations become

$$\begin{aligned}\frac{dg_{\pm\kappa}}{dr}\mp\frac{\kappa}{r}g_{\pm\kappa}+\frac{(E-V+mc^2)}{\hbar c}f_{\pm\kappa}=0,\\ \frac{df_{\pm\kappa}}{dr}\pm\frac{\kappa}{r}f_{\pm\kappa}+\frac{(E-V-mc^2)}{\hbar c}g_{\pm\kappa}=0.\end{aligned} \tag{A14}$$

We have not used this notation because the partial waves (A9) and (A10) are not eigenfunctions of k.

2. Calculation of Coulomb Functions

Mott and Massey have given the Coulomb functions in terms of confluent hypergeometric functions.[23] We use instead the more rapidly convergent series solution given by Elton:[28]

$$\begin{aligned}G_j=x^{s_j}N_j\sum_{m=0}^{\infty}a_m^{(j)}x^m,\\ F_j=x^{s_j}N_j\sum_{m=0}^{\infty}b_m^{(j)}x^m,\end{aligned} \tag{A15}$$

where

$$s_j=\pm\rho_j=\pm[(j+\tfrac{1}{2})^2-\gamma^2]^{\frac{1}{2}}.$$

The positive sign gives the regular solution, and the negative sign the irregular solution. The coefficients of the series are given by

$$a_0=1, \quad b_0=\gamma/(s_j+j+\tfrac{1}{2}), \tag{A16}$$

together with the recurrence relations:

$$\begin{aligned}m(m+2s_j)a_m^{(j)}=-\gamma a_{m-1}^{(j)}\\ -(s_j+m+j+\tfrac{1}{2})b_{m-1}^{(j)},\\ m(m+2s_j)b_m^{(j)}=-\gamma b_{m-1}^{(j)}\\ +(s_j+m-j-\tfrac{1}{2})a_{m-1}^{(j)}.\end{aligned} \tag{A17}$$

The normalization, obtained by comparison with Mott and Massey's solutions, is

$$N_j=\frac{s_j}{|s_j|}\frac{2^{s_j}|\Gamma(s_j+i\gamma)|}{\Gamma(2s_j+1)}\left[\frac{(j+\tfrac{1}{2})(j+\tfrac{1}{2}+s_j)}{2}\right]^{\frac{1}{2}}e^{\frac{1}{2}\pi\gamma}. \tag{A18}$$

3. Numerical Integration of the Radial Dirac Equations

We use a step-by-step procedure based on derivatives rather than differences. Let y_n, y_n', y_n'', $\cdots$ be a function and its derivatives at $x=x_n$. Alternative approximate formulas, given by Milne,[29] for y_{n+1} at $x_{n+1}=x_n+h$ are

$$y_{n+1}=y_n+\tfrac{1}{2}h(y_n'+y_{n+1}'), \tag{A19}$$

$$y_{n+1}=y_n+\tfrac{1}{2}h(y_n'+y_{n+1}')+(1/12)h^2(y_n''-y_{n+1}''), \tag{A20}$$

$$y_{n+1}=y_n+\tfrac{1}{2}h(y_n'+y_{n+1}')+(1/10)h^2(y_n''-y_{n+1}'')+(1/120)h^3(y_n'''+y_{n+1}'''). \tag{A21}$$

The respective errors are of order $h^3y'''/12$, $h^5y^{(5)}/720$, $h^7y^{(7)}/100\,800$. The method can easily be extended to take more derivatives into account. We use Eq. (A20) to obtain the results of Part III.

Since Eqs. (21) are linear,[30] we may solve Eqs. (A19–A21) exactly for y_{n+1} in terms of y_n. Let y_n be a column matrix composed of $F_{j,n}$ and $G_{j,n}$

$$y_n=\begin{pmatrix}F_j\\ G_j\end{pmatrix}_n. \tag{A22}$$

Then from Eqs. (21), the derivatives of y_n can be represented by matrices acting on y_n:

$$y_n'=A_ny_n, \quad y_n''=B_ny_n, \quad y_n'''=C_ny_n. \tag{A23}$$

For example,

$$A_n=\begin{pmatrix}-(j+\frac{1}{2})/x_n & (1-v_n)\\ -(1-v_n) & (j+\frac{1}{2})/x_n\end{pmatrix}. \tag{A24}$$

The solutions of Eqs. (A19–A21) are given by

$$y_{n+1}=\left(1-\frac{h}{2}A_{n+1}\right)^{-1}\left(1+\frac{h}{2}A_n\right)y_n, \tag{A25}$$

$$y_{n+1}=\left(1-\frac{h}{2}A_{n+1}+\frac{h^2}{12}B_{n+1}\right)^{-1}\times\left(1+\frac{h}{2}A_n+\frac{h^2}{12}B_n\right)y_n, \tag{A26}$$

$$y_{n+1}=\left[1-\frac{h}{2}A_{n+1}+\frac{h^2}{10}B_{n+1}-\frac{h^3}{120}C_{n+1}\right]^{-1}\times\left[1+\frac{h}{2}A_n+\frac{h^2}{10}B_n+\frac{h^3}{120}C_n\right]y_n. \tag{A27}$$

[28] L. R. B. Elton, Proc. Phys. Soc. (London) **A66**, 806 (1953). There is a sign error in Elton's Eq. (3.14).

[29] W. E. Milne, *Numerical Solution of Differential Equations* (John Wiley and Sons, Inc., New York, 1953), pp. 76–78.

[30] When this method is applied to nonlinear differential equations y_{n+1} is obtained from y_n by an iteration procedure.

We can make some estimates of the errors involved in using this method. Inside the turning point (which is at $x \cong j$), any small errors made in an integration step will bring in a small amount of irregular function. However, in this region the regular function increases rapidly with increasing x, while the irregular function decreases rapidly. Thus, in this region, the effect of a small error tends to be damped quickly. Of course the normalization near the origin may differ from that outside the turning point because of these errors, but that does not affect the present calculations since we need only the ratio (F_j/G_j) at the fitting-on radius.

Outside the turning point the error in the phase can be estimated by replacing the Eqs. (21) by the equations

$$g'=-f, \quad f'=+g, \tag{A28}$$

which have the solutions

$$g=\cos x, \quad f=\sin x.$$

Equations (A19–A21) have the solution[31]

$$g=\cos\lambda x, \quad f=\sin\lambda x,$$

where

$$\lambda=1-h^2/12,$$
$$\lambda=1-h^4/720,$$
$$\lambda=1-h^6/100\,800,$$

respectively. The total phase error in a distance L is therefore

$$\delta\phi=h^2L/12,$$
$$\delta\phi=h^4L/720,$$
$$\delta\phi=h^6L/100\,800,$$

for the three approximations.

If we require $\delta\phi<10^{-4}$, for $L=8$ we find in the respective cases:

$$h<10^{-2}, \quad h<0.3, \quad h<1.$$

The interval that would be required using Eq. (A19) is prohibitively small. With Eq. (A20) there is more computing work at each step of the integration, but the interval is reasonable. One could not use such a large interval with Eq. (A21) as estimated here because of the variation of A_n with x. With a smaller interval Eq. (A21) may be useful in obtaining greater accuracy.

[31] This was pointed out to us by Professor L. I. Schiff.

PHYSICAL REVIEW VOLUME 95, NUMBER 2 JULY 15, 1954

High-Energy Electron Scattering and Nuclear Structure Determinations. II*†‡

R. HOFSTADTER, B. HAHN,§ A. W. KNUDSEN, AND J. A. MCINTYRE
Department of Physics and W. W. Hansen Laboratories of Physics, Stanford University, Stanford, California

(Received April 1, 1954)

Elastic scattering measurements have been carried out with electrons in Au^{197} at energies of 84, 126, 154, and 183 Mev and in Pb^{208} at 84, 153, and 186 Mev. Diffraction effects are observed which appear to vary with momentum and angular position as if a fundamental parameter $p\sin(\theta/2)$ were equal to a constant for a given diffraction feature. Such a behavior would be predicted by the Born approximation. A comparison of the scattering in Au^{197} and Pb^{208} suggests that inelastic scattering does not materially influence the scattering curves presented. The appearance of diffraction effects indicates a model more nearly uniform in charge density than early tentative conclusions based on Born approximation calculations.

I. INTRODUCTION

IN the first paper of this series with the above title[1] experimental electron scattering curves were presented for several materials at 125 Mev. Elastic profiles were shown, the apparatus was described, various checks on the experimental information were discussed, and other relevant information was given. A preliminary attempt to explain the at-that-time unexpected absence of prominent diffraction peaks was made in terms of a first-order Born approximation calculation for various nuclear charge distributions.[1,2] These approximate calculations led to a tentative interpretation which indicated a smooth decrease of charge density from the center to the outer regions of heavy nuclei such as gold and lead. It must be borne in mind that the conventional values of nuclear radius (for example, root-mean-square values) were retained in this interpretation.

It has recently been shown by Yennie, Wilson, and Ravenhall[3] that an accurate phase shift calculation for

* The research reported in this document was supported jointly by the U. S. Office of Naval Research and the U. S. Atomic Energy Commission, and by the U. S. Air Force through the Office of Scientific Research of the Air Research and Development Command.
† Aided by a grant from the Research Corporation.
‡ This material was presented in part at the New York Meeting of the American Physical Society in January, 1954 [Phys. Rev. 94, 773 (1954)].
§ Visiting Post Doctoral Research Fellow of the Schweizerische Arbeitsgemeinschaft in Mathematik und Physik, Switzerland.
[1] Hofstadter, Fechter, McIntyre, Phys. Rev. 92, 978 (1953). We shall refer to this paper as I.
[2] L. I. Schiff, Phys. Rev. 92, 988 (1953).
[3] Yennie, Wilson, and Ravenhall, Phys. Rev. 92, 1325 (1953).

a more conventional nuclear model with uniform charge density and a sharp edge provides elastic scattering curves with washed-out minima and maxima for nuclei with $Z \cong 80$. For copper ($Z=29$) the minima and maxima are pronounced and the Born approximation is more pertinent although not completely reliable even in this case. The calculations of Yennie *et al.*, and also those of Baranger,[4] carried out by a less accurate method, therefore implied that perhaps the experimental data can be fitted by a uniform, or nearly uniform, model. In any case, it became apparent immediately that more experimental and theoretical information would be required before definite conclusions on the type of charge distribution could be made. The tentative interpretation which led to a strong taper at the center has to be abandoned although the early suggestion of a taper at the edge is confirmed (see below).

It has been a major goal of our program to carry out elastic scattering at different energies in order to provide more than one "fix" on a given nucleus. For this reason we have presently continued the earlier studies and in this paper we give the experimental curves for Au^{197} and Pb^{208} at several energies.[5]

Since the first energy level in the Pb^{208} nucleus is at 2.6 Mev it is possible with the energy resolution of our spectrometer magnet to select only elastically scattered electrons.[6] In contrast, in the Au^{197} nucleus there is an energy level below 100 kev, and electrons exciting this level could not be rejected as inelastically scattered electrons by our apparatus. If one then assumed that inelastic scattering events significantly modified the gold angular distribution, it would be very unlikely that the gold and lead angular distributions would be similar. Experimental evidence of such a similarity would thus be evidence for a negligible contribution of inelastic scattering from gold.

II. APPARATUS

The main features of the experimental apparatus have been described in I (pp. 979 and 980). Some recent additions and improvements in the apparatus are noted below. A remotely controlled uranium slit at the exit of the analyzing magnet has been added. A beam "sniffer" which indicates small horizontal shifts in the position of the beam emerging from the second deflecting (refocusing) magnet has also been added. This is an ionization chamber split vertically in two with the readings of each half balanced against the other, and the slit being located on the beam line. The sniffer is used to control the beam manually from time to time as the occasion demands. The analyzing magnet current

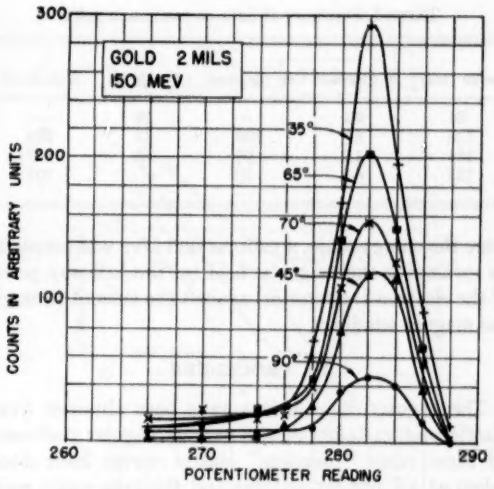

FIG. 1. Representative elastic scattering curves at 150 Mev in gold. The ordinates of the individual curves are unrelated.

is now regulated to better than 0.1 percent by means of electronic control of the generator field winding.

The analyzing magnet has also been rewound with hollow conductor square copper rod so that its upper bending limit is now 195 Mev, whereas it was previously about 150 Mev. The focusing properties at the highest energies have not been studied carefully although they are presumably not bad judging by the quality of the elastic curves. However, the magnet shows increasing saturation at the high energies so that the current scale is no longer proportional to energy. In order to deter-

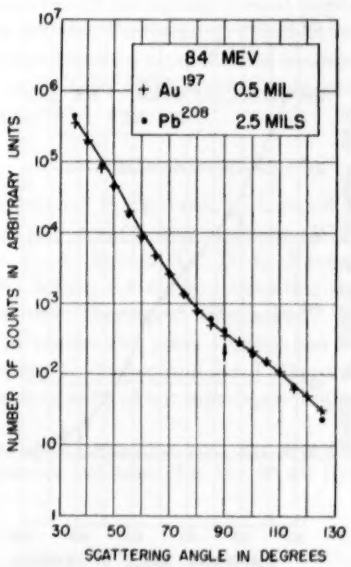

FIG. 2. Elastic scattering in Au^{197} and Pb^{208} at 84 Mev. The arrow marks an estimate of the angular position of a diffraction washed-out minimum. Curves normalized arbitrarily.

[4] E. Baranger, Phys. Rev. **93**, 1127 (1954). We wish to thank Mrs. Baranger for early communication of her results.

[5] The 96-percent pure Pb^{208} sample was obtained from the Isotopes Division, U. S. Atomic Energy Commission, Oak Ridge, Tennessee.

[6] We have recently observed inelastic electron scattering peaks in beryllium and other materials at 190 Mev.

TABLE I. Summary of data on minima in gold.

Energy (Mev)	θ_I (degrees)	θ_{II} (degrees)	$E \sin(\theta_I/2)$	$E \sin(\theta_{II}/2)$
84	90	...	59	...
126	51	109	55	103
154	45	90	58	109
183	...	70	...	105

mine the energy scale, a calibration curve was prepared by measuring the magnetic field (at the half-way point of the electron trajectories) against the current through the magnet windings.

III. PROCEDURE

The angular distributions have been obtained from elastic profiles taken at the various angular positions. In most cases "complete" elastic curves have been taken at all angular settings and the area under each elastic curve has been plotted as an individual point in the angular distribution. As an example, a few members in a set of elastic curves are shown in Fig. 1. In this case the energy spread in the incident 150-Mev beam was 0.5 percent, the thickness of the gold foil was 2 mils. The exit slit of the spectrometer was set at a width corresponding to 0.5 percent in energy and the entrance slit was $\frac{3}{4}$ in. wide and $\frac{3}{4}$ in. high at a distance of 11 in. from the center of the scattering foil. In the case of Pb^{208} the measurements have usually been made with five points straddling the center of the peak instead of a complete elastic curve. The best energy resolution realized to date with the analyzing magnet is 0.28 percent at 125 Mev.

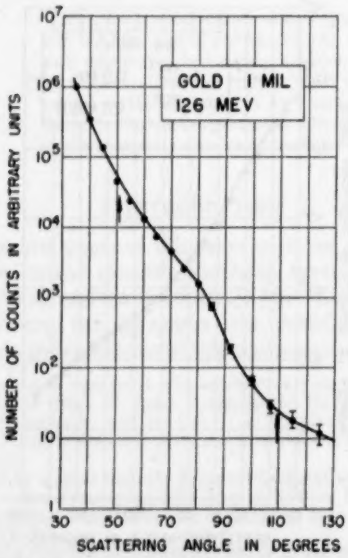

FIG. 3. Elastic scattering in Au^{197} at 126 Mev. The arrows mark an estimate of the angular position of diffraction washed-out minima.

IV. RESULTS

Experiments were carried out at 84, 126, 154, and 183 Mev in Au^{197} and at 84, 153, and 186 Mev in Pb^{208}. The angular distributions so obtained are shown in Figs. 2, 3, 4, and 5. In Figs. 2, 4, and 5 both the lead and gold data are plotted, while in Fig. 3 only the gold data appear. The statistical errors are also shown in Fig. 3 and are typical of those obtained at the other energies. It is clear from these curves that the angular distributions for lead and gold are identical within the accuracy of the experiments, and it may therefore be presumed that inelastic processes contribute a negligible amount to the angular distributions. The newer data are also more consistent internally than the data in paper I and the study in gold at 126 Mev has therefore been repeated. The agreement is quite good and the slight differences observed are within the old experimental errors.

The data for gold and lead show clearly the signs of washed-out diffraction structure. The 84-Mev data for

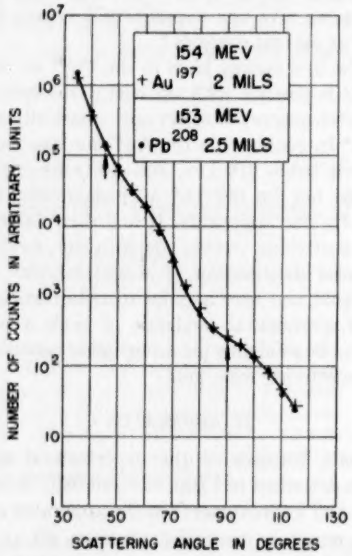

FIG. 4. Elastic scattering in Au^{197} and Pb^{208} at 154 and 153 Mev, respectively. The arrows mark estimates of the angular positions of diffraction washed-out minima. Curves normalized arbitrarily.

gold and lead show a washed-out minimum near 90°. At 126 Mev in gold there is a similar point at 51° and a second washed-out minimum at 109°. At 154 Mev the first "minimum" appears near 45° and a second more pronounced one at 90°. The second "minimum" at 154 Mev falls at 90° where we found the first "minimum" at 84 Mev, an energy close to one-half of 154 Mev. At 183 Mev the first "minimum" has moved near 35° and is not clearly visible. The second one has now moved to about 70°. Hence it is now possible to trace the diffraction structure through many scattering

curves at different energies. The diffraction peaks and valleys are not prominent but nevertheless are definite, as shown by a "form factor" plot of Fig. 6 in which the point charge calculations have been divided into the experimental curves at the various energies. It is to be noted that a uniform charge distribution with square edge[2] gives an appearance somewhat like the experimental data but with more pronounced diffraction features.

Table I shows a summary of the data on "minima" in gold. From these it may be seen that the product

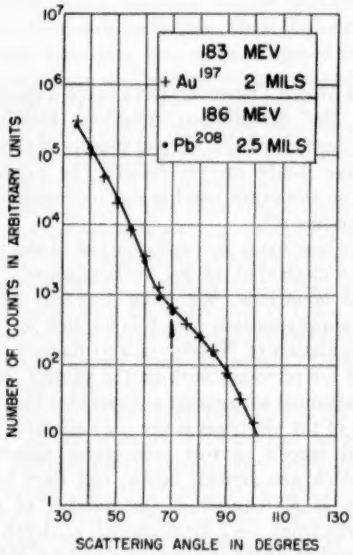

FIG. 5. Elastic scattering in Au^{197} and Pb^{208} at 183 and 186 Mev, respectively. The arrow marks an estimate of the angular position of a diffraction washed-out minimum. Curves normalized arbitrarily.

$E\sin\theta/2\cong 57$, where E is the energy in Mev ($E=pc$ at these energies), for the first "minimum" in all the gold and lead curves. The product $E\sin\theta/2\cong 106$ for the second "minimum." These figures imply a nuclear radius for a uniformly charged model, $R=r_0A^{\frac{1}{3}}$, where $r_0=(1.1\pm0.1)\times10^{-13}$ cm for both Au^{197} and Pb^{208} where we have used the curves of Yennie *et al.*[3] Therefore the charge density is considerably higher than that given by previous models where $r_0=1.45\times10^{-13}$ cm. A rounded-off model gives a better fit than the uniform, but as yet not an exact fit of the experimental data.[7,8] Similar

[7] Yennie, Ravenhall, and Wilson, preceding paper [Phys. Rev. **95**, 500 (1954)].

[8] Brenner, Brown, and Elton (to be published). We wish to thank Prof. R. E. Peierls for early communication of these results.

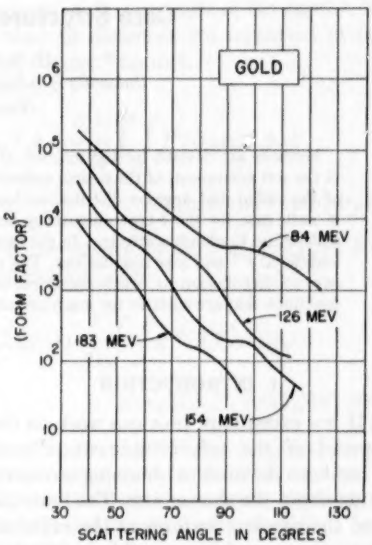

FIG. 6. The squares of form factors plotted against angle for gold at 84, 126, 154, and 183 Mev. The ordinate is obtained by plotting the quotient of the observed scattering by the point charge scattering curve. The ordinates of individual curves are unrelated.

conclusions concerning a smaller nuclear size have been drawn recently from the measurements of Fitch and Rainwater[9] and Pidd, Hammer, and Raka.[10]

A model such as a Gaussian or exponential will not explain simultaneously the scattering data at 126 and 183 Mev because the theoretical curves for such peaked distributions fall off too rapidly toward large angles at the higher energies. Furthermore, the observed diffraction structure implies a type of finite boundary rather than the smooth taper which predicts an entirely smooth scattering curve.[3,7]

ACKNOWLEDGMENT

We are grateful to Professor L. I. Schiff for many interesting and fruitful conversations. We wish to thank Dr. D. R. Yennie, Dr. D. G. Ravenhall, and Mr. R. N. Wilson for many stimulating discussions concerning their theoretical calculations. We should also like to express our great appreciation to Mr. B. Chambers, Mr. V. Prosper, and Mr. J. Fregeau for their help in building parts of our experimental apparatus.

[9] V. L. Fitch and J. Rainwater, Phys. Rev. **92**, 789 (1953).

[10] Pidd, Hammer, and Raka, Phys. Rev. **92**, 436 (1953).

Core Structure in Soft Component Showers

H. S. GREEN AND O. BERGMANN
University of Adelaide, Adelaide, South Australia, Australia
(Received December 16, 1953)

Methods are devised for the solution of the integro-differential equations for the evolution and spread of the soft component of the cosmic radiation, avoiding approximations made in earlier work. The behavior of the radial and angular distribution functions is analyzed near their origins and coefficients are found in each case for the δ-type singularity arising from particles, which together with their ancestors have suffered no Coulomb scattering. In the case of the radial-distribution function for electrons only, there are additional r^{-1} and $\log r$ singularities. The contribution of these singularities is compared with that of the over-all distribution by rough numerical computations. Expressions are given for the over-all distribution functions that are suitable for machine computations.

1. INTRODUCTION

WITH few exceptions, previous work on the radial spread of the soft component of cosmic-ray showers has been devoted to obtaining moments of the distribution about the shower axis. The lower moments are indeed the simplest features of the radial distribution to investigate, and it is possible in principle to reconstruct the distribution function completely from a knowledge of its moments. Obviously, however, the moments depend only very insensitively on the values of the distribution function near the center, and this makes it almost impossible in practice to determine from them the behavior of the radial distribution near the shower axis. Similar considerations apply to the angular distribution of the cosmic-ray particles with respect to the shower axis. If only an independent method were available to determine directly the behavior of the radial distribution function at small distances, and the angular distribution function at small angles, the difficulty mentioned would disappear. It is the purpose of this paper to provide and apply such a method.

The early workers in the field agree that the radial distribution function must be singular at the shower axis. Euler and Wergeland[1] found a dependence of r^{-1} on the distance r, which was adopted by Molière,[2] though his own calculation gave a dependence like $r^{-\frac{1}{2}}$. Later[3] Molière stated without proof that the radial distribution function for electrons should behave as $r^{-\frac{1}{2}}$, but that for photons as r^{-1}, near the shower axis. Bethe,[4] however, suggested that a more precise method should give a variation like $r^{-4/3}$ for the electrons, and Blatt[5] on qualitative grounds, concluded that Molière's function was not sufficiently peaked. Reconstructions of the distribution function from the moments (e.g., that of Eyges and Fernbach[6]) have generally relied on the correctness of Molière's function near the origin. Green and Messel,[7] however, have made a quantitative study of the distribution function, showing that Molière's theory contains several sources of error which throw grave doubt on his result. The experimental evidence[8] on the other hand is not inconsistent with a dependence like r^{-1}.

We have now made an *exact* analysis of the problem, using a new method of solving the fundamental integro-differential equations. We have avoided the use of Landau's approximation, which is implicit in the exact formal calculation of Nishimura and Kamata,[9] as well as most of the previous work on the subject. We have, however, assumed with earlier authors that the Coulomb scattering of the electrons is the only effective cause of the lateral spread of soft component showers. Our results, which are derived below, can then be stated as follows. If $R^{(i)}(r,z)rdr$ is the number of particles ($i=1$ for electrons, $i=2$ for photons), at depth z in the medium, and at distance between r and $r+dr$ from the shower axis, then

$$R^{(1)}(r,z)=A^{(1)}(z)[r^{-1}\delta(r)+2\alpha\rho(z)(3\varphi r)^{-1}+2\{\alpha\rho(z)\}^2(3\varphi)^{-2}\ln r]+E^{(1)}(r,z), \quad (1)$$

$$R^{(2)}(r,z)=A^{(2)}(z)r^{-1}\delta(r)+E^{(2)}(r,z), \quad (2)$$

where $A^{(1)}(z)$ and $A^{(2)}(z)$ are functions of the depth, evaluated below, and $E^{(1)}(r,z)$ and $E^{(2)}(r,z)$ are functions which are finite for $r=0$; these are most easily evaluated using the moments of the distributions. In (1), α is the total cross section[10] for Coulomb scattering by an atom of the medium of mass density $\rho(z)$; φ is the minimum scattering angle, which depends on the energy of the electron concerned. Further, if $\Theta^{(i)}(\theta,z)\theta d\theta$ is the number of particles whose paths make an angle between θ and $\theta+d\theta$ with the shower axis, then

$$\Theta^{(i)}(\theta,z)=B^{(i)}(z)\theta^{-1}\delta(\theta)+F^{(i)}(\theta,z), \quad (3)$$

[1] H. Euler and H. Wergeland, Astrophysica Norwegica **3**, 165 (1940).
[2] G. Molière, *Cosmic Radiation*, as edited by W. Heisenberg (Dover Publications, New York, 1946).
[3] G. Molière, Phys. Rev. **77**, 715 (1950).
[4] H. Bethe, Phys. Rev. **59**, 684 (1941).
[5] J. M. Blatt, Phys. Rev. **75**, 1584 (1949).
[6] L. Eyges and S. Fernbach, Phys. Rev. **82**, 23 (1951).
[7] H. S. Green and H. Messel, Phys. Rev. **88**, 331 (1952).
[8] Cocconi, Tongiorgi, and Greisen, Phys. Rev. **76**, 1020 (1949).
[9] J. Nishimura and K. Kamata, Progr. Theoret. Phys. (Japan) **7**, 185 (1952).
[10] This cross section is made dimensionless by multiplication with the radiation length and division by the mass of an atom of the medium.

where $F^{(1)}(\theta,z)$ and $F^{(2)}(\theta,z)$ are finite for $\theta=0$. It is assumed that the showers are initiated by a single particle or spectrum of particles directed along the shower axis; the functions $A^{(i)}(z)$ and $B^{(i)}(z)$ depend on the incident spectrum, and also the density distribution of the medium.

It will be noticed that the essence of the above results is a separation of the singularities of the distribution functions from the main continuous distributions. A clear physical interpretation can be given to each of the singular terms, as follows. The $\delta(r)$ and $\delta(\theta)$ singularities arise from particles whose ancestors have suffered no Coulomb scattering. Since the cross section for Coulomb scattering is so large compared with those for pair production and bremstrahlung (in the effective photon energy range), the coefficients $A^{(i)}(z)$ and $B^{(i)}(z)$ must obviously be relatively small at all except small depths and high energies; the main contribution to them comes from photons which are produced early in the cascade process and then travel a considerable distance without producing a pair. The additional singularities in $R^{(1)}(r,z)$ arise from electrons whose ancestors have also suffered no Coulomb scattering, but which have themselves been scattered once or twice. All other particles contribute to the main continuous distribution, which has no singularity at the origin, though it may be considerably peaked.

The conclusion to be drawn from this paper is, therefore, that earlier workers were correct in supposing that the distribution functions are singular at their origins, though the exact nature of the singularities was wrongly assigned; and that the singular contributions to the distribution functions are, at ordinary atmospheric depths and relatively low energies, unimportant. In determining the distribution functions from their moments, it is therefore permissible under these conditions to assume an expansion in terms of orthogonal polynomials finite at the origin. This conclusion is itself of considerable practical importance, but we believe that our method also makes possible the direct computation by modern methods of the distribution functions without use of the moments. We do in fact derive explicit formulas for $R^{(i)}(r,z)$ and $\Theta^{(i)}(\theta,z)$ in the form of series, the computation of about 70 terms of which would suffice numerically, even to a depth of 24 cascade units.

2. SOLUTION OF THE DIFFUSION EQUATIONS

For the formulation of the fundamental integro-differential equations, the reader is referred to a recent paper of Messel and Green.[11] Let $f^{(i)}(\mathbf{p},\mathbf{r})(2\pi p^2)^{-1}\times dp_1dp_2dp_3dr_1dr_2$ be the probability of finding a particle of the ith kind ($i=1$ for electrons, 2 for photons) with momentum $\mathbf{p},d\mathbf{p}$ at a vector displacement $\mathbf{r}$ from the foot of the shower axis assumed vertical (so that $z=-r_3+$constant is a measure of the depth). We shall suppose that all distances are measured in radiation lengths (42.8 g cm^{-2} for air).

Further, let

$$g^{(i)}(k_1,k_2,T,p,z)=\frac{1}{2\pi}\int\int f^{(i)}(r_1,r_2,T,p,z)\times\exp\{i(k_1r_1+k_2r_2)\}dr_1dr_2, \quad (4)$$

where T is the tangent of the angle between p and the downward vertical, and

$$h^{(i)}(k,\lambda_1,\lambda_2,p,z)=\frac{1}{2\pi}\int\int g^{(i)}(k,T_1,T_2,p,z)\times\exp\{i(\lambda_1T_1+\lambda_2T_2)\}dT_1dT_2, \quad (5)$$

where $T_1=T\cos\beta=(kp)^{-1}(k_1p_1+k_2p_2)$ and $T_2=T\sin\beta$. The angles are supposed to be small, so that there is little difference between the tangent, the sine, and the angle itself. Then $h^{(i)}$ satisfies the equation

$$\frac{1}{\rho(z)}\left\{\frac{\partial h^{(i)}(p)}{\partial z}+k\frac{\partial h^{(i)}(p)}{\partial\lambda_1}\right\}+A^{(i)}h^{(i)}(p)=\sum_{j=1}^{2}\int_p^\infty dp_1h^{(j)}(p_1)V^{(j,i)}(p_1,p,\lambda), \quad (6)$$

where $\rho(z)$ is the mass density of the atoms of the medium, $A^{(i)}$ is the total cross section[10] for collision of a particle of the ith kind with an atom, and $V^{(j,i)}(p_1,p,\lambda)$ which depends only on $\lambda=(\lambda_1^2+\lambda_2^2)^{\frac{1}{2}}$, is defined by

$$V^{(j,i)}(p_1,p,\lambda)=\int_0^\infty W^{(j,i)}(p_1,p,\tau)J_0(\lambda\tau)\tau d\tau, \quad (7)$$

where $W^{(j,i)}(p_1,p,\tau)dp\tau d\tau$ is the differential cross section[10] for the production, at an angle $\tan^{-1}\tau$ with the primary, of a particle of the ith kind, as a result of the encounter of a particle of the jth kind with an atom. We take

$$A^{(i)}=\alpha^{(i)}+\alpha\delta_{i1},$$
$$V^{(j,i)}(p_1,p,\lambda)=p_1^{-1}v^{(j,i)}(p/p_1)+2\alpha\delta(p_1-p)\int_1^\infty dx x^{-3}J_0(\lambda\varphi x)\delta_{i1}, \quad (8)$$

where $\alpha^{(1)}$ and $\alpha^{(2)}$ are the total cross sections for bremstrahlung and pair production, respectively, and α the total cross section for Coulomb scattering; $\varphi=0.0073Z^{-\frac{1}{3}}m_ec/p$ is the minimum angle for the Coulomb scattering of an electron of momentum p. The maximum angle for Coulomb scattering has been given the value $\pi/2$ since it does not sensitively enter into the results; this could not be done using Landau's approximation, which amounts to replacing $J_0(\lambda\varphi x)$ by $1-\frac{1}{4}(\lambda\varphi x)^2$.

[11] H. Messel and H. S. Green, Proc. Phys. Soc. (London) **A66**, 1009 (1953).

We shall obtain two different solutions of (6), the first of which is useful for calculating the contribution to the distribution functions from particles whose ancestors have been scattered only a few times; these ancestors must have been photons with long lives, and electrons, if any, with short lives. These will predominate at *very* short distances from the shower axis. Afterwards we shall obtain a second solution which is more useful for the analysis of the singularities, and also for calculating the over-all distribution functions.

The first solution, which is useful in the numerical evaluation of the coefficients $A^{(i)}$ and $B^{(i)}$ of Eqs. (1), (2), and (3), is obtained by taking a Mellin transform of (7). The details of this procedure are well known (see reference 7), and we therefore state only the result

$$\frac{1}{\rho(z)}\left(\frac{\partial H^{(i)}}{\partial z}+k\frac{\partial H^{(i)}}{\partial \lambda_1}\right)+\alpha\delta_{i1}H^{(i)}=B^{(i)}H^{(3-i)} -D^{(i)}\delta_{i1}H^{(i)}+\frac{\alpha\delta_{i1}}{2\pi i}\int dv_1 H^{(i)}(v_1)E(v-v_1), \quad (9)$$

where

$$H^{(i)}(v)=\int_0^\infty h^{(i)}(p)p^{v-1}dp, \quad (10)$$

$$E(x)=(p\varphi)^{x-2}(\tfrac{1}{2}\lambda_1)^x\Gamma(-\tfrac{1}{2}x) \times\{(2-x)\Gamma(1+\tfrac{1}{2}x)\}^{-1}. \quad (11)$$

The functions $B^{(i)}(v)$ and $D^{(i)}(v)$ are the same as in reference 7; the integration with respect to v_1 in (9) is to be performed along a path normal to the real axis such that $0<R(v_1-v)<\frac{3}{2}$. Let

$$H_j=H^{(1)}+\xi_j H^{(2)}, \quad (12)$$

where ξ_1 and ξ_2 are the roots of the equation

$$B^{(2)}\xi^2+(D^{(2)}-D^{(1)}-\alpha)\xi-B^{(1)}=0. \quad (13)$$

Then the equation satisfied by H_j is

$$\frac{1}{\rho(z)}\left(\frac{\partial H_j}{\partial z}+k\frac{\partial H_j}{\partial \lambda_1}\right) =-S_jH_j+\frac{\alpha}{2\pi i}\int dv_1 H^{(1)}(v_1)E(v-v_1), \quad (14)$$

where

$$S_j=D^{(1)}+\alpha-\xi_jB^{(2)}, \quad (15)$$

and one will have

$$H^{(i)}=\Gamma_1{}^{(i)}H_1+\Gamma_2{}^{(i)}H_2, \quad (16)$$

with

$$\xi_2{}^{-1}\Gamma_1{}^{(1)}=-\xi_1{}^{-1}\Gamma_2{}^{(1)}=-\Gamma_1{}^{(2)}=\Gamma_2{}^{(2)}=(\xi_2-\xi_1)^{-1}. \quad (17)$$

It follows from (14) that

$$H_j=\exp(-S_jl)H_j(l=0)+\int_0^l dl_1\exp\{-S_j(l-l_1)\} \times\frac{\alpha}{2\pi i}\int dv_1 H^{(1)}(l=l_1,\lambda_1=\lambda_1')E(v-v_1,\lambda_1=\lambda_1'), \quad (18)$$

where $l(z)=\int_0^z\rho(z)dz$ and $\lambda_1'=\lambda_1+k(z_1-z)$ if $l_1=l(z_1)$. Equations (16) and (18) can be combined to give a single integral equation in $H^{(i)}$, which is soluble by iteration. The nth term obtained in the iteration process represents particles whose electronic ancestors have suffered just n Coulomb scatterings. The total cross section for Coulomb scattering (α) is large compared with the $B^{(i)}$ and $D^{(i)}$, and one has, therefore, very nearly

$$\xi_1=-B^{(1)}/\alpha,\quad \xi_2=\alpha/B^{(2)},\quad \xi_2-\xi_1=\alpha/B^{(2)}, \quad S_1=\alpha=4.65\times10^5,\quad S_2=D^{(2)}=0.774. \quad (19)$$

When l is large, H_1 is negligible compared with H_2, so that

$$H^{(1)}=\alpha^{-2}B^{(1)}B^{(2)}H_2 \quad \text{and} \quad H^{(2)}=\alpha^{-1}B^{(2)}H_2.$$

The method of obtaining the radial and angular distribution functions from $h^{(i)}$ and $H^{(i)}$ will be described later. Owing to the relative magnitude of α, however, the iteration procedure described above converges extremely slowly for the main distribution, and we therefore proceed to develop an alternative method of solution of (6). The latter equation is written in the form

$$\frac{1}{\rho(z)}\left(\frac{\partial h^{(i)}}{\partial z}+k\frac{\partial h^{(i)}}{\partial \lambda_1}\right)=\alpha h^{(i)}\{K(\varphi\lambda)-1\}\delta_{i1}+Q^{(i)}, \quad (20)$$

where

$$K(y)=2\int_1^\infty dx x^{-3}J_0(xy), \quad (21)$$

and

$$Q^{(i)}=\sum_{j=1}^{2}\int_p^\infty dp_1 p_1{}^{-1}v^{(j,i)}(p/p_1) \times\{h^{(j)}(p_1)-\delta_{ij}h^{(j)}(p)\}. \quad (22)$$

This form of the equation makes it clear that, although the integral $\alpha^{(1)}=\int_p^\infty dp_1 p_1{}^{-1}v^{(1,1)}(p/p_1)$ diverges at the lower limit, $Q^{(i)}$ is finite and the singularity therefore disappears.

Equation (20) is integrated, regarding $Q^{(i)}$ temporarily as a known function of z and λ_1. It is also a function of p and λ_2, but the dependence on p is not important at the moment, and we shall set $\lambda_2=0$, since this does not prevent the subsequent determination of the angular and radial distribution functions. Thus, $\lambda_1=\lambda$ and the solution is

$$h^{(i)}=\exp\left\{\alpha\int_0^z\rho(z-\zeta)[K\{\varphi(\lambda-k\zeta)\}-1]d\zeta\delta_{i1}\right\} \times h^{(i)}(z=0)+\int_0^z\rho(z-\zeta_1) \times\exp\left\{\alpha\int_0^{\zeta_1}\rho(z-\zeta)[K\{\varphi(\lambda-k\zeta)\}-1]d\zeta\delta_{i1}\right\} \times Q^{(i)}(z-\zeta_1,\lambda-k\zeta_1)d\zeta_1. \quad (23)$$

When (22) is substituted in (23) one obtains what is, in effect, an integral equation for the determination of $h^{(i)}$, which will be solved by an iteration procedure. The solution thus obtained is

$$h^{(i)}=\sum_{n=0}^{\infty}\int_{p}^{\infty}dp_1p_1^{-1}u^{(j,i)}(p/p_1)\int_{p_1}^{\infty}dp_2p_2^{-1}u^{(k,j)}(p_1/p_2)\times\cdots\int_{p_{n-1}}^{\infty}dp_np_n^{-1}u^{(l,s)}(p_{n-1}/p_n)\times Z_n^{(i,j,k\cdots l)}(p,p_1,p_2,\cdots p_n)h^{(l)}(z=0), \quad (24)$$

where $j, k, \cdots s, l$ are summed over the values 1 and 2,

$$u^{(j,i)}(p/p_1)=v^{(j,i)}(p/p_1)-\alpha^{(i)}\delta(1-p/p_1), \quad (25)$$

and

$$Z_n^{(i,\cdots l)}(p,\cdots p_n)=\int_0^{l}dl_1\int_0^{l_1}dl_2\cdots\int_0^{l_{n-1}}dl_n\times\exp\left\{\alpha\int_0^{l_1}\rho(z-\zeta)[K\{\varphi(\lambda-k\zeta)\}-1]d\zeta\delta_{i1}+\alpha\int_{l_1}^{l_2}\rho(z-\zeta)[K\{\varphi_1(\lambda-k\zeta)\}-1]d\zeta\delta_{j1}+\cdots+\alpha\int_{l_n}^{s}\rho(z-\zeta)[K\{\varphi_n(\lambda-k\zeta)\}-1]d\zeta\delta_{l1}\right\}, \quad (26)$$

where $\varphi_n=p\varphi/p_n$.

The nth term of this solution represents the contribution to the over-all distribution of particles whose ancestry involves precisely n bremstrahlung and pair production processes. In the next section we shall isolate the singularities from the nth term, and obtain their sum with respect to n. We do not propose to compute the over-all distribution functions, but shall discuss here only the convergence of the series (24) in order to determine the practicability of doing so.

Observe first that (24) is essentially a series expansion of the distribution function in powers of the cross sections for bremstrahlung and pair production, so that the convergence of the series for a given depth z will depend on the relative number of particles whose ancestry involves n such processes. We shall therefore calculate the ratio $r_n(z)$ of the number of particles whose ancestry has suffered more than n processes to the total number of particles, at depth z, assuming a power law spectrum for the energies. The value of n for which this ratio is less than, say, 0.01 will give the number of terms in (24) which have to be taken into account to obtain sufficient numerical accuracy.

The average number of electrons $N^{(i)}(v,l)$ with a given energy, at a depth of l radiation lengths, produced by an incident spectrum of electrons with the integral power law exponent $v-1$ is[12]

$$N^{(i)}(v,l)=\text{const}\times\exp\{-\tfrac{1}{2}(D^{(1)}+D^{(2)})l\}\cdot B^{(2)}\eta^{-1}\sinh(\tfrac{1}{2}\eta l), \quad (27)$$

$$\eta=\{(D^{(2)}-D^{(1)})^2+4B^{(1)}B^{(2)}\}^{\frac{1}{2}}.$$

Now $B^{(1)}$, $B^{(2)}$, $D^{(1)}$, and $D^{(2)}$, which are functions of v, are defined linearly in terms of the bremstrahlung and pair production cross sections, so if $N^{(i)}(v,l)$ is expanded in powers of l, the term proportional to l^n will be the number of particles whose ancestry has been involved in n multiplication processes. Hence, neglecting $\{\frac{1}{2}(D^{(1)}+D^{(2)}-\eta)l\}^n$ compared with $\{\frac{1}{2}(D^{(1)}+D^{(2)}+\eta)l\}^n$ and approximating $\sinh(\frac{1}{2}\eta l)$ by $\frac{1}{2}\exp(\frac{1}{2}\eta l)$ one has, for $l>2$,

$$r_n(l)=\sum_{m=n}^{\infty}(m!)^{-1}\{-\tfrac{1}{2}(D^{(1)}+D^{(2)}+\eta)l\}^m\times\exp\{\tfrac{1}{2}(D^{(1)}+D^{(2)}-\eta)l\}.$$

If one substitutes the values $B^{(1)}=0.628$, $B^{(2)}=0.648$, $D^{(1)}=1.310$ and $D^{(2)}=0.774$ which correspond to $v=2.5$, and uses Stirling's approximation for $m!$, one finds that $r_n(l)\ll 0.01$ if $n=3l$.

Since l never exceeds 25 in the atmosphere, it would seem that the computation of $h^{(i)}$ or its transform $f^{(i)}$, from (24), is well within the capacity of modern methods of computation, especially when it is considered that each term of the summation is obtained from the previous one by the same set of elementary operations.

3. ISOLATION OF THE SINGULARITIES

It follows directly from (4) and (5) that

$$h^{(i)}(k,0,0,p,z)=\frac{1}{2\pi}\int\int\int f^{(i)}(r\cos\theta,r\sin\theta,T,p,z)\times TdTd\theta J_0(kr)rdr. \quad (28)$$

Hence, the radial distribution functions are given by

$$R^{(i)}(r,p,z)=\frac{1}{2\pi}\int\int f^{(i)}(r\cos\theta,r\sin\theta,T,p,z)TdTd\theta=\int_0^{\infty}h^{(i)}(k,0,0,p,z)J_0(kr)kdk. \quad (29)$$

Similarly, from (4) and (5) one has

$$h^{(i)}(0,\lambda,0,p,z)=\frac{1}{2\pi}\int\int\int f^{(i)}(r_1,r_2,T,p,z)\times dr_1dr_2J_0(\lambda T)TdT, \quad (30)$$

so that the angular distribution functions are given by

$$\Theta^{(i)}(T,p,z)=\frac{1}{2\pi}\int\int f^{(i)}(r_1,r_2,T,p,z)dr_1dr_2=\int_0^{\infty}h^{(i)}(0,\lambda,0,p,z)J_0(\lambda T)\lambda d\lambda. \quad (31)$$

[12] See L. Janossy, *Cosmic Rays* (Oxford University Press, London, 1948).

We shall now show that $h^{(1)}(k,0,0,p,z)$ can be expressed in the form

$$h^{(1)}(k,0,0,p,z)=A^{(1)}[1+2\alpha\rho(z)(3\varphi k)^{-1}(1-e^{-\beta k}) +2\{\alpha\rho(z)\}^2(3\varphi k)^{-2}(1-e^{-\beta k})^2]+a^{(1)}(k), \quad (32)$$

where $A^{(1)}$ depends only on p and z, and $a^{(1)}(k)$, which also depends on p and z, is such that the integral $\int_0^\infty a^{(1)}(k)kdk$ converges. It will then follow from (29) that

$$R^{(1)}(r,p,z)=A^{(1)}[r^{-1}\delta(r)+2\alpha\rho(z)(3\varphi)^{-1} \times\{r^{-1}-(r^2+\beta^2)^{-\frac{1}{2}}\}+2\{\alpha\rho(z)\}^2(3\varphi)^{-2} \times\{-\ln r+2\ln(\beta+(\beta^2+r^2)^{\frac{1}{2}})-\ln(2\beta+(4\beta^2+r^2)^{\frac{1}{2}})\}] +\int_0^\infty a^{(1)}(k)J_0(kr)kdk, \quad (33)$$

where the last term is finite for $r=0$. This will verify the result (1).

The dependence of $R^{(i)}$ on r and $\Theta^{(i)}$ on T for very small values of r and T, respectively, is determined by the dependence of $h^{(i)}$ on k and λ for very large values of k and λ. We have, therefore, to examine the dependence of $Z_n^{(i,\cdots t)}(p,p_1,\cdots p_n)$ defined by (26), on k and λ for large values of these arguments. First consider the typical integral,

$$I_n=\int_{\zeta_n}^{\zeta_{n+1}}\rho(z-\zeta)K\{\varphi_n(\lambda-k\zeta)\}d\zeta, \quad (34)$$

which it contains.

The k dependence of the integral I_n can be investigated by setting $\lambda=0$. This will enable one to discuss the singularities in the *radial* distribution functions. When k is large, the slowly varying factor $\rho(z-\zeta)$ can be replaced by $\rho(z-\zeta_n)$, and

$$I_n=\rho(z-\zeta_n)\{\zeta_n I(\zeta_n\varphi_n k)-\zeta_{n+1}I(\zeta_{n+1}\varphi_n k)\}, \quad (35)$$

where

$$I(u)=2\int_1^\infty dy\int_1^\infty dx x^{-3}J_0(xyu). \quad (36)$$

If we use the formula $x^nJ_{n-1}(x)=(d/dx)\{x^nJ_n(x)\}$, this integral can be developed asymptotically as follows:

$$I(u)=-2u^{-2}J_2(u)-14u^{-3}J_3(u)-118u^{-4}J_4(u)\cdots, \quad (37)$$

which behaves like $u^{-5/2}\cos(u-\frac{1}{4}\pi)$ for large values of u. In the exceptional case, when $\zeta_n=0$, one has, instead of (35),

$$I_0=\rho(z)\{(\tfrac{3}{2}\varphi k)^{-1}-\zeta_1 I(\zeta_1\varphi k)\}; \quad (38)$$

this behaves like k^{-1} for large values of k. It is clear from these considerations that the first integral in the exponent of (26) is the essential one for large values of k and the whole exponent behaves like

$$2\alpha\rho(z)(3\varphi k)^{-1}\delta_{i1} -\alpha\{(l-l_1)\delta_{i1}+(l_1-l_2)\delta_{j1}+\cdots+l_n\delta_{t1}\}, \quad (39)$$

where $l=l(z)$ and $l_r=l(z-\zeta_r)$.

This result means that very near the shower-axis the radial distribution is determined by particles whose ancestors have not been scattered; though in the case of electrons, they may have been scattered themselves.

The k^{-1} dependence of the approximate exponent (39) does not reproduce the true behavior of the exponent of (26) for small values of k, and we shall therefore approximate $Z_n^{(i,j,\cdots t)}(p_1\cdots p_n)$ instead by

$$Z_n^{(i,\cdots t)}(p_1\cdots p_n)=\int_0^l dl_1\int_0^{l_1}dl_2\cdots\int_0^{l_{n-1}}dl_n \times\exp[2\alpha\rho(z)(3\varphi k)^{-1}(1-e^{-\beta k})\delta_{i1} -\alpha\{(l-l_1)\delta_{i1}+\cdots+l_n\delta_{t1}\}], \quad (40)$$

for large values of k and $\lambda=0$. The type of singularity resulting, is of course in no way dependent on this special assumption. The value of β will be assigned later, in such a way as to give correctly the total number of electrons which have been once scattered.

By expanding the factor $\exp[2\alpha\rho(z)(3\varphi k)^{-1}(1-e^{-\beta k})]$ in (40) as a power series in α, one sees immediately that $h^{(1)}(k,0,0,p,z)$ has the form (32); so that (33) follows. Similarly $h^{(2)}(k,0,0,p,z)$ for large values of k, is of the form

$$h^{(2)}(k,0,0,p,z)=A^{(2)}+a^{(2)}(k), \quad (41)$$

where $\int_0^\infty a^{(2)}(k)kdk$ converges. This, substituted in (29), leads to the formula (2) showing that there is no singularity in the radial distribution function for the photons, apart from the δ-type singularity on the shower axis itself. The constants $A^{(i)}$ are given by

$$A^{(i)}=\sum_{n=0}^\infty\int_p^\infty dp_1 p_1^{-1}u^{(j,i)}(p/p_1)\cdots \times\int_{p_{n-1}}^\infty dp_n p_n^{-1}u^{(t,s)}(p_{n-1}/p_n)\int_0^l dl_1\cdots\int_0^{l_{n-1}}dl_n \times\exp[-\alpha\{(l-l_1)\delta_{i1}+\cdots+l_n\delta_{t1}\}]h^{(t)}(p_n,l=0). \quad (42)$$

This formula can be evaluated most easily by observing that $A^{(i)}$ is the contribution to $h^{(i)}(k,0,0,p,z)$ arising from particles which, together with their ancestors, have suffered no scattering. It is therefore to be obtained by applying an inverse Mellin-transform to our formula (16) and dropping the second term in substituting from (18). If the spectrum of the incident particle obeys an *integral* power law with exponent $\nu-1$, so that $h^{(i)}(l=0)=h_0^{(i)}p^{-\nu}$, the result can be written down immediately; it is, very nearly

$$A^{(i)}=\Gamma_2^{(i)}(\nu)\exp\{-S_2(\nu)l\}\cdot\{h_0^{(1)}+\xi_2(\nu)h_0^{(2)}\}p^{-\nu}. \quad (43)$$

The value of β introduced in (40) can be assigned by observing that according to (33), the number of electrons which have been scattered once, but whose ancestors have not been scattered is

$$2A^{(1)}\alpha\rho(z)(3\varphi)^{-1}\int_0^\infty [r^{-1}-(r^2+\beta^2)^{-\frac{1}{2}}]rdr = 2\beta A^{(1)}\alpha\rho(z)(3\varphi)^{-1}.$$

But the probability of finding an electron at any level which has been once scattered since its creation must practically the same as that of finding one which has not been scattered. The value of β is therefore

$$\beta=3\varphi\{2\alpha\rho(z)\}^{-1}. \tag{44}$$

To determine the singularities in the *angular* distribution, one sets $k=0$ and examines the dependence of $h^{(i)}(0,\lambda,0,p,z)$ on λ for large values of λ. For $k=0$, one has

$$Z_n^{(i,\cdots i)}(p,\cdots p_n)=\int_0^l dl_1\cdots\int^{l_{n-1}} dl_n \times\exp[\alpha\{K(\varphi\lambda)-1\}(l-l_1)\delta_{i1}+\cdots +\alpha\{K(\varphi_n\lambda)-1\}l_n\delta_{i1}]. \tag{45}$$

For large values of $y=\varphi_n\lambda$, one has the asymptotic expansion

$$K(y)=-\{2y^{-1}J_1(y)+8y^{-2}J_2(y)+48y^{-3}J_3(y)+\cdots\},$$

showing that $K(y)\to 0$ as $y^{-\frac{1}{2}}\sin(y-\frac{1}{4}\pi)$. Thus

$$h^{(i)}(0,\lambda,0,p,z)=A^{(i)}+b^{(i)}(\lambda), \tag{46}$$

where $\int_0^\infty b^{(i)}(\lambda)\lambda d\lambda$ converges. This result substituted into (31), verifies our formula (3). Thus there is no singularity in the angular distribution functions, apart from the δ-type singularity arising from particles which, together with their ancestors, have suffered no Coulomb scattering.

4. NUMERICAL RESULTS AND DISCUSSION

Only in the case of the radial distribution functions for the electrons do the singularities contribute to the density off the shower-axis. This conclusion is, of course, a consequence of our assumption that no scattering takes place in bremstrahlung and pair-production. But since earlier authors made the same assumption any other result which they obtained can only be attributed to errors in their calculations. An obvious source of error is the use of Landau's approximation but though it is difficult to analyze the exact effect of this approximation, the less singular behavior which it involves of the exponent in our calculations would lead one to expect a less peaked singularity at the shower axis. Possibly our δ-type singularity would be replaced by something like $r^{-4/3}$ if Landau's approximation were used, though we have not succeeded in verifying this.

TABLE I.

l	1	2	4	6	12	24
A	0.1×10^{-9}	1.7×10^{-10}	1.9×10^{-11}	2.6×10^{-12}	1.2×10^{-14}	5.7×10^{-19}
B	1.6×10^{-10}	7.4×10^{-11}	3.4×10^{-11}	2.0×10^{-11}	6.2×10^{-12}	3.3×10^{-13}

The physical interpretation of the singularities which we have separated from the distribution functions might lead one to suppose that they cannot be an important feature of the gross distributions. To assess their importance, we have made a rough comparison of the density of the electrons arising from the singularities with the over-all density at a short distance from the shower axis. We have assumed that our formula (33) giving the density associated with the singularities holds approximately even for $r\gg\beta$. We have also assumed that the over-all density falls off roughly as $\exp[-br]$ where the contributions from the singularities are neglected. The value of the constant b can be determined from the calculation of the mean square distance of the electrons from the shower axis, made by Green and Messel,[7] together with the well-known values for the average number of electrons at any given depth. For this purpose, a power law spectrum of photons has been assumed with $v=2.5$. In Table I we give in row A the average density of 100 $\pm\frac{1}{2}$ Mev-electrons contributed by the singular terms at a distance of 1 m from the shower-axis. In row B, we give for comparison, the density of electrons contributed by the gross distribution with the same energy, which is effectively constant over an area of several meters around the shower axis.

The spectrum is normalized so that the number of photons with energy greater than 100 Mev in the incident distribution is 1.5×10^{-2}. If the incident spectrum consists of electrons instead of photons, the figures in row A would have to be decreased by the factor 7.1×10^{5}, owing to the Coulomb scattering which usually takes place before bremsstrahlung can occur.

The figures refer to an isothermal atmosphere at 0° centigrade, so that $l=24$ corresponds to sea level approximately in the real atmosphere. It can be seen that the singularities for the energy and distance considered are negligible at sea level. But for heights above $l=3.8$ approximately, they play an increasingly important part. The r^{-1} dependence of the density on the distance from the shower axis extends only for a distance of a few cm at 100 Mev. Beyond this, the contributions of the singularities to the density falls more rapidly and actually varies as r^{-3} at 1 m, if the formula (33) is used.

Since an incident spectrum of particles has been considered it is well to point out that the existence of singularities in the distribution functions depends on the assumption that they all have the same direction. This is only one of the unphysical properties, attributed to the incident distribution, which have been taken over from the work of previous authors.

Polarization in High-Energy Elastic Nucleon-Nucleus Scattering*

BERTRAM J. MALENKA†
Harvard University, Cambridge, Massachusetts
(Received April 14, 1954)

The proposal to explain the comparatively large polarization observed in high-energy elastic proton-nucleus scattering by means of the spin-orbit interaction used in the shell model of the nucleus is examined. Three simple examples are considered in first Born approximation. The approximate magnitude and the approximate location of the maximum polarization for 340-Mev nucleons on carbon is in rough agreement with experiment. However, regions of negative polarization also seem to be predicted by the theory. Finally, an approximate method to calculate the polarization for high energy and small scattering angle is suggested.

I. INTRODUCTION

RECENT experiments[1–4] in the double scattering of high-energy protons by a nucleus indicate a considerably larger amount of spin polarization in the emerging proton beam than is observed in proton-proton scattering. These experiments also seem to indicate that the largest asymmetry occurs in the range of energy and scattering angle where the scattering can be expected to be mostly elastic.[5] In a previous communication,[5] the author suggested that these results might be explained by means of the spin-orbit interaction used in the shell model of the nucleus. This suggestion also has been advanced independently by other authors.[6,7] Some of the consequences will be elaborated here.

In the nuclear shell model,[8,9] it has been shown that the observed shell structure of nuclei can be explained by introducing a relatively strong spin-orbit interaction in the potential well model of the nucleus. We make the additional assumption that for elastic nucleon-nucleus scattering essentially the same spin-orbit force that acts on a bound nucleon also acts on the nucleon being elastically scattered by the nucleus. Since the strength of this interaction depends on the spin orientation of an incident nucleon relative to its orbital momentum, the scattered nucleon beam will be spin-polarized. For an unpolarized incident beam, the double scattering experiments referred to above which measure the right-left asymmetry of the second scattered nucleon beam are used to determine the amount of polarization.

We therefore suppose that the nucleus exerts a potential H' on the incident nucleon. This potential is of the form

$$H'=(1+i\epsilon)V_0(r)+V_1(r)\tfrac{1}{2}\boldsymbol{\sigma}\cdot\mathbf{r}\times(-i)\nabla, \quad (1)$$

where the parameter ϵ is introduced to take account of nuclear absorption.[10] At 100 Mev, the value of ϵ is around $\frac{1}{2}$ and apparently slowly increases with higher energies.[11] The $V_0(r)$ is a central potential well and $V_1(r)$ describes the radial dependence of the spin-orbit interaction. The magnitude of $V_1(r)$ should be adjusted so that it gives the correct order of doublet splitting when calculated by bound state perturbation theory,[12] that is,

$$\Delta E=E_{l+\frac{1}{2}}-E_{l-\frac{1}{2}}=\langle\psi_{E,l}(r),\, V_1(r)\psi_{E,l}(r)\rangle(l+\tfrac{1}{2}), \quad (2)$$

where $\psi_{E,l}(r)$ is the radial part of a bound state wave function for the unperturbed central nuclear potential well. According to Mayer,[8] ΔE should be roughly about -2 Mev for large l, say l about 5.

For an interaction given by (1), we assume that we can express the elastic scattering amplitude in the form[13]

$$f(\theta)=f_0(\theta)+\boldsymbol{\sigma}\cdot\mathbf{n}f_1(\vartheta), \quad (3)$$

where $\mathbf{n}$ is a unit vector defined by

$$\mathbf{k}_0\times\mathbf{k}=\mathbf{n}k^2\sin\theta, \quad (4)$$

where $\mathbf{k}_0$ and $\mathbf{k}$ are the initial and final nucleon propagation vectors. For an unpolarized incident beam, the polarization is then

$$P(\theta)=\frac{\frac{1}{2}\,\mathrm{Tr}[f^\dagger(\theta)\boldsymbol{\sigma}\cdot\mathbf{n}f(\theta)]}{\frac{1}{2}\,\mathrm{Tr}[f^\dagger(\theta)f(\theta)]}=\frac{f_0^*(\theta)f_1(\theta)+f_0(\theta)f_1^*(\theta)}{|f_0(\theta)|^2+|f_1(\theta)|^2}, \quad (5)$$

where the trace is taken over the spin space. With this definition of $\mathbf{n}$, $P(\theta)>0$ corresponds to more nucleons with spin up being scattered to the left and $P(\theta)<0$ more with spin down being similarly scattered. We note that the differential cross section for single elastic scattering which is just the denominator of (5) depends on the sum of the absolute squares of the scattering

* This work was partially supported by the joint program of the U. S. Office of Naval Research and the U. S. Atomic Energy Commission.
† After September, 1954, at Washington University, St. Louis, Missouri.
[1] Oxley, Cartwright, and Rouvina, Phys. Rev. **93**, 806 (1954).
[2] Marshall, Marshall, and Carvalho, Phys. Rev. **93**, 1431 (1954).
[3] Chamberlain, Segrè, Tripp, Wiegand, and Ypsilantis, Phys. Rev. **93**, 1430 (1954).
[4] J. M. Dickson and D. C. Salter at Harwell, as reported in the Proceedings of the 1954 Rochester Conference on High Energy Physics (University of Rochester Press, Rochester, to be published).
[5] B. J. Malenka, Bull. Am. Phys. Soc. **29**, No. 4, 32 (1954).
[6] E. Fermi, Nuovo cimento (to be published).
[7] W. Heckrotte and J. V. Lepore, Phys. Rev. **94**, 500 (1954).
[8] M. G. Mayer, Phys. Rev. **78**, 16 (1950).
[9] Haxel, Jensen, and Suess, Ann. Physik **128**, 295 (1950).
[10] R. E. LeLevier and D. S. Saxon, Phys. Rev. **87**, 40 (1952).
[11] I. I. Shapiro and J. M. Teem (private communication).
[12] B. J. Malenka, Phys. Rev. **86**, 68 (1952).
[13] See for instance, J. Schwinger, Phys. Rev. **73**, 407 (1948) or L. Wolfenstein, Phys. Rev. **75**, 1664 (1949).

amplitudes, whereas $P(\theta)$ is sensitive to their relative phases and accordingly can have negative values.

From the shell model, we know that $V_0(r)$ is some modified square well extending a distance of the order of the nuclear radius. The depth of this well appears to be in the vicinity of 30 Mev, although current optical model calculations seem to indicate that for high-energy elastic nucleon-nucleus scattering, the effective well depth may be considerably reduced.[11] However, the radial dependence of $V_1(r)$ is not as well determined since several functions of r will yield approximately the right order of doublet splitting in (2) when the magnitude of $V_1(r)$ is suitably adjusted. The forms suggested so far for the radial dependence either assume an approximately uniform effect,[12] in which case $V_1(r)$ is itself some sort of modified square well, or represent an estimate the effect of a core acting on a nucleon,[14,15] in which case $V_1(r)$ approximately has the form $r^{-1}d\phi/dr$, where $\phi(r)$ characterizes the collective action of the core. The resulting form of the second category also includes a generalization of the relativistic Thomas effect which when unmodified gives a doublet splitting which is too small.[16] Here $V_1(r)$ would be proportional to $r^{-1}dV_0/dr$.

II. BORN APPROXIMATION

Since the range of energies used in the polarization experiments are relatively high and since the absorption parameter ϵ at these energies is larger than $\frac{1}{2}$, we can expect a first Born approximation calculation of the scattering amplitudes to give approximately quantitatively correct results for the polarization.†

For this approximation, we can use Eq. (5) directly. However, in many cases, it becomes convenient to make the rearrangement

$$f_0(\theta)=(1+i\epsilon)f_0'(\theta), \tag{6}$$

$$f_1(\theta)=i\tfrac{1}{2}\lambda^2k^2\sin\theta f_1'(\theta), \tag{7}$$

where λ is the nucleon Compton wavelength, and where $f_0'(\theta)$ and $f_1'(\theta)$ are now real scattering amplitudes which are calculated in first Born approximation from the real potentials $V_0(r)$ and $\mathcal{V}_1(r)=-\lambda^{-2}\int rV_1(r)dr$. The latter potential is obtained by partial integration in $f_1(\theta)$. The expression (5) for $P(\theta)$ then becomes

$$P_0(\theta)=\frac{\epsilon\lambda^2k^2\sin\theta f_0'(\theta)f_1'(\theta)}{(1+\epsilon^2)[f_0'(\theta)]^2+\frac{1}{4}\lambda^4k^4\sin^2\theta[f_1'(\theta)]^2}. \tag{8}$$

In this form, it can be readily shown that $P_0(\theta)$ reaches its optimum value for the scattering angles, θ_0, which satisfy the equation

$$(1+\epsilon^2)[f_0'(\theta_0)]^2=\tfrac{1}{4}\lambda^4k^4\sin^2\theta[f_1'(\theta_0)]^2. \tag{9}$$

The maximum and minimum values of $P_0(\theta)$ are then

$$P_0(\theta_0)=\pm\epsilon/(1+\epsilon^2)^{\frac{1}{2}}, \tag{10}$$

provided that θ_0 exists in the interval from 0 to π.

The effect of also including a shielded Coulomb interaction would be to add the Coulomb amplitude $f_c(\theta)$ to $f_0(\theta)$. Since this amplitude is real, it will only enter in the denominator of $P_0(\theta)$. It can be easily verified that except at very small angles, the contribution of the Coulomb term is comparatively quite small, so that neglecting it will not essentially alter any of the results presented in this paper.

As an elementary example of a uniform spin-orbit effect, we consider the potential defined by

$$\begin{aligned} &V_0(r)=-U_0, \quad V_1(r)=-U_1=-\alpha_0U_0, \quad r\leq R,\\ &V_0(r)=0, \qquad\quad V_1(r)=0, \qquad\qquad\quad r>R. \end{aligned} \tag{11}$$

The resulting expression for $P_0(\theta)$ is then

$$P_0^{(0)}(\theta)=\frac{\epsilon\alpha_0kR\cos\tfrac{1}{2}\theta j_1(2kR\sin\tfrac{1}{2}\theta)j_2(2kR\sin\tfrac{1}{2}\theta)}{(1+\epsilon^2)j_1^2(2kR\sin\tfrac{1}{2}\theta)+\frac{1}{4}\alpha_0^2k^2R^2\cos^2\tfrac{1}{2}\theta j_2^2(2kR\sin\tfrac{1}{2}\theta)}, \tag{12}$$

where j_1 and j_2 are regular spherical Bessel functions.

In Fig. 1, we have plotted $P_0^{(0)}(\theta)$ for carbon at 340 Mev using a nuclear radius $R=3.2\times10^{-13}$ cm. The value of the absorption part of the well, ϵU_0, was taken to be about 16 Mev which is consistent with an optical model determination of this term from the sum of np and pp total cross sections. We also took U_0 to be about 27 Mev to facilitate comparison with reference 6. This gives $\epsilon\approx0.6$ and from (10), a maximum polarization of approximately 51 percent. Finally from (2) and reference 12, we estimated U_1 to be about $\frac{1}{2}$ Mev and hence $\alpha_0\approx0.02$.

If we consider a generalization of the relativistic Thomas effect, in first Born approximation, we find that we can permit $V_0(r)$ to be any potential well where

$$V_1(r)=-\alpha_1\lambda^2\frac{1}{r}\frac{d}{dr}V_0(r). \tag{13}$$

Then $\mathcal{V}_1(r)=\alpha_1V_0(r)$ and $f_1'(\theta)=\alpha_1f_0'(\theta)$, so that

$$P_0^{(1)}(\theta)=\frac{\epsilon\alpha_1\lambda^2k^2\sin\theta}{1+\epsilon^2+\frac{1}{4}\alpha_1^2\lambda^4k^4\sin^2\theta}, \tag{14}$$

[14] J. Keilson, Phys. Rev. 82, 759 (1951).
[15] J. Hughes and K. J. LeCouteur, Proc. Phys. Soc. (London) 63, 1219 (1951).
[16] B. H. Flowers in *Progress in Nuclear Physics*, Editor, O. R. Frisch (Academic Press, Inc., New York, 1952), Vol. 2, p. 271.

† We might note that at high energies the magnitude of $V_1(r)$ decreases and ϵ increases. However, as long as their product is smaller than the incident kinetic energy, the first Born approximation can be expected to be valid, and for large ϵ, contain the principal contribution to the polarization.

giving a polarization that is independent of the shape of $V_0(r)$. This expression for $P_0^{(1)}(\theta)$ agrees with that obtained by Fermi[6] for a square well. The $P_0^{(1)}(\theta)$ of (14) is plotted in Fig. 2 for an estimated $\alpha_1 \approx 15$.

Finally, we consider a simple example such as might be associated with the effect of a nuclear core interacting with a single nucleon. Here we again let

$$V_0(r) = -U_0, \quad r \leq R$$
$$V_0(r) = 0, \quad r > R \tag{15}$$

and take

$$V_1(r) = -\frac{\lambda^2}{r}\frac{d}{dr}\mathcal{U}_1(r), \tag{16}$$

where

$$\mathcal{U}_1(r) = -\alpha_2 U_0, \quad r \leq bR,$$
$$\mathcal{U}_1(r) = -\alpha_2 U_0 (bR/r) e^{-\mu(r-bR)}, \quad r > bR. \tag{17}$$

The resulting $P_0(\theta)$ is

$$P_0^{(2)} = \frac{\epsilon b^2 \alpha_2 \lambda^2 k^2 \sin\theta\, j_1(2kR\sin\tfrac{1}{2}\theta)\psi(k,bR,\theta)}{(1+\epsilon^2) j_1^2(2kR\sin\tfrac{1}{2}\theta) + \tfrac{1}{4} b^4 \alpha_2^2 \lambda^4 k^4 \sin^2\theta \psi^2(k,bR,\theta)}, \tag{18}$$

where

$$\psi(k,bR,\theta) = j_1(2kbR\sin\tfrac{1}{2}\theta) + (\mu bR)^{-1}[1+(2k/\mu)^2 \sin^2\tfrac{1}{2}\theta]^{-1} \times [\sin(2kbR\sin\tfrac{1}{2}\theta) + (2k/\mu)\sin\tfrac{1}{2}\theta \cos(2kbR\sin\tfrac{1}{2}\theta)]. \tag{19}$$

The behavior of (18) is plotted in Fig. 3 for $\alpha_2 \approx 15$, $\mu^{-1} = 1.4 \times 10^{-13}$ cm and $b \approx 0.7$.

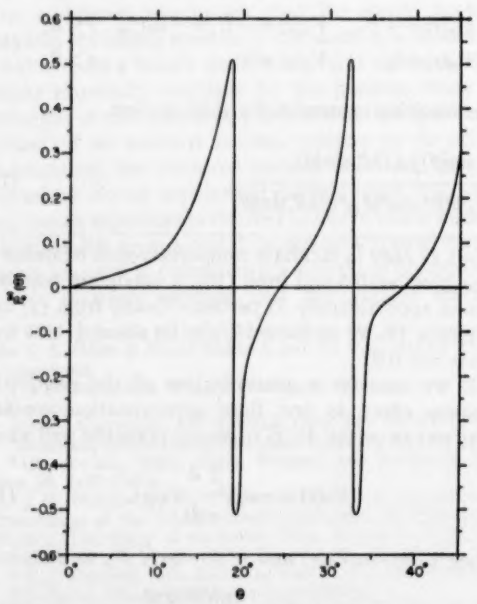

FIG. 1. The polarization as a function of scattering angle as plotted from Eq. (12).

Of the three examples considered, $P_0^{(1)}(\theta)$ and $P_0^{(2)}(\theta)$ appear to best fit the data of Chamberlain *et al.*[3] which indicate a maximum polarization at about 10°. The $P_0^{(0)}(\theta)$ has its first maximum at about 20°. The successive maxima in $P_0^{(0)}(\theta)$ and $P_0^{(2)}(\theta)$ would not be too readily detectable by present methods since they occur at the larger angles where the assumed unpolarized inelastic collisions become important and effectively reduce the observable asymmetry. A characteristic of this theory seems to be the presence of regions of negative polarization following the first maximum, the exception being the first Born approximation of the Thomas-like interaction where the $f_0'(\theta)$ and $f_1'(\theta)$ are proportional to each other, but presumably even here a more exact calculation would show regions of negative polarization.[17] The data referred to in this paper do not show any change in sign of polarization. However, since the experiments do not completely cover the regions where $P_0(\theta)$ can be negative, this possibility

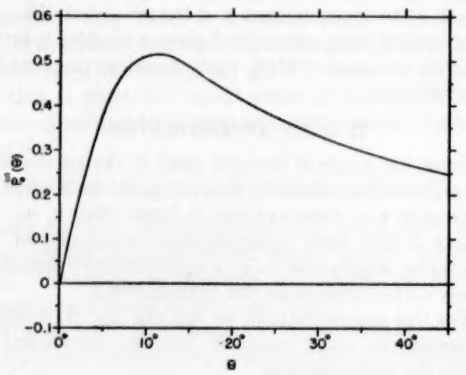

FIG. 2. The polarization as a function of scattering angle as plotted from Eq. (14).

cannot be ruled out. In general, increasing the incident nucleon energy tends somewhat to compress the graphs, towards the lower angles and decreasing the energy stretches them, so that at higher energies the regions of negative polarization may be in the more observable range of the lower scattering angles although the width of these regions may possibly become narrower.‡

The relative magnitudes α of the spin-orbit interaction were only estimated approximately. However, the condition for stationary α is just Eq. (9) for determining $P_0(\theta_0)$ so that small changes in α will leave the location

[17] A phase shift calculation shows that this is indeed the case. E. Fermi (private communication), and Snow, Sternheimer, and Yang, Phys. Rev. **94**, 1073 (1954).

‡ It is also possible that the experimental resolution is such that narrow regions of negative polarization cannot be readily detected. In this respect, we note that a more exact calculation which rounds off the potential wells involved also makes the regions of negative polarization considerably narrower as has been demonstrated by W. Heckrotte (private communication). For heavier nuclei, it may be possible to eliminate the regions of negative polarization altogether; R. M. Sternheimer (private communication).

of optimum polarization relatively unchanged. The magnitude of the maximum polarization is of the proper order, but the figure of 51 percent is not too significant and rather is an approximate lower limit on the maximum polarization. Actually, some of the current optical model calculations mentioned[11] above seem to indicate an $\epsilon \approx 1.2$ for carbon at 340 Mev. This would increase the optimum polarization for $P_0(\theta)$ to about 77 percent.

III. SMALL-ANGLE APPROXIMATION

In an attempt to find an approximate treatment more accurate than the first Born approximation, yet less laborious than a phase shift calculation, we again notice that the high-energy elastic polarization experiments are carried out predominantly at relatively small scattering angles. A procedure which takes advantage of these properties for calculating the scattering amplitude has been suggested[18] and is essentially followed below.

The exact scattering amplitude may be written symbolically as

$$f(\theta)=-\frac{k}{2\pi\hbar v}\int \exp(-i\mathbf{k}\cdot\mathbf{r})\left(\mathbf{r}\left|H'\frac{1}{1-GH'}\right|\mathbf{r}'\right)\times\exp(i\mathbf{k}_0\cdot\mathbf{r}')(d\mathbf{r})(d\mathbf{r}'), \quad (20)$$

where G is the free nucleon Green's function. If we use the expansion

$$[1-GH']^{-1}=1+GH'+GH'GH'+\cdots \quad (21)$$

then $f(\theta)$ is expressed in terms of the Born series. Using cylindrical coordinates with the z axis parallel to $\mathbf{K}=\frac{1}{2}(\mathbf{k}_0+\mathbf{k})$ and evaluating each term of the Born series in the approximation of high energy and small scattering angle,[19] we find that the sum can be written in the form

$$f(\theta)=\frac{ik}{2\pi}\int_0^{2\pi}d\phi\int_0^{\infty}\rho d\rho\exp[-i(\mathbf{k}-\mathbf{k}_0)\cdot\boldsymbol{\varrho}]\times\{1-\exp[2i\delta_0(\rho)+i\delta_1(\rho)\boldsymbol{\sigma}\cdot\boldsymbol{\varrho}\times\mathbf{K}]\}, \quad (22)$$

where

$$\delta_0(\rho)=-\frac{1+i\epsilon}{\hbar v}\int_0^{\infty}V_0([\rho^2+z^2]^{\frac{1}{2}})dz,$$
$$\delta_1(\rho)=-\frac{1}{\hbar v}\int_0^{\infty}V_1([\rho^2+z^2]^{\frac{1}{2}})dz. \quad (23)$$

The expression for $f(\theta)$ can be regarded as a modification of the optical model to include the spin-orbit term provided that a suitable averaging over spin-space is understood. We can write Eq. (22) in the form of Eq. (3) by making use of the commutation properties of the σ and subsequently carrying out the angle integration.

[18] R. J. Glauber, Phys. Rev. **91**, 459 (1953).
[19] See Appendix.

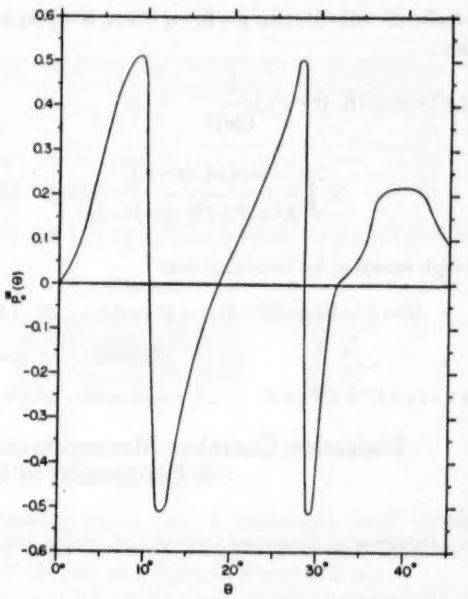

FIG. 3. The polarization as a function of scattering angle as plotted from Eq. (18).

We find that

$$f_0(\theta)=ik\int_0^{\infty}\rho d\rho[1-e^{2i\delta_0}\cos(|\mathbf{K}|\rho\delta_1)]J_0(|\mathbf{k}-\mathbf{k}_0|\rho),$$
$$f_1(\theta)=ik\int_0^{\infty}\rho d\rho e^{2i\delta_0}\sin(|\mathbf{K}|\rho\delta_1)J_1(|\mathbf{k}-\mathbf{k}_0|\rho), \quad (24)$$

where $|\mathbf{K}|=\frac{1}{2}|\mathbf{k}_0+\mathbf{k}|=k\cos\frac{1}{2}\theta$ and $|\mathbf{k}-\mathbf{k}_0|=2k\sin\frac{1}{2}\theta$. If we keep only terms linear in δ_0 and δ_1, we obtain the first Born approximation scattering amplitudes such as were used to obtain the results of Sec. II. Presumably, using the scattering amplitudes of (24) instead of a first Born approximation in Eq. (5) would enable us to obtain a better approximation for $P(\theta)$, although as yet, no completely satisfactory estimate of the errors involved in this approximation has been carried out.

The author wishes to take this opportunity to thank K. Strauch for numerous conversations about the current polarization experiments and R. J. Glauber for several interesting discussions.

APPENDIX

The summation of the Born series of (21) is carried out by employing an approximate free particle Green's function[20] for high energy and small angle propagation. To do this, in the usual form of the Green's function

$$G(\mathbf{r},\mathbf{r}')=\frac{1}{(2\pi)^3}\int\frac{\exp[i\mathbf{p}\cdot(\mathbf{r}-\mathbf{r}')]}{p^2-(k^2+i\epsilon)}(d\mathbf{p}), \quad (A.1)$$

[20] This treatment follows the unpublished work of reference 18.

we make the substitution $\mathbf{p}=\mathbf{K}+\mathbf{q}$ where $\mathbf{K}=\frac{1}{2}(\mathbf{k}_0+\mathbf{k})$. Then

$$G(\mathbf{r},\mathbf{r}')=\exp[i\mathbf{K}\cdot(\mathbf{r}-\mathbf{r}')]\frac{1}{(2\pi)^3}\times\int\frac{\exp[i\mathbf{q}\cdot(\mathbf{r}-\mathbf{r}')]}{K^2+q^2+2\mathbf{K}\cdot\mathbf{q}-k^2-i\epsilon}(d\mathbf{q}). \quad (A.2)$$

At high energies, by assuming that

$$K^2-k^2=k^2(\cos^2\tfrac{1}{2}\theta-1)=-k^2\sin^2\tfrac{1}{2}\theta\approx-q^2 \quad (A.3)$$

and taking the z axis parallel to $\mathbf{K}$, we obtain

$$G(\mathbf{r},\mathbf{r}')\approx\exp[i\mathbf{K}\cdot(\mathbf{r}-\mathbf{r}')]\frac{1}{16\pi^3k}\times\int\frac{\exp[i\mathbf{q}\cdot(\mathbf{r}-\mathbf{r}')]}{q_z-i\epsilon}(d\mathbf{q}) \quad (A.4)$$

and when evaluated in cylindrical coordinates for positive $\epsilon\to0$, this becomes

$$\begin{aligned} &G(\mathbf{r},\mathbf{r}')\approx\tfrac{1}{2}ik^{-1}\exp[i|\mathbf{K}|(z-z')]\delta(\varrho-\varrho'), && z>z',\\ &G(\mathbf{r},\mathbf{r}')\approx0, && z<z'. \end{aligned} \quad (A.5)$$

PHYSICAL REVIEW VOLUME 95, NUMBER 2 JULY 15, 1954

Ionization Chamber Measurements at 10 600 Feet of the Absorption of the *N* Component in Carbon and Hydrocarbon*

ROBERT H. REDIKER†
Department of Physics and Laboratory for Nuclear Science, Massachusetts Institute of Technology, Cambridge, Massachusetts
(Received April 12, 1954)

A detector consisting of a lead-shielded ionization chamber with Geiger counters above and below the chamber is described. The charged N component of energy of several tens of Bev is detected.

The absorption of the charged N component in carbon is much smaller than that predicted from the absorption in air. This phenomenon may be explained by the fact that π mesons or other unstable particles which are produced in nuclear interactions can give rise to further nuclear interactions.

Approximate values for the interaction mean free path of N rays in carbon have been obtained. These values depend on the number of shielded counters below the ionization chamber which are struck. For zero counters discharged, the mean free path is 136 ± 12 g cm^{-2} and seems to decrease as the requirement on the number of shielded counters struck is increased. The interaction mean free paths in carbon are compared to previous results in lead.

The absorption of the N component in oil indicates a cross section of the hydrogen nucleus much smaller than that corresponding to the range of nuclear forces.

Events with large pulses from the ionization chamber or with multiple discharge of shielded counters below the chamber are more likely to be associated with the nucleonic component of extensive air showers.

I. INTRODUCTION

THE results reported here were obtained in a continuation of previous experiments[1–6] performed with a lead-shielded ionization chamber and an array of Geiger-Mueller counters above the lead shield. The time coincident pulses of the ionization chamber and of the Geiger counters recorded the arrival of penetrating ionizing particles which could produce ionization bursts below the lead shield. In a preceding paper[4] (referred to in what follows as I) we were able to separate the total burst rate recorded by the detector into two parts: one which arises from electromagnetic interactions of μ mesons, and another which arises from nuclear interactions of the so-called N component of cosmic rays.

The reader is referred to I for a discussion of the processes by which the bursts are produced. From the latitude effect observed with similar apparatus[5] and from correlation of the observed counting rate with the energy spectrum of the producing radiation, the mean energy of the detected radiation is determined to be about 10^{10} ev. This is in agreement with the energy transfer necessary to produce the smallest detected ionization burst (see I).

In the experiment described in I, we measured the absorption in air and in lead of the N component responsible for the detected bursts. We also obtained information about the collision mean free path for this radiation in lead.

In the present experiment, performed at 10 600 feet, we have extended the results of I to carbon and hydrocarbon absorbers. We have also investigated the absorption of the N component associated with extensive air showers.

* This work was supported in part by the joint program of the U. S. Office of Naval Research and the U. S. Atomic Energy Commission.

† Now at Lincoln Laboratory, Massachusetts Institute of Technology, Cambridge, Massachusetts.

[1] Bridge, Rossi, and Williams, Phys. Rev. **72**, 257 (1947).
[2] Bridge, Hazen, and Rossi, Phys. Rev. **73**, 179 (1948).
[3] Bridge, Hazen, Rossi, and Williams, Phys. Rev. **74**, 1083 (1948).
[4] H. Bridge and B. Rossi, Phys. Rev. **75**, 810 (1949).
[5] McMahon, Rossi, and Burdett, Phys. Rev. **80**, 157 (1950).
[6] H. Bridge and R. Rediker, Phys. Rev. **88**, 206 (1952).

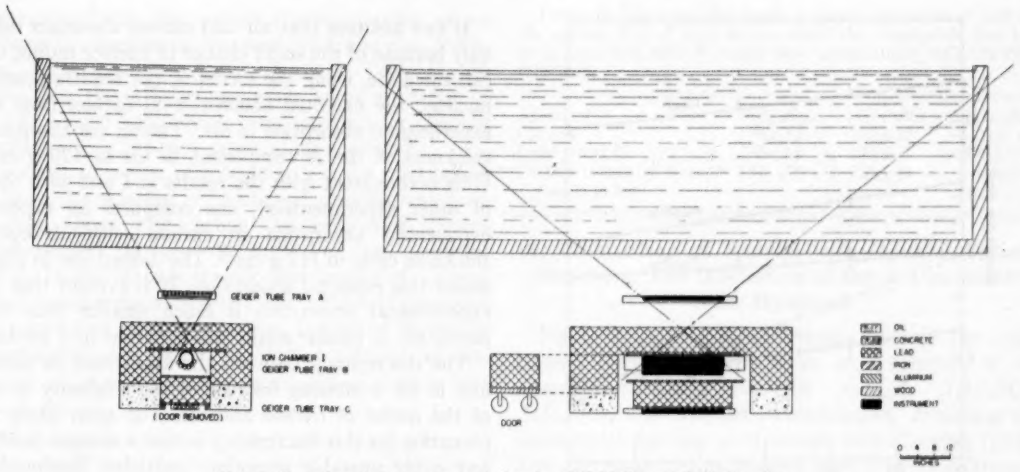

FIG. 1. Experimental arrangement showing full 85.5-g cm^{-2} oil absorber.

II. EXPERIMENTAL ARRANGEMENT

With one exception, the experimental arrangement shown in Fig. 1 was identical to the arrangement used in I at 10 600 feet. The one difference was that in this experiment 171 g cm^{-2} of lead rather than 142 g cm^{-2} of lead was placed between tray A and the ionization chamber. This lead served as the producing layer for most of the bursts observed in the ionization chamber. Not shown in Fig. 1 is the extension tray E, a counter tray of 0.15 square meters placed 3 meters from the detector and at the same height as the lower counter in tray B.

TABLE I. The coincidences whose rates were investigated as a function of absorber thickness.[a,b]

$A1$	Coincidence between pulse in Geiger Tray A and ionization burst in chamber.
$A1B$	Coincidence between pulses in Geiger Trays A and B and ionization burst in chamber.
A_1IB	Same as AIB except that only one Geiger tube in Tray A was struck.
$AIBC$	Coincidence between pulses in Geiger Trays A, B, and C and ionization burst in chamber.
A_1IBC	Same as $AIBC$ except that only one Geiger tube in Tray A was struck.
$AIBC_0$	Coincidence between pulses in Geiger Trays A and B and ionization burst in chamber, in anticoincidence with pulse from Tray C.
A_1IBC_0	Same as $AIBC_0$ except that only one Geiger tube in Tray A was struck.
$AIBC_1$	Same as $AIBC$ except that only one Geiger tube in Tray C was struck.
A_1IBC_1	Same as $AIBC$ except that only one Geiger tube in each of the Trays A and C was struck.
$AIBC_2$	Same as $AIBC$ except that at least two Geiger tubes in Tray C were struck.
A_1IBC_2	Same as $AIBC$ except that at least two Geiger tubes in Tray C were struck and only one Geiger tube in Tray A was struck.

[a] The symbol E after any of the coincidences listed above indicates a simultaneous pulse in the extension Geiger Tray E. Thus $AIBE$ is a coincidence between pulses in Geiger Trays A, B, and E and ionization burst in the chamber.

[b] The size of ionization-burst voltage pulses from the chamber are given in terms of the voltage pulse caused by a polonium α particle (5.30 Mev) near the wall of the chamber. The relative size is indicated by the subscript following I. I_m means the voltage due to the ionization burst was larger than m times the pulse due to the polonium α particle.

Directly above tray A one could stack different thicknesses of carbon or place a wooden tank which could be filled with different amounts of oil.

In what follows we shall concern ourselves with the various categories of events listed in Table I. In interpreting the results obtained for these events the following characteristics of the detector should be kept in mind. Requiring a coincidence between the ionization chamber I and a counter in tray B excluded low-energy interactions whose secondary particles failed to emerge from the wall of the ionization chamber. Requiring a coincidence between I and more than one C counter insured that the event causing the ionization burst in I was one in which penetrating particles were produced. In this manner, as we have shown in I, we are able to detect the N component alone. A coincidence with a counter in the extension tray, E, indicated that the detected event was associated with an air shower. It was shown in I and is evident from the results to be presented here that these events are produced by interactions of the penetrating particles in air showers.

III. RESULTS

(1) The Experimental Data

Coincidence rates have been obtained for the various categories of events listed in Table I for four thicknesses of the carbon absorber and four thicknesses of the oil absorber. These rates have been corrected for fluctuations in barometric pressure. The maximum barometric correction was of the order of six percent. The coincidence rates have also been corrected for accidental electronic coincidences and for overlap of pen marks on the recording tape from which most of the data were obtained (see I). Both these corrections are of the order of one percent and tend to cancel since they are of opposite sign.

In addition, the coincidence rates which arise from electromagnetic interactions of μ mesons (to be called

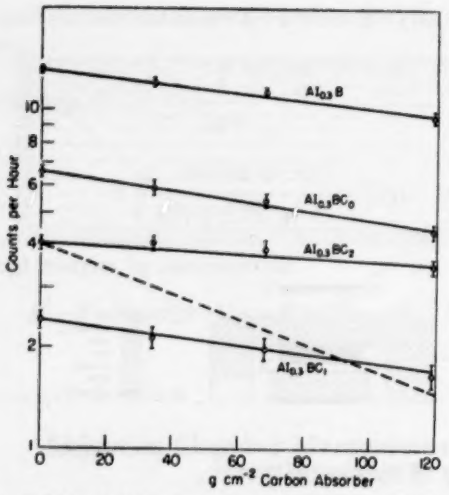

FIG. 2. The coincidence rate due to N bursts is plotted as a function of the carbon absorber thickness for the $AI_{0.3}B$, $AI_{0.3}BC_0$, $AI_{0.3}BC_1$, and $AI_{0.3}BC_2$ events. The dashed line shows the absorption $e^{-x/117}$ that would be expected from the model of the semitransparent nucleus and from the experimental value of the absorption thickness in air.

μ bursts) have been separated from the coincidence rates which are due to interactions of the N component (to be called N bursts). The method by which this separation was accomplished has been discussed in detail in paper I.

(2) Absorption of the N Component in Carbon

Figure 2 shows semilogarithmic plots of the coincidence rates due to N bursts as a function of absorber thickness for the $AI_{0.3}B$, $AI_{0.3}BC_0$, $AI_{0.3}BC_1$, and $AI_{0.3}BC_2$ events. (See Table I for an explanation of the symbols used to describe the different events.)

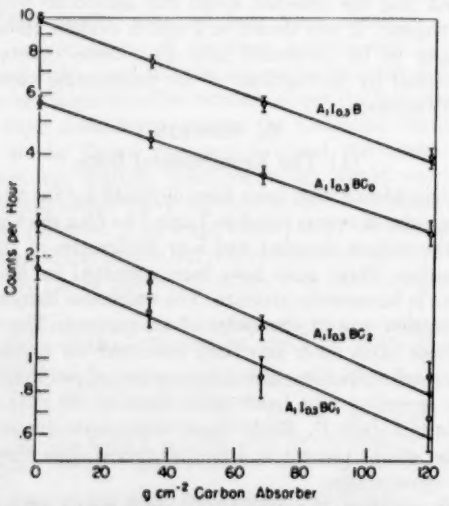

FIG. 3. The reduction of the $A_1I_{0.3}$ type of coincidence rates due to N bursts with addition of carbon absorber.

If one assumes that air and carbon absorbers differ only because of the small change in nuclear radius, one can calculate, using the model of the semitransparent nucleus, the expected absorption in carbon from the experimental absorption in air.[7] Taking the absorption thickness of the N component in air as 120 g cm^{-2} (this is consistent with the results in I and with those of other experimenters), one computes an expected exponential absorption in carbon with absorption thickness close to 117 g cm^{-2}. The dashed line in Fig. 2 shows this expected absorption. It is evident that the experimental absorption is much smaller than that predicted. A similar result was reported in I for lead.

The discrepancy between the absorption in carbon and in air is striking because of the similarity in size of the nuclei of carbon and air. The most likely explanation for this discrepancy is that π mesons (and/or any other unstable secondary particles) produced in high-energy nuclear interactions give rise to further nuclear interactions which produce the observed coincidences. While in air a large percentage of these π mesons decay before colliding with nuclei, in carbon almost all of them will interact before decaying. Thus the total number of interacting particles is greater under an air-plus-carbon absorber than under an equivalent thickness of air alone.[8]

(3) The Collision Mean Free Path of the N Component in Carbon

In this section we shall discuss the variation with absorber thickness of the rates of those coincidence events in which one and only one counter in tray A was struck (A_1 events). This requirement rules out many detected events in which the incident particle has interacted in the absorber. If all events associated with interactions in the absorber could be eliminated from the data, the measured absorption would yield directly the collision mean free path of the incident radiation. It seems likely that the above condition is not completely satisfied by the A_1 requirement (see I), and thus the measured mean free paths are somewhat longer than the actual collision mean free paths.

Figure 3 shows semilogarithmic plots of the coincidence rates due to N bursts as a function of carbon absorber thickness for the $A_1I_{0.3}B$, $A_1I_{0.3}BC_0$, $A_1I_{0.3}BC_1$, and $A_1I_{0.3}BC_2$ events. The mean free paths have been determined from a least-squares

[7] See B. Rossi, *High Energy Particles* (Prentice-Hall, Inc., New York, 1952) for a detailed discussion of this point.

[8] Another possible explanation for the difference in the absorption curves in air and condensed materials is the geometric coherence of particles produced in the condensed absorber. A nuclear interaction that takes place in the absorber may produce two or more secondary particles which then produce the observed coincidence only because of their striking the detecting equipment simultaneously. If the same interaction occurred in air, the secondary particles would in most cases be so widely separated at the detector that no such coincidence would be possible. An experiment investigating this effect was reported in I. The results show that this explanation is most unlikely.

treatment of the data under the assumption of an exponential decrease of the rates with absorber thickness. These mean free paths, shown in Table II, are larger than the collision mean free paths in carbon of 65–100 g cm^{-2} which have been reported for charged particles which produce penetrating showers.[9–11]

In order to reduce lifetime effects in the comparison of the results obtained in I with lead absorber and those obtained above with carbon absorber, wood spacers were inserted between the layers of lead absorber (see I). In this manner the effective density of the lead absorber was reduced to 5.16 g cm^{-3}. Table II compares the mean free paths in carbon, computed from the experimental absorption in lead according to the model of the semitransparent nucleus,[7] with the

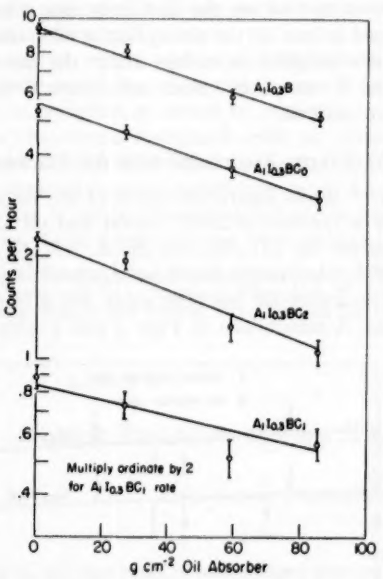

FIG. 4. The reduction of the $A_1I_{0.3}$ type of coincidence rates due to N bursts with addition of oil absorber.

experimental carbon results. Only the mean free paths for the $A_1I_{0.3}BC_0$ coincidence rates seem to be consistent with this nuclear model. This may indicate an experimental difficulty rather than a shortcoming of the nuclear model. Figure 8 of I and Fig. 3 show that in both lead and carbon, the absorption of the $A_1I_{0.3}BC_0$ coincidence rate can be fit very well by an exponential. On the other hand these two figures show that in lead and carbon, exponential absorption curves for the $A_1I_{0.3}BC_1$ and $A_1I_{0.3}BC_2$ rates are not fit well by the experimental points. It may be that the A_1 requirement for these events is not sufficient to eliminate the effects of secondary particles produced in the absorber.

[9] G. Cocconi, Phys. Rev. **76**, 984 (1949).
[10] Walker, Walker, and Greisen, Phys. Rev. **80**, 546 (1950).
[11] R. R. Brown, Phys. Rev. **87**, 999 (1952).

TABLE II. The mean free paths in g cm^{-2} of carbon or lead for the various $A_1I_{0.3}B$ type events under the assumption that the rates associated with N bursts vary exponentially with absorber thickness.

Absorber	$A_1I_{0.3}BC_0$	$A_1I_{0.3}BC_1$	$A_1I_{0.3}BC_2$
Carbon	136±12	122±22	111±11
Lead (from I)	225±14	292±41	286±23
Carbon calculated from results in lead	154_{-18}^{+20}	226±43	220±24

(4) Comparison of Results with Oil and Carbon Absorbers. The Interaction of the N Component with Hydrogen

Figure 4 shows semilogarithmic plots of the coincidence rates due to N bursts as a function of oil absorber thickness for the $A_1I_{0.3}B$, $A_1I_{0.3}BC_0$, $A_1I_{0.3}BC_1$, and $A_1I_{0.3}BC_2$ coincidences. Assuming an exponential decrease of the rates with absorber thickness, the mean free paths have been determined from a least-squares treatment of the data. Since these coincidences require that only one tube in tray A be discharged, these mean free paths given in Table III(e) are approximations to the interaction mean free paths in oil of the charged N rays incident from the atmosphere (see Sec. III. 3).

From the experimental data on the carbon absorption we have computed the collision mean free path in oil[12] under the following assumptions on the interaction cross section, σ_{Np}, between the particles of the N component and hydrogen nuclei: (a) $\sigma_{Np}=0$; (b) $\sigma_{Np}=25\times10^{-27}$ cm^2 (this corresponds to the cross section for p-p scattering at several hundred Mev); (c) $\sigma_{Np}=60\times10^{-27}$ cm^2 (this corresponds to a proton radius $r=\hbar/m_\pi c$, where m_π is the mass of the π meson); (d) σ_{Np} as determined for the different events from the absorption in carbon and the model of the semitransparent nucleus assuming $\sigma_{Np}=\sigma_{Nn}$,[13] i.e., assuming the interaction cross section of the N rays with neutrons and protons to be equal.

TABLE III. The mean free paths in g cm^{-2} of oil for the various $A_1I_{0.3}B$ type coincidences under the assumption that the rates associated with N bursts vary exponentially with absorber thickness. Mean free paths calculated from the results in carbon and with various assumed hydrogen interaction cross sections are compared with the experimental result.

	$A_1I_{0.3}BC_0$	$A_1I_{0.3}BC_1$	$A_1I_{0.3}BC_2$
(a) Calculated with $\sigma_{Np}=0$	156±14	140±25	128±13
(b) Calculated with $\sigma_{Np}=25\times10^{-27}$ cm^2	121±8	110±16	102±8
(c) Calculated with $\sigma_{Np}=60\times10^{-27}$ cm^2	90±5	85±9	80±5
(d) Calculated with σ_{Np} as determined from experimental absorption in carbon	129±13	115±23	104±12
(e) Experimental	146±16	167±38	108±12

[12] The chemical analysis of the diesel oil used as absorber was by weight: hydrogen 13.1 percent, carbon 84.0 percent, oxygen 2.6 percent, and sulfur 0.3 percent.
[13] These cross sections are (17.2±2.1, 20.2±5.6, 23.5±3.9) $\times10^{-27}$ cm^2 for the $A_1I_{0.3}BC_0$, $A_1I_{0.3}BC_1$, and $A_1I_{0.3}BC_2$ events, respectively.

The results are compared in Table III with the experimental findings. One sees that while any of the assumptions (a), (b), or (d) is consistent with the experimental data, assumption (c) is ruled out. We thus conclude that the cross section for interaction of N particles with protons is not much larger than 25×10^{-27} cm^2 and could be zero.

Two uncertainties must be kept in mind in interpreting this result. First, if the energy and angular distribution of secondaries produced when the N component interacts with carbon nuclei are very different from those resulting when it interacts with hydrogen nuclei, then the efficiency of detecting an interaction in the absorber might be quite different for the two kinds of interactions. If in the interactions with hydrogen nuclei the secondaries are emitted in a very narrow cone in the laboratory system, it is conceivable that all the secondary particles could pass through a single counter in tray A and the interaction would be missed. In this case the experimental cross section would be too small. Similarly, the requirement that only one counter in tray A be discharged would not eliminate elastic scattering,[14] including charge exchange, of neutrons by the hydrogen nuclei in the absorber. Experimentally there is very little information either on the angular distribution of the secondary particles emitted in nucleon-nucleon collisions or on the possibility of elastic scattering. While the present experiment can give no indication as to elastic scattering, if the angular distribution is to explain the small observed cross section for the interaction of N particles with protons, the secondaries must be concentrated in a cone of half-angle smaller than 1.1 degrees. (This is the half-angle subtended by a counter in tray A at the middle of the oil absorber.)

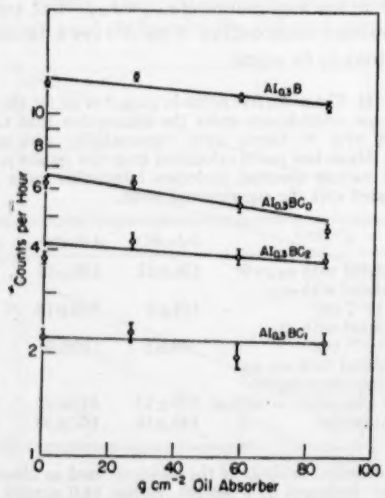

FIG. 5. The coincidence rate due to N bursts is plotted as a function of oil absorber thickness for the $AI_{0.3}$ type of events.

[14] By elastic scattering we mean scattering in which no new particles are produced.

Secondly, one should realize that the interaction cross sections determined for carbon above and for lead in I are considerably smaller than the corresponding cross sections determined with penetrating shower detectors (see Sec. III. 3 and paper I). While part of this discrepancy may be caused by the general inadequacy of the A_1 requirement in ruling out all events in which the incident particle interacts in the absorber, it is difficult to explain the entire discrepancy on this basis.

Figure 5 shows semilogarithmic plots of the coincidence rates due to N bursts as a function of oil absorber thickness for the $AI_{0.3}B$, $AI_{0.3}BC_0$, $AI_{0.3}BC_1$, and $AI_{0.3}BC_2$ coincidence events. A comparison of Figs. 5 and 4 with the corresponding Figs. 2 and 3 for absorption in carbon indicates that regardless of whether or not we require that only one counter be discharged in tray A, the absorption in oil is consistent with the absorption in carbon under the assumption that the N component does not interact with the hydrogen nucleus.

(5) Events Associated with Air Showers

Figure 6 shows logarithmic plots of the coincidence rates as a function of both carbon and oil absorber thickness for the $AI_{0.3}BE$, $AI_{0.3}BC_0E$, $AI_{0.3}BC_1E$, and $AI_{0.3}BC_2E$ coincidences. For these air-shower associated events, no separation has been made into μ bursts and N bursts. A comparison of Figs. 2 and 5 with Fig. 6

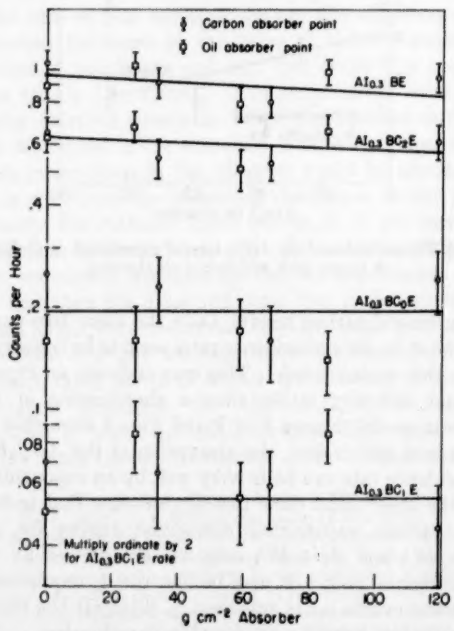

FIG. 6. The coincidence rate is plotted as a function of the oil absorber thickness and the carbon absorber thickness for the events associated with air showers, $AI_{0.3}BE$, $AI_{0.3}BC_0E$, $AI_{0.3}BC_1E$, and $AI_{0.3}BC_2E$. For these events, no separation has been made into N bursts and μ bursts.

shows that the variation of the rates with absorber thickness is independent within statistics of the requirement that the events be associated with an air shower. This result is in agreement with the conclusion reached in I that these events associated with the discharge of counters in the extension tray are due to the N rays in air showers.[16–17] While the electrons discharge the extension tray, the N rays through their nuclear interactions give rise to the AIB coincidences as in the case of unassociated events.

Two or more counters in the shielded tray C were struck in 65 percent of the $AI_{0.3}B$ events associated with air showers, but were struck in only 30 percent of the $AI_{0.3}B$ events not associated with air showers. This result is in agreement with other observations showing that large penetrating showers are more frequently associated with air showers than are small penetrating showers.[17]

The rate of events associated with air showers in which only one tube in tray A is struck ($A_1I_{0.3}BE$ events) is negligible, as would be expected.

Since the events associated with air showers are believed to be due to the N component, they have not been subtracted from the coincidence rates. An analysis of the data in terms of unassociated events would not alter any of the conclusions we have obtained above.

[16] Cocconi, Tongiorgi, and Greisen, Phys. Rev. **75**, 1063 (1949).
[16] G. Cocconi and V. C. Tongiorgi, Phys. Rev. **79**, 730 (1950).
[17] Greisen, Walker, and Walker, Phys. Rev. **80**, 535 (1950).

(6) The Pulse-Height Distribution

Data were also obtained for the events listed in Table I for different minimum voltage pulses from the ionization chamber. In addition to the coincidences with the $I_{0.3}$ pulses, results were obtained for coincidences with $I_{0.6}$, $I_{0.9}$, $I_{1.2}$ pulses (see Table I for definition of these terms). In agreement with I these results indicate that within the experimental errors the shape of the pulse-height distributions for a given coincidence event is independent of the absorber thickness. Thus the pulse-height distributions given in I apply here.

The pulse-height distributions for events associated with air showers are much flatter than those for events not associated with air showers. Thus, while only (6.7 ± 0.6) percent of the $AI_{0.3}B$ coincidences are associated with air showers, (14 ± 2) percent of the $AI_{1.2}B$ coincidences are associated with air showers.[18]

The experiment discussed in this paper was performed at the Inter-University High Altitude Laboratory at Echo Lake, Colorado. The author wishes to thank Professor Bruno Rossi for his continual and generous help and encouragement. Much of the apparatus was designed by Dr. H. S. Bridge, whose continued interest in this work is greatly appreciated. The author was fortunate in having the assistance of Mr. Daniel T. Anderson in performing the experiment.

[18] These results are for 0 g cm^{-2} oil absorber.

PHYSICAL REVIEW VOLUME 95, NUMBER 2 JULY 15, 1954

Cosmic Radiation at Very High Altitudes Near the Geomagnetic Equator*

MARTIN A. POMERANTZ†
Bartol Research Foundation of the Franklin Institute, Swarthmore, Pennsylvania
(Received March 16, 1954)

During an extensive series of balloon-flights near the geomagnetic equator in India, intensity-depth curves have been obtained with the standard quadruple coincidence counter trains, containing various thicknesses of interposed absorber (4.0 cm, 7.5 cm, and 17.7 cm of Pb), previously utilized at high latitudes. A rather pronounced difference occurs between the two stations at Aligarh, Uttar Pradesh ($\lambda=18°$ N) and Bangalore, Mysore ($\lambda=3°$ N). The primary flux values, extrapolated to the "top of the atmosphere" from data obtained with instruments containing 7.5 cm of Pb, are 0.032 ± 0.001 and 0.024 ± 0.001 cm^{-2} sec^{-1} sterad^{-1}, respectively.

A maximum appears in all of the curves, and the general features, as well as the absorption characteristics of the cosmic rays in the upper atmosphere, are in accord with expectation. The effective absorption length in lead, approximately 290 g cm^{-2}, remains unchanged when the geomagnetic cut-off energy of the primary protons is increased from 1.4 Bev to 14.2 Bev. The intensity of mesons having energies exceeding 260 Mev is determined from the data by invoking Messel's theory of the nucleon cascade, and this yields results which are in excellent agreement with the available experimental facts.

The primary magnetic-rigidity spectrum averaged over the range 2.1 Bv to 15.4 Bv is $N(>pc/Ze)=0.68(1+pc/Ze)^{-1.4}$, based upon the present measurements at 52° N and 3° N. However, the data recorded within the equatorial region require a higher value of the corresponding exponent in the differential distribution if the usual assumptions are valid. This effect may be attributable to an irregularity in the primary spectrum, contributions from trapped orbits and albedo, or local magnetic anomalies.

The ratio of intensities in the horizontal and vertical directions at high altitudes is practically equal at 52° N and 3° N, although it would have been expected to increase near the equator in view of the decrease previously observed north of 52°.

I. INTRODUCTION

INVESTIGATIONS of the variation with latitude of the intensity and properties of various components of the cosmic radiation have yielded a considerable amount of information regarding the primary particles. In particular, the only direct method available for the

* Assisted by the U. S. Office of Naval Research and by the U. S. Atomic Energy Commission. Field expedition sponsored by National Geographic Society.

† Fulbright Professor, Muslim University, Aligarh, U. P., India, 1952–53.

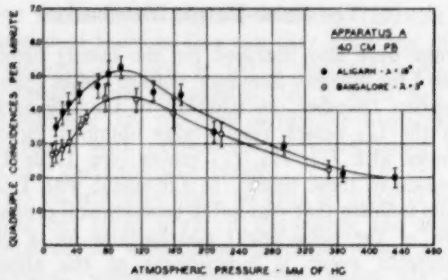

FIG. 1. Vertical counting rate as a function of atmospheric pressure, at two stations in India, for cosmic rays penetrating 4.0 cm of Pb. The experimental points represent the combined data obtained in separate balloon flights.

determination of the distribution in energy of the bulk of incoming protons utilizes observations of the vertical intensity at the highest accessible altitudes at different latitudes. On the basis of geomagnetic theory, which defines the corresponding minimum momenta required for arrival, the energy spectrum can be determined,

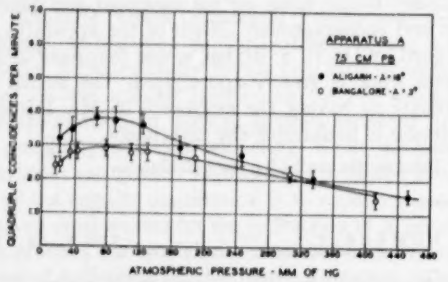

FIG. 2. Vertical counting rate *vs* atmospheric pressure, for particles having residual ranges exceeding 7.5 cm of Pb. The maximum observed at 3° and 18° does not appear at high latitudes.

subject, however, to certain qualifications imposed by the assumptions which must be invoked.

Thus, the measurements obtained by Winckler *et al.*[1] with balloon-borne instruments at atmospheric depths of 15 g/cm², and by Van Allen and Singer[2] with rockets indicated that the primary spectrum could be represented by a power law in which the total flux of particles having energy exceeding E is approximately inversely proportional to E, where 14 Bev$>E>$2 Bev for protons. This is consistent with the results of an analysis by Neher[3] in terms of the energy flux brought in by the primary cosmic radiation.

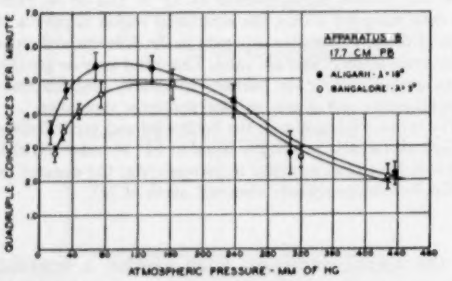

FIG. 3. Variation of counting rate with atmospheric pressure, for particles traversing 17.7 cm of Pb.

Hilberry's[4] earlier measurements on extensive showers as well as more recent underground experiments[5] indicated that the exponent in a simple power-law spectrum is higher at higher energies. It has also been demonstrated that a marked departure occurs at the low-energy end of the spectrum.[6] Therefore, despite the fact that the data obtained at different latitudes on the average appeared to be adequately represented by a straight line on a log-log plot of intensity *vs* threshold energy, the possibility of deviations from this general gross behavior was not precluded. As a matter of fact, vertical coincidence measurements obtained in India by Neher and Pickering[7] in 1939–40 had revealed no difference between the intensity-depth curves at 3° N and 17° N, a result which was then regarded as direct evidence for a banded structure in the primary cosmic-ray spectrum as predicted by the atom-annihilation hypothesis for the origin of cosmic rays proposed by Millikan, Neher, and Pickering.[8] A systematic program of balloon flights with the same standardized equipment which had previously been extensively utilized at higher latitudes[9] was therefore undertaken near the geomagnetic equator not only to determine whether this condition still prevails, but also to examine in some detail the energy dependence of various properties of the primary cosmic rays.

II. EXPERIMENTAL PROCEDURE

The data reported in the present paper were obtained in India during the series of balloon flights summarized in Table I. The ascents were conducted during three periods, initially at Aligarh, Uttar Pradesh (geomagnetic latitude 18° N), next at Bangalore, Mysore (geomagnetic latitude 3° N), and finally, again at Aligarh. The experiments were performed with quadruple-coincidence counter trains in two different geometrical arrangements designated A and B. These were utilized to obtain, as a function of atmospheric depth, measurements of the intensity of those cosmic-ray particles at very high altitudes having a minimum residual range of 4.0 cm, 7.5 cm, or 17.7 cm of Pb, respectively. The general techniques have previously been described in detail.[10] Numerous measurements had already been

[1] Winckler, Stix, Dwight, and Sabin, Phys. Rev. **79**, 656 (1950).
[2] J. A. Van Allen and S. F. Singer, Phys. Rev. **78**, 819 (1950).
[3] H. V. Neher, *Progress in Cosmic Ray Physics* (North Holland Publishing Company, Amsterdam, 1952), p. 301.
[4] N. Hilberry, Phys. Rev. **60**, 1 (1941).
[5] Barrett, Bollinger, Cocconi, Eisenberg, and Greisen, Revs. Modern Phys. **24**, 133 (1952).
[6] For a discussion of this matter see, e.g., M. A. Pomerantz and G. W. McClure, Phys. Rev. **86**, 542 (1952).
[7] H. V. Neher and W. H. Pickering, Phys. Rev. **61**, 407 (1942).
[8] Millikan, Neher, and Pickering, Phys. Rev. **61**, 397 (1942).
[9] Reference 6, and earlier publications cited therein.
[10] M. A. Pomerantz, Electronics **24**, 88 (1951).

obtained[9] at high altitudes with type *A* at Churchill, Manitoba (geomagnetic latitude 69° N) and with both types at Swarthmore, Pennsylvania (geomagnetic latitude 52° N), as well as in the lower atmosphere.[11] The geometrical factors[12] whereby all counting rates in the accompanying curves may be reduced to absolute unidirectional intensities are summarized in Table II.

III. RESULTS AND DISCUSSION

A. Intensity *vs* Altitude Curves

Intensity *vs* altitude curves were obtained with vertical quadruple-coincidence counter trains of Type *A* containing 4.0 cm Pb and 7.5 cm Pb, respectively, and Type *B* containing 17.7 cm Pb. The data obtained in separate flights were in satisfactory agreement. The composite results, obtained by combining all of the data for a specific altitude interval during both ascent and descent of the several individual instruments, are plotted in Figs. 1, 2, and 3.

The most striking result, which is immediately apparent in all cases, is that a rather pronounced latitude effect occurs between 18° N and 3° N. Furthermore, each of the curves exhibits a distinct maximum which does not appear at high latitudes when the interposed absorber exceeds approximately 5 cm of Pb.

As is seen in Fig. 1, in the equatorial region the intensity of particles having a residual range exceeding 4 cm of Pb is maximum at an atmospheric depth of approximately 100 mm of Hg. Previous experiments had indicated that at 52° N the maximum occurs at 50 mm of Hg, whereas at 69° N the curve flattens off at low pressures. These observations are in accord with the expectation that an increase in the low-energy limit of the primaries is accompanied by an increase in the amount of interposed absorber required to remove the maximum in the total vertical intensity *vs* altitude curve. Moreover, it is not surprising that the maximum in the atmospheric transition curve shifts towards the top of the atmosphere as the average energy of the primaries is reduced.

The maximum with 7.5 cm of Pb interposed in the counter train is rather flat in the vicinity of 80 mm of Hg (Fig. 2). At the higher latitudes, in contrast, the intensity increases monotonically with altitude. Although conflicting conclusions regarding the latter point had appeared,[13] the recent experiments of Pullar and Dymond[14] have unambiguously confirmed this result and have resolved this question.[15]

A peak is also present in the intensity-depth curve of particles which can penetrate at least 17.7 cm of Pb, again representing an appreciable change from the behavior at 52° N. The slope near the "top of the atmosphere" is actually greater in this case than with the smaller thicknesses of absorber. The counting rates in Fig. 3 are not directly comparable with those in Figs. 1 and 2, but may be normalized by the factors listed in Table II.

Table I. Balloon-flight summary.

Flight No.	Date	Station	Absorber, cm Pb	Zenith angle	Ceiling altitude, feet
2 *A*	12–28–52	Aligarh	7.5	0°	88 000
3 *A*	12–31–52	Aligarh	7.5	0°	85 000
4 *A*	1– 8–53	Aligarh	7.5	0°	85 000
5 *A*	1–18–53	Aligarh	7.5	0°	102 000
6 *A*	3–25–53	Bangalore	7.5	0°	87 000
7 *A*	3–27–53	Bangalore	7.5	0°	51 000
8 *A*	3–30–53	Bangalore	7.5	0°	88 000
9 *A*	4– 2–53	Bangalore	7.5	0°	90 000
10 *A*	4–13–53	Bangalore	7.5	90°	89 000
11 *A*	4– 7–53	Bangalore	7.5	90°	78 000
12 *A*	5– 5–53	Bangalore	4.0	0°	86 000
13 *A*	5– 6–53	Bangalore	4.0	0°	98 000
14 *A*	5–28–53	Aligarh	4.0	0°	83 000
15 *A*	5–27–53	Aligarh	4.0	0°	70 000
17 *A*	6– 6–53	Aligarh	4.0	0°	95 000
1 *B*	1–29–53	Aligarh	17.7	0°	85 000
2 *B*	3– 3–53	Aligarh	17.7	0°	100 000
3 *B*	3–31–53	Bangalore	17.7	0°	84 000
4 *B*	5– 2–53	Bangalore	17.7	0°	80 000

Inasmuch as a coincidence train containing 203 g cm^{-2} of Pb counts predominantly protons having energies exceeding $E=4.5\times10^8$ ev and mesons with energies greater than 2.6×10^8 ev, the computations of Messel[16] on the development of the nucleon cascade may be utilized to determine the meson intensity throughout the upper atmosphere. Assuming a primary proton power-law spectrum with $\gamma=1.1$, Messel has calculated the vertical intensity of protons with energy greater than E for various values of the ratio E_c/E (where E_c=geomagnetic cut-off energy) as a function of atmospheric depth. In Fig. 4 are plotted the curves $H(\lambda)$ representing the observed vertical intensity penetrating 203 g cm^{-2} of Pb at 3° N and at 52° N, as well as the corresponding theoretical curves $P(\lambda)$ for protons, from Messel's theory. For the present purposes, the simplifying approximation is made that the extrapolated intensity at the "top of the atmosphere" consists

Table II. Geometrical factors for converting counting rates to absolute particle intensities. p is defined by: $I(\theta,h,t)=I(0,h,t)\times\cos^p\theta$; h represents atmospheric depth, t thickness of interposed absorber.

Instrument	Effective length, l cm	Effective width, w cm	Separation, L cm	$\varphi=N(0,h,t)/I(0,h,t)$ $p=2$	$p=1$	$p=0$
A	19.4	0.9	11.5	1.23	1.29	1.45
B	19.4	2.3	26.6	2.33	2.50	2.52
φ_B/φ_A				1.90	1.94	1.74

[9] M. A. Pomerantz, Phys. Rev. **75**, 1721 (1949).
[11] Reference 11 contains a complete discussion of these factors.
[13] M. L. Vidale and M. Schein, Phys. Rev. **81**, 1065 (1951); M. Vidale, *ibid.* **88**, 266 (1952).
[14] J. D. Pullar and E. G. Dymond, Phil. Mag. **44**, 565 (1953).
[15] E. G. Dymond in *Progress in Cosmic Ray Physics* (North Holland Publishing Company, Amsterdam, 1954), Vol. 2, Chap. 3.
[16] H. Messel in *Progress in Cosmic Ray Physics* (North Holland Publishing Company, Amsterdam, 1954), Vol. 2, Chap. 4.

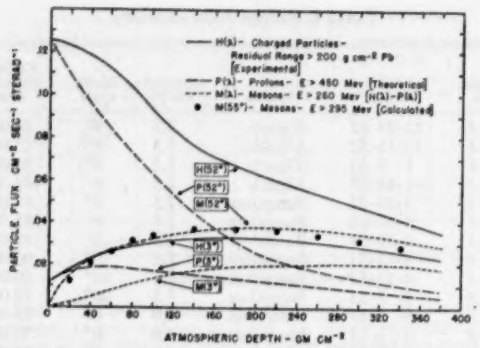
H(λ)- Charged Particles- Residual Range > 200 g cm⁻² Pb [Experimental]
P(λ)- Protons- E > 450 Mev [Theoretical]
M(λ)- Mesons- E > 260 Mev [H(λ)-P(λ)]
M(55°)- Mesons- E > 295 Mev [Calculated]
H(52°)
P(52°)
M(52°)
H(3°)
P(3°)
M(3°)
PARTICLE FLUX CM⁻² SEC⁻¹ STERAD⁻¹
ATMOSPHERIC DEPTH - GM CM⁻²

FIG. 4. Particle flux as a function of atmospheric depth at 52° N and 3° N. $H(\lambda)$ represents the total hard component penetrating 203 g cm^{-2} of Pb, $P(\lambda)$ is obtained from Messel's theory of the nucleon cascade (see reference 16), and $M(\lambda)$ is the difference between them, consisting principally of mesons having energies above 260 Mev. The black dots indicate the calculated meson flux at 55° N as derived by Clark from Sands' production spectrum (see reference 19).

exclusively of primary protons at both latitudes. The general features would not be greatly modified by a detailed analysis which, in any event, could not be undertaken at present in view of limitations imposed by both theoretical and experimental considerations.

The approximate intensity of mesons having energies exceeding 260 Mev, $M(\lambda)$, is obtained by subtracting $P(\lambda)$ from $H(\lambda)$. Although the meson curves at 52° N and 3° N both display quite flat maxima, the intensity increases much more rapidly with atmospheric depth at the higher latitude, where the average primary energy is lower. The proton and meson intensities are equal at 165 g cm^{-2} at 52° N, and 122 g cm^{-2} at 3° N. There is striking agreement between the $M(52°)$ curve and the points derived from Sands[17] production spectrum by Clark.[18] Clark's proton curves, which when added to the computed meson and alpha-particle curves yield the counting rates observed in his investigations of the hard component (divided experimentally into two groups according to whether or not the traversing particle produced a nuclear interaction in the absorber, thereby triggering side counters), however, lead to a net result for protons having energies exceeding 0.5 Bev which lies above $P(52°)$ plotted in terms of the present data. This arises from the fact that Clark's values of the flux penetrating 20 cm of Pb in the upper atmosphere at 55° N are about 50 percent higher than those indicated by curve $H(52°)$, although they coincide at lower altitudes. A similar trend is indicated in related measurements of the total intensity.[19] It should be emphasized that these considerations do not apply to the predicted meson curve, which does not involve balloon-flight data.

On the other hand, the *shape* of the curve representing the total intensity of protons with $E>0.5$ Bev, deduced from Clark's analysis, is in excellent agreement with $P(\lambda)$ as given by Messel.

Using Messel's earlier computations based upon $\gamma=1.7$, Pullar and Dymond[14,15] derived the meson flux from measurements of the hard component (range>90 g cm^{-2} Pb) at high latitudes. If the corresponding calculations were applied to the present equatorial data, the theoretical proton curve would actually exceed the observed hard component curve (Fig. 2). The maximum counting rate due to protons alone would be 3.3 at 100 mm of Hg, as compared with the observed rate of 2.9 counts per minute which includes both protons and mesons. In contrast, the revised theory with $\gamma=1.1$ would doubtless provide a reasonable result from this qualitative point of view, although the detailed calculations with the parameters applicable to this set of conditions have not been performed.

B. Absolute Primary Flux

In Table III are listed values of the absolute particle flux near the geomagnetic equator, as reported by various investigators. The intensity at balloon altitude measured by Winckler *et al.* (W, 3 cm Pb, 15 g/cm^2) and the present author (P, 4 cm Pb, 10 mm Hg) are in

TABLE III. Absolute vertical intensity measurements near geomagnetic equator.

Geomagnetic latitude	Particle flux, cm^{-2} sec^{-1} sterad^{-1}	Author*	Absorber	Atmospheric depth
0°	0.027±0.001	W	3 cm Pb	15 g/cm^2
0°	0.031±0.001	W	0	15 g/cm^2
0°	0.021±0.001	W	3 cm Pb	Top-extrapolated
0°	0.028±0.004	V	0	Rocket
3°	0.0227	R	10 cm Pb	Top-extrapolated
3°	0.029±0.002	P	4 cm Pb	10 mm Hg
3°	0.028±0.002	P	7.5 cm Pb	20 mm Hg
3°	0.025±0.001	P	4 cm Pb	Top-extrapolated
3°	0.024±0.001	P	7.5 cm Pb	Top-extrapolated
19°	0.0364	R	10 cm Pb	Top-extrapolated
20°	0.031±0.001	W	3 cm Pb	15 g/cm^2
20°	0.024±0.001	W	3 cm Pb	Top-extrapolated
18°	0.039±0.002	P	4 cm Pb	10 mm Hg
18°	0.036±0.002	P	7.5 cm Pb	20 mm Hg
18°	0.034±0.001	P	4 cm Pb	Top-extrapolated
18°	0.032±0.001	P	7.5 cm Pb	Top extrapolated

Latitude ratio	Author	Absorber	Atmospheric depth
$I(19°)/I(3°)=1.60$	R	10 cm Pb	Top-extrapolated
$I(20°)/I(0°)=1.15$	W	3 cm Pb	15 g/cm^2
$I(20°)/I(0°)=1.14$	W	3 cm Pb	Top-extrapolated
$I(18°)/I(3°)=1.28$	P	4 cm Pb	10 mm Hg
$I(18°)/I(3°)=1.29$	P	7.5 cm Pb	20 mm Hg
$I(18°)/I(3°)=1.39$	P	4 cm Pb	Top-extrapolated
$I(18°)/I(3°)=1.37$	P	7.5 cm Pb	Top-extrapolated
$I(52°)/I(3°)=7.1$	P	7.5 cm Pd	Top-extrapolated

* These references are as follows. W: Winckler, Stix, Dwight, and Sabin, Phys. Rev. 79, 656 (1950); V: J. A. Van Allen and A. V. Gangnes, Phys. Rev. 78, 50 (1950); R: Rao, Balasubrahmanyan, Gokhale, and Pereira, Phys. Rev. 91, 764 (1953); P: Present author.

[17] M. Sands, Technical Report No. 28, Laboratory of Nuclear Science and Engineering, Massachusetts Institute of Technology, 1949 (unpublished).

[18] M. A. Clark, Phys. Rev. 87, 87 (1952).

[19] M. A. Clark, Technical Report No. 59, Laboratory of Nuclear Science and Engineering, Massachusetts Institute of Technology, 1952 (unpublished).

agreement, although the value at the "top of the atmosphere" obtained by extrapolation[20] appears to be slightly higher in the latter case. The rocket determination by Van Allen and Gangnes is also in accord within the statistical uncertainties, as is the extrapolated value reported by Rao *et al.*

The situation at 18° is somewhat different, however, and the present result (P, 4 cm Pb, 10 mm Hg) is considerably higher than Winckler's (W, 3 cm Pb, 15 g/cm²) at ceiling altitude at 20°. This difference is increased by extrapolation to zero pressure. The corresponding extrapolated flux measurement by Rao *et al.* at 19° is even higher.

It is of interest to note that, insofar as it is meaningful to compare absolute flux determinations by different investigators, the measurements over India (P, R) differ from those over the Pacific Ocean (W, V) in a sense which is in accord with that theoretically expected to arise from the eccentricity of the terrestrial dipole. As a consequence of the fact that the dipole which represents the earth's magnetic field is off-center, the minimum momentum required for a primary to reach the earth in the vertical direction at 3° in India should be slightly less than that at the geomagnetic equator in the area where Winckler conducted his flights, and higher than that in the region where the rocket was fired. However, Millikan and Neher's world survey[21] revealed that the minimum intensity at sea level does not coincide with the region of maximum threshold energy determined by these considerations, but occurs about 65° west of this position, close to the point at which the horizontal component of the real magnetic field at the surface of the earth is maximum. The intensity at sea level at the geomagnetic equator is actually slightly lower in India than in the Western Hemisphere.

C. Primary Energy Spectrum

The most frequently quoted expressions relating the latitude dependence of the measured vertical intensity to the corresponding cutoff determined from geomagnetic theory are listed in Table IV. The exponents indicated represent the present series of determinations of the flux at the "top of the atmosphere" as listed in Table III.

TABLE IV. Summary of power-law expressions based upon data obtained at 52° N and 3° N.

Variable	Geomagnetic cutoff[a]		Integral spectral distribution
	$\lambda=52°$	$\lambda=3°$	
Magnetic rigidity, pc/Ze	2.1 Bv	15.4 Bv	$N(>pc/Ze)=0.68(1+pc/Ze)^{-1.2}$ $N(>pc/Ze)=0.37(pc/Ze)^{-1.6}$
Proton energy, E_p	1.4 Bev	14.2 Bev	$N(>E_p)=0.46(1+E_p)^{-1.1}$ $N(>E_p)=0.23(E_p)^{-0.6}$
Energy per nucleon ($A=2Z$), E/A	0.4 Bev	6.8 Bev	$N(>E/A)=0.26(1+E/A)^{-1.2}$

[a] Obtained by applying theoretical factors taking into account the asymmetry of the earth's dipole to the values given by R. A. Alpher, J. Geophys. Research **55**, 437 (1950).

TABLE V. Differential magnetic rigidity distributions based upon data obtained at 18° N and 3° N.

Limiting cone	Geomagnetic cutoff, pc/Ze		Differential spectral distribution
	$\lambda=18°$	$\lambda=3°$	
Main cone	13.8 Bv	15.4 Bv	$dN(pc/Ze)=k(1+pc/Ze)^{-4.0}d(pc/Ze)$
Störmer +earth's shadow cone	12.6 Bv	15.4 Bv	$dN(pc/Ze)=k(1+pc/Ze)^{-3.1}d(pc/Ze)$

Analysis of the geomagnetic effects is independent of the composition of the primary cosmic radiation when the cutoffs are expressed in terms of magnetic rigidity, pc/Ze, which is therefore the most relevant quantity for the present purposes. At the geomagnetic equator and at latitudes above 35° the lower limit is effectively defined by the Störmer plus earth's shadow cones which determine the least rigidity a charged particle must possess to be allowed to enter from a given direction. In the intermediate region there exists a penumbral region between this lower limit and that value of rigidity determined by the main cone, which if exceeded assures admission. The region about geomagnetic latitude 18° is characterized by great uncertainty regarding the contribution of the penumbral region. The statement is usually made that the penumbral region is practically dark at latitudes below about 15°, so that the main cone is essentially the total allowed cone.[22] Between 15° and 35°, the allowed and forbidden regions of the penumbra are presumed to be of equal importance, but quantitative predictions are exceedingly difficult to propound. Detailed theoretical investigation[23] has indicated that at 20°, the main cone is still quite important in determining the minimum rigidity which is permitted to enter in the vertical direction. It is not possible to predict the contribution of the penumbral region to the cosmic-ray intensity at 18° in India. However, it is not expected to be appreciable.[24] Thus, the value of the exponent, $(\gamma+1)$, in the differential magnetic-rigidity distribution (Table V) is -4.0 in the interval $pc/Ze=13.8$–15.4 Bv as compared with -2.2 averaged over the range between 2.1 Bv and 15.4 Bv, and there appears to be a departure from the assumed simple power law. This might be accounted for by the presence of a considerable flux of particles having energies less than that defined by the main cone. This would have to be attributed to a difference in the contributions from trapped orbits and albedo at different latitudes in India, which apparently does not occur at the longitudes where Winckler's flights were conducted. On the other hand, the form of the primary

[20] Extrapolated values were not specifically stated in reference W of Table III, but have been derived by the present author from the published data.

[21] R. A. Millikan and H. V. Neher, Phys. Rev. **50**, 15 (1936).

[22] M. S. Vallarta, Phys. Rev. **74**, 1837 (1948).

[23] R. A. Hutner, Phys. Rev. **55**, 614 (1939).

[24] M. S. Vallarta (private communication).

spectrum itself might be the origin of the observed effect. If this is the case and if the generally accepted geomagnetic theory is employed to determine the cutoff at the various stations, there remains a discrepancy between the absolute flux measurements at 18° in India and 20° in the Pacific Ocean.

D. Absorption Coefficients

Comparison of the data obtained with different thicknesses of absorber interposed in the counter train reveals the manner in which the absorption of the cosmic radiation at high altitudes depends upon the energy of the incoming particles. The curves in Fig. 5 indicate the general trends which are followed, although their precise shapes are not significant owing to the statistical uncertainties entering into the differences between counting rates. The greatest absorption of the softer components (residual range between 4.0 and 7.5 cm Pb) occurs deeper in the atmosphere at low latitudes where the average primary energy is higher. Furthermore, at low latitudes the more penetrating component (17.7 cm Pb>range>7.5 cm Pb) appears to be hardening as it proceeds downward into the atmosphere, contrary to the situation at high latitudes.

The effective absorption length in lead, determined from the data obtained with the larger amounts of interposed absorber, is about 290 g cm^{-2} at 52°, 18°, and 3°. Thus, the interaction mean free path does not change when the energy of the primary protons is increased from 1.4 Bev to 14.2 Bev.

The variation in the atmosphere of the new radiation which appears between 3° and 18° is similarly represented by differences as shown in Fig. 6. These curves show the altitude dependence of the intensity of the incoming particles and their progeny capable of penetrating 4.0 cm Pb, 7.5 cm Pb, and 17.7 cm Pb, respectively, which are present at 18° but not at 3°.

E. Horizontal Intensity

Flights with counter trains oriented horizontally were conducted only at Bangalore, and the results are plotted in Fig. 7. The bump at about 75 mm of Hg repeated consistently and appears to represent a real phenomenon, despite the fact that one is hesitant to attach significance to apparent fine structure in intensity-depth curves of this type.

The altitude variation of the ratio of horizontal to vertical intensities is shown in Fig. 8. It is quite remarkable that this factor is almost the same, at the highest altitude attained, at 52° and 3°. The latitude effect of the horizontal component is almost as great as that of the vertical. The bump at 75 mm Hg can probably be ascribed to air showers, which undoubtedly contribute considerably to the counting rate of this arrangement, especially at such depths.

Earlier experiments had revealed no difference in the horizontal intensity between 52° N and 69° N, and this result was interpreted as an indication that low-energy primaries (i.e., near the geomagnetic cutoff at 52°) do not contribute appreciably to the horizontal intensity. As has been noted previously,[6] the particles recorded at high altitudes by a coincidence counter train inclined at a zenith angle of 90° are predominantly secondaries produced by essentially downward-moving primaries. If the more energetic primaries were more efficacious in producing horizontally-directed secondaries, the horizontal/vertical ratio should be higher at 3° N than at 52° N. Thus, the present measurements indicate that the multiplicity for production of wide-angle events is independent of energy for protons between 1.4 Bev and 15.5 Bev, in contrast with the conclusion based upon the northern experiments. This constitutes a dilemma.

IV. CONCLUSIONS

The existence of a large variation with latitude of the primary cosmic-ray intensity between 3° N and 18° N in India has been established, although the explanation for earlier observations to the contrary is not clear. Although appreciable fluctuations in the intensity of low-energy particles are sometimes ob-

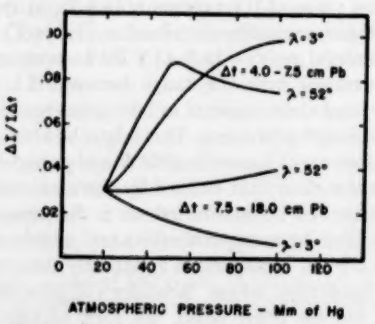

FIG. 5. Variation with atmospheric pressure, at 3° N and 52° N, of the absorption coefficient of two groups of cosmic rays, having residual ranges of 4.0–7.5 cm of Pb and 7.5–18.0 cm of Pb, respectively.

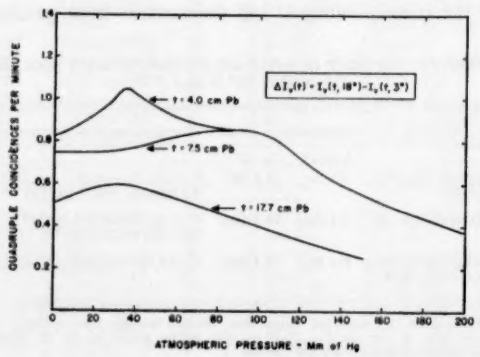

FIG. 6. Counting rate vs atmospheric pressure, for particles (having ranges exceeding 4.0 cm of Pb, 7.5 cm of Pb and 17.7 cm of Pb, respectively) which are present in India at 18° N but not at 3° N.

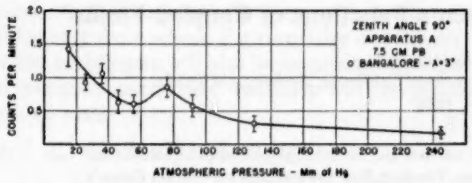

FIG. 7. Horizontal counting rate as a function of atmospheric pressure for cosmic rays penetrating 7.5 cm of Pb at 3° N.

served[25,26] at high altitudes, time variations in the intensity of particles having rigidities exceeding the geomagnetic cutoff in the equatorial regions are presumably much smaller.[26]

The intensity-depth curves, as well as the absorption characteristics of the cosmic rays at high altitudes, are in accord with expectation in terms of the change with latitude of the average energy of the primaries. The nucleon cascade theory developed by Messel appears to be in harmony with the experimental results.

The latitude effect observed in India is greater than that expected on the basis of the customary assumptions and reliance on standard geomagnetic theory. This may be indicative of the nature of the spectrum at the upper limit of the field-sensitive region for vertical incidence; alternatively, the possibility of local magnetic anomalies or contributions from trapped orbits and albedo must be considered. Unless very special conditions prevail the latter explanation does not appear tenable, particularly in view of the results of the beautiful experiments reported recently by Winckler and Anderson.[27] Utilizing a Čerenkov detector, they determined that, at $\lambda=40°$ N, the albedo is not more than 5 percent of the incident flux, for particles of $\beta>0.7$ in any upward direction. This is too small by a factor of at least four to resolve the discrepancy between the observed east-west asymmetry and that predicted from the primary spectrum and geomagnetic theory. Also, according to new calculations by Treiman,[28] the contribution arising from the trapped orbits of a solar dipole field is appreciably smaller than had been indicated earlier.[29] Moreover, as a consequence of Liouville's theorem, the intensity of trapped particles is constant

[25] M. A. Pomerantz and G. W. McClure, Phys. Rev. **87**, 240 (1952).
[26] Neher, Peterson, and Stern, Phys. Rev. **90**, 655 (1953).
[27] J. R. Winckler and K. Anderson, Phys. Rev. **93**, 596 (1954).
[28] S. B. Treiman, Phys. Rev. **93**, 544 (1954).
[29] Kane, Shanley, and Wheeler, Revs. Modern Phys. **21**, 51 (1949).

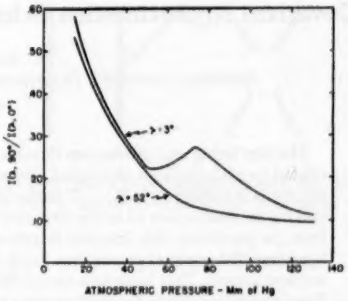

FIG. 8. Ratio of intensity in the horizontal direction to that in the vertical direction at 52° N and 3° N, as a function of atmospheric pressure.

throughout the accessible bounded volume of space. The irregularity in the spectrum indicated by the present experiments may be related to the aforementioned inconsistency among the other geomagnetic effects.

The intensity in the horizontal direction does not exhibit as much latitude variation as would have been anticipated from qualitative considerations involving the observations at northern latitudes. Thus, a simple picture of this phenomenon is inadequate to account for the observed results.

V. ACKNOWLEDGMENTS

It is a pleasure to thank the National Geographic Society for its continuing support in sponsoring the field expedition, and Dr. Lyman J. Briggs for his constant encouragement. Appreciation is expressed to Aligarh Muslim University, with which the author was privileged to be affiliated during the year 1952–53 under the Fulbright program, and to the Vice-Chancellor, Dr. Zakir Hussain, for the hospitality extended to us. The facilities of the Physics Department, which participated actively in the project, were made available through the helpful cooperation of Professor P. S. Gill. The author is also indebted to the Indian Institute of Science, Bangalore, for providing facilities and assistance, and especially to Professor R. S. Krishnan. The active assistance particularly of S. P. Agarwal, H. S Hans, R. N. Mathur, Y. Prakash, T. J. Tidd, A. E. Viele, and many others too numerous to mention individually, contributed materially to the successful completion of the balloon-flight program. Finally, the author is grateful to Dr. W. F. G. Swann for his constant interest and encouragement.

Covariant Approximation Scheme for Green's Functions of Coupled Fields*

R. ARNOWITT AND S. GASIOROWICZ
Radiation Laboratory, Department of Physics, University of California, Berkeley, California
(Received April 15, 1954)

The scattering and production Green's functions for one nucleon and an arbitrary number of mesons are related by an infinite set of coupled linear integral equations. The first N of these equations contain Green's functions involving $0, 1, 2, \cdots N$ external meson lines. The set of equations may be cut off at any point by making an assumption as to the structure of the Green's function with the highest number of external meson lines. In particular this function is approximated by decomposing it into products of lower-order Green's functions, the physical assumption being that one of the mesons interacts weakly with the remaining meson-nucleon system. This leads to a closed set of equations which are linear if vacuum polarization is neglected. Examples of successive approximations are derived. The formalism is also applied to the two-nucleon case and to the three-fields problem, the latter being treated in a manifestly gauge-covariant manner.

I. INTRODUCTION

RECENT investigations of the problem of the interaction between the meson and nucleon fields have been aimed at dispensing with methods suited only to weakly coupled systems. In particular, attention has been centered upon covariant two-body equations[1] (in which the approximation of a perturbation expansion of the interaction operator is made), and on the non-adiabatic three-dimensional Tamm-Dancoff method[2] (where the approximation consists of setting the amplitudes for systems containing more than a given number of particles to zero). While the Bethe-Salpeter approach is a covariant one, a serious drawback lies in its perturbation treatment of the interaction term. Not only is the convergence of this in grave doubt, but one has no criteria for deciding how many (and which) irreducible graphs are to be included for the description of a given process. In the Tamm-Dancoff scheme no perturbation approximation is used. Here again however, there is no guide enabling one to determine at what number of particles the infinite set of equations should be cut off. Furthermore, as has recently been pointed out,[3] the lack of symmetry between the "crossed" and "uncrossed" diagrams at any stage of the approximation in the meson-nucleon case will yield an incorrect zero energy limit for the exchange scattering.

The purpose of this paper is to utilize a new approximation procedure for dealing with the Green's functions appropriate to a given problem. Taking cognizance of the relationship between the vertex operator and kernels involving external meson lines, a system of coupled integral equations for these Green's functions may be written down. Following a suggestion of Neuman,[4] we treat one of the mesons as interacting weakly with the rest of the system by decomposing the highest Green's function considered into products of lower Green's functions, thus cutting off the infinite set of equations. This scheme has the advantages of being Lorentz covariant (and for photon processes, gauge covariant), of containing no perturbation features, and of providing some physical insight into the meaning of the approximation. The basic symmetry of the Green's functions in the meson variables avoids the difficulty with the exchange scattering mentioned above. If certain aspects of vacuum polarization are neglected, the resulting equations are linear.

In the following section the formalism is developed in connection with the meson-nucleon system. Later sections deal with its applicability to the two-nucleon and the three-fields problems.

II. ONE-NUCLEON SYSTEMS

(A) Definitions and Notation

The equations of motion for the pseudoscalar meson operator ϕ_i and the nucleon field operator ψ interacting via symmetric pseudoscalar coupling in the absence of external fields are

$$(\gamma p+m+g\gamma_5\tau_i\phi_i)\psi=0, \tag{2.1}$$

$$(p^2+\mu^2)\phi_i+\tfrac{1}{2}g[\bar{\psi},\gamma_5\tau_i\psi]=0, \tag{2.2}$$

where $p_\mu=-i\partial/\partial x_\mu$.[5] A generalized Green's function governing processes involving n nucleons and m external meson lines may be defined as follows.

$$G(x_1\cdots x_n, x_1'\cdots x_n'; \xi_1\cdots\xi_m) = i^{n+[m/2]}\langle(\psi(x_1)\cdots\psi(x_n)\bar{\psi}(x_1')\cdots\bar{\psi}(x_n') \times\phi(\xi_1)\cdots\phi(\xi_m))_+\rangle\times\epsilon(x_1\cdots x_n'), \tag{2.3}$$

where, for any Heisenberg operator $F(x)$, the symbol $\langle F(x)\rangle$ stands for $\langle\mathrm{vac}\sigma_1|F(x)|\mathrm{vac}\sigma_2\rangle/\langle\mathrm{vac}\sigma_1|\mathrm{vac}\sigma_2\rangle$; σ_1 and σ_2 represent two spacelike surfaces at $\pm\infty$, respectively; $[m/2]$ is the integral part of $m/2$; $\epsilon(x_1\cdots x_n')$ is $+1$ for an even permutation of the order of the times $x_0\cdots x_{0n}'$ and -1 for an odd permutation. The spinor and isotopic indices have been suppressed. In this

* This work was performed under the auspices of the U. S. Atomic Energy Commission.

[1] J. Schwinger, Proc. Natl. Acad. Sci. U. S. 37, 452, 455 (1951); E. E. Salpeter and H. A. Bethe, Phys. Rev. 84, 1232 (1951).

[2] Dyson, Schweber, and Visscher, Phys. Rev. 90, 372 (1953).

[3] M. Gell-Mann and M. L. Goldberger (private communication from M. L. Goldberger).

[4] M. Neuman, Phys. Rev. 92, 1021 (1953). The formalism developed below is closely related to that of Dr. Neuman's paper.

[5] Throughout the paper the notation is that of J. Schwinger (reference 1). Thus, $\{\gamma_\mu,\gamma_\nu\}=-2\delta_{\mu\nu}$; $\gamma_5^2=-1$.

section we shall concern ourselves with problems involving only one nucleon. For simplicity of notation the nucleon coordinates will also be suppressed and matrix multiplication over these variables will be assumed. Thus we write

$$G(\xi_1\cdots\xi_m)=i^{1+[m/2]}\langle(\psi(x)\bar{\psi}(x')\phi(\xi_1)\cdots \times\phi(\xi_m))_+\rangle\epsilon(x-x'). \quad (2.4)$$

It will also be found useful to define the quantity $\gamma(\xi)$:

$$(x|\gamma_\delta\tau_i(\xi)|x')=\gamma_\delta\tau_i\delta(x-x')\delta(\xi-x'). \quad (2.5)$$

(B) Derivation of the Green's Functions Equations[6a]

We begin by obtaining the equation for the one-nucleon, no-meson Green's function. Operating on the quantity G with $(\gamma p+m)$ and invoking the equations of motion (2.1), one finds

$$(\gamma p+m)G(xx')=\delta(x-x')-ig\gamma_\delta\tau_i \times\langle(\psi(x)\bar{\psi}(x')\phi_i(x))_+\rangle\epsilon(x-x'), \quad (2.6)$$

where $\delta(x-x')$ arises from the time derivative of the discontinuity of G. Referring to (2.3) we notice that the last term on the right-hand side is equal to $-g\gamma_\delta\tau G(xx';x)$, so that (2.6) may be rewritten as

$$(\gamma p+m)G=1-g\int\gamma(\xi)G(\xi)d\xi, \quad (2.7)$$

where $(x|1|x')=\delta(x-x')$. By proceeding in a similar manner, the equation for $G(\xi)$ may be obtained:

$$(\gamma p+m)G(\xi)=ig\int\gamma(\xi')G(\xi'\xi)d\xi'. \quad (2.8)$$

No term corresponding to $\delta(x-x')$ appears here since $\langle\phi(\xi)\rangle=0$ in the absence of external meson fields. The application of $(\gamma p+m)$ to $G(\xi'\xi)$ leads to the appearance of the quantity $i\langle(\phi_i(\xi)\phi_j(\xi'))_+\rangle$, to be denoted by $\mathcal{G}_{ij}(\xi\xi')$ [the one-meson (no-nucleon) Green's function], as well as $G(\xi''\xi'\xi)$:

$$(\gamma p+m)G(\xi'\xi)=\mathcal{G}(\xi'\xi)-g\int\gamma(\xi'')G(\xi''\xi'\xi)d\xi''. \quad (2.9)$$

The next equation in the scheme is

$$(\gamma p+m)G(\xi''\xi'\xi)=ig\int\gamma(\xi''')G(\xi'''\xi''\xi'\xi)d\xi'''. \quad (2.10)$$

The equation for $\mathcal{G}$ may easily be obtained by operating with $(k^2+\mu^2)$ (where $k_\mu=-i\partial/\partial\xi_\mu$) upon $\mathcal{G}$ and using (2.2). Thus,

$$(k^2+\mu^2)\mathcal{G}(\xi\xi')=\delta(\xi-\xi')+g\,\mathrm{Tr}\gamma(\xi)G(\xi'). \quad (2.11)$$

We may mention at this point that the substitution of (2.8) into (2.7) and (2.11) yields Eqs. (1″a) and (1″b) of Neuman.[4]

$$(\gamma p+m)G=1-ig^2\int\gamma(\xi)G_0\gamma(\xi')G(\xi'\xi)d\xi d\xi', \quad (2.12a)$$

$$(k^2+\mu^2)\mathcal{G}(\xi\xi')=\delta(\xi-\xi')+ig^2 \times\mathrm{Tr}\int\gamma(\xi)G_0\gamma(\xi'')G(\xi''\xi')d\xi''. \quad (2.12b)$$

We shall denote by $\mathcal{G}_0(\xi\xi')$ the solution of (2.11) with the second term on the right omitted.

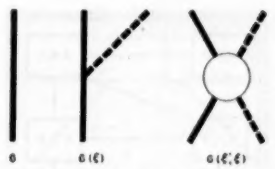

FIG. 1. The first three Green's functions with the time ordering arranged so that a minimum number of lines occur at a given time.

(C) The Approximation Scheme

The functions G, $G(\xi)$, $G(\xi,\xi')$, etc., of the preceding section govern rigorously the motion of one nucleon and various numbers of mesons, the functions with an odd number of meson indices referring to the *production* of at least one meson (rather than a *scattering*). Thus G is the propagation function for a nucleon with all possible self-energy processes occurring. As is customarily done, we shall represent such "clothed" particles by thick lines. In Fig. 1 we give the diagrammatic representations of the first few Green's functions with the times arranged so that a minimum number of "thick lines" occur at a given time. We also notice that any Green's function may be symbolically represented by a set of three indices (x,y,z) where $x=$ the number of nucleons, $y=[m/2]$ where m is the number of meson variables, and the number $z=1$ or 0 depending on whether m is odd or even. The sum of these three indices yields the maximum number of thick lines in the corresponding diagrams time-ordered as in Fig. 1.

Equations (2.7), (2.8), (2.9), etc., coupling the various Green's functions may be schematically represented by an array of linking "boxes" [labeled by (x,y,z)], each box describing a particular Green's function (Fig. 2). The scheme proposed consists of limiting oneself in a given calculation to a finite number of thick lines which corresponds to a finite portion of the array of "boxes." If this is done, one in general obtains N equations involving $N+1$ unknowns, the last Green's function $G(\xi_1\cdots\xi_N)$ having one more line than the number allowed by the scheme. Following the suggestion made by Neuman,[4] the last function is now treated approximately. The scheme utilized is to factor this function into products of Green's functions already appearing in the equations, some of these being replaced by their zeroth order forms so that the number of thick lines does

[6a] Similar equations have been derived by J. Schwinger, unpublished lecture notes, Harvard University.

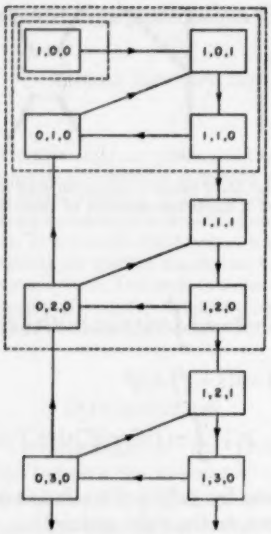

FIG. 2. Schematic representation of Green's function couplings. The dashed boxes show the kernels included for one, two, and three "thick lines," respectively.

not exceed the maximum allowed. Such a factorization may, of course, be carried out in a number of ways. A procedure that appears most reasonable at low energies is the factoring out, in a symmetric fashion, of a single meson propagation function: $G(\xi_1\cdots\xi_N)\simeq G(\xi_1\cdots\xi_{N-2})\mathcal{G}(\xi_{N-1}\xi_N)+\cdots$. The physical interpretation of this procedure is that one of the mesons does not interact strongly with the remaining meson-nucleon complex.

(D) Examples of Approximations

(i) *Zeroth Approximation*

To this order one allows only one thick line. Since, in (2.7), $G(\xi)$ has two lines and its factorization in the absence of an external meson field gives zero $[G(\xi)\simeq G\langle\phi(\xi)\rangle=0]$, Eq. (2.7) reduces to

$$(\gamma p+m)G_0=1, \tag{2.13}$$

the equation for the noninteracting nucleon kernel.

(ii) *First Approximation*

In this approximation we still restrict ourselves to one line. Here we break up

$$G(\xi\xi')=G\mathcal{G}_0(\xi\xi'), \tag{2.14}$$

which corresponds to the explicit assumption of no meson-nucleon scattering. Inserting (2.14) in (2.12a) one obtains:

$$(\gamma p+m)G=1-ig^2\times\left[\int\gamma(\xi)\mathcal{G}_0(\xi\xi')G_0\gamma(\xi')d\xi d\xi'\right]G. \tag{2.15}$$

The G defined by the foregoing equation has previously been studied[6] in order to ascertain its effect on the suppression of pairs in meson-nucleon scattering. It is to be noted that in the present scheme, its use in any discussion of the meson-nucleon equation would be inconsistent due to the approximation made in Eq. (2.14).

(iii) *Second Approximation*

Here we consider the case of two thick lines, i.e., the second set of boxes (Fig. 2), described by Eqs. (2.7), (2.8), (2.9), and (2.11). We approximate the three-line quantity appearing here by

$$G(\xi''\xi'\xi)\simeq G(\xi'')\mathcal{G}_0(\xi'\xi)+G(\xi')\mathcal{G}_0(\xi\xi'')+G(\xi)\mathcal{G}_0(\xi''\xi'). \tag{2.16}$$

Eliminating $G(\xi)$ in terms of $G(\xi\xi')$ via (2.8) and substituting into (2.9) one obtains an equation for $G(\xi\xi')$:

$$\begin{aligned}G(\xi'\xi)=&G_0\mathcal{G}_0(\xi'\xi)-ig^2\int G_0\gamma(\xi'')\\&\times G_0\gamma(\xi''')G(\xi'''\xi'')\mathcal{G}_0(\xi'\xi)d\xi''d\xi'''\\&+ig^2G_0\,\mathrm{Tr}\int\mathcal{G}_0(\xi\xi'')\gamma(\xi'')\\&\times G_0\gamma(\xi''')G(\xi'''\xi')d\xi''d\xi'''\\&-ig^2\Big\{\int G_0\gamma(\xi'')G_0\gamma(\xi''')[G(\xi'''\xi')\mathcal{G}_0(\xi''\xi)\\&+G(\xi'''\xi)\mathcal{G}_0(\xi''\xi')]d\xi''d\xi'''\Big\}.\end{aligned} \tag{2.17}$$

The second and third terms on the right-hand side of (2.17) are only self-energy structures on external lines and may therefore be absorbed into the first term. In obtaining (2.17), use was made of Eqs. (2.12a, b).

The quantity $G(\xi''\xi'\xi)$ describes one-meson production in a meson-nucleon scattering process. The approximation (2.16) does not allow a *real* production of this type to occur since $G(\xi)$ has vanishing matrix elements between states conserving energy-momentum. Experimentally the meson-production cross section in meson-nucleon collisions appears to be very small up to energies $\sim$1 Bev. Thus this approximation may be adequate at low energies, since one may hope that any expected rise in the matrix element for virtual production at energies $\gg$1 Bev (in intermediate states) will be damped by the energy denominators.

An integral equation for $G(\xi)$, which quantity is closely related to the vertex operator, may be derived in this approximation. Substituting (2.16) into (2.9) and

[6] Brueckner, Gell-Mann, and Goldberger, Phys. Rev. **90**, 476 (1953); Karplus, Kivelson, and Martin, Phys. Rev. **90**, 1072 (1953).

eliminating $G(\xi\xi')$ in (2.8) via (2.9) one obtains

$$G(\xi)=ig\int G_{0\gamma}(\xi')G_0\Big[\mathcal{G}_0(\xi'\xi)+ig^2\int \mathcal{G}_0(\xi\xi'')\,\mathrm{Tr}\gamma(\xi'')G(\xi)d\xi''\Big]d\xi'-ig^2\int G_{0\gamma}(\xi')G_{0\gamma}(\xi'')[G(\xi'')\mathcal{G}_0(\xi'\xi)+G(\xi')\mathcal{G}_0(\xi\xi'')+G(\xi)\mathcal{G}_0(\xi''\xi')]d\xi'd\xi''. \quad (2.18)$$

(iv) Third Approximation

In this case, we eliminate $G(\xi''\xi'\xi)$ in (2.9) via (2.10) and decompose the Green's function $G(\xi'''\cdots\xi)$ so as to allow no more than two thick lines:

$$\begin{aligned}G(\xi'''\xi''\xi'\xi)\simeq&[G(\xi'''\xi'')-G\mathcal{G}(\xi'''\xi'')]\mathcal{G}(\xi'\xi)\\&+[G(\xi'''\xi')-G\mathcal{G}(\xi'''\xi')]\mathcal{G}(\xi''\xi)\\&+[G(\xi'''\xi)-G\mathcal{G}(\xi'''\xi)]\mathcal{G}(\xi''\xi')\\&+[G(\xi''\xi')-G\mathcal{G}(\xi''\xi')]\mathcal{G}(\xi'''\xi)\\&+[G(\xi''\xi)-G\mathcal{G}(\xi''\xi)]\mathcal{G}(\xi'''\xi')\\&+[G(\xi'\xi)-G\mathcal{G}(\xi'\xi)]\mathcal{G}(\xi'''\xi'')\\&+G[\mathcal{G}(\xi'''\xi'')\mathcal{G}(\xi'\xi)+\mathcal{G}(\xi'''\xi')\\&\times\mathcal{G}(\xi''\xi)+\mathcal{G}(\xi'''\xi)\mathcal{G}(\xi''\xi')]. \quad (2.19)\end{aligned}$$

The first terms in (2.19) represent the diagrams in which only one meson can propagate independently. Since $G(\xi'''\xi''\xi'\xi)$ must also include the possibility of two disconnected meson lines, the second set of terms must be added in. Equation (2.19) may be rewritten as follows:

$$\begin{aligned}G(\xi'''\xi''\xi'\xi)\simeq&[G(\xi'''\xi'')\mathcal{G}(\xi'\xi)+G(\xi'''\xi')\mathcal{G}(\xi''\xi)\\&+G(\xi'''\xi)\mathcal{G}(\xi''\xi')]\\&+[\{G(\xi''\xi')-G\mathcal{G}(\xi''\xi')\}\mathcal{G}(\xi'''\xi)\\&+\{G(\xi''\xi)-G\mathcal{G}(\xi''\xi)\}\mathcal{G}(\xi'''\xi')\\&+\{G(\xi'\xi)-G\mathcal{G}(\xi'\xi)\}\mathcal{G}(\xi'''\xi'')]. \quad (2.20)\end{aligned}$$

The first three terms are the ones appearing in the second approximation. Substituting (2.20) into (2.10), one sees that in this case the three remaining terms allow single-meson production in a meson-nucleon collision. The approximation made in (2.20) assumes that two real mesons and a nucleon do not form a closely bound system, or, for a different time ordering, one is neglecting two-meson production in meson-nucleon scattering. An equation for the meson-nucleon Green's function may easily be derived and is linear when vacuum polarization effects (closed loops) are neglected. Some of the lowest-order diagrams included in this approximation are shown in Fig. 3.

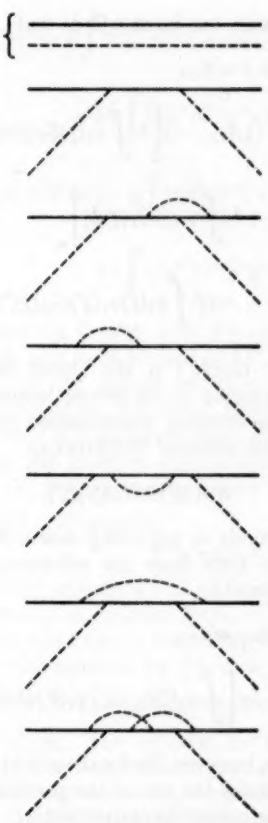

FIG. 3. Some of the lower-order diagrams included in the third approximation. The corresponding "crossed" diagrams also appear, as the Green's function is symmetric in the meson variables.

III. TWO-NUCLEON SYSTEMS

The formalism developed in Sec. II can easily be applied to the two-nucleon problem. The quantity of central interest is the two-nucleon, no-meson Green's function G_{12} defined by

$$G_{12}=-\langle(\psi(x_1)\psi(x_2)\bar{\psi}(x_1')\bar{\psi}(x_2'))_+\rangle\epsilon,$$
$$\epsilon=\epsilon(x_1-x_2)\epsilon(x_1-x_1')\epsilon(x_1-x_2')\times\epsilon(x_1'-x_2)\epsilon(x_1'-x_2')\epsilon(x_2-x_2'). \quad (3.1)$$

As before we will denote the two-nucleon, m-meson kernel by $G_{12}(\xi_1\cdots\xi_m)$.

We begin by operating with $(\gamma_1 p_1+m)$ on G_{12} to obtain

$$(\gamma_1 p_1+m)G_{12}=(1_1G_2)_{\Lambda}-g\int\gamma_1(\xi)G_{12}(\xi)d\xi, \quad (3.2)$$

where in general

$$(x_1x_2|A_{\Lambda}|x_1'x_2')=(x_1x_2|A|x_1'x_2')-(x_1x_2|A|x_2'x_1'). \quad (3.3)$$

In (3.2) the inhomogeneous term comes from the two nonvanishing discontinuities in the time derivative of

(3.1). Continuing, one further finds that

$$(\gamma_1 p_1+m)(\gamma_2 p_2+m)G_{12}$$
$$=(1_1 1_2)_\Lambda - g\Big[1_1\int\gamma_2(\xi)G_2(\xi)d\xi + 1_2\int\gamma_1(\xi)G_1(\xi)d\xi\Big]_\Lambda$$
$$-ig^2\int\gamma_1(\xi)\gamma_2(\xi')G_{12}(\xi\xi')d\xi d\xi'. \quad (3.4)$$

The quantity $G_{12}(\xi\xi')$ is the kernel describing the scattering of a meson by the two-nucleon system, or, for a different time ordering, double-meson production in a nucleon-nucleon collision. The breakup

$$G_{12}(\xi\xi')\cong G_{12}\mathcal{G}_0(\xi\xi'), \quad (3.5)$$

which corresponds to neglecting meson-deuteron scattering, yields, aside from the self-energy terms, the familiar equation[7]

$$(\gamma_1 p_1+m)(\gamma_2 p_2+m)G_{12}$$
$$=\{1_1 1_2\}_\Lambda - ig^2\Big[\int\gamma_1(\xi)\mathcal{G}_0(\xi\xi')\gamma_2(\xi')d\xi d\xi'\Big]G_{12}. \quad (3.6)$$

In our scheme, however, the breakup (3.5) is incomplete in that it contains but one of the possible "two lines" structures. The correct decomposition is

$$G_{12}(\xi\xi')\cong G_{12}\mathcal{G}_0(\xi\xi')+\{G_1[G_2(\xi\xi')-G_2\mathcal{G}_0(\xi\xi')] + G_2[G_1(\xi\xi')-G_1\mathcal{G}_0(\xi\xi')]\}. \quad (3.7)$$

The additional terms may be interpreted as a kind of "impulse approximation" to the meson-deuteron scattering kernel, in that the meson interacts with only one nucleon at a time. The substitution of (3.7) into (3.4) yields (neglecting self-energy terms):

$$(\gamma_1 p_1+m)(\gamma_2 p_2+m)G_{12}$$
$$=\{1_1 1_2\}_\Lambda - ig^2\Big[\int\gamma_1(\xi)\mathcal{G}_0(\xi\xi')\gamma_2(\xi')d\xi d\xi'\Big]G_{12}$$
$$-ig^2\int\gamma_1(\xi)\gamma_2(\xi')\{G_1[G_2(\xi\xi')-G_2\mathcal{G}_0(\xi\xi')] + 1\leftrightarrow 2\}_\Lambda d\xi d\xi'. \quad (3.8)$$

Continuing with the scheme, one may obtain the rigorous equation for $G_{12}(\xi\xi')$:

$$(\gamma_1 p_1+m)(\gamma_2 p_2+m)G_{12}(\xi\xi')$$
$$=[1_1 1_2\mathcal{G}(\xi\xi')]_\Lambda - g\Big\{1_1\int\gamma_2(\xi'')G_2(\xi''\xi'\xi)d\xi''+1\leftrightarrow 2\Big\}_\Lambda$$
$$-ig^2\int\gamma_2(\xi''')\gamma_1(\xi'')G_{12}(\xi'''\xi''\xi'\xi)d\xi''d\xi'''. \quad (3.9)$$

In an elimination of $G_{12}(\xi\xi')$ in (3.4) via (3.9), the first three terms on the right-hand side of (3.9) give "impulse" contributions, while the last term includes the effects due to the nucleon-nucleon binding. Making the breakup of $G_{12}(\xi'''\xi''\xi'\xi)$ analogous to (3.7) in (3.9) yields an integral equation for $G_{12}(\xi\xi')$.[8]

IV. THREE-FIELD SYSTEMS

The introduction of the electromagnetic field permits the extension of the technique outlined above to such problems as photoproduction, nuclear Compton effect, and the nucleon magnetic moments. In order to exhibit the gauge invariance of the scheme, we shall in this section deal only with manifestly gauge-covariant quantities. The three-field equations of motion are:

$$(\gamma p+m-e\gamma_\mu TA_\mu+g\gamma_5\tau_i\phi_i)\psi=0, \quad (4.1)$$
$$[(p-eSA)^2+\mu^2]\phi_i=-\tfrac{1}{2}g[\bar\psi,\gamma_5\tau_i\psi], \quad (4.2)$$
$$p^2A_\mu-p_\mu p_\lambda A_\lambda=\tfrac{1}{2}e[\bar\psi,\gamma_\mu\psi], \quad (4.3)$$

where $T=\frac{1}{2}(1+\tau_3)$ and

$$S=\begin{pmatrix}0 & i & 0\\ -i & 0 & 0\\ 0 & 0 & 0\end{pmatrix}.$$

In the succeeding development ξ will be used to denote the meson coordinate, η the photon coordinate, and

$$(x|\gamma_\mu(\eta)|x')=\gamma_\mu T\delta(x-x')\delta(\eta-x'). \quad (4.4)$$

The equation obeyed by the one-nucleon Green's function is

$$(\gamma p+m)G=1-g\int\gamma(\xi)G(\xi)d\xi+e\int\gamma(\eta)G(\eta)d\eta, \quad (4.5)$$

where

$$G(\eta)=i\langle(\psi(x)\bar\psi(x')A(\eta))_+\rangle\epsilon(x-x') \quad (4.6)$$

and is not a gauge covariant quantity. The corre-

[7] In its wave function form, the equation analogous to (3.6) in quantum electrodynamics has been investigated by J. Goldstein, Phys. Rev. **91**, 1516 (1953), for the case of vanishing total energy. See also R. Arnowitt and S. Gasiorowicz, Phys. Rev. **94**, 1057 (1954).

[8] In view of the experimental results favoring two-meson production in nucleon-nucleon collisions at energies ~1 Bev, it would seem that a decomposition of $G_{12}(\xi\xi')$ as in (3.7) is not a good approximation, and the effects included in (3.9) will have to be taken into account. It is interesting to note that in terms of a perturbation expansion, (3.9) contains the two-pair fourth-order potentials, which have previously been shown to be large.

sponding gauge covariant kernel is[9]

$$G^c(\eta)=i\langle(\psi(x)\bar{\psi}(x')A(\eta))_+\rangle\epsilon(x-x')$$
$$-i\langle A(\eta)\rangle\langle(\psi(x)\bar{\psi}(x'))_+\rangle\epsilon(x-x')$$
$$=G(\eta)-GA(\eta). \tag{4.7}$$

Introducing $G^c(\eta)$ into (4.5) one obtains

$$(\gamma p+m)G=1-g\int\gamma(\xi)G(\xi)d\xi+e\int\gamma(\eta)G^c(\eta)d\eta$$
$$+e\left[\int\gamma(\eta)A(\eta)d\eta\right]G, \tag{4.8}$$

i.e.,

$$[\gamma(p-eTA)+m]G$$
$$=1-g\int\gamma(\xi)G(\xi)d\xi+e\int\gamma(\eta)G^c(\eta)d\eta, \tag{4.9}$$

in which form the gauge invariance of the equation is clearly exhibited.

Proceeding as before, the kernels $G(\xi)$ and $G^c(\eta)$ obey the equations:

$$(\gamma\pi+m)G(\xi)=ig\int\gamma(\xi')G(\xi'\xi)d\xi'$$
$$-ie\int\gamma(\eta')G^c(\eta'\xi)d\eta', \tag{4.10}$$

$$(\gamma\pi+m)G^c(\eta)=ig\int\gamma(\xi')G^c(\xi'\eta)d\xi'$$
$$-ie\int\gamma(\eta')G^c(\eta'\eta)d\eta', \tag{4.11}$$

where $\pi_\mu=p_\mu-eTA_\mu$, and the covariant photoproduction and Compton kernels are

$$G^c(\xi'\eta)=G(\xi'\eta)-iA(\eta)G(\xi'), \tag{4.12}$$

$$G^c(\eta'\eta)=G(\eta'\eta)-iA(\eta)G^c(\eta')$$
$$-iA(\eta')G^c(\eta)-iA(\eta)A(\eta')G, \tag{4.13}$$

respectively. The meson-nucleon scattering, photoproduction, and Compton scattering functions further obey the equations:[10]

$$(\gamma\pi+m)G(\xi'\xi)=\mathcal{G}(\xi'\xi)-g\int\gamma(\xi'')G(\xi''\xi'\xi)d\xi''$$
$$+e\int\gamma(\eta'')G^c(\eta''\xi'\xi)d\eta'', \tag{4.14}$$

$$(\gamma\pi+m)G^c(\eta'\xi)=-g\int\gamma(\xi'')G^c(\xi''\eta'\xi)d\xi''$$
$$+e\int\gamma(\eta'')G^c(\eta''\eta'\xi)d\eta'', \tag{4.15}$$

$$(\gamma\pi+m)G^c(\eta'\eta)=\mathcal{G}^c(\eta'\eta)-g\int\gamma(\xi')G^c(\xi'\eta'\eta)d\xi'$$
$$+e\int\gamma(\eta'')G^c(\eta''\eta'\eta)d\eta'', \tag{4.16}$$

with definitions for $\mathcal{G}^c(\eta'\eta)$, $G^c(\eta''\xi'\xi)$, $G^c(\eta''\eta'\xi)$, and $G^c(\eta''\eta'\eta)$ analogous to (4.12) and (4.13).

In cutting off the infinite set of equations, it is necessary to decompose the higher meson and photon Green's functions in a gauge-invariant manner, that is, break them up into products of gauge-invariant quantities. Thus in the first approximation we set

$$G(\xi'\xi)\cong G\mathcal{G}(\xi'\xi);\quad G^c(\eta'\xi)\cong 0;$$
$$G^c(\eta'\eta)\cong G\mathcal{G}^c(\eta'\eta). \tag{4.17}$$

Eliminating $G(\xi)$ and $G^c(\eta')$ in (4.9) via (4.10) and (4.11), one obtains an equation for G, involving $\mathcal{G}(\xi'\xi)$, $\mathcal{G}^c(\eta'\eta)$, and $G_0{}^c\equiv(\gamma\pi+m)^{-1}$. Neglecting vacuum polarization effects, the equation for $\mathcal{G}^c(\eta'\eta)\equiv\mathcal{G}_0{}^c(\eta'\eta)$ is

$$q^2\mathcal{G}_{\mu\nu}{}^c(\eta'\eta)-q_\mu q_\lambda\mathcal{G}_{\lambda\nu}{}^c(\eta'\eta)=\delta_{\mu\nu}\delta(\eta'-\eta), \tag{4.18}$$

where $q_\mu=-i\partial/\partial\eta_\mu$. The equation for $\mathcal{G}(\xi'\xi)$ will be considered in connection with the next approximation.

In the second approximation, the production kernels of equations (4.14) to (4.16) are decomposed:

$$G(\xi''\xi'\xi)\cong G(\xi'')\mathcal{G}(\xi'\xi)+\text{symm. terms}, \tag{4.19}$$

$$G^c(\eta''\xi'\xi)\cong G^c(\eta'')\mathcal{G}(\xi'\xi)+G\mathcal{G}^c(\eta''\xi'\xi), \tag{4.20}$$

$$G^c(\eta''\eta'\xi)\cong G(\xi)\mathcal{G}^c(\eta''\eta'), \tag{4.21}[11]$$

$$G^c(\eta''\eta'\eta)\cong G^c(\eta'')\mathcal{G}^c(\eta'\eta)+\text{symm. terms}. \tag{4.22}$$

By the use of Eqs. (4.10) and (4.11), the production kernels (4.19) to (4.22) may be expressed in terms of scattering kernels, which when substituted into (4.14) to (4.16) yield three equations coupling the meson-nucleon scattering, photoproduction, and Compton scattering Green's functions:

$$G(\xi'\xi)=G\mathcal{G}(\xi'\xi)-ig^2\int G_0{}^c\gamma(\xi'')G_0{}^c\gamma(\xi''')$$
$$\times[\mathcal{G}(\xi''\xi)G(\xi'''\xi')+\mathcal{G}(\xi''\xi')G(\xi'''\xi)]d\xi''d\xi'''$$
$$+ieg\int G_0{}^c\gamma(\xi'')G_0{}^c\gamma(\eta'')[\mathcal{G}(\xi''\xi)G^c(\eta''\xi')$$
$$+\mathcal{G}(\xi''\xi')G^c(\eta''\xi)]d\eta''d\xi''$$
$$+e\int G_0{}^c\gamma(\eta'')\mathcal{G}^c(\eta''\xi'\xi)Gd\eta'', \tag{4.23}$$

[9] The structure of $G^c(\eta)$ arises naturally using the variational definition of Schwinger. We shall henceforth denote $\langle A(\eta)\rangle$ simply by $A(\eta)$.

[10] These equations have also been obtained by M. Neuman by using the variational derivative techniques (private communication).

[11] The term involving $\mathcal{G}^c(\eta''\eta'\xi)$ is absent, since we have explicitly neglected vacuum polarization. This type of kernel describes the two-photon decay of the neutral meson.

$$G^c(\eta'\xi)=-ig^2\int G_0{}^c\gamma(\xi''')G_0{}^c\gamma(\xi'')$$
$$\times\mathcal{G}(\xi'''\xi)G^c(\eta'\xi'')d\xi''d\xi'''$$
$$+ieg\int G_0{}^c\gamma(\xi'')G_0{}^c\gamma(\eta'')$$
$$\times\mathcal{G}(\xi''\xi)G_0{}^c\mathcal{G}^c(\eta''\eta')d\xi''d\eta''$$
$$+ieg\int G_0{}^c\gamma(\eta'')G_0{}^c\gamma(\xi'')$$
$$\times\mathcal{G}^c(\eta''\eta')G(\xi''\xi)d\xi''d\eta''$$
$$-g\int G_0{}^c\gamma(\xi'')\mathcal{G}^c(\eta'\xi''\xi)Gd\xi''-ie^2\int G_0{}^c\gamma(\eta'')$$
$$\times G_0{}^c\gamma(\eta''')\mathcal{G}^c(\eta''\eta')G^c(\eta'''\xi)d\eta''d\eta''', \quad (4.24)$$

$$G^c(\eta\eta')=G\mathcal{G}^c(\eta\eta')+ieg$$
$$\times\int G_0{}^c\gamma(\eta'')G_0{}^c\gamma(\xi'')[G^c(\xi''\eta')\mathcal{G}^c(\eta''\eta)$$
$$+G^c(\xi''\eta)\mathcal{G}^c(\eta''\eta')]d\xi''d\eta''-ie^2$$
$$\times\int G_0{}^c\gamma(\eta'')G_0{}^c\gamma(\eta''')[G^c(\eta'''\eta')\mathcal{G}^c(\eta''\eta)$$
$$+G^c(\eta'''\eta)\mathcal{G}^c(\eta''\eta')]d\eta''d\eta'''. \quad (4.25)$$

It remains to evaluate $\mathcal{G}(\xi\xi')$ and $\mathcal{G}^c(\eta\xi\xi')$. Starting with Eq. (4.2) we obtain

$$(k^2+\mu^2)\mathcal{G}(\xi'\xi)$$
$$=\delta(\xi'-\xi)+ieS\langle(\{k,A(\xi')\}\phi(\xi')\phi(\xi))_+\rangle$$
$$-ie^2S^2\langle(A(\xi')A(\xi')\phi(\xi')\phi(\xi))_+\rangle. \quad (4.26)$$

Introducing the notation $S(\xi,\eta)=S\delta(\xi-\eta)$ and the covariant derivative $\bar{k}_\mu=k_\mu-eSA_\mu$, (4.26) may be written in the form

$$(\bar{k}^2+\mu^2)\mathcal{G}(\xi'\xi)$$
$$=\delta(\xi'-\xi)+e\int\{S(\eta\xi'),\bar{k}\}\mathcal{G}^c(\xi'\xi\eta)d\eta$$
$$+ie^2\int S(\eta'\xi')S(\eta\xi')\mathcal{G}^c(\xi'\xi\eta'\eta)d\eta d\eta'. \quad (4.27)$$

Similarly,

$$(\bar{k}^2+\mu^2)\mathcal{G}^c(\xi'\xi\eta)$$
$$=-ie\int\{S(\eta'\xi'),\bar{k}\}\mathcal{G}^c(\xi'\xi\eta'\eta)d\eta'$$
$$+ie^2\int S(\eta''\xi')S(\eta'\xi')\mathcal{G}^c(\xi'\xi\eta''\eta'\eta)d\eta'd\eta''. \quad (4.28)$$

If terms of order e only are kept, the above quantities satisfy the equations

$$(\bar{k}^2+\mu^2)\mathcal{G}(\xi'\xi)=\delta(\xi'-\xi), \quad (4.29)$$

$$(\bar{k}^2+\mu^2)\mathcal{G}^c(\xi'\xi\eta)=-ie\int\{S(\eta'\xi'),\bar{k}\}$$
$$\times\mathcal{G}(\xi'\xi)\mathcal{G}_0{}^c(\eta'\eta)d\eta'. \quad (4.30)$$

To lowest order in e, (4.23) to (4.25) becomes

$$G(\xi'\xi)=G\mathcal{G}_0(\xi'\xi)-ig^2\int G_0{}^c\gamma(\xi'')$$
$$\times G_0{}^c\gamma(\xi''')[\mathcal{G}_0(\xi''\xi)G(\xi'''\xi')$$
$$+\mathcal{G}_0(\xi''\xi')G(\xi'''\xi)]d\xi''d\xi''', \quad (4.31)$$

$$G^c(\eta'\xi)=-ig^2\int G_0{}^c\gamma(\xi''')G_0{}^c\gamma(\xi'')$$
$$\times\mathcal{G}_0(\xi'''\xi)G^c(\xi''\eta')d\xi''d\xi'''$$
$$+ieg\int G_0{}^c\gamma(\xi'')G_0{}^c\gamma(\eta'')$$
$$\times\mathcal{G}_0(\xi''\xi)G^c(\eta''\eta)d\xi''d\eta''$$
$$+ieg\int G_0{}^c\gamma(\eta'')G_0{}^c\gamma(\xi'')$$
$$\times\mathcal{G}_0{}^c(\eta''\eta')G(\xi''\xi)d\xi''d\eta''$$
$$+ieg\int G_0{}^c\gamma(\xi'')\mathcal{G}_0(\xi''\xi''')\{S(\eta''\xi'''),\bar{k}\}$$
$$\times\mathcal{G}(\xi'''\xi)\mathcal{G}_0{}^c(\eta''\eta)Gd\eta''d\xi''d\xi''', \quad (4.32)$$

$$G^c(\eta'\eta)=G\mathcal{G}_0{}^c(\eta'\eta)+ieg\int G_0{}^c\gamma(\eta'')$$
$$\times G_0{}^c\gamma(\xi'')[G^c(\xi''\eta')\mathcal{G}_0{}^c(\eta''\eta)$$
$$+G^c(\xi''\eta)\mathcal{G}_0{}^c(\eta''\eta')]d\eta''d\xi''$$
$$-ie^2\int G_0{}^c\gamma(\eta'')G_0{}^c\gamma(\eta''')[\mathcal{G}_0{}^c(\eta'''\eta')\mathcal{G}_0{}^c(\eta''\eta)$$
$$+\mathcal{G}_0{}^c(\eta'''\eta)\mathcal{G}_0{}^c(\eta''\eta')]G_0{}^cd\eta''d\eta'''. \quad (4.33)$$

It should be noted that a knowledge of the meson-nucleon scattering Green's function is required for the solution of the photoproduction equation, and the latter for the nuclear Compton effect. Since the equations are gauge-covariant, one may, of course, choose any gauge, in particular the usual Lorentz gauge.

V. CONCLUSION

In the preceding sections an attempt has been made to outline a procedure for obtaining a closed set of

covariant equations describing meson processes in an approximate fashion. The approximation does not depend for its validity on the weakness of the coupling between the meson and the nucleon fields, but rather on the correctness of the conjectured form of the highest-order Green's function appearing in a subset of the rigorous equations. More explicitly, since any subset of the rigorous equations correctly describes the whole theory, a knowledge of the Green's function containing the highest number of variables in such a set allows one in principle to calculate any physical process. The approximation made is to assume that one of the mesons in the highest Green's function does not interact with the remaining meson-nucleon structure. The successive approximations allow more and more mesons to interact closely with the nucleon. Although it seems mathematically impossible at this stage to prove convergence, the scheme appears reasonable in view of the fact that highly multiple meson production is not observed experimentally.

A remark should be made on the consistency of the decomposition scheme. The rules for making the breakup apply only to the first Green's function that is not treated rigorously. The question arises whether the equations containing the higher Green's functions are then consistent. It can be shown that, to make them so, one must make the same physical assumptions in these equations as are implied by the original breakup. For example, if the decomposition (2.14) is substituted into (2.9), consistency is obtained, provided one assumes $G(\xi''\xi'\xi)\cong G(\xi'')\mathcal{G}_0(\xi'\xi)$. Comparison with (2.16) shows that this term appears there along with two other terms which give rise to meson-nucleon scattering. The latter, however, must be neglected in accordance with the assumptions leading to (2.14), namely that no meson-nucleon scattering be allowed.

The neglect of vacuum polarization effects in the low-energy region seems reasonable. For high energies, however, one might expect the incident meson to interact mainly with the meson cloud around the nucleon, and hence polarization effects would predominate. It is possible to rearrange the equations so that these effects are more explicitly exhibited, while the direct meson-nucleon interaction is de-emphasized.

Unlike the approximation in the Tamm-Dancoff method, the number of mesons and pairs present is not limited to a fixed number. This is due mainly to the covariance of the approach, which allows the "bending back" of nucleon lines in time.[12] The covariance allows as a consequence a preservation of the symmetry in meson indices of the Green's functions, with the resulting inclusion of equal numbers of crossed and uncrossed graphs in the same approximation. There is, of course, the serious practical drawback of having to solve inhomogeneous four-dimensional equations for the Green's functions rather than three-dimensional wave equations; on the other hand, the boundary conditions are clearly defined when dealing with the kernels.

In order to get a qualitative feeling for the equations, we have examined the problem of π^+-p scattering in the second approximation in a very crude fashion. Equation (2.18) was simplified by neglecting vacuum polarization and dropping terms which yield only self-energy contributions to the external lines.[13] Rewriting the integral equation in momentum space, an ansatz was made that the solution be expressible in terms of a product of the lowest-order perturbation expression times a slowly varying function, which could be taken out of the integral.[14] The resulting algebraic equation was solved for the slowly varying function, which was found to be expressible in terms of the second-order mass and vertex operators. Substitution of this result into Eq. (2.17) yielded an expression for the meson-nucleon Green's function. In this particular case, a perturbation theory renormalization of the second-order mass and vertex operators gave the same result as a term-by-term renormalization of the perturbation solution of (2.18) followed by the "slowly varying approximation" applied to the resulting finite residue which was then resumed. With a coupling constant $g^2/4\pi\cong 1-3$ the low-energy data may be fitted roughly. However, no particular emphasis should be placed on this result since it is by no means clear that the first step of such an iteration procedure approximates the true solution, or even that the iteration converges.

The renormalization used in the above example is basically unsatisfactory because of its limited applicability. In addition, it is questionable whether the renormalizations of the external lines[13] are consistent with those carried out on the approximate solution of the integral equation. The general problem of renormalizing the entire approximation scheme is being investigated by the authors in collaboration with Dr. S. Bludman.

It is a pleasure to acknowledge stimulating discussions with Dr. J. V. Lepore and Dr. M. Neuman.

[12] The scheme resembles more closely a Tamm-Dancoff procedure in "proper time."

[13] These contributions were assumed to renormalize the masses and Green's functions on the outgoing lines.

[14] This may be viewed as the first step of an iteration procedure. Thus, if the solution obtained below is written as $G_1(\xi)=G_0(\xi)f_1$, where f_1 is the slowly varying function, then the next ansatz would be $G_2(\xi)=G_1(\xi)f_2$, where now f_2 is to be taken out of the integral.

Time-Dependent Variational Principle*

SAUL ALTSHULER† AND J. F. CARLSON‡
Department of Physics and Institute for Atomic Research, Iowa State College, Ames, Iowa
(Received April 5, 1954)

A variational principle for the transition amplitude is derived for interactions which are explicitly time-dependent. The form is similar to the Schwinger variational principle for the transition amplitude in stationary state collision theory.

ALTHOUGH time-dependent variational principles for scattering processes have been treated[1] in the past, no explicit attention seems to have been given to problems in which the interaction potential is time-dependent. An important example of this viewpoint in scattering theory, useful in the case of heavy particle collisions, is the well-known impact parameter method[2,3] in which the incident particle is regarded as a moving center of force, and the standard Dirac method of variation of constants is employed to compute the effective cross section for excitation. This quantity is the integral

$$\int\int |a_b(\infty)|^2 dXdY, \tag{1}$$

where $a_b(t)$ is the probability amplitude containing the impact parameter, $(X^2+Y^2)^{\frac{1}{2}}$. We show that $a_b(\infty)$ can be exhibited as a variational principle in a form which resembles the Schwinger variational principle for the transition amplitude in the stationary state theory.[4,5]

We begin with the pair of integral equations:

$$\begin{aligned}\psi_a^{(+)}(t)&=\Phi_a(t)+\frac{1}{i\hbar}\int_{-\infty}^{t}\exp\left[\frac{i}{\hbar}H_0(t'-t)\right]\\&\qquad\times V(t')\psi_a^{(+)}(t')dt',\\ \psi_b^{(-)}(t)&=\Phi_b(t)+\frac{1}{i\hbar}\int_{\infty}^{t}\exp\left[\frac{i}{\hbar}H_0(t'-t)\right]\\&\qquad\times V(t')\psi_b^{(-)}(t')dt',\end{aligned} \tag{2}$$

which satisfy $[i\hbar(\partial/\partial t)-H_0]\psi^{(\pm)}(t)=V(t)\psi^{(\pm)}(t)$, while the Φ's describe the time development of the system in the absence of interaction. It is to be observed that upon specializing to the stationary state picture by removing the explicit time-dependence of the interaction and fixing the energy of the system, the integrations over time lead readily to the familiar stationary state integral equations:

$$u_a^{(\pm)}=\varphi_a+\frac{1}{E_a\pm i\epsilon-H_0}Vu_a^{(\pm)}, \tag{3}$$

where

$$\psi_a^{(\pm)}(t)=\exp\left(-\frac{i}{\hbar}E_at\right)u_a^{(\pm)},$$

and

$$\Phi_a(t)=\exp\left(-\frac{i}{\hbar}E_at\right)\varphi_a.$$

Here, the small positive ϵ arises by introducing the factor $\exp[(\pm)\epsilon t'/\hbar]$ in order to define the integrals in (2). This corresponds to Lippman's and Schwinger's adiabatic decrease in the interaction strength, and the plus and minus signs automatically account for diverging or converging scattered waves.

Upon making a measurement on the system in the state $\psi_a^{(+)}(t)$, the amplitude which corresponds to observing the state $\Phi_b(t)=\exp[(-i/\hbar)H_0t]\Phi_b(0)$ is given by

$$\begin{aligned}a_b(t)&=\Phi_b^{\dagger}(t)\psi_a^{(+)}(t)\\&=\Phi_b^{\dagger}(t)\Phi_a(t)+\frac{1}{i\hbar}\int_{-\infty}^{t}\Phi_b^{\dagger}(0)\exp\left(\frac{i}{\hbar}H_0t\right)\\&\qquad\times\exp\left(\frac{i}{\hbar}H_0(t'-t)\right)V(t')\psi_a^{(+)}(t')dt'\\&=\frac{1}{i\hbar}\int_{-\infty}^{t}\Phi_b^{\dagger}(t')V(t')\psi_a^{(+)}(t')dt',\end{aligned} \tag{4}$$

if we regard the $\Phi_n(0)$ as forming an orthonormal set of eigenfunctions describing the free system. Moreover, if $\Phi_n(0)=\varphi_n$, that is, $\Phi_n(t)=\exp[(-i/\hbar)E_nt]\varphi_n$, where $H_0\varphi_n=E_n\varphi_n$, then (4) is precisely the amplitude obtained by the method of variation of constants.

Let us now rewrite the pair of Eqs. (2) after first forming the Hermitian adjoint of $\psi_b^{(-)}(t)$. That is,

$$\begin{aligned}\psi_a^{(+)}(t)&=\Phi_a(t)+\frac{1}{i\hbar}\int_{-\infty}^{\infty}\exp\left[\frac{i}{\hbar}H_0(t'-t)\right]\\&\qquad\times\eta(t'-t)V(t')\psi_a^{(+)}(t')dt',\end{aligned} \tag{5}$$

---

* Contribution No. 320 from the Institute for Atomic Research and Department of Physics, Iowa State College, Ames, Iowa. Work was performed in part in the Ames Laboratory of the U. S. Atomic Energy Commission.

† The research reported in this paper has been sponsored in part by the Geophysical Research Directorate of the Air Force Cambridge Research Center, Air Research and Development Command.

‡ Deceased, April 5, 1954.

[1] B. A. Lippman and J. Schwinger, Phys. Rev. **79**, 469 (1950).

[2] N. F. Mott, Proc. Cambridge Phil. Soc. **27**, 553 (1931).

[3] J. W. Frame, Proc. Cambridge Phil. Soc. **27**, 511 (1931).

[4] J. Schwinger, *Lectures on Nuclear Physics*, Harvard University, 1947 (unpublished).

[5] S. Altshuler, Phys. Rev. **89**, 1278 (1953).

$$\psi_b^{(-)\dagger}(t)=\Phi_b^{\dagger}(t)+\frac{1}{i\hbar}\int_{-\infty}^{\infty}\psi_b^{(-)\dagger}(t')V^{\dagger}(t')\eta(t-t')\times\exp\left[-\frac{i}{\hbar}H_{\text{op}}(t'-t)\right]dt'. \quad (6)$$

Here,

$$\eta(t'-t)=1;\quad t'<t$$
$$=0;\quad t'>t.$$

We now multiply Eq. (6) from the right by $V(t)\psi_a^{(+)}(t)$, Eq. (5) from the left by $\psi_b^{(-)\dagger}(t)V^{\dagger}(t)$, and integrate over t, obtaining

$$\int_{-\infty}^{\infty}dt\psi_b^{(-)\dagger}(t)V(t)\psi_a^{(+)}(t)=\int_{-\infty}^{\infty}dt\Phi_b^{\dagger}(t)V(t)\psi_a^{(+)}(t)+\frac{1}{i\hbar}\int_{-\infty}^{\infty}\int_{-\infty}^{\infty}dtdt'\psi_b^{(-)\dagger}(t')V^{\dagger}(t')\times\exp\left[-\frac{i}{\hbar}H_0(t'-t)\right]\eta(t-t')V(t)\psi_a^{(+)}(t), \quad (7)$$

and

$$\int_{-\infty}^{\infty}dt\psi_b^{(-)\dagger}(t)V^{\dagger}(t)\psi_a^{(+)}(t)=\int_{-\infty}^{\infty}dt\psi_b^{(-)\dagger}(t)V^{\dagger}(t)\Phi_a(t)+\frac{1}{i\hbar}\int_{-\infty}^{\infty}\int_{-\infty}^{\infty}dtdt'\psi_b^{(-)\dagger}(t)V^{\dagger}(t)\times\exp\left[\frac{i}{\hbar}H_0(t'-t)\right]\eta(t'-t)V(t')\psi_a^{(+)}(t'). \quad (8)$$

Upon interchanging variables in the double integral of (7), and considering the class of problems for which V is Hermitian, the following reciprocity relation is established:

$$\frac{1}{i\hbar}\int_{-\infty}^{\infty}dt\Phi_b^{\dagger}(t)V(t)\psi_a^{(+)}(t)=\frac{1}{i\hbar}\int_{-\infty}^{\infty}dt\psi_b^{(-)\dagger}(t)V(t)\Phi_a(t). \quad (9)$$

The second term on the right is just

$$\lim_{t\to-\infty}\psi_b^{(-)\dagger}(t)\Phi_a(t),$$

the asymptotic amplitude for observing the state $\Phi_a^{\dagger}(t)$ when a measurement is made upon the system in the state $\psi_b^{(-)\dagger}(t)$. From (9) and (8) we form the functional

$$\Lambda=\frac{\left(\int_{-\infty}^{\infty}dt\Phi_b^{\dagger}(t)V(t)\psi_a^{(+)}(t)\right)\left(\int_{-\infty}^{\infty}dt\psi_b^{(-)\dagger}(t)V(t)\Phi_a(t)\right)}{\int_{-\infty}^{\infty}dt\psi_b^{(-)\dagger}(t)V(t)\psi_a^{(+)}(t)-\frac{1}{i\hbar}\int_{-\infty}^{\infty}\int_{-\infty}^{\infty}dtdt'\psi_b^{(-)\dagger}(t)V(t)\exp\left[\frac{i}{\hbar}H_0(t'-t)\right]\eta(t'-t)V(t')\psi_a^{(+)}(t')}, \quad (10)$$

which, for exact $\psi_a^{(+)}(t)$ and $\psi_b^{(-)}(t)$, is equal to $a_b(\infty)$ and is stationary with respect to arbitrary, independent variations of these wave functions. That is, the requirement that Λ be stationary with respect to arbitrary variations of $\psi_a^{(+)}(t)$ and $\psi_b^{(-)}(t)$ leads to the integral Eqs. (5) and (6), as can be demonstrated in a straightforward manner.

For application of the variational principle it is convenient to choose the configuration representation in which by standard transformation theory the Green's function, $(1/i\hbar)\exp[(i/\hbar)H_0(t'-t)]\eta(t'-t)$, becomes

$$G(\mathbf{r},t;\mathbf{r}',t')\equiv\left(\frac{1}{i\hbar}\exp\left[\frac{i}{\hbar}H_0(t'-t)\right]\eta(t'-t)\right)_{\mathbf{r},\mathbf{r}'}=\frac{1}{i\hbar}\sum_n\varphi_n(\mathbf{r})\varphi_n^{*}(\mathbf{r}')\exp\left[\frac{i}{\hbar}E_n(t'-t)\right]\eta(t'-t), \quad (11)$$

where the $\varphi_n(\mathbf{r})$ are the complete, orthonormal set of eigenfunctions of the operator H_0. Consequently,

$$\Lambda=\frac{\left(\int_{-\infty}^{\infty}dt\int d\tau\Phi_b^{\dagger}(\mathbf{r},t)V(\mathbf{r},t)\psi_a^{(+)}(\mathbf{r},t)\right)\left(\int_{-\infty}^{\infty}dt\int d\tau\psi_b^{(-)\dagger}(\mathbf{r},t)V(\mathbf{r},t)\Phi_a(\mathbf{r},t)\right)}{\int_{-\infty}^{\infty}dt\int d\tau\psi_b^{(-)\dagger}(\mathbf{r},t)V(\mathbf{r},t)\psi_a^{(+)}(\mathbf{r},t)-\int_{-\infty}^{\infty}dt\int_{-\infty}^{\infty}dt'\int d\tau\int d\tau'\psi_b^{(-)\dagger}(\mathbf{r},t)\times V(\mathbf{r},t)G(\mathbf{r},t;\mathbf{r}',t')V(\mathbf{r}',t')\psi_a^{(+)}(\mathbf{r}',t')}. \quad (12)$$

The trial functions which recommend themselves are $\psi_a^{(+)}(\mathbf{r},t)=\Phi_a(\mathbf{r},t)$ and $\psi_b^{(-)}(\mathbf{r},t)=\Phi_b(\mathbf{r},t)$, and where the $\Phi_a(\mathbf{r},t)$ and $\Phi_b(\mathbf{r},t)$ are further specialized to be the unperturbed stationary states. From analogy with stationary state applications[5] it would appear legitimate to expect this choice of trial solution to provide amplitudes superior to those obtained in the second Born approximation.

PHYSICAL REVIEW VOLUME 95, NUMBER 2 JULY 15, 1954

Integral Equations of Quantized Field Theory

H. S. GREEN
University of Adelaide, Adelaide, South Australia
(Received February 15, 1954)

A systematic method is developed for the solution of the integral equations of quantized field theory. It is first shown how to generalize these equations for any number of fermions in interaction with a boson field, and then how to apply the renormalization procedure to the resulting equations. A method of approximation to the solution of the "renormalized" equations is described, which yields divergence-free covariant scattering amplitudes, analogous to the Tamm-Dancoff amplitudes. It is shown that the nth order Tamm-Dancoff amplitudes do not approach limiting values for large n, and that the procedure does not therefore converge; but that a somewhat modified procedure would probably do so. Singularities in the scattering amplitudes, regarded as functions of the coupling constant, are related to the existence of bound states.

1. INTRODUCTION

MOST problems arising in quantum electrodynamics can be satisfactorily solved by perturbation methods. As Dyson[1] among others has pointed out, this is not because the renormalized perturbation series for scattering amplitudes converge; it just happens that the fine-structure constant is small enough to give these series an asymptotic character. In the meson theory of nuclear forces, the coupling constant is much larger and the perturbation series give no reliable quantitative predictions. Attention has therefore been directed to the solution of the integral equations of field theory by other methods.

The integral equations for quantum electrodynamics were first described, though not explicitly formulated, by Dyson.[2] Schwinger[3] later gave a formal derivation of the integral equations which was independent of perturbation theory, which has been used recently by Edwards[4] to obtain a very approximate solution of one of the integral equations. No systematic method of solving the integral equations, apart from the perturbation method, however, has yet been described. Meanwhile an apparently quite different nonperturbation approach to the same problem has been made via what is generally known as the Tamm-Dancoff method. Originally this method suffered from the inconvenience that it was incapable of a completely covariant formulation, but Dyson[5] has recently established a connection between covariant amplitudes and the corresponding Tamm-Dancoff amplitudes, and Cini[6] and Fubini[7] have considered covariant modifications of Tamm-Dancoff equations.

In spite of their very different appearance, the Tamm-Dancoff equations are closely related to the integral equations of Dyson and Schwinger. They have hitherto suffered from the same defect that no way has been found for the application to them of the renormalization procedure. Methods so far proposed for the elimination from them of the divergences either do not work, or would not work in higher approximation. The author has therefore considered in the present paper the question of "renormalizing" the integral equations, and devised a method by which this can be explicitly carried out.

Unfortunately the integral equations in their "renormalized" form are hopelessly nonlinear, and an exact solution of them is impossible. The Tamm-Dancoff method of approximation, however, has the great merit that it produces only linear integral equations which can be solved by standard methods. Of these, Fredholm's method has the advantage that one knows in advance that the solution will converge. Hence, if one applies the Tamm-Dancoff method to the solution of the "renormalized" integral equations, one is certain of obtaining a meaningful result at every stage of approximation. This, of course, no more guarantees the convergence of the method than the efficacy of the renormalization procedure guaranteed the convergence of the perturbation method; and it will in fact be shown that Tamm-Dancoff amplitudes of arbitrarily large but finite order will not closely approximate the exact scattering ampli-

[1] F. J. Dyson, Phys. Rev. **85**, 631 (1952); Proc. Roy. Soc. (London) **A207**, 395 (1951).
[2] F. J. Dyson, Phys. Rev. **75**, 1736 (1949).
[3] J. S. Schwinger, Proc. Natl. Acad. Sci. U. S. **37**, 452, 455 (1951).
[4] S. F. Edwards, Phys. Rev. **90**, 284 (1953).
[5] F. J. Dyson, Phys. Rev. **91**, 1543 (1953).
[6] M. Cini, Nuovo cimento **10**, 526 (1953).
[7] S. Fubini, Nuovo cimento **10**, 851 (1953).

tudes. The nature of this calamity, however, suggests a remedy.

To make our method of determining scattering amplitudes quite general, we first derive a generalization of Schwinger's integral equations for an arbitrary number of fermions in interaction with a boson field. It is shown how to eliminate the divergences from these integral equations, and then how to apply a Tamm-Dancoff type of approximation to reduce them to linear form.

2. DERIVATION OF THE INTEGRAL EQUATIONS

Consider as a preliminary step the equation

$$[i\nabla - m - f\gamma\cdot a(x)]K(x,x_0)=\delta_+(x-x_0), \tag{1}$$

where $\nabla=\gamma_\lambda(\partial/\partial x_\lambda)$, m is a fermion mass, and $f\gamma\cdot a(x)$ denotes $e\gamma_\lambda a^\lambda(x)$, $g\gamma_b a_b(x)$, or some similar expression. It determines the Green's function $K(x,x_0)$ for a single fermion in interaction with an external field; $a(x)$ is arbitrary but unquantized, so that no interaction is yet introduced of the fermion with itself or any other fermion. The subscript $+$ to the δ function may be dropped, according to Feynman,[8] if m is given an infinitesimal imaginary part. We shall work mainly in the momentum representation, and accordingly write

$$\begin{aligned} K(x,x_0)&=\textstyle\sum_p K(p)\exp[-ip\cdot(x-x_0)],\\ a(x)&=\textstyle\sum_k a_k\exp[-ik\cdot(x-x_0)], \end{aligned} \tag{2}$$

within any large but finite region of space *and time*. For convenience units will be chosen so that the velocity of light, Planck's constant $\hbar$, and also the volume of the 4-dimensional region considered are all unity. Then (1) becomes

$$(\not{p}-m-f\gamma\cdot\textstyle\sum_k a_k E_k)K(p)=1, \tag{3}$$

where $\not{p}=\gamma_\lambda p^\lambda$ and E_k is the incremental operator which satisfies $E_k p=(p+k)E_k$, $E_kE_l=E_{k+l}$, etc., so that $E_kK(p)=K(p+k)$. For a system of n fermions, Eq. (3) is replaced by

$$\prod_{r=1}^{n}[\not{p}^{(r)}-m-f\gamma^{(r)}\cdot\textstyle\sum_k a_k E_k{}^{(r)}]K_n[p^{(1)},\cdots p^{(n)}]=1, \tag{4}$$

which, since the fermions do not interact, has the solution

$$K_n[p^{(1)},\cdots p^{(n)}]=K[p^{(1)}]\cdots K[p^{(n)}]. \tag{5}$$

It should be noticed that, whereas $K(p)$ is represented by a simple Dirac matrix with 2 spinor suffixes, $K_n[p^{(1)},\cdots p^{(n)}]$ is a *direct* product of n such factors and its representative has therefore $2n$ spinor suffixes; in (4), $\not{p}^{(r)}$ and $\gamma^{(r)}$ form matrix products with $K[p^{(r)}]$ but not with the other factors of K_n.

Our object in this section will be to determine how Eq. (4) should be modified to take into account not only the interactions of the n fermions with the external field, but also their mutual interactions and self interactions. We shall freely use the ideas of Feynman[8] in doing so, though one could no doubt obtain the same result by generalizing the rigorous field-theoretical method of Schwinger.[3]

The perturbation solution of (4) is

$$K_n=\prod_{r=1}^{n}\Big\{\sum_{s=0}^{\infty}\{[\not{p}^{(r)}-m]^{-1}f\gamma^{(r)}\cdot\textstyle\sum_k a_k E_k{}^{(r)}\}^s[\not{p}^{(r)}-m]^{-1}\Big\} \tag{6}$$

in which the sth term in the summation gives the probability amplitude that the rth particle will interact s times with the external field, within the region considered. Now consider the effect of applying the operator $-D_k(\partial^2/\partial a_k\cdot\partial a_{-k})$ to the right-hand side of (6), where D_k is the probability amplitude for the transmission of a boson with momentum k; this will remove factors a_k and a_{-k} in all possible ways, summing the results after multiplication by $-D_k$. So, according to Feynman, $-\frac{1}{2}\sum_k D_k(\partial^2K_n/\partial a_k\cdot\partial a_{-k})$ must be the probability amplitude for the fermions to interact any number of times with the external field, and just once among themselves. Similarly, $(s!)^{-1}[-\frac{1}{2}\sum_k D_k(\partial^2/\partial a_k\cdot\partial a_{-k})]^sK_n$ is the probability amplitude for the fermions to interact any number of times with the external field, and just s times among themselves. Therefore,[9]

$$G_n=\exp[-\tfrac{1}{2}\textstyle\sum_k D_k(\partial^2/\partial a_k\cdot\partial a_{-k})]K_n \tag{7}$$

is the probability amplitude for any number of external, and any number of mutual interactions. This is the Green's function which we wished to obtain. Regarded as a function of the a_k's, it has the property of a generating function for all scattering amplitudes involving n fermions. For, if G_n is developed in powers of the a_k's, thus:

$$G_n=\sum_{b(k)}G_n{}^*[b(k)]\textstyle\prod_k[b(k)!]^{-1}(a_k)^{b(k)}, \tag{8}$$

$G_n{}^*[b(k)]$ will be the exact scattering amplitude for the interaction of the set of n fermions with a boson distribution containing $b(k)$ bosons with momentum k. This is what one will primarily wish to calculate.

It should be remarked at this point that, if one wishes to take account of fermion loops, it is not sufficient to set $D_k=(k^2-\mu^2)^{-1}$, where μ is the boson mass; as shown by Schwinger,[3] D_k is a function of the a_k's, defined by

$$\{k^2-\mu^2+\mathrm{spur}[f\gamma\cdot E_{-k}\textstyle\sum_p(\partial/\partial a_k)G_1(\not{p})]\}D_k=1. \tag{9}$$

Like m, μ is given an infinitesimal imaginary part to ensure that all bosons will carry positive energy.

The expression (7) for G_n is very formal, and in practice it is better to make use of the equation, analogous to (9), which is satisfied by G_n; this is obtained by applying

[8] R. P. Feynman, Phys. Rev. **76**, 769 (1949).

[9] The author has received a preprint of a paper entitled "Field Equations in Functional Form" by S. F. Edwards and R. E. Peierls, which contains, in effect, a derivation of (7) from (10), for the special case $n=1$. Mention is made of a reverse derivation by T. H. R. Skyrme.

the operator $\exp\{-\frac{1}{2}\sum_k D_k(\partial^2/\partial a_k\cdot\partial a_{-k})\}$ to the Eq. (4) for K_n. Bearing in mind the operational form of Taylor's theorem $f(x+h)=\exp(hd/dx)f(x)$, the result is clearly

$$\prod_{r=1}^{n}[\not{p}^{(r)}-m-f\gamma^{(r)}\cdot\sum_k(a_k-D_k\partial/\partial a_{-k})E_k^{(r)}]G_n=1. \quad (10)$$

This will be written, for future convenience, in the form

$$\prod_{r=1}^{n}\{\not{p}^{(r)}-m-f[\gamma_k^{(r)}\cdot a_k-D_k\gamma_{-k}^{(r)}\cdot\partial/\partial a_k]\}G_n=1, \quad (11)$$

where $\gamma_k^{(r)}$ is short for $\gamma^{(r)}E_k^{(r)}$, and summation over repeated momentum suffixes is understood (as for tensor suffixes in general relativity theory).

A perturbation solution of Eq. (11) is readily obtained, thus:

$$G_n=\prod_{r=1}^{n}[\sum_{s=0}^{\infty}\{[\not{\mathbf{p}}^{(r)}-m]^{-1}f[\gamma_k^{(r)}\cdot a_k-D_k\gamma_{-k}^{(r)}\cdot\partial/\partial a_k]\}^s(\not{p}^{(r)}-m)^{-1}] \quad (12)$$

and one can verify directly that this solution generates the Feynman probability amplitudes in their usual form. The validity of the operational procedures used to derive (11) is thereby checked, but the solution itself has not much application except in quantum electrodynamics, owing to the fact that it is at best only semiconvergent. There do exist, however, various ways of transforming semiconvergent series to convergent series, and our main hope of obtaining meaningful results from field theories with medium or strong coupling seems to depend on finding such a way which is applicable to (12). An alternative way of posing the same problem is to demand a nonperturbation solution of (11). The task is complicated by the fact that even the individual terms on the right-hand side of (12) are not meaningful until they have been "renormalized." It is obviously desirable, if not necessary, to adapt the renormalization procedure to Eq. (11) as it stands, to have reasonable hope of obtaining any other solution in a meaningful form. This will be attempted in the following section.

3. THE "RENORMALIZATION" OF THE INTEGRAL EQUATIONS

It will be found that for the "renormalization" of Eq. (11), one needs to consider, in the first instance, only the special case with $n=1$. We shall therefore consider first

$$[\not{p}-m-f(\gamma_k a_k-D_k\gamma_{-k}\cdot\partial/\partial a_k)]G(p)=1. \quad (13)$$

According to Dyson[9] and Ward,[10] the divergences can be eliminated from this equation by writing ZG for G, YD_k for D_k, $Y^{\frac{1}{2}}a_k$ for a_k, $Y^{-\frac{1}{2}}f$ for f, and $m-\delta m$ for m, where Y, Z, and δm are suitably chosen constants. The result is

$$Z[\not{p}-m+\delta m-f(\gamma_k\cdot a_k-D_k\gamma_{-k}\cdot\partial/\partial a_k)]G(p)=1. \quad (14)$$

To make Z and δm precise, it is necessary to impose two conditions on $G(p)$, which can be formulated as follows. Let

$$\Gamma(p)=\{[G(p)]^{-1}\}_0 \quad (15)$$

denote the value of $[G(p)]^{-1}$ when all the a_k's are given the value zero; it is the reciprocal of Dyson's "renormalized" $S_F'(p)$. Also let

$$\Gamma_k(p)=-\{(\partial/\partial a_k)[fG(p)]^{-1}\}_0 \quad (16)$$

denote as usual the vertex function. Then δm and Z are to be chosen so that

$$\Gamma(q)=\not{q}-m, \quad \Gamma_0(q)=\gamma, \quad (17)$$

if q is a momentum satisfying $q^2=m^2$.

The elimination of Z and δm from (14) was attempted first by Utiyama, Sunakawa, and Imamura,[11] who, however, were compelled to resort to the perturbation expansion which it is the purpose of the method to avoid. A partial elimination has recently been effected by the author,[12] and this will now be carried to completion.

Equation (14) is first multiplied by $[G(p)]^{-1}$ from the right, the result being

$$Z[\not{p}-m+\delta m-f\gamma_k\cdot a_k+fD_k\gamma_{-k}\cdot(\partial G/\partial a_k)G^{-1}]=G^{-1}. \quad (18)$$

On account of the free operators E_k which are concealed in γ_k and $\gamma_{-k}(\partial G/\partial a_k)$, this step is not as trivial as it might appear; strictly it involves the expansion of the left-hand side of (14) in powers of the a_k's, separating the terms proportional to $\prod_k(a_k)^{b(k)}$, which are then multiplied from the right by $\{G[p+\sum_k b(k)k]\}^{-1}$, and finally reforming the equation. If

$$V(p)=[G(p)]^{-1}, \quad V_k(p)=-(\partial/\partial a_k)[fG(p)]^{-1}, \quad (19)$$

Eq. (18) becomes

$$V=Z(\not{p}-m+\delta m-f\gamma_k\cdot a_k)+Af^2D_k\gamma_{-k}\cdot GV_k. \quad (20)$$

Hence,

$$V_j=Z\gamma_j+Z\gamma_{-k}\cdot W_{jk}, \quad (21)$$

where

$$W_{jk}=-f(\partial/\partial a_j)(D_kGV_k). \quad (22)$$

[No summation over k is implied on the right-hand side of (22)]. In contrast with Γ_j, V_j represents a vertex at which any number of interactions with the external field may occur. The significance of W_{jk} is best described by saying that $(W_{jk}-f^2D_kGV_kGV_j)G$ is the amplitude for Compton scattering in an external field.

[9] J. C. Ward, Proc. Phys. Soc. (London) **A64**, 54 (1951); J. C. Ward, Phys. Rev. **78**, 182 (1950).

[11] Utiyama, Sunakawa, and Imamura, Progr. Theoret. Phys. (Japan) **8**, 77 (1952).

[12] H. S. Green, Proc. Phys. Soc. (London) **A66**, 873 (1952). A formal method applicable also to theories with scalar or pseudoscalar coupling was given by J. C. Ward, Phys. Rev. **84**, 897 (1951).

The elimination of Z from the second term on the right-hand side of (21) can be carried out in the following way. A new operator X_{jk} is defined in terms of W_{jk} by the equation

$$X_{jk}=W_{jk}-W_{-ik}X_{ji}. \tag{23}$$

This is formally an integral equation, with kernel W_{-ik} to determine X_{jk} when W_{jk} is known.[13] In practice, however, it never has to be solved because X_{jk} represents the same Feynman diagrams as W_{jk}, with the exception of all those which are reducible, in the sense that they can be obtained by joining simpler graphs end to end. In any approximate method of solving the integral equations, the solution X_{jk} of (23) will therefore be obtainable by inspection, being in fact a simpler expression than W_{jk} itself. Now, if one multiplies Eq. (23) on the left by $Z\gamma_{-k}$ and uses (21), one has

$$Z\gamma_{-k}\cdot X_{jk}=Z\gamma_{-k}\cdot W_{jk}-(V_{-i}-Z\gamma_{-i})X_{ji},$$

or, changing i to k in the last term,

$$Z\gamma_{-k}\cdot W_{jk}=V_{-k}X_{jk}. \tag{24}$$

Hence, (21) may be written

$$V_j=Z\gamma_j+V_{-k}X_{jk}. \tag{25}$$

This has the same form as an equation derived by Edwards,[4] who, however, did not define X_{jk} except in terms of perturbation series. The observation that X_{jk} represents a class of *irreducible* Compton-type graphs makes it clear that the summation (integration), implied by the double occurrence of the suffix k in (25), will not introduce any divergence which is not removable by the subtraction of a single constant $(1-Z)\gamma_j$.

The final elimination of Z from (25) involves the use of the second of Eqs. (17), from which it follows that

$$V_j(\boldsymbol{p})=\gamma_j+[V_j(\boldsymbol{p})-\Gamma_0(q)E_j](m+\boldsymbol{q})/(2m)+[V_j(\boldsymbol{p})-\Gamma_0(-q)E_j](m-\boldsymbol{q})/(2m). \tag{26}$$

Into the right-hand side of this equation one substitutes

$$V_j(\boldsymbol{p})-\Gamma_0(\pm q)E_j=V_{-k}(\boldsymbol{p})X_{jk}(\boldsymbol{p})-\Gamma_{-k}(\pm q)F_{0k}(\pm q)E_j, \tag{27}$$

where $F_{jk}(\boldsymbol{p})=[X_{jk}(\boldsymbol{p})]_0$ is what $X_{jk}(\boldsymbol{p})$ reduces to when the a_k's are set equal to zero. The result is a version of (21) from which the divergences have been explicitly cancelled.

A similar procedure can now be applied to Eq. (20). One first uses (25) to rewrite it in the form

$$V=Z(\boldsymbol{p}-m+\delta m)-fV_ka_k+f^2(V_{-k}-V_{-j}X_{-kj})D_kGV_k+fV_{-j}X_{kj}a_k. \tag{28}$$

Such divergences as arise from the summations in the last two terms of (28), taken together, can be removed by the subtraction of a single linear function of $\boldsymbol{p}$, $(1-Z)(\boldsymbol{p}-m+\delta m)$. To carry out the subtraction explicitly, use is made of the formula

$$V(\boldsymbol{p})=\boldsymbol{p}-m+\{V(\boldsymbol{p})-[1+(p_\lambda-q_\lambda)(\partial/\partial q_\lambda)]\Gamma(q)\}\times(m+\boldsymbol{q})/(2m)+\{V(\boldsymbol{p})-[1-(p_\lambda+q_\lambda)\times(\partial/\partial q_\lambda)]\Gamma(-q)\}(m-\boldsymbol{q})/(2m), \tag{29}$$

which follows directly from the first of Eqs. (17). Into the right-hand side of this equation, one substitutes from (28) and the equation

$$\Gamma(\pm q)=Z(\pm q-m+\delta m)+f^2[\Gamma_{-k}(\pm q)-\Gamma_{-j}(\pm q)F_{-kj}(\pm q)]D_kS(\pm q)\Gamma_k(\pm q), \tag{30}$$

to which it reduces, where all the a_k's vanish and $\boldsymbol{p}=\pm q$. The divergences then cancel, leaving an equation explicitly free of infinities.

It should be noticed that the freedom from divergences of the equations finally obtained is dependent on two or more terms, which separately contain divergent integrals, being evaluated together in such a way that the divergences cancel. There are various ways of doing this without risk of ambiguity in solving the equations; when the interaction $f\boldsymbol{\gamma}\cdot\boldsymbol{a}(x)$ contains a term of the type $e\gamma_\lambda\cdot a^\lambda(x)$, as in electrodynamics, one can most simply reduce (29) with the help of the identity[12]

$$\Gamma(\boldsymbol{p})-\Gamma(q)=(q-\boldsymbol{p})\cdot\Gamma_{q-\boldsymbol{p}}(\boldsymbol{p}). \tag{31}$$

In other cases, a relativistic cut-off procedure may be used consistently in the confidence that the cut-off constant cannot appear in any solution obtained.

The elimination of the infinities from the Eq. (9) after renormalization is complicated in meson theories because one has to introduce a direct interaction between the mesons to compensate for divergences introduced by the indirect interaction via pair production and annihilation. This complication will be avoided by ignoring fermion loops in the subsequent discussion, though of course they should be taken into account. The approximation involved amounts to setting $(k^2-\mu^2)$ for D_k. The generalization of the theory of this section to the many fermion problem will be discussed in Sec. 6. Meanwhile, we shall consider the principles involved in solving the equations already obtained.

4. TAMM-DANCOFF EQUATIONS AND THEIR TRANSFORMATION TO DIVERGENCE-FREE FORM

We shall now consider what can be done to obtain a solution of (14). There is little hope of solving this equation explicitly, involving as it does the infinitely many variables a_k, since this is not possible even for the much simpler Eq. (3). But from a formal point of view, (14) is a partial differential equation in the a_k's and requires a set of boundary conditions for the complete specification of its solution. The only obvious condition to impose is that G should be a regular function of a_k for

[13] X_{-jk} and $-W_{-jk}$ are reciprocal functions of the boson momenta in the sense of Volterra: see E. T. Whittaker and G. N. Watson's *Modern Analysis* (Cambridge University Press, London, 1940), Sec. 11.22.

$a_k=0$, and this makes a solution in the form

$$G=S-fS_ka_k+\tfrac{1}{2}f^2S_{kl}a_ka_l-\tfrac{1}{6}f^3S_{jkl}a_ja_ka_l+\cdots,$$
$$S=(G)_0,\quad S_k=-f^{-1}(\partial G/\partial a_k)_0, \tag{32}$$
$$S_{kl}=f^{-2}(\partial^2G/\partial a_k\partial a_l)_0,$$

a practical necessity. When this is substituted into (14), one obtains the infinite chain of equations

$$Z(\not p-m+\delta m)S=Zf^2D_f\gamma_{-j}\cdot S_j+1, \tag{33}$$

$$Z(\not p-m+\delta m)S_k+Z\gamma_kS=Zf^2D_f\gamma_{-j}\cdot S_{jk} \tag{34}$$

$$Z(\not p-m+\delta m)S_{kl}+Z(\gamma_kS_l+\gamma_lS_k)=Zf^2D_f\gamma_{-j}\cdot S_{jkl}, \tag{35}$$

etc. In order to solve this sequence of equations, it must be terminated by introducing some approximation on account of which one of the terms on the right-hand side either vanishes or can be simplified. The result will be a set of integral equations with the great advantage that it is linear in the unknowns and is therefore soluble in principle by existing methods. The Tamm-Dancoff method proceeds in this way.

We shall introduce here not the usual Tamm-Dancoff method, but an obviously covariant modification of it which may be described as follows. In the coordinate representation, an open 3-dimensional surface drawn through any point on the fermion trajectory will intersect a number of meson lines. The minimum number of meson lines intersected by such a variable surface depends only on the point on the fermion line selected. Configurations in which this minimum number exceeds a certain value n will be left out of consideration in the nth order approximation of the method adopted here. Thus, for example, S_{jkl} will certainly vanish in the second-order approximation.

To apply the method, it is necessary to know whether a particular meson is emitted or absorbed; this is possible if the sign of the 4th component of its momentum vector is given. We shall, therefore, henceforth adopt the convention that the 4th component of a momentum vector is always positive, replacing k by $-k$, etc., where necessary in the foregoing. The nth order approximation to any expression A_{-jkl} involving momentum suffixes will be denoted by $A_{-jkl}^{(n)}$. It is now easy to formulate rules concerning the nth order approximation to products of such expressions. One has, for instance, $(A_{-jkl}B_{ij})^{(n)}=A_{-jkl}^{(n-1)}B_{ij}^{(n)}$. The general rule is that the difference between the order of a factor and the order of the term in which it occurs is the sum of the number of unrepeated positive suffixes to the right of the factor and the number of unrepeated negative suffixes to the left of the factor. (The suffix to a factor D_j is ignored for this purpose, and a suffix to the right or left of the factor is repeated if it occurs also in the factor itself).

The approximation procedure just described affects the value of the renormalization constants Z and δm. Since $S_j^{(0)}=0$, it follows from (33) that $Z^{(0)}=1$ and $\delta m^{(0)}=0$, and

$$S^{(0)}=(\not p-m)^{-1}. \tag{36}$$

Similarly, from (34) one has

$$S_k^{(1)}=-(\not p-m)^{-1}\gamma_kS^{(1)}, \tag{37}$$

and by substitution in (33),

$$Z^{(1)}(\not p-m-\delta m^{(1)})S^{(1)}$$
$$=-f^2D_f\gamma_{-j}(\not p-m)^{-1}\gamma_jS^{(1)}+1. \tag{38}$$

It is fairly easy to eliminate the divergent constants $Z^{(1)}$ and $\delta m^{(1)}$ from (38), but in the higher order approximations, the elimination of the divergences is impossible with the Eqs. (33)–(35) etc., in their original form. Looking over the considerations of the previous section, the reason is obvious: it is G^{-1}, rather than G, which is easily "renormalized."

One is thus led to consider the expansion

$$V=G^{-1}=\Gamma-f\Gamma_ka_k+\tfrac{1}{2}f^2\Gamma_{kl}a_ka_l-\cdots, \tag{39}$$

in preference to (32). There certainly exists a set of simple relations between the coefficients of the two series:

$$S=\Gamma^{-1},\quad S_k=-S\Gamma_kS,$$
$$S_{kl}=-S(\Gamma_{kl}-\Gamma_kS\Gamma_l-\Gamma_lS\Gamma_k)S, \tag{40}$$

etc., but the Γ's are the only quantities to which the renormalization procedure can be directly applied. A particular case of this can be seen in the work of Fubini,[7] who proposed using the relation

$$S_{-kl}^{(2)}=-S^{(1)}[\Gamma_{-kl}^{(2)}-\Gamma_{-k}^{(1)}S^{(0)}\Gamma_l^{(1)}$$
$$-\Gamma_l^{(2)}S^{(2)}\Gamma_{-k}^{(2)}]S^{(1)} \tag{41}$$

to calculate the second-order approximation to the amplitude for meson-nucleon scattering, as defined above. [The method he suggested for obtaining a divergence-free $\Gamma_l^{(2)}$, however, does not work; the Eq. (47) below must be used].

The equations satisfied by the coefficients Γ, Γ_k, Γ_{kl}, etc., of (39) can be obtained either by substituting (40) in (33)–(35) etc., or more directly by substituting (39) in (20). They are

$$\Gamma=Z(\not p-m+\delta m)+Zf^2D_k\gamma_{-k}\cdot S\Gamma_k, \tag{42}$$

$$\Gamma_k=Z\gamma_k+Zf^2D_f\gamma_{-j}\cdot S(\Gamma_{jk}-\Gamma_kS\Gamma_j), \tag{43}$$

$$\Gamma_{kl}=Zf^2D_f\gamma_{-j}\cdot S(\Gamma_{jkl}-\Gamma_{kl}S\Gamma_j-\Gamma_kS\Gamma_{jl}-\Gamma_lS\Gamma_{jk}$$
$$+\Gamma_kS\Gamma_lS\Gamma_j+\Gamma_lS\Gamma_kS\Gamma_j), \tag{44}$$

etc. All the equations of this section have an obvious geometrical interpretation.

In proceeding from (33)–(35) to (42)–(44) the equations have lost their linear character. Fortunately this is restored by the method of approximation which has been suggested. Thus, (42) and (43) yield

$$\Gamma^{(n)}=Z^{(n)}[\not p-m+\delta m^{(n)}]$$
$$+Z^{(n-1)}f^2D_k\gamma_{-k}\cdot S^{(n-1)}\Gamma_k^{(n)}, \tag{45}$$

and

$$\Gamma_k^{(n)}=Z^{(n-1)}\gamma_k+Z^{(n-2)}f^2D_j\gamma_{-j}\cdot S^{(n-2)}[\Gamma_{jk}^{(n)}-\Gamma_k^{(n-1)}S^{(n-1)}\Gamma_j^{(n)}], \quad (46)$$

which are linear in the unknowns if $S^{(n-1)}$ and $\Gamma_k^{(n-1)}$ [and $S^{(n-2)}$] are supposed to be already determined.

For small values of n, no difficulty arises in eliminating the divergence from the equations thus obtained. As an example, (46) reduces for $n=2$ to

$$\Gamma_k^{(2)}=Z^{(1)}\gamma_k-f^2D_j\gamma_{-j}\cdot S^{(0)}\Gamma_k^{(1)}S^{(1)}\Gamma_j^{(2)}, \quad (47)$$

since, as may be seen from (44), $\Gamma_{kl}^{(2)}$ vanishes. The cancelling of the divergence $[Z^{(1)}-1]\gamma_k$ from a corresponding divergence in the second term is now readily effected. But in higher approximations it is necessary to adhere closely to the method of the previous section. Setting the a_k's equal to zero, the function W_{jk} defined by (22) reduces to

$$R_{jk}=f^2D_jS(\Gamma_{jk}-\Gamma_kS\Gamma_j), \quad (48)$$

and X_{jk} to F_{jk}, where, according to (23),

$$F_{jk}=R_{jk}-R_{-ik}X_{ji}. \quad (49)$$

Instead of the Eq. (46), one will use

$$\Gamma_j^{(n)}=Z^{(n-1)}\gamma_j+\Gamma_{-k}^{(n)}F_{jk}^{(n)}, \quad (50)$$

in which $F_{jk}^{(n)}$ is supposed to be already known. Also, from (28) with the a_k's set equal to zero, one has

$$\Gamma^{(n)}=Z^{(n)}(\not{p}-m+\delta m)+f^2[\Gamma_{-k}^{(n)}-\Gamma_{-j}^{(n)}F_{-kj}^{(n)}]D_kS^{(n-1)}\Gamma_k^{(n)}. \quad (51)$$

The exact order in which the various functions can be determined will be indicated in the next section.

5. SOLUTION OF THE EQUATIONS

To discuss systematically the principles involved in the solution of the system of equations already obtained, it will be necessary to introduce a new general class of scattering amplitudes, typified by $L(j_1\cdots j_r,k_1\cdots k_s)S$, where the factor S, inserted for convenience, is defined in (32). Here $j_1\cdots j_r$ denote the energy-momenta of external bosons absorbed by the fermion considered, in the order of their absorption along the fermion line; $k_1\cdots k_s$ denote the energy-momenta of external bosons emitted by the fermion, in the *reverse* order of their emission along the fermion line. Since the j's and k's represent boson momenta, they would appear in the foregoing discussion as suffixes, the k's prefixed by a negative sign. But to obtain functions of the type hitherto considered, one would have to sum $L(j_1\cdots j_r,k_1\cdots k_s)$ over all permutations of the j's and k's.

We shall wish also to consider the function $L_m^{(n)}(j_1\cdots j_r,k_1\cdots k_s)$ which represents a contribution to $L(j_1\cdots j_r,k_1\cdots k_s)$ from certain configurations: namely, those for which (in the coordinate representation) the minimum number of boson lines intersected by an open 3-dimensional surface through any point on the fermion line is never less than m nor greater than n. It accordingly represents an nth order approximation, of the type already considered, to a function $L_m(j_1\cdots j_r,k_1\cdots k_s)$ representing configurations in which at least m bosons are always "present." It should be noticed that $L_m(j_1\cdots j_r,k_1\cdots k_s)$ vanishes if $m>r$ or $m>s+1$. For $m=0$, L_m reduces to the total scattering amplitude L, and can be expressed in the form

$$L_0(j_1\cdots j_r,k_1\cdots k_s)=L_1(j_1\cdots j_r,k_1\cdots k_s)+L_1(j_1\cdots j_r,-)SL_1(-,k_1\cdots k_s). \quad (52)$$

Since $S^{(n)}=[\Gamma^{(n)}]^{-1}$ can be expressed in terms of $L_1^{(n)}(j,-)$, $L_2^{(n)}(j,k)$, $L_1^{(n)}(-,k)$ and $S^{(n-1)}$ with the help of (51), the problem of obtaining $L_0^{(n)}$ is reduced in principle to that of obtaining $L_1^{(n)}$ and $L_2^{(n)}$, when $L_m^{(n-1)}$ ($m=0$, 1, 2 etc.) are assumed to be already determined.

The equations satisfied by the newly defined functions can be inferred from those of the previous section. It follows from (40), (43), and (44), for example, that

$$L_1^{(2)}(j,k)=S^{(1)}[\gamma_{-k}S^{(0)}\gamma_j-f^2D_l\gamma_{-k}S^{(0)}\gamma_jL_1^{(2)}(l,k)], \quad (53)$$

and (47) may be written

$$L_1^{(2)}(j,-)=S^{(1)}[Z^{(1)}\gamma_j-f^2D_l\gamma_{-k}S^{(0)}\gamma_jL_1^{(2)}(l,-)]. \quad (54)$$

Any of these equations has an adjoint, obtained by reversing the order of the factors in any product, and interchanging the j's and k's in $L_m^{(n)}(j_1\cdots j_r,k_1\cdots k_s)$. Equations of this type can of course be written down at once from graphical considerations similar to those used in formulating the Bethe-Salpeter equation.[14] In fact, analytical relations can be obtained in this way which one would not easily discover otherwise, though they are relatively easy to prove analytically when known. For example, one has

$$L_2^{(3)}(j_1j_2,k_1k_2)=L_1^{(2)}(j_1,k_2)L_1^{(2)}(j_2,k_1)-f^2L_1^{(2)}(j_1,l)D_lL_2^{(3)}(j_2l,k_1k_2), \quad (55)$$

$$L_2^{(3)}(j_1j_2,k)=L_1^{(2)}(j_1,k)L_1^{(2)}(j_2,-)-f^2L_1^{(2)}(j_1,l)D_lL_2^{(3)}(j_2l,k), \quad (56)$$

and

$$L_1^{(3)}(j_1j_2,k_1k_2)=L_0^{(2)}(j_1,k_2)L_0^{(3)}(j_2,k_1)-f^2L_0^{(2)}(j_1,l)D_lL_1^{(3)}(j_2l,k_1k_2), \quad (57)$$

$$L_1^{(3)}(j_1j_2,k)=L_0^{(2)}(j_1,k)L_0^{(2)}(j_2,-)-f^2L_0^{(2)}(j_1,l)D_lL_1^{(3)}(j_2l,k), \quad (58)$$

$$L_1^{(3)}(j,k)=L_0^{(2)}(-,k)L_0^{(2)}(j,-)-f^2L_0^{(2)}(-,l)D_lL_1^{(3)}(jl,k). \quad (59)$$

To continue, one has

$$\begin{aligned}L_3^{(4)}&(j_1j_2j_3,k_1k_2k_3)\\&=L_2^{(3)}(j_1j_2,k_2k_3)L_1^{(2)}(j_3,k_1)-f^2[L_2^{(3)}(j_1j_2,k_3l)\\&\quad+L_2^{(3)}(j_1j_2,lk_3)]D_lL_2^{(3)}(j_3l,k_1k_2)\\&\quad+f^4[L_2^{(3)}(j_1j_2,il)+L_2^{(3)}(j_1j_2,li)]\\&\qquad\times D_iD_lL_3^{(4)}(j_3il,k_1k_2k_3),\end{aligned} \quad (60)$$

[14] E. E. Salpeter and H. A. Bethe, Phys. Rev. **84**, 1232 (1951).

etc. Though the equations become more complicated as one proceeds, their mode of formation is fairly obvious.

The computation of successively higher approximations to L_m in this way involves nothing worse than the computation of convergent integrals and the solution of integral equations of the general type

$$\varphi_\lambda(j,l)=f_\lambda(j,l)+\int K_{\lambda\mu}(j,k)\varphi_\mu(k,l)dk, \qquad (61)$$

where j, k, and l represent sets of momenta $j_1,\cdots j_r$, $k_1\cdots k_r$, and $l_1\cdots l_s$, the integration $\int\cdots dk$ denotes integration over all components of the 4-vectors $k_1\cdots k_r$, and λ, μ are spinor suffixes summed from $1\cdots 4$ when repeated in any term. This is a somewhat generalized form of Fredholm's equation, the solution of which is

$$\varphi_\lambda(j,l)=f_\lambda(j,l)+D^{-1}\int D_{\lambda\mu}(j,k)f_\mu(k,l)dk, \qquad (62)$$

where

$$D=1-\int K_{\lambda\lambda}(k,k)dk+(2!)^{-1}\times\int\int\begin{vmatrix}K_{\lambda\lambda}(k,k)K_{\mu\lambda}(k',k)\\K_{\lambda\mu}(k,k')K_{\mu\mu}(k',k')\end{vmatrix}dkdk'-(3!)^{-1}\int\int\int\cdots, \qquad (63)$$

and

$$D_{\lambda\mu}(j,k)=K_{\lambda\mu}(j,k)-\int\begin{vmatrix}K_{\lambda\mu}(j,k)K_{\nu\mu}(k',k)\\K_{\lambda\nu}(j,k')K_{\nu\nu}(k',k')\end{vmatrix}dk'+(2!)^{-1}\int\int\cdots. \qquad (64)$$

The series in (63) and (64) are *absolutely convergent*, provided the integral $\int\int|K_{\lambda\mu}(k,k')|^2dkdk'$ exists; and the only difficulty in satisfying this condition arises in connection with Eqs. (53) and (54), which will be discussed presently. It follows that the only singularities in $\varphi_\lambda(j,l)$, which are not already present in $f_\lambda(j,l)$ or the kernel, arise from the vanishing of D. When $D=0$, there is no solution of (61), though there does exist a solution of the corresponding homogeneous equation

$$\varphi_\lambda(j,l)=\int K_{\lambda\mu}(j,k)\varphi_\mu(k,l)dk, \qquad (65)$$

which is of the type proposed by Salpeter and Bethe[14] for bound states.

We shall accordingly take the point of view that any zero of $D_n^{(n+1)}$—the value of D corresponding to a kernel K formed from $L_{n-1}^{(n)}$—is associated with a bound state of the fermion and n bosons (a hyperon in nuclear theory). This point of view is justified by the fact that amplitudes, solutions of (65), exist for the creation of such bound states through the successive absorption of n bosons by the "bare" fermion. The states so defined are highly idealized because the true amplitudes do not describe exclusively configurations in which the number of bosons "present" varies within such narrow limits. An actual hyperon will fluctuate continually between the ideal state and other ideal states; such fluctuations, however, are virtual and may be regarded as self-energy processes of the hyperon concerned. The suggestion is simply that all processes, both real and virtual, can be conveniently interpreted in terms of transitions of the fermion between states, in any particular one of which the number of virtual bosons "present" is either n or $n+1$.

It should be noticed that $D_n^{(n+1)}$ is a function of w^2, where w is the resultant energy momentum vector of the system of the fermion with its n or $n+1$ bosons, and that for sufficiently large values of w^2, $D_n^{(n+1)}$ is complex. The roots of the equation $D_n^{(n+1)}(w^2)=0$ are therefore of the form $w^2=(M_n^{(n+1)}+iN_n^{(n+1)})^2$, where $M_n^{(n+1)}$ may be regarded as the mass of the ideal hyperon and $N_n^{(n+1)}$ as its reciprocal lifetime—which may be very large. The effect of virtual transitions to other ideal states will be to modify the mass value and lifetime so determined. So far as transitions to states with fewer bosons "present" are concerned, one can allow for this by solving the equation $D_1^{(n+1)}(w^2)=0$ instead of $D_n^{(n+1)}(w^2)=0$; but to take into account transitions to states with more than n bosons "present," one would have to raise the order of approximation of the kernel from which $D_1^{(n+1)}$ is formed.

It is known[15] that the right-hand side of (63) can be obtained by expanding the exponential, and regrouping the terms so obtained, on the right-hand side of

$$D^*=\exp\Big[-\int K_{\lambda\lambda}(j,j)dj-\tfrac{1}{2}\int\int K_{\lambda\mu}(j,k)K_{\mu\lambda}(k,j)djdk-\tfrac{1}{3}\int\int\int K_{\lambda\mu}(j,k)K_{\mu\nu}(k,l)\times K_{\nu\lambda}(l,j)djdkdl-\cdots\Big]. \qquad (66)$$

In fact, $D=D^*$ within the range in which the exponent of (66) is meaningful. The "first" zero of D therefore corresponds to the radius of convergence of the series in (66), and can be obtained by solving the equation

$$\int^{(n)}\cdots\int K_{\lambda\mu}(j_1,j_2)K_{\mu\nu}(j_2,j_3)\cdots\times K_{\omega\lambda}(j_n,j_1)dj_1\cdots dj_n=1 \qquad (67)$$

[15] See E. Hellinger and O. Toeplitz, *Integralgleichungen* (Teubner, Leipzig, 1928), Sec. 11.

for sufficiently large values of n. The identity of D and D^*, within their common range of significance, enables one to see the connection between Fredholm's and Liouville's solutions of (61), for

$$D_{\lambda\mu}{}^*(j,k)=D^*\Big[K_{\lambda\mu}(j,k)+\int K_{\lambda\mu}(j,l)K_{\mu\nu}(l,k)dl+\cdots\Big] \quad (68)$$

defines a function which, where it exists, is equivalent to that defined by (64).

We return now to the consideration of the difficulties, additional to those resolved by ordinary renormalization procedures, which arise in the solution of (52) and (53), as well as similar equations of higher order. The kernel for both (52) and (53) is

$$K(j,k)=-f^2S^{(1)}(w-j)\gamma_{-k}D_kS^{(0)}(w-j-k)\gamma_j,$$

and the integrals $\mathrm{spur}\int K(j,j)dj$, $\mathrm{spur}\iint K(j,k)\times K(k,j)djdk$, which appear in Fredholm's solution of these equations are logarithmically divergent. Let the divergent parts of these integrals, constants chosen so that the convergent remainders vanish when $w^2=m^2$, be C_1, C_2, C_3, etc. Then it is clear from (66) that if $\exp(C_1+\frac{1}{2}C_2+\frac{1}{3}C_3+\cdots)D^*$ is expanded and the terms of the expansion suitably regrouped, the divergences will cancel identically. Also, if $\exp(C_1+\frac{1}{2}C_2+\frac{1}{3}C_3+\cdots)\times D_{\lambda\mu}{}^*(j,k)$ is expanded and the terms of the expansion regrouped, the divergences will cancel identically. In the solution of (53), but not of (52), additional divergences appear; these, however, can be eliminated by standard renormalization methods, in the course of which the divergent constant Z is reduced to 1.

One indisputable conclusion, which can be drawn from the above considerations, is that the singularities in the Tamm-Dancoff amplitudes are all associated with the existence of (not necessarily observable) bound states. If $L_m{}^{(n)}$ approached a limiting value L_m when n became very large, it could be concluded immediately that all singularities in the exact amplitudes were likewise associated with bound states of the type contemplated. Unfortunately $L_m{}^{(n)}$ does not approach a limiting value, as we shall immediately demonstrate.

It is sufficient for our purpose to notice a contribution to the amplitude for the scattering of a single boson by a fermion, namely $-f^2S\Gamma_j'S\Gamma_{-k}'S$, where Γ_j' is defined by

$$\Gamma_j'=Z'\gamma_j-f^2\gamma_{-l}D_lS^{(0)}\Gamma_j'S^{(0)}\gamma_l. \quad (69)$$

This is an equation of the type whose explicit solution was attempted by Edwards; he obtained a solution of the homogeneous equation for a particular case, but nothing corresponding to the general Fredholm solution—probably because of the divergences, not removed by ordinary renormalization procedure, which have already been noticed in connection with the similar Eq. (53). Now the nth order approximation to the solution of (69) is a polynomial of the nth degree in f^2. The general solution does not approach a limiting value for large n, as one can infer from the mere existence of a solution of the homogeneous equation with $Z'=0$.[16]

To discover the physical reason for this failure of the Tamm-Dancoff method, it should be noticed that (69) is an equation of Fredholm's type, and the divergence of the solution when expressed as a power series in f^2 is a consequence of the existence of a zero of the Fredholm denominator corresponding to the kernel $-f^2D_j[\gamma_{-\rho}S^{(0)}]_{\lambda\mu}[S^{(0)}\gamma_j]_{\sigma\rho}$. The latter is precisely the lowest order approximation to the kernel of the original Bethe-Salpeter equation for bound states of a pair of fermions. The vanishing of the particular Fredholm denominator we are considering is therefore associated with the existence of such bound states. Fermion pairs in a bound state can be created in the vacuum, and these will influence the amplitudes for scattering of bosons by a single fermion. Quite generally the existence of bound states of a system of n fermions will spoil the convergence of the Tamm-Dancoff method applied to a single fermion. Very probably the existence of such bound states is also the *only* cause of failure of the approximation method we have examined; if this is conceded, two conclusions may be drawn. Firstly, the singularities in scattering amplitudes—which are the prime cause of the failure of the perturbation series—are all associated in one way or another with transitions, real or virtual, to bound states. Secondly, if account could be taken of bound states involving any number of fermions, the failure of the Tamm-Dancoff method of approximation applied to the single fermion problem would be removed. Without attempting a detailed solution of the problems thus raised, we shall therefore briefly examine the generalization of the previous considerations to systems of more than one fermion.

6. THE MANY-FERMION PROBLEM

The interaction of a system of n fermions with a boson field is completely described by the generating function G_n, which is the solution of Eq. (11). This equation, when formally renormalized, assumes the form

$$Z^n\prod_{r=1}^{n}\{\not{p}^{(r)}-m+\delta m-f[\gamma_k{}^{(r)}\cdot a_k-D_k\gamma_{-k}{}^{(r)}\cdot(\partial/\partial a_k)]\}G_n=1. \quad (70)$$

One can write down immediately a partial solution of (70), which effectively reduces the many-fermion problem to the single-fermion problem already considered; it is

$$Z\{\not{p}^{(n)}-m+\delta m-f[\gamma_k{}^{(n)}\cdot a_k-D_k\gamma_{-k}{}^{(n)}\cdot(\partial/\partial a_k)]\}G_n=G_{n-1}. \quad (71)$$

[16] At the particular value of the total energy for which Edwards solved the equation, the Fredholm denominator vanishes for a rather large value of the coupling constant, which would have to be exceeded before the perturbation series diverged. At other energies the divergence would occur sooner. See also J. S. Goldstein, Phys. Rev. **91**, 1516 (1953) and a paper by the author to appear soon in Proc. Phys. Soc. (London) **A**.

As a matter of interest, one can construct from this the Schrödinger-like equation

$$Z\sum_{r=1}^{n}\{p^{(r)}-m+\delta m-f[\gamma_k^{(r)}\cdot a_k - D_k\gamma_{-k}^{(r)}\cdot(\partial/\partial a_k)]\}G_n=\sum_{r=1}^{n}G_{n-1}^{(r)}, \quad (72)$$

where $G_{n-1}^{(r)}$ is the function G_{n-1} with a set of energy-momenta $p^{(1)}\cdots p^{(n)}$, excluding $p^{(r)}$, as its arguments. This last equation, though more symmetrical, is not fully equivalent to (71), which is therefore to be preferred.

In considering (71) further, we shall write p for $p^{(n)}$ and γ_k for $\gamma_k^{(n)}$ for the sake of simplicity and to avoid confusion with the notation developed in the previous two sections. It will be found convenient also to set

$$G_n=GG_{n-1}H_n, \quad (73)$$

where G is the function of p, i.e., $p^{(n)}$, considered exclusively in No. 3 and No. 4. When (73) is substituted into (72), and use is made of the equation satisfied by G, (72) reduces to

$$G_{n-1}H_n+ZfD_k\gamma_{-k}\cdot G[(\partial G_{n-1}/\partial a_k)H_n + G_{n-1}(\partial H_n/\partial a_k)]=G_{n-1}. \quad (74)$$

Dividing by G_{n-1} on the left and H_n on the right gives

$$H_n^{-1}=1-ZfD_k\gamma_{-k}\cdot G[(\partial G_{n-1}^{-1}/\partial a_k)G_{n-1} + H_n(\partial H_n^{-1}/\partial a_k)]. \quad (75)$$

Here $Z\gamma_{-k}$ may be replaced by $\Gamma_{-k}-\Gamma_{-l}X_{-kl}$, completing the elimination of the divergent constants.

The functions most easily expressed in a divergence-free form are clearly the coefficients U, U_k, etc., in the expansion

$$H_n^{-1}=U-fU_ka_k+\tfrac{1}{2}f^2U_{kl}a_ka_l-\cdots. \quad (76)$$

When these coefficients have been determined, it will be possible to determine G_n in the form

$$G_n=GG_{n-1}U^{-1}\{1+f[U_k+\tfrac{1}{2}f(U_kU^{-1}U_1 + U_1U^{-1}U_k-U_{kl})a_l]a_kU^{-1}+\cdots\}. \quad (77)$$

The equations satisfied by U, U_k, etc., are easily written down from (75); one has

$$U=1+Zf^2D_k\gamma_{-k}\cdot S(P_k+U^{-1}U_k), \quad (78)$$

$$U_l=Zf^2D_k\gamma_{-k}\cdot S_lS(P_k+U^{-1}U_k) + Zf^2D_k\gamma_{-k}\cdot S[P_{kl}+U^{-1}(U_{kl}-U_lU^{-1}U_k)], \quad (79)$$

etc., if

$$(\partial G_{n-1}^{-1}/\partial a_k)G_{n-1}=P_k-fP_{kl}a_l+\cdots. \quad (80)$$

The Eqs. (78), (79), etc., are very closely analogous to those connecting Γ, Γ_l, etc., and this fact alone suggests that they should be soluble by an approximation procedure similar to that developed in No. 4. Thus, for example, (78) yields at the nth approximation

$$U^{(n)}=1+Zf^2D_k\gamma_{-k}\cdot S^{(n-1)}\{P_k^{(n)}+[U^{(n-1)}]^{-1}U_k^{(n)}]. \quad (81)$$

One has, accordingly, at one's disposal at least one method of solving the equations which does not depend on a perturbation expansion at any stage.

The method thus sketchily indicated for the solution of the many-nucleon problem leaves one still very far from an exact convergent solution to even the single-fermion problem. What is needed to carry one further is a system of classifying the bound states which arise in many-fermion-boson interactions, and a somewhat less restricted method of approximation which ultimately takes all such states into account. There is reasonable hope that these can be found; but until they are found, one will not be able to say with certainty whether the exact equations of field theory are soluble in principle, or not.

The author acknowledges the assistance of Mr. I. E. McCarthy in proving a few of the formulas of this paper, and discussions with Dr. J. C. Ward.

Letters to the Editor

PUBLICATION of brief reports of important discoveries in physics may be secured by addressing them to this department. The closing date for this department is five weeks prior to the date of issue. No proof will be sent to the authors. The Board of Editors does not hold itself responsible for the opinions expressed by the correspondents. Communications should not exceed 600 words in length and should be submitted in duplicate.

Anisotropy of Cyclotron Resonance of Holes in Germanium*

R. N. DEXTER, *Lincoln Laboratory, Massachusetts Institute of Technology, Cambridge, Massachusetts, and University of Wisconsin, Madison, Wisconsin*

AND

H. J. ZEIGER AND BENJAMIN LAX, *Lincoln Laboratory, Massachusetts Institute of Technology, Cambridge, Massachusetts*

(Received June 1, 1954)

SEVERAL investigators[1,2] have reported cyclotron resonance of holes and electrons in germanium at liquid helium temperatures. Recently, we have performed similar experiments at 8900 and 23 000 Mc/sec using infrared instead of rf excitation of carriers. This technique considerably improved the quality of the data because very low rf power levels could be used, thus avoiding rf ionization and the resulting changes in carrier concentration with dc magnetic field. These experiments were carried out on oriented single crystal samples of p- and n-type germanium which had room temperature resistivities of about 40 ohm-cm.

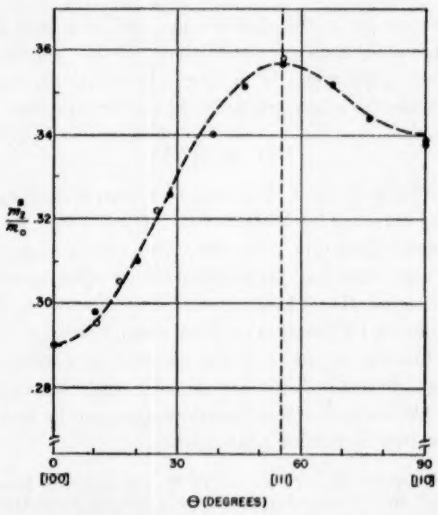

FIG. 1. The ratio of m_2^* to m_0 as a function of the angle θ between the [100] direction and the magnetic field in the (110) plane. The open and solid circles are experimental points taken at 23 000 and 8900 Mc/sec, respectively. The dashed curve is a theoretical function, Eq. (2).

With rf impact ionization, the two hole resonances in germanium, corresponding to effective masses of $m_1^*=0.04$ (m_0 and $m)_2^*=0.3m_0$ (m_0 is the free electron mass) showed no directional effects.[1,2] Under infrared excitation and very low rf excitation, we have observed anisotropy in the cyclotron resonance associated with the holes of effective mass m_2^*, as shown in Fig. 1.

The cyclotron resonance associated with the holes of small effective mass was approximately isotropic with $m_1^*=0.042m_0$. However, there were indications of a slight anisotropy with minimum effective mass when the magnetic field was in the [111] direction.

When infrared excitation was used, the intensity of the high-mass resonance was about eight times that of the low-mass one. The collision times for the two kinds of holes, as calculated from the line widths, were about equal. A typical value of collision time was about 6×10^{-11} seconds.[3]

The two resonances were interpreted in terms of a model for the top of the valence band in germanium[4] in which the energy E as a function of the wave vector, $\mathbf{k}$, is

$$E=(\hbar^2/2m_0)\times\{ak^2\pm[bk^4+c(k_x^2k_y^2+k_x^2k_z^2+k_y^2k_z^2)]^{\frac{1}{2}}\}, \quad (1)$$

where a, b, and c are constants. The plus and minus signs are associated with m_1^* and m_2^*, respectively. The radical was expanded to first order (the second order term in the expansion would contribute about 7 percent) and a perturbation method gave the frequencies for cyclotron motion. To first order, the effective masses for resonance with the magnetic field in the (110) plane, assuming $\mathbf{k}\cdot\mathbf{H}=0$, have the form

$$m^*=m_0\{A+B(1-3\cos^2\theta)^2\}, \quad (2)$$

where A and B are constants depending only on a, b, and c, which appear in Eq. (1). The constants, evaluated by fitting to the low-field peak and the high-field peaks in the [100] and [111] directions, are $a=13.6$, $b=83$, and $c=126$. An anisotropy in m_1^* of about 2 percent was predicted from these values. This prediction is consistent with the observations.

According to the above interpretation, the constant energy surfaces of the Brillouin zone near the top of the valence band in germanium are two sets of surfaces centered about $k=0$. These surfaces are nearly spherical for the holes of mass m_1^*. For the holes of mass m_2^*, they are perturbed spherical surfaces, protruding outward along the [111] axes.

We would like to express our thanks to Professor H. Brooks for his helpful suggestions concerning germanium band structure. We are happy to acknowledge interesting discussions with Drs. E. N. Adams, II,

and Esther Conwell. Thanks are due Dr. D. Tuomi for orienting the samples, and other members of the solid state groups of Lincoln Laboratory for their assistance.

* The research in this document was supported jointly by the Army, Navy, and Air Force under contract with the Massachusetts Institute of Technology.

[1] Dresselhaus, Kip, and Kittel, Phys. Rev. **92**, 547 (1953).

[2] Lax, Zeiger, Dexter, and Rosenblum, Phys. Rev. **93**, 1418 (1954).

[3] This is an approximate upper limit since the resonance line is presumably broadened by distribution of velocities in the direction of the magnetic field.

[4] C. Kittel, Phys. Rev. **94**, 768 (1954); H. Brooks (private communication); W. Shockley, Phys. Rev. **78**, 173 (1950).

Kinetic Properties of the Domains in Rochelle Salt*

Toshio Mitsui and Jiro Furuichi
Faculty of Science, Hokkaido University, Sapporo, Japan
(Received May 17, 1954)

As has been previously reported by the present writers,[1] the relation between the propagation velocity v of the domain wall in Rochelle salt and the electric field E is in general given by

$$\gamma v = 2P_s(E - E_0),$$

where P_s is the saturation polarization and both γ and E_0 are constants. Further investigations have proved that γ is structure-sensitive as well as E_0 and that the temperature dependency of the relation is as shown in Fig. 1. The fact that the curves are almost parallel to each other suggests that γ is roughly proportional to P_s, i.e.,

$$\gamma = \alpha P_s,$$

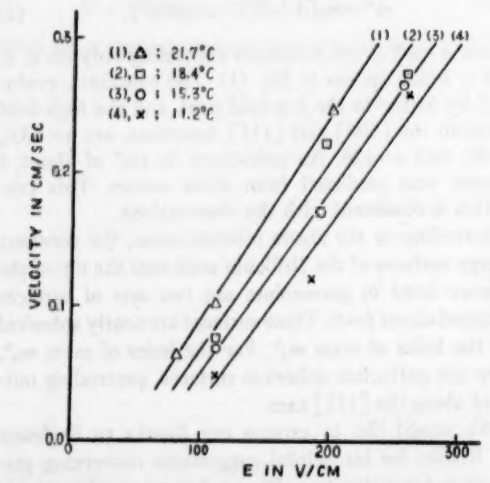

FIG. 1. Propagation velocity of the domain wall as a function of the electric field and the temperature.

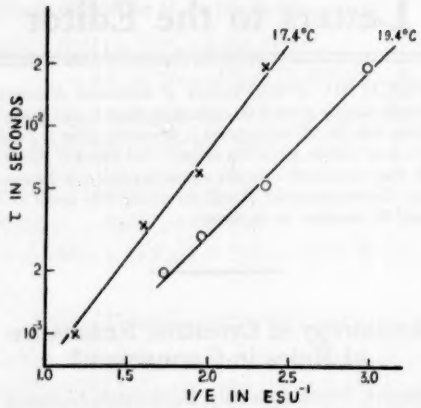

FIG. 2. Relation between the relaxation time for nucleation of the domain, τ, and the electric field, E. The ordinate, is scale logarithmic.

where α is a structure-sensitive constant. This relation implies that γ is proportional to the structure change of the crystal due to the passage of the wall, since the spontaneous deformation y_s is proportional to P_s.

As has been reported by M. Marutake[2] and T. Nakamura,[3] many new domains appear when an electric field is applied along the a axis. The writers' observations have revealed that the new domains come into view at the same places in the crystal when application and withdrawal of the field are repeated, a fact suggesting that the nucleation of the domain takes place at some crystal imperfections. The relaxation time of the appearance of the new domains was measured by means of a rotating sector and a square-wave voltage as in the case of the study of the propagation velocity of the wall.[1] It has been found that the relaxation time τ can be expressed well by the equation

$$\tau = \tau_0 \exp(C/E),$$

where both τ_0 and C are constants, analogously to the results obtained by Merz[4] for $BaTiO_3$ (see Fig. 2). The measured values of C have the same order of magnitude with each other and in general decrease with increasing temperature above 15°C.

A detailed discussion of these results will appear in the *Journal of the Physical Society of Japan*. The writers wish to thank Dr. P. W. Anderson for his valuable discussions and for information on the research at the Bell Telephone Laboratories.

* This work has been supported by the Scientific Research Expenditure and the Scientific Research Subsidy of the Ministry of Education

[1] T. Mitsui and J. Furuichi, Phys. Rev. **90**, 193 (1953).

[2] M. Marutake, J. Phys. Soc. Japan **7**, 25 (1952).

[3] T. Nakamura, Repts. Inst. Sci. and Technol., Univ. Tokyo **7**, 113 (1953).

[4] W. J. Merz, Phys. Rev. (to be published).

Infrared Absorption Spectrum of Germanium*

L. H. HALL,† J. BARDEEN, AND F. J. BLATT
Department of Physics, University of Illinois, Urbana, Illinois
(Received May 24, 1954)

WE have calculated the optical absorption by valence electrons in pure germanium for "direct" and "indirect" transitions to the conduction band. The "direct" transitions are those in which the valence electron absorbs a photon, the propagation vector **k** of the electron remaining essentially constant. In the case of the "indirect" transitions the electron absorbs a photon and also suffers a substantial change of its **k** vector, momentum conservation being achieved by the absorption or emission of a phonon.

The band structure which was assumed for this calculation is shown in Fig. 1, and is based on previous calculations of Herman,[1] and Herman and Callaway,[2] and on cyclotron resonance experiments.[3,4] It is evident from this structure that the long wavelength absorption limit for the direct transitions occurs at a wavelength $\lambda_d=0.86$ microns, corresponding to the energy difference $E_{c0}-E_v=1.45$ ev, and that this wavelength is shorter than the long-wavelength limit for the indirect transitions $\lambda_i=1.8$ microns, corresponding to the energy difference $E_c-E_v=0.7$ ev.

Because the indirect transitions are of second order as compared to the direct transitions, one may expect that the probability for the former is less than the probability for the latter. If the probability for the indirect transitions is many orders of magnitude smaller than for the direct transitions, the former could not be observed, and the long wavelength limit of the absorption spectrum would appear at $\lambda=\lambda_d$. If, however, the probability for indirect transitions is reduced by only a few orders of magnitude in relation to the direct transitions, a tail at the long wavelength end of the spectrum should appear, the ultimate absorption limit being at $\lambda=\lambda_i$.

The calculation follows the usual time-dependent perturbation procedure. One obtains the following expressions for the rate of absorption of energy by direct and indirect transitions, respectively:

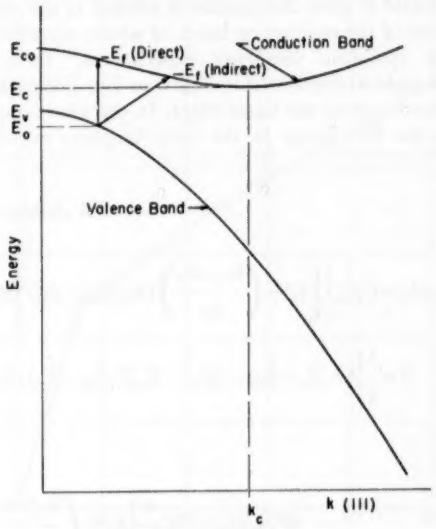

FIG. 1. Assumed band structure of germanium.

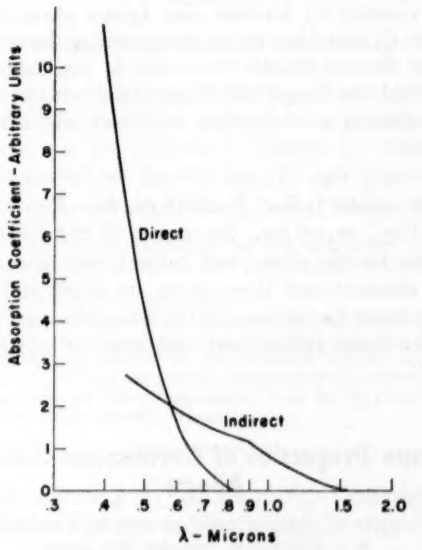

FIG. 2. Absorption coefficients for "direct" and "indirect" transitions as functions of wavelength. The ordinates have been chosen such that $A_d(\lambda_d-\Delta\lambda)/A_i(\lambda_i-\Delta\lambda)=10$.

$$W_d=\int\int\left\{\frac{2\pi t}{\hbar^2}\delta\left[(E_f-E_0-\hbar\omega)\frac{t}{\hbar}\right]\right\}\{|H'|^2\}\left\{\frac{8\pi\omega^2 d\omega}{(2\pi c)^3}\right\}\left\{\frac{1}{4\pi^2}\left(\frac{2m_v}{\hbar^2}\right)^{\frac{3}{2}}(E_v-E_0)^{\frac{1}{2}}dE_0\right\}, \quad (1)$$

$$W_i=N\int\int\int\left\{\frac{2\pi t}{\hbar^2}\delta\left[(E_f-E_0-\hbar\omega)\frac{t}{\hbar}\right]\right\}\{|H''|^2\}\left\{\frac{8\pi\omega^2 d\omega}{(2\pi c)^3}\right\}$$

$$\times\left\{\left(\frac{1}{4\pi^2}\right)^2\left(\frac{2m_v}{\hbar^2}\right)^{\frac{1}{2}}\left(\frac{2m_c}{\hbar^2}\right)^{\frac{3}{2}}[(E_v-E_0)(E_f-E_c)]^{\frac{1}{2}}\,dE_0dE_f\right\}. \quad (2)$$

The factor N gives the number of minima in the energy surfaces of the conduction band, of which, according to recent cyclotron resonance experiments,[4] there are either eight as illustrated in Fig. 1, or four if the energy minima occur at the band edges. In the above expressions the first factor in the curly brackets expresses, through the delta function, the conservation of energy requirement; the second factor is the square of the matrix element for the transition, the third factor gives the density of photon states, and the final factor the appropriate density of electron states. These expressions can be reduced to

$$W_d(\omega)d\omega = C_1\frac{2m_v}{\hbar}(E_v-E_0)^{\frac{1}{2}}\omega d\omega, \tag{3}$$

$$\left.\begin{aligned} W_i(\omega)d\omega = C_1C_2\left\{\left[k_e^2+\left(\frac{m_e+m_v}{\hbar^2}\right)(E_v+\hbar\omega-E_e)\right]B+\frac{2(m_v-m_e)}{3\hbar^2}[(E_{c0}-E_c)(E_v+\hbar\omega-E_{c0})]^{\frac{3}{2}}\right\}\frac{d\omega}{\omega} \\ B=\frac{1}{4}\left\{[3(E_v+\hbar\omega)-2E_{c0}-E_e][(E_{c0}-E_c)(E_v+\hbar\omega-E_{c0})]^{\frac{1}{2}}\right. \\ \left.+(E_v+\hbar\omega-E_e)^2\tan^{-1}\left(\frac{E_{c0}-E_e}{E_v+\hbar\omega-E_{c0}}\right)^{\frac{1}{2}}\right\} \end{aligned}\right\};\ \lambda\leq\lambda_d, \tag{4a}$$

$$W_i(\omega)d\omega = C_1C_2\frac{\pi}{8}\left\{k_e^2+\left(\frac{m_e+m_v}{\hbar^2}\right)(E_v+\hbar\omega-E_e)\right\}(E_v+\hbar\omega-E_e)^2\frac{d\omega}{\omega};\ \lambda\geq\lambda_d. \tag{4b}$$

The constant C_1 involves only known physical constants; C_2 contains a factor characterizing the strength of the electron-phonon interaction in the conduction band and also the quantity N already referred to above. Free electron wave functions have been used throughout.

By using Eqs. (3) and (4) and the following parametric values[2-4]: $E_{c0}-E_v=0.75$ ev, $E_{c0}-E_v=1.45$ ev, $m_v=0.3m_e$, $m_e=0.2m_e$, the shapes of the absorption spectra for the direct and indirect transitions have been obtained, and these curves are shown in Fig. 2. An estimate for the ratio of the absorption coefficients for the direct and indirect transitions at wavelength $\lambda_d-\Delta\lambda$ and $\lambda_i-\Delta\lambda$, respectively, gives

$$A_d(\lambda_d-\Delta\lambda)/A_i(\lambda_i-\Delta\lambda)\sim 10.$$

These results appear to be in qualitative agreement with experimental observations of absorption in thin films of germanium by Brattain and Briggs.[5] Details of the calculation will soon be published in this journal.

* Supported in part by contract with the U. S. Office of Naval Research.

† On leave from the University of California at Santa Barbara, California.

[1] F. Herman, Phys. Rev. **88**, 1210 (1952).
[2] F. Herman and J. Callaway, Phys. Rev. **89**, 518 (1953).
[3] Dresselhaus, Kip, and Kittel, Phys. Rev. **92**, 827 (1953).
[4] Dexter, Zeiger, Lax, and Rasenblum, Phys. Rev. **95**, 597 (1954).
[5] W. H. Brattain and H. B. Briggs, Phys. Rev. **75**, 1705 (1949).

Some Properties of Germanium-Silicon Alloys

EVERETT R. JOHNSON AND SCHUYLER M. CHRISTIAN
RCA Laboratories, Princeton, New Jersey

(Received May 3, 1954)

PREPARATION of homogeneous alloys of germanium-silicon has been reported by Stöhr and Klemm[1] and by Wang and Alexander.[2] We have prepared a series of germanium-silicon alloys by a process of homogenization at high temperatures and have determined composition, density, lattice constant, and forbidden band gap. All alloys were homogeneous within the precision of the x-ray measurements. Absolute values of composition of the material were determined by analyzing for germanium polarographically.[3] This method of analysis, with silicon as the sole chemical impurity, is believed to be accurate to better than ±1 percent. Forbidden band widths were determined optically, on samples normalized to 0.020-in. thickness. The band width was taken as the energy corresponding to the value of the absorption which is exhibited by germanium at its accepted band width (0.72 ev). At this point the absorption coefficient was 22.7 cm^{-1}. All absorption curves had slopes which were similar to that of pure germanium.[4]

In Table I is summarized the data obtained on these alloys. Figure 1 shows the variation of lattice constant with composition and agrees within experimental error with that obtained by Stöhr and Klemm.[1] Lattice constant measurements indicate that one should observe a nonlinear variation of density with composition due to the small volume difference between germanium and silicon. However, our measurements of density and composition are not sufficiently sensitive to detect this. Consequently, a plot of density *versus* composition

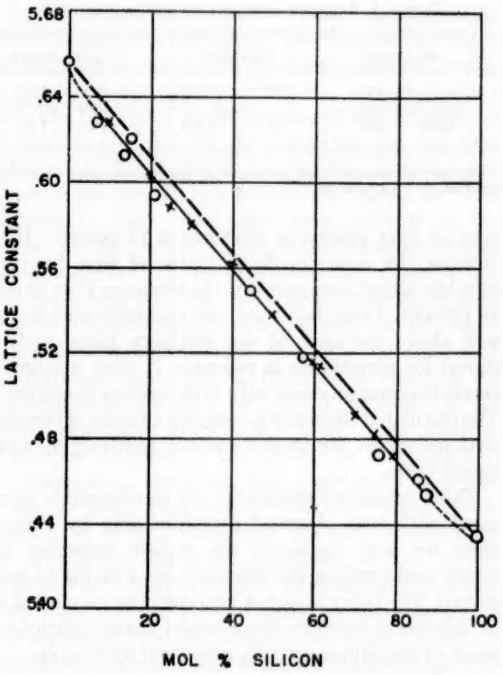

FIG. 1. Variation of lattice constant with mol percent silicon. × = Values given by Stöhr and Klemm corrected to the more modern values of lattice constant for pure Ge and Si. O = Values of lattice constant measured and reported herein.

is linear within experimental error. This indicates that density is adequate for determining composition of homogeneous material, within a few percent. In Fig. 2 is plotted band gap *versus* composition. As can be seen a marked change in slope occurs at approximately 10 mol percent silicon. The alloys containing less than 12 mol percent silicon were single-crystal specimens while

TABLE I. Summary of data obtained in germanium-silicon alloys.

Designation	Density	Lattice constant	Mol percent silicon	Forbidden band width (ev)
GS-23	2.80	5.461	85.8	1.15
GS-25	2.72	5.454	87.4	1.16
GS-26	3.03	5.473	75.7	1.13
GS-29	3.62	5.518	57.5	1.08
GS-30	3.95	5.549	44.3	1.05
GS-31	4.86	5.620	15.0	0.94
GS-34	4.89	5.613	13.5	0.93
GS-37	4.70	5.593	22.9	0.94
D-28	—	—	7.2[a]	0.83
D-31	—	—	4.3[a]	0.78
D-39	—	—	6.0[a]	0.81
D-40-*G*	—	5.626	12.6[a]	0.91
D-40-*S*	—	—	4.2[a]	0.78
D-40-*T*	—	—	7.4[a]	0.82
D-41	—	—	8.2[a]	0.84
200-*S*	—	—	0.7[a]	0.73
Ge	5.323	5.657	—	0.72
Si	2.328	5.434	—	1.20

[a] Determined spectrographically as $x \pm 0.1x$ mol percent.

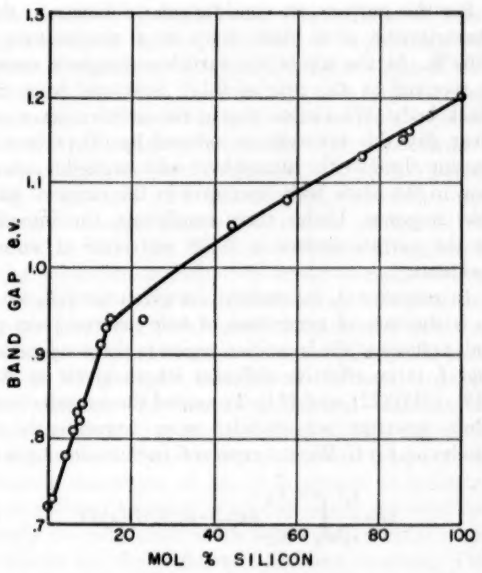

FIG. 2. Variation of energy gap with mol percent silicon.

those containing more than 12 mol percent were polycrystalline.

The authors wish to thank Dr. James A. Amick for x-ray analyses, Dr. Henry B. DeVore for optical measurements, and Dr. Marvin C. Gardels for chemical analyses.

[1] Herbert Stöhr and Wilhelm Klemm, Z. anorg. u. allgem. Chem. **241**, 4, 305–424 (1939).

[2] C. C. Wang and B. H. Alexander, Am. Inst. Mining Met. Engrs., Symposium on Semiconductors, New York City, February 15–18, 1954 (unpublished).

[3] M. C. Gardels (to be published).

[4] The slopes of those curves obtained on polycrystalline specimens differed slightly from the single crystalline specimens. However, sufficient information on polycrystalline samples was obtained to indicate that the general appearance of the curve shown in Fig. 2 would not change appreciably if all the data had been obtained on single crystalline specimens.

Use of Silicon *p-n* Junctions for Converting Solar Energy to Electrical Energy

R. L. CUMMEROW
Knolls Atomic Power Laboratory, Schenectady, New York*
(Received June 1, 1954)

CHAPIN[1] has reported experiments using silicon *p-n* junctions to convert solar radiation into electrical energy. He reports attaining an efficiency of 4 percent with such a device. The writer[2] has recently developed relations for the efficiency of *p-n* junctions as power converters in terms of the fundamental experimentally determined constants of semiconducting materials. These equations are given for monochromatic radiation. It is interesting to extend these calculations to the solar spectrum with a silicon *p-n* junction.

For this purpose, we consider solar radiation as that characteristic of a black body at a temperature of 5760°K. At the top of the earth's atmosphere energy is received at the rate of 0.135 watt/cm² from this black body. We assume that at the earth's surface on a clear day this intensity is reduced by 20 percent in passing through the atmosphere with negligible alteration in the black body spectrum in the range of junction response. Under these conditions, the intensity at the earth's surface is 0.108 watt/cm² at normal incidence.

In reference 2, expressions are given for g_0L, where g_0 is the rate of generation of hole-electron pairs per unit volume at the transition region in the *p-n* junction, and L is an effective diffusion length given by Eqs. (19), (21), (22), and (23). To extend these results to the sun's spectrum we consider more conveniently the product $g_0L=G$. We can express G in the following way:

$$G=\frac{r_s^2}{r_0^2}\int_0^{\lambda_c}\frac{N_\lambda}{S_\lambda}\exp(-d/S_\lambda)L(\lambda)d\lambda. \qquad (1)$$

In this expression, N_λ is the number of photons per unit wavelength per unit area in the black-body spectrum assumed above, S_λ is the reciprocal absorption coefficient for photons of wavelength λ, d is the depth of the junction below the irradiated surface, $L(\lambda)$ is the effective diffusion length, λ_c is the cutoff wavelength in the semiconductor corresponding to the width of the band gap, and r_s and r_0 are the radii of the sun and the earth's orbit, respectively.

Moss[3] gives a curve of absorption coefficient *versus* wavelength for silicon. For the very high absorption region at the shorter wavelengths, Eq. (1) simplifies to

$$G=\frac{r_s^2}{r_0^2}\operatorname{sech}(d/L_p)\int_0^{\lambda_c}N_\lambda d\lambda, \qquad (2)$$

where we use electrodes which reflect the minority carriers at the surfaces of the semiconducting material and assume that we are irradiating *n*-type material of depth d, and where the diffusion length of the holes (minority carrier) is L_p. The value of the integral in Eq. (2) has been worked out and is given in graphical form by Benford.[4]

For the longer wavelength regions of the spectrum, it is necessary to evaluate the integral [Eq. (1)] numerically or graphically. For silicon, using Moss' absorption coefficient *versus* wavelength, the approximation (2) is good from very short wavelengths up to about 0.87μ. From 0.87μ to 1.1μ a graphical evaluation of Eq. (1) is employed.

Table I shows the constants assumed for the silicon *p-n* junction. Using the approximation for the sun's spectrum described above, the constants shown in Table I, and the calculated value of $G=2.25\times10^{17}$ $cm^{-2}sec^{-1}$, we find from Eqs. (27) and (28) of reference 2 that the efficiency of conversion (neglecting reflection loss) of solar energy to electrical is 17 percent. If we increase the intensity by a factor of four by some suitable optical arrangement, the efficiency rises to only 18 percent. From this result we conclude that we are well above the knee of the efficiency curve such as shown for germanium in reference 2, since a large increase in power produces very little increase in efficiency. The calculated efficiency is lower by a factor of two than that calculated for monochromatic radiation of wavelength 0.87μ.

TABLE I. Assumed constants for silicon junction.[a]

Mobilities		Lifetimes		Conductivities	
μ_n	μ_p	τ_n	τ_p	σ_n	σ_p
(cm^2/volt sec)		(sec)		(ohm^{-1} cm^{-1})	
1200	400	10^{-5}	10^{-5}	1.0	1.0

[a] It was also assumed that the square of the concentration for intrinsic material, $n_i^2=2.5\times10^{26}$ cm^{-6}.

These calculated efficiencies are in reasonable agreement with that observed experimentally by Chapin, since we have neglected the surface reflection loss which could reduce the efficiency by a factor as great as two. The other factor of two could be accounted for in differences between the assumed characteristics and those of the silicon actually employed by Chapin.

* Operated by the General Electric Company for the U. S. Atomic Energy Commission.

[1] D. M. Chapin, Am. Inst. Mining Met. Engrs., Symposium on Semiconductors, February 15, 1954 (unpublished).
[2] R. L. Cummerow, Phys. Rev. **95**, 16 (1954).
[3] T. S. Moss, *Photoconductivity in the Elements* (Academic Press, Inc., New York, 1952), p. 113.
[4] F. E. Benford, Gen. Elec. Rev. **46**, 377, 433 (1943).

Power Efficiency for the Photovoltaic Effect in a Germanium Grown Junction*

RALPH P. RUTH AND JAMES W. MOYER
Knolls Atomic Power Laboratory,† Schenectady, New York

(Received May 25, 1954)

IT is known that the short-circuit photovoltaic current of an unbiased *p-n* junction increases linearly with the intensity of the incident radiation except for very large intensities. The open-circuit photovoltage also increases with the incident intensity, but at a rate which decreases for large intensities.[1] A consideration of the current-voltage characteristic of a typical rectifying junction indicates that the photocurrent for maximum power delivered to an external resistive load must vary with incident intensity in much the same way that the short-circuit photocurrent does; the photovoltage for maximum power must follow more closely the dependence of the open-circuit photovoltage. Thus, the efficiency of conversion of incident power into maximum power delivered to the external load should increase with incident intensity in a manner similar to that of the open-circuit photovoltage, provided the intensity is not too large.

A disk-shaped germanium crystal,[2] approximately six mm in diameter and slightly less than one mm thick, was cut from an ingot with the grown junction parallel to the faces and approximately 0.1 mm from the *n* face. The resistivity of the *n* material was in excess of 20 ohm-cm and that of the *p* material was less than one ohm-cm. The radiation was incident normal to the *n* face of the crystal; this surface was etched for these experiments. Fine wire leads were soldered to the centers of the parallel faces; each electrode covered less than one tenth of the area of the face. Observations were made both with the continuous spectrum supplied by a 3200°K photoflood lamp and with the exit beam of a quartz monochromator. Intensity variation with the continuous spectrum was obtained by changing the lamp-to-crystal distance. A shutter in front of the crystal permitted observations to be made immediately upon exposure of the crystal to the radiation; all observations described here were made with the crystal at room temperature. For both types of observation a vacuum thermopile was used to determine the appropriate radiation intensities at the crystal surface. For a given incident intensity the external current and voltage were measured as functions of the load resistance; the photocurrent was measured with a low-resistance galvanometer and the photovoltage with a high-impedance vacuum-tube voltmeter. The point of maximum power was selected by inspection of the resulting power-*vs*-load resistance curve.

Figure 1 shows the observed efficiency of conversion of incident power into maximum delivered power as a function of the incident radiation intensity for radiation of four different compositions. The inset is the low-intensity portion of the figure with the vertical scale expanded. The dependence for the white radiation from the tungsten lamp is given by curve *A*. Curve *B* is for the part of this radiation beyond 0.9 μ as transmitted by an infrared filter. Curve *C* shows the relationship for the tungsten lamp radiation between 0.7 μ and 1.1 μ as transmitted by a glass color filter. Curve *D*, which appears only in the inset, represents the efficiency data for low intensities of wavelength 1.65μ as obtained with the monochromator. It is seen that, in all four cases, the power efficiency increases with incident intensity over a large range of intensities. The dependence is nearly linear for low intensities (i.e., below about 0.005 watt/cm^2) and becomes approximately logarithmic for larger intensities. This is similar to the manner in which the open-circuit photovoltage varies with the incident intensity.[1] As would be expected from a consideration of the current-voltage characteristic of a *p-n* junction, it was found that the load resistance for maximum power remained approximately the same (200 to 300 ohms for this crystal) for low intensities but decreased with increasing incident radiation intensity to about 25 ohms for the highest intensity used.[3] It will be noted that for white radiation (curve *A*) an efficiency maximum of nearly $\frac{1}{2}$ percent is indicated for an incident intensity of approximately 0.1 watt/cm^2 (nearly the magnitude of the solar constant); for larger intensities the observed power efficiency decreases. This occurs in the same high-intensity region in which the beginning of a current saturation effect was observed for both the short-circuit and the maximum-power conditions. No efficiency maximum is indicated for any of the other data.

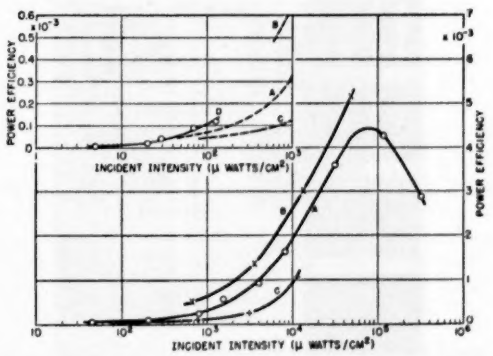

FIG. 1. Efficiency of germanium grown junction in converting power received in incident radiation into maximum power in external resistive load. *A*. White radiation from incandescent tungsten source. *B*. Radiation of *A* beyond 0.9 μ. *C*. Radiation of *A* between 0.7 μ and 1.1 μ. *D*. Radiation of wavelength 1.65 μ.

The curves shown in Fig. 1 represent lower limits for the power efficiencies, since the data presented are given in terms of incident power and not in terms of the power absorbed by the germanium crystal at its surface. As the reflecting power of germanium in the wavelength regions involved here is the order of 0.5,[4] it follows that the efficiencies of conversion of *absorbed* power are roughly twice those shown in Fig. 1.

An effective quantum efficiency appreciably less than unity was observed for this crystal. The relative photocurrent response of the crystal to an equal-energy spectrum of low intensity is shown in Fig. 2. The energy sensitivity at the peak response point is approximately three times that at 1.0 μ; the sensitivity per incident photon at the peak is nearly twice that at 1.0 μ. The relative responses, for a given incident intensity, in-

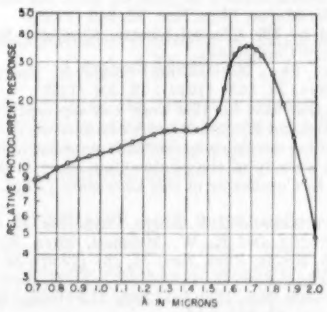

FIG. 2. Relative photocurrent response of germanium grown junction to an equal-energy source.

dicated by the curves of Fig. 1 are consistent with the spectral sensitivity data of Fig. 2. Utilizing the short-circuit photocurrents, found by extrapolation to zero external resistance, and the corresponding measured intensities it was possible to calculate the effective quantum efficiencies for both the monochromator measurements and the direct-radiation measurements. The peak response region between 1.65 μ and 1.70 μ corresponds to approximately 0.3 electron-hole pairs produced per incident photon. If approximate values for the optical constants of germanium[4] are applied to the data of Fig. 2 the general shape of the response curve is not appreciably altered, but the peak response then corresponds to an effective quantum efficiency of approximately 0.5 electron-hole pairs per absorbed photon and the 1.0 μ region to approximately 0.3. These effective quantum efficiencies, although verified on several occasions, are decidedly less than the value of unity generally accepted for the photovoltaic process at a p-n junction.[5] The discrepancy can be attributed to excessive recombination of the generated charges at the crystal surfaces and to an effective series ohmic resistance at the electrode contacts on the crystal.

The relatively small effective quantum efficiency does not affect the validity of the results reported; it does, however, restrict the magnitudes of the power efficiencies observed. Had an effective quantum efficiency of approximately unity been observed in the peak response region the curves of Fig. 1 would indicate power efficiencies from 2½ to four times those shown. This would correspond to efficiencies of conversion of *absorbed* power five to eight times those indicated in Fig. 1. For the white radiation of curve *A* this would mean a maximum power efficiency of approximately two percent. For the infrared radiation of curve *B* an efficiency of three percent or more is indicated, since there is no evidence of a maximum in the intensity range shown. It appears not unreasonable to presume that efficiencies of seven or eight percent could be realized with a junction better suited to this application.

* This investigation was described, in slightly different form, in a paper presented at the Rochester, New York, meeting of the American Physical Society on June 18, 1953. See Ralph P. Ruth and James W. Moyer, Phys. Rev. **92**, 846 (1953).

† Operated by the General Electric Company for the U. S. Atomic Energy Commission.

[1] H. Y. Fan, Phys. Rev. **75**, 1631 (1949); M. Becker and H. Y. Fan, Phys. Rev. **75**, 1631 (1949); **78**, 301 (1950).

[2] The junction used for this work was supplied by Dr. R. N. Hall of the General Electric Research Laboratory.

[3] A theoretical development of these empirical relationships is contained in a study of the photovoltaic effect in p-n junctions made by R. L. Cummerow of this laboratory [Phys. Rev. **95**, 16 (1954)].

[4] W. H. Brattain and H. B. Briggs, Phys. Rev. **75**, 1705 (1949); K. Lark-Horovitz and K. W. Meissner, Phys. Rev. **76**, 1530 (1949); H. B. Briggs, Phys. Rev. **77**, 287 (1950); M. Becker and H. Y. Fan, Phys. Rev. **76**, 1530 (1949); D. G. Avery and P. L. Clegg, Proc. Phys. Soc. (London) **B66**, 512 (1953); H. B. Briggs, J. Opt. Soc. Am. **42**, 686 (1952).

[5] F. S. Goucher, Phys. Rev. **78**, 816 (1950). See also B. J. Rothlein, Sylvania Technologist **4**, 86 (1951).

Magnetic Domains in Cobalt by the Longitudinal Kerr Effect*

CHARLES A. FOWLER, JR., AND EDWARD M. FRYER
Department of Physics, Pomona College, Claremont, California
(Received May 24, 1954)

THE longitudinal Kerr effect was recently employed by the authors to successfully photograph the magnetic domains in a single crystal of silicon iron.[1] The domains in that specimen were unusually large (1–3 mm wide) and the question remained as to how applicable the technique would be for examining the very much smaller domains usually encountered in ordinary ferromagnetic crystals. Partly to answer this question, we have undertaken to photograph the domains in a (10·0) surface of a single crystal of hexagonal cobalt, which was known from powder pattern evidence to contain antiparallel domains lying in the direction of the c axis, the direction of easy magnetization.

No data on the longitudinal Kerr effect in cobalt were available, but the normal polar case in cobalt is reported to rotate the plane of polarization by about 20 minutes, which is about the same magnitude as for the normal polar case in iron.[2] The polar effect in cobalt had been employed by Williams, Wood, and Foster to photograph the mottled structure characteristic of the end-on view of domains terminating in a basal plane normal to the c axis.[3] We therefore first sought to measure the longitudinal Kerr rotation for the cobalt specimen by using the photoelectric technique previously described.[1] The rotation, a maximum when the light is incident at about 60°, measured 3.5

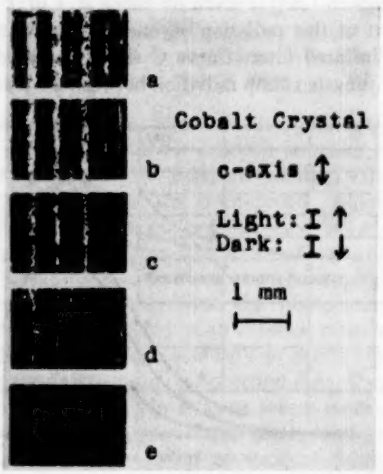

FIG. 1. Photographs of the domain behavior in a (10·0) surface as the applied field is increased from zero in (a) to a value sufficient to produce saturation in (e). The direction of the field is toward the bottom of the page.

minutes at saturation. This value is sufficiently close to the 5 minutes found in silicon iron to assure enough contrast for photographing antiparallel domains.

Employing essentially the same experimental arrangement that was described for our silicon iron investigation,[1] we have succeeded in obtaining reasonably satisfactory photographs of the domain structure in a (10·0) surface of the hexagonal cobalt crystal. Figure 1 is a series of such photographs of a small portion of the surface, taken as the originally demagnetized specimen is subjected to a gradually increasing field. The photocell monitor indicated that the domain changes were characteristically discrete and sporadic, and the pictures reveal that certain domains tend to persist while others are changing. The figure shows that these cobalt domains are a small fraction of a millimeter wide, at least an order of magnitude smaller than those we had photographed in silicon iron.

Certain of the domains appear unsharp and fuzzy at the edges, and this results directly from inability to perfectly superpose the correcting "reversed flat" on the domain negative in order to reduce the photographic "surface noise," a problem first encountered in the silicon iron work.[1,4] Whereas the troublesome small surface imperfections only partially obscured the large silicon iron domains, they practically obliterate the very much smaller cobalt domains. Thus the negative-positive superposition technique that was so useful in the silicon iron work becomes absolutely essential in obtaining satisfactory photographs of the cobalt domains. Figure 2 shows uncorrected photographs of the demagnetized and the saturated specimen, the "reversed flat" corrector, and the same two photographs after correction. It is to be emphasized that the surface was electrolytically polished to a mirror smoothness, and that the rough appearance results simply from the unusual conditions of photography, conditions that cause even the smallest pit, wave, or depression to

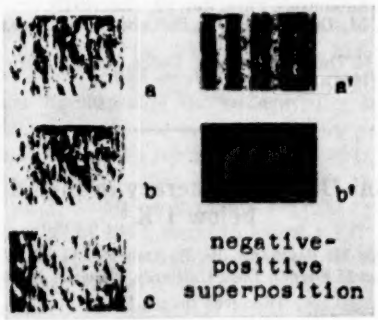

FIG. 2. Reduction of "surface noise" by negative-positive superposition. Uncorrected photographs of domain structure when the crystal is (a) demagnetized and (b) saturated. (c) is the "reversed flat," a positive of (b). Photographs (a') and (b') are corrected pictures made by superposing (c) on (a) and (b), respectively.

FIG. 3. Further enlargement of a domain photograph, permitting estimate of resolution limit.

stand out in the uncorrected photograph with a contrast that rivals or exceeds the contrast between adjacent domains.

Some estimate of the resolution limit can be made from Fig. 3 which is a further enlargement of one of the photographs. The light domain at the right measuring less than 0.05 mm is well resolved, and an examination of the walls themselves suggests that a width of approximately 0.01 mm is about the limit in this photograph. The sharpness is somewhat improved if the surface area to be corrected by the superposition technique is limited, for the smaller the area the more nearly perfect can be the matching.

This investigation is continuing with the objective of observing the interesting cobalt transition at about 275°C where the c axis ceases to be the axis of easy magnetization and becomes the direction of most difficult magnetization.[5] The authors are indebted to R. J. Williams and R. M. Bozorth for the loan of the cobalt crystal and for helpful discussions concerning the work.

* Supported by the Office of Naval Research.

[1] C. A. Fowler and E. M. Fryer, Phys. Rev. **94**, 52 (1954).
[2] *International Critical Tables* (McGraw-Hill Book Company, Inc., New York, 1929), first edition, Vol. VI, p. 435.
[3] Williams, Foster, and Wood, Phys. Rev. **82**, 119 (1951).
[4] C. A. Fowler and E. M. Fryer, J. Opt. Soc. Am. **44**, 256 (1954).
[5] R. M. Bozorth, *Ferromagnetism* (D. Van Nostrand Company, Inc., New York, 1951), p. 555.

Ultrasonic Measurements in Magnetically Cooled Helium*

C. E. CHASE AND MELVIN A. HERLIN
Department of Physics and Research Laboratory of Electronics, Massachusetts Institute of Technology, Cambridge, Massachusetts
(Received May 19, 1954)

MEASUREMENTS have been made of the absorption of ordinary "first" sound in liquid helium at a frequency of 12.1 Mc/sec and at temperatures down to 0.1°K. A pulse technique similar to that employed earlier by one of the authors[1] was used. The results of one demagnetization are shown in Fig. 1.

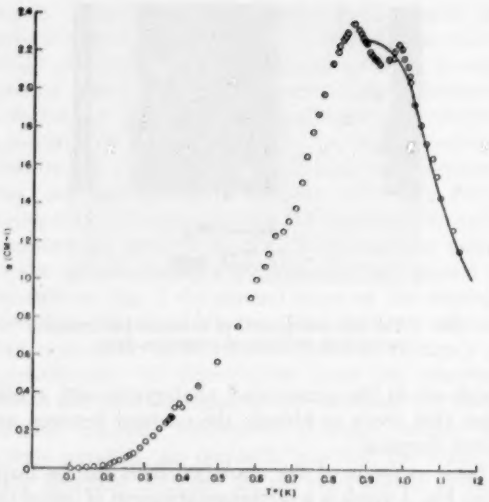

FIG. 1. Attenuation of sound in liquid helium. Solid curve, earlier results (reference 1); circles, present results (12.1 Mc/sec).

The circles represent the experimental points; the full curve indicates the results of earlier measurements.[1] The twin maxima in the attenuation in the neighborhood of 0.9°K are clearly resolved, and provide direct evidence for the existence of two distinct relaxation times in agreement with the prediction of Khalatnikov.[2,3] A full report will be published shortly.

* This work was supported in part by the Signal Corps; the Office of Scientific Research, Air Research and Development Command; and the Office of Naval Research; and in part by the International Business Machines Corporation.

[1] C. E. Chase, Proc. Roy. Soc. (London) **A220**, 116 (1953).
[2] I. M. Khalatnikov, J. Exptl. Theoret. Phys. (U.S.S.R.) **20**, 243 (1950).
[3] I. M. Khalatnikov, J. Exptl. Theoret. Phys. (U.S.S.R.) **23**, 8 (1952).

Remark Concerning the Absolute Value of Avogadro's Number

M. E. STRAUMANIS
Department of Metallurgy, School of Mines and Metallurgy, University of Missouri, Rolla, Missouri
(Received May 17, 1954)

IN an earlier article[1] it was proposed to accept for x-ray work the value of

$$N_0 = 0.602567 \times 10^{24} \text{ (phys) or } 0.602403 \times 10^{24} \text{ (g mole)}^{-1} \text{ (chem)} \quad (1)$$

for Avogadro's number, for reasons explained in detail in the article.

DuMond and Cohen[2] have recommended the value

$$N_{\text{universal}} = (0.602472 \pm 0.000036) \times 10^{24} \text{ (g mole)}^{-1} \text{ (phys)} \quad (2)$$

for the same and other purposes. However they did not mention that their method of computation gave also a new conversion factor,[3] $\lambda_g/\lambda_s = 1.002063$, instead of the now generally accepted value 1.00202. If the new factor is used for the computation of N_0 by the author's Eq. (4)[1] for calculation of N_0 from N_s (Siegbahn's Avogadro number), the following value is obtained:

$$N_0' = (0.602489 \pm 0.000030) \times 10^{24} \text{ (g mole)}^{-1}, \quad (3)$$

which agrees completely with (2) within the error limits. The agreement between (2) and (3) shows that in both cases $(\lambda_g/\lambda_s)^3 \times N$ is the same within the error limits, and that the x-ray crystal density method is by no means less accurate than other exact methods. Furthermore, if $(\lambda_g/\lambda_s)^3$ and N are used simultaneously in one term, as for instance for the calculation of x-ray molecular weight, density, or the number of molecules per unit cell, both recommendations (1) and (2) are identical, and give the same result.

However, it is questionable whether the new conversion factor of 1.002063 will be accepted in x-ray spectroscopy and in precision determination of lattice parameters. It seems to the author that a new conversion factor will not be accepted until it is substantiated by new precision measurements of x-ray wavelengths by means of gratings. Until such time as a new conversion factor is generally accepted, to avoid confusion, it seems desirable to use the old conversion factor of 1.00202. By substituting this factor for λ_g/λ_s in Eq. (4),[1] the above-mentioned Avogadro number (1) is obtained (physical or chemical scale). This N_0 therefore, was, and still is, recommended for x-ray work because it is in correct relationship with the accepted conversion factor of 1.00202 and Siegbahn's Avogadro number N_s, which was used for the computation of the fundamental value for the lattice spacing of calcite, and consequently for the determination of x-ray wavelengths.

[1] M. E. Straumanis, Phys. Rev. **92**, 1155 (1953).
[2] J. W. M. DuMond and E. R. Cohen, Phys. Rev. **94**, 1790 (1954).
[3] J. W. M. DuMond and E. R. Cohen, Revs. Modern Phys. **25**, 691, 706 (1952).

Fermi-Dirac Degeneracy in Liquid He^3 below 1°K*

WILLIAM M. FAIRBANK, W. B. ARD, AND G. K. WALTERS
Department of Physics, Duke University, Durham, North Carolina
(Received June 1, 1954)

THE temperature dependence of the nuclear magnetic susceptibility of liquid He^3 has been measured directly down to 0.23°K by observing the strength of the nuclear magnetic resonance absorption signal. In a previous communication[1] we reported measure-

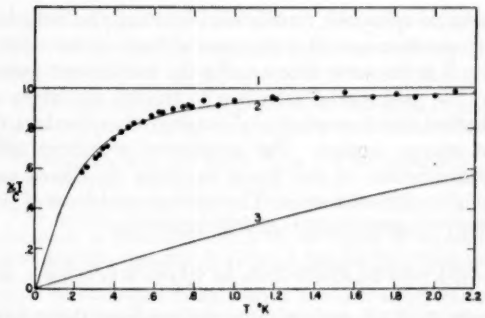

FIG. 1. Plot of $\chi T/C$ *vs* T. (χ = molar nuclear magnetic susceptibility of He^3, T = absolute temperature, C = normalizing Curie constant.) Curve 1 represents the Curie law expected from Boltzmann statistics, curve 3 represents an ideal Fermi-Dirac gas with the same density and atomic mass as liquid He^3 ($T_0 = 5°$), curve 2 represents an ideal Fermi-Dirac gas with a degeneracy temperature $T_0 = 0.45°K$. The dots represent the experimental points.

ments in the gas at 4.2°K and in the liquid down to 1.2°K. These measurements give an answer to the much discussed[2–12] question of the extent to which liquid He^3 behaves as an ideal Fermi-Dirac gas. At sufficiently low temperatures the spins of the particles of an ideal Fermi-Dirac gas would be expected to line up antiparallel and this would cause the spin magnetic susceptibility to deviate from the classical $1/T$ Curie law and finally to become temperature independent.

The experimental results below 2.1°K are shown in Fig. 1. It is seen that the data fall between curve 1, the classical Curie curve, and curve 3, the curve for an ideal Fermi-Dirac[3,13] gas with a degeneracy temperature $T_0 = (h^2/8mk)(3N/\pi V)^{\frac{2}{3}} = 5°K$, calculated for an ideal Fermi-Dirac gas of the same density[15] and atomic mass as He^3. Curve 2 is the curve for a Fermi-Dirac gas with a degeneracy temperature of 0.45°K, arbitrarily selected to give the best fit of the data. It appears from this experiment that the nuclear spins of liquid He^3 line up antiparallel as would be expected of a degenerate ideal Fermi-Dirac gas, but at temperatures an order of magnitude lower, the ordinate in Fig. 1 being a measure of the fraction of the He^3 nuclear spins that have become saturated.

In order to normalize the susceptibility measurements we have made use of our previously published data[1] above 1.2°K. We reported that above 1.2°K the molar susceptibility, calculated from the measured volume susceptibility using the published density measurements[14] of 1949, seems to follow a $1/T$ law indicating no apparent degeneracy. Kerr,[15] using the larger amounts of He^3 now available at Los Alamos, has remeasured the density of liquid He^3 to an estimated accuracy of ±0.3 percent. When these latest values of the density are used to recalculate the data, a possible 4 percent deviation from Curie's law is indicated at 1.2°K. The data in Fig. 1 have been so normalized. However, this incipient degeneracy at 1.2°K is not outside possible experimental error which we estimate to be ±5 percent for χT. In calculating the data of Fig. 1, the density of liquid He^3 has been assumed to be constant below 1°K.

The nuclear resonance techniques used in this experiment and the method of calculating the susceptibility from these measurements have been discussed previously.[1] The He^3 sample, 20 cc of He^3 gas at STP, was obtained from the Stable Isotope Division of the Oak Ridge National Laboratory and was concentrated by us by fractional distillation to better than 99 percent purity. Temperatures below 1°K were obtained by adiabatic demagnetization of 25 grams of potassium chrome alum, pressed around a copper rod. This copper rod served as a thermal contact with the He^3 cavity which was located six inches from the salt. The temperature was measured by means of a carbon resistor independently calibrated against the susceptibility of the paramagnetic salt as determined by ballistic measurements. An independent check of the temperature, within an accuracy of 10 percent, was made by placing a salt containing protons in direct contact with the He^3 and measuring the strength of the nuclear magnetic resonance signal from the protons as a function of temperature.

The spin-lattice relaxation time T_1 was found to be 30 seconds over the temperature range from 0.23°K to 1.2°K. In a previous experiment in which the only surfaces in contact with the He^3 were the Pyrex walls of the container,[1] T_1 was determined to be 200 sec at 1.2°K. We therefore conclude that the relaxation time in the present experiment was primarily determined by interaction with the surfaces in contact with the He^3, such as the copper walls, the coil, and the salt used for proton measurements, rather than by the spin-spin interaction of the He^3 nuclei.

We are deeply indebted to Professor F. London for his intense interest in this experiment and for his frequent theoretical advice. His untimely death came just after the initial results below 1°K were obtained. We are also indebted to Professor Walter Gordy and Dr. H. Dehmelt who were co-workers with us in the early stages of this experiment. We wish to thank Mr. W. D. McCormick and Mr. E. J. Lynch for aid in taking the measurements and Mr. T. C. Chen for aid in the calculations.

* This project has been supported by contracts with the Ordnance Corps, Department of the Army. These results were presented as a postdeadline paper at the American Physical Society meeting in Washington, April 29–May 1, 1954.

[1] Fairbank, Ard, Dehmelt, Gordy, and Williams, Phys. Rev. **92**, 208 (1953).
[2] I. Pomeranchuk, J. Exptl. Theoret. Phys. (U.S.S.R.) **20**, 919 (1950).
[3] L. Goldstein and M. Goldstein, J. Chem. Phys. **18**, 538 (1950).
[4] E. M. Lifshitz, J. Exptl. Theoret Phys. (U.S.S.R.) **21**, 659 (1951).
[5] K. S. Singwi, Phys. Rev. **87**, 540 (1952).
[6] J. G. Daunt, Advances in Physics **1**, 209 (1952).
[7] Weinstock, Abraham, and Osborne, Phys. Rev. **89**, 787 (1953).
[8] T. C. Chen and F. London, Phys. Rev. **89**, 1038 (1953).

[9] Hammel, Laquer, Sydoriak, and McGee, Phys. Rev. **86**, 432 (1952).
[10] G. de Vries and J. G. Daunt, Phys. Rev. **93**, 631 (1954).
[11] T. R. Roberts and S. G. Sydoriak, Phys. Rev. **93**, 1418 (1954).
[12] Osborne, Abraham, and Weinstock, Phys. Rev. **94**, 202 (1954).
[13] J. McDougall and E. C. Stoner, Trans. Roy. Soc. (London) **A237**, 67 (1938).
[14] Grilly, Hammel, and Sydoriak, Phys. Rev. **75**, 1103 (1949).
[15] E. C. Kerr, at Third International Conference on Low Temperature Physics and Chemistry, The Rice Institute, December 17–22, 1953 (unpublished) (also private communication).

Spin-Orbit Interaction and the Effective Masses of Holes in Germanium*

G. Dresselhaus, A. F. Kip, and C. Kittel
Department of Physics, University of California, Berkeley, California

(Received April 23, 1954; revised manuscript received May 21, 1954)

We reported[1] earlier the observation of cyclotron resonance of electrons and holes in germanium crystals; in particular, we reported the observation of two approximately isotropic effective masses for holes, $m^*/m=0.04$ and 0.3. The association of these masses with the motion of holes has been confirmed by experiments at K band with circularly polarized radiation, which also reveal a structure to the $m^*=0.3m$ resonance. These experiments, which will be published shortly, determine the sign of the charge carrier. The questions which arise are: (1) Why are there two masses? (2) Why can the masses be resolved, in view of the warped nature of energy surfaces[2] near degenerate points? (3) Why are the masses so light? We consider these questions below.

(1) Herman and Callaway[3] have carried out calculations suggesting that the top of the valence band in germanium occurs at the center of the Brillouin zone and is threefold degenerate, corresponding to p bonding orbitals on the Ge atoms. We suggest that spin-orbit interaction[4] is responsible for the observation of essentially two, rather than three, masses. The top of the valence band has point group symmetry properties related to atomic $p_{\frac{1}{2}}$ states and is quadruply degenerate, but in crystals with a center of symmetry the contact is that of two double-degenerate bands. There is therefore a possibility of two different masses. The band arising from atomic $p_{\frac{1}{2}}$ states is lower (for holes) by perhaps 500 to 2000 cm^{-1}, as estimated from atomic spectra and by a suggested interpretation of the infrared absorption[5] of $p-$Ge.

(2) We have carried out for this proposed level scheme a general second-order perturbation determination of the energy surfaces near $\mathbf{k}=0$, following the method of Shockley.[2] The calculation hinges largely on symmetry properties of the bands and is *not* based on a strong-binding model. The perturbation is

$$H'=\hbar\mathbf{k}\cdot[(\mathbf{p}/m)+\zeta(\mathbf{S}\times\mathbf{r}], \quad (1)$$

where the spin-orbit term is not important; its inclusion however does not alter the general form of the result. Here $\mathbf{k}$ is the wave vector and $\mathbf{p}$ the momentum operator. We paid special attention to tracing the origin of spherical and nonspherical (warping) contributions to the energy surface. The symmetry properties and representations of the bands as given by Elliott are useful in this connection. The most general form of the energy to second order may be written as

$$E(k)=Ak^2\pm[B^2k^4+C^2(k_x^2k_y^2+k_y^2k_z^2+k_z^2k_x^2)]^{\frac{1}{2}}, \quad (2)$$

where A, B, C, are constants derived from the matrix elements of H' connecting the valence band edge (representation Γ_{8g}) with other states. It turns out that the principal nonspherical perturbation (which enters through C) arises from the perturbation by a state with antibonding s character (Γ_{7u}) which is separated[3] from Γ_{8g} by some 6 ev. The spherical perturbations A, B arise principally from the antibonding $p_{\frac{1}{2}}$ and $p_{\frac{3}{2}}$ states (Γ_{6u},Γ_{8u}) which are separated from Γ_{8g} by 0.7–0.8 ev. The perturbations involve the usual energy denominator, so that the spherical terms could be larger than the nonspherical, but other arguments suggest that the differences may not be great.

Nonspherical energy surfaces give cyclotron resonance if the tube mass[6] on a plane in $\mathbf{k}$ space perpendicular to the magnetic field is independent of the energy. Otherwise, an accelerated electron will enter a tube of different period, and the phase will be destroyed. With the nonspherical term, it is possible to define for certain field directions two sets of tubes for which cyclotron resonance is possible. With the field parallel to the [100] axis, and $C^2\ll 4B^2$, the two resonances on a single energy surface are separated by

$$\Delta\omega\cong\omega_0\frac{C^2}{16B}\left(\frac{2m}{\hbar^2}\right)\frac{m^*}{m}, \quad (3)$$

to first order. For strong warping only one of the lines will be strong.

Our preliminary measurements with H in the [100] direction indicate that there are actually two peaks near $m^*/m=0.3$, with a separation $\Delta\omega/\omega_0\approx 0.2$, which leads to the rough estimate $B^2/C^2\approx 1$. For the $0.04m$ effective mass we would then estimate $\Delta\omega/\omega_0\approx 0.03$, which cannot be resolved at present. The $0.3m$ structure should be somewhat anisotropic.

(3) The spherical terms in the energy are quite large, as the perturbing levels are unusually close. It is quite reasonable that the masses should be light: the coefficients A, B will be $\gg\hbar^2/2m$.

It appears that it is possible to account for the features of the hole resonances, as observed up to the present. The effect of spin-orbit interaction on the electron cyclotron resonance is to lift the degeneracy of the antibonding p band so that the $p_{\frac{1}{2}}$ band is lowest. The ellipsoid model proposed for $n-$Ge by Meiboom and

Abeles[7] and Lax and co-workers[8] probably would not work unless the degeneracy, in this case along ⟨111⟩ axes, where lifted by the spin-orbit interaction.

* This work has been assisted in part by the National Science Foundation (G. Dresselhaus), and by the U. S. Office of Naval Research and the U. S. Signal Corps.

[1] Dresselhaus, Kip, and Kittel, Phys. Rev. **92**, 827 (1953).
[2] W. Shockley, Phys. Rev. **78**, 173 (1950).
[3] F. Herman and J. Callaway, Phys. Rev. **89**, 518 (1953).
[4] We were led to a recognition of the importance of spin-orbit interaction in semiconductors from the results of experiments on electron spin resonance in silicon. A detailed theoretical analysis of spin-orbit effects by Dr. R. J. Elliott will shortly be submitted for publication in this journal. It may be noted that spin-orbit splittings in heavy semiconductors may be comparable with the energy gap separation.
[5] A. H. Kahn (to be published).
[6] W. Shockley, Phys. Rev. **79**, 191 (1950).
[7] S. Meiboom and B. Abeles, Phys. Rev. **93**, 1121 (1954).
[8] Lax, Zeiger, Dexter, and Rosenblum, Phys. Rev. **93**, 1418 (1954).

Nuclear Spin and Hyperfine Structure Interaction of the 3.1-hr Cs^{134} Isomer*

V. W. Cohen and D. A. Gilbert
Brookhaven National Laboratory, Upton, New York
(Received June 2, 1954)

WE have performed an atomic beam magnetic resonance[1] experiment on the 3.1-hr isomer of Cs^{134}. The results of this experiment indicate that $I=8$ in units of h, and $\Delta\nu=3675.6\pm0.6$ Mc/sec.

The apparatus is of the "flop-in" type in which one observed those atoms which have undergone the transition in the homogeneous magnetic field for which $[I+\frac{1}{2}, -(I+\frac{1}{2})]\rightleftarrows[I+\frac{1}{2}, -(I-\frac{1}{2})]$. At very weak magnetic fields this transition frequency is linear in H and is independent of $\Delta\nu$, depending only upon I. At intermediate fields the dependence upon $\Delta\nu$ becomes significant and is given accurately by the modified Breit-Rabi[1] expression permitting one to calculate $\Delta\nu$.

The Cs^{134m} for each run was prepared by irradiating approximately 100 mg of CsCl in the Brookhaven reactor for about 9 hours. It was then placed in a Monel oven with freshly cut chips of metallic barium. At about 450°C a strong steady beam of Cs atoms emerged from the oven. The focused atoms, selected by a 0.004-in. slit, are allowed to impinge for an arbitrary time interval upon a thin, flat tungsten target upon which they are adsorbed. The target could then be removed via an airlock and its activity measured with a proportional counter, thus giving a measure of the focused beam intensity for one set of magnetic field and frequency conditions. For deposition times of the order of five minutes counting rates of approximately 70 counts/min at the peak with a background of about 15 counts/min were obtained. The magnetic field was calibrated by observing the rf spectrum of Cs^{133} and using $\Delta\nu^{133}=9192.76$ Mc/sec as given by Kusch and Taub.[2]

TABLE I. Observed resonances.

Cs^{133} (Mc/sec)	Cs^{134m} (Mc/sec)
1.990	0.940
4.504	2.125
9.995	4.750
15.252	7.325
29.865	14.612
48.850	24.540
99.500	53.582±0.010
213.500	136.280±0.010

The frequencies at which Cs^{134m} resonances were observed are given in Table I along with the calibrating frequencies of Cs^{133}. The lower-frequency results serve to establish the spin. The constant $\Delta\nu^{134m}$ was calculated for the two highest field runs as given in the table. These combine to give a value of 3675.6±0.6 Mc/sec. Using the value[3] 0.731 for g_I of Cs^{133} and neglecting any hfs anomaly, we calculate the magnetic moment of Cs^{134m} to be $\mu=1.10\pm0.01$, with the sign undetermined.

The available proton-neutron configurations, agreeing with the measured spin, on the basis of the shell model[4] are $d_{5/2}$, $h_{11/2}$ and $g_{7/2}$, $h_{11/2}$. In the limit of a strict $J-J$ coupling two-particle wave function, the magnetic moments calculated for these two pure states are +2.72 nm and −0.35 nm, respectively. Thus it would appear that a mixed configuration, such as suggested by de-Shalit and Goldhaber,[5] is necessary to account for the magnitude of the observed moment. The proper admixture would then be 53 percent $(g_{7/2}, h_{11/2})$ and 47 percent $(d_{5/2}, h_{11/2})$ with the theory predicting a positive sign. In this connection it is interesting to note that no combination of "stripped"[6] moments for the proton and neutron, calculated from pure states, yields a magnetic moment in agreement with the observed value. Furthermore, if one analyzes the data of Bellamy and Smith[7] concerning the ground state of Cs^{134}, one finds that the above conclusion also holds here. Thus it would appear that the magnetic moments of Cs^{134} and Cs^{134m} make rather a strong case for the use of mixed configurations if one restricts the discussion to single proton-single neutron wave functions.

The authors wish to express their thanks to Dr. M. Goldhaber and Dr. J. Weneser of the Laboratory for the helpful suggestions on the interpretation of these data.

* Work performed under auspices of U. S. Atomic Energy Commission.

[1] J. M. B. Kellogg and S. Millman, Revs. Modern Phys. **18**, 323 (1946).
[2] P. Kusch and H. Taub, Phys. Rev. **75**, 1477 (1949).
[3] Kusch, Millman, and Rabi, Phys. Rev. **55**, 1176 (1939).
[4] Mayer, Moszkowski, and Nordheim, Revs. Modern Phys. **23**, 315 (1951).
[5] A. de-Shalit and M. Goldhaber, Phys. Rev. **92**, 1211 (1953).
[6] I. Talmi, Phys. Rev. **83**, 1248 (1951).
[7] E. H. Bellamy and K. F. Smith, Phil. Mag. **44**, 33 (1953).

Nuclear Spin and Magnetic Moment of 3.1 hr Cs^{134m}

L. S. Goodman and S. Wexler
Argonne National Laboratory, Lemont, Illinois
(Received June 1, 1954)

THE atomic beam magnetic resonance method has been used to measure the spin, hyperfine structure constant, and magnetic moment of the radioactive nucleus 3.1-hr Cs^{134m}. The apparatus constructed for this purpose incorporated the magnet design of Nagle,[1] but contained a movable compartment for rapid insertion and pumpdown of sources, and a detector compartment, removable through vacuum locks, making possible the collection of the radioactive atoms on disks at liquid nitrogen temperatures. The beam intensity of the active species was determined by counting, in a windowless flow counter, the 100-kev conversion electrons of Cs^{134m} from the deposit formed during constant exposure time.

The "flop-in" method of Zacharias[2] was employed to detect the low-field $[F=I+\frac{1}{2},\ m_F=-F\leftrightarrow F=I+\frac{1}{2},\ m_F=-(F-1)]$ transitions in both the active nuclide and inactive Cs^{133} in the beam. Collected in Table I are

Table I. Observed low-field resonance frequencies in Cs^{134m} and Cs^{133}.

ν_{133} (Mc/sec)	ν_{134m} (Mc/sec)
9.365	4.480
17.220	8.295
43.940	21.934
90.937	48.403
164.105	97.140

the resonances in Cs^{134m} found in magnetic fields determined by observing resonances of the same transition in Cs^{133} ($I=7/2$, $\Delta\nu=9193$ Mc/sec). In general, each frequency value is an average of the results of two experiments. A typical curve of a resonance in Cs^{134m} appears in Fig. 1.

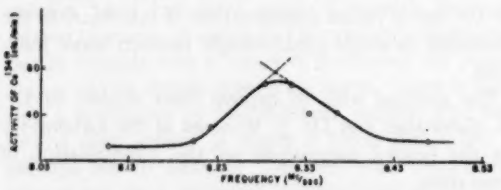

Fig. 1. A typical curve of a resonance in Cs^{134m}.

In sufficiently low magnetic fields the frequency at which the $F=I+\frac{1}{2},\ m_F=-F\leftrightarrow m_F=-(F-1)$ transition is observed is given to a high degree of approximation by[3]

$$\nu=1.400\frac{H}{I+\frac{1}{2}}+\left(1.400\frac{H}{I+\frac{1}{2}}\right)^2\frac{2I}{\Delta\nu},$$

where ν is the low-field transition defined above (in Mc/sec), H is the magnetic field (in gauss), I is the nuclear spin (in units of $\hbar$), and $\Delta\nu$ is the hyperfine structure constant (in Mc/sec). Solution of this equation using the first two pairs of data of Table I gives unambiguously a spin of 8 and $\Delta\nu\approx 3600$ Mc/sec. From the Fermi relation,[4]

$$\Delta\nu_{134m}/\Delta\nu_{133}=\frac{(2I_{134m}+1)\mu_{134m}}{I_{134m}}\cdot\frac{I_{133}}{(2I_{133}+1)\mu_{133}},$$

the magnetic moment, μ_{134m}, was then calculated to be 1.1 nm ($\mu_{133}=+2.58$ nm). At higher magnetic fields the approximate low-field equation is no longer valid, and the complete Breit-Rabi relation[5] is used to arrive at a more precise value of the hfs constant. Our best estimate at present is $\Delta\nu_{134m}=3662$ Mc/sec, based on the highest pair of frequencies listed in Table I and assuming that μ_I is positive in sign. The magnetic moment is then more precisely calculated to be 1.10 nm. Further experiments at higher frequencies are being conducted to establish the algebraic sign of the moment.

We wish to thank J. A. Dalman, whose numerous contributions of ingenious design have made possible the surmounting of the difficult technique problems inherent in this experiment and for his great assistance in the performance of the experiments. Acknowledgment is also gratefully made of the extensive design work of H. W. Ostrander and of the advice of and consultation with D. E. Nagle, which gave great impetus to the project in its initial stages.

[1] D. E. Nagle, thesis, Massachusetts Institute of Technology, 1947 (unpublished).
[2] J. R. Zacharias, Phys. Rev. **61**, 270 (1942).
[3] Davis, Nagle, and Zacharias, Phys. Rev. **76**, 1068 (1949).
[4] E. Fermi, Z. Physik **60**, 320 (1930).
[5] G. Breit and I. I. Rabi, Phys. Rev. **38**, 2082 (1931).

Decay of Cs^{134m} (3.1 hr)

A. W. Sunyar, J. W. Mihelich, and M. Goldhaber
Brookhaven National Laboratory, Upton, New York*
(Received June 2, 1954)

THE discovery reported in the two preceding letters,[1,2] that Cs^{134m} (3.1 hr), has a spin of 8 units ($\hbar$), reopens the question of its correct decay scheme. It was previously shown that this isomer decays by a 128-kev transition, identified as an $E3$ transition from its K conversion coefficient.[2] As the ground state of Cs^{134} has a measured spin of 4 units,[4] and as no β rays are observed from Cs^{134m}, it was considered likely that the metastable state has a spin of 7 units.[5] Because of the discrepancy between this value and the now directly measured value of 8 units for the

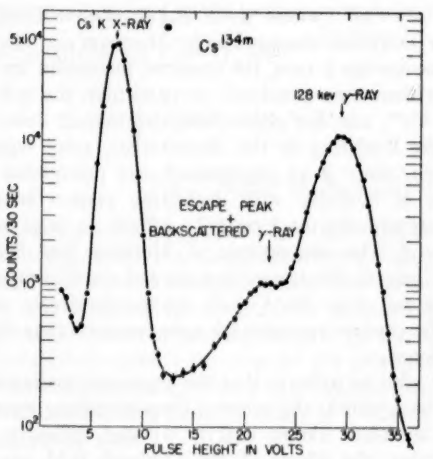

FIG. 1. Scintillation counter spectrum of Cs^{134m}, showing 128-kev γ ray and K x-rays accompanying K internal conversion.

spin, we have redetermined the K conversion coefficient of the 128-kev transition. The method was the same as previously described: x_K/γ ratio,[3] but an improved scintillation spectrometer was used (see Fig. 1). The $E3$ character of the 128-kev transition was confirmed. We find $\epsilon_K = 2.6 \pm 0.3$, whereas the theoretical values are $\alpha_2 \approx 0.61$, $\alpha_3 \approx 2.8$, $\alpha_4 \approx 14$.

It thus appears probable that the previously made tacit assumption of a single step (γ_1) from the metastable state to the ground state is incorrect, and that γ_1 is followed by a "hidden" low-energy transition (γ_2). We therefore searched for low-energy γ rays with a proportional counter and found indeed a 10.5 ± 0.7 kev γ ray (γ_2) of low intensity (see Fig. 2); $\gamma_2/x_K \approx 2 \times 10^{-2}$, $\epsilon_{tot} \approx 200$. From the recently calcluated absolute L_I and L_{II} conversion coefficients,[6] and the approximate empirical[7] and theoretical[8] L-subshell ratios (Table I)

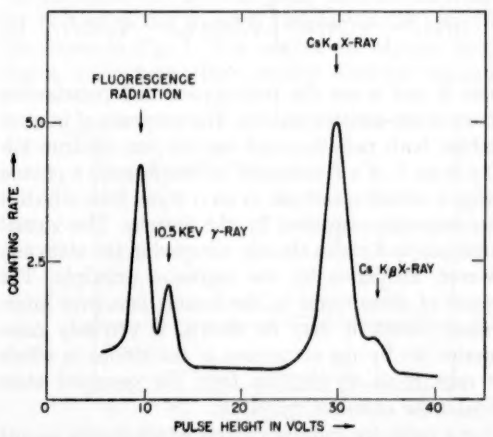

FIG. 2. Proportional counter spectrum showing 10.5-kev γ ray. An average of a counting rate meter trace is shown. Fluorescence radiations from the brass walls of the counter are also present.

TABLE I. Theoretical L conversion coefficients for γ_2.

	α_1	β_1	α_2	β_2
L_I[a]	~5.3	~76	~40	$\sim 1.7 \times 10^4$
L_{II}[a]	~5	~6.5	$\sim 10^4$	$\sim 10^2$
L_{III}[b]	[~10]	[~0.3]	$[\sim 1.8 \times 10^4]$	—
L_{total}	~20	~83	$\sim 2.8 \times 10^4$	$\sim 1.8 \times 10^4$

[a] Extrapolated values from tables of Rose, Goertzel, and Swift (reference 6).
[b] Estimated from L_{II} conversion using L_{II}/L_{III} values of Gellman, Griffith, and Stanley (reference 8) at 14.5 kev and $Z = 49$.

the best agreement is obtained for an $M1$ transition (with a probable admixture of $\lesssim 0.5$ percent $E2$, depending on the amount of M conversion). These conversion data alone cannot rule out the alternative assignment (99 percent) $E1+1$ (percent $M2$), which would, however, lead to unlikely parity assignments. The 10.5-kev γ ray and L radiations presumed to come from the internal conversion of the 10.5-kev transition, were found to be in coincidence with the 128-kev unconverted γ ray ($T_{1/2} \lesssim 10^{-7}$ sec). Thus, the following sequence of spins and parities: $4+$, $5+$, $8-$ (see Fig. 3),

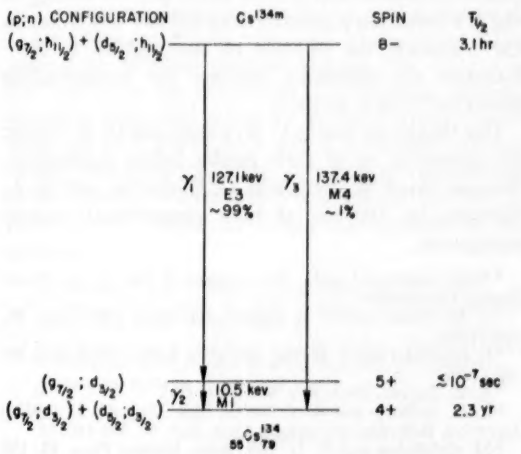

FIG. 3. Proposed decay scheme of Cs^{134m}. The most plausible configurations for the odd proton and odd neutron leading to the observed spins and compatible with the measured magnetic moments are shown.

is compatible with the experimental evidence. From these assignments and from the empirical formula for $M4$ lifetimes[9] a crossover transition (γ_3), $8- \xrightarrow{M4} 4+$, with an energy $\gamma_1+\gamma_2 = 138.5$ kev and an intensity of ~0.5 percent should be expected. A search for the crossover transition with a 180° permanent magnet spectrograph was indeed successful, showing K, L, and M conversion electrons and yielding an energy $E_3 = 137.4 \pm 0.5$ kev. An improved value for the energy of γ_1 was obtained, $E_1 = 127.1 \pm 0.5$ kev. The energy difference between these two transitions could be estimated more accurately as $E_2 = E_3 - E_1 = 10.3 \pm 0.4$ kev, in good agreement with the value found directly for γ_2.

The crossover transition was too weak to permit an accurate estimate of its electron intensities. Comparing its K and L electrons to the M electrons of the "stop over" 127-kev transition, we find for the intensity of the crossover transition 0.8 ± 0.5 percent, in good agreement with the expectations for a one-particle transition $h_{11/2}\rightarrow d_{3/2}$. The K/L ratio was found to be 2 ± 1.3, which is more consistent with the empirical K/L ratio[9] for an $M4$ than for an $E4$ transition.

The most plausible shell model configurations for the odd proton and odd neutron of $_{55}Cs^{134}{}_{79}$ are shown in Fig. 3. Mixed states are expected,[10] since $d_{5/2}$ and $g_{7/2}$ proton levels in Cs nearly coincide in energy. These configurations indicate that, in contrast to the $M4$ and $M1$ transitions, the $E3$ transition of Cs^{134m} should be "forbidden" as a one-particle transition, both because the particle making the transition is a neutron, and because in strict j-j coupling the transition is forbidden; it is indeed one of the slowest known $E3$ transitions,[9] with an $|M|^2\approx10^{-6}$.

It is interesting to note that the addition of a proton to Xe^{133} leads to a lowering of the energy difference between metastable and ground state, i.e., the energy of the $M4$ transition is reduced from 232 kev to 137 kev in Cs^{134}, whereas the addition of two protons to Xe^{133} increases the difference between the corresponding states to 275 kev[5] in Ba^{135}.

Our thanks are due to V. W. Cohen and D. A. Gilbert for informing us of their results before publication. We also thank W. Bernstein, G. Harbottle, and M. L. Perlman for the use of their proportional counter equipment.

* Work performed under the auspices of the U. S. Atomic Energy Commission.

[1] V. W. Cohen and D. A. Gilbert, this issue, Phys. Rev. **95**, 569 (1954).
[2] L. Goodman and S. Wexler, preceding Letter, Phys. Rev. **95**, 570 (1954).
[3] A. W. Sunyar, Phys. Rev. **83**, 864 (1951).
[4] E. H. Bellamy and K. F. Smith, Phil. Mag. **44**, 33 (1953); Jaccarino, Bederson, and Stroke, Phys. Rev. **87**, 676 (1952).
[5] M. Goldhaber and R. D. Hill, Revs. Modern Phys. **24**, 179 (1952).
[6] Rose, Goertzel, and Swift (privately circulated tables).
[7] J. W. Mihelich, Phys. Rev. **87**, 646 (1952).
[8] Gellman, Griffith, and Stanley, Phys. Rev. **85**, 944 (1952).
[9] M. Goldhaber and A. W. Sunyar, Phys. Rev. **83**, 906 (1951).
[10] A. de-Shalit and M. Goldhaber, Phys. Rev. **92**, 1211 (1953).

Radiative Capture of Orbital Electrons

R. J. Glauber and P. C. Martin
Harvard University, Cambridge, Massachusetts

(Received June 1, 1954)

THE continuous spectra of γ rays accompanying orbital electron capture have recently been measured for a number of elements.[1-3] These have thus far been compared with a theoretical spectrum of the form $x(1-x)^2$ (where $x=E/E_{max}$), obtained under highly simplified assumptions by Morrison and Schiff.[4] For low-energy γ rays, the observed intensities are far higher than those predicted. In particular, the spectra Fe^{55}, Cs^{131}, and Ge^{71} have been determined down to energies bordering on the characteristic x-ray region; in each, there is an unexplained and precipitous increase of intensity with decreasing photon energy. Deviations from the form $x(1-x)^2$ are, in fact, to be expected. The assumptions of Morrison and Schiff, that Coulomb effects may be neglected and that capture occurs only from the K-shell, are quantitatively valid only for capture processes far more energetic than those mentioned.

We wish to indicate that the above approximations may be avoided; the internal bremsstrahlung spectra may be found almost exactly without difficulty. In particular, the effects of the Coulomb field can be treated precisely. When this is done, the spectrum of magnetic dipole radiation accompanying K capture is found indeed to have the form $x(1-x)^2$, for all energies of interest. Further considerations show the remaining and dominant part of the observed low-energy radiation to be electric dipole in character and to arise from the capture of electrons from P states.

We assume that the electron capture process is an allowed one, with a matrix element of the most general form,

$$H_e=\sum_\lambda c^{(\lambda)}\langle T_\mu{}^{(\lambda)}\rangle(\bar{\chi}(0)T_\mu{}^{(\lambda)}\psi(0)), \qquad (1)$$

in which $\psi(0)$ and $\chi(0)$ are the electron and neutrino wave functions evaluated at the nucleus, the $c^{(\lambda)}$ are linear combination coefficients for the various β-coupling operators $T_\mu{}^{(\lambda)}$, and $\langle T_\mu{}^{(\lambda)}\rangle$ is a nuclear matrix element. The radiative transition of an electron from the state $\psi_i(\mathbf{r})$ to the state $\psi_f(\mathbf{r})$ has the familiar matrix element[5]

$$(H_R)_{fi}=-e(2\pi/k)^{\frac{1}{2}}\int\bar{\psi}_f(\mathbf{r})e_\mu\gamma_\mu e^{-i\mathbf{k}\cdot\mathbf{r}}\psi_i(\mathbf{r})d\tau, \qquad (2)$$

where $\mathbf{k}$ and $\mathbf{e}$ are the propagation and polarization vectors of the emitted photon. The processes of interest combine both radiation and capture; an electron initially in an S or a P state will ordinarily emit a photon during a virtual transition to an S state, from which it is subsequently captured by the nucleus. The virtual transitions to S states already occupied in the atom are, however, forbidden by the exclusion principle. The absence of these terms in the summations over intermediate states, it may be shown, is precisely compensated for by the occurrence of transitions in which the capture of an electron from the occupied state precedes the radiative transition.

For a radiative capture process which leaves vacant an initially occupied state $\psi_n(\mathbf{r})$ (with $E_n<0$), the expressions (1) and (2) may be shown, after some re-

arrangement, to lead to the total matrix element

$$M=(ie/m)(2\pi/k)^{\frac{1}{2}}\sum c^{(\lambda)}\langle T_\mu{}^{(\lambda)}\rangle$$

$$\times\int(\bar{\chi}(0)T_\mu{}^{(\lambda)}\mathcal{G}_{E_n-k}(0,\mathbf{r})$$

$$\times e^{-i\mathbf{k}\cdot\mathbf{r}}\mathbf{e}_\eta(\partial_\eta-\tfrac{1}{2}\sigma_{\eta\rho}k_\rho)\psi_n(\mathbf{r}))d\tau, \quad (3)$$

in which $\sigma_{\eta\rho}=(i/2)[\gamma_\eta,\gamma_\rho]$ and $k_\rho=(\mathbf{k},k)$. The function $\mathcal{G}_{E_n-k}(0,\mathbf{r})$, which is a Green's function for the second order Dirac equation, implicitly embodies the summation over intermediate states. It is quite adequately approximated in the present context, by the simpler nonrelativistic Green's function for the propagation of an electron with energy E_n-k in a Coulomb field. The latter function is defined in terms of Coulomb wave functions $\varphi_j(\mathbf{r})$ as

$$G_{E_n-k}(0,\mathbf{r})=\sum_j\frac{\varphi_j(0)\varphi_j{}^*(\mathbf{r})}{E_j-E_n+k}. \quad (4)$$

Since this expression has spherical symmetry about the origin, it is easily evaluated by solving the appropriate radial Schrödinger equation. The occurrence of a particularly tractable form for the Coulomb Green's function stems from the fact that electron capture necessarily takes place at the center of force. The solution is found to contain a Whittaker function and has integral representation,

$$G_{E_n-k}(0,\mathbf{r})=(m\beta/\pi)e^{-\beta r}\int_0^\infty e^{-2\beta ru}\left(\frac{1+u}{u}\right)^{Z/\beta a_0}du, \quad (5)$$

for $k-E_n>Z^2$ Rydbergs, where $\beta=[2m(k-E_n)]^{\frac{1}{2}}$, and a_0 is the Bohr radius.

With the expression (5), the integrations required to find the matrix element (3) may be carried out analytically. The resulting γ-ray spectra for capture from the various significant electron shells have been calculated for Fe^{55} which has an energy release[1] of 220 kev. They are shown in Fig. 1. The spectra for capture from S states, aside from their slightly different maximum energies, have the general shape $x(1-x)^2$. The P-state spectra are by comparison quite weak at high energies and extremely intense near the characteristic x-ray lines. The processes responsible for the intensity peaks are ones in which capture of an S electron is followed by a radiative transition from a higher P state. They differ from the normal and highly probable course of electron capture and subsequent emission of characteristic x-rays only by relaxation of the requirement of energy conservation in the intermediate state. The P state spectra of Fig. 1 may, in fact, be thought of as representing the extreme wings of the characteristic x-ray lines.

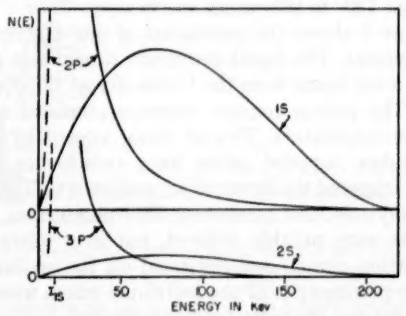

FIG. 1. Gamma-ray spectra for radiative capture from various electron shells of Fe^{55}. The characteristic x-ray region lies below I_{1S}, the K-shell ionization energy.

For a given energy release, the intensities of the P-state spectra increase relative to those of the S states roughly as the square of the nuclear charge. Hence for Ge^{71} and Cs^{131} the P-state contributions should dominate all save the upper ends of the spectra. The shapes observed[2] corroborate this. Screening of the Coulomb field will act to reduce somewhat the intensities of spectra from the $n=2$ and 3 shells and will be taken into account in seeking quantitative agreement with experiment.

The analysis described may be applied equally well to forbidden transitions which will be characterized in general by differing spectrum shapes. The capture in Fe^{55} for which log ft equals 6.1, is evidently allowed, but quite unfavored, a fact which might be anticipated from the shell model since $\Delta l=2$. A detailed account of the techniques employed including an examination of the effects of screening is in preparation. We wish to thank Dr. T. Berlin for calling this problem to our attention.

[1] L. Madansky and F. Rasetti, Phys. Rev. **94**, 407 (1954).
[2] B. Saraf, Phys. Rev. **94**, 642 (1954); also work on Ge^{71} [B. Saraf, Phys. Rev. **95**, 97 (1954)].
[3] Emmerich, Singer, and Kurbatov, Phys. Rev. **94**, 113 (1954).
[4] P. Morrison and L. I. Schiff, Phys. Rev. **58**, 24 (1940).
[5] We employ units in which $\hbar=1$, $c=1$.

Proton-Neutron Coincidences in the High-Energy Photodisintegration of Lithium*

M. Q. BARTON AND J. H. SMITH
Department of Physics, University of Illinois, Champaign, Illinois
(Received June 1, 1954)

WHEN photons with energies of several hundred Mev interact with complex nuclei, they eject high-energy protons and neutrons in greater numbers than compound nucleus formation can explain. The cross sections and angular distributions of such reactions indicate a direct interaction between the photons and individual nucleons. Of the various models proposed to explain these results, perhaps the most appealing is the "pseudodeuteron" model discussed by Levinger.[1] Several experiments have tended to confirm

this theory,[2] but the clearest proof would seem to be the observation of the simultaneous ejection of a proton and a neutron in the photodisintegration of a complex element. We have recently observed coincident protons and neutrons from lithium irradiated with 265-Mev bremsstrahlung from the University of Illinois betatron.

In our experiment a proton counter consisting of a series of five organic scintillators was set at 76.5° to the x-ray beam. Pulse heights photographed from an oscillograph in three of the organic scintillators allowed an almost unambiguous identification of the particle and its energy. Protons in the energy range 65 Mev to about 200 Mev were observed in the same betatron run. When this counter was run by itself, electrons, mesons, meson stars, and protons were all clearly distinguished. This counter is more adequately described in the accompanying letter on the photodisintegration of deuterium.

In order to observe coincident protons and neutrons a counter 4 inches in diameter by 10 inches long filled with terphenyl in phenylcyclohexane was placed behind 2 inches of lead on the side of the beam opposite the proton counter. A coincidence between this counter and the proton telescope triggered the sweep of the oscillograph used for photographing the pulse heights. The pulse height distribution in the proton telescope clearly indicated that only protons were in coincidence with neutrons on the other side of the beam.

A further check on the two-body nature of such interactions was made by swinging the neutron counter in angle. Figure 1 shows the number of coincidences from a lithium target as a function of the neutron counter angle. A definite angular correlation is observed. The angular correlation from deuterium is shown for comparison. The equality of the peak angles gives striking confirmation of the two-body nature of the interaction. The broadening of the lithium curve is about what would be expected from the internal momentum distribution of the "pseudodeuteron" in the nucleus.

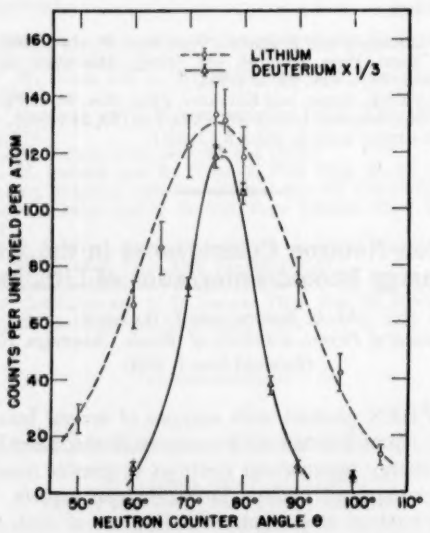

FIG. 1. Neutron-proton coincidences as a function of the angle of the neutron counter. The proton counter is fixed at 76.5°. The lithium ordinate is in most cases the actual number of counts observed. The deuterium curve has been normalized for number of atoms in the beam and reduced by a factor of three to facilitate comparison.

In a supplementary experiment with A. O. Hanson and T. Yamagata described in an accompanying letter, the liquid deuterium target was used to measure the efficiency of our neutron counter as 6.8 percent. We can then estimate that 53 percent of all photoprotons from lithium have a correlated neutron. If the probability of subsequent interactions in the nucleus is taken into account, the possibility remains that all photoprotons in this energy range are produced in such a two-body process.

We have observed this effect qualitatively in beryllium, carbon, boron, nitrogen, and oxygen targets.

The data presented in this letter are at best preliminary, and quantitative conclusions are subject to considerable uncertainty. However, the qualitative existence of correlated protons and neutrons in the high-energy photoeffect leaves little doubt of the basic correctness of the "pseudodeuteron" model for at least a large fraction of the interactions.

* This work was supported in part by the joint program of the Office of Naval Research and the U. S. Atomic Energy Commission.

[1] J. S. Levinger; Phys. Rev. **84**, 43 (1951).

[2] J. W. Weil and B. D. McDaniel, Phys. Rev. **92**, 391 (1953). See this paper for other references.

Photodisintegration of Deuterium by 265-Mev Bremsstrahlung

T. YAMAGATA, M. Q. BARTON, A. O. HANSON, AND J. H. SMITH
Department of Physics, University of Illinois, Urbana, Illinois

(Received June 1, 1954)

WE have measured the differential cross section of the photodisintegration of deuterium at 45°, 75°, and 120° in laboratory coordinates.

Figure 1 shows the schematics of our experimental arrangement. The liquid deuterium target[1] was placed in the x-ray beam from the University of Illinois betatron. The proton counter telescope consisted of five organic scintillators. Two of them, viewed by 931-A phototubes, supplied pulses for a coincidence circuit which triggered the sweep of an oscilloscope. The other three crystals were viewed by 5819 phototubes. Their outputs were suitably delayed, put in a mixing and integrating circuit, and displayed on the oscilloscope. 35-mm photographs of the individual traces were later projected and the pulse heights measured.

In most cases, pulses from protons, mesons, and electrons are readily distinguishable, since particles differing

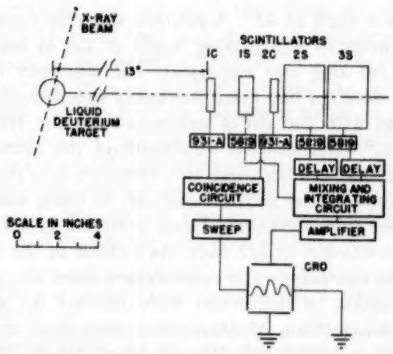

FIG. 1. Sketch showing size of scintillators in proton counter and block diagram of associated electronics.

in mass have different correlations between the three pulses recorded on the film. In Fig. 2, a typical plot of the pulse heights in $1-S$ *vs* those in $2-S$ is shown. It is seen that the points make three distinct groups. The outermost group is protons, whereas the middle and the innermost are mesons and electrons, respectively.

As can be seen in Fig. 2, protons with sufficient energy to pass through $2-S$ might be confused with lower energy protons or meson stars except for the third pulse. The plot of the second *vs* the third pulse heights shows a pattern similar to Fig. 1 and serves for the necessary identification.

The energy of a proton was determined by measurement of the height of the second or the third pulse, according as the proton stopped in the second crystal or entered the third one. The energy loss in these two crystals was calculated as a function of the initial photon energy, and taking into account the light output efficiency of the crystal[2] and nonlinearity of the chain amplifiers, a pulse height *vs* photon energy curve was established. For the calibration, the maximum energy losses in these crystals were assigned to the highest pulses. It was also possible to shift the energy scale by putting an aluminum absorber between the first two scintillators.

The number of protons found in a certain energy bin had to be corrected for scattering effects. Two attempts were made to account for the nuclear scattering. The first was to use the geometrical cross section as the nuclear scattering cross section. An isotropic angular distribution was assumed in the center-of-mass coordinates. The portion of protons which miss the $2-C$, $2-S$, or $3-S$ crystals (referring to Fig. 1) were calculated. This correction reaches a maximum value of 17.6 percent. Since the error due to nuclear scattering

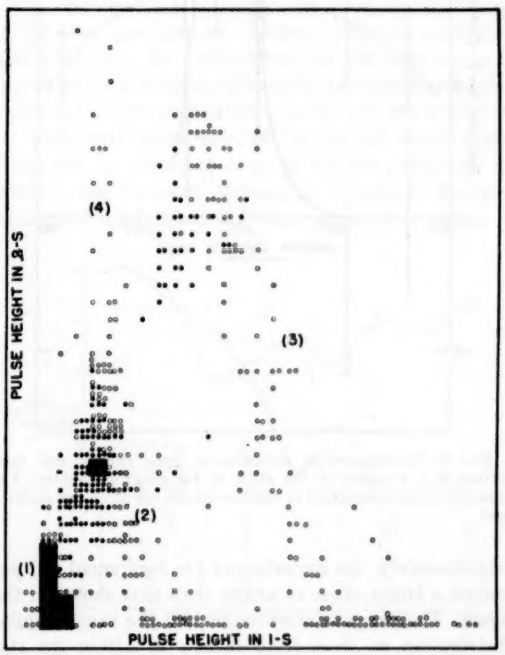

FIG. 2. Correlation of pulse heights in $1-S$ and $2-S$. Each point represents an event with pulse heights in $1-S$ and $2-S$ indicated by position on the chart. A solid circle indicates there is a pulse present in the last crystal $3-S$. Its height is not indicated. Electrons, mesons, and protons form distinct groups labeled 1, 2, and 3, respectively. Group 4 probably represents meson stars. Regions too dense to show individual events have been blackened in.

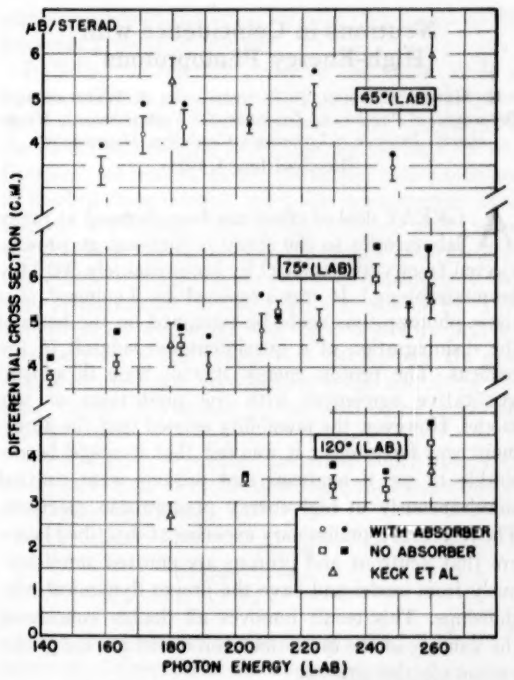

FIG. 3. Differential cross section of the photodisintegration of deuterium at 45°, 75°, and 120° in laboratory coordinates. Open points are corrected using geometrical cross sections. Solid points are corrected on a basis of neutron scattering cross sections.

is large, a second correction using the total cross section for neutron scattering as given by Taylor *et al.*,[3] was used, which represents an upper limit on the correction.[4] In this case, the maximum correction amounted to 28.3 percent. Coulomb scattering and multiple scattering effects were not corrected for, because they were found much smaller than the nuclear scattering effect.

Figure 3 shows graphs of our results. The open and the solid points correspond to the first and second type correction, respectively. The indicated standard deviations are due to the counting statistics only. They are in general consistent with the results of Keck *et al.*,[5] which are also plotted on the graphs. The values are not very consistent in the highest-energy bin. This is not surprising, since the scattering effects are the largest there, and also since the value there is very sensitive to the maximum energy of the bremsstrahlung.

[1] E. A. Whalin and R. A. Reitz, Rev. Sci. Instr. (to be published).
[2] J. B. Birks, Proc. Phys. Soc. (London) **A64**, 1814 (1951).
[3] A. E. Taylor and E. Wood, Phil. Mag. **44**, 95 (1953).
[4] H. de Carvalho found recently that nuclear scattering cross sections for protons and neutrons agreed well at high energies. [Cosmic-Ray Symposium at Purdue University, Indiana, May, 1954 (unpublished).]
[5] Keck, Littauer, O'Neill, Perry, and Woodward, Phys. Rev. **93**, 824 (1954).

Neutrons in Coincidence with High-Energy Photoprotons*

H. Myers, A. Odian, P. C. Stein, and A. Wattenberg
Department of Physics and Laboratory for Nuclear Science, Massachusetts Institute of Technology, Cambridge, Massachusetts
(Received June 1, 1954)

A GREAT deal of effort has been devoted at many laboratories to the study of high-energy protons ejected from various nuclei by approximately 300-Mev bremsstrahlung.[1] It was proposed by Levinger[2] that these photoprotons could be explained on the basis of the disintegration of a quasi-deuteron subunit in the nucleus. The proton energy spectra were in general qualitative agreement with the predictions of this model. However, the possibility existed that the agreement was fortuitous[1]; it was felt that it would be desirable to see if neutrons and protons were emitted simultaneously in high-energy photoproton reactions. The results of a preliminary experiment described below are that neutrons and protons are emitted simultaneously from nuclei and have the proper dynamical relationships. This result removes all doubts concerning the validity of the quasi-deuteron model for the photoproton ejection process.

A proton telescope consisting of three scintillators was employed with an energy spread of about 10 Mev at 135 Mev. In these measurements the proton detector was fixed at 45°. A neutron detector consisting of a cylinder of scintillating liquid 10 cm in diameter and 30 cm long was employed. The efficiency of the neutron detector had been previously determined to be 9 percent with the aid of neutrons from the Harvard cyclotron. Measurements were made of the number of coincidences between these two detectors as a function of the angle of the neutron counter. In these measurements the bremsstrahlung beam from the M.I.T. synchrotron was run at 325 Mev. As a check of the equipment the neutron-proton coincidences from the photodisintegration of deuterium were studied by a $D_2O - H_2O$ subtraction. Measurements were then made of the neutron-proton coincidences from carbon. The results of both of these measurements are shown in Fig. 1.

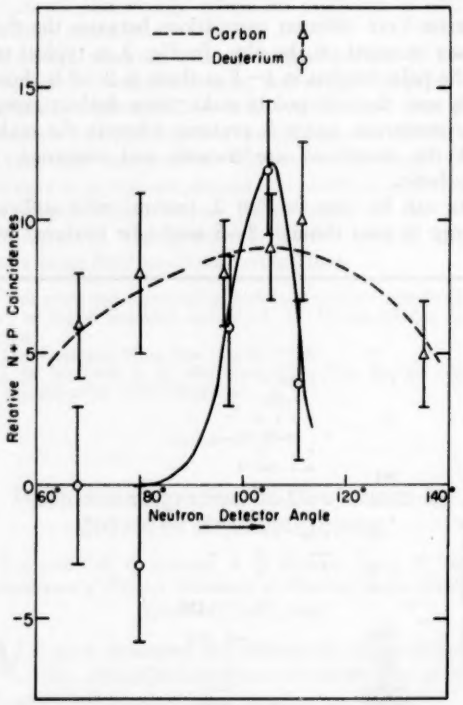

FIG. 1. Neutron-proton coincidences from carbon and deuterium as a function of the angle of the neutron counter. The coincidences are expressed in relative counts per atom per monitor unit.

Unfortunately, the mounting of the equipment did not permit a larger range of angles than that shown in the figure. The oxygen coincidences had the same angular distribution as those from carbon to within the statistics obtained. The accidental coincidence rate was measured and found to be negligible.

If one assumes that the neutrons are emitted in an angular cone around the angle predicted for the neutrons from deuterium and if one assumes that the angular distribution does not extend appreciably beyond the

range investigated, one finds that there are about 1.2 neutrons in coincidence with every proton from carbon. The fact that this is greater than unity could be explained by poor statistics, or by the fact that the solid angle subtended by the neutron counter is no doubt due to a lead housing surrounding it. Further investigations are being made of this phenomenon with better geometry; however, the authors feel that most of the time neutrons and protons are emitted simultaneously from carbon and oxygen at these high energies.

* This work was supported in part by the joint program of the U. S. Office of Naval Research and the U. S. Atomic Energy Commission.

[1] Feld, Godbole, Odian, Scherb, Stein, and Wattenberg, Phys. Rev. 94, 1000 (1954). See this paper for references to other work.
[2] J. S. Levinger, Phys. Rev. 84, 43 (1951).

Diffuse Surface Optical Model for Nucleon-Nuclei Scattering*

ROGER D. WOODS AND DAVID S. SAXON
University of California, Los Angeles, California and National Bureau of Standards, Los Angeles, California
(Received May 24, 1954)

WE report some first results of calculations of the differential cross section for the elastic scattering of 20-Mev protons by medium and heavy nuclei, assuming that the nuclear part of the interaction is described by a spinless, spherically symmetric, complex potential. These calculations, which are accomplished by numerical integration of the partial wave radial equations for values of L up to 13, are performed on SWAC, the National Bureau of Standards Western Automatic Computer. The time required to obtain a complete differential cross section, tabulated at 5° intervals, is 15 to 20 minutes.

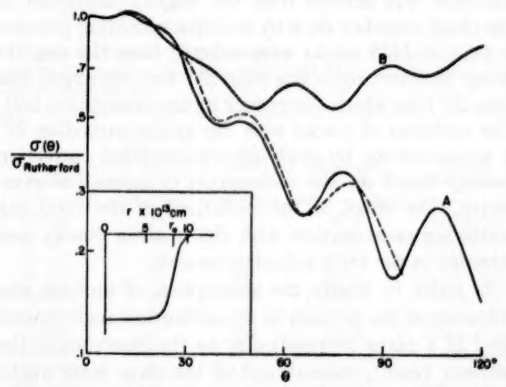

FIG. 1. Elastic scattering of 22-Mev protons by Pt relative to Rutherford scattering. The dashed curve is the experimental result of Cohen and Neidigh (see reference 3), the normalization of which is somewhat uncertain. Curve A is calculated for a diffuse surface model with $V=38$ Mev, $W=9$ Mev, $r_0=8.24\times10^{-13}$ cm, and $a=0.49\times10^{-13}$ cm. The shape of the well is shown in the small drawing at the lower left. Curve B is calculated for a square well of comparable size and depth.

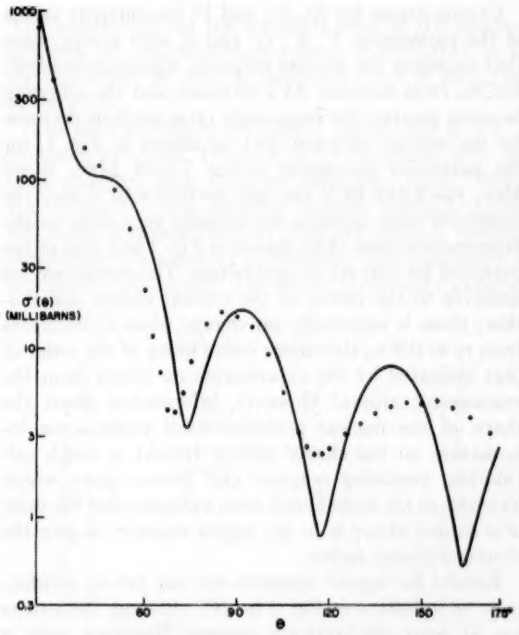

FIG. 2. Elastic scattering of 18-Mev protons by Ni. The experimental points are those of Dayton (see reference 1). The curve was calculated for a diffuse surface model with $V=40$ Mev, $W=10$ Mev, $r_0=5.3\times10^{-13}$ cm, and $a=0.35\times10^{-13}$ cm.

Initially, the complex potential was taken to be a square well with all of the nuclear charge essentially on the nuclear surface; this because of the simplicity of the model and because of its apparent success for Al.[1] However, for heavier nuclei, the square well results are in marked disagreement with the experimental cross sections of Gugelot,[1] Burkig and Wright,[2] and Cohen and Neidigh.[3] In particular, the square well predicts scattering at larger angles which is considerably too large as illustrated in Fig. 1 for the case of Pt. This disagreement, which has also been noted by others,[4] persists even if the square well parameters are permitted to vary over an extensive range and if the nuclear charge is assumed to be distributed over the nuclear volume.

Consequently, a nuclear potential which decreases smoothly to zero is now being studied, the assumed form of this potential being

$$V(r)=\frac{V+iW}{1+e^{(r-r_0)/a}},$$

where r_0 is a measure of the nuclear size and a determines the diffuseness of the nuclear surface. The Coulomb part of the interaction is taken to be that arising from a uniform charge distribution over a sphere of radius r_1 (not necessarily equal to r_0).

Computations for Al, Ni, and Pt for different values of the parameters V, W, r_0, and a, with $r_1=r_0$, show that rounding the nuclear potential significantly modifies the cross sections. As a increases and the rounding becomes greater, the large-angle cross sections decrease for the heavier elements and, as shown in Fig. 1, for the particular parameter values $V=38$ Mev, $W=9$ Mev, $r_0=8.24\times10^{-13}$ cm and $a=0.49\times10^{-13}$ cm, the computed cross sections are actually very close to the experimental ones. Also shown in Fig. 1 is a plot of the potential for this set of parameters. The results are *not* sensitive to the radius of the nuclear charge distribution; there is essentially no change when r_1 decreases from r_0 to $0.8\,r_0$, this latter value being of the order of that indicated by the experiments on x-rays from the mu-mesonic atoms.[5] However, information about the shape of the nuclear potential itself yields some information on the charge radius. Indeed, a rough calculation, assuming neutron and proton gases which fill states to the same Fermi level, indicates that the value of a quoted above is in the region required to give the observed charge radius.

Results for lighter elements are not yet so satisfactory, as indicated in Fig. 2 for Ni, although the results are at least qualitatively correct. However, only a limited range of the parameters has so far been investigated. Further computations are now in progress.

It is planned to extend the calculations to other elements and to other energies. It is also planned to calculate differential cross sections for the elastic scattering of neutrons in this energy region[6] using the same model.

* The preparation of this paper was sponsored (in part) by the Office of Naval Research.

[1] R. E. Le Levier and D. S. Saxon, Phys. Rev. **87**, 40 (1952); P. C. Gugelot, Phys. Rev. **87**, 525 (1952). Later results of I. E. Dayton, kindly communicated to us by Professor Gugelot prior to publication, showed that this success was fortuitous since the Al cross sections contained much deeper and narrower minima than had previously been reported.

[2] J. W. Burkig and B. T. Wright, Phys. Rev. **82**, 451 (1951).

[3] B. I. Cohen and R. V. Neidigh, Phys. Rev. **93**, 282 (1954). These results were kindly communicated to us prior to publication.

[4] F. Rohrlich and D. M. Chase, Phys. Rev. **94**, 81 (1954).

[5] V. L. Fitch and J. Rainwater, Phys. Rev. **92**, 789 (1953); L. N. Cooper and E. M. Henley, Phys. Rev. **92**, 801 (1953).

[6] Some preliminary results of experiments by J. H. Coon on the elastic scattering of 14-Mev neutrons from several elements have been kindly supplied prior to publication by Dr. J. H. Coon and Dr. R. Thomas.

Neutron-Proton Scattering at 300 Mev*

J. De Pangher†
Radiation Laboratory, Department of Physics, University of California, Berkeley, California

(Received June 1, 1954)

A WILSON cloud chamber,[1,2] containing only hydrogen and water vapor, was photographed stereoscopically in a magnetic field[3] of strength 22 000 gauss to obtain data[2,4] on the protons scattered by 300-Mev neutrons. Certain selection criteria were adopted for the measurements of the tracks, which were obtained in two runs at the Berkeley cyclotron. A lower limit of 155 Mev was set on the neutron energy for a track to be accepted. Definite regions of the cloud chamber were chosen for the measurements in each of the two runs. Tracks whose dip angles exceeded 50° were excluded from measurement. The scatter angle was generally limited to 85°, although a few trackes were measured with angles up to 86° to make sure no 85° tracks were missed.

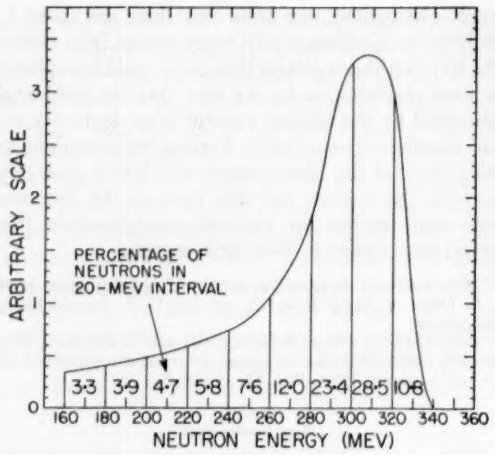

FIG. 1. The unfolded neutron energy spectrum from 340-Mev protons in a $1\frac{3}{4}$-in. thick LiD target. Errors of measurement were taken from the original data by an error-unfolding process.

The energy spectrum for the neutrons that were produced in a LiD target, $1\frac{3}{4}$ in. thick, by 340-Mev protons inside the cyclotron is shown in Fig. 1. This spectrum was derived from the original histogram of the cloud-chamber data by an error-unfolding process. A total of 1435 tracks were selected from the angular group (scatter angles less than 85° and dip angles less than 25°) for which the energy measurements are best. The omission of tracks with dip angles exceeding 25° is accounted for by applying a geometrical correction factor,[5] based on the assumption of azimuthal symmetry. The effect of the variation[6] of the total n-p scattering cross section with the neutron energy was included in the error-unfolding process.

In order to justify the assumption of uniform distribution of the protons in the azimuthal angle (measured in a plane perpendicular to the direction of the neutron beam), tabulations[2] of the data were made. Figure 2 shows the azimuthal distribution for dip angles less than 40° and for neutron energies above 200 Mev. Tracks with dip angles greater than 40° fall into the excluded region and are not tabulated. The number of tracks for any square or partial square is given inside the square. The numbers within any vertical column

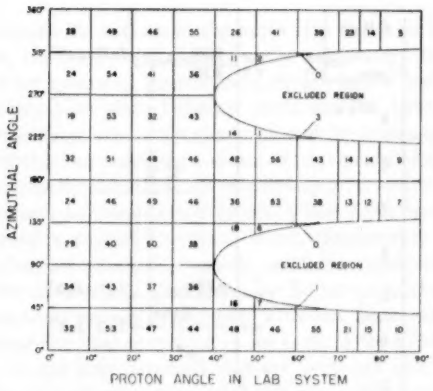

FIG. 2. Azimuthal distribution for dip angles less than 40°. Neutron energies are greater than 200 Mev.

and contained in whole squares should agree within the limitations imposed by the statistical errors of measurement. A consideration of these data shows that the assumption of uniformity of the azimuthal distribution is valid.

Table I lists the angular distribution data, based on 2057 tracks, for the neutrons in the center-of-mass system. The data are limited to neutrons with energies above 200 Mev and to protons with dip angles less than 40°. The geometrical correction factor has the value unity for proton deflection angles less than 40°, but above 40° the value of this factor rises steadily up to the value 2.25 at 90°. By assuming a total n-p cross section of 35 mb, it is possible to calculate the differential cross section from the total weighted number of tracks. However, the standard statistical errors in the differential cross section are based on the uncorrected number of tracks in the 10-degree angular intervals.

TABLE I. Angular distribution of neutrons in center-of-mass system for neutron energies above 200 Mev and for proton dip angles less than 40°.

Angle	Number of tracks first run	Number for both runs	Weighted number	mb per steradian
10–20	26	37	82.2	3.83±0.63
20–30	42	56	121.9	3.48±0.47
30–40	50	86	181.0	3.81±0.41
40–50	70	102	205.2	3.50±0.35
50–60	66	107	200.7	2.96±0.29
60–70	70	98	173.5	2.31±0.23
70–80	63	102	161.8	2.02±0.20
80–90	78	112	155.6	1.89±0.18
90–100	75	116	125.0	1.51±0.14
100–110	104	166	166.0	2.07±0.16
110–120	114	163	163.0	2.17±0.17
120–130	90	170	170.0	2.51±0.19
130–140	114	179	179.0	3.06±0.23
140–150	118	193	193.0	4.06±0.29
150–160	98	165	165.0	4.71±0.37
160–170	81	139	139.0	6.48±0.55
170–180	36	66	66.0	9.14±1.12

The upper limit on the standard error in the neutron angle in the center-of-mass system is estimated to be ±3.0°, while the average standard error is estimated to be ±1.5°.

The data contained in Table I are plotted in Fig. 3 in histogram form. They are to be compared with the data obtained with counters by Kelly, Leith, Segrè, and Wiegand,[7] who reported neutron energies (about 260 Mev) somewhat smaller than the neutron energies measured in the present experiment. The agreement is considered satisfactory. The special point was computed

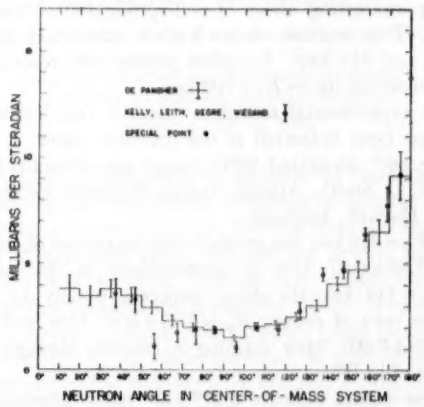

FIG. 3. Two sets of data are displayed here, the cloud chamber work (histogram) and the experimental points of Kelly *et al.* on the angular distribution of neutrons in the center-of-mass system. The meaning of the special point is given in the text.

from a smooth curve drawn through the counter data to illustrate how the cloud chamber with its selected 10-degree channel width would depict this rapidly changing portion of the angular-distribution curve. The cloud-chamber data extended into smaller neutron angles than do the counter data and clearly show a marked departure from symmetry about 90° in contrast to the 90-Mev data,[8,9] which exhibit symmetry about 90°.

Thanks are due to Professor W. M. Powell, who suggested this problem, and whose encouragement and interest in the progress of the work have been a constant inspiration to this writer.

* This work was performed under the auspices of the U. S. Atomic Energy Commission.

† Now at the Hanford Atomic Products Operation, General Electric Company, Richland, Washington.

[1] J. De Pangher, Phys. Rev. **83**, 894 (1951).
[2] J. De Pangher, University of California Radiation Laboratory Report UCRL-2153, March, 1953 (unpublished).
[3] W. M. Powell, Rev. Sci. Instr. **20**, 403 (1949).
[4] J. De Pangher, Phys. Rev. **92**, 1084 (1953).
[5] Brueckner, Hartsough, Hayward, and Powell, Phys. Rev. **75**, 555 (1949).
[6] Mott, Guernsey, and Nelson, Phys. Rev. **88**, 15 (1952).
[7] Kelly, Leith, Segrè, and Wiegand, Phys. Rev. **79**, 96 (1950).
[8] O. Chamberlain and J. W. Easley, Phys. Rev. **94**, 208 (1954).
[9] C. Y. Chih and W. M. Powell (private communication).

Gamma Rays from the $Si^{29}(p,\gamma)P^{30}$ Reaction

P. M. Endt, J. C. Kluyver, and C. van der Leun
Physisch Laboratorium der Rijksuniversiteit, Utrecht, Netherlands
(Received May 18, 1954)

In a preceding paper[1] energy measurements have been described of gamma rays from the $Mg^{26}(p,\gamma)Al^{26}$ reaction, giving information the on position and isobaric spin of the Al^{26} ground state and first excited state.

The $Si^{29}(p,\gamma)P^{30}$ reaction has now been studied to obtain data on the lowest states in P^{30}, a missing link in the interesting series of self-conjugated $A=4n+2$ nuclei. This reaction shows known resonances at $E_p=326$ and 414 kev.[2] No other pronounced resonances were observed up to $E_p=700$ kev.

The experimental technique used in this investigation has been indicated in the previous paper. A thin (16 $\mu g/cm^2$) separated $Si^{29}O_2$ target was obtained from Dr. M. L. Smith, Atomic Energy Research Establishment, Harwell, England.

At $E_p=326$ kev the ground-state transition of energy $E_{\gamma 1}=5.86\pm0.07$ Mev is predominant in the decay. At $E_p=414$ kev the decay proceeds mainly by two gamma rays of energy $E_{\gamma 2}=5.27\pm0.07$ Mev and $E_{\gamma 3}=0.688\pm0.007$ Mev forming a cascade through the first level in P^{30}.

These values indicate a $P^{30}-Si^{30}$ mass difference of 4.28 ± 0.06 Mev in agreement with the less accurate mass difference adopted in our recent review article.[3] The first level in P^{30} is well fixed at 0.688 ± 0.007 Mev, as $E_{\gamma 3}$ was measured by comparison to the 0.661-Mev gamma-ray from Cs^{137}, and the 0.511-Mev annihilation line. A first level in this region was also indicated from the $Si^{29}(d,n)P^{30}$ reaction.[4] The resonance levels are at 5.87 ± 0.07 and 5.95 ± 0.07 Mev above the ground state.

The energy difference of 4.97 Mev between the first level in P^{30} and the Si^{30} ground state is about equal to the value (4.87 Mev) computed from the Coulomb energy difference (taking a nuclear radius of $R=1.38\times10^{-13}\times A^{\frac{1}{3}}$ cm) and the neutron-proton mass difference. The first level of P^{30} is thus identified as the lowest $T=1$ state with spin $J=0$ and even parity.

The $T=0$ ground state of P^{30} is, according to the shell model, expected to have $J=0^+$ or 1^+, although $J=1^+$ is more probable from analogy with the ground state of the deuteron. The fact that gamma transitions are observed between the P^{30} first excited state and the ground state then fixes the ground-state spin as $J=1^+$, as $0\rightarrow0$ transitions are forbidden.

As the Si^{29} spin is $\frac{1}{2}^+$, the resonance levels in P^{30} have spin 0^+, 0^-, 1^+, 1^-, or 2^-, because the capture of protons with $l_p=2$ or higher is very improbable at these low energies. The remarkable absence of the ground-state transition in the decay from the 5.97-Mev level can best be explained by assigning $J=1^-$, $T=0$ to this level. Electric dipole radiation to the ground state is then prohibited by the isotopic spin selection rule of Radicati.[5] However, an assignment of $J=2^-$ to the resonant level cannot be excluded altogether. In this case the ground-state transition would be $E1$ but isobaric spin forbidden, to be compared with an $M2$ transition to the first excited state. The spin, parity, and isotopic spin assignments derived from these arguments are shown in Fig. 1.

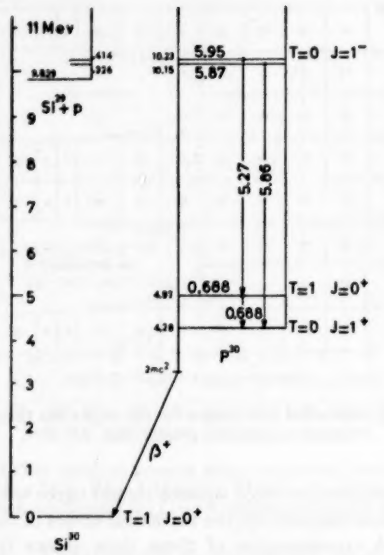

FIG. 1. Levels in P^{30} found from $Si^{29}(p,\gamma)P^{30}$.

[1] Kluyver, van der Leun, and Endt, Phys. Rev. (to be published).
[2] R. Tangen, Kgl. Norske Videnskab. Selskabs, Forh. Skrifter No. 1 (1946).
[3] P. M. Endt and J. C. Kluyver, Revs. Modern Phys. **26**, 95 (1954).
[4] Mandeville, Swann, Chatterjee, and Van Patter, Phys. Rev. **85**, 193 (1952).
[5] L. A. Radicati, Phys. Rev. **87**, 521 (1952).

Heat Generation in the Earth by Solar Neutrinos

A. M. Cormack
Physics Department, University of Cape Town, Rondebosch, Cape Town, South Africa
(Received May 3, 1954)

In the course of the carbon cycle in the sun, an enormous number of neutrinos are generated, and the only possible mechanism by which they may be absorbed in the sun is inverse beta decay. The cross section for this process is of the order of 10^{-44} cm^2 and is too small to cause any appreciable absorption of neutrinos, hence they must nearly all leave the sun and this results in a flux of about 7.4×10^{10} neutrinos/

cm² sec at the surface of the earth. By the same argument, these will contribute hardly any energy to the earth by means of inverse beta decay, but if inelastic collisions take place between neutrinos and electrons, the energy given to the electrons will be dissipated in the earth, thus providing a source of heat over and above those usually considered in geophysics.

Inelastic collisions can only take place if the neutrino possesses a magnetic moment which can interact with the electron magnetic moment, and the cross section for the process has been given by Bethe[1] as a function of neutrino magnetic moment. This has been used to estimate the heat generated in the earth in the following way. It has been assumed that the neutrinos produced in the sun are monoenergetic with an energy equal to their average energy (about $2mc^2$), and that they are produced at the center of the sun which is considered to be a polytropic gas sphere of polytropic index 3. A very simple form of transfer theory has been used to estimate the degeneration of neutrino energy due to inelastic collisions taking place in their passage outwards through the sun, and the earth has been assumed to consist of iron. The resulting heat generation in the earth (H ergs/g sec) as a function of the neutrino magnetic moment (n Bohr magnetons) is shown in Fig. 1. It is

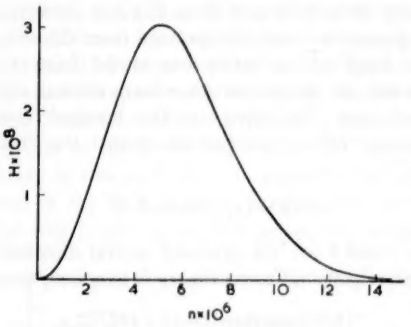

FIG. 1. The heat generation, H ergs/g sec in the earth as a function of the neutrino magnetic moment, n Bohr magnetons.

obvious that H may be small for one of two reasons: either because n is so large that nearly all the neutrino energy is dissipated in the sun, or because n is so small that both sun and earth are effectively transparent to neutrinos.

Nahmias[2] has set an upper limit to n of 1.8×10^{-4}, so that the possibility of the peak value of heat generation (3.05×10^{-8} erg/g sec) is not excluded, since the curve of Fig. 1 decreases steadily with increasing n beyond the range shown. This peak figure is nearly twice the heat generated in iron meteorites by natural radioactivity as determined by Paneth. It is generally assumed that the amount of heat produced in the earth's core by radioactivity is about the same as in iron meteorites.

Further details will be published elsewhere, including an attempt to set limits to the neutrino magnetic moment by establishing an upper limit to the amount of heat generated in the earth's core by the inelastic collision process.

[1] H. A. Bethe, Proc. Cambridge Phil. Soc. **31**, 108 (1935).
[2] M. E. Nahmias, Proc. Cambridge Phil. Soc. **31**, 90 (1935).

Some Pile Neutron Cross Sections of Isotopes of Americium, Berkelium, Californium, and Element 99†

B. G. HARVEY, H. P. ROBINSON, S. G. THOMPSON, A. GHIORSO, AND G. R. CHOPPIN
Radiation Laboratory and Department of Chemistry, University of California, Berkeley, California
(Received May 20, 1954)

IN recent experiments[1–4] designed to produce new isotopes of the heaviest elements by neutron bombardments in the Materials Testing Reactor, approximate values have been obtained for several neutron capture cross sections. Neutron flux values were obtained from measurements made by the MTR operating staff. However, the neutron flux in a given position in the reactor is by no means constant, so that, as always, flux uncertainties represent the greatest source of error in most of the measurements.

After bombardment, the target material and products were carefully separated from activities due to fission products and impurities. The chemical separation methods, involving both precipitation and ion-exchange techniques, will be described in a separate report.[5] The product nuclei whose yields were measured were in all cases properly identified by means of their chemical and nuclear properties.

In some cases, the amount of the nuclide being bombarded changed drastically during the course of the experiment, since it was itself being produced from lighter nuclei. In these cases, the (otherwise laborious) calculations were made with the electronic analog computer GADAC developed for this purpose in this laboratory.[6]

TABLE I. Summary of results.

Nuclide bombarded	Target	Product measured	Number of experiments	σ (barns)
Am^{243}	Almost monoisotopic Am^{243}	Am^{244}	3	140±50
Bk^{249}	Monoisotopic Bk^{249}	Bk^{250}	2	1100±300
Bk^{249}	Monoisotopic Bk^{249}	Bk^{249} (i.e., Bk^{249} destruction)	1	
Cf^{249}	Monoisotopic Cf^{249}	Cf^{250}	1	270
Cf^{249}	Mixed Cf isotopes, $Cf^{249,250,251,252}$	Cf^{249} (i.e., Cf^{249} destruction)	1	~900 (fission plus capture)
Cf^{252}	$Cf^{249,250,251,252}$	99^{255}	1	30
Cf^{254}	Long bombardment of Pu^{239}	100^{255}	1	<2
99^{253}	Mixed Cf isotopes, $Cf^{249,250,251,252}$	100^{254}	1	160
99^{254}	Long bombardment of Pu^{239}	100^{255}	1	<15

The results are summarized in Table I.

The fission cross section of Cf^{249}, by difference between its total and capture cross sections, is about 630 barns. The ratio of σ_f/σ_c is thus about 2.3. This number is entirely consistent with the calculated binding energy, 6.33 Mev,[7] of the ingoing neutron.[8,9]

The cross sections of Cf^{254} and 99^{254} are given only as limits because it is not known how much of the 100^{255} is formed by $Cf^{254}(n,\gamma)Cf^{255}\xrightarrow{\beta^-}99^{255}\xrightarrow{\beta^-}100^{255}$ and how much by $99^{254}(n,\gamma)99^{255}\xrightarrow{\beta^-}100^{255}$. If the capture cross section of 99^{254} is zero, then that of Cf^{254} would need to be approximately 2 barns, while if the cross section of Cf^{254} is zero, then that of 99^{254} would need to be approximately 15 barns. The yield of 100^{255} is accounted for by cross sections which are related by the approximate equation $\sigma_{Cf^{254}}+0.1\sigma_{99^{254}}=1.4$.

We wish to express our gratitude to Professor Glenn T. Seaborg for his interest in this work. We are particularly indebted to the staff of the Phillips Petroleum Company at the MTR for their assistance in making neutron bombardments.

† This work was performed under the auspices of the U. S. Atomic Energy Commission.

[1] Ghiorso, Thompson, Choppin, and Harvey, Phys. Rev. **94**, 1081 (1954).
[2] Choppin, Thompson, Ghiorso, and Harvey, Phys. Rev. **94**, 1080 (1954).
[3] Harvey, Thompson, Ghiorso, and Choppin, Phys. Rev. **93**, 1129 (1954).
[4] Thompson, Ghiorso, Harvey, and Choppin, Phys. Rev. **93**, 908 (1954).
[5] S. G. Thompson *et al.*, J. Am. Chem. Soc. (to be published).
[6] H. P. Robinson and G. O. Brink (unpublished).
[7] Calculated by R. A. Glass, Ph.D. thesis (to be published).
[8] J. R. Huizenga and R. B. Duffield, Phys. Rev. **88**, 959 (1952).
[9] G. T. Seaborg, Phys. Rev. **88**, 1429 (1952).

Thermal Neutron Capture Cross Sections of Hydrogen, Boron, and Silver*

F. R. Scott, D. B. Thomson, and W. Wright†
Los Alamos Scientific Laboratory, Los Alamos, New Mexico
(Received December 7, 1953; revised manuscript received June 2, 1954)

A RELATIVELY simple and direct measurement of the neutron-proton capture cross section has been made by the determination of the mean life of thermal neutrons in a finite water geometry. This method was used first by Manley, Haworth, and Luebke[1] and more recently by von Dardel and Waltner.[2] The present scheme differs from these previous methods in the use of a variable volume together with a modification of the sigma pile method.[3] A pulsed neutron source was obtained from the (γ,n) and (γ,f) reactions in uranium using a betatron. Figure 1 is a schematic drawing of the physical layout. The uranium, covering one end of the tank, acted as a plane source of neutrons and shielded the detector from the intense x-ray burst from the betatron. The geometry was a stainless steel tank 36 in. long, 24 in. wide, and 36 in. high. Five surfaces, including the water surface, were covered with Cd sheets and paraffin blocks. The front surface facing the uranium was covered only with Cd. A General Electric B^{10}-lined proportional counter $1\frac{1}{2}$ in. in diameter and $13\frac{1}{2}$ in. long was used as the thermal neutron detector and was placed at various positions in the geometry. For all of the present measurements, the counter was centered in the water 5 inches from the front surface.

An eight-channel electronic time analyzer recorded the thermal neutron density as a function of time. This analyzer was calibrated against a standard 100-kc oscillator before and after each run. A semilogarithmic plot of the data, corrected for variation in channel widths, gave the thermal neutron mean life after a small correction for the effect of the counter. All of the exponential plots were straight within statistics indicating no measurable background.

The counter correction was obtained by placing one, two, and three similar B^{10}-lined counters close together and by observing the change in the measured neutron lifetime due to a change in the number of counters. By extrapolation, this gave a correction of $+10\pm3$ μsec due to the presence of one counter in a water geometry 20 in.$\times$24 in.$\times$36 in. Counter corrections for other geometries were extrapolated from this value.

The depth of the water was varied from 9 to 20 inches and the thermal neutron mean life was obtained for each case. The inverse of this lifetime (corrected for counter effect) was plotted against the "buckling factor,"

$$B^2=(\pi/a)^2+(\pi/b)^2,$$

where a and b are the extended lateral dimensions. If a single velocity diffusion theory is assumed, then

$$(1/t)\,(\text{measured})=(1+B^2L^2)\Sigma_a v,$$

where L is the diffusion length, Σ_a the macroscopic absorption cross section, and v the velocity of the thermal neutrons. As the size of the system approaches infinity, $B^2\to0$ and

$$1/t=\Sigma_a v.$$

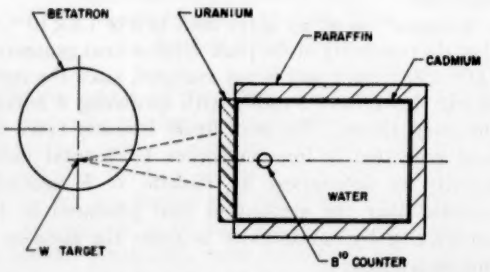

FIG. 1. A schematic diagram of the experimental layout.

Also from the slope of $1/t$ *vs* B^2,

$$\frac{d}{dB^2}\left(\frac{1}{t}\right)=\frac{L^2}{t_\infty}=Dv.$$

Figure 2 shows the results of these measurements. The ordinate intercept gives a mean life of $t_\infty=213\pm4$ μsec for thermal neutrons in an infinite water medium. The slope of the line, together with this lifetime, gives a diffusion length $L=2.85\pm0.05$ cm and a transport mean free path $\lambda_t=0.525\pm0.010$ cm. This mean life can be transformed into a thermal neutron-proton absorption cross section of $\sigma_H=0.323\pm0.008$ barn at a neutron velocity of 2200 meters per second. This cross section is low by 2 percent as compared with $\sigma_H=0.329\pm0.004$ obtained by Hamermesh, Ringo, and Wexler,[4] by measuring $\sigma_B/\sigma_H=2292\pm27$ and using a boron cross section of 755 ± 3 barns. Recently, Carter, Palevsky, Myers, and Hughes[5] have measured the boron cross section with the slow chopper at Brookhaven and boric acid powder obtained from Ringo. If their value of 749 ± 4 barns is used in the ratio obtained by Hamermesh *et al.*, a value of $\sigma_H=0.327\pm0.004$ is obtained. Our result for hydrogen agrees with this value within experimental error.

Also, the thermal neutron capture cross section of boron (mined in California) was determined by measuring the thermal neutron lifetime in various water concentrations of anhydrous boric acid. Figure 3 shows the measured variation in the decay constant as a function of the concentration. Besides a geometry correction due to the finite water tank and the counter correction, it was necessary to correct for the presence of water in the B_2O_3 powder. By titration, the boron content was found to be 29.9 percent by weight, indicating a deficiency of 3.88 percent of boron in the powder.

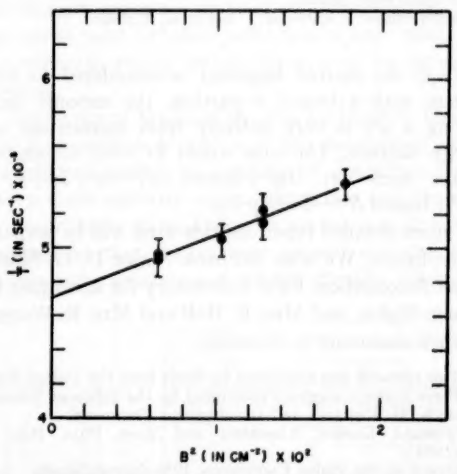

FIG. 2. A plot of the thermal neutron decay constant as a function of the buckling factor B^2. All points have been corrected for the effect of the detector.

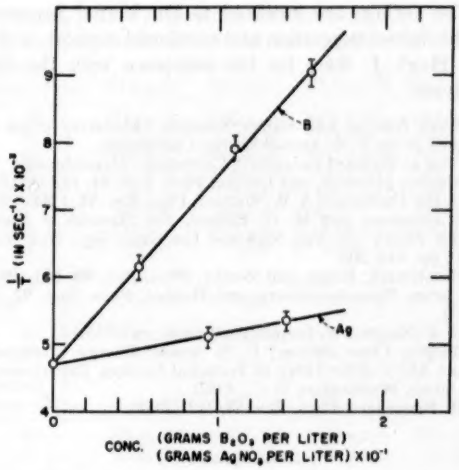

FIG. 3. Thermal neutron decay constant as a function of B_2O_3 and AgCl concentrations. All points have been corrected for geometry and detector effects.

A boron thermal neutron capture cross section $\sigma_B=744\pm20$ barns was found from the slope of the boron line in Fig. 3. This result, which is independent of the hydrogen cross section, is within the experimental error of other recently reported measurements.[5,6] The boron to hydrogen ratio of $\sigma_B/\sigma_H=2303\pm50$ is in good agreement with the results of Hamermesh, Ringo, and Wexler.[4]

The thermal neutron capture cross section in silver was measured in the same manner. Figure 3 shows a plot of the variation of the thermal neutron decay constant as a function of the silver concentration. This concentration was obtained by dissolving $AgNO_3$ crystals in the tank. The silver concentration was measured by precipitating AgCl from a given volume of the solution with HCl. The concentration of silver obtained from titration of AgCl was within the 2 percent measurement error of the concentration obtained from weighing the $AgNO_3$. The measured thermal neutron capture cross section of silver was $\sigma_{Ag}=58.0\pm2$ barns after correcting for the 1.78 ± 0.05 barns neutron capture cross section in nitrogen.[7] This result compared favorably with 56 ± 4 barns as reported by Pomerance[8] who used 95 barns for the gold cross section as a standard. Recently, the gold cross section has been measured to be 98.7 ± 0.6 barns[5] which alters the silver cross section as reported by Pomerance to 58.2 ± 4 barns.

Although the lifetime method of measuring thermal neutron cross sections is not as accurate as the pile oscillator or slow chopper methods, it does afford a relatively direct measurement of macroscopic thermal neutron cross sections in large geometries, and the results obtained are compatible with results by other means.

The authors are indebted to Dr. Vernal Josephson for his initial suggestion and continued support, and to Dr. Hugh J. Karr for his assistance with the time analyzer.

* Work done at Los Alamos Scientific Laboratory under the auspices of the U. S. Atomic Energy Commission.

† Now at Harvard University, Cambridge, Massachusetts.

[1] Manley, Haworth, and Luebke, Phys. Rev. **61**, 152 (1942).
[2] G. von Dardel and A. W. Waltner, Phys. Rev. **91**, 1284 (1953).
[3] S. Glasstone and M. G. Edlund, *The Elements of Nuclear Reactor Theory* (D. Van Nostrand Company, Inc., New York, 1952), pp. 116, 203.
[4] Hamermesh, Ringo, and Wexler, Phys. Rev. **90**, 603 (1953).
[5] Carter, Palevsky, Myers, and Hughes, Phys. Rev. **92**, 716 (1953).
[6] G. R. Ringo *et al.* (unpublished data), $\sigma_B = 755 \pm 3$.
[7] *Neutron Cross Sections*, U. S. Atomic Energy Commission Report AECU-2040 (Office of Technical Services, Department of Commerce, Washington, D. C., 1952).
[8] H. Pomerance, Phys. Rev. **88**, 412 (1952).

Heavy Unstable Particles in Stripped Emulsions*

J. Crussard, M. F. Kaplon, J. Klarmann, and J. H. Noon
University of Rochester, Rochester, New York

(Received May 18, 1954)

A SEARCH for heavy unstable particles has been made in 400 μ and 600 μ stripped emulsions flown at balloon altitude, at 41° and 55° geomagnetic latitudes. The events listed in Table I have been observed, and also one τ meson and four K-type decays having secondaries of minimum ionization but giving no other significant information about their decay products.

The following remarks refer to the events in Table I.

(1) $K_\pi{}^+$ must be another example of the decay $\tau^+ \rightarrow \pi^+ + 2\pi^0$ which had been previously assumed from our first observed case.[1] On the whole, 7 similar cases have presently been found in different places.[2]

(2) The value found for the mass of $K_\mu{}^+$, $(980 \pm 130)m_e$, does not favor the assumption that these particles giving slow μ's as decay products are heavier than the τ.

(3) At 80 μ from its stopping point, the particle K_1 suffers a very large angle scattering (137°) with an energy loss of about 40 Mev, indicating a nuclear interaction.

(4) Though no proper calibration has been made, the measurements on the secondary of K_2 seem to indicate a π rather than a μ.[3]

(5) The mass measurements on the seven K particles (not including $K_\pi{}^+$) give: 660 ± 210, 850 ± 125, 1060 ± 260, 1030 ± 160, 980 ± 130, 1020 ± 300, 968 ± 220. This distribution agrees with its mean value, which is $m/m_e = 927 \pm 66$.

(6) The Q value of the τ found here (73.85 ± 1 Mev) is in agreement with the mean value $Q = 74.7 \pm 0.3$ Mev obtained from the τ's observed in different laboratories.[2]

TABLE I. Observations of unstable particles.

Event	Origin[a]	Primary range (mm)	Mass (m_e)[b]	Secondaries
$K_\pi{}^+$	$2+0p$	13.8	1060 ± 100 (*SR* and *IR*)	π^+ of 4.6 mm range. The normal $\pi - \mu - \beta$ decay at rest is observed. $E_{\pi^+} = 15.2 \pm 0.27$ Mev.
$K_\mu{}^+$	$2+3p$	20.2	980 ± 130 (*IR*)	μ^+ of 16.63 mm range ($\mu - \beta$ at rest is observed) $E_\mu = 28.0$ Mev. This cannot be a $\pi - \mu$ decay in flight; the mass is 187 ± 30 from *SI* at the start.
K_1	$25+5h$	$2.3+0.08$	1020 ± 300 (*SI*)	$I/I_0 \simeq 1$ (steeply dipping)
K_2	outside	31.8	968 ± 220 (*SR*)	$I/I_0 = 1.19 \pm 0.03$ $p\beta c = 140 \pm 8$ Mev. $m/m_e = 272 \pm 25$, using the Bristol calibration
τ	$5+0n$	61.3	870 ± 215 (*SR*)	π^+ of 87 μ, stopping, $E = 1.5 \pm 0.03$ Mev; π^- of 19.6 mm, stopping $E = 35.4 \pm 0.59$ Mev; $\pi^\pm$, outgoing. $E = 36.7 \pm 0.62$ Mev; giving $Q = 73.6 \pm 1$ Mev. From momentum balance: $Q = 75.3 \pm 3$ Mev. Mean value: $Q = 73.85 \pm 1.0$ Mev.
$\Lambda^\pm$	$25+5n$	1.8	2390 ± 490 (*SI*)	Decay in flight. Secondary $I/I_0 = 1.015 \pm 0.05$. $p\beta c = 195 \pm 30$ Mev. If it is a π, $E_\pi = 128 \pm 24$ Mev. If $\Lambda^\pm \rightarrow N + \pi^\pm$, $Q = 116 \pm 50$ Mev.
Excited fragment	$18+4p$	0.089	$4 \leq Z \leq 6$	Proton, $E = 6.6$ Mev. Proton, $E = 5.5$ Mev. Alpha, $E = 27$ Mev. (There is a momentum unbalance of 395 Mev/c, opposite the α particle.)

[a] The type of the originating stars are given, following the Bristol notation; h means heavy primary.
[b] In this column, S: scattering; I: ionization; R: range.

(7) If the excited fragment is considered to be a nucleus with a bound Λ^0-particle, the mesonic decay (giving a π^0) is very unlikely from momentum and energy balance. The case would fit with nonmesonic decays such as: $(Be^8 + \text{bound } \Lambda^0) \rightarrow 3n + 2p + \alpha$, or $(Be^7 + \text{bound } \Lambda^0) \rightarrow 2n + 2p + \alpha$.

A more detailed report on this work will be prepared in the future. We wish to thank Major D. G. Simons of the Aeromedical Field Laboratory for arranging the balloon flights, and Miss B. Hull and Mrs. R. Wargotz for their assistance in scanning.

* This research was supported by funds from the United States Air Force under a contract monitored by the Office of Scientific Research, Air Research and Development Command.

[1] Crussard, Kaplon, Klarmann, and Noon, Phys. Rev. **93**, 253 (1954).
[2] Report on the Padua Conference, 1954 (unpublished).
[3] However, it would not agree with an assumed decay $\theta^\pm \rightarrow \pi^\pm + \pi^0$, for which $p\beta c = 168$ Mev and $I/I_0 = 1.11$, if $\theta^\pm$ has the mass of the θ^0.

Total Cross Sections for High-Energy Neutrons*

VAUGHN CULLER AND R. W. WANIEK
Cyclotron Laboratory, Harvard University, Cambridge, Massachusetts
(Received May 3, 1954)

IN measurements of total cross sections for high-energy neutrons, detectors accepting neutrons of relatively wide ranges of energy have been used. By utilizing the known spectrum of the neutron beam and the threshold acceptance energy values of the detectors an effective energy has been stated to about 2 percent.[1] A scintillation counter telescope allows the use of considerably narrower energy acceptance bands in the determination of total cross sections.[2] The increased resolution of such a telescope makes it a suitable instrument to analyze the variation of total cross sections as a function of energy as well as permitting a more precise determination of the effective energy.

By means of such a telescope, a good-geometry attenuation experiment has been performed with neutrons produced from a $\frac{1}{4}$-in. beryllium target bombarded by the 110-Mev internal proton beam of the Harvard 95-in. synchrocyclotron.[3] The neutron beam, collimated by pipes of rectangular cross section (so chosen to give maximum counting rate for a given energy resolution), was first monitored by a triple coincidence scintillation counter telescope of neutron threshold energy approximately 35 Mev (Fig. 1). Then the neutron beam, attenuated by samples of various elements, passed through a second rectangular collimator and its intensity was determined by another scintillation counter telescope. The second telescope (which counted exchange protons following the conventional polyethylene-carbon subtraction method) consisted of 8 plastic scintillators mounted on 1*P*21 photomultipliers. Five, six, seven, and eightfold coincidences were used, with the resultant energy bands determined by range differences.

The values of the cross sections are listed in Table I.[4] The cross section of hydrogen was determined from a polyethylene-carbon subtraction, of deuterium from a heavy water-ordinary water subtraction and of oxygen by an ordinary water-hydrogen subtraction. It is to be emphasized that the energies quoted and the errors given are the absolute and not the effective values. The statistics of the cross sections are counting statistics only; other sources of error are believed negligibly small.

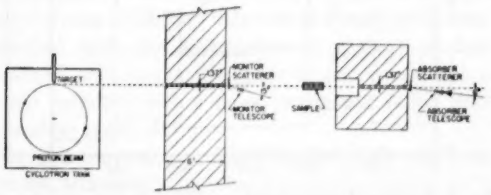

FIG. 1. Geometry of the experiment.

TABLE I. Total cross sections for neutrons. (10^{-27} cm^2).

Neutron energy (Mev)	94.8±1.5	98.6±2.5	102.0±0.76	107.9±5
Pb	4628±87	4595±63	4407±121	4736±209
Fe	1947±48	1874±37	1734±81	1946±184
Si	1136±52	1067±42	1041±92	925±218
Al	1067±29	1046±23	920±50	1064±126
O	721±13	675±9	649±14	668±42
C	518±6	494±4	466±7	508±18
D	110±7	108±5	81±9.9	62±21.9
H	77±5	76±3	80±7	59±16
Neutron energy (Mev)	**77.7±1.3**	**82.2±3**	**86.8±1.4**	**100.7±12**
Pb	4910±164	4957±98	4905±107	4569±46
C	614±31	585±17	602±19	518±7
Neutron energy (Mev)	**61.5±1.7**	**66.8±3.5**	**72.1±1.7**	**93.5±19**
Pb	4590±225	4551±160	4647±193	4605±121
C	674±62	671±42	601±41	521±79

In the case of lead, confirmation of the "Harwell dip"[1] is observed at the lower energy points.

Acknowledgments are due G. Tirellis and G. Bouchard for their assistance during the experiment and in the analysis of the data.

* Supported by a joint program of the U. S. Office of Naval Research and the U. S. Atomic Energy Commission.
[1] A. E. Taylor and E. Wood, Phil. Mag. **44**, 95 (1953).
[2] Vaughn Culler and R. W. Waniek, Phys. Rev. **87**, 221 (1952).
[3] R. W. Waniek and Vaughn Culler, Phys. Rev. **95**, 659 (1954).
[4] Total cross sections of C and Fe far high-energy neutrons have also been obtained by B. Ragent, University of California Radiation Laboratory Report UCRL-2337, 1953 (unpublished).

Element 100 Produced by Means of Cyclotron-Accelerated Oxygen Ions

HUGO ATTERLING, WILHELM FORSLING, LENNART W. HOLM, LARS MELANDER, AND BJÖRN ÅSTRÖM
Nobel Institute of Physics, Stockholm, Sweden
(Received May 18, 1954)

THE beam of high-energy $(O^{16})^{6+}$ ions produced by the 225-cm cyclotron of this institute[1] has been used to bombard uranium targets. An alpha activity which is ascribed to an isotope of element 100 has been found among the transmutation products formed in this way.

Uranium metal was irradiated for several hours with the internal oxygen beam, at a radius of 85 cm. At this radius the maximum attainable energy of $(O^{16})^{6+}$ ions is roughly 180 Mev. Measurements were made of the intensity of oxygen ions reaching this radius with energies greater than 60 Mev, the best beam being about 0.03 microampere. For the production of californium as a reference element the uranium target was irradiated

for some hours with $(C^{12})^{6+}$ ions before the oxygen bombardment. Carbon dioxide was used as source gas for the production of both kinds of ions, and the selection of bombarding particle was made by adjusting the magnetic field to the corresponding resonance value.

The surface layer of the uranium target was dissolved and carriers were added. The separation of actinides and lanthanides was performed by lanthanum fluoride precipitation and ion exchange chromatography.[2] The identification of element 100 was established from its position relative to that of californium in the eluate.

The alpha activity was measured by means of an ionization chamber and a 16-channel pulse analyzer. The measurements were started about two hours after the end of the irradiations. In the element-100 eluate fraction, up to 20 alpha disintegrations of energy 7.7 Mev were usually found, decaying with a half-life of about half an hour. According to alpha systematics a probable mass number corresponding to these data is 250.

The first positive results were obtained on February 19. The work is still in progress.

We express our gratitude to the head of the institute, Professor Manne Siegbahn, for his continuous interest. Professor John O. Rasmussen, Jr., cooperated with us in the early development of this project during part of 1953, and his valuable advice is gratefully acknowledged. Our thanks are also due the cyclotron crew and other members of the technical staff.

[1] H. Atterling, Arkiv Fysik **7**, 503 (1954). This paper is a preliminary report on the acceleration of carbon, nitrogen, and oxygen ions in the 225-cm cyclotron.

[2] E.g., Street, Thompson, and Seaborg, J. Am. Chem. Soc. **72**, 4832 (1950).

Interactions of High-Energy Neutrons in Molybdenum*

E. G. Silver and R. W. Waniek
Cyclotron Laboratory, Harvard University, Cambridge, Massachusetts
(Received May 10, 1954)

In the past, decisive evidence obtained from stars induced by neutrons in nuclear emulsions was obscured by the ambiguity in the identification of the nucleus involved in the interaction.[1,2] To obviate this difficulty we have resorted to the use of thin filaments embedded in Ilford G5 electron sensitive emulsions.[3,4] The technique required the overcoming of various problems which will be discussed in a publication to appear elsewhere. In this letter we intend to present the results obtained from emulsions with embedded molybdenum wires of 28 microns diameter. We selected this material because of its favorable position between silver and bromine and for its desirable mechanical properties. The plates were exposed in good geometry to the neutron beam obtained by internal bombardment of a $\frac{1}{4}$-in. beryllium target with the proton beam of the 95-in. synchrocyclotron. The target was located at the 70-Mev radius and the neutrons were collimated in the forward direction and then passed through a hardener (32 cm of polyethylene) before impinging into the plates. We searched for events originating in molybdenum by scanning along the wires and measured the spatial angle and the true range, discriminating between particles with single and double charge. 250 events were analyzed. Each range was corrected for self absorption in the wire as a function of the azimuth and dip angles. The shrinkage was virtually eliminated from these emulsions and the residual amount was properly taken into account in computing both the range and the spatial angle. The range spectrum presented contains only singly-charged particles (Fig. 1). Under the reasonable assumption that they are protons, the two peaks appearing in our histogram would correspond to energies of about 3 and 6 Mev, respectively. The conventionally calculated Coulomb barrier for the molybdenum nucleus is of about 9 Mev. In addition, the range spectrum of the doubly-charged particles, assumed to be predominantly alphas, showed a similar

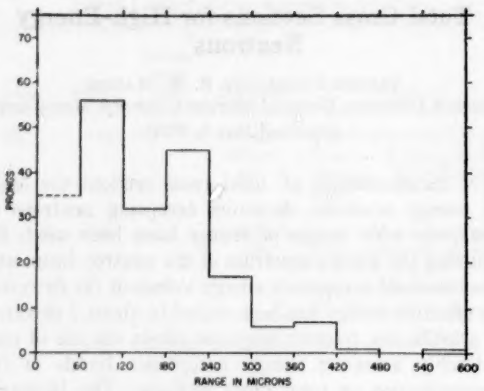

Fig. 1. Range histogram of singly-charged particles.

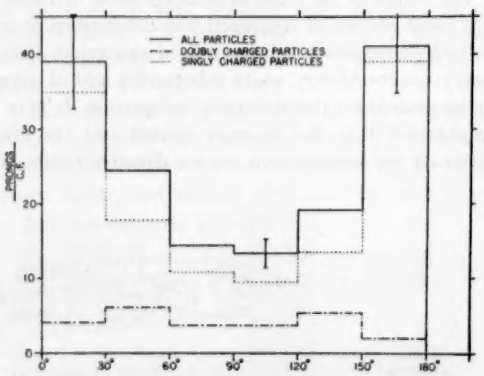

Fig. 2. Number of prongs *versus* spatial angle corrected for solid angle. (C.F. is the correction factor for the solid angle.)

distribution of particles emitted below the barrier. The angular distribution (Fig. 2) represents a histogram of the number of particles per unit solid angle plotted *versus* spatial angle. Calculations indicate that scattering in the wire for the lowest-energy protons emerging, should amount to no more than 8° in the average. Since self-absorption energy losses are a function of the azimuth and dip angle, we have considered the correction necessary to compensate for the loss of low-energy tracks emitted nearly parallel to the wire axis. We have found this correction to fall well within the statistics. Additional small corrections may be introduced due to the existence of a small "shadow volume" above and below the wire which is inaccessible to scanning.

Similar experiments with tungsten and Nylon filaments and at different energies are in progress.

* This work was supported by the joint program of the U. S. Office of Naval Research and the U. S. Atomic Energy Commission.

[1] R. W. Waniek and Taiichiro Ohtsuka, Phys. Rev. **89**, 1307 (1953).
[2] R. W. Waniek and Taiichiro Ohtsuka, Phys. Rev. **91**, 1574 (1953).
[3] G. P. S. Occhialini, Nuovo cimento **8**, 341 (1951).
[4] E. G. Silver and R. W. Waniek, Phys. Rev. **94**, 769 (1954).

Polarization of Nucleons Elastically Scattered from Nuclei*

R. M. STERNHEIMER
Brookhaven National Laboratory, Upton, New York
(Received May 25, 1954)

IT has been shown by several authors[1–4] that the observed polarization[5–7] of protons of energy 200-400 Mev elastically scattered from nuclei can be accounted for by the assumption of a spin-orbit coupling of reasonable magnitude. In previous calculations[3] of the polarization of 316-Mev protons scattered from Be, it was found that the polarization P is positive inside the first diffraction minimum, becomes negative at $\sim 17°$, and becomes positive again for larger scattering angles θ ($\sim 21°$). Although the order of magnitude of the observed P could be explained, the experiments of Marshall *et al.*[6] and of Chamberlain *et al.*[7] do not seem to give support to an oscillatory behavior of P. The previous calculations were carried out using a square well potential. It was suggested by E. Fermi and C. N. Yang that the oscillatory behavior of P may be directly connected with the assumption of a sharp nuclear boundary, and might disappear if one would use a nuclear potential with a more progressive falloff near the nuclear radius R.[8]

For this purpose, the following harmonic oscillator potential was used,

$$V = V_0(1 - r^2/R^2), \tag{1}$$

where V_0 is a constant. The calculations were again carried out for 316-Mev nucleons on Be, using the same parameters of the optical model[9,10] as in I, i.e., $R = 3.2 \times 10^{-13}$ cm, $k_1 = 0.86 \times 10^{13}$ cm^{-1}, $K = 1.7 \times 10^{13}$ cm^{-1}, corresponding to a complex well of depth $\bar{V} = -(13 + i25.6)$ Mev. V_0 was so chosen that the average $\langle V \rangle$ of (1) over the nuclear volume equals $\bar{V}$. We have

$$\langle V \rangle = (3/R^3) \int_0^R V_0(1 - r^2/R^2) r^2 dr = \tfrac{3}{5} V_0. \tag{2}$$

Thus V_0 was taken as $(5/2)\bar{V} = -(32.5 + i64)$ Mev.

For the spin-orbit coupling, two models were assumed which correspond to those considered in I. The potential functions for these models will be written $-U_{1,2}(r)\mathbf{l}\cdot\boldsymbol{\sigma}$, where $\hbar\mathbf{l}$ and $\hbar\boldsymbol{\sigma}/2$ are the orbital and the spin angular momenta of the nucleon. $U_1(r)$ was taken proportional to the real part of $(1/r)(dV/dr)$ in accordance with the form of the Thomas precession. Thus U_1 is a constant u_1 independent of r. U_2 is assumed concentrated at the center of the nucleus. The approximate form of U_2 is

$$U_2(r) \cong u_2(R/r)^2(1 - r^2/R^2). \tag{3}$$

The main term δ_{L0} of the phase shift corresponding to V is given by

$$\delta_{L0} = \frac{kV_0}{2T} \int_0^{(R^2 - y^2)^{\frac{1}{2}}} \left(1 - \frac{x^2 + y^2}{R^2}\right) dx = \frac{V_0 kR}{3T} \left(1 - \frac{y^2}{R^2}\right)^{\frac{3}{2}}, \tag{4}$$

where k = wave number, T = kinetic energy, x and y are coordinates with respect to the center of the nucleus; x is along the incident direction of the nucleon, and $y = (l + \frac{1}{2})/k$. One obtains for the phase shifts $\delta_l^{\pm}$ of the two models,

$$(\delta_l^{\pm})_1 = -\frac{5}{3} R \left(\frac{iK}{2} + k_1\right) \left[1 - \frac{(l+\frac{1}{2})^2}{k^2 R^2}\right]^{\frac{3}{2}} \pm \frac{5k\epsilon_1(l+\frac{1}{2})}{6T(L+\frac{1}{2})} \left[R^2 - \frac{(l+\frac{1}{2})^2}{k^2}\right]^{\frac{3}{2}}, \tag{5}$$

$$(\delta_l^{\pm})_2 = -\frac{5}{3} R \left(\frac{iK}{2} + k_1 \pm \frac{k\epsilon_2}{2T}\right) \left[1 - \frac{(l+\frac{1}{2})^2}{k^2 R^2}\right]^{\frac{3}{2}}, \tag{6}$$

where L is the largest integer $< kR$, and $\epsilon_{1,2}$ are parameters which measure the strength of the spin-orbit coupling. We have $\epsilon_{1,2} = \frac{3}{5} u_{1,2}(L + \frac{1}{2})$.

The calculations of P from the $\delta_l^{\pm}$ were carried out using Eqs. (3)–(6) of I. Figure 1 shows $P(\theta)$ for the potential $U_1(r)$ with $\epsilon_1 = 4$, 7.5, 12, and 15 Mev. It is seen that P remains positive throughout the range of θ. The same is shown by Fig. 2 which presents $P(\theta)$ as obtained from $U_2(r)$ with $\epsilon_2 = 4$, 7.5, and 15 Mev. Thus

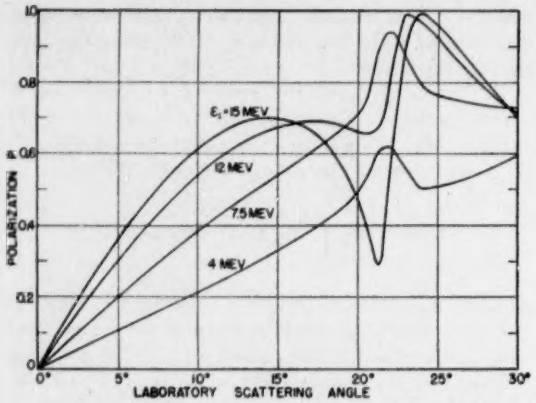

FIG. 1. Polarization P as a function of scattering angle for various ϵ_1 calculated from potential U_1 [Eq. (5)] for 316-Mev protons scattered from Be. The spin-independent part of the potential is $V_0(1-r^2/R^2)$.

the assumption of a gradual nuclear boundary, which is also supported by electron scattering experiments,[11] has the effect of wiping out the negative region of P near 20°. A plausible explanation of this result is obtained by referring to the curves of $P(\theta)$ obtained in I for the square well. It is seen that the areas in which $P<0$ are considerably smaller than those in which $P>0$. Since the positions of negative P are correlated with the value of R, one expects that if R is effectively smeared out, some average P is obtained which is positive throughout the first diffraction minimum.

From Figs. 1 and 2 it is seen that the result of Marshall *et al.*[6] that $P(14°)\cong 0.6$ can be fitted with $\epsilon_1\cong 10$ Mev (i.e., $u_1\cong 1.23$ Mev) or $\epsilon_2\cong 14$ Mev (i.e., $u_2\cong 1.73$ Mev). Figure 3 shows the differential cross section $\langle d\sigma/d\Omega\rangle$ averaged over spin directions for $U_2(r)$ with $\epsilon_2=0$, 4, 7.5, and 15 Mev. These results are similar to those shown in Fig. 3 of I for the square well. However,

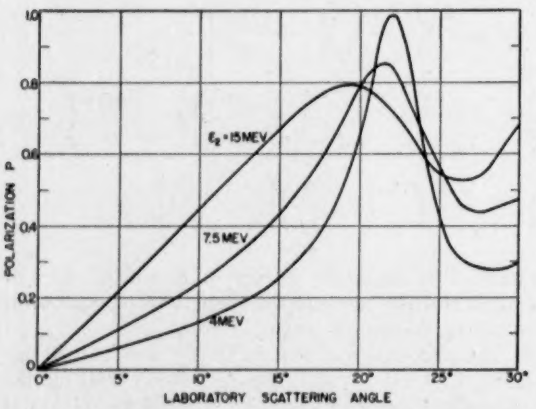

FIG. 2. Polarization P as a function of scattering angle for various ϵ_2 calculated from potential U_2 [Eq. (6)] for 316-Mev protons scattered from Be. The spin-independent part of the potential is $V_0(1-r^2/R^2)$.

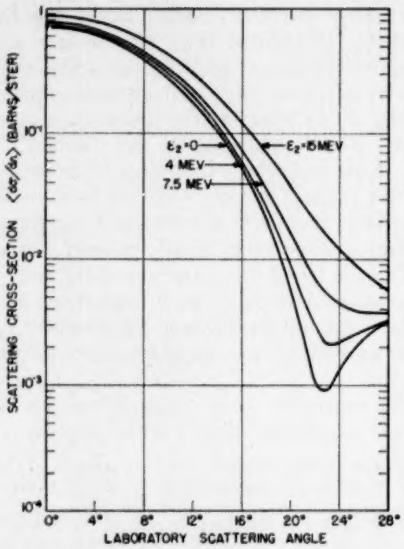

FIG. 3. Differential scattering cross section $\langle d\sigma/d\Omega\rangle$ averaged over spin directions for 316-Mev protons scattered from Be. The curves were calculated from potential U_2 for various ϵ_2.

the diffraction minima for $\epsilon_2=0$ and 4 Mev are less deep, as a result of the fact that the potential of Eq. (1) tends to fill in the minima, even in the absence of spin-orbit coupling. The values of the total diffraction cross section σ_d are: $\sigma_d=70$, 76, 84, and 113 mb for $\epsilon_2=0$, 4, 7.5, and 15 Mev, respectively.

The present results for Be were confirmed by similar calculations for Cu and Pb at 316 Mev, using Taylor's[10] radii, $R=5.80\times10^{-13}$ cm and 8.12×10^{-13} cm, respectively, and the same values of k_1 and K as for Be. Both for $U_1(r)$ and $U_2(r)$, it was found that P remains positive throughout the region of the first diffraction minimum, and up to 19° for Cu and 13° for Pb.

It can be concluded that the polarization in the region of the first diffraction minimum is very sensitive to the radial dependence of the nuclear potential, and gives additional information on the radial falloff besides that provided by a measurement of $\langle d\sigma/d\Omega\rangle$ as a function of θ. If it is established experimentally that P does not change sign near the first diffraction minimum, then agreement can be obtained by assuming the rounded-off potential of Eq. (1).

I would like to thank Professor R. Serber, Dr. G. A. Snow, and Dr. C. N. Yang for several helpful discussions and comments.

* Work done under the auspices of the U. S. Atomic Energy Commission.

[1] E. Fermi, Nuovo cimento **11**, 407 (1954).
[2] W. Heckrotte and J. V. Lepore, Phys. Rev. **94**, 500 (1954).
[3] Snow, Sternheimer, and Yang, Phys. Rev. **94**, 1073 (1954). This letter will be referred to as I.
[4] B. J. Malenka, Phys. Rev. **95**, 521 (1954).
[5] Oxley, Cartwright, and Rouvina, Phys. Rev. **93**, 806 (1954).
[6] Marshall, Marshall, and de Carvalho, Phys. Rev. **93**, 1431 (1954), and private communication.

[7] Chamberlain, Segrè, Tripp, Wiegand, and Ypsilantis, Phys. Rev. **93**, 1430 (1954), and private communication.
[8] While these calculations were in progress, Dr. W. Heckrotte sent us preliminary results of calculations of the polarization of 300-Mev nucleons scattered from carbon. Some of these calculations were carried out with the harmonic oscillator potential and gave results similar to those obtained here.
[9] Fernbach, Serber, and Taylor, Phys. Rev. **75**, 1352 (1949).
[10] T. B. Taylor, Phys. Rev. **92**, 831 (1953).
[11] Hofstadter, Fechter, and McIntyre, Phys. Rev. **92**, 978 (1953); L. I. Schiff, Phys. Rev. **92**, 988 (1953).

Statistical Mechanics and the Overhauser Nuclear Polarization Effect*

C. KITTEL
Department of Physics, University of California, Berkeley, California
(Received May 27, 1954)

OVERHAUSER[1] has discovered the remarkable result that under appropriate conditions the population distribution of nuclear spins in a metal among the nuclear magnetic sublevels is determined essentially by the magnitude of the electronic magnetic moment μ_B, rather than by the nuclear moment μ_I. His conditions are that the electron spin resonance of the condition electrons should be saturated, and that the principal spin-lattice relaxation mechanism of the nuclear spins should be the $\mathbf{I}\cdot\mathbf{s}$ hyperfine coupling with the conduction electrons. The predicted enhancement of nuclear polarization on saturating the electron resonance has been detected experimentally by Carver and Slichter.[2] Overhauser arrived at his result by a detailed kinetic calculation. The purpose of this note is to establish briefly the connection of the result with the general principles of statistical mechanics and with the second law of thermodynamics.

The canonical ensemble in statistical mechanics describes the distribution of a small sub-system A of a large system $A+B$, as a function of the energy of the remainder B of the system. It is important for our purpose to recall in Gibbsian language the argument which gives the Boltzmann distribution ratio $P^+/P^- = \exp[-2\mu_I H/kT]$ for nuclei of spin $I=\frac{1}{2}$ in thermal equilibrium in a static magnetic field H. The nuclear and electron spin systems will be treated as A, while the reservoir B consists of the crystal lattice and the translational energy of the conduction electrons. We consider what happens when one nuclear spin is reversed. With $\mathbf{I}\cdot\mathbf{s}$ coupling dominant,[3] an electron spin must simultaneously turn the other way. The energy change of the combined spin systems is $2(\mu_B-\mu_I)H$ and is balanced by a corresponding change $-2(\mu_B-\mu_I)$ in the translational energy of a conduction electron. We are interested in the effect of a nuclear spin flip alone, and therefore we are to look at the system at a later time when the reversed electron has been restored to its original direction with energy change $-2\mu_B H$ by means of a relaxation process[4] not involving the nuclear spin. The net effect of the reversal of a nuclear spin is to change the energy of the reservoir B by $-2(\mu_B-\mu_I)H + 2\mu_B H = 2\mu_I H$. This energy change in the reservoir B changes the volume of phase space accessible to the reservoir, and the later change gives directly the canonical distribution of the sub-system A. It is to be noted that we have no interest in processes in which the restoration of the original electron spin orientation is accompanied by the restoration of the nuclear spin.

When the system is not in thermal equilibrium, but is flooded with rf power to saturate completely the conduction electron spin resonance, the corresponding net energy change in the reservoir on reversing one nuclear spin is now $-2(\mu_B-\mu_I)H$, instead of $2\mu_I H$. The reason is simple: the restoration of the electron spin to its original direction now occurs by the action of the rf field, instead of by a relaxation process. This is the significance of rf saturation. The magnetic energy change $-2\mu_B H$ is provided by the rf field instead of by the reservoir B. The reservoir had its energy changed by $-2(\mu_B-\mu_I)H$ at the beginning when the nuclear and electron spins flipped at the same time, and this is now the only energy change suffered by the reservoir in connection with the total process. The distribution of the sub-system reflects the energy change $-2(\mu_B-\mu_I)H$ of the reservoir, so that the population of the nuclear magnetic sublevels is now given by $P^+/P^- = \exp[2(\mu_B-\mu_I)H/kT]$ under rf saturation of the electron resonance. This demonstrates the enhancement of the nuclear polarization and agrees with the original result of Overhauser.

The discussion may be generalized to treat polarization of a nuclear spin system which suffers spin-lattice relaxation by dipolar or hyperfine interaction with an rf-saturated electron spin system. We let f_B denote the fraction of the spin-lattice relaxation processes of the nuclear spin system which are accompanied by an electron spin change in the opposite sense (I^-S^+ type interaction), while f_F denotes the fraction accompanied by an electron spin change in the same sense (I^-S^- type interaction). Then the nuclear population ratios are

$$P^+/P^- = \exp\{2[(f_B-f_F)\mu_B-\mu_I]/kT\},$$

under saturation conditions, when $S=I=\frac{1}{2}$. As noted also by Bloch, the enhancement effect is not necessarily restricted to metals. It may even be possible to observe the effect in materials with a low concentration of single unpaired electrons. The irradiation of hydrogenous material might introduce suitable centers for proton polarization.

It may be noted that saturation of the spin resonance associated with a zero-field splitting may also enhance polarization. We exhibit the simplest case, taking $f_B=1$, $S=1$, and an electronic zero-field splitting ΔE in an axial crystalline electric field. Then $P^+/P^- = \exp[\Delta E/kT]$, provided that the resonance at

$h\nu = \Delta E$ is saturated. Nuclear electric quadrupole splitting of a second nuclear species with $I=1$ could be substituted for the electronic system, if ΔE were large enough to be useful.

I am indebted to Professor F. Bloch for helpful discussions.

* Assisted in part by the National Science Foundation.

[1] A. W. Overhauser, Phys. Rev. **92**, 411 (1953); an elementary kinetic derivation of Overhauser's principal result has been given by F. Bloch, Stanford meeting of the American Physical Society [Phys. Rev. **93**, 944 (1954)].

[2] T. R. Carver and C. P. Slichter, Phys. Rev. **92**, 212 (1953).

[3] W. Heitler and E. Teller, Proc. Roy. Soc. (London) **A155**, 637 (1936); see also J. Korringa, Physica **16**, 601 (1950).

[4] It is thought at present that the most important process of conduction electron spin relaxation may be by spin reversal during electron collisions with phonons and lattice imperfections, as discussed by R. J. Elliott, Phys. Rev. (to be published).

Nuclear Scattering of Gamma Rays below Meson Threshold*

G. E. Pugh,† D. H. Frisch, and R. Gomez
Department of Physics and Laboratory for Nuclear Science, Massachusetts Institute of Technology, Cambridge, Massachusetts

(Received June 1, 1954)

USING an energy-sensitive gamma-ray detector (which will be described soon in an article for the *Review of Scientific Instruments*) we have made preliminary measurements, at 90° and 135°, of the absolute gamma-ray scattering cross section for Be, C, Al, Cu, Sn, Pb, and Bi in the energy range from 35 to 130 Mev. The work was done in the bremsstrahlung beam of the M.I.T. synchrotron using targets about $\frac{1}{4}$ radiation length thick. The maximum beam energy was kept just below meson threshold to prevent confusion with decay gamma rays from the π^0 meson.

A standard coincidence, anticoincidence telescope with a lead converter was used to identify the gamma ray. The telescope was followed by a very large liquid scintillator which integrates the energy loss of the electron pair in its volume and thus estimates the energy of the gamma ray. The pulse height response of the counter to monoenergetic events, ranging from 25 to 150 Mev, was measured using electrons of known energy to simulate gamma rays (note the family of curves in Fig. 1A).

By using the known bremsstrahlung spectrum of the synchrotron, the efficiency of the converter, and the measured response of the counter to any energy event, it is possible to predict the response of the counter for any arbitrary scattering cross section.

In exact analogy with atomic x-ray scattering, the differential cross section was taken as: $d\sigma/d\Omega = \sigma^0[Z^2f^2 + (1-f^2)Z]$, where σ^0 is the individual-particle cross section and f is the nuclear analog of the atomic structure factor given by

$$f=\int_0^\infty \frac{\sin kr}{kr}\,4\pi r^2\frac{\rho(r)}{Z}\,dr.$$

Response curves were computed for a uniform distribution $[\rho(r)=\text{const}]$ of protons in nuclei of radii $R=R_0A^{\frac{1}{3}}\times10^{-13}$ cm. In Fig. 1 the curves (a) $R_0=0.8$, (b) $R_0=1.1$, (c) $R_0=1.4$ were obtained by using for σ^0 the classical Thompson individual-proton cross section:

$$\sigma_p{}^0(\text{Thompson})=\tfrac{1}{2}(e^2/mc^2)^2(1+\cos^2\theta).$$

For elements heavier than aluminum the agreement with this classical Thompson scattering is as good as the statistics of the experiments. The results point to $R_0=1.1\pm0.2$.

In the lighter elements there is a clear disagreement which corresponds to too large a backward scattering of high-energy photons. Careful analysis of the data on Be and C enables us to deduce an experimental σ^0 which gives a best fit to the data, when R_0 is taken as 1.1. The ratio of this $\sigma_{(n+p)}{}^0$ "obs" to $\sigma_p{}^0$ Thompson together with a rough estimate of its statistical band of error is plotted in Fig. 2. The statistics are far from conclusive, but the trend of the data suggests that the

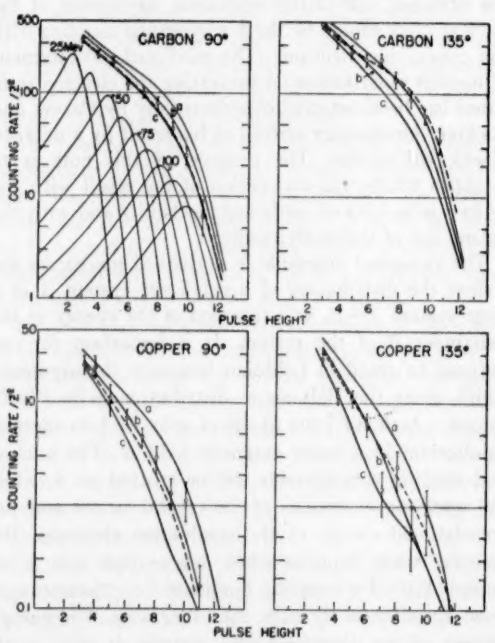

FIG. 1. Typical data for one light and one heavy element. Curves *a*, *b*, and *c* are theoretical response curves of counts *vs* pulse height computed using Thompson scattering only by a uniform distribution of free, classical protons in a nucleus of radius $R=R_0A^{\frac{1}{3}}\times10^{-13}$. (a) $R_0=0.8$; (b) $R_0=1.1$; and (c) $R_0=1.4$. The dotted curves are identical with (b) except that they use the modified Thompson cross section $\sigma_{(n+p)}{}^0$ "obs" shown in Fig. 2. The theory and experiment are on the same absolute scale; neither ordinate nor abscissa is normalized arbitrarily.

anomalous effects may be considerably quenched in heavy elements.

Classically, the large backward scattering can be explained by attributing a frequency-dependent magnetic susceptibility to the nucleons with a resonance at the meson absorption peak. The parameters of such a resonance can be determined from the total magnetic dipole absorption of a deuteron at meson resonance and from the resonant half-width. The ratio of 135° to 90° scattering predicted by this simple model is in agreement with the experiment.

The apparent reduction in scattering at 90° could be attributed to a large radius ($R_0=1.3$ for C; $R_0=1.6$ for Be) for light elements, and/or to the electric susceptibility of the nucleons. A classical resonance calculation for electric dipole meson production predicts a reduction in the 90° cross section comparable with what is observed.

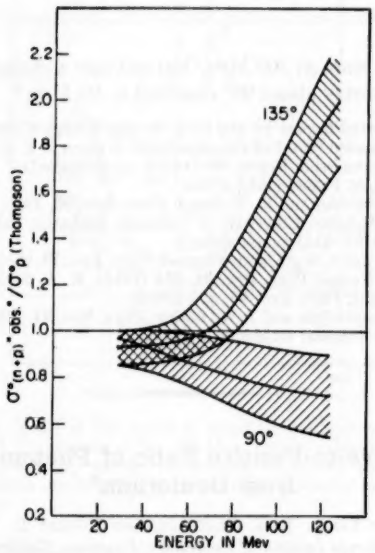

FIG. 2. Ratio of the "neutron+proton" γ-ray cross section "observed" in Be and C to the classical proton Thompson cross section.

Thus far, no experiments have been done to separate neutron and proton effects on the scattering cross section. In view of the alleged charge independence of photomeson reactions, it seems reasonable that both contribute equally to the anomalous scattering. That is why a deuteron was used in the calculation of magnetic dipole oscillator strength.

A more sophisticated phenomenological calculation for protons just received from Gell-Mann, Goldberger, and Thirring is likewise in agreement with the data, provided that only protons give anomalous effects. If the neutrons contribute comparably to the anomalous scattering, then their scattering amplitudes seem to be a factor of two larger than fits the data. This disagreement may indicate some quenching of meson effects in complex nuclei. However, more accurate data, including probably a hydrogen-deuterium comparison, is necessary before such conclusions can be drawn experimentally.

* This work was supported in part by the joint program of the U. S. Office of Naval Research and the U. S. Atomic Energy Commission.

† Eastman Fellow.

Small-Angle Neutron-Proton Scattering at 400 Mev*

A. J. HARTZLER, R. T. SIEGEL, AND W. OPITZ†
Carnegie Institute of Technology, Pittsburgh, Pennsylvania

(Received May 24, 1954)

THE previously reported[1] differential n-p scattering measurements at 400 Mev have now been extended to cm neutron scattering angles below 40°. In this region the energy of the recoil protons is too low for detection with a scintillation telescope, so an arrangement for observing the scattered neutrons has been used. The properties of the neutron beam, details of collimation, and the monitoring arrangement were described in reference 1. For the small-angle measurements the diameter of the beam was reduced slightly to 2½ in. at the scatterer, which was at least 4 in.×4 in. in all cases. Extra lead shielding was also added near the scattering table to reduce neutron background.

Two types of scatterers were used, one of liquid hydrogen in a Styrofoam container and the other a pair of polythene and graphite plates which contained equal numbers of carbon atoms. The data taken with the two sets were in agreement, and both are included in the results quoted in Table I.

The apparatus is shown in Fig. 1. A thin (0.48 cm) anticoincidence counter (A), 7.6 cm wide by 10 cm high, screened out charged particles from the scatterer region. Following it were a polythene converter, 2.5 ×5.0×7.6 cm, which was centered 64.5 cm from the scatterer and determined the solid angle; a 3×6×½ cm stilbene crystal (B); 5.08 cm of Cu absorber; a 4×6×½

TABLE I. Relative n-p cross sections at small angles, normalized to $d\sigma/d\Omega=1.00$ at 40°. Column B contains results obtained with a neutron detector; column D those measured with a recoil proton telescope.

A Lab angle Θ	B Relative $(d\sigma/d\Omega)_{c.m.}$	C C.m. angle θ	D Relative $(d\sigma/d\Omega)_{c.m.}$
5.8	1.12±0.63	12.7	
6.8	1.33±0.14	15	
9.1	0.92±0.11	20	
13.8	0.85±0.17	30	
18.5	1.00±0.07	40	1.00±0.06
23.0	1.05±0.13	50	1.01±0.04
27.8	0.63±0.12	60	0.75±0.02

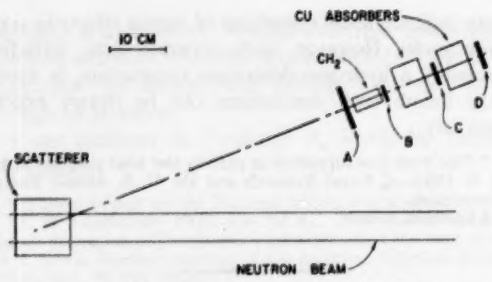

FIG. 1. Plan of neutron beam and detector for small-angle n-p scattering.

cm crystal (C); a second (variable) Cu absorber; and a $5\times10\times\frac{1}{2}$ cm crystal (D). Charged particles produced in the converter were counted by B, C, D in coincidence ($\tau=10^{-8}$ sec). The copper absorber between C and D was adjusted at every angle to the thickness necessary to impose a 365-Mev low-energy cutoff on the primary neutron beam.

At each angle the efficiency of the detector compared with that at 18.5° was computed with the aid of (a) high-energy n-p data,[1-3] (b) the efficiency *vs* proton energy measured for the telescope $B-C-D$ arranged in a sequence similar (but not identical) to that used here. Experimental confirmation of the calculated efficiencies was obtained by comparing the cm scattering from 40°–60° with the previous measurement obtained with a recoil proton telescope. (Column D of Table I).

The results with statistical standard deviations from counting are listed in Table I. Here the observed scattered-neutron counting rates (corrected for detector efficiency) have been transformed into the center-of-mass system and normalized to 1.00 at 40°.

Figure 2 and Table II show all our n-p results, extrapolated to 0° as shown and normalized to a total cross section of 33 mb.[4] The slow angular dependence of the cross section for small θ and its rapid variation near 180° are in qualitative agreement with the cloud-chamber work at 300 Mev,[3] but indicate a change from the symmetry about 90° observed at 90 Mev.[5]

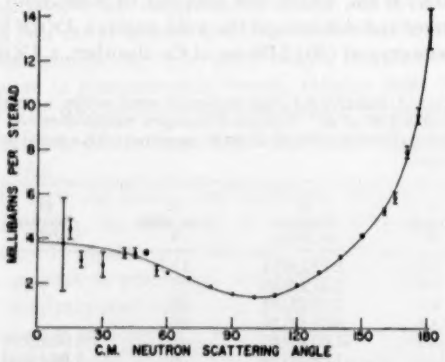

FIG. 2. Differential scattering cross section for 400-Mev neutrons on protons.

TABLE II. Absolute differential n-p scattering cross sections at 400 Mev. Errors are standard deviations computed for all known sources except the uncertainty in the total cross section (33 mb).

C.m. angle θ	$d\sigma/d\Omega$ (mb/sterad)	C.m. angle θ	$d\sigma/d\Omega$ (mb/sterad)
12.7	3.73±2.10	100	1.42±0.06
15	4.43±0.46	110	1.50±0.08
20	3.07±0.37	120	1.94±0.08
30	2.84±0.57	130	2.50±0.09
40	3.33±0.20	140	3.21±0.09
45	3.35±0.20	150	4.17±0.11
50	3.38±0.12	160	5.25±0.14
55	2.56±0.23	165	5.82±0.22
60	2.48±0.08	170	7.93±0.28
70	2.22±0.09	175	9.57±0.34
80	1.85±0.06	180	13.49±0.91
90	1.54±0.06		

* Supported in part by the U. S. Atomic Energy Commission. A more detailed report of this experiment is given in U. S. Atomic Energy Commission Report NYO-6566 (unpublished).

† Fulbright Fellow (1953–1954).

[1] A. J. Hartzler and R. T. Siegel, Phys. Rev. **95**, 185 (1954).

[2] J. De Pangher, University of California Radiation Laboratory Report UCRL-2153 (unpublished).

[3] Kelly, Leith, Segrè, and Wiegand, Phys. Rev. **79**, 96 (1950).

[4] V. A. Nedzel, Phys. Rev. **94**, 174 (1954); R. A. Schluter and S. C. Wright, Phys. Rev. **95**, 639 (1954).

[5] O. Chamberlain and J. W. Easley, Phys. Rev. **94**, 208 (1954), have used a similar technique at 90 Mev.

Negative-to-Positive Ratio of Photomesons from Deuterium*

MATTHEW SANDS, J. G. TEASDALE, AND ROBERT L. WALKER
California Institute of Technology, Pasadena, California

(Received June 1, 1954)

PREVIOUS measurements of the yields of positive and negative pions from the interaction of photons with deuterium indicated that the negative-to-positive ratio is about one for photon energies up to 300 Mev.[1] The ratio has now been measured for mesons of various energies and angles produced by the 500-Mev bremsstrahlung of the Caltech synchrotron.

The magnetic spectrometer used earlier in this laboratory for the detection of positive mesons from hydrogen[2] has been employed in this experiment to select particles of a particular momentum, angle, and sign of charge produced in a high pressure deuterium target by the photon beam. The total angular aperture in the plane of the beam was 20°, and the momentum interval selected was 10 percent of the center value.

For the angles and momenta of this work, most of the particles counted were mesons. Those electrons transmitted by the magnet at low fields were distinguished from mesons by their smaller energy loss in the counters. High-energy electrons were few except at

the forwardmost angle where they contributed in the worst case about 20 percent of the total counting rate. Since positive and negative electrons of high energy are produced in equal number, and since the negative-to-positive ratio for mesons is close to one, the electron contamination contributes a small error in the observed ratio. Corrections have been made for the effect. Protons that were selected by the spectrometer magnet did not have sufficient energy to penetrate the counters used.

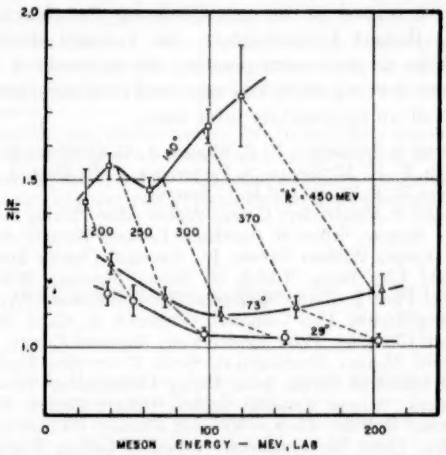

FIG. 1. Ratio of the yields of negative and positive mesons produced in deuterium by 500-Mev bremsstrahlung, plotted against laboratory energy for various laboratory angles. The errors shown are standard deviations due primarily to counting statistics.

The observed counts have been corrected for backgrounds taken without deuterium in the target, for accidental coincidences, and for the effect of 1.4 percent of hydrogen impurity in the target gas. All of the corrections together modify the observed ratios by a few percent, at most.

The decay of the pions in flight smears somewhat the effective momentum resolution of the apparatus. A preliminary estimate of the magnitude of the effect indicates that the distortions in the energy curve amount to less than the statistical errors at any point. More detailed calculations are in progress. Any significant corrections will be made in the final report of this work.

The results for the negative-to-positive ratio, corrected as described, are given in Fig. 1. We plot N_-/N_+, the ratio of the yield of negative mesons to that of positive mesons, against the laboratory energy of the mesons for three laboratory angles. The points which would correspond to the same photon energy "k" if the mesons arose from interactions of photons with free nucleons at rest are connected by broken lines.

The results indicate that the photoproduction of mesons is greater from neutrons than from protons, particularly at backward angles. The qualitative features of the result are predicted by pseudoscalar meson theory in weak-coupling (as well as by other theories).[3] The numerical values predicted for the negative-to-positive ratio are, however, considerably larger than those reported here. The experimental values are, on the other hand, larger than would be expected from coupling solely through the magnetic moments of the nucleons.

The absolute yields observed in these experiments will be included in the final report of this work.

* This work was supported in part by the U. S. Atomic Energy Commission.

[1] White, Jacobson, and Schultz, Phys. Rev. **88**, 836 (1952); R. Littauer and D. Walker, Phys. Rev. **86**, 836 (1952); Luckey, Jenkins, and Wilson, Phys. Rev. **91**, 468 (1953).

[2] Walker, Teasdale, and Peterson, Phys. Rev. **92**, 1090 (1953).

[3] K. Brueckner and M. Goldberger, Phys. Rev. **76**, 1725 (1949); K. Brueckner, Phys. Rev. **79**, 641 (1950); R. Marshak, *Meson Physics* (McGraw-Hill Book Company, Inc., New York, 1952).

Proceedings of the American Physical Society

Minutes of the 1954 Spring Meeting at Washington, D. C., April 29 and 30, and May 1, 1954

(Corresponding to *Bulletin of the American Physical Society*, Volume 29, no. 4)

THE 1954 Spring meeting of the American Physical Society was held among the surroundings and in the manner that have become familiar in the past few years. The dates were the last two days of April and the first of May. The Sheraton Park provided one more hall for our sessions than the year before, the Shoreham one fewer, the National Bureau of Standards the same number as before. Mostly the halls seemed adequate to the audiences; there were occasional exceptions. The programme set a new record in number (406) of contributed papers, the registration (1904) did not. As is normal at our Washington meetings, nuclear physics and theoretical physics were by far the most abundantly represented parts of our field among the contributed papers, and physicists from the Washington area supplied a goodly share of the invited papers. In nuclear physics, in addition to invited papers on various topics, there was a Symposium on polarization of nucleons by scattering. There was a group of invited papers in electron physics, another in biophysics, and our Division of Chemical Physics provided a third, its title being "Chemical applications of radiofrequency spectroscopy."

The multifarious tasks of the Local Committee were performed with a competence which disguised their difficulty. Its experienced and extremely capable Chairman, Hugh Odishaw, captained a group including D. F. Bleil of Naval Ordnance Laboratory, W. C. Hull of Naval Research Laboratory, C. K. Jen of the Applied Physics Laboratory of Johns Hopkins University, R. J. Seeger of the National Science Foundation, Howard Tatel of the Department of Terrestrial Magnetism of the Carnegie Institution of Washington, and R. D. Huntoon and H. H. Rosen of the National Bureau of Standards. Homage is paid to all of these institutions for the help that they gave us, the National Bureau of Standards above all.

The banquet of the Society was held on Friday evening in the Grand Ballroom of the Shoreham Hotel, H. A. Bethe presiding. The attendance was 306. P. Debye of Cornell University, E. R. Piore of the Office of Naval Research, Edoardo Amaldi of "CERN" and the University of Rome gave the speeches of the evening. J. Robert Oppenheimer received a standing ovation.

The Council convened on Thursday afternoon. It elected to Fellowship nine candidates and to Membership 104 candidates. Their names follow.

The Council empowered the President to appoint an Assistant Secretary and an Assistant Treasurer, to assure that the functions of either office may be carried on when the respective officer is traveling or indisposed. The President has since appointed W. W. Havens, Jr., and S. L. Quimby to the respective positions.

With regard to the case involving the clearance of J. Robert Oppenheimer, the Council decided to make no statement pending the outcome of the current investigation, but expected to make a statement at an appropriate later time.

Elected to Fellowship: E. P. Blizard, A. D. Callihan, W. N. English, F. K. McGowan, S. Pasternack, J. B. Platt, L. D. Roberts, R. P. Shutt, and R. L. Sproull.

Elected to Membership: George Wilbur Allen, *Irving Ames, Henry Aroeste, *Elliot H. Auerbach, Leonard Bernard Auerbach, Casper William Barnes, Jr., *Leonard Charles Beavis, *Donald Elro Bedo, *Ulrich H. Bents, Abraham William Berger, Paul J. Blatz, Robinson Derry Burbank, *Walter Stephen Byrnes, Ugo Camerini, *Frederick E. Card, Beryl Edward Clotfelter, Peter Aldrich Cole, Maynard Cowan, Jr., Clarence Marion Cunningham, *Scott Crittenden Daubin, *John Litchfield Davis, Irvin Henry DeBarbieris, *Howard Diamond, *Samuel Franklin Eccles, *Robert Everett Ellis, *Seymour Epstein, *George Kenneth Farney, William Gene Fateley, *John G. Fetkovich, Edmund George Franzak, *David H. Freeman, *Earl Wayne Friesen, *Clayton Frederick Giese, *Walter Gilbert, *William Livingston Gordon, *Richard Anton Griener, Stephen Graham Hamilton, Orin Chester Hansen, Jr., Hubert Heffner, *Harold William Hemstreet, Jr., *Theodore E. Hopkins, *James F. Hornig, *David Franklin Hotz, *Susumu Ishiwata, Gordon Leroy Johnson, *Stanley Ross Jones, *James Francis Kenney, Hans Otto Kneser, George D. Kohler, Adolph Theodor Krebs, Jacob Leeder, Robert S. Leonard, *Elliott Hershel Lieb, *Anthony Joseph Lomazzo, *Victor Flores Maldonado, *Paul C. Martin, Tommy French McCraw, Ronald Alexander McGee, *Kirk Warren McVoy, James Alexander Morrison, *J. Harry Mortenson, Francis Joseph Murray, *Richard Bennet Murray, David Herman Navon, *Theodore J. Newman, *Pablo Leopoldo Okhuysen, *Edward Davis Orenstein, James Overmeyer, Karlis Voldemars Ozols, William Francis Palmer, Richard H. Parker, *Donald Edward Parks, George John Pearson, *Charles Patton Poole, Edith Frances Reilly, *Marion Colburn Rinehart, Robert William Rufle, *George Janeway Safford, Morris Salkoff, Herbert Henry Sauer, Benjamin Frank Scherr, Sanford B. Schwartz, William Corr Shaw, Russell Dowell Shelton, Meyer Silver, Floy Wilking Smith, John Leslie Stephenson, Robert Carl Swyers, Frank Robert Tangherlini, Yoshinosuke Terashima, Jacques Georges Thirion, James Chilton Thompson, Ernest C. Tsivoglou, Charles Henry Townes, Leopoldo Benjamin Valdes, *D. O. Van Ostenburg, Michael Waldner, Orson Joseph Wallace, Elliott H. Weinberg, Mervin Claude Werst, George W. Wetherill, *John Widmer Winchester, *George Kenneth Yates, and *Hugh David Young.

Karl K. Darrow, *Secretary*
American Physical Society
Columbia University
New York 27, New York

Statement Issued on Behalf of the Council of the American Physical Society, Released to Press as of Saturday Afternoon June 12, 1954

The Council of the American Physical Society is deeply perturbed by the considerations used by the "Gray Board" in withdrawing the clearance of Dr. J. Robert Oppenheimer, while at the same time attesting to his loyalty and discretion. Many members of the American Physical Society have known and worked with Dr. Oppenheimer for many years and as a consequence of this association have great confidence in the value of Dr. Oppenheimer as a public servant. The Council of the American Physical Society is, for obvious reasons, in no position to render a judgment whether Dr. Oppenheimer meets the present requirements of the Atomic Energy Commission for clearance. There is, however, one matter of principle which emerges as a serious problem from the majority report of the Gray Board, upon which we feel it a duty to comment.

The chief new charges against Dr. Oppenheimer arose from the advice he gave on request and his subsequent attitude concerning the H-bomb. This question was a very difficult technical and policy matter on which opinions widely differed, with many men of assured loyalty and competence sharing Dr. Oppenheimer's views. Charges based on policy disagreement appear to be customary in Russia, but we regard them as not only morally reprehensible but also very harmful to our national welfare. If a man whose advice is sought must fear that his potential utility to the government may be challenged because his reasoned recommendations later become politically unpopular, he may be tempted to give advice that is politically safe rather than technically valid.

The opinion rendered by the majority of the Gray Board leaves this important question in doubt. While clearing Dr. Oppenheimer of all specific charges raised against him in connection with the H-bomb development, they reprimand him for his "lack of enthusiasm" for the programme after it was officially adopted. To require such subservience to an official viewpoint as a proof of trustworthiness is to prevent the development of the best thought.

There can be little doubt that the majority report of the Gray Board will have an adverse effect upon the ultization of scientists in the government. It is to be hoped that these issues will be clarified by the Atomic Energy Commission in the course of its final ruling on Dr. Oppenheimer's clearance.

H. A. BETHE, *President*
American Physical Society

Errata Pertaining to Papers C1, F5, F13, H9, JA18, K12, KA14, Q16, QA10, RA5, S11, SA6, V3, V5, VA3, W10, and Y10

C1, by L. H. Johnston, E. A. Day, and J. H. Williams. In line 11, accelerated should read accelerator.

F5, by I. H. Solt, Jr., and M. W. P. Strandberg. In line 9. $g=2.0012\pm0.0002$ at 300°K and 78°K should read $g=2.0013\pm0.0002$ at 300°K and 78°K. In line 17, 11.5 gauss should read 12.4 gauss.

F13, by A. Bennett. A footnote should be added, reading, "Supported by the Office of Naval Research."

H9, by M. Avramy Melvin. The title should read "The Law of Impact for Generally Shaped Bodies."

JA10, by G. Birnbaum and A. A. Maryott. In line 12, ($\alpha=3.1\times10^{-5}$) should read ($\alpha=1.5\times10^{-4}$).

K12, by S. Koslov, V. Fitch, and J. Rainwater. In line 18, 206.36 and 208.22 should read 207.67 and 209.99.

KA14, by E. H. Daggett and G. R. Grove. In line 6, Po^{102} should read Po^{210}.

Q16, by F. Ajzenberg, W. Franzen, and J. G. Likely. In line 11, 10.6 Mev should read 18.6 Mev.

QA10, by P. T. Landsberg. The last two sentences of the abstract should be omitted.

RA5, by J. S. Levin and D. J. Hughes. Instead of the last sentence, read: The 4.9 and 61-ev levels in Au^{197}, and the 23-ev level[2] in Hg^{198} all have radiation widths about 5 times larger. The strong dependence of Γ_γ on atomic weight in this group of elements indicates that radiation widths are influenced by nuclear shell structure.

S11, by Leonard A. Mann, Ray A. Grandey, and Arnold F. Clark. In Table I, fourth column, 33.6 should read 28.0. In lines 8, 9, and 10, "The total cross section···is constant within statistical error" should read "The total cross section ···decreases geometrically with increase of energy of the pion."

SA6, by G. A. Bartholomew, F. Brown, H. E. Gove, A. E. Litherland, and E. B. Paul. In lines 14 and 15, "···and that the 10.80 Mev states is probably 3.2+" should read "···and that the 10.80 Mev state is probably 3.2−."

V3, by Joseph Callaway. The centered equation should read:

$$V(r)=\frac{0.576e^2}{\frac{4}{3}\pi\rho_-(n)^{\frac{1}{3}}+5.1}.$$

V5, by L. C. Biedenharn, R. L. Gluckstern, and M. H. Hull, Jr. In line 10, $\hbar^{-1}$ should be η^{-1}.

VA3, by K. M. Siegel, A. H. Halpin, and A. L. Maffett. In lines 4 and 5, steamfunction should read streamfunction.

W10, by W. Baer. In line 11, 66.3 should read 69.6. In line 12, 77.5, 87.2, 107.9 should read 81.3, 89.7, 112.8.

Y10, by D. Nagle, J. Marshall, L. Marshall, and W. Skolnik. The last sentence of the abstract should be omitted. The next to the last sentence should read: "The present results, from a single cyclotron run, seem to show for deuterium a behavior similar to that of hydrogen."[1]

PROGRAMME

THURSDAY MORNING AT 10:00

Shoreham, Main Ballroom

(BRYCE CRAWFORD, JR., presiding)

Symposium of the Division of Chemical Physics

Chemical Applications of Radio-Frequency Spectroscopy

A1. Molecular-Beam Studies of Molecules. N. F. RAMSEY, *Harvard University.* (35 min.)

A2. Structural Determinations by Nuclear Magnetism. H. S. GUTOWSKY, *University of Illinois.* (35 min.)

A3. Chemical Applications of Nuclear Magnetic Resonance. M. E. PACKARD, *Varian Associates.* (35 min.)

A4. Recent Applications of Microwave Spectroscopy to the Study of Molecules. C. H. TOWNES, *Columbia University.* (35 min.)

Business Meeting of the Division of Chemical Physics

(To be convoked during Session A whenever the Chairman shall see fit.)

THURSDAY MORNING AT 10:00

Sheraton Park, Continental Room

(DAVID PINES presiding)

Nonmetallic Solids, I (Including Semiconductors)

B1. Thermal Conductivity of Semiconductors. A. NEAVES AND D. TER HAAR,* *St. Andrews University, Scotland.*—Using methods due to Wilson[1] and Makinson[2] we have evaluated the electronic thermal conductivity K_e and the lattice thermal conductivity K_g for the case of semiconductors, when to a first approximation we can use a Maxwell distribution for the conduction electrons. As far as K_g is concerned, Sommerfeld and Bethe[3] have shown that the main contribution arises from the changed lattice distribution function, if we are dealing with metals. In the case of semiconductors the change in the electron distribution function is, however, important.

* On leave of absence at Purdue University.
[1] A. H. Wilson, Proc. Cambridge Phil. Soc. **37**, 371 (1937).
[2] R. E. B. Makinson, Proc. Cambridge Phil. Soc. **38**, 474 (1938).
[3] A. Sommerfeld and H. Bethe, Handbuch der Physik **242**, 333 (1933).

B2. Electronic Thermal Conduction in Semiconductors. P. J. PRICE, *Watson Laboratory.*—A temperature gradient in a semiconductor leads to gradients of the carrier concentrations, and hence to carrier diffusion currents

$$\mathbf{N}_1=\mathbf{N}_2=-\frac{\sigma_1\sigma_2}{\sigma_1+\sigma_2}\left(\frac{k}{e^2}\right)\left[\frac{\Delta}{kT}+3+\gamma_1+\gamma_2\right]\text{grad}T, \qquad (1)$$

where Δ is the energy gap between the bands, and the (thermal diffusion) factors γ_1 and γ_2 are each $\frac{1}{2}$ for pure lattice scattering. (We have assumed nondegeneracy in the electron and hole distributions, and neglected any "impurity band" transport effects.) Each electron-hole pair transports annihilation energy Δ, as well as band energy of order kT; and hence the carrier flow contributes, to the thermal conduction

$$K_{\text{flow}}=\frac{\sigma_1\sigma_2}{\sigma_1+\sigma_2}\left(\frac{k}{e^2}\right)\left[\frac{\Delta^2}{kT}+\alpha\Delta+\beta kT\right], \qquad (2)$$

where α and β again depend on the scattering processes. For silicon and germanium, the term in Δ^2 of (2) could attain about 0.3 watt units at their melting points. There is thus the possibility of minima, at high temperatures, in the total thermal conductivities.

B3. Comparison of Hall and Magnetoresistance Phenomena in InSb with those in Germanium.* T. C. HARMAN, R. K. WILLARDSON, AND A. C. BEER, *Battelle Memorial Institute.*—Studies of Hall coefficients and resistivities as functions of temperature and of magnetic field reveal interesting differences in the behavior of p-type InSb[1] and p-type germanium.[2] The effects in InSb are adequately explained by an extension of Harding's work to include arbitrary concentrations of both p- and n-type carriers. The shift in temperature of the Hall coefficient crossover, the Hall coefficient maximum, and the magnetoresistance maximum with magnetic field can be predicted. No maxima in magnetoresistance *versus* temperature were observed in high-purity p-type germanium (80°K to 600°K). Furthermore, the shift of the Hall coefficient crossover temperature with magnetic field in germanium is in the opposite direction from that in InSb; a behavior at variance with predictions from the two-carrier model. Experimental values of $\Delta R/R_0$ and $\Delta\rho/\rho_0$ are shown as functions of temperature for InSb and germanium. Results are compared with calculated values given in terms of an implicit temperature parameter $n_1\mu_1/n_2\mu_2$.

* Supported in part by the Wright Air Development Center.
[1] Willardson, Beer, and Middleton, Phys. Rev. **93**, 912(A) (1954); O. Madelung, Z. Naturforschr. **8a**, 791 (1953).
[2] W. C. Dunlap, Phys. Rev. **71**, 471 (1947); **79**, 286 (1950); **82**, 329 (1951).

B4. Application of a Three-Carrier Model to the Hall Effect in Germanium. R. K. WILLARDSON, T. C. HARMAN, AND A. C. BEER, *Battelle Memorial Institute.*—Recent cyclotron resonance observations[1] on p-type germanium at 4°K have indicated the existence of positive holes with effective masses of 0.04m and 0.30m. An appreciable difference in mobility of these two p-type carriers may therefore be expected. In fact, the mobility of the holes of lower effective mass should be significantly greater than that of the electrons ($m^*=0.11$m). The presence of this additional p-type carrier of high mobility can explain why the Hall coefficient changes with increasing magnetic field from positive to negative in the neighborhood of the crossover point. Furthermore, the unusually large changes in extrinsic Hall coefficient with magnetic field are explained. In particular, the rapid decrease with increasing magnetic field of the Hall coefficient at 80°K for fields below 1000 gauss[2] is accounted for. Initial calculations indicate a reasonably good fit of experimental data is obtained by taking the mobility of the holes with the lower effective mass to be about five times that of the ordinary hole mobility. The contribution of these carriers is about 20 percent of the observed p-type conductivity.

[1] Dresselhaus, Kip, and Kittel, Phys. Rev. **92**, 827 (1953).
[2] Harman, Willardson, and Beer, "Note on Hall coefficient in germanium," submitted for publication as a letter to the editor of Phys. Rev.

B5. Radioactive and Photoelectric $p-n$ Junction Power Sources. W. G. PFANN AND W. VAN ROOSBROECK, *Bell Telephone Laboratories.*—An electrical power source can be made by bombarding a $p-n$ junction with beta particles so that electron-hole pairs produced by radiation are separated by the junction field.[1] Such radioactive cells have been constructed; equations for maximum output power W and efficiency F, applicable to photocells also, have been derived; and a detailed study of the factors which limit W and F has been completed. F increases with the source-current I_θ of separated charges and with the zero-voltage junction resistance R_0. While I_θ increases with amount and activity of the isotope and energy of its radiation, it is limited by self-absorption in the isotope and the need for keeping beta energies below the threshold for formation of lattice defects in the semiconductor. These factors materially limit W and F for $Sr^{90}-Y^{90}$ cells. Of germanium and silicon cells made with $Sr^{90}-Y^{90}$, cell currents were higher for germanium, because of longer diffusion lengths and shorter beta range; but cell powers were higher for silicon, because of larger R_0. Operating at -10°C increased the power of a germanium cell by a factor of 24.

[1] P. Rappaport, Phys. Rev. **93**, 246 (1954).

B6. Some Electrical Properties of Several Silicon-Germanium Alloys.* L. DAVIS, JR., G. A. DEMARS, L. G. RUBIN, AND W. D. STRAUB, *Ratheon.*—Large crystallites of Si–Ge alloys ranging in composition from 14 percent to 84 percent Ge were obtained from melts that were cooled from above the solidus to below the liquidus at the rate of 2°C per hour. The lattice constants of several samples were determined from density measurements and powder patterns and checked the values of Stor and Klemm[1] within 0.1 percent. The x-ray line widths indicated a spread of 2 percent to 16 percent in sample compositions, the larger spreads coming in the high Ge content samples. Measurements of intrinsic resistivity *versus* temperature resulted in energy gap values of $E_G=1.13$ ev for the compositional range 14 percent–50 percent Ge and $E_G=1.02$ ev for 62 percent–84 percent Ge. All samples were p type with Hall hole mobilities of about 550 cm²/volt sec for the 62 percent–74 percent Ge range and about 250 for the 14 percent–34 percent Ge range. In general, the measurements were performed on single crystal samples.

* Work supported in part by U. S. Bureau of Ships, Air Corps, and Signal Corps.
[1] H. Stor and W. Klemm, Z. anorg. Chem. **241**, 305.

B7. Anisotropy of Cyclotron Resonance in Germanium.* Part I Theory. BENJAMIN LAX, H. J. ZEIGER, AND R. N. DEXTER, *Lincoln Laboratory.*—Calculations by Shockley,[1] Herman, and others[2] on the band structure of germanium suggested that the energy surfaces for the conduction band in k space might consist of six ellipsoids of revolution with principal axes along the [100] directions. Experimental results on cyclotron resonance in n-type germanium at microwave frequencies and liquid helium temperatures indicate that the surfaces are eight ellipsoids of revolution with principal axes along the [111] directions. Based on this model, equations of motion for electrons in the conduction band are written in terms of a longitudinal mass m_1 and a transverse mass m_2. Expressions are obtained for the effective mass for an arbitrary orientation of dc magnetic field with respect to the crystalline axis. These allow the determination of m_1 and m_2 from the positions of the magnetic resonance peaks. Theoretical expressions are developed for the rf absorption as a function of dc magnetic field, for arbitrary orientation of magnetic field and rf electric field with respect to the crystalline axes. From the resonance line shapes, the relaxation time for scattering of conduction band electrons can be estimated.

* The research reported in this document was supported jointly by the Army, Navy, and Air Force under contract with the Massachusetts Institute of Technology.
[1] W. Shockley, Phys. Rev. **90**, 491 (1953).
[2] F. Herman, Phys. Rev. **88**, 1210 (1952); F. Herman and J. Callaway, Phys. Rev. **89**, 518 (1953).

B8. Anisotropy of Cyclotron Resonance in Germanium.* Part II Experiment. R. N. DEXTER, H. J. ZEIGER, BENJAMIN LAX, AND E. S. ROSENBLUM, *Lincoln Laboratory.*—Experiments have been performed on cyclotron resonance in ~40 ohm-cm p-type and n-type single crystals of germanium. Measurements were made at liquid helium temperatures at microwave frequencies of 8895 Mc per second and 23 650 Mc per second. The germanium sample was mounted in a rectangular cavity, and the power absorbed in the cavity was detected by a recording spectrometer. Observations were made as a function of dc magnetic field for various orientations of the magnetic field in the (110) plane. At an rf electric field of about ~4 volts/cm in the sample "breakdown" was observed. A relaxation oscillation, associated with "breakdown" and "quenching," appeared at this critical field. For cyclotron resonance the electric field in the sample was maintained at ~0.1 volt/cm, well below the "breakdown" field. P-type germanium resonance showed no directional anisotropy and the results were in agreement with those previously reported.[1] The n-type germanium resonance curves showed distinct anisotropy effects. Good agreement between theory and experiment was obtained for values of longitudinal mass $m_1=1.3\ m_0$ and transverse mass $m_2=0.08\ m_0$.

* The research in this document was supported by the Army, Navy, and Air Force under contract with the Massachusetts Institute of Technology.
[1] Dresselhaus, Kip, and Kittel, Phys. Rev. **92**, 827 (1953).

B9. A. C. Photoconductivity in Phosphors.* J. J. DROPKIN AND S. ORGEL,† *Polytechnic Institute of Brooklyn.*—An ac method has been used to determine the resistance and capacitance of a number of phosphors under uv and ir irradiation for the frequency range 20 to 100 cps. The phosphor R and C decrease with increasing frequency. The behavior of both R and C are accurately described by a Debye dispersion equation of the type given by Koops[1] for grain conduction. (Other mechanisms give the same equations.) The asymptotic value of the resistance for increasing frequency is proportional to the interelectrode distance, inversely proportional to the square root of uv intensity, and inversely proportional to the ir intensity. The kinetics of photoconduction in phosphors indicate that the asymptotic resistance can therefore be used as a measure of the photoresistance of the phosphor.

* Supported in part by the U. S. Office of Naval Research.
† Present address: 102 Court F, West Lafayette, Indiana.
[1] C. G. Koops, Phys. Rev. **83**, 121 (1951).

B10. X-Ray Production of F Centers in NaCl and LiF.* R. C. HERMAN, L. L. MADOR,† R. F. WALLIS, AND M. C. WILLIAMS, *Applied Physics Laboratory, The Johns Hopkins University.*—The relative energy loss of a heterogeneous x-ray beam has been calculated as a function of depth of penetration in NaCl and LiF crystals, and compared with curves of *F*-center absorption obtained by scanning in depth, perpendicular to the x-ray beam, crystals x-rayed for various times at 30 or 50 kv. It is found that *F*-center production in NaCl is proportional to the energy loss for short x-ray exposures. For longer exposures *F*-center production efficiency decreases, although no saturation has yet been obtained. After 24-hour exposures an anomalous increase in production is observed near the x-rayed face. On the other hand, for LiF the *F*-center production efficiency is almost constant, and the absorption-depth curves fall off more steeply than the calculated energy loss curves. This discrepancy might result from luminescence effects which are more pronounced than in NaCl, or might indicate a difference in mechanism for the production of *F* centers in LiF. The technique for measuring, perpendicular to the direction of the x-ray beam, the absorption of essentially homogeneous *F*-center concentrations is useful for the quantitative study of growth and decay effects.

* This work was supported by the Bureau of Ordnance, Department of the Navy.
† Now at Research Division, National Distillers Products Corporation, Cincinnati, Ohio.

B11. Effects of Preparation and Temperature on the Response of NaI Phosphors.* C. O. MUEHLHAUSE, E. DER MATEOSIAN, AND MICHAEL MCKEOWN, *Brookhaven National Laboratory.*—Phosphors of NaI with and without Tl were grown both by the method of Bridgman and of Kyropoulos.[1] Pulse height *vs* temperature curves were measured for both alpha particles and electrons in the temperature range from 77°K to 300°K. These data were taken with a Dumont 6292 photomultiplier and an 0.8 μs rise time linear amplifier having an input integrating time of $\sim$20 μs. It was found that the ratio of the pulse height per unit energy of the alpha particle to that of the electron was dependent on both the method of preparing the phosphor and on the temperature of its operation. In some cases, this ratio was observed to be greater than unity. The data also suggested that the effects of Tl activation are important at temperatures above $\sim$175°K. At temperatures below $\sim$160°K luminescent centers other than those due to Tl play an important role. Phosphors that were grown too rapidly exhibited an anomalous resolution which was not a monotonic function of the temperature. At temperatures below $\sim$100°K faster fluorescent components were observed than have been reported previously.[2]

* Research performed under the auspices of the U. S. Atomic Energy Commission.
[1] S. Kyropoulos, Z. anorg. u. allgem. Chem. **154**, 308 (1926).
[2] J. Bonanomi, J. Rossel, Helv. Phys. Acta **24**, 310 (1951). J. Bonanomi, Helv. Phys. Acta **25**, 725 (1952).

B12. Ionic Conductivity and X-Ray Coloration of Alkali Halides. F. A. CUNNELL AND E. E. SCHNEIDER,* *University of Durham, England.*—Extensive investigations of the structure sensitive ionic conductivity down to 100°C of pure crystals of LiF, NaCl, KCl, KBr, KI, and crystals of KCl−Sr and NaCl−Mn have been carried out with a dc method allowing the direct observation of polarization effects on a CRO. The experiments have revealed consistent deviations from a linear $\log\sigma - 1/T$ relation and a significant lowering of the conductivity following either heat treatment (quenching) or x-ray coloration of the crystals. These results and those on the magnitude and duration of the polarization have been interpreted in terms of an effective block structure of single crystals resulting from a nonuniform distribution of imperfections. Experiments on the correlation between ionic conductivity and darkenability by x-rays, as affected by heat treatment and divalent impurity content, have lent further support to these ideas.

* 1953–54 at Duke University, Durham, North Carolina.

B13. Thermal Restoration of Color Centers at Low Temperature. R. V. HESKETH AND E. E. SCHNEIDER,* *University of Durham, England.*—X-ray colored crystals of KCl can be partially bleached at liquid nitrogen temperature by irradiation in the *F* band. During such bleaching an absorption peak appears at 8750A. When during subsequent gradual heating the *F* and V_1 absorptions are observed, a pronounced peak appears at −100°C in both "absorption glow curves" indicating that *F* centers and V_1 centers are temporarily restored and subsequently destroyed by thermally activated recombination. The thermal bleaching can be prevented and the restored absorptions be arrested by recooling from −100°C to liquid nitrogen temperature. The formation of the V_1 band on warming (conditional on *F* irradiation at low temperature) is particularly remarkable in the case where the crystal after x-raying had been raised to room temperature so that at the beginning of the experiment it did not contain any V_1 centers at all. The experiments suggest that the electrons released by low-temperature *F* bleaching are trapped in metastable centers (possibly associated with the peak at 8750A) which also contain a positive hole, and that the thermal breakup of these centers yields *F* and V_1 centers in close proximity to each other.

* 1953–54 at Duke University, Durham, North Carolina.

B14. Phosphorescence of and Energy Storage in Some Ultraviolet Emitting Phosphors.* C. E. MANDEVILLE AND H. O. ALBRECHT, *Bartol Research Foundation.*—Measurements of the phosphorescent decay of uv excited NaCl−Tl show its uv and visible emission bands to decay by distinctly differing laws, whereas the bands of KCl−Tl under α particle and uv excitation appear to have approximately the same mode of decay. The "light storage" properties of NaCl−Ag have been investigated as a function of silver concentration. The photostimulated emission of x-ray excited thick crystals of NaCl−Ag has a maximum at a silver concentration of a few tenths of a percent by weight and shows a marked decline at concentrations as great as one percent by weight. The energy storage properties of x-rayed beryllium oxide have been observed. By drawing short photostimulated bursts of uv from the phosphor at least once every 48 hours over a period of days, it has been concluded that BeO retains in deep traps stored electrons for a greater time (thermal escape is less probable) than does NaCl−Ag of the most favorable silver concentration. The absolute emission of BeO under both excitation and photostimulation is less than that of NaCl−Ag, but the BeO is powdered and thus has poor transmission properties.

* Assisted by the joint program of the U. S. Office of Naval Research and the U. S. Atomic Energy Commission.

B15. Effect of Pressure on the Optical Absorption of the Activator in a Luminescent Solid. PETER D. JOHNSON AND FERD E. WILLIAMS, *General Electric Research Laboratory.*—The optical absorption spectrum of thallium-activated potassium chloride has been measured at pressures to 2000 kg/cm^2. The absorption band corresponding to the $^1S_0 \rightarrow {}^3P_1{}^0$ transition of Tl^+ shifts 4A to longer wavelengths. The spectral shift can be calculated from the theory of luminescence of KCl:Tl[1] recognizing that the occupation probabilities of accessible atomic configurations of the activator system are dependent on pressure and the transition energy for a particular configuration is not. The probability $Q(\epsilon,P)$ of the transition energy ϵ at the configuration q with the applied pressure P is $Q(\epsilon,P) = Q_0(\epsilon)\exp\{[AP/kT][q-(AP/2K)]\}$, where $Q_0(\epsilon)$ is the probability of the transition energy ϵ with no applied pressure, A is the effective area of the activator system and K

is the force constant determined from the quantitative configuration coordinate model. The area A is determined by assuming that the pressure acts hydrostatically on six pistons each of cross section equal to the cross sectional area of the Cl^-. The theoretical shift in absorption is 5A to longer wavelengths.

[1] F. E. Williams, J. Chem. Phys. **19**, 457 (1951); J. Phys. Chem. **57**, 780 (1953).

B16. Light Decay from Electroluminescent Phosphors.* S. H. AUTLER AND W. F. ROAT, *Lincoln Laboratory.*—A series of studies has been made on powdered electroluminescent phosphors. The phosphors which were of the ZnS:Cu:Pb blue-green type were excited by sharp pulses of current of the order of a microsecond in duration. The pulse of light which followed each current pulse was detected by a photomultiplier after passing through a monochromator. The decay of the light intensity was recorded for several thousand microseconds and was thus observed during a period when the plate was not being excited. The decay rate depended on the wavelength of the light, but in all cases the light fell off much slower than either a linear or bimolecular process would predict. A second current pulse applied in the same direction before the light has ceased completely results in a momentary decrease in output. This suggests that, before emission occurs, electrons must diffuse back to the emission centers from which they have been pulled by the original electric field. Irradiating the phosphor with infrared has marked effects upon its light output and this will be discussed.

* The research in this document was supported by the U. S. Army, Navy, and Air Force under contract with the Massachusetts Institute of Technology.

THURSDAY MORNING AT 10:00

Shoreham, West Ballroom

(E. C. CREUTZ presiding)

Apparatus of Nuclear Physics, I

C1. Proposed Design of a 50-Mev Proton Linear Accelerator.* L. H. JOHNSTON, E. A. DAY, AND J. H. WILLIAMS, *University of Minnesota and Midwest Accelerator Conference.*—Requirements for the injection of protons into a multi-billion volt alternating gradient accelerator indicate the following desirable properties: (a) high energy to minimize frequency modulation and effects of space charge, gas scattering, and remanent guide field; (b) small energy spread and good collimation to allow capture of injected protons into small aperture; (c) large pulse currents. An Alvarez-type single-cavity accelerated with the following characteristics is proposed. Injector energy ½ Mev, length 80 feet, radio-frequency 200 megacycles, peak rf power 6 megawatts, maximum repetition rate 1 per second, rf pulse length 200 microseconds, proton pulse length as required by alternating gradient machine, output energy 50.0±0.2 Mev, anticipated instantaneous current more than 0.1 milliamperes. Steel vacuum enclosure with bonded copper lining also serves as resonant cavity. Diameter tapered from 42 in. to 36 in. to maintain uniform 6-in. diameter drift tubes. Magnetic quadrupole lenses inside each drift tube provide radial focussing. Initial proton aperture 1 centimeter, final 2 centimeters. Anticipated beam diameter 1 centimeter, angular deviation ±1 milliradian.

* Partially supported by the U. S. Atomic Energy Commission.

C2. Ionization Loading of Electrostatic Generators. C. M. TURNER, *Brookhaven National Laboratory.**—Back streaming electrons in a positive ion acceleration tube generate x-rays upon striking materials at the anode end of the tube. Recent tests show that ionization of the high-pressure insulating gas used in electrostatic generators by this x-ray flux, contributes significantly to the well known difficulties which accompany the application of high potentials to an acceleration tube. Not only is the charging current requirement increased excessively by this extraneous ion load, but ions precipitated onto the potential grading hoop system upset the otherwise uniform gradient along it and thereby invite sparking. The ratio of these ionization currents to the primary back electron current can be as high as 40 at 2 million volts and 150-psig tank pressure. Variations of anode geometry from a simple steel plate to a composite of beryllium and lead designed to minimize x-ray production and maximize x-ray absorption, increased the voltage limitation on the 8 foot long acceleration tube in the rebuilt Brookhaven National Laboratories research electrostatic generator from 2.5 million to close to 4 million.

* Work performed under the auspices of the U. S. Atomic Energy Commission.

C3. Rf Cockcroft-Walton Generator for Neutron Production.* R. A. PECK, JR., *Brown University.*—A 200-kev deuteron accelerator has been constructed for spectroscopy of relatively low-yield (n,p) reactions, utilizing the $D+T$ reaction for neutron production. The high-voltage source is of the rf Cockcroft-Walton type[1] and consists of six doubler units sealed in oil-filled plastic drums. The stack of doublers is excited by a 45-kc oscillator (20-kv peak) and each unit provides 40-kv dc, without power load. Ripple components[2] and dc output have been observed at frequencies of 45 kc, 800 cps, and 60 cps. Voltage output under load improves markedly with change from 60 to 800 cps but changes little above 800 cps. The ion source is of the rf type and has produced currents up to 15 ma, with higher currents apparently obtainable if desired;[3] several milliamperes (at 200 kev) have been obtained on a 10-cm² target blank. Some features of design and construction will be discussed and performance characteristics described.

* Supported in part by the U. S. Atomic Energy Commission.
[1] J. R. Woodyard, Rev. Sci. Instr. **22**, 705 (1951) and UCRL-694.
[2] E. Everhart and P. Lorrain, Rev. Sci. Instr. **24**, 221 (1953).
[3] H. P. Eubank, Phys. Rev. **92**, 853 A (1953).

C4. A Pressurized 500-Kilovolt High-Frequency Cockcroft-Walton Accelerator.* PAUL LORRAIN, R. BÉIQUE, P. GILMORE, P. E. GIRARD, A. BRETON, AND P. PICHÉ, *Université de Montréal.*—A 24-stage high-frequency Cockcroft-Walton accelerator (1), (2) has been built which accelerates positive ions to 500 kev. For compactness, it is pressurized at 10 psig in a tank 38 inches in diameter and 53 inches long. A single oscillator and power amplifier unit is used to feed the voltage multiplying circuit, the filament transformers, and the power supplies for the source and the extracting electrode. There are no moving parts, aside from control rods which serve to direct and focus the beam, burn the source on and off, and admit

gas to the source while the accelerator is in operation. A PIG-type ion source is used (3), (4). Focussing is obtained by means of a single extraction electrode which operates as an *einzel* lens.

* Supported in part by Canadian Atomic Energy Control Board.
[1] Paul Lorrain, Rev. Sci. Instr. **20**, 216 (1949).
[2] Edgar Everhart and Paul Lorrain, Rev. Sci. Instr. **24**, 221 (1953).
[3] Paul Lorrain, Can. J. Research **A25**, 338 (1947).
[4] Paul Lorrain, Helv. Phys. Acta **XII**, 497 (1948).

C5. Particle Selection Technique Used at the M.I.T. Cyclotron.* F. A. ASCHENBRENNER, *M.I.T.*—The particle selective counter consists of a thin plastic scintillation counter which measures dE/dx of the reaction particles and a NaI(Tl) counter which measures the remaining energy of the reaction particles after they pass through the thin counter. The product $E \cdot dE/dx$ which is proportional to the mass over a limited energy range is taken electronically and displayed on one axis of an oscilloscope. The energy is displayed on the other axis. The product and energy pulses are also sent through two pulse height analyzers. Output pulses from the analyzers actuate a coincidence circuit. The coincidence pulses trigger the intensity grid of the oscilloscope when the pulses on the two axes are at their maxima. Time exposure photographs of the oscilloscope show separate lines representing the resolved particles of different mass and also individual particle energy groups. The bias and gate of the product analyzer can then be adjusted so that only one type of particle is counted. The other analyzer can then be used to obtain the energy spectrum of the type of particle selected.

* This work has been supported in part by the joint program of the U. S. Office of Naval Research and the U. S. Atomic Energy Commission.

C6. Microtrons (Electron Cyclotrons for X and K Band Operation) II.[1] H. F. KAISER, *Naval Research Laboratory.*—Three microtrons under study and development will be discussed: (1) a K band (24 Kmc) microtron which has been observed to operate in a low-energy mode; (2) a general purpose X band (9375 mc/sec) microtron which is being used to test microtron ideas and is suitable for electron and x-ray experimental research, including studies on extracted electron beams; (3) a high-power 1-megwatt X band microtron incorporating experience gained in design and operation of X band microtrons to-date. Development of the K band microtron depends at present on improvement of resonators and increase of available power, both of which are feasible. The X band microtron is easily operated with commercially available magnetrons and forms an easily operated and dependable accelerator for energies of several Mev.

[1] H. F. Kaiser, Phys. Rev. **91**, 456 (1953); J. Franklin Inst., Feb., 1954.

C7. Phase Properties of the Deflected Ion Beam from a Fixed-Frequency Cyclotron. M. JAKOBSON, *Montana State University,* AND J. H. MANLEY, *University of Washington.*—The duration of the ion burst and the phase of the dee voltage as the deflected ion beam emerges from the University of Washington Cyclotron has been investigated. This knowledge is necessary for the measurement of reaction energies with a time of flight spectrometer. The ions were detected by means of a stilbene crystal mounted on a 1P21 photomultiplier. The photomultiplier signals were sent to the vertical amplifier of a 517 Tektronix. A rf pickup coil at the deflector provided the horizontal sweep and time base. The ions are sharply defined in phase at threshold. As the dee voltage is increased above threshold, and with the magnetic field tuned to resonance, the duration of the ion burst increases rapidly at first, then approaches a constant value. The ions emerge earlier in time as the magnetic field is *increased* through resonance. As different turns appear, a jump in time of arrival of the ions occurs. The phases of the emerging ions have been obtained by numerical integration and are in agreement with measurements.

C8. Betatron Orbit Stability as a Function of n. G. C. BALDWIN, F. R. ELDER, AND W. F. WESTENDORP, *General Electric Research Laboratory.*—Experiments are in progress with a small betatron with symmetrical magnetic circuit and polepiece profile designed to produce a guide field exponent $n=0.7$ constant over a wide annular region. With low rate pulsed operation, n can be varied linearly from 0.5 to 0.9 by concentric polepiece windings excited by a current transformer. Reduced output and weak x-radiation throughout the acceleration cycle, indicating instability, are observed for discrete n values of 0.53, 0.56, 0.64, 0.75, >0.84. Theoretical analysis shows these to be the result of interaction with azimuthal guide field variations.[1]

[1] D. M. Denison and T. Berlin, Phys. Rev. **69**, 542 (1946); D. Judd, Ph.D. thesis, California Institute of Technology (1950).

C9. Spectral Distribution Curves of the Far Ultraviolet Radiation from the Cornell Synchrotron.* D. H. TOMBOULIAN AND P. L. HARTMAN, *Cornell University.*—Based on Schwinger's[1] theory, numerical calculations have been carried out for the purpose of comparison with recent[2] experimental observations of the electromagnetic radiation emitted by high-energy electrons. Tentative intensity distributions curves have been obtained from the spectrograms on the basis of certain assumptions regarding the distribution of energy among the different order spectra produced by the grating. Utilizing the narrow emission bands of certain light elements as the incident radiation, a determination of the actual grating response is in progress. More complete reduction of the experimental data must await the outcome of the current work on the efficiency of the grating.

* Supported by the Office of Ordnance Research, U. S. Army.
[1] J. S. Schwinger, Phys. Rev. **75**, 1912 (1949).
[2] P. L. Hartman and D. H. Tomboulian, Phys. Rev. **91**, 1577 (1953).

C10. A Gaseous Scintillation Counter. C. EGGLER AND C. M. HUDDLESTON, *Argonne National Laboratory* (introduced by Louis A. Turner).—A photomultiplier tube has been used to measure the light emitted by argon and certain other gases when excited by α particles. A thin film of plastic color shifter has proved effective for converting spectral lines in the far ultraviolet into the region of photocathode sensitivity. Preliminary experiments, using a simple geometrical arrangement and a Pu source of known activity, indicate a counting efficiency approaching 100 percent. Pulse-height analysis strongly suggests the possibility of using a gaseous scintillation counter for heavy-particle spectral analysis.

C11. Measurement of the Time Jitter in BF_3 Counters. O. D. SIMPSON, *Phillips Petroleum Company.**—Time jitter or the variations in time delay after a neutron is absorbed until the α pulse is recorded has been measured for some commercial BF_3 counters. The gamma rays from the 470 kev level in Li^7 were detected by means of NaI crystal α photomultiplier and used to trigger an oscilloscope trace. By measuring the α-particle pulse number-time distribution, the time jitter was determined. A counter of 2-in. diameter, 60 cm of Hg BF_3, and 2-mil center wire showed variations of $2\frac{1}{2}$ μsec (the time between 50 percent of maximum probability values). A counter of 1-in. diameter, 65-cm Hg BF_3, and a 6-mil center wire showed variations of 0.5 ± 0.1 μsec. Factors involved in BF_3 counting characteristics are discussed with emphasis upon fast neutron chopper detectors.

* Work carried out under contract with the U. S. Atomic Energy Commission.

C12. Scintillation Detector for Thermal and Epithermal Neutrons. K. H. SUN, P. R. MALMBERG, AND F. A. PECJAK, *Westinghouse Research Laboratories.*—Thermal and epithermal

neutron detection by scintillation counters as compared with that by gas-filled counters has the advantages of simplicity, ruggedness, compact geometry, and better time resolution. Gamma insensitive neutron phosphors made from mixtures of boron-containing substances and ZnS−Ag have been investigated in great detail recently.[1–4] A phosphor of this type has been prepared from a glycerol borate plastic containing 20 weight percent boron mixed with du Pont 1410 (10 micron) ZnS−Ag. The low viscosity of the melted boron plastic at 200°C facilitates the thorough mixing with the ZnS−Ag which is essential to optimum counting efficiency and permits molding of the phosphor into any desired shape. Using disk-shaped phosphors and a Du Mont 6292 photomultiplier, optimum counting rates have been observed for a ZnS−Ag to boron plastic ratio of 2 and a thickness of about 1 mm. Estimated counting efficiencies for thermal neutrons greater than 10 percent have been attained using ordinary boron. A much greater efficiency is expected with enriched B^{10}.

[1] Palevsky, Muether, and Stolovy, Bull. Am. Phys. Soc. **28**, No. 6, 16 (1953).
[2] C. O. Muehlhause, BNL 242 (T-38). Also BNL 1953 Ann. Rep., p. 10.
[3] D. E. Alburger, BNL 1233.
[4] Gatti, Germagnoli, Persano, and Zimmer, Nuovo cimento (9), **9**, 1012–21 (1952).

C13. Vapor Expansion Chamber Using Pure Water. I. J. E. HOPSON AND C. E. NIELSEN, *Ohio State University.*—A cloud chamber operating on pure water vapor has been built and operated. Provisions have been made for having a volume defined expansion of vapor, free from condensation nuclei and air, into a vacuum. Some important operating points are: a. by pumping on water it can be caused to supply vapor free of condensation nuclei. b. The chamber will hold a vacuum in the micron range thereby assuring the purity of the operating vapor. c. During expansion the vapor must not be in contact with a free liquid surface. d. After each expansion the entire system is pumped out and a new supply of vapor is used. Thus there are no reevaporation nuclei left in the chamber. e. The present chamber operates from an initial pressure of from one to two centimeters of mercury; thus, it is ideal for the study of low-energy ionizers. f. With suitable valves and vacuum pump the time interval between useful expansions can be less than 15 seconds. g. Clear alpha-particle tracks without background with a ratio of final to initial volumes of 1.7 with the initial temperature of the water at that of the room were observed.

C14. Vapor Expansion Chamber Using Ammonia and Water. II. R. P. CAREN AND C. E. NIELSEN, *Ohio State University.*—The vapor expansion method of cloud-chamber operation in which after each expansion into an evacuated volume the chamber is refilled with clean vapor was tried with an ammonium hydroxide vapor source; good tracks were obtained. With this method of operation there is simultaneous cooling of the vapor in the chamber and heating of the vapor entering the expansion volume, and sensitive time characteristics approach those of Wilson chamber expansion to constant pressure. Expansion of the vapor in the chamber is less than in the Wilson chamber with the same ratio of final to initial volume, and the temperature ratio, given by $T_1/T_2=(V_2/V_1)^p$, is here found by using $p=(\gamma-1)/\gamma$. Pressure may be varied by varying the concentration of ammonia in the vapor source. In experiments involving stopping power the similarity of ammonia and water makes vapor composition relatively unimportant. This chamber is simple in construction, requires no clearing expansions, and may be operated at any desired pressure above the vapor pressure of water.

C15. Vapor Expansion Chamber Using Pure Gases at Low Temperatures. III. C. E. NIELSEN AND J. E. HOPSON, *Ohio State University.*—A cloud chamber operated as described in the preceding abstracts has been cooled in liquid nitrogen and used with nitrogen vapor. With the ratio of final to initial volume constant, supersaturation obtained has been varied by varying the amount of undersaturation of the vapor before expansion. Ion tracks are observed from a minimum supersaturation of about two and one-half up to the maximum supersaturation of about five obtainable with the present apparatus. Uniform condensation on vapor aggregates is negligible in this range of supersaturation. Experiments with oxygen and argon are in progress; it is found that no condensation occurs in clean oxygen with supersaturations up to about six, the maximum yet studied. At these temperatures evaporation from the vapor source is so slow that an effective expansion is possible with a pool of liquid in the chamber. One could therefore use a Wilson chamber if it were desired. Droplets in nitrogen grow very rapidly, so that if tracks are to be photographed, the time delay between track formation and exposure must be made unusually short.

THURSDAY MORNING AT 10:00

Sheraton Park, Burgundy Room

(B. T. MATTHIAS presiding)

Low-Temperature Physics

D1. The Effect of Temperature Scales on Low-Temperature Calorimetric Data. J. R. CLEMENT, *Naval Research Laboratory.*—In correlating calorimetric and elastic data via Born-von Kármán theory, the Debye characteristic temperature for the lattice heat is usually the basis of comparison. For such correlations, a reliable estimate of the uncertainty in the absolute value of the caloric results is important. This fact has led to an investigation of the effect of uncertainties in the liquid helium vapor pressure-temperature scale on the absolute reliability of calorimetric data below 4.2°K. Certain apparent "anomalies" in some older data can be practically eliminated by correcting the data from the temperature scale in use at the time of the original experiments to the presently accepted (1949) scale. Furthermore, uncertainties in Debye temperatures deduced from data based on the 1949 scale have been considered in view of measured deviations from this scale.[1,2] For a hypothetical material having an electronic heat equal to the lattice heat at 10°K, an error in Debye temperature as large as 15 percent may occur around 1.5°K.

[1] J. Kistemaker, Physica **12**, 272 (1946).
[2] L. D. Roberts and R. A. Erickson, Phys. Rev. **91**, 488 (1953).

D2. Methods of Spinning Rotors at Low Temperatures.* J. W. BEAMS AND J. B. BREAZEALE, *University of Virginia.*—Two methods of spinning rotors at high speeds at liquid helium temperatures are described. In the first method, the

rotor is spun inside a tubular vacuum chamber on the end of a vertical small diameter, long, stainless steel hypodermic needle tube. The hypodermic needle shaft and rotor are driven and supported by an air-driven, air-supported turbine[1] located above the chamber. The chamber is sealed by a vacuum gland around the shaft. Vibrations in the long shaft are suppressed by properly spaced Teflon guides and special dampers. The rotor may be evacuated through the hollow shaft. In the second method the rotor is suspended inside a glass vacuum chamber by the axial magnetic field of a solenoid.[2] The solenoid is outside and coaxial with the Dewars containing the cooling liquids. The rotors are accelerated and driven around a vertical axis by a rotating magnetic field in a way similar to that of the armature of an induction or synchronous motor. The latter method is preferable if slight heating is to be avoided. In both methods the chambers surrounding the rotors are cooled by liquid helium surrounded by liquid nitrogen. Applications of the methods will be discussed.

* Supported by the Office of Ordnance Research.
[1] Beams, Revs. Modern Phys. **10**, 245 (1938).
[2] Beams, Young, and Moore, J. Appl. Phys. **17**, 886 (1947).

D3. The Magnetic Dependence of the Thermoelectric Power of Bismuth at Low Temperatures. J. BABISKIN AND M. C. STEELE, *Naval Research Laboratory.*—Measurements have been made on the thermoelectric power of polycrystalline bismuth wire (0.020-in. diam, 10 in. long, 99.98 percent purity) against copper as a function of temperature and magnetic field at liquid helium temperatures. The lower junction was maintained at 4.2°K in liquid helium. The temperature of the upper junction (which was above the bath) ranged from 4.2°K to 10°K and was measured by a calibrated carbon thermometer. The thermoelectric power was found to vary from $6\mu v/°K$ at 5°K to $11\mu v/°K$ at 9°K in zero field. Upon applying a uniform longitudinal magnetic field of 70 gauss, the thermoelectric power increased ~10 percent. This is a much larger effect than that observed previously[1] at room temperature in stronger magnetic fields. Further increase of the field showed that thermoelectric power increased less rapidly and appeared to approach saturation at ~400 gauss, when the upper junction was at ~8°K. Preliminary measurements have also been made on a bismuth single crystal in transverse and longitudinal magnetic fields. While the thermoelectric power at zero field was somewhat higher than for the wire, fields up to 100 gauss produced much more pronounced effects than for the wire.

[1] C. W. Heaps, Phys. Rev. **31**, 648 (1928).

D4. The Temperature Variations of the Elastic Constants of Copper Single Crystals from 4.2°K to 300°K. JOHN GAFFNEY AND W. C. OVERTON, JR., *Naval Research Laboratory.*—Using a previous developed cryogenic technique[1] together with an ultrasonic pulse technique, we have measured the adiabatic elastic constants of oriented single crystals of copper from 4.2°K to 300°K. The room temperature measurements are in excellent agreement with those of Lasarus,[2] while at 4.2°K the values of C_{11}, C_{12}, and C_{44} were found to exceed those at room temperature by 4.8 percent, 2.8 percent, and 8.6 percent, respectively. The experimental technique, measured crystal thickness corrections, and uncertainties of the elastic constants will be discussed. The Hooke's law atomic force constants for nearest and next-nearest neighbor interaction for the copper lattice have been obtained from these elastic constants by the relations $\alpha = ac_{44}$ and $\gamma = a(C_{11} - C_{12} - C_{44})/4$ where "a" is the lattice constant. The extrapolated value of γ/α at 0°K is -0.0946.

[1] W. C. Overton, Jr. and R. T. Swim, Phys. Rev. **84**, 758 (1951). W. C. Overton, Jr., thesis, Rice Institute, 1950.
[2] D. Lasarus, Phys. Rev. **76**, 545 (1949).

D5. Correlation Techniques for Testing the Born-von Kármán Theory of Specific Heats. W. C. OVERTON, JR., AND J. R. CLEMENT, *Naval Research Laboratory.*—Two essentially independent elements enter the complete theory of the lattice heat of a crystalline solid: (1) specific heat calculations using vibration spectra based on Born-von Kármán theory, and (2) an atomic model relating the microscopic atomic force constants, α and γ, to the macroscopic elastic c_{ij}'s. Critical testing of the complete theory requires both experimental caloric and elastic data, a combination not generally available. An apparent failure of the theory would not be traceable specifically to either of the two theoretical elements by the usual testing procedures. With the appropriate theoretical calculations, one phase of our technique critically tests element (1) independently, requires only caloric data, and yields numerical values of α and γ. These calorically deduced values of α and γ may then be compared with values derived from the experimental c_{ij}'s through any atomic model,[1,2] this comparison providing an independent test of element (2). The atomic model used by Leighton[1] has been verified experimentally for copper, for which the necessary low-temperature elastic constants[3] are available.

[1] R. B. Leighton, Revs. Modern Phys. **20**, 165 (1948).
[2] J. de Launay, J. Chem. Phys. **21**, 1975 (1953).
[3] W. C. Overton, Jr. and J. Gaffney (to be published).

D6. The Thermal Conductivity of Gallium Single Crystals at Low Temperatures.* HARMON H. PLUMB AND JULES A. MARCUS, *Northwestern University.*—The principal thermal conductivities of Gallium single crystals were measured in the liquid hydrogen and helium temperature range using helium gas thermometers. Gallium of 99.94 percent purity, obtained from the Aluminum Company of America, was grown into cylindrical single crystals (3 mm in diameter and 10 cm in length) by a method similar to that described by Powell.[1] For each specimen, the cylinder axis was parallel to one of the three principal crystallographic directions to within 5°. For one set of crystals the maxima of the thermal conductivity occurred at 6°K and yielded the ratio $c:a:b$ as 1:2:4.5 with the value 3.8 watt/cm°K for the conductivity in the c direction. Another set with maxima at 4°K yielded the ratio $c:a:b$ as 1:3.7:—with the value 10.6 watt/cm°K for the c direction. In the liquid helium range the thermal conductivity fell off rapidly with temperature extrapolating to zero at $T = 0$°K for all crystals. In the liquid hydrogen region both sets of crystals yielded a ratio of approximately 1:3:6 (as compared with 1:3.2:7 for electrical conductivities[1]) with the value 0.4 watt/cm°K for the conductivity in the c direction at 20°K.

* Supported by the National Science Foundation.
[1] R. W. Powell, Proc. Roy. Soc. (London) **A209**, 525 (1951).

D7. The Electrical and Thermal Conductivity of Magnesium and a Magnesium Alloy at Low Temperatures. D. A. SPOHR* AND R. T. WEBBER, *Naval Research Laboratory.*—The minimum of electrical resistance found at low temperatures in some of the dilute alloys of magnesium[1] is sufficiently pronounced to make possible a search for a corresponding effect in the thermal conductivity. We have measured the electrical and thermal conductivity over the temperature range 1.5 to 20°K in two polycrystalline specimens: (1) "pure" Mg, and (2) Mg−0.043 percent Mn. The pure specimen showed a slight minimum in electrical resistance and a thermal conductivity which followed, within experimental error, the dependence on temperature ($1/K = 1/AT + BT^2$) usually found in pure metals in this temperature range.[2,3] The dilute alloy specimen showed a much more pronounced electrical resistance minimum (ρ increased about 10 percent as the temperature was lowered from 4.2 to 1.4°K) and an exactly corresponding depression of the thermal conductivity so that the Lorenz ratio ($K\rho/T$) maintained a value of $(2.64 \pm 0.02) \times 10^{-8}$ (Volt/°K)^2

at temperatures below 4°K. These conclusions are in qualitative agreement with those reported recently by Herlin.[4]

* Now on leave at Clarendon Laboratory, Oxford.
[1] H. E. Rorschach, Jr. and M. A. Herlin, Proc. Schenectady Cryogenics Conf., p. 151 (Schenectady, New York, 1952).
[2] K. Mendelssohn and H. M. Rosenberg, Proc. Phys. Soc. (London) **A65**, 385 (1952).
[3] Kemp, Sreedhar, and White, Proc. Phys. Soc. (London) **A66**, 1077 (Nov. 1, 1953).
[4] Paper presented by M. A. Herlin at the Third Intern. Conf. of Low Temp. Phys. and Chem., Houston, Texas [December, 1953 (unpublished)].

D8. The Thermal Conductivity of Indium-Thallium Alloys at Liquid Helium Temperatures. RONALD J. SLADEK,* *University of Chicago.*—The thermal conductivity of indium specimens containing 0, 5, 15, 20, 30, 38, and 50 atomic percent Tl have been measured as a function of temperature down to 1.3°K and as a function of applied magnetic fields below T_c. The normal state results agree at least qualitatively with the quasi-free electron theory of metals, and the superconducting state results agree with Hulm's suggestion that superconducting electrons do not scatter phonons.[1] A thermal resistivity maximum was found to accompany the isothermal destruction of superconductivity by either a longitudinal or a transverse magnetic field in specimens containing 15 percent Tl or more.[2] Scattering of phonons at boundaries between superconducting and normal regions of the specimen may be responsible for this effect.

* U. S. Atomic Energy Commission predoctoral fellow, 1951–1953. Present address: Westinghouse Research Laboratories.
[1] J. K. Hulm, Proc. Roy. Soc. (London) **A204**, 98 (1950).
[2] R. J. Sladek, Phys. Rev. **91**, 1280 (1953).

D9. The Low-Temperature Magnetization of Two Cerium Salts. WARREN E. HENRY, *Naval Research Laboratory.*—The $^2F_{5/2}$ ground state of Ce^{+++} with one unpaired f electron is of interest because any crystalline electric field asymmetry leaves the essential Kramers degeneracy.[1] A low-lying doublet[2] in Ce^{+++} exhibiting no hyperfine structure is convenient for low-temperature demagnetizations. Thus a sphere of small crystals of cerous nitrate hexahydrate has been magnetized to practical saturation, using a method previously described.[3] If M is plotted against H/T, superposition of magnetic isotherms is observed. A Brillouin function for $J_z=\pm\frac{1}{2}$ and $g=2.1$ seems applicable in the range, 1.3°–4.2°K, for fields up to 60 000 gauss. Similar magnetization of $3Mg(NO_3)_2\cdot 2Ce(NO_3)_3\cdot 24H_2O$ was performed. Although this salt is magnetically more dilute than cerous nitrate, nonsuperposition of isotherms is observed. Since marked anisotropy[4] has already been observed for a single crystal of the double salt, a discussion will be given on the possible role of a crystalline anisotropy field in the observed nonsuperposition of isotherms.

[1] J. H. Van Vleck, *Electric and Magnetic Susceptibilities* (Oxford University Press, London, 1932), p. 296.
[2] R. J. Elliott and K. W. H. Stevens, Proc. Roy. Soc. (London) **215**, 437 (1952); W. G. Penney and R. Schlapp, Phys. Rev. **41**, 194 (1932).
[3] W. E. Henry, Phys. Rev. **87**, 229 (1952).
[4] Cooke, Duffus, and Wolf, Phil. Mag. **44**, 6 (1953); K. S. Krishnan and A. Mookherji, Phil. Trans. Roy. Soc. **A237**, 135 (1938).

D10. The de Haas-van Alphen Effect in Zinc at Liquid Oxygen Temperatures. TED G. BERLINCOURT AND M. C. STEELE, *Naval Research Laboratory.*—Recently, McClure and Marcus[1] measured the magnetic susceptibility of zinc in magnetic fields up to 9.5 kilogauss and found a field dependence in χ_{11}, the component of susceptibility parallel to the hexagonal axis, at temperatures as high as 85°K. We have extended these measurements to 25 kilogauss in the temperature range 55 to 90°K and have observed oscillations in χ_{11} equally spaced in reciprocal field as is characteristic of the de Haas-van Alphen effect. However, in the range investigated the period of oscillation β/E_0 is not temperature independent, as it is below 20°K,[2] but increases with increasing temperature. For example, β/E_0 is 6.7×10^{-5} gauss^{-1} in the region 2 to 20°K and rises to 9.8×10^{-5} gauss^{-1} at 55.4°K and 13.4×10^{-5} gauss^{-1} at 70°K. Such a temperature dependence might arise from alteration of the overlap of the pertinent Brillouin zone by the Fermi surface brought about by thermal expansion of the crystal.

[1] J. W. McClure and J. A. Marcus, Phys. Rev. **84**, 787 (1951).
[2] L. Mackinnon, Proc. Phys. Soc. (London) **B62**, 170 (1949).

D11. An Estimate of the Lifetime of Positrons in Superconductors. M. DRESDEN, *University of Kansas.*—It has been suggested[1] that there might be two factors which would cause the annihilation characteristics of positrons in superconductors to be different from those in normal conductors. Preliminary experiments of Talley and Stump[2] and Millett[3] appear to indicate some such effects. One of the factors involved, the change in the *ortho-para* positronium conversion rate has been investigated. It was found advantageous to use the collective description of the electron gas as given by Bohm and Pines. The estimated conversion rate depends rather sensitively on the (unknown) wave function of the system. On the basis of the qualitative nature of this wave function one may conclude that the long-lived component of the positron life time should become longer with decreasing temperature, to a limit of about 3.10^{-7} sec. The precise temperature dependence of this life time should give rather detailed information about the wave function in the superconductive state.

[1] M. Dresden, Phys. Rev. (to be published).
[2] Talley and Stump, Bull. Am. Phys. Soc. **29**, 2 Abstract G9.
[3] Millett, Bull. Am. Phys. Soc. **29**, 2 Abstract G8.

D12. (Abstract withdrawn.)

D13. Effect of Pressure on the Superconducting Transition of Tin.* M. GARBER AND D. E. MAPOTHER, *University of Illinois.*—The shift in the superconducting transition curve under hydrostatic pressure has been measured for a pure single crystal ellipsoid of tin. Pressures up to 100 atmos were applied with liquid helium and the superconducting transition observed by a sensitive ballistic induction technique. Our measurements give a value of -0.0065 ± 0.0002 gauss/atmos. This value is within the range recently reported by Fiske.[1] The transition curve measured at 1 atmos is observed to be lowered by about 0.1 gauss by several applications at helium temperature of the maximum pressure. This may explain why previously reported shifts[2,3] (in which the method used prevented cycling the pressure at low temperature) are generally 15 to 20 percent greater than those of the present work.

* This work supported in part by the Office of Ordnance Research.
[1] M. D. Fiske, Houston Low Temperature Conference.
[2] Kan, Sudovstov, and Lazarew, J. Exptl. Theoret. Phys. U. S. S. R. **18**, 825 (1948).
[3] P. F. Chester and G. O. Jones, Phil. Mag. **44**, 1281 (1953).

D14. Superconductivity of a Precipitation Hardening Aluminum Alloy.* R. E. MOULD† AND D. E. MAPOTHER, *University of Illinois.*—Measurements of the critical magnetic field down to about 0.8°K have been made on a precipitation hardening Al alloy (Al plus about 1.1 percent Mg_2Si) in various conditions of heat treatment. In the hardened condition the H_c *vs* T curve is displaced parallel to itself in the direction of lower temperatures, the effect being superficially similar to the isotope effect and about the magnitude of the largest isotope shifts observed. This shift can be understood in terms of the stress field produced by the Mg_2Si which precipitates as submicroscopic particles, coherent with the parent Al lattice.[1] In the quenched condition (Mg and Si in supersaturated solid solution) and in the fully annealed condition (Mg_2Si precipitated and stresses released) the H_c *vs* T curves closely reproduced those of pure Al. The width of the observed transitions indicates that the stress field in the hardened alloy is quite uniform.

* This work was supported in part by the Office of Ordnance Research.
† On leave from Preston Laboratories, Butler, Pennsylvania.
[1] A. H. Geisler and J. K. Hill, Acta Cryst. 1, 238–252 (1948).

D15. The Attenuation of Second Sound in Liquid Helium II. W. B. HANSON* AND J. R. PELLAM, *National Bureau of Standards.*—A continuous wave technique was used for the measurement of the temperature amplitude attenuation coefficient or second sound in the temperature range from 1.25°K to 2.17°K. The high frequencies employed (from 100 kc/sec to 268 kc/sec), and the low second sound velocity gave rise to a well defined beam of second sound, thus obviating the need for containing walls in the second sound cell. The frequency squared dependence of the attenuation was quantitatively verified and good agreement with the latest variant of Khalatnikov's theory was obtained for both the magnitude of the attenuation and its temperature dependence. The expected rapid rise in attenuation near the λ point was observed.

* Submitted in partial fulfillment of the requirements for the degree of Doctor of Philosophy from George Washington University.

D16. An Atomic Theory of Liquid Helium. D. TER HAAR, *St. Andrews University, Scotland.**—Under the above title Feynman[1] has recently published two papers in which he shows how one can approximate the exact partition function in such a manner that one can study possible transitions. It is shown how one can derive an approximate partition function similar to the one obtained by Feynman through neglecting the noncommutability of the potential energy operator and the kinetic energy operator, using a method introduced by Kramers in the theory of the equation of state.[2] In this way one gets an explicit expression for the density function entering Feynman's partition function.

* On leave of absence at Purdue University.
[1] R. P. Feynman, Phys. Rev. 91, 1291, 1301 (1953).
[2] For a description of this method, see: D. ter Haar, *Elements of Statistical Mechanics* (Rinehart and Company, Inc., New York, 1954), pp. 184–188.

THURSDAY MORNING AT 10:00

Sheraton Park, Caribar Room

(E. FEENBERG presiding)

Theoretical Physics, I: Nuclear Theory

DA1. Effect of Nuclear Charge on Internally Produced Pairs. G. K. HORTON AND E. PHIBBS, *University of Alberta.*—The angular distribution of internally created pairs has been used with increasing frequency to study the energy levels of light nuclei. Apart from the exact calculations of Jaeger and Hulme of the total cross section for $Z=84$, the only available theoretical estimates of the transition probabilities are those based on the 1st Born approximation. It can easily be seen that this is not adequate when little kinetic energy is available for one of the components of the pair. This often cannot be avoided, as in No^{254} where a continuous β spectrum only leaves about 0.28 Mev kinetic energy for the positrons. We have calculated the angular distribution of pairs using the Coulomb wave functions dicussed previously by one of us.[1] The results for electric and magnetic dipole, and electric quadrupole transitions, nuclear charges from 10–50, and transition energies varying from one Mev to seven Mev, with various distributions of the energy among the positron and the electron, will be presented. Significant deviations from the 1st Born approximation results have been found. A comparison with the available experimental evidence will be made.

[1] G. K. Horton and R. T. Sharp, Phys. Rev. 89, 885 (1953).

DA2. Energy Levels in a Spheroidal Well. STEVEN A. MOSZKOWSKI, *University of California, Los Angeles.*—The problem of the energy levels in a deformed nucleus was first discussed by Rainwater,[1] who treated the nuclear potential as a spheroidal well with infinitely high walls. Let the axes of the spheroid be $R(1+d)$, $R(1+d)^{-\frac{1}{2}}$, and $R(1+d)^{-\frac{1}{2}}$. Then the energy levels are given by: $E_N=E_N^{(0)}+dE_N^{(1)}+d^2E_N^{(2)}$. $E_N^{(0)}$ is the energy of a nucleon in a spherical well of radius R. $E_N^{(1)}$ was calculated by Rainwater as function of the quantum numbers n, l, and m. Spin orbit coupling was not taken into account. An explicit formula for the next term $E_N^{(2)}$ has now been derived for the above case by solution of the wave equation in spheroidal coordinates. The results of these calculations can be applied to various features of nuclear structure; e.g., the contribution of kinetic energy to surface energy, and the trend of quadrupole moments with nucleon number.

[1] J. Rainwater, Phys. Rev. 79, 432 (1950).

DA3. Refinement of the Uniform Model.* EVERETT MARK HAFNER, *Cavendish Laboratory and University of Rochester.*—Wigner's theory of the symmetric Hamiltonian is applied to a description of the energies of 60 states in light nuclei of even mass, $4 \leq A \leq 40$. In addition to the usual assumptions of this model, we make two new ones (*i*) that the theory applies to 0+ states, and (*ii*) that the nuclear volume over which interaction integrals are to be taken is of the form $(a+bA^{\frac{1}{3}})$, where a and b are approximately constant over the entire region, and accurately constant over local regions. To a first approximation, interaction integrals are determined empirically by examining the *relative* energies of 0+ configurations differing by 2 neutrons, assuming that $a=0$ and $b=1.47\times10^{-13}$ cm. We then seek a second approximation by fitting the *absolute* energies of 19 of the known 0+ ground states. We find that the 12 remaining known 0+ states (10 of which are excited, including the states at 2.72 Mev in B^{12}, 7.68 in C^{12}, and 6.05

in O^{16}) are given accurately. The model predicts the energies of 29 states as yet unmeasured. The nuclear radii to which we are led are in agreement with those given by neutron scattering.

* Research supported by the National Science Foundation.

DA4. Theory of Elastic Scattering of Alpha Particles by Heavy Nuclei. J. S. BLAIR, *University of Washington.*—A semiclassical model is used to interpret recent experiments of Farwell and Wegner[1] on the elastic scattering of 15–40 Mev alpha particles by heavy nuclei. In this model the outgoing lth partial wave is assumed to vanish if the corresponding classical turning point is less than the radius of the nucleus plus that of the alpha particle; otherwise it has a phase characteristic of pure Coulomb scattering. The theory predicts that the sum of nuclear and alpha particle radii is approximately equal to the classical apsidal distance evaluated at the energy for which the experimental cross section is one quarter of the corresponding Rutherford cross section. There is fairly good agreement between the calculated and experimental cross sections.

[1] G. W. Farwell and H. Wegner, Phys. Rev. (to be published).

DA5. Numerical Calculation of the Stripping Angular Distribution.* W. TOBOCMAN AND M. KALOS, *Cornell University.*—Calculations of the (dp) cross section which include the Coulomb interaction are being carried out with the help of an I. B. M. card programmed computer. So far we have calculated two cases—one in which the neutron is captured with orbital angular momentum $l=0$ and the other corresponding to angular momentum $l=2$. We find that the only effect of the Coulomb interaction in the $l=0$ case is to enhance the second peak of the angular distribution of the liberated protons. The effect of taking the Coulomb interaction into account for the $l=2$ case is to displace the peak of the angular distribution to larger angles and to broaden the peak somewhat. The calculations are being extended to other cases, and the effects due to the interaction of the protons with the residual nucleus and the scattering of the incident deuteron beam will also be included.

* Supported by the joint program of the U. S. Office of Naval Research and the U. S. Atomic Energy Commission.

DA6. Coulomb Effects in Deuteron Stripping.* N. AUSTERN, *Cornell University,* AND S. T. BUTLER, *Australian National University.*—We have now succeeded in finding a simple and accurate approximation scheme for including the nuclear Coulomb field into the deuteron stripping calculation. Fourier expansion of the hypergeometric function parts of the Coulomb wave functions yields the stripping amplitude in the form of a rapidly converging series of, essentially, non-Coulomb stripping amplitudes. The interpetation of the formulas is very direct, and it is easy to see that the Coulomb effects tend not to give large changes in the angular distribution.

* Supported by the joint program of the U. S. Office of Naval Research and the U. S. Atomic Energy Commission.

DA7. Isotopic Spin Factors in Nuclear Reactions.* R. J. DRACHMAN† AND D. C. PEASLEE, *Columbia University.*—Heavy-particle reactions among low states of light nuclei should exhibit statistical factors for isotopic spin in the following way: $\Gamma_{A\times B}=kP\gamma^2C_x^2$. Here C_x is a Clebsch-Gordan coefficient between the isotopic spins of the nuclear states A, B and the emitted particle x; and k, P, γ^2 are the usual particle wave number, penetration factor, and reduced width. Since $C_x^2\leq 1$, isotopic spin conservation generally makes a further reduction in Γ. Experimental evidence for C_x^2 may be obtained by comparing the observed Γ_p and Γ_n for excitation of equivalent compound nuclear states with $T_B=T_A+\frac{1}{2}$. In this case $C_n^2/C_p^2=(2T_A+1)$. Application of these and related considerations will be made to p and n reactions on Li^7.

* Work supported in part by the research program of the U. S. Atomic Energy Commission.
† National Science Foundation Predoctoral Fellow.

DA8. Supermultiplet Evidence from Isotopic Spin Spacing.* D. C. PEASLEE, *Columbia University.*—Let $\Delta(TT')=E(T)-E(T')$ be the energy difference between the lowest states of isotopic spins T and T' in a given nucleus. From β-decay energies and Coulomb-energy estimates, derived from other β-decay energies, we can estimate Δ for light nuclei where isotopic spin should be relatively valid. $\Delta(\frac{3}{2}\frac{1}{2})$ and $\Delta(10)$ for even-even nuclei show a general tendency to decrease with increasing A but remain in the range 5–15 Mev. In striking contrast, $\Delta'(10)$ for odd-odd nuclei is small ($\lesssim\frac{1}{2}$ Mev for $A>18$) and even slightly negative for $A>30$. This qualitative difference is in accord with a supermultiplet structure in which nucleon-nucleon forces are not very spin dependent. On a strict j-j coupling model, however, $\Delta'(10)\approx 0$ implies that $\Delta(TT')\approx 0$ for $T'<T\leq(j+\frac{1}{2})$. The observed values of Δ are thus additional evidence in support of supermultiplet structure in light nuclei.

* Work supported by the research program of the U. S. Atomic Energy Commission.

DA9. Spin Correlations in Neutron Scattering by Gases. A. C. ZEMACH AND R. J. GLAUBER, *Harvard University.*—Spin correlations within a molecule, resulting from the symmetry requirement imposed by nuclear statistics, are well known to affect the scattering of low-energy neutrons. The additional interference terms which arise in the presence of identical nuclei are proportional to the incoherent rather than the coherent scattering cross sections. These effects have been evaluated for polyatomic molecules by an elaboration of a technique described earlier.[1] The complementary symmetries of the spatial and spin dependences of the wave functions permit separation of the required averages over spin and spatial orientations, although the wave functions are not themselves separable. It is thereby shown explicitly that the effects of correlation are quite small in most polyatomic molecules, save at very low temperatures. Typical results, assuming thermal equilibrium, are that the cross section in the forward direction is reduced by 1 percent in gaseous methane at 45°K and by 6 percent in gaseous ammonia at 200°K. These figures decrease rapidly with increasing temperature.

[1] A. C. Zemach and R. J. Glauber, Bull. Am. Phys. Soc. **29**, No. 1, 53 (1954).

DA10. Reorientation of Aligned Nuclei. N. R. STEENBERG,* *National Research Council, Canada.*—It is known that magnetic couplings in the intermediate state affect angular correlations. When nuclei aligned at low temperatures decay by, for example, a β-γ cascade such couplings (external field and hfs) may be expected to influence the degree of alignment of the γ-emitting state and thus the angular distribution. This effect can be conveniently incorporated into the statistical matrix of the γ-emitting state. In many cases of experimental interest the ionic state is a doublet having anisotropic hfs, $(AS_xI_x+BS_xI_x+BS_yI_y)$. Then when $kT<A$ and the lifetime, τ, of the intermediate state is not long a very explicit expression for the degree of nuclear alignment Δ of the γ-emitting can be derived. This is dependent on the external field, the magnetic moment of the intermediate state and on τ, and is immediately applicable to the angular distribution. It is found (1) that reorientation may either increase or decrease Δ, (2) that a strong external field cancels the effect altogether, and (3) where $B=0$ the coupling has no effect on Δ. Where τ is very long, Δ tends to a finite limit.

* National Research Laboratories Postdoctorate Fellow.

DA11. Nuclear Shapes at Half-Filled Shells. BENJAMIN SEGALL, *University of California, Berkeley.*—In the coupled individual-particle collective-mode model of the nucleus,[1] the centrifugal pressure of the individual particles (or holes) in excess of a closed shell distorts the nucleus spheroidally. The

addition of "particles" into a shell, in general, tends to make the shape increasingly oblate, while an increase in the number of "holes" causes the shape to become more prolate. A question that arises is whether in the transition between regions of oblate-shape stability to regions of prolate-shape stability (i.e., at a half-filled shell), the nucleus takes on an axially symmetric or an asymmetric deformation. Calculations were carried out for the $J=5/2$, $7/2$, $9/2$, and $11/2$ shells assuming a strong interaction between the particles and surface, and the results showed that the ground state energies for half-filled shell nuclei are essentially independent of shape. The fact that the symmetric shape is not decidedly favored implies that the "strong coupling approximation" of Bohr and Mottleson[1] is inapplicable in these cases. Thus the simple rotational spectra and large separation of rotational and vibrational levels resulting from that approximation would not be expected to arise.

[1] A. Bohr, Kgl. Danske Videnskab. Mat. fys. Medd. **26**, No. 14 (1952); and A. Bohr and B. Mottelson, Kgl. Danske Videnskab. Mat.-fys. Medd. **27**, No. 16 (1953).

DA12. Level Structure of Li^6.* D. H. LYONS AND A. M. FEINGOLD, *University of Pennsylvania*.—The splitting produced by the tensor force of the S and D states of Li^6 has been computed by a variational method which includes the effect of configuration interaction.[1] It is found that the tensor force contributes, on the average, about 12 Mev to the binding energy, the major part coming from excited configurations. In addition, the ^3D states are split in essentially the same manner as would result from a vector-type force in first order. A total multiplet splitting of 5 Mev is obtained, with the $^3D_3$ state lowest. The tensor force also separates the $^1S_0$ and $^3S_1$ states and the $^1D_2$ and ^3D states, giving a final level structure for Li^6 in qualitative agreement with the known experimental data.

* Supported in part by the joint program of the U. S. Office of Naval Research and the U. S. Atomic Energy Commission.
[1] A. M. Feingold, Ph.D. thesis, Princeton University, 1952.

DA13. Pairing Effects in the Coulomb Energies of Mirror Nuclei.* I. TALMI AND B. C. CARLSON, *Princeton University*.—The Coulomb energies of the mirror nuclei have been written by Feenberg and Goertzel[1] in the form $E_c(Z)=\frac{1}{2}Z(Z-1)a+[Z/2]b$, where $[Z/2]$ is the largest integer not exceeding $Z/2$. The first term represents an average Coulomb interaction, and the second term is a pairing energy. If a and b were strictly constant, the difference between the members of a mirror pair would be $\Delta_1(Z)=E_c(Z)-E_c(Z-1)=(Z-1)a+\frac{1}{2}[1+(-1)^Z]b$. When Δ_1 is plotted directly, or after division by $Z-1$, the pairing effects become inconspicuous at higher Z because of the unequal weighting of a and b. This can be avoided by taking second differences, $\Delta_2(Z)=\Delta_1(Z)-\Delta_1(Z-1)=a+(-1)^Zb$, and the experimental data are sufficiently accurate to justify this procedure. A plot of second differences shows that the pairing effects do not disappear at higher Z, and that some evidence of shell structure appears at $Z=6$, 8, 14, and 20. More accurate data would be particularly desirable for S^{31} and Cl^{33}. Theoretical estimates of a and b will be discussed.

* Supported by the Higgins Scientific Trust Fund and the U. S. Atomic Energy Commission.
[1] E. Feenberg and G. Goertzel, Phys. Rev. **70**, 597 (1946).

THURSDAY MORNING AT 10:00

NBS, East Building

(L. S. TAYLOR presiding)

Invited Papers

E1. Radiation and the Dynamics of Cell Division. CORNELIUS TOBIAS, *University of California, Berkeley*. (45 min.)

E2. Effects of Irradiating Small Fractions of Individual Dividing Cells (motion pictures). R. E. ZIRKLE, *University of Chicago*. (45 min.)

E3. Molecular Structure and Biological Control Mechanism. CYRUS LEVINTHAL, *University of Michigan*. (45 min.)

THURSDAY AFTERNOON AT 2:15

Shoreham, West Ballroom

(N. F. RAMSEY presiding)

Magnetic Resonance and Allied Topics

Invited Paper

F1. Electronic Wave Functions in Metals in Relation to Nuclear Magnetic Resonance. HARRY JONES, *Imperial College (London) and Carnegie Institute of Technology*. (30 min.)

Contributed Papers

F2. Method for Detection of Pure Quadrupole Resonances.* P. J. BRAY, *Rensselaer Polytechnic Institute*.—The very sensitive dispersion detection technique employed by Gutowsky[1] in magnetic moment measurements would require a tracking receiver for application to quadrupole resonance detection. However, the quench frequency of a self-quenched super-

regenerative oscillator depends logarithmically on signal amplitude and, since it is about a thousandth of the oscillation frequency, does not present tracking problems. In present experiments, a convenient harmonic of the quench frequency of a frequency modulated self-quenching superregenerative oscillator is detected with an HRO 60 receiver. AM slope detection of the expected quadrupole resonance modulation of the quench frequency is used with oscilloscope presentation of the receiver output. The presented signal is a dispersion-type curve for each super-regenerative side-band detection of the quadrupole resonance. Signal-to-noise ratios obtained with this detection method surpass those achieved in this laboratory[2,3] with plate-current-detection techniques. Signal-to-noise comparisons and quadrupole resonance data obtained with this quench variation method will be given.

* Research supported by the Rensselaer Polytechnic Institute Research Grants Committee.
[1] Gutowsky, Meyer, and McClure, Rev. Sci. Instr. **24**, 644 (1953).
[2] P. J. Bray and P. J. Ring, J. Chem. Phys. **21**, 2226 (1953).
[3] P. J. Bray and D. Esteva, J. Chem. Phys. (to be published).

F3. Intensities of the Zeeman Components of Quadrupole Transitions in Sodium Chlorate.* YU TING AND DUDLEY WILLIAMS, *Ohio State University.*—The Zeeman pattern of the Cl^{35} nuclear quadrupole transition is a single crystal of sodium chlorate has been studied in a field of 6000 gauss. The shifts of the observed lines from the zero-field frequency for various orientations of the crystal in the external field were in close agreement with theoretical predictions.[1] At orientations in which the angle between one direction of electric-field symmetry and the direction of H field approached 90°, rapid changes in the intensities of the observed components were noted. Two of the four Zeeman components diminished in intensity and disappeared at 90°. The other two Zeeman components increased in intensity and reached a maximum at 90°. The transformation matrix, which diagonalizes the total Hamiltonian at this orientation (with zero electric field asymmetry factor), can be obtained in closed form. The calculated probability of magnetic dipole transitions shows that the disappearance of the components in question is indeed to be expected.

* Supported by Office of Scientific Research, Air Research and Development Command, Baltimore, Maryland.
[1] C. Dean, Ph.D. thesis, Harvard University (1952).

F4. Random Pulses and Electron-Spin Line Widths in Metals.* D. L. FALKOFF, *Brandeis University and Lincoln Laboratory.*—Dyson[1] has given a theory which accounts well for the observed[2] line width and line shape for electron-spin resonance in plates of lithium and sodium which are thick in comparison with the skin depth. By treating the diffusion of the conduction electrons, the absorption line for the bulk samples was found to depend on the diffusion time T_D, which a conduction electron spends in the skin depth as well as on the skin relaxation time T_2. But for samples not much larger than the skin depth, it is more appropriate to consider the random motion of the individual conduction electrons in and out of the skin depth rather than the average diffusion. Analysis of the resulting random time series shows that the line width can also depend on the mean recurrence time T_r between successive sojourns in the skin depth. This effect will depend on the ratio of sample width to skin depth.

* The research in this abstract was supported jointly by the U. S. Army, Navy, and Air Force under contract with the Massachusetts Institute of Technology.
[1] Unpublished Harvard Lecture, January 4, 1954.
[2] G. Feher and T. W. Griswold, Bull. Am. Phys. Soc., **28**, No. 7, 18 (1953).

F5. Conduction Electron Spin Resonance Absorption in Sodium.* I. H. SOLT, JR., AND M. W. P. STRANDBERG, *M.I.T.*—In order to understand more clearly the degree of spin-orbit coupling experienced by the conduction electrons in metals, an accurate measurement has been made of the g value of the spin resonance absorption in sodium. Colloidal suspensions of sodium particles (less than 4 microns in size), ultrasonically dispersed in paraffin wax, were investigated at 9000 Mc/sec. The measured g values are $g=2.0012\pm0.0002$ at 300°K and 78°K, and $g=2.0014\pm0.0002$ at 4°K. These values disagree outside the range of experimental error with the value of 2.0019 calculated by Yafet.[1] Line-shaped and line-width measurements were also made. The observed line shape was asymmetric and could be explained as the sum of the real and imaginary parts of the susceptibility where the imaginary part had a Lorentz shape. The line width at the half-power points of the imaginary part of the susceptibility was 11.5 gauss at room temperature and decreased linearly with temperature. This corresponds to a relaxation time of about 5×10^{-9} sec at room temperature.

* This work was supported in part by the U. S. Army Signal Corps, the Air Materiel Command, and the U. S. Office of Naval Research.
[1] Y. Yafet, Phys. Rev. **85**, 478 (1952).

F6. Paramagnetic Resonance Absorption in Ammonium Chrome Alum.* CHARLES F. DAVIS, JR., AND M. W. P. STRANDBERG, *M.I.T.*—A study has been made of the paramagnetic resonance absorption in diluted single crystals of ammonium chrome alum at room temperature. Work was done at X, S, and K band and at various orientations of the crystal. These data have been checked with the theoretical predictions of line intensity and position (based on the assumption that the chromium ion is in an electric field of trigonal symmetry). Paramagnetic resonance spectra of single ammonium chrome alum crystals at 77°K have been studied in an attempt to explain the anomalous two splittings of the ground state.

* This work was supported in part by the U. S. Army Signal Corps, the Air Materiel Command, and the U. S. Office of Naval Research.

F7. Paramagnetic Resonances in Glasses.* R. H. SANDS,† J. TOWNSEND, AND H. P. HOOD,‡ *Washington University.*—Work has been in progress for the past year and one-half on paramagnetic absorption spectra in glasses. Samples containing known amounts of impurities, furnished us by the Corning Glass Works, have been studied by means of a microwave spectrometer operating near 9000 Mc/sec. These and other samples show absorption lines lying close to apparent g values of 2, 4, and 6. These three lines do not always occur in the same sample. A tabulation of these g values will be presented together with representative line shapes. The influence of Stark splittings on the line shapes will be discussed and some theoretical results shown.

* Assisted by the joint program of the U. S. Office of Naval Research and the U. S. Atomic Energy Commission.
† Heermann-Mallinckrodt Fellow.
‡ Research and Development Division Corning Glass Works, Corning, New York.

F8. Paramagnetic Resonance in Organic Free Radicals at Low Fields.* R. S. CODRINGTON, J. D. OLDS, AND H. C. TORREY, *Rutgers University.*—We have measured the magnetic resonance line shapes of the solid organic free radicals: diphenylpicryl hydrazyl, tri-p-anisylaminium perchlorate and tri-p-aminophenylaminium perchlorate as a function of magnetic field at the frequencies 0.8, 1.5, 4, 8, and 15 Mc. At 15 Mc all show two Lorentz shaped resonances symmetrically disposed about zero field with full widths between inflection points of 2.0, 0.68, and 0.33 oersteds, respectively. As the frequency is lowered, the resonances merge in each case to form a single absorption maximum at zero field. For each radical the entire shape is accurately predicted by a set of Bloch equations modified so that longitudinal relaxation is parallel and transverse relaxation perpendicular to the instantaneous field direction. The usual Bloch equations give completely erroneous results at low frequencies. In every case the oscillating field was sufficiently small that no longitudinal

relaxation effects were observed. For each radical a single T_2 obtained from the width at 15 Mc sufficed to reproduce all details of the shapes. The resonance lines of these radicals at 9 300 Mc are significantly wider than at 15 Mc probably due to diamagnetic anisotropy at high fields.

* Supported by the U. S. Office of Naval Research.

F9. Paramagnetic Resonance Absorption of $VOSO_4 \cdot 5H_2O$. M. B. PALMA,* M. U. PALMA,* AND D. PALUMBO, *University of Palermo* (introduced by M. W. P. Strandberg).—The microwave paramagnetic resonance absorption (in X band) of the V^{++++} ion in vanadylsulphate has been examined at the Institute of Physics of the University of Palermo. This ion is, together with the Ti^{+++} ion, the only example of paramagnetic ions of the iron group which have only one electron in the 3d shell. In the salts in which it has been studied, the Ti^{+++} does not show any absorption at room temperature because of the very short relaxation time.

The experimental results and their theoretical interpretation will be given. Further experiments at different frequencies and temperatures are being carried out at the Microwave Spectroscopy Laboratory, Research Laboratory of Electronics, M.I.T.

* Now at Research Laboratory of Electronics, M.I.T.

F10. Magnetic Resonance Enhancement in a Multilevel System.* JAMES H. BURGESS,† *Washington University* (introduced by G. E. Pake).—In any system with more than two energy levels one can cause the steady state population distribution to depart from its thermal equilibrium value by applying a perturbation affecting only a single pair of levels. Thus other observable transitions of the system will be altered in intensity. For those transitions involving one of the perturbed pair there will be a first-order broadening. The free radical $ON(SO_3)_2^=$ exhibits a hyperfine structure of six levels which can be examined by magnetic resonance techniques.[1] Calculations show that other π transition intensities are enhanced or diminished depending upon the transition saturated. Experiments at 31 gauss yield, for the most favorable case, an enhancement ratio of 1.2 in substantial agreement with calculations. Besides a small constant broadening, a "bump" occurs which shifts with the saturation oscillator frequency in a field sweeping experiment. When centered in the line the "bump" increases the width by a factor of 1.8. Curves will be shown and possible explanations for the "bump" discussed.

* Assisted by the joint program of the U. S. Office of Naval Research and the U. S. Atomic Energy Commission.
† Washington University Fellow.
[1] Townsend, Weissman and Pake, Phys. Rev. **89**, 606 (1953).

F11. Nuclear Magnetic Resonance in Some Solid Hydrocarbons. F. A. RUSHWORTH,* *Union College* (introduced by Harold E. Way).—The nuclear magnetic resonance spectra and spin-lattice relaxation times have been measured for the protons in *n*-pentane, *n*-hexane and cyclo-pentane at temperatures down to 70°K. Molecular motion in the solid state was found in all three cases. For *n*-petane and *n*-hexane the results indicated a reorientation process of the methyl groups at the ends of the molecules, governed by an activation energy of 2.8 kcal/mole. The absorption lines had not broadened to their theoretical rigid widths at the lowest temperatures reached, although the reorientation frequencies at these temperatures were considerably smaller than the line widths. In the case of cyclopentane the lattice was effectively rigid below about 120°K. The uncertainties involved do not allow a distinction to be drawn between the plane and puckered molecular models. Above the temperature of the first transition (122.4°K) considerable molecular motion was occurring, the molecules probably rotating with spherical symmetry. At higher temperatures the second moment of the line shape decreased still further to a very low value, and it is suggested that the molecules were diffusing bodily through the lattice.

* On leave from University of St. Andrews, Scotland.

F12. Magnetic Moment of the First-Excited State of Pb^{204}. V. KROHN AND S. RABOY, *Argonne National Laboratory.*—The effect of a magnetic field on an angular correlation pattern[1] was used to measure the magnetic moment of the first excited state (370 kev) of Pb^{204}. The technique used involved measuring the coincidence rate at 135° and 225° as a function of the magnetic field applied perpendicular to the plane of the two counters. The 905-kev gamma ray was delayed by about 0.4 μsec and the coincidence resolving time was 0.13 μsec. The ratio of the coincidence rates at the two angles as a function of Larmor frequency was calculated by integrating Eq. (74) of Abragam and Pound[2] over the experimental time limits. A value of $g = +0.04 \pm 0.02$ was obtained by comparison of the calculated curve with the experimental data.

[1] Aeppli, Alberg-Schönberg, Frauenfelder, and Scherer, Helv. Phys. Acta **25**, 339 (1952).
[2] A. Abragam and R. Pound, Phys. Rev. **92**, 943 (1953).

F13. Measurements of the Distribution of Velocities in Potassium Molecular Beams. A. BENNETT,* *Carnegie Institute of Technology.*—Extensive measurements of velocity distributions in beams of potassium atoms have been made under various conditions of oven pressure and slit geometry. The measurements confirm the modified Maxwell distribution in the beam, except that the proportion of slow molecules is considerably smaller than that expected for a Maxwell distribution at the source; this deficiency increases with increasing oven pressure and with decreasing molecular velocity. The deficiency is less if the oven slit is a hole in a thin wall than if it is a long canal. The velocity selector comprised two slotted discs, rotated at constant speed; the phase angle between discs was varied to vary the transmitted velocity. The detector was a surface ionization gauge with platinum filament. The results were corrected for the finite width of the selector slits and are believed accurate to within two percent of the maximum amplitude of the spectrum. Calculations show that the sensitivity of the apparatus should be sufficient to observe the distribution of velocities of a molecular beam after reflection from a solid surface.

* Now at Westinghouse Research Laboratories.

THURSDAY AFTERNOON AT 2:15

Shoreham, Main Ballroom

(J. A. HIPPLE presiding)

Apparatus of Nuclear Physics, II; Other Topics in Nuclear Physics

FA1. Scattered Radiation Contribution to Depth Dose Data for 35- and 90-Mev Synchrotron X-Rays. J. BOAG AND B. ZENDLE, *National Bureau of Standards.*—Cavity ionization measurements were made in a masonite phantom of the doses along the central axis due to annular x-ray beams of different radii. Two sets of measurements were made, one with 90-Mev

synchrotron x-rays and a 14.5-meter target to phantom distance and the other with 35 Mev and a 4.5 meter distance. The data are being used to interpret depth dose measurements[1] made with an anthracene crystal and a 14 cm diameter, 39-Mev betatron x-ray beam possessing a nonuniform radial intensity distribution. When this beam is corrected to a plane uniform beam of infinite extent by means of the scattered radiation data, the dose at 45-cm depth is increased about 20 percent. This type of correction to cavity ionization depth dose measurements permits an absolute evaluation at these x-ray energies of the ergs per gm absorbed for 1 esu per cc of ionization measured in water. The scattered radiation data are also useful in interpreting narrow beam-large ionization chamber transition curves.[2]

[1] B. Zendle and H. W. Koch (to be published).
[2] Blocker, Kenney, and Panofsky, Phys. Rev. **79**, 419 (1950).

FA2. The Oxidation Yield of the Ferrous Sulfate Dosimeter by X-Rays.* W. BERNSTEIN, J. WEISS, AND J. B. H. KUPER, *Brookhaven National Laboratory.*—A variety of values have been reported for the absolute yield, G (ferrous ions oxidized per 100 ev of ionizing radiation absorbed in the solution), for the ferrous sulfate dosimeter. Measurement[1] of the energy absorbed by calorimetric and cathode-ray bombardment techniques give a G of 15.8; ionization-chamber measurements vary between 15 and 21. This disagreement between the individual ionization chamber measurements and collectively with the other methods led to this investigation.

A parallel plate ionization chamber and a solution cell with identical sensitive volumes were constructed from polystyrene. 3×10^{-3} M ferrous sulfate in 0.8 NH_2SO_4 solutions were used. The ionization chamber was designed in accordance with the Bragg-Gray principle; extrapolation to zero spacing eliminated the edge effect. The stopping power correction for polystyrene was verified by the use of an identical aluminum chamber for which the average ionization potential is known. The energy, W, to produce one ion pair in air was determined to be 34.4 ev in terms of Jesse's[2] values for A and N_2. The G value obtained was 16.0 ± 0.5, in good agreement with the calorimetric and cathode ray bombardment measurements.

* Work performed under the auspices of the U. S. Atomic Energy Commission.
[1] J. Saldick and A. O. Allen, J. Chem. Phys. (to be published).
[2] W. P. Jesse and J. Sadanski, Phys. Rev. **90**, 1120 (1953).

FA3. Magnetic Spectrograph for Nuclear Disintegration Studies.* W. W. BUECHNER, C. P. BROWNE, H. ENGE,† M. MAZARI,‡ AND C. D. BUNTSCHUH, *M.I.T.*—A sector-type, uniform-field, analyzing magnet has been constructed, following a design proposed by Bainbridge.[1] The entrance and exit faces of the magnet are sections of a circle of radius 50 cm. The magnet gap is one-half inch. The target or source of particles is located approximately 50 cm from the entrance face. Particles with radii of curvature between 37 and 56 cm in the magnetic field emerge from the exit face and are detected on a photographic plate, each exposure covering a range of approximately a factor of 2 in particle energy. With polonium alpha particles and a total acceptance angle of 0.1 radian in the gap plane, peaks of half-width <2 mm are obtained over a length of 75 cm along the plate. The dispersion varies along the plate but is approximately 0.1 percent in energy per mm. The magnet is mounted so it can be rotated about an axis through the source, the angular range being 135 degrees. The spectrographs will be used in conjunction with the ONR electrostatic accelerator.

* This work has been supported by the joint program of the U. S. Office Naval Research and U. S. Atomic Energy Commission.
† Now at the University of Bergen, Norway.
‡ On leave from the National University of Mexico.
[1] K. T. Bainbridge, Solvay Report, 7th Congress in Chemistry, 1947.

FA4. MTR Fast Chopper. R. G. FLUHARTY, *Phillips Petroleum Company.**—A fast neutron chopper (Brookhaven type (*1*)) has been installed at the Materials Testing Reactor and is in successful operation. The resolution is at least 0.1 μsec/m, and for energies below 300 ev, the counting rate is 5000 counts/hr/1 μsec channel. This is about 25 times that quoted by Brookhaven (*2*). The detectors used are 28, 1″ diameter, Al-walled BF_3 proportional counters filled to 65 cm pressure. The counters hang vertically in a 5, 4, 3, 5, 4, 5 array so the neutron path length in the counters is 6″. The "time jitter" of the detectors is 0.5 ± 0.1 μsec (*3*). Present operation uses a 15-meter flight path, but greater distances are planned as a means of using the high flux. The neutron spectrum and use of the instrument to study known resonances will be discussed.

* Work carried out under contract with the U. S. Atomic Energy Commission.
[1] Seidl, Hughes, and Palevsky, Phys. Rev. **89**, 897(A) (1953).
[2] Hughes, Seidl, Palevsky, and Levin, Phys. Rev. **90**, 363(A) (1953).
[3] Simpson, abstract C11.

FA5. MTR Time-of-Flight Instrumentation. D. R. DE BOISBLANC AND K. A. MCCOLLOM, *Phillips Petroleum Company** (introduced by R. L. Doan).—Time-of-flight instrumentation has been designed for use with the MTR Fast Chopper. The circuits used with other fast choppers were not directly applicable because of the loss of information arising from high counting rates expected at the MTR. A well-known time division principle employing two ring scalers in a 10×10 array establishes 100 consecutive channels of equal time duration. A novel feature of the circuitry reduces the dead time between channels to substantially zero by a means not requiring extremely fast pulse rise times. Channel widths of 0.5, 1.0, 2.0, 5.0, 10, and 20 microseconds are available. A continuously adjustable time delay of 0-1000 microseconds initiated by a light pulse in synchronism with the neutron burst is provided. The run-through of the 100 channels commences at the end of the time delay period. Provisions are included for total detector, total channel, in-pile monitor, and background counts.

* Work carried out under contract with the U. S. Atomic Energy Commission.

FA6. Ionization of Pure Gases and Mixtures of Gases by 5-Mev Alpha Particles. T. E. BORTNER AND G. S. HURST, *Oak Ridge National Laboratory.*—In this experiment the charge produced in a large ionization chamber, by the complete stopping of Pu^{239} alpha particles, was measured by a standard null method. From the charge produced the number of ion pairs n was deduced and W defined by the equation $W=E/n$, where E is the energy used in forming the n ion pairs, was computed. The results for a number of pure gases, among them He at 46 ev will be shown. Our results of W for mixtures of gases is described by the formula

$$1/W_m=[(1/W_1)-(1/W_2)]Z+(1/W_2),$$

where $Z=P_1/(P_1+aP_2)$ and W_m is the W for the gas mixture having two components of pressure P_1 and P_2 with W values for the pure gases equal to W_1 and W_2, respectively. It was found that the W value for gas mixtures did not vary linearly for some gases. In a mixture of N_2 and O_2 the a factor is 1.06. The values for a for the mixtures will be given in tabular form.

FA7. Energy Expenditure per Ion Pair in Solids. E. J. STERNGLASS, *Westinghouse Research Laboratories.*—Since the ionization density produced by an electron beam of energy V entering a solid has a pronounced maximum at a mean depth $\bar{d}$ due to scattering of the primaries, and the ejected electrons are absorbed exponentially in metals,[1] the energy expended per ionization $\bar{E}_0$ is obtainable from measurements of Δ, the number of secondaries escaping per incident primary. The internal secondaries are initially randomly directed, and essentially all those reaching the surface can escape as the

surface dipole barrier is small. $\bar{d}$ increases approximately as V.[3] Accordingly,

$$\Delta = [V/\bar{E}_0][0.5 \exp(-\beta V^{\frac{1}{2}})],$$

where β is a characteristic constant. Using available data on the secondary yield of 33 metallic and semiconducting elements corrected for backscattering, values of $\bar{E}_0$ were found to be of the same order as for gases, varying periodically with Z from about 20–35 ev, independent of V or the ionization potential.

[1] E. J. Sternglass, "The phenomenon of secondary electron emission from homogeneous solids," thesis, Cornell, 1951; also Report of 13th Annual Electronics Conference, M.I.T. (1953).
[2] N. Bohr, Danske Videnskab. Selskab. **18**, No. 8, (1948), Chaps. 3 and 5.

FA8. Range and Specific Ionization for High-Energy Protons in Nuclear Emulsions. O. HEINZ, *University of California, Berkeley.**—Stacks of nuclear emulsion varying in thickness from 18.35 g/cm² to 56.83 g/cm² were exposed in the external proton beam of the Berkeley cyclotron, and the average specific ionization dT/dx [in Mev(g/cm²)$^{-1}$] was measured by determining the equivalent thickness of Cu needed to remove the same amount of energy from the beam as a given thickness of emulsion. The energies range from 230 to 320 Mev. The emulsion stacks consisted of layers of 200μ Ilford C-2 stripped emulsions of average density 3.81±0.01 g/cm². The specific ionization was found to be 1.5 percent higher for emulsion than for Cu measured over the same energy interval. From these data the ratio of the mean ionization potentials for emulsion and Cu was determined as $I_E/I_{Cu}=0.89\pm0.09$. The range of 342.5-Mev protons in emulsion was found to be 92.68±0.25 g/cm² which is 1.1 percent lower than the measured range of the same beam in Cu (93.65±0.20 g/cm²). The measured range in emulsion is about 1.5 percent shorter than the value calculated by Vigneron (and extended to higher energies by Barkas). They assumed 332 ev as the mean ionization potential of emulsion. This work was done under the auspices of the U. S. Atomic Energy Commission.

* Now at Bell Telephone Laboratories.

FA9. The Stopping Powers of Metals for Low-Energy Protons.* D. W. GREEN, J. N. COOPER, AND J. C. HARRIS, *Ohio State University.*—The stopping powers for gold, antimony, tin, and manganese have been measured for protons with energies from 400 to 1000 kev by a modification of the technique of Madsen and Venkateswarlu.[1] Thin films of the metals were evaporated directly on thin layers of lithium fluoride which served as targets for the proton beam from a Van de Graaff generator. The resultant displacements of the lithium and fluorine (p,γ) resonances were measured. The curve for the stopping power of gold lies about 10 percent above that of Kahn.[2] A plot of the logarithm of the atomic stopping power as a function of the logarithm of Z reveals that these data and those for copper, selenium, silver, lead, and bismuth as previously reported[3] lie very near a straight line.

* Supported in part by the U. S. Atomic Energy Commission through a contract with the Ohio State University Research Foundation.
[1] C. B. Madsen and P. Venkateswarlu, Phys. Rev. **74**, 648 and 1782 (1948).
[2] D. Kahn, Phys. Rev. **90**, 503 (1953).
[3] Green, Cooper, and Harris, Bull. Am. Phys. Soc. **29**, No. 1, 27 (1954).

FA10. Penetration of 6-Mev Gamma Rays in Lead and Iron. K. SHURE, P. A. ROYS, AND J. J. TAYLOR, *Westinghouse Electric Corporation, Atomic Power Division.*—Measurements of the relative dose rate from 6-Mev gamma-ray source have been taken in water and in air through lead and iron. The lead varied in thickness from zero to eight inches and the iron varied from zero to twelve inches in one-inch steps. The source of the 6-Mev gamma rays was N^{16} produced by circulating demineralized water through the high flux region of the Materials Testing Reactor. The water was then piped to a tightly wound coil of Saran tubing in the form of a flat cylindrical disc which served as a source plate. The anthracene scintillation detector was moved along the axis of the cylindrical disk. The output current from the photomultiplier, which was a measure of the dose rate, was read on a low drift ac electrometer. The relative dose rate has been calculated by the Spencer-Fano[1] method utilizing the results of the joint NBS-NDA computational program.[2] The calculated results agree fairly well with the experimental results.

[1] L. V. Spencer and U. Fano, J. Research Natl. Bur. Standards **46**, 446 (1951); Phys. Rev. **81**, 464 (1951).
[2] Goldstein, Wilkins, and Spencer, Phys. Rev. **89**, 1150 (1953); NDA Memo 15C-20 (1953).

FA11. Calculations on the Penetration of High-Energy Electrons.* L. V. SPENCER, *National Bureau of Standards.*—The Boltzmann equation for electron diffusion and degradation in an infinite homogeneous medium, assuming continuous energy loss and plane geometry, has been reduced by Lewis to a chain of equations in terms of the quantities

$$I_{1n}(t) = \int_{-\infty}^{\infty} dz z^n \int_{4\pi} d\Omega P_1(\cos\vartheta) I(t,\vartheta,z),$$

where $I(t,\vartheta,z)$ is the flux of electrons with residual range t and obliquity ϑ at a distance z from the source plane. Lewis wrote down formal expressions for the $I_{1n}(t)$ but did not use them to reconstruct spatial distributions. We have calculated spatial distributions by utilizing (1) a simple recursion relation existing between the quantities

$$I_{1n}{}^p = \int_0^{\infty} dt t^p I_{1n}(t),$$

which enables easy calculation of $I_{0n}{}^p$ for comparatively large n; and (2) the fact that the trend of the $I_{0n}{}^p$ for large n (corresponding to the deep penetration tail of $I(t,\vartheta,z)$) agrees with that obtained from a function similar to Yang's thin foil distribution.

* Work supported by the U. S. Office of Naval Research.

FA12. The Transmission of Monoenergetic Positrons and Electrons. H. H. SELIGER, *National Bureau of Standards, and The University of Maryland.*—The transmission as a function of thickness of absorber of monoenergetic positrons and electrons with energies up to 400 Kev has been measured in aluminum and in silver. The absorber forms the window of a 2π proportional flow counter whose counting efficiency is better than 99 percent down to a few hundred electron volts. Particles from a radioactive source are focused into a beam by a 90 degree magnetic analyzer with an energy resolution better than 5 percent. The beam, with a half angle of divergence of 2 degrees, impinges perpendicularly upon the absorber window of the 2π counter so that the total transmission is measured, independent of the forward angle of emergence or of the partial energy loss. In this type of geometry, positrons appear to be more strongly absorbed than electrons in medium and thick absorbers. Possible reasons for the difference between these results and those of other workers[1,2] will be presented. This work is continuing.

[1] K. A. Baskova and B. S. Dzhelepov, Doklady Akad. Nauk. S.S.S.R. **77**, 1001 (1951).
[2] Chang, Cook, and Primakoff, Phys. Rev. **90**, 544 (1953).

FA13. A Formula for Nuclear Masses in Terms of the Electron Mass Involving only Rational Numbers for Light Nuclei. ENOS E. WITMER, *University of Pennsylvania.*—The mass of any nucleus in any state may be represented by Mm, where m is the rest mass of the negative electron. We surmise that M is always an integral multiple of 1/256. For $A \leq 11$, M in the ground state is given in almost all cases to within ±0.1 by the formula

$$M = (7/2)^6 A - (139/64)AB(A)f_1(Z) + (23/64)f_2(A,N). \quad (1)$$

Here $AB(A)$ is always an integer and is 1, 3, 9, 28, 30, 36, 42, and 56 for A from 1 to 8, respectively. $f_1(0)=0$ and $f_1(Z)=1$ for $Z\geq 1$. $f_2(A,N)$ is always an integer and some of the formulas for it are

$$f_2(A,0)=0;\quad f_2(A,1)=1;\quad f_2(A,2)=A+1. \qquad (2)$$

Formula (1) gives the masses of the neutron and proton exactly, m is 0.000548 770 2859 amu.

FA14. Scattering of X-Rays by Nuclei.* G. PUGH,† D. H. FRISCH, AND R. GOMEZ, *M.I.T.*—Bremsstrahlung x-rays of energies from 50 to 135 Mev, produced by the M.I.T. synchrotron, are being scattered from lithium, beryllium, carbon, aluminum, copper, tin, and lead. The x-rays scattered at 45°, 90°, or 135° produce electron pairs in an 0.1-inch lead converter. The total energy of these electrons is measured with a large terphenylcyclohexylbenzene scintillation counter. Preliminary cross sections at 90° are approximately equal to the coherent sum of Thomson scattering by Z free protons in a density distribution which—if uniform—has a radius of between 0.8 and $1.4A^{\frac{1}{3}}\ 10^{-13}$ cm.

* This work has been supported in part by the joint program of the U. S. Office of Naval Research and U. S. Atomic Energy Commission.
† Eastman Fellow.

FA15. Angular Dependence of Annihilation Quanta from the Magnetic Substates of Triplet Positronium.* R. M. DRISKO, *University of Pittsburgh.*—The calculation by Ore and Powell[1] of the angular distribution and spectrum of the annihilation quanta from triplet positronium has been repeated without averaging over spin. The relative number of quanta per unit solid angle and per unit energy interval is found to be $[(1\pm\cos^2\theta)F(k)\pm(1-3\cos^2\theta)f(k)]$, where θ is the angle between the quantization axis and the direction of observation of the quantum, and k is the energy of the quantum in units mc^2. The upper sign refers to the combined and equal contributions of the $m=\pm 1$ substates, the lower to the $m=0$ substate. $F(k)$ is the energy spectrum defined as in reference 1 but with mass set equal to unity.

$$f(k)=\frac{k}{2(2-k)^2}-\frac{(1-k)}{(2-k)^3}\ln(1-k)-\frac{4(1-k)}{k^3}-\frac{(2-k)^2}{2k^3}-\frac{3(2-k)(1-k)}{k^4}\ln(1-k).$$

From this formula, when $\theta=90°$ the $m=0$ substate contributes more than $\frac{1}{4}$ of the quanta, an effect recently observed by Hughes and Marder.[2] Formulas for the polarization and angular correlations of the quanta will also be presented.

* This work was carried out at Carnegie Institute of Technology under U. S. Atomic Energy Commission Predoctoral Fellowship.
[1] A. Ore and J. Powell, Phys. Rev. **75**, 1696 (1949).
[2] See accompanying abstract FA16 by Marder, Hughes, and Wu.

FA16. Effect of Angular Dependence of Annihilation Radiation of Orthopositronium in a Magnetic Field.* S. MARDER, V. W. HUGHES, AND C. S. WU, *Columbia University.*—An effect of the angular dependence of the annihilation radiation from the magnetic substates of orthopositronium has been observed in an experiment similar to that of Deutsch and Dulit.[1] Quanta due to positron annihilation were observed at a direction of 90° to a magnetic field. The fraction of orthopositronium decaying by three-quantum annihilation, f, can then be computed, and at high values of the field f was found to be less than $\frac{1}{4}$. The value $\frac{1}{4}$ is expected statistically since only annihilation radiation of the $M=0$ substate is affected by the field. Our observation is understandable if the angular distribution of the annihilation radiation from the different magnetic substates is considered. Angular distribution formulas are given in the accompanying abstract by R. Drisko. The ratio of singlet to triplet decay rates can be computed from values of f *vs* the field, after corrections are made for the angular distribution. Our data yield $\lambda_s/\lambda_t=1289$ with a statistical probable error of ±14 percent. This result agrees with the theoretical value 1115.[2]

* This work partially supported by the U. S. Atomic Energy Commission.
[1] M. Deutsch and E. Dulit, Phys. Rev. **84**, 601 (1951).
[2] A. Ore and J. Powell, Phys. Rev. **75**, 1696 (1949).

THURSDAY AFTERNOON AT 2:15

Sheraton Park, Continental Room

(D. E. ALBURGER presiding)

Radioactive Nuclei, I

G1. Beta End-point Energies and Half-Lives for Some Mirror Transitions.* W. A. HUNT, R. M. KLINE, AND D. J. ZAFFARANO, *Iowa State College.*—The positron spectra and half-lives of some short-lived nuclides formed by (γ,n) reactions induced by 70-Mev x-ray irradiation have been reexamined,[1] using an improved scintillation spectrometer with a fast 100-channel pulse-height analysis system[2] and cyclic timing equipment with the synchrotron.[3] Beta spectra from P^{32}, Y^{90}, Cl^{34}, and Li^8 were used for energy calibration, and good statistics were obtained in the half-life measurements. Results are summarized as follows:

Nuclide	End point (Mev)	Half-life (seconds)	ft (seconds)
Mg^{23}	2.95±0.07	10.7 ±0.7	3600± 500
Si^{27}	3.76±0.08	4.05±0.10	4000± 450
S^{31}	4.50±0.10	2.40±0.07	5150± 600
Ca^{39}	6.10±0.15	0.90±0.05	7250±1000

* Work supported by the U. S. Atomic Energy Commission.
[1] F. I. Boley and D. J. Zaffarano, Phys. Rev. **84**, 1059 (1951).
[2] Hunt, Rhinehart, Weber, and Zaffarano, Rev. Sci. Instr. (to be published).
[3] P. L. Phipps, M.S. thesis, Iowa State College, 1953 (unpublished).

G2. New Isotope Identification Program on the Oak Ridge 86-inch Cyclotron. T. H. HANDLEY AND B. L. COHEN, *Oak Ridge National Laboratory.*—The large currents of 22-Mev protons, the large fluxes of high-energy neutrons they produce, the ready accessibility of enriched stable isotopes, and an auxiliary project on rare earth purification have formed the basis for a program of search for new radioactive isotopes with the Oak Ridge 86-inch cyclotron. Activities are produced by (p,n), $(p,2n)$, $(p,3n)$, (p,pn), (p,α), $(p,\alpha n)$, $(p,2p)$, (n,p), and (n,α) reactions. An empirical systematics of the excitation functions and cross sections for these reactions has been worked out and has been a valuable aid in evaluating impurity problems, in determining mass assignments, and in estimating upper and lower limits to half-lives not observed. Equipment and techniques have been developed for detecting activities between one second and 10^7 years. A total of ten new radioactive species (including seven in the rare earth region) have been positively identified, and seven assignments in recent isotope tables have been disproven. Beta and gamma radia-

tions from all new isotopes have been studied by scintillation spectrometry.

G3. Superallowed Transitions in $4n$-type Nuclides. M. BOLSTERLI AND E. FEENBERG, *Washington University.**—Recent experimental work[1] on radioactive $4n$-type nuclides indicates the presence of superallowed components in the decay of Sc^{40}, Cl^{32}, P^{28}, A^{36}, and Na^{20}. Partial half-lives for the superallowed components can be estimated from available information on dn thresholds, Coulomb energies, β^+ and γ energies and the ft values of the image β^- transitions. In the superallowed component $|\int 1|^2=2$ and $|\int \dot{\sigma}|^2$ can be computed for special coupling schemes. The ft values estimated for the superallowed components are generally consistent with $|\int 1|^2+|\int \sigma|^2>2$.

* Assisted in part by the joint program of the U. S. Office of Naval Research and the U. S. Atomic Energy Commission.
[1] Glass, Jensen, and Richardson, Phys. Rev. **90**, 320 (1953); Glass and Richardson, Bull. Am. Phys. Soc. **28**, No. 7, B3 (1953); A. C. Birge, Phys. Rev. **85**, 753 (1952); L. W. Alvarez, Phys. Rev. **80**, 519 (1950).

G4. Production of Be^7 in High-Energy Reactions.* J. HUDIS, E. BAKER, AND G. FRIEDLANDER, *Brookhaven National Laboratory.*—Cross sections will be reported for the formation of Be^7 in the bombardment of C, Al, Cu, Ag, and Au in the Cosmotron with protons in the Bev energy range. In the case of C the cross section stays substantially constant (near 12 mb) from 1.0 to 2.2 Bev, and is approximately the same in this energy range as at 340 Mev.[1] For the other target elements investigated, the excitation curves show a rise with increasing proton energy and the slopes of the curves increase with increasing Z. At 2.2-Bev proton energy, the cross sections are all of the same order of magnitude, between 1 and 10 mb. The data indicate that, except possibly in the case of C targets, Be^7 is formed not as a residue of nucleon evaporations, but by direct ejection.

* Research carried out under the auspices of the U. S. Atomic Energy Commission.
[1] L. Marquez and I. Perlman, Phys. Rev. **81**, 953 (1951).

G5. The Inner Bremsstrahlung in A^{37} and Ge^{71}.* BABULAL SARAF, *Bartol Research Foundation.*—The experimentally observed spectrum (by scintillation spectrometer) of the inner bremsstrahlung from A^{37} has been compared with the theoretical spectrum, after correcting for the detection efficiency, ratio of full energy peak to Compton distribution, and $I-$x-ray escape peak. The comparison shows good agreement from approximately 300 kev to the end point of the spectrum, but at low energies the emission seems to be larger than the theoretical predictions. The absolute source strength of A^{37} has been measured by proportional counter, and it has been found that the emission probability for the higher-energy part of the spectrum is in agreement with the theory within the probable error of about 30 percent. The spectrum of Ge^{71} has been studied down to 20 kev. It has been found that the emission below ~100 kev is much larger than the theoretical value and exceeds considerably the probable errors. The absolute source-strength has been measured by counting a known fraction of x-rays in a scintillation spectrometer. The emission probability above 100 kev is here also found to be in agreement with the theory within the probable error of about 30 percent.

* Assisted by the joint program of the U. S. Office of Naval Research and the U. S. Atomic Energy Commission.

G6. Double Vacancies in the K Shell Associated with K-Electron Capture in A^{37}.* J. A. MISKEL AND M. L. PERLMAN, *Brookhaven National Laboratory.*—The pulse-height spectrum produced by the decay of A^{37} in a proportional counter was analyzed to determine the probability, per K-electron capture, for the production of a double vacancy in the K shell. The double vacancy is produced by promotion of the second K electron to a bound state or to the continuum. In these experiments both processes could be observed; the measurements included events in which the kinetic energies of the promoted electrons were in the range zero to 4.0 kev. Eighty-four percent of the theoretically predicted total effect should occur in this energy interval. The data, appropriately corrected, give for the probability of double K vacancy production per K capture, in the energy interval investigated, $4.8\pm0.8\times10^{-4}$. The result is substantially in agreement with the value calculated from theory.

* Research carried out under the auspices of the U. S. Atomic Energy Commission.

G7. The β Spectrum of K^{42}.* L. KOERTS, A. SCHWARZSCHILD, R. GOLD, AND C. S. WU, *Columbia University.*—The composite β spectrum of K^{42} has been investigated in the magnetic coincidence spectrometer. The high-energy group exhibits the shape of the unique first-forbidden transition and gives an upper energy limit of 3.56 Mev, which agrees with previous investigations.[1] The lower-energy group is investigated by means of the magnetic coincidence spectrometer. The gamma ray is detected by a NaI scintillation counter with a 4′ lucite light pipe. It is particularly interesting to study the shape of the low-energy β group since the results of the $\beta-\gamma$ angular correlation of K^{42} [2] requires a major contribution of the B_{ij} term from the theoretical interpretation based on the single tensor interaction alone. However, the Kurie plot of the coincidence β spectrum is linear from its upper energy limit of 1.97 Mev to about 0.5 Mev within the statistical fluctuations. It can be concluded that the contribution from the B_{ij} term is not overwhelming. Auxiliary experiments show that the excess of electrons below this energy could be attributed to the finite thickness (~1 mg/cm²) and large area ($r=0.8$ cm) of the evaporated source.

* This work partially supported by the U. S. Atomic Energy Commission.
[1] F. Shull and E. Feenberg, Phys. Rev. **75**, 1768 (1949).
[2] D. T. Stevenson and M. Deutsch, Phys. Rev. **84**, 1071 (1951).

G8. Gamma Radiation from K^{42}. N. H. LAZAR AND P. R. BELL, *Oak Ridge National Laboratory.*—The gamma radiation emitted in the decay of K^{42} was investigated in a $3''\times3''$ right circular cylinder of NaI (Tl) mounted on a Dumont K-1197 photomultiplier. A previously unreported gamma ray at 0.309 Mev was found. From a comparison of its decay with that of the 1.52 Mev gamma ray, it is thought to follow a weak branch of the K^{42} decay. In order to see this gamma ray, the bremsstrahlung from the high-energy beta rays (3.5 Mev) had to be eliminated. This was done by means of a NaI (Tl) absorber whose pulses were placed in anticoincidence with the signal. By this means, inner bremsstrahlung to ~0.2 Mev and degraded radiation from the absorber, as well as external bremsstrahlung from the stopping of the beta rays, were eliminated. It is suggested that a similar technique using an organic anticoincidence absorber might be useful in other applications, for example, in the examination of inner bremsstrahlung.

G9. On the Disintegration of K^{43}. TORSTEN LINDQVIST* AND ALLAN C. G. MITCHELL, *Indiana University.*†—The nuclear spectrum of K^{43} (22.0 hr) has been studied with the help of a magnetic lens spectrograph. K^{43} decays to Ca^{43} emitting five gamma rays having energies 0.369, 0.627, 0.219, 0.393, and 1.00 Mev, the last three being weak. Five beta-ray groups were found, of energies 1.839, 1.218, 0.827, 0.460, and 0.243 Mev, with relative abundance of 1.6, 5.4, 83.1, 5.4, and 4.5 percent, respectively. A disintegration scheme is proposed. The K^{43} was prepared by the reaction $A^{40}(\alpha,p)K^{43}$.

* Supported by the joint program of the U. S. Office of Naval Research and the U. S. Atomic Energy Commission.
† On leave from Physics Department, University of Uppsala, Sweden.

G10. The Disintegration of Ga^{70}.† M. E. BUNKER, J. W. STARNER, AND J. P. MIZE, *Los Alamos Scientific Laboratory.*—The radiations of Ga^{70} (20.3 min) have been investigated with

beta- and gamma-scintillation spectrometers. The radioactive samples were produced by thermal neutron irradiation of gallium oxide enriched in Ga^{69} (98.42 percent). The principle mode of decay is by a ground-state beta transition of energy 1.65 Mev.[1] Examination of the gamma spectrum revealed the existence of two weak gamma rays of energy 1.04±0.01 Mev and 0.174±0.005 Mev. Coincidences have been observed between these gamma rays. The 1.04-Mev gamma, which is involved in <1 percent of the disintegrations, is several times more intense than the 0.174-Mev gamma. On the basis of these facts and the results of $\beta-\gamma$ coincidence studies, it is concluded that there are two weak beta groups leading from Ga^{70} to excited levels in Ge^{70} at 1.04 and 1.21 Mev above the ground state. Log *ft* calculations based on preliminary intensity measurements suggest that both of these low-energy beta transitions are of the allowed type.

† Work performed under the auspices of the U. S. Atomic Energy Commission.
[1] S. K. Haynes, Phys. Rev. **74**, 423 (1948).

G11. The Isomeric States in $_{32}Ge^{75}$ and $_{32}Ge^{77}$. S. B. BURSON, W. C. JORDAN, AND J. M. LEBLANC, *Argonne National Laboratory.*—Neutron irradiation of Ge^{74} and Ge^{76} produces isomeric states in Ge^{75} and Ge^{77}. Using enriched isotopes, we have studied these activities by means of a scintillation coincidence spectrometer and electron spectrographs. Ge^{75m}: The metastable state in Ge^{75} decays with a half-life of 49±2 seconds. The scintillation spectrometer showed one gamma ray of 142±3 kev and no beta rays. *K* and *L* internal conversion lines were observed from which the energy was assigned as 138.5±1.0 kev. (K/L estimated >3.) Ge^{77m}: Ge^{77m} decays with a half-life of 52±2 seconds. The scintillation spectrometer showed two gamma rays of 159±3 kev and 215±3 kev of nearly equal intensity. (No conversion lines were observed.) These radiations are not in coincidence but the 215-kev gamma ray is in coincidence with a beta ray whose maximum energy was found to be about 2.7 Mev from absorption measurements. The 159-kev gamma ray is not in coincidence with beta radiation. Thus Ge^{77m} decays by at least two processes—a 159-kev transition to the ground state of Ge^{77} and a 2.7-Mev beta ray to a 215-kev excited state in As^{77}.

G12. New Isomers in Br and Cl. GERTRUDE SCHARFF-GOLDHABER AND MICHAEL MCKEOWN, *Brookhaven National Laboratory.**—A systematic search for isomeric transitions with lifetimes of the order of seconds is being carried out by activation with neutrons from the Brookhaven reactor. So far two new activities have been established: (a) In various Cl compounds a γ transition of 660±20 kev with $T_{\frac{1}{2}}=1.0\pm0.2$ sec was found. Bombardment of enriched Cl isotopes[1] showed the activity in the Cl^{37} sample with a cross section of ~5 mb for "pile neutrons." (b) In Br a γ transition of 210±10 kev with $T_{\frac{1}{2}}=5.0\pm0.2$ sec appeared. With the help of enriched isotopes[1] the activity was shown to be produced in the Br^{79} sample with a cross section of ~10 mb for "pile neutrons."

* Under the auspices of the U. S. Atomic Energy Commission.
[1] The enriched isotopes were obtained from Oak Ridge National Laboratory.

G13. Implications of Photonuclear Effect in Zr^{90}. P. AXEL AND J. D. FOX, *University of Illinois.*—The yields of 4.4 minute Zr^{89m} and 78 hour Zr^{89}, both formed from Zr^{90} during betatron irradiation of natural zirconium, have been studied as a function of energy. At any energy E, slightly above its 12.3-Mev threshold E_{th}, the yield of spin ½ Zr^{89m} is approximately proportional to $(E-E_{th})^3$. In contrast, the yield of the spin 9/2 ground state was anomalously small; no activity was detected for betatron energies between the ground-state threshold and the 588-kev isomeric level. The experiment would have detected 1 percent of the yield expected from photonuclear reactions involving small spin changes. These data give direct experimental proof that (1) photonuclear thresholds are sometimes high because the ground-state transition is unobservable and (2) gamma-ray emission predominates over the emission of high angular momentum neutrons which have energies up to 550 kev. This experiment also implies that quantitative photonuclear yield studies can give information about (1) competition between gamma ray and neutron emission, (2) spin changes, (3) relative density of nuclear energy levels of different spins, and (4) the multipolarity of gamma rays absorbed by nuclei.

G14. Radiations from Cd^{115} (43-Days).* JAGDISH VARMA,† *Bartol Research Foundation.*—The disintegration scheme of Cd^{115} has been studied by several groups of investigators with varying results. The data of the present measurements show that three gamma rays are emitted in de-excitation of levels in In^{115} at 0.95, 1.28, and 1.43 Mev. The quantum energies are 1.28, 0.95, and 0.485 Mev, the latter two in cascade. Beta-ray spectra terminate at all levels of In^{115}. The 150-Kev transition between the two higher excited states was not detected in the single counting rate or by coincidence methods. These results are in agreement with those of Engelkemeir.[1]

* Assisted by the joint program of the U. S. Office of Naval Research and the U. S. Atomic Energy Commission.
† Research Fellow, Bartol; permanent address Morena (M.B.) India.
[1] D. W. Engelkemeir, Argonne National Laboratory Report 4717 (April, 1952).

G15. The Disintegration of I^{126}.* MORRIS L. PERLMAN AND JOAN WELKER, *Brookhaven National Laboratory.*—The radiations from I^{126} have been studied with the aid of a coincidence spectrometer. The active material, produced by fast neutron irradiation of KIO_3, was concentrated by means of a Szilard-Chalmers separation. In the electron-capture decay of I^{126} a gamma ray of energy 0.74 Mev was found to occur in cascade with the previously known[1,2] 0.65-Mev gamma ray. The cross-over transition also was observed. In the negative beta decay a gamma ray of energy 0.48 Mev occurs in cascade with the previously known[1,2] 0.38-Mev gamma ray; here also a cross-over is observed. The relative abundances of these transitions and of the positron transitions and the maximum energy of the positron spectrum were measured. This information, combined with the previously measured ratio of electron-capture decay to beta decay and with the ratio of the abundances of the 0.85-Mev and 1.24-Mev[1,2] beta rays is sufficient to give the abundances of all observed transitions in the decay scheme. Both the *ft* values and the electron capture to positron ratio for the ground-state transition indicate that I^{126} has spin 2 and negative parity in agreement with the assignments neutron $h_{11/2}$ proton $g_{7/2}$.

* Research carried out under the auspices of the U. S. Atomic Energy Commission.
[1] M. L. Perlman and G. Friedlander, Phys. Rev. **82**, 440 (1951).
[2] Marty, Langevin, and Hubert, J. phys. radium **14**, 671 (1953).

G16. *K*-Conversion Electron—Gamma Angular Correlation in Sn^{117}. ROBERT K. GOLDEN AND SHERMAN FRANKEL, *University of Pennsylvania.**—Sn^{117m} was produced by irradiating separated Sn^{116} in the Oak Ridge Low Intensity Testing Reactor. Because of the low specific activity it was necessary to use thick sources and correct the data for electron multiple scattering.[1] Four sources of average thickness 0.35, 0.70, 1.5, and 2.1 mg/cm² were prepared by evaporation onto glass (<0.25 mg/cm²) films. Thickness distributions of all sources were determined by densitometry of radiograms. The experimental angular correlation coefficients, when plotted *vs* the multiple scattering correction factor, followed a straight line which extrapolated correctly to zero correlation at infinite thickness, verifying the accuracy of the scattering correction for large source thicknesses. A least squares fitting of these data extrapolated to $a_2=-0.136\pm0.005$ at zero source thickness, requiring a mixture of M_1 and E_2 in the second $d_{\frac{1}{2}}\rightarrow s_{\frac{1}{2}}$

transition. Comparing this value with the no mixture coefficient (corrected for geometry) of -0.156 ± 0.001 requires a ratio of electric intensity to total intensity δ^2 of 0.0015 ± 0.0005. Details of the extensive scattering corrections will be given.

* This work supported in part by the Office of Ordnance Research.
[1] S. Frankel, Phys. Rev. **83**, 673 (1951).

G17. A Mixed $E1+M2$ Gamma Transition in Nd^{144}.† ROLF M. STEFFEN, *Purdue University.*—An accurate measurement of the angular correlation of the two cascade gamma rays emitted by Nd^{144} yielded the following correlation function: $W(\theta)=1-(0.210\pm0.015)P_2(\cos\theta)$; $A_4<0.01$. This correlation is consistent with the angular momentum assignment 1–2–0 of Alburger and Kraushaar.[1] Nevertheless the first transition is a mixture of dipole (99.9 percent) and quadrupole (0.1 percent) radiation ($\delta=\pi$). The second transition is by pure quadrupole radiation. Polarization direction correlation measurements[2] indicate an over-all parity change in this cascade. The most reasonable parity assignment is 1 (odd)—2 (even)—0 (even), which necessitates the assumption of an $E1+M2$ mixture for the first gamma transition. As compared to the predictions of the independent particle model, the intensity of the $E1$ transition is then reduced by a factor of about 1000. The parity and angular momentum assignments are in good agreement with the intensity of the strong crossover transition.

† Supported by the U. S. Atomic Energy Commission.
[1] D. E. Alburger and J. J. Kraushaar, Phys. Rev. **87**, 448 (1952).
[2] J. N. Brazos and D. M. Roberts (to be published).

THURSDAY AFTERNOON AT 2:15

NBS, East Building

(F. G. BRICKWEDDE presiding)

Chemical and General Physics

H1. Role of the Principal Quantum Number (n) in the Calculation of the Radii of Ions with Low (1^+,2^+,3^+,4^+) Valence. N. EFREMOV, *1061 Intervale Avenue, New York, New York.*—The ion C^{4+}—the smallest among the tetravalent ions—is the primary ion for the calculation and its ordinate[1] is $(n+11)=12$, whereas its abscissa $K(C^{4+})=n=1$. The K value increases by 1 with decreasing atomic number of an element by 1, e.g., $K(C^{4+})=1$, whereas $K(B^{3+})=2$, etc. Consequently, for the next tetravalent ion Si^{4+} which belongs to the Ne-period ordinata as well abscissa will increase by 1. E.g., let us consider the ordinate and abscissas for the quadrupole group of ions with low valence, belonging to the Ne period. The

Ions	Na^{1+}	Mg^{2+}	Al^{3+}	Si^{4+}
Abscissa K	$(n+3)$	$(n+2)$	$(n+1)$	n
Abscissa K	5	4	3	2
Ordinate	$(n+11)$	$(n+11)$	$(n+11)$	$(n+11)$
Ordinate	13	13	13	13
Number of portions $=K(n+11)$	65	52	39	26
Ionic radii in A	0.95	0.76	0.57	0.38

formula for calculation is: $R_i(X)=/(n+11)K/P$, e.g., $R_i(Al^{3+})=39P=0.57$A. Thus n is ordinata for ions with high[1] valence and abscissa (K) for tetravalent ions.

[1] See Bull. Am. Phys. Soc. **29**, No. 3 (1954).

H2. Deviations from Additivity of the Intermolecular Field at High Densities.* L. JANSEN AND Z. I. SLAWSKY,† *University of Maryland.*—The induced dipole field of an assembly of neutral atoms or molecules is additive up to the second order of approximation with respect to isolated pairs. Non-additive terms have been evaluated in the attractive field between three atoms by Axilrod[1] and in the repulsive field between three helium atoms by Rosen.[2] At high densities the deformation of the electron clouds by the repulsive part of the potential field cannot be neglected in the zero-order wave functions for the induced dipole interaction. Using the model of a caged molecule and approximating the effect of the repulsive forces by a boundary condition, it is shown that a non-additive effect exists in the induced dipole field, resulting in a considerable weakening of the attractive field between two molecules. For argon the calculated internal energy on the assumption of additivity of the intermolecular field is too negative by about 100 cal/mole at a density of 600 Amagat.

* Supported by the U. S. Office of Naval Research.
† On the Staff of the Naval Ordnance Laboratory.
[1] B. M. Axilrod, J. Chem. Phys. **17**, 1349 (1949); **19**, 719 (1951).
[2] P. Rosen, J. Chem. Phys. **21**, 1007 (1953).

H3. The Effect of Intermolecular Forces on the Rapid Expansion of a Gas from an Initial Condition of Very High Density and Temperature.* J. M. DAWSON AND Z. I. SLAWSKY,† *University of Maryland.*—Measurements of the expansion rates of nitrogen with initial pressures between 300 atmos and 1000 atmos and initial temperature of 27°C show that clearly in this region the effect of intermolecular forces is to retard the expansion as compared with an ideal gas. In this region the internal energy of nitrogen is negative. It was believed that if the expansion was started in a region of positive internal energy the effect would be an increase in the expansion rate. Since no data was available for a real gas with large internal energy it was impossible to check this experimentally. Therefore, calculations of the expansion rates were made using the results of the high density and temperature free volume calculations of W. Fickett and William W. Wood. Results of these calculations showed as expected that the expansion rate was increased with respect to an ideal gas.

* Supported by the U. S. Office of Naval Research.
† On the staff of the Naval Ordnance Laboratory.

H4. A General Method for High-Speed Machine Computation of Ideal Gas Thermal Properties. The Diatomic Free Radicals of the Isotopic Hydrides.* LESTER HAAR AND A. S. FRIEDMAN, *National Bureau of Standards.*—The partition functions for the free radicals are obtained in closed form. They include terms to account for the special low-temperature effects arising with these molecules, in particular when the ground states are $^2\pi$ states. For the light molecules the splitting of the ground state is further complicated by the uncoupling of the electronic spin to the nuclear axis. In addition the partition function includes first-order corrections for rotation-vibration coupling, rotational stretching, and vibrational anharmonicity. Tables of thermal properties are computed with the aid of the NBS digital computer at 80 temperature intervals from 50° to 5000°K. The results for OH are compared with the term by term computations of the unexpanded partition function available for this molecule.[1]

* Sponsored in part by the U. S. Atomic Energy Commission Division of Research.
[1] Glatt, Adams, and Johnston, O.S.U. Tech. Report No. TR 316-5.

H5. Double Bond Character of the Carbon Chlorine Bond. R. BERSOHN, *Cornell University.*—Double bond character of

the carbon chlorine bond was first proposed by Pauling and co-workers to explain the shortening and lowered reactivity of conjugated C=Cl bonds. From the bond lengths Pauling deduced a double bond character of 15 percent for the C−Cl bond in vinyl chloride. From the quadrupole coupling asymmetry parameter η, Goldstein and Bragg deduced the value of 4 percent. All the published asymmetry data for C−Cl bonds can be explained on the assumption of weak coupling of the Cl π electrons with the C π electrons. The effect of the Cl atoms can then be treated as a weak perturbation on the aromatic system; molecular orbital theory has been used to calculate the double bond character and hence η for a variety of molecules. It is found that η is about 0.10 for linkages of the type

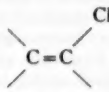

but about 0.25 for

H6. Dielectric Constant of Dioctyl Phthalate Smoke.* H. C. THACHER, JR., AND PAUL B. DORAIN, *Indiana University.*—The difference in dielectric constant between thermally dispersed dioctyl phthalate smokes before and after filtration was measured with a Birnbaum microwave refractometer[1] operating at 9385 Mc/sec. The results fit the equation $\Delta\epsilon/c = 10.8 \times 10^{-10} - 6.86 \times 10^{-12} c$, where c is the concentration of smoke in mg/m³. The dielectric constant difference $\Delta\epsilon$ appears to be independent of particle size. According to the simple theory[2] $\Delta\epsilon/c$ should have the constant value 10.3×10^{-10}, in good agreement with the limiting value for the experimental results. The decrease in $\Delta\epsilon/c$ at higher concentration is much larger than would be expected from the Clausius-Mosotti equation.

* Supported by the Chemical Corps Medical Laboratories.
[1] G. Birnbaum, Rev. Sci. Instr. **21**, 169 (1950).
[2] H. C. Thacher, Jr., J. Phys. Chem. **56**, 795 (1952).

H7. A Precision Double-Focusing Mass Spectrometer.* T. L. COLLINS, T. T. SCOLMAN, AND A. O. NIER, *University of Minnesota.*—A large double-focusing mass spectrometer has been constructed and is now operating. The machine utilizes a 90° electrostatic analyzer followed by a 60° magnetic analyzer with radii of 20 and 16 inches, respectively. The ion-optical design is similar to smaller spectrometers in use in this laboratory.[1] The electronic control system utilizes a small spectrometer with a modulated beam. A second major control system senses the position of the beam directly after the electrostatic analyzer in order to regulate the 35 kilovolt accelerating potential. Major mechanical features include object and image slits completely adjustable for position, width, and rotation through a single sylphon. The resolution exceeds 1 in 25 000.

* Supported by the National Science Foundation and the joint program of the U. S. Office of Naval Research and the U. S. Atomic Energy Commission.
[1] A. O. Nier and T. R. Roberts, Phys. Rev. **81**, 507 (1951).

H8. Electron Impact Studies of Isotopic Oxygen and Carbon Dioxide Molecules.* OLIVER A. SCHAEFFER AND HENRY R. OWEN, *Brookhaven National Laboratory.*—The relative changes in the probability of bond breaking following electron impact has been studied for the molecules $O^{16}O^{16}$ and $O^{16}O^{18}$; $O^{16}C^{12}O^{16}$, $O^{16}C^{13}O^{16}$, and $O^{16}C^{12}O^{18}$. The experimental results were obtained with a 60° mass spectrometer employing a source designed to equalize the collection efficiency of the fragment ions formed. The experimental results are compared with a calculation based on a "vertical" transition mechanism for the electron impact process. In the case of oxygen the experimental ratio of bond breaking in $O^{16}O^{16}$ divided by that in $O^{16}O^{18}$ was 0.98 compared to a calculated ratio of 0.97. The formation of C^{13+} from $C^{13}O_2^{16}$ was found to be 1.010 times larger than the formation of C^{12+} from $C^{12}O_2^{16}$; while the formation of $C^{13}O^{16+}$ was found to be 0.96 times as large as the formation of $C^{12}O^{16+}$ from the respective molecules. The calculated values for these two quantities are 1.013 and 0.98, respectively. Similar agreement was found for the processes in the $O^{16}C^{12}O^{18}$ molecule. The calculation adequately describes the electron impact process studied, even though for some processes fragmentation of the heavier molecule is predominant, while for other processes the fragmentation of the lighter molecule is predominant.

* Work performed under the auspices of the U. S. Atomic Energy Commission.

H9. The Law of Impact for Stiff Bodies. M. AVRAMY MELVIN, *Florida State University.*—The usual method of measuring the coefficient of restitution e with two pendular balls is not very accurate. Also it is not known (though generally assumed) that the approximate constancy of e, for a given material, will extend to noncentral collisions of two aspherical bodies. To test the constancy of e with accuracy, we made experiments with a pair of impacting Kater pendula with various mass distributions. The results (for steel) show that, with given unequal mass distributions, e may vary considerably from constancy (e.g., from 0.199 to 0.051) as the kinetic energy before impact E is varied. There is a tendency for the value of e to decrease with increasing value of E. The interpretation is discussed elsewhere. A practical inference which may be drawn from the present investigation is that f, the ratio of kinetic energy to that before impact, *is generally a better empirical constant than e.* For many materials e, though variable, is appreciably smaller than 1. In such cases f depends primarily upon the mass distribution and may be calculated therefrom while inserting a rough average value for e. f as measured stays very nearly constant for any given mass distribution and agrees very well with the calculated value.

H10. Some Aspects of the Dynamics of Waterdrop Collisions with Solids. OLIVE G. ENGEL, *National Bureau of Standards.*—Little information exists in regard to the stages of collision and flow of a water drop when it impinges against a solid surface. The radial flow in the impact plane was mapped chemically at the National Bureau of Standards and high-speed pictures of the collision incident have been made. Pictures taken at a rate of about 10 000 frames per second show that the water drop is very little deformed before it enters into radial flow. The top of the drop essentially appears not to know that the bottom has struck. An equation for the impact pressure has been developed which takes into account the spherical shape of the drop and its property of flow. Evidence exists which indicates that values of the pressure calculated from this equation are of the right order of magnitude. The diameter of the radial flow has been measured at known intervals of time. An equation for the radius of flow as a function of time has been developed on the assumption that the kinetic energy of the drop is converted to surface energy. Consideration has been given to the possible existence of cavitation in the radial flow. Schlieren pictures of the flow have been taken.

H11. Drop Size Distribution and Visibility in Clouds and Rain.* SHEPARD BARTNOFF, *Tufts College.*—The analysis of two sets of drop size distributions in natural clouds and one set of drop size distributions in rain indicates that the coefficient C in Trabert's visibility equation, $V = (C\rho\bar{r})/W$, is a function of the breadth of the distribution. In this equation, $\bar{r}$ is mean linear radius, ρ density, and W liquid water content.

As pointed out by Atlas and Bartnoff,[1] a more useful equation is found to be $V=(K\rho d_0)/W$, where d_0 is the median volume diameter. The usefulness of the Atlas and Bartnoff equation is supported by the present analysis, which verifies that the coefficient K is nearly independent of the breadth of the drop-size distribution and which indicates that the value $K=1.2$ found by Atlas and Bartnoff for natural clouds also holds for rain.

* This work is supported by a contract with the Air Force Cambridge Research Center.

[1] D. Atlas and S. Bartnoff, J. Meteorol. 10, 143–148 (1953).

H12. (Abstract withdrawn.)

H13. (Abstract withdrawn.)

H14. The JAINCOMP-C and -D Digital Computers. DONALD H. JACOBS AND MILTON E. PUGH, *The Jacobs Instrument Company.*—JAINCOMP–C is a very compact high speed electronic digital computer of the all-electronic all-parallel design developed in earlier JAINCOMP computers. Its addition time is 8 μsec, and it is capable of solving an equation involving 200 3-address operations (involving 9 continuous variables and 70 adjustable constants) in 0.1 sec. It was developed for real-time control use, and special input and output equipment was developed with it. Its program is contained on an electronically scanned punched card holding 128 24-bit instructions and having an access time of 1 microsecond per instruction. Adjustable constants are also stored on electronically scanned punched cards, and intermediate results are stored in JAINCOMP-type magnetic core registers having an access time of 3 μsec per word. Word length is 24 bits. Nine semimagnetic registers are provided as buffer storage for variable inputs. The entire computer, which is entirely of plug-in construction, fits in a cabinet $21\frac{1}{2}\times24\frac{1}{2}\times27\frac{1}{2}$ in. A completely automatic system of continuous functional checking is built in. JAINCOMP–D (designed but not constructed) is a general-purpose high-capacity version of JAINCOMP–C. Differences are (a) 36 bit words, (b) large memory: 1024 36-bit words of magnetic storage plus magnetic tape plus other types, and (c) much greater flexibility: can be controlled from punched card or magnetic tape or from memory, all interchangeable.

THURSDAY AFTERNOON AT 2:15

Sheraton Park, Burgundy Room

(M. H. HEBB presiding)

Nonmetallic Solids. II

I1. Growth of CdI_2 Crystals. J. B. NEWKIRK, *General Electric Research Laboratory* (introduced by D. Turnbull).—An experimental study of CdI_2 crystals growing in aqueous solution gave evidence which supports hypotheses of Fisher, Fullman, and Sears concerning the origin of growth steps on crystal surfaces. Self-perpetuating growth steps were observed to form spontaneously on the hexagonal face of an apparently perfect crystal which was growing in the edgewise direction only. As proposed by the above authors, this could result from disregistry of lattice planes where they meet after growing around a dirt particle that had been trapped by the advancing edge of the crystal. Spiral growth steps also formed at the point of contact where two randomly oriented crystals meet edge to edge. Motion pictures are presented which illustrate the above effects.

I2. The Influence of Covalence on Ion Ordering and Distortion in Spinels. I.* A. L. LOEB AND J. B. GOODENOUGH, *Lincoln Laboratory.*—In previous attempts to explain the cation distribution in spinel lattices on the basis of elastic and electrostatic energies, covalence was resorted to in order to account for the preference of certain cations for tetrahedral sites. A later treatment, based on the perturbation of *d*-shells by a crystalline field due to surrounding ions, is limited by the assumption of ionic lattice elements. A mechanism based on covalent bonding due to overlap of hybrid orbitals is proposed here to predict the cation distribution and related properties of spinels. Cations in tetrahedral sites usually bond through tetrahedral sp^3 orbitals; in octahedral sites cations are bound ionically, or covalently through either octahedral d^2sp^3 or planar dsp^2 bonds. In the last case the cation is bound covalently to four oxygen ions at the corners of a square, and ionically to two oxygen ions on an axis normal to the square, so that tetragonal distortion of the lattice results. Covalence decreases the electrostatic and modifies the elastic energies. A covalent exchange mechanism is proposed for the indirect interaction between incomplete *d* shells.

* The research reported in this and the following abstract was supported jointly by the U. S. Army, the U. S. Navy, and the U. S. Air Force under contract with the Massachusetts Institute of Technology.

I3. Measurement of the Elastic Constants of Cobalt and of Cobalt Zinc Ferrite Crystals. H. J. MCSKIMIN, A. J. WILLIAMS, AND R. M. BOZORTH, *Bell Telephone Laboratories.*—The 5 elastic constants of hexagonal cobalt have been determined using pulse modulated ultrasonic waves which are reflected back and forth within the crystal. Frequencies between 15 and 30 Mc/sec were used. Values of the constants were derived from 11 measurements of wave velocities for longitudinal and shear modes in 3 crystals, using a phase comparison technique. At 25°C the constants (all in 10^{12} dynes/cm^2) are: $c_{11}=3.071\pm0.5$ percent, $c_{12}=1.650\pm0.5$ per-

cent, $c_{12}=1.027\pm1.5$ percent, $c_{13}=3.581\pm0.5$ percent, $c_{44}=0.755\pm0.5$ percent. These are based on a density of 8.836. The volume compressibility is calculated to be 0.526×10^{-12} cm²/dyne, a value close to that obtained by extrapolating Bridgman's 1949 results to zero pressure. Similar measurements for cubic cobalt zinc ferrite ($Co_{0.32}Zn_{0.32}Fe_{2.3}O_4$) give at 30°C (in 10^{12} dynes/cm²): $c_{11}=2.66$, $c_{12}=1.53$, $c_{44}=0.78$, based on density 5.43.

I4. The Equation of State and the Thermal Dependence of the Elastic Coefficients of Crystalline Argon. JOHN H. HENKEL, *Brown University* (introduced by R. B. Lindsay).—An interaction potential of the form $(A/R^{10})-(B/R^6)$ for two argon atoms is assumed. The values of A and B are evaluated using the heat of sublimation and the lattice constant at temperature $T=0$°K and pressure $p=0$. By assuming that each atom moves in a potential field due to all the other atoms at rest in their mean positions a theory is developed for anharmonic vibrations using the perturbation theory for a harmonic oscillator. The partition function for each argon atom is obtained and the equation of state is calculated. The specific heat equation obtained represents a correction to the Einstein form. The specific heats at constant pressure are calculated as a function of temperature and deviate from the experimental ones by only 3 percent at low temperatures (15°K–30°K) and only 1 percent at higher temperatures. The isothermal elastic coefficients C_{11}, C_{12}, and C_{44} are calculated by Born's method without neglecting the part played by the thermal energy. The Cauchy relation is found to be invalid, C_{44} being about twice C_{12} at the higher temperatures.

I5. Vibration Spectra of Crystal Lattices. MELVIN LAX AND JOEL L. LEBOWITZ, *Syracuse University*.—The frequency distribution $g(\nu)$ of a crystal is approximated by combining Van Hove's[1] determination of the analytical nature of $g(\nu)$, and Montroll's method of moments.[2] The function $g(\nu)$ is represented by an expression with the correct behavior at the singularities and at the maximum and minimum frequencies. The behavior between singular points is adjusted smoothly by leaving n undetermined parameters. These parameters are then fixed by using the correct first n moments. As a test, this procedure was applied to the two dimensional square lattice with nearest and next nearest neighbor interactions, solved exactly for a particular case by Montroll.[3] The assumed distribution function had the right form at the end points, contained terms of the appropriate logarithmic form and a jump function (with known coefficients). It also included Legendre polynomials with unknown coefficients, which were determined by the moments. The difference between the exact and approximate distribution functions was a few percent using only the zeroth moment (normalization). Using higher moments produced a gradual increase in accuracy.

[1] L. Van Hove, Phys. Rev. **89**, 1189 (1953).
[2] E. W. Montroll, J. Chem. Phys. **10**, 218 (1942).
[3] E. W. Montroll, J. Chem. Phys. **15**, 575 (1947).

I6. Solid Surface Studies by Total Reflection of X-Rays.* L. G. PARRATT, *Cornell University*.—Analysis of the shape of the curve of reflected x-ray intensity *vs* glancing angle in the region of total reflection provides a method of studying certain structural properties of the mirror surface about 10 to a few hundred Angstroms deep. The theory, extended to treat any (small) number of stratified homogeneous media, is used as a basis of comparison. Curves for evaporated copper on glass are studied as an example. These curves probably can be explained by assuming that the copper (exposed to atmospheric air at room temperature) has completely oxidized about 150A deep. If oxidation is less than about 100A deep, there probably exists an electron density minimum just below an internal oxide seal. This seal, perhaps 50A below the nominal surface plane, arrests further oxidation of more deeply-embedded loose-packed copper crystallites. All measurements to date have been carried out under laboratory atmospheric conditions which do not allow satisfactory separation or control of the physical and chemical variables involved. Under better control, the method seems promising.

* This research was supported by the U. S. Air Force through the Office of Scientific Research of the Air Research and Development Command.

I7. Equipment for the Measurement of Very Small X-Ray Scattering Cross Sections.* W. W. BEEMAN AND R. H. NEYNABER, *University of Wisconsin*.—A rotating anode, water-cooled, x-ray tube, vacuum-scattering chamber, and proportional counter detector will be described. With slits furnishing an angular resolution of ±14 minutes, a copper anode, and 30 Kv and 100 ma on the tube, over 10^9 effective (i.e., taking into account window absorption and counter efficiency) CuKα photons per second illuminate the scattering sample. Background counting rates, with the sample removed, are one-half count per second. Absolute scattering cross sections are measured by calibrating the geometry at small angles with a gas scatterer. Under the above conditions of operation a two centimeter path of air at STP furnishes over 120 counts per second. Angular measurements may be made from a lower limit determined by the slit resolution (about 1 degree scattering angle with the above slits) up to 110°. Possible applications include the measurement of scattering from gases, liquids and imperfect lattices away from Bragg angles. With a scattering sample of cold worked nickel and an iron anode we have verified the small-angle vacancy scattering first reported by Blin and Guinier. Counting rates are about 20 counts per second.

* Research supported by the Wisconsin Alumni Research Foundation, the U. S. Office of Naval Research and the U. S. Office of Scientific Research, Air Research and Development Command.

I8. Propagation of Displacement in a Solid, Having a Crystalline Structure with Bistable States.* C. F. PULVARI, *The Catholic University of America*.—Displacement in function of field and temperature has been extensively treated in bistable crystalline solids such as $BaTiO_3$. This paper offers a theory for displacement in function of field and duration of acting field. A continuous bistable potential barrier has an unstable intermediate state. Such a barrier can be represented by a function $\varphi(\eta, U)$ being a fourth-order polynomial of η where U denotes the activation energy as a parameter, and η the displacement vector. The equation of displacement is given by $m(d^2\eta/dt^2)=(\partial\varphi/\partial\eta)$, where m is the mass of the displaced particle. From the results the onset of unelastic displacement and the propagation of polarization is obtained.

* This work is supported by a U. S. Air Force Contract.

I9. Granular Structure of Barium Titanate Ceramic.* JOHN L. SAMPSON, EDWARD E. ALTSHULER, AND CHARLES R. MINGINS, *Tufts College*.—The granular structure of barium titanate in polycrystalline ceramic form has been investigated using the electron microscope. It is found that the grain size is considerably different at a fired surface from what it is in the interior, so that an estimate of scattering or diffusion of energy in a piece of ribbon would be in error if the grain size observed at the surface were used. Very small regular striae are sometimes found; they may be associated with lattice vibrations at phase transition. "Natural" surfaces have been compared with etched surfaces and with surfaces which have been worked in various ways. Observations have also been made on grown crystals.

* Part of an investigation sponsored by the U. S. Army Ordnance Corps.

I10. On Counting Lattice Frequencies. HERBERT B. ROSENSTOCK, *U. S. Naval Research Laboratory*.—Van Hove[1] has traced the singularities[2] in the frequency spectra of

crystals to the "critical points" (points where all $\partial\omega^2/\partial k_i$ vanish) of the frequency in wave number space, and shown that the periodicity of a 3-dimensional crystal alone implies the existence of at least 8 critical points. Whenever ω^2 may be written as a function of the $c_i=\cos k_i$ alone, it follows that 8 critical points are located at the corners of the half-periodicity cube. Others may be found by studying $\omega^2(c)$ on the edges and surfaces of the cube, where the secular determinant simplifies greatly; the behavior inside may be inferred with little ambiguity from that on the surfaces by simple topological considerations. Though the "shape" of the frequency distribution is thus determined, its absolute value anywhere is not. For this, Montroll's approximate method,[3] when modified to take account of the singularities, appears to give adequate results without excessive labor. Preliminary results for the simple, f.-c., and b.-c. cubic lattice will be given.

[1] L. Van Hove, Phys. Rev. **89**, 1189 (1953).
[2] See H. B. Rosenstock and G. F. Newell, J. Chem. Phys. **21**, 1607 (1953) and references therein.
[3] E. W. Montroll, J. Chem. Phys. **10**, 218 (1942); J. Chem. Phys. **11**, 481 (1943).

I11. Calculation of Electrostatic Lattice Potentials, Including Ionic Overlap. JOSEPH BIRMAN, *Sylvania Electric Products, Inc.*—It is necessary to know the electrostatic lattice potential at some point r in an ionic crystal in order to calculate electronic energy levels at a vacancy, activation energy for ionic diffusion, and similar quantities. The conventional method of calculation, due to Ewald,[1] proceeds by shrinking the ions down to point singularities whose charge equals the net charge of the ion. It will be shown how a slight modification of Ewald's method enables one to calculate the lattice potentials in a more realistic lattice, namely one where the ions are represented as point positive cores (nucleus plus tightly bound inner electrons), surrounded by a Gaussian valence electron density. This valence electron density is normalized to give the ion its correct net charge, the half-width chosen in one of a number of ways, depending on the accuracy desired. The effect of increasing the half-width (and therefore the overlap) of the ions will be illustrated by showing the effect of overlap on the self-potential (Madelung Constant) of an NaCl structure.

[1] M. Born and M. G. Mayer, *Handbuch der Physik 24/2* (Julius Springer, Berlin, 1933), p. 711.

I12. Thermal Ionization of Impurities in Polar Crystals. H. D. VASILEFF, *Sylvania Electric Products, Inc.*—A general expression for the thermal ionization rate of an impurity in a polar crystal has been derived. The interaction energy of the trapped electron with the optical vibrational modes was assumed to be linear in the normal vibrational coordinates of the lattice. The eigenvalue equations and perturbation of the Born-Oppenheimer adiabatic potential method were employed. The method of O'Rourke[1] was applied, giving a result in agreement with that of Huang and Rhys.[2] It was found that a multiphonon transition is due fundamentally to a nonzero value of the configurational constant S. A simplified expression for the rate can be obtained only for very low temperatures.

[1] R. C. O'Rourke, Phys. Rev. **91**, 265 (1953).
[2] K. Huang and A. Rhys, Proc. Roy. Soc. (London) **A204**, 406 (1950).

THURSDAY AFTERNOON AT 2:15

Sheraton Park, Caribar Room

(JOHN TINLOT presiding)

Theoretical Physics, II: High-Energy Scattering

IA1. Internal Pair Production in the Radiative Absorption of π^- Mesons by Hydrogen Atoms. W. WADA, *Naval Research Laboratory.*—Using the standard field theoretical method the internal pair-production coefficient for the radiative absorption of slow π^- mesons by hydrogen atoms has been calculated. The probability per second that the pair production takes place, as a function of the emergent neutron energy, is found to have a sharp maximum in the close vicinity of the maximum neutron kinetic energy (9.2 Mev). The ratio of the total probability for the pair production to the radiative absorption probability is found to be of the order of magnitude of the fine structure constant in agreement with experiment.[1] Although a pseudoscalar meson field with a pseudoscalar coupling is employed for our calculation, a pseudovector coupling is also expected to give a similar ratio by virtue of the equivalence theorem. The distribution of angles between pairs is being calculated at the energy of the neutron for which the pair production probability is maximum and will be presented.

[1] Sargent, Rinehart, Cornelius, Lederman, and Rogers, Bull. Amer. Phys. Soc. **28**, No. 6, 13 (1953).

IA2. Approximate Equations for Meson-Nucleon Systems. RICHARD ARNOWITT AND S. GASIOROWICZ, *University of California, Berkeley.*—The scattering and production Green's functions for one nucleon and an arbitrary number of mesons are related by an infinite set of coupled linear integral equations. The first N of these equations contain Green's functions involving 0, 1, 2, $\cdots$ N external meson lines. Experimentally no closely bound states of one nucleon with a large number of real mesons appear to exist. This suggests the approximation of factoring the Green's function with N external meson lines into products of lower Green's functions, as recently proposed by M. Neuman. In particular one may do this by breaking off a single meson propagation function in a symmetric fashion. If vacuum polarization effects are neglected, the resulting equations remain linear. Taking $N=1$ leads to the lowest order perturbation result. $N=2$, which involves the breakup of the meson-nucleon Green's function (i.e., neglecting the meson-nucleon interaction) leads to the S_F' function of Brueckner, Gell-Mann, and Goldberger. Taking $N=3$ means ignoring meson production in meson-nucleon scattering, etc. In the last case an integral equation involving only the meson-nucleon kernel may be derived. Approximate solutions will be discussed. This work was performed under the auspices of the U. S. Atomic Energy Commission.

IA3. Meson Production in Meson-Proton Scattering. M. S. NELKIN* AND H. A. BETHE, *Cornell University.*—The integral equation for meson-nucleon scattering in the lowest Tamm-Dancoff approximation[1] is considered for $E>M+2\mu$. If the two meson, one nucleon energy denominator in the kernel is evaluated as a δ_+ function, then the Goldberger[2] scattering amplitude evaluated on the energy shell gives the tangent of

the complex phase shift. If the imaginary part of the phase shift is small, then the imaginary part of the integral equation can be reduced to a form identical to the real part except for the behavior of the inhomogeneous term at small momenta. If this difference is ignored, the ratio σ(production)/σ(scattering) can be calculated without solving the integral equation, and turns out to be less than 1 percent at 400 Mev. Numerical results will be given, and the validity of the approximations used examined.

* National Science Foundation predoctoral fellow.
[1] Dyson, Schweber, and Visscher, Phys. Rev. **90**, 372(A) (1953).
[2] M. L. Goldberger, Phys. Rev. **84**, 929 (1951).

IA4. Meson-Meson Effects in Meson Nucleon Scattering. MARC H. ROSS, *Brookhaven National Laboratory.**—Experimental information is becoming available at present which enables a phenomenological test of the suggestion that meson-meson interaction plays an important role in meson nucleon scattering. We assume that the interaction (a) between the incoming meson and the nucleon's proper field, can be represented by a potential, common to all angular momenta, of long range, i.e., of order meson compton wave length; and that the direct meson nucleon interaction (b) is of short range. In addition to phase shifts obtained directly from scattering differential cross sections, we consider indirect phase shift information from various near zero energy experiments and from comparison of meson photoproduction with scattering at all energies. The present data suffice only to determine the shallow attractive well for (a) with $T=\frac{3}{2}$. A specific prediction providing a test of the model is attractive D wave phase shifts (for $T=\frac{3}{2}$) around 250 Mev of magnitude considerably larger than one might expect from (b) alone. Of greater significance at present are general implications of the problem: (1) It seems quite possible that a separation of effects (a) and (b) exists. Thus continued and improved low-energy scattering experiments are of great interest. (2) Great caution should be exercised in comparing a meson theoretical calculation of (b) alone with experimental results.

* Work done under the auspices of the U. S. Atomic Energy Commission.

IA5. Pion-Nucleon S Phase Shifts at Low Energy.* H. P. NOYES, *University of Rochester.*—Bernardini *et al.* have shown[1,2] that their recent results on the photoproduction of charged pions in hydrogen and deuterium near threshold, combined by detailed balancing with Panofsky's results for the absorption of π^- mesons in hydrogen, give $\alpha_1-\alpha_3=0.16p/\mu c$ $(1^+-0.25)$, where α_1 and α_3 are the S phase shifts of isotopic spin $\frac{1}{2}$ and $\frac{3}{2}$, respectively. This is in clear contradiction with the value obtained by *linear* extrapolation from the results of the pion scattering experiments at Columbia at 65 Mev and at Rochester at 40 Mev,[1] which is $0.33p/\mu c$. It is, however, explicable in terms of the S wave potential model proposed by Marshak as extended by Woodruff, which gives $0.2p/\mu c$, using the following parameters: $I=\frac{1}{2}$; $V=V_0\exp(-r/r_0)$; $V_0=-105$ Mev; $r_0=0.65\times10^{-13}$ cm. $I=\frac{3}{2}$; $V=+\infty$, $r\leq r_e$ $=0.54\times10^{-13}$ cm; $V=V_0\exp-(r-r_e)/r_0$, $r>r_e$; $V_0=-187$ Mev; $r_0=0.60\times10^{-13}$ cm. A least squares analysis of the 40 Mev pion-nucleon scattering data will be presented and the resulting limitations on the values of the phase shifts and the parameters of the model will be discussed.

* Supported by the U. S. Atomic Energy Commission.
[1] *Proceedings of the Fourth Annual Rochester Conference*, University of Rochester, Physics Department, 1954.
[2] Bull. Am. Phys. Soc. **29**, No. 1, G4 (1954).

IA6. Electron Scattering from Nuclei. G. T. TRAMMELL, *Oak Ridge National Laboratory.*—To aid in the theoretical evaluation of the high-energy electron-heavy nucleus elastic scattering experiments of Hofstadter and collaborators,[1] the Oak Ridge electronic digital computer (ORACLE) is being used for the calculation of the scattering cross sections from several assumed nuclear charge distributions. The results obtained will be presented.

[1] Hofstadter, Fechter, and McIntyre, Phys. Rev. **92**, 978 (1953).

IA7. High-Energy Electron Scattering. J. MAYO GREENBERG, *Rensselaer Polytechnic Institute.*—An investigation of nucleonic distribution in the nucleus by scattering of electrons whose wavelength is sufficiently small to demonstrate some structural detail is being conducted by Hofstadter and coworkers at Stanford University. The analysis of the experimental results is hampered by the fact that it is necessary to perform tedious phase shift calculations for various trial models of the nucleus. The scattering approximation of Montroll and Greenberg[1] seems particularly suitable to the high-energy electron scattering problem. Calculations which are essentially based on an application of this method using the Dirac equation are presented and compared with exact results of Yennie *et al.*, using phase shift analysis.

[1] E. W. Montroll and J. M. Greenberg, Phys. Rev. **86**, 889 (1952).

IA8. Coulomb Energy and Nuclear Radius. B. JANCOVICI, *Princeton University* (introduced by E. P. Wigner).—The discrepancy between the values $(1.45\times10^{-13}A^{\frac{1}{3}}$ cm) for the nuclear radii derived from mirror nuclei and those $(1.2\times10^{-13}A^{\frac{1}{3}}$ cm) derived from μ-mesonic atoms was investigated. The calculation was based on the shell model with a square well potential, the depth of which was adjusted to fit the experimental binding energy of the last nucleon. The radius of the well was chosen to fit the mesonic atom data. These depend on the mean square radius of the total charge distribution. The Coulomb energy difference ΔE_c of the β transition was computed, including exchange terms. ΔE_c can be expressed in terms of r_e defined by $\Delta E_c=1.2Ze^2/(r_e10^{-13}A^{\frac{1}{3}}$ cm). For (O^{15},N^{15}) the computed r_e is 1.29, the experimental value 1.41. In F^{17}, the last proton is outside the closed shells and, hence, loosely bound. The computed ΔE_c is smaller and gives r_e $=1.37$; however, the experimental r_e is 1.52 in this case. Therefore, the experimental discontinuity in r_e at the closure of the p shell is reproduced by the model but the computed absolute values of r_e remain too small.

IA9. Interpretation of Scattering of High-Energy Nucleons by Complex Nuclei.* I. I. SHAPIRO AND J. M. TEEM,† *Harvard University.*—The Glauber[1] procedure has been used to calculate angular distributions of protons scattered elastically from C and Al at 96 Mev. Comparison with recent experimental results[2] has been made. The Coulomb potential for a uniformly charged nucleus was used, combined with a complex square well of width $r_0A^{\frac{1}{3}}+r_1$, the first term representing the electromagnetic radius and the second the extension of size due to nuclear forces. The well parameters were taken to be those for neutron scattering. They were obtained by a "best fit" of energy dependent total cross sections, known absorption cross sections, and elastic cross sections at 84 Mev. The well depths, assumed independent of A, have variations with energy similar to Taylor's.[3] Investigations of neutron scattering using other potential forms, e.g., Gaussian, to determine edge effects of the square well, will also be discussed.

* Assisted by the joint program of the U. S. Office of Naval Research and the U. S. Atomic Energy Commission.
† National Science Foundation Predoctoral Fellow.
[1] R. J. Glauber, Phys. Rev. **91**, 459 (1953).
[2] K. Strauch and F. Titus, Bull. Am. Phys. Soc. **29**, No. 1 (1954), abstract T6.
[3] T. B. Taylor, Phys. Rev. **92**, 831 (1953).

IA10. Nuclear Cross Sections and the Size of the Nucleus.* WARREN HECKROTTE, *University of California, Berkeley.*—The experiments of Millburn *et al.* at this laboratory on the determination of the inelastic nuclear cross sections for high-energy deuterons yield the following expression for the cross

section as a function of the mass number of the target nuclei: $\sigma=\pi(1.68A^{\frac{1}{3}}+0.64)^2\times10^{-26}$ cm^2. It may readily be shown that this implies the value $R=1.68\times A^{\frac{1}{3}}\times10^{-13}$ cm for the nuclear radius and $R_D=2.56\times10^{-13}$ cm for the mean separation of the particles in the deuteron. To understand further this result for the nuclear radius, the total nuclear cross sections for 90-Mev neutrons have been interpreted in terms of a non-square well nuclear density distribution. Taking for numerical simplicity a parabolic shape, the radius (measured to the edge of the distribution) that is obtained is $R=1.60\times A^{\frac{1}{3}}\times10^{-13}$ cm. The significance of this result and the experimental result as compared with other determinations of the nuclear radius will be discussed.

* This work was performed under the auspices of the Atomic Energy Commission.

IA11. Nuclear Radii and Transparencies from Inelastic Cross-Section Measurements. I. Method.* G. P. MILLBURN, *University of California, Berkeley,* AND W. BIRNBAUM, W. E. CRANDALL, AND L. SCHECTER, *California Research and Development Company.*—The total inelastic cross sections for high-energy protons, deuterons, He^3 particles, and alpha particles accelerated in the 184-inch cyclotron were measured by an attenuation technique. Integral range curves for various absorbers were measured and analyzed to account for the secondary charged particles present in the beam of attenuated particles. A relation between the inelastic cross sections of protons and deuterons permits a straightforward analysis of the curves for deuterons and yields the stripping cross sections. Corrections for multiple scattering and true path length in the absorber were applied to the data.

* Supported by the U. S. Atomic Energy Commission.

IA12. Nuclear Radii and Transparencies from Inelastic Cross-Section Measurements. II. Interpretation.* W. E. CRANDALL, W. BIRNBAUM, AND L. SCHECTER, *California Research and Development Company,* AND G. P. MILLBURN, *University of California, Berkeley.*—The inelastic cross sections for multi-nucleon bombarding particles fit a relation, $\sigma_a=\pi(a_a A^{\frac{1}{3}}+R_a)^2$, where a_a and R_a depend upon the bombarding particle. To obtain an expression in which the nuclear radius appears explicitly, further simplifying assumptions are introduced for loosely bound multi-nucleon system, such as deuterons and He^3 particles, allowing the inelastic cross section to be expressed in the form, $\sigma_a=\pi(a_0A^{\frac{1}{3}}+R_a)^2(1-\tau^a)$, where $a_0A^{\frac{1}{3}}$ may be interpreted as the radius of the struck nucleus, including a highly transparent fringe region, and τ is the average transparency of this nucleus to the individual nucleons of the bombarding nucleus.

* Supported by the U. S. Atomic Energy Commission.

IA13. Polarization in Scattering by Nuclei at High Energies.* B. J. MALENKA, *Harvard University.*—Recent experiments indicate a considerable polarization in high-energy proton scattering by the larger nuclei. It is suggested that this effect can be principally explained by assuming a simple spin-orbit interaction of the form and magnitude required in the theory of shell structure. An initial approach to this problem is carried out by treating the spin interaction term in Born approximation. A more accurate approximation is obtained if we note that the polarization effect has been observed at comparatively small scattering angles. This permits us to treat the scattering problem with polarization by making use of a technique introduced by Glauber[1] which effectively sums the complete Born series for high-energy and small-angle potential scattering. A rough preliminary calculation appears to indicate that the maximum polarization occurs for an appropriate range of scattering angle.

* Partially supported by the joint program of the U. S. Office of Naval Research and the U. S. Atomic Energy Commission.

[1] R. J. Glauber, Phys. Rev. 91, 459 (1953).

IA14. Polarization Effects in High-Energy Proton-Deuteron Scattering. S. TAMOR, *University of California, Berkeley.*—Recent experiments on the polarization of high-energy protons scattered from light elements[1,2] (Be, C) indicate considerably larger effects than those obtained in p-p and n-p scattering.[1-3] Since calculations[4,5] of polarization in p-p and n-p scattering using tensor interactions give reasonable agreement with experiment it is interesting to investigate whether the polarization from more complex nuclei can be described in terms of the same nucleon-nucleon forces with inclusion of interference and spin-correlation effects. Using a formalism already described,[6] calculations have been carried out on the polarization produced in elastic proton-deuteron scattering at 240 Mev. A significant enhancement of the polarization is obtained, especially at larger angles. A detailed discussion of results will be presented. This work was performed under the auspices of the U. S. Atomic Energy Commission.

[1] C. L. Oxley *et al.*, Phys. Rev. 91, 419 (1953).
[2] O. Chamberlain *et al.*, Phys. Rev. (to be published).
[3] L. F. Wouters, Phys. Rev. 84, 1069 (1951).
[4] D. R. Swanson, Phys. Rev. 89, 749 (1953).
[5] L. J. B. Goldfarb and D. Feldman, Phys. Rev. 88, 1099 (1952).
[6] S. Tamor, Phys. Rev. 93, 227 (1954).

FRIDAY MORNING AT 9:30

NBS, East Building

(R. T. BIRGE presiding)

Invited Papers in Electron Physics

J1. Survey of Characteristic Energy Losses of Electrons. L. MARTON, *National Bureau of Standards.* (30 min.)

J2. Electron Interaction in Solids. DAVID PINES, *University of Illinois.* (30 min.)

J3. Some Fundamental Processes of Gaseous Electronics. L. B. LOEB, *University of California, Berkeley.* (40 min.)

J4. Buildup Processes in Sparks and Positive Corona. L. H. FISHER, *New York University.* (30 min.)

FRIDAY MORNING AT 9:30

Sheraton Park, Burgundy Room

(W. W. WATSON presiding)

Spectra from X-Rays through Microwaves

JA1. *K*-Absorption Edge Studies of Compounds. H. P. HANSON, *University of Texas*, AND J. R. KNIGHT, *University of Florida*.—A series of *K*-absorption edge curves have been obtained for various compounds of the elements $Z=25$ through $Z=30$. The fluorides, chlorides, oxides and sulfides of these metals were investigated. The significant trends which were observed in the data will be discussed in terms of the homopolar nature of the bonding and the decreasing number of vacancies in the *d* shell.

JA2. X-Ray Absorption in Solid Argon.* JACK SOULES† AND C. H. SHAW, *The Ohio State University*.—The structure of the argon *K*-absorption edge at 3.86A has been investigated under high resolving power using the two crystal x-ray spectrometer with calcite crystals. Solid argon films of controllable thickness were prepared by freezing the gas onto a Beryllium window backed by liquid helium. A proportional counter detector and pulse height analyzer permitted the use of high x-ray tube voltage without the confusion of second order effects. Data were obtained for argon in both the gaseous and solid states. Previous work[1] on the gas absorption is confirmed and extended to interpret the electron band structure of the solid.

* Supported by the U. S. Office of Naval Research.
† DuPont Fellow, 1952–53.
[1] L. G. Parratt, Phys. Rev. **56**, 295 (1939).

JA3. *L*-Absorption Spectrum of Silicon and Silicon Dioxide.* D. E. BEDO AND D. H. TOMBOULIAN, *Cornell University*.—Following a method described previously,[1] absorption measurements have been carried out in the spectral region extending from 60A to 200A. Absorbers were prepared by evaporation on a glass substrate treated with "Victo-wet." Deposited films sprayed with Zapon were floated off and suitably mounted. Preliminary measurements on Si show a repeatable absorption edge at 124.5A to be identified with the $L_{2,3}$ discontinuity. A similar edge appears in the case of SiO_2, but its position is shifted towards shorter wavelengths by 8A. No measurements have been reported on the absorption by the semiconductor or its dioxide in the soft x-ray region. However, a similar shift in the edge is revealed in a study[2] of the *K*-absorption spectrum of Si and SiO_2. In conjunction with the available information on the *L*-emission band of Si, the present measurements lead to the value of 0.8 ev as an estimation of the energy gap in the semiconductor.

* Supported by the Office of Ordnance Research, U. S. Army.
[1] D. H. Tomboulian and E. M. Pell, Phys. Rev. **83**, 1196 (1951).
[2] V. P. Barton and G. A. Lindsay, Phys. Rev. **71**, 406 (1947).

JA4. An Extension of the Extreme Ultraviolet Solar Spectrum. F. S. JOHNSON, J. D. PURCELL, AND R. TOUSEY, *Naval Research Laboratory*.—New spectra of the sun were obtained on February 2, 1954 from a rocket between 80 and 104 km altitude. All ten exposures show the Lyman alpha line of hydrogen (1216A) in emission and several are greatly overexposed. The continuum was photographed to 1750A. The Schumann-Runge bands of oxygen appear in the continuum with intensity depending on altitude. On the highest exposure traces of the continuum can be seen between 1100 and 1300A at the wavelengths of the O_2 transmission windows. Except for this, the continuum below 1750A was entirely absorbed by the O_2 present above 104 km. The spectrograph was kept directed at the sun by means of the pointing control developed and constructed by the University of Colorado[1] and made available by the U. S. Air Force. Fog due to stray light was reduced, so as not to swamp the extreme ultraviolet, by using a plastic grating, made by removing the aluminum from a Bausch and Lomb replica, and by focusing the sun on the slit with a mirror of quartz whose reflectance increases below 2000A, reaching a maximum[2] of approximately 20 percent near 1200A.

[1] Stacey, Stith, Nidey, and Pietenpol, Electronics **27**, 149 (1954).
[2] R. Tousey, Phys. Rev. **57**, 1060 (1940).

JA5. Pressure Shift in Helium λ5875.* JOHN R. HOLMES AND LEON PAPE, *University of Southern California*.—Using a Fabry-Perot interferometer, pressure shift in λ5875($2\,^3P - 3\,^3D$) of He^4 was looked for over a pressure range from 5×10^{-3} to 20 mm in a helium atmosphere. A mean shift of 0.0074 cm^{-1} toward lower frequency at the higher pressure was found. As this is within the experimental error it is concluded that over the above pressure range pressure shift is not likely to falsify significantly isotope shift measurements in the helium spectrum, in disagreement with Fred, Tomkins, Brody, and Hamermesh.[1]

* Supported partly by the U. S. Office of Naval Research.
[1] Fred, Tomkins, Brody, and Hamermesh, Phys. Rev. **82**, 406 (1951).

JA6. Spectroscopic Isotope Shift in Hf I and Hf II. J. A. COLLINSON AND W. W. WATSON, *Yale University*.—We have observed the hyperfine structure of some 70 Hf I and 20 Hf II lines in the range 2870–4900A. This structure is in every case either a line which appears single or a doublet (roughly 0.030–0.050 K) whose components are of the proper relative intensities to be produced by isotopes 178 and 180. The doublets are sometimes in the "negative" sense. In Hf I, the shifts are consistent with the tentative analysis of that spectrum[1] and indicate that the same electron configuration, presumably $5d^26s^2$ of the ground state, is responsible for all seven of the low-energy levels. Rasmussen[2] reported λλ 4837 and 4800 as single and λ 4655 as split, while we find λ 4837 double. In Hf II,[3] the double electron transition of λ 3134.72 ($5d6s^2\,{}^2D_{3/2}$—$5d^26p\,{}^4G_{5/2}$) exhibits structure substantially larger than that in any other line.

[1] W. F. Meggers and B. F. Scribner, J. Research Natl. Bur. Standards **4**, 169 (1930).
[2] E. Rasmussen, Naturwiss. **23**, 69 (1935).
[3] W. F. Meggers and B. F. Scribner, J. Research Natl. Bur. Standards **13**, 625 (1934).

JA7. Isotope Shift in the Li I Spectrum. RAYMOND H. HUGHES, *University of Wisconsin*.*—The previous work[1] on the isotope shift in the spectrum of the neutral lithium atom, in which the $2S-2P$ and $2P-3D$ transitions were studied in the hollow cathode spectra from separate isotopes[2] with the aid of a Fabry-Perot interferometer, has been extended to

TABLE I.

	$n=2$	3	4	5
$ns\,{}^2S_{1/2}$	$+0.037\pm0.007$	$+0.010\pm0.005$	$+0.003\pm0.005$	
$np\,{}^2P_{1/2,3/2}$	-0.119 ± 0.003			
$nd\,{}^2D_{3/2,5/2}$		$+0.002\pm0.006$	$+0.000\pm0.003$*	0.000 ± 0.003*

* Basis for assignment of the $2P$ shift.

include the transitions between the $2P$ and the $3S$, $4S$, $4D$, $5D$ levels. The specific shifts (i.e., the residuals after correcting for the normal reduced mass effect) have been determined with respect to the limit Li II $1s^2\ ^1S_0$ as a reference point, and are listed in Table I. The + sign means that the corrected Li^7 level lies farther below $^1S_0$ than the Li^6. The errors shown are limit errors. Meissner's values for the $3D$, $4D$, and $5D$ doublet separations have been confirmed.[3]

* Supported partly by Office of Ordnance Research, U. S. Army.
[1] Raymond H. Hughes, Phys. Rev. **91**, 457(A) (1953).
[2] Obtained on loan from the Y-12 plant, Oak Ridge National Laboratory on U. S. Atomic Energy Commission allocation.
[3] Meissner, Mundie, and Stelson, Phys. Rev. **74**, 932 (1948).

JA8. The Vibrational Spectrum of Fluorotrichloroethylene.* D. E. Mann and Earle K. Plyler, *National Bureau of Standards.*—The infrared spectrum of gaseous $FClC{:}CCl_2$ has been observed in the range 3–50 microns. The Raman spectrum of the liquid has also been obtained. A complete and satisfactory vibrational assignment has been achieved. The planar fundamentals occur at 1645, 1181, 988, 857, 520, 407, 250, 174, and 144 cm^{-1}; the out-of-plane vibrations appear at 537, 358, and 123 cm^{-1}. Thermodynamic functions have been calculated.

* This work has been supported in part by the U. S. Office of Naval Research.

JA9. Microwave and Far Infrared Atmospheric Water-Vapor Absorption. T. F. Rogers, *Air Force Cambridge Research Center.*—Recent measurements and analyses[1] of rotation-vibration water vapor absorption bands have provided term values from which more accurate and extended calculations of long wavelength rotational transitions can be made.[2] Peak intensities of all predicted H_2O lines from 0–60 cm^{-1} and HDO from 0–35 cm^{-1} have been obtained for a 1 percent vapor concentration in air at 760 mm and 293°. The Van Vleck-Weisskopf modified Lorentz equation has been employed to calculate the complete absorption spectrum to 35 cm^{-1} for H_2O and 15 cm^{-1} for HDO. For the 0–15 cm^{-1} region, the H_2O absorption spectrum has further been calculated for several heights well into the troposphere thereby allowing estimates of total vertical absorption to be made.

[1] Benedict, Claasen, and Shaw, J. Research Natl. Bur. Standards **49**, 91 (1952); Taylor, Benedict and Strong, J. Chem. Phys. **20**, 1884 (1952); Benedict, Gallar, and Plyler, J. Chem. Phys. **21**, 1301 (1953).
[2] King, Hainer, and Cross, Phys. Rev. **71**, 433 (1947); J. H. Van Vleck, Phys. Rev. **71**, 425 (1947).

JA10. Microwave Absorption in Compressed Gases. G. Birnbaum and A. A. Maryott, *National Bureau of Standards.*—The weak absorption due to the wings of the rotational lines of HCl and HBr was measured in the pressure region 0–20 atmos by a cavity resonator method at a wavelength of 1.28 cm. Also measured were mixtures of each of these gases with He, H_2, A, N_2, CH_4, SF_6, and CO_2 at pressures up to 45 atmos. For self broadening the absorption varied nearly as p^2, and for foreign broadening the absorption varied linearly with the pressure of foreign gas, except in the case of $HX-CO_2$ mixtures. Absorption was found in the nonpolar gas CO_2 by itself ($\alpha=3.1\times10^{-6}$ cm^{-1} at 45 atmos); possible reasons for this absorption are examined. The relative pressure broadening abilities of the foreign gases were compared with those obtained from measurements at 1.28 cm on the inversion spectrum of CH_3Cl. The broadening ability increased in the order He, H_2, A, N_2, CH_4, SF_6, and CO_2 with respect to all three polar gases. Correlation of broadening ability with the polarizability and quadrupole moment of the perturber is examined.

JA11. A Microwave Spectral Series of Deuterated Hydrogen Peroxide.* J. T. Massey, C. I. Beard, and C. K. Jen, *The Johns Hopkins University.*—From the observation of more than one hundred microwave absorption lines of deuterated hydrogen peroxide,[1] a spectral series consisting of thirteen $\Delta J=0$ transitions has been established by their Zeeman and Stark effects. The frequencies of these lines converge in a smooth manner toward the high-frequency series limit at 37 526 mc/s. All lines show measurable π splitting with the magnetic field and the measured g-factor plot is representable by a function which increases with frequency. The Stark components, showing in each case a $\Delta J=0$ pattern, increase in number consecutively from line to line as the frequency is decreased. The minimum J value at the limit is most probably 4 with a possible uncertainty of ±1. The isotopic species of the series has not yet been determined with certainty. From the Zeeman calculations, it seems plausible to assume that it is an HDO_2 series. Calculation of the energy levels using the potential barrier derived from the H_2O_2 spectrum,[1] indicates that this series might come from the $n=1$ torsional vibrational state of HDO_2.

* This work was supported by the U. S. Bureau of Ordnance, Department of the Navy, under Contract NOrd 7386.
[1] J. T. Massey and D. R. Bianco, J. Chem. Phys. (to be published).

JA12. Pressure Broadening of Cyanogen Bromide in the Microwave Region.* Ralph Trambarulo, Henry Lackner, Paul Moser, and Harold Feeny, *University of Delaware.*—The self-broadening of the $J=2$ to 3, $F=5/2$ to $7/2$ and $7/2$ to $9/2$ rotational transition of cyanogen bromide at 24.6 Kmc was investigated as a function of temperature and pressure by a method previously described.[1] This transition consists of a number of hyperfine lines which were not resolved on our spectrometer. Corrections were made for multiplet line structure and also for the mode curvature of the microwave source. The line-breadth parameter is 27.1 Mc/mm at room temperature, and the temperature variation is proportional to $T^{-1.6}$ giving an apparent collision diameter which varies with temperature. The interpretation of these results is now in progress.

* Supported by the U. S. Air Force, through the Office of Scientific Research of the Air Research and Development Command.
[1] Feeny, Moser, Lackner, and Smith, J. Chem. Phys. (to be published).

JA13. Microwave Spectrum of OCS.* Martin Peter and M. W. P. Strandberg, *M.I.T.*—The $J=1\rightarrow J=2$ transition of OCS has been studied with a microwave spectroscope designed for high sensitivity and high resolution. The line $v_2=1$ has been found at 0.85 ± 0.1 Mc/sec above the $v_1=2$ line. This is the frequency predicted with the α_2 value determined from infrared spectra by Thompson,[1] and agrees with his value within his limits of error. Several quadrupole components of OCS^{33} in the states $v_1=1$; $v_2=1$, $l=\pm1$; and $v_2=2$ have also been measured and analyzed.

* This work was supported in part by the U. S. Signal Corps, the Air Materiel Command, and the U. S. Office of Naval Research.
[1] The authors are indebted to Professor H. W. Thompson of St. John's College, Oxford, for his kindness in making his data available to them before publication.

JA14. Selection Rules in the Microwave Magnetic Resonance Spectrum of Oxygen.* M. Tinkham and M. W. P. Strandberg, *M.I.T.*—The X-band paramagnetic resonance spectrum of molecular oxygen consists of about 120 lines of observable intensity for magnetic fields below 12 kilogauss. Forty of these lines have been identified by rather tedious calculations. To aid in identifying the others, we have used a circularly polarized radiation field in the cavity containing the sample gas. This field is provided by exciting the two degenerate orthogonal TE_{111} modes in a cylindrical cavity 90° out of phase. This field configuration gives pure circularly polarized radiation only along the axis. Averaging H^2 over the cavity, 52 percent is circular in one sense, 4 percent is circular in the other sense, and 44 percent is axial. Comparison of the two observed spectra with the two senses of rotation unambiguously separates $\Delta M=\pm1$, 0 transitions. The results

are that approximately 95 lines have $\Delta M=+1$, the rest have $\Delta M=-1$. The absence of $\Delta M=0$ lines is consistent with detailed calculations which show that their intensities should be down by a factor of at least 100. Another result of the identification is that about two-thirds of the lines observed have the "forbidden" $\Delta J=\pm 2$. They are allowed here because J is not a good quantum number in the presence of the magnetic perturbation.

* This work was supported in part by the U. S. Signal Corps, the Air Materiel Command, and the U. S. Office of Naval Research.

JA15. Effects of the Deviation of O_2 from Hund (b).* M. W. P. STRANDBERG AND M. TINKHAM, *M.I.T.*—The rotational Hamiltonian of the oxygen molecule, including the spin-spin interaction, is not exactly diagonal in the Hund (b) representation $|J^2,J_z,K^2,S^2)$ where $\mathbf{J}=\mathbf{K}+\mathbf{S}$. Hence K is not a good quantum number, and three points should be made. First, the intensities of the oxygen spin triplet spectrum at 5 mm are not exact as given by Van Vleck. He has used the matrix elements of S_Z in the Hund (b) representation rather than in the representation which diagonalizes the Hamiltonian. Thus inference of the breadths of the oxygen lines from the observed pressure and intensity, using the Van Vleck formulas, is only approximate. Exact calculation shows that such a procedure will overestimate the actual line width for low K transitions. Second, lines "forbidden" under the previous analysis now become allowed. For example, the three lowest frequency lines corresponding to changes in $K=1\rightarrow 3$ are predicted to be at 368, 522 Mc/sec, 424, 787 Mc/sec, and 487, 274 Mc/sec, with intensities respectively of 0.64×10^{-6} cm^{-1}, 38×10^{-6} cm^{-1}, and 17×10^{-6} cm^{-1}, assuming the same $\Delta\nu$ as the 5-mm lines. Third, the weak field Zeeman splittings will not exactly follow the simple vector model predictions for Hund (b).

* This work was supported in part by the U. S. Signal Corps, the Air Materiel Command, and the U. S. Office of Naval Research.

JA16. Air-Guided Propagation of Short Radio Waves Around the Earth Bulge.* THOMAS J. CARROLL, *Lincoln Laboratory*.—If the normal air be treated as a homogeneous, linear,[1] or curvilinear graded dielectric layer surmounting a perfectly reflecting curved earth, then the effect of the dielectric air layer in overcoming the earth curvature can be worked out rather completely and the field calculated in good agreement with experiment at least as far as 400 miles. Conventional airless 4/3 earth theory is adequate only out to a few tens of miles beyond the horizon, because of the neglect of the reflective effect of coherent scattering by the air dielectric. The calculation illustrates the great power in this classical problem of the complex eigenvalue method as evolved by quantum mechanicians, as well as the limitations of WKB methods pointed out by Bremmer for electromagnetic waves. The presence of the normal air layer, hitherto neglected except for its refractive effect, can thus be proved to have considerable practical importance to radio technology.

* Supported jointly by the U. S. Army, Navy, and Air Force under contract with the Massachusetts Institute of Technology.
[1] T. J. Carroll and R. M. Ring, Lincoln Laboratory Technical Report 38.

FRIDAY MORNING AT 9:30

Shoreham, West Ballroom

(J. B. PLATT presiding)

Meson Scattering; Meson Absorption; Mesonic Atoms

K1. The Parity of the Pion.* WILLIAM CHINOWSKY AND JACK STEINBERGER, *Columbia University*.—The best evidence presently available for the negative relative parity of pion and nucleon comes from the experiments of Panofsky *et al.*[1] which show, indirectly, that the process $\pi^-+D\rightarrow 2N$ is allowed, even when the initial system is in an S state. The reaction itself has, however, not been observed before. In this experiment, π^- mesons came to rest in a cylinder of liquid deuterium, 3 in. in diameter$\times 3\frac{1}{4}$ in. high. The two 70 Mev neutrons are detected in liquid scintillation counters $2\frac{1}{2}$ in. in diameter and 2 in. along the direction of motion of the neutron. The efficiency of each counter for the detection of such neutrons is $\sim$5 percent. We discriminate against charged particles and high-energy γ rays by means of anticoincidence counters, and against low energy γ rays and neutrons by means of pulse height requirements. N-N coincidences are measured as a function of the angle subtended by the two detectors at the target. The observed coincidence rate is peaked at 180° with an angular width which is just the resolution of the apparatus. The absolute intensity can be estimated, and roughly agrees with that predicted by Panofsky. The experiment therefore confirms the evidence that the pion is not scalar.

* This work was performed under the joint program of the U. S. Office of Naval Research and the U. S. Atomic Energy Commission.
[1] Panofsky, Aamodt, and Hadley, Phys. Rev. **81**, 565 (1951).

K2. Charge Exchange Scattering of Stopped π^- Mesons in Deuterium.* JACK STEINBERGER AND WILLIAM CHINOWSKY, *Columbia University*.—Using an arrangement similar to that of the preceding abstract, we have searched for neutral mesons produced by π^- mesons stopped in D_2, according to the reaction

$$\pi^-+D\rightarrow\pi^0+N+N_0. \quad (1)$$

The neutral mesons were to be detected by observing the two π^0 decay γ rays in coincidence in two telescopes, each consisting of two $4\frac{1}{2}$ in. diameter scintillation counters with $\frac{3}{4}$ in. polyethylene absorber between them. A $\frac{1}{4}$ in. Pb converter is in front of each telescope. This system is insensitive to the neutrons from the competing process $\pi^-+D\rightarrow 2N$. We find a small number of $\gamma-\gamma$ coincidences, corresponding to a fractional rate for process (1) of 0.0008 ± 0.0003. We believe, however, that such a rate can be accounted for by an expected small hydrogen impurity in the deuterium.

* This work was performed under the joint program of the U. S. Office of Naval Research and the U. S. Atomic Energy Commission.

K3. (Abstract withdrawn.)

K4. Total Cross Sections for Scattering of Positive Pions by Hydrogen.* J. BLASER, J. ASHKIN, F. FEINER, J. GORMAN, AND M. O. STERN, *Carnegie Institute of Technology.*—External π^+ beams of energies ranging from 135 to 197 Mev have been used for the measurement of total cross sections by an attenuation experiment. Liquid hydrogen as well as CH_2 and C were used as scatterers. Possible errors introduced by contamination of the π^+ beam by protons have been eliminated by use of time of flight and pulse-height selection. The corrected cross sections have typical uncertainties of ±5 percent and rise from 120 mb at 135 Mev to 200 mb for energies between 170 to 196 Mev. They follow very well the curve representing three times the total cross section for π^- scattered on hydrogen.[1] This supports the idea of the dominant role played by the state of angular momentum 3/2 and isobaric spin 3/2.

* Research partially supported by the U. S. Atomic Energy Commission.
[1] Ashkin *et al.*, Phys. Rev. (to be published).

K5. π^- P Collisions at 1.5 Bev. I.* W. D. WALKER, J. CRUSSARD, AND M. KOSHIBA, *University of Rochester.*—About 70 $\pi^- P$ collisions have been found from scanning G-5 emulsions exposed to the Brookhaven Cosmotron. The criteria for acceptance and rejection of these interactions will be discussed. The results at the present time are as shown in Table I. The angular distributions from these interactions will be discussed. In general the proton (or neutron) almost always go backward in the center of mass system. The π^- goes forward and the secondary meson usually goes out at an angle of the order of 120° with respect to the π^-.

TABLE I.

Products	No. cases
π^-+P	16
$\pi^-+P+\pi^0$	31
$\pi^++\pi^-+N$	11
π^0+N $2\pi^0+N$ $\Lambda^0+\theta^0$	13
$\pi^++2\pi^-+P$	1

* This work was assisted by the U. S. Atomic Energy Commission.

K6. π^- Interactions at 1.5 Bev. II.* J. CRUSSARD, W. D. WALKER, AND M. KOSHIBA, *University of Rochester.*—In the course of scanning for the $\pi^- - P$ collisions of the previous abstract many other interactions were found. A mean free path of 25 cm was obtained with about 25 percent of the interactions being diffraction scatterings of 1°–2°. Several interactions seemed to be interpretable as $\pi^- - N$ interactions. These interactions consisted usually of a large angle deflection of the π^- with only a β emerging from the vertex of the interaction. The results are given in Table I. Interactions with light nuclei have been subdivided as to whether 0, 1, 2, 3π mesons emerge from the interaction. The results of these studies show qualitative agreement with the results of the $\pi^- - P$, and $\pi^- - N$ interactions as to the relative number of the different interactions except in one respect. There is an indication of another process which may be a many body collision in the nucleus.

TABLE I.

Products	No. cases
π^-+N $\pi^-+N+\pi^0$	36
$2\pi^-+P$	7
$\pi^++2\pi^-+N$	1

* Assisted by the U. S. Atomic Energy Commission.

K7. Scattering of 145-Mev π^+ by Hydrogen in Emulsion. JAY OREAR, *University of Chicago,* AND C. H. TSAO, J. J. LORD, AND A. B. WEAVER, *University of Washington.*—Standard Ilford G5 plates have been exposed to a flux of 7.7×10^5 particles per cm^3 in the 145-Mev (nominal energy) external π^+ beam of the Chicago cyclotron. About two pion-proton scatterings can be found and measured per hour using area scanning techniques.[1] The possibility of obtaining a large number of events will make feasible a determination of the phase shifts more accurate than previously obtained. As of February 15, 54 events had been analysed to give a total cross section of (169±23) millibarns. The mean pion energy will be determined from events where the proton stops in the emulsion. So far too small a number of such events have been found to make an accurate determination. Least squares analysis of the angular distribution in the barycentric system gives $d\sigma/d\omega = (5.0\pm2.5) - (6.8\pm3.6)\cos\chi + (25.2\pm10.0)\cos^2\chi$ in millibarns per steradian. This curve gave a good fit to the data lumped into six experimental points each containing nine events. With improved statistics this experiment offers the possibility of detecting d-wave phase shifts. We hope to improve the statistics by at least a tenfold increase of the data.

[1] Jay Orear, Phys. Rev. 92, 156 (1953).

K8. High-Energy Electrons in the Capture of μ^- Mesons by Complex Nuclei.* S. LOKANATHAN, J. STEINBERGER, AND H. B. WOLFE, *Columbia University.*—We have searched for high-energy electrons produced in the reactions $\mu^-+p\rightarrow p+e^-$ and $\mu^-+n\rightarrow n+e^-$. These electrons are expected to have an energy distribution peaked near 100 Mev, and to have an average energy of 85 Mev. μ^- mesons produced in the Columbia University cyclotron were stopped in targets of several materials. The electrons were to be observed in a three-counter telescope in delayed coincidence with the incoming meson. The system was calibrated by means of the electrons from normal μ^- decay, and then absorber was inserted to discriminate against these. No positive evidence for the reaction was found. The fraction of *captured* muons which result in electrons is (0.007±0.031) for Al, (−0.0007±0.0047) for Cu, and (−0.0014±0.0043) for Cd. We can therefore place an upper limit of 0.003 on this fraction. This implies that the strength of the coupling, g^2, for this type of β-decay process is at least 2000 times smaller than that of the dominant capture reaction.

* This work was performed under the joint program of the U. S. Office of Naval Research and the U. S. Atomic Energy Commission.

K9. Production of Neutrons by Negative μ Mesons Stopped in Various Absorbers.* D. R. JONES, *Washington University.*† —Measurements of the production of neutrons by negative mesons which stop and interact in two materials, sodium and magnesium, are reported. The mean number of neutrons emitted per interaction was measured and found to be 0.6 ±0.2 for magnesium and 1.0±0.4 for sodium, where the uncertainties quoted include an estimated contribution from systematic sources as well as those of a statistical nature.

The data confirm that relative neutron production in magnesium is less than in lead, but show that it is not zero. Neutron production in sodium is also shown to be nonzero and probably greater than in magnesium, though less than in lead. In the course of the experiment a value of $1.18^{+0.18}_{0.14}$ μsec (statistical) was found for the mean life of negative μ mesons in sodium.

* Supported by the joint program of the U. S. Office of Naval Research and the U. S. Atomic Energy Commission.
† Now at the University of Cincinnati.

K10. X-Rays from π Mesic Atoms.* A. D. McGuire, M. Camac, M. L. Halbert, and J. B. Platt, *University of Rochester.*—The π^- meson beam of the University of Rochester 240 Mev synchrocyclotron was used to study the x-rays produced by pion transitions between atomic bound states. Particular attention was paid to the $2p-1s$ transitions. Well collimated, magnetically analyzed 50 Mev π^- mesons were detected by a 3 fold counter telescope and allowed to stop in various materials of low Z. The resulting x-rays were detected by a NaI scintillation counter in time coincidence with the telescope. The energy loss in the NaI crystal was recorded using a 25 channel pulse-height selector. The transitions were identified on the basis of pulse height in the NaI counter which was calibrated with known energy x-rays from radioactive sources. The probability that a stopped π^- meson makes a $2p-1s$ radiative transition was measured for mesons stopping in Be, B, C, N, and O. Preliminary results are 0.21, 0.14, 0.065, 0.04 and 0.01, respectively, with an error of 0.02 in each case. Account was taken of (1) and NaI counter efficiency and solid angle, (2) attenuation and scattering of the x-rays in leaving the stopping material, and (3) muon and electron contamination of the pion beam.

* Work supported by the U. S. Atomic Energy Commission.

K11. Energy Measurements of Meson X-Rays.* M. B. Stearns, M. Stearns, L. Leipuner, and S. DeBenedetti, *Carnegie Institute of Technology.*—The critical absorption technique is being used to study the x-ray energy of the $2p-1s$ transition of pions captured in beryllium. Since a small energy shift could be contributed by secondary effects (Compton degradation, fluorescent x-rays) other lines of similar energy were examined. The π-Phosphorus M-line computed for a point nucleus (without polarization and radiative corrections) is below the stated value[1] of the K edge of cerium ($Z=58$) for $m_\pi/m_e=272.5$, and above it for $m_\pi/m_e=273$. Comparative absorption measurements in successive elements show that it is above this edge. This indicates that the Compton degradation does not appreciably affect the result and gives a lower limit for the meson mass. Similar measurements show that the π-Fluorine L-line and μ-Beryllium K-line fall between the predicted edges. The π-Beryllium K-line should fall 330 volts above the edge of Neodymium ($Z=60$) for $m_\pi/m_e=273$. Instead, the experiments indicate that it lies below this edge, an effect possibly connected to a repulsion between the nucleus and the pion in the $1s$ state. Measurements of energies of other lines are in progress.

* Supported by the U. S. Atomic Energy Commission.
[1] Hill, Church, and Mihelich, Rev. Sci. Instr. **27**, 523 (1952).

K12. Mass of the μ^- Meson from Mesonic X-Rays.* S. Koslov, V. Fitch, and J. Rainwater, *Columbia University.*—The precise measurement of mesonic atom x-ray energies in the 15–90 kilovolt range has been applied to the determination of negative meson masses. A filter technique using thin filters of various elements between the NaI (Tl) crystal of a scintillation spectrometer[1] and the mesonic atom allows a statement to be made as to whether the x-ray energy for a transition with small natural line width lies above or below the photoelectric K-shell absorption limit in a particular filter element. The precision of an upper or lower limit for the x-ray energy is thus equivalent to high-precision absorption limit measurements.[2] $2p-1s$, $3d-2p$, and $4f-3d$ mesonic transitions in various elements have been selected for their proximity to K-absorption limits. Energy level shifts due to nuclear penetration are small in the particular transitions used. Preliminary results indicate that the mass of the μ^- meson is between 206.36 and 208.22 electron masses (subject to quantum electrodynamic corrections). Measurements now in progress indicate that closer assignments of the μ^- mass limits are possible and will be reported. This method is also being applied to the mass of the π^- meson.

* This work was performed under the joint program of the U. S. Office of Naval Research and the U. S. Atomic Energy Commission.
[1] V. Fitch and J. Rainwater, Phys. Rev. **92**, 789 (1953).
[2] Y. Cauchois and H. Hulubei, *Table de Constantes Selectionnes Longuers D'Onde Des Emissions X Et Des Discontinuities D'Absorption X* (1947).

Friday Morning at 9:30

Sheraton Park, Continental Room

(M. L. Perlman presiding)

Radioactive Nuclei, II

KA1. Disintegration of Ce^{139}. C. H. Pruett and R. G. Wilkinson, *Indiana University.**—The radiations of 140-day Ce^{139} have been examined with a 180° magnetic spectrometer and a coincidence gamma-scintillation spectrometer. Sources were prepared from deuteron activated lanthanum. The electron spectrum consists only of Auger electrons and conversion electrons corresponding to the K, L, and M conversion of a single gamma ray at 166 kev. No positrons were found. The $K/L+M$ ratio was found to be 6.6 and the ratio of Auger electrons to K conversion electrons was 0.34. The simple nature of the decay was confirmed by the scintillation pulse height spectrum. Only photoelectron peaks resulting from LaKα x-rays and the 166-kev gamma ray were present. The results of a scintillation coincidence experiment, when combined with the beta-ray spectrometer data yield a value the K-conversion coefficient consistent with an M-1 classification of the gamma ray. This was further substantiated by delayed coincidence measurements, the results of which place a lower limit of 10^{-8} sec on the lifetime of the single excited state.

* Supported by the joint program of the U. S. Office of Naval Research and U. S. Atomic Energy Commission.

KA2. Anisotropic Gamma Radiation from Aligned Ce^{141} Nuclei.* E. Ambler, R. P. Hudson, *National Bureau of Standards,* and G. M. Temmer, *Department of Terrestrial Magnetism.*—We have observed a fourteen percent anisotropy in the counting rate of the 143-kev gamma ray following beta decay of Ce^{141}. The alignment was achieved by the method of

Bleaney (zero residual field), using three single crystals of cerium-magnesium nitrate, reaching demagnetization temperatures of about 0.003°K.[1] The alignment occurs in a *plane* rather than along an axis, as predicted.[2] Scintillation counter A was located in that plane and counter B at right angles to it. Some twelve demagnetizations gave essentially identical results for the 400-second warm-up period, showing the decay of the anisotropy. No effect was observed when the counters viewed the sample at 45° and 135° to the alignment plane. The fact that counting rate A was higher permits us to conclude that the gamma-ray transition in Pr^{141} is predominantly magnetic dipole. Internal conversion data[3] admit both $M1$ and $E2$ transitions ($7/2^+ \rightarrow 5/2^+$). The gamma ray in Pr^{141} is also very weakly Coulomb-excited ($E2$ process)[4] supporting our observations. Estimates of the magnetic moment of Ce^{141} will be made.

* Assisted by the U. S. Office of Naval Research.
[1] J. M. Daniels and F. N. H. Robinson, Phil. Mag. **44**, 630 (1953).
[2] R. J. Elliott and K. W. H. Stevens, Proc. Roy. Soc. (London) **A215**, 437 (1952).
[3] E. Kondaiah, Phys. Rev. **83**, 471 (1951).
[4] G. M. Temmer and N. P. Heydenburg, Phys. Rev. **93**, 351 (1954).

KA3. The Disintegration of Pm^{150}.*† VERA KISTIAKOWSKY FISCHER, *University of California and U. S. Naval Radiological Defense Laboratory.*—The gamma rays of the 2.7 hour half-life isotope Pm^{150} have been investigated with a "grey wedge" scintillation spectrometer in coincidence either with a proportional counter or with a scintillation counter and single channel pulse-height analyzer. Beta-ray spectrometer studies previously reported[1] show 2.01- and 3.00-Mev negatrons to be emitted. More than ten gamma rays ranging in energy from 0.14 to 2.4 Mev are observed in coincidence with the two beta particles. Their energies will be given and a possible decay scheme will be discussed. Some conclusions on the beta decay stability of Nd^{150} will be drawn.

* This work was sponsored in part by the U. S. Atomic Energy Commission.
† The completion of this study was made possible by the Sarah Berliner fellowship (1953–54) of the American Association of University Women.
[1] Vera Kistiakowsky, Phys. Rev. **87**, 859–60 (1952).

KA4. Lifetime Measurements of Fast E2 Transitions in Even-Even Nuclei. A. W. SUNYAR, *Brookhaven National Laboratory.**—A delayed coincidence scintillation spectrometer of short resolving time has been utilized in half-life determinations of a number of fast[1] $E2$ transitions in even-even nuclei. Our results are summarized in Table I. With the exception of the Po^{210} transition, all transitions are between the 2+ first excited state and the 0+ ground state of even-even nuclei. A consideration of the matrix elements for all $E2$ transitions of measured lifetime in even-even nuclei shows a smooth variation of the matrix element with Z. Maximum matrix elements occur near $Z=68$. The matrix elements reduce as the proton number increases toward the magic number 82. At $Z=84$, the matrix element for the Po^{210} transition is large.

TABLE I.

Nucleus	E (kev)	$T_{1/2} \times 10^9$ seconds
Sm^{152}	122	1.40
Hf^{180}	93	1.39
W^{182}	100	1.27
Os^{188}	155	0.65
Po^{210}	46.4[2]	1.52

* Work done under the auspices of the U. S. Atomic Energy Commission.
[1] M. Goldhaber and A. W. Sunyar, Phys. Rev. **83**, 906 (1951).
[2] Mihelich, Schardt, and Segrè (private communication).

KA5. Low-Energy Transitions in Gadolinium and Related Rare-Earth Activities.* E. L. CHURCH,† *Argonne National Laboratory,* AND M. GOLDHABER, *Brookhaven National Laboratory.*—The neutron-capture conversion-electron spectrum of gadolinium has been investigated with a 180°-focusing beta-ray spectrograph. Transitions of 79.1, 181.7 and 88.8, 198.7 kev were observed using normal gadolinium. Comparison with a target having its isotopic constitution altered by long-term neutron bombardment indicates the assignment of the above pairs of transitions to $_{64}Gd^{156}$ and $_{64}Gd^{156}$, respectively. Comparison of fission-product and normal europium activities assigns transitions of 121.8, 244.3 and 123.4, 247.7 kev to $_{62}Sm^{152}$ and $_{64}Gd^{154}$, respectively. The electric-quadrupole character of these transitions will be discussed with reference to the collective model. Levels in Gd^{156} were also populated by beta decay from 14.0±1.0-day Eu^{156} formed by neutron capture in long-lived Eu^{155}. The decay of Eu^{155} excites strong transitions of 59.8, 86.3, and 105.1 kev in $_{64}Gd^{155}$. Reported gammas of ~130 kev are due to a misinterpretation of the conversion lines of a Eu^{156} impurity. The decay of Gd^{153} yields transitions of 69.4, 97.3, and 103.1 kev in $_{63}Eu^{153}$. Only the first and last of these are seen following the decay of Sm^{153}. Possible decay schemes of these nuclei will be considered. (Absolute energy uncertainties ~0.5 kev.)

* Based in part on a doctoral investigation carried out at Brookhaven, 1951–1952.
† On loan from Frankford Arsenal, Philadelphia, Pennsylvania.

KA6. Radiations from Ho^{164}.* H. N. BROWN,† F. B. SMITH, AND R. A. BECKER, *University of Illinois.*—Samples of holmium oxide and metallic holmium, irradiated with 22-Mev x-rays, yielded a 36.7±0.5-minute activity which was attributed to Ho^{164}. This is consistent with the values given in the table of K. Way.[1] Pulse-height measurements, with NaI (Tl) and a proportional counter, indicated the presence of radiation of energies 37, 46, 73, and 90 kev. Magnetic spectrometer data yielded conversion electrons consistent with $90-L$, $90-M$, $73-K$, $73-L$, $73-M$, $37-L$, $(37-M+90-K)$, $46-L$, and $46-M$ superimposed upon a beta continuum with end-point 990±30 kev. The continuum is consistent with two groups separated by about 90 kev. Pulse-height measurements of coincidences showed gamma-gamma coincidences: 46–73, 46–46, and 37–46, and beta-gamma coincidences involving 90- and 49-kev radiation The 49-kev radiation was attributed to characteristic erbium x-rays. Most of the 46-kev radiation is thought to be characteristic x-rays from dysprosium, consistent with K-capture branching of the parent nucleus. All radiations followed, within experimental error, the 36-minute half-life. Tentative level schemes will be discussed.

* Supported in part by the U. S. Atomic Energy Commission and U. S. Office of Naval Research. The Ames Laboratory is to be thanked for rare earth samples.
† National Science Foundation fellow.
[1] Nuclear Data, Natl. Bur. Standards Circ. 499.

KA7. The Disintegration of Ta^{182}. J. W. MIHELICH, *Brookhaven National Laboratory.**—The excited levels of W^{182} reached by β emission from Ta^{182} and electron-capture from Re^{182} have been investigated using scintillation counters, β spectrometers, and coincidence techniques. Multipolarity assignments have been made for all transitions. The data indicate that of the eight possible partial level arrangements suggested by Muller *et al.*,[1] using their accurate energy determinations, only (b) of Fig. 14[1] is reasonable. It has been established that the 100-kev transition from the first excited 2+ level is in coincidence with the γ rays of 1121 and 1188 kev, but not with the one of 1223 kev. It is probable that the level designated as "f"[1] has an excitation energy of 1223 kev and that the transitions of 1121 and 1223 kev proceed from it, while the transition of 1188 kev proceeds from level "a" at 1291 kev, and that this level is responsible for the lifetime of 1.03×10^{-9} sec recently observed.[2]

* Work done under the auspices of the U. S. Atomic Energy Commission.
[1] Muller, Hoyt, Klein, and DuMond, Phys. Rev. **88**, 775 (1952).
[2] A. W. Sunyar, Phys. Rev. (to be published).

KA8. Gamma-Ray Studies of Re^{186}.* J. P. HURLEY AND P. S. JASTRAM, *Washington University.*—A study has been made of the decay scheme of Re^{186}, using a scintillation coincidence spectrometer, in an attempt to resolve the apparently contradicting results of the magnetic spectrometer and the beta-gamma angular correlation measurements: the pronounced (70 percent) beta-gamma anisotropy which should result from a first-forbidden unique transition is not found. A test of the possibility that the correlation is attenuated by interaction between the nuclear magnetic dipole or electric quadrupole moment with the magnetic field of the electron shell is afforded by the angular correlation between the gamma rays which cascade through the state in question. This work is now in progress with preliminary results indicating that both transitions are electric quadrupole and requiring that the spin assignments be 0–2–2 for the ground state and the two excited states of Os^{186}.

* Supported by the joint program of the U. S. Office of Naval Research and the U. S. Atomic Energy Commission.

KA9. The Beta Spectra of Re-186 and Re-188.* DONALD GUSS, LAWRENCE KILLION, AND F. T. PORTER, *Washington University.*—The 14-cm radius of curvature 180° spectrometer has been used to reinvestigate in detail the shapes of the beta spectra of Re-186 and Re-188. For Re-186 the assumption that the ground-state transition (1064±4-kev end point) has the allowed shape yields a spectrum for the first inner group which does not have an allowed shape. Application of the ($\Delta I=2$, yes) unique correction factor gives a linear FK plot for the first inner group with end-point energy 928±12 kev in good agreement with the observed 137-kev gamma ray from the 1st excited state in the even-even daughter Os-186. For the ground-state transition log ft = 7.71; for the transition to the first excited state log $(2I_f+1)ft=8.35$. These results suggest assignment of zero spin and odd parity for ground state of Re-186 rather than spin 1.[1] For Re-188 no analysis has been found that will yield an unambiguous interpretation of the measured spectra. It appears possible that both of the principal beta groups have nonallowed shapes.

* Supported by the joint program of the U. S. Office of Naval Research and U. S. Atomic Energy Commission.
[1] F. R. Metzger and R. D. Hill, Phys. Rev. **82**, 646 (1951).

KA10. The Radiations of Ir^{192m}.* J. P. MIZE, J. W. STARNER, AND M. E. BUNKER, *Los Alamos Scientific Laboratory.*—An investigation of the radiations accompanying the radioactive decay of Ir^{192m} (1.42-min) has been performed with a NaI(Tl) scintillation spectrometer and an aluminum-lined proportional counter. An interest in this isomer was prompted by the previously reported gamma-ray continuum accompanying the decay of Ir^{192m} and the proposed interpretation of the continuum as being engendered by "two-quantum" emission.[1,2] Examination of the photon spectrum revealed the presence 57.4-kev quanta, iridium L x-rays, and a low-intensity continuum extending to ~50 kev. From a measurement of the relative intensities of the 57.4-kev quanta and the iridium L x-rays produced by interval conversion of the 57.4-kev transition, we have calculated the L-shell conversion coefficient of this gamma ray. If one assumes that the gamma-transition is $E3$, then $\alpha_L \simeq 750$. On the basis of absorption and coincidence measurements, the continuum is attributed to bremsstrahlung produced by conversion electrons from the highly converted 57.4-kev gamma ray.

* Work done under the auspices of the U. S. Atomic Energy Commission.
[1] Goldhaber, Muehlhause, and Turkel, Phys. Rev. **71**, 372 (1947).
[2] E. der Mateosian and M. Goldhaber, Phys. Rev. **82**, 115 (1951).

KA11. The Decay of Pt^{199}. J. M. LEBLANC, J. M. CORK,* AND S. B. BURSON, *Argonne National Laboratory.*—The beta and gamma rays associated with the decay of 30-min Pt^{199} have been studied using 180° photographic spectrometers and a 10-channel coincidence scintillation spectrometer. The beta rays were studied by measuring their attenuation in Al. Sources were obtained by irradiating normal PtO in the Argonne heavy water reactor. Nine gamma rays of energies 0.07, 0.197, 0.246, 0.316, ~0.48, 0.54, 0.71, 0.78, and 0.96 were found to decay with a 30-min half-life and are therefore assigned to this activity. Conversion electron lines were obtained for the 0.197, 0.246, and 0.316-Mev gamma rays. The results of beta-gamma coincidence measurements indicate that the 0.197, 0.246, 0.316, and 0.54-Mev gamma-rays are in coincidence with beta rays having an end point energy of about 1.2. Gamma-gamma coincidences will be discussed.

* University of Michigan.

KA12. The Decay of Hg^{195}.* C. H. BRADEN, E. T. PATRONIS, JR., AND L. D. WYLY, *Georgia Institute of Technology.*—We have investigated the Hg activities produced by the bombardment of Au with protons in the Oak Ridge 86-in. cyclotron. Hg was chemically separated from Au and Pt. Scintillation counters were used to determine the gamma spectrum of the decay. Protons slowed to 12 Mev produced an activity showing a weak 280-kev gamma line in addition to a 130-kev line and a strong line of about 70 kev. The 130-kev line is definitely associated with the K-capture decay of Hg^{197}. The fact that other known lines in the decay of Hg^{197} were not resolved is attributed to the strong internal conversion. Bombardment with 20-Mev protons produced an activity that shows gamma lines of 1200 kev (very weak), 810 (weak), 580 (weak), and 270 (strong). The latter three lines all decay with the same half life of approximately 42±5 hours and are all in coincidence with the strong x-ray line of about 70 kev. The 1200-kev line seems to also decay with the same half-life, but owing to the low intensity our measurements are not precise. We assign these lines to the decay of Hg^{195} produced by the Au $(p,3n)$ Hg^{195} reaction. The decay of Hg^{195} therefore gives rise to Au^{195} which is known to decay with a half-life of 183 days. A separation of Au from the Hg after a few weeks shows a Au activity of long half-life.

* Supported in part by a grant from the National Science Foundation.

KA13. Resonance Fluorescence with Nuclei: Tl^{203}.* F. R. METZGER AND W. B. TODD, *Bartol Research Foundation.*—Hg^{203} decays to the ground state of Tl^{203} by the emission of a beta ray followed by a 280-kev gamma ray. The 280-kev gamma rays were used to irradiate thallium in an attempt to observe resonance fluorescence. In order to utilize the recoil momentum distribution produced by the beta-ray emission, gaseous sources of Hg^{203} were used. However, the lifetime of the 280-kev state turned out to be longer than the collision time of the Tl^{203*} ions in the mercury vapor. Thus most of the recoiling Tl^{203*} nuclei had reached thermal equilibrium before they emitted the 280-kev radiation. The increase in counting rate observed upon heating of the Hg^{203} sources to 900 degrees centigrade was therefore almost completely due to the thermal Doppler broadening of the 280-kev line. Based on preliminary measurements with two different sources the lifetime τ_γ for the 280-kev transition is estimated as $(1\pm0.4)\times10^{-9}$ sec. From Weisskopf's formula[1] one estimates for a 280-kev magnetic dipole transition a lifetime of 1.5×10^{-12} sec.

* Assisted by the joint program of the U. S. Office of Naval Research and the U. S. Atomic Energy Commission.
[1] V. F. Weisskopf, Phys. Rev. **83**, 1073 (1951).

KA14. Gamma-Ray Spectrum of Po^{209}. E. H. DAGGETT AND G. R. GROVE, *Mound Laboratory.**—A polonium sample was produced at ORNL by the bombardment of bismuth targets with 20-Mev protons. The sample contained a mixture of the polonium isotopes of mass 208 and 209 with a negligible amount of Po^{192}. Measurements were made of the isotopic ratio from the molecular spectrum and the alpha activity by calorimetry. The spectrum obtained with a NaI

(Tl) crystal and pulse-height analyser showed the existence of gamma rays with energies of about 270, 570, and 865 kev. The 803-kev gamma ray of Po^{210} was not detectable. This spectrum is attributed to Po^{209} since there is no gamma radiation from Po^{208}.[1] The intensity of the 865-kev gamma ray relative to the gamma ray of a calibrated Po^{210} sample was estimated to be about 7.5×10^{-3} quanta per 209 alpha particle. Coincidence measurements between various pairs of gamma rays indicated that only the 270- and 570-kev quanta were in cascade and existed with about the same relative intensity as the 865-kev gamma ray.

* Mound Laboratory is operated by Monsanto Chemical Company for the United States Atomic Energy Commission.
[1] Templeton, Howland, and Perlman, Phys. Rev. **72**, 758 (1947).

KA15. The $\alpha-\gamma$ Angular Correlation in the Decay of Ra^{224}, Ra^{226}, and Pu^{238}. J. C. D. MILTON AND J. S. FRASER, *Chalk River Laboratories.*—The angular correlation of the 241-, 186-, and 45-kev γ rays from the first excited states of the daughter nuclei following the α decay of Ra^{224}, Ra^{226}, and Pu^{238} have been measured using NaI detectors with pulse-height selection for both radiations and a coincidence resolving time of 1.4×10^{-8} sec. The data were taken automatically at 5° or 15° intervals between 90° and 220°. A weighted least squares fit to $W(\theta)=1+A_2P_2(\cos\theta)+A_4P_4(\cos\theta)$ gave for Ra^{224}, Ra^{226}, and Pu^{238}, respectively: $A_2=0.534\pm0.014$, 0.490 ± 011, 0.330 ± 037; $A_4=-1.739\pm0.023$, -1.299 ± 0.023, -1.145 ± 0.065. The errors shown are statistical only. Angular resolution corrections have been applied. The transitions are of the type 0–2–0 for which the theoretical values are $A_2=0.714$, $A_4=-1.714$. That the quadrupole moment is responsible for the deviations from theory is indicated by the facts that A_4 is attenuated less than A_2,[1] and that the attenuation increases with increasing neutron number.[2] The effect of the chemical constitution of the sources was not investigated. They were evaporated from solution on mica 1 mgm/cm² thick: the Ra^{224} from radiothorium in HNO_3, Ra^{226} from radium in HCl and Pu^{238} from plutonium in HNO_3.

[1] A. Abragam and R. V. Pound, Phys. Rev. **92**, 943 (1953).
[2] K. W. Ford, Phys. Rev. **90**, 29 (1953).

KA16. Gamma Radiation from the Decay of UX_2 (Pa^{234}). W. G. CROSS AND T. A. EASTWOOD, *Chalk River Laboratories.*—The gamma rays from the decay of UX_2 have been measured with a NaI scintillation spectrometer. Lines were observed at 0.758 ± 0.010, 0.998 ± 0.010, 1.49 ± 0.03, 1.7 ± 0.06 and 1.84 ± 0.03 Mev, with respective relative intensities of 0.65, 1.00, 0.03, 0.03, and 0.1. Between 0.3 and 0.7 Mev no nuclear gamma ray was observed with relative intensity greater than 0.1, the limit of detection being set by the relatively strong bremsstrahlung spectrum. No $\gamma-\gamma$ coincidences were detected between the 0.998- and 0.758-Mev lines. The 0.998-Mev radiation occurs in 1 percent of the disintegrations. An upper limit of 2×10^{-3} per disintegration was obtained for the emission of γ rays between 0.78 and 0.83 Mev, for which conversion electrons have been reported.[1,2] The observed γ intensities are considerably smaller than would be required to fit the β spectrum analysis made by Heerschap *et al.*[3]

[1] Bradt, Heine, and Scherrer, Helv. Phys. Acta **16**, 455 (1943).
[2] Heerschap, Hok, and Sizoo, Physica **16**, 767 (1950).

FRIDAY MORNING AT 9:30

Shoreham, Main Ballroom

(P. H. ABELSON presiding)

Electric Excitation of Nuclei; Photonuclear Reactions

Invited Paper

L1. Coulomb Excitation of Nuclear Energy Levels by Alpha-Particles. G. M. TEMMER, *DTM, Carnegie Institution of Washington.* (30 min.)

Contributed Papers

L2. Electric Excitation of Mn^{55} with Protons. HANS MARK, CLYDE MCCLELLAND, AND CLARK GOODMAN,* *M.I.T.*—Thin (20- and 40-kev) targets of Mn evaporated on Pb were bombarded with monoenergetic protons from the Rockefeller Generator. The yield of the 133-kev γ ray[1] was measured as a function of proton energy E_p between 0.550 and 2.40 Mev. From 0.55 to 1.0 Mev the normalized yield fits the characteristic electric quadrupole excitation function fairly well. Above 1.0 Mev, the yield shows marked resonances indicating compound nucleus formation. Five γ rays, having energies of 133, 420, 505, 650, and 975 kev, were observed at $E_p=2.12$ Mev. The 133 kev γ ray comes from the first excited state of Mn^{55}. The 420- and 975-kev γ rays probably come from[2] $Mn^{55}(p,n,\gamma)Fe^{55}$. The origin of the 505- and 650-kev γ rays is not yet certain. Measurement of the absolute cross section of the excitation of the 133-kev γ ray at low proton energies is in progress.

* This work has been supported by the joint program of the U. S. Office of Naval Research and the U. S. Atomic Energy Commission.
[1] Reported as 128 kev by G. M. Temmer and N. P. Heydenburg, Bull. Am. Phys. Soc. **29**, 10 (1954).
[2] P. H. Stelson and W. M. Preston, Phys. Rev. **82**, 655 (1951).

L3. Electric Excitation of Gold.* J. EISINGER, C. F. COOK, AND C. M. CLASS, *Rice Institute.*—The gamma-ray spectrum obtained from the electric excitation of gold has been studied using protons accelerated by the 5.5-Mev Van de Graaff. At a bombarding energy of 3-Mev, lines at 191, 279 and 555 kev were observed. The thin target yield curves of the 279- and 555-kev lines have been measured between 2 and 5 Mev and were found to lie substantially above the theoretical curves[1] at the high energies as was found by Goldburg and Williamson.[2] The angular distributions of these lines were also obtained. The data for the 279-kev radiation can be fitted by $1-0.19\cos^2\theta$ and the distribution of the 555-kev radiation is $1+0.21\cos^2\theta$. The latter distribution agrees with theory[1] if it is assumed the excited state has a spin of 7/2.

* Work supported by the U. S. Atomic Energy Commission.
[1] K. Alder and A. Winther, Phys. Rev. **91**, 1578 (1953).
[2] W. I. Goldburg and R. M. Williamson, Bull. Am. Phys. Soc. **29**, No. 1, 10 (1954).

L4. Coulomb Excitation of Gold. W. I. GOLDBURG, S. A. COX, AND R. M. WILLIAMSON, *Duke University.*—A further study has been made of the strongest gamma rays (277±5 kev

and 545±8 kev) resulting from the Coulomb excitation of gold by four Mev protons.[1] The anisotropy of the 277-kev gamma ray is −15±5 percent; this agrees best with a 7/2→5/2 $M1$ transition. The 545-kev gamma-ray anisotropy is +25±5 percent in agreement with a 7/2→3/2 $E2$ transition. Coincidence counting equipment of 0.1 μsec resolving time has been used to determine that the number of coincidences between the 277 kev and a possible 268-kev cascade gamma is less than 5 percent of the number of 277-kev transitions.[2] Hence, we are led to the conclusion that the lower-energy gamma ray goes to the ground state and is the same one observed from beta-decay experiments[3] to occur at 279 kev—in spite of the observed angular distribution. The coincidence of the 137-kev and the 166-kev gamma rays in Ta was verified. A more careful survey of weaker lines from a spectroscopically pure gold sample is now in progress.

* This work supported by the U. S. Atomic Energy Commission.
[1] W. I. Goldburg and R. M. Williamson, Bull. Am. Phys. Soc. **29**, No. 1, 10 (1954).
[2] K. Alder and A. Winther, Phys. Rev. **91**, 1578 (1953).
[3] J. W. Mihelich and A. de-Shalit, Phys. Rev. **91**, 78 (1953).

L5. Coulomb Excitation *vs* Compound Nucleus Formation in the Lighter Elements. N. P. Heydenburg and G. M. Temmer, *DTM, Carnegie Institution of Washington.*—We have obtained thin target excitation curves for gamma-ray emission from low-lying excited states of F^{19},[1] Na^{23}, Mn^{55}, Fe^{57}, and Ge^{73} under alpha-particle bombardment up to 3.5 Mev. In the cases of F^{19} and Na^{23} we also followed the 1.28-Mev and 1.83-Mev gamma rays resulting from the $(\alpha,p\gamma)$ reactions, coming from Ne^{22*} and Mg^{26*}, respectively. Fe^{57} and Ge^{73} were enriched samples (to 59 percent and 78 percent, respectively) obtained from Oak Ridge. All targets were evaporated on thin nickel foil. The $(\alpha,p\gamma)$ reactions give a measure of the compound nucleus formation and show that the targets were thin. We observed the Coulomb and/or inelastic excitation of the 113-kev and 196-kev levels in F^{19}, the 446-kev level in Na^{23}, the 128-kev level in Mn^{55}, the 122-kev line coming from the 136-kev level in Fe^{57}, and a 68-kev line in Ge^{73} (obviously not the 68-kev $M4$ transition which is not seen in the As^{73} decay.[2] The excitation of the reaction gamma rays and the inelastic (Coulomb) gamma rays are strikingly different. The thin target yields are in good agreement with the simple theory of Coulomb excitation for $E2$ transition.[3]

[1] G. M. Temmer and N. P. Heydenburg, Phys. Rev. **93**, 351 (1954); and Phys. Rev. (to be published).
[2] Welker, Schardt, Friedlander, and Howland, Phys. Rev. **92**, 401 (1953).
[3] K. Alder and A. Winther, Phys. Rev. **91**, 1578 (1953).

L6. Photodisintegration of Deuterium by 95-Mev Bremsstrahlung.* Lew Allen, Jr.,† and A. O. Hanson, *University of Illinois.*—Investigation of the deuterium photoeffect has been continued using betatron x-rays of 95-Mev maximum energy. The target volume was defined by tungsten slits. The photoprotons were detected by stacks of 600μ pellicles placed at seven angles between 20° and 160°. Proton energies were determined by range measurements and separated into five energy bins. The statistical error of each differential cross section is less than 10 percent. The curve of total cross section *versus* photon energies between 20 and 65 Mev is in agreement with calculations by Marshall and Guth and Schiff for central forces of 50 percent exchange character. The angular distributions are well fitted by $f(\theta)=(\alpha+\sin^2\theta)(1+2\beta\cos\theta)$, where α varies from 0.12 at 20 Mev to 0.8 at 62 Mev, and β is about $\frac{1}{3}$ (V_P/C).

* This work is supported in part by the joint program of the U. S. Office of Naval Research and the U. S. Atomic Energy Commission.
† Captain, U. S. Air Force, assigned USAF Institute of Technology.

L7. Fine Structure of the $O^{16}(\gamma,n)O^{15}$ Activation Curve.* B. M. Spicer, A. S. Penfold, and J. Goldemberg, *University of Illinois.*—The activation curve has been measured from threshold to 19 Mev by counting the O^{15} positron activity induced in cylinders of compressed boric acid. The curve shows discontinuities in slope at energies 15.60, 15.97, 16.45, 16.68, 16.86, 16.94, 17.04, 17.43, 17.54, 17.66, 17.72, 17.88, 18.48, 18.73, 18.91 Mev. These results will be compared to those of Montalbetti and Katz,[1] who find breaks at 15.6, 15.9, 16.7, 16.9, 17.1, 18.4, 18.7 Mev. The relative positions of these breaks can be reproduced to within ±10 kev. Operating stability of the betatron was often better than ±6 kev, with periodic deterioration to ±30 kev. The absolute energy scale was calibrated by determining thresholds for the $C^{12}(\gamma,n)C^{11}$, $O^{16}(\gamma,n)O^{15}$, $Cu^{63}(\gamma,n)Cu^{62}$ reactions, taken as 18.72, 15.61, 10.65 Mev, respectively, and is believed accurate to ±20 kev. The activation curve was also measured behind 1 electronic absorption length of water. Detailed information will be presented regarding the interpretation of these curves.

* Supported in part by the joint program of U. S. Office of Naval Research and U. S. Atomic Energy Commission.
[1] R. Montalbetti and L. Katz, Can. J. Phys. **31**, 798 (1953).

L8. Photo Protons from Cobalt.* M. E. Toms, H. Gerardo, and W. E. Stephens, *University of Pennsylvania.*—The photoprotons ejected from a 0.7-mil cobalt foil by the bremsstrahlung x-rays from a 24-Mev betatron have been observed in nuclear emulsions. The angular distribution shows a slight forward asymmetry consistent with the results of Mann, Halpern, and Rothman.[1] The energy distribution is consistent with that calculated from an evaporation process. In contrast to copper[2] which has similar thresholds, no evidence was found for photodeuterons. However, there is approximately one photo alpha particle for every 54 photoprotons. Further details will be presented.

* Supported in part by the joint program of the U. S. Office of Naval Research and the U. S. Atomic Energy Commission.
[1] Mann, Halpern, and Rothman, Phys. Rev. **87**, 146 (1952).
[2] Byerly and Stephens, Phys. Rev. **83**, 54 (1951).

L9. The $In^{115}(\gamma,\gamma')In^{115m}$ Cross Section.* J. L. Burkhardt† and E. J. Winhold, *M.I.T.*—The photoexcitation yield of the 4.5 hr isomeric state in In^{115} has been measured at a series of energies from 2 to 14 Mev. Stacked foils were exposed directly in the electron beam from the M.I.T. linear accelerator. A lower limit to the photon absorption cross section is obtained from this measurement. Even though an unknown fraction of the excited nuclei decay to the ground state and are not detected, the experimental data may give an indication of the actual shape of the absorption cross section in the region below particle emission thresholds. The cross section computed from the observed yield curve exhibits a strong maximum at about 8 Mev, as has been reported by others.[1] In the low-energy region the cross section appears to rise continuously, its slope increasing rapidly with increasing energy. At 5 Mev the cross section is about ten percent of the peak value.

* This work was supported by the joint program of the U. S. Office of Naval Research and U. S. Atomic Energy Commission.
† National Science Foundation Predoctoral Fellow.
[1] Goldemberg and Katz, Phys. Rev. **90**, 308 (1953).

L10. Angular Distributions of Photodeuterons.* D. A. Edwards, B. Wolfe, A. Silverman, and J. W. DeWire, *Cornell University.*—The angular distributions of energetic deuterons emitted from various nuclei upon exposure to 300-Mev bremsstrahlung are being investigated, employing a technique reported previously by DeWire, Silverman, and Wolfe.[1] Preliminary results indicate that the angular distributions of deuterons of 40-Mev average energy are roughly the same as those for photoprotons of that energy, for the four elements studied thus far: C, Cu, Ag, and Pb. The ratios of the number of deuterons to the number of protons per unit energy interval at 90° have been measured for Be, Al, Mo, and W in addition to the four elements mentioned in the foregoing. These ratios increase with A from 0.12 for C to 0.24 for Pb (with ten percent statistics); the ratio for Be is 0.21. The

ratios at 90° for C, Cu, and Pb are in agreement with the results reported earlier.[1]

* Supported by the joint program of the U. S. Office of Naval Research and the U. S. Atomic Energy Commission.
[1] DeWire, Silverman, and Wolfe, Phys. Rev. **92**, 519 (1953).

L11. Systematics of Photoproton Yields. E. V. WEINSTOCK AND J. HALPERN, *University of Pennsylvania.*—The photoproton yields from the elements Ta, Pt, Pb, W, and Au have been determined for betatron bremsstrahlung bombardment at 22-Mev peak energy by the use of zinc sulfide detectors[1] and a 50-μsec betatron pulse duration. The yields, as measured in photoprotons per mole per roentgen, are as follows: Ta, 5.7×10^4; Pt, 2.9×10^4; Pb, 5.8×10^4; W, 5.2×10^4; and Au, 1.9×10^4. These values, along with previous determinations,[1] permit a study of general behavior of photoproton yields for Z values throughout the periodic table. Comparisons with calculations based on the evaporation model[2] show good agreement with experimental trends up to a Z of 50, after which the measured yields are too high by factors ranging from 10 to 10^4. Calculations based on the direct photoelectric process[3] give better agreement, though still too low by a factor of 10.

[1] A. K. Mann and J. Halpern, Phys. Rev. **82**, 733 (1951).
[2] J. M. Blatt and V. F. Weisskopf, *Theoretical Nuclear Physics* (John Wiley and Sons, Inc., 1950), pp. 340–79.
[3] E. D. Courant, Phys. Rev. **82**, 703 (1951).

L12. Energy Dependence of Some Photonuclear Reactions.* T. T. SUGIHARA† AND I. HALPERN,‡ *M.I.T.*—The relative yields of some selected radionuclides formed by the irradiation of arsenic with 140-Mev and 320-Mev bremsstrahlung have been measured. Radiochemical isolation of Ga, Cu, Ni, and Co, as well as an aliquot of the arsenic target, led to the following relative yields at 140 Mev and 320 Mev, respectively: As^{74}, 1050, 1050; As^{73}, 110, 110; Ga^{73}, 0.3, 0.5; Ga^{72}, 0.9, 1.2; Ga^{70}, 8.4, 9.5; Ga^{68}, 4.2, 7.6; Ga^{66}, 0.2, 0.7; Cu^{67}, 0.1, 0.2; Cu^{64}, 0.3, 2.5; Cu^{61}, <0.1, 0.6; Ni^{66}, <0.02, 0.05; Ni^{65}, 0.08, 0.1; Co^{61}, 0.09, 0.2; Co^{55}, <0.02, 0.1. Irradiations were monitored with Cu foil and yield values are relative to the saturation Cu^{64} activity produced in the foil. As the maximum energy of the synchrotron is reduced, the yields of nuclides far from the target are decreased. The isotope of maximum yield for a given Z seems to shift to the neutron-rich side at the lower energy. This may be related to increased α emission at lower energy. The difference in yields at the two energies and the difference bremsstrahlung spectrum suggest that the major contribution to the 320-Mev yields of copper, and probably those of lower Z, comes from quanta of energy greater than 140 Mev.

* Supported in part by the U. S. Atomic Energy Commission.
† Now at Department of Chemistry, Clark University.
‡ Now at Department of Physics, University of Washington.

FRIDAY MORNING AT 9:30

Sheraton Park, Caribar Room

(F. J. DYSON presiding)

Theoretical Physics, III: Field Theory

M1. Electromagnetic Interaction of Particles of Spin $\frac{3}{2}$. SURAJ N. GUPTA, *Purdue University* (introduced by F. J. Belinfante).—It is well known that if we consider the interaction of charged particles of spin 0, $\frac{1}{2}$, and 1 with the electromagnetic field, the divergencies in the case of spin $\frac{1}{2}$ are less severe than those in the case of spin 0 or 1. In fact, confining ourselves to mass and charge (or field strength) renormalizations, we can remove all the divergencies only in the case of charged particles of spin $\frac{1}{2}$. Since it is not known what the situation is for any other particles of half-integral spin, we have investigated the interaction of charged particles of spin $\frac{3}{2}$ with the electromagnetic field. We have used the Fierz-Pauli theory for a field of spin $\frac{3}{2}$, and it is found that the quantization of such a field can be carried out without any special difficulty. It is also possible to obtain the usual rules for the contribution of any Feynman diagram in this case. A preliminary investigation shows that the divergencies in this case are even stronger than those in the case of charged particles of spin 1.

M2. Quantized Linear Theory of Gravitation. I. F. J. BELINFANTE AND J. C. SWIHART, *Purdue University.*—We have quantized the Lorentz-covariant linear gravitational theory reported on earlier,[1] with choice of constants $b=q=0$, $C=1$, while the coefficients a, $f=-\xi a$, and K provisionally are arbitrary. The Lorentz-covariance of the canonical commutation relations has been proved by considering infinitesimal Lorentz transformations. As our old choice of the Lagrangian density would make the interaction part of the energy density T^{00} non-Hermitian, we must introduce new variables by a canonical transformation before an interaction representation can be defined. We have found appropriate new canonical variables for ψ and for the canonical conjugates of $h_{\lambda\mu}$. After expressing T^{00} in the new variables, its interaction part becomes hermitian. Also, the old expression $\psi^\dagger(1+\frac{1}{2}h_{0\mu}\alpha^\mu)\psi$ for the probability density, when expressed in the new variables, becomes simply $\psi^\dagger\psi$. While the new ψ is no undor[2] in Heisenberg representation, the new and not the old ψ becomes an undor in the interaction representation. We are now proving the integrability of the generalized Schroedinger equation for this interaction representation.

[1] Abstracts, Phys. Rev. **90**, 357 and **91**, 500 (1953).
[2] F. J. Belinfante, Physica **6**, 849 (1939).

M3. Quantized Linear Theory of Gravitation. II.* J. C. SWIHART AND F. J. BELINFANTE, *Purdue University.*—We perform another canonical transformation, from the $h_{\mu\nu}$ variables and their canonical conjugates $p^{\mu\nu}$ to new canonical variables (no tensors) $y_{\mu\nu}$ and $z_{\mu\nu}$, by $y_{00}=-\frac{1}{2}h_\nu{}^\nu$, $y_{jj}=-h_{jj}+h_{00}+\frac{1}{2}h_\nu{}^\nu$, $y_{0j}=h_{0j}$, $(j=1,2,3;\ \mu,\nu=0,1,2,3;\ \mu<j;\ z_{\mu\nu}$ in terms of $p_{\mu\nu}$ similarly). The Fourier coefficients of $y_{\mu\nu}$ and $z_{\mu\nu}$ are expressed in terms of annihilation operators $a_{\mu\nu}(\mathbf{k})$ and their conjugates. With z axis $\|\mathbf{k}$ we introduce $b_{11}=(a_{11}-a_{22})/\sqrt{2}$, $b_{22}=(a_{11}+a_{22})/\sqrt{2}$, further $b_{\mu\nu}=a_{\mu\nu}$, and occupation numbers $n_{\mu\nu}(\mathbf{k})=b_{\mu\nu}{}^*b_{\mu\nu}$. An auxiliary condition $(\nabla_\nu h_\mu{}^\nu+R\nabla_\mu h_\nu{}^\nu)^{(+)}\Psi=0$ is postulated for eliminating negative energies from $H_g=\Sigma_{\mathbf{k}}\hbar ck[\Sigma_{(j\le l)}n_{jl}(\mathbf{k})-\Sigma_\mu n_{0\mu}(\mathbf{k})]+$constant. Thence $\langle n_{13}\rangle-\langle n_{01}\rangle=\langle n_{23}\rangle-\langle n_{02}\rangle=\langle n_{22}\rangle-\langle n_{03}\rangle=0$ for a Gupta metric, while $\langle n_{33}\rangle-\langle n_{00}\rangle=0$ if $(1+4R)^2=4\xi-1$. As $T^{\mu\nu}$ in general does not satisfy the corresponding conservation law, Ψ in the auxiliary condition must be taken in Heisenberg while $h_\mu{}^\nu$ in interaction representation. The condition is thus imposed on incident gravitons only. A static central gravitational field yet satisfies it, if $a=\frac{1}{4}$ (thence deflection of light along sun 1.75″),

and if $\xi=\frac{1}{2}-4K+16K^2$, $R=2K-\frac{1}{2}$. With $K=1/16$ this would yield Einstein's values for the observable effects.

* Supported in part by National Science Foundation.

M4. Quantum Theory of Gravitation.* PETER G. BERGMANN, *Syracuse University.*—Once the equations of the gravitational field have been cast into the canonical form, their actual quantization may be attempted with the help of standard perturbation theory, in order to answer such questions as the collision cross section for two gravitons. Unfortunately, the Hamiltonian is of infinitely high degree in the field variables, and so it would seem as if a time-dependent theory should lead to an infrared catastrophe even in a first-order calculation. It now appears as if the adoption of a particular set of coordinate conditions would reduce the Hamiltonian to a polynomial, albeit of a very high degree. For instance, there are first-order processes that involve in a single collision two photons and six gravitons. In purely gravitational interactions a first-order process may involve as many as eleven gravitons. It may be possible to reduce these figures further by additional transformations, but they show at least that first-order processes involving infinite numbers of gravitons may be completely eliminated.

* Research supported by the U. S. Office of Naval Research.

M6. Hyperquantization of Feynman Amplitudes. F. COESTER, *The Institute for Advanced Study.*—Mathews and Salam[1] and Freese[2] have studied differential equations for Feynman amplitudes which follow from the field equations and a suitable formal definition of the amplitudes in terms of Heisenberg fields. These equations can be cast into an extremely simple form by a hyperquantization procedure which leads to an occupation number representation for the set of all Feynman amplitudes. The relation between the amplitudes and the occupation number representation is quite similar to that between the Fock amplitudes and the occupation number representation commonly used in field theory. Formal solutions of the new equations will be given which can be renormalized explicitly. The well-known results of perturbation theory as well as the integral equations for the amplitudes can be easily derived from these formal solutions.

[1] P. T. Mathews and A. Salam, Proc. Roy. Soc. (London) **221**, 128 (1954).
[2] E. Freese, Z. Naturforsch. **8a**, 776 (1953).

M7. Isotopic Spin Conservation and a Generalized Gauge Invariance.* C. N. YANG† AND R. MILLS, *Brookhaven National Laboratory.*—The conservation of isotopic spin points to the existence of a fundamental invariance law similar to the conservation of electric charge. In the latter case, the electric charge serves as a source of electromagnetic field; an important concept in this case is that a gauge invariance which is closely connected with (1) the equation of motion of the electromagnetic field, (2) the existence of a current density, and (3) the possible interactions between a charged field and the electromagnetic field. We have tried to generalize this concept of gauge invariance to apply to isotopic spin conservation. It turns out that a very natural generalization is possible. The field that plays the role of the electromagnetic field is here a vector field that satisfies a nonlinear equation even in the absence of other fields. (This is because unlike the electromagnetic field this field has an isotopic spin and consequently acts as a source of itself.) The existence of a current density is automatic, and the interaction of this field with any fields of arbitrary isotopic spin is of a definite form (except for possible terms similar to the anomalous magnetic moment interaction terms in electrodynamics).

* Work performed under the auspices of the U. S. Atomic Energy Commission.
† On leave of absence from the Institute for Advanced Study, Princeton, New Jersey.

M8. Conservation Theorems in Modified Electrodynamics.* J. W. DETTMAN AND A. SCHILD, *Carnegie Institute of Technology.*—A system of interacting particles with variable rest masses is considered,[1] whose motion is governed by a variational principle of the form

$$\delta\tfrac{1}{2}\sum_{ab}\int_{-\infty}^{\infty}\int_{-\infty}^{\infty}\Lambda(\xi_{ab}{}^{\mu},\dot{x}_a{}^{\mu},\dot{x}_b{}^{\mu})du_a du_b=0. \qquad (1)$$

Here $x_a{}^{\mu}$ are the space-time coordinates of particle a, $\xi_{ab}{}^{\mu}=x_a{}^{\mu}-x_b{}^{\mu}$, $\dot{x}_a{}^{\mu}=dx_a{}^{\mu}/du_a$, and u_a is a physically significant parameter along the world line of a, the variable rest mass m_a being defined by $m_a{}^2=\dot{x}_a{}^{\mu}\dot{x}_{a\mu}$. For suitable choices of the interaction function Λ, it has been shown[1] that, when the particles are at distances large compared to the classical electron radius, the new theory reduces to classical electrodynamics, and that the variable rest masses m_a become constants of motion. The conservation laws of energy-momentum and of angular momentum for systems governed by (1) are derived from the Lorentz invariance of Λ.

* Assisted by Air Research and Development Command, U. S. Air Force.
[1] A. Schild, Phys. Rev. **92**, 1099 (1953).

M9. Variance Properties of a General Field Operator. P. H. FANG, *Catholic University of America.*—Consider a class of operator functions $S(x,p)$, $[p=-i(\partial/\partial x)]$, which satisfies the following equation under a transformation operator T, $TS(x,p)=tS(x,p)$; here t is the eigenvalue of T; in this case, S is called t-variant. In particular, when $t=1$, one has invariance, a condition usually required in ordinary quantum mechanics for certain T's. Four types of transformation are studied, namely, the Lorentz transformation T_L, the Hermitian transformation T_H, the Fourier transformation T_F, and the reciprocity transformation T_R. In the case of T_F, $T_F{}^4=1$, and $t_F=\pm 1, \pm i$. The connection of t_F with t_L, t_H, and t_R is established, from which, respectively, the character of the light cone, the property of eigenvalue of $S(x,p)$, and the connection of $S(x,p)$ in the space-time space and momentum-energy space is obtained. Yukawa and Rayski's nonlocal field theory and Born's mass-spectrum problem of elementary particles are considered in relation to this larger class of transformations.

M10. Superselection Rule Regarding Spinor Particle Numbers. SATOSI WATANABE, *U. S. Naval Postgraduate School.*—Consider a unitary transformation U which transforms the state function Ψ into $U\Psi$ and all physical quantities Q (including interaction Hamiltonian) into UQU^{-1}. If the interaction type is such that the total number of spinor particles (which may or may not belong to the same field) can change only by an integral multiple of an integer n, then we have $UQU^{-1}=Q$ if we take $U=U_n=\Pi_s{}^{\infty}(1-N_s+\omega_n N_s)$

$=\Pi_i{}^{*}\omega_n{}^{N_i}$. N_i is the particle number operator of eigenstate i of the spinor fields, and ω_n is any one of the nth roots of unity. Then, Ψ and $U\Psi$ are physically indistinguishable from each other, whatever physical quantities may be used for the intended detection. If we take $\omega_n=\exp(2\pi i/n)$, the eigenvalues of U_n become n different nth roots of unity, thus dividing the entire Hilbert space into n disconnected subspaces. On account of Lorentz invariance, n is limited to even numbers. Thus W.W.W.'s superselection rule[1] ($n=2$) has a general validity. W.W.W.'s original proof is based on a particular situation: $R^TR^{-1}=U_2$.[2] In case $n=0$ (heavy particles?), the superselection rule with any arbitrary n will hold.

[1] Wick, Wightman, and Wigner, Phys. Rev. **88**, 101 (1952).
[2] See Eq. (8.15), S. Watanabe, Phys. Rev. **84**, 1008 (1951).

M11. Invariance and Isotopic Spin. A. W. STERN, *Flushing 56, N. Y. C.*—A recent attempt to incorporate the concept of isotopic spin into the formalism of a consistent theory instead of using this concept as a shorthand way of distinguishing between the neutron and proton states of the nucleon has been made by Pais. His work employs a six-dimensional manifold, that is, it involves the familiar space time of four dimensions *plus* an isotopic spin or ω space of two dimensions. The six dimensions are not all on an equal footing. There are phenomena, electromagnetic and Coulomb interactions, which are functions of the space-time variables but not of the ω variables. Thus we have two different kinds of space, which is a way of introducing heterogeneity in the continuum. There is an infinite number of particle states in the mass spectrum of Pais' new theory. Although they are extremely short-lived, some of the mass states may nevertheless manifest themselves in very high-energy scattering and particle production phenomena. Selection rules, symmetry principles, and invariant properties are absolute only in the simplest and isolated systems, and may be violated in the presence of perturbing fields. They are only relative in complex systems, such as a system which would embrace nucleons, π mesons, and the light particles all together.

M12. On the Formulation of Quantum Electrodynamics in Minkowski Space. T. A. WELTON, *Oak Ridge National Laboratory.*—A formulation of quantum electrodynamics has been found which is completely analogous to the elementary nonrelativistic quantum mechanics. A study is made of a hypothetical system of particles moving in a Minkowski space of four completely equivalent dimensions, with a fifth variable analogous to the time in nonrelativistic calculations. The particles move only under the action of external forces, which, however, are specified by certain noncommuting amplitudes. Mass values and transition probabilities, as well as wave functions, although noncommuting quantities, are simply calculated by the methods of elementary wave mechanics. To obtain physical answers, appropriate averages must first be taken of the noncommuting preliminary answers, and a simple analytic continuation must be performed in which the real mass constant for the hypothetical particles is made purely imaginary. In this way a one-to-one correspondence is established between the results of calculations in the hypothetical space and actual physical phenomena. All elementary results agree completely with those of conventional formulations. The description of pair production is thus far ambiguous, but results of a promising formulation will be presented. Relativistic corrections to the Lamb shift have also been calculated and will be presented. These differ essentially from previous calculations.

M13. Properties of Hypothetical Atoms Composed of Magnetic Poles. ARTHUR E. RUARK, *University of Alabama.*—There is need for some numerical discussion of the properties of hypothetical atoms, presumably unstable, composed of monopoles. In order to assess the possibility of detecting such entities, in case they exist, attention will be given to the Dirac type and to poles having strength g equal to the electron charge. See also the abstract of a talk before the 1954 meeting of The Southeastern Section, in which the latter monopole type is discussed on the basis of generalized electromagnetic equations symmetrical in respect to charges and poles.

M14. A Completed Quantum Theory. IRVING STEIN, *Wayne University.*—Preliminary work has been completed on a modified quantum theory, from which the standard theory can be derived and in which there is no indeterminacy. The modified theory is based upon the assumption that the state vectors associated with given particles actually describe the kinematical and dynamical properties of the particles. It is then found that the classical kinematical variables are generally not appropriate as quantum-mechanical kinematical variables. Based upon the assumed reality of the state vectors, it is found that the observables of Dirac are the quantum-mechanical variables. Three further postulates are made: (1) each particle has simultaneously a value of every state vector permitted by the field and therefore also of every associated observable, each a kinematical degree of freedom of the particle. (2) The time-dependent Schroedinger equation holds for each of the state vectors. (3) The state vectors are all related to each other by a measure. The measure of the 'distance' of the state vectors is given by the angle in Hilbert or function space between one state vector and the conjugate of the other state vector. Thus, the kinematical variables are not independent variables since they are related to each other through the statistics of the standard theory. The theory is a field theory of kinematical variables.

FRIDAY AFTERNOON AT 2:00

Shoreham, Main Ballroom

(E. O. HULBURT presiding)

Invited Papers in Nuclear Physics

N1. Experimental and Theoretical Studies of Levels in Lead 206. D. E. ALBURGER, *Brookhaven National Laboratory.* (30 min.)

N2. Recent Progress in Microtron Research. H. F. KAISER, *Naval Research Laboratory.* (30 min.)

N3. Classical Field Theory of Nuclei. EDWARD TELLER, *University of California, Berkeley.* (45 min.)

FRIDAY AFTERNOON AT 2:00

NBS, East Building

(A. V. ASTIN presiding)

Invited Papers in General and Low-Temperature Physics

O1. Recent Determinations of the Velocity of Light. HAROLD LYONS, *National Bureau of Standards.* (30 min.)

O2. Electron-Diffraction Studies of Internal Motion in Molecules. I. L. KARLE, *Naval Research Laboratory.* (30 min.)

O3. Atomic Theory of the Lambda Transition in Liquid Helium. D. TER HAAR, *St. Andrews University, Scotland.* (30 min.)

O4. Superconducting Compounds. B. T. MATTHIAS, *Bell Telephone Laboratories.* (30 min.)

O5. Magnetic Measurements Below 1° Kelvin. R. P. HUDSON, *National Bureau of Standards.* (30 min.)

FRIDAY AFTERNOON AT 2:00

NBS, Materials and Testing

(H. D. HAGSTRUM presiding)

Electrostatic and Electron Physics

OA1. A New Technique for Solving Three-Dimensional Electron Optics Potential Problems with Axial Symmetry. JENNY E. ROSENTHAL, *Du Mont Laboratories.*—The need for a new approach for solving 3-dimensional potential problems is discussed since standard techniques of separating variables and then expanding the solution in terms of products of known functions cannot be applied—even in principle—to many cases of boundary value problems with discontinuous boundaries. It is shown that methods based on complex potential can be extended from ordinary 2-dimensional problems to 3-dimensional problems with axial symmetry. Such an extension suggests a different type of expansion for the potential function satisfying Laplace's equation in cylindrical coordinates. This expansion has the advantage that every term in it has the proper behavior at infinity, i.e. (in the usual notation), goes to zero as $C\{Z^2+r^2\}^{-\frac{1}{2}}$. Special cases are considered and the possibility is discussed of using them to build up solutions of more difficult problems.

OA2. An Automatic Electrostatic Field Plotter. DAVID H. ANDREWS, *U. S. Naval Materiel Laboratory* (introduced by Robert J. Wohl).—Rapid electrostatic field plots are automatically made using the resistive paper technique combined with a commercial "$X-Y$" recorder, providing easily and quickly a graphic presentation of the equipotential lines for any desired electrode configuration. Experimental verification of its accuracy is shown by a comparison of the equipotential lines drawn by this plotter with those obtained from an electrolytic tank. The underlying principles for modification of an "$X-Y$" recorder to accomplish this purpose are stated and details given for the particular recorder used. A description of the techniques used in the preparation of the sample electrode systems and in the operation of the plotter is given. Several illustrative field plots are shown together with the application of the plotter to a typical cathode-ray tube electron gun.

OA3. Excitation and Separation of Pure High-Order Modes in Large High-Q Cavities. C. T. ZAHN AND W. G. SCHWEITZER, JR., *National Bureau of Standards.*—A successful method for suppressing undesired modes is presented. It is based on mathematical properties of the wave equation: (1) particular solutions extend analytically throughout all space, and (2) nodal surfaces divide space into elementary cells. Each particular, or "master" mode pattern thus defines an infinite variety of cavities having a common frequency, namely, all those corresponding to the addition of adjacent cells. These principles can be used to great advantage in microwave techniques. By suitable choice of "complex cavity", devices can be obtained with remarkable transducing, filtering, or suppressing properties. Such complex cavity-systems are amenable to extraordinarily simplified theoretical calculations. By an experimental application of the foregoing ideas to a cylindrical system it was possible to excite a very large cavity in a *well-separated* axially symmetric transverse electric mode of frequency 20 000 megacycles per second, and having about 50 radial nodes and 100 longitudinal. The *observed* Q was slightly less than *one million.*

OA4. Time Delay in Secondary Emission.* M. H. GREENBLATT, *RCA Laboratories.*—An experiment to measure the time delay in secondary emission in as direct a manner as possible was performed. The experiment consists of producing short bursts of primary electrons, allowing these primaries to strike a secondary emission target, and examining the resultant bursts of secondary electrons. The short primary pulses are produced by deflecting an electron beam at 400 mc across a circular aperture. The electrons that get through bombard a secondary emissive surface. The bursts of secondaries are analyzed by synchronously deflecting them across a fluorescent screen or presentation electrode. The time dispersion of the secondary pulse is thus made to correspond to an intensity modulation on the face of the tube. The measurements show that any broadening of the primary pulse by the secondary emission process is less than 7×10^{-11} sec and is probably much less.

* Work supported by U. S. Atomic Energy Commission.

OA5. Forward-Backward Ratio of Secondary Emission Produced by 1.3-Mev Electrons.* M. A. POMERANTZ, J. F. MARSHALL, AND R. A. SHATAS, *Bartol Research Foundation.*—A new method for measuring the secondary-electron emission from thin targets bombarded by energetic electrons permits

the independent determination of the yield from both faces of the target foil through which the primary electrons pass with negligible energy loss. The experimental arrangement comprises essentially a sandwich consisting of the target interposed between a pair of closely spaced thin metallic foils, the electrostatic potentials of which can independently be defined. From various combinations of the 9 equations relating the 9 observed target currents to the corresponding potential configurations, the yields from the two faces of the specimen can be determined. Such an analysis in the case of a 11 mg/cm^3 Ni target provides a value for the ratio of the yield in the forward direction (i.e., same as incident beam) to that in the backward direction, $\delta_F/\delta_B = 1.05 \pm 0.13$, where the indicated uncertainty is inherent in the present method of measuring currents. Although the targets were only chemically cleaned, this result was unaffected by interchanging front and back surfaces by a rotation of the sandwich in vacuum.

* Assisted by the U. S. Office of Naval Research and by the U. S. Office of Ordnance Research.

OA6. Target-Thickness Dependence of Delta-Ray Emission Produced by 1.3-Mev Electrons.* J. F. MARSHALL, R. A. SHATAS, AND M. A. POMERANTZ, *Bartol Research Foundation.*—The yield of energetic secondaries (delta rays) emitted from thin foils bombarded by 1.3-Mev electrons has been determined as a function of target thickness for Al and Ni in the range 2 mg cm^{-2} to 70 mg cm^{-2}, the upper limit being imposed by uncertainties introduced by the stopping of multiply-scattered primaries. In accordance with expectation, the yield increases with thickness from 0.5 percent to 2 percent in the case of Al of the aforementioned thicknesses. On the basis of the assumption that the lattice electrons can be regarded as free in the present analysis, and by invoking a range-energy relationship for treating the escape of the delta-rays, the yields have been computed. The theoretical absolute values are only slightly higher than the experimental results, and the observed data are in good agreement with the shape of the calculated yield *vs* thickness curves. Furthermore, the difference in yields per mg cm^{-2} of Al and Ni is in accord with theory, as is the similarity between Ni and Cu.

* Assisted by the U. S. Office of Ordnance Research and by the U. S. Office of Naval Research.

OA7. Characteristic Energy Loss of Electrons.* LEWIS B. LEDER AND L. MARTON, *National Bureau of Standards.*—Measurement of the energy loss of 30–35 kev electrons in solids reported at the last New York meeting[1] has been continued. Energy loss values obtained for several new materials will be reported. In particular, comparison will be made of the characteristic energy losses for metals and the metal compounds. Also, the apparatus has since been improved so that we can now measure not only the energy loss spectra, but also relative intensities and cross sections for the events.

* This work was supported by the U. S. Office of Naval Research.
[1] Lewis B. Leder and L. Marton, Bull. Am. Phys. Soc. **29**, No. 1, 40 (1954).

OA8. Electron Scattering in Solids at 20 kev,* L. MARTON, TOMMY F. MCCRAW, AND J. AROL SIMPSON, *National Bureau of Standards.*—The apparatus for measuring large-angle scattering of electrons described at an earlier meeting[1] has been made automatic. Energy and intensity spectra at angular intervals of 0.002 radians are measured in two seconds by sweeping the scattered electron beam magnetically. A complete run over 30 degrees can be made in eight minutes. Intensity and energy distributions have been obtained for several metals, in some cases through an angle of 30 degrees.

* This work was supported by the U. S. Office of Naval Research.
[1] L. Marton, Phys. Rev. **87**, 200(A) (1952).

OA9. The Phenomena of Plasma Resonance.* K. S. W CHAMPION AND S. C. BROWN, *M.I.T.*—Plasma resonance is associated with the transmission of externally applied high-frequency electromagnetic waves through a plasma. Two types of resonance will be discussed. The first, impedance resonance, occurs when the E field at a point has a relative maximum. The second, dielectric resonance, occurs when the dielectric constant is zero at the point considered. Impedance resonance occurs when $ne^2/m\epsilon_0\omega^2 = 1$ and dielectric resonance when $ne^2/m\epsilon_0(\nu_c^2+\omega^2) = 1$, where n represents the electron density and ν_c the electron collision frequency. At low pressures, when $\nu_c^2 \ll \omega^2$, the two types of resonance coincide, but they differ at high pressures. Impedance resonance corresponds to greatest ionization and excitation rates. Above dielectric resonance the transmitted electromagnetic waves are strongly attenuated and there is a reflected wave. A special tunable 100 Mc/sec resonant cavity was designed so that discharges above plasma resonance could be produced in relatively large volumes. Discharges were obtained which, under the appropriate conditions, exhibited the properties of impedance and dielectric resonance.

* This work was supported in part by the Signal Corps, the Air Materiel Command, and the U. S. Office of Naval Research.

OA10. Magneto-Hydrodynamic Flows in Hydrogen and Helium.* W. R. ATKINSON, R. G. FOWLER, AND W. R. HOLDEN, *University of Oklahoma.*—An electrically energized shock tube was used to produce a stream of luminous conductive gas. Two aspects of the interaction between this flow and a stationary magnetic field were observed. First, eddy currents induced in the moving plasma produced a field that augmented the static field in the region ahead of the advancing ion front. The resulting field can be described as similar to the static field except that each line of force is pushed downstream by the advancing ion front which resists penetration by the field to an extent determined by the conductivity. This field alteration was studied by observing the voltage induced in external coils. Secondly, alterations in the flow produced by the field were studied by a rotating mirror. Again plasma eddy currents opposed relative motion between the field and the plasma which consequently lost flow energy and gained heat energy that increased the luminosity. This attenuation of flow velocity at times produced a receding shock originating at the boundary of the magnetic field. Further experiments indicated that expansion in the shock tube may be influenced by the inherent magnetic fields of the initial heating current.

* This work was supported by the U. S. Office of Naval Research.

OA11. Motion of Arc Cathode Spot in a Magnetic Field. ROBERT M. ST. JOHN AND J. G. WINANS, *University of Wisconsin.*—The retrograde motion of the cathode spot of an arc in a transverse magnetic field[1] can be associated with electrostatic forces on positive ions produced by electron impact. A cathode spot assembly consisting of a group of electrons in the cathode, a positive ion sheath separated by a dark space from the cathode, and an electron cloud between the positive ion sheath and anode is postulated. Electrons after acceleration through the cathode dark space would travel a curved path due to the magnetic field and produce new positive ions on the forward (direction of magnetic force) side of the cathode spot. These new positive ions would be attracted by the cathode spot assembly with a resultant force that would cause them to overshoot the positive ion sheath before being pulled into the cathode to start a new spot in the retrograde direction. Addition of an inert gas reduces the mobility of positive ions to the order of that of the cathode electrons thus permitting forward motion of the cathode spot assembly to reduce the overshooting. Higher pressures would cause a forward spot motion.

[1] J. D. Cobine and C. J. Gallagher, Elec. Eng. **68**, 469 (1949).

OA12. An Electron Spectrometer for the Study of Inelastic Collision Cross Sections.* E. N. LASSETTRE, A. S. BERMAN, S. SILVERMAN, AND M. E. KRASNOW, *The Ohio State University.*—An electron spectrometer, an improved version of an instrument previously used in this laboratory, is described which is suitable for the determination of electron impact energy spectra and relative electronic collision cross sections. A velocity analyzer of the type described by Yarnold and Bolton,[1] with a resolving power of 2500, is employed. Scattered current is detected by a particle counter of the electron multiplier type developed by J. S. Allen.[2] The instrument has been used in the study of inelastic collision cross sections at scattering angles above 3.5°, incident kinetic energies of 400–600 ev, and excitation energies less than 80 ev. Cross sections are placed on an absolute basis by comparing the scattering with that for the $1^1s \rightarrow 2^1P$ transition in helium and using the theoretical cross sections (unpublished calculations by Lassettre and Jones) for the helium scattering. The construction, operation, and capabilities of the above instrument will be discussed.

* The research reported in this paper has been sponsored by the Geophysics Research Directorate of the Air Force Cambridge Research Center, Air Research and Development Command.
[1] G. D. Yarnold and H. C. Bolton, J. Sci. Instr. Britain **26**, 38 (1949).
[2] J. S. Allen, Rev. Sci. Instr. **18**, 739 (1947).

OA13. Electronic Collision Cross Sections and Oscillator Strengths for Oxygen in the Schumann-Runge Region.* E. N. LASSETTRE, S. SILVERMAN, AND M. E. KRASNOW, *The Ohio State University.*—Using the apparatus and techniques described in a concurrent abstract the electronic collision cross sections for the energy loss range 6.5 to 10.7 electron volts in oxygen have been determined. In this region the spectrum has two peaks, one at 8.44 electron volts, corresponding to the Schumann-Runge continuum, and the other at 9.94 electron volts. Electronic collision cross sections were determined for the peak at 8.44 volts for angles ranging from 3.5 to 9.5 degrees with incident electron energies of 519 and 611 volts, and for the 9.94-volt peak from 3.5 to 8 degrees with an incident electron energy of 518 volts. From these data generalized oscillator strengths have been calculated, and extrapolated to give optical oscillator strengths. For the 8.44-volt peak the differential optical oscillator strength obtained in this way is 0.17, and the integrated optical oscillator strength from 6.5 to 9.3 volts is 0.23. For the 9.94-volt peak the differential optical oscillator strength is 0.038 and the integrated optical oscillator strength is 0.025. The results for the 8.44-ev transition will be compared with the optical determinations on the Schumann-Runge continuum.

* The research reported in this paper has been sponsored by the Geophysics Research Directorate of the Air Force Cambridge Research Center, Air Research and Development Command.

OA14. Scattering of H^- Ions in the Range 20–400 ev.* E. E. MUSCHLITZ, JR., *University of Florida.*—A new ion source designed for the production of negative ions coupled with a 90° mass spectrometer has been utilized for obtaining beams of negative ions. Collimated beams of H^- ions, 2 mm in diameter and with intensities up to 10^{-12} ampere, have been obtained. Differential pumping and electrostatic focusing have been employed in the same manner as in previous work with positive ion beams.[1] Scattering cross sections have been determined for collisions of H^- ions in hydrogen at pressures of 10^{-1} to 10^{-3} mm Hg using the method of Simons and co-workers.[2]

* Supported by U. S. Office of Naval Research.
[1] Simons, Francis, Fontana, and Jackson, Rev. Sci. Instr. **13**, 419 (1942).
[2] Simons, Muschlitz, and Unger, J. Chem. Phys. **11**, 307 (1943).

OA15. Experimental Determination of Charge Transfer Cross Sections. W. F. SHERIDAN AND J. A. DILLON, JR., *Air Force Cambridge Research Center,* AND S. N. GHOSH,* *Wentworth Institute.*—Cross sections for charge transfer reactions between ions and neutral atoms and molecules have been measured in the energy range from 50 to 850 ev. The ion source and collimator consists of a modified Bennett-type mass spectrometer, and the collection chamber is similar to that used by Keene.[1] Cross sections for symmetrical reactions involving noble gases are in good agreement with previously reported values. The values for helium are of the same magnitude as those of Hasted[2] and others rather than the higher values obtained by extrapolating the results of Keene and Meyer. For N_2^+, N_2, and N_2^+, A reactions, cross sections are generally larger than those for O_2^+, O_2, and O_2^+, A reactions in agreement with predictions based on the Frank-Condon principle.

* Part of this research was supported by the Geophysics Research Directorate, Air Force Cambridge Research Center, Air Research and Development Command.
[1] J. P. Keene, Phil. Mag. **40**, 369 (1949).
[2] J. B. Hasted, Proc. Roy. Soc. (London) **A205**, 421 (1951).

FRIDAY AFTERNOON AT 2:00

Sheraton Park, Continental Room

(L. R. HAFSTAD presiding)

Neutron Physics, I: Neutron Scattering

P1. A System for Measuring Flight Times of Fast Neutrons. CONWAY W. SNYDER AND VINCENT E. PARKER,* *Oak Ridge National Laboratory.*—For determining the energies of neutrons from nuclear reactions and scattering, a flight-time apparatus has been built. Neutrons are produced in pulses 10 millimicroseconds or less in length by sweeping the ion beam one million times per second past a slit ahead of the neutron-producing target, and are detected by a liquid scintillator and photomultiplier at a distance of one to ten meters. Current pulses from the target and photomultiplier pulses are amplified, equalized, clipped, and fed into a 1*N*26 crystal diode which acts as a fast coincidence circuit. Flight times are measured by inserting lengths of coaxial cable in the neutron detector channel to obtain coincidence. A subsequent slow coincidence can also be used to permit pulse-height selection of the photomultiplier pulses. Preliminary tests with neutrons produce in *d-n* and other reactions indicate that the flight times of monoenergetic neutrons can be measured to better than 5 millimicroseconds.

* Research Participant from Louisiana State University.

P2. Time of Flight Measurements of Inelastic Neutron Scattering. GERARD K. O'NEILL, *Cornell University.*—With a technique which has been described previously,[1] the energy distributions of neutrons inelastically scattered from 14.6 Mev by C, Al, Cu, Sn, and Pb have been measured. Three-point angular distributions for the process in C, Al, and Pb were also obtained. 14.6-Mev $T(d,n)\alpha$ neutrons, whose direc-

tions and origin times were obtained from their accompanying alphas, scattered in a thin slab. Scattered neutrons above 0.5 Mev were detected after traversing 50 to 100 cm, and their flight times were measured by a direct-reading analyzer having nine 4.6 millimicrosecond channels. Working distance was limited by scatterer-in backgrounds, scatterer-out background exceeding 20 percent only for light elements. The over-all resolution was 0.25 Mev at 1 Mev, 1 Mev at 2.5 Mev. In favorable cases 14-Mev elastically-scattered neutrons were resolved from decay gamma rays. Nuclear temperatures obtained are in general agreement with photographic plate results.[2] Angular distributions were isotropic within statistical errors. A possible extension of the method to higher resolution, with an anticoincidence alpha counter to remove random background due to undesired neutrons, will be discussed.

[1] G. K. O'Neill, Phys. Rev. **92**, 853 (1953).
[2] E. R. Graves and L. Rosen, Phys. Rev. **89**, 343 (1953).

P3. Inelastic Scattering of 4.3-Mev Neutrons by Fe^{56}.* B. JENNINGS, J. B. WEDDELL, *Westinghouse Research Laboratories*, AND R. L. HELLENS, *Westinghouse Electric Corporation*.—The neutron spectrum from the scattering of 4.3-Mev neutrons by iron has been measured at 90° by the proton recoil photographic method. Two exposure geometries were employed; one, similar to that of Stelson and Preston,[1] used a 2×2 cm cylindrical scatterer. The second, with a different collimator and with a flat plate scatterer 6.4 mm thick, leads to a lower relative background, and is the basis of the following preliminary results. The neutron energies fall into groups corresponding to energy levels in Fe^{56} at 0.85, 2.1, 2.7, and perhaps 3.0 Mev. The total elastic cross section, using the Bartol[2] angular distribution measurement at 3.7 Mev, is estimated at 2.6±0.6 barns. The inelastic cross sections for the first three levels, assuming isotropic distribution, are estimated at 0.9±0.3, 0.4±0.2, and 0.2±0.1 barn, respectively. The errors stated include statistics, an estimate of track measurement uncertainties, and the incomplete determination of the background.

* Assisted by the joint program of U. S. Office of Naval Research and U. S. Atomic Energy Commission.
[1] P. H. Stelson and W. M. Preston, Phys. Rev. **86**, 132 (1952).
[2] W. D. Whitehead and S. C. Snowdon, Phys. Rev. **92**, 114 (1953).

P4. De-Excitation Gamma Rays from Inelastic Scattering of Neutrons.* GORDON L. GRIFFITH, *Westinghouse Research Laboratories*.—In conjunction with the direct measurements of the inelastic neutrons, observations have been made of the de-excitation gamma rays. The detector was a NaI(Tl) scintillation counter shielded from direct neutrons by a lead cone and surrounded by a ring of the scattering material being investigated. Pulse-height spectra for several elements have been obtained and the observed gamma rays correspond in general to previously known transitions. In those cases where both neutron and gamma-ray measurements have been made transition assignments are usually positive. Cross section determinations can not be made from the gamma ray measurements because of the multiple scattering in the large scatterers used.

* Jointly supported by U. S. Office of Naval Research and U. S. Atomic Energy Commission.

P5. Inelastic Scattering of Neutrons by Ba^{137} and Hg^{199}.* C. P. SWANN AND F. R. METZGER, *Bartol Research Foundation*.—The production by inelastic scattering of neutrons of the 527-kev isomeric level of Hg^{199} and of the 661-kev isomeric level of Ba^{137} have been studied. Neutrons were produced by bombarding a 50-kev lithium target with protons accelerated in the large Bartol Van de Graaff. The cross section for the production of the 13/2+ level of Hg^{199} increases sharply at 620±10-kev mean neutron energy indicating a level at about 90 kev above the metastable state. Below 620 kev the observed activity decreases with increasing neutron energy and is attributed mainly to fast neutron capture by Hg^{198}. At 620 kev the cross section corresponds to about one mb. Several other breaks indicate higher excited states in Hg^{199}. The 11/2-level of Ba^{137} has been excited with mean neutron energies as low as 670±10 kev indicating direct formation of the metastable state. The experimental cross section at 150 kev above the threshold is about 5 mb which is an order of magnitude smaller than the theoretical estimate based on the compound nucleus model.[1]

* Supported in part by the U. S. Atomic Energy Commission and in part by the joint program of the U. S. Office of Naval Research and the U. S. Atomic Energy Commission.
[1] W. Hauser and H. Feshbach, Phys. Rev. **87**, 366 (1952).

P6. Neutron Inelastic Scattering.* ROBERT M. KIEHN† AND CLARK GOODMAN, *M.I.T.*—Neutron inelastic scattering cross sections of Fe, Al, Cr, Ni, Pb, and Bi have been measured with ~20-kev resolution for neutron energies between 0 and 2.7 Mev. A NaI(Tl) gamma-ray spectrometer inside a hollow, conical scatterer measured the monoenergetic gamma rays emitted by the excited nucleus. The cross sections are in good agreement with predictions based on the Hauser-Feshbach theory. The energies of the first few excited states of the nuclei were found to be in good agreement with values obtained by other methods. New levels were found in Bi at 895±25 and 1560±35 kev. Levels at 200, 410, and 630 kev were also observed as a result of inelastic scattering within the detector.

* This work was supported by the joint program of the U. S. Office of Naval Research and the U. S. Atomic Energy Commission.
† Gulf Oil Corporation Fellow, now at Los Alamos Scientific Laboratory.

P7. Neutron Inelastic Scattering in Ta and I.* JANET B. GUERNSEY† AND CLARK GOODMAN, *M.I.T.*—Preliminary results indicate that the 136.5-kev first rotational state in Ta can be excited by 1.1-Mev neutrons. This observation may be interpreted by the Bohr-Mottelson theory[1] as an inelastic process without the formation of a compound nucleus. The detection of the 136-kev gammas, at neutron energies below 1 Mev, is made difficult by the presence of capture gamma radiation in NaI of about 150 kev. There is also evidence of gamma radiation from a low-lying state in I at about 46 kev presumably resulting from inelastic scattering. This level as well as the 200-, 410-, and 630-kev levels[2] has been assigned to I as a result of experiments using an I scattering cone.

* This work was supported by the joint program of the U. S. Office of Naval Research and the U. S. Atomic Energy Commission.
† On leave from Wellesley College.
[1] A. Bohr and B. R. Mottelson, Danske Videnskb. Selskab. Math.-fys. Medd. **27**, 158 (1953).
[2] See preceding abstract.

P8. Neutron-Capture Gamma-Ray Spectra.* MELVIN REIER, *Brookhaven National Laboratory*, AND MORRIS H. SHAMOS, *Physics Department, New York University*.—The low-energy component of the gamma-ray spectra, resulting from thermal neutron capture, was investigated by measuring the distribution of pulse heights incident upon a single NaI crystal and supplementing the information obtained this way by utilizing the Compton scattering technique.[1] Data in the region from about 100 kev to 2 Mev will be presented for a number of elements and will be discussed in terms of the proposed decay schemes. The following gamma rays have been observed:

Element	
Vanadium	2 unresolved lines at about 0.82, 0.64, 0.43.
Cobalt	1.82, 1.48, 0.82, 0.65, 0.289, 0.237.
Copper	0.280, 0.202.
Titanium	1.75, 2 unresolved lines between 1.53 and 1.58, 1.39.
	2 unresolved lines between 1.06 and 1.10, 0.334.
Iron	2 unresolved lines between 1.55 and 1.68, 0.355.
Chromium	2.13, 1.07, 0.815, 0.740.
Gold	0.248.
Manganese	0.308, 0.266, 0.206, 0.098.
Iodine	0.255.

* Research performed under the auspices of the United States Atomic Energy Commission.
[1] Hofstadter and McIntyre, Phys. Rev. **78**, 619 (1950).

P9. The Gamma-Ray Spectrum from the Inelastic Scattering of Fast Neutrons in Iron.* D. L. LAFFERTY, L. A. RAYBURN, AND T. M. HAHN, *University of Kentucky.*—A complex spectrum of gamma rays has been obtained from the inelastic scattering of fast neutrons in iron. The source of fast neutrons was the $D-D$ reaction produced by the University of Kentucky Low-Voltage Accelerator. A ring-type geometry allowed the background to be subtracted from the total spectrum yielding the iron spectrum. An analysis of the pulse-height distribution from a NaI scintillation spectrometer reveals the presence of lines corresponding to energies of 2.66, 2.21, 2.10, 1.78, 1.70, 1.59, 1.40, 1.24, 1.098, 0.989, 0.892, 0.851, 0.675, and 0.462 Mev.

* Sponsored by the Office of Ordnance Research, U. S. Army.

P10. Gamma Rays Produced by the Inelastic Scattering of D−D Neutrons in Cu, Al, and Mg.* L. A. RAYBURN, D. L. LAFFERTY, AND T. M. HAHN, *University of Kentucky.*—Monoenergetic neutrons from the $H^3(d,n)$ He^3 reaction were used to bombard scatterers of Cu, Al, and Mg in the form of rings surrounding a gamma-ray spectrometer. The gamma rays resulting from inelastic scattering of the neutrons in the scatterers were detected by a spectrometer consisting of a NaI(Tl) crystal mounted on a DuMont 6292 photomultiplier tube. A single-channel differential pulse-height analyzer was used to analyze the pulses from the photomultiplier. No shielding was used between the neutron source and the NaI crystal. The gamma spectrum for each scatterer obtained by subtracting the background counting rate from the counting rate with scatterer in place will be presented.

* Sponsored by the Office of Ordnance Research, U. S. Army.

P11. Gamma Radiation from Interaction of 3.1-Mev Neutrons. V. E. SCHERRER, B. A. ALLISON, AND W. R. FAUST, *Naval Research Laboratory.*—Neutrons from the $D(d,n)$ He^3 reaction were allowed to fall on radiators made of aluminum, manganese, zirconium, arsenic, and bismuth. Various gamma-ray lines have been identified and correlated with established levels for the nuclei concerned. Estimates of the gamma-ray production cross section have been made for each radiator material.

P12. Differential Cross Section for Elastic Scattering of Neutrons from Nitrogen. C. H. JOHNSON AND J. L. FOWLER, *Oak Ridge National Laboratory.*—Neutrons produced by the $T(p,n)$ He^3 reaction were elastically scattered from a cylindrical sample of LiN_3 and detected by a propane recoil counter. The neutron energy spread resulting from the tritium gas target was 40 kev. The counter was shielded from the direct neutrons by paraffin slabs and was biased to have an approximate constant detecting efficiency for neutrons scattered at all angles from nitrogen. Background was found by scattering neutrons from a can containing the same amount of lithium as the original scatterer. Differential cross sections were measured over the region of $\cos\varphi$ (center-of-mass angle) from $+0.9$ to -0.7 at energies below 1.6 Mev (0.80, 1.28, 1.54 Mev). For $\cos\varphi<0.5$ the distributions are essentially isotropic in agreement with results found by observing nitrogen recoil energies in a counter.[1] At 1.28 and 1.54 the differential neutron measurements show an increased cross section for $\cos\varphi>0.5$. For this forward scattering, that is for low-energy recoils, the nitrogen recoil counter is not reliable. An interpretation of the resonance distributions will be discussed.

[1] Fowler, Johnson, and Risser, Phys. Rev. 91, 441A (1953).

P13. Sphere Measurements of Neutron Inelastic Collision Cross Sections.* ROBERT C. ALLEN, *Los Alamos Scientific Laboratory.*—With a monoergic neutron source and an energy-discriminating neutron detector, the transmission of a sphere is a measure of the inelastic collision cross section. Neutrons up to 1.5 Mev are obtained from the $T(p,n)$ He^3 source with the 2.5-Mev Los Alamos electrostatic accelerator. The neutron detector is a small high-pressure hydrogen recoil proportional counter. The counter, which has a cylindrical counting volume one-half inch in length and one-half inch in diameter, can be placed inside a sphere of one and one-quarter inches diameter. With an argon hydrogen filling of ten atmospheres a good differential pulse-height distribution is obtained. Some results of the inelastic collision cross section as a function of energy and of the inelastic neutron spectrum will be discussed.

* Work done under the auspices of the U. S. Atomic Energy Commission.

FRIDAY AFTERNOON AT 2:00

Shoreham, West Ballroom

(ARTHUR ROBERTS presiding)

Meson Production

PA1. Photoproduction of π^+ Mesons near Threshold.* L. S. OSBORNE, Y. GOLDSCHMIDT-CLERMONT,† AND G. PARKER, *M.I.T.*—Nuclear emulsions were exposed in a gas hydrogen target[1] through which was passed the γ-ray beam from the 340-Mev electron synchrotron. The plates were scanned and rescanned for stopped π^+ mesons and identified by the $\pi-\mu$ decay. The scanning efficiency is estimated at better than 90 percent. Meson angles and ranges were converted to angles and energies in the center-of-mass system. In this system the angular distribution was roughly spherically symmetric. The average differential cross sections between 60° and 120° (center of mass) were

Meson energy in c of m system	$(d\sigma/d\tau)\times10^{30}$ cm²
2–5 Mev	2.4±0.3
5–6.5 Mev	2.6±0.8

* This work was supported in part by the joint program of the U. S. Office of Naval Research and U. S. Atomic Energy Commission.
† Now at Physikalisches Institut-ETH, Zurich, Switzerland.
[1] Goldschmidt-Clermont, Osborne, and Scott, Phys. Rev. 89, 329 (1953).

PA2. Determination of Photo Cross Sections from Bremsstrahlung Activation Curves.* A. S. PENFOLD AND J. E. LEISS, *University of Illinois.*—When a photon-induced reaction is investigated by irradiating with bremsstrahlung, the number of reactions is related to the cross section for the reaction through the activation integral

$$a(E_0)=\int_0^{E_0} P(E_0,E)\sigma(E)dE.$$

The problem of obtaining staisfactory practical solutions of this equation has been investigated with the Illinois digital computer. The 0° thin target bremsstrahlung equation due to Schiff[1] was used as the kernel, $P(E_0,E)$. Two general types of solutions have been investigated; the first in terms of integral operators, and the second in terms of matrix operators. Explicit forms of some of these operators will be shown and the applicability of the solutions and their relation to previously published solutions will be discussed. The effect of

variations in $P(E_0,E)$ and of statistical errors in $\alpha(E_0)$ will be discussed.

* Supported in part by the U. S. Office of Naval Research, U. S. Atomic Energy Commission, and the National Science Foundation.
[1] L. I. Schiff, Phys. Rev. **83**, 252 (1951).

PA3. Photoproduction of π^+ Mesons from Hydrogen.* J. E. Leiss and C. S. Robinson, *University of Illinois.*—The photoproduction of π^+ mesons from liquid hydrogen has been investigated using the activation curve method of the preceding abstract. Activation curves were obtained in a five-channel range telescope, by varying the betatron energy in 10-Mev steps from 140 to 300 Mev. Beyond 90° lab most counts represent π^+ mesons. Protons are dynamically excluded. The electron flux, including positrons from decay of mesons stopped in the target, is small and is subtracted on the basis of measurements below the meson counting threshold. These conclusions were confirmed with nuclear emulsions. Analysis of the activation curves yields values of the cross section for photon energies above the counting threshold in each channel. Comparison of different channels, after correction for multiple scattering, allows extrapolation of the results to zero absorber thickness. The cross section at 107°, 149°, and 165° (c.m.) has been determined from 200 to 300 Mev. The results at 107° and 149° agree essentially with other experiments. The cross section at 165° is about 15 percent lower than at 149°.

* Supported in part by the U. S. Office of Naval Research, U. S. Atomic Energy Commission, and National Science Foundation.

PA4. Photoproduction of π^+ Mesons from Hydrogen near Threshold.* C. S. Robinson and J. E. Leiss, *University of Illinois.*—The activation curve method of the two preceding abstracts has been extended to energies near threshold by counting positrons from decay of mesons stopped in the target. A small x-ray beam passed through a target of sufficient size to stop most mesons created by photons up to 30 Mev above threshold. A telescope of 4-inch diameter scintillators was placed at 140°. At this angle pair electron background from hydrogen was small. A preliminary activation curve was obtained for hydrogen from a carbon-paraffin difference, by varying the betatron energy in 5-Mev steps from 130 to 220 Mev. This curve was analyzed to obtain the total cross section. Above 180-Mev photon energy an appreciable correction for mesons escaping from the target was necessary. This correction can be made accurately if an angular distribution of emitted mesons is assumed. These preliminary results are in agreement with a total cross section proportional to meson momentum up to 180 Mev, and with the results of Goldwasser and Bernardini.[1] An experiment with liquid hydrogen is being prepared.

* Supported in part by U. S. Office of Naval Research, U. S. Atomic Energy Commission, and National Science Foundation.
[1] Goldwasser and Bernardini, Bull. Am. Phys. Soc. **25**, No. 1, 18 (1954).

PA5. Yield of π^+-Mesons by 335-Mev Protons as a Function of Atomic Number. J. Merritt and D. Hamlin, *University of California, Berkeley.*—The relative differential cross section $d^2\sigma/dEd\Omega$ was measured for the production of π^+ mesons at $0°\pm4°$ by 335-Mev protons on D, C, Cu, and Pb. The observed π^+ meson energies were 52, 88, and 147 Mev for C, Cu, and Pb. For D the meson spectrum from 40 to 140 Mev was observed. The mesons were counted electronically from signals generated in a trans-stilbene crystal telescope. Identification of the π^+ meson depended upon a fast coincidence in the first two crystals plus the $\pi-\mu$ decay in the third crystal of the telescope.[1] For C, Cu, and Pb the relative yield per nucleus can be explained by proton and meson attenuation within the nucleus. The attenuation of protons and mesons is consistent with mean free paths which have been measured in other experiments for protons and mesons in nuclear matter. This work was done under the auspices of the U. S. Atomic Energy Commission.

[1] Hamlin, Jakobson, Merritt, and Schulz, Phys. Rev. **84**, 857 (1) (1951).

PA6. π^+ Production in Hydrogen by 437-Mev Protons.* T. H. Fields, J. G. Fox, J. A. Kane, R. A. Stallwood, and R. B. Sutton, *Carnegie Institute of Technology.*—The differential cross section for the process $p+p\rightarrow\pi^++d$ has been measured using a fast coincidence technique which detects both emergent particles. The target was liquid hydrogen, and the solid angle was defined by the meson counter. Absorption curves were taken on both the mesons and the deuterons. The contribution to the counting rate from the reaction $p+p\rightarrow\pi^++p+n$ is believed negligible since the deuteron range curve indicates no component corresponding to slow protons, and since the counting rate does not depend on the solid angle of the deuteron counter as long as the meson counter defines the solid angle. Measurements have been made at c.m. angles of 30°, 50°, and 90° yielding cross sections of 0.192, 0.121, and 0.039 mb/sterad, respectively, with statistical errors of about 7 percent. These points can be well fitted by an angular distribution of $(0.20\pm0.02+\cos^2\theta)$ and yield a total cross section of 1.35 ± 0.13 mb. These values are in good agreement with those on the inverse reaction[1] for π^+ spin $=0$. Work on the reaction $p+p\rightarrow\pi^++p+n$ is in progress.

* Work supported in part by U. S. Atomic Energy Commission.
[1] Durbin, Loar, and Steinberger, Phys. Rev. **84**, 581 (1951).

PA7. Pion Production by 440-Mev Protons Incident upon Hydrogen and Carbon.* Arthur H. Rosenfeld,† *University of Chicago.*—The energy spectrum of pions produced in $P-P$ collisions has been measured at three angles using 440-Mev protons. About half the time bound deuterons are formed. $d\sigma/d\Omega\propto(0.15\pm0.05+\cos^2\theta)$; $\sigma=(4.26\pm0.9)$ mb. If charge independence applies to pion production in nucleon-nucleon collisions, then there are only three independent cross sections whose excitation functions have been given by Watson and Brueckner.[1] All available data are compiled and agree well with the theory. One of the three cross sections is small; the other two are normalized separately to fit the data. We find $\sigma(P+P\rightarrow n^++D)=1.0\text{ mb}\times\eta^3$, where η is the c.m. pion momentum in units of μc. The experimental ratio $\sigma(P+P\rightarrow n^++N+P)/\sigma(P+P\rightarrow n^++D)$ seems slightly larger than predicted by Watson. We find $\sigma(P+P\rightarrow n^0)=0.22\text{ mb}\times\eta^6$. The energy spectrum of n^+ and n^- produced in a carbon target at 90° lab. has also been measured. We find $(d\sigma/d\Omega)_{90°}=(0.83\pm0.11)$ mb/sterad, and a n^+/n^- ratio of 7.2 ± 1.5.

* Work supported in part by the U. S. Office of Naval Research.
† National Science Foundation Fellow.
[1] K. M. Watson, Phys. Rev. **88**, 1163 (1952).

PA8. The Production of Positive and Negative Pions in Beryllium by 1.0 and 2.3-Bev Protons.* S. J. Lindenbaum and Luke C. L. Yuan, *Brookhaven National Laboratory.*—The momentum spectrum and relative cross section for the production of negative and positive pions in beryllium by 1.0-Bev protons was observed at a 32° laboratory angle in a manner similar to that reported[1] for 2.3-Bev protons. Assuming that beryllium is a light enough nucleus so that one is essentially observing the elementary proton-nucleon meson production, the pion spectra in the c.m. system show a peak at ~100 Mev for both 1.0 and 2.3-Bev incident protons. The results disagree with the Fermi statistical theory predictions.[2] Although the inclusion of the apparent pion-nucelon resonance interaction in the final state statistical weights would possibly explain the 2.3-Bev results, the similarity of 1.0-Bev and 2.3-Bev spectra suggests that this resonance state may play a

fundamental role in these processes. R. Serber has suggested that a shake-off from the meson cloud could explain the results.

* Work performed under the auspices of the U. S. Atomic Energy Commission.
[1] Luke C. L. Yuan and S. J. Lindenbaum, Phys. Rev. (to be published).
[2] Christian and Yang, B. N. L. Report, December, 1953.

PA9. Neutral Pion-Deuteron Production in High-Energy n-p Collisions.* ROBERT A. SCHLUTER, *University of Chicago.*—The reaction $n+p \rightarrow D+\pi^0$ has been observed in a high-pressure hydrogen diffusion cloud chamber. Deuterons are identified by a technique of ionization measurement in conjunction with momentum measured in the 10 500 gauss magnetic field. Several cases of internally converted π^0 gamma-rays confirm the method of identification. The flux and spectrum of the 400±25 Mev neutron beam of the Chicago synchrocyclotron are measured by proton recoils observed simultaneously. The ratio of deuterons to protons of laboratory angle $\leqq 30°$ representing neutrons of >350 Mev, is 0.047 ±0.015. Using published data on n-p scattering, the total cross section is 0.6±0.2 mb, agreeing, within the accuracy of the measurements, with the prediction of charge independence that the ratio of this reaction to $p+p \rightarrow D+\pi^+$ should be $\frac{1}{2}$. The angular distribution of the pions will be presented.

* Supported by the U. S. Office of Naval Research and the U. S. Atomic Energy Commission.

PA10. Negative Pion Production in n-p Collisions.* S. C. WRIGHT AND R. A. SCHLUTER, *University of Chicago.*—We have studied the production of π^- mesons in n-p collisions by bombarding a high-pressure hydrogen diffusion cloud chamber with 400±25 Mev neutrons from the Chicago synchrocyclotron. With the same incident beam the reaction $n+p \rightarrow D+\pi^0$ (see previous abstract) is favored by a factor $\left(3.8^{+1.9}_{-1.4}\right)$ compared to $n+p \rightarrow \pi^-+2p$. In the center-of-mass coordinate system there appears to be no strong correlation between the two protons. Details of the energy and angular distributions of the product particles will be presented.

* Supported by the U. S. Office of Naval Research and the U. S. Atomic Energy Commission.

FRIDAY AFTERNOON AT 2:00

Sheraton Park, Burgundy Room

(C. C. LAURITSEN presiding)

Reactions of Transmutation. I

Q1. $(p,2n)$, $(p,2p)$, (p,t), $(p,\mathrm{He_3})$, and (p,f) Cross Sections and Excitation Functions. B. L. COHEN, G. H. MCCORMICK, T. H. HANDLEY, AND E. NEWMAN, *Oak Ridge National Laboratory.*—Cross sections and excitation functions for several $(p,2n)$, $(p,2p)$, (p,t), $(p, \mathrm{He_3})$, and (p,f) reactions have been measured using 22-Mev protons from the internal circulating beam of the ORNL 86-inch cyclotron. $(p,2n)$ excitation functions in medium weight elements show an energy dependence corresponding to a nuclear temperature of about 2 Mev, but the absolute cross sections are smaller than can be understood from existing theories by large factors. The ratio of $(p,2p)$ to (p,pn) cross sections is approximately as predicted by statistical theory; this indicates that Coulomb barriers are quite effective in suppressing the emission of low-energy protons, and that the phenomenon of excessive charged particle emission is not strongly evident in "second particle" emission from nuclear reactions. The difference in level densities by a factor of four between even-even and odd-odd nuclei is quite evident from this data. The cross sections for the (p,t) reaction in iron and the $(p, \mathrm{He_3})$ reaction in zinc are about equal to, and about ten times less than, respectively, the predictions of the statistical theory. The (p,f) cross sections in U^{238} and U^{235} are about equal to the total reaction cross section at all energies up to 22 Mev, but in Th^{232}, it is only about 60 percent as large.

Q2. Neutron Thresholds from (d,n) and (p,n) Reactions.* C. F. COOK, T. W. BONNER, AND J. B. MARION, *The Rice Institute.*—The two counter technique for detecting neutron thresholds has been used to study (d,n) and (p,n) reactions. A slow neutron counter and a conventional long counter are arranged to subtend the same solid angle with the neutron source. The ratio of counts in the slow counter to counts in the long counter exhibits a sharp rise at the thresholds and then falls off almost exponentially with increasing neutron energy. Resonances in the compound nucleus are exhibited by both counters, but the ratio remains unchanged. This method has been applied to $C^{13}(d,n)N^{14}$. A broad level at 3.28-Mev deuteron energy has been observed. This level corresponds to an excited state in N^{14} of 8.16 Mev. The observed half-width was about 300 kev. Results from bombardment of B^{10} and B^{11} will also be presented.

* Supported by the U. S. Atomic Energy Commission.

Q3. Angular Distribution of Deuterons from (p,d) Reactions in Light Nuclei.* J. B. REYNOLDS AND K. G. STANDING,† *Princeton University.*—Deuterons resulting from the bombardment of various elements with 18-Mev protons were observed, using a method developed by one of us.[1] The angular distribution of deuterons from the reaction $X(p,d)Y$ can be fitted with a theoretical (Butler) curve calculated for the inverse reaction $Y(d,p)X$. Angular distributions were observed for reactions leading to the following final nuclei, Y: Li^6, $r_0=5.0$; Li^{6*}(2.19 Mev); Be^8, $r_0=3.0$; B^9, $r_0=4.5$; B^{9*}(2.4 Mev), $r_0=4.7$; B^{10}; F^{18}, $r_0=5.0$; Al^{26}. Values of Butler's r_0 (in units of 10^{-13} cm) are given as obtained by comparing theory and experiment. In all cases, except F^{18} and Al^{26}, the angular momentum ln carried away from the target nucleus by the pickup neutron was unity. For F^{18} and Al^{26}, ln = 0 and 2, respectively. From these results it can be concluded that X and Y have opposite parity for all of the above reactions except the last two for which X and Y have the same parity.

* This work was supported by the U. S. Atomic Energy Commission and The Higgins Scientific Trust Fund.
† Now at the University of Manitoba, Winnipeg, Canada.
[1] K. G. Standing, Phys. Rev. (to be published).

Q4. Comparison of the Reactions $H^1(H^2\pi^+)H^3$ and $H^1(H^2\pi^0)He^3$ as a Test of Charge Independence. KENNETH C. BANDTEL, WILSON J. FRANK, RICHARD MADEY, AND BURTON J. MOYER, *University of California, Berkeley.*—A comparison study of these reactions is of interest because of the conclusions that can be drawn with regard to the conservation of isotopic spin, or in other words, the principle of charge

independence of nuclear forces. Conservation of isotopic spin predicts that the value of the differential cross section for the H^2 reaction will be twice that for the He^3 reaction. A liquid deuterium target was bombarded by 340-Mev protons from the Berkeley 184-in. synchrocyclotron. The reaction $H^1(H^2\pi^+)H^3$ has been studied previously[1] by utilizing the difference in time of flight between the π^+ and the H^3. In addition, E and dE/dx for the H^3 and He^3 particle is measured. These pulses are displayed in succession on the sweep of a Tektronix 517 scope. They are photographed and the pulse heights are then read off the film. Both final products are detected in case of the H^2 reaction. Only the He^3 particle is detected because of the uncertainty in the efficiency of a γ-ray counter. A comparison of the two cross sections can be obtained under the same conditions, thus eliminating many systematic errors. Preliminary results are not inconsistent with the predicted ratio. This work was done under the auspices of the U. S. Atomic Energy Commission.

[1] Frank, Bandtel, Madey, and Moyer, Phys. Rev. (to be published).

Q5. Fast Neutron Scintillation Spectra of $Li^6(n,\alpha)H^3$ in LiI(Eu). J. H. NEILER, F. MUCKENTHALER, AND JAMES SCHENCK, *Oak Ridge National Laboratory.*—Pulse-height spectra produced by the $Li^6(n,\alpha)H^3$ reaction in LiI(Eu) crystals of several activator concentrations have been obtained for neutrons of 2.3, 3.6, 5.0, and 16.7 Mev. Although the spectra exhibit good resolution for both thermal and fast neutrons, the fast neutron reaction produces a band rather than a line. Such a shape is to be expected if the pulse height *versus* energy response of the crystal to alpha particles is nonlinear for the alpha energies produced in this reaction. The data indicate that the pulse height produced by tritons is greater than that of electrons of the same energy. A possible explanation of this effect, which depends upon the self-absorption of the emitted light of LiI(Eu) crystals, will be presented.

Q6. Reaction Particles from 14.5-Mev Deuteron Bombardment of Li^7 and Li^6.* S. H. LEVINE, R. S. BENDER, J. N. MCGRUER, AND W. F. VOGELSANG, *University of Pittsburgh.*—Observations have been made of the angular distributions of charged particles resulting from the deuteron bombardment of natural lithium. 14.5-Mev deuterons were incident upon a thin Li target and outgoing particles were analyzed with a magnetic spectrometer. The detector was a CsI crystal and the particles were identified by pulse-height analysis and by their ranges in foils. The following reactions were observed:

Reaction	Levels (Mev)
$Li^7(d,t)Li^6$	g.s., 2.187
$Li^7(d,d)Li^7$	g.s., 0.478, 4.61
$Li^7(d,p)Li^8$	g.s., 1.0, 2.28
$Li^7(d,He^6)He^4$	g.s., 1.71
$Li^7(d,d)He^5$	g.s.
$Li^6(d,He^5)He^4$	g.s.
$Li^6(d,p)Li^7$	g.s., 0.478, 6.56

Present data when compared with Butler curves favor $l=1$ transfer for the two triton groups and the He^3 group corresponding to the ground state of He^5.

* Work done at the Sarah Mellon Scaife Radiation Laboratory and assisted by the Joint Program of the U. S. Office of Naval Research and the U. S. Atomic Energy Commission.

Q7. The $Li^7(d,p)Li^8$ Yield Curve.* STANLEY BASHKIN, *State University of Iowa.*—The S.U.I. mevatron was used to measure the cross section for the $Li^7(d,p)Li^8$ reaction from $E_d=700$ kev to 3200 kev. Previously reported resonances[1] at 750 kev and 1000 kev appeared at 812 kev and 1040 kev, respectively; no evidence of the reported resonance at 1400 kev was found. The yield rises rapidly from 1200 kev to 1500 kev, less rapidly to 1900 kev, and is flat thereafter to 3200 kev. The decay betas from Li^8 ($t_{\frac{1}{2}}=0.8$ sec) were detected with a thin NaI(Tl) crystal coupled to a 5819 photomultiplier. A strongly energy-dependent background of neutron capture γ rays increased from one tenth of the beta counts at 700 kev to seven times the beta counts at 3200 kev. The betas passed through an electromagnet before reaching the detector. When the field was off, background and betas were counted. When the field was on, the betas were deflected to one side and only the undisturbed background was recorded. The difference in readings gave the number of betas.

* Supported in part by the U. S. Atomic Energy Commission.
[1] Baggett and Bame, Phys. Rev. 85, 434 (1952).

Q8. The $Li^7(He^3,p)Be^9$ Reaction. W. E. KUNZ, C. D. MOAK, AND W. M. GOOD, *Oak Ridge National Laboratory.*—The following competitive processes were investigated in the bombardment of a $Li_2{}^7SO_4$ target with He^3:

$$He^3+Li^7\rightarrow B^{10}\rightarrow Be^9+H^1+11.19 \text{ Mev} \quad (1)$$

$$Be^8+H^3+11.75 \quad (2)$$

$$Li^6+He^4+13.32 \quad (3)$$

$$2He^4+H^1+n+9.61. \quad (4)$$

A NaI crystal spectrometer was used to study these reactions. Spectrometer calibration was obtained from the 14.7-Mev protons produced by $He^3(d,p)He^4$. Absorbers were used to distinguish different particles. The spectrum consisted of a continuum of protons and alphas from (4) on which was superposed 4 sharp particle groups and a single broad particle group. The most consistent interpretation of the particle groups is that each group consists of protons. Only a trace of reaction (2) was evident and reaction (3) was easily discerned. If indeed all the proton groups come from (1) then Be^9 would have the following states: ground, 1.87, 2.58, 3.24, and a broad state as 4.89.

Q9. A Proton Recoil Telescope for Observing Neutron Spectra. CARROLL C. TRAIL* AND C. H. JOHNSON, *Oak Ridge National Laboratory.*—A proton recoil telescope has been constructed to measure the neutron spectrum from the $Li^7(d,n)Be^8$ reaction. The neutrons impinge upon a polyethylene radiator and protons recoiling in the forward direction give rise to proportional counter pulses and terminate in a NaI scintillation counter. The photomultiplier impulses are analyzed by a multichannel pulse sorter which is gated by coincidences between the scintillation counter pulses and the proportional counter pulses. Polyethylene radiators of different thicknesses are mounted upon a wheel inside the counter. Radiator thicknesses were selected so that the energy spread of the recoil protons could be limited to 5 percent of the incident neutron energies for energies greater than 3 Mev. The efficiency of the counter for these radiators is 5×10^{-4}. The neutron spectrum of the $Li^7(d,n)Be^8$ reaction has been studied at 0°. Preliminary results with 10 percent statistics indicate only one excited state of Be^8 below 9 Mev.

* Graduate student at Texas A. and M. College working under an Oak Ridge Institute of Nuclear Studies fellowship.

Q10. Resonance Near the $Li^7(p,n)$ Threshold.* H. W. NEWSON AND J. H. GIBBONS, *Duke University.*—The total neutron yield has been measured as a function of proton energy from threshold to about 2.4 Mev. The resulting curve was normalized to that of Taschek and Hemmendinger.[1] The two curves agree well except near threshold where there is a rapid rise for a few kilovolts until the yield becomes practically constant at a proton energy of 1.900 Mev. Dividing the cross section by the neutron velocity in the center-of-mass system, it is apparent that there is a resonance near threshold; the curve has a maximum at 1.888 Mev which is evidently due to

target thickness and proton energy spread. Correcting for these effects it is evident there is no true maximum but the curve appears slightly flatter near threshold than at higher energies. The peak found by Bashkin and Richards[2] at 1.87 Mev is probably due to the same resonance; a resonance in this general region has been predicted by Breit and Bloch.[3]

* Work supported by U. S. Atomic Energy Commission.
[1] R. Taschek and A. Hemmendinger, Phys. Rev. **74**, 373 (1948).
[2] S. Bashkin and H. T. Richards, Phys. Rev. **84**, 1129 (1951).
[3] G. Breit and I. Bloch, Phys. Rev. **74**, 397 (1948).

Q11. The Be^9+He^3 Reactions. C. D. MOAK, W. M. GOOD, AND W. E. KUNZ, *Oak Ridge National Laboratory.*—The charged particle spectrum for the case of He^3 on Be^9 has been measured with a NaI charged particle spectrometer. The following reactions were observed:

$$Be^9+He^3 \rightarrow B^{11}+H^1+10.32 \text{ Mev} \quad (1)$$

$$\rightarrow Be^8+He^4+18.90 \text{ Mev}. \quad (2)$$

In addition, neutron measurements indicate that the following reaction takes place:

$$Be^9+He^3 \rightarrow C^{11}+n^1+7.56 \text{ Mev}. \quad (3)$$

In reaction (1) the proton spectrum shows the excited states already reported in the case of $B^{10}(d,p)B^{11}$.[1] The presence of α particles in the spectrum has been verified through the use of Al absorbers placed between the target and the NaI crystals. The charged particle spectra and thin target yield measurements will be presented.

[1] Van Patter, Buechner, and Sperduto, Phys. Rev. **82**, 248 (1951).

Q12. Capture Gamma Rays from 315-Kev Proton Bombardment of Be^9.* R. R. CARLSON AND E. B. NELSON, *State University of Iowa.*—A three crystal scintillation spectrometer detected 6.7 ± 0.15, 6.0 ± 0.15, 5.1 ± 0.1, and 4.7 ± 0.15 Mev gamma rays with relative intensities (±25 percent) of 0.15, 0.40, 1.00, and 0.45, respectively. These energies correspond to transitions in B^{10} from the capture state at 6.87 ± 0.04 Mev to the ground state and low-lying levels at 0.72, 1.74, and 2.15 Mev.[1] The observed relative intensities and the known spins and parities[1] of the ground state and 1.74-Mev excited state of B^{10} imply spin one for the capture state. A thick target yield of $(1.2\pm0.3)\times10^{-10}-5.1$ Mev gammas per proton was found by comparison with the fluorine gamma-ray yield. Combined with the thin target excitation function,[2] this gives the cross section at resonance (336 kev) for the emission of 5.1-Mev gamma radiation as $(1.2\pm0.4)\times10^{-29}$ cm^2. A single-crystal spectrometer, limited to 2 Mev, detected 0.72 ± 0.02, 1.03 ± 0.03, and 1.43 ± 0.03 Mev gamma rays corresponding to transitions between low-lying levels in B^{10}.

* Supported in part by the U. S. Atomic Energy Commission.
[1] F. Ajzenberg and T. Lauritsen, Revs. Modern Phys. **24**, 321 (1952).
[2] S. E. Hunt, Phys. Rev. **87**, 902 (1952).

Q13. Gamma-Gamma Correlation in $Be^9(d,n)B^{10*}(\gamma)B^{10}$. S. M. SHAFROTH* AND S. S. HANNA, *The Johns Hopkins University.*†—The 2.86- and 0.72-Mev gamma rays from the $Be^9(d,n)B^{10*}(\gamma)B^{10}$ reaction were detected in coincidence. Two sodium iodide scintillation counters were employed, followed by pulse-height analysis and coincidence detection. Thick beryllium targets were used with a bombarding energy of 0.66 Mev. If θ_1 and θ_2 denote the angles of the 2.86- and 0.72-Mev gamma rays, respectively, measured with respect to the beam, and ϕ the dihedral angle between them, the correlation function may be expressed by $W(\theta_1,\theta_2,\phi)$. The following measurements were obtained:

	A_2
$W(\pi/2,\theta_2,\pi)$	0.05 ± 0.03
$W(\theta_1,\pi/2,\pi)$	0.05 ± 0.03
$W(\theta_1,2\pi/3,\pi)$	0.04 ± 0.05
$W(\pi/2,\theta_1,\pi/2)$	-0.01 ± 0.05
$W(\theta_1,\pi/2,\pi/2)$	-0.03 ± 0.05

A_2 is the coefficient in the expression $1+A_2\cos^2\theta$, where θ is either θ_1 or θ_2 (in the third correlation $\theta=\theta_1+\pi/6$). Spin assignments to the states in B^{10} will be discussed on the basis of these results.

* Now at Northwestern University.
† Supported by the U. S. Atomic Energy Commission.

Q14. Magnetic Analysis Indicating Charge Symmetry in the Reaction $Be^9(p,\alpha)Li^6$. R. MALM AND D. R. INGLIS, *Argonne National Laboratory.*—Alphas from $Be^9(p,\alpha)Li^6$ corresponding to the ground state and first excited state of Li^6 show no sign of resonance as the proton energy passes through 2.565 Mev where the transition to the second excited state, the 3.58-Mev state having $T=1$, shows a known gamma resonance. This is consistent with charge symmetry or with conservation of isobaric spin T if the resonant state is assumed to have $T=1$. The observations were made with a 16-inch radius, two-dimensional focusing, magnetic spectrometer the construction and performance of which will be described.

Q15. The Angular Distribution of 12-Mev and 16-Mev Gamma Rays from Proton Bombardment of Boron.* H. H. GIVIN, G. K. FARNEY, T. M. HAHN, AND B. D. KERN, *University of Kentucky.*—The angular distributions of 12- and 16-Mev gamma rays from the reaction $B^{11}(p,\gamma)C^{12}$ have been measured as a function of proton bombarding energy up to 2 Mev. Thin targets were used and corrections were made for the absorption of gamma rays by the tantalum target backing. At each proton energy, the gamma-ray spectrum was obtained at each of seven angles. Angular distributions of the 12- and 16-Mev components were determined from appropriate integrations of the spectrum. Expressing the angular distributions in the form $1+A\cos\theta+B\cos^2\theta$, tentative values of the coefficients at representative energies are shown:

E_p (kev)	A_{16}	B_{16}	A_{12}	B_{12}
700	−0.05	0.18	0.03	−0.13
1000	−0.03	0.14	0.11	0.06
1200	0.02	0.15	0.16	0.09
1400	0.05	0.20	0.17	0.08
1600	0.00	0.24	0.18	0.13

* Sponsored by the Office of Ordnance Research, U. S. Army.

Q16. Neutrons from the Proton Bombardment of B^{10}.† F. AJZENBERG, *Boston University,* AND W. FRANZEN* AND J. G. LIKELY, *Princeton University.*—A B^{10} target, 200-kev thick, has been bombarded with 17.3-Mev protons from the Princeton cyclotron. The resultant neutrons have been studied by means of Ilford C-2 emulsions, 200 and 400 microns thick, mounted approximately 4.5 inches from the target and at five angles to the incident beam. Preliminary measurements at 30, 120, and 150 degrees (2200 tracks) indicate a ground-state Q value of -4.35 ± 0.2 Mev, giving a mass defect for C^{10} of 10.6 Mev, in fairly good agreement with beta-decay results.[1] The data also indicate an excited state of C^{10} at 3.4 Mev and unresolved levels at higher excitation energies.

† This work has been supported in part by the U. S. Air Force through the Office of Scientific Research and in part by the joint program of the U. S. Office of Naval Research and the U. S. Atomic Energy Commission.
* Now at the University of Rochester.
[1] R. Sherr and J. B. Gerhart, Phys. Rev. **91**, 909 (1953).

FRIDAY AFTERNOON AT 2:00

Sheraton Park, Caribar Room

(G. E. UHLENBECK presiding)

Theoretical Physics, IV: Statistical Mechanics

Invited Paper

QA1. The Excluded-Volume Problem. ROBERT J. RUBIN, *Applied Physics Laboratory, Johns Hopkins University.* (30 min.)

Contributed Papers

QA2. Equations of Motion of Coupled Ordered and Dissipative Systems.* J. L. JACKSON, *Applied Physics Laboratory, The Johns Hopkins University.*—J. Weber has investigated[1] in detail the exchange of energy between an ordered system and a dissipative system. The ordered system considered was an ideal electrical oscillator (condenser and inductance) and the dissipative system a generalized circuit element of the type described by Callen and Welton.[2] It has been found possible to derive the equations of motion (in this case the Kirchoff laws) for such coupled systems from the Hamiltonian. Two Kirchoff equations are nonstatistical in nature and are obtained directly as two of the Hamilton equations. The third Kirchoff equation, the one involving the voltage drop across the dissipative system, is a statistical one and is valid only within the limits of first-order perturbation theory. The coefficients in the differential equation for the current through the dissipative system involve exactly the impedances calculated previously by this author.[3]

* This work was supported by the Bureau of Ordnance, Department of the Navy.

[1] J. Weber, Phys. Rev. **90**, 977 (1953).
[2] H. B. Callen and T. A. Welton, Phys. Rev. **83**, 34 (1951).
[3] J. L. Jackson, Phys. Rev. **87**, 471 (1952).

QA3. Solution of the Transport Equation for the Case of Slab Geometry.* J. LEHNER AND G. M. WING, *Los Alamos Scientific Laboratory* (introduced by F. C. Hoyt).—We consider the one velocity flow of neutrons in a uniform infinite slab of thickness $2a$ immersed in a vacuum. Assuming isotropic scattering, the linearized Boltzmann equation may be written

$$-\mu\frac{\partial N}{\partial x}(x,\mu,t)-\sigma N+\frac{c}{2}\int_{-1}^{1}N(x,\mu',t)d\mu'=\frac{1}{v}\frac{\partial N}{\partial t}$$

with $N(\pm a,\mu,t)=0$, $\mu\lesseqgtr 0$. It has long been customary to assume that there exists a complete infinite set of eigenfunctions $N_i(x,\mu,t)=e^{\alpha_i t}n_i(x,\mu)$ in terms of which the initial value problem may be solved. It is proved that this is false, and that the set of eigenfunctions is always finite but nonempty. A solution to the initial value problem is obtained as a sum over this finite set plus an integral. The behavior of this integral for large time is determined.

* Work done under the auspices of the U. S. Atomic Energy Commission.

QA4. On the Principle of Minimum Entropy Production. MARTIN J. KLEIN AND PAUL H. E. MEIJER, *Case Institute of Technology.**—The characterization of the steady state in irreversible processes as the state of minimum entropy production is one of the most interesting aspects of irreversible thermodynamics. We have attempted to derive this property of the steady state by applying the methods of statistical mechanics. The particular model considered was the Knudsen gas: two identical vessels, containing the same ideal gas, maintained at temperatures T and $T+\delta T$, respectively, are connected by a small opening. Using the stochastic equations for the time rates of change of the occupation numbers in the containers, and generalizing a method developed by Thomsen,[1] we have been able to prove that the steady state corresponds to a minimum value of dS/dt. It was essential to include the entropy contributions of the two heat baths (T and $T+\delta T$). The results can be put in a form parallel to that given by Casimir[2] and give some insight into the heat of transport.

* Supported by a grant from the National Science Foundation

[1] J. S. Thomsen, Phys. Rev. **91**, 1263 (1953).
[2] H. B. G. Casimir, Revs. Modern Phys. **17**, 343 (1945).

QA5. Dynamical Behavior of Collective Coordinates in the New Approach to the Many-Body Problem. GEORGE J. YEVICK, *Stevens Institute of Technology*, AND JEROME K. PERCUS, *Columbia University.*—To eliminate the nonlinearity in the dynamical equations of motion for many interacting particles, we[1] have utilized collective coordinates to develop an equivalent but linear theory. As further verification of the equivalence between the oscillator Lagrangian and the true Lagrangian, we have explicitly calculated the equations of motion for the x_i using the collective Lagrangian. We can then show that these equations of motion reduce to the correct set by precisely the same choice of fictitious oscillator masses and frequencies required for conformability between the two Lagrangians. In so doing, we were driven to use many collective coordinates q_k with wavelengths much smaller than the mean interparticle spacing, in order to adequately represent the interparticle potential. Clearly these q_k's cannot represent organized behavior and must be the reservoir for the chaotic thermal energy of the system. The coupling between the low and high q_k's is due principally to the velocity dependent potentials which are treated in the theory as perturabations. The influence of these coupling terms on the degradation of energy from the low to the high k is now being considered as the mechanism for irreversibility.

[1] See Bull. Am. Phys. Soc. **29**, No. 1, Abstracts U4 and U5 (1954).

QA6. Domain of Action of Collective Coordinates in the New Approach to the Many-Body Problem. JEROME K. PERCUS, *Columbia University*, AND GEORGE J. YEVICK, *Stevens Institute of Technology.*—In order to evaluate the classical partition function using the new collective coordinate approach to the many body problem, and even more important, in order to set up the quantum mechanical problem for the collective coordinates, it is paramount to determine the domain of action of the collective coordinates. As a possible approach to this difficult problem, we have been making a comparison between the classical partition functions in x space and q space. We expand $V(x_i-x_j)$ by means of its Fourier coefficients V_k. With a multiple Maclaurin expansion of the two partition functions using variables $(1/T)$ and V_k (T denotes the absolute temperature), an equating of coefficients allows us to compute successive mixed moments of the q_k's. Making the assumption of separability of q space into a product of two-dimensional spaces, we can evaluate these moments, and thus the q-space distribution, by means of a

generating function. This results in a new expression for the classical partition function which has been obtained by neglecting certain combinations of terms because of the properties of the V_k's and the fact that we have only a finite number of k's. This partition function is now being analyzed.

QA7. Statistical Aspects of the Second Law of Thermodynamics. C. D. GREEN AND D. TER HAAR,* *St. Andrews University, Scotland.*—Extending previous investigations[1] to more physical models mean life times and mean times of recurrence for nonequilibrium situations are calculated. The models investigated include the Ehrenfests' two-dimensional wind-wood model,[2] a one-dimensional model with a velocity distribution, models with isotropic scattering and a model with a one-dimensional Maxwell distribution.

* On leave of absence at Purdue University.
[1] D. ter Haar and C. D. Green, Proc. Phys. Soc. (London) **A66**, 153 (1953).
[2] P. and T. Ehrenfest, Anz. Math. Wiss. **4**, part *32* (1911).

QA8. Simplified Model of a Stationary Nonequilibrium Process.* HARRY L. FRISCH AND JOEL L. LEBOWITZ, *Syracuse University.*—A Gibbs ensemble will describe a stationary process if the Liouville equation of the system is modified by additional terms describing the stochastic interaction with surroundings, provided the surroundings are at different temperatures. In that case there will be a flux of energy through the system whose ensemble average does not vanish. Probably the simplest model of such a process is a single one-dimensional particle traveling back and forth between two large pistons having different mean energies of vibration. Because even this model leads to a rather involved integral equation, we have simplified it further by assuming that some of the reflections from the pistons are as from rigid walls, with the remainder (a fixed percentage of all reflections) leading to a redistribution of velocity independent of the incident velocity. This redistribution may be thought of as a surface adsorption with subsequent release. This new model is mathematically so simple that the solutions of the integro-differential equation can be obtained in full by relatively elementary methods. The results will be presented.

* This research was supported by Office of Scientific Research.

QA9. The Quantum-Mechanical Molecular Distribution Functions in a One-Dimensional Fluid Composed of Hard Spheres.* ROBERT J. RUBIN, *Applied Physics Laboratory, The Johns Hopkins University.*—The Schrödinger equation for N hard sphere molecules of mass m and diameter b in a one-dimensional box of length $a>Nb$ is identical with that for one particle of mass m in a special region of an N-dimensional cube. Consider a set of N orthogonal axes y_i and the N-dimensional cube with one corner at the origin, whose edges are in the direction of the coordinate axes and of length $a-Nb$. The polyhedron-like region is that portion of the cube such that $0\leqslant y_1\leqslant\cdots\leqslant y_i\leqslant\cdots\leqslant y_N\leqslant a-Nb$ and $y_i=x_i-(i-\frac{1}{2})b$, where x_i is the coordinate of the ith molecule. The eigenvalue and eigenfunction of a particular stationary state are

$$E_K=\sum_{K_i\neq K_j}^{N}\frac{K_i^2\hbar^2}{8m(a-Nb)^2},\quad \psi_K=D\left[\left(\frac{2}{a-Nb}\right)^{\frac{1}{2}}\sin\frac{K_i\pi y_j}{a-Nb}\right]$$

where $D[\ ]$ is an $N\times N$ determinant. The probability per unit length that any molecule will be at x is

$$\rho^{(1)}(x)=\langle\bar{\psi}_K\sum_{n=1}^{N}\delta(x_n-x)\psi_K\rangle.$$

* This work was supported by the Bureau of Ordnance, Department of the Navy, under Contract NOrd-7386.

QA10. Statistical Mechanics of Temperature-Dependent Energy Levels. P. T. LANDSBERG, *University of Pennsylvania, and University of Aberdeen, Scotland.**—The method of the Gibbs ensemble does not apply to systems whose energy levels E_i depend on the temperature. As a generalization, suppose that $\exp(-E_i/kT)$ be replaced by $\exp(-f_i)$ when the basic relations for the ensemble are set up. f_i is some function of E_i and T. The total energy, entropy (S), free energy (F) per system, as averaged over the ensemble, are now given by generalizations of the usual equations. The restriction that this ensemble shall lead to the usual laws of thermodynamics must still be imposed. In particular, the condition $(\partial F/\partial T)_{V,N}+S=0$ yields a complicated condition which involves the E's, the f's, and their temperature derivatives. If $f_i=E_i/kT$, one finds that the Gibbs ensemble is suitable for physical systems only if $(\partial E_i/\partial T)_{V,N}$, as averaged over the ensemble, is known to vanish. If $f_i=\int[E_i(T)/kT^2]dT$, as proposed by Rushbrooke,[1] the system must satisfy another more complicated relation. It would appear, therefore, that a more far-reaching generalization than that given by Rushbrooke, or possibly even that given by the class of ensembles which we have discussed here, will be required to deal adequately with system whose energy levels may be arbitrary functions of the temperature.

* Assisted by the U. S. Office of Naval Research.
[1] G. S. Rushbrooke, Trans. Faraday Soc. **36**, 1055 (1940).

QA11. Can a Well-Informed Heat Engine (WHE) Have Free Will? JEROME ROTHSTEIN, *Columbia University.*—WHE defined: physical system with measuring apparatus, effector apparatus to operate on environment and self, and internal programming whereby operations are performed on environment and self as a function of information input and internal state. Theorem: arbitrary operationally defined behavior is realizable in principle by WHE.[1] Query: within WHE's universe U (close system containing WHE) can WHE perform measurements permitting him to predict his future behavior? Answer: no. Proof: WHE interacts with rest of U so prediction of WHE behavior requires determination of state ϕ of U. Initial less perfect knowledge of U corresponds to entropy $S(U)>S(\phi)$, in fact $S(\phi)=0$ for pure state required for prediction. If answer yes, 2nd law violated, therefore no. Conclusion: it is impossible for a WHE contained in a closed system to decide, on the basis of measurements made by means wholly contained in the system, between the alternatives (a) the behavior of WHE is determinate (b) the behavior of WHE is indeterminate, i.e., relative to U WHE has "free will."

[1] J. Rothstein, Phys. Rev. **86**, 620(A) (1952).

FRIDAY EVENING AT 7:00

Shoreham, Main Ballroom

(H. A. BETHE presiding)

Banquet of the American Physical Society

After-dinner speakers: E. R. PIORE AND P. DEBYE

SATURDAY MORNING AT 9:30

Shoreham, Main Ballroom

(H. A. BETHE presiding)

Symposium on Polarization of Nucleons by Scattering

R1. High-Energy Experiments on Polarization of Protons. CLYDE WIEGAND, *University of California, Berkeley.* (30 min.)

R2. Polarization of High-Energy Protons. JOHN MARSHALL, *University of Chicago.* (30 min.)

R3. Polarization in Neutron-Proton Collisions. JOHN TINLOT, *University of Rochester.* (30 min.)

R4. Theoretical Considerations about Polarization Experiments. LINCOLN WOLFENSTEIN, *Carnegie Institute of Technology.* (30 min.)

SATURDAY MORNING AT 9:30

Sheraton Park, Continental Room

(H. H. BARSCHALL presiding)

Neutron Physics, II; Neutron Resonances

RA1. Total Neutron Cross Sections in the Kilovolt Region: Tl^{203} and Tl^{205}.* J. H. GIBBONS AND H. W. NEWSON, *Duke University.*—The use of a high-resolution neutron collimation-detection system,[1,2] used in conjunction with a Van de Graaff accelerator and the $Li^7(p,n)$ reaction, has been successful in the isotopic assignment of several Tl resonances in the region 3–80 kev neutron energy. For example, the resonance at 5 kev seems to be due to Tl^{203}, whereas the 17.5-kev peak and at least one peak between 50 and 60 kev are due to Tl^{205}. The Tl^{205} average level spacing seems to be several times that of Tl^{203}. The enriched Tl^{203} sample, which made these measurements possible, was loaned by the Stable Isotopes Division, Oak Ridge National Laboratory. Time permitting, other recent measurements will be presented.

* Work supported by the U. S. Atomic Energy Commission.

[1] J. H. Gibbons and H. W. Newson, Phys. Rev. **91**, 209A (1953).

[2] J. H. Gibbons, Bull. Am. Phys. Soc. **29**, 36 (1954).

RA2. Neutron Capture Measurements with the G. E. Betatron Velocity Selector. R. D. ALBERT, M. L. YEATER, AND E. R. GAERTTNER, *Knolls Atomic Power Laboratory.**—The capture of neutrons in a sample is measured by time coincidence detection of the emitted capture photons.[1] Level densities thus obtained are

Sample	Au	Mo	Ta	Sm_2O_3	Gd_2O_3
Number of levels	7	4	13	16	9
Energy range (ev)	58–186	43–153	10–100	8–95	20–62

Levels separated by 4 ev at 100 ev are resolved. The observed counting rate of photons emitted by a sample having a ratio σ_ϵ/σ_T of capture to total cross section is given by $f(E)\langle\eta^2V(V-1)\rangle_{Av}\sigma_\epsilon/\sigma_T(1-\bar{T})$ where $f(E)$ is the neutron intensity, η the detector efficiency, V the gamma-ray multiplicity, and $\bar{T}$ is the transmission broadened by instrumental resolution. This relation is valid as long as a neutron scattered in the target has small probability of being subsequently capture. The factor $f(E)\langle\eta^2V(V-1)\rangle_{Av}$ is determined by a low-energy measurement where $\sigma_\epsilon \cong \sigma_T$, and $\bar{T}=0$. $f(E)$ is measured with a boron counter. On the assumption that $\langle\eta^2V(V-1)\rangle_{Av}$ is independent of energy, one obtains $\Gamma_\gamma/\Gamma(1-\bar{T})$ as a function of energy for each resonance. Conventional procedures developed for area analysis of transmission data may be applied to obtain resonance parameters.

* Operated by the General Electric Company for the U. S. Atomic Energy Commission.

[1] R. D. Albert and E. R. Gaerttner, Phys. Rev. **91**, 451(A) (1953).

RA3. Resonance Scattering of Ag and Au.* R. E. WOOD,† *Brookhaven National Laboratory.*—The resonance scattering of Ag and Au has been measured below 10 ev, using thin samples and the scattering pipe technique of Borst.[1] On the basis of the observed scattering data and the available total cross section data, the total angular momentum of the compound nucleus in the resonant state has been uniquely determined as follows: $I=1$ ($g=\frac{1}{2}$) for the 5.2-ev resonance of Ag, and $I=2$ ($g=\frac{3}{4}$) for the 4.91-ev resonance of Au. These assignments are in disagreement with the results of Tittman and Sheer[2] in the case of Au, and are in agreement with the results of Sheer *et al.*[3] in the case of Ag. The method of analysis will be given and parameters of the resonances will be discussed.

* Research performed under the auspices of the U. S. Atomic Energy Commission.

† Doctoral candidate from the University of Utah.

[1] L. B. Borst, Phys. Rev. **90**, 859 (1953).

[2] J. Tittman and C. Sheer, Phys. Rev. **83**, 746 (1951).

[3] Sheer, Moore, Rainwater, and Havens, Columbia Nuclear Physics Progress Report, June 1952.

RA4. Self-Indication Measurement of σ_{to} for the 5.2-ev Neutron Resonance in Silver.* J. E. DRAPER AND C. P. BAKER, *Brookhaven National Laboratory.*—This measurement was made using the pulsed 60-inch cyclotron to deliver a neutron burst of 0.7 μsec in each 540 μsec interval, and a 64 channel time-of-flight analyzer to distinguish neutron energies. The detector was a thin silver (n,γ) radiator viewed by six shielded NaI gamma detectors (in fast twofold coincidence to minimize background which was 0.03 of the resonance peak with thick samples). The counting rate *vs.* neutron flight time over a 4.3-meter flight path was taken (a) with only the silver radiator in position and (b) with the addition of the same thickness of silver absorber in good geometry. The ratio of the areas in the resonance for (b) and (a) constitutes the transmission which depends only on σ_{to} and not on the width Γ. Six silver thicknesses were used ranging $N\sigma_{to}$ from 0.24 to 120 to check the fit of data with theory. Preliminary analysis gives $\sigma_{to}=33\,000\pm3000$ barns (isotopic). The analysis of data taken at a resolution of 0.2 μsec/m for silver resonances up to 100 ev is in progress. The influences of Doppler broadening, scattering in the radiator, and wing area will be discussed.

* Research performed under contract with the U. S. Atomic Energy Commission.

RA5. Measurements of Neutron Resonance Parameters in U, Th, Hg, and Au.* J. S. LEVIN AND D. J. HUGHES,† *Brookhaven National Laboratory.*—Several neutron resonances in U, Th, Hg, and Au have been investigated with the Brookhaven fast chopper and their parameters determined. Three methods of analysis were used; "shape" analysis, "area" analysis, and a method[1] based on an analysis of the interference between resonance scattering and potential scattering. All of these analyses are corrected for the effects of Doppler broadening. The parameters of the 6.70±0.06-ev resonance in U^{238} were found to be $\sigma_0=23\,000\pm3000$ b, $\Gamma=25\pm2$ mv, $\Gamma_n=1.5\pm0.1$ mv, $\sigma_0\Gamma=595\pm30$ bev, $\sigma_0\Gamma^2=15.2\pm0.7$ bev.[2] The radiation width of this level is therefore 23.5±2 mv, which is the smallest value reported for any resonance. The 22, 24, and 71-ev resonances in Th^{232} also have very small radiation widths. The 4.9 and 61-ev levels in Au^{197}, and the 23-ev level[2] in Hg^{198} of Γ_γ on atomic weight in this group of elements indicates that radiation widths are influenced by nuclear shell structure.

* Work carried out under contract with U. S. Atomic Energy Commission.
† At present a Fulbright Professor at Cambridge University.
[1] Kato, Hughes, and Levin, Phys. Rev. **93**, 930 (1954).
[2] Isotopic assignment of this resonance made by L. M. Bollinger, private communication.

RA6. Parameters of Neutron Resonances in Cs, In, Sn, Pr.* R. S. CARTER AND J. A. HARVEY, *Brookhaven National Laboratory.*—The neutron resonance cross section structure of cesium, indium, tin, and praseodymium has been investigated in the energy interval 3 to 400 ev using the Brookhaven fast chopper. Wherever possible thick and thin samples were run to determine Γ from which a value for Γ_γ could be obtained. The average Γ_γ for each element was obtained and used in the calculation of Γ_n for each resonance. The ratio of the average reduced neutron width to the average level spacing per spin state ($\bar{\Gamma}_n^0/\bar{D}$) was determined for each element. Ten resonances were found below 300 ev in Cs^{133}. For the seven resonances below 160 ev, $\bar{D}=50$ ev per spin state and $\bar{\Gamma}_n^0/\bar{D}=0.7\times10^{-4}$. Twenty-two resonances were found below 150 ev in normal indium (4.2 percent In^{113}, 95.8 percent In^{115}). Below 50 ev, $\bar{D}=17$ ev per isotope and spin state. Separated isotopes of In are now being studied. Seven resonances were found below 150 ev in normal tin. One is in Sn^{119}, two in Sn^{117}, one in Sn^{116}, and none in Sn^{120}. The remaining three have not yet been identified. The large spacing agrees with the results obtained at 1 Mev.[1] Four resonances were found in Pr below 360 ev giving a value for $\bar{D}$ of about 200 ev per spin state.

* Work carried out under contract with the U. S. Atomic Energy Commission.
[1] Hughes, Garth, and Levin, Phys. Rev. **91**, 1423 (1953).

RA7. Neutron Resonances in Holmium, Thulium, and Lutetium.* V. E. PILCHER, R. S. CARTER, AND A. STOLOVY, *Brookhaven National Laboratory.*—Neutron transmission measurements of holmium, thulium, and lutetium in the energy region 3–300 ev have been carried out using the Brookhaven fast chopper. With the present resolution it is felt that all resonances have been resolved up to 100 ev. It has been possible to analyze most of the observed resonances for the individual Breit-Wigner parameters by making use of two different sample thicknesses. The analysis, in all cases, is based on the measurement of the area above a transmission dip, with corrections for Doppler broadening. In holmium, 19 resonances have been observed, giving an average level spacing ($\bar{D}$) of 12 ev per spin state. A value of Γ_n has been calculated for each resonance, making use of a best value of Γ_γ (assumed constant). The ratio $\bar{\Gamma}_n^0/\bar{D}$ for holmium is found to be 2.8×10^{-4}. In thulium, 17 resonances were found, giving an average level spacing of 14 ev per spin state. Preliminary calculations give a $\bar{\Gamma}_n^0/\bar{D}$ of 1.7×10^{-4}. Analysis of data on lutetium is now in progress.

* Work carried out under contract with U. S. Atomic Energy Commission. These samples were loaned to us by Dr. F. H. Spedding of the Ames Laboratory.

RA8. Variation of the $\bar{\Gamma}_n^0/\bar{D}$ Ratio with Atomic Weight.* J. A. HARVEY, C. E. PORTER, AND D. J. HUGHES,† *Brookhaven National Laboratory.*—The black-nucleus model[1,2] predicted a value of $\sim1.4\times10^{-4}$ for the ratio of the average of the reduced neutron width of low-energy neutron resonances for a given spin state of the compound nucleus to the average of the level spacing of that spin state. According to several recent theories[3–5] this ratio depends upon the size of the target nucleus and has pronounced maxima at atomic weights corresponding to size-resonances. In the cloudy-crystal-ball model[3] this ratio can vary from about $(0.2\text{–}8)\times10^{-4}$. A careful study has been made of the parameters of the resonances up to 100–200 ev for many nuclei above atomic weight 100. A peak in the width-to-spacing ratio of only twice the black-nucleus value is found about mass 160. Around mass 120 and above mass 190 the ratio is 0.8×10^{-4}. A discussion of this discrepancy will be given.

* Work carried out under contract with the U. S. Atomic Energy Commission.
† At present a Fulbright Professor at Cambridge University.
[1] Feshbach, Peaslee, and Weisskopf, Phys. Rev. **71**, 145 (1947).
[2] H. Feshbach and V. F. Weisskopf, Phys. Rev. **76**, 1550 (1949).
[3] Feshbach, Porter, and Weisskopf, U. S. Atomic Energy Commission Report NYO-3076, 1953 (unpublished).
[4] A. Bohr and B. R. Mottelson, Danske Vidensk. Selskab. Mat.-fys. Medd. **27**, No. 16 (1953).
[5] R. G. Thomas, private communication.

RA9. Analyses of Neutron Resonances in the Zinc Isotopes. D. A. DAHLBERG AND L. M. BOLLINGER, *Argonne National Laboratory.*—Using the Argonne fast neutron "chopper," measurements have been made on the cross section of normal zinc and samples enriched in Zn^{64}, Zn^{66}, Zn^{67}, and Zn^{68} over the energy range from 150–10 000 ev. An isotopic assignment was made for all resonances observed in normal zinc. Resonance widths Γ were obtained by finding values of Γ which give calculated areas above the transmission dips that are equal to the experimentally measured areas, and by curve fitting using the Breit-Wigner one-level formula. The results obtained are shown in Table I. No resonances were observed in Zn^{66} below 10 kev.

TABLE I.

E_0	Isotopic assignment	g (assumed)	Γ
225 ev	67	½	1.3 ev
455	67	½	10
530	68	1	10
1620	67	½	19
2300	67	½	29
2750	64	1	70
4600	64	1	56

RA10. Total Neutron Cross Sections of Bi and Mn. L. M. BOLLINGER, R. R. PALMER, AND D. A. DAHLBERG, *Argonne National Laboratory.*—The Argonne fast neutron "chopper" was used to measure the total neutron cross sections of Bi and Mn in the energy range 200 to 10 000 ev. In Bi, the resonances at 810 and 2370 ev, for which widths of 5.3 and 19 ev were measured, were both observed to have the characteristic *S*-wave scattering shape. For manganese, the first three resonances at 337, 1080, and 2360 ev, were intensively studied. Assuming *S*-wave scattering, the measured peak cross section of the 2360-ev resonance implies that its J value must be 3. An unusual behavior was observed for the cross section in the neighborhood of the 1080-ev resonance which can be interpreted as being caused by interference between resonances. This interpretation implies $J=3$ for the 1080-ev level and $J=2$ for the 337-ev level. Cross-section curves calculated with the above J assignments reproduce every qualitative feature of the measured curves, but no choice of level widths gives

complete quantitative agreement. In particular, the width required to fit the data near the base of the 337-ev resonance is greater than that needed near its peak.

RA11. Further Applications of the "Internal Source" Scintillation Spectrometer. E. DER MATEOSIAN, *Brookhaven National Laboratory.**—"Internal source" scintillation spectrometry is performed by means of the usual methods of scintillation spectrometry with the exception that a NaI—Tl crystal is used in which is dissolved the source of radiations under investigation. Obvious advantages of incorporating the radioactive material into the crystal are that one obtains a 4π geometry, almost 100 percent efficiency for ionizing particles and soft photons and the absence of "window" and source thickness corrections. In previous publications we have described the application of this technique to the study of two-step isomeric transitions, beta decay, alpha-particle decay, and L and K orbital electron capture. The method has now been used to determine the neutron capture cross section for the recently observed successive neutron capture in Ta^{181}; i.e., $Ta^{181}+n\rightarrow Ta^{182}+n\rightarrow Ta^{183}$. A comparison of the amounts of Ta^{182} and Ta^{183} formed allows one to calculate a value for the neutron capture cross section for the second step, which we find to be $59\,000\pm10\,000$ barns. A further application has been made to the study of Cd^{113m} which decays by means of the emission of a 575-kev beta ray.

* Work accomplished under the auspices of the U. S. Atomic Energy Commission.

RA12. Neutron Multiplicity from Spontaneous Fission of Uranium. K. W. GEIGER AND D. C. ROSE, *Research Council of Canada.*—Metallic uranium[1] was placed in a paraffin pile containing two $^{10}BF_3$ neutron counters. The amplifier was blocked by a gate circuit which opened for 320 μsec after the first neutron of an event was collected. This time is about twice as long as the mean life of thermal neutrons in the pile. The number of neutrons during this interval was recorded and gives therefore information concerning the actual number of neutrons released in one fission event. The efficiency of the pile was found using the known neutron rate from spontaneous fission of U, 1.65×10^{-2} neutrons sec^{-1} g^{-1}.[2] Without further assumptions the method does not give the mean neutron multiplicity directly but the higher moments of the multiplicity spectrum. A Poisson distribution for the multiplicity spectrum fits our data well and gives an average of 2.2 ± 0.2 neutrons per spontaneous fission. This value is in good agreement with the mean multiplicity from other methods.

[1] Loaned by Atomic Energy of Canada Limited.
[2] D. F. Littler, Proc. Phys. Soc. (London) **A65**, 203 (1952).

SATURDAY MORNING AT 9:30

Shoreham, West Ballroom

(BRUNO ROSSI presiding)

Cosmic Rays

S1. Galactic r-f Radiation and Cosmic-Ray Electrons.* S. B. TREIMAN AND M. BLUME, *Princeton University.*—It has been suggested[1] that our spiral arm is permeated by a magnetic field directed along the arm and of magnitude $\sim6\times10^{-6}$ gauss. Such a field would cause cosmic-ray electrons to radiate, partly in the radio-frequency range. A calculation of this effect has been made for an assumed electron energy spectrum of the form const$\times E^{-2}$, with a "cutoff" at 1.5 Bev. (The results are not sensitive to the choice of the exponent.) Comparison with the observed r-f intensities coming from the galactic background leads us then to an estimate of f_{max}, the upper limit on the fraction of electrons in the cosmic radiation. We find $f_{max}\approx0.2$. Inasmuch as direct measurements give an upper limit of only a few percent,[2] this result is not in itself very interesting. However, we point out that for the magnetic field configuration envisaged in reference 1, the bremsstrahlung should be strongly polarized. The apparent experimental absence of polarization permits us then to lower the estimate of f_{max} by at least an order of magnitude, limited only by the accuracy of polarization measurements.

* Supported in part by the U. S. Office of Naval Research and the U. S. Atomic Energy Commission.
[1] S. Chandrasekhar and E. Fermi, Astrophys. J. **118**, 113 (1953).
[2] Critchfield, Ney, and Oleska, Phys. Rev. **85**, 461 (1952).

S2. Acquirement of Cosmic-Ray Energies by Betatron Action.* W. F. G. SWANN, *Bartol Research Foundation.*—In a cylindrically symmetrical problem with magnetic field along the axis of z and changing with time, the energy of a particle is shown to increase continually if $E-\dot{r}H/c$ is greater than zero, E being the tangential electric field, and $\dot{r}$ the radio velocity. It follows, moreover, that if $E>H$, a particle can never loop except around the origin of symmetry. The situation is discussed in relation to galactic magnetic fields. Spacial conductivity plays a role in cosmic-ray problems concerning acquirement of energy. It is pointed out that there is an upper limit nec to the spacial current density where n is the number of ions per cc, and e is the electronic charge. The implication of this limitation in cosmic-ray problems is discussed.

* Assisted in part by the joint program of the U. S. Office of Naval Research and the U. S. Atomic Energy Commission.

S3. Solar-Connected Variations of the Cosmic Rays. P. MORRISON, *Cornell University.*—Three apparently distinct variations of cosmic-ray intensity in time can be ascribed to solar phenomena: (1) large sudden increases of low-energy cosmic-rays at the time of exceptional solar flares, (2) world-wide decreases in cosmic-ray intensity, lasting for days, and correlated roughly with magnetic storms, (3) irregular maxima and minima showing a marked 27d recurrence. The Chicago group has demonstrated that the increases of type (1) correspond to cosmic-ray particles emitted from roughly the solar direction and that less extreme flares also emit cosmic-ray particles but in smaller numbers. Events of type (2) can be explained as the consequences of emission from the active sun of diffuse clouds of ionized hydrogen bearing a turbulent magnetic field. If such clouds are sufficiently large and carry appropriate fields they will sweep the interplanetary volume free of cosmic-ray particles, which randomly diffuse into the clouds until steady-state density is reached. With parameters reasonable for these events, the steady state is reached in days. The observed decreases are interpreted as times when the earth is immersed in such an empty cloud. Similar, but less unusual clouds emitted from solar active regions, and partly filled at formation with solar-flare generated cosmic-rays, can account for type (3) changes as well.

S4. Storm Decrease of the Cosmic Radiation at the Pole. S. F. SINGER, *University of Maryland.*—A large decrease in the cosmic-ray intensity has been observed in the immediate vicinity of the geomagnetic pole for the first time, in association with similar variations at other geomagnetic latitudes. Hence the explanation of the cosmic storm decrease in terms of a magnetic redistribution due to an equatorial ring current becomes quite unlikely. It is possible to account for the effect either by a general deceleration of the cosmic radiation in the vicinity of the earth or by a decrease in their number or by both. Experiments will be discussed which may allow one to distinguish among these possibilities.

S5. The Flux of Primary Cosmic-Ray Heavy Nuclei at the Equator. R. F. HOURD, J. R. FLEMING, AND J. J. LORD, *University of Washington.*—Nuclear emulsions have been exposed in the stratosphere in connection with the U. S. Office of Naval Research sponsored project Churchy. The plates were exposed by Skyhook balloon for 6.6 hours at elevations from 90 000 to 94 000 feet and at geomagnetic latitude 10°N. A sandwich of 6 Ilford G-5 emulsions 600 microns in thickness were employed having only thin tissue paper between adjacent emulsions. The sandwich of emulsions with surfaces vertical were placed in a thin aluminum container along with thermal insulation. The outside plates of the sandwich were scanned for heavy tracks. The tracks were then identified by range, delta rays, grain counting, and the photoelectric determination of their width. Making corrections for geometry and absorption, the primary flux of particles having $Z \geq 10$ was found to be 0.44 ± 0.08 per sterad per second per square meter. The corresponding flux of C, N, O, and F nuclei was 2.3 ± 0.5. In addition, while it is difficult to make corrections for secondary Li, Be, and B it does appear that their relative abundance is even slightly greater than that reported by the Bristol group for latitude 55°N.

S6. A Čerenkov Counter Measurement of Fast Multiply Charged Cosmic Rays.* JOHN LINSLEY, *University of Minnesota.*—Additional results have been obtained with an improved version of the Čerenkov counter-cloud chamber apparatus which yielded a recently reported measurement of the flux of primary cosmic-ray alpha particles.[1] Instead of merely triggering the cloud chamber, the Čerenkov counter signals were displayed on a cathode-ray tube which was intensified by a gate from the geometry-defining Geiger-counter telescope so that pulse heights were recorded on continuously moving film. Sufficiently large gated signals, triggered the cloud chamber, provided it was sensitive at the time, so the event that caused the signal could be examined in some detail in such cases. Use of a larger multiplier permitted more rapid accumulation of data, and steps were taken to reduce perturbation of the flux that was measured by the material in the apparatus. Data were obtained during two Skyhook balloon flights at geomagnetic latitude 40°. The flux of fast alpha particles at that latitude will be reported, and information will be presented relating to primaries with Z greater than two.

* The research was supported in part by the joint program of the U. S. Atomic Energy Commission and the U. S. Office of Naval Research.
[1] Bull. Am. Phys. Soc. **29**, 59 (1954).

S7. Fragmentation of Heavy Primary Nuclei of the Cosmic Radiation into Light Elements.* J. H. NOON AND M. F. KAPLON, *University of Rochester.*—Interactions of heavy primary nuclei with carbon, oxygen, and hydrogen nuclei of plastic (cellulose acetate) have been studied to determine the proportion of light elements (Li,Be,B) produced as fast fragments. A vertical stack of stripped emulsions and plastic sheets was flown at Minnesota (55° geomagnetic) for 9 hours at 102 000 ft. Twelve 400μ Ilford G-5 emulsions (6 in.×4 in.), 11 200μ G-5–200μ G-0 emulsions and 11 plastic sheets were arranged in 11 sets of triads. In tracing 800 heavy primaries ($Z \geq 6$) through the stack, 15 interactions were found to occur in the plastic and in 8 cases light elements were produced as fast fragments. The probability for fragmentation into light elements thus obtained agrees with a previous calculation on the basis of a simple geometrical model using data from heavy primary interactions with nuclei of photographic emulsion.[1] This information is important in estimating what proportion of the observed flux of light elements at a given depth in the atmosphere comes from interaction of heavy primaries with nitrogen and oxygen of the residual atmosphere.

* This research was supported in part by the U. S. Air Force under Contract AF 18(600)-380 monitored by the Office of Scientific Research, Air Research and Development Command.
[1] Noon, Kaplon, and Ritson, Phys. Rev. **92**, 1585 (1953).

S8. The Interaction of Cosmic-Radiation Heavy Primaries in Lead.* Y. EISENBERG, *Cornell University.*—An emulsion "cloud chamber" consisting of lead plates and photographic emulsions was flown for 10 hours at a depth of 18 g/cm^2 from the top of the atmosphere. 508 tracks of primaries of charge $Z \geq 6$ traversing a total amount of 16 meters of lead were followed through the entire stack and the interaction mean free path was measured as a function of the mass number of the incident particles. The best fit to the experimental points is obtained by assuming a geometric cross section $\sigma = \pi(R_1 + R_2)^2$, $R = R_0 A^{\frac{1}{3}}$ and $R_0 = 1.2 \times 10^{-13}$ cm the interactions were studied in greater detail. The energy spectrum of the primary radiation was determined, the fragmentation of the incident particles was measured, and the relative abundance of the various charge groups at the top of the atmosphere was deduced.

* Supported in part by the U. S. Atomic Energy Commission and the U. S. Office of Naval Research.

S9. Nuclear Size and Cross Sections at Cosmic-Ray Energies.* ROBERT W. WILLIAMS, *Princeton University.*—Recent measurements of the absorption cross section of various nuclei for 1.4-Bev neutrons[1] have yielded nuclear radii which are quite close to those inferred from the electromagnetic experiments. The results of several cosmic-ray investigations have shown that cross sections for neutrons and protons in the "penetrating-shower" region (energy up by one order of magnitude) are consistently larger than could be inferred on a uniform-density nuclear model A nonuniform model ("fuzzy edge") is used here to reconcile partially the two sets of data and infer a nucleon-nucleon cross section in the high-energy domain.

* Supported by the U. S. Office of Naval Research and the U. S. Atomic Energy Commission.
[1] Hill, Coor, Hornyak, Smith, and Snow, Bull. Am. Phys. Soc. **29**, 54 (1954).

S10. Observations on the High-Energy Soft Cascade.* M. KOSHIBA AND M. F. KAPLON, *University of Rochester.*—The use of stripped emulsion stacks affords an excellent opportunity to study the soft cascade process in detail. In order to specify with some certainty the initial conditions of the cascade and to introduce no selection bias, it is appropriate to study the soft showers originating from the decay photons of neutral π mesons emitted in high-energy nuclear interactions. Soft showers which appear to originate from a single electron or photon in the emulsion may be accompanied by one or more photons; further, for these showers there may be a detection bias favoring those showers with the largest fluctuations.

We have studied the soft cascades initiated by the decay π^0 photons of a very high-energy nuclear interaction. For the showers of low initial energy the cascade seems to develop in accord with the predictions of shower theory; on the other hand for showers of very high initial energy ($\gtrsim 100$ Bev), the trident process seems to play an important role in the initial

development.[1] Detailed shower developments will be presented and the trident process discussed.

* This research was supported in part by the U. S. Air Force under a contract monitored by the Office of Scientific Research, Air Research and Development Command.
[1] Evidence for this was presented by Dr. P. Freier at the Duke Conference on Cosmic Radiation.

S11. Cross Sections for Meson-Induced Stars in Ilford G5 Nuclear Emulsions.* LEONARD A. MANN, RAY A. GRANDEY, AND ARNOLD F. CLARK, *Carnegie Institute of Technology.*—Ilford G5 plates were exposed to pion beams of various energies. The mean free paths and prong distributions for the stars formed in the emulsion are listed in Table I. The negative

TABLE I.

Pion	Energy (mev)	No. of stars	Mean free path (cm)	Average No. of prongs per star
π^+	110	369	33.6±1.7	3.1
π^-	110	349	...	2.7
π^+	155	400	31.1±1.7	3.2
π^-	155	1454	27.9±1.7	2.6
π^-	210	770	29.8±0.9	3.0

pion plates were "area scanned," the positive pion plates were scanned linearly. The total cross section corrected for the Coulomb barrier, taken at 10 Mev, is constant within statistical error. The errors quoted are standard deviations based upon the number of stars and the estimate of the length of track scanned.

S12. Cosmic-Ray μ Meson—Low-Energy Differential Range Spectrum.* A. FAFARMAN AND M. H. SHAMOS, *New York University.*—The differential range spectrum of cosmic-ray μ mesons has been investigated in the region from 0 to 410 gm/cm² Pb. The apparatus comprised a GM counter tray "*A*" (30×50 cm²) and a 3-liter tank of liquid scintillator "*B*" (15 cm diameter×20 cm deep) with variable thickness of absorber between the two. Delayed coincidences *A B B* (delayed 0.5 to 8.0 μsec) were used to identify mesons stopping in the tank; for each such event the delay between *B* and *B* (delayed) was recorded by a 4 channel delay discriminator. The possibility of a contribution to the counting rate from the photomultiplier after-pulsing was investigated and found to be zero. The spectrum decreases monotonically with decreasing energy and shows no irregularity: (several minima have been observed in this portion of the spectrum by investigators using the anticoincidence method which they attributed to electrons and/or protons). Although only relative readings were taken, the method is adaptable to a precision determination of the *absolute* differential range spectrum of low-energy mesons, a region of the spectrum where some uncertainty exists.[1] The delay data yields for the natural mixture of sea level cosmic-ray μ mesons a mean life in carbon of 2.14±0.07 μsec.

* Research assisted by the U. S. Atomic Energy Commission and the U. S. Office of Naval Research.
[1] C. M. York, Phys. Rev. **85**, 998 (1952).

S13. Pairs Formed by Bremsstrahlung of Great Energy. I. Experimental. D. T. KING AND M. M. BLOCK,* *Naval Research Laboratory.*—In cosmic-ray experiments on electromagnetic phenomena of high energy there is a possibility of confusion between electron pairs created directly by fast electrons[1] (tridents) and bremsstrahlung pairs materializing indistinguishably close to the track of the parent particle. In nuclear emulsions, pairs originating within ~0.2 micron from their parent track are generally unresolvable from tridents. In order to examine this effect, we have measured for 200 examples the projected orthogonal distance between the origin of a bremsstrahlung pair and the nearest thin parallel track. Twenty-six emulsions were exposed to the cosmic radiation at altitudes exceeding 95 000 ft at geomagnetic latitude 55°N for six hours. The energies of the incident electrons considered were between 0.1 and 10 Bev. The experimental proximity distribution has been compared to the theoretical distribution to be described in the following paper. From these data we estimate the fraction of apparent tridents among the bremsstrahlung pairs to be about 6 percent.

* On military leave of absence from Duke University, Durham, North Carolina.
[1] Hooper, King and Morrish, Phil. Mag. **42**, 304 (1951).

S14. Pairs Formed by Bremsstrahlung of Great Energy. II. Theoretical Separation Distribution. M. M. BLOCK* AND D. T. KING, *Naval Research Laboratory.*—The distribution in orthogonal separation between the point of materialization of a bremsstrahlung pair and the track of the parent electron has been derived. Since the major contribution to the proximity distance in nuclear emulsions usually arises from the multiple coulomb scattering of the parent particle, we have not considered the angle of emission due to the radiative collision. The calculations have been made for the experimental conditions described in the preceding paper and satisfactory agreement with those results has been found. The analysis enables us to determine the fraction of bremsstrahlung pairs which materialize within a given distance from the path of the parent electron. The fraction experimentally unresolvable from tridents is found to increase rapidly with increasing energy of the incident particle. Thus, for a primary energy of 100 Bev and a path length of 0.5 radiation units in the emulsion, it is found that this fraction is ~70 percent.

* On military leave of absence from Duke University, Durham, North Carolina.

S15. Ratio of π^-/π^+ Meson Production in Cosmic-Ray Disintegrations of Emulsion Nuclei. HERMAN YAGODA, *National Institutes of Health.*—In the examination of 1–2 mm thick G5 emulsions[1] exposed in the stratosphere 531 σ stars and 121 $\pi\mu$ decays were observed to originate in stars or decay processes. The π^-/π^+ ratio exhibits a strong energy dependence. When corrected for π^- mesons which only produce neutrons and Auger electrons on capture, the variation with energy is

T_π (Mev)	0–5	7.5±2.5	12.5±2.5	27.5±12.5
π^-/π^+	16.1±2.6	5.4±0.8	3.6±0.7	2.4± 0.5

At the highest kinetic energies under consideration the π^-/π^+ ratio appears to approach 2, rather than unity as indicated by Mei and Pickup.[2] One example of the coplanar decay of a charged tau meson into three pions has been observed. Two of the secondaries terminate giving $E_{\pi^-}=3.9$ Mev and $E_{\pi^+}=29$ Mev. The energy of the third particle is estimated at 45±5 Mev from the grain density along 3400 microns of recorded track. The mass of the tau meson based on a Q value of 78±5 Mev is 984±10m_e.

[1] H. Yagoda, Phys. Rev. **85**, 891–900 (1952).
[2] J. Y. Mei and E. Pickup, Can. J. Phys. **30**, 430–7 (1952).

SATURDAY MORNING AT 9:30

Sheraton Park, Burgundy Room

(W. W. BUECHNER presiding)

Reactions of Transmutation, II

SA1. Pickup Reactions $B^{10}(n,d)Be^9$ for 14-Mev Neutrons.* F. L. RIBE AND J. D. SEAGRAVE, *Los Alamos Scientific Laboratory.*—Measurements have been made of the yields and angular distribution of deuterons resulting from the bombardment of B^{10} by 14-Mev neutrons. The spectrum of charged reaction products was measured by means of a coincidence-telescope spectrometer consisting of two proportional counters and a thin NaI scintillator. The telescope was rotated to obtain measurements at various angles. Deuterons corresponding to the ground state and 2.43-Mev excited state of Be^9 were identified by measurements of both their energy and dE/dx values. The ground-state angular distribution was found to match the expected Butler inverse-stripping curve for $l_p=1$. The Butler analysis for the excited-state deuterons also gave $l_p=1$, corresponding to odd parity and spin 3/2, 5/2, 7/2, or 9/2 for the first-excited state of Be^9. In particular, the spin value 1/2, to be expected from the $L-S$ coupling model, is excluded. The cross sections, integrated from zero to 90 degrees (center-of-mass), are 21 ± 3 and 16 ± 2 millibarns, respectively, for the ground- and excited-state reactions.

* Work done under the auspices of the U. S. Atomic Energy Commission.

SA2. Cross Sections for the Reactions $C^{12}(p,pn)(n,2n)C^{11}$. S. D. WARSHAW, R. A. SWANSON, AND A. H. ROSENFELD, *The University of Chicago.*—The cross section for the reaction $C^{12}(p,pn)C^{11}$ has been measured at two energies, one above and one below that at which a dip has been observed at Berkeley.[1] At 387 ± 16 Mev the cross section is 43.6 ± 2.2 mb. This value does not fall on an extrapolation of the Berkeley result. However, at 283 ± 14 Mev we find 48.9 ± 2.5 mb which agrees with Berkeley within experimental error. The error of our experiment comes almost entirely from the uncertainty of the calibration of the C^{11} counter. The reproducibility of a single measurement was better than 1 percent so that the relative slope of the cross section as a function of energy is accurately determined. Using the same C^{11} counting techniques, the cross section for the $(n,2n)$ reaction is found to be 17.9 ± 1.4 mb for the Chicago neutron beam. For this beam, studied by Yodh,[2] the energy region from 300 to 440 Mev contains about one-half the neutron flux—peaked at about 400 Mev—with the remainder nearly uniformly distributed down to 20 Mev. This cross section may be compared with 20.0 ± 4 mb for a spectrum peaked at 90 Mev[3] and indicates that the cross section is probably nearly constant with energy.

[1] Aamodt, Petersen, and Phillips, Phys. Rev. **88**, 739 (1952).
[2] G. B. Yodh (to be published).
[3] R. L. Mather and H. F. York, quoted in reference 1. See also McMillan and York, Phys. Rev. **73**, 262 (1948).

SA3. Excitation Function for $C^{12}(D;\ p,2n)C^{11}$, $C^{12}(He^3;\ 2p,2n)C^{11}$, and $C^{12}(\alpha;\ 2p,3n)C^{11}$.* W. BIRNBAUM AND W. E. CRANDALL, *California Research and Development Company*, G. P. MILLBURN AND R. V. PYLE, *University of California, Berkeley.*—The carbon-11 activity *versus* range for monoergic beams of 340-Mev protons, 190-Mev deuterons, 490-Mev He^3 particles, and 380-Mev alpha particles are compared and from the known attenuation cross section for these particles and the excitation function for $C^{12}(p,pn)C^{11}$ reaction,[1] similar excitation functions for the multi-nucleon particles are obtained.

* Supported by the U. S. Atomic Energy Commission.
[1] Aamodt, Petersen, and Phillips, Phys. Rev. **88**, 739 (1952).

SA4. Energy Levels of C^{13} by Inelastic Alpha Scattering.† D. W. MILLER, V. K. RASMUSSEN, AND M. B. SAMPSON, *Indiana University.*—The previously reported[1] investigation of the inelastic scattering of 22-Mev alpha particles by carbon has been extended. Recoil nuclei from elastic scattering and from inelastic scattering with excitation of the 4.43-Mev level have been observed at forward angles. No recoils in which the C^{12} had been excited to the 7.7-Mev level were observed. From the observed intensity of the corresponding inelastic alphas, the probability that a C^{13} nucleus excited to the 7.7-Mev state will decay to Be^8+He^4 is estimated to be greater than $\sim$80 percent. At forward angles the alpha spectrum corresponding to 8 to 16 Mev excitation of C^{13} has been investigated. A weak group leaving C^{13} excited to 12.7 Mev and an intense broad group with several peculiar characteristics are observed. No other group with intensity greater than 10 percent that of the alpha group leaving C^{13} in the 9.6-Mev state can be detected above the continuum due to $C^{13*}\rightarrow Be^8+He^4$. The broad group is found only at angles less than 20°. It may possibly be explained by inelastic scattering, leaving C^{13} in a number of overlapping states between 9 and 11.7 Mev.

† Supported by the joint program of the U. S. Office of Naval Research and the U. S. Atomic Energy Commission.
[1] Rasmussen, Miller, Carmichael, and Sampson, Phys. Rev. **92**, 852 (1953).

SA5. Energy Levels in C^{14} and N^{14}.* R. D. BENT, R. W. BONNER, AND R. F. SIPPEL, *The Rice Institute.*—The gamma radiation from the bombardment of a 50 percent $C^{13}-C^{12}$ target with four-Mev deuterons has been measured with a lens-type pair spectrograph. The energies of internally converted pairs were measured with a resolution of 2.7 percent. Strong gamma-ray lines were observed at 3.10, 3.42, 4.96, 5.12, 5.74, 6.14, and 6.72 Mev. Weaker lines were observed at 3.7, 3.9, 4.48, 6.48, 7.11, and 7.37 Mev. The intensity of the 6.72-Mev line relative to that at 6.14 Mev was increased by a factor of 3 when the bombarding energy was increased from 2 to 4 Mev. A probable interpretation of the lines are: those at 3.10, 3.7, and 3.9 are from the reaction $C^{13}(d,p)^*C^{13}$; The line at 4.48 Mev from the reaction $C^{13}(d,\alpha)^*B^{11}$ or a cascade in $^*N^{14}$; the lines at 4.96, 5.12, and 5.74 from the reaction $C^{13}(d,n)^*N^{14}$; the line at 6.14 Mev from $C^{13}(d,p)^*C^{14}$. The radiation of the four highest energies may be either from excited states of C^{14} or N^{14}.

* Supported by the U. S. Atomic Energy Commission.

SA6. Resonances in Proton Bombardment of C^{13}. G. A BARTHOLOMEW, F. BROWN, H. E. GOVE, A. E. LITHERLAND, AND E. B. PAUL, *Chalk River Laboratories.*—The Chalk River electrostatic generator has been used to study the reaction $C^{13}(p\gamma)N^{14}$. An elemental carbon target (25 percent enriched in C^{13}) was used. Gamma rays were detected in a 2 in. by 2 in. diameter NaI crystal and a Dumont 6292 photomultiplier. Gamma-ray resonances were found at proton energies of 0.36, 0.53, and 0.64 Mev corresponding to levels in N^{15} observed at 10.53, 10.69, and 10.80 Mev in the $N^{14}(dp)N^{15}$ reaction.[1] At each resonance the ground state γ ray and a peak corresponding to γ rays of about 5.3 Mev are easily distinguished. From the angular distribution of the ground-state γ ray it may be deduced that the 10.69 Mev state is 3/2− and that the 10.80-Mev state is probably 3/2+. In the region of the known (pn) resonances ($Ep=1.17$, 1.31, 1.66 Mev) the ground-state γ

ray is observed but is not strongly resonant. The angular distributions of the ground-state γ ray and the emitted neutrons favor the assignment of $1/2-$ for the 1.17 Mev resonance.

Sperduto, Buechner, Elkind, and Fader, Phys. Rev. **91**, 473 (1953).

SA7. Scintillation Counter Study of Gamma Rays from Proton Capture in Sodium. E. B. NELSON, E. H. GEER, AND R. R. CARLSON, *State University of Iowa.**—The spectrum of the gamma rays produced by the resonant capture of 305 kev protons by sodium[1] has been studied with a single crystal scintillation spectrometer having a resolution of 21 percent at 6 Mev, and with a three crystal pair spectrometer having a resolution of 7 percent at 6 Mev. Gamma-ray energies were determined with an accuracy of 2 percent and cascades were identified by coincidence measurements. The energies of the gamma rays and cascades are consistent with transitions between known levels of Mg^{24}. Goldberg *et al.*[2] have determined the spin and parity of the 11.99 Mev Mg^{24} capture state to be $2+$ by a study of the elastic scattering of alpha particles by Ne^{20}. Our results on the intensity of the gamma rays and their angular distribution are consistent with this assignment. We do not observe direct gamma transitions to the ground state nor alpha decay of the capture state, the alpha decay presumably being inhibited by barrier penetrability.

* Supported in part by the U. S. Atomic Energy Commission.
[1] H. Casson, Phys. Rev. **89**, 809 (1953).
[2] E. Goldberg (private communication).

SA8. Gamma-Ray Resonances in the Proton Bombardment of Na^{23}.* N. P. BAUMANN,† F. W. PROSSER, JR.,† AND R. W. KRONE, *University of Kansas.*—Previous work in this laboratory[1] failed to show any resonances in the Mg^{24} compound nucleus from 12.453 Mev to 12.667 Mev, with the exception of a resonance at $E_p=0.874$ Mev attributed to a F^{19} target contamination. This agreed essentially with the earlier work of Burling.[2] However, the elastic scattering of alpha particles from Ne^{20} at Wisconsin[3] has indicated resonances in Mg^{24} at 12.481, 12.499, 12.531, and 12.601 Mev. A careful resurvey of this region has shown several small resonances agreeing in part with those found at Wisconsin. Pulse-height distributions of the emitted gamma rays have been carried out with a single-crystal spectrometer for several of these resonances and gamma-ray energies have been assigned. Great care was taken to eliminate F^{19} contamination on the targets insofar as possible. The excitation curve, pulse-height distributions, and decay schemes will be shown and discussed.

* Work supported in part by the U. S. Office of Naval Research.
† National Science Foundation Predoctoral Fellows.
[1] Phys. Rev. (to be published).
[2] R. L. Burling, Phys. Rev. **60**, 340 (1941).
[3] E. Goldberg (private communication).

SA9. Some Spin Assignments and Partial Width Measurements of Resonances in S^{32} from the Reaction $P^{31}(p\gamma)S^{32}$. H. E. GOVE, E. B. PAUL, A. E. LITHERLAND, AND G. A. BARTHOLOMEW, *Chalk River Laboratories.*—The angular distributions of some of the gamma rays from the $P^{31}(p\gamma)S^{32}$ reaction have been measured at seventeen resonances[1,2] in the range of proton energies 0.5–2.5 Mev. The partial widths for emission of the gamma rays to the ground and first-excited states of S^{32} have been measured at twelve of these resonances. For six of the resonances at which the ground state transition is predominant the angular distribution is consistent with the assignment $J=1\pm$ for the compound state. The partial widths for these dipole transitions lie between 0.1 ev and 10 ev. In the case of the 1.89 Mev resonance the total width is 24 kev, which suggests formation by P-wave protons. This would indicate that the measured partial width of 5 ev for the emission of the ground-state gamma ray is the partia width for electric dipole emission.

[1] H. E. Gove and E. B. Paul, Phys. Rev. **92**, 852 (1953).
[2] Smith, Cooper, and Harris, Bull. Am. Phys. Soc. **29**, 12 (1954).

SA10. Capture Gamma-Ray Studies Using a Scintillation Coincidence Spectrometer. ARTHUR RECKSIEDLER AND BERNARD HAMERMESH, *Argonne National Laboratory.*—Utilizing a collimated neutron beam from the Argonne heavy water reactor and two NaI(Tl) crystals, coincident gamma rays from the reactions $Cl^{35}(n,\gamma)Cl^{36}$ and $Cd^{113}(n,\gamma)Cd^{114}$ have been studied. Previous studies indicated that several possible two-step branches were present in the capture gamma decay schemes of these isotopes.[1,2] One 20-channel and one single-channel pulse-height analyzer were used with a coincident circuit having a resolving time of 5 microseconds. In chlorine, the 0.778-Mev gamma ray was found to be in coincidence with the 7.77-Mev gamma ray. Another possible line was observed at 0.725 ± 0.010 Mev. Other two-step cascades which were confirmed were the 1.15 Mev–7.42 Mev and 1.59 Mev–6.98 Mev branches. In cadmium, the 0.558 Mev–8.48 Mev branch was confirmed. Since the instrument has poor resolution in the high-energy range compared with a pair spectrometer, the values assigned to the more energetic gamma-rays of the cascades are the values reported by Kinsey *et al.*

[1] B. Hamermesh and V. Hummel, Phys. Rev. **88**, 916 (1952).
[2] Kinsey, Bartholomew, and Walker, Phys. Rev. **85**, 1012 (1952).

SA11. (d,p) Reactions of Ca^{42} and Ca^{44}.† C. M. BRAAMS,* *M.I.T.*—Thin targets of calcium oxide have been bombarded with deuterons from the MIT–ONR electrostatic generator, and the spectra of protons emitted at 90 degrees to the incident beam have been observed with the annular magnetic spectrograph and Eastman NTA nuclear emulsions. Enriched samples of $CaCO_3$ were obtained from the U. S. Atomic Energy Commission; Ca^{42} was concentrated to 64 percent and Ca^{44} to 98 percent. Targets were made by evaporating CaO onto Formvar films. The Q value for the (d,p) reaction to the ground state of Ca^{43} is 5.70 Mev; we have seen excited states in Ca^{43} at 0.38, 0.61, 1.00, and 1.40 Mev. For Ca^{45}, the ground-state Q value is 5.19 Mev; excited states are seen at 0.18, 1.43, 1.89, 2.24, 2.39, and 2.84 Mev. Quoted numbers are accurate to ±0.02 Mev. We intend to make more accurate measurements and to extend this work to higher excitations.

† This work has been supported by the joint program of the U. S. Office of Naval Research and the U. S. Atomic Energy Commission.
* Fellow of the Elsevier Foundation, Amsterdam, The Netherlands.

SA12. Excitation Function for $Fe^{56}(n,p)Mn^{56}$.* J. TERRELL AND D. M. HOLM, *Los Alamos Scientific Laboratory.*—The $Fe^{56}(n,p)Mn^{56}$ cross section has been measured as a function of neutron energy in the ranges 3 to 5 and 12 to 18 Mev. It is planned to extend the energy coverage of these measurements. Preliminary data indicates a maximum cross section in the region 12 to 14 Mev. The cross section at 5 Mev is about 1 percent of this maximum value, and for lower energies decreases rapidly.

* Work done under the auspices of the U. S. Atomic Energy Commission.

SA13. (Abstract withdrawn.)

SA14. Measurement of (p,xn) Cross Sections in Bismuth. R. E. BELL, *McGill University.**—Absolute cross sections of the reactions $(p,3n)$, $(p,5n)$, $(p,6n)$, and $(p,7n)$ in bismuth have been measured for proton energies ranging from 20 to 85 Mev. Bismuth foils (~80 mg/cm²) were irradiated in the circulating beam of the McGill synchrocyclotron, together with Teflon foils (~25 mg/cm²) to serve as proton flux monitors through the known $C^{12}(p,pn)C^{11}$ cross section. The polonium electron-capture activities from the (p,xn) reactions in bismuth were determined absolutely by counting the $K-X$ rays with a thin NaI(Tl) counter. The C^{11} activity of the monitor foils was measured by counting the annihilation quanta with a NaI(Tl) counter of known efficiency. The overall accuracy is estimated at 15 percent. The $(p,3n)$ cross section plotted as a function of energy forms a nearly symmetrical curve peaking at 0.85 barn at 28 Mev, with a half width of 12.5 Mev, dropping to less than 10 percent of its peak value by 49 Mev. The $(p,5n)$ cross section has a peak of ~0.75 barn at 49 Mev. The $(p,6n)$ and $(p,7n)$ cross-section peaks are somewhat lower, and decrease only slowly above 70 Mev. This unsymmetrical behavior shows the increasing importance of fast nucleon cascade processes as the energy is increased (see following abstract).

* On loan from Chalk River Laboratories.

SA15. Schematic Calculation of (p,xn) Cross Sections of Heavy Elements.* J. DAVID JACKSON, *McGill University.*—Calculations have been made of (p,xn) and (p,pxn) cross sections of heavy elements for energies up to 100 Mev. Complete compound nucleus formation was assumed for proton energies below 30 Mev, while at higher energies the reaction probabilities for the prompt (cascade) processes and the residual nucleus excitation distributions were taken from the Chalk River Monte Carlo calculations at 60 and 90 Mev.[1] The evaporation process was handled in a simplified manner, neglecting charged particle evaporation and assuming a constant nuclear temperature (this schematic model for evaporation can be solved essentially exactly). Averaging over the Monte Carlo distributions leads to the (p,xn) and (p,pxn) cross sections as functions of incident proton energy. Comparison with the experimental data for bismuth (see preceding abstract) shows that the theory and experiment can be brought into good general agreement at least up to $x=7$, by taking $R\simeq 7.7\times 10^{-13}$ cm, $T\simeq 1.85$ Mev while $B\simeq 7.4$ Mev where R is the nuclear radius, T is the nuclear temperature, and B is the average neutron binding energy.

* Supported by Atomic Energy of Canada, Limited.

[1] McManus, Sharp, and Gellmann, Bull. Am. Phys. Soc. **28**, No. 6 (1953), and private communication.

SA16. The Angular Distribution of U^{235} Fragments from Neutron-Induced Fission as a Function of Incident Neutron Energy. J. E. BROLLEY, JR., W. C. DICKINSON, AND R. L. HENKEL, *Los Alamos Scientific Laboratory.*—We have employed a double ionization chamber to extend our previously reported investigations[1] to 20 Mev. A common high-voltage electrode served a Frisch-grid chamber and a parallel plate chamber. A 0.9 mg/cm² Au foil, on which was evaporated a 0.5 mg/cm² layer of $U^{235}O_3$, was mounted on the Frisch-grid side of the common electrode. This electrode was honeycombed with holes to serve as a collimator. Those fragments traversing the collimating passages created a gate pulse for the amplifier of the gridded chamber. Only coincident pulses in the two chambers were counted. To attain complete symmetry between the 0° and 90° angular settings, the collimator holes were inclined at 45° to the electrode normal. The ratio R of the fission cross section at 0° to that at 90° for various neutron energies produced at the large Los Alamos Van de Graaff generator is given in Table I; earlier measurements with thermal and 14.3-Mev neutrons are included. At 7.5 Mev relative fission cross sections were measured at 0°, 15°, 30°, 60°, and 90°. The distribution satisfies $\sigma_f(\theta)\sim[1+0.07\times\cos^2\theta+0.29\cos^4\theta]$.

TABLE I.

E_n (Mev)	0	2.5	4.6	7.5	14.3	20.4
R	0.99±0.05	1.02±0.05	1.13±0.06	1.36±0.05	1.27±0.08	1.11±0.09

[1] W. C. Dickenson and J. E. Brolley, Jr., Phys. Rev. **90**, 388 (1953).

SATURDAY MORNING AT 9:30

NBS, East Building

(R. M. BOZORTH presiding)

Magnetism

T1. A Generator of Linearly Varying Current for an Electromagnet.* JOHN LEVINSON, *Alfred University.*—An all-electronic generator suitable for an electromagnet of 10 to 100 ohms resistance has been constructed and used in experiments on the magnetization of ferrites. Combined with automatic recording equipment, it has eliminated the need for manual setting of field values and the subsequent plotting of the dependent variables against the field. The current varies with time between adjustable limits up to plus or minus three amperes, the positive and negative limits not being necessarily equal. Characteristics desired were: (a) smoothness of variation, (b) high order of linearity in passing through zero current, and (c) cycling frequencies of 1, 3, and 10 cycles per minute, variable by about 50 percent. Circuit diagrams are presented showing how these characteristics were incorporated in the generator.

* Supported by the U. S. Office of Naval Research.

T2. Statistics of a Face-Centered Cubic Ferromagnet. E. DEMPSEY AND D. TER HAAR,* *St. Andrews University.*—

The variational method of Kramers and Wannier[1] for evaluating the partition function of the two-dimensional Ising model of a ferromagnet is extended to include next nearest as well as nearest neighbor interactions for a simple cubic ferromagnet.[2] Putting the interaction between nearest neighbors equal to zero leads to the equations for the Ising model of a face-centered cubic lattice involving nearest neighbor interactions only. These equations are solved by series expansions both for temperatures above and below the Curie temperature and series expansions for the partition function, configurational energy and configurational specific heat are obtained.

* On leave of absence at Purdue University.
[1] H. A. Kramers and G. H. Wannier, Phys. Rev. **60**, 252 (1941).
[2] Compare B. Martin and D. ter Haar, Physica **18**, 569 (1952).

T3. A Method of Measuring the Magnetic Properties of Ferromagnetic Materials by Means of the Hall Effect.* SIMON FONER,† *Carnegie Institute of Technology.*—The method described here is based on the assumption of the empirical formulation of the Hall effect in ferromagnetics, $e_H = R_0 H + R_1 M$, where e_H is the Hall electric field per unit current density, H is the magnetizing field, R_0 and R_1 are two constants of the material investigated and M is the magnetization. Measurements of e_H as a function of magnetic induction B may be used to determine R_0 and R_1. These constants are then used to calculate M as a function of B and therefore H. Since R_1 may be quite large for some materials, the changes in M may be greatly magnified. The method is independent of the demagnetizing factor and can be used to examine the magnetic hardness or domain size effect (a/H terms) in detail since any linear variation of M with H is absorbed by the R_0 term. The data for Armco iron at room temperature,[1] has been examined in detail. Any H dependent part of $\partial 4\pi M/\partial H$ as large as one gauss per oersted can be detected. The results generally agree with previous data obtained by other methods.

* Supported by the U. S. Office of Naval Research.
† Now at the Lincoln Laboratory.
[1] S. Foner and E. M. Pugh, Phys. Rev. **91**, 20 (1953).

T4. Magnetic Domains in Cobalt by the Longitudinal Kerr Effect.* CHARLES A. FOWLER, JR., AND EDWARD M. FRYER, *Pomona College.*—The Kerr magneto-optic effect has been successfully employed to photograph the antiparallel domains lying in those surfaces of a single cobalt crystal that contain the c axis, which is the direction of easy magnetization. The technique has been modified only slightly from that used by the authors in photographing the much larger domains of a silicon iron specimen.[1] Changes of the surface domain configuration as the crystal is carried from the demagnetized state to saturation can be observed. The saturated character of individual domains in the demagnetized specimen is demonstrated by a photoelectric record of local Kerr rotations. The photographic technique of negative-positive superposition, developed to improve the sharpness of the silicon iron photographs by reducing background, is essential in photographing the smaller cobalt domains. Other difficulties that attend the higher magnification are discussed.

* Supported by the U. S. Office of Naval Research.
[1] Fowler and Fryer, Revs. Modern Phys. **25**, 33 (1953); Phys. Rev. (to be published).

T5. Ferrimagnetic Resonance in Sintered Masses. DAVID PARK, *Williams College.**—Three factors must be considered in making a theory of this process in the absence of any steady external field. There are many crystallites, oriented at random; the crystallites will have different characteristic resonant frequencies, and they will interact with their neighbors. In order to approximate to a solution, we assume that the behavior of the group of neighbors of any crystallite X approximates that of the whole sample, and then find what this behavior must be in order that, at the same time, it be average over all X. Formulas for μ' and μ'' are then determined by what statistical distribution is assumed to characterize the resonant properties of the various crystallites. The results show most of the features of the observed data. Details will be given in the following talk.

* Work supported by the Sprague Electric Company.

T6. Domain Rotation in Sintered Nickel Ferrite. FIELDING BROWN AND CHARLES L. GRAVEL, *Sprague Electric Company.*—The complex permeability spectrum of sintered nickel ferrite has been measured between 2 mc and 3000 mc, and its dependence on maximum sintering temperature has been observed. Samples were prepared by pressing together fully reacted particles of nickel ferrite and sintering to various temperatures in the range 960–1350°C. The unsintered powder-wax samples show an absorption maximum at 2000 mc, in rough agreement with the theory of ferrimagnetic resonance,[1] and which moves smoothly to lower frequencies as the material is sintered to higher temperatures. The susceptibility at low frequency, χ_0, is found to be inversely proportional to the frequency at which susceptibility is reduced to one-half this value, ω_0, in agreement with the theory of Snoek[2] for domain rotations. Since domain wall resonance predicts a different relationship ($(\chi_0)^{\frac{1}{2}}\alpha\omega_0^{-1}$) and since the crystallite size is very small in our samples, thus restricting possible domain wall relaxation to frequencies much higher than ω_0, the dispersion mechanism has been identified with domain rotation in an effective anisotropy field.

[1] F. Brown and D. Park, Phys. Rev. **93**, 381 (1954).
[2] J. L. Snoek, Philips Tech. Rev. **8**, 353 (1946).

T7. The Calculation of Ferromagnetic and Antiferromagnetic Curie Temperatures. H. A. BROWN AND J. M. LUTTINGER, *University of Michigan.**—Two well-known methods, both based on a Heitler-London approximation, have been used by Weiss[1] and Opechowski[2] to calculate Curie temperatures for spin $\frac{1}{2}$. Both methods have now been extended to higher spin. The Opechowski method requires only the calculation of traces of products of spin matrices as functions of the spin quantum number. The Weiss method is slightly modified in that, instead of finding the energy levels of the cluster exactly and then expanding the partition function in powers of the internal and applied fields, one obtains the series expansion directly by utilizing the fact that the partition function is a trace. The technique is equivalent to using perturbation theory and allows one to bypass the problem of diagonalizing a $(2S+1)$ by $(2S+1)$ matrix. The ferromagnetic Curie temperatures found by the Weiss method approach those of the third Opechowski approximation for high spin. An approximate model, in which spins are considered as classical vectors, has also been used in both methods and equivalent results found for high spin. Work is proceeding on the fourth and fifth Opechowski approximations.

* Work supported in part by the Wisconsin Alumni Research Foundation.
[1] P. R. Weiss, Phys. Rev. **74**, 1493 (1948).
[2] W. Opechowski, Physica **4**, 181 (1937); V. Zehler, Z. Naturforsch. **5a**, 344 (1950).

T8. The Spherical Model of an Antiferromagnet.* B. S. GOURARY AND R. W. HART, *The John Hopkins University.*—The sphericalization technique is adapted to the calculation of the partition function of a body centered cubic lattice of spins with isotropic antiferromagnetic interaction between nearest and second nearest neighbors. Two transition points are obtained. The usual Curie point transition from the paramagnetic state to the antiferromagnetic state (caused by the sticking of the saddle point) leads to an antiferromagnetic state with ordering either of the first kind or of the second kind,[1] depending on the value of the ratio of the second nearest neighbor interaction to the nearest neighbor interac-

tion. In addition, a transition from one kind of ordering to the other can occur if the ratio of the interactions varies with the temperature. Mathematically, this transition occurs because the largest eigenvalue of the interaction matrix becomes degenerate at the temperature at which the ratio of the interactions attains a certain critical value. These results are in qualitative agreement with molecular field theory.[2]

* Work supported by the Bureau of Ordnance, U. S. Navy.
[1] J. H. Van Vleck, J. phys. radium **12**, 262 (1951).
[2] J. S. Smart, Phys. Rev. **90**, 55 (1953).

T9. Neutron-Magnetic Diffraction Studies of Lanthanum, Calcium Manganites. W. C KOEHLER AND E. O. WOLLAN, *Oak Ridge National Laboratory.*—A study has been made of the magnetic structures of a series of perovskite type compounds varying in composition from (100 percent La) MnO_3 to (100 percent Ca) MnO_3. In the composition range from about (0.9 La, 0.1 Ca) to (0.5 La, 0.5 Ca) the compounds are ferromagnetic with Curie temperatures ranging from near room temperature downward, in agreement with the magnetic measurements of Jonker and Van Santen.[1] The neutron diffraction studies show a series of different antiferromagnetic structures for compositions outside the above mentioned range and a coexistence of ferro and antiferromagnetic structures in the 0.9 La to 0.5 La composition range. The antiferromagnetic structures can at least partially be accounted for on the basis of magnetic cells which involve doubling of the chemical cell (a) along one axis, (b) along two axes, and (c) along three axes. The details of the proposed magnetic cells, their interrelations and their relation to composition and to the valence states of the manganese ions will be discussed.

[1] G. H. Jonker and J. H. Van Santen, Physica **16**, 337 (1950).

T10. Magnetostrictive Effects in α-Fe_2O_3. H. M. A. URQUHART* AND J. E. GOLDMAN, *Carnegie Institute of Technology.*—In a previous communication[1] magnetostrictive effects in antiferromagnetic α-Fe_2O_3 near the anisotropy transition were reported. The linear dependence on applied magnetic field of the temperature at which these effects disappear suggested that the transition temperature may be field dependent. Recent neutron diffraction studies[2] did not show such a dependence. Extension of our measurements to include the angular dependence of the distortion together with independent data on the magnetization[3] have suggested an explanation of the observed phenomena in terms of the possible existence of antiferromagnetic domains. The spin system senses the magnetic field through the accompanying unbalanced spins (parasitic ferromagnetism) which above the transition appears to follow the applied magnetic field when both are in the (111) plane. One cannot, however, unambiguously ascertain whether the antiferromagnetic part follows the field or sets itself perpendicular thereto. Our measurements suggest that the crystalline anisotropy in the high-temperature orientation is very much smaller than in the low-temperature system in agreement with recent observations of Anderson *et al.*

* Now at University of Pittsburgh.
[1] H. Urquhart and J. E. Goldman, Phys. Rev. **91**, 435 (1953).
[2] Corliss, Hasting, and Goldman, Phys. Rev. **93**, 893 (1954).
[3] C. Guillaud, J. phys. radium **12**, 489 (1951).

T11. Lattice Parameters of the $FeFe_{(2-x)}Cr_xO_4$ Spinel System.* H. J. YEARIAN, J. M. KORTRIGHT, AND R. H. LANGENHEIM, *Purdue University.*—Spinels of the $FeFe_{(2-x)}Cr_xO_4$, $0 \leqslant x \leqslant 2$, system have been made by reduction of the corresponding sesquioxide solid solution at 1180°C, 1100°C, and 950°C and the lattice parameters determined at room temperature. The solutions of approximately stoichiometric composition have lattice parameters which vary with x in a nonlinear manner from 8.396 ± 0.002A at $x=0$ to 8.376 ± 0.002A at $x=2$. The four essentially linear segments comprising the total curve are interpreted as follows: from $x=0$ to $x=0.3$ the structure is completely inversed; from $x=1.28$ to $x=2.0$ it is completely normal; between these regions reversion from the inversed to the normal form occurs in two successive stages. Oxygen-rich spinels crystallized at 950°C show the same general variations of parameter but the region of complete inversion extends to approximately $x=0.6$.

* Supported by the U. S. Office of Naval Research and Project SQUID.

SATURDAY MORNING AT 9:30

Sheraton Park, Caribar Room

(P. G. BERGMANN presiding)

Theoretical Physics, V: Field Theory and Interactions

U1. Properties of Bethe-Salpeter Wave Functions. G. C. WICK, *Carnegie Institute to Technology.*—The analytic character of the relativistic wave function of a two-body system[1] in a bound state as a function of the "relative time" variable, or of the Fourier conjugate variable p_0 can be inferred from the definition of the wave function[2] plus some simple stability requirements. The analytic continuation of the wave function to imaginary values of p_0 is possible, and allows one to throw some light on the eigenvalue problem. Variational methods will be discussed. An example of an exact solution with $E+0$ will be exhibited.

[1] H. A. Bethe and E. E. Salpeter, Phys. Rev. **82**, 309 (1951); **84**, 1232 (1951); J. Schwinger, Proc. Natl. Acad. Sci. U. S. **37**, 452, 455 (1951).
[2] M. Gell-Mann and F. Low, Phys. Rev. **84**, 350 (1951).

U2. Solutions of a Bethe-Salpeter Equation. R. E. CUTKOSKY, *Carnegie Institute of Technology.*—The Bethe-Salpeter equation in the ladder approximation, for the case of two scalar particles of equal mass interacting through a massless scalar field, is studied with the methods previously discussed.[1] At zero energy the equation may be transformed by the method of Fock,[2] and the solutions given by the spherical harmonics on a five-dimensional sphere. At energies different from zero a complete set of solutions may be obtained by an integral representation method.[1] The degeneracy of the eigenvalues will be discussed.

[1] G. C. Wick, preceding Abstract.
[2] V. Fock, Z. Physik **98**, 145 (1935); M. Levy, Proc. Roy. Soc. (London) **A204**, 145 (1950).

U3. Classical Limit of Pseudoscalar Coupling. W. E. THIRRING, *Institute for Advanced Study.*—The pseudoscalar coupling is approximated by the Hamiltonian $H=U(\rho_3 M+\rho_1 g\phi)+H^{\text{mes}}$ where M=nucleon mass, ϕ=meson field, U=source density with radius a. ρ is treated as a classical vector obeying the appropriate equations of motion. The free

gyration of ρ is quenched by the asymmetrical form of the coupling. The gyration forced by an incident meson wave causes scattering and photoabsorption. For $(g^2/4\pi)\ll 1$ the cross sections for scattering (σ_s) and photoproduction (σ_a) at low energies coincide with the perturbation theoretical values. For $(g^2/4\pi)\gg 1\sigma_s$ is independent of g and of the order a^2. The ratio between σ_p and σ_s is c^2v/g^2 for all g. The agreement with experiment, therefore, is worse for large values of g. A connection between a and M, g is not obtained as there is no consistent renormalization of a one nucleon theory. The results for charge symmetrical coupling are similar. Although the connection between this calculation and the complete field theory is questionable, it may indicate that a possible suppression of σ_s at large values of g will suppress σ_p, too. This point seems to be a serious disagreement between pseudoscalar theory and experiment.

U4. On the Factorable Neutron-Proton Interaction. YORIKO YAMAGUCHI AND YOSHIO YAMAGUCHI, *University of Illinois.*—The two body Schrdöinger equation can be solved exactly for a factorable nuclear potential with momentum matrix elements of the form $(\mathbf{p}|V|\mathbf{p}')=\lambda g(\mathbf{p})g(\mathbf{p}')$. Simple examples for (*i*) ^1S-interaction, $g(\mathbf{p})=(\beta^2+p^2)^{-1}$, and (*ii*) eigen ^3S-interaction, $g(\mathbf{p}) = (\beta^2 + p^2)^{-1} - 8^{-1}\{(\sigma^n\mathbf{p})(\sigma^n\mathbf{p})p^{-2} - (\sigma^n\sigma^n)\}\times t\beta^2(\gamma^2+p^2)^{-2}$, have been investigated in detail. The deuteron D-state probability and quadrupole moment, and $k\cot\delta$ for $N-P$ scattering have been expressed in analytic forms and fitted by adjusting the parameters β, γ and t. The $N-P$ scattering up to 100 Mev can be fitted fairly well using (*i*) and (*ii*) alone. The photo-disintegration of the deuteron has also been analyzed with consideration of the gauge-invariance problem. The total cross section (E.D. plus M.D.) agrees with the observed data[1] up to photon energies of ~60 Mev, but the angular distribution has too small an isotropic component. The D-wave function of the deuteron becomes important with increasing photon energy. Consideration of thermal neutron capture by hydrogen confirms Austern's conclusion[2] that an interaction magnetic moment is needed.

[1] Allen, Hanson, and Whalin (private communication).
[2] N. Austern, Phys. Rev. **92**, 670 (1953).

U5. General Conditions on the Scattering Matrix. M. L. GOLDBERGER, *Princeton University,* M. L. GELLMAN, *University of Chicago,* AND W. E. THIRRING, *Institute for Advanced Study.*—Van Kampen[1] has discussed the limitations which may be imposed on the S matrix by certain causality requirements. His treatment has been reformulated in a simple and entirely quantum mechanical manner. Our method is readily generalizable to treat the problem of scattering of particles with rest mass. The fundamental idea is to demand that any expectation value of the commutator of two field operators must vanish for two points separated by a space-like interval. The special problem considered is a quantized field interacting with a given external field. The latter is supposed to be exactly zero outside a certain domain. The most powerful statements which are independent of the size of the region of interaction can be made for the forward scattering amplitude. They give a relation connecting the real part of the forward scattering amplitude and the total cross section. Sum rules of the familiar Kramers-Kronig form can be derived without reference to the scattering mechanism. Applications of these relations to scattering of γ rays by atoms, photonuclear reactives, scattering of photons by nucleons will be discussed. Generalizations of the results for the case of two coupled quantized fields are considered.

[1] Van Kampen, Phys. Rev. **89**, 1072 (1953).

U6. Nuclear Rotational Levels and the μ-Mesic Atom. B. A. JACOBSOHN, *University of Washington.*—Nuclei which, according to the Bohr-Mottelson collective model,[1] possess low-lying rotational excitations can be excited with relative ease by the electric field of a μ meson in an inner Bohr orbit. Since the energy differences between different μ states are large, the meson can be considered to be in a single orbit. However for heavy nuclei which are far removed from closed-shell configurations, the nuclear levels are closely spaced and are connected by large quadrupole matrix elements. The coupled system is one in which the stationary states correspond to the μ in a single orbit and the nucleus existing in mixtures of several states. The lifetimes of these states are determined by the meson transitions. Calculations of the effect on the $2p\rightarrow 1s$ line have been carried out using the collective model.[1] The result is that this line is split into several components with a shifted center of gravity. In favorable cases, the splitting may be as much as several hundred kilovolts. The effect can probably be ignored in those cases which have been investigated experimentally up to the present.[2]

[1] A. Bohr and B. R. Mottelson, Kgl. Danske Videnskab. Selskab Mat.-fys. Medd. **27**, No. 16 (1953).
[2] V. L. Fitch and J. Rainwater, Phys. Rev. **92**, 789 (1953).

U7. Red-shifts in the Spectra of Celestial Bodies. E. FINLAY-FREUNDLICH, *University Observatory, St. Andrews, Scotland* (introduced by D. ter Haar).—It is shown that red-shifts occurring in the spectra of B- and O-stars are too large to be gravitational red-shifts such as are predicted by the theory of relativity. It is suggested that the red-shifts may be due to a loss of energy in the radiation field of the stars. If $\Delta\nu/\nu$ is the fractional change of frequency of the lines, T the temperature of the radiation field, l the length of path traversed through the radiation field, the following relation holds: $\Delta\nu/\nu=-AT^4l(A)$, where A is a constant. It is shown that formula (A) can account for red-shifts observed in the spectra of O, B, A, supergiant M, W-R stars and of the sun. In addition to the red-shift given by formula (A) the data from the sun and from Sirius B (a white dwarf) seem to suggest that there exists an additional gravitational red-shift which is, however, only a fraction (about one-fifth) of the red-shift predicted by the theory of relativity.

U8. Classical Radiation from Moving Charges. SIDNEY A. BLUDMAN, *University of California, Berkeley.*—For an arbitrarily moving charged particle, a coordinate system can be introduced in which the particle remains permanently at rest and the spatial axes are not rotated. Maxwell's equations can be solved in these curvilinear coordinates: the field is coulombic and the Poynting flux vanishes so that, by this coordinate transformation, the radiation field has been transformed away. The equations of motion for particles reveal, of course, the non-inertial character of this coordinate system. On transforming back to an inertial system, the conventional formula for the field of an arbitrarily moving charge is obtained. The radiation damping force is shown to transform as a vector under conformal transformations so that it vanishes only for the uniformly accelerated motions generated from rest by the conformal group. In linear accelerators this uniform acceleration obtains and the small amount of energy radiated is due entirely to changes in the acceleration energy of the particle. This work was performed under the auspices of the U. S. Atomic Energy Commission.

U9. Dyson's New Tamm-Dancoff Method. ABRAHAM KLEIN,* *Harvard University.*—The three-dimensional formalism proposed by Dyson,[1] though attractive in many respects, poses several questions that remain to be clarified. Since the method employs covariant amplitudes with all times set equal, one might expect to find a simple relationship between the equations obtained from a covariant treatment and Dyson's equations, after the elimination of higher amplitudes. For the one-particle problem, a three-dimensional equation for a stationary state can be deduced from the

covariant one without approximation and compared with the new T.-D. equation, since simple rules can be given for constructing the latter to any approximation. The kernels agree only to lowest order, which explains the renormalizability of Dyson's equation in that order, but casts doubt upon the renormalizability of the equation as a whole by available methods. Similar remarks obtain for the two-particle problem. Further, the simple example of a two-component spinor field interacting with a boson field—the true and free vacuum states are then equal—provides evidence against the validity of Dyson's rule for prescribing that the comparison state for all energies is the vacuum state.

* Society of Fellows.
[1] F. J. Dyson, Phys. Rev. 91, 1543 (1953).

U10. Exchange Current Effects in the Deuteron. J. BERNSTEIN AND A. KLEIN,* *Harvard University.*—Recent treatments by Villars[1] and Deser[2] of corrections to the quadrupole moment of the deuteron arising from nucleon recoil upon emission of a meson has led to values of 10 percent and more. Though one might expect *a priori* that one is dealing with a dynamic effect which vanishes when nucleon recoil is neglected in intermediate states (as found by Villars), the effective current operator found by Deser does not show this behavior. Since this discrepancy arises from the difference in treatment, we have reexamined the problem by all available methods: (a) canonical transformation, (b) Tamm-Dancoff method, (c) covariant two-nucleon equation. Methods (b), and (c) indicate an ambiguity which is the analogue of that arising in the problem of computing fourth order nuclear forces from gradient coupling, and results of the character of those found by both previous authors can be obtained under suitable approximations. Formulas and results will be presented and discussed.

* Society of Fellows.
[1] F. Villars, Phys. Rev. 86, 476 (1952).
[2] S. Deser, Phys. Rev. 92, 1452 (1953).

U11. Two-Body Forces and Nuclear Saturation. I. Method. K. BRUECKNER, C. LEVINSON, AND H. MAHMOUD, *Indiana University.**—The investigation of nuclear saturation for potentials for which Born approximation is valid is a relatively simple problem. For the rapidly varying and nonmonotonic potentials of pseudoscalar meson theory, however, variational methods using independent particle trial functions are grossly inadequate. The problem can be approached using more general variational functions with interparticle correlation; the evaluation of the resulting expressions is very difficult since indirect correlations involving many more than two particles become important at high densities. An alternative procedure has been developed which allows a rather straightforward evaluation of the many-body energy even when the potentials are of great complexity. This method depends on an approximation, valid in the limit of very many scatterers, which leads to an exact solution (a degenerate Fermi gas) for the coherent particle motion. In this case the many body potential energy can be simply expressed in terms of the low energy scattering amplitudes so that details of the two-body potential configuration are unimportant. The method also allows evaluation of correction terms arising from incoherent contributions to the particle motion. These corrections indicate the extent to which the coherent wave motion differs from an independent particle motion.

* Supported in part by the National Science Foundation and the Joint Program of the U. S. Office of Naval Research and the U. S. Atomic Energy Commission.

U12. Two-Body Forces and Nuclear Saturation. II. Results. C. LEVINSON, K. BRUECKNER, AND H. MAHMOUD, *Indiana University.**—The method described in the previous abstract has been applied to the two-body potentials given by pseudoscalar meson theory when the effects of nucleon pair formation are assumed to be small. In this approximation the many body forces of the theory are negligible. These potentials give an excellent fit to the low energy scattering parameters of the two-nucleon system and also an approximately correct description of scattering up to 90 Mev. They are characterized by repulsive cores of radii 0.3–$0.4\hbar/\mu c$ and quite weak interactions in odd states. The many body energy has been evaluated neglecting the tensor contributions which average to zero in first approximation. The result shows saturation at an energy per particle (neglecting Coulomb energy) of 12 Mev at a nuclear radius $1.15\times10^{-13}A^{\frac{1}{3}}$ cm. The position and magnitude of the saturation minimum in the energy are rather sensitive to the repulsive cores in P states which were taken to be $0.4\hbar/\mu c$ for the above result. The repulsive forces which lead to the saturation arise principally from the effect of the repulsive cores on the S-wave scattering, the phase shifts changing sign at high energy. The method has also been applied to potentials of the Levy type in which the odd-state potentials are rather strong and attractive.

* Supported in part by the National Science Foundation and the Joint Program of the U. S. Office of Naval Research and the U. S. Atomic Energy Commission.

SATURDAY AFTERNOON AT 1:30

Sheraton Park, Caribar Room

(E. P. WIGNER presiding)

Theoretical Physics, VI: Atoms and Electrons

V1. Electronic Polarizabilities of Ions from the Hartree-Fock Wave Functions.* R. M. STERNHEIMER, *Brookhaven National Laboratory.*—The electronic polarizability α can be written as a sum of terms of the type $a\int_0^\infty u_0u_1rdr$, where a=coefficient, u_0 and u_1 are r times the radial part of the unperturbed wave function and the perturbation, respectively, for a particular shell and excitation. α has been calculated for 14 ions using the Hartree-Fock wave functions for u_0. For the He-like ions, an analytic expression for u_1 can be obtained, if the $1s$ wave functions of Löwdin[1] are used. For the heavier ions, the differential equations for the u_1 were solved numerically. The most important term of α arises from the excitation of $nl\rightarrow l+1$, were n and l are the principal and azimuthal quantum number of the highest filled subshell. The calculated values of α for most cases lie between 1 and 1.5 times the experimental values. Values have also been obtained for the quadrupole polarizability which measures the quadrupole moment induced in the ion by the field of an external charge.

* Work done under the auspices of the U. S. Atomic Energy Commission.
[1] P. O. Löwdin, Phys. Rev. 90, 120 (1953).

V2. A Perturbation Calculation of Elastic Exchange Scattering of Electrons by Hydrogen Atoms.* SIDNEY BOROWITZ, *New York University.*—We consider the elastic exchange scattering of electrons by hydrogen atoms. If the mass of the proton is considered infinite, one can take as a perturbation either the interaction of the electron with both particles of the scatterer (asymmetric perturbation), or merely the interaction between the two electrons (symmetric perturbation). We have treated the latter case to first order. This method leads to integrals which can be evaluated exactly, after suppressing terms which seem to arise from the logarithmic phase factors in the asymptotic behavior of unscreened Coulomb wave functions. The results indicate that the symmetric perturbation calculation gives a completely different energy dependence for the exchange scattered amplitude than does the asymmetric perturbation calculation.[1]

* Research supported by contract with Air Force Cambridge Research Center Air Research and Development Command.
[1] Corinaldesi and Trainor, Nuovo cimento **9**, 1952.

V3. An Approximate Correlation Potential. JOSEPH CALLAWAY, *Princeton University.*—The success of Slater's free electron approximation to the exchange potential[1] suggests a similar approach to the correlation energy. Wigner's formula for the correlation energy of a free electron gas[2] is to be modified by making the density of electrons a function of position, and gives as a correlation potential to be added to Hartree or Hartree-Fock equations (for electrons of positive spin):

$$V(r)=\frac{0.576e^2}{(3/8\pi\rho(r))^{\frac{1}{3}}+5.1}.$$

Here ρ_- is the local density of electrons of negative spin. Applications of this formula to ferromagnetism are in progress. For iron at the observed lattice spacing, this formula indicates correlation effects are too small compared to the exchange potential to alter the predictions of the energy band theory of ferromagnetism.

* National Science Foundation Predoctoral Fellow.
[1] J. C. Slater, Phys. Rev. **81**, 385 (1951).
[2] E. P. Wigner, Phys. Rev. **46**, 1002 (1934).

V4. SCF Treatment of Unclosed Shells, Operators Containing Spin, and Radial Correlation. PAUL F. WACKER, *Catholic University of America.*—In computing the energy of states belonging to degenerate spin-space symmetry species, configurations or combinations of configurations belonging to all but one subspecies may be disregarded. Hence, a single determinant may often be used. The energy is then given[1] by $tr(\mathbf{H}+\frac{1}{2}tr_{2,4}(\mathbf{j}-\mathbf{j}^{[2,4]})\boldsymbol{\rho})\boldsymbol{\rho}$. The ith spin-orbital eigenvector $\mathbf{C}i$ of a Hartree-Fock treatment[2] is a solution of $\mathbf{FC}i=f_i\mathbf{SC}i$, where $\mathbf{F}=\frac{1}{2}\mathbf{H}+\frac{1}{2}tr_{2,4}(\mathbf{j}-\mathbf{j}^{[2,4]})\boldsymbol{\rho}$, f_i is an eigenvalue, and $\mathbf{S}$ is the spin-orbital overlap matrix. If the Hamiltonian contains spin, these equations automatically include a perturbation treatment of the spin effects. If Russell-Saunders coupling occurs, α or β spin may be assigned to each spin orbital, simplifying the equations. The nonzero halves of the eigenvectors are then given by $\mathbf{F}_{\alpha\alpha}\mathbf{C}i_\alpha=f_i\mathbf{S}\mathbf{C}i_\alpha$ and $\mathbf{F}_{\beta\beta}\mathbf{C}i_\beta=f_i\mathbf{S}\mathbf{C}i_\beta$, where S is the overlap matrix for spatial orbitals, while $\mathbf{F}_{\alpha\alpha}$ and $\mathbf{F}_{\beta\beta}$ are diagonal quadrants of the $\mathbf{F}$ matrix. Since a different spatial orbital is assigned to each electron, these equations treat "radial" correlation. If correlation is neglected, further simplification results.

[1] Wacker, Phys. Rev. **91**, 465A, 429 (1953).
[2] Roothaan, Revs. Modern Phys. **23**, 69 (1951).

V5. Coulomb Wave Functions for Large Values of the Parameter η. L. C. BIEDENHARN, R. L. GLUCKSTERN, AND M. H. HULL, JR., *Yale University.**—Current interest in nuclear reactions involving heavy charged particles and in Coulomb excitation of nuclei has pointed up the need for Coulomb wave functions for large values of the parameter $\eta=ZZ'e^2/(\hbar v)$. The Coulomb functions commonly denoted[1] by $F_L(\rho)$, $G_L(\rho)$, as well as their derivatives $F_L'(\rho)$, $G_L'(\rho)$, have been represented, therefore, by power series expansions in $\hbar^{-1}$ at the classical turning point $\rho_L=\eta+[\eta^2+L(L+1)]^{\frac{1}{2}}$ and at $\rho_0=2\eta$ somewhat as in earlier work of others[2] primarily at $L=0$. The usefulness of this type of expansion is apparent from the fact that one or two terms suffice to reproduce numerical results[3] for $L=0$ at ρ_0 with $10\leq\eta\leq200$, as has been pointed out by Newton.[3] Expansions applicable for large L at $\rho=\rho_0$ have also been obtained. In addition, approximate wave functions for arbitrary values of ρ in the vicinity of ρ_L will be presented.

* Assisted by the Office of Ordnance Research, U. S. Army and by the joint program of the U. S. Office of Naval Research and the U. S. Atomic Energy Commission.
[1] Yost, Wheeler, and Breit, Phys. Rev. **49**, 174 (1936).
[2] J. K. Tyson, thesis, MIT, (1948); T. D. Newton, Chalk River Project report CRT-526 (1952); Feshbach, Shapiro, and Weisskopf, NYO-3077 (1953).
[3] W. D. Barfield and A. A. Broyles, Phys. Rev. **88**, 892 (1952).

V6. (Abstract withdrawn.)

V7. W.K.B. Approximation through the Turning Point. A. A. BROYLES, *The Rand Corporation.*—The W.K.B. approximation is quite useful for many wave functions at some distance from the classical turning point. The infinity at the turning point may be removed without serious damage to the approximation at other points by multiplying the energy or the potential by a constant S near unity. This constant is determined on each side of the turning point so that the resulting approximation and its derivatives match at the turning point. The method was tried on hydrogen bound wave functions for the outside turning point using a normalization integral equal to

$$\frac{1}{2}\int_{R_1}^{R_2}\frac{1}{(\epsilon-U)^{\frac{1}{2}}}dR$$

where R_1 and R_2 are the turning points. This is equivalent to replacing the cosine squared by $\frac{1}{2}$. Inside the turning point, the energy ϵ was multiplied by S_i and outside, the potential, U, was multiplied by S_0. The phase $-\pi/4$ was replaced by

$$\phi=-(\pi/4)+(n-l+\tfrac{1}{2})\pi-\int_{R_1}^{R_2}(S_i\epsilon-U)^{\frac{1}{2}}dR.$$

V8. Calculation of Potential from the Transit Time.* JERRY SHMOYS AND SAMUEL N. KARP, *New York University.*—The potential is calculated from the transit time of a particle crossing a potential well. The particle is assumed to move according to the classical laws of motion. Similarly, the charge density of the ionosphere could be calculated from the transit time of a radio pulse through a series of ionospheric layers; to do this one would have to assume that the pulse moves with the group velocity of the medium, and that the medium is lossless. The potential thus calculated is not unique but this deficiency turns out not to be too serious. The method involves the use of the Mellin transform of the transit time with respect to energy (or frequency). Some quantities characterizing the well can be obtained from the Mellin trans-

form directly, i.e., without calculating the inverse transform. The procedure is illustrated by the case of an exponential well.

* This work was performed at the Institute of Mathematical Sciences, New York University and was supported in part by the U. S. Air Force, Air Force Cambridge Research Center, Air Research and Development Command.

V9. A Simplifying Approximation for Determining Cascade Shower Distributions. BAYARD RANKIN, *University of California, Berkeley, California.*—The state of an electron-photon shower at depth x is specified (ignoring lateral spread) by the parameters $(I, \epsilon, N, \mathbf{E}, \lambda)$ representing, respectively, the initial energy, the energy below which particles are not observed, the number of particles, an N-dimensional energy vector, and the ordering of electrons and photons among the energy components of $\mathbf{E}$. The ordering parameter λ will have 2^N permissible values. It is possible to solve directly for the probability $P(N, \Delta\mathbf{E}, \lambda)$ of the set of states with energies contained in $\Delta\mathbf{E}=(\mathbf{E}, \mathbf{E}+\epsilon\mathbf{1})$. One solves simultaneously for all probabilities, $P(N, \Delta\mathbf{E}, \lambda)$, with common $(N, \Delta\mathbf{E})$ and different λ and uses recurrence relations for probabilities with different $(N, \Delta\mathbf{E})$. This has been done assuming energy-dependent bremsstrahlung, materialization, collision loss, and multiple scattering, and assuming ϵ/I is small. (UCRL Report 2322.) Unfortunately, the simultaneous set of $P(N, \Delta\mathbf{E}, \lambda)$ for fixed $(N, \Delta\mathbf{E})$ may be large. To limit the number of unknowns, one can choose for $x \to 0$ an ordering parametrization (different for different $(N, \Delta\mathbf{E})$) such that $P(N, \Delta\mathbf{E}, \lambda)$ is smooth (or quadratic) as a function of λ. Once this smoothness is established, it should persist as x increases. Now for each $(N, \Delta\mathbf{E})$ only the three x-dependent coefficients in the quadratic function are unknown and the solution is expressible in 3×3 matrices.

V10. Pair Production and Bremsstrahlung in the Field of an Electron. F. ROHRLICH, *State University of Iowa.*—The exact differential cross section for pair production by gamma rays in the field of an electron is obtained. The calculation neglects neither recoil nor exchange effects and does not assume the initial electron to be at rest. Therefore, the result gives also the differential cross section for bremsstrahlung in electron-electron collisions (for equal signs of the charges), provided suitable signs are changed and a different density of final states is employed. The integration of these cross sections will be discussed. The results can be compared with previous exact calculations by Votruba[1] and approximate calculations by Borsellino[2] who neglects exchange. The final formulas given by Borsellino are incorrect.

[1] V. Votruba, Bull. intern. acad. tcheque sci. **49**, 19 (1948); Phys. Rev. **73**, 1468 (1948).
[2] A. Borsellino, Nuovo cimento **4**, 112 (1947).

V11. Theoretical Energy and Angular Distributions of Bremsstrahlung Electrons.* PHILIP T. MCCORMICK,† *University of Notre Dame.*—The Bethe-Heitler triple differential bremsstrahlung cross section[1] has been integrated over the angles of the radiated photon to obtain the distribution in energy and angle of the scattered electron. The calculation has been carried out exactly using a pure Coulomb field and preliminary numerical results for the electron energy-angle distributions have been obtained for incident electrons of kinetic energies corresponding to momenta of 2 mc, 4 mc, 6 mc, 10 mc, and 20 mc scattered at angles of 30°, 60°, 90°, 120°, and 150° with the direction of the incident electrons. Because the calculation was lengthy, further checks on it are being planned in order to assure the correctness of the results.

* This work was submitted by Philip T. McCormick in partial fulfillment of the requirements for the Ph.D. degree at the University of Notre Dame.
† Now at DePaul University, Chicago, Illinois.
[1] W. Heitler, *The Quantum Theory of Radiation* (Oxford University Press, London, 1949), second edition, p. 164.

V12. Interference Effects in the Annihilation Process.* G. GIBSON AND P. STEHLE, *University of Pittsburgh.*—The two-photon annihilation process has been considered in the limit of small velocities for a positron incident on a localized two-electron system. We have treated the situation where one electron annihilates with the positron, while the state of the second electron is altered by the removal of the first. If the electrons are initially in a singlet state, then the absolute square of the transition amplitude is of order β^2 for the triplet annihilating state, and of order $1+\beta^2$ for the singlet annihilating state. However, these are two processes not leading to the same final state for the surviving electron. In order to have interference it is necessary that neither of the initial electron states be orthogonal to the final electron state, and that the Fourier transforms of both electron states are finite for the momentum required of the annihilating electron by the conservation laws. If the electrons are initially in a triplet state, they have symmetric roles in the annihilation, and interference effects may result from electron exchange. This effect is being investigated for annihilation in multielectron atoms.

* Work done at the Sarah Mellon Scaife Radiation Laboratory and assisted by the Joint Program of the U. S. Office of Naval Research and the U. S. Atomic Energy Commission.

V13. Electromagnetic Scattering by Dielectric Bodies.* MARSHALL H. COHEN, *The Ohio State University.*—The field scattered by a dielectric body may be approximated by using Rumsey's "reaction method"[1] and volume polarization currents. This method gives a phase and amplitude for the assumed current, with respect to the incident field, and leads directly to the variational equations used by Lurye.[2] Calculations for the echo width of a lossless circular cylinder have been made and compared with the exact solution. The cylinder is one free-space wavelength in diameter and a plane wave is incident normally on it. There are three major conclusions. It is important to have a good current assumption because different ones give substantially different results. The current $Ae^{-ik_1x}+Be^{ik_1x}$, where k_1 is the propagation constant of the medium and A and B are determined by the reaction equations, gives very good results over the first resonance region. The reaction method gives better results than the classical iterated integral equation solution,[3] for the same amount of labor.

This work was done under a contract between Wright Air Development Center and the Ohio State University Research Foundation.
[1] V. H. Rumsey, "The reaction concept in electromagnetic theory," Phys. Rev. (to be published).
[2] J. R. Lurye, "Electromagnetic Scattering Matrices of Stratified Anisotropic Media," Report EM-11, Mathematics Research Group, New York University.
[3] D. R. Rhodes, "On the Theory of Scattering by Dielectric Bodies," Report 475-1 Antenna Laboratory, Ohio State University.

V14. High-Speed Computation of Angular Momentum Functions. ALBERT SIMON, *Oak Ridge National Laboratory.*—The Racah function $W(abcd; ef)$[1] has proven to be an invaluable tool in the general treatment of angular distributions of nuclear reactions, angular correlation, etc. A complete table of the numerical values of this function, up to the limits $a, c \leq 15/2$; $b, d \leq 9/2$; $e \leq 3$; $f \leq 8$, has been obtained by a UNIVAC calculation and will be published shortly. Some general aspects of the method of computation and the form of presentation will be discussed. The circumstance that a partial table of these functions was computed earlier[2] by the use of desk machines permits an illuminating comparison of labor involved. An entirely similar routine is needed for the computation of the Clebsch-Gordan coefficients. Such a table has been prepared with the restriction that none of the arguments be larger than 9/2. Extension of these tables to higher limits would be trivial and will be done if a sufficient demand exists. The X[3] and G functions[4] are needed for the more general problems of polarization in nuclear reactions, radiation from aligned nuclei, etc.

[1] G. Racah, Phys. Rev. **62**, 438 (1942).
[2] L. C. Biedenharn, U. S. Office of Naval Research Laboratory Report 1098.
[3] U. Fano, U. S. National Bureau of Standards Report-1214; A. Simon and T. A. Welton, Phys. Rev. **90**, 1036 (1953).
[4] A. Simon, Phys. Rev. **92**, 1050 (1953).

SATURDAY AFTERNOON AT 1:30

Sheraton Park, Burgundy Room

(J. O. HIRSCHFELDER presiding)

Fluid Dynamics

Invited Papers

VA1. Theory of Turbulent Diffusion. F. N. FRENKIEL, *Applied Physics Laboratory, Johns Hopkins University.* (30 min.)

VA2. On the Interaction of Shock Waves. OTTO LAPORTE, *University of Michigan.* (30 min.)

Contributed Papers

VA3. Ideal Flow and Creeping Motion. K. M. SIEGEL AND A. H. HALPIN, *University of Michigan,* AND A. L. MAFFETT, *Gettysburg College.*—It is shown that any ideal fluid steam-function when multiplied by a radial distance squared yields a nontrivial solution to the equation of creeping motion. Similarly this creeping motion solution can be used to find a new ideal fluid solution. This scheme shows that we can find expansions which do not depend on the separability of the original partial differential equation. All presently known solutions of creeping-motion boundary-value problems can be obtained in this manner.

VA4. A Spatial Spectrum for Turbulent Shear Flow. WILLEM V. R. MALKUS, *Woods Hole Oceanographic Institution.*—A statistical mechanical criterion for steady-state fluid dynamics has yielded the approximate principle that the turbulent motion in shearing flow maximizes the rate of dissipation. This principle is applied to determine the spatial spectrum of momentum transport in channel flow, subject to the stability constraint that an arbitrary smallest scale of motion contributes to this transport. The predicted spectrum leads to a "velocity defect law," a "logarithmic velocity law," and an analytic description of the "boundary layer," not as separate deductions, but as a single expression from one solid boundary to the other. This theory has one parameter, the minimum eddy size. That relation between minimum eddy size and Reynolds number which gives best agreement with the observations is determined.

VA5. Numerical Solution of a Spherical Blast Wave. HAROLD L. BRODE, *The Rand Corporation.*—The strong shock, point source, similarity solution[1] was used as initial conditions in a numberical integration of the differential equations of gas motion in Lagrangian form. The technique of Von Neumann and Richtmyer[2] which introduces an artificial viscosity was employed. The solutions were carried from two thousand atmospheres down to one tenth atmospheres peak overpressure. Results include pressure, density, particle velocity, and position as functions of time over a graduated space grid of ninety divisions. The problem was coded for both the ORDVAC and the IBM-701 high speed computers, and was repeated both with an ideal gas assumption and with a more detailed equation of state. A study was made of the effects of such factors as the shock width, the initial shock strength, the space and time grid sizes, the sphericity, the stability, the loss of significance and some other features of the numerical computation.

[1] J. Von Neumann, AECD-2860, "Shock Hydrodynamics and Blast Waves," Los Alamos Scientific Laboratory, October 28, 1944.
[2] J. Von Neumann and R. D. Richtmyer, J. Appl. Phys. **21**, 232 (1950).

VA6. General Relations in a Fluid Convection Theory. II. Conditions for Flow-Patterns. F. T. ROGERS, JR., *University of South Carolina.*—Attention has been called[1] to the role of repetitive flow-patterns (whether cellular or columnar) in the problem of the onset of convection in a fluid in a porous medium and heated from below. Reference 2 summarizes the problem for a nonstatic thermal environment and temperature-dependent viscosity. It is found that if the basic differential equations for the thermodynamic-hydrodynamic interrelationship are approached (in the sense of least squares) through trigonometric series of finite length, a straightforward course is open for calculation of the dimensionless quantity, E^2D^2, which characterizes the repetitive flow pattern. Moreover a way is found for solution of the larger problem by the requirements of consistency. In even the one-term-series approximation it appears that if the flow-pattern is repetitive, then the flow-"cell" dimensions are in part dependent upon the temperature-dependence of viscosity.

[1] Paper read at the Oak Ridge meeting, April, 1954.
[2] F. T. Rogers, Jr., J. Appl. Phys. **24**, 877 (1953).

VA7. Upstream Effects Induced by a Jet Exhausting from the Base of a Body of Revolution. J. L. POTTER AND N. M. SHAPIRO, *Ordnance Missile Laboratories.*—An experimental investigation of the flow upstream of the base of a body of revolution in a subsonic stream with and without a jet exhausting from the base is described. From evidence furnished by surveys of pressure and velocity distribution in the flow, it is seen that a jet issuing from the base of a body induces acceleration of the fluid approaching the base, the magnitude of this effect varying with axial and radial distance from the jet exit as well as other theoretically predicted parameters. The significance of this phenomenon is demonstrated by its influence on the load distribution on stabilizing fins located near the base of a body.

SATURDAY AFTERNOON AT 1:30

Sheraton Park, Continental Room

(J. A. DE JUREN presiding)

Neutron Physics, III

W1. Cross Section for Producing High-Energy Neutrons from Carbon Targets Bombarded by Protons, Deuterons, and He^3 Particles.* L. SCHECTER AND W. E. CRANDALL, *California Research and Development Company,* AND G. P. MILLBURN AND J. ISE, *University of California, Berkeley.*—The differential cross section, $d\sigma/d\Omega$, for producing neutrons with energy in excess of 20 Mev from carbon targets bombarded by 340-Mev protons, 190-Mev deuterons, and 490-Mev He^3 particles were measured. The absolute cross sections were determined by counting identical carbon targets and neutron detector foils in the same geometry and utilizing the known excitation functions for the neutron and bombarding particles.

* Supported by the U. S. Atomic Energy Commission.

W2. Total Cross Sections for High-Energy Neutrons.* R. W. WANIEK AND VAUGHN CULLER, *Harvard University.*—A good geometry attenuation experiment for measuring the total nuclear cross sections of various elements has been performed with neutrons produced from a ¼-in. beryllium target bombarded by the 110-Mev internal proton beam of the Harvard 95-inch synchrocyclotron. The neutron beam collimated by pipes of rectangular cross section was first monitored by a triple coincidence scintillation counter telescope. Then the beam was attenuated by samples of various elements and the resultant intensity determined by another scintillation counter telescope. By the selection of three, four, five and six-fold coincidences energy bands of approximately 5-Mev absolute total width were defined. The effective energy spread is therefore considerably smaller. Cross sections of hydrogen, deuterium, carbon, oxygen, aluminum, silicon, iron, and lead have been measured and the results will be presented.

* Supported by the joint program of the U. S. Office of Naval Research and the U. S. Atomic Energy Commission.

W3. Photoneutron Cross Sections in He, N, O, F, Ne and A. G. A. FERGUSON, J. HALPERN, R. NATHANS, AND P. F. YERGIN, *University of Pennsylvania.*—The apparatus previously reported[1] for the direct detection of neutrons from (γ,n) reactions induced by betatron bremsstrahlung has been modified to permit cross section determinations using gaseous targets at 100 atmospheres pressure. Results from oxygen are consistent with other determinations.[2] The remaining elements, representing new results, show the familiar giant dipole resonance for the photoneutron process. Helium has a resonance peak at 24 Mev with a 4-Mev half-width, a peak cross section of 1.25 millibarns and an integrated cross section of 6 Mev-millibarns. The other elements show behaviors consistent with the systematics reported[3] for (γ,n) reactions. The lower the Z of the element, however, the greater is the difference between the observed integrated cross sections for $(\gamma,n)+(\gamma,p)+(\gamma,pn)$ reactions and the sum rules. An explanation of this result in terms of various models will be proposed.

[1] Halpern, Mann, and Nathans, Rev. Sci. Instr. **23**, 678 (1952).
[2] Montalbetti, Katz, and Goldemberg, Phys. Rev. **91**, 659 (1953).
[3] R. Nathans and J. Halpern, Phys. Rev. **92**, 207 (1953).

W4. Photoneutron Angular Distributions. K. GELLER, J. HALPERN, AND PAUL F. YERGIN, *University of Pennsylvania.*—The angular distributions of photoneutrons produced by 22 Mev bremsstrahlung on Pb, Ag, and Cu have been measured using a lucite-zinc sulfide fast neutron detector.[1] The results do not show any significant nonisotropy. If the distributions are fitted to the form $A+B\sin^2\theta$, the value of B/A consistent with the data for any of the elements could not exceed 0.12. If we make approximate estimates of the neutron energy distributions for two different models, the evaporation model and Courant's direct photoeffect model,[2] and if we assume that all of the nonisotropic component is the result of direct photoeffect, and take into account the measured energy sensitivity of the type of detector used,[3] then the cross section for direct photoeffect production of the nonisotropic component is not more than 1 percent of the total cross section for Cu, and must be considerably less for Ag and Pb, for which the data is better.

[1] W. F. Hornyak, Rev. Sci. Instr. **23**, 264 (1952).
[2] E. D. Courant, Phys. Rev. **82**, 703 (1951).
[3] W. D. Whitehead and S. C. Snowdon, Phys. Rev. **92**, 114 (1953).

W5. Total Cross Section of O_2 for Cold Neutrons.* R. M. EISBERG, H. PALEVSKY, M. E. RICKEY, AND T. I. TAYLOR, *Brookhaven National Laboratory.*—The total cross section of O_2 for neutrons has been measured in the neutron wavelength range 5A to 10A. A beam of cold neutrons from the Brookhaven pile was "chopped" into a series of bursts by a rotating cadmium shutter. The neutron time of flight over a 5 meter path between the shutter and a BF_3 filled proportional counter was recorded in a 12 channel analyzer. A 3.5 meter long target vessel was placed in the beam in good geometry with respect to the detector and the beam attenuation due to filling the target with 10 atmospheres of purified O_2 was measured. Backgrounds were measured by inserting a 0.010-in. cadmium foil in the beam. The temperature and pressure of the O_2 were measured to ¼ percent and the molecular density was computed from the Beattie-Bridgeman equation of state. The standard deviation of the cross section due to counting statistics were generally less than 1 percent. Corrections were made for the finite resolution of the time of flight analyzer. The measured cross section falls on a smooth curve passing through the following points: 14.5 barns at 5.00A, 19.6 barns at 7.71A, 23.4 barns at 10.00A.

* Work carried out under contract with U. S. Atomic Energy Commission.

W6. Magnetic Scattering of Cold Neutrons by Gaseous Oxygen.* H. PALEVSKY AND R. M. EISBERG, *Brookhaven National Laboratory.*—The scattering of neutrons by gaseous oxygen arises from the nuclear and magnetic interactions. The magnetic scattering is incoherent and does not interfere with the nuclear scattering;[1] therefore the total neutron cross section of the oxygen molecule is simply the sum of the magnetic and nuclear cross sections. In the wavelength region of interest the nuclear cross section can be accurately calculated[2] using the known free atom cross section of oxygen.[3] The experiment was performed by measuring the total neutron cross section for gaseous oxygen as described in the previous abstract. For the energy region investigated it is expected that the magnetic scattering is very nearly all elastic and therefore the wavelength variation of the magnetic scattering depends only on the spatial distribution of the magnetic moment in the oxygen molecule. For unity form factor the calculated magnetic cross section is 4.53 barns.[2] Subtracting the nuclear cross section from the measured cross section gives a smooth curve passing through 2.2 barns at 5A, 3.36 at 7.7A, and 3.8

at 10A. The shape of this curve indicates that the scattering is mostly elastic.

* Work carried out under contract with the U. S. Atomic Energy Commission.
[1] O. Halpern and M. H. Johnson, Phys. Rev. **55**, 898 (1939).
[2] O. Halpern and J. Appleton, Phys. Rev. **90**, 869 (1953).
[3] Harvey, Hughes, and Goldberg, Phys. Rev. **87**, 220 (1953).

W7. Neutron Moderation in SiO_2. JAY TITTMAN, *Schlumberger Well Surveying Corporation.*—The spatial distribution of In resonance neutrons about a point Ra-Be source has been measured in an essentially infinite silica medium under conditions similar to those previously reported.[1] The moderator consisted of a cubical pit 8 ft on an edge filled with 99.8 percent pure silica sand of density 1.61 ± 0.02 g/cm^3. A thin-walled Al tube allowed insertion of the source and Al sheaths running through the moderator provided slots for foil positioning. Standard foil counting technique was used to establish the resonance 54-min saturation activity, including corrections for 4.5-hr activity induced by inelastic scattering and 54-min activity induced by kilovolt region neutrons.[2] Edge effects were shown to be negligible over the region studied. The data are fit by a simple Gaussian slowing down density for $2000 < r^2 < 10\,000$ cm^2, corresponding to an effective age $\tau = 1900 \pm 90$ cm^2. The second-order solution to the transport equation[3] then provides agreement with the experimental results down to $r^2 = 0$ and out to $r^2 = 17\,000$.

[1] J. Tittman and F. F. Johnson, Phys. Rev. **91**, 452 (1953).
[2] Roberts, Hill, and McCammon, Phys. Rev. **80**, 6 (1950).
[3] R. E. Marshak, Revs. Modern Phys. **19**, 213 (1947).

W8. Slowing-Down of Neutrons in Hydrogenous Moderators. P. F. ZWEIFEL AND H. HURWITZ, JR., *Knolls Atomic Power Laboratory.**—The age-diffusion approximation to the Boltzmann equation is inaccurate for neutrons slowing down in hydrogenous moderators because of the large neutron energy loss per neutron-proton collision. A program is under way to compare more elaborate calculational methods for a sinusoidal variation of neutron flux with position. Such a distribution is pertinent to reactor calculations and to the Fourier analysis of the neutron distribution from a point source. The methods include the spherical harmonic method[1] and an improvement on this method in which the system of equations is made finite by neglecting higher harmonics in the hydrogen scattering function rather than in the neutron flux.[2] A simpler but less accurate method in which the nonisotropic component of the hydrogen scattering is assumed not to change the neutron energy[3] has been included in the comparison. Numerical results for the Fourier transform of the slowing-down density from a point source of fission neutrons in water are presented, and results for the second spatial moment are compared.

* Operated for the U. S. Atomic Energy Commission by the General Electric Company.
[1] R. E. Marshak, Revs. Modern Phys. **19**, 200 (1947); G. C. Wick, Z. Physik **121**, 702 (1943); these methods may be shown to be equivalent.
[2] Bethe, Tonks, and Hurwitz, Phys. Rev. **80**, 11 (1950); G. C. Wick, Phys. Rev. **75**, 738 (1949); D. Selengut (private communication).
[3] This method, as applied to reactor calculations, has been suggested by D. Selengut and G. Goertzel.

W9. Standards for Thermal Neutron Capture Measurements. G. R. RINGO AND S. WEXLER, *Argonne National Laboratory.*—Comparison of the capture cross section of boron measured at Argonne with that measured at Brookhaven, Harwell, and Stockholm has shown excellent agreement with the Brookhaven results but not with the other two. Evidence of pronounced isotopic abundance variation was looked for and not found. There was also no evidence of disagreement in chemical analysis. The burden of the discrepancies which were several times the probable errors of the measurements is thus thrown on the physical measurements. Since the Argonne and Brookhaven results agree so well and are between the other two values, it is likely that the average of the Argonne and Brookhaven values, 752 barns for 2200 m/sec neutrons, is reliable to 1 percent. Although isotopic abundance ratios of boron have been reported to vary as much as 4 percent, none was found more than 1 percent from the Argonne standard in this study.

W10. Migration Areas of Po–Be Neutrons in H_2O–Zr Mixtures. W. BAER, *Westinghouse Electric Corporation.*—The spatial distribution of Po–Be neutrons moderated by water and zirconium has been measured for four water-zirconium volume ratios. Neutrons are detected by a $\frac{1}{4}$ in. diameter $\times$ 1 in. long enriched BF_3 counter, and data are taken with the counter bare and cadmium covered. Using the second and fourth moments of the spatial distribution, the mean square slowing down lengths below the cadmium cutoff are determined experimentally. From these results, the migration areas M^2 are evaluated. For pure water $M^2 = 66.3$ cm^2; and for Zr/H_2O ratios of 0.25, 0.50, and 1.00, $M^2 = 77.5$, 87.2, 107.9 cm^2, respectively. The energy spectrum of the source has been determined experimentally, and a calculation made of the value of M^2 for the pure water case using the Marshak formula.[1] This calculation assumes only elastic scattering, and that the oxygen scattering is isotropic in the laboratory system. The theoretical value of M^2 is found to be 60.9 cm^2 for pure water. This value is 10 percent lower than the experimental measurement of M^2, and is presumed to be largely due to the anisotropy in the forward direction of neutron scattering from oxygen.[2]

[1] R. E. Marshak, Revs. Modern Phys. **19**, 209 (1947).
[2] Baldinger, Huber, and Procter, Helv. Phys. Acta **25**, 142 (1952).

SATURDAY AFTERNOON AT 1:30

Shoreham, Main Ballroom

(R. W. THOMPSON presiding)

Strange Particles of the Cosmic Rays

Invited Paper

X1. Positrons from Decay of Mu Mesons. RYOKUCHI SAGANE, *University of California, Berkeley.* (30 min.)

Contributed Papers

X2. Observations on Unstable Particles in Photographic Emulsion.* M. F. KAPLON, J. CRUSSARD, J. KLARMANN, AND J. NOON, *University of Rochester.*—Further evidence is presented for the existence of the alternate decay mode of the τ^+ meson.[1] A particle with a mass value of $1060 \pm 100\ m_e$, originating from a star classified as either $2+1_0$ or $2+0_p$, is observed

to decay into a π^+ meson of 15.2 Mev energy. Two cases of the normal 3 charged π decay of the τ meson are observed, one of which gives a precise Q value of 73.85 ± 1 Mev; it is noted that the τ meson mass is identical within experimental errors to that of the θ^0 meson.[3] A K meson is observed to be produced from a star with a total visible prong energy of 850 Mev; this may suggest a low production threshold. Another K meson is observed to suffer large angle inelastic scattering at low energy ($\sim$40 Mev) implying a direct nuclear interaction of this particle. Q values for 2 prong stars consisting of π^- mesons and protons will be reported; among these is a value of 37.8 ± 0.6 Mev,[3] corresponding to a Λ_0 decay.

* This research was supported in part by the U. S. Air Force under a contract monitored by the Office of Scientific Research, Air Research and Development Command.
[1] J. Crussard *et al.*, Phys. Rev. 93, 253 (1954).
[2] The latest value reported by Thompson for the θ^0 at the Fourth Annual Rochester Conference was $965\pm10m_e$.
[3] In excellent agreement with a value of 37.7 ± 0.5 Mev reported by P. Fowler at the Fourth Annual Rochester Conference.

X3. Decay of a Heavy Neutral Particle. R. A. HOWARD, P. M. FITZPATRICK, H. E. HOFFMAN, AND J. S. URBAN, *University of Oklahoma.*—A V-shaped track has been found in a 400 micron Ilford G-5 emulsion exposed* to cosmic rays at 99 000 feet. The vertex of the V is 949 microns from a star of 19 prongs and is approximately coplanar with the star center. One branch of the V represents a particle which comes to rest in the emulsion after a distance of 962 microns. The other branch of the V has a smaller grain density and passes out of the emulsion without noticeable scattering after traveling 466 microns. Preliminary measurements indicate that the particle which came to rest had a mass at least equal to that of a proton, while the other particle was a meson. If one interprets this event as the emission from the star center of a neutral particle which subsequently decays into a proton and a meson then the Q is much lower than that of a Λ^0 decay. Careful remeasurements are underway to determine the masses and momenta of the decay particles with as high precision as is possible.

* Plates flown through courtesy of the General Mills Company and the U. S. Office of Naval Research.

X4. Charged Heavy Mesons from Nuclear Collisions. L. VOYVODIC, *National Research Council, Canada.*—Unstable heavy charged particles have occasionally been observed to arise from nuclear disintegrations in the energy region of several Bev. Two examples of such events are described, observed in 1000 micron Ilford G5 emulsions exposed in stratosphere balloon flights. After production in a star of type $1+21n$, a K particle of 8-mm residual range in emulsion decays at rest, yielding a secondary particle of 1.5 times plateau ionization. The rest mass obtained from range, ionization, and scttering on this probable kappa meson is 950 ± 150 m_e. In the second event an H particle, with mass 2100 ± 300 m_e, is produced in a star of type $0+9_p$. After traversing 12-mm emulsion the particle decays in flight near the end of its range, giving a secondary track at, or very near, plateau ionization.

X5. Magnetic Cloud Chamber Observation of V-Particles. I. Charged V-Particles.* Y. B. KIM, J. R. BURWELL, H. O. COHN, C. J. KARZMARK, AND R. W. THOMPSON, *Indiana University.*—The large magnetic chamber[1] (illuminated volume 22 in. high, 11 in. wide, and 5 in. deep situated in uniform field of 7000 gauss) has now been in operation for about 460 days at sea level with penetrating shower trigger requiring two or more particles below the chamber. Stereoscopic photographs of about 3000 penetrating showers (visible multiplicity of at least 3) have been obtained among which are found 146 examples of neutral V events and 63 examples of angular deflection without visible recoil. The nature of these deflections will be discussed; preliminary classification indicating that 29 of the 63 are decays of charged V particles (10 positive; 19 negative). The data is in the process of analysis and the results will be reported. In one example, R-423, the charged secondary is identified to be a negative pion (by $\pi-\mu$ decay) with a transverse momentum of 101 Mev/c.

* Assisted by the U. S. Office of Ordnance Research and by grant of the Frederick Gardner Cottrell Fund of the Research Corporation.
[1] Thompson, Buskirk, Etter, Karzmark, and Rediker, Phys. Rev. 90, 329 (1953).

X6. Magnetic Cloud Chamber Observations of V-Particles. II. Status of Work on the θ^0 Meson.* R. W. THOMPSON, J. R. BURWELL, H. O. COHN, R. W. HUGGETT, AND C. J. KARZMARK, *Indiana University.*—Twenty-two neutral V events, exclusive of Λ^0 decay, have now been analyzed. The Q-curve plot of the data suggests in a natural way that twenty cases are examples of decay of the θ^0 (formerly called $V_1^{0\,1}$)$\rightarrow\pi^\pm+(\pi^\mp$ or $\mu^\mp)$, and thus confirm earlier evidence[1] for this particle and decay scheme. Within the limited statistics, the decay is isotropic in the C.M. system. With $m_\tau=139.7$ Mev, no revision of our earlier $Q(\pi,\pi)$ value of 214 ± 5 Mev is yet required, $M(\pi,\pi)=966\pm10$ m_e. There are two anomalous cases, 328[1] and R-439, which may indicate an alternate decay mode of the θ^0 (for example, $\theta^0\equiv\tau^0\rightarrow\pi^\pm+\pi^\mp+\pi^0$; or $\theta^0\rightarrow\pi+\mu+\nu$) or the decay of some new type of heavy neutral particle. These two cases would, of course, be explained if the main θ^0 decay mode were a 3-body process, but in view of the fit of the 20 "normal" cases, this appears to be an unlikely possibility unless the energy spectrum of the neutral particle in that 3-body process is very markedly different from the spectrum expected from statistical considerations.

* Assisted by the U. S. Office of Ordnance Research and by grant of the Frederick Gardner Cottrell Fund of the Research Corporation.
[1] Thompson, Buskirk, Etter, Karzmark, and Rediker, Phys. Rev. 90, 1122 (1953).

X7. Production of V^0 Particles in Copper.* D. R. HARRIS AND A. L. HODSON, *Princeton University.*—A cloud chamber containing a $1\frac{1}{2}$ inch thick centrally located copper plate has been operated in a magnetic field at mountain altitude (10 800 feet).[1] The chamber was expanded following a coincidence corresponding to three or more minimum ionizing particles passing through each of three proportional counter trays. Two of these trays were below the cloud chamber and one was immediately under the central copper plate in the cloud chamber. 28 V^0 particles were observed to originate in interactions in the copper plate and to decay in the cloud chamber. Events in which these V^0's were produced have been analyzed as to the nature of the producing particles and compared to events in which V^0's were not observed. An analysis is shown for the calculation of momentum from a conical projection of a particle's track in a uniform magnetic field with transverse components.

* Supported by the U. S. Office of Naval Research and the U. S. Atomic Energy Commission.
[1] J. Ballam *et al.*, Phys. Rev. 91, 1019–1020 (1953).

X8. Momentum of S-Particle Secondaries.* D. WILLARD, *M.I.T.*—We have made a statistical analysis of the scattering angles in lead plates of the charged secondary particles from eighteen S particles observed in the M.I.T. multiplate cloud chamber. Under the assumption that all secondaries have the same momentum, we found that the most likely value[1] of the momentum is 249 $(1\pm0.05\pm0.07)$ Mev/c if all secondaries are mu mesons; 264 $(1\pm0.05\pm0.07)$ Mev/c if all secondaries are pi mesons. 0.05 is the standard error (relative) arising from experimental errors. 0.07 is the standard error (relative) arising from the statistical nature of the theory. We shall present the method of analysis and discuss the manner in which our results can be interpreted.

* Research supported in part by the joint program of the U. S. Office of Naval Research and the U. S. Atomic Energy Commission.
[1] S. Olbert, Phys. Rev. 87, 319 (1952); Annis, Bridge, and Olbert, Phys. Rev. 89, 1216 (1953); Bridge, Peyrou, Rossi, and Safford, Phys. Rev. 90, 921 (1953).

X9. Recent Results on *S* Particles.* H. S. BRIDGE, H. COURANT, B. DAYTON, H. C. DESTAEBLER, JR., B. ROSSI, AND D. WILLARD, *M.I.T.*—This paper presents a summary of recent results on charged heavy mesons which have been observed to stop and decay in the M.I.T. multiplate cloud chamber. The data include information on the ranges of the charged decay products and on the frequency and angular distribution of the associated photons.

* Research supported in part by the joint program of the U. S. Office of Naval Research and the U. S. Atomic Energy Commission.

X10. An Unusual Cosmic-Ray Event.* H. C. DESTAEBLER, JR., H. S. BRIDGE, H. COURANT, AND B. ROSSI, *M.I.T.*—We have observed a most unusual cosmic-ray event in the M.I.T. multiplate cloud chamber. A slow, heavy particle stops in one of the brass plates and produces 3 electron cascades. There is no other visible product. The showers diverge at wide angles and appear to be initiated by photons. Lower limits for the energies of the 3 showers are about 20, 130, and 590 Mev. More likely values are 160, 220, and 925 Mev. One might perhaps explain this event in terms of known particles, by assuming that the stopped particle is a negative heavy meson which undergoes nuclear absorption, thus transforming practically all of its energy into gamma rays. However, the masses of known heavy mesons do not appear to be quite sufficient to account for the observed energy release. If the event is a decay process, the conservation of momentum requires that a fourth unseen particle was emitted. In this case the lower limit for the total energy release is about 1200 Mev. The large value of the energy release raises the question as to whether the event may be interpreted in terms of an annihilation process.

* Research supported in part by the joint program of the U. S. Office o Naval Research and the U. S. Atomic Energy Commission.

SATURDAY AFTERNOON AT 1:30

Shoreham, West Ballroom

(JOHN MARSHALL presiding)

Nucleonic Scattering

Y1. Proton-Proton Cross Section at 95 Mev.* U. E. KRUSE† AND J. M. TEEM,‡ *Harvard University*.—The differential cross section for scattering of protons by hydrogen has been measured using the external proton beam of the Harvard cyclotron. Coincidences between the two protons scattered from targets of polyethylene and polystyrene were measured with suitable subtraction for the contribution from carbon. The number of incident protons was measured by means of a Faraday cup. The beam energy was determined by measuring the range in aluminum. The angular distribution from 90° to 40° in the center-of-mass system as determined in this way was found to be 4.6 mg/sterad at 90° and showed a slight rise toward small angles. Further checks are being planned using liquid hydrogen targets.

* Supported by the joint program of the U. S. Office of Naval Research and the U. S. Atomic Energy Commission.
† Society of Fellows.
‡ National Science Foundation Predoctoral Fellow.

Y2. Proton-Proton Scattering Near the Interference Minimum.* ROBERT L. ZIMMERMAN, DAVID H. FRISCH, AND DANIEL I. COOPER,† *M.I.T.*—The differential proton-proton scattering cross section at 45° in the laboratory system has been remeasured in the energy region from 350 to 420 kev. To calibrate the machine energy the alpha particles from the 340-kev $F^{19}(p,\gamma\alpha)$ reaction were observed in the same geometry and with the same proportional counters used in the proton scattering experiment. To do this a trace of fluorine-containing gas was mixed with the hydrogen in the scattering chamber. High current densities were obtained with the aid of an electro static alternating gradient lens above the scattering chamber. The interference minimum in the ratio to the Mott cross section was found to occur at 382.7±1.5 kev, giving an *S*-wave phase shift at this energy of $\delta_0 = 0.2529 \pm 0.0011$ radians in agreement with our preliminary measurements.[1] The combination of our observation with the Wisconsin data[2] alone seems to exclude a static potential with a repulsive core. Such a conclusion agrees with an analysis by Yovits *et al.*[3] of data from a wide range of energies.

* Supported by the joint program of the U. S. Office of Naval Research and the U. S. Atomic Energy Commission.
† Now at Bell Telephone Laboratories.
[1] Cooper, Frisch, and Zimmerman, Phys. Rev. **90**, 339 (1953).
[2] Yovits, Smith, Hull, Bengston, and Breit, Phys. Rev. **85**, 540 (1952) survey and interpret all the data and quote the unpublished results of a thorough investigation by Heydenburg and Little in the low-energy region.
[3] Worthington, McGruer, and Findley, Phys. Rev. **90**, 899 (1953).

Y3. $p-p$ Scattering in Nuclear Emulsions.* S. K. KAO AND A. F. CLARK, *Carnegie Institute of Technology*.—A flux of two million protons per cm² with an energy of 420±20 Mev passed through Ilford G-5 nuclear plates. The 200 micron thick emulsions are area-scanned for elastic p-p collisions which are identified by (a) an estimate of the corresponding grain densities along the tracks, (b) coplanarity of the tracks, (c) the proper angles. If we limit the azimuthal angles to less than 45°, the measurements on coplanarity angles are accurate to between 1 to 2°, and that of the angle between the scattered and recoiled protons to between ½ to 1°. The azimuthal angle is the angle between the plane of the plate and the plane of the event. Measurements of events and computations indicate that, with this angular resolution, quasielastic events will constitute only a small fraction of the elastic events. These background events are due to interaction with protons bound in a heavy nucleus. Forty-one acceptable events have been identified. Scanning is continuing to build up statistics.

* Supported in part by the U. S. Atomic Energy Commission.

Y4. The External Proton Beam of the Carnegie Synchrocyclotron.* J. A. KANE, R. A. STALLWOOD, R. B. SUTTON, T. H. FIELDS, AND J. G. FOX, *Carnegie Institute of Technology*.—A few percent of the internal proton beam of the synchrocyclotron emerges from the machine without benefit of a deflector or a scatterer. It emerges uniformly in azimuth with an energy of about 450 Mev. After passing through a

collimator 30 ft from the machine, its intensity is about 2×10^6/cm²/sec. Here the energy is 437 Mev due to degradation in the window and air. The beam is monitored with an ionization chamber similar to that of Chamberlain *et al.*[1] The contamination is about 5 percent of the total flux, and consists of a lower energy "tail" of protons which is essentially zero below 370 Mev. Three separate methods have been used to study this contamination (a) measurement of the angle between scattered protons in p-p elastic scattering; (b) measurement of the angular distribution of Cerenkov radiation from the beam traversing glass;[2] (c) a differential range technique using a coincidence-anticoincidence counter telescope. Scattering measurements indicate no left-right asymmetry, and thus the beam is presumed to be unpolarized.

* Work supported in part by the U. S. Atomic Energy Commission.
[1] Chamberlain, Segré, and Wiegand, Phys. Rev. **83**, 923 (1951).
[2] R. L. Mather, Phys. Rev. **84**, 181 (1951).

Y5. Proton-Proton Scattering at 437 Mev.* R. B. Sutton, T. H. Fields, J. G. Fox, J. A. Kane, W. E. Mott, and R. A. Stallwood, *Carnegie Institute of Technology*.—Proton-proton scattering data, previously reported,[1] obtained by detecting the scattered and recoil protons in coincidence, using targets of CH_2 and C, were carefully checked and satisfactory agreement obtained. Additional data were taken with a liquid hydrogen target by two methods; in one the scattered and recoil protons were detected in coincidence as before for 90° and 50°; in the other only the higher-energy proton was detected using a two-counter coincidence telescope. At small angles enough copper was placed between the counters to absorb everything except elastically scattered protons. The detection efficiency of this telescope was measured in the direct beam with appropriate absorbers to reduce its energy. The relative values of the cross sections are as follows (the errors are from counting statistics):

C.M. angle	90°	65.3°	50.5°	36.4°	30°	27.8°	25.2°	16.6°
CH_2 target	1.00	1.03±0.03		1.16±0.03	1.16±0.03		1.24±0.03	
H_2	1.00		1.09±0.03			1.17±0.05		1.19±0.06

* Supported in part by the U. S. Atomic Energy Commission.
[1] Mott, Sutton, Fox, and Kane, Phys. Rev. **90**, 712 (1953).

Y6. The Total $p-p$ Cross Section Above 400 Mev. A. M. Shapiro, C. P. Leavitt, and F. F. Chen, *Brookhaven National Laboratory*.—The $p-p$ total cross section at six energies between 0.4 and 1.3 Bev has been measured in a program to study the energy variation of this cross section up to 3 Bev. A polyethylene-carbon difference method was employed in conjunction with a fast-coincidence counter telescope and magnetic analysis of the 32° scattered proton beam from a Be target in a Cosmotron straight section. The meson contamination was less than 1 percent. The momentum resolution was about ±4 percent. Transmission measurements were made with various values of θ, the half-angle subtended by the rear counter at the center of the absorber, from 1.9° to 8.3°. The cross sections at each energy were plotted against θ^2, and each total cross section was found by straight-line extrapolation to 0°. The preliminary cross sections are given below.

E (Mev):	410	535	615	830	1075	1275
σ_t (mb):	27	32	38	49	49	47

These values have been corrected for multiple Coulomb scattering in the absorber. The error in each of these points is approximately 2 mb. The sharp rise in the cross section from 400 to 800 Mev may be associated with an increase in the inelastic (meson production) cross section.

Y7. Pickup Deuterons Produced from 95-Mev Protons. W. Selove, *Harvard University*.*—Deuterons produced by the interaction of the external beam of the Harvard cyclotron were detected in a scintillation-counter range telescope. Deuterons were separated from other charged particles by simultaneous measurement of range and specific ionization, and the energy distribution measured for deuterons above about 50 Mev, with a resolution of a few percent. Results will be reported of measurements which have been made at several angles with beryllium and carbon, and at one angle with aluminum, silicon, copper, and lead. Calculations are being made as to the nucleon distributions which can be inferred from the experimental results.

* On leave to Radiation Laboratory, University of California, Livermore California.

Y8. A Search for Polarization in Charge Exchange Scattering.* H. Bradner and R. E. Donaldson, *University of California, Berkeley*.—A refinement of Wouters'[1] experiment is being made to investigate the asymmetry produced by polarization in double exchange scattering of protons on C or Ta targets. Neutrons are produced in the first scatterer by the internal proton beam of the 184-inch cyclotron. These neutrons are converted in the second scatterer outside the shielding and recorded by two coincidence telescopes. The two telescopes are positioned by an unpolarized beam and all subsequent angular changes are made with the first scatterer. The results to date are:

Targets	1st angle	Counter angle ±6°	Bombarding energy Mev	Rejection energy Mev	$C=\frac{R-L}{R+L}$ percent
Ta	17°	25°	190	90	−1.4±1.6
C	17°	25°	190	110	0.5±2.9
C	35°	35°	245	90	5.2±3.0

Quoted errors are statistical probable errors plus an estimated one percent systematic error. An investigation is now being made on a 10°, 330-Mev initial scattering and on a single charge exchange scattering with a known polarized beam.[2]

* Supported by the U. S. Atomic Energy Commission.
[1] L. F. Wouters, Phys. Rev. **84**, 1069 (1951).
[2] Chamberlain, Segre, Tripp, Wiegand, and Ypsilantis, Phys. Rev. (to be published).

Y9. Polarization of 170-Mev Neutrons.* A. Roberts, J. Tinlot, and E. M. Hafner, *University of Rochester*.—A beam of 240-Mev protons strikes an internal target, T_1, and a set of neutron collimators is placed at the angle $\theta_1=29°$ (lab). Neutrons scatter from a radiator, T_2, and recoil protons are observed in a triple telescope at the angle θ_2 in a horizontal plane, to the left or right of the neutron axis. The telescope has a small acceptance angle (~2°) determined by brass slits, and is accurately mounted on a selsyn-driven turntable whose angular position can be read to 1′. The telescope contains an absorber whose thickness is varied with angle in such a way as to set a neutron threshold of 120 Mev at all angles. An additional internal target, producing forward neutrons on the same axis, is used to check the symmetry. Preliminary measurements have been made at angles $\theta_2=12$, 20, 30, 45, and 55 degrees, using T_1-T_2 combinations Be−CH_2, Be−C, C−CH_2, and C−C. We find that the Be−H asymmetry goes through a maximum of about 5 percent at 30°, and through zero near 45°. The Be−C asymmetry behaves differently, remaining positive up to 55°.

* Supported by the U. S. Atomic Energy Commission.

Y10. Polarization of 310-Mev Protons by Deuterium.* D. Nagle, J. Marshall, L. Marshall, and W. Skolnik, *The University of Chicago*.—The polarization of deuterium for 310-Mev protons has been examined as a function of angle in a preliminary measurement. Protons in an equilibrium

cyclotron orbit of 322-Mev average energy were polarized by scattering at 14° from an internal beryllium target. A scattered beam of 314-Mev protons emerging through the heavy shield were found to be 60 percent polarized as estimated from the asymmetry of a second scattering at 14° from beryllium in the experimental area. The asymmetry of scattering of this beam from liquid deuterium was examined from 8° to 36° aboratory angle, from which data the polarization of deuterium for this range of angles was estimated. The present results, from a single cyclotron run, seem to show a rather different behavior for deuterium than for hydrogen.[1] The polarization of deuterium shows little tendency to decrease with increasing angle, and in particular remains large at 90° in the baricentral system of the nucleon-scattered proton.

* Research supported by a joint program of the U. S. Office of Naval Research and the U. S. Atomic Energy Commission.
[1] Chamberlain, Segre, Tripp, Wiegand, and Ypsilantis; Marshall, Marshall, and de Carvalho, Phys. Rev. (to be published).

Y11. Elastic Proton-Deuteron Scattering at 95 Mev.* J. M. TEEM† AND U. E. KRUSE,‡ *Harvard University.*—The differential cross section for the elastic scattering of 95-Mev protons by deuterons has been measured at eighteen angles between 60° and 172° (center-of-mass) to a statistical accuracy of 3–5 percent. For scattering angles larger than 115° the elastic events were observed by identifying the recoil deuteron, using a telescope of counters which simultaneously measured its range and specific ionization. A CD_2-C subtraction was employed, but over most of the angular range the carbon contribution was reduced by requiring a coincidence between the scattered proton and the deuteron in the range-specific ionization telescope. For the smaller angles a range analysis of the protons in coincidence with particles at the recoil deuteron angle made possible an unambiguous separation of elastic and inelastic events. The absolute cross section was determined by the Faraday cup method. Comparison will be made with previous experiments on the scattering of neutrons and protons by deuterons.

* Supported by the joint program of the U. S. Office of Naval Research and the U. S. Atomic Energy Commission.
† National Science Foundation Predoctoral Fellow.
‡ Society of Fellows

Y12. Neutron-Proton Scattering at 91 Mev.* R. H. STAHL, *Harvard University.*—The differential cross section for the scattering of neutrons by protons has been measured suing an external neutron beam from the Harvard cyclotron with an effective energy of 91 Mev. The proton target was a 3-cm diameter cylinder of liquid hydrogen in a 0.0006 in. Be–Cu foil container. Recoil protons were counted with good angular resolution in a scintillation telescope between 59° and 176° in the center-of-mass system. A similar telescope fixed at 140° with CH_2 radiator served as a beam monitor sensitive to variations in the neutron beam. Special attention was given to large angle scattering, and to the apparent asymmetry of scattering about 90°.

* Supported by a joint program of the U. S. Atomic Energy Commission and the U. S. Office of Naval Research.

Y13. Nuclear Internal Momentum Distributions.* J. M. WILCOX AND B. J. MOYER, *University of California, Berkeley.*—The nuclear internal momentum distributions of protons in light nuclei have been studied with the 340-Mev scattered proton beam from the synchrocyclotron. The two protons from a quasielastic scattering event are detected in coincidence, and the energy of one of them is magnetically analysed. In the limit of the impulse approximation, conservation of energy and momentum can be employed to solve for the momentum of the struck proton. The best fit to the experimental data for beryllium was obtained with a Gaussian momentum density distribution with a $1/e$ value of about 20 Mev. Fermi (rectangular) and Chew-Goldberger distributions did not fit as well. Qualitative differences were observed between lithium, beryllium, and boron.

* This work was done under the auspices of the U. S. Atomic Energy Commission.

Y14. Scattering of 10 Mev Protons on Magnesium and Carbon.* G. E. FISCHER, *University of California, Berkeley.*—In order to study the mechanism of excitation of nuclear levels by inelastic scattering, a scattering chamber of 36 in. diameter was constructed. The deflected beam of the Berkeley 60-in. cyclotron was brought out of the shielding by means of strong focusing magnets. Particles from the nuclear reactions were detected by either of two systems, a quadruple proportional counter telescope, or a coincidence crystal spectrometer. Energy resolution was of the order of 2.5 percent. The angular distribution of protons from the reactions $C^{13}(p,p^1)C^{13*}$ $Q=-4.47$ and $Mg^{24}(p,p^1)Mg^{24*}$ $Q=-1.38$ was found to be peaked in the forward direction. The elastic scattering of protons on the above nuclei were also studied and interference minima found. Two new levels are believed to have been found in Mg^{24}. Work on Si^{28} and Be^9 is in progress.

* This work was done under the auspices of the U. S. Atomic Energy Commission.

Y15. Proton Bremsstrahlung and High-Energy Gamma Emission from Carbon. DAVID COHEN, BURTON J. MOYER, HARLAN SHAW, AND CHARLES WADDELL, *University of California, Berkeley.*—A 180° pair spectrometer, similar to that here employed previously in π^0 experiments, capable of spectrum analysis in the range 10–150 Mev, has been employed in a study of the bremsstrahlung from bombardment of nuclei by high-energy protons below threshold for π^0 production. The bremsstrahlung is apparently appropriate to the $(E/2-h\nu)^{\frac{1}{2}}(d\nu/\nu)$, modified by nucleon momentum distributions, which is expected from electric dipole radiation in $N-P$ collisions. Superimposed upon the bremsstrahlung in the case of carbon nuclei is a strong line emission at 15.2 ± 0.2 Mev. This line emission is present over a variation in proton bombarding energy from 30–340 Mev; and it is also produced by deuteron bombardment of B^{11}, but not of B^{10}. It is believed to belong to a C^{13} nuclear transition for which disintegration into three alphas is forbidden by either parity or isotopic spin selection rules.

Y16. Elastic Scattering of Alpha Particles by Heavy Nuclei.* GEORGE W. FARWELL AND HARVEY E. WEGNER,† *University of Washington.*—The elastic scattering of alpha particles by Ag, Ta, Pb, and Th has been studied at energies of 13 to 42 Mev. Variation of cross section with energy at a scattering angle of 60° is similar to that previously reported for Au.[1] At low energies, the cross section for each material follows the Coulomb dependence. At higher energies, the cross section falls rapidly as the alpha-particle energy increases, following the empirical formula $\sigma(E)=\sigma(E_0)\exp[-K(E-E_0)]$. The critical energy E_0 increases with Z. The coefficient K is about 0.26 Mev^{-1} and is nearly the same for all elements studied. Interpretation of results in terms of a semiclassical strong absorption model due to Blair[2] leads to values of the sum of nuclear radius and alpha radius in agreement with the empirical formula $D=(1.50A^{\frac{1}{3}}+1.5)10^{-13}$ cm.

* Partially supported by the U. S. Atomic Energy Commission.
† Now at Brookhaven National Laboratory.
[1] George W. Farwell and Harvey E. Wegner, Phys. Rev. (to be published).
[2] J. S. Blair, abstract following.

SATURDAY AFTERNOON AT 1:30

NBS, East Building

(S. MILLMAN presiding)

Solid-State Physics, III, Mostly Metals

Invited Paper

Z1. Noise in Semiconductors, Rectifiers, and Transistors. R. L. PETRITZ, *Naval Ordnance Laboratory.* (30 min.)

Contributed Papers

Z2. Electronic Quadrupole-Quadrupole Interactions in Cerium Metal.* J. M. KELLER AND E. KOENIGSBERG,† *Iowa State College.*—Electronic multipoles arise from the charge density of electrons in incomplete atomic shells. Interactions between multipoles about different atoms are principally quadrupole-quadrupole (*Q-Q*). For rare earth metals, the *Q-Q* interactions of the 4*f* shell electrons are of the same order of magnitude as the crystal field (charge-multipole) interactions. The *Q-Q* contributions to the electronic energy and specific heat at temperatures below 20°K cannot be neglected. We have investigated these contributions for hexagonal cerium, treating the conduction electrons as a uniform negative charge distribution. Measured values of specific heat[1] cannot be reproduced by a theory including crystal fields but ignoring *Q-Q* interactions. Nor is the disagreement removed by including *Q-Q* effects, but assuming different electronic states distributed at random among the lattice sites. It is probable that the specific heat anomalies are associated with breakdown of some type of ordering. Including *Q-Q* interactions, ordered arrangements of electrons in the crystals have been found, with energies considerably lower than for random electron arrangement. In all the ordered arrangements studied, electrons of two different orientations are located in alternating crystal planes.

* Work supported by the U. S. Atomic Energy Commission.
† Now at Midwest Research Institute.
[1] Parkinson, Simon, and Spedding, Proc. Roy. Soc. (London) **A207**, 137 (1951).

Z3. Axial Ratios in Hexagonal Metals. J. W. MCCLURE,* *University of Chicago.*—A theoretical study has been made of the deviations of the axial ratios of hexagonal metal crystals from the ideal close-packing value. The procedure followed was to express the shearing stress in the close-packed configuration as an expectation value, using a method similar to that of Fuchs and Peng.[1] This yielded a generalized virial theorem. Introducing the Hartree-Fock approximation and making use of commutation relations allowed us to express the stress as a sum of three terms: (1) an integral taken over the surface of an atomic polyhedron, which can be interpreted as a "kinetic stress" due to the electrons; (2) a lattice sum of electrostatic interactions, which is quite small; and (3) an exchange contribution. In the weak potential case (1) reduces to the estimates of Jones[2] and Goodenough,[3] while in the more general case it has the same qualitative behavior. A rough estimate of (3) showed that it was appreciable and thus should be taken into account.

* National Science Foundation Predoctoral Fellow.
[1] K. Fuchs and H. W. Peng, Proc. Roy. Soc. (London) **A180**, 451 (1942).
[2] H. Jones, Phil. Mag. **41**, 663 (1950).
[3] J. B. Goodenough, Phys. Rev. **89**, 282 (1953).

Z4. An Analysis of the Forbes Bar Method for Measuring the Thermal Conductivity of Metals.* JOSEPH M. CLIFFORD AND R. B. SAWYER, *Lehigh University.*—Hogan and Sawyer[1] calculated the conductivity of a specimen from the results of two experiments: a measurement of the power required to maintain the specimen at a uniform temperature above that of the surrounding furnace, and a measurement of the temperature along the specimen with one end heated. Newton's law of cooling was assumed in both experiments; the heat-transfer coefficient calculated from the first was used, in the second, to obtain the lateral heat loss from the specimen. However, since the heat-flow patterns in the insulation surrounding the specimen are different in the two experiments, the heat-transfer coefficient calculated from the first experiment is not strictly applicable to the second. Calculation of the temperature distribution within the specimen and the insulation during the second experiment leads to conductivities which, in some cases, are appreciably smaller than those previously reported. Revised conductivities will be shown for AISI stainless steel types 347 and 446.

* Supported by the Office of Ordnance Research, U. S. Army.
[1] C. L. Hogan and R. B. Sawyer, J. Appl. Phys. **21**, 177 (1952).

Z5. High-Speed Transient Dynamic Analysis.* JOHN C. LINDSAY† AND A. V. MASKET, *The University of North Carolina.*—The transient dynamic analyzer developed at Chapel Hill has been employed to measure the forces during the penetration of mild steel, aluminum, and a composite of steel and aluminum by ogival and cylindrical projectiles. Accuracy is generally better than 5 percent. Values of a real material deceleration as large as 10^6 g or greater are easily measured during the impact. Details of the method and typical results will be presented.

* Supported by the U. S. Office of Naval Research.
† Now with E. I. du Pont de Nemours and Company.

Z6. Volume Changes in Substitutional Alloys. A. W. ROSS AND D. TER HAAR,* *St. Andrews University, Scotland.*—The coefficient of volume expansion of a linear chain consisting of equal numbers of A and B atoms has been evaluated. The potential energies for AA, BB and AB pairs are assumed to be $v_{AA}=v_{BB}=A+B(r-r_1)^2$, $V_{AB}=C+B(r-r_2)^2$, where $r_2<r_1$, corresponding to the smallest volume for a completely ordered state, and where C is chosen such that the ordered state is the state present at absolute zero. It is found that dL/dT varies roughly as the specific heat. In the case of a simple cubic lattice the expansion coefficient shows a discontinuity at the Curie point.

* On leave of absence at Purdue University.

Z7. Small Angle X-Ray Scattering from Cold-Worked Al–Ag and Al–Zn Alloys.* J.-P. JAN AND J. S. KOEHLER, *University of Illinois.*—Alloys of high purity Al with 30 wt percent Ag were annealed in the one phase region, quenched and reduced to half the original thickness by cold rolling. Non cold-worked samples give a small angle scattering identi-

cal to the one observed by Walker and Guinier,[1] corresponding to spherical clusters of Ag atoms, with a radius of gyration of 10A. Cold-worked samples exhibit a strong anisotropy effect, corresponding to an elongation of the Ag clusters in the direction of rolling. The ratio of the radii of gyration parallel and perpendicular to the following direction is 1.4. Similar results were obtained from larger amounts of cold work and Al-30 wt percent Zn. The anisotropy increases with the amount of cold work. The growth of the clusters on aging in the first stage of precipitation is isotropic in a non cold-worked specimen. In a cold-worked specimen, the clusters became more isotropic on aging.

* Supported by the U. S. Atomic Energy Commission, the U. S. Office of Ordnance Research and the «Bourse Bonjour» of the University of Lausanne, Switzerland.
[1] C. B. Walker and A. Guinier, Acta Metallurgica 1, 568 (1953).

Z8. Resistivity of Ordered and Disordered Copper-Gold Alloys at Low Temperatures.* E. PASSAGLIA AND W. F. LOVE, *University of Pennsylvania.*—The resistivity of copper-gold alloys of composition 25, 37.5, 50, 62.5, and 75 atomic percent gold has been measured as a function of temperature from room temperature to 4.2°K in states slowly cooled and rapidly quenched from above the ordering temperatures for this system. The room temperature resistivities agree with those previously obtained by Johansson and Linde.[1] The residual resistances are high in both the quenched and slowly cooled states, but the ratio of the residual resistance to the ice point resistance was found to be appreciably lower in the slowly cooled states for the 25 percent and 50 percent compositions. The other compositions showed no such difference in the residual resistance ratio. The resistivity data was analyzed using the Gruneisen[2] function. Values of the Debye temperature calculated in this manner were found to be strongly temperature dependent, but no appreciable difference was found between quenched and slowly cooled states. Hysteresis anomalies of the order of 1 percent were found in the neighborhood of 225°K.

* Supported by the U. S. Atomic Energy Commission.
[1] C. H. Johansson and J. O. Linde, Ann. Physik 25, 1 (1936).
[2] E. Gruneisen, Ann Physik. 16, 530 (1933).

Z9. Electronic Energy of Ordered Alloys. EDWARD W. HART, *General Electric Research Laboratory.*—The change of electronic energy of an alloy for small departures from perfect ordering can be formulated as equivalent to an impurity problem. If the departure of the lattice potential from that for perfect long range order is considered as a perturbation on the perfect lattice, the energy change per misplaced atom can be estimated by first-order perturbation theory. The principal part of the energy shift of the band functions appears as a rigid band shift. For an idealized one-dimensional diatomic lattice of alternating atomic specie, the energy change per defect is positive for the lowest energy band and is negative for states in the next higher band. It should be emphasized that the stabilizing effect of the ordered state which may arise in this way is demonstrable only for departures from perfect order in the ordered phase and does not compute the relative energy of the disordered phase. It is unnecessary for the treatment reported here to assume an equivalent lattice of weighted means of atomic potentials although it can be shown by the present treatment that this assumption is a good first approximation in the ordered phase.

Z10. Lattice Distortion and X-Ray Diffraction Intensities in Dilute Solid Solutions.* WILLIAM J. TAYLOR, *Ohio State University.*—It is assumed that: (1) the solute atoms are randomly distributed in (substitutional or interstitial) sites $\mathbf{r}_\alpha$; (2) the mean ratio of solute atoms to sites is z; (3) a solute atom at $\mathbf{r}_\alpha$ displaces a lattice atom at $\mathbf{r}_j$ by an amount $\mathbf{u}_{j\alpha}$ depending only on $\mathbf{r}_j-\mathbf{r}_\alpha$; (4) the total displacement of the lattice atom at $\mathbf{r}_j$ is $\mathbf{u}_j=\Sigma_\alpha\mathbf{u}_{j\alpha}$ where the sum extends over all solute atoms. The Laue-Bragg diffraction by the lattice depends on the effective scattering power $f_j\langle\exp(i\mathbf{k}\cdot\mathbf{u}_j)\rangle_{Av}$, where f_j is the atomic scattering power (corrected for thermal vibration), $\mathbf{k}$ is the diffraction vector, and the angular brackets indicate an average over-all solute atom configurations. An application of the Markoffian theory of random processes yields the exact result $\langle\exp(i\mathbf{k}\cdot\mathbf{u}_j)\rangle_{Av}=\exp\{-z\Sigma_\alpha[1-\cos\times(\mathbf{k}\cdot\mathbf{u}_{j\alpha})]\}$, where the sum on the right extends over all solute atom sites. The sum converges, and the remainder for $|\mathbf{r}_j-\mathbf{r}_\alpha|$ greater than several interatomic distances can be approximated adequately as a Fresnel integral by inserting the elastic theory formula for a spherical strain, $\mathbf{u}_{j\alpha}=A(\mathbf{r}_j-\mathbf{r}_\alpha)/|\mathbf{r}_j-\mathbf{r}_\alpha|^3$, where A is determined by the lattice expansion. An experimental program has been initiated to determine whether inversion of this expression is capable of yielding the displacements for $|\mathbf{r}_j-\mathbf{r}_\alpha|$ too small for elastic theory to apply.

* Supported by the Aeronautical Research Laboratory, Wright Air Development Command.

Z11. A Neutron Diffraction Study of the Copper-Manganese System. DAVID MENEGHETTI AND S. S. SIDHU, *Argonne National Laboratory.*—A neutron diffraction study of a series of continuous solid solutions of manganese in copper up to 85 atomic percent manganese has been made. It shows that at compositions above 13 atomic percent manganese, a broad peak appears in the region of (100) reflection of the face-centered cubic lattice. A correlation of this peak with the magnetic attraction of the alloys indicates that it is at least in part due to short-range magnetic order. Its intensity decreases at compositions greater than about 50 atomic percent. At compositions greater than about 69 atomic percent manganese a sharp diffraction line occurs at the position of a (110) reflection of the face-centered cubic unit cell. This line is temperature dependent and vanishes at 380°K. It is proposed that this reflection arises from an antiferromagnetic coupling between manganese atoms as the manganese concentration becomes predominant. No long-range crystal ordering was observed in these samples. The neutron patterns of the furnace-cooled samples did not change by heat treatment of the alloys for a period of three days at 750°C and followed by quenching in water.

SATURDAY AFTERNOON AT 1:30

NBS, Materials and Testing

(R. T. BIRGE presiding)

Post-Deadline Papers, If Any

SUPPLEMENTARY PROGRAMME

SP1. Microtron Maximum Particle Energy.* H. F. KAISER, *Naval Research Laboratory.*—The maximum particle energy attainable by a microtron may be increased in several ways: (a) simple enlargement of the magnetic pole area with operation at a given energy gain per turn; (b) increase of gain per turn by higher powered resonators; (c) increase of operating frequency allowing use of higher magnetic resonant fields,[1] and (d) combination with other types of accelerating processes at possible expense of reduced net duty factor. The last mentioned may consist in (1) modification of the microtron to include a local guide field which may be time-modulated and superposed on the static field in the region of a final particle orbit with the object of trapping the charge in this orbit and accelerating it in synchronous fashion as the local field grows. (2) the microtrons final orbit may be caused to take a rectilinear path and be injected into a larger acceleration structure (conventional or strong-focusing accelerators). The problems involved in these two approaches will be examined and discussed.

* To be given at the end of Session C if the Chairman rules that time permits.

[1] H. F. Kaiser, Phys. Rev. **87**, 183 (1952); **91**, 456 (1953); J. Franklin Inst., February, 1954.

SP2. Nuclear Masses as Rational Multiples of the Electron Mass. ENOS E. WITMER, *University of Pennsylvania.**—The mass of any nucleus in any state may be represented by Mm, where m is the rest mass of the negative electron. M appears to be always an integral multiple of 2^{-n}, where n is a positive integer or zero. Furthermore it seems probable that $n \leq 8$ always. In any case the application of the latter idea to all the existing data has produced remarkable agreements and remarkable results. Thus the nuclear mass of O^{16} is found to be $29148(13/128)m$, which yields $m = 0.000548\ 770\ 2859$ amu by taking account of the binding energy of the electrons. Using this value of m on the nuclear masses recently published by Bainbridge yields the following M-values that are astoundingly close to integers.

Nucleus	M-value
Li^7	12786.00006 ± 0.0474
C^{13}	20065.9998 ± 0.0437
O^{18}	27340.0007 ± 0.0237
F^{19}	30983.0003 ± 0.0200

For $A \leq 17$ there are 25 nuclear masses with a probable error of $\pm 0.051m$ or less. The probability of this situation arising by chance is only 3×10^{-9}.

* To be given at the end of Session FA if the Chairman rules that time permits.

SP3. Suppression of Pair Effects in Nuclear Forces. ABRAHAM KLEIN,* *Harvard University.*†—One can think of the fourth-order nuclear potential (exchange of two mesons) as the virtual scattering of a meson by each nucleon. The adiabatic limit can be viewed as the limit in which the nucleon transfers zero four-momentum during each interaction with the meson field. It follows that the fourth-order pair potential, including radiative corrections, is given exactly by the perturbation theory result if the "bare" coupling constant is replaced by the renormalized one defined by the meson-nucleon scattering experiment in the limit of zero kinetic energy and meson mass. This gives $g^2/4\pi = 0.36 - 2$, which may be interpreted as a suppression of pair production in the sense that the coupling constant required to account for the P-wave effects (and the S wave in photomeson production) is an order of magnitude larger. Higher-order pair potentials are not given simply by the perturbation result with the above value for the coupling constant. Though a considerable class of radiative corrections is thus included (finite), radiative corrections to multiple vertices, constituting an increasing class of corrections in higher order, are omitted. The effect of such terms can be estimated at present only by perturbation methods.

* Society of Fellows.

† To be given at the end of Session U if the Chairman rules that time permits.

Author Index to Papers Presented at the 1954 Washington Meeting

Ajzenberg, F., W. Franzen, and J. G. Likely—Q16
Alberger, D. E.—N1
Albert, R. D., M. L. Yeater, and E. R. Gaerttner—RA2
Allen, Lew, Jr., and A. O. Hanson—L6
Allen, Robert C.—P13
Ambler, E., R. P. Hudson, and G. M. Temmer—KA2
Andrews, David H.—OA2
Arnowitt, Richard and S. Gasiorowicz—IA2
Aschenbrenner, F. A.—C5
Atkinson, W. R., R. G. Fowler, and W. R. Holden—OA10
Austern, N. and S. T. Butler—DA6
Autler, S. H. and W. F. Roat—B16
Axel, P. and J. D. Fox—G13
Babiskin, J. and M. C. Steele—D3
Baer, W.—W10
Baldwin, G. C., F. R. Elder, and W. F. Westendorp—C8
Bandtel, Kenneth C., Wilson J. Frank, Richard Madey, and Burton J. Moyer—Q4
Bartholomew, G. A., F. Brown, H. E. Gove, A. E. Litherland, and E. B. Paul—SA6
Bartnoff, Shepard—H11
Bashkin, Stanley—Q7
Baumann, N. P., F. W. Prosser, Jr., and R. W. Krone—SA8
Beams, J. W. and J. B. Breazeale—D2
Bedo, D. E. and D. H. Tomboulian—JA3
Beeman, W. W. and R. H. Neynaber—I7
Belinfante, F. J. and J. C. Swihart—M2
Bell, R. E.—SA14
Bennett, A.—F13
Bent, R. D., R. W. Bonner, and R. F. Sippel—SA5
Bergmann, Peter G.—M4
Berlincourt, Ted G. and M. C. Steele—D10
Bernstein, J. and A. Klein—U10
Bernstein, W., J. Weiss, and J. B. H. Kuper—FA2
Bersohn, R.—H5
Beidenharn, L. C., R. L. Gluckstern, and M. H. Hull, Jr.—V5
Birman, Joseph—I11
Birnbaum, G. and A. A. Maryott—JA10
Birnbaum, W., W. E. Crandall, G. Millburn, and R. V. Pyle—SA3
Blair, J. S.—DA4
Blaser, J., J. Ashkin, F. Feiner, J. Gorman, and M. O. Stern—K4
Block, M. M. and D. T. King—S14
Bludman, Sidney A.—U8
Boag, J. and B. Zendle—FA1
Bollinger, L. M., R. R. Palmer, and D. A. Dahlberg—RA10
Bolsterli, M. and E. Feenberg—G3
Borowitz, Sidney—V2
Bortner, T. E. and G. S. Hurst—FA6
Braams, C. M.—SA11
Braden, C. H., E. T. Patronis, Jr., and L. D. Wyly—KA12
Bradner, H. and R. E. Donaldson—V8
Bray, P. J.—F2
Bridge, H. S., H. Courant, B. Dayton, H. C. DeStaebler, Jr., B. Rossi, and D. Willard—X9
Brode, Harold L.—VA5
Brolley, J. E., Jr., W. C. Dickinson, and R. L. Henkel—SA16
Brown, Fielding and Charles L. Gravel—T6
Brown, H. A. and J. M. Luttinger—T7
Brown, H. N., F. B. Smith, and R. A. Becker—KA6
Broyles, A. A.—V7
Brueckner, K., C. Levinson, and H. Mahmoud—U11
Buechner, W. W., C. P. Browne, H. Enge, M. Mazari, and C. D. Buntschuh—FA3
Bunker, M. E., J. W. Starner, and J. P. Mize—G10
Burgess, James H.—F10
Burson, S. B., W. C. Jordan, and J. M. LeBlanc—G11
Burkhardt, J. L. and E. J. Winhold—L9
Callaway, Joseph—V3
Caren, R. P. and C. E. Nielsen—C14
Carlson, R. R. and E. B. Nelson—Q12
Carroll, Thomas J.—JA16
Carter, R. S. and J. A. Harvey—RA6
Champion, K. S. W. and S. C. Brown—OA9
Chinowsky, William and Jack Steinberger—K1
Church, E. L. and M. Goldhaber—KA5
Clement, J. R.—D1
Clifford, Joseph M. and R. B. Sawyer—Z4
Codrington, R. S., J. D. Olds, and H. C. Torrey—F8
Coester, F.—M6
Cohen, B. L., G. H. McCormick, T. H. Handley, and E. Newman—Q1
Cohen, David, Burton J. Moyer, Harlan Shaw, and Charles Waddell—Y15
Cohen, Marshall H.—V13
Collins, T. L., T. T. Scolman, and A. O. Nier—H7
Collinson, J. A. and W. W. Watson—JA6
Cook, C. F., T. W. Bonner, and J. B. Marion—Q2
Crandall, W. E., W. Birnbaum, and L. Schecter—IA12
Cross, W. G. and T. A. Eastwood—KA16
Crussard, J., W. D. Walker, and M. Koshiba—K6
Cunnell, F. A. and E. E. Schneider—B12
Cutkosky, R. E.—U2
Daggett, E. H. and G. R. Grove—KA14
Dahlberg, D. A. and L. M. Bollinger—RA9
Davis, Charles F., Jr., and M. W. P. Strandberg—F6
Davis, L., Jr., G. A. deMars, L. G. Rubin, and W. D. Straub—B6
Dawson, J. M. and Z. I. Slawsky—H3
deBoisblanc, D. R. and K. A. McCollom—FA5
Dempsey, E. and D. ter Haar—T2
der Mateosian, E.—RA11
DeStaebler, H. C., Jr., H. S. Bridge, H. Courant, and B. Rossi—X10
Dettman, J. W. and A. Schild—M8
Dexter, R. N., H. J. Zeiger, Benjamin Lax, and E. S. Rosenblum—B8
Drachman, R. J. and D. C. Peaslee—DA7
Draper, J. E. and C. P. Baker—RA4
Dresden, M.—D11
Drisko, R. M.—FA15
Dropkin, J. J. and S. Orgel—B9
Edwards, D. A., B. Wolfe, A. Silverman, and J. W. DeWire—L10
Efremov, N.—H1
Eggler, C. and C. M. Huddleston—C10
Eisberg, R. M., H. Palevsky, M. E. Rickey, and T. I. Taylor—W5
Eisenberg, Y.—S8
Eisinger, J., C. F. Cook, and C. M. Class—L3
Engel, Olive G.—H10
Fafarman, A. and M. H. Shamos—S12
Falkoff, D. L.—F4
Fang, P. H.—M9
Farwell, George W. and Harvey E. Wegner—V16
Ferguson, G. A., J. Halpern, R. Nathans, and P. F. Yergin—W3
Fields, T. H., J. G. Fox, J. A. Kane, R. A. Stallwood, and R. B. Sutton—PA6
Finlay-Freundlich, E.—U7
Fischer, G. E.—Y14
Fischer, Vera Kistiakowsky—KA3
Fisher, L. H.—J4
Fluharty, R. G.—FA4
Foner, Simon—T3
Fowler, Charles A., Jr., and Edward M. Fryer—T4
Frenkiel, F. N.—VA1
Frisch, Harry L. and Joel L. Lebowitz—QA8
Gaffney, John and W. C. Overton, Jr.—D4
Garber, M. and D. E. Mapother—D13
Geiger, K. W. and D. C. Rose—RA12
Geller, K., J. Halpern, and Paul F. Yergin—W4
Gibbons, J. H. and H. W. Newson—RA1
Gibson, G. and P. Stehle—V12
Givin, H. H., G. K. Farney, T. M. Hahn, and B. D. Kern—Q15
Goldberger, M. L., M. L. Gellman, and W. E. Thirring—U5
Goldburg, W. I., S. A. Cox, and R. M. Williamson—L4
Golden, Robert K. and Sherman Frankel—G16
Gourary, B. S. and R. W. Hart—T8
Gove, H. E., E. B. Paul, A. E. Litherland, and G. A. Bartholomew—SA9
Green, C. D. and D. ter Haar—QA7
Green, D. W., J. N. Cooper, and J. C. Harris—FA9
Greenberg, J. Mayo—IA7
Greenblatt, M. H.—OA4
Griffith, Gordon L.—P4
Guernsey, Janet B. and Clark Goodman—P7
Gupta, Suraj N.—M1
Guss, Donald, Lawrence Killion, and F. T. Porter—KA9
Gutowsky, H. S.—A2
Haar, Lester and A. S. Friedman—H4
Hafner, Everett Mark—DA3
Handley, T. H. and B. L. Cohen—G2
Hanson, H. P. and J. R. Knight—JA1

Hanson, W. B. and J. R. Pellam—D15
Harman, T. C., R. K. Willardson, and A. C. Beer—B3
Harris, D. R. and A. L. Hodson—X7
Hart, Edward W.—Z9
Harvey, J. A., C. E. Porter, and D. J. Hughes—RA8
Heckrotte, Warren—IA10
Heinz, O.—FA8
Henkel, John H.—I4
Henry, Warren E.—D9
Herman, R. C., I. L. Mador, R. F. Wallis, and M. C. Williams—B10
Hesketh, R. V. and E. E. Schneider—B13
Heydenburg, N. P. and G. M. Temmer—L5
Holmes, John R. and Leon Pape—JA5
Hopson, J. E. and C. E. Nielsen—C13
Horton, G. K. and E. Phibbs—DA1
Hourd, R. F., J. R. Fleming, and J. J. Lord—S5
Howard, R. A., P. M. Fitzpatrick, H. E. Hoffman, and J. S. Urban—X3
Hudis, J., E. Baker, and G. Friedlander—G4
Hudson, R. P.—O5
Hughes, Raymond H.—JA7
Hunt, W. A., R. M. Kline, and D. J. Zaffarano—G1
Hurley, J. P. and P. S. Jastram—KA8
Jackson, J. David—SA15
Jackson, J. L. QA2
Jacobs, Donald H. and Milton E. Pugh—H14
Jacobsohn, B. A.—U6
Jakobson, M. and J. H. Manley—C7
Jan, J.-P. and J. S. Koehler—Z7
Jancovici, B.—IA8
Jansen, L. and Z. I. Slawsky—H2
Jennings, B., J. B. Weddell, and R. L. Hellens—P3
Johnson, C. H. and J. L. Fowler—P12
Johnson, F. S., J. D. Purcell, and R. Tousey—JA4
Johnson, Peter D. and Ferd E. Williams—B15
Johnston, L. H., E. A. Day, and J. H. Williams—C1
Jones, D. R.—K9
Jones, Harry—F1
Kaiser, H. F.—C6, N2, SP1
Kane, J. A., R. A. Stallwood, R. B. Sutton, T. H. Fields, and J. G. Fox—Y4
Kao, S. K. and A. F. Clark—Y3
Kaplon, M. F., J. Crussard, J. Klarmann, and J. Noon—X2
Karle, I. L.—O2
Keller, J. M. and E. Koenigsberg—Z2
Kiehn, Robert M. and Clark Goodman—P6
Kim, Y. B., J. R. Burwell, H. O. Cohn, C. J. Karzmark, and R. W. Thompson—X5
King, D. T. and H. M. Block—S13
Klein, Abraham—U9, SP3
Klein, Martin J. and Paul H. E. Meijer—QA4
Koehler, W. C. and E. O. Wollan—T9
Koerts, L., A. Schwarzschild, R. Gold, and C. S. Wu—G7
Koshiba, M. and M. F. Kaplon—S10
Koslov, S., V. Fitch, and J. Rainwater—K12
Krohn, V. and S. Raboy—F12
Kruse, U. E. and J. M. Teem—V1
Kunz, W. E., C. D. Moak, and W. M. Good—Q8
Lafferty, D. L., L. A. Rayburn, and T. M. Hahn—P9
Landsberg, P. T.—QA10
LaPorte, Otto—VA2
Lassettre, E. N., A. S. Berman, S. Silverman, and M. E. Krasnow—OA12
——, S. Silverman, and M. E. Krasnow—OA13
Lax, Benjamin, H. J. Zeiger, and R. N. Dexter—B7
Lax, Melvin and Joel L. Lebowitz—I5
Lazar, N. H. and P. R. Bell—G8
LeBlanc, J. M., J. M. Cork, and S. B. Burson—KA11
Leder, Lewis B. and L. Marton—OA7
Lehner, J. and G. M. Wing—QA3
Leiss, J. E. and C. S. Robinson—PA3
Levin, J. S. and D. J. Hughes—RA5
Levine, S. H., R. S. Bender, J. N. McGruer, and W. F. Vogelsang—Q6
Levinson, C., K. Brueckner, and H. Mahmoud—U12
Levinson, John—T1
Levinthal, Cyrus—E3
Lindenbaum, S. J. and Luke C. L. Yuan—PA8
Lindqvist, Torsten and Allan C. G. Mitchell—G9
Lindsay, John C. and A. V. Masket—Z5
Linsley, John—S6
Loeb, A. L. and J. B. Goodenough—I2
Loeb, L. B.—J3
Lokanathan, S., J. Steinberger, and H. B. Wolfe—K8
Lorrain, Paul, R. Béique, P. Gilmore, P. E. Girard, A. Breton, and P. Piché—C4
Lyons, D. H. and A. M. Feingold—DA12
Lyons, Harold—O1
Malenka, B. J.—IA13
Malkus, Willem V. R.—VA4
Malm, R. and D. R. Inglis—Q14
Mandeville, C. E. and H. O. Albrecht—B14
Mann, D. E. and Earle K. Plyler—JA8
Mann, Leonard A., Ray A. Grandey, and Arnold F. Clark—S11
Marder, S., V. W. Hughes, and C. S. Wu—FA16
Mark, Hans, Clyde McClelland, and Clark Goodman—L2
Marshall, J. F., R. A. Shatas, and M. A. Pomerantz—OA6
Marshall, John—R2
Marton, L.—J1
——, Tommy F. McCraw, and J. Arol Simpson—OA8
Massey, J. T., C. I. Beard, and C. K. Jen—JA11
Matthias, B. T.—O4
McClure, J. W.—Z3
McCormick, Philip T.—V11
McGuire, A. D., M. Camac, M. L. Halbert, and J. B. Platt—K10
McSkimin, H. J., A. J. Williams, and R. M. Bozorth—I3
Melvin, M. Avramy—H9
Meneghetti, David and S. S. Sidhu—Z11
Merritt, J. and D. Hamlin—PA5
Metzger, F. R. and W. B. Todd—KA13
Mihelich, J. W.—KA7
Millburn, G. P., W. Birnbaum, W. E. Crandall, and L. Schecter—IA11
Miller, D. W., V. K. Rasmussen, and M. B. Sampson—SA4
Milton, J. C. D. and J. S. Fraser—KA15
Miskel, J. A. and M. L. Perlman—G6
Mize, J. P., J. W. Starner, and M. E. Bunker—KA10
Moak, C. D., W. M. Good, and W. E. Kunz—Q11
Morrison, P.—S3
Moszkowski, Steven A.—DA2
Mould, R. E. and D. E. Mapother—D14
Muehlhause, C. O., E. der Mateosian, and Michael McKeown—B11
Muschlitz, E. E., Jr.—OA14
Nagle, D., J. Marshall, L. Marshall, and W. Skolnik—Y10
Neaves, A. and D. ter Haar—B1
Neiler, J. H., F. Muckenthaler, and James Schenck—Q5
Nelkin, M. S. and H. A. Bethe—IA3
Nelson, E. B., E. H. Geer, and R. R. Carlson—SA7
Newkirk, J. B.—I1
Newson, H. W. and J. H. Gibbons—Q10
Nielsen, C. E. and J. E. Hopson—C15
Noon, J. H. and M. F. Kaplon—S7
Noyes, H. P.—IA5
O'Neill, Gerard K.—P2
Orear, Jay, C. H. Tsao, J. J. Lord, and A. B. Weaver—K7
Osborne, L. S., Y. Goldschmidt-Clermont, and G. Parker—PA1
Overton, W. C., Jr. and J. R. Clement—D5
Packard, M. E.—A3
Palevsky, H. and R. M. Eisberg—W6
Palma, M. B., M. U. Palma, and D. Palumbo—F9
Park, David—T5
Parratt, L. G.—I6
Passaglia, E. and W. F. Love—Z8
Peaslee, D. C.—DA8
Peck, R. A., Jr.—C3
Penfold, A. S. and J. E. Leiss—PA2
Percus, Jerome K. and George J. Yevick—QA6
Perlman, Morris L. and Joan Welker—G15
Peter, Martin and M. W. P. Strandberg—JA13
Petritz, R. L.—Z1
Pfann, W. G. and W. van Roosbroeck—B5
Pilcher, V. E., R. S. Carter, and A. Stolovy—RA7
Pines, David—J2
Plumb, Harmon H. and Jules A. Marcus—D6
Pomerantz, M. A., J. F. Marshall, and R. A. Shatas—OA5
Potter, J. L. and N. M. Shapiro—VA7
Price, P. J.—B2
Pruett, C. H. and R. G. Wilkinson—KA1
Pugh, G., D. H. Frisch, and R. Gomez—FA14
Pulvari, C. F.—I8
Ramsey, N. F.—A1
Rankin, Bayard—V9
Rayburn, L. A., D. L. Lafferty, and T. M. Hahn—P10
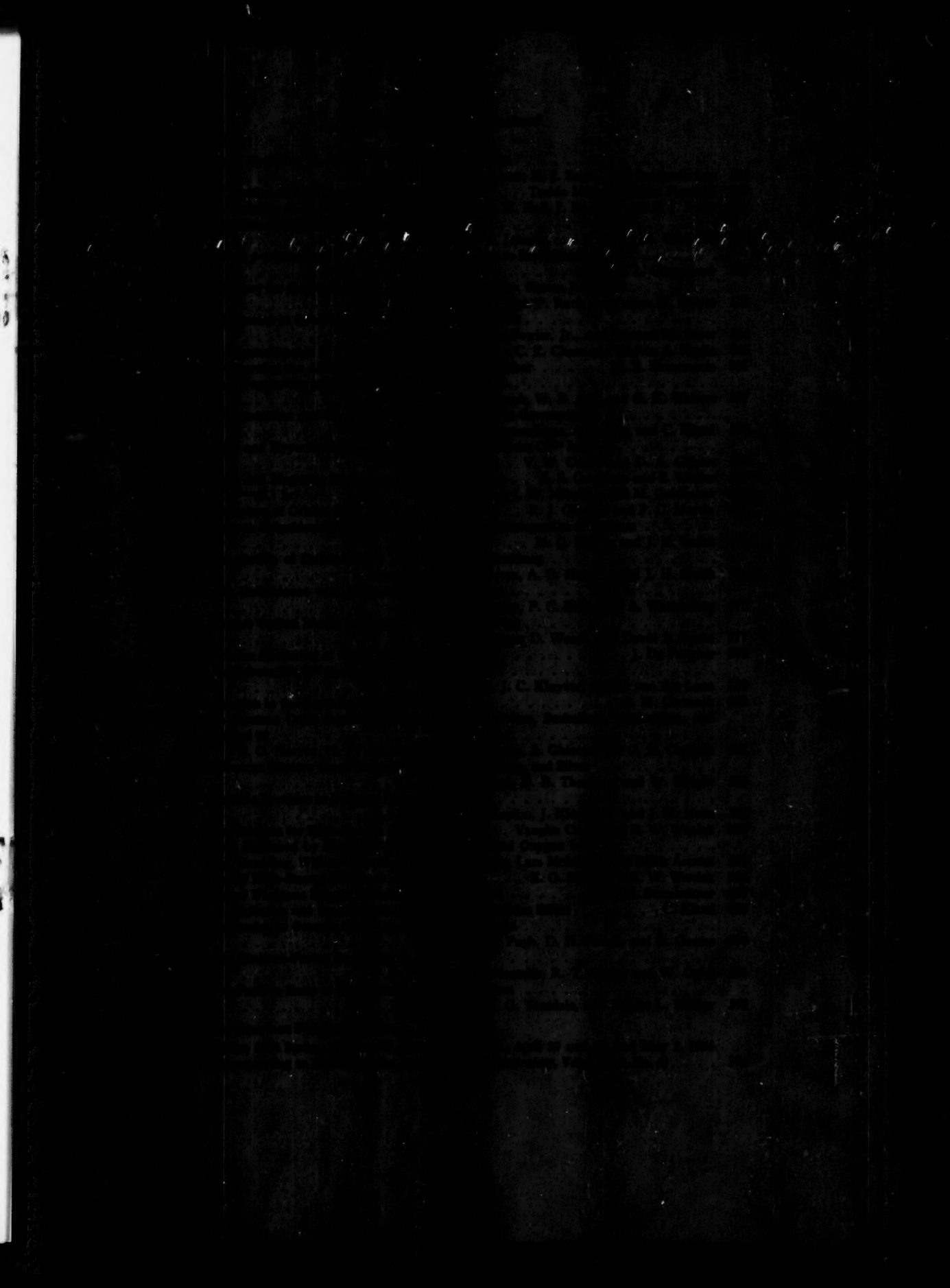
Recknagel, Arthur and Bernard Hamermesh—SA10
Reier, Melvin and Morris H. Shamos—P8
Reynolds, J. B. and K. G. Standing—Q3
Ribe, F. L. and J. D. Seagrave—SA1
Ringo, G. R. and S. Wexler—W9
Roberts, A., J. Tinlot, and E. M. Hafner—Y9
Robinson, C. S. and J. E. Leiss—PA4
Rogers, F. T.—VA6
Rogers, T. F.—JA9
Rohrlich, F.—V10
Rosenfeld, Arthur H.—PA7
Rosenstock, Herbert B.—I10
Rosenthal, Jenny E.—OA1
Ross, A. W. and D. ter Haar—Z6
Ross, Marc H.—IA4
Rothstein, Jerome—QA11
Ruark, Arthur E.—M13
Rubin, Robert J.—QA1, QA9
Rushworth, F. A.—F11
Sagane, Ryokuchi—X1
Sampson, John L., Edward E. Altshuler, and Charles R. Mingins—I9
Sands, R. H., J. Townsend, and H. P. Hood—F7
Saraf, Babulal—G5
Schaeffer, Oliver A. and Henry R. Owen—H8
Scharff-Goldhaber, Gertrude and Michael McKeown—G12
Schecter, L., W. E. Crandall, G. P. Millburn, and J. Ise—W1
Scherrer, V. E., B. A. Allison, and W. R. Faust—P11
Schluter, Robert A.—PA9
Segall, Benjamin—DA11
Seliger, H. H.—FA12
Selove, W.—Y7
Shafroth, S. M. and S. S. Hanna—Q13
Shapiro, A. M., C. P. Leavitt, and F. F. Chen—Y6
Shapiro, I. I. and J. M. Teem—IA9
Sheridan, W. F., J. A. Dillon, Jr., and S. N. Ghosh—OA15
Shmoys, Jerry and Samuel N. Karp—V8
Shure, K., P. A. Roys, and J. J. Taylor—FA10
Siegel, K. M., A. H. Halpin, and A. L. Maffet—VA3
Simon, Albert—V14
Simpson, O. D.—C11
Singer, S. F.—S4
Sladek, Ronald J.—D8
Snyder, Conway W. and Vincent E. Parker—P1
Solt, I. H., Jr., and M. W. P. Strandberg—F5
Soules, Jack and C. H. Shaw—JA2
Spencer, L. V.—EA11
Spicer, B. M., A. S. Penfold, and J. Goldemberg—L7
Spohr, D. A. and R. T. Webber—D7
Stearns, M. B., M. Stearns, L. Leipuner, and S. DeBenedetti—K11
Stahl, R. H.—V12
Steenberg, N. R.—DA10
Steffen, Rolf M.—G17
Stein, Irving—M14
Steinberger, Jack and William Chinowsky—K2
Stern, A. W.—M11
Sternglass, E. J.—FA7
Sternheimer, R. M.—V1
St. John, Robert M. and J. G. Winans—OA11
Strandberg, M. W. P. and M. Tinkham—JA15
Sugihara, T. T. and I. Halpern—L12
Sun, K. H., P. R. Malmberg, and F. A. Pecjak—C12
Sunyar, A. W.—KA4
Sutton, R. B., T. H. Fields, J. G. Fox, J. A. Kane, W. E. Mott, and R. A Stallwood—Y5
Swann, C. P. and F. R. Metzger—P5
Swann, W. F. G.—S2
Swihart, J. C. and F. J. Belinfante—M3
Talmi, I. and B. C. Carlson—DA13
Tamor, S.—IA14
Taylor, William J.—Z10
Teem, J. M. and U. E. Kruse—Y11
Teller, Edward—N3
Temmer, G. M.—L1
ter Haar, D.—D16, O3
Terrell, J. and D. M. Holm—SA12
Thacher, H. C., Jr., and Paul B. Dorain—H6
Thirring, W. E.—U3
Thompson, R. W., J. R. Burwell, H. O. Cohn, R. W. Huggett, and C. J. Karzmark—X6
Ting, Yu and Dudley Williams—F3
Tinkham, M. and M. W. P. Strandberg—JA14
Tinlot, John—R3
Tittman, Jay—W7
Tobias, Cornelius—E1
Tobocman, W. and M. Kalos—DA5
Tomboulian, D. H. and P. L. Hartman—C9
Toms, M. E., H. Gerardo, and W. E. Stephens—L8
Townes, C. H.—A4
Trail, Carroll C. and C. H. Johnson—Q9
Trambarulo, Ralph, Henry Lackner, Paul Moser, and Harold Feeny—JA12
Trammell, G. T.—IA6
Treiman, S. B. and M. Blume—S1
Turner, C. M.—C2
Urquhart, H. M. A. and J. E. Goldman—T10
Varma, Jagdish—G14
Vasileff, H. D.—I12
Voyvodic, L.—X4
Wacker, Paul F.—V4
Wada, W.—IA1
Walker, W. D., J. Crussard, and M. Koshiba—K5
Waniek, R. W. and Vaughn Culler—W2
Warshaw, S. D., R. A. Swanson, and A. H. Rosenfeld—SA2
Watanabe, Satosi—M10
Weigand, Clyde—R1
Weinstock, E. V. and J. Halpern—L11
Welton, T. A.—M12
Wick, G. C.—U1
Wilcox, J. M. and B. J. Moyer—Y13
Willard, D.—X8
Willardson, R. K., T. C. Harman, and A. C. Beer—B4
Williams, Robert W.—S9
Witmer, Enos E.—FA13, SP2
Wood, R. E.—RA3
Wolfenstein, Lincoln—R4
Wright, S. C. and R. A. Schluter—PA10
Yagoda, Herman—S15
Yamaguchi, Yoriko and Yoshio Yamaguchi—U4
Yang, C. N. and R. Mills—M7
Yearian, H. J., J. M. Kortright, and R. H. Langenheim—T11
Yevick, George J. and Jerome K. Percus—QA5
Zahn, C. T. and W. G. Schweitzer, Jr.—OA3
Zemach, A. C. and R. J. Glauber—DA9
Zimmerman, Robert L., David H. Frisch, and Daniel I. Cooper—Y2
Zirkle, R. E.—E2
Zweifel, P. F. and H. Hurwitz, Jr.—W8